

SOCIETY OF PETROLEUM ENGINEERS



FUNDAMENTALS OF DRILLING ENGINEERING

Robert F. Mitchell
Stefan Z. Miska

SPE TEXTBOOK SERIES VOL. 12

Fundamentals of Drilling Engineering

Fundamentals of Drilling Engineering

Editors:

Robert F. Mitchell

Halliburton

Stefan Z. Miska

University of Tulsa

Contributors:

Bernt S. Aadnoy, *University of Stavanger*

Neal Adams, *Neal Adams Services*

John W. Barker, *ExxonMobil*

J.C. Cunha, *Petrobras America*

Alfred W. Eustes III, *Colorado School of Mines*

Ross L. Kastor, *Antelope Engineering*

Vassilios C. Kelessidis, *Technical University of Crete*

Roberto Maglione, *Eni SpA*

Stefan Z. Miska, *University of Tulsa*

Robert F. Mitchell, *Halliburton*

Evren Ozbayoglu, *University of Tulsa*

Jim Powers, *ExxonMobil*

Ronald Sweatman, *Halliburton*

Society of Petroleum Engineers

© Copyright 2011 Society of Petroleum Engineers

All rights reserved. No portion of this book may be reproduced in any form or by any means, including electronic storage and retrieval systems, except by explicit, prior written permission of the publisher except for brief passages excerpted for review and critical purposes.

Manufactured in the United States of America.

ISBN 978-1-55563-207-6
ISBN 978-1-55563-338-7 (Digital)

Society of Petroleum Engineers
222 Palisades Creek Drive
Richardson, TX 75080-2040 USA

<http://www.spe.org/store>
books@spe.org
1.972.952.9393

Preface

Drilling engineering is a multidisciplinary subject, including a broad spectrum of topics in engineering, geology, chemistry, and physics. A general textbook must cover all these topics at greater than superficial depth and with reasonable balance in an abbreviated form. This is not an easy task. For instance, a well-known book on drilling fluids fills more than 600 pages, while *Fundamentals of Drilling Engineering* must cover similar topics in only 60 pages. Similar problems of topic selection, condensation, and presentation must be solved for each of the other disciplines covered in the textbook. Because the book must be useful for introductory studies, intermediate studies, and post-graduate studies, each topic not only must cover elementary concepts but also include more advanced topics.

The specific chapter topics covered in this book include the following:

- **Rotary Drilling.** This chapter describes the basics of rotary drilling; there are a number of elementary problems posed, suitable for an introductory course on drilling.
- **Introduction to Geomechanics in Drilling.** The objective of this chapter is to introduce the basic concepts of geomechanics related to drilling, including wellbore stability and the selection of suitable mud weights.
- **Drilling Fluids.** This chapter describes the types, functions, formulation, and testing of drilling fluids.
- **Cementing.** This chapter describes the primary objectives of cementing, the formulation and testing of cement, and methods for cement placement.
- **Drilling Hydraulics.** This chapter describes how wellbore pressures are calculated in a variety of scenarios, such as circulation and surge pressures.
- **Rotary Drilling Bits.** This chapter discusses bit types and selection criteria, factors affecting bit wear and drilling rate, and optimization of bit performance.
- **Casing Design.** This chapter addresses the types and functions of casing strings and the methods used for the selection, sizing, and design of well completions.
- **Directional Drilling.** This chapter presents directional well trajectory design, the control of the well path while drilling, and methods for modeling the torque and drag forces on a drillstring.
- **Fundamentals of Drillstring Design.** This chapter presents descriptions of the components of a drillstring, determination of the forces and moments in the drillstring, the effect of wellbore pressures on drillstring forces, and overall drillstring design.
- **Drilling Problems.** This chapter presents specific drilling problems and their solutions, including lost circulation, well control, recovery of broken drillstring components, and stuck drillpipe.

Most important among the first drilling engineering textbooks was *Applied Drilling Engineering*, written by Adam T. Bourgoyne, Keith Millheim, Martin Chenevert, and F.S. Young, which was published in 1986. A second edition was published in 1991 and remains available today, and almost every drilling engineer has a copy of the “red book” on his or her bookshelf. This landmark publication summarized the state of the art of scientific drilling that was developed in the 1945–1980 time period. A survey of the academic community tells us that this text is considered the most comprehensive of available textbooks, that it represents a good mix of theory and practice, that it is clear and easily understood, and that the example problems are effective teaching aids.

Fundamentals of Drilling Engineering is intended to be the successor to *Applied Drilling Engineering*. Why do we need a new book, and why change the title? No matter how you calculate the age of the latter work, it is at least 20 years old. Not many technical books can remain state of the art for 20 years or more, and this book is no exception; drilling technology has changed (significantly, in some areas) over the last 20 years. Further, the authors of *Applied Drilling Engineering* had a vision of the drilling engineering practices of the future; in many ways, the industry has taken different, unanticipated directions. The basic approach to drilling engineering has also moved from “rules of thumb” and correlations to a more fundamental, physics-based science, and there are many examples of this older style in that textbook. Some topics, such as torque-drag drillstring analysis, extended-reach wells, and underbalanced drilling, have taken on an importance not anticipated by the authors.

Drilling fluids and cementing technologies have evolved to solve new problems, notably environmental and disposal concerns. Geological topics cover wellbore pressures but miss other important problems, such as wellbore stability. Cuttings transport analysis has progressed far since the first book's publication. Other topics of modern importance, such as environmental, health, and safety issues, are completely absent from that textbook. Nevertheless, it will remain available, both as a useful source of information and as a historical document describing the state of the art of drilling engineering during a period of rapid technological development.

While the past 20 years have produced explosive growth in new technologies in the drilling industry, the greatest change has been the greatly increased use of computer analysis in exploration, well design, planning, and reporting. In the mid-1980s, when *Applied Drilling Engineering* was first published, computer applications were largely confined to "mainframe" or "minicomputers" not generally available to drilling engineers on a daily basis. The personal computer was still too primitive to be useful for engineering calculations, and drilling engineering calculations were still in the "hand calculation" stage. Any calculation that could not be summarized on the back of a file card was considered too complex to be useful. The first IBM PC was introduced in 1981, and with the introduction of the Intel 80386 chip in 1986, personal computers became capable of intense engineering calculations. In 2011, most routine engineering calculations are done with commercial software packages on personal computers. The effective and correct use of these programs is a new teaching problem for the petroleum industry, especially considering the large turnover in manpower expected over the next decade.

How do you replace a classic textbook, and why change the name? First, you don't replace it. *Applied Drilling Engineering* still has value. Because *Applied Drilling Engineering* will remain available for the foreseeable future, the new textbook would necessarily need a new name. One problem with the original name is that it is somewhat misleading in that it suggests a collection of drilling applications, rather than the fundamentals of drilling engineering it actually contains. To correct this potential misunderstanding, the word "Fundamentals" is prominent in the name of the new textbook. Second, to produce a worthy successor to *Applied Drilling Engineering*, we have taken the same approach used by the industry to drill a well—that is, we assembled a drilling team. Drilling engineering covers a widely diverse set of disciplines, and no single person can be an expert in all areas. Thus, the drilling team has experts in drilling fluids, cementing, geology, drillbits, and other areas. The editors sought out experts in industry and academia to contribute to this new textbook. The following pages give brief biographical information on each of these authors. This book could not have been produced without their efforts.

Robert F. Mitchell
Houston

Notes from the Editors

A Note on Prerequisites

This book is intended primarily for junior and senior petroleum engineering students in a four-year university-level type of program. Some parts also can be useful for graduate students as well as practicing engineers. We have assumed that the readers have successfully completed courses in calculus and differential equations, fluid mechanics and thermodynamics, engineering static, dynamics, and mechanics of materials. In general, a good understanding of conventional Newtonian mechanics (both fluid and solid) is sufficient for solving most drilling engineering problems, but some parts (e.g., those discussed in Chapters 3 and 4) also require a good background in chemistry that may be found in many textbooks at the bachelor's level. Most developments are furnished with derivations followed by numerical examples. Careful review of example problems is highly recommended before working on the "solve at home" types of problems provided at the end of each chapter.

We certainly hope that this book will also inspire the readers to study more advanced topics, as addressed in the recently published SPE book *Advanced Drilling and Well Technology*.

A Note About Units

An engineer or student new to drilling engineering will encounter the most peculiar collection of units to be found in any discipline. One reason for these odd units is that drilling engineering first developed as a craft. Wells have been drilled for millennia, and for much of that time, drilling has been a craft, not a science. The young driller learned his craft as a roughneck on a drilling rig and, as he acquired experience and seniority, eventually was put in charge of a drilling rig. Wells were successfully drilled because of the driller's intuition in anticipating and experience in solving problems.

Drilling engineering did not really exist as an engineering science before approximately 1945. Measurements were made with tools convenient to the driller. Mud weight would be measured in pounds of mud per gallon because the driller likely had a gallon bucket in which to weigh the mud. The origins of the 42-gal oil barrel are obscure, but some historical documents indicate that around 1866, early oil producers in Pennsylvania, USA decided they needed a standard unit of measure to convince buyers that they were getting a fair volume for their money. They agreed to base this measure on the more-or-less standard 40-gal whiskey barrel, but added an additional 2 gal to ensure that any measurement errors would always be in the buyer's favor. Drilling companies outside of the United States adopted metric units as well, measuring well depth in meters, volumes in liters, and diameters in centimeters.

We have to contend with this odd assortment of units because for almost any engineering calculation, unit conversion will be necessary. For instance, the exact formula for calculating hydrostatic pressure for a constant density fluid is:

$$\Delta p = \rho g \Delta Z, \quad (1)$$

where p is pressure, ρ is density, g is the acceleration of gravity, and Z is true vertical depth. Field units are psi for pressure, lbm/gal for density, and feet for depth. To reconcile these units, the equation has to be rewritten:

$$\Delta p = 0.05195 \rho \Delta Z \quad (2)$$

This mysterious coefficient 0.05195 equals $12/231$, where 231 is the number of cubic inches in a gallon and 12 is the number of inches in a foot. The acceleration of gravity g is given in the unfamiliar unit of 1 lbf/lbm.

A more challenging calculation is dynamic pressure:

$$p = \rho v^2, \quad (3)$$

where p is pressure, ρ is density, and v is velocity. Field units are psi for pressure, lbm/gal for density, and ft/sec for velocity. To reconcile these units, the equation has to be rewritten:

$$p = 0.001615 \rho v^2. \quad (4)$$

This coefficient 0.001615 equals $12/(231 \times 32.17)$, where 231 is the number of cubic inches in a gallon, 12 is the number of inches in a foot, and 32.17 is the acceleration of gravity in ft/sec^2 . Notice that it is necessary to

convert the field unit density to a consistent unit of density in this equation, but this time the conversion is the acceleration of gravity in ft/sec^2 , not 1 lbf/lbm. The potential pitfall is the confusion of weight with mass.

We have tried, in this text, to keep equations in the form of Eq. 1 or Eq. 3 and to avoid the use of equations like Eq. 2 and Eq. 4. The drawback to Eqs. 1 and 3 is that we must convert units. It would be preferable to have measurements in a system of units such that we wouldn't have to convert each property to a different unit to make a correct calculation.

There are systems of units, called consistent units, which have the properties we desire. The system most commonly used is the SI system of units, based on the metric system. There exist consistent English units systems as well, but they are even more obscure than drilling engineering units and are not commonly used. The SI units and conversion factors can be found in *The SI Metric System of Units and SPE Metric Standards*, published by SPE. It is highly unlikely that drillers will adopt this system, but the scientific world uses it as a matter of course.

When making engineering calculations, the safest approach is to convert all properties to SI units, perform the calculation, and then convert the result back to field units. With practice, some calculations (such as Eq. 1) become so familiar that one would simply use the coefficient 0.052. With computer programs and spreadsheets, use of SI units is particularly easy, and we recommend their use. For instance, Eq. 3 in SI units can be calculated with no concern about gravity constants whatsoever.

For a proposed list of standard symbols for drilling engineering, please refer to the Appendix that begins on page 677.

Acknowledgments

While working on this book, particularly on Chapters 8 and 9, I received help from many students, staff, and faculty collaborating with me under the auspices of the University of Tulsa Drilling Research Projects (TUDRP). I would also like to express my appreciation to the students in my Advanced Drilling course for their constructive feedback. Comments and suggestions from Texas A&M University students related to Chapter 9 are also greatly appreciated. I also wish to thank those students who helped to develop figures and verify calculations. I am very grateful to all member companies of TUDRP for their financial assistance and the guidance and technical support of their representatives. Their contributions to my research help make it possible to formulate new and useful concepts and to educate young, talented engineers. Ms. Paula Udwin deserves special thanks for her support and help with the typing of Chapters 8 and 9. I am deeply thankful to my wife Anna for her many years of continual support, understanding, and patience.

Stefan Miska
Tulsa

First, I would like to acknowledge the influence of John Thorogood on the inception and development of this text and the companion text, *Advanced Drilling and Well Technology*. Second, I would like to thank the authors for their efforts in making this text technically sound and state of the art. They have performed an important service to the industry. Stefan and I both appreciate the help and support of SPE and the SPE staff, especially Jennifer Wegman.

Robert F. Mitchell
Houston

About the Authors

Robert F. Mitchell is a Halliburton Technology Fellow in the Drilling and Evaluation Division of Halliburton. He has published more than 80 papers on wellbore and well completion problems, including wellbore thermal/flow simulation, drillstring mechanics, tubing buckling analysis, arctic well completions, tubular stress analysis, and geomechanics. Principal technical accomplishments include the first deep permafrost thaw subsidence casing design, the comprehensive analysis of the post-buckling equilibrium of tubulars, and the accurate prediction of dynamic surge pressures. Mitchell wrote the Casing and Tubing Design chapter for the textbook *Petroleum Well Construction*, was the Drilling Engineering volume editor for SPE's *Petroleum Engineering Handbook*, and was an editor of and contributor to the SPE book *Advanced Drilling and Well Technology*. He has served as a technical editor for *Applied Mechanics Reviews*, the *Journal of Energy Resources Technology*, *SPE Computer Applications*, and *SPE Journal* and as Executive Editor for *SPE Drilling & Completion*. Mitchell was vice president of Enertech Engineering and Research Company from 1980 to 1996 and worked at Exxon Production Research Co from 1973 to 1980. He holds BA, MME, and PhD degrees from Rice University and is a registered professional engineer in Texas. Mitchell received the 2005 SPE Drilling Engineering Award and is an SPE Distinguished Member.

Stefan Z. Miska is currently the Jonathan Detwiler Endowed Chair Professor of the McDougall School of Petroleum Engineering and Director of the Tulsa University Drilling Research Projects (TUDRP) at the University of Tulsa. He holds MS and PhD degrees from the University of Mining and Metallurgy in Cracow, Poland; recently, he was awarded the title of Professor of Technical Sciences by the president of Poland. Over the years, Miska has taught at his alma mater, the Norwegian Institute of Technology, and New Mexico Tech. In 1992, he joined the University of Tulsa as chair of its Petroleum Engineering Department. Miska has published more than 170 technical papers and contributed to several books. He was involved in the successful design and development of a downhole, turbine-type motor for air drilling and has been instrumental in the development of research facilities for wellbore hydraulics at simulated downhole conditions. He also has made contributions to the development of new buckling concepts and the axial force transfer in extended-reach drilling. Miska's current research interests are focused on wellbore hydraulics, mechanics of tubulars, and directional drilling. He is involved with SPE in many capacities, including serving as a Technical Editor for *SPE Drilling & Completion* and as a member of the Drilling and Completions Advisory Committee. He was the recipient of the 2000 SPE Distinguished Petroleum Engineering Faculty Award and the 2004 SPE Drilling Engineering Award. He is also an SPE Distinguished Member.

Bernt S. Aadnøy is Chairman and Professor of Petroleum Engineering at the University of Stavanger; he previously worked for Phillips Petroleum, Rogaland Research, Statoil, and Saga Petroleum. Aadnøy has published more than 130 papers, mostly on rock mechanics and well technology. He is the author of several books, including *Mechanics of Drilling*, *Modern Well Design*, and *Petroleum Rock Mechanics*, and he served as editor of the SPE book *Advanced Drilling and Well Technology*. He also has served as a Technical Editor for *SPE Drilling & Completion*, *SPE Journal*, and the *Journal of Petroleum Science and Engineering*. Aadnøy holds a mechanical engineering degree from Stavanger Tech., a BS degree in mechanical engineering from the University of Wyoming, an MS degree in control engineering from the University of Texas, and a PhD degree in petroleum rock mechanics from the Norwegian Institute of Technology. He was the recipient of the 1999 SPE Drilling Engineering Award.

Neal Adams has more than 39 years of oil industry experience. Having started his career as a roughneck and floorhand on drilling and workover rigs, he has developed a worldwide reputation as a leading specialist in safety, well control, drilling and production, training, and problem solving. He is the author of numerous books and technical papers and has been an active member of SPE for 30 years; his contributions include serving as a Distinguished Lecturer (1982–1983), on the Board of Directors of the Gulf Coast Section, Program Committee for the SPE Annual Technical Conference and Exhibition, and chapter author for SPE's *Petroleum Engineering Handbook, Volume II: Drilling Engineering*. Adams holds an MS degree in petroleum engineering from the University of Houston. He is a registered engineer in Texas and Oklahoma.

John W. Barker is a retired engineer, formerly with ExxonMobil Development Co. At ExxonMobil, he was a staff engineer and worked with offshore drilling operations for more than 20 years. Barker holds a BS degree in civil engineering from Texas A&M University.

J.C. Cunha is Well Operations Manager for Petrobras America in Houston. His career spans engineering and management positions on several projects in South America, the Gulf of Mexico, Africa, and the Caribbean. Cunha wrote one of the chapters in SPE's book *Advanced Drilling and Well Technology* and is the author of more than 30 SPE papers. Cunha has served on several SPE committees and was selected as a 2010-2011 SPE Distinguished Lecturer. He holds a civil engineering degree from Juiz de Fora Federal University, Brazil, an MS degree from Ouro Preto University, Brazil, and a PhD degree in petroleum engineering from the University of Tulsa.

Alfred William Eustes III is an associate professor in the Petroleum Engineering Department at the Colorado School of Mines, where he researches and teaches a variety of drilling, completion, and workover-related topics. His research specialties include drilling and completion engineering and operations, as well as experimental and drilling model research. Eustes is a registered professional engineer with the state of Colorado and has 32 years of drilling, completion, workover, and production engineering and operations experience, 9 of which were with Arco Oil and Gas Co. Since then, he has been involved in drilling operations from the Rocky Mountains to Alaska and with the DOE at Yucca Mountain and Hanford. He advised NASA regarding extra-terrestrial drilling issues and the National Science Foundation with respect to ice coring and drilling. Eustes holds a BS degree in mechanical engineering from Louisiana Tech University, an MS degree in mechanical engineering from the University of Colorado at Boulder, and a PhD degree in petroleum engineering from the Colorado School of Mines.

Ross Kastor is president of Antelope Engineering and is also a lecturer in the College of Engineering at the University of Houston. Kastor was employed by Shell Oil Co. from 1950 to 1991. He holds BS and MS degrees from Ohio State University.

Vassilios C. Kelessidis is an associate professor of drilling engineering and fluid mechanics in the Mineral Resources Engineering Department at the Technical University of Crete, Greece. Previously, he worked for more than 8 years in various technical and research positions in Anadrill Schlumberger, Dowell Schlumberger, and Schlumberger Cambridge Research. His expertise is in drilling fluid properties and drilling hydraulics, multiphase gas/liquid and solid/liquid flow, cuttings transport, drilling simulation, and development of novel drilling techniques. Kelessidis has published more than 65 technical papers with more than 200 citations and holds one patent. He holds a diploma from Aristotelian U. of Thessaloniki, Greece, an MS degree from Oregon State University, and a PhD degree from the University of Houston, all in chemical engineering.

Roberto Maglione is currently working for Eni SpA, Agip Division; he has covered different positions in drilling and completion operations, production laboratories, and R&D both in Milan, Italy, and abroad. Presently, he is a consultant on drilling operations and drilling fluids hydraulics and rheology. Maglione is the author or co-author of more than 80 technical papers related to several aspects of drilling operations, such as hydraulic optimization, surge and swab, well control problems, drilling fluids rheology and hydraulics, heat transfer, and multiphase fluid flow, as well as two books on drilling fluids rheology. Maglione holds an MS degree in mining engineering from the Polytechnic of Turin and is a registered professional engineer in Italy.

Evren M. Ozbayoglu is an associate professor of petroleum engineering at the University of Tulsa. Previously, he was a faculty member at the Middle East Technical University in Ankara, Turkey from 2002 to 2009. His work interests are focused primarily on topics related to drilling engineering. Ozbayoglu holds BS and MS degrees from the Middle East Technical University and a PhD degree from the University of Tulsa.

Jim Powers works in the Drilling Technical group of ExxonMobil Development Company; he has worked for more than 20 years in the areas of tubular design and threaded connection qualification, including more than 5 years of experience drilling land and platform wells. Powers has participated in API standards development for more than 20 years, serving as chairman of Subcommittee 5, which stewards tubular goods. He holds a BS degree in mechanical engineering from Rice University.

Ron Sweatman is Chief Technical Professional specializing in cementing, well integrity, reservoir conformance, borehole strengthening, lost circulation control, drilling trouble zone diagnostics, and CO₂ EOR/CCS technologies in Halliburton's Global Business and Technical Solutions group based in Houston. He has more than 42 years of experience, including 6 years in cement manufacturing and 36 years in well construction, production, and injection applications, with assignments in field laboratory testing services, field/office engineering, operations/area management, and regional/corporate technical support groups. Sweatman is the author of more than 50 technical publications and 29 patents. He holds a degree in chemistry from Louisiana State University and a degree in petroleum engineering from the University of Southwestern Louisiana and has served on many SPE, API, ISO, IADC, IEA, and other industry committees.

Contents

Preface	v
Notes from the Editors	vii
Acknowledgments	ix
About the Authors	x
1. Introduction to Rotary Drilling	1
1.1 Foreword	1
1.2 History of Drilling	1
1.3 The Drilling Team	5
1.4 Drilling Rigs	7
1.5 Drilling Rig Systems	15
1.6 Marine Drilling	36
1.7 Drilling Cost Analysis	40
2. Introduction to Geomechanics in Drilling	55
2.1 Borehole Stability Analysis for Vertical Wells	55
2.2 Borehole Stability Analysis for Inclined Wells	73
2.3 General Methodology for Analysis of Wellbore Stability	76
2.4 Empirical Correlations	80
3. Drilling Fluids	87
3.1 Introduction	87
3.2 A Brief History of Drilling Fluids	87
3.3 Functions of Drilling Fluids	89
3.4 Drilling-Fluid Categories	90
3.5 Clay Chemistry	95
3.6 Estimating Drilling Fluid Properties	98
3.7 Testing of Drilling Fluids	108
3.8 Solids Control	124
3.9 Health, Safety, and Environmental (HSE) Considerations	129
4. Cementing	139
4.1 Composition of Portland Cement	140
4.2 Cement Testing	141
4.3 Standard and Nonstandard Drilling Cements	145
4.4 Cement Additives	149
4.5 Cement Placement Techniques	160
4.6 Well Parameters Affecting Cement Design and Operations	173
5. Drilling Hydraulics	179
5.1 Introduction to Drilling Hydraulics	179
5.2 Hydrostatic Pressure Calculations	180
5.3 Steady Flow of Drilling Fluids	194
5.4 Rheological Models of Drilling Fluids	206
5.5 Laminar Flow in Pipes and Annuli	218
5.6 Turbulent Flow in Pipes and Annuli	245
5.7 Frictional Pressure Drop in an Eccentric Annulus	260

5.8	Frictional Pressure Drop With Pipe Movement	265
5.9	Calculating Steady-State Pressures in a Wellbore	267
5.10	Dynamic Surge and Swab Pressures	273
5.11	Cuttings Transport	279
6.	Rotary Drilling Bits	311
6.1	Introduction	311
6.2	Bit Types	312
6.3	Manufacturing and Design of Bits	317
6.4	IADC Bit-Classification System	326
6.5	IADC Bit Dull-Grading System	331
6.6	Rock-Failure Mechanism During Drilling	336
6.7	Wear Mechanism	342
6.8	ROP	352
6.9	Economics	363
6.10	Bit-Operation Practices	368
7.	Casing Design	385
7.1	Introduction	385
7.2	Casing Manufacture	387
7.3	Casing Standardization	388
7.4	Line Pipe	391
7.5	Strength of Materials	391
7.6	Casing-Tube Performance Properties	397
7.7	Corrosion	405
7.8	Casing Connections	407
7.9	Casing-Program Selection and Design	417
7.10	Probabilistic Reliability-Based Design of Casings	433
7.11	Computer-Based Design of Casings	434
7.12	Casing Stability	436
7.13	Special Casing-Design Considerations	441
8.	Directional Drilling	449
8.1	Fundamentals of Directional-Well Trajectory Design	449
8.2	Deviation Control	477
8.3	Tool-Deflection Orientation	511
8.4	Method of Vectors and Its Application to Directional Drilling	522
8.5	Torque-and-Drag Modeling and Calculations for 2D Well Profiles	538
8.6	Torque-and-Drag Modeling for 3D Well Profiles	557
9.	Fundamentals of Drillstring Design	585
9.1	Introduction	585
9.2	Drill Collars	585
9.3	Drillpipe and Tool Joints	596
9.4	Load Capacity of Drillpipe	610
9.5	Drillstring Design	615
10.	Drilling Problems	625
10.1	Lost Circulation	625
10.2	Well Control	631
10.3	Pipe Sticking and Fishing Operations	654
	Appendix—Proposed Standard Symbols for Drilling Engineering	677
	Author Index	681
	Subject Index	687

Chapter 1

Introduction to Rotary Drilling

J.C. Cunha, Petrobras, and Ross Kastor, Antelope Engineering

The objectives of this chapter are to introduce the student to the rotary-drilling process, familiarize the student with the basic rotary-drilling equipment, and introduce the student to fundamental operational procedures and drilling cost evaluation.

1.1 Foreword

Envision an amazing source of energy whose location is known but not easily accessible. Now imagine that this energy will be used to provide means of transportation for every person living on Earth. In addition, envision that this incredible energy will also allow every product, natural or industrialized, to be transported from or into virtually any place on the face of our planet. As a consequence of that, this energy will somehow be an important part of every venture in every country of the world.

No matter the nature of the business, it will, in some way, depend on that energy. You may think about any industrial enterprise, any large or small commercial endeavor, the construction industry, the entertainment or the tourism industries, and even the processes involved in producing other types of energy. Regardless of the venture, this extraordinary energy will always be necessary and almost every individual living on Earth, even in the most remote locations, will certainly depend on it.

Regrettably, the source of this energy is not located in a place of easy access. Concealed beneath millions of tons of rocks, trapped deep below ground, many thousands of meters under Earth's surface, this energy often is located in areas of very difficult access or even offshore, under very deep waters. Nevertheless, due to its importance in our lives, no matter the location or the depth, in some way we will have to find a means to establish a path between the energy source and the surface.

Somehow, in a notable work of engineering, a well will be drilled connecting the energy source to the surface. This well will have the necessary strength to withstand the enormous pressures produced by the adjacent rocks. It will prevent any damage to the surrounding environment. It will be outfitted with modern equipment to allow production in a safe and nondetrimental way.

The planning and execution of this remarkable work of engineering is the job of drilling engineers.

1.2 History of Drilling

Drilling for oil and gas is not new. Even though the modern techniques, equipment, and methods that are going to be described in this book are completely different from the ones used in the prehistoric era of the industry, there is evidence of wells purposely drilled for production of hydrocarbons as early as A.D. 347 in China. Also, there are reports of oilwell drilling activities in Japan by A.D. 600.

The first oil well drilled in Europe dates back to 1745 in Pechelbronn, France, where petroleum mining from oil sands had been taking place since 1498. After that, many wells were drilled, mostly using rudimentary hand tools, in Europe, North America, and Asia where an oil well was drilled in 1848 on the Aspheron Peninsula northeast of Baku. Following the Baku well, various shallow oil wells were drilled in Europe during the next decade.

There are many different versions about where the first well of the modern oil industry was drilled. Depending on the historian, locations and dates will vary widely. Also, there are many different depictions about what should be considered a *modern* well and what would differentiate it from a well that, even though it has produced oil, was not actually drilled having that as a primary goal. In this chapter, without dueling about whom, where, and when, which would be rather ineffectual, we will mention some important milestones and pioneers that have contributed to the advancement of the modern oil industry in those early days.

In 1858, in Oil Springs (then part of the township of Enniskillen), Ontario, Canada, a rudimentary 49-ft (14.93-m) well was dug by James Miller Williams with the intention to produce “kerosene” for lamps. Even though this is considered to be one of the pioneer ventures of the North American oil industry, the Williams well did not represent any significant advance as far as drilling technology is concerned.

A true milestone for the drilling industry and probably the world’s most widely recognized drilling milestone occurred in 1859. In that year, in Titusville, Pennsylvania, USA, Edwin L. Drake (**Fig. 1.1**) drilled what is, so far as known or documented, the first well purposely planned for oil in the United States. Even though there is evidence of oil and gas wells that had been drilled in the United States for as long as 40 years prior to the Drake well, most of those early wells were actually originally drilled in search of potable water or brine.

In the nineteenth century, cable tool rigs (see **Fig. 1.2**) were in widespread use in North America. Cable tool rigs pounded through soil and rock to drill the well by repeatedly dropping a heavy iron bit attached to a cable. Using a 6-hp steam engine (see **Fig. 1.3**) to power his cable tool drilling equipment, Drake drilled a well 69.5 ft deep (21.18 m) that initially produced oil at a rate believed to be from 8 to 10 B/D. **Fig. 1.4** presents some of the tools used in cable drilling.

Immediately after that first success, many other wells followed, causing the oil industry—and particularly its drilling segment—to experience an unprecedented growth.

1.2.1 Development of Rotary Drilling—The Modern Era. Percussion drilling was widely used by the oil industry until the 1930s. Even though there are archaeological records of the Egyptians using rotary drilling mechanisms as early as 3000 B.C., the process was little used in the early days of the industry because of its complexity compared to percussion drilling.

During the 1890s, Patillo Higgins, a mechanic and self-taught geologist, tried to prove his theory about the existence of oil at a depth of approximately 1,000 ft (305 m) below a salt dome formation south of Beaumont in eastern Jefferson County, Texas, USA. He gathered funding from various partners and drilled three wells, including one using a cable tool rig, but all three holes did not reach the proposed final depth because unconsolidated sand at a depth of approximately 400 ft (122 m) caused all three wells to be lost.

In 1899 Higgins partnered with Captain Anthony Francis Lucas, an engineer and navy officer who had immigrated to America a few years earlier, to try again to drill a proper test well in the region. Their first try, a well drilled in July 1899, was yet another disappointment, with the well being lost due to the same unstable sands that



Fig. 1.1—Edwin L. Drake (Giddens 1975). Used with permission from the Pennsylvania Historical and Museum Commission Drake Well Museum Collection, Titusville, Pennsylvania.

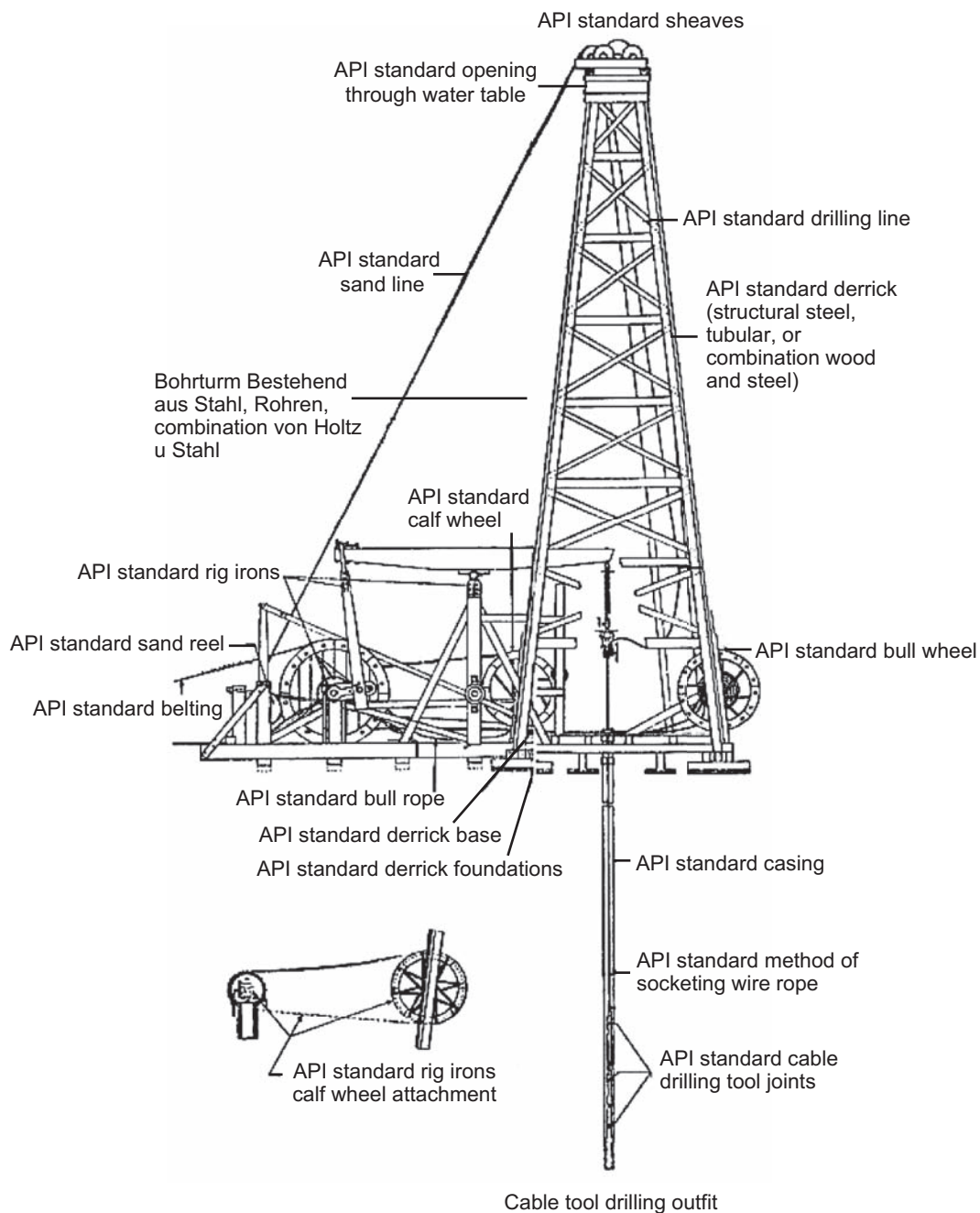


Fig. 1.2—Cable-tool rig schematic. After Brantley (1940).

caused the previous failures. Their second well, however, the fifth try in the region, finally succeeded in reaching the objective.

With operations initiated on 27 October 1900, the Lucas Spindletop well reached its final depth on 8 January 1901, and two days later, when a new drilling bit was being run into the well, it started flowing with an amazing and unprecedented rate of nearly 100,000 BOPD (Fig. 1.5), which at that time represented more than the entire oil production of the United States.

The Lucas Spindletop well, besides establishing the presence of large hydrocarbon deposits in the region, also demonstrated the viability of using rotary drilling rigs to drill oil wells in soft formations where cable tools could not be effectively used except at very shallow depths.

There is some disagreement about the final depth of the Lucas well. Captain Lucas stated that the final depth was 1,160 ft (353.55 m), while Al Hamill, the drilling contractor for the well, in an article written 50 years later

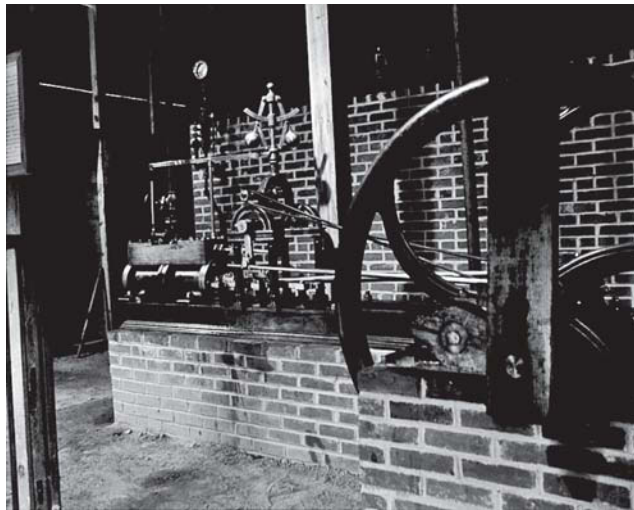


Fig. 1.3—Steam engine (Brantley 1971). Reprinted courtesy of Gulf Publishing.

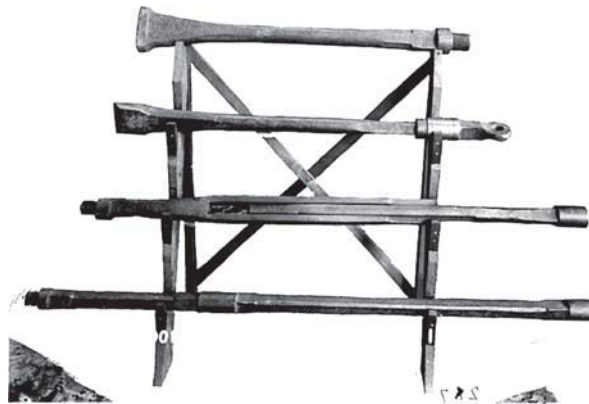


Fig. 1.4—Cable drilling tools (Brantley 1971). Reprinted courtesy of Gulf Publishing.



Fig. 1.5—The Lucas Spindletop well (circa January 1901). From Brantley (1971). Reprinted courtesy of Gulf Publishing.

reported the final depth as 1,020 ft (310.88 m). Nevertheless, more significant than the controversy is the importance of this well for the oil industry.

The well was drilled using the most advanced technology known, and after its initial uncontrolled geyser-like production, it was capped, allowing production to restart in a safe and controlled way. The Lucas well is considered by many as the birth of the modern oil industry. The fact that it had its operations initiated by the end of the last year of the nineteenth century and concluded on the very first days of the twentieth century just adds more symbolic meaning to this true milestone of an industry that changed the world.

1.3 The Drilling Team

Modern well drilling is an activity that involves many specialists and usually various companies. The expertise and number of engineers and technicians involved in the planning and execution of a drilling operation will depend on the type of well being drilled, its purpose, the well location, its depth, and the complexity of the operation.

A well drilled with the purpose of discovering a new petroleum reservoir is called an *exploration* (or *wildcat*) well. Wildcat wells are the very first ones drilled in a certain unexplored area. After a wildcat well has shown the potential of a reservoir to be productive, appraisal wells may be drilled to obtain more information about the reservoir and its extension. Once a newly discovered reservoir is considered economically viable, a development plan is established and *development* wells are drilled to produce the oil and gas present in the reservoir.

Besides the most common exploration and development wells, special wells may be drilled for a variety of purposes including stratigraphic tests and blowout relief (see Chapter 10). **Fig. 1.6** presents an overall classification of wells according to their purpose.

The rights for a company to explore a certain area must be secured before any activity is carried out. Due to the high risk involved in the business, it is not uncommon to have two or more companies forming a consortium for the venture. Normally in that case, one company—the operating partner—will lead the operation while the other partners, who will have proportional participation in all expenses and profits, may or may not have a say on the operational procedures depending on the clauses accorded in the joint operating agreement (often referred to as the JOA).

Prior to any drilling activity, seismic and geologic studies are carried out in order to determine the best location for the first exploration well. Those studies are performed by a company's geological team, which usually is responsible for recommending locations for wildcat wells, while the reservoir team will be responsible, on a later phase, for locating development wells. In either situation, the drilling team will be responsible for the planning and execution of the operation including its budget (cost estimation) and contingency plans.

Leading a drilling operation is not an easy task. Normally, the oil company that owns the exploration rights for the area, or the operating partner in case of a consortium, assembles a drilling team that in turn will prepare the detailed well design and the drilling program and establish operational procedures according to local regulations and the company's own health, safety, and environment (HSE) policy. This is done in order to conduct drilling operations in the most safe, clean, and economical way.

The drilling operation itself generally will be carried out by a drilling contractor that may be hired specifically for a certain well or on a long-term contract. The contractor will be responsible for performing the operations according to the well program using the equipment and procedures specified in the contract.

Prior to the initiation of the drilling operations, the wellsite must be prepared to receive the drilling rig and all other related equipment. The specific type of work for wellsite preparation will depend on the location and

<u>Objective</u>	<u>Trajectory</u>	<u>Environment</u>
<ul style="list-style-type: none"> • Exploration <ul style="list-style-type: none"> ◦ Wildcat ◦ Appraisal ◦ Extension • Development • Injection • Special purpose <ul style="list-style-type: none"> ◦ Stratigraphic ◦ Blowout relief 	<ul style="list-style-type: none"> • Vertical • Directional <ul style="list-style-type: none"> ◦ Inclined ◦ Horizontal ◦ Long reach ◦ Special design 	<ul style="list-style-type: none"> • Onshore • Offshore

Fig. 1.6—Well classification.

the infrastructure present. Offshore operations in unexplored areas may require a seafloor survey to determine the feasibility of installation of subsea equipment. Some onshore areas may require extensive preparation, and remote areas, without any infrastructure, may require costly and time-consuming preparation including road construction. **Fig. 1.7** shows an offshore location in the North Sea, an operation in western Canada, and another in Brazil's Amazon jungle.

During drilling operations, the operator will have at least one representative, usually a drilling engineer or technician, responsible for ensuring that operational standards are being followed by the drilling contractor and other service contractors involved in the process. Depending on the importance of the well, the operator may be represented by a team of specialists including engineers, geologists, drilling-fluid specialists, and others. The operator's representatives, besides ensuring that the well program is properly executed, will also be responsible for on-site decisions regarding minor adjustments or major changes to the drilling program that may be necessary due to unpredicted conditions.

During well drilling, various services will be needed depending on the type of well and its complexity. Common services required for oilwell drilling are related to drilling fluids (Chapter 3), directional drilling (Chapter 8), casing and cementing (Chapters 4 and 7), drilling bits (Chapter 6), and well logging (which is beyond the scope of this book). **Fig. 1.8** presents a typical drilling structural organization. The drilling engineer recommends the drilling procedures that will allow the well to be drilled as safely and economically as possible. In many cases, the

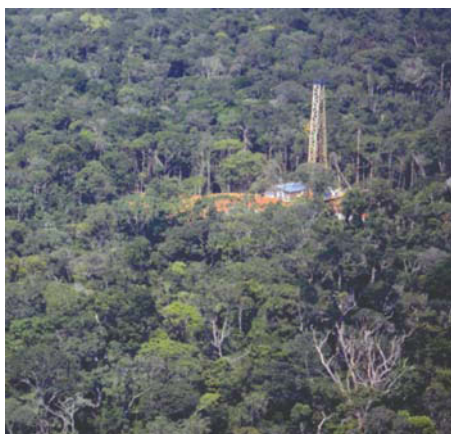


Fig. 1.7—Drilling operations in the Chinook Field, Gulf of Mexico (courtesy of Petrobras), Alaska (courtesy of Minerals Management Service), and Brazil's Amazon jungle (courtesy of Petrobras).

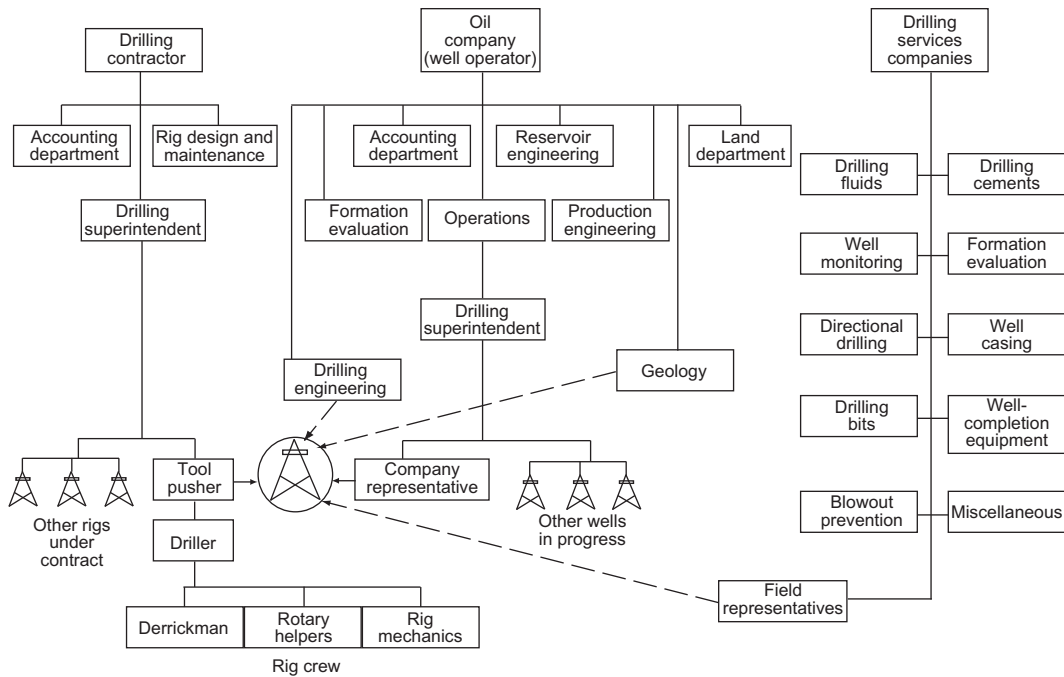


Fig. 1.8—Typical drilling rig organization (Bourgoyne et al. 1986).

original well plan must be modified as drilling progresses because of unforeseen circumstances. These modifications also are the responsibility of the drilling engineer. The company representative, using the well plan, makes the on-site decisions concerning drilling operations and other services needed. Rig operation and rig personnel supervision are the responsibility of the tool pusher or drilling supervisor.

1.4 Drilling Rigs

Currently, rotary drilling is the standard oilwell drilling method for the drilling industry, with almost all operations being performed by rotary-drilling rigs. Rigs will vary widely in size, drilling capability, level of automation, and environment in which they can operate. Nevertheless, the basic rotary-drilling process is the same for all types of rigs as shown in Fig. 1.9.

The well is drilled using a bit that, under a downward force and rotation, breaks the rock into small pieces. The force is provided by the weight of pipes placed above the drilling bit, while rotation generally is provided at surface by equipment that rotates the *drillstring*, which in turn transmits rotation to the bit. As the bit drives into the ground, deepening the well, new pipes are added to the drillstring. The small pieces of rock (*cuttings*), resulting from the bit action, are transported to surface by a fluid (*drilling fluid* or *mud*) that is constantly pumped into the hollow drillstring all the way to the bottom of the hole, where it passes through small orifices placed at the bit, and returns to surface carrying the cuttings through the annular space formed between the well and the drillstring. Once reaching the surface, the cuttings are separated from the fluid, which is treated for reuse.

Generally, rotary rigs are classified as either land rigs or marine rigs. Fig. 1.10 shows rig classification under those categories.

1.4.1 Land Rigs. Land rigs, in a broad sense, can be categorized as conventional and mobile. Mobile rigs tend to be more easily transported, while the conventional rigs will take longer to be moved from one location to another.

Conventional rigs normally use a standard derrick that needs to be built on location before drilling the well and is usually dismantled before moving to the next location. In the past, quite often the derrick was left standing above the well after it began production in case workovers became necessary; however, today's modern rigs are usually built so that the derrick can be easily disassembled and moved to the next wellsite. There also are special rigs that are built in a way that rig pieces, when disassembled, will never exceed a certain weight, allowing transportation by helicopter. Those rigs, also called *helitransportable* rigs, are used in remote areas with no road infrastructure and also on jungle operations.

Mobile rigs have a cantilever derrick or a portable mast that is raised and lowered as a whole rather than being constructed piecemeal. The rig-up and rig-down operation is less time-consuming than on conventional rigs.

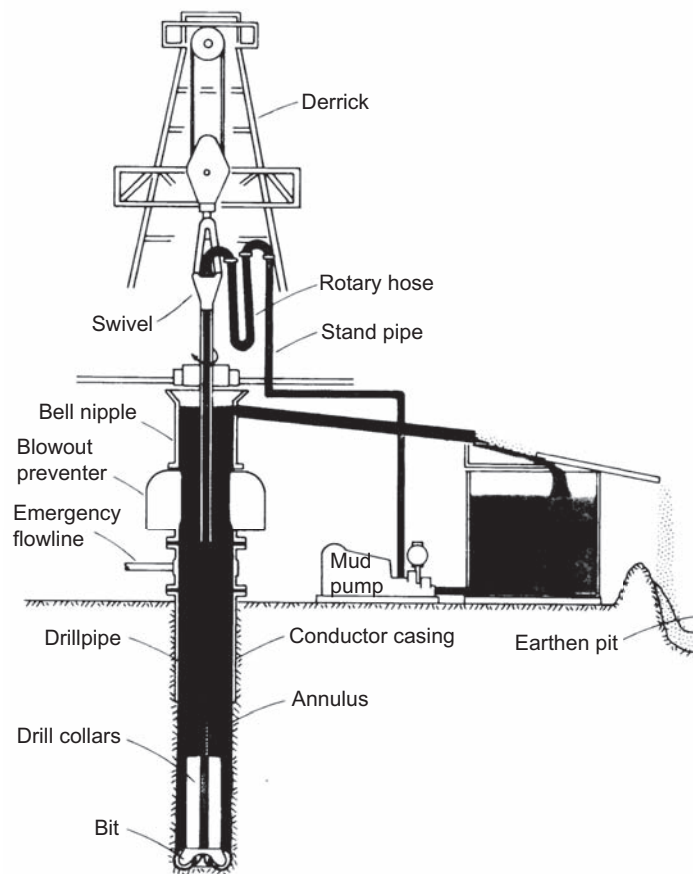


Fig. 1.9—The rotary drilling process (Bourgoyne et al. 1991).

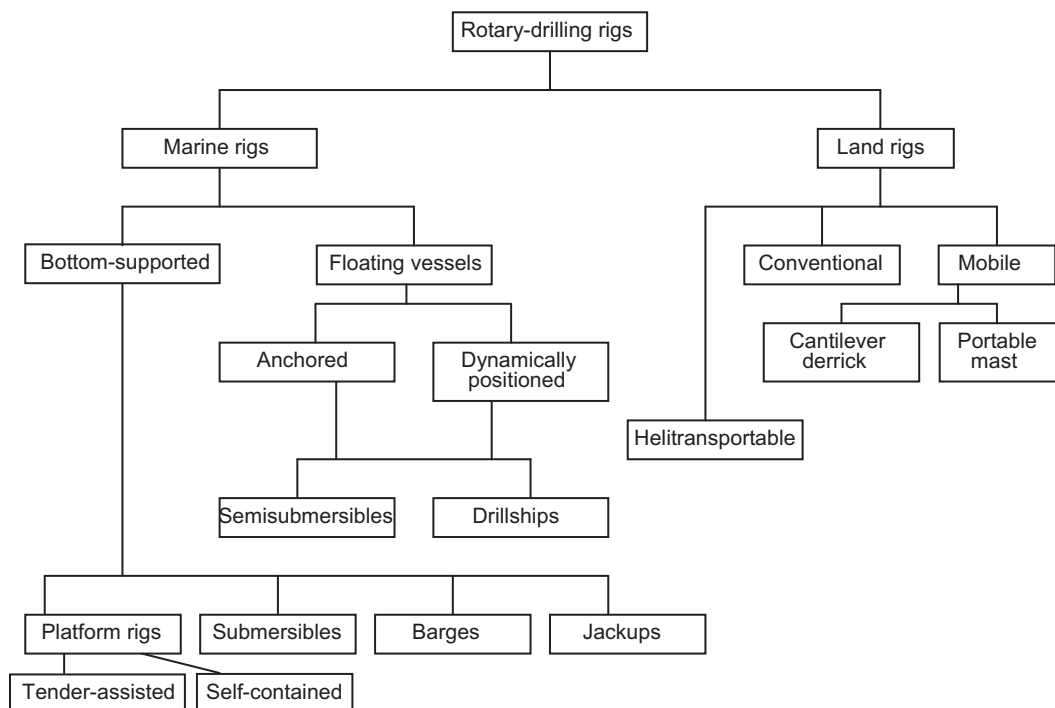


Fig. 1.10—Rotary-rig classification (Bourgoyne et al. 1986).

Generally, all important rig components are skid-mounted and can be transported and reconnected easily. The cantilever derrick has its components assembled horizontally on the ground and then is raised using the rig hoisting equipment (see **Fig. 1.11**).

Rigs with portable masts usually are mounted on a truck together with its hoisting system. Upon arrival on location, the telescoped portable mast is easily raised to vertical and extended to its fully operational position. **Fig. 1.12** shows a mobile rig with portable mast.

Besides portability, another important feature for a rig is its maximum operating depth, which is closely related to its derrick loading capacity. A variety of rig types are available in the market with maximum depth capacity ranging from less than 3,000 ft (~900 m) up to 30,000 ft (~9000 m) and beyond. A typical rig specification sheet



Fig. 1.11—Rig with cantilever derrick (Derrick Engineering Company 2010).



Fig. 1.12—Mobile rig with portable mast (GEFCO 2007). Courtesy of GEFCO.

is shown in **Fig. 1.13**. These specifications must be used to evaluate and compare rigs of various contractors before selecting the right one for an upcoming well. Information contained in the rig specifications generally addresses the following items:

- Derrick type
- Drawworks type
- Maximum operating depth
- Hookload capacity
- Mud pumps (number, manufacturer, horsepower)
- Engines (type, horsepower)
- Topdrive or rotary table
- Well-control equipment
- Fishing tools
- Main rig equipment information
- Drillstring and accessories
- Circulating system and mud-processing equipment
- Miscellaneous equipment

The rig specification usually contains a schematic of the rig's layout so that the rigsite can be properly prepared. This information is of extreme importance in certain areas where logistic or environmental conditions may drastically limit the drillsite area.

1.4.2 Marine Rigs. The beginning of the oil industry was marked by the development of oil fields located on land. Even though there were indications of existence of underwater oil reservoirs in lakes and oceans, the easier logistics for land developments and the abundance of onshore reservoirs precluded offshore ventures in those earlier years. When the industry started moving offshore, the first wells were drilled near shore using regular land drilling rigs over wharfs or artificial islands. Modern offshore drilling started in the mid-1940s, when offshore wells started to be drilled in shallow waters from fixed platforms. Today, marine drilling activity is an important segment of the industry, with offshore rigs carrying amazing technological developments.

Fixed platforms require a large up-front investment, for they first must be constructed and transported to a specified location. Obviously, such investment should be made only after there is reasonable assurance about the presence of commercial oil and/or gas accumulations. This reality pushed the industry to develop mobile drilling vessels—rigs that could be used for exploration drilling and, afterward, drill the subsequent production wells or be moved to another location. Less than a decade after offshore wells started to be drilled from fixed platforms, movable, submersible offshore drilling barges were introduced. The portability of these drilling vessels created a major increase in the attractiveness of offshore drilling.

Besides portability, another important characteristic of an offshore drilling unit is its maximum water depth of operation. There are rigs that can drill only in very shallow waters, while some modern drilling vessels can drill in very deep oceans.

Offshore drilling rigs can be bottom-supported or floating vessels. A submersible drilling barge (**Fig. 1.14**) is a bottom-supported vessel typically used in 8 to 20 ft of water (3 to 6 m). In order to operate, the barge is towed to the location and sunk to the bottom by flooding various vessel compartments. After conclusion of the drilling operation, the water is pumped out of the compartments, allowing the rig to float so that it can be moved to the next location. The barge usually is designed as a fully self-contained vessel. In addition to a complete drilling rig, it has sleeping quarters for the crew and ancillary personnel and galley facilities. Crew boats are used for transportation between the rig and the nearest docking facility and for emergency evacuation of personnel. Water depth and weather limit the areas for submersible barge operation. A minimum water depth of 6 to 8 ft (2 to 3 m) is required for vessel draft during transport to the location. The upper range on the water depth can be extended to 40 ft (12 m) if a shell mat or pad is built as a support base for the barge. Quite often, the shell pad is required due to poor seafloor supporting capabilities.

Drilling barges are widely used in areas such as the Gulf of Mexico and the Niger basin marsh areas, and in coastal waters immediately adjacent to land areas. Specially dredged channels may be required in marshes where no other access is available. These channels, or canals, may add significantly to the well costs. Barges are not used when wave height exceeds 5 ft (1.5 m).

The discovery of significant petroleum reserves in an offshore area usually requires the installation of a production platform to extract the reserves economically. A number of wells are drilled directionally from the platform to exploit the reservoir. This approach is more cost-effective, in most cases, than using many single-well platforms with vertical wells.

Technical Specifications of Rig QGI	Brakes
Rig Name Queiroz Galvão 1 QG 1	Electromagnetic Baylor model 6032 Elmago.
Place of Manufacture USA	Crown Block
Year of Manufacture 1980	Skytop Brewster 7 sheaves 60"
Manufacturer Skytop Brewster	Blocks
Model NE 95	Skytop Brewster 400
Type Electric SCR	Swivel
	National P 500
Drilling Capacity	Hook
5000 mts. With 5" Drill pipe.	Hydrahook 500 ton
Rig Driving Force	Drill String and Accessories
4 Each Caterpillar D-398 TA coupled up with 4 generators, Each with 1000 KVA totaling 4000 KVA	Drill Pipe 5" 2500Mts Grade S135
1 Each SCR system IPS Model 2.200	Drill Pipe 3½" 1000Mts Grade "G"
2 Each Centrifuge Pumps 6" x 8" for Mud Hoppers driven by 2 electric motors 75 hp. With 1750 rpm.	Drill Collars 9½" 4
2 Each Centrifuge Pumps 6" x 8" to super charge mud pumps driven by 2 electric motors 75 hp 1750rpm.	Drill Collars 8" 21
2 Each Centrifuge Pumps 6" x 8" for solids extraction equipment driven by 2 electric motors 75 hp 1750rpm.	Drill Collars 6½" 30
1 each Hydraulic tong unit driven by 1 electric motor 60 hp.	Drill Collars 4¾" 15
2 each air compressors driven by 2 each electric motors 30 hp.	Hevi-Wate 5" 21
1 each Koomey Accumulator driven by 1 electric motor 25 hp	Hevi-Wate 3½" 50
4 each Centrifuge pumps driven by 4 electric motors 20 hp	Float subs for each Diameter
5 each mud mixers driven by 5 electric motors 20 hp.	Stabilisers for each Diameter
2 each Centrifuge pumps for Degasser and trip tank 2 motors 10 hp	Roller Reamers for each Diameter
2 each sale shakers driven by 2 electric motors 5 hp	Junk Baskets 12¼" and 8½"
Mud cleaner driven by 3 hp motor	Kelly Cocks and Kelly Valve for 5¼" hex Kelly
4 each lubrication pumps driven by 4 electric motors 3 hp	Protectors 100 for casing on drill pipe
	Subs 1 Each set of subs for all Diameters
Industrial Safety and Pollution Control	Fishing Tools
H ₂ S Detection System, MAS, Model 580	Overshots 11¼" FS, 8 1/8" FS, and 5¼"
Sensibility 10 ppm, Alarm, 3 Sensors, Flow line, Shale Shaker and rig floor.	Jars 7¼", 6½", 4¼"
Complete set of fire extinguishers	Bumpers 7¼", 6½", 4¼"
Water treatment plant to attend the camp	Rig Intensifiers 7¼", 6½", 4¼"
Bug Blower installed on rig floor.	Safety Joints 7¼", 6½", 4¼"
	Raper Taps 7¼", 6½", 4¼"
Capacity of fuel and water	Reverse circulating junk basket 11¼" 77/s" 5¼"
Diesel tanks 2 each 30 M ³	Magnets 11½" 81/s" 5¼"
Water Potable 1 Each 5 M ³	Impression Block 11½" 81/s" 5¼"
Industrial Water 2 Each 20 M ³	Junk Mill 12¼" 8½" 61/s"
	Spears for 9½/s" casing and 7" casing
Circulating System and mud processing equipment	Casing Equipment
3 Each Triplex mud pumps 1300 hp National 10P-130	Elevators Side Door 20" 133/s" 95/s" 7" 150 ton
2 Each water pumps Diesel independent Duplex 70 hp each	Pick up Elevators 20" 133/s" 95/s" 7"
2 Each Derrick Shale Flow Line Cleaner Plus Stock of screens to attend each situation	1 Set Spiders 350 ton Pneumatic for 133/s", 95/s" and 7"
1 Each Desander Demco 4" x 10 cones	Manual Slips for 20" 133/s" 95/s" 7"
1 Each Mud Cleaner Brandt Single	Rig Tongs to suit 20" 133/s" 95/s" 7" casing
Centrifuge: manufacturer brandt, model HS 3400, horsepower 50, driving by horsepower 15	Hydraulic Tongs lamb 16000 with heads for 133/s", 95/s" and 7"
1 Each Degasser Drilco See-flow.	Stabbing Board installed in Mast
1 Each sand Trap with 2 divisions and individual outlets for cleaning.	Instruments and Recorders
1 Each slug pit 75 Brls	1 Each set of Pit volume indicators with complete alarm system.
5 Each Mud Mixers and 6 Mud guns	Drilling Instruments
4 Each Mud Tanks total stock 1650 bbl	Weight indicator, rotary torque indicator, connection torque indicator, pump stroke counters, RPM counter, Pit volume totalizer, Pump pressure gauges.
2 Each mixing Hoopers with individual lines to each tank and mud guns	Geolograph
1 Each Mud Laboratory with running water for analysis	Totco, Model DR6WPT 6 pin recorder
1 Each baroid kit 821	Deviation recorders, 0-8, 0-16 Degrees
BOP and Well Control System	Communication System
Cameron 135/s" x 10000 psi triple ram preventers being 1 single and 1 double Ram sets for 23/s", 21/s", 3½/s", 5", 7", 9½/s" and blinds.	Complete internal telephone system 10 points
1 each kill Line 2" x 10000 psi with 2 manual valves and 1 check. Valve Cameron.	Accommodation
1 each Principal choke line 31/s" with 2 manual valves and 1 hydraulic closing valve. Flex line hook up to choke line.	The camp houses are equipped to accommodate up to 70 people, Kitchen, mess hall, bathrooms, store rooms and recreation room.
1 each secondary choke line 21/s" with 2 manual valves. Rigid hook up to choke line.	Logistic Equipments
Choke Manifold 10000 psi with 2 manual chokes and 1 hydraulic choke 31/s" x 10000 psi.	1 Each D 6 Caterpillar tractor
1 each Accumulator Koomey type 80 180 gallon capacity.	1 Each crane track type GROVE 20/22 ton.
1 each hydraulic test pump Koomey 10000 psi to test BOP	1 Each Pick up Toyota double cabin with 4 wheel drive.
1 each Trip Tank with a capacity of 20 Brls closed in system with visual and alarm readouts.	Fishing Tools QGI
Inside BOP to suit 5" and 3½" drill pipe.	OVERSHOT 11¼" TYPE FS. # C-12822
25 Mts. Chiksans 2" and Lo torq valves.	EXTENSION 42" 1
1 Each poor boy Degasser Vertical.	OVERSHOT 8 1/8" # C-5222/032
	EXTENSION 42" # A-5223
Principal Rig Equipment	OVERSIZED GUIDE 15" 1
Rotary Table	OVERSIZED GUIDE 11 ½" A-5229
Skytop Brewster 27½"	OVERSHOT 77/s" #5227
Ezy Torque	EXTENSION 42" B-2106
Drilco type D 150,000 Ft/lbs	OVERSHOT 5¼" 8975/006
Kelly Spinner	EXTENSION 42" 8976/040
International AGC-2 Air	FISHING JAR 7¼" 1
Wire Line Unit	FISHING JAR 6¼" 1
Matthey 5000 Mts	FISHING JAR 4¼" 1
Cat Lines	JAR INTENSIFIER 4¼" 1
2 Each ingersoll rand 7500lbs, 4000lbs.	FISHING BUMPER 8" 1
Draw works	FISHING BUMPER 6¼" 1
Skytop Brewster, NE-95 375 ton 1500hp,	FISHING BUMPER 4¼" 1
Drilling Line 13/s" equipped with Crown O Matic	MAGNET 11" 1
	MAGNET 8½" 1
HOTST CAPACITY LB. x 1,000	MAGNET 5 ¾" 1
DRUM CLUTCH	JUNK BASKET 8½" 1
LO	LO 1st 599 719 828
LO	LO 2nd 459 551 635
LO	HI 1st 330 396 456
LO	HI 2nd 237 285 328
HI	LO 1st 165 198 228
HI	LO 2nd 126 152 175
HI	HI 1st 91 109 125
HI	HI 2nd 65 78 90
	JUNK BASKET 12¼" 1
	JUNK BASKET 17½" 1
	REVERSE CIRCULATING JUNK BASKET 8" 1
	REVERSE CIRCULATING JUNK BASKET 5¼" 1
	IMPRESSION BLOCK 10" 1
	IMPRESSION BLOCK 6" OD 1
	TAPER TAP 7¼" TAPER 1¾" TO 4¼" 1
	TAPER TAP 61/s" TAPER 13/16" TO 31/16" 1
	JUNK MILL 12¼", 8½" and 61/s" 1 each
	SAFETY JOINT 7¼" 1
	CASING SPEAR 9/s" and 7" 1 each
	KANGAROO 12¼" 1
	KANGAROO 8½" 1

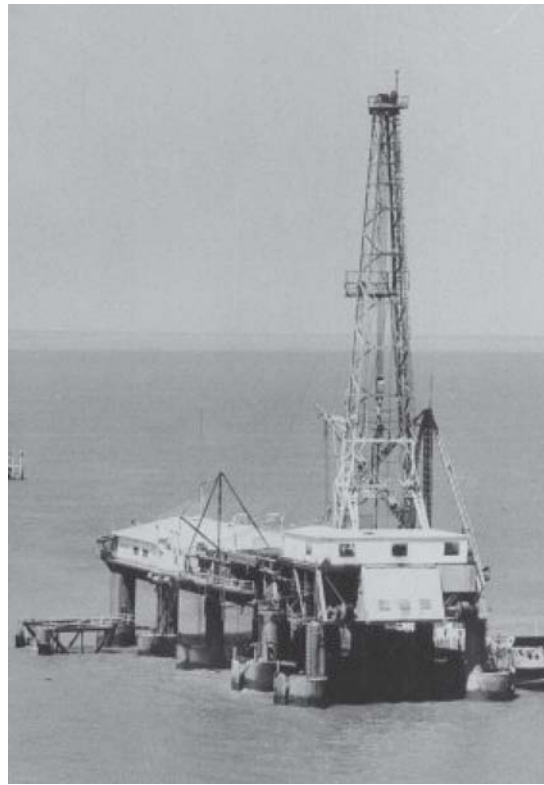


Fig. 1.14—Submersible drilling barge “Mr. Charlie,” circa 1954.

Rigs that drill from platforms can be fully self-contained or tender-supported. If the production platform is sufficiently large, all drilling equipment and personnel can stay on the rig. Alternatively, a floating tender is used if the platform working area or load capacity is restricted.

Fixed platforms (**Fig. 1.15**) are usually of jacket-type construction and are supported by piling. There are also areas, with firmer bottom sediments, where massive concrete structures are built and simply placed on the bottom. In both cases there will be a large structure running from the seafloor all the way to surface. Obviously, installation of such large structures will be possible only up to a certain water depth because construction and transportation of platforms for very deep areas would be either extremely expensive or technically unfeasible. Normally, fixed platforms are used for development of fields in water depths up to 1,500 ft (460 m). Slender and lighter platforms, the so-called *compliant towers*, may be installed in deeper areas. Those platforms have a flexible tower as opposed to the relatively rigid structures of the regular fixed platforms.

Normally, the main purpose of fixed platforms is to remain in place permanently after drilling has been concluded, producing and processing the oil and gas from the wells. Actually, there are fields where the wells are drilled previously by another drilling vessel and it is only afterward that a fixed structure is installed and the wells are tied back to the platform to initiate production.

When fixed platforms are used for drilling operations, the drilling equipment may either remain in place for future use in some necessary well intervention or it may be removed for use elsewhere. In the latter case, if well intervention or new drilling jobs are necessary, the required equipment has to be reinstalled.

The primary and most widely used bottom-supported marine vessel for oilwell drilling is the *jackup rig* (**Fig. 1.16**). Unlike fixed platforms, jackups are designed primarily for drilling operations. As with any bottom-supported rig, jackups cannot operate in a deepwater environment. Water depths will vary from a few feet to approximately 350 ft (~106 m).

The principal components are a barge-type unit and three to five legs capable of supporting the vessel when positioned over the seafloor. When moving between locations, the legs are up in the air, allowing the barge to float. Upon arrival at the new location, the legs are jacked down to contact the seafloor, and the barge is raised into the air. When drilling is completed, the rig is lowered to the water level, the legs are raised, and the rig is towed to the next location. It is not uncommon to have some difficulty removing the legs from loosely consolidated, sticky subseafloor soils; therefore, most rig legs are equipped with water-jetting systems to help release the legs.

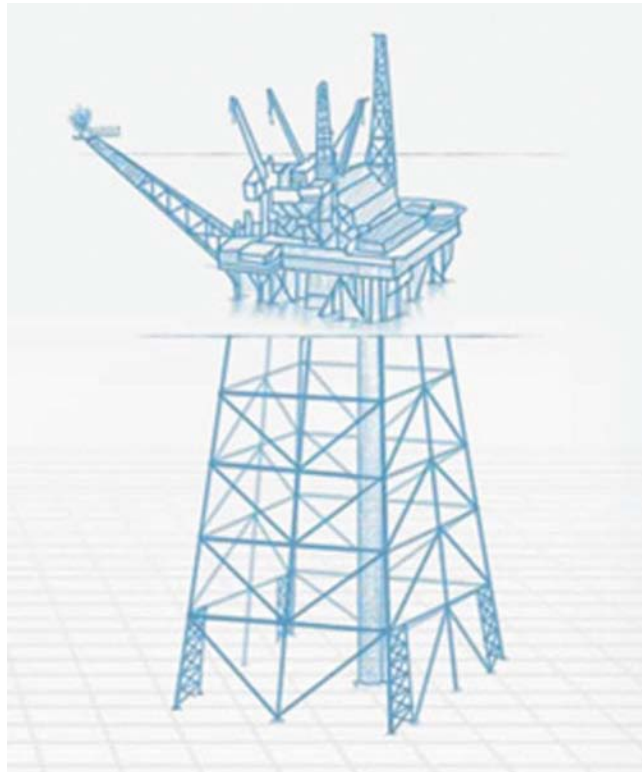


Fig. 1.15—Typical fixed-platform structure. Courtesy of Petrobras.



Fig. 1.16—Jackup rig. Courtesy of Maersk Drilling.

The rig is self-contained and carries all drilling equipment, materials, life-support systems, and crew quarters. The barge usually is divided into two or three decks. The top deck contains the rig, pipe racks, and occasionally the living quarters. The lower decks contain all support drilling equipment, such as pumps and mud systems, and the auxiliary barge equipment. Even though they are self-contained, jackups and most drilling rigs do not have enough load capability and space to carry all equipment, chemicals, water, pipes, and other miscellaneous materials necessary to drill a well. Usually rigs will have enough capability to carry everything necessary to keep the operation going for a certain period of time, at least a week, but supply boats will continually travel back and forth, bringing new equipment and supplies and carrying away equipment no longer needed.

Floating rigs such as drillships and semisubmersible platforms do not rest on the seafloor. As such, these rigs are not restricted by the length of the rig's legs for maximum operating water depth. Normally these rigs are more expensive than jackups and are used in areas where, due to the water depth, jackups cannot operate. For station keeping while drilling, these rigs use either an anchoring system or a dynamic positioning (DP) system.

The semisubmersible drilling unit usually has two lower hulls that provide flotation. When drilling, the ballasted lower hulls, filled with water, grant stability to the rig. After conclusion of the drilling operation, the water is pumped out of the compartments and the rig can be moved to the next location. Anchored semisubmersible rigs (**Fig. 1.17**) are held in place by huge anchors that, combined with the submerged portion of the rig, provide great stability, allowing the rig to be used in turbulent offshore waters.

There are semisubmersible rigs that use a dynamic positioning system. This system uses electric motors installed in the hulls that allow propelling of the rig in any direction. A computer system, using satellite positioning technology and sensors located near the wellhead, commands the motors, ensuring that the ship will be kept directly above the subsea wellhead at all times.

Drillships use a ship-type vessel as the primary structure to support the rig. It may be a converted seagoing vessel or, most commonly, a specially designed drilling vessel. Most drillships are self-propelled, not requiring oceangoing tugs for transportation between locations. Semisubmersible rigs generally are not self-propelled.

New-generation drillships usually are dynamically positioned, but there are also anchored vessels. Anchored drillships (**Fig. 1.18**) normally are built with a central turret where the anchoring system is installed. This allows vessel rotation around the central turret in order to always keep the ship facing the waves, reducing wave action.

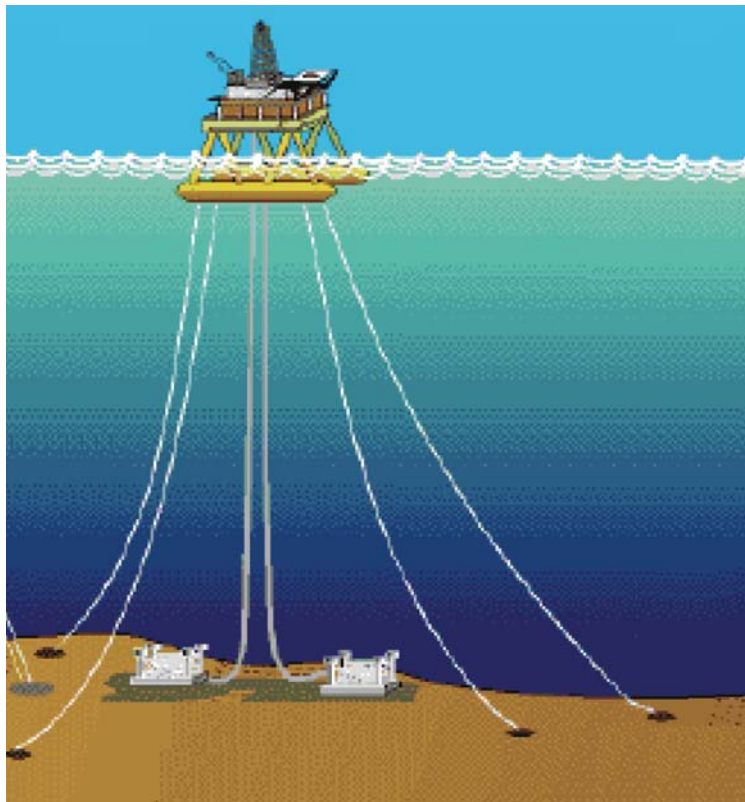


Fig. 1.17—An anchored semisubmersible drilling rig [after Aadnøy et al. (2009)].



Fig. 1.18—An anchored drillship (Lake 2006).

Even though floating drilling vessels are designed to minimize motion due to ocean waves and tides, the ship will never be totally motionless. To eliminate the effect of rig heave and allow penetration control during drilling operations, motion compensators are installed on the rig's hoisting system.

Water depth records on offshore drilling operations are broken regularly. Large hydrocarbon accumulations in offshore reservoirs as well as increasing oil prices have made expensive deepwater exploration attractive for many companies. Semisubmersible rigs have already drilled in water depths exceeding 8,000 ft (~2440 m), while dynamically positioned drillships have already drilled in water depths greater than 10,000 ft (~3000 m).

Deepwater rigs (**Fig. 1.19**) carry up-to-date technology and a high level of automation. Some will have dual activity with two derricks installed, which will allow drilling operations by one derrick and assemblage of equipment for the next drilling phase by the other.

Other types of stationary platforms where drilling can take place are the tension leg platform (TLP) and spar platform. Spar platforms and TLPs are primarily production structures that may have drilling capability. Even though these types of vessels are classified as floating structures, they must be differentiated from the common floating drilling vessels since they are designed to be stationary production platforms.

A TLP is a floating deepwater-compliant structure designed for offshore hydrocarbon production with its hull moored to the ocean floor by high-strength cables, giving the platform vertical and lateral stability. The drilling equipment and production facilities, as well as crew quarters, are installed at surface on top of the structure.

The spar platform concept comprises a huge cylindrical steel hull that supports both the drilling operations and production facilities. Compartments on the upper portion of the cylinder provide buoyancy, while water-filled tanks on the bottom give weight and stability. The hull is attached to the seafloor by catenary mooring systems.

1.5 Drilling Rig Systems

As mentioned in Section 1.4, rigs will vary widely in size, drilling capability, level of automation, appearance, method of deployment, and environment in which they can operate. Nevertheless, the basic drilling equipment for the rotary-drilling process will be present in all rigs.



Fig. 1.19—A modern ultradeepwater drillship operating in Campos Basin, Brazil (courtesy of Petrobras SA).

Drilling rigs are used to construct the well. This includes drilling the hole, lowering and cementing the casing, and providing the means to perform various auxiliary functions such as logging and well testing. Modern rigs have complex equipment and require experienced personnel for efficient operations. If improperly selected, the rig can be the cause of low penetration rates, formation damage due to poor solids control, and, ultimately, high well costs.

Proper rig selection is important for the safety, efficiency, and cost of the well. The correct procedure for rig selection is to consider the various loads that will be placed on the equipment and to select the most cost-effective rig that will satisfy these requirements. Drilling contractors provide detailed rig specifications for this purpose. When these specifications are compared with the well prognosis, the proper rig can be selected.

Rig selection is not completely quantitative. Although the objective is to select the most cost-effective rig that will drill the well, some other factors must be considered, including

- Technical design requirements
- Rig's manpower (i.e., experience and training)
- Track record
- Logistics
- Rigsite requirements

Occasionally a company will use a certain rig even if it is not the most suitable, due to nontechnical reasons including market availability and long-term contractual commitments.

Drilling rigs have six basic systems. During drilling operations, all six systems are necessary and there is high interaction between them. Traditionally, rig systems are classified as

- Power system
- Hoisting system
- Circulating system
- Rotary system
- Well-control system
- Well-monitoring system

Additionally, floating offshore rigs will have a seventh system comprising special marine equipment required to deal with the particularities of offshore drilling.

1.5.1 Rig Power System. Drilling rigs—and their support vessels in the case of a barge or floating vessel—have high power requirements. Equipment that requires power includes the drawworks, mud pumps, rotary system, and life-support system. The power loading may be continuous or intermittent.

The power system on a drilling rig usually consists of a prime mover as the source of power and some means to transmit the power to the end-use equipment. The prime movers used in the current drilling industry are diesel engines.

Most rig power is consumed by the hoisting and fluid-circulating systems. The other rig systems have much smaller power requirements. Since the hoisting and circulating systems generally are not used simultaneously, the

same engines can perform both functions. Total power requirements for most rigs are from 1,000 to 3,000 hp (750 to 2,200 kW).

Power is transmitted via one of the following systems:

- Mechanical drive
- Direct-current (DC) generator and motor
- Alternating-current (AC) generator, silicon-controlled rectifier (SCR), and DC motor

The most widely used system on new rigs or large marine rigs is the AC-SCR system, also called the *diesel-electric* system. Diesel-electric rigs are those in which the main rig engines are used to generate electricity. Electric power is transmitted easily to the various rig systems, where the required work is accomplished through use of electric motors. DC motors can be wired to give a wide range of speed-torque characteristics that are extremely well suited for the hoisting and circulating operations. Electric power allows the use of a relatively simple and flexible control system. The driller can apply power smoothly to various rig components, thus minimizing shock and vibration problems.

Most early drilling rigs used a mechanical drive system to transmit power from the engines to the operating equipment such as the drawworks and pumps. The drive system consists of gears, chains, or belts that are attached to the engines' shafts and couple the output of two or more engines. Torque converters are attached to the shafts to increase the range of output revolutions per minute (rev/min) and also to improve engine life by absorbing equipment-induced power-train shock loads.

The weaknesses of the mechanical drive systems are as follows:

- Shock loading to the engine
- Inability to produce high torque at low engine rev/min, which becomes a compounded problem as higher workloads continue to decrease engine rev/min
- Difficulty in providing low torque output due to minimum engine idle speeds and gear ratios
- Power loss through the gears and chains

Power system performance characteristics generally are stated in terms of output horsepower, torque, and fuel consumption for various engine speeds. The shaft power P_{sp} developed by an engine is obtained from the product of the angular velocity of the shaft ω and the output torque T :

$$P_{sp} = \omega T. \quad (1.1)$$

The overall power efficiency η_{sp} determines the rate of fuel consumption \dot{m}_f at a given engine speed. Fuel consumption times the heating values H of the fuel, for internal-combustion engines, gives the heat energy input per unit time (power) to the engine, Q :

$$Q = \dot{m}_f H. \quad (1.2)$$

Since the overall power system efficiency η_{sp} is defined as the power output per power input, then

$$\eta_{sp} = \frac{P_{sp}}{Q}. \quad (1.3)$$

Example 1.1—Power and Efficiency of an Engine. A diesel engine gives an output torque of 1,740 ft-lbf at an engine speed of 1,200 rev/min. If the fuel consumption rate is 31.5 gal/hr, what is the output power and overall efficiency of the engine?

Solution. The angular velocity ω is given by

$$\omega = 2\pi(1,200) = 7,540 \text{ rad/min.}$$

The power output can be computed using Eq. 1.1

$$P_{sp} = \omega T = \frac{7,540 (1,740) \text{ ft} \cdot \text{lbf/min}}{33,000 \text{ ft} \cdot \text{lbf/min/hp}} = 398 \text{ hp} = 297 \text{ kW.}$$

Since the fuel type is diesel, the density is 7.2 lbm/gal and the heating value H is 19,000 Btu/lbm. Thus, the fuel consumption rate \dot{m}_f is

$$\dot{m}_f = 31.5 \text{ gal/hr} (7.2 \text{ lbm/gal})(1 \text{ hr}/60 \text{ min}) = 3.78 \text{ lbm/min}.$$

The total heat energy consumed by the engine is given by Eq. 1.2

$$\begin{aligned} Q &= \dot{m}_f H = 3.78 \text{ lbm/min}(19,000 \text{ Btu/lbm})(779 \text{ ft} - \text{lbf/Btu})/33,000 \text{ ft} - \text{lbf/min/hp} \\ &= 1695 \text{ hp} (1,264 \text{ kW}). \end{aligned}$$

Thus, the overall efficiency of the engine at 1,200 rev/min given by Eq. 1.3 is

$$\eta_{sp} = \frac{P_{sp}}{Q} = \frac{397.5}{1695.4} = 0.234 \text{ or } 23.4\%$$

1.5.2 Hoisting System. The hoisting system is a vital component of the rig equipment. It provides a means for vertical movement of pipe in the well (i.e., to lower or raise drillstrings, casings, and other equipment into or out of the well). The principal items in the hoisting system are as follows:

- Drawworks
- Block and tackle
- Derrick and substructure
- Ancillary equipment such as elevators, hooks, and bails

Two of the most recognizable and routine drilling operations performed with the hoisting system are called *making a connection* and *making a trip*. Making a connection refers to the periodic process of adding a new joint of drillpipe as the hole deepens. Making a trip refers to the process of removing the drillstring from the hole to change a portion of the bottomhole assembly and then lowering the drillstring back to the hole bottom. One of the main reasons to make a trip is to change a dull bit. In that case, the entire drillstring is pulled out of the well (*trip out*) so the used bit can be changed to a new one. After that the string is lowered into the well again (*trip in*) so the drilling process can resume.

Drawworks. The drawworks is the equipment that uses the energy from the power system to apply a force to the cable (see Fig. 1.20a). In practical terms, it reels in the cable (*drilling line*) on the drum to lift the pipe. In addition, it allows the cable to be spooled out as the pipe is lowered into the well. The drawworks must have an effective brake system to control the heavy pipe loads and a cooling system to dissipate large amounts of frictional heat generated during braking.

The draw works drum is grooved to accommodate a certain cable size. Several layers of the line overlap on the drum. Occasionally, the line becomes damaged due to accelerated wear if it is wrapped improperly on the drum during the reeling process.

An effective braking system must be used on the drum. In some cases, 500-ton loads must be decelerated quickly and held in place. A commonly used braking system on mechanical rigs is the hydrodynamic type. The braking is provided by water being impelled in a direction opposite to the rotation of the drum.

Electric rigs often use an electromagnetic (eddy current) brake in addition to a breaking action generated by the drive motors on the drawworks. The braking is provided by two opposing magnetic fields. The magnitude of the magnetic fields is dependent on the speed of rotation and the amount of external excitation current. The brake is directly coupled to the drawworks shaft. The electric brake alone cannot stop the drawworks, but it does take much of the load off the mechanical brake.

The drawworks transmission provides a means for easily changing the direction and speed of the traveling block.

Block and Tackle. The block and tackle is the primary link between the drawworks and the loads that will be lowered into or raised out of the wellbore. It is composed of the crown block, the traveling block, and the drilling line. The arrangement and nomenclature of the block and tackle used on rotary rigs are shown in Fig. 1.20a. The principal function of the block and tackle is to provide a mechanical advantage, which permits easier handling of large loads. The mechanical advantage MA_{br} of a block and tackle is simply the load supported by the traveling block, F_{tb} , divided by the load imposed on the drawworks, the tension in the fast line, F_{fl} :

$$MA_{bt} = \frac{F_{tb}}{F_{fl}} \quad \dots \quad (1.4)$$

The load imposed on the drawworks is the tension in the fast line. The ideal mechanical advantage, which assumes no friction in the block and tackle, can be determined from a force analysis of the traveling block. Consider the free-body diagram of the traveling block as shown in Fig. 1.20b. If there is no friction in the pulleys, the tension in the drilling line is constant throughout. Thus, a force balance in the vertical direction yields

$$N_{tb}F_{fl} = F_{tb},$$

where N_{tb} is the number of lines strung through the traveling block. Solving this relationship for the tension in the fast line and substituting the resulting expression in Eq. 1.4 yields

$$MA_{bti} = \frac{F_{tb}}{F_{tb}/N_{tb}} = N_{tb},$$

which indicates that the ideal mechanical advantage of the block-and-tackle system, MA_{bti} , is equal to the number of lines strung between the crown block and traveling block. The use of 6, 8, 10, or 12 lines is common, depending on the loading condition.

The input power P_{bt} of the block and tackle is equal to the drawworks load F_{fl} times the velocity of the fast line, v_{fl} :

$$P_{bt} = F_{fl}v_{fl} \quad \dots \quad (1.5)$$

The output power, or hook power, P_h , is equal to the traveling block load F_{tb} times the velocity of the traveling block, v_{tb} :

$$P_h = F_{tb}v_{tb} \quad \dots \quad (1.6)$$

For a frictionless block and tackle, $F_{tb} = N_{tb}F_{fl}$. Also, since the movement of the fast line by a unit distance tends to shorten each of the lines strung between the crown block and traveling block by only $1/N_{tb}$ times the unit distance, then $v_{tb} = v_{fl}/N_{tb}$. Thus, a frictionless system implies that the ratio of output power to input power is equal to 1.

Of course, in an actual system, there is always a power loss due to friction. Values of block-and-tackle efficiency will vary and depend on various conditions including the number of lines strung through the traveling block. The greater the number of lines, the lesser the efficiency.

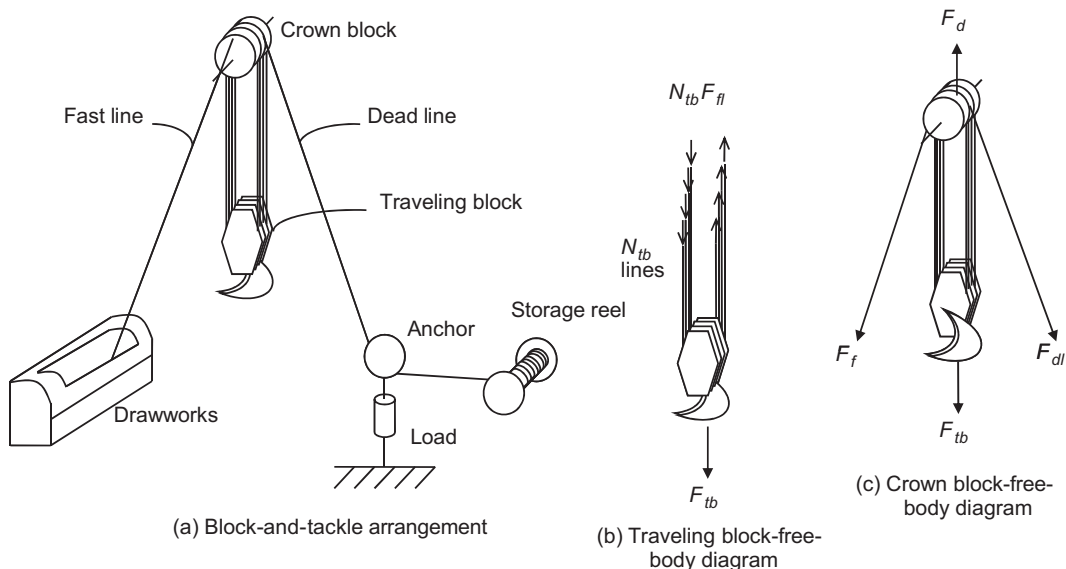


Fig. 1.20—Schematic of drawworks and block and tackle (Bourgoyne et al. 1986).

API RP9B (2005) contains the following standard efficiency relation:

$$\eta_{bt} = \frac{(K^{N_L} - 1)}{K^{N_{Sh}} N_L (K - 1)}, \quad \dots \quad (1.7)$$

where

η_{bt} = block-and-tackle efficiency

K = friction factor (approximately 1.04)

N_L = number of lines strung

N_{Sh} = number of rolling sheaves (normally, $N_{Sh} = N_L$)

Table 1.1 indicates η_{bt} values for various pulley systems.

Knowledge of the block-and-tackle efficiency permits calculation of the actual tension in the fast line for a given load. Because the power efficiency is given by

$$\eta_{bt} = \frac{P_h}{P_{sp}} = \frac{F_{tb} v_{tb}}{F_{fl} v_{fl}} = \frac{F_{tb} v_{fl} / N_{tb}}{F_{fl} v_{fl}} = \frac{F_{tb}}{F_{fl} N_{tb}},$$

the tension in the fast line is

$$F_{fl} = \frac{F_{tb}}{\eta_{bt} N_{tb}}. \quad \dots \quad (1.8)$$

The above equation can be used to select drilling-line size. However, a safety factor should be used to allow for line wear and shock loading conditions.

The line arrangement used on the block and tackle causes the load imposed on the derrick to be greater than the hookload. As shown in Fig. 1.20c, the load F_d applied to the derrick is the sum of the hookload F_{tb} , the tension in the dead line, F_{dl} , and the tension in the fast line, F_{fl} :

$$F_d = F_{tb} + F_{fl} + F_{dl}. \quad \dots \quad (1.9a)$$

If the load, F_{tb} , is being hoisted by pulling on the fast line, the friction in the sheaves is resisting the motion of the fast line and the tension in the drilling line increases from F_{tb}/N_{tb} at the first sheave (dead line) to $F_{tb}/\eta_{bt} N_{tb}$ at the last sheave (fast line). Substituting these values for F_f and F_s in Eq. 1.9a gives

$$F_d = F_{tb} + \frac{F_{tb}}{\eta_{bt} N_{tb}} + \frac{F_{tb}}{N_{tb}} = \left(\frac{1 + \eta_{bt} + \eta_{bt} N_{tb}}{\eta_{bt} N_{tb}} \right) F_{tb}. \quad \dots \quad (1.9b)$$

Drilling Line. Drilling rigs have many applications for wire rope. The more common uses are as drilling lines and guideline tensioners. The drilling line connects to the drawworks and the dead line anchor. It is pulled through the crown and traveling block sheaves so the traveling block can be raised or lowered as necessary.

The crown block and traveling block consist of sheaves designed for use with wire rope. The crown block is stationary and is located at the top of the derrick. The traveling block is free to move and has a hook, bails, and elevators attached to the bottom for latching to the pipe. Both blocks have 4–12 sheaves. The number of lines strung varies with load, with fewer on shallow wells and maximum for heavy loads.

TABLE 1.1—EFFICIENCY FACTORS FOR BLOCK-AND-TACKLE SYSTEM ($K = 1.04$) (Bourgoyne et al. 1986)	
Number of Lines, N_L	Efficiency, η_{bt}
4	0.908
6	0.874
8	0.842
10	0.811
12	0.782
14	0.755

Wire rope is made from cold-drawn carbon steel of various grades, depending on the strength required. API *Spec 9A/ISO 10425* (2004) covers wire rope grades and construction. The classification of the various grades is as follows:

- Extra improved plow steel (EIPS)
- Improved plow steel (IPS)
- Plow steel (PS)
- Mild plow steel (MPS)

The primary element of wire rope is the individual wires. Wires are carefully selected, sized, and helically placed together, forming a precise geometric pattern that forms the strand. After stranding, the strands are helically placed together around a core to form wire rope (see **Fig. 1.21a**). The helix may be right-handed or left-handed (see Fig. 1.21b). The proper way to measure the wire-rope diameter is shown in Fig. 1.21c. The core may be a fiber rope (either naturally grown fibers or synthetic fibers), a plastic core, a spring steel core, a multiple-wire strand, or an independent wire rope core (IWRC). The IWRC is the most widely used because it resists crushing and distortion.

The nominal strength of wire rope depends on the materials used in construction, the number of strands and wires, and the size of the rope. The grade of steel utilized in the construction is a key factor in ultimate breaking strength. Most wire ropes are made using IPS. In addition, EIPS provides 10% extra strength over IPS, with EE-IPS providing another 10% strength over EIPS.

Table 1.2 presents nominal breaking strength for various wire rope diameters. In the table there are specifications for cables with fiber core and IWRC. The 6×19 classification indicates a cable of six strands with 19 wires per strand.

Drilling line does not tend to wear uniformly over its length. The most severe wear occurs at the pickup points in the sheaves and at the lap points on the drum of the drawworks. The pickup points are the points in the drilling line that are on the top of the crown block sheaves or the bottom of the traveling block sheaves when the weight of the drillstring is lifted from its supports in the rotary table during tripping operations. The rapid acceleration of the heavy drillstring causes the most severe stress at these points. The lap points are the points in the drilling line where a new layer or lap of wire begins on the drum of the drawworks.

Drilling line is maintained in good condition by following a scheduled slip-and-cut program. Slipping the drilling line involves loosening the dead line anchor and placing a few feet of new line in service from the storage reel. Cutting the drilling line involves removing the line from the drum of the drawworks and cutting off a section of line from the end. Slipping the line changes the pickup points, and cutting the line changes the lap points. The line is sometimes slipped several times before it is cut. Care must be taken not to slip the line a multiple of the distance

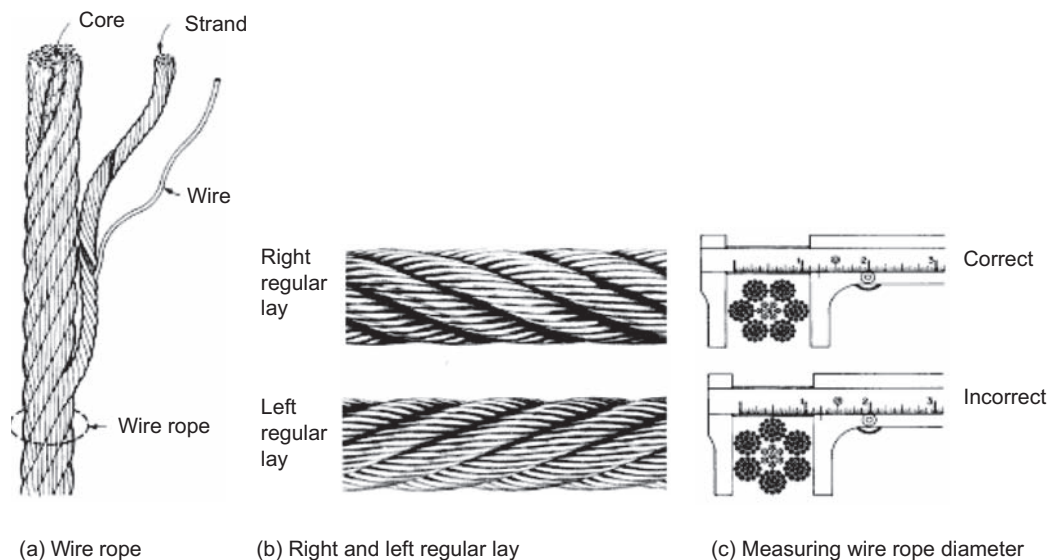


Fig. 1.21—(a) Wire rope: wire, strand, and core; (b) right and left regular lay; and (c) measuring wire rope diameter [from API Spec. 9 (2004)]. Reproduced courtesy of the American Petroleum Institute.

TABLE 1.2—NOMINAL BREAKING STRENGTH OF 6 × 19 WIRE ROPE (Bourgoyne et al. 1986)							
Rope Diameter		Approximate Weight (lbm/ft)		Nominal Strength (tons)			EEIPS IWRC
(in.)	(mm)	Fiber Core	IWRC	IPS IWRC	Fiber Core	IWRC	
1/4	6.5	0.105	0.116	2.94	3.20	3.40	3.74
5/16	8.0	0.164	0.18	4.58	4.69	5.27	5.80
3/8	9.5	0.236	0.26	6.56	6.71	7.55	8.31
7/16	11.0	0.32	0.35	8.89	9.09	10.2	11.2
1/2	13.0	0.42	0.46	11.5	11.8	13.3	14.6
9/16	14.5	0.53	0.59	14.5	14.9	16.8	18.5
5/8	16.0	0.66	0.72	17.7	18.3	20.6	22.7
3/4	19.0	0.95	1.04	25.6	26.2	29.4	32.3
7/8	22.0	1.29	1.42	34.6	35.4	39.8	43.8
1	26.0	1.68	1.85	44.9	46.0	51.7	56.9
1 1/8	29.0	2.13	2.34	56.5	57.9	65.0	71.5
1 1/4	32.0	2.63	2.89	69.4	71.0	79.9	87.9
1 3/8	35.0	3.18	3.50	83.5	85.4	96.0	106.0
1 1/2	38.0	3.78	4.16	98.9	101.0	114.0	125.0
1 5/8	42.0	4.44	4.88	115	118.0	132.0	146.0
1 3/4	45.0	5.15	5.67	133	136.0	153.0	169.0
1 7/8	48.0	5.91	6.50	152	155.0	174.0	192.0
2	52.0	6.72	7.39	172	176.0	198.0	217.0
2 1/8	54.0	7.59	8.35	192	197.0	221.0	243.0
2 1/4	58.0	8.51	9.36	215	220.0	247.0	272.0
2 3/8	60.0	9.48	10.4	239	244.0	274.0	301.0
2 1/2	64.0	10.5	11.6	262	269.0	302.0	332.0
2 3/4	70.0	12.7	14.0	314	321.0	361.0	397.0

between pickup points; otherwise, points of maximum wear are just shifted from one sheave to the next. Likewise, care must be taken when cutting the line not to cut a section equal in length to a multiple of the distance between lap points.

In *API RP 9B* (2005), API has adopted a slip-and-cut program for drilling lines. The parameter adopted to evaluate the amount of line service is the ton-mile. A drilling line is said to have rendered 1 ton-mile (14.3 MJ) of service when the traveling block has moved 1 US ton (0.91 Mg) a distance of 1 mile (1.6 km). Note that for simplicity, this parameter is independent of the number of lines strung. Ton-mile records must be maintained in order to employ a satisfactory slip-and-cut program. The number of ton-miles between cutoffs will vary with drilling conditions and drilling-line diameter and must be determined through field experience. In hard-rock drilling, vibration problems may cause more rapid line wear than when the rock types are relatively soft. Ton-miles between cutoffs typically range from approximately 500 (7,150 MJ) for 1-in.-diameter drilling line to approximately 2,000 (28,600 MJ) for 1.375-in.-diameter drilling line.

Calculation and recording of ton-miles is tedious work. Normally, devices that automatically accumulate the ton-miles of service are available in the rigs. The device will constantly measure the loads being applied to the cable as well as the length of displacement.

Derrick and Substructure. The derrick and substructure play an important role in drilling operations. The derrick provides the height necessary for the hoisting system to raise and lower the pipe. The greater the height, the longer the section of pipe that can be handled and, thus, the faster a long string of pipe can be inserted into or removed from the hole. Derricks can handle sections called stands, which are composed of two, three, or four joints of drillpipe. Because common drillpipes are between 8 and 10 m long (approximately 26 to 33 ft), a derrick designed to handle three-drillpipe stands will be taller than a 10-story building.

The substructure provides the height required for the blowout preventer stack on the wellhead below the rig floor. The derrick and the substructure must have enough strength to support all loads, including the hook load, pipe set in the derrick, and wind loads.

1.5.3 Circulating System. The fluid-circulating system provides hydraulic power to the drilling fluid so that it can be pumped from surface into the drillstring, travel all the way down the bottom of the hole, and then return to surface through the annulus, carrying the rock cuttings produced by the action of the bit against the rock. **Fig. 1.22** shows a schematic of the typical path of the drilling fluid in a regular drilling operation.

The main components of the rig's circulating system are the mud pumps, mud pits, mud-mixing equipment, and contaminant-removal equipment.

Mud pumps are designed for pressure output, flow rate, and horsepower requirements. High pressures are required to circulate heavy muds in deep wells and to optimize hole cleaning below the bit. Flow rate must exceed a minimum required to clean the hole. This usually is not a limiting criterion for most operations except when drilling large-diameter surface hole sections. Maximum available pump horsepower is sometimes used in surface holes or when operating downhole motors.

Most mud pumps currently used in the drilling industry are duplex or triplex positive-displacement pumps. The duplex double-acting pump has two liners with valves on both ends of the liners. Fluid is displaced from the liner on the forward and backward strokes of the rod plunger (**Fig. 1.23a**). On the forward stroke of each piston, the volume displaced, V_{dfs} , depends on the liner diameter, d_{dpl} , and the stroke length, L_{dst} , and is given by

$$V_{dfs} = \frac{\pi}{4} d_{dpl}^2 L_{dst}.$$

On the backward stroke the volume, V_{dbs} , also depends on the rod diameter, d_{dpr} , and is given by

$$V_{dbs} = \frac{\pi}{4} (d_{dpl}^2 - d_{dpr}^2) L_{dst}.$$

Thus, the total volume, V_{dp} , displaced per complete pump cycle by a pump having two cylinders is given by

$$V_{dp} = 2(V_{dfs} + V_{dbs})\eta_{dpv} = \frac{\pi}{2} (2d_{dpl}^2 - d_{dpr}^2) L_{dst} \eta_{dpv}, \quad \dots \dots \dots (1.11)$$

where η_{dpv} is the volumetric efficiency of the pump.

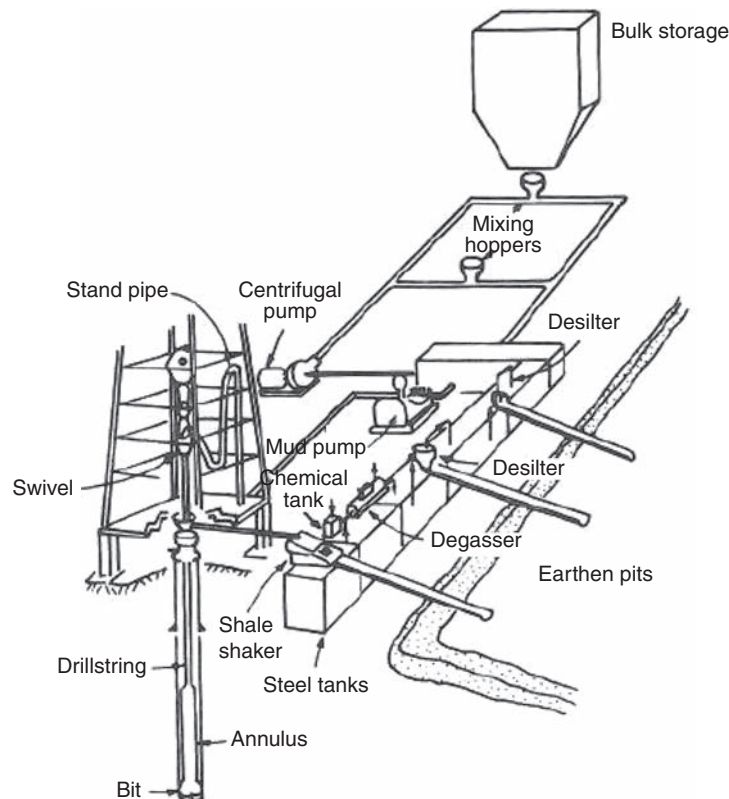


Fig. 1.22—Schematic of drilling-fluid path (Bourgoyne et al. 1991).

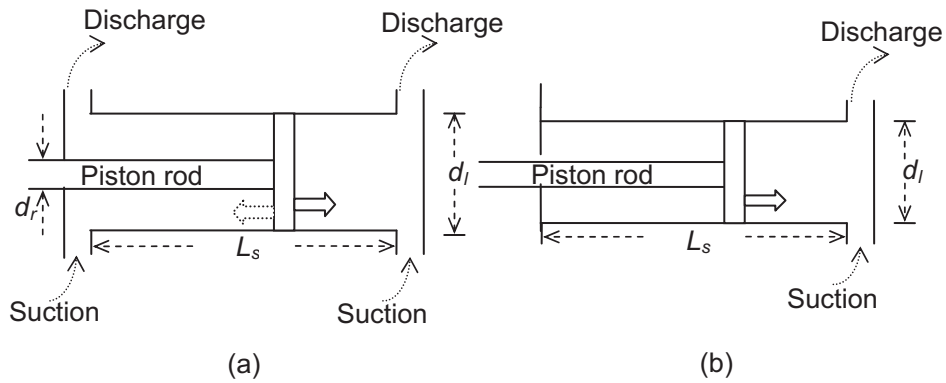


Fig. 1.23—Schematic of (a) duplex double-acting pump and (b) triplex single-acting pump.

Triplex pumps are lighter and more compact than duplex pumps, their output pressure pulsations are not as great, and they are cheaper to operate. For these reasons, modern rigs use triplex pumps. One single-action piston of a triplex pump is shown in Fig. 1.23b. The volume displaced by each piston V_{tst} during one complete pump cycle is given by

$$V_{tst} = \frac{\pi}{4} d_{ipl}^2 L_{tst}$$

Thus, the volumetric output for a complete cycle of a triplex pump, V_{tp} , is as follows:

$$V_{tp} = \frac{3\pi}{4} d_{ipl}^2 L_{tst} \eta_{tpv} \quad (1.12)$$

The flow rate q of the pump is obtained by multiplying the single-cycle volumetric output by the number of cycles, N , per unit time.

Pumps are rated for hydraulic power, maximum pressure, and maximum flow rate. If the inlet pressure of the pump is essentially atmospheric pressure, the increase in fluid pressure moving through the pump is approximately equal to the discharge pressure. The hydraulic power output of the pump is equal to the discharge pressure times the flow rate. The hydraulic power developed by the pump is given by

$$P_H = \Delta p q \quad (1.13)$$

For a given hydraulic power level, the maximum discharge pressure and flow rate can be varied by changing the stroke rate and liner size. A smaller liner will allow the operator to obtain a higher pressure, but at a lower rate.

Example 1.2—Duplex Pump Factor. Compute the pump factor, V_{dp} , in units of barrels per stroke for a duplex pump having 6.5-in. liners, 2.5-in. rods, 18-in. strokes, and a volumetric efficiency of 90%.

Solution. The pump factor for a duplex pump can be determined using Eq. 1.11:

$$V_{dp} = \frac{\pi}{2} (2d_{dpl}^2 - d_{dpr}^2) L_{dst} \eta_{dpv} = \frac{\pi}{2} [2(6.5)^2 - (2.5)^2] (18) (0.90) = 199 \text{ in.}^3/\text{stroke}.$$

Recall that there are 231 in.³ in a US gallon and 42 US gallons in a US barrel. Thus, converting to the desired field units yields

$$1991 \text{ in.}^3/\text{stroke} \left(\frac{\text{gal}}{231 \text{ in.}^3} \right) \left(\frac{\text{bbl}}{42 \text{ gal}} \right) = 0.205 \text{ bbl/stroke} = 0.0326 \text{ m}^3/\text{stroke}$$

Pump Suction Design. Pump suction requirements are an often-neglected consideration in mud-pump planning, which can seriously reduce the efficiency of the pump. If the mud pump cannot gain access to the proper volume of mud as needed, its output will be less than expected for a particular pump rate. The two common types of suction systems are atmospheric and supercharged.

The pump suction system common in early drilling operations used atmospheric pressure in conjunction with the hydrostatic pressure of the fluid in the mud pits to force the drilling fluid into the suction valves of the pump. The hydrostatic pressure must overcome inertia forces and friction pressures of the fluid in the lines. Obviously, long suction lines with many bends significantly decrease the effectiveness of the system. In addition, gas-cut or high-viscosity fluids impede the system's good operation.

Optimum input requirements increase as the pump stroke rates increase. Under most conditions, a flooded or atmospheric suction system cannot meet the upper demands.

A more successful method of fulfilling mud-pump suction needs is the use of centrifugal pumps as boosters (superchargers or prechargers). The addition of a supercharger offers many advantages including elimination of shock loads, smoother operation, increased bearing life, and higher-speed operation. The supercharger also enables the mud pump to better handle gas-cut or aerated mud, giving better filling.

Pulsation Dampeners. Improved pumping characteristics can be expected when a pulsation dampener (surge chamber) is added to the discharge line. The surge chamber contains a gas in the upper portion, which is separated from the drilling fluid by a flexible diaphragm. The surge chamber greatly dampens the pressure surges developed by the positive-displacement pump. A dampener helps to utilize most of the available pump horsepower. It accomplishes this by increasing the speed at which the pump can run without the problems of knocking and accompanying pressure surges. The extra speed advantage is the basic reason to use a dampener, but other advantages include the following:

- Stabilizes pressures in the suction line
- Allows the use of longer suction lines or smaller-diameter lines
- Makes suction from deeper pits possible
- Allows the use of heavier muds
- Allows the use of higher-temperature muds

Most operators prefer to run pulsation dampeners on the discharge end of the pump. The discharged drilling fluid is under high pressure and, as it is forced out of the liners it places significant surge pressures on the equipment. The pulsation dampeners are designed to absorb most of these surges and to reduce the wear of the other surface circulating equipment.

Centrifugal Pumps. The centrifugal pump (see **Fig. 1.24**) plays an important role in the circulating system. Among its applications are supercharging the rig pumps, pumping fluid to mud-mixing equipment and to the solids-control equipment, and performing ancillary functions such as pumping water and cleaning tanks.

Centrifugal pumps will not perform satisfactorily with gaseous or high-viscosity fluids. The primary component of a centrifugal pump is an impeller that accelerates the fluid into the discharge line.

Drilling-Fluid-Handling Equipment. The drilling fluid is handled by a variety of equipment during the normal drilling process. Each item must be evaluated to determine if it will meet the job requirements for the upcoming well. The handling equipment includes the mud pits (tanks for drilling-fluid storage), solids-control equipment, gas-control system (degasser), and chemical-treatment systems.

Mud pits are required for holding an excess volume of drilling fluid at surface. This surface volume allows time for settling of the finer rock cuttings and for the release of entrained gas bubbles not mechanically separated. Also, in the event of some drilling-fluid losses to underground formations, this fluid loss is replaced by mud from the surface pits.

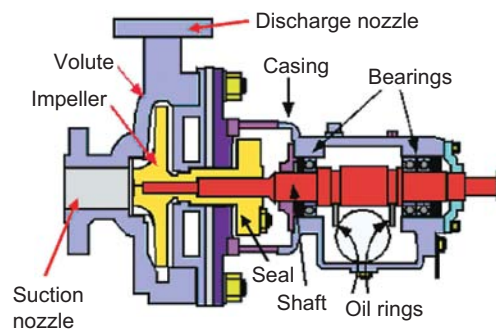


Fig. 1.24—Centrifugal pump diagram (Sahdev 2008).

The mud-pit system and the arrangement of the mud-handling equipment on the pits is a design consideration for the drilling-fluid engineer. This fact is particularly pertinent in land drilling operations if rental solids-control equipment is used. Offshore rigs are usually limited with respect to space availability and, in most cases, the pit system will have a dedicated position for the special equipment.

Drilling operations during the early days of the industry used earthen pits to contain the mud. The fluid from the well was discharged in one end of the pit, and the mud pump suction line was located in the other end of the pit. The surface area was large enough that solids could settle to the bottom of the pit before entering the pump suction line.

Earthen pits were replaced by steel pits for several reasons, including increasingly severe environmental regulations that made mandatory a very comprehensive treatment of discarded fluids and rock cuttings so that no harm is done to the environment. In addition, steel pits are easier to move with the rig, compared to the effort required to build new earthen pits. Also, certain denser and more-viscous fluids require special solids-control equipment that can be located only on steel pits.

During drilling operations, the discharged fluid from the well enters the pits and is processed through several types of solids-removal equipment, including the shale shakers, sand trap, degasser, desilting hydrocyclone, desanding hydrocyclone, centrifuges, and mud cleaners. After the treatment, the fluid will eventually re-enter the suction line and repeat the cycle.

Removal of undesirable solids from the drilling fluid is important to improve drilling performance and consequently reduce drilling costs. Fluids properly treated will

- Increase drilling rates by enhancing cuttings removal
- Provide better bit hydraulics due to lower fluid viscosity
- Avoid premature wear on surface equipment such as lines and the mud pumps' liners

In addition, formation damage will be reduced. A fluid with a high percentage of solid particles may invade and block the formation's pore channels, reducing the reservoir permeability.

Solids are removed from the mud system by settling, screening, centrifuging, or dilution. Settling is ineffective in most cases due to weighted mud systems or lack of time for gravity segregation. Dilution is expensive with heavy-mud systems. The principles employed for most commonly used solids-removal equipment are screening, centrifuging, or a combination of both.

The shale shaker is the most important component of the solids-control equipment. It removes the major portion of all drilled solids circulated out of the well. It also removes the large cuttings that would plug the other equipment.

Although many manufacturers produce shale shakers, the designs are quite similar. Mud flows from the well flowline into the "possum belly," or mud box. The possum belly has a lower bypass gate so that mud can flow directly into the sand trap and pits in case the screens are plugged with viscous fluids or solids. Depending on the openings in the screen mesh, the mud and small-diameter particles fall through the screen and exit at the discharge chute. The vibrating, or rotating, assembly on the screen causes the larger particles to move along to the end and off the screen.

Various screen arrangements are available on common shakers. Multiple-screen shakers are widely used and can offer better solids removal. The particle separation with a multiple-deck screen is determined by the finest-mesh screen, which is usually the bottom screen. The size separation with the parallel arrangement is determined by the coarsest screen size.

Screening surfaces used in solids-control equipment are generally made of woven wire screen cloth in many different sizes and shapes. Characteristics of the screen cloth that must be considered by the drilling engineer are mesh size and the shape and size of openings. Mesh is defined as the number of openings per linear inch.

A sand trap is a small compartmented section of the first pit immediately adjacent to the shale shaker. The effluent from the shale shaker flows to the sand trap. Its purpose is to allow settling of heavy particles such as sand or shale cuttings that escaped removal by the shaker screen.

Hydrocyclones (desilters and desanders) remove most of the solids in the 16- to 100- μm range. Because some barite falls within these sizes, the desilters and desanders cannot be used cost-effectively on weighted systems unless a fine-mesh screen is used below the cyclone to remove the barite from the underflow. (Barite is a solid purposely added to muds to increase mud density.)

A hydrocyclone (**Fig. 1.25**) consists of a conical shell with a small opening at the bottom for underflow discharge, a larger opening at the top for liquid discharge through an internal vortex finder, and a feed nozzle on the side of the body near the wide end of the cone. The fluid enters the cyclone under pressure from a centrifugal pump. High fluid velocity causes the particles to rotate rapidly within the main chamber of the cyclone. Light, fine solids and the liquid phase of the fluid tend to spiral inward and upward for discharge through the liquid outlet.

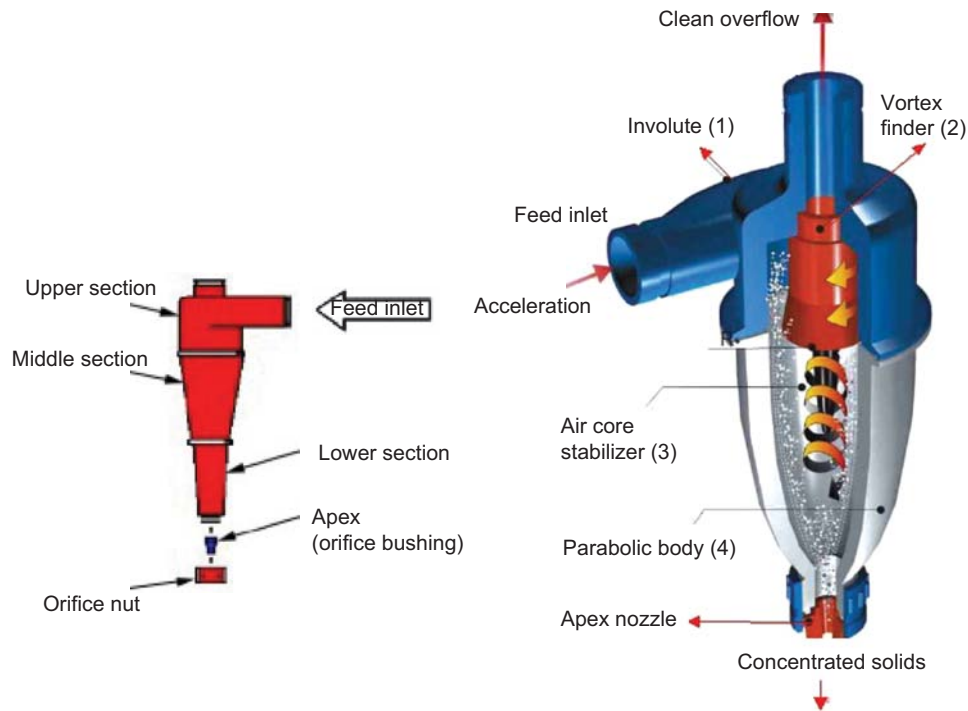


Fig. 1.25—Hydrocyclone (GN Solids 2009–2010). Courtesy of Tangshan Guanneng Machiner Equipment Co. Ltd.

Heavy, coarse solids and the liquid film around them tend to spiral outward and downward for discharge through the solids outlet.

Oilfield cyclones commonly vary from 4 to 12 in. (10 to 30 cm) in size and may be arranged in a parallel, multicone system. The size measurement refers to the inside diameter of the largest cylindrical section of the cone. The diameter of the cone usually controls throughput capacity and the size of solids that can be removed.

Centrifuges are used to remove colloid-sized solids (5 μm) from weighted water-based muds. The decanting centrifuge is the most commonly used type (Fig. 1.26). Unlike screens, cyclones, and mud cleaners that operate continuously on the full mud circulating volume, centrifuges operate intermittently on a small fraction of the circulating volume, usually 5–10%.

A decanting centrifuge consists of a conveyor screw inside a cone-shaped bowl that is rotated at very high speeds (1,500–2,500 rev/min). The drilling fluid usually is diluted with water and then pumped into the conveyor. As the conveyor rotates, the fluid is thrown out of the feed ports into the bowl. The centrifugal force on the mud pushes the heavy, coarse particles against the wall of the bowl, where the scraping motion of the conveyor screw moves them toward the solids discharge port. The light, fine solids tend to remain in suspension in the pools between the conveyor flutes and are carried to the overflow ports along with the liquid phase of the mud.

Mud cleaners were developed in the early 1970s in response to a need for equipment to effectively remove fine drilled solids from weighted muds without excessive loss of barite and fluid. The cleaners use a combination of desilting hydrocyclones and a very fine-mesh vibrating screen to remove fine drilled solids while returning valuable mud additives and liquids to the active system.

After the drilling fluid has passed through a shale shaker to remove the large cuttings, the mud is pumped into the cyclones on the mud cleaner. These cyclones clean the mud and discharge the finest solids and liquid phase into the next pit downstream. The solids discarded out of the bottom of the cyclones are deposited on a screen. Drilled solids larger than the screen are discarded into the waste pit. The remaining solids, which include most of the barite, pass through the screen and are discharged into the next downstream pit. The size of particles separated by a mud cleaner depends primarily on the mesh of the screen used in the particular unit.

Several manufacturers of solids-control equipment have developed complete packages of skid-mounted solids-control devices and all supporting tanks, piping, pumps, motors, and accessories. These unitized systems provide excellent solids control, efficiency, and ease of transportation and installation. They can create a “closed” system for ecologically sensitive drilling sites. Because the unit is designed as a complete system, all pieces of equipment including pumps and motors are sized properly to provide maximum efficiency in the smallest amount of space. Piping is designed for optimum fluid handling with the shortest practical suction and discharge lines.

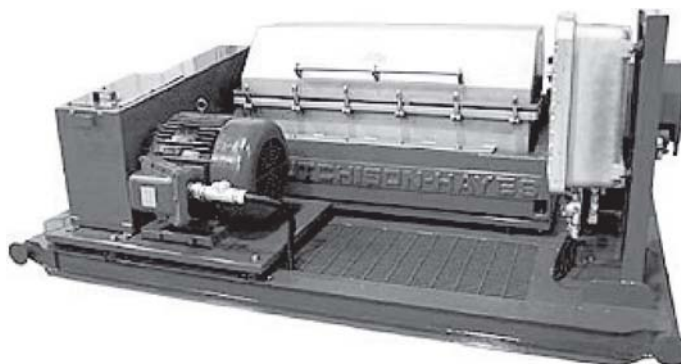


Fig. 1.26—Decanting centrifuge (Hutchison-Hayes Separation 2011). Used with permission from Hutchison-Hayes Separation, Inc.

Components of unitized systems can vary, depending on the manufacturer and the particular drilling application. Most include one or more of the basic separation devices installed in series, including screen shaker, degasser, desander, mud cleaner, and centrifuge. Desilting requirements usually are met by blocking the mud-cleaner screens and operating them as desilters when appropriate. Sand traps and agitators also are standard equipment in most units. In some cases, clay-removal cyclones may be used in place of or in addition to centrifuges.

When the amount of entrained formation gas leaving the settling pit becomes too great, it can be separated using a degasser. A vacuum chamber degasser is shown in **Fig. 1.27**. A vacuum pump mounted on top of the chamber removes the gas from the chamber. The mud flows across inclined flat surfaces in the chamber in thin layers, which allows the gas bubbles that have been enlarged by the reduced pressure to be separated from the mud more easily. Mud is drawn through the chamber at a reduced pressure of approximately 5 psia (35 kPa) by a mud jet located in the discharge line.

Pressures in a Wellbore. Calculation of static fluid pressure is most suitable for hand calculation, since velocity is zero and no time-dependent effects are present. The general equation for the static fluid pressure Δp calculation is given by:

$$\Delta p = \int_{\Delta s} \rho g \cos(\phi) ds, \quad (1.14)$$

where ρ is the density of the fluid, g is the gravity constant, ϕ is the angle of inclination of the wellbore (measured from the vertical), and s is the measured depth of the well. The simplest version of Eq. 1.14 is the case of an incompressible fluid with constant density ρ :

$$\Delta P = \rho g \Delta Z, \quad (1.15)$$

where ΔZ is the change in true vertical depth (i.e., hydrostatic head). For constant slope wellbore trajectories, ΔZ equals $\cos(\phi)\Delta s$.

Example 1.3—Static Pressure in a Wellbore. Calculate the static mud density required to prevent flow from a permeable stratum at 12,200 ft if the pore pressure of the formation fluid is 8,500 psig.

Solution. The common field unit for mud density is lbm/gal (pound per gallon, or ppg). Because we want pressure in psig, we need to convert Eq. 1.15 into field units of ppg, psig, and feet. Eq. 1.15 converts to:

$$\Delta p(\text{psig}) = \rho(\text{lbm/gal}) \frac{\text{gal}}{231 \text{ in.}^3} \frac{12 \text{ in.}}{\text{ft}} g \left(\frac{\text{lbf}}{\text{lbm}} \right) \Delta Z(\text{ft}) = 0.05195 \rho(\text{lbm/gal}) \Delta Z(\text{ft})$$

Note that the gravity constant for lbm is 1 lbf/lbm—that is, 1 pound mass weighs 1 pound force. Solving the equation for density:

$$\rho = \frac{8,500 \text{ psig}}{0.05195(12,200 \text{ ft})} = 13.4 \text{ lbm/gal}$$



Fig. 1.27—Vacuum-chamber degasser (Derrick Equipment 2010).

Example 1.4—Pressures in a Deviated Well. A 20,000 ft well is drilled vertically to 3,000 ft, and the remainder of the well is drilled at a 50° angle to the vertical. If the wellbore fluid is 10.5 lbm/gal, what is the pressure at 10,000 ft?

Solution. For the first 3,000 ft, the measured depth s equals the true vertical depth Z , so the pressure at 3,000 ft is

$$\Delta p(3,000 \text{ ft}) = 0.05195(10.5 \text{ lbm/gal})(3,000 \text{ ft}) = 1,636 \text{ psig}$$

The remainder of the interval from 3,000 ft to 10,000 ft is inclined 50°, so the true vertical depth increment is:

$$\Delta Z(3,000 \text{ ft to } 10,000 \text{ ft}) = \cos(50^\circ)(10,000 - 3,000) \text{ ft} = 0.6428(7,000) \text{ ft} = 5,000$$

The resulting pressure at 10,000 ft is:

$$\Delta p(10,000 \text{ ft}) = 1,636 \text{ psig} + 0.05195(10.5 \text{ lbm/gal})(5,000) \text{ ft} = 4,090 \text{ psig} = 28,200 \text{ kPa}$$

1.5.4 The Rotary System. The rotary system includes all of the equipment used to achieve bit rotation. Originally, the main driver in the system of all rigs was the rotary table. The main parts of the rotary system with a rotary table are the swivel, kelly, and drillstring.

The rotary swivel (**Fig. 1.28**) serves two important functions in the drilling process. It is a connecting point between the circulating system and the rotary system. It also provides a fluid seal that must absorb rotational wear while holding pressure. The upper section of the swivel has a bail for connection to the elevator hook, and the gooseneck of the swivel provides a downward-pointing connection for the rotary hose.

The kelly is the first section of pipe below the swivel. The outside cross section of the kelly is square or (most commonly) hexagonal to permit it to be gripped easily for turning. Torque is transmitted to the kelly through kelly bushings, which fit inside the master bushing of the rotary table. The kelly thread is right-handed on the lower end and left-handed on the upper end to permit normal right-hand rotation of the drillstring.

During drilling operations, in every connection, a new pipe is added below the kelly. To avoid premature wear in the kelly's threads, a kelly saver sub is used between the kelly and the first joint of drillpipe. Kelly cock valves are located on either end of the kelly.

Modern rigs use a topdrive to replace the kelly, kelly bushings, and rotary table. Drillstring rotation is achieved through hydraulic or electric motors. One type of topdrive is shown in **Fig. 1.29**.

Topdrives are suspended from the hook and can travel up and down the derrick. This will allow drilling to be done with stands of pipes, instead of single joints, which will save considerable time. Comparing with the conventional process, where a new pipe must be added to the drillstring after the length of just one joint has been drilled, using a topdrive system, a new connection will occur only after the length of one stand (two, three, or four pipes) has been drilled.

Besides saving time, a system with a topdrive enables the driller to re-initiate fluid circulation or drillstring rotation faster while tripping, which reduces the chance of problems such as stuck pipe.



Fig. 1.28—(a) Rotary swivel (Steven M. Hain Company, Inc. 2010); used with permission from Steven M. Hain Company, Inc.; (b) rotary swivel (courtesy of OSHA).

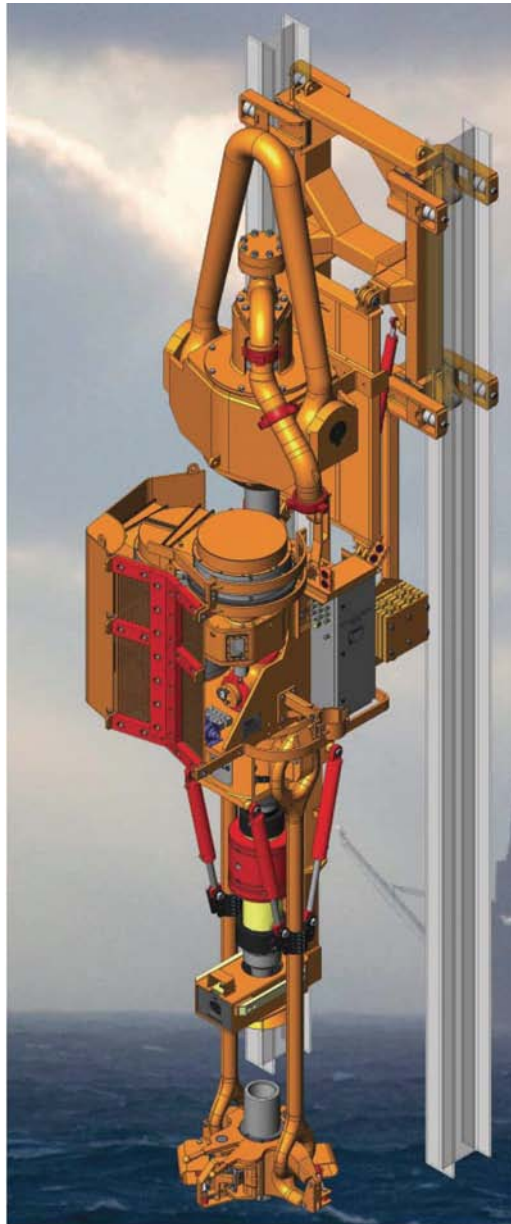


Fig. 1.29—Topdrive (*Bull. 20310* 2008).

The drillstring connects the surface equipment with the drill bit at the bottom of the well. The rotary table, or the topdrive, rotates the drillstring and, consequently, rotation is transmitted to the bit.

The drillstring is basically composed of two major portions, the drillpipes and the *bottomhole assembly* (BHA) (see **Fig. 1.30**). Drillpipes (Fig. 1.30b) are specified by outside diameter, weight per foot, steel grade, and length range. Drillpipes are classified by API in the following length ranges: Range 1 is 18 to 22 ft (5.5 to 6.7 m), Range 2 is 27 to 30 ft (8 to 9 m), and Range 3 is 38 to 45 ft (12 to 14 m).

Range 2 drillpipe is used most commonly. Since each joint of pipe has a unique length, the length of each joint must be measured carefully and recorded to allow a determination of total well depth during drilling operations.

The drillpipe joints are fastened together in the drillstring by means of tool joints (Fig. 1.30a). The portion of the drillpipe to which the tool joint is attached has thicker walls than the rest of the drillpipe to provide for a stronger joint. This thicker portion of the pipe is called the *upset*. If the extra thickness is achieved by decreasing the inside diameter, the pipe is said to have an internal upset. If the extra thickness is achieved by increasing the outside diameter, the pipe is said to have an external upset. A tungsten carbide hardfacing sometimes is manufactured on the outer surface of the tool joint box to reduce the abrasive wear of the tool joint by the borehole wall when the drillstring is rotated.

The BHA is the lower section of the drillstring. Even though a BHA may have many different tubulars depending on the complexity of the operation, most of the BHA is composed of drill collars (Fig. 1.30c). The drill collars are thick-walled, heavy steel tubulars used to apply weight to the bit. The buckling tendency of the relatively thin-walled drillpipe is too great to use it for this purpose. The smaller clearance between the borehole and the drill collars helps to keep the hole straight. Stabilizers (**Fig. 1.31**) often are used in the drill collar string to assist in keeping the drill collars centralized. Other types of tubulars used include shock absorbers and drilling jars. In addition, heavyweight drillpipes, a type of drillpipe with thicker walls, are commonly placed on top of the BHA to make the transition between the heavier drill collars and the drillpipes.

1.5.5 The Well-Control System. The well control system prevents the uncontrolled flow of formation fluids from the wellbore. When the bit penetrates a permeable formation that has a fluid pressure in excess of the hydrostatic pressure exerted by the drilling fluid, formation fluids will begin displacing the drilling fluid from the well. The flow of formation fluids into the well in the presence of drilling fluid is called a *kick*.

The well-control system enables the driller to

- Detect the kick
- Close the well at the surface
- Circulate the well under pressure to remove the formation fluids and increase the mud density

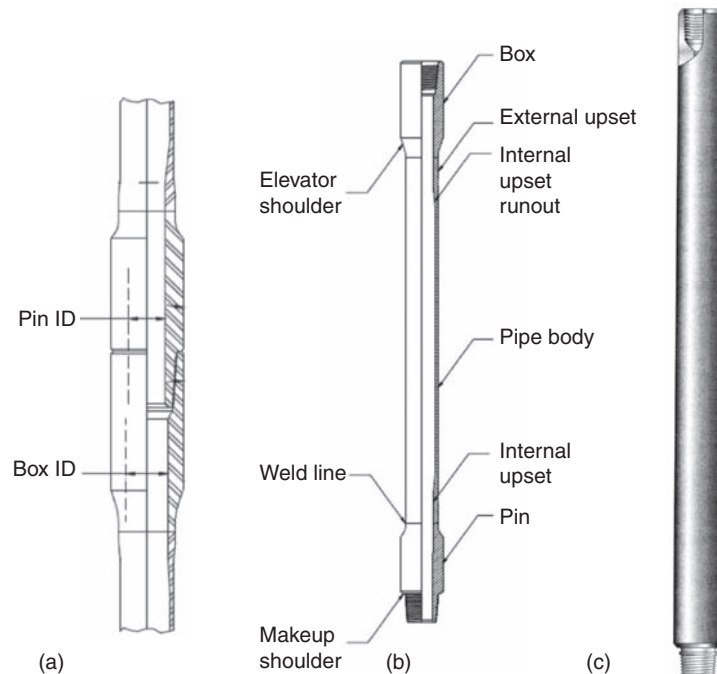


Fig. 1.30—(a) Drillpipe tool joint; (b) drillpipe; (c) drill collar. Parts (a) and (b) are from Aadnoy et al. (2009).



Fig. 1.31—Drillstring stabilizer (National Oilwell Varco 2010a).

- Move the drillstring up and down with the well closed
- Divert the flow away from rig personnel and equipment

Failure in detecting a kick or a malfunction in the well-control system may result in an uncontrolled flow of formation fluids into the wellbore. This unwanted fluid production is called a *blowout*. A blowout is arguably the worst disaster that can occur during drilling operations. Blowouts can cause loss of lives, drilling equipment, the well, much of the oil and gas reserves in the underground reservoir, and can cause damage to the environment. Thus, the well-control system is one of the more important systems on the rig.

Kick detection during drilling operations usually is achieved by use of a pit-volume indicator or a flow indicator. Both devices can detect an increase in the flow of mud returning from the well over that which is being circulated by the pump.

Pit volume indicators usually employ floats in each pit that are connected by means of pneumatic or electrical transducers to a recording device on the rig floor. The recording device indicates the volume of all active pits. High- and low-level alarms can be preset to turn on lights and horns when the pit volume increases or decreases significantly. An increase in surface mud volume indicates that formation fluids may be entering the well. A decrease indicates that drilling fluid is being lost to an underground formation.

Mud-flow indicators are used to help detect a kick more quickly. The more commonly used devices are somewhat similar in operation to the pit-level indicators. A paddle-type fluid-level sensor is used in the flowline. In addition, a pump-stroke counter is used to sense the flow rate into the well. A panel on the rig floor displays the flow rate into and out of the well. If the rates are appreciably different, a gain or loss warning will be given.

While making a trip, circulation is stopped and a significant volume of pipe is removed from the hole. Thus, to keep the hole full, mud must be pumped into the hole to replace the volume of pipe removed. Kick detection during tripping operations is accomplished through use of a hole fill-up indicator. The purpose of the fill-up indicator is to measure accurately the mud volume required to fill the hole. If the volume required to fill the hole is less than the volume of pipe removed, a kick may be in progress.

Small trip tanks provide the best means of monitoring hole fill-up volume. Trip tanks usually hold 10 to 15 bbl (1.6 to 2.4 m³) and have 1-bbl (0.16 m³) gauge markers. Periodically, the trip tank is refilled using the mud pump. The required fill-up volume is determined by periodically checking the fluid level in the trip tank. When a trip tank is not installed on the rig, hole fill-up volume should be determined by counting pump strokes each time the hole is filled. The level in one of the active pits should not be used since the active pits are normally too large to provide sufficient accuracy.

The flow of fluid from the well caused by a kick is stopped by use of well-control devices called *blowout preventers* (BOPs). The BOP will close the well and hold well pressure, consequently impeding new fluid from entering the wellbore.

Multiple BOPs with different purposes are used in a well. This arrangement is called a BOP *stack*. The reason for using a BOP stack is to enable the system to close the well and stop the flow of unwanted fluid into the wellbore under all drilling conditions. The well-control system must enable well closure while drilling, tripping in or out of the hole, running casing, and even when there is no drillstring inside the well.

When the drillstring is in the well, movement of the pipe without releasing well pressure should be allowed to occur. In addition, the BOP stack should allow fluid circulation through the well annulus under pressure. These objectives usually are accomplished by using several ram preventers and one annular preventer.

An example of a ram preventer is shown in Fig. 1.32. Ram preventers have two packing elements on opposite sides that close by moving toward each other. Pipe rams have semicircular openings that match the diameter of pipe sizes for which they are designed. Thus, the pipe ram must match the size of pipe currently in use. If more than one size of drillpipe is in the hole, additional ram preventers must be used in the BOP stack. Rams designed to close when no pipe is in the hole are called *blind rams*. Blind rams will flatten drillpipe if inadvertently closed with the drillstring in the hole but will not stop the flow from the well. Shear rams are blind rams designed to shear the drillstring when closed. This will cause the drillstring to drop in the hole and will stop flow from the well. Shear rams are closed on pipe only when all pipe rams and annular preventers have failed or, in the case of offshore drilling, when an emergency dictates that the drilling vessel must abandon the location. In that case, the blind ram is intentionally activated, and an emergency disconnection is made. This operation will be described



Fig. 1.32—Double ram preventer (© Cameron 2006).

later in Section 1.6. Ram preventers are available for working pressures of 2,000, 5,000, 10,000, and 15,000 psig (14,000, 35,000, 70,000, 100,000 kPa).

Annular preventers, sometimes called *bag-type* preventers, stop flow from the well using a ring of synthetic rubber that contracts around the pipe, preventing fluid passage and sealing the annulus. The rubber packing conforms to the shape of the pipe in the hole. Most annular preventers also will close an open hole if necessary. A cross section of one type of annular preventer is shown in Fig. 1.33. Annular preventers are available for working pressures of 2,000, 5,000, and 10,000 psig (14,000, 35,000, 70,000 kPa).

Both ram and annular BOPs are closed hydraulically. In addition, the ram preventers have a screw-type locking device that can be used to close the preventer if the hydraulic system fails. The annular preventers are designed so that once the rubber element contacts the drillstring, the well pressure helps to hold the preventer closed.

Modern hydraulic systems used for closing BOPs are high-pressure fluid accumulators similar to those developed for aircraft fluid-control systems. The accumulator is capable of supplying sufficient high-pressure fluid to close all of the units in the BOP stack at least once and still have a reserve. Accumulators with fluid capacities of 40, 80, or 120 gal (0.15, 0.30, or 0.45 m³) and maximum operating pressures of 1,500 or 3,000 psig (10,000 or 20,000 kPa) are common. The accumulator is maintained by a small pump at all times, so the operator has the ability to close the well immediately, independent of normal rig power. For safety, standby accumulator pumps are maintained that use a secondary power source.

The accumulator is equipped with a pressure-regulating system. The ability to vary the closing pressure on the preventers is important when it is necessary to *strip pipe* into the hole. Stripping the pipe means moving the pipe with the preventer closed. A pipe may be stripped either into or out of the well. If a kick is taken during a trip, it is best to strip back to bottom to allow efficient circulation of the formation fluids from the well. The application of too much closing pressure to the preventer during stripping operations causes rapid wear of the sealing element. The usual procedure is to reduce the hydraulic closing pressure during stripping operations until there is a slight leakage of well fluid.

Stripping is accomplished most easily using the annular preventer. However, when the surface well pressure is too great, stripping must be done using two pipe ram preventers placed far enough apart for external-upset tool joints to fit between them. The upper and lower rams must be closed and opened alternately as the tool joints are lowered through.

Space between ram preventers used for stripping operations is provided by a drilling spool. Drilling spools also are used to permit attachment of high-pressure flowlines to a given point in the stack. These high-pressure flowlines make it possible to pump into the annulus or release fluid from the annulus with the BOP closed. A conduit used to pump into the annulus is called a *kill line*. Conduits used to release fluid from the annulus may include a choke line, a diverter line, or simply a flowline. All drilling spools must have a large enough bore to permit the next string of casing to be put in place without removing the BOP stack.

The BOP stack is attached to the casing using a casing head. The casing head is welded or connected to the first string of casing cemented in the well. It must provide a pressure seal for subsequent casing strings placed in the well. Also, outlets are provided on the casing head to release any pressure that might accumulate between casing strings.

The control panel for operating the BOP stack usually is placed on the derrick floor for easy access by the driller. The controls should be marked clearly and identifiably with the BOP stack arrangement used. Modern and safer rigs will have at least one other control panel located far from the rig floor. This panel will be used in case it is necessary, for safety reasons, to evacuate personnel from the rig floor.

The arrangement of the BOP stack varies considerably. The arrangement used depends on the magnitude of formation pressures in the area and on the type of well-control procedures used by the operator. API presents several recommended arrangements of BOP stacks, including *Spec. 16A* (2004), *Spec. 16C* (1993), and *Spec. 16D* (2004). Fig. 1.34 shows two typical BOP stack arrangements, showing several types of rams, annular preventers,

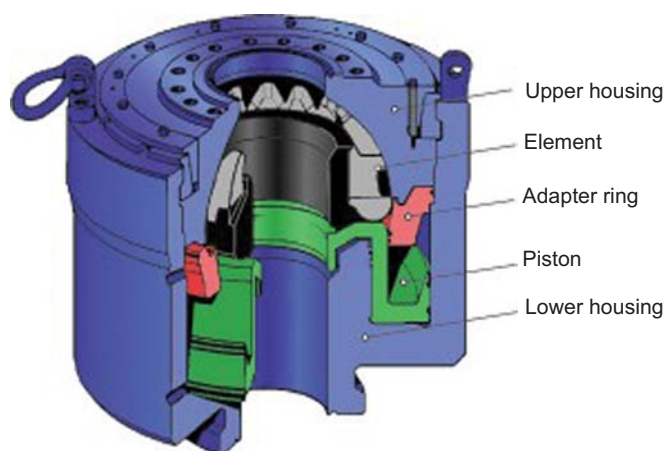


Fig. 1.33—Annular preventer. Courtesy of National Oilwell Varco.

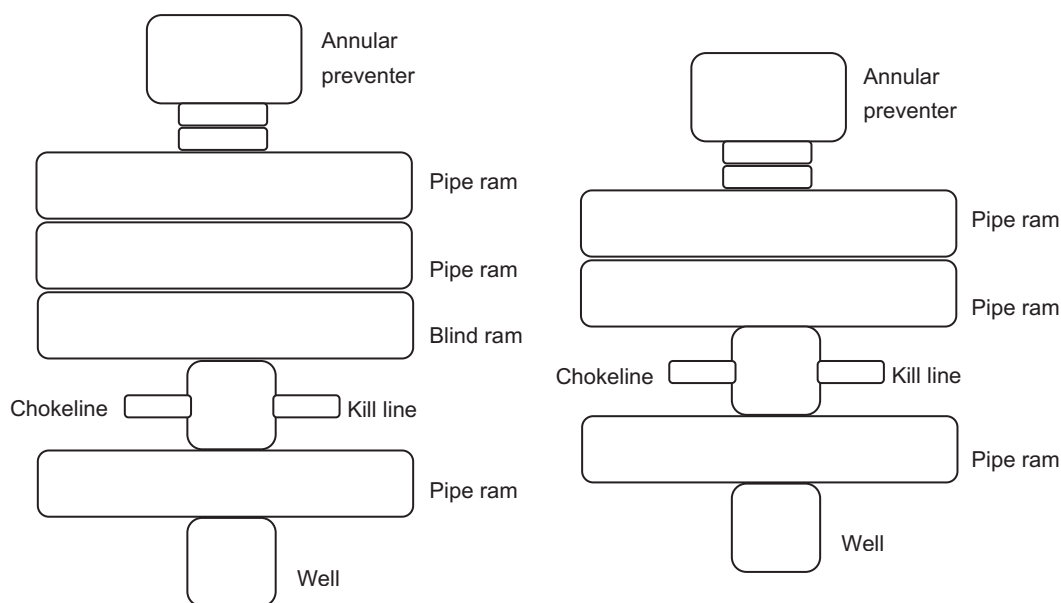


Fig. 1.34—BOP stack arrangements.

drilling spools, and flowlines. In some cases, it may be desirable to conduct drilling operations with surface pressure on the annulus. A rotating head, which seals around the kelly at the top of the BOP stack, must be used when this is done. Rotating heads most commonly are employed when air or gas is used as a drilling fluid.

When the drillstring is in the hole, the BOP stack can be used to stop only the flow from the annulus. Several additional valves can be used to prevent flow from inside the drillstring. These valves include *kelly cocks* (i.e., valves inside the kelly) and *inside BOPs*. Generally, an upper kelly cock having left-hand threads is placed above the kelly, and a lower kelly cock having right-hand threads is placed below the kelly. The lower kelly cock also is called a *drillstem valve*. Two kelly cocks are required because the lower position might not be accessible in an emergency if the drillstring is stuck in the hole with the kelly down.

An *inside BOP* is a valve that can be placed in the drillstring if the well begins flowing during tripping operations. Inside BOPs can use a ball valve or dart-type valve (check valve), as shown in **Fig. 1.35**. An inside BOP should be placed in the drillstring before drillpipe is stripped back in the hole because it will permit mud to be pumped down the drillstring after reaching the bottom of the well. Inside BOPs are installed when needed by screwing into the top of an open drillstring with the valve or dart in the open position. Once the BOP is installed, the valve can be closed or the dart released.

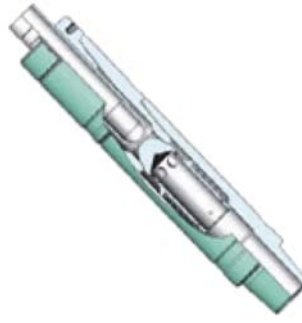


Fig. 1.35—Inside BOP with dart-type valve (National Oilwell Varco 2010b).

A high-pressure circulating system is used for well-control operations. The kick normally is circulated from the well through an adjustable choke. The adjustable choke is controlled from a remote panel on the rig floor. Sufficient pressure must be held against the well by the choke so that the bottomhole pressure in the well is maintained slightly above the formation pressure. Otherwise, formation fluids would continue to enter the well.

Mechanical stresses on the emergency high-pressure flow system can be quite severe when handling a kick. The rapid release of large volumes of fluid through the surface piping frequently is accompanied by extreme vibrational stresses. Thus, care should be taken to use the strongest available pipe and to anchor all lines securely against reaction thrust. Also, some flexibility in the piping to and from the wellhead is required. The weight of all valves and fittings should be supported on structural members so that bending stresses are not created in the piping. Because of fluid abrasion, the number of bends should be minimized. The bends required should be sweep-turn bends rather than sharp “L” turns, or should have an abrasion-resistant target at the point of fluid impingement in the bend.

API has several recommended choke manifold arrangements for 2,000-, 3,000-, 5,000-, 10,000-, and 15,000-psig (14,000, 21,000, 34,000, 69,000, and 100,000 kPa) working pressure systems (*Spec. 16C* 1993). In addition to these recommendations, well operators have developed many other, optional designs.

1.5.6 Well-Monitoring System. An optimal drilling operation requires close control over a number of parameters. Even though the drilling program may have recommendations related to drilling parameters, it is mandatory that rig personnel (e.g., driller, drilling supervisor, drilling and mud engineer) keep track of the operation development at all times in order to make necessary adjustments and to quickly detect and correct drilling problems.

A modern rig will have devices that display and simultaneously record most of the important parameters related to the drilling operation. Parameters that cannot be determined automatically, such as mud properties, will be measured, recorded, and controlled constantly as well. Some of the most important parameters include

- Well depth
- Weight on bit
- Rotary speed
- Rotary torque
- Pump pressure
- Pump rate
- Fluid-flow rate
- Flow return
- Rate of penetration
- Hookload
- Fluid properties (e.g., density, temperature, viscosity, gas and sand content, salinity, solids content)
- Pit level

Monitoring of these important parameters, together with reliable historical records of previous similar operations, will assist the driller in predicting and detecting possible drilling problems. Monitoring the mud system is an important task that must be fulfilled to maintain well control. The mud gives warning signs and indications of kicks that can be used to reduce the severity of the kicks by early detection, avoiding a large influx of gas into the wellbore. Additionally, if the system is properly monitored, other drilling problems such as lost circulation can be minimized.

Moreover, good records of various aspects of the drilling operation also can aid geological, engineering, and supervisory personnel. Today, modern rigs carry centralized well-monitoring systems that can be housed in the engineer's office and/or in the geologist's office at the rigsite. Besides, if desired, advancements in satellite communications allow installation of monitoring systems in places far from the rigsite.

These monitoring units provide detailed information about the formation being drilled and the fluids being circulated to the surface in the mud, and they centralize the record keeping of drilling parameters. The mud logger carefully inspects rock cuttings taken from the shale shaker at regular intervals and maintains a log describing their appearance. Additional cuttings are labeled according to their depth and are saved for further study by the paleontologist. The identification of the microfossils present in the cuttings assists the geologist in correlating the formations being drilled. Gas samples removed from the mud are analyzed by the mud logger using a gas chromatograph. The presence of a hydrocarbon reservoir often can be detected by this type of analysis.

With the development of downhole tools specially designed for well inclination and direction control, operations in directional wells became much more efficient. These tools are run together with the BHA and will constantly send information to surface regarding the position of the well. Measurement-while-drilling (MWD) tools normally use a mud pulser that sends information to the surface by means of coded pressure pulses in the drilling fluid contained in the drillstring. Chapter 8 provides information on MWD equipment.

1.6 Marine Drilling

Drilling wells offshore, from a floating vessel, requires special equipment and procedures. Even though the drilling operation itself is similar to onshore drilling, special equipment is required to hold the vessel on location over the borehole and to compensate for the vertical, lateral, and tilting movements caused by wave action against the vessel.

In the past, most floating vessels were held on location by anchors. However, to anchor a drillship or a semisubmersible in deep water using conventional anchors and cables or chains is virtually impossible. Consider an operation at a water depth of 2000 m (6,560 ft). The cables or chains connecting the anchor with the vessel would have to be huge in order to support the large tensions. Consequently, the vessel space required to store the cables must also be very large. Further, the operation to position the anchors would be very difficult, probably unfeasible. Even though there are some reports (Maksoud 2002) of deepwater mooring, this was achieved with special cables made of polyester and a mooring system that used a special suction anchor system. This system needs the support of other boats to handle the anchors and cables. On the other hand, a dynamically positioned drillship can move to the location and get positioned using only its own equipment; no additional support is needed.

Conventional anchored vessels are limited to just a few hundred meters of water depth. When the ocean bottom is too hard for conventional anchors, anchor piles are driven or cemented in boreholes in the ocean floor. The vessel is moored facing the direction from which the most severe weather is anticipated. Certain drillships are designed to be moored from a central turret containing the drilling rig. In this case, the ship will rotate about the turret so that it always faces incoming waves. Most mooring systems are designed to restrict horizontal vessel movement to approximately 10% of the water depth for the most severe weather conditions; however, horizontal movement can be restricted to approximately 3% of the water depth for the weather conditions experienced 95% of the time. As many as 12 anchors are used in a mooring system. For anchored vessels, motion problems are more severe for drillships than for semisubmersibles. However, drillships usually are easily operated and can be moved rapidly from one location to the next.

For deep and ultradeep water, where anchoring systems are not feasible, an anchorless system was developed. In this case, the vessel has large *thrusters* (**Fig. 1.36**), units capable of holding the drilling vessel on location without anchors. This system is called *dynamic positioning* (DP), and it works to counteract the forces to which the drilling vessel is subjected while on location. The wind, waves, and maritime currents will tend to displace the vessel from its station. Sensors at the vessel detect these actions and require the thrusters to counteract the forces accurately. The entire system is controlled by two independent computer systems. In addition, manual position and heading control is also available. **Table 1.3** shows the classification of DP systems according to standards established by the International Maritime Organization (IMO). **Fig. 1.37** shows a DP control room, and **Fig. 1.38** shows a diagram of the basic elements of a DP system.

Even though DP systems are designed mainly for use in water depths in excess of 700 m (2,300 ft), there are cases in which DP vessels (semisubmersibles or drillships) have been used in lesser depths due to their practicality and time-saving capability.

A special derrick design must be used for drillships because of the tilting motion caused by wave action. The derrick of a drillship often is designed to withstand as much as a 20° tilt with a full load of drillpipes standing in the derrick. Also, special pipe-handling equipment is necessary to permit tripping operations to be made safely during rough weather. This equipment permits drillpipe to be laid down quickly on a pipe rack in doubles or

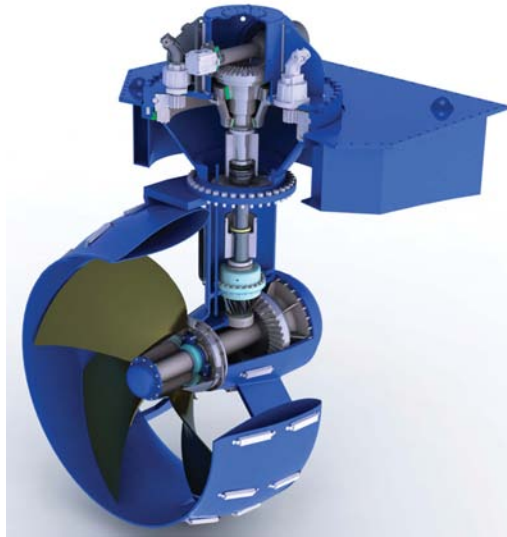


Fig. 1.36—Thruster with controllable-pitch propeller (Thrustmaster of Texas 2010).

TABLE 1.3—IMO DP CLASSIFICATION [after MSC/Circ. 645 (1994)] Reproduced courtesy of the International Maritime Organization	
IMO DP Class	Description
Class 1	Automatic and manual position and heading control under specified maximum environmental conditions.
Class 2	Automatic and manual position and heading control under specified maximum environmental conditions, during and following any single fault excluding loss of a compartment. (Two independent computer systems.)
Class 3	Automatic and manual position and heading control under specified maximum environmental conditions, during and following any single fault including loss of a compartment due to fire or flood. (At least two independent computer systems with a separate backup system.)



Fig. 1.37—DP control room. Courtesy of Keith Wyatt, Converteam.

triples rather than supported in the derrick. A block guide track also is used to prevent the traveling block from swinging in rough weather.

Normally, in marine operations from floating vessels, the wellhead and BOPs are placed at the seafloor. A marine riser conducts the drilling fluid from the ocean floor to the drilling vessel. A flex joint at the bottom of the marine riser allows lateral movement of the vessel. The vertical movement of the vessel is allowed by a slip joint placed at the top of the marine riser. The riser is secured to the vessel by a pneumatic tensioning system. To reduce tension requirements in long and heavy riser strings, buoyant sections made of light material are added to the riser system.

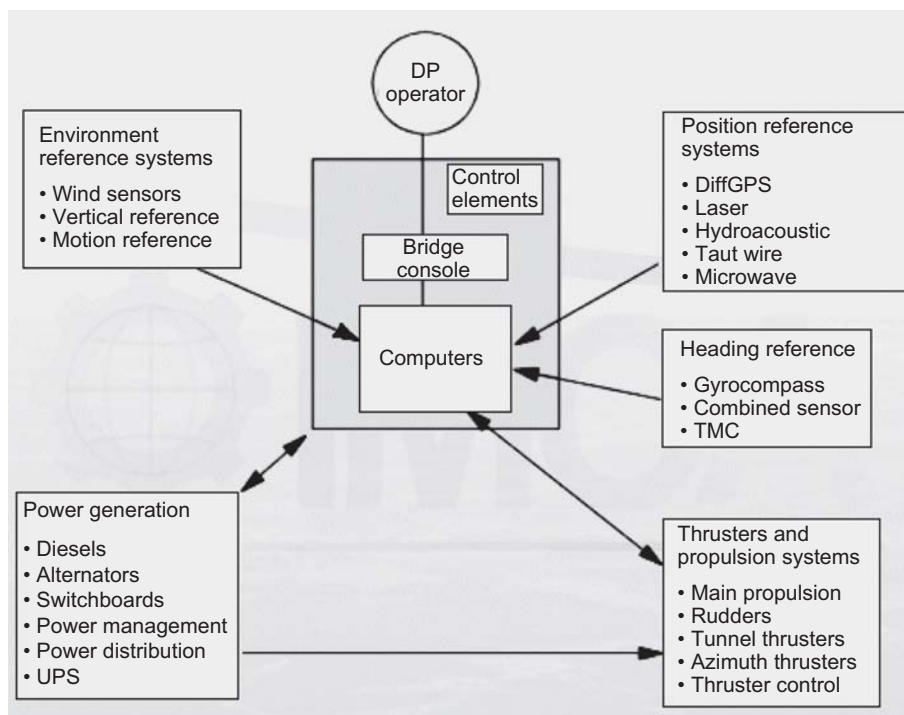


Fig. 1.38—The elements of a DP system (IMCA 2003). Courtesy of the International Marine Contractor Association.

To keep the drillstring from suffering the effects of the vertical movement of the vessel and to keep the weight on bit constant, types of surface-motion-compensating equipment called *heave compensators* have been developed. A constant hookload is maintained through use of a pneumatic tensioning device on the traveling block.

As mentioned before, the BOP stack for a floating drilling operation normally is placed on the ocean floor below the marine riser. However, in recent years, alternatively, a system with a slim high-pressure riser system and a surface BOP has been developed. Even though a subsea BOP could be considered the standard drilling procedure, a number of wells (DeLuca 2005) have been drilled lately using surface BOPs.

The subsea BOP ensures that the well can be closed even in severe weather, such as a hurricane. In such extreme conditions, the BOP can be closed and the marine riser disconnected from the top of the BOP system, allowing the vessel to go to a safer place. Later, when weather conditions get back to normal, the vessel returns to the location and the riser is reconnected to the BOP so that the operation can resume. If the drillstring is in the well and an emergency disconnection is necessary, the BOP's shear ram is used to cut off the drillpipe. Then, the BOP's blind ram also is closed, keeping the well shut. Later, after the reconnection, the portion of the drillstring remaining in the well can be fished (special tools are used to retrieve the original drillpipe), the damaged pipe substituted, and the operation resumed.

Another feature of the subsea system is that identical hydraulically operated connectors often are used above and below the BOP stack. This makes it possible to add on an additional BOP stack above the existing one in an emergency.

Offshore drilling operations differ from onshore drilling in various aspects, including *well spud-in* (initiating a well), in which the differences in equipment and operating procedures are considerable. For drilling operations from floating vessels, this difference is even more significant. Various schemes have been developed for offshore well spud-in. To illustrate those differences, let us analyze initial drilling operations for a shallow-water well drilled from a jackup rig and a deepwater well drilled from a floating DP vessel. Note that the sequence of operations presented for both cases does not represent the only possible way to initiate a well because these operations can vary depending on the type of rig and equipment used.

In a jackup rig, the first section may be drilled using, for example, a 26-in. bit coupled with a 36-in. hole opener. This first section normally is not long, and when concluded, a 30-in. conductor is run into the well and cemented. The 30-in. conductor (**Fig. 1.39**) has an internal profile that allows support, at mudline, for the next casing, normally a 20-in. surface casing. Alternatively, the conductor could be jetted instead of cemented. In the case of jetting, the initial well section is drilled by the action of water jets positioned at the lower end of the conductor. When the planned depth is reached, the conductor is already in place.

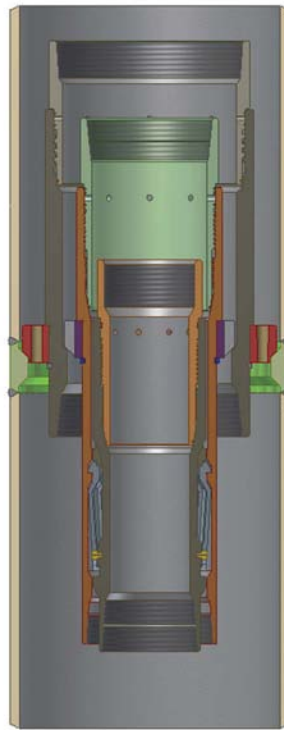


Fig. 1.39—MLH Mud Line Suspension System (photo courtesy of GE Oil & Gas).

After this first phase is concluded, the conductor is cut below the rotary table, and the first wellhead and a diverter is installed at its top so that the drilling operation can resume. The next section is drilled using, for example, a 26-in. bit, and afterward a 20-in. casing will be run and cemented. Note that this casing has its weight supported by the 30-in. conductor at mudline, avoiding unnecessary loads to the rig.

The 20-in. casing, when cemented in place, also is cut below the rotary table, allowing a wellhead and BOP to be installed on its top. After that, drilling operation resumes, with each section being drilled and its associated casing being run and cemented in a similar fashion. Normally, the first low-pressure BOP, installed on top of the 20-in. casing, is changed after the next casing is run, so that high-pressure safety equipment can be installed. Note that, because all safety and wellhead equipment is installed at surface, subsequent operations are quite similar to onshore drilling.

When drilling from a floating vessel, normally the wellhead and BOPs are installed close to seafloor and are called a *subsea system*. There are many different wellhead and subsea BOP configurations. One type of design, which has been in use since the early 1980s, involves the installation at seafloor of two guide bases. The first one, called the *temporary* guide base, is a heavy steel structure with an opening in the center and four cables, called *guidelines*, surrounding the central hole and extending back to the vessel, where a constant tension is maintained in the cables.

With the temporary base in position, a drillstring with the first drill bit is lowered to the seafloor, and the first section of the well is drilled. Commonly, a remotely operated vehicle (ROV) is used to monitor the operation. The ROV has a camera that transmits the view of the action to a monitoring station located at surface on the drilling vessel.

After conclusion of drilling, the first casing is run into the well with the *permanent* guide base attached to its top, and, as the casing is placed in position, the permanent guide base is landed on the temporary base (**Fig. 1.40**).

After the first well section is concluded, a second section is drilled, also without a BOP system. A marine riser may be installed in the wellhead housing of the previous casing; if so, a diverter system is installed at surface to deal with the possible hazards associated with drilling into shallow gas zones. This will allow formation fluids to be diverted away from the rig in an emergency.

After drilling, the conductor casing is lowered into the hole with a high-pressure subsea wellhead housing attached to its top. The wellhead housing internal profile (see Fig. 1.40) is designed to receive subsequent casing strings. The BOP stack is lowered and latched into the top of the wellhead, and the marine riser then can be deployed and latched into the BOP.

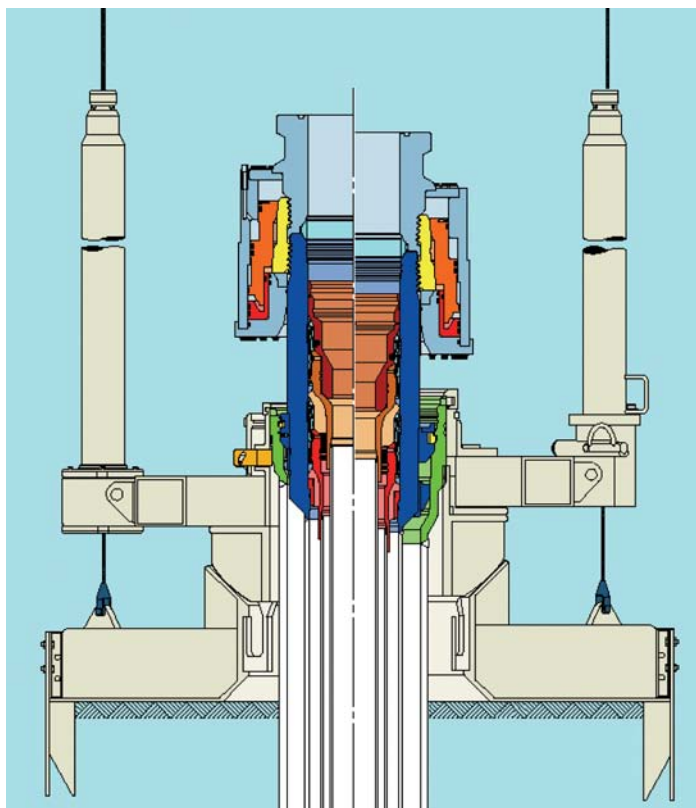


Fig. 1.40—SS10 subsea system with temporary and permanent guide base (courtesy of Drill-Quip).

As can be seen from the above sequence of operations, well startup from a floating vessel can be very time-consuming, which directly affects well cost because daily rates for floating vessels tend to be especially high. This situation is more noticeable for deepwater drilling, where the tripping operations to install subsea equipment at seafloor take even longer.

Recently, modern subsea systems and procedures were specially developed for deepwater drilling. These systems allow the operator, in one trip, to run the first large-bore casing and its wellhead housing and, after jetting it in place, to immediately start drilling the second well section without tripping back to surface. The sequence of operation for deepwater well spud-in is as follows (see **Fig. 1.41**):

- Run the conductor and its wellhead housing and jet it in place.
- Release the running tool and drill ahead with the bit and BHA previously connected with the running string and positioned inside the conductor.
- After conclusion of drilling, retrieve the drillstring and the running tool to surface.
- Run the next casing with the high-pressure wellhead. The casing is run with a running tool connected to the wellhead, and casing length is calculated so that, when the casing shoe is in place, the wellhead is landed on the wellhead housing. After landing the wellhead, cement the casing and then retrieve the running tool and running string back to surface.
- Run the BOP with the riser already connected on its top. The BOP is then landed on the high-pressure wellhead.
- With the BOP and riser in place, the operation to drill the next section can be carried out.

1.7 Drilling Cost Analysis

Drilling is the most visible of the many faces of the oil industry and may represent up to 40% of the entire exploration and development costs (Cunha 2002) of a field. Drilling engineers play a major role in well planning, not only designing the well but also recommending efficient and safe drilling procedures for routine rig operations such as drilling-fluid treatment, pump operation, bit selection, drilling parameters, and casing and cement programs. Drilling engineers also are responsible for preparing contingency plans that will be used in case any

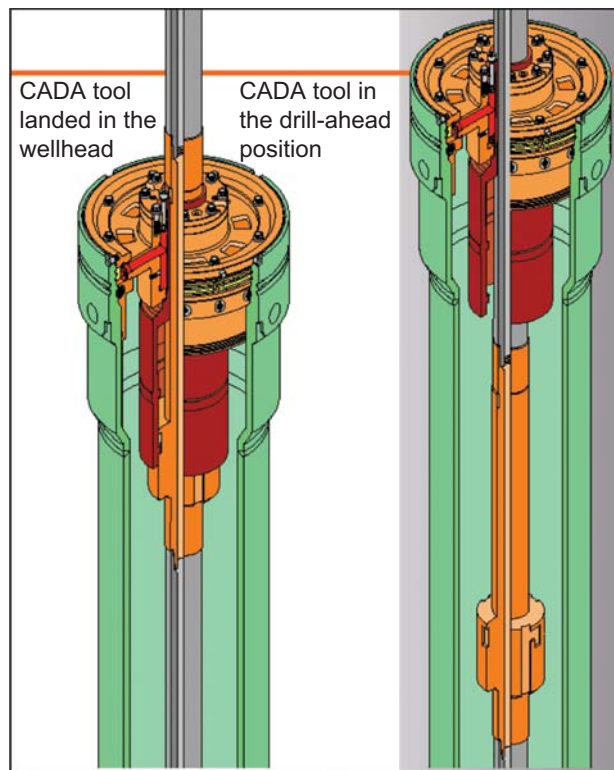


Fig. 1.41—Cam-actuated drill-ahead (CADA) tool (courtesy of Dril-Quip).

problems are encountered during the drilling operation. This entire process, which should be carried out taking into consideration safety and environmental constraints and regulations, must ultimately be as efficient and inexpensive as possible.

The final cost of a well depends on many factors, but clearly good well planning represents a major step toward cost-efficiency. In addition, the drilling team should be attentive during well drilling to keep track of the development of operations and promptly act if changes are needed. In this section, we will discuss existing methods for drilling cost analysis as well as ways to optimize costs during drilling operations.

1.7.1 Drilling Cost Prediction. One of the most challenging tasks for the drilling engineer is to predict well costs, either for a single exploration well or for a number of development wells on a drilling campaign. Normally, a decision about when and where a well will be drilled is made far in advance of operation startup. It is important for companies to have a reasonable cost estimate so that a proper budget can be prepared, with the necessary funds being set aside for the operation. Also, most exploration ventures are very risky, presenting a high possibility of resulting in “dry wells.” Because of this, it is very common in modern industry for companies to make joint ventures to explore a new area. In such cases, normally one company is responsible for the operations (the operating partner), while others share the costs and eventually the associated profits of the project. In this common case, the operator must present to the partners an authorization for expenditure (AFE) with the expected cost of drilling, which will allow the partners also to include those predicted expenses on their own budgets. An AFE usually includes a provision for contingency costs, and it is expected that operators will have the necessary expertise to predict well costs that will not exceed 20% of the initially predicted budget. In some cases, such as the evaluation of a given tract of land available for lease, only an approximate cost estimate is required. In other cases, such as in a proposal for drilling a new well, a more detailed cost estimate is required.

Drilling costs depend primarily on well location and well depth. External factors, such as abnormal rig market conditions, also may influence cost. The location of the well governs the costs of preparing the wellsite and moving the rig to the location. Remote locations, with no roads or infrastructure, will certainly result in a higher final well cost. Also, a wildcat well drilled in a place far from the regions where rigs are concentrated will have a significant part of its costs spent on rig mobilization and demobilization. For example, an operator may have to pay millions of dollars just to bring a deepwater drillship from the Gulf of Mexico to the African west coast. Additionally, if the region does not have a developed market, all costs, including crew, boat, and helicopter rentals,

well-monitoring services, housing, routine maintenance, drilling-fluid treatment, and rig supervision, will be considerably higher.

The depth of the well will govern the lithology that must be penetrated and, thus, the time required to conclude the well. Traditionally, oil companies have in their database a source of historical drilling/cost data presented by type of well, region, and well depth. In addition, there are companies that specialize in collecting drilling data around the world and compiling them in a database that can be used by drilling engineers when planning and budgeting well operations.

Drilling costs tend to increase exponentially with depth, and it is a good policy for drilling engineers to rely on past data to estimate drilling time and cost for future operations.

When enough data are available for a certain region, it is possible to assume a relationship between cost, C_{dc} , and depth, s , as proposed in Bourgoyne (1986).

$$C_{dc} = a_{dc} \exp(b_{dc}s), \quad (1.16)$$

where the constants a_{dc} and b_{dc} depend primarily on the well location.

Example 1.5—Well Cost Estimation. Fig. 1.42 presents data of depth and cost for a series of wells drilled in the same region. Assuming all external conditions remained the same, estimate the cost for two new wells with depths of 13,550 ft (4130 m) and 19,500 ft (5943 m).

Solution. From the data in Fig. 1.42 it is possible to perform a least-squares curve fit (see Appendix) where a_{dc} equals USD 803,210 and b_{dc} equals $4.9 \times 10^{-5} \text{ ft}^{-1}$. Fig. 1.43 shows a cost vs. depth chart for the area and the resulting exponential curve.

Once the parameters of the curve are established, the predicted costs are easily obtained as

$$C_{dc} = 803,210 \exp(4.9 \times 10^{-5} \times s).$$

For $s = 13,550$ ft,

$$C_{dc} = 803,210 \exp(4.9 \times 10^{-5} \times 13,550) = \text{USD } 1.56 \text{ million}.$$

For $s = 19,500$ ft,

$$C_{dc} = 803,210 \exp(4.9 \times 10^{-5} \times 19,500) = \text{USD } 2.09 \text{ million}.$$

When a number of similar wells have been drilled in a region (e.g., in a development campaign in which all wells have approximately the same depth and casing program), prediction of future wells is simpler. Data from the completed wells may be used to estimate time and costs of future wells. In such a case, it is important, when analyzing the data, to keep in mind the order in which the wells were drilled, because it is well known that, keeping all external conditions constant, there will be a tendency to have an improved performance as the drilling campaign progresses. This improvement is part of a learning process and can be mathematically described by learning curves (Teplitz 1991). This useful concept can be used in many petroleum engineering processes, including prediction of drilling performance and well cost (Ikoku 1978). If enough data are available, a curve can be drawn relating wells drilled with drilling performance (or well cost). Then the drilling engineer can use the curve to predict future well costs. The learning curve can be mathematically represented by

$$C_{lc} = a_{lc} n_w^{b_{lc}}, \quad (1.15)$$

where C_{lc} represents the “learning curve” cost of the well or cost per foot, a_{lc} and b_{lc} are constants, and n_w represents the well number (ordered by the first well drilled to the last) or the cumulative footage drilled.

One problem with this formula is that well cost continues to decrease the more wells that are drilled, whereas, in reality, there will be a minimum cost for the ideal trouble-free well. We could devise a more complex formula, such as:

$$C_{lc} = C_{\min} + a_{lc} n_w^{b_{lc}},$$

Well	Depth	Cost	ln Cost	Depth*ln Cost	(ln Cost)^2	Depth^2	Cost Estimate
1	12550	1,480,500	14.21	178309.0	201.86	157502500	1,481,868
2	12560	1,482,500	14.21	178468.1	201.90	157753600	1,482,592
3	12800	1,500,000	14.22	182028.5	202.24	163840000	1,500,058
4	12950	1,490,000	14.21	184075.0	202.05	167702500	1,511,079
5	12980	1,515,000	14.23	184717.4	202.52	168480400	1,513,293
6	13000	1,513,000	14.23	184984.9	202.48	169000000	1,514,770
7	13250	1,530,000	14.24	188690.3	202.80	175562500	1,533,364
8	13780	1,560,000	14.26	196505.5	203.35	189888400	1,573,540
9	14250	1,600,000	14.29	203568.6	204.08	203062500	1,610,048
10	14250	1,650,000	14.32	204007.1	204.96	203062500	1,610,048
11	15000	1,700,000	14.35	215192.1	205.81	225000000	1,670,068
12	16500	1,800,000	14.40	237654.4	207.45	272250000	1,796,903
13	16580	1,810,000	14.41	238898.5	207.61	274896400	1,803,932
14	17000	1,850,000	14.43	245321.8	208.24	289000000	1,841,287
15	17240	1,840,000	14.43	248691.8	208.09	297217600	1,862,979
16	18000	1,950,000	14.48	260700.1	209.77	324000000	1,933,370
17	18200	1,960,000	14.49	263689.9	209.92	331240000	1,952,332
18	18200	1,900,000	14.46	263124.0	209.02	331240000	1,952,332
19	18750	2,020,000	14.52	272223.9	210.79	351562500	2,005,443
Totals	287840		272.38	4130851	3904.94	4452261400	
	avg(lnCost)	14.34					
	beta1	4.9E-05			a=exp(beta0)	803,210	
	beta0	13.60			b=beta1	4.9E-05	

Fig. 1.42—Spreadsheet calculation of “least squares” fit.

which has the proper behavior for large n_w , but at a higher computational cost. A simpler approach would take the last wells drilled and calculate their average cost and the standard deviation. The average \pm twice the standard deviation should give the approximate cost range for 95% of the remaining wells. If the standard deviation is high, you are still on the learning curve, and you will not be able to predict accurately the future well costs. Further, if you make major changes in your operations, your predictions will no longer be valid.

Example 1.6—Statistical Well Cost Estimation. Given the table with the costs of 20 wells drilled in the same field with approximately the same final depth, determine the estimated costs for the next two wells to be drilled in the field.

Solution. Take Wells 15 through 20 and calculate the average cost and the standard deviation. A spreadsheet for this calculation is given in Fig. 1.44. The average well cost is USD 2.94 million and the standard deviation is USD 40,000, only 1.4% of the average cost of a well in the last six wells drilled. Because there is not much variation in well cost, we can feel relatively confident that the next two wells will cost between USD 2.9 and 3.0 million. Further, we are rather high on the learning curve and should not expect much more cost saving.

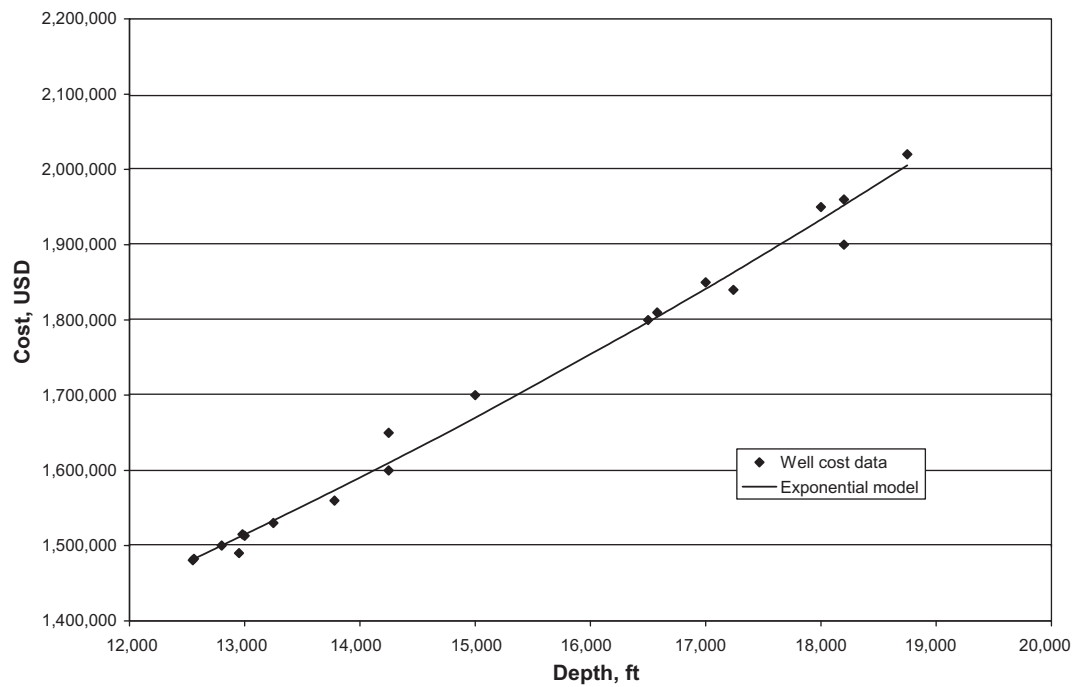


Fig. 1.43—Example 1.5: well cost vs. depth.

Well	Cost (USD)	(C-Cavg)^2
15	2,997,800	3147210000
16	2,932,800	79210000
17	2,966,800	630010000
18	2,891,800	2490010000
19	2,957,500	249640000
20	2,903,500	1459240000
Total	17,650,200	8055320000
Average cost	2,941,700	USD
Variance	1611064000	
Standard deviation	40,138	USD
Minimum cost (95%)	2,861,424	USD
Maximum cost (95%)	3,021,976	USD

Fig. 1.44—Spreadsheet statistics for Wells 15 through 20 (Example 1.6).

Lease: _____ Well No. _____					AFE No.: _____		
Field: _____ County: Offshore State: _____					Original #: _____		
Proposed TD: _____ Objective: _____					Supplement #: _____		
Legal Location: _____					Budget Period: _____		
Code		DHC to drill well to 24,000' md/tvd			Dry Hole	Completion	
BCP	ACP				Cost (BCP)	Cost (ACP)	TOTAL
ESTIMATED INTANGIBLE DRILLING COST							
		Surveys and Permits			\$0		\$0
		Surface Damages					
		Location			\$0		\$0
		Location Cleanup	Rate	Days	Days		\$0
		Rig Move (Mob & Demob.)			\$0		\$0
		Drilling Cost - Turnkey					\$0
		Drilling Cost - Daywork	219000	45		\$9,789,300	\$9,789,300
		Fuel/Water (Rig/Boats)	\$19,100	45		\$853,770	\$853,770
		Transportation (Boats/Air/Trucking)			\$1,966,800		\$1,966,800
		Rental Tools/Equipment/Rental Repairs			\$360,550		\$360,550
		Bits			\$226,880		\$226,880
		Drilling Mud/Chemicals/Mud Engineer			\$2,742,050		\$2,742,050
		Mud and Sample Logging			\$201,150		\$201,150
		Directional Drilling Service/Tools/Motors/Surveys			\$511,815		\$511,815
		MWD/LWD/PWD			\$447,000		\$447,000
		Cement and Cementing Services			\$668,500		\$668,500
		Casing Crews and Tools			\$450,000		\$450,000
		Fishing Operations			\$50,000		\$50,000
		Logging - Open Hole			\$0		\$0
		Completion Rig Cost			\$0		\$0
		Perforating, Cased Hole Logging TCP, CBL			\$0		\$0
		Acidizing and Fracturing (frac pack)			\$0		\$0
		Sand Control GP			\$0		\$0
		Testing, BHP Surveys, Etc.			\$0		\$0
		Completion Fluid and Filtering			\$0		\$0
		Contract Labor			\$1,500		\$1,500
		Rig Supervisor+Drilling Engr.+Ops. Geol.			\$268,200		\$268,200
		Dock/Dispatcher/Communication/Catering			\$248,085		\$248,085
		P&A/T&A			\$0		\$0
		Pipe Inspection			\$130,000		\$130,000
		Overhead			\$547,870		\$547,870
		Insurance/Taxes			\$0		\$0
		Misc. (Disposal/Boat Cleaning/ROV/True Training/Other)			\$892,950		\$892,950
		Contingencies			\$561,567		\$561,567
TOTAL INTANGIBLES					\$20,917,986	\$0	\$20,917,986
ESTIMATED TANGIBLE COSTS							
		Drive Pipe	369	36	\$200.00	\$73,730	\$73,730
		Conductor	3,545	20	\$71.40	\$253,120	\$253,120
		Surface Casing	3,030	16	\$71.00	\$215,130	\$215,130
		Intermediate Casing	10,353	13 5/8	\$60.41	\$625,395	\$625,395
		Drilling Liner	0	9 5/8	\$36.56	\$0	\$0
		Production Liner				\$0	\$0
		Production Casing				\$0	\$0
		Production Tubing				\$0	\$0
		Casing Equipment/Service/Contingencies			\$120,000		\$120,000
		Wellhead Equipment/MLS Equip.			\$660,000		\$660,000
		Subsurface Production Equipment (Packers & SCSSV & GP)				\$0	\$0
		Pumping Unit and Installation				\$0	\$0
		Rods and Downhole Pump				\$0	\$0
		Tank Batteries				\$0	\$0
		Separators, Heaters, Dehydrator, etc.				\$0	\$0
		Flow Lines, Fittings and Connections				\$0	\$0
		Caisson and/or Protective Structure				\$0	\$0
		Labor - Production Equipment				\$0	\$0
		Contingencies			0%	\$2,000	\$2,000
TOTAL TANGIBLES					\$1,949,375	\$0	\$1,949,375
TOTAL DRILLING AND COMPLETION COSTS					\$22,867,361	\$0	\$22,867,361
PERCENT WORKING INTEREST					100.0000%	100.0000%	100.0000%
TOTAL WORKING INTEREST WELL COST					\$22,867,361	\$0	\$22,867,361
Approved: _____							

Fig. 1.45—AFE for an offshore well in the Gulf of Mexico.

Normally, when accurate drilling-cost prediction is needed, a cost analysis based on a detailed well plan must be made. The cost of tangible well equipment (such as casing) and the cost of preparing the surface location usually can be predicted accurately. Also, the cost per day of the drilling operations can be estimated from considerations of rig rental costs, other equipment rentals, transportation costs, rig supervision costs, and others. The time required to drill and complete the well is estimated on the basis of rig-up time, drilling time, trip time, casing placement time, formation evaluation and borehole survey time, completion time, and trouble time. Trouble time includes time spent on hole problems such as stuck pipe, well-control operations, and formation fracture. Major time expenditures always are required for drilling and tripping operations.

TABLE 1.4—TIME DISTRIBUTION FOR GULF OF MEXICO DEEPWATER WELL		
Operation Description	Days	Percentage
Normal operation (except drilling)	44.40	37
Drilling	34.80	29
Lost time—operation problems	14.40	12
Lost time—service company equipment	3.60	3
Lost time—rig equipment	3.60	3
Weather-related problems	9.60	8
Plugging and abandoning	3.60	3
Rig moving, positioning	6.00	5
Total	120.00	100

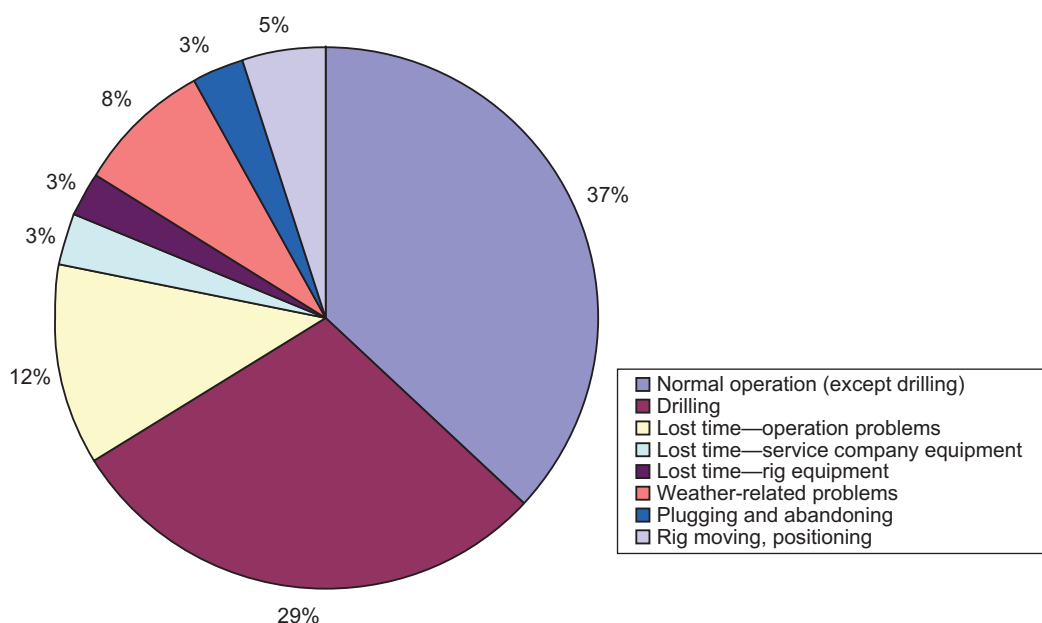


Fig. 1.46—Time distribution for the Gulf of Mexico deepwater well referenced in Table 1.4.

Engine Speed (rev/min)	Torque (ft-lbf)	Fuel Consumption (gal/hr)
1,200	1,400	25.3
1,000	1,550	19.7
800	1,650	15.7
600	1,700	12.1

After gathering all information, the drilling engineer is then equipped to prepare the AFE. AFEs vary significantly in format and amount of information contained. Normally, each company will have its own customized AFE form. An example of an AFE for an offshore well in the Gulf of Mexico is shown in **Fig. 1.45**. The provision of an extra percentage of the total predicted cost for “Contingencies” is customary. This amount is set aside for costs related to unexpected drilling problems such as mud contamination, lost circulation, stuck drillstring, broken drillstring, or ruptured casing. Also, geological uncertainties are always present, and eventually a well may end up being deeper than originally predicted, which will increase the final well cost. As experience is gained in an area, more-accurate predictions of drilling time can be obtained, and consequently better AFEs can be prepared.

In addition to predicting the time requirements for drilling and tripping operations, time requirements for other planned drilling operations also must be estimated. These additional drilling operations usually can be broken into the general categories of

- Wellsite preparation
- Rig movement and rigging up
- Formation evaluation and borehole surveys
- Casing placement
- Well completion
- Drilling problems

The cost associated with wellsite preparation and moving the rig on location depends primarily on the terrain, the distance of the move, and the type of rig used. The cost of formation evaluation depends on the number and cost of the logs and tests scheduled plus rig time required to condition the drilling fluid and run the logs and tests. The time required to run, cement, and test casing depends primarily on the number of casing strings, casing depths, diameters, and weights per foot. These costs also must include the rig time required for running and cementing the casing strings, rigging up the surface equipment for each casing size, and perhaps changing the drill-pipe or drill collar sizes to accommodate the new hole size. The cost of completing the well depends on the type of completion used, and this cost estimate is often made by the completion/production engineer.

On many wells, a large portion of the well cost may be related to unexpected drilling problems such as mud contamination, lost circulation, stuck drillstring, broken drillstring, or ruptured casing. These unforeseen costs cannot be predicted with accuracy and, in some cases, are not included in the original cost estimate. Requests for additional funds then must be submitted whenever a significant problem is encountered. However, long-range economic decisions concerning a drilling program in a given area should include average well costs due to drilling problems. **Table 1.4** shows an actual time distribution for operations in a deepwater well in the Gulf of Mexico. **Fig. 1.46** is the graphical representation of the operation time distribution for the same well.

Problems

- 1.1 What are the major differences between percussion drilling and the modern rotary-drilling process?
- 1.2 List the classification of wells according to their objective, trajectory, and environment.
- 1.3 List the main types of rotary-drilling rigs for onshore and offshore environments.
- 1.4 What are the main systems present in a drilling rig?
- 1.5 The following test data were obtained on a diesel engine.
 - (a) Compute the brake horsepower at each engine speed.
Answer: 319.9, 295.1, 251.3, and 194.2 hp.
 - (b) Compute the overall engine efficiency at each engine speed.
Answer: 0.235, 0.278, 0.297, and 0.298.
 - (c) Compute the fuel consumption in gallons/day for an average engine speed of 800 rev/min and a 12-hour workday.
Answer: 188.4 gal/D.
- 1.6 An intermediate casing string is to be cemented in place at a depth of 10,000 ft. The well contains 10.5 lbm/gal mud when the casing string is placed on bottom. The cementing operation is designed so that the 10.5-lbm/gal mud will be displaced from the annulus by (1) 300 ft of 8.5 lbm/gal mud flush, (2) 1,700 ft of 12.7 lbm/gal filler cement, and (3) 1,000 ft of 16.7 lbm/gal high-strength cement. The high-strength cement will be displaced from the casing with 9-lbm/gal brine. Calculate the pump pressure required to completely displace the cement from the casing.

Answer: The complex well fluid system is illustrated in **Fig. 1.47**. The hydrostatic pressure balance is written by starting at the known pressure and moving through the various fluid sections to the point of the unknown pressure. When moving down through a section, ΔZ is positive, and the change in hydrostatic pressure is added to the known pressure; conversely, when moving up through a section, ΔZ is negative, and the change in hydrostatic pressure is subtracted from the known pressure.

$$\Delta P_1 = 0.05195(10.5 \text{ lbm/gal})(7,000 \text{ ft}) = 3,818 \text{ psig}$$

$$\Delta P_2 = 0.05195(8.5 \text{ lbm/gal})(300 \text{ ft}) = 132 \text{ psig}$$

$$\Delta P_3 = 0.05195(12.7 \text{ lbm/gal})(1,700 \text{ ft}) = 1,122 \text{ psig}$$

$$\Delta P_4 = 0.05195(16.7 \text{ lbm/gal})(1,000 \text{ ft}) = 868 \text{ psig}$$

$$\Delta P_5 = 0.05195(9 \text{ lbm/gal})(-10,000 \text{ ft}) = -4,676 \text{ psig}$$

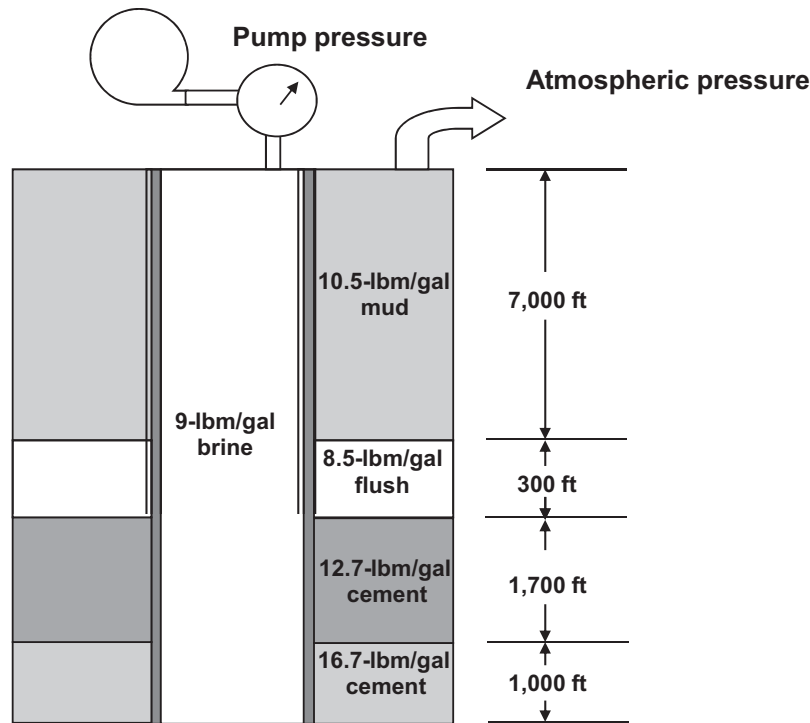


Fig. 1.47—Complex well fluid system.

Pump pressure = $\sum \Delta P_i = 1,264$ psig.

- 1.7 A very simple drilling cost formula (Bourgoyne 1986) to evaluate the efficiency of a bit run can be written by associating the depth interval drilled during the bit run, Δs , the rotating time during the bit run, t_{rot} , the nonrotating time during the bit run, t_{con} , and the trip time, t_{tr} . This drilling formula is

$$C_{br} = \frac{C_{bit} + C_{rig}(t_{rot} + t_{con} + t_{tr})}{\Delta s},$$

where C_{br} is the drilling cost per unit depth, C_{bit} is the bit cost, and C_{rig} is the fixed operating cost of the rig per unit time, independent of the alternatives being evaluated. The nonrotating time t_{con} is the time to connect new pipes to the drillstring as drilling progresses. On the basis of the information provided above, solve the following:

A recommended bit program is being prepared for a new well using bit-performance records from nearby wells. Drilling-performance records for three bits are shown for a thick limestone formation at 9,000 ft. Determine which bit gives the lowest drilling cost if the operating cost of the rig is USD 2,300/hr, the trip time is 7 hours, and the connection time is 2 minutes per connection. Assume that each of the bits is operated at near the minimum cost per foot attainable for that bit.

Bit	Bit Cost (USD)	Rotating Time (hours)	Connection Time (hours)	Mean Penetration Rate (ft/hr)
A	800	14.8	0.1	13.8
B	4,900	57.7	0.4	12.6
C	4,500	95.8	0.5	10.2

Answer: For Bit A, the cost per foot is:

$$C_{br} = \frac{800 + 400(14.8 + 0.1 + 7)}{13.8(14.8)} = 46.8 \text{ USD/ft}$$

Similarly for Bit B:

$$C_{br} = \frac{4,900 + 400(57.7 + 0.4 + 7)}{12.6(57.7)} = 42.6 \text{ USD/ft}$$

Finally, for Bit C:

$$C_{br} = \frac{4,500 + 400(95.8 + 0.5 + 7)}{10.2(95.8)} = 46.9 \text{ USD/ft}$$

Bit B with a cost of 42.6 USD per ft.

- 1.8 Solve the problem presented in Example 1.2 (Section 1.5.2, “Hoisting System”) assuming the well is 14,880 ft deep and the drilling fluid has a density of 12 lbm/gal. In addition, assume that the BHA is composed of eight stands of 7×3-in. drill collars. All other variables remain the same.
- 1.9 List the main parameters that should be controlled and measured by the well-monitoring system while drilling a well.
- 1.10 Explain the main characteristics of a DP system.
- 1.11 Repeat what was done in Example 1.7 (Section 1.7.1 “Drilling Cost Prediction”) using the following tables:

<u>Well Order</u>	<u>Cost (USD)</u>
1	26,385,420
2	27,895,500
3	26,430,250
4	24,355,400
5	23,215,560
6	22,450,090
7	20,345,600
8	21,095,600
9	19,455,900
10	19,600,080
11	19,155,400
12	18,890,900
13	18,750,000
14	18,930,080
15	18,345,890

<u>Well Order</u>	<u>Cost (USD)</u>
1	17,895,040
2	15,935,400
3	16,890,900
4	15,455,090
5	14,999,890
6	14,750,980
7	14,020,760
8	13,987,650
9	14,230,890
10	13,678,650
11	13,545,780

Use Wells 10–15 for the first table and Wells 7–11 for the second table. What cost range should be expected, everything else being equal? What does the standard deviation tell you about the learning curve?

Answer for the First Table: The average well cost is USD 18.9 million. Well cost should vary between approximately USD 19.1 million and USD 18.1 million. The standard deviation is approximately USD 418,000, which is approximately 2.2% of the average total cost. We should not expect much cost improvement.

Answer for the Second Table: The average well cost is USD 13.9 million. Well cost should vary between USD 13.3 million and USD 14.4 million. The standard deviation is USD 277,000, or approximately 2.0% of the average total cost. Again, we should not expect much cost improvement.

Nomenclature

a_{dc}	=	constant used in curve-fitting drilling cost vs. depth, USD
a_{lc}	=	constant used in “learning curve” drilling cost, USD
b_{dc}	=	constant used in curve-fitting drilling cost vs. depth, (1/L), 1/ft (1/m)
b_{lc}	=	constant used in “learning curve” drilling cost, dimensionless
C_{dc}	=	estimated cost from curve-fitting drilling cost vs. depth, USD
C_{bit}	=	bit cost, USD
C_{br}	=	drilling cost per unit depth for bit run, USD/ft (USD/m)
C_{lc}	=	estimated well cost based on “learning curve” concepts, USD
C_{min}	=	minimum possible cost to drill a well, USD
C_{rig}	=	fixed operating cost of rig per unit time, USD/day
d_{dpl}	=	diameter of liner in duplex pump, (L), in. (cm)
d_{dpr}	=	diameter of rod in duplex pump, (L), in. (cm)
d_{tpl}	=	diameter of liner in triplex pump, (L), in. (cm)
F_d	=	force on derrick, (mL/t ²), lbf (N)
F_{fl}	=	force in fast line, (mL/t ²), lbf (N)
F_{dl}	=	force in static line (dead line), (mL/t ²), lbf (N)
F_{tb}	=	force (weight) carried by the traveling block, (mL/t ²), lbf (N)
g	=	gravity constant, (L/t ²), lbf/lbm, (m/s ²)
H	=	heating value of fuel, (L ² /t ²), Btu/lbm (kJ/kg)
K	=	friction factor, dimensionless
L_{dst}	=	stroke length on duplex pump, (L), in. (cm)
L_{tst}	=	stroke length on triplex pump, (L), in. (cm)
MA_{bt}	=	real mechanical advantage of block-and-tackle system, dimensionless
MA_{bti}	=	ideal mechanical advantage of frictionless system, dimensionless
\dot{m}_f	=	mass rate of fuel consumption, (m/t), lbm/min (kg/s)
N	=	number of data points in statistical analysis, dimensionless
N_L	=	number of lines strung in block-and-tackle system, dimensionless
N_{Sh}	=	number of rolling sheaves (normally, $N_{Sh} = N_L$) in block-and-tackle system, dimensionless
N_{tb}	=	number of lines strung between crown block and traveling block, dimensionless
n_w	=	well number (e.g., $n_w = 10$ means well number 10)
P_{sp}	=	shaft power, (m ² L/t ³), hp (kW)
P_h	=	output power (hook power) of block-and-tackle system, (m ² L/t ³), hp (kW)
P_H	=	hydraulic power of a pump, (m ² L/t ³), hp (kW)
P_{bt}	=	input power to block-and-tackle system, (m ² L/t ³), hp (kW)
Q	=	heat input from fuel consumption, (m ² L/t ³), hp (kW)
s	=	measured depth, (L), ft (m)
s_i	=	initial drilled depth of bit run, (L), ft (m)
t_{con}	=	nonrotating time (e.g., the time to connect new pipes to the drillstring)
t_{rot}	=	rotating time during the bit run
t_s	=	average time required to handle one stand of drillpipe during tripping operations
t_{tr}	=	time of tripping operations required to change bit
T	=	torque, (m ² L/t ²), ft-lbf (Nm)
V_{dbs}	=	volume per stroke of back stroke of duplex pump, (L ³), bbl/stroke (m ³)
V_{dp}	=	total volume per stroke of a duplex pump, (L ³), bbl/stroke (m ³)
V_{dfs}	=	volume per forward stroke of duplex pump, (L ³), bbl/stroke (m ³)
V_{tst}	=	volume per stroke of single cylinder of a triplex pump, (L ³), bbl/stroke (m ³)
V_{tp}	=	total volume per stroke of a triplex pump, (L ³), bbl/stroke (m ³)

v_{tb}	=	velocity of traveling block, (L/s), ft/s (m/s)
v_{fl}	=	velocity of fast line, (L/s) , ft/s (m/s)
$\{x_i, y_i\}$	=	i th pair of numbers in a data set
\bar{x}	=	average value of x_p $i=1..N$
\bar{y}	=	average value of y_p $i=1..N$
Z	=	true vertical depth, (L), ft (m)
β_0, β_1	=	coefficients for best straight line fit to data $\{x_i, y_i\}$, $i=1..N$
Δp	=	pressure change, (L/m-t ²), psi (bar)
Δs	=	change in measured depth, (L), ft (m)
ΔZ	=	change in true vertical depth, (L), ft (m)
ρ	=	density, (m/L ³), ppg, (kg/m ³)
η_{bt}	=	block-and-tackle efficiency, dimensionless
η_{sp}	=	shaft power efficiency, dimensionless
η_{dpv}	=	volumetric efficiency of a duplex pump, dimensionless
η_{tpv}	=	volumetric efficiency of a triplex pump, dimensionless
ϕ	=	angle of wellbore with the vertical, dimensionless, degrees (rad)
ω	=	angular velocity, (1/t)

Subscripts

bt	=	block-and-tackle
bti	=	deal block-and-tackle
d	=	derrick
dc	=	drilling cost estimate
dl	=	dead line
dp	=	duplex pump
dpl	=	duplex pump liner
db	=	duplex pump backward stroke
dfs	=	duplex pump forward stroke
dpr	=	duplex pump rod
dst	=	duplex pump stroke
f	=	fuel
fl	=	fast line
h	=	hook
H	=	hydraulic
lc	=	learning curve
min	=	minimum
r	=	rig
sp	=	shaft power
tb	=	traveling block
tp	=	triplex pump
tpl	=	triplex pump liner
tst	=	triplex pump stroke
w	=	well

Abbreviations

AC	alternating current
AFE	authorization for expenditure
API	American Petroleum Institute
BHA	bottomhole assembly
BOP	blowout preventer
DC	direct current
DP	dynamic positioning
EEIPS	extra extra improved plow steel

EIPS	extra improved plow steel
IMO	International Maritime Organization
IPS	improved plow steel
IWRC	independent wire rope core
MPS	mild plow steel
MWD	measurement while drilling
PS	plow steel
ROV	remotely operated vehicle
SCR	silicon-controlled rectifier
TLP	tension-leg platform

References

- Aadnoy, B.S., Cooper, I., Miska, S.Z., Mitchell, R.F., and Payne, M.L. 2009. *Advanced Drilling and Well Technology*, Chap. 7. Richardson, Texas: SPE.
- API Spec 9/ISO 10425, *Specification for Wire Rope*, 25th edition. February 2004. Washington, DC: API.
- Bourgoyne, A.T. Jr., Millheim, K.K., Chenevert, M.E., and Young, F.S. Jr. 1986. *Applied Drilling Engineering*. Textbook Series, SPE, Richardson, Texas **2**: 2.
- Bourgoyne, A.T., Millheim, K.K., Chenevert, M.E., and Young, F.S. 1991. *Applied Drilling Engineering* (revised printing), Textbook Series, SPE, Richardson, Texas **2**.
- Brantley, J.E. 1940. *History of Oil Well Drilling*, first edition, 122. New York City: AIME.
- Brantley, J.E. 1971. *History of Oil Well Drilling*, 48, 58, 232–238. Houston: Gulf Publishing Company.
- Bull. 20310, 750ECIX 1350TopDrive. 2008. Tesco, http://www.tescocorp.com/data/1/rec_docs/588_20310e_750_ECIX_1350_topdrive_web.pdf. Downloaded 23 December 2010.
- Cameron. 2006. TL Blowout Preventer, http://www.coopercameron.com/content/products/product_detail.cfm?pid=2791&bunit=dps (accessed 28 December 2010).
- Cunha, J.C. 2002. Effective Prevention and Mitigation of Drilling Problems. *World Oil & Gas Technologies, Volume 2* (September): 28–34.
- DeLuca, M. 2005. Surface BOP Maintaining Its Niche. *Offshore Engineer* **30** (2): 19–22.
- Derrick Engineering Company. 2010. For Sale: Oil Field Masts and Substructures, Drill Rigs Available for Immediate Sale, <http://www.derrickengineering.com/classifieds.htm> (accessed 16 December 2010).
- Derrick Equipment Company. 2010. Vacu-Flo Degasser, <http://www.derrickequipment.com/Images/Documents/VacuFloDegasserRevJune2010.pdf>. Downloaded 21 December 2010.
- GEFCO. 2007. SpeedStar SS-135, <http://www.gefco.com/ss135drillingrig.htm> (accessed 16 December 2010).
- GN Solids Control Oilfield Equipment. 2009–2010. Introduction of hydrocyclones in desander and desilter, <http://oilfield.gnsolidscontrol.com/hydrocyclones-in-desander-and-desilter/> (accessed 20 December 2010).
- Giddens, P.G. 1975. Edwin L. Drake and the Birth of the Petroleum Industry. Historic Pennsylvania Leaflet No. 21, eds. S.W. Higginbotham and Donald H. Kent. Harrisburg, Pennsylvania: Pennsylvania Historical and Museum Committee.
- Hutchison-Hayes Separation. 2011. Decanting centrifuge, http://www.hutch-hayes.com/5500_centrifuge_standard.htm (accessed 11 January 2011).
- IMCA. 2003. Principals of DP. In Marine Division publication *Introduction to DP*, Section 2, <http://www.imca-int.com/divisions/marine/reference/intro02.html>.
- Ikoku, C.U. 1978. Application of Learning Curve Models to Oil and Gas Well Drilling. Paper SPE 7119 presented at the SPE California Regional Meeting, San Francisco, 12–14 April. DOI: 10.2118/7119-MS.
- Lake, L.W. ed. 2006. *Petroleum Engineering Handbook, Vol. II*, Chap. 14, II-607. Richardson, Texas: SPE.
- Maksoud, J. 2002. Deepwater Nautilus Sets Another World Record in the GOM, Polyester Mooring Extends Rated-Depth Capability. *Offshore International* **62** (10): 62–63.
- MSC/Circ.645 (*Maritime Safety Committee Circular 645*), *Guidelines for vessels with dynamic positioning systems*. 1994. London: International Maritime Organization.
- National Oilwell Varco. 2010a. Drilling Stabilizers, http://www.nov.com/Downhole/Drilling_Tools/Drilling_Stabilizers.aspx (accessed 28 December 2010).
- National Oilwell Varco. 2010b. Drilling Check Valves, http://www.nov.com/Downhole/Drilling_Tools/Drilling_Check_Valves.aspx (accessed 28 December 2010).
- RP9B, *Application, Care and Use of Wire Rope for Oil Field Service*, 12th edition. June 2005. Washington, DC: API.

- Sahdev, M. 2008. Centrifugal Pumps: Basic Concepts of Operation, Maintenance, and Troubleshooting, Part I. The Chemical Engineers' Resource Page, <http://www.cheresources.com/centrifugalpumps3.shtml> (accessed 21 December 2010).
- Spec 16A/ISO 13533. 2004. *Specification for Drill Through Equipment* (includes Supplement/Errata dated November 2004), 3rd edition, June 2004. Washington, DC: API.
- Spec 16C. 1993. *Choke and Kill Systems*, 1st edition, January 1993. Washington, DC: API.
- Spec 16D. 2004. *Control Systems for Drilling Well Control Equipment and Control Systems for Diverter Equipment*, 2nd edition, July 2004. Washington, DC: API.
- Teplitz, Charles J. and Carlson, John G.. 1991, *The Learning Curve Deskbook: A Reference Guide to Theory, Calculations, and Applications*. Westport, Connecticut, USA: Greenwood Publishing Group/Quorum Books.
- Thrustmaster of Texas, Inc. 2010. Azimuth Thrusters, [http://www.thrustmastertexas.com/products/azimuth Thrusters.html](http://www.thrustmastertexas.com/products/azimuth%20Thrusters.html) (accessed 21 January 2011).
- The Oil and Asphalt Industry Has a Rich History in Canada. 1988. *Asphalt Magazine* (a publication of the Asphalt Institute, Lexington, Kentucky) **12** (3): 14–15.
- Will, S. 1999. Compliant Towers: The Next Generation. *Offshore International* **59** (7): 82–84.
- Zwillinger, Daniel, ed. 1996. *CRC Standard Mathematical Tables and Formulae*, 30th edition. Boca Raton, Florida: CRC Press, 601–603, 626.

Appendix—Simple Statistics and Least-Squares Fit

Given a set of N data pairs $\{x_i, y_i\}$, the following formula, from Zwillinger (1996), gives the “best” fit to this data:

$$y = \beta_0 + \beta_1 x, \quad \dots \quad (\text{A-1})$$

where

$$\beta_1 = \frac{N \sum_{i=1}^N x_i y_i - \left(\sum_{i=1}^N x_i \right) \left(\sum_{i=1}^N y_i \right)}{N \sum_{i=1}^N x_i^2 - \left(\sum_{i=1}^N x_i \right)^2} \quad \dots \quad (\text{A-2})$$

and

$$\beta_0 = \bar{y} - \beta_1 \bar{x}$$

$$\bar{y} = \frac{\sum_{i=1}^N y_i}{N} = \text{the average value of } y$$

$$\bar{x} = \frac{\sum_{i=1}^N x_i}{N} = \text{the average value of } x. \quad \dots \quad (\text{A-3})$$

The variance and the standard deviation are calculated in the following way:

$$\text{Variance of } x = \frac{\sum_{i=1}^N (x_i - \bar{x})^2}{N - 1}$$

$$\text{Standard deviation of } x = \sqrt{\text{Variance of } x}, \quad \dots \quad (\text{A-4})$$

where \bar{x} is the average value of x .

These formulas are easy to use on a spreadsheet, or you may have a math software package or spreadsheet that already has them programmed.

SI Metric Conversion Factors

bbl	×	1.589 873	E – 01 = m ³
ft	×	3.048*	E – 01 = m
gal	×	3.785 412	E – 03 = m ³
gal/hr	×	3.785 412	E – 03 = m ³ /h
gal/min	×	2.271 247	E – 01 = m ³ /h

hp	×	7.460 43	E – 01 = kW
in.	×	2.54*	E + 00 = cm
in. ³	×	1.638 706	E + 01 = cm ³
lbf	×	4.448 222	E + 00 = N
lbm	×	4.535 924	E – 01 = kg
mile	×	1.609 344	E + 00 = km
psi	×	6.894 757	E + 00 = kPa
ton-mile	×	1.459 972	E + 00 = M kg-m
US ton	×	0.907 185	E + 00 = Mg

*Conversion factor is exact.

Chapter 2

Introduction to Geomechanics in Drilling

Bernt S. Aadnøy, University of Stavanger

The objective of this chapter is to introduce the student to the basic concepts of geomechanics related to drilling, including wellbore stability in vertical and horizontal wells and the selection of suitable mud weight to enhance wellbore stability.

2.1 Borehole Stability Analysis for Vertical Wells

This chapter offers an introduction to geomechanics. It is divided into three sections; the first two sections focus, first, on vertical wells and, second, on inclined wells. The last section addresses general methodology, for more advanced analysis. The first two sections will give the student basic knowledge because we study the simplest conditions. For deviated wells we must consider a 3D perspective, a more general and complex analysis. These issues are addressed in the last section. There are many aspects of geomechanics, including, for instance, rock mechanics and soil mechanics. For those who want to go deeper into the subject, there is a special reference section of recommended reading at the end of the chapter.

2.1.1 Description of the Problem. Stability of boreholes became an important issue in the early 1980s when long, highly inclined wells were evolving, to be able to drain large reservoirs from single offshore platforms. Bradley (1979) is considered the person who introduced analytic borehole stability analysis to the oil industry. From that time, geomechanics has evolved as a petroleum discipline, and today a geomechanical analysis is often conducted for more complex wells, in order to reduce risk and cost.

In this chapter we will focus on the understanding of the physics of borehole stability. One objective is to promote physical understanding. This is an introductory text to borehole mechanics seen from a drilling perspective. The major drilling challenge that relates to borehole mechanics is the stability of the wellbore.

Several well problems often arise during drilling:

- A circulation loss occurs when the volume of returned mud is less than the volume of mud pumped. Circulation losses are unplanned events that usually must be resolved before drilling can continue. Circulation losses also may lead to loss of well control, resulting in a blowout, or lead to difficulty in cleaning the borehole, which may eventually lead to a stuck drillstring. One remedy is to reduce the mud weight. We will develop a fracturing model to analyze these problems.
- Mechanical borehole collapse often occurs at low borehole pressures, such as happens with too low mud weight or during circulation losses or if the well is swabbed in while tripping pipe. The remedy is often to increase wellbore pressure, usually by increasing the mud weight.
- Particularly in shales, chemical effects may induce hole enlargement or collapse. When water-based drilling fluids are used, the shale may react with the mud filtrate (fluid that penetrates the wellbore wall), deteriorating the borehole. Oil-based muds are often better on hole collapse, but more difficult if circulation losses arise.

There are many publications presenting various empirical correlations for borehole stability, mainly addressing fracturing. However, in the last decades an analytic approach has emerged, wherein the problems are analyzed

using the principles of classical mechanics. The advantage is that the various problems can be seen from a common reference frame. This chapter will provide an introduction to the mechanics approach.

Fig. 2.1 illustrates some common drilling problems. The mud weight or the bottomhole pressures are often a compromise between well control and borehole stability. We will present methods to establish the optimum mud weight.

It is observed that 10–20% of the time spent on a well is due to unplanned events. These events often have a root in borehole stability. Knowing that the worldwide drilling budgets are many billion dollars, we understand therefore that borehole instability is a very costly problem. **Table 2.1** shows the unplanned time spent on an exploration well in the North Sea.

The unplanned events in Table 2.1 are mostly related to borehole stability. Some wells have lower downtime, but if severe problems arise, they are often very time-consuming to solve. The average statistic must of course include problem wells.

2.1.2 Units and Equations. First we will define our reference frames. Pressures are defined in terms of the hydrostatic head at a given depth, or

$$P = \rho g Z. \quad (2.1)$$

Here P is the wellbore pressure, ρ is the mud density, g is the gravity constant, and Z is the true vertical depth. The drilling industry uses the mud density as a reference. For simple comparison to the mud weight, we use equivalent density instead of pressure. Another advantage of the equivalent density is that it takes out the depth element. It is defined as

$$\rho_e = \frac{P}{gZ}. \quad (2.2)$$

In metric units, the gradient equation becomes

$$\gamma_e \text{ (SG)} = \frac{P \text{ (bar)}}{0.098 \times Z \text{ (m)}}, \quad (2.3)$$

where

$$\gamma_e = \frac{\rho_e}{\rho_{\text{water}}}$$

The unit SG denotes specific gravity, the ratio of the actual density to the density of water. For most drilling applications, the gradient is preferred because it is depth-independent and can be directly compared to the static mud weight. However, during transient fluid processes such as cement displacement and circulating out a kick, it is advised to use pressures instead of gradients.

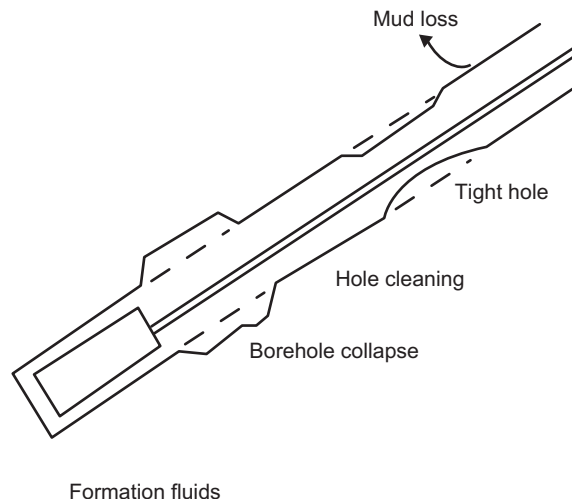


Fig. 2.1—Typical borehole problems.

TABLE 2.1—EXAMPLE OF UNPLANNED EVENTS	
Unplanned Event	Time Used to Cure
Mud losses	2.5 days
Tight hole, reaming	0.3 days
Squeeze cementing	2.5 days
Fishing	0.3 days
Total time loss	5.6 days
Percent of well time	5.6 days / 30 days = 19%

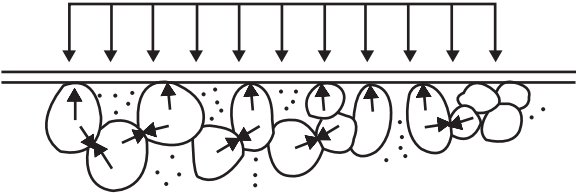


Fig. 2.2—Illustration of effective stresses.

2.1.3 In-Situ Stresses. All rocks are subjected to stresses at any depth. It is a convention in the petroleum industry to define these stresses as follows:

- A vertical principal stress, usually the overburden stress σ_v . This results from the cumulative weight of the sediments above a given point. Usually this is obtained from bulk density logs or from the density of cuttings.
- Two principal horizontal stresses, the maximum horizontal stress σ_H and the minimum horizontal stress σ_h . The magnitudes of these are obtained from leakoff data or other measurements.

Note that we use the sign convention of compressive stress as positive, a convenience since we usually are dealing with compressive stresses. We assume that these principal stresses are always vertical and horizontal. Furthermore, we assume the following stress states:

- In a relaxed depositional-basin environment, the two horizontal stresses are smaller than the overburden stress, a so-called normal fault stress state: $\sigma_h < \sigma_H < \sigma_v$. The two horizontal stresses are often similar and equal to 70–90% of the overburden stress.
- Tectonic stresses may arise due to faulting or plate tectonics. Two different states may exist:
 - Strike-slip fault stress state: $\sigma_h < \sigma_v < \sigma_H$
 - Reverse fault stress state: $\sigma_v < \sigma_h < \sigma_H$

Most oil fields are located in sedimentary basins and are in normal fault stress states. This will form the basis for the following development. However, before looking at the actual borehole mechanics, we need to consider other properties of porous media. Regarding stresses, Terzaghi (1943) defined the effective stress principle: The total stress is the sum of the pore pressure and the stress in the rock matrix, or

$$\sigma_{\text{total}} = \sigma' + P_{\text{pore}} \quad \dots \dots \dots (2.4)$$

where we have indicated the effective stress as σ' . This is illustrated in **Fig. 2.2**. Imagine that the total load on the wellbore wall is the mud pressure inside the borehole. This load is taken up by the stresses in the rock matrix plus the pore pressure. When we study failure of rock, we always compute the effective stresses, which apply to the rock itself.

Example 2.1—In-Situ Stresses.

1. At a given depth in a sedimentary basin, the overburden stress is equal to 1.95 SG from density logs. From fracturing data, the horizontal stresses are defined as 1.75 and 1.77 SG. What type of stress state exists in this field? Is this what you would expect in a sedimentary basin?
2. Another well is drilled in a tectonic setting. The overburden stress is given as 1.81 SG, whereas the two horizontal stresses are estimated to be 1.92 and 1.64 SG. What stress state is this?

3. If there is normal pore pressure in 1 and 2, compute the effective stresses, also called the rock matrix stresses.

Solution.

1. The stress ratios are

$$\frac{\sigma_h}{\sigma_v} = \frac{1.75 \text{ SG}}{1.95 \text{ SG}} = 0.90 \quad \frac{\sigma_H}{\sigma_v} = \frac{1.77 \text{ SG}}{1.95 \text{ SG}} = 0.91.$$

Because both stress ratios are smaller than 1, we have a normal fault stress state. This is the expected stress state in a sedimentary basin.

2. Now the stress ratios are: $\frac{\sigma_h}{\sigma_v} = \frac{1.64 \text{ SG}}{1.81 \text{ SG}} = 0.91$ $\frac{\sigma_H}{\sigma_v} = \frac{1.92 \text{ SG}}{1.81 \text{ SG}} = 1.06$.

In this case, one horizontal stress is smaller than the overburden stress, whereas the other horizontal stress is larger than the overburden stress. This is a strike/slip stress state, which may be caused by a tectonic event such as an earthquake.

3. A normal pore pressure is often defined as the density of seawater, 1.03 SG. The effective stresses for 1 and 2 are:

$$\frac{\sigma'_h}{\sigma'_v} = \frac{(1.75 - 1.03) \text{ SG}}{(1.95 - 1.03) \text{ SG}} = \frac{0.72 \text{ SG}}{0.92 \text{ SG}} = 0.78 \quad \frac{\sigma'_H}{\sigma'_v} = \frac{(1.77 - 1.03) \text{ SG}}{(1.95 - 1.03) \text{ SG}} = \frac{0.74 \text{ SG}}{0.92 \text{ SG}} = 0.80$$

$$\frac{\sigma'_h}{\sigma'_v} = \frac{(1.64 - 1.03) \text{ SG}}{(1.81 - 1.03) \text{ SG}} = \frac{0.61 \text{ SG}}{0.78 \text{ SG}} = 0.78 \quad \frac{\sigma'_H}{\sigma'_v} = \frac{(1.92 - 1.03) \text{ SG}}{(1.81 - 1.03) \text{ SG}} = \frac{0.89 \text{ SG}}{0.78 \text{ SG}} = 1.14$$

We observe that the stress ratios change values but are still within the definition of the stress states. The effective stresses are the stresses acting on the rock matrix when we exclude the pore pressure. Because we are concerned with failure of the rock matrix, we have to use effective stresses. This principle will be implemented in the borehole failure models that follow.

2.1.4 Pore Pressures. Sedimentary rocks are usually porous. The pores usually are filled with water, which is the most abundant fluid. In oil and gas reservoirs, the water is locally replaced with hydrocarbons.

The pore pressure is an important parameter for several reasons. First, it is important for the production of hydrocarbons and for determining whether the reservoir can be produced naturally or if artificial lift is required. The pore pressure is also important for borehole stability because of the effective stress principle (Eq. 2.4).

In sedimentary rocks such as sandstones, the pore pressure can be measured directly with logging tools. However, shales are nearly impermeable, so there exist no direct methods to measure the pore pressure here. Instead, the pore pressure is inferred from drilling data and from various logs. The methods used are beyond the scope of this chapter, but the interested student is referred to Bourgoyne (1986), Chapter 6.

It should be noted that there is a large uncertainty in the pore pressure prediction of these indirect methods. In the reservoir, direct measurements are considered accurate. Because the pore pressure profile has a direct bearing on the selection of the casing depths, the uncertainty should be understood. Remember also that if a homogeneous tight shale has a high pore pressure, it cannot flow and therefore cannot lead to a well-control incident.

In general, a caprock is required to create overpressure. There are several different mechanisms that create abnormal pore pressures. Some mechanisms are

- Buoyancy, where the lightest fluid moves to the top and the heaviest to the bottom
- Rock compaction of a closed volume
- Consolidation effects
- Chemical effects

The buoyancy effect is considered a dominating mechanism, and it is always present in a reservoir. In the following examples, we will explore the pressures throughout an oil and gas reservoir as shown in **Fig. 2.3**.

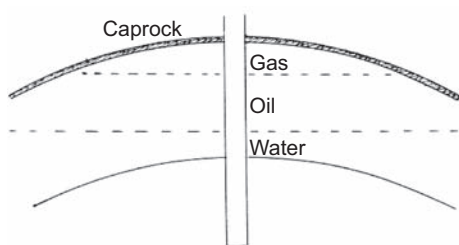


Fig. 2.3—Trapped hydrocarbons.

Example 2.2—Pore Pressure From Measurements. Fig. 2.3 shows hydrocarbons trapped in a sandstone reservoir under an arch-shaped caprock. A well is drilled through the reservoir, and multiple pore pressure measurements are made throughout the reservoir, except through the caprock, which acts as a seal. **Table 2.2** summarizes the pore pressure measurements. We will plot the data and evaluate the results. The results are shown in **Fig. 2.4**.

Depth (m)	Pressure (bar)	Fluid
1500	(151.4)	(Caprock)
1550	170.7	Gas
1580	172	Gas
1620	172.6	Gas
1680	173	Oil
1700	174.6	Oil
1740	179.5	Oil
1800	182.7	Oil
1850	186.7	Water
1900	191.8	Water

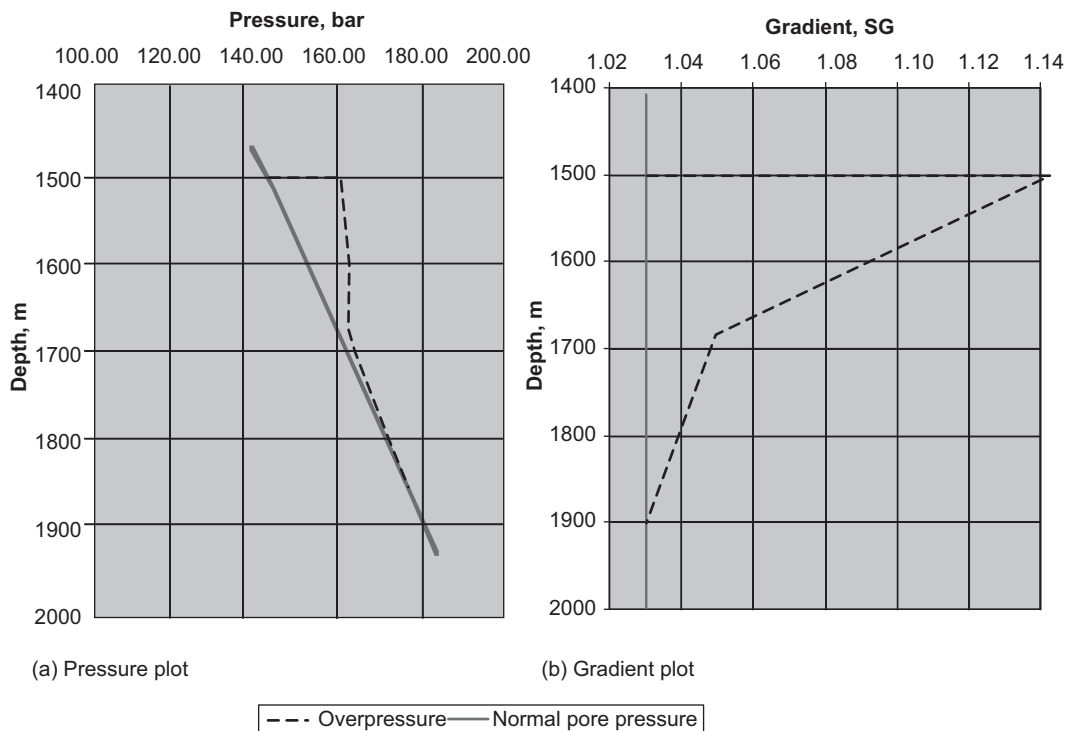


Fig. 2.4—Plots of measured pore pressures.

Solution. Above 1500 m and below 1900 m, we assume a normal pore pressure. In the interval in between, hydrocarbons have migrated upward and are captured below the caprock. The pressure at any point in the reservoir is equal to the normal pressure below minus the weight of the hydrocarbons to the point of interest. As an example, the pore pressure at 1700 m is

$$P_o = 0.098 \times 1.03 \text{ SG} \times 1900 \text{ (m)} - 0.098 \times 0.88 \text{ SG} \times [1900 \text{ (m)} - 1700 \text{ (m)}] = 174.5 \text{ bar}$$

This shows that the reservoir has overpressure below the caprock, but normal pressure at the bottom of the reservoir. During production, the water front moves upward, leading to reduced pore pressures above the water front.

Measured pore pressures are often missing, and we must rely on indirectly obtained pore pressures from logs. These are often uncertain because they are not calibrated. In the event that we have competent shales with negligible permeability, zero flow potential may be assumed when evaluating the well-control risk.

Example 2.3—Pore Pressure. The gradient plot in Fig. 2.5 is from a well in the North Sea. Assume that the caprock is located at the 9⁵/₈-in. casing point at 2350 m. Call this location point B. Furthermore, assume that there is vertical communication down to 2600 m. Call this location point A.

1. Using the pore pressure data, calculate the density of the oil in the reservoir in this interval.
2. Assume that the fluid in the depth interval A–B is not oil, but condensate of density 0.5 SG. Compute the pore pressure in this interval for the new values of fluid density.

Solution.

1. From Fig. 2.5 the following pore pressure gradients are read:
 - 1.57 SG in point B at a depth of 2350 m
 - 1.50 SG in point A at a depth of 2600 m

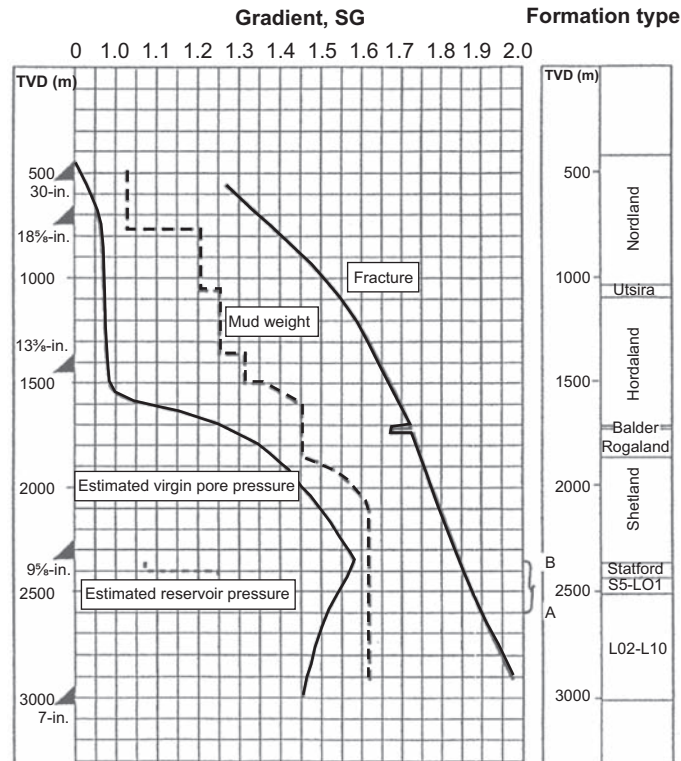


Fig. 2.5—Gradient plot from a well in the North Sea.

The pressures at these positions are

$$P_B = 0.098 \times 1.57 \text{ SG} \times 2350 \text{ m} = 361.6 \text{ bar}$$

$$P_A = 0.098 \times 1.50 \text{ SG} \times 2600 \text{ m} = 382.2 \text{ bar.}$$

The difference in pressure is

$$P_B - P_A = 382.2 \text{ bar} - 361.6 \text{ bar} = 20.6 \text{ bar.}$$

This hydrostatic pressure reduction is caused by the weight of the oil column acting over the depth interval. The relative density of the oil is then

$$\gamma_e = \frac{P_B - P_A}{0.098(Z_B - Z_A)} = \frac{20.6 \text{ bar}}{0.098 \times 250 \text{ m}} = 0.84 \text{ SG}$$

2. We assume the same gradient and pressure at point A as used above. The pressure here is 382.2 bar. If we assume condensate of 0.5 SG, the pressure at point B will be

$$P_B = 382.2 \text{ bar} - 0.098 \times 0.5 \text{ SG}(2600 \text{ m} - 2350 \text{ m}) = 370 \text{ bar.}$$

This corresponds to a gradient of:

$$\gamma_e = \frac{370 \text{ bar}}{0.098 \times 2350 \text{ m}} = 1.61 \text{ SG}$$

2.1.5 Fracturing. In this section, we will present the borehole mechanics model used in the oil industry. The first part assumes simple conditions, as found in relaxed sedimentary basins, such as equal horizontal in-situ stresses and also a vertical borehole. Later we will present more-complex scenarios.

There are two different mechanics approaches used in the oil industry:

- Classical mechanics approach. We assume an infinite plate with a hole in the middle. This hole represents the wellbore. (See **Fig. 2.6.**) For fracturing and collapse analysis during drilling, this is the method used.
- Fracture mechanics approach, assuming that a fracture already exists. This is used in stimulation operations where massive fracturing and reservoir stimulation take place, and relates to boreholes that are already fractured. This will not be pursued in this chapter.

The plate in **Fig. 2.6** is subjected to external loading defined by the in-situ stresses. The borehole is the hole in the middle. At the borehole wall, for the special case $\sigma_H = \sigma_h$, three different stresses exist as illustrated in **Fig. 2.7**:

• The radial stress is given by the mud pressure: $\sigma_r = P_w$ (2.5a)

• The tangential stress, or hoop stress: $\sigma_\theta = 2\sigma_h - P_w$ (2.5b)

• The axial stress, or vertical stress: $\sigma_z = \text{constant}$ (2.5c)

The tangential stress depends on the horizontal stress. The factor 2 is called a stress concentration factor and is due to the circular geometry of the borehole. If the borehole has an oval shape or some other noncircular shape, higher stress concentration factors often arise. If $\sigma_H \neq \sigma_h$, then σ_θ would vary with θ (we will learn more about this in Section 2.2.1). Also, observe that the borehole pressure directly affects the tangential stress.

For this special case, we observe from Eqs. 2.5a and 2.5b that the sum of the radial and tangential borehole stresses is constant. A consequence of this is that at high borehole pressures the tangential stress is low, whereas at low borehole pressure the tangential stress is high.

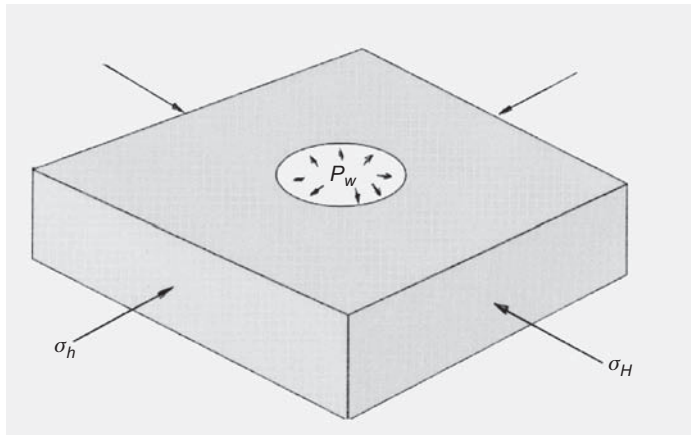


Fig. 2.6—Classical mechanics approach: an infinite plate with a hole in the middle [from Aadnoy (1996)].

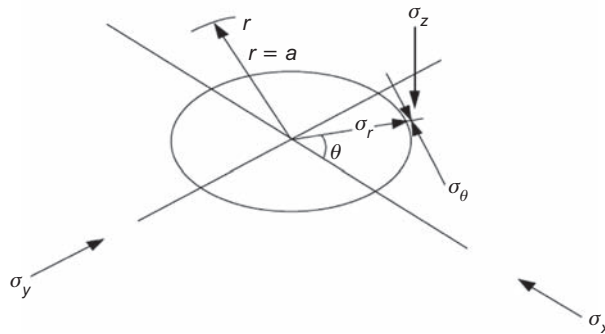


Fig. 2.7—Stresses acting on the borehole wall [from Aadnoy (1996)].

Fig. 2.8 visualizes the effects of varying the borehole pressure. If the mud weight applies the same load as the stresses before the hole was drilled, there is no disturbance, as illustrated in Fig. 2.8a. If the borehole pressure is lower than the in-situ stresses, the borehole will shrink, or actually fail in collapse (Fig. 2.8b), because of the high hoop stress that is created with low borehole pressures. Finally, Fig. 2.8c illustrates that with a high borehole pressure, the hole will expand until it fails or fractures.

Fig. 2.8 shows the expected fracture gradients for a relaxed depositional basin. In general, the fracture pressure increases with depth as the overburden stress and the horizontal stresses increase with depth. However, sometimes we encounter loss zones where this trend no longer applies. For deviated wells, the fracture gradient is expected to decrease with increased wellbore inclination, as shown in Fig. 2.8. At present, we will analyze vertical wells only; deviated wells will be covered later in this chapter.

When the borehole pressure is increased, the wellbore wall will eventually fail. Mud losses may occur through the resulting fracture. Borehole fracturing is a tensile failure, because the tangential stress goes into tension. Rocks generally have low tensile strength. Often tiny cracks and fissures exist in the rock body, or are created during the drilling operation. It is therefore a common assumption to neglect rock tensile strength. Fracturing is defined as the pressure at which the effective hoop stress is zero. For a vertical well with equal horizontal in-situ stresses,

$$\sigma_\theta - P_o = 2\sigma_h - P_w - P_o = 0, \quad \dots\dots\dots (2.6a)$$

or

$$P_{wf} = 2\sigma_h - P_o. \quad \dots\dots\dots (2.6b)$$

For unequal horizontal in-situ stresses, the fracturing pressure becomes

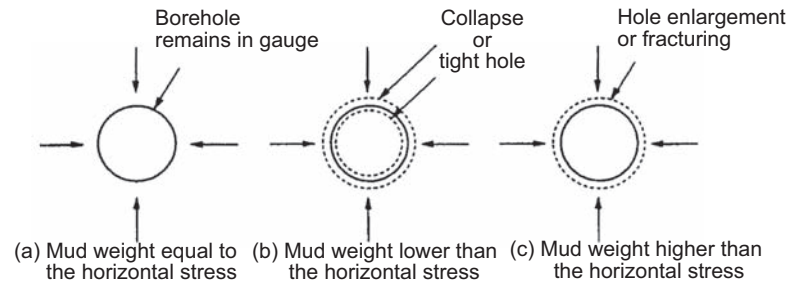


Fig. 2.8—Borehole response to borehole pressure.

$$\sigma_{\theta} - P_o = 3\sigma_h - \sigma_H - P_w - P_o, \quad \dots\dots\dots (2.7a)$$

or

$$P_{wf} = 3\sigma_h - \sigma_H - P_o, \quad \dots\dots\dots (2.7b)$$

Example 2.4—Fracturing.

1. Assume that we have a 1100-m-deep vertical well. At this depth, the overburden stress gradient is 1.9 SG, while the two horizontal stresses are 1.51 SG. There exists a normal pore pressure of 1.03 SG in the formation. Determine the fracturing pressure for the borehole.
2. Further interpretation of the well data reveals that the two horizontal stresses are actually different. Using the same overburden stress as above, but assuming that the horizontal stresses are equal to 1.61 and 1.45 SG, respectively, compute the fracture pressure now.
3. Discuss the effect of anisotropic stresses—that is, equal horizontal stresses vs. different horizontal stresses. Which gives highest fracture pressure?

Solution.

1. Using Eq. 2.6, the fracturing pressure is

$$P_{wf} = 2 \times 1.51 \text{ SG} - 1.03 \text{ SG} = 1.99 \text{ SG}.$$

2. The new fracture pressure becomes

$$P_{wf} = 3 \times 1.45 \text{ SG} - 1.61 \text{ SG} - 1.03 \text{ SG} = 1.71 \text{ SG}.$$

3. In the discussion, include if a difference in stresses leads to a lower fracture gradient. Conversely, do equal in-situ stresses lead to a stronger well?

Often we perform a leakoff test (LOT) or a formation integrity test after each casing string is cemented in place. The purpose is to ensure that the formation is sufficiently strong, and that the cement has sufficient integrity such that the next section can be drilled. This leakoff test is our main parameter to estimate the magnitude of the in-situ stresses.

Fig. 2.9 shows the general trends for the fracture gradient in a depositional basin. The fracturing pressure increases with depth, and it decreases with borehole inclination. The reason for the latter is that the in-situ stresses are different. For a vertical well, there are two nearly equal horizontal stresses acting on the wellbore. For a horizontal well, the overburden stress and the horizontal stress are acting on the borehole, creating an anisotropic stress state.

The LOT. This pressure test is very important for the drilling of wells. After each casing is installed and cemented in place, a hydraulic test is performed. This is called the LOT. To allow further drilling, this must show adequate hole strength to drill the next openhole section. When the cement is hardened around the casing, the casing shoe is drilled 4–6 m into the new formation below the shoe. Then the well is shut in and the borehole is

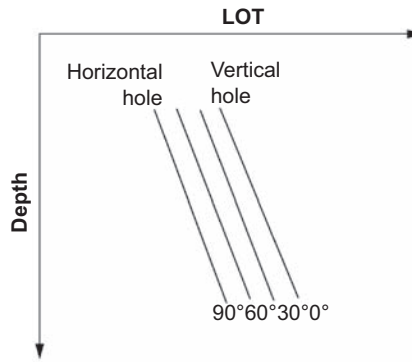


Fig. 2.9—Fracture gradients for relaxed depositional basin [from Aadnoy (1996)].

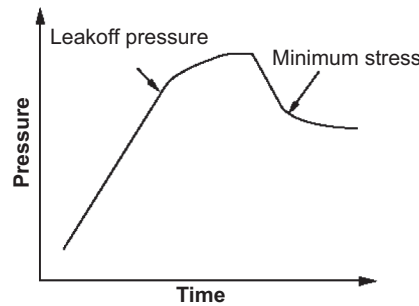


Fig. 2.10—Pressure plot during leakoff test.

pressurized, usually using the cement pump. The pressure that builds up in the annulus is shown in **Fig. 2.10**. The initial linear slope is due to the compressibility of the drilling fluids in the borehole. When the pressure buildup deviates from the straight line, we assume that a fracture initiates in the borehole wall. This is commonly defined as the LOT point. Beyond this point, the pump is stopped and the pressure drop is observed. It is common to assume that the point where the pressure curve changes slope indicates the minimum horizontal stress; however, this interpretation is debated.

The Optimal Mud Weight. In a typical well, we have a pore pressure prognosis, an overburden stress prognosis, and several LOT data. To develop this information into a predictive tool, we must estimate the horizontal stresses. From Eq. 2.6, we obtain

$$\sigma_h = \frac{1}{2}(P_{wf} + P_o). \quad \dots\dots\dots (2.8)$$

With the assumptions given, the horizontal stress is actually the midpoint between the fracture pressure and the pore pressure. For this reason, it is often called *the median-line principle*. **Fig. 2.11** shows an example. The oil industry has commonly used a mud weight barely exceeding the pore pressure, as shown in the left stepped curve in **Fig. 2.11**. When borehole stability analysis became invoked, a high mud weight like the right stepped curve was often recommended to reduce the tangential stress and, hence, the collapse potential of the well. This often led to fluid-loss problems instead. The middle stepped curve gave better results because it is based on the idea of minimum disturbance of the stresses acting on the borehole. This is explained in the following.

Before the well was drilled, a horizontal stress state σ_h existed in the rock. During drilling, the rock that was in the hole is replaced with drilling mud. If the drilling mud creates the same stress, there is no disturbance in stresses. However, a lower mud weight sets up a compressive tangential stress, and a higher mud weight sets up a lower tangential stress. A mud weight equal to the horizontal stress level is actually the optimal mud weight for the well. We therefore often start a new well program using the median-line principle for mud weight. This mud weight must be modified for several reasons:

- The mud density in a well section is constant, but the stresses and pore pressure change with depth. The mud weight is therefore a compromise over a depth interval.
- Wells often have potential fluid-loss zones. The mud weight selection must consider this.

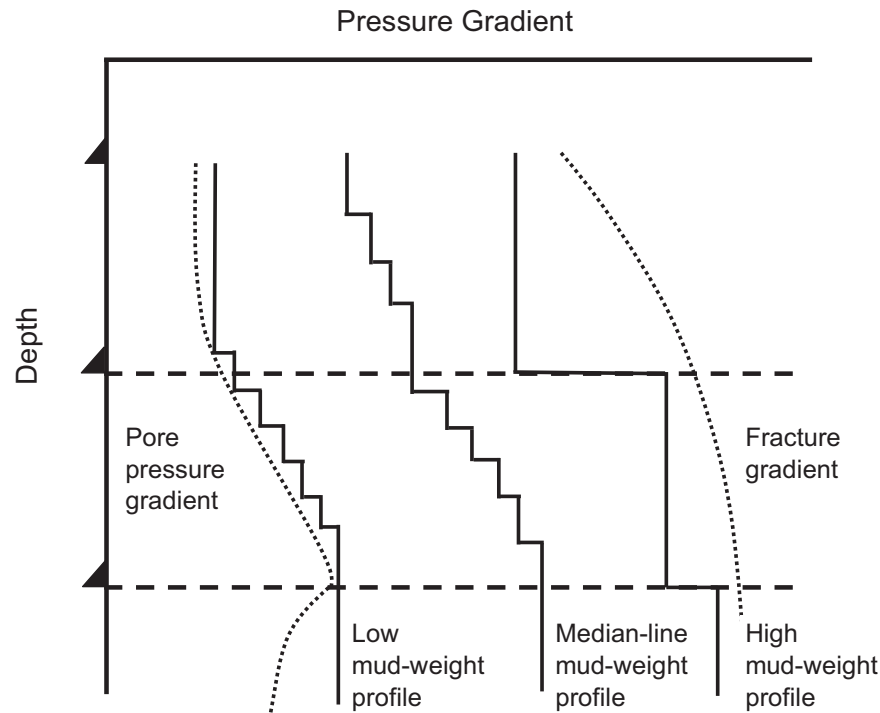


Fig. 2.11—Alternative mud-weight schedules.

- In directional wells, differential sticking (higher wellbore pressure presses the drillstring against lower pore pressure) can result in a stuck drillstring. This risk can be reduced by reducing the mud weight.
- In exploration wells, sometimes the mud weight is kept close to the pore pressure (tagging the pore pressure). This is one method to establish a more correct pore pressure curve than the prognosis.
- Mud cost may be of concern.

Fig. 2.11 shows three mud weight selection principles: low mud weight, median-line mud weight, and high mud weight. Recent experience favors the median-line method.

The median-line principle is a simple tool to establish an optimal mud-weight schedule, taking into account the concerns discussed above. Aadnoy (1996) reports a reduction in tight holes and backreaming after invoking this principle.

Example 2.5—Optimal Mud Weight. Fig. 2.12 shows a pressure gradient prognosis for a well. There are two sand stringers, and it has a sand reservoir. The rest of the borehole consists of shales. Assuming a relaxed depositional basin, do the following:

1. Draw a curve that estimates the horizontal stress level.
2. In the interval between the two casing points, suggest a mud weight profile. Lists concerns that add constraints to this plan.

Solution.

1. Draw a figure similar to Fig. 2.9 using Fig. 2.10. The horizontal stress estimate is the midpoint between the fracturing curve and the pore pressure curve.
2. The mud weight should not be changed continuously. From a practical perspective, the mud engineer may increase mud weight every 4–6 hours. Propose 3 to 4 mud weight increases in the interval. At the top of the new well section, it is common to start with a mud weight below the median line for two reasons. A low mud weight gives a longer pressure increase in the LOT plot of Fig. 2.8, leading to better interpretation, and a gradual increase from a lower mud weight will gradually expand the borehole, possibly leading to less tight hole. In a deviated well, hole cleaning and stuck pipe are of particular concern. Two permeable sand stringers are exposed in the interval. For a given inclination, the upper is most critical because the

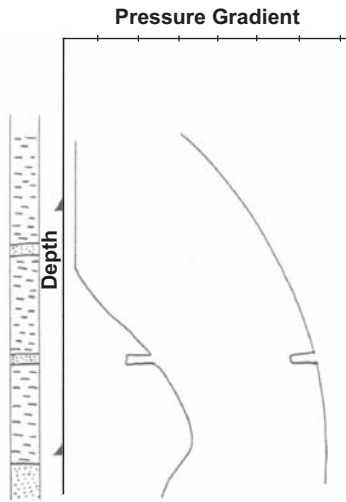


Fig. 2.12—Pressure gradient prognosis.

pore pressure is lowest. Here the highest differential pressure between the mud pressure and the pore pressure will arise. In these cases, we must consider the highest allowable mud weight to avoid differential sticking. Other remedies include using small and lightweight drilling assemblies and a thin mud cake.

2.1.6 Borehole Collapse. Borehole collapse typically takes place at lower borehole pressures. The high stress contrast between the high hoop stress and the low borehole pressures gives rise to a high shear stress. Therefore, collapse is defined as a *shear failure*.

Sometimes tight holes occur, which may require frequent wiper trips or reaming. This can, in certain wells, lead to stuck drillstring or difficulties in landing the casing string. There are many reasons for a tight hole; for example, dogleg severity (high wellbore curvature) can contribute, or simply inward creep of the borehole wall, also aided by shale swelling.

Most boreholes will enlarge over time. This is often a time-dependent collapse phenomenon. Problems caused by hole enlargement include difficulties in removing rock fragments and drilled cuttings from the borehole, or a reduced quality of the logging operation or cement placement behind casing strings. It is important to understand that a tight hole and borehole collapse are similar events; in one case, the hole may yield, while in the latter case, an abrupt failure may occur. If rock cavings are seen in the mud returns, the correcting action is usually to increase the mud weight, thereby reducing the hoop stress.

Fig. 2.13 shows a typical collapse failure. The shear failure planes are curved because of the circular geometry of the hole. As shown in Fig. 2.13a, the shear planes connect, resulting in rock fragments falling into the borehole.

If the external borehole stresses are equal, the collapsed hole will retain a circular shape, as seen in Fig. 2.13b. However, if the stresses are different, an elongated borehole will result. For a vertical well, the longer hole axis will point in the direction of the minimum in-situ stress. This is often used as a method to assess the direction of the minimum horizontal stress from caliper logs, and it is called *breakout analysis*. This method usually is not applied for deviated wells because it is believed that the drillstring rotation may provide an upward bias for an elongated borehole.

Shear Failure. Before analyzing borehole collapse, we must define the failure mechanism, which is a shear failure. Strength data are obtained from cores as shown in Fig. 2.14. Core samples are subjected to a constant confining pressure and loaded axially until they fail. This process is repeated for various confining pressures. The failure behavior depends on the loading state—that is, the confining pressure level. An example of such laboratory tests is shown in Table 2.3.

There are many details that must be considered when testing core plugs. This discussion will not be pursued here, but the reader is referred to Cook and Edwards (2009). For a given rock plug test, the data from the test are the maximum compressive stress; the minimum stress, which is the confining pressure; and the pore pressure inside the plug. Here we will show how these pressures are used for modeling.

The failure data from Table 2.3 are plotted in Fig. 2.15. Six core plugs are tested to failure for various confining pressures. We show the data in a Mohr-Coulomb plot. Along the horizontal axis, the failure and the confining pressure for each test are marked, and a circle is made between these points. A line is drawn on top of all circles. This is the failure line, which we will use in our collapse analysis.

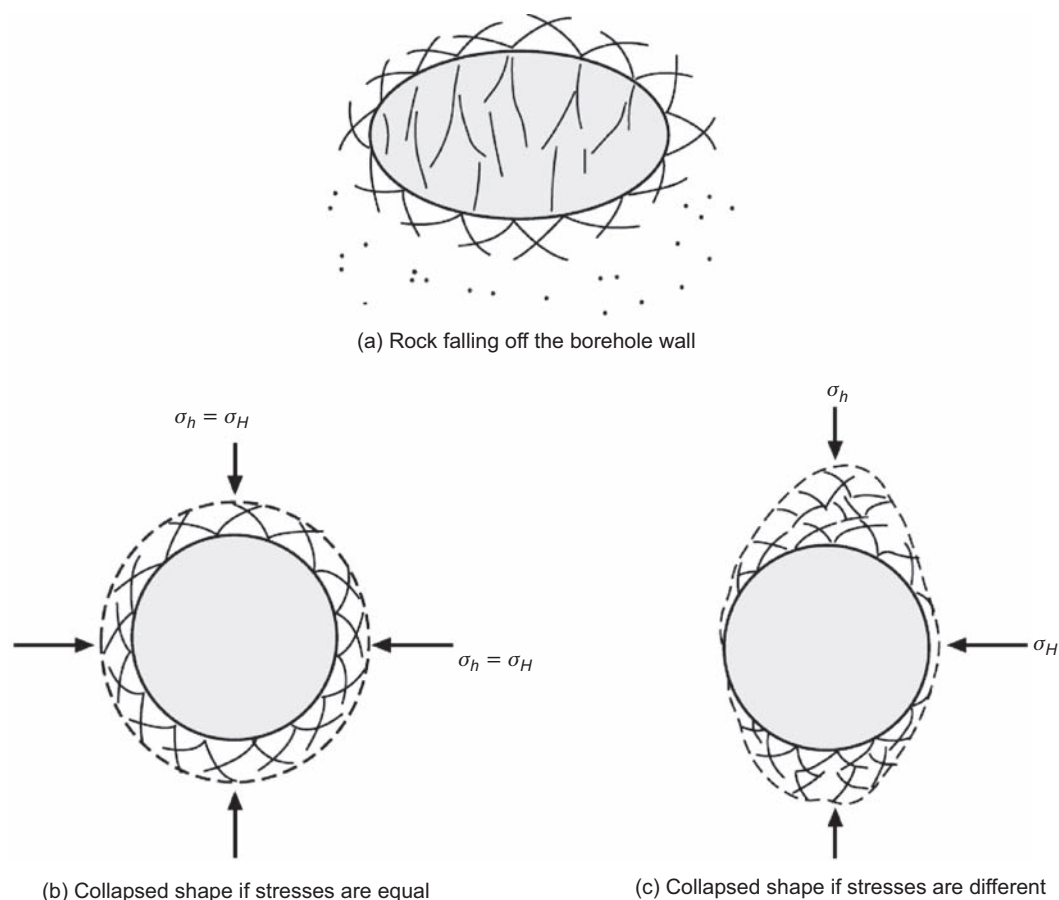


Fig. 2.13—Collapse of borehole wall.

If the stress state for an application falls below the failure line, the specimen is intact. However, crossing the failure line, the specimen will fail. The laboratory-obtained data from Table 2.3 can be modeled with many other failure models. We will restrict the discussion to the most common model.

The Mohr-Coulomb Shear Model. In a 2D stress state, the stresses can be described by means of Mohr's circle. This is done by constructing a circle with a diameter equal to the difference between the maximum and the minimum stress at failure.

The Mohr-Coulomb failure model is this failure line, which mathematically can be expressed as

$$\tau = \tau_0 + \sigma' \tan \phi. \quad (2.9)$$

The failure line is established from laboratory-obtained data as shown above. To apply this failure model to a well, we must derive expressions for the stresses acting on the wellbore. Fig. 2.16 shows the stresses at failure.

In the Fig. 2.16, we use effective stresses. Inspection of the figure reveals that the coordinates (τ, σ') at failure are defined by the following equations:

$$\tau = \frac{1}{2}(\sigma'_1 - \sigma'_3) \cos \phi. \quad (2.10a)$$

$$\sigma' = \frac{1}{2}(\sigma'_1 + \sigma'_3) - \frac{1}{2}(\sigma'_1 - \sigma'_3) \sin \phi. \quad (2.10b)$$

The models above are expressed in terms of principal stresses. The maximum principal stress is the tangential stress and the minimum principal stress is the wellbore pressure. The derivation will be shown later. Inserting Eq. 2.10 into the Mohr-Coulomb failure model, Eq. 2.9, and the borehole stresses from Eq. 2.5 (equal horizontal stresses), results in the following equation for the critical collapse pressure:

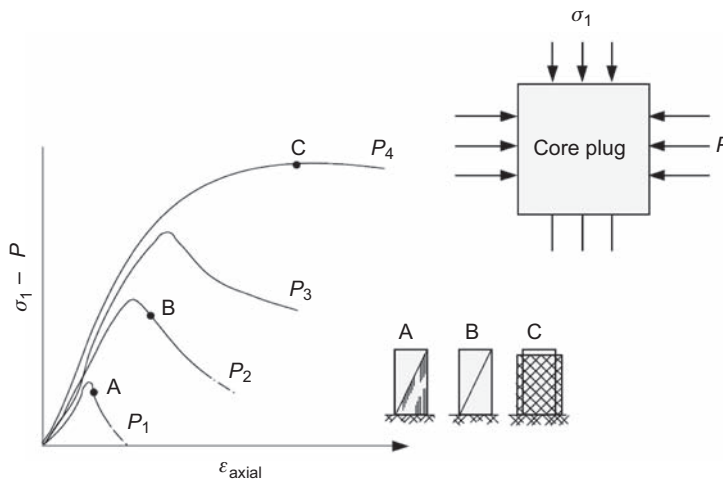


Fig. 2.14—Shear strength from core samples [from Aadnoy (1996)].

TABLE 2.3—TRIAxIAL STRENGTH DATA FOR LEUDERS LIMESTONE		
Test No.	Confining Pressure, σ_3 (bar)	Yield Strength, σ_1 (bar)
1	0	690
2	41	792
3	69	938
4	138	1069
5	207	1248
6	310	1448

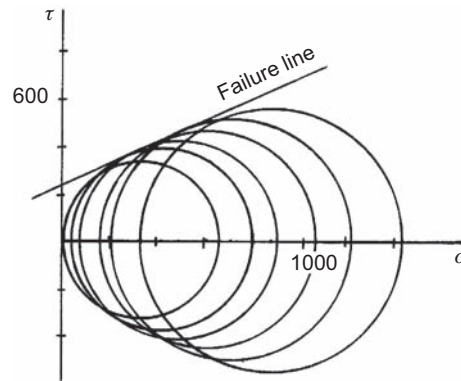


Fig. 2.15—Mohr-Coulomb failure model for data of Table 2.3 [from Aadnoy (1996)].

$$P_{wc} = \sigma_h (1 - \sin \phi) - \tau_0 \cos \phi + P_o \sin \phi. \quad \dots \dots \dots (2.11)$$

The Mohr-Coulomb model contains two material properties. The angle ϕ is defined as the angle of internal friction. Sandstone, for example, will exhibit friction along a shear plane because the grains will restrict motion. This is true whether the sand grains are cemented or not. The cohesive strength τ_0 , on the other hand, reflects the degree of cementation of the material.

Although simple, Eq. 2.11 shows the interrelationships that cause mechanical wellbore collapse. A high formation stress and a high pore pressure induce collapse. High cohesive strength or the cementation of the rock actually resists collapse. Loose sands have no cohesive strength and therefore have a high collapse pressure. Therefore, the borehole might be subjected to sand production. A high angle of internal friction also opposes collapse.

The fracture angle on the plug specimen shown in Fig. 2.16 can be determined from the following expression:

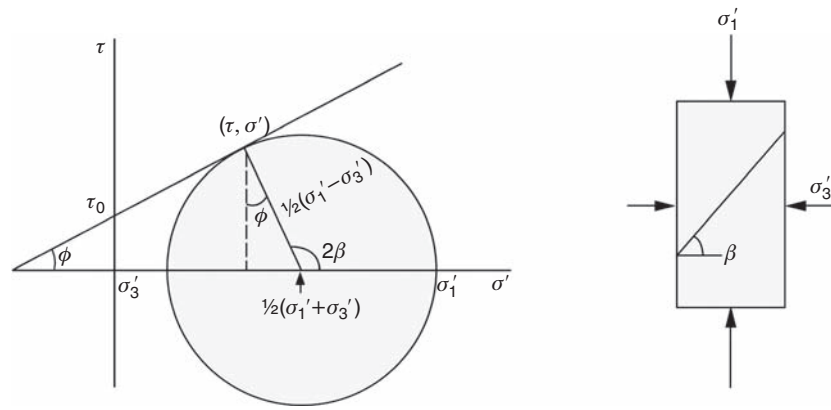


Fig. 2.16—Stresses at failure for the Mohr-Coulomb failure model [from Aadnoy (1996)].

$$\beta = 45^\circ + \frac{\phi}{2}. \quad \dots\dots\dots (2.12)$$

We will show the mechanisms that lead to mechanical hole collapse by referring to the three borehole stresses given in Eq. 2.5. Because we are considering porous media, we will define them in terms of effective stresses:

$$\text{Radial effective stress:} \quad \sigma'_r = P_w - P_o. \quad \dots\dots\dots (2.13a)$$

$$\text{Tangential effective stress:} \quad \sigma'_\theta = 2\sigma_h - P_w - P_o. \quad \dots\dots\dots (2.13b)$$

$$\text{Vertical effective stress:} \quad \sigma'_v = \sigma_v - P_o. \quad \dots\dots\dots (2.13c)$$

Example 2.6—Stresses on the Borehole Wall. Plot the radial, the tangential, and the vertical stress for the following stress state:

$$\sigma_h = 1.5 \text{ SG}, \sigma_v = 1.7 \text{ SG}, P_o = 1.03 \text{ SG}$$

Solution. Inserting these data into Eq. 2.13 results in the data shown in **Table 2.4**; these data are furthermore plotted in **Fig. 2.17**.

We observe from Example 2.6 that the vertical (axial) stress component is constant regardless of the borehole pressure, while the radial and tangential stresses vary with the borehole pressure. Of course, the radial stress is given by the borehole pressure itself, so the key parameter is the tangential stress, or the hoop stress. In the following, we will illustrate how these stresses relate to failure of the borehole.

At low borehole pressure, the difference between the radial and the tangential effective stresses controls failure because this stress contrast gives rise to shear stresses. We see that for the lowest borehole pressure gradient (P_{w1}), this difference is largest. At P_{w2} , the difference is smaller, but we observe that at high pressures (P_{w3}), the stress difference again increases. But here the borehole fails in a tensile mode. Fracturing is a tensile failure.

The three cases from Fig. 2.17 are shown in a Mohr-Coulomb plot in **Fig. 2.18**. The straight line is a failure envelope obtained from triaxial testing of cores. We see that P_{w2} and P_{w3} are well below the failure envelope, and

TABLE 2.4—EFFECTIVE STRESSES FOR VARIOUS MUD WEIGHTS			
Borehole pressure gradient (SG)	$P_{w1} = 1.1$	$P_{w2} = 1.4$	$P_{w3} = 1.75$
Radial effective stress	0.07	0.37	0.72
Tangential effective stress	0.87	0.57	0.22
Vertical effective stress	0.67	0.67	0.67

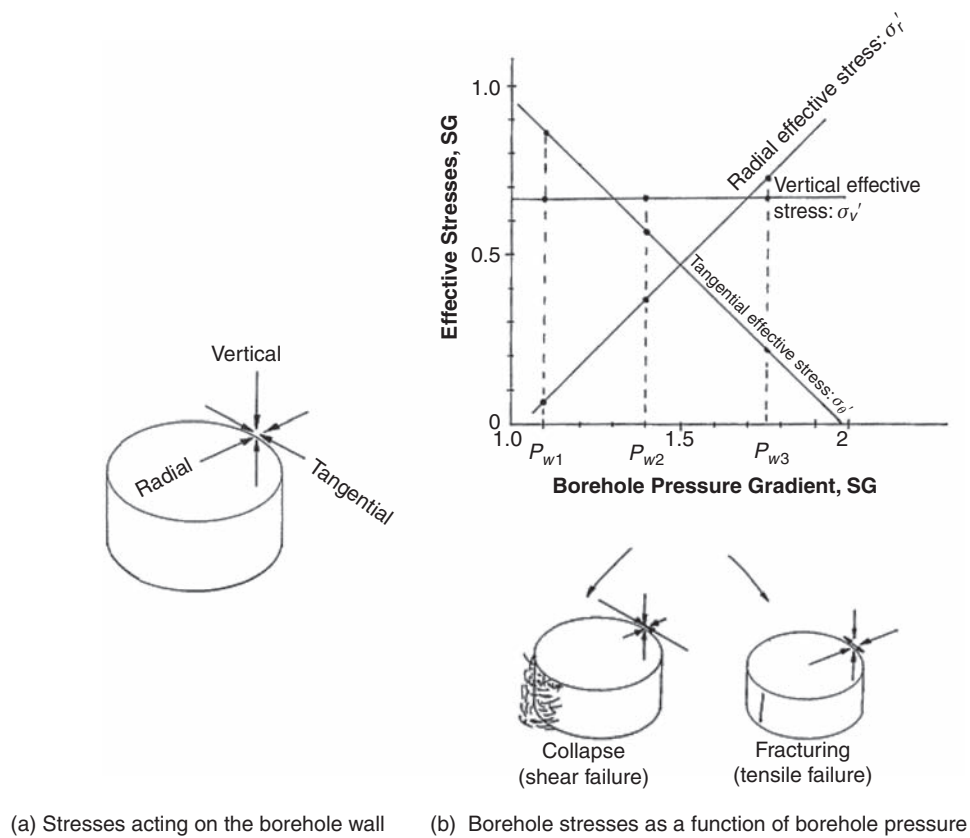


Fig. 2.17—Stresses on the wellbore wall [from Aadnøy (1996)].

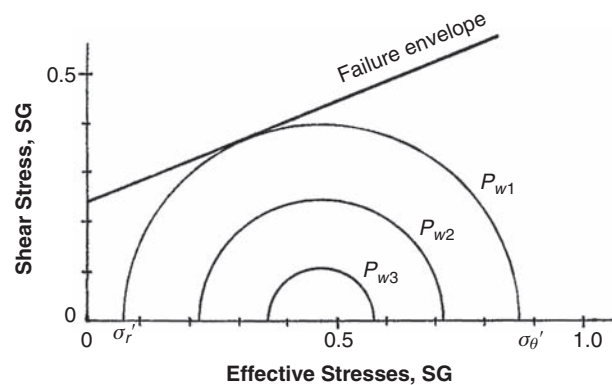


Fig. 2.18—Mohr-Coulomb representation of the three cases in Example 2.6.

the hole should therefore be stable for these borehole pressures. However, P_{w1} approaches the failure envelope, and at this point the stress loading is equal to the strength of the rock. The borehole will fail at this point.

Example 2.7—Borehole Collapse. A vertical well is subjected to equal horizontal stresses. The following data apply:

Horizontal stress:	1.5 SG
Pore pressure:	1.03 SG
Angle of internal friction:	30°
Rock cohesive strength:	0.4 SG

1. Compute the critical collapse pressure for the wellbore.
2. During drilling, one observes that the rock is not consolidated, because sand particles drop out of the wellbore wall. Compute the critical collapse pressure now.

Solution. This problem has equal horizontal in-situ stresses. For this case, Eq. 2.11 can be used to predict the critical collapse pressure.

1. The critical collapse pressure is with the data given:

$$P_{wc} = 1.5(1 - \sin 30^\circ) - 0.4 \cos 30^\circ + 1.03 \sin 30^\circ = 0.92 \text{ SG.}$$

2. If the rock is not consolidated, the cohesive strength is zero. The critical collapse pressure now becomes:

$$P_{wc} = 1.5(1 - \sin 30^\circ) + 1.03 \sin 30^\circ = 1.27 \text{ SG.}$$

This example illustrates the importance of the degree of consolidation of the rock. When there is no cementation, the well will collapse at a higher pressure than for a consolidated rock. Sand production during production is similar to wellbore collapse and can be analyzed the same way.

Interpretation of Caliper Logs. We have just shown that the borehole pressure plays a key role in collapse failures of boreholes. Often the remedy is to increase the borehole pressure—that is, to lower the shear stress as shown in Fig. 2.17. We also have briefly introduced the elements of stresses and rock strength. Unfortunately, often we do not have sufficient stress and rock strength information to perform a detailed collapse analysis.

However, we have many caliper logs from boreholes, showing hole enlargement. In this chapter, we will take advantage of these to analyze the field data in an empirical way. First, we will analyze a vertical exploration well in the southern North Sea.

Example 2.8—Exploration Well. During drilling of a vertical exploration well, some borehole collapse took place. Although the collapse was not very pronounced, there was difficulty landing the production casing and the liner. Remedial work such as reaming, hole cleaning, and under-reaming took considerable time before the well was successfully finished.

Fig. 2.19 shows the information for the well. We observe that the 12¼-in. hole section is abnormally long, 2000 m. Also, there is normal pore pressure down to 2800 m. The well has a low pore pressure gradient profile. Also shown are the mud weights used, the overburden stress gradient obtained from integration of density logs, and the measured leakoff values below each casing shoe.

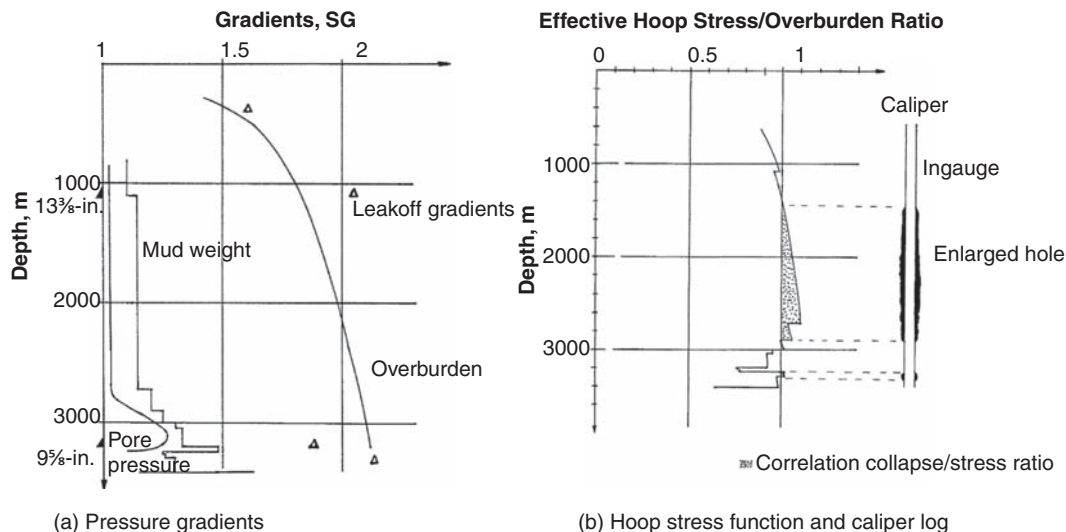


Fig. 2.19—Pressure gradients and caliper log for the exploration well.

Solution. In the foregoing, we have seen that the well will reach a critical pressure and collapse as the mud weight is lowered, and we have seen that the tangential (or hoop) stress is the key parameter. We will now calculate the hoop stress for this well and correlate with the caliper log. We will use the results of an analysis of the well, which concluded that the horizontal stress level is approximately 80% of the overburden stress for this well. The effective stresses from Eq. 2.13 can then be written

$$\sigma'_r = P_w - P_o. \quad (2.14a)$$

$$\sigma'_\theta = 2\sigma_h - P_w - P_o = 2 \times 0.8 \times \sigma_v - P_w - P_o. \quad (2.14b)$$

$$\sigma'_v = \sigma_v - P_o. \quad (2.14c)$$

We want to depth-normalize the data. For example, if we calculate the effective hoop stress and divide by the effective overburden stress, we expect a vertical trend. This ratio can be obtained from Eq. 2.14, as follows:

$$\frac{\sigma'_\theta}{\sigma'_v} = \frac{2 \times 0.8 \times \sigma_v - P_w - P_o}{\sigma_v - P_o}. \quad (2.15)$$

Fig. 2.19 shows Eq. 2.15 plotted using the field data. Also, the caliper log is shown. We observe that there is a very good correlation as the hole is collapsed for $\sigma'_\theta/\sigma'_v > 1$, but the hole is basically in gauge if this ratio is lower. At the bottom of the 12¼-in. section of Fig. 2.19, we observe that the mud weight has been increased. The result is an in-gauge hole. However, in the 8½-in. section, the mud weight was temporarily reduced, and some collapse took place. Maintaining a higher mud weight for the remainder of the drilling operation resulted in an in-gauge hole.

From the evaluation of Fig. 2.19, we can state that the critical collapse pressure was reached when $\sigma'_\theta/\sigma'_v = 1$. Solving Eq. 2.15 for this condition results in

$$P_{wc} = 0.6\sigma_v. \quad (2.16)$$

Actually, the solution to this evaluation of this particular well is that the mud weight should be higher than 60% of the overburden stress. This curve is shown in **Fig. 2.20**. It is seen that only a slight increase in mud weight would probably have resulted in a more in-gauge hole. Also, from Fig. 2.20 we see that the overburden stress gradient is systematically increasing with depth, which also is reflected in the horizontal stress state. The mud weight, however, is kept nearly constant, which implies that the shear stress acting on the hole wall is increasing with depth.

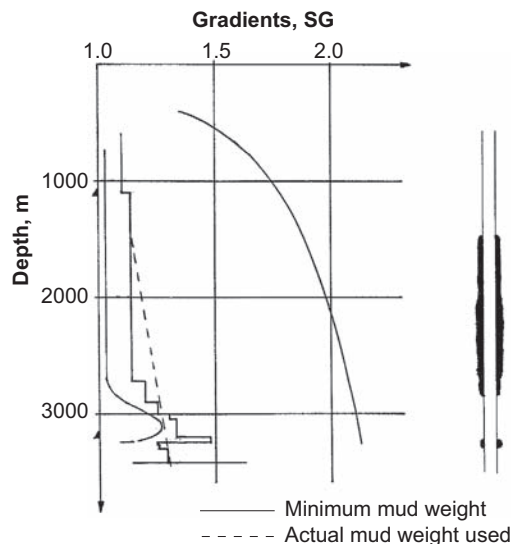


Fig. 2.20—Results of the analysis showing critical mud weight to avoid collapse.

Inspection of Fig. 2.19a indicates that when the external loading (the in-situ stresses) increases with depth, the mud weight should be increased correspondingly. When maintaining a constant mud weight with depth the tangential stress is increasing, leading to collapse of the borehole wall.

2.1.7 Water-Based vs. Oil-Based Drilling Fluids. These two types of drilling fluids have very different behavior. In recent years, the oil-based drilling fluid has gained popularity, but the present environmental movement brings water-based drilling fluids back. They both have their advantages and disadvantages as briefly discussed here.

Water-based drilling fluids use water as the continuous phase. Additives are used to change density and viscosity and to control filtrate losses. Also, chemical compatibility with the rock is important. Water-based drilling fluids are cheap. They also are good for curing mud losses. By pumping coarse bridging materials (called lost-circulation material), mud losses often are cured. It is believed that the main mechanism is that in water-wet formations, filtrate losses occur, leaving dense particles in the mud in the fracture. The main disadvantage with water-based drilling fluids is that they are reactive to clays and lead to time-dependent borehole problems. The hole size often increases with time in shales.

Oil-based drilling fluids use oil as the continuous phase. Lower well friction is one of the advantages with oil-based drilling fluids. They are therefore often used in long-reach wells where friction is a critical parameter. Usually the borehole does not show time-dependent deterioration as with water-based fluids. The capillary pressure prevents oil from invading a water-wet rock.

There is, however, one disadvantage with oil-based drilling fluids. If circulation losses arise during drilling, it is often difficult to stop the losses. A severe loss situation can be quite time-consuming to cure. One main mechanism is that there is little or no filtrate loss toward the water-wet rock, such that the drilling-fluid viscosity will not increase and the oil-based mud will continue opening the fracture.

2.2 Borehole Stability Analysis for Inclined Wells

We have so far discussed vertical wells. Many wells today are deviated. This complicates the picture, which is now three-dimensional, and one has to properly account for the effects of wellbore deviation. In the following sections, the general methodology will be presented. We will first define the general equations for stresses around a borehole.

2.2.1 The Kirsch Equations. In the previous derivation, we have studied the stresses at the borehole wall. Now we will investigate the stress state in the rock formation. The following equations define this (Aadnoy and Chenevert 1987):

$$\begin{aligned} \sigma_r = & \frac{1}{2}(\sigma_x + \sigma_y) \left(1 - \frac{a^2}{r^2}\right) + \frac{1}{2}(\sigma_x - \sigma_y) \left(1 + 3\frac{a^4}{r^4} - 4\frac{a^2}{r^2}\right) \cos 2\theta, \\ & + \tau_{xy} \left(1 + 3\frac{a^4}{r^4} - 4\frac{a^2}{r^2}\right) \sin 2\theta + \frac{a^2}{r^2} P_w \end{aligned} \quad (2.17a)$$

$$\begin{aligned} \sigma_\theta = & \frac{1}{2}(\sigma_x + \sigma_y) \left(1 + \frac{a^2}{r^2}\right) - \frac{1}{2}(\sigma_x - \sigma_y) \left(1 + 3\frac{a^4}{r^4}\right) \cos 2\theta \\ & - \tau_{xy} \left(1 + 3\frac{a^4}{r^4}\right) \sin 2\theta - \frac{a^2}{r^2} P_w \end{aligned} \quad (2.17b)$$

$$\sigma_z = \sigma_{zz} - 2\nu(\sigma_x - \sigma_y) \frac{a^2}{r^2} \cos 2\theta - 4\nu\tau_{xy} \frac{a^2}{r^2} \sin 2\theta. \quad (2.17c)$$

$$\tau_{r\theta} = \left[\frac{1}{2}(\sigma_x - \sigma_y) \sin 2\theta + \tau_{xy} \cos 2\theta \right] \left(1 - 3\frac{a^4}{r^4} + 2\frac{a^2}{r^2}\right). \quad (2.17d)$$

$$\tau_{rz} = \left(\tau_{xz} \cos \theta + \tau_{yz} \sin \theta \right) \left(1 - \frac{a^2}{r^2}\right). \quad (2.17e)$$

$$\tau_{\theta z} = \left(-\tau_{xz} \cos \theta + \tau_{yz} \sin \theta \right) \left(1 + \frac{a^2}{r^2} \right). \quad (2.17f)$$

At the borehole wall ($r = a$), the above equations reduce to

Radial stress:

$$\sigma_r = P_w. \quad (2.18a)$$

Tangential stress:

$$\sigma_\theta = \sigma_x + \sigma_y - P_w - 2(\sigma_x - \sigma_y) \cos 2\theta - 4\tau_{xy} \sin 2\theta. \quad (2.18b)$$

Axial stress, plane strain:

$$\sigma_z = \sigma_z - 2\nu(\sigma_x - \sigma_y) \cos 2\theta - 4\nu\tau_{xy} \sin 2\theta. \quad (2.18c)$$

Axial stress, plane stress:

$$\sigma_z = \sigma_{zz}. \quad (2.18d)$$

Shear stress:

$$\tau_{\theta z} = 2(\tau_{yz} \cos \theta - \tau_{xz} \sin \theta). \quad (2.18e)$$

$$\tau_{rz} = \tau_{r\theta} = 0. \quad (2.18f)$$

Eq. 2.18 is used for most borehole stability analysis because the formation fails at the borehole wall. That is, the stresses are usually highest on the borehole wall, so therefore it will fail here first. The plane stress solution (vertical stresses remain constant) for the axial stress usually is used because of simplicity. The difference between the plane stress and plane strain solutions (wellbore displaces only in the horizontal plane) is usually negligible.

Example 2.9—Stresses Into the Formation. Assume that $\sigma_x = \sigma_y$ and $\tau_{xy} = \tau_{xz} = \tau_{yz} = 0$. Plot the stresses from Eq. 2.17 for various r/a ratios. At what r/a ratio is the borehole no longer affecting the in-situ stresses?

Solution. Note the symmetry between the radial and the tangential stresses. The effect of the borehole diminishes for the r/a ratio between 5 and 10. We usually state that the stress concentration effect of the borehole extends 5 radii into the rock.

2.2.2 Deviated Boreholes and Stresses in Three Dimensions. Deviated boreholes are in general subjected to a more complex stress state than vertical wells, even in a sedimentary basin. The reason is that if horizontal stresses are equal for a vertical well, the stresses normal to the hole will change when the well becomes inclined.

In applications of the Kirsch equations given above, often one assumes a horizontal and vertical in-situ stress field. The borehole, however, may take any orientation. Therefore, one must define equations to transform the in-situ stresses to the orientation of the borehole.

It is common in the oil industry to assume three principal in-situ stresses: the vertical or overburden stress σ_v , and the maximum and minimum horizontal stresses, σ_H and σ_h . **Fig. 2.21** shows the most important stresses. The input stresses are the in-situ stresses σ_v , σ_H , and σ_h . Because the borehole may take any orientation, these stress must be transformed to a new coordinate system, x , y , z , where we observe stresses as σ_x , σ_y , σ_z . The directions of the new stress components are given by the borehole inclination from vertical, ϕ , the geographical azimuth, α , and the position on the borehole wall from the x axis, θ . One of the properties of this transformation is that the y axis is always parallel to the plane formed by σ_H and σ_h .

The following equations define all transformed stress components:

$$\sigma_x = \left(\sigma_H \cos^2 \alpha + \sigma_h \sin^2 \alpha \right) \cos^2 \phi + \sigma_v \sin^2 \phi. \quad (2.19a)$$

$$\sigma_y = (\sigma_H \sin^2 \alpha + \sigma_h \cos^2 \alpha). \quad (2.19b)$$

$$\sigma_z = (\sigma_H \cos^2 \alpha + \sigma_h \sin^2 \alpha) \sin^2 \phi + \sigma_v \cos^2 \phi. \quad (2.19c)$$

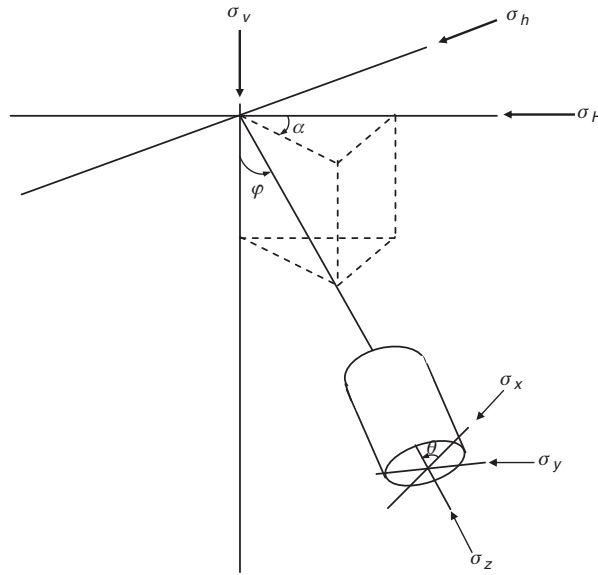


Fig. 2.21—Orientation of borehole relative to the in-situ stresses.

$$\tau_{yz} = \frac{1}{2}(\sigma_h - \sigma_H) \sin 2\alpha \sin \varphi. \quad (2.19d)$$

$$\tau_{xz} = \frac{1}{2}(\sigma_H \cos^2 \alpha + \sigma_h \sin^2 \alpha - \sigma_v) \sin 2\varphi. \quad (2.19e)$$

$$\tau_{xy} = \frac{1}{2}(\sigma_h - \sigma_H) \sin 2\alpha \cos \varphi. \quad (2.19f)$$

With this, all equations are defined that are required to analyze failures of boreholes. This analysis will be demonstrated in the following example.

Example 2.10—Stress Transformations. Using the stress transformation equations from Eq. 2.19, do the following:

1. Assume that the two horizontal in-situ stresses are equal. Write the resulting equations. See if any shear components disappear. Also, see if the stress state becomes independent of the azimuth.
2. Define all three principal in-situ stresses as equal. Write the resulting equations. Is there any directional dependence on azimuth and inclination? What would you call this stress state?

Solution.

1. Letting $\sigma_h = \sigma_H$, Eq. 2.19 becomes

$$\sigma_x = \sigma_h \cos^2 \varphi + \sigma_v \sin^2 \varphi$$

$$\sigma_y = \sigma_h$$

$$\sigma_z = \sigma_h \sin^2 \varphi + \sigma_v \cos^2 \varphi$$

$$\tau_{yz} = \tau_{xy} = 0$$

$$\tau_{xz} = (\sigma_h - \sigma_v) \sin 2\varphi$$

The stress state is isotropic in the horizontal plane. We observe that the transformed stresses are no longer dependent on the azimuth of the borehole. This is the simplest case in a relaxed depositional basin, where the borehole stability is the same in all geographical directions for a given wellbore inclination.

2. If $\sigma_h = \sigma_H = \sigma_v$, Eq. 2.19 reduces to

$$\begin{aligned}\sigma_x &= \sigma_h \\ \sigma_y &= \sigma_h \\ \sigma_z &= \sigma_h \\ \tau_{yz} &= \tau_{xz} = \tau_{xy} = 0.\end{aligned}$$

This is a fully hydrostatic stress state, equal to a static fluid pressure acting equally in all directions. For deeper parts of the Earth's crust, this stress state is called *lithostatic*. However, at shallower parts of the crust where hydrocarbons are found, this stress state rarely exists.

2.3 General Methodology for Analysis of Wellbore Stability

In this section, the general methodology for borehole stability analysis will be presented for both fracturing and collapse. This is valid for all stress states (normal, strike-slip, and reverse) and for all borehole orientations.

The calculation procedure is as follows:

- Calculate the stresses in the direction of the borehole.
- Insert these data into the borehole stress equations.
- Determine the point on the borehole wall where failure will occur.
- Implement a failure model.
- Compute borehole pressure at failure.

In the following sections, the general methodology for failure analysis will be presented both for fracturing and collapse.

Assuming that we know the in-situ stress state, we must transform these to the orientation of the borehole by using Eq. 2.19. The transformed stresses may then be inserted into the stress equations (Eq. 2.18).

Now we have expressions for the stresses at the borehole wall, or the stress state in the adjacent formation. Usually the borehole pressure is unknown at this stage. The object is often to determine the critical pressure that leads to failure of the borehole.

2.3.1 Principal Borehole Stresses. To solve for the critical pressure, the stresses discussed above are inserted into the failure criteria for the borehole. Remember, however, to use effective stresses by subtracting the pore pressure. This applies only for normal stresses, not for shear stresses.

The borehole wall is subjected to normal stresses and shear stresses. It is common to find the maximum normal stress by defining a direction (plane) where the shear stresses vanish. The resulting stresses are called principal stresses. At the borehole wall, these are

$$\sigma_1 = P_w \quad \dots \quad (2.20a)$$

$$\sigma_2 = \frac{1}{2}(\sigma_\theta + \sigma_z) + \frac{1}{2}\sqrt{(\sigma_\theta - \sigma_z)^2 + 4\tau_{\theta z}^2} \quad \dots \quad (2.20b)$$

$$\sigma_3 = \frac{1}{2}(\sigma_\theta + \sigma_z) - \frac{1}{2}\sqrt{(\sigma_\theta - \sigma_z)^2 + 4\tau_{\theta z}^2} \quad \dots \quad (2.20c)$$

After calculating the principal stresses above, the subscripts are often interchanged such that 1 always refers to the maximum compressive principal stress, 2 to the intermediate, and 3 to the least principal stress. Typical principal stresses are

$$\begin{aligned}\text{Fracturing:} \quad \sigma_1 &= P_w \\ \sigma_3 &= \frac{1}{2}(\sigma_\theta + \sigma_z) - \frac{1}{2}\sqrt{(\sigma_\theta - \sigma_z)^2 + 4\tau_{\theta z}^2} \quad \dots \quad (2.21a)\end{aligned}$$

$$\begin{aligned}\text{Collapse:} \quad \sigma_1 &= \frac{1}{2}(\sigma_\theta + \sigma_z) + \frac{1}{2}\sqrt{(\sigma_\theta - \sigma_z)^2 + 4\tau_{\theta z}^2} \\ \sigma_3 &= P_w \quad \dots \quad (2.21b)\end{aligned}$$

2.3.2 Borehole Fracturing. The borehole will fracture when the minimum effective principal stress reaches the tensile rock strength σ_t . This is expressed as

$$\sigma'_3 = \sigma_3 - P_o = \sigma_t. \quad (2.22)$$

Inserting Eq. 2.21a into Eq. 2.22, the critical tangential stress is given by

$$\sigma_\theta = \frac{\tau_{\theta z}^2}{\sigma_z - \sigma_t - P_o} + P_o + \sigma_t. \quad (2.23)$$

Inserting the equation for the tangential stress, Eq. 2.18b, the critical borehole pressure is given by

$$P_w = \sigma_x + \sigma_y - 2(\sigma_x - \sigma_y) \cos 2\theta - 4\tau_{xy} \sin 2\theta - \frac{\tau_{\theta z}^2}{\sigma_z - \sigma_t - P_o} - P_o - \sigma_t. \quad (2.24)$$

There is another unknown for the general case. The fracture may not arise in the direction of the x or y axis because of shear effects. To resolve this issue, Eq. 2.24 is differentiated to define the extreme conditions ($dP_w / d\theta = 0$).

The normal stresses are in general much larger than the shear stresses. Neglecting second-order terms, Eq. 2.25 defines the position on the borehole wall for the fracture:

$$\tan 2\theta = \frac{2\tau_{xy}}{(\sigma_x - \sigma_y)}. \quad (2.25)$$

The final fracture equation is obtained by inserting the angle from Eq. 2.25 into Eq. 2.24.

The general fracturing equation is now defined. It is valid for all cases, arbitrary directions, and anisotropic stresses, but must in general be solved by numerical methods.

If symmetric conditions exist, all shear stress components may vanish. In these cases, the fracture may take place at one of the following conditions: $\sigma_H = \sigma_h$; $\gamma = 0^\circ$; $\alpha = 0^\circ, 90^\circ$. It is also common to assume that the rock has zero tensile strength because it may contain cracks or fissures. Inserting these conditions, the fracturing equation becomes

$$P_w = 3\sigma_x - \sigma_y - P_o - \sigma_t \quad \text{for } \sigma_x < \sigma_y \text{ and } \theta = 90^\circ, \quad (2.26a)$$

$$P_w = 3\sigma_y - \sigma_x - P_o - \sigma_t \quad \text{for } \sigma_y < \sigma_x \text{ and } \theta = 0^\circ. \quad (2.26b)$$

These equations simply say that a fracture will initiate normal to the least stress and will propagate in the direction of the largest normal stress.

Also, observe that assuming a maximum and a minimum stress normal to the borehole wall and vanishing shear stresses, the general fracturing equation becomes

$$P_w = 3\sigma_{\min} - \sigma_{\max} - P_o - \sigma_t. \quad (2.27)$$

Example 2.11—Fracture Pressure vs. Borehole Inclination. Assume that the following data exist for a well:

Overburden stress:	$\sigma_v = 100$ bar
Horizontal stress:	$\sigma_H = \sigma_h = 90$ bar
Pore pressure:	$P_o = 50$ bar
Borehole inclination:	$\phi = 40^\circ$

Borehole azimuth:	$\alpha = 165^\circ$
Tensile rock strength:	$\sigma_t = 0$
Rock Poisson's ratio:	$\nu = 0.25$

Determine the fracture pressure for a vertical well and for the deviated well given above.

Solution. For the vertical well, the in-situ stresses relate directly to the borehole direction and become $\sigma_x = \sigma_y = 90$ bar. The fracture pressure is determined directly by Eq. 2.27 and is

$$P_{wf} = 2\sigma_x - P_0 = 2 \times 90 - 50 = 130 \text{ bar.}$$

For the inclined well, the stresses must first be transformed to the orientation of the wellbore by Eq. 2.19. The result is

$$\begin{aligned}\sigma_x &= 94.13 \text{ bar} \\ \sigma_y &= 90 \text{ bar} \\ \sigma_z &= 95.87 \text{ bar} \\ \tau_{xz} &= -4.92 \text{ bar} \\ \tau_{yz} &= \tau_{xy} = 0.\end{aligned}$$

These data are again inserted into the equations for the borehole stresses, which become

$$\begin{aligned}\text{Radial stress:} \quad \sigma_r &= P_w \\ \text{Tangential stress:} \quad \sigma_\theta &= 184.13 - P_w - 8.26 \cos 2\theta \\ \text{Axial stress, plane strain:} \quad \sigma_z &= 95.87 - 2.07 \cos 2\theta \\ \text{Shear stress:} \quad \tau_{\theta z} &= -9.84 \sin \theta\end{aligned}$$

The angle θ from the x axis at which the fracture starts (see Fig. 2.21) must be determined. Eq. 2.25 for these particular data results in $\theta = 0^\circ$, and Eq. 2.24 reduces to Eq. 2.26b. The fracturing pressure now becomes

$$P_{wf} = 3 \times 90 - 94.13 - 50 = 125.9 \text{ bar.}$$

We observe that the fracturing pressure decreases with increased borehole inclination. This is a general trend. However, for anisotropic stress states, this behavior may differ.

2.3.3 Borehole Collapse. While fracturing occurs at high borehole pressures, collapse is a phenomenon associated with low borehole pressures. This can be seen from Eq. 2.21b. At low borehole pressures, the tangential stress becomes large. Since there now is a considerable stress contrast between the radial and the tangential stress, a considerable shear stress arises. If a critical stress level is exceeded, the borehole will collapse in shear.

The maximum principal stress (from Eq. 2.21b) is dominated by the tangential stress and is given by

$$\sigma_1 = \frac{1}{2}(\sigma_\theta + \sigma_z) + \frac{1}{2}\sqrt{(\sigma_\theta - \sigma_z)^2 + 4\tau_{\theta z}^2}, \quad \dots \dots \dots (2.28)$$

and the minimum principal stress (from Eq. 2.21b) is given by

$$\sigma_3 = P_w. \quad \dots \dots \dots (2.29)$$

Differentiating the maximum principal stress equation, Eq. 2.28, we can determine the position on the borehole wall at which the collapse will occur. This is complicated because there are many implicit functions in

Eq. 2.28. For the case above with vanishing shear stresses, it turns out that the collapse position on the borehole wall is 90° from the position of fracture initiation. Invoking this angle into Eq. 2.28, the collapse stress is obtained.

If symmetric conditions exist, all shear stress components may vanish. In these cases, the collapse failure may take place at one of the following conditions: $\sigma_H = \sigma_h$, $\varphi = 0^\circ$, $\alpha = 0^\circ$ or 90° . Inserting these conditions into Eq. 2.26, the borehole pressure causing highest tangential stress is

$$\sigma_1 = 3\sigma_y - \sigma_x - P_w \quad \text{for} \quad \sigma_x < \sigma_y \text{ and } \theta = 0^\circ, \dots\dots\dots (2.30a)$$

$$\sigma_1 = 3\sigma_x - \sigma_y - P_w \quad \text{for} \quad \sigma_y < \sigma_x \text{ and } \theta = 90^\circ, \dots\dots\dots (2.30b)$$

or, in general,

$$\sigma_1 = 3\sigma_{\max} - \sigma_{\min} - P_w, \dots\dots\dots (2.31)$$

These equations simply say that borehole collapse will initiate in the direction of the minimum horizontal in-situ stress. Eq. 2.31 is strictly valid if the borehole direction is aligned with the in-situ stress direction.

Having obtained expressions for the maximum and the minimum principal stress, a failure model must be defined. An example will demonstrate the application.

Example 2.12—Collapse Pressure vs. Inclination. Compute the critical pressure that will cause mechanical borehole collapse for the well given in Example 2.4. The remaining data are cohesive strength $\tau_0 = 60$ bar, and angle of internal friction $\phi = 30^\circ$.

Solution. We will use the Mohr-Coulomb model of Eq. 2.9. From Example 2.4, the transformed in-situ stresses become

$$\sigma_x = 94.13 \text{ bar}$$

$$\sigma_y = 90 \text{ bar}$$

$$\sigma_z = 95.87 \text{ bar}$$

$$\tau_{xz} = 4.92 \text{ bar}$$

$$\tau_{yz} = \tau_{xy} = 0$$

$$P_o = 50 \text{ bar}$$

Comparing these data with the equations above, we see that the maximum principal stress is defined by Eq. 2.30b:

$$\sigma_1 = 3 \times 94.13 - 90 - P_w = 192.39 - P_w.$$

The minimum principal stress is equal to the borehole pressure.

The failure model is defined by Eqs. 2.9 and 2.10, which become

$$\tau = \frac{1}{2}(\sigma'_1 - \sigma'_3) \cos \varphi = \tau_0 + \left[\frac{1}{2}(\sigma'_1 + \sigma'_3) - \frac{1}{2}(\sigma'_1 - \sigma'_3) \sin \varphi \right] \tan \varphi.$$

Inserting the numbers above, the critical collapse pressure is found from

$$\tau = \frac{1}{2}(192.39 - 2P_w) \cos 30^\circ = 60 + \left[\frac{1}{2}(92.39) - \frac{1}{2}(192.39 - 2P_w) \sin 30^\circ \right] \tan 30^\circ,$$

or

$$P_{wc} = 21.14 \text{ bar}.$$

Example 2.12 demonstrates the calculation method for borehole collapse. However, the student should evaluate the physical significance of the result. The critical collapse pressure above is lower than the pore pressure. In reality, an inward flow would occur, for example, during underbalanced drilling. The calculation method above is valid only if the collapse (or well) pressure is higher than the pore pressure, or if the rock is impermeable.

When the borehole pressure is lower than the pore pressure, and we have a permeable formation, flow occurs from the formation into the borehole. This means that the pore pressure at the borehole wall is equal to the borehole pressure. Inserting this condition ($P_o = P_w$) into the principal stress equations, the result is

$$\sigma'_1 = 3 \times 94.13 - 90 - P_w - P_w = 192.39 - 2P_w$$

$$\sigma'_3 = P_w - P_w = 0$$

The failure model defined by Eqs. 2.9 and 2.10 now becomes

$$\tau = \frac{1}{2}(192.39 - 2P_w)\cos 30^\circ = 60 + \left[\frac{1}{2}(92.39) - \frac{1}{2}(192.39 - 2P_w)\sin 30^\circ \right] \tan 30^\circ,$$

The numerical solution to this equation is a negative pressure, a clearly unrealistic solution. For practical purposes the well may at most be emptied—that is,

$$P_{wc} = 0 \text{ bar.}$$

These calculations have relevance to the emerging activities toward underbalanced drilling and sand production. An inward flow into the borehole actually stabilizes the formation because the pore pressure is reduced locally.

2.4 Empirical Correlations

Many correlations have been used in the oil industry to enable the transfer of knowledge from one well to another. Some of these are just simple correlations, whereas others are based on models or physical principles. Although many correlations are still useful, others are replaced by more fundamental engineering methods that have evolved in recent years. It also should be stated that there is significant potential in exploring the geology from various aspects. Here, we will briefly discuss some of the classical correlation methods still in use.

The first factor to discuss is the drillability, which is actually a normalized rate of penetration.

2.4.1 Drillability Correlations. In its simplest form, the rate of penetration R (m/hr, ft/hr) is modeled as a function of supplied energy:

$$R = (k)(\text{WOB})(N), \dots\dots\dots (2.32)$$

where WOB is the bit force, N is the rotary speed, and the factor k represents the drillability. In a soft rock, R is high and k is high. Conversely, in a hard rock R and k are small for the same bit force and rotary speed. The drillability is actually an instant measure of the rock properties at the face of the drillbit. It is presently the only information obtained at the drillbit face during drilling.

By computing the drillability, we can create a log that tells us something about the rock; some interesting information can be obtained if we understand the relationships.

Fig. 2.22 shows an example from an underground blowout in the North Sea. The well had been flowing for a year before it was killed with a relief well. The drillabilities for the two wells were compared, and they were identical until the wells were approximately 6 m apart. The increase in drillability in the relief well is believed to be caused by a considerable underground flow over a period of 1 year. This information is important for the planning of the relief well and the target size for the relief well. Inside this region of increased drillability, the drilling assembly was homing in towards the flowing well.

Drillability also has been used to estimate pore pressures for many years. There is usually a considerable uncertainty in pore-pressure estimation; pore pressure in shales cannot be measured, but in permeable rocks like sandstones, real pressure measurements can be used to calibrate pore-pressure curves. A common method is to compute sound transit time from seismic records. During drilling, the drillability is also used as an indicator of pore pressure. Well known is the so-called d -exponent developed by Jorden and Shirley (1966); during drilling, the following parameter is computed:

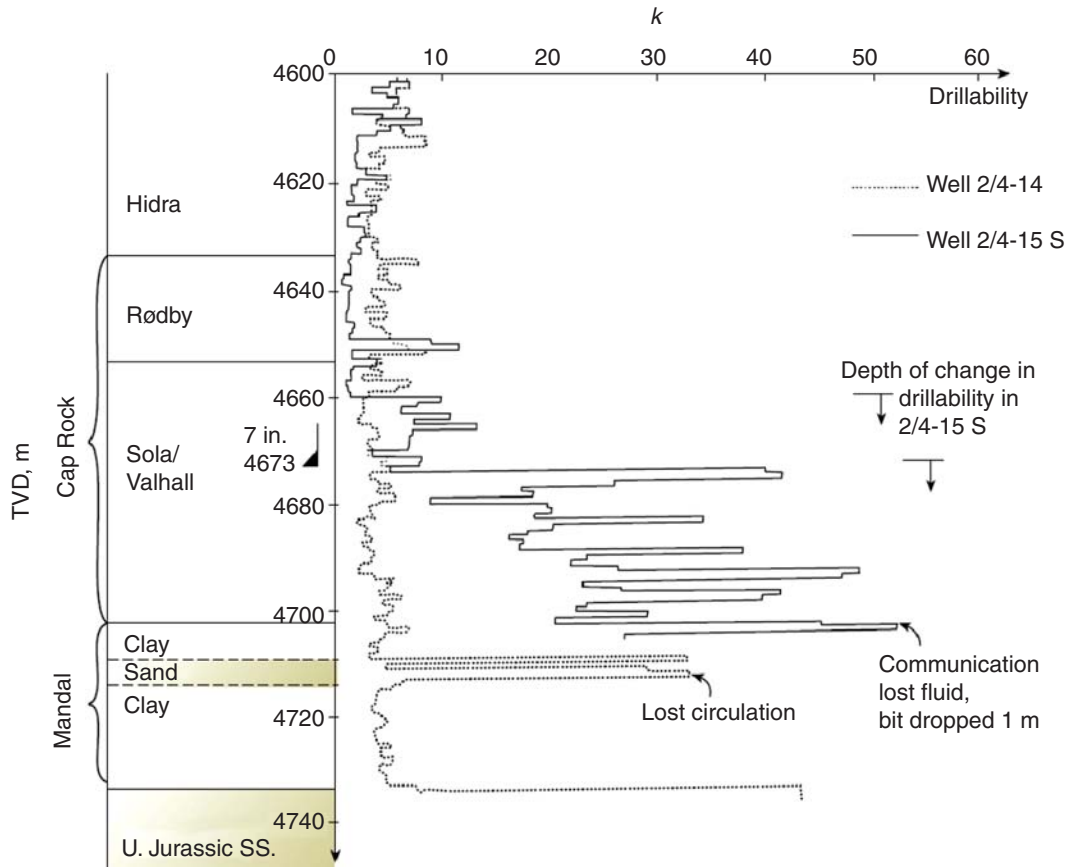


Fig. 2.22—Drillabilities for the blowing well and the relief well. From Aadnoy (2010).

$$d_{\text{exp}} = \frac{\log\left(\frac{R}{60N}\right)}{\log\left(\frac{12W}{1000d_b}\right)} \quad (2.33)$$

The parameters are the same as in Eq. 2.32, and the bit diameter is d_b (in.). A number of corrections are proposed to this equation, and it is still in use in the oil industry.

The d -exponent is actually a drillability equation in logarithmic form. If a weak rock is encountered, both drilling rate and drillability increase. Conversely, a hard rock slows down the drilling rate and causes the drillability to decrease.

During drilling, a trend line is established for the d -exponent. If this starts to deviate from the trend, it can be associated with some of the following factors:

- Bit wear. Rock bits wear gradually, and the drilling efficiency may reduce gradually; an abrupt drop in drillability may be caused by drillbit or roller cone failure.
- If drillability increases relative to the trend line, it may be a pore-pressure indicator. Reservoir rock below the caprock often has higher drillability because it is weaker and more porous.

Hareland and Hoberock (1993) developed a method to estimate the rock strength from drillability data; the result is used as input data for wellbore stability analysis.

The concept of drillability has been used to a small extent in drilling. For the foreseeable future, there is considerable potential for further applications of drillability; drilling optimization is one such area.

2.4.2 Fracture Pressure Correlations. In order to predict fracture pressures and pore pressures, a number of correlations have been derived over the years. Although some of these are valid for the places in which they

were derived, a number of correlations based on various physical assumptions have been seen to have a more general applicability; many of these have been developed in the Gulf of Mexico region. It is interesting to see how understanding of the fracture problem gradually evolved.

Hubbert and Willis (1957) developed a very useful correlation; they assumed that the horizontal stress in a relaxed basin should be one-third to one-half of the overburden stress. Although we today know that this value is too low, their correlation is still effective. Matthew and Kelly (1967) modified this model by introducing a “matrix stress coefficient,” which implied that the stress ratios were not constant with depth. Pennebaker (1968) related the overburden gradient to geologic age and established “effective stress ratio” relationships. Pennebaker also correctly found that the fracture gradient is related to the overburden stress gradient.

Eaton (1969) introduced the Poisson effect by defining the horizontal stress as a result of the overburden stress. The correlation coefficient for this case was actually Poisson’s ratio. Finally, Christman (1973) extended this work to an offshore environment.

At first glance, the five methods listed above look different; however, Pilkington (1978) compared these methods and found that they were very similar. By introducing the same correlation coefficient, all five models can be defined by the following equation:

$$P_{wf} = K(\sigma_v - P_o) + P_o \quad (2.34)$$

Pilkington also used field data and showed that Eq. 2.34 basically gave the same result as each of the five models. Most of these models were developed in the Texas-Louisiana area, where they still may serve; however, in the early 1980s, wellbore inclination increased, and because the empirical correlations could not handle this, continuum mechanics was introduced. In addition to handling the directions of inclined wells it also opened up for various stress states. Any relaxed or tectonic setting can now be handled by using classical mechanics.

2.4.3 Pore-Pressure Correlations. Pore pressure is a key factor in petroleum production, and it also has a significant effect on well construction and wellbore stability. Typically, 70% of the rock we drill is shale or clay; as discussed, these rocks are usually impermeable, and it is therefore not possible to measure pore pressure—pressure measurements are made in the reservoir.

We need a pore-pressure curve to select mud weights and casing points. The pore-pressure curves inferred from many sources are used as absolute; of course, underbalanced drilling in a tight shale will not lead to a well kick. So if we could guarantee that there were no permeable stringers, we could drill the well with a mud weight below the pore pressure. Unfortunately, such a guarantee is unlikely.

From this discussion, it is clear that pore pressure from logs and other sources is not accurate unless it is calibrated (e.g., with a pressure measurement). This is usually not the case, so pore-pressure curves in general have significant uncertainty.

In many cases, correlations serve well as predictive tools for new wells. Consistency is important here; if, for example, Eq. 2.34 is used to establish a correlation, the same equation should be used to develop predictions for new wells. One should be careful when mixing various correlations because the results may not be representative for the actual wells.

For further work on pore-pressure estimation, the reader is referred to the literature on petrophysical interpretation.

Problems

2.1 In-Situ Stresses

Given leakoff data from three wells (see **Table P-1**), determine the following:

TABLE P-1—LEAKOFF DATA					
Data set	Leakoff (SG)	Pore pressure (SG)	Overburden (SG)	Depth (m)	Inclination (degrees)
1	1.51	1.03	1.62	890	0
2	1.35	1.21	1.76	1124	30
3	1.27	1.30	1.80	1540	39

TABLE P-2—EFFECTS OF INCREASED MUD WEIGHT

Effect	Advantage	Debatable	Disadvantage
Reduced borehole collapse	<input type="checkbox"/>	<input type="checkbox"/>	<input type="checkbox"/>
Reduced fill	<input type="checkbox"/>	<input type="checkbox"/>	<input type="checkbox"/>
Poor pore pressure estimation	<input type="checkbox"/>	<input type="checkbox"/>	<input type="checkbox"/>
Increased lost circulation	<input type="checkbox"/>	<input type="checkbox"/>	<input type="checkbox"/>
Reduced washout	<input type="checkbox"/>	<input type="checkbox"/>	<input type="checkbox"/>
Expensive mud	<input type="checkbox"/>	<input type="checkbox"/>	<input type="checkbox"/>
Increased differential sticking	<input type="checkbox"/>	<input type="checkbox"/>	<input type="checkbox"/>
Reduced pressure variations	<input type="checkbox"/>	<input type="checkbox"/>	<input type="checkbox"/>
Reduced drilling rate	<input type="checkbox"/>	<input type="checkbox"/>	<input type="checkbox"/>
Reduced tight hole	<input type="checkbox"/>	<input type="checkbox"/>	<input type="checkbox"/>
Reduced clay swelling	<input type="checkbox"/>	<input type="checkbox"/>	<input type="checkbox"/>

- For the two last wells, compute the expected leakoff pressures as if they were vertical. Please state assumptions.
- Estimate the in-situ stress state based on the LOT values. Please state all assumptions.
- Plot a curve that defines the fracture pressure for a vertical and a horizontal well over the depth interval.

2.2 Pore Pressure

In the planning of a new well, the geologist identifies a significant uncertainty in the estimation of the pore pressure profile. The following data were used:

Depth: 1800 m
 Estimated pore pressure: 1.23 SG
 Reservoir interval: 1800–2000 m

- Determine the density of the oil in the reservoir. Assume waterdrive. What is the expected pore pressure gradient at the bottom of the reservoir?
- After many discussions with colleagues, the geologist decides that the reservoir section most probably covers the interval 1800–2100 m. Assume the same oil density, and compute the pressure gradients at the top and bottom of the reservoir now.
- Where would you perforate your production casing? When water breakthrough occurs after some time of production, a workover is called for. Where would you perforate now?

2.3 Mud Weight Limits

- Define the two classical limits for the mud weight. What are the failure mechanisms?
- Using a simple fracturing equation, define a mud-weight selection criterion. What is this criterion called?
- Define two advantages of using this criterion. Also, define two concerns.

2.4 Selection of Optimal Mud Weight

Assume that we use low mud weight. If we increase the mud weight, determine if the following effects of higher mud weight constitute an advantage or a disadvantage. If the effect is debatable, explain why.

2.5 Establishing a Fracture Prognosis

We are planning a new exploration well, and have no reference information.

- Make an overburden stress gradient curve assuming that the bulk density of the rock is 2.0 SG. Plot to 2000 m depth. Also, plot the pore pressure gradient curve assuming normal pore pressure to 1000 m and a linear increase to 1.3 SG at 2000 m.
- An LOT of 1.8 SG is obtained at a depth of 1500 m. Determine the horizontal in-situ stress in the rock.

2.6 Borehole Stability

The following data apply for a well:

Overburden stress: 110 bar
 Horizontal stresses: 100 bar

Pore pressure:	65 bar
Well inclination:	60°
Well azimuth.:	75° clockwise from North
Rock cohesive strength:	30 bar
Rock frictional angle:	30°

- Determine the fracturing pressure for a vertical well and for the well given above.
- Determine the critical collapse pressure for a vertical well and for the well given above.

It is decided that a well should be drilled underbalanced through the reservoir. The objective is to minimize particle invasion and skin effects. The drilling rig is equipped with a rotating blowout preventer for this purpose. The new condition is that the borehole pressure matches the pore pressure. This must be taken into account in the effective stress principle.

Use the same data as above, and assume that the well pressure is 40 bar during the operation.

- Determine the collapse pressure now for the (vertical) well.
- Is the underbalance reducing or increasing the collapse resistance of the borehole? Explain why.

Nomenclature

a	=	borehole radius, L, in. [cm]
g	=	gravity constant, L/t^2 , lbf/lbm [m/s^2]
P	=	pressure, $m/L-s^2$, psi [bar]
P_A	=	pressure at depth Z_A , $m/L-s^2$, psi [bar]
P_B	=	pressure at depth Z_B , $m/L-s^2$, psi [bar]
P_o	=	pore pressure, $m/L-s^2$, psi [bar]
P_w	=	borehole pressure, $m/L-s^2$, psi [bar]
P_{wc}	=	critical collapse pressure, $m/L-s^2$, psi [bar]
P_{wf}	=	fracturing pressure, $m/L-s^2$, psi [bar]
r	=	radius, L, in. [cm]
Z	=	true vertical depth, L, ft [m]
Z_A	=	true vertical depth of Point A, L, ft [m]
Z_B	=	true vertical depth of Point B, L, ft [m]
α	=	borehole azimuth, radians
β	=	shear failure direction on core plugs, radians
γ_e	=	equivalent specific gravity of the wellbore fluids, dimensionless
φ	=	borehole inclination, radians
θ	=	position on borehole wall from x axis, radians
ρ	=	density, m/L^3 , lbf/ft ³ [kg/m^3]
ρ_e	=	equivalent mud density of the wellbore fluids, m/L^3 , lbf/ft ³ [kg/m^3]
ρ_{mud}	=	mud density, m/L^3 , lbf/ft ³ [kg/m^3]
ρ_{water}	=	density of water, m/L^3 , lbf/ft ³ [kg/m^3]
σ	=	normal stress, $m/L-s^2$, psi [bar]
σ'	=	rock effective stress, $m/L-s^2$, psi [bar]
σ_h	=	minimum horizontal stress, $m/L-s^2$, psi [bar]
σ_H	=	maximum horizontal stress, $m/L-s^2$, psi [bar]
σ_{max}	=	maximum principal normal stress, $m/L-s^2$, psi [bar]
σ_{min}	=	minimum principal normal stress, $m/L-s^2$, psi [bar]
σ_r	=	radial stress, $m/L-s^2$, psi [bar]
σ'_r	=	radial effective stress, $m/L-s^2$, psi [bar]
σ_v	=	overburden stress, $m/L-s^2$, psi [bar]
σ'_v	=	overburden effective stress, $m/L-s^2$, psi [bar]
σ_x	=	normal stress, x coordinate direction, Cartesian coordinates, $m/L-s^2$, psi [bar]
σ_y	=	normal stress, y coordinate direction, Cartesian coordinates, $m/L-s^2$, psi [bar]
σ_z	=	normal stress, z coordinate direction, cylindrical coordinates, $m/L-s^2$, psi [bar]
σ_{zz}	=	normal stress, z coordinate direction, Cartesian coordinates, $m/L-s^2$, psi [bar]
σ_θ	=	tangential stress, $m/L-s^2$, psi [bar]
σ'_θ	=	tangential effective stress, $m/L-s^2$, psi [bar]

τ	=	shear stress, m/L-s ² , psi [bar]
τ_0	=	cohesive rock strength, m/L-s ² , psi [bar]
τ_{rz}	=	shear stress, r plane in the z direction, cylindrical coordinates, m/L-s ² , psi [bar]
$\tau_{r\theta}$	=	shear stress, r plane in the θ direction, cylindrical coordinates, m/L-s ² , psi [bar]
τ_{xy}	=	shear stress, x plane in the y direction, Cartesian coordinates, m/L-s ² , psi [bar]
τ_{yz}	=	shear stress, y plane in the z direction, Cartesian coordinates, m/L-s ² , psi [bar]
$\tau_{\theta z}$	=	shear stress, θ plane in the z direction, cylindrical coordinates, m/L-s ² , psi [bar]
ν	=	Poisson's ratio for the rock matrix, dimensionless
ϕ	=	angle of internal friction for rocks, radians

References

- Aadnoy, B.S. 2010. *Modern Well Design: Second Edition*. Leiden: Francis and Taylor.
- Aadnoy, B.S. 1996. *Modern Well Design*. Rotterdam, The Netherlands: A.A. Balkema.
- Aadnoy, B.S. and Chenevert, M.E. 1987. Stability of Highly Inclined Boreholes. *SPE Drill Eng* **2** (4): 364–374.
- Bradley, W.B. 1979. Failure of Inclined Boreholes. *J. of Energy Resources Technology Trans.* **102**: 232–239.
- Cook, J. and Edwards, S. 2009. Geomechanics and Wellbore Stability. In *Advanced Drilling and Well Technology*, ed. B.S. Aadnoy et al. Richardson, Texas: SPE.
- Christman, S.A. 1973. Offshore Fracture Gradients. *J. Pet. Tech* **25** (8): 910–914. SPE-4133-PA. DOI: [10.2118/4133-PA](https://doi.org/10.2118/4133-PA).
- Eaton, B.A. 1969. Fracture Gradient Prediction and Its Application in Oilfield Operations. *J. Pet. Tech.* **21** (10): 1353–1360. SPE-2163-PA. DOI: [10.2118/2163-PA](https://doi.org/10.2118/2163-PA).
- Hareland, G. and Hoberock, L.L. 1993. Use of Drilling Parameters to Predict In-Situ Stress Bounds. Paper SPE/IADC 25727 presented at the SPE/IADC Drilling Conference, Amsterdam, 22–25 February. DOI: [10.2118/25727-MS](https://doi.org/10.2118/25727-MS).
- Hubbert, M.K. and Willis, D.G. 1957. Mechanics of Hydraulic Fracturing. *Trans., AIME* **210**: 153–168. SPE-686-G.
- Jorden, J.R. and Shirley, O.J. 1966. Application of Drilling Performance Data to Overpressure Detection. *J. Pet. Tech.* **18** (11): 1387–1394. SPE-1407-PA. DOI: [10.2118/1407-PA](https://doi.org/10.2118/1407-PA).
- MacPherson, L.A. and Berry, L.N. 1972. Predictions of Fracture Gradients. *The Log Analyst* (October 1972) 12.
- Matthews, W.R. and Kelly, J. 1967. How to Predict Formation Pressure and Fracture Gradient From Electric and Sonic Logs. *Oil and Gas J.* (20 February).
- Pennebaker, E.S. 1968. An Engineering Interpretation of Seismic Data. Paper SPE 2165 presented at the SPE Annual Meeting, Houston, 29 September–2 October. DOI: [10.2118/2165-MS](https://doi.org/10.2118/2165-MS).
- Pilkington, P.E. 1978. Fracture Gradients in Tertiary Basins. *Petroleum Engineer International* (May): 138–148.
- Terzaghi, K. 1943. *Theoretical Soil Mechanics*. New York City: John Wiley.

Further Reading and Advanced Topics

- Aadnoy, B.S. and Djurhuus, J. 2009. Normalization and Inversion Methods. In *Advanced Drilling and Well Technology*, ed. B.S. Aadnoy et al. Richardson, Texas: SPE.
- Bourgoyne, A.T. Jr., Millheim, K.K., Chenevert, M.E., and Young, F.S. Jr. 1986. *Applied Drilling Engineering*. Textbook Series, SPE, Richardson, Texas **2**: 2.
- Fjaer, E., Holt, R., Raaen, A.M., Horsrud, P., and Risnes, R. 2008. *Petroleum Related Rock Mechanics*, second edition. *Developments in Petroleum Science*, 53. Amsterdam: Elsevier Science Publishers.

Page Intentionally Left Blank

Please Keep Scrolling To Continue

Chapter 3

Drilling Fluids

A.W. Eustes III, Colorado School of Mines

The purposes of this chapter are to present (1) the primary functions of the drilling fluid, (2) the test procedures used to determine whether the drilling fluid has suitable properties for performing these functions, and (3) the common additives used to obtain the desirable properties under various well conditions.

3.1 Introduction

The success of the rotary-drilling process (completion of an oil or gas well) and its cost depend substantially on three important factors:

- The bit penetrating the rock
- The cleaning the bit face and transport of the cuttings to surface
- The support of the borehole

The drilling fluid used affects all of these critical items. The drilling-fluid density and ability to penetrate rock have an effect on the rate of penetration. The hydraulic energy expended on the bottom of the hole and the viscosity and flow rate of the fluid affect the cuttings transport. And the density of the fluid and its ability to form a layer on the wellbore (wall cake) affects the wellbore stability and support. It is often said that the majority of the problems in drilling are related in some manner or another to the drilling fluid.

The drilling engineer is concerned with the selection and maintenance of the drilling fluid because of its relation to most drilling operational problems. The cost of the drilling fluid, commonly known as “drilling mud” or simply “mud,” is comparatively small as compared to the rig or casing costs; but, the selection of the proper fluid and the testing and control of its properties has considerable effect on the total well cost. The additives needed to create and maintain the fluid properties can be expensive. In addition, the penetration rate of the rotary bit and operational delays caused by circulation loss, stuck drillpipe, caving shale, and the like are significantly affected by the drilling-fluid properties. Fluid properties also profoundly influence the rig days needed to drill the total depth (TD) (Bourgoyne 1991; Darley and Gray 1988).

3.2 A Brief History of Drilling Fluids

Like many aspects of modern well construction, the first modern drilling fluid—little more than muddy water—was used at Spindletop in south Beaumont, Texas, USA to drill through unconsolidated sands (Clark and Halbouty 1980). However, the Chinese used water as a “softening” agent while drilling wells several hundred feet in depth as early 600 BCE (Darley and Gray 1988). The practice of circulating fluid while drilling was introduced and patented in England in 1845 by Robert Beart (Beart 1845).

While clay-based muds were helpful in establishing a wall cake and stabilizing unconsolidated sands, they did not provide a way to control subsurface pressures. In 1926, noted Louisiana geologist Ben K. Stroud patented a “means for controlling the flow of gas, oil and water under pressure from the well.” His “invention” was a “compound consisting of iron oxide, barium sulfate, lead concentrate, and mercury mixed in the

desired proportion and quantities according to the character of the well being bored” (Stroud 1926). Barite was soon identified as the best weighting material for drilling purposes because it is inert and comparatively nonabrasive.

The addition of high specific gravity weighting material to drilling fluid created the need for a reliable suspending agent. Bentonite was already in use in the 1920s as a cement component. Seeing its usefulness for well drilling, one manufacturer packaged and sold “Plastiwate,” 95% of which was barite, with 5% bentonite added for suspension purposes (Darley and Gray 1988). Finely ground, premium-grade Wyoming sodium bentonite is now the standard viscosifier and primary fluid-loss-control agent in most freshwater base muds. One of its key functions has not changed since 1928: promoting hole stability in poorly consolidated formations.

Approximately 85% of the barite sold in the United States is used as a weighting agent in drilling fluids. The third largest market for bentonite (behind kitty litter and foundry sand manufacturers) is the oil and gas drilling industry. The production specifications of barite, bentonite, and attapulgite (saltwater clay) for use in drilling fluids are specified by the American Petroleum Institute (API) (*API Spec. 13A*).

The early simple drilling fluids quickly gave way to increasingly “engineered” systems. To better protect the target formations, additives were developed for improved rheology and fluid-loss control, shale inhibition, and resistance to contamination. Laboratory and field-test procedures became more sophisticated as drilling-fluid companies and oil and gas operators sought correlations between surface measurements and downhole conditions. Under conditions in which bentonite and other clay additives proved inadequate, organic and synthetic polymers were substituted as viscosifiers and fluid-loss-control agents. Low-solids and solids-free polymer formulations are the basis for drill-in fluid systems, which are commonly used for drilling horizontal well production intervals.

One of the major turning points in drilling-fluids technology was the introduction of invert emulsion oil-based fluids (OBFs) in the 1960s (although true oil muds were used much earlier in California and Texas). The improvement in drilling performance, compared to that of water-based fluids, was impressive. These OBFs (typically formulated with diesel) were naturally inhibitive and enabled high rates of penetration. However, heightened concerns over environmental issues in the late 1970s led state and federal regulatory agencies to prohibit the overboard discharge of whole mud and drill cuttings offshore when diesel is in the drilling fluid (Bleier 1993). The risk of causing serious harm to fish populations together with transportation and disposal issues rising from continued use of oil- and diesel-based fluids offshore significantly curtailed their use in the Gulf of Mexico (GOM) and other offshore locations. Diesel OBFs are still commonly used in on-land drilling operations and, if disposal processes are properly monitored and carried out, are used under certain circumstances offshore.

Synthetic-based fluids (SBFs) were developed and introduced around 1990. These fluids retained the good drilling-performance characteristics of traditional OBFs, yet complied with the stringent regulations governing offshore fluid and cuttings disposal. After a decade of evolving SBF development, internal olefin- (IO) and ester-based fluids emerged as reliably “safe” drilling fluids, based on a prolonged period of testing and data collection coordinated by the Environmental Protection Agency (EPA), Minerals Management Service (MMS), API/National Offshore Industries Association (NOIA), and several drilling-fluids companies.

As drilling operations began moving into deeper water in the 1990s, typical SBF formulations were challenged by temperatures ranging from the near-freezing seabed to 400°F at TD. The development of a clay-free SBF in 2001 allowed operators to control rheological properties over this temperature range, with no sacrifice in drilling performance (Whitson and McFadyen 2001). Because of its flat rheological profile, this ester/IO-blend fluid also helped reduce deepwater risks associated with high equivalent circulating densities (ECDs) and surge pressures, particularly while running and cementing casing strings.

Underbalanced drilling increased in favorability throughout the 1990s and led to the refinement of pneumatic (air, mist, and foam) drilling methods. This type of drilling has been successful in certain mature fields, in low pressure formations, and particularly in hard, dry rock. Though these methods are not adaptable for all downhole environments and require close management of ignition and explosion risks, producing formations are not as likely to be damaged by pneumatic drilling. Less complicated completions and fewer subsequent workover operations are also among the benefits. The absence of drilling fluid eliminates the need for a mud-handling system, and disposal issues related to drilling fluid and drill cuttings are greatly reduced.

Sustained drilling in ultradeepwater locations and the emergence of energy production capabilities in extremely remote geographical locations continue to influence drilling-fluid-system design and packaging. While traditional drilling-fluid formulations are still commonly used, advanced modeling and testing tools available today make it possible to create a single “fit-for-purpose” drilling-fluid system without incurring unacceptable cost increases.

3.3 Functions of Drilling Fluids

The functions of a drilling fluid can be categorized as follows:

- Cuttings transport
 - Clean under the bit
 - Transport the cuttings up the borehole
 - Release the cuttings at the surface without losing other beneficial materials
 - Hold cuttings and weighting materials when circulation is interrupted
- Physicochemical functions
- Cooling and lubricating the rotating bit and drill string
- Fluid-loss control
 - Wall the newly drilled wellbore with an impermeable cake for borehole support
 - Reduce adverse and damaging effects on the formation around the wellbore
- Control subsurface pressure
- Support part of the drillstring and casing weight
- Ensure maximum logging information
- Transmit hydraulic horsepower to the rotating bit (Magcobar 1972)

3.3.1 Cuttings Transport. The drilling fluid should be able to remove rock fragments or cuttings from beneath the drilling bit, transport them up the wellbore drillstring annulus, and permit their separation at the surface using solids-control equipment. The density and viscosity of the drilling fluid are the properties that control the process of lifting particles that fall down through the flowing fluid by the effect of gravity. The fluid must also have the ability to form a gel-like structure to hold cuttings and weighting materials when circulation is interrupted.

Horizontal and high-angle wells require specialized fluid formulations and “sweep” protocols to minimize the risk of barite sag (in which the barite slurry separates downhole) and of low-side cuttings settling, both of which can lead to stuck pipe and loss of the well. The lubricity of the drilling fluid is also a key factor in controlling torque and drag in these types of operations.

3.3.2 Physicochemical Functions. The drilling-fluid system should remain stable when exposed to contaminants and hostile downhole conditions. Among the common natural contaminants are reactive drill solids, corrosive acid gases (e.g., H_2S), saltwater flows, and evaporites (e.g., gypsum). The cement used in setting casing and liner strings is also a contaminant to some water-based muds. Wells in certain areas have extremely high bottomhole temperatures, at times approaching 500°F, and, likewise, arctic locations may expose the drilling fluid to subzero temperatures at surface.

3.3.3 Cooling and Lubricating the Rotating Bit and Drillstring . The drilling mud cools and lubricates when the rotating bit drills into the bottom of the hole and when the drillstring rotates against the wellbore walls. The fluid should have the ability to absorb the heat generated by the friction between metallic surfaces and formation. In addition, the fluid should not adversely affect the bit life nor increase the torque and drag between the drillstring and the borehole.

3.3.4 Fluid-Loss Control. The bit removes lateral support of the drilled wellbore and is immediately replaced by the drilling fluid until the casing is set with cement. The stability of uncased sections of the borehole is achieved by a thin, low-permeability filter cake formed by the mud on the walls of the hole. Also, the cake seals pores and other openings in formations caused by the bit, thereby minimizing liquid loss into permeable formations.

Poor fluid-loss control can cause surge (an increase in wellbore pressure under a bit from running into the hole), swab (a decrease in wellbore pressure under a bit from running out of the hole), and circulation-pressure problems (known as ECD). Loss of circulation increases the drilling-fluid cost and the potential for the inflow of fluids (gas, oil, or water) from formations. High viscosity and high gel strength may cause excessive pressure in the borehole, as well.

The drilling fluid should not negatively affect the production of the fluid-bearing formation. That is, the drilling mud is designed to reduce adverse effects on formation around the wellbore. In contrast, the fluid must assist in the collection and interpretation of electrical-log information.

3.3.5 Control Subsurface Pressure. A drilling fluid is the first line of defense against well-control problems. The drilling fluid balances or overcomes formation pressures in the wellbore. Typically, this is accomplished with

weighting agents such as barite, although there are other chemicals that can be used. In addition, surface pressure can be exerted to give the equivalent pressure needed to balance a formation pressure.

An overbalanced condition occurs when the drilling fluid exerts a higher pressure than the formation pressure. An underbalanced condition occurs when the drilling fluid exerts a lower pressure than the formation pressure. Therefore, in underbalanced drilling operations, the borehole is deliberately drilled with a fluid/pressure combination lower than the formation pressure. A balanced condition exists if the pressure exerted in the wellbore is equal to the formation pressure.

3.3.6 Help Support the Drillstring and Casing Weight. Any time a material is submerged in a fluid in a gravitational field, there is a reaction that offsets the force that gravity exerts. This is often called buoyancy, although there are a lot of misconceptions related to this term. Nonetheless, in heavily weighted situations, this “buoyancy force” can assist by offsetting some of the weight of a drillstring or casing. This offset is dependent upon the density of the fluid, with higher-density fluids giving more of an offset and lower density “fluids” (e.g., air) not helping much, if at all.

3.3.7 Ensure Maximum Logging Information. The drilling fluid has a profound impact on the electrical and acoustical properties of a rock. Because these properties are what logging tools measure, it is imperative that the correct selection of wireline logging tool or logging-while-drilling (LWD) tool for a given drilling fluid be made. Or, lacking that, then the correct drilling fluid must be used for a given logging tool. In addition, the drilling fluid should facilitate retrieval of information by means of cuttings analysis.

3.3.8 Transmit Hydraulic Horsepower to the Rotating Bit. The hydraulic force is transmitted to the rotating bit when the fluid is ejected through the bit nozzles at a very high velocity. This force moves the rock fragments or cuttings away from the drilled formation beneath the bit. In directional-drilling operations, the hydraulic force powers the downhole hydraulic motor and turns electric-power generators (turbines) for measurement-while-drilling (MWD) and LWD drillstring equipment.

3.4 Drilling-Fluid Categories

According to the *World Oil* annual classification of fluid systems, there are nine distinct categories of drilling fluids in use today (World Oil 2002). Five categories include freshwater systems, one category covers saltwater systems, two categories include oil- or synthetic-based systems, and the last category covers pneumatic (air, mist, foam, gas) “fluid” systems. In the following text, these fluids will be discussed in detail.

3.4.1 Classification of Drilling Fluids. The principal factors governing the selection of type (or types) of drilling fluids to be used on a particular well are

- The characteristics and properties of the formation to be drilled
- The quality and source of the water to be used in building the fluid
- The ecological and environmental considerations

Continuous-Phase Classification. Drilling fluids are categorized according to their *continuous* phase so that there are

- Water-based fluids
- OBFs
- Pneumatic (gas) fluids

Consider a drop of a drilling fluid. If one could go from a point in one phase to any other point in that same phase, then it is said to be continuous. If one had to cross one phase to get back to the previous phase, then that phase is discontinuous. Solids are always a discontinuous phase. Therefore, drilling fluids are designated by their continuous phase.

Water-based drilling muds are the most commonly used fluids, while oil-based muds are more expensive and require more environmental considerations. The use of pneumatic drilling fluids (i.e., air, gas, and foam) is limited to depleted zones or areas where the formations are low pressured (although with underbalanced-drilling equipment, higher pressured zones can now be drilled without the need of pneumatic drilling fluids). In water-based fluids, the solid particles are suspended in water or brine, while in oil-based muds the particles are suspended in oil. When pneumatic drilling fluids are used, the rock fragments or drill cuttings are removed by a high-velocity stream of air or natural gas. Foaming agents are added to remove minor inflows of water (Darley and Gray 1988).

Water-Based Fluids. The majority of wells are drilled with water-based drilling fluids. The base fluid may be fresh water, saltwater, brine, or saturated brine. A typical water-based mud composition is illustrated in **Fig. 3.1**.

Water-based drilling fluids range from native muds to lightly treated fluids to the more heavily treated, inhibitive fluids. They are divided into three major subclassifications:

- Inhibitive
- Noninhibitive
- Polymer

Inhibitive fluids retard clay swelling (i.e., the ability of active clays to hydrate is greatly reduced). For this reason, inhibitive fluids are used for drilling hydratable-clay zones. The ability of the formation to absorb water is not inhibited when noninhibitive fluids are used. The term noninhibitive refers to the lack or absence of those specific ions (sodium, calcium, and potassium) that are present in inhibitive fluids. Inhibitive fluid systems do not use chemical dispersants (thinners) or inhibitive ions, but native waters. Polymer fluids may be inhibitive or noninhibitive depending upon whether an inhibitive cation is used.

Saltwater Drilling Fluids. Saltwater drilling fluids are used for shale inhibition and for drilling salt formations. They are also known to inhibit hydrates (ice-like formations of gas and water) from forming, which can accumulate around subsea wellheads and well-control equipment, blocking lines and impeding critical operations.

Inhibitive Drilling Fluids. Inhibitive drilling fluids are designed to reduce chemical reactions between the drilling fluid and the formation. Fluid formulations containing sodium, calcium, and/or potassium ions minimize shale hydration and swelling. Gypsum (“gyp”) drilling fluids are used for drilling anhydrite and gypsum formations. In known H_2S environments, a high pH water-based fluid treated with scavengers, or an OBF with 4–6 ppb of excess lime, usually is the recommended drilling-fluid system.

Incorporating up to 10% oil in a water-based fluid to improve lubricity and inhibition was a long-standing drilling practice; however, the availability of glycol additives and high performance SBFs makes oil additions unnecessary. Furthermore, disposal of water-based fluids containing a measurable percentage of oil is closely regulated.

Organic and Synthetic Polymers. Organic and synthetic polymers are used to provide viscosity, fluid-loss control, shale inhibition, and prevention of clay dispersion in freshwater- or saltwater-based drilling fluids. Most polymers are very effective even at low concentrations and can be run by themselves or added in small quantities to enhance or extend bentonite performance. Specially developed high-temperature polymers are available to help overcome gelation issues.

Polymers function in several ways. Some polymers actually hydrate and swell in much the same manner as conventional clay materials. By doing this they thicken the water phase, making the escape of this water into the formation or into the clay structure more difficult, thereby preventing swelling. Large, high molecular-weight polymers will bond onto clay surfaces and literally surround and isolate the clay/shale particle. This is referred to as encapsulation.

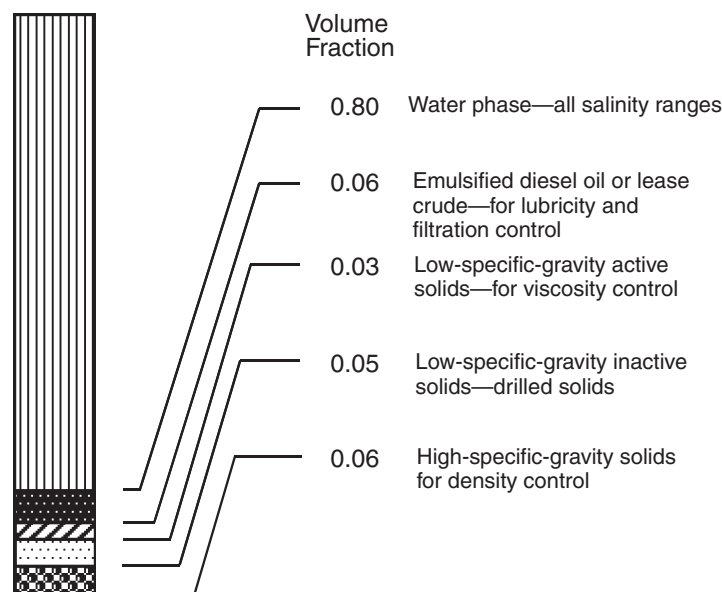


Fig. 3.1—Composition of 11-lbm/gal water-based mud (Bourgoyne et al. 1991).

Smaller polymers with low molecular weight will attach to exposed broken-edge bond sites and block the intrusion of hydrating water from the continuous phase. Free water can still bond to exposed surfaces, but the interior regions of the clays will not be wetted or expanded.

A recently developed inhibitive polymer system relies on nonionic materials that behave in much the same way as inhibitive water-based muds, because of hydrogen bonding. The advantage of this system is the ability to maintain a moderate concentration without raising the viscosity to undesirable levels. Excess polymeric material remains available to handle freshly drilled solids.

Membrane-Efficient Water-Based Drilling Fluids. Wellbore instability predominantly occurs in shales that overlay reservoirs and is an industrywide problem that affects exploration through to development drilling. Shales are fine-grained with high clay content, low permeability, and are chemically reactive with incompatible drilling fluids. The significant drilling fluid/shale interaction mechanisms are hydraulic or mud-pressure penetration, chemical potential, and swelling/hydration stresses.

When drilling with improperly designed drilling fluids, shales without effective osmotic membranes progressively imbibe water, which leads to mud-pressure penetration. Consequently, the net radial mud support changes over a period of time and near-wellbore formation pore pressure increases. This reduces formation strength and leads to borehole instability.

Past efforts to develop improved water-based fluids for shale drilling have been hampered by a limited understanding of the drilling fluid/shale interaction phenomenon. Recent studies of fluid/shale interactions have produced new insights into the underlying causes of borehole instability, and these studies suggest new and innovative approaches to the design of water-based drilling fluids for drilling shales (Tare 2002).

In most cases, the two most relevant mechanisms for water transport into and out of shale are the hydraulic-pressure difference between the wellbore pressure (drilling-fluid density) and the shale pore pressure; and the chemical potential difference (i.e., the water activity) between the drilling fluid and the shale.

The fine pore size and negative charge of clay on pore surfaces cause argillaceous materials to exhibit membrane behavior. The efficiency is a measure of the capacity of the membrane to sustain osmotic pressure between the drilling fluid and shale formation.

If the water activity of the drilling fluid is lower than the formation water activity, an osmotic outflow of pore fluid from the formation, because of the chemical potential mechanism, will lessen the increase in pore pressure resulting from mud-pressure penetration. If the osmotic outflow is greater than the inflow as a result of mud-pressure penetration, there will be a net flow of water out of the formation into the wellbore. This will result in the lowering of the pore fluid pressure below the in-situ value. The associated increase in the effective mud support will lead to an improvement in the stability of the wellbore.

One of the key parameters that can be manipulated to increase the osmotic outflow is membrane efficiency. The osmotic outflow increases with increasing membrane efficiency. In most conventional water-based fluids, the membrane efficiency is low. Therefore, even if the water activity of the drilling fluid is maintained significantly lower (with a high salt concentration) than the shale-water activity, the osmotic outflow may be negligible because of the low membrane efficiency.

As a result of extensive testing, three new generations of water-based drilling fluid systems with high membrane efficiencies (greater than 80%) have been developed, including a 12% NaCl system that generated a membrane efficiency of approximately 85%. Such systems hold promise for operations where OBFs and SBFs are unsuitable or prohibited because of drilling conditions and/or regulations.

OBFs. Normally, the high salinity water phase of an invert emulsion or SBF helps stabilize reactive shale and prevent swelling. However, drilling fluids formulated with diesel- or synthetic-based oil and no water phase are used to drill long shale intervals where the salinity of the formation water is highly variable. By eliminating the water phase altogether, the all-oil drilling fluid preserves shale stability throughout the interval. These drilling-fluid systems are commonly used in eastern Venezuela to drill the Caripita shale, which may be up to 10,000 ft thick.

Diesel and mineral oil OBFs—also called “invert emulsions”—are inhibitive, resistant to contaminants, stable at high temperatures and pressures, lubricious, and noncorrosive. A typical oil-based-mud composition is illustrated in **Fig. 3.2**. Onshore, they are the fluids of choice for drilling troublesome shale sections, extended-reach wells that would be otherwise prone to pipe-sticking problems, and dangerous HP/HT H_2S wells. The drilling efficiency of an OBF system can save days, perhaps weeks, on the time required to drill the well.

These fluid systems are also subject to stringent disposal regulations because of their toxicity. Mineral-oil formulations are considered less toxic than diesel-based fluids, but not a suitable alternative where “greener” SBFs are available. The use of diesel- or mineral-oil-based fluids is absolutely prohibited in some areas.

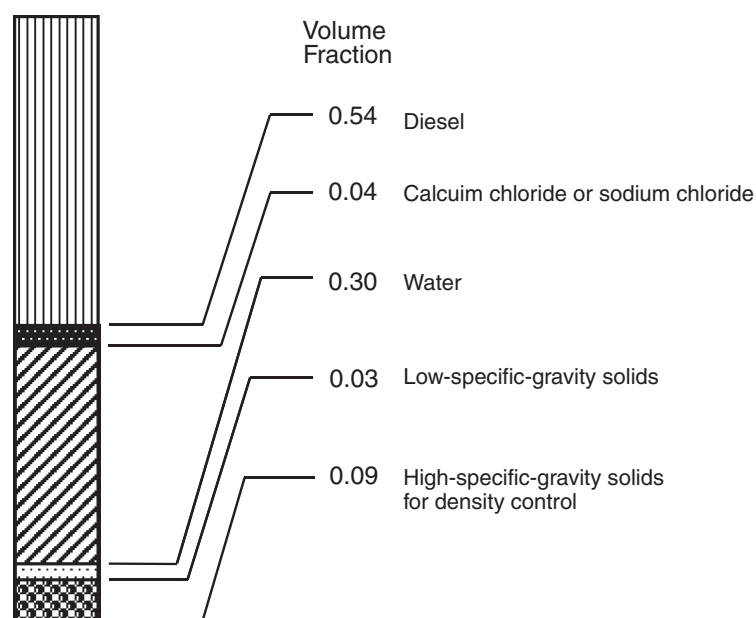


Fig. 3.2—Composition of 11-lbm/gal oil-based mud (Bourgoyne et al. 1991).

The oil/water ratios typically range from 90:10 to 60:40, though both oil and water percentages can be increased beyond these ranges. Generally, the higher the percentage of water, the thicker the drilling fluid. High salinity levels in the water phase dehydrate and harden reactive shales by imposing osmotic pressures.

The basic components of an invert-emulsion fluid include diesel or mineral oil, brine (usually calcium chloride), emulsifiers, oil-wetting agents, organophilic clay, filtration-control additives, and slaked lime. Relaxed OBFs are formulated without filtration-control additives and have a loose emulsion.

The primary emulsifiers are calcium-based soaps. Secondary emulsifiers enhance temperature stability and are tall oils. In order to make the clays and lignites oil soluble, a tallow derivative is grafted onto them. The tallow derivative is primarily responsible for extremely high viscosities at low temperatures, making traditional invert-emulsion muds unsuitable for deepwater applications.

SBFs. Synthetic-based drilling fluids were developed to provide the highly regarded drilling-performance characteristics of conventional OBFs while significantly reducing the toxicity of the base fluid. Consequently, SBFs are used almost universally offshore and they continue to meet the increasingly rigorous toxicity standards imposed by regulatory agencies.

The cost-per-barrel for an SBF is considerably higher than that of an equivalent-density water-based fluid, but because synthetics facilitate high ROPs and minimize wellbore-instability problems, the overall well-construction costs are generally less, unless there is a catastrophic lost-circulation occurrence.

Emulsion-Based Drilling Fluids (EBFs). In early 2002, an SBF formulated with an ester/IO blend became widely used, especially in deepwater operations where temperatures range from 40 to 350°F on a given well. The fluid contains no commercial clays or treated lignites; rheological and fluid-loss-control properties are maintained with specially designed fatty acids and surfactants. The system provides stable viscosity and flat rheological properties over a wide range of temperatures.

Gel strengths develop quickly, but are extremely shear-sensitive. As a result, pressures related to breaking circulation, tripping or running casing, cementing, and ECD are significantly lower than pressures that occur with conventional invert emulsion fluids. Lost circulation incidents appear to occur less frequently and with a lesser degree of severity where EBFs are used.

The EBF performs well from an environmental perspective and has met or surpassed stringent oil-retained-on-cuttings regulations governing cuttings discharge in the GOM. The EBF is highly water- and solids-tolerant and responds rapidly to treatment.

Pneumatic Drilling Fluids. Pneumatic drilling fluids are most commonly used in dry, hard formations such as limestone or dolomite. In pneumatic drilling-fluid systems, air compressors circulate air through the drillstring and up the annulus to a rotating head. The return “fluid” is then diverted by the rotating head to a flowline leading some distance from the rig to protect personnel from the risk of explosion. Gas from a pressured natural gas

source nearby may be substituted for air. Both air and gas drilling are subject to downhole ignition and explosion risks. Sometimes, nitrogen—either from cryogenic sources or generated using membrane systems—is substituted for the pneumatic fluid. Pneumatic drilling fluids are considered to be nondamaging to productive formations.

Silicate-Based Drilling Fluids. Field applications of sodium silicate drilling fluids indicate that they appear to provide a sealing effect within shale pore throats and may also increase membrane efficiency (the mobility of solutes through a shale pore network) (Mody 1993). Contact with calcium or magnesium ions, or the decrease in pH caused by dilution of fluid filtrate with pore fluid, may cause the electrolytes to precipitate (Bland 2002). Shale permeability is therefore reduced. However, the excellent shale inhibition characteristics of silicate drilling-fluid systems may be outweighed by other perceived deficiencies in lubricity, thermal stability, and the necessity for a high pH.

Typically, the silicate-based fluid system creates a physical membrane, which, in conjunction with the soluble sodium silicate or potassium silicate, provides primary shale inhibition. The wellbore becomes pressure-isolated so that filtrate invasion is minimal. Polyglycols may provide secondary inhibition, improve lubricity and filtration control, and stabilize the drilling fluid's physical properties. Polyglycols can withstand the high pH environment of silicate fluids better than conventional lubricants that may hydrolyze at high pH.

Silicate-based fluids have been used successfully in drilling highly reactive gumbo clays in the top hole interval and as an alternative inhibitive fluid in areas where invert-emulsion fluids are prohibited. They may also be useful for drilling highly dispersible formations such as chalk and have been used to stabilize unconsolidated sands.

3.4.2 Drilling Fluid Additives. Water-based drilling fluids consist of a mixture of solids, liquids, and chemicals, with water being the continuous phase. Solids may be active or inactive. The active (hydrophilic) solids such as hydratable clays react with the water phase, dissolving chemicals and making the mud viscous. The inert (hydrophobic) solids such as sand and shale do not react with the water and chemicals to any significant degree. Basically, the inert solids, which vary in specific gravity, make it difficult to analyze and control the solids in the drilling fluid (i.e., inert solids produce undesirable effects).

Broad classes of water-based drilling-fluid additives are in use today. Clays, polymers, weighting agents, fluid-loss-control additives, dispersants or thinners, inorganic chemicals, lost-circulation materials, and surfactants are the most common types of additives used in water-based muds. Clays and polymers were discussed in Section 3.4.1.

Weighting Agents. The most important weighting additive in drilling fluids is barium sulfate (BaSO_4). Barite is a dense mineral comprising barium sulfate. The specific gravity of barite is at least 4.20 g/cm³ to meet API specifications for producing mud densities from 9 to 19 lbm/gal. However, a variety of materials have been used as weighting agents for drilling fluids including siderite (3.08 g/cm³), calcium carbonate (2.7–2.8 g/cm³), hematite (5.05 g/cm³), ilmenite (4.6 g/cm³), and galena (7.5 g/cm³).

Fluid-Loss-Control Additives. Clays, dispersants, and polymers such as starch are widely used as fluid-loss-control additives. Sodium montmorillonite (bentonite) is the primary fluid-loss-control additive in most water-based drilling fluids. The colloidal-sized sodium-bentonite particles are very thin and sheetlike or platelike with a large surface area, and they form a compressible filter cake. Inhibitive mud systems inhibit the hydration of bentonite and greatly diminish its effectiveness. Therefore, bentonite should be prehydrated in fresh water before being added to these systems. The larger and thicker particles of sodium montmorillonite do not exhibit the same fluid-loss-control characteristics.

Thinners or Dispersants. Although the original purpose in applying certain substances called thinners was to reduce flow resistance and gel development (related to viscosity reduction), the modern use of dispersants or thinners is to improve fluid-loss control and reduce filter cake thickness. The term dispersant is frequently used incorrectly to refer to deflocculants. Dispersants are chemical materials that reduce the tendency of the mud to coagulate into a mass of particles or “floc cells” (i.e., the thickening of the drilling mud resulting from edge-to-edge and edge-to-face association of clay platelets). In addition, some dispersants contribute to fluid-loss control by plugging or bridging tiny openings in the filter cake. For this reason, some dispersants such as lignosulfonate (a highly anionic polymer) are more effective than others as fluid-loss reducers (IMCO 1981).

Quebracho is a type of tannin that is extracted from certain hardwood trees and used as a mud thinner. It also can be added to mud to counteract cement contamination. High pH is required for quebracho to dissolve readily in cold water. Therefore, quebracho should be added with caustic soda in equal proportions by weight of 1 part of caustic soda to 5 parts quebracho. Concentration of quebracho varies between 0.5 and 2 lbm/bbl. Safety considerations for mixing these fluids (or any fluid and solid) must be observed.

Lost-Circulation Materials. In mud parlance, losses of whole drilling fluid to subsurface formation are called lost circulation. Circulation in a drilling well can be lost into highly permeable sandstones, natural or induced formation fractures, and cavernous zones; such a loss is generally induced by excessive drilling-fluid pressures. Drilling mud flowing into the formation implies a lack of mud returning to the surface after being pumped down a well.

An immense diversity of lost-circulation materials have been used. Commonly used materials include:

- Fibrous materials such as wood fiber, cotton fiber, mineral fiber, shredded automobile tires, ground-up currency, and paper pulp
- Granular material such as nutshell (fine, medium, and coarse), calcium carbonate (fine, medium, and coarse), expanded perlite, marble, formica, and cottonseed hulls
- Flakelike materials such as mica flakes, shredded cellophane, and pieces of plastic laminate

Darley and Gray (1988) include an additional group of lost-circulation materials—slurries. Hydraulic cement, diesel oil-bentonite-mud mixes, and high-filter-loss drilling muds harden (increase strength) with time after placement.

Surfactants or Surface-Active Agents. A surface-active agent is a soluble organic compound that concentrates on the surface boundary between two dissimilar substances and diminishes the surface tension between them. The molecular structure of surfactants is made of dissimilar groups having opposing solubility tendencies such as hydrophobic and hydrophilic. They are commonly used in the oil industry as additives to water-based drilling fluid to change the colloidal state of the clay from that of complete dispersion to one of controlled flocculation. They may be cationic (dissociating into a large organic cation and a simple inorganic anion), anionic (dissociating into a large organic anion and a simple inorganic cation), or nonionic (long chains of polymer that do not dissociate) (Darley and Gray 1988).

Surfactants are used in drilling fluids as emulsifiers, dispersants, wetting agents, foamers and defoamers, and to decrease the hydration of the clay surface. The type of surfactant behavior depends on the structural groups of the molecules.

Various Other Additives. There are a plethora of other additives for drilling fluids. Some are used for pH control—that is, for chemical-reaction control (inhibit or enhance) and drill-string-corrosion mitigation. There are bactericides used in starch-laden fluids (salt muds in particular) to kill bacteria. There are various contaminate reducers such as sodium acid polyphosphate (SAPP) used while drilling cement to bind up calcium from the cement cuttings. There are corrosion inhibitors, especially H_2S scavengers. There are defoamers to knock out foaming and foaming agents to enhance foaming. There are lubricants for torque-and-drag reduction as well as pipe-freeing agents for when a drill string is stuck.

3.5 Clay Chemistry

The key to understanding drilling fluids is to understand clay chemistry. And to really understand clay chemistry, the understanding of particle sizes is critical.

3.5.1 Particle Sizes. The common size of a given particle is usually measured in microns (μm). This is 0.001 mm or 3.937×10^{-5} in. Particles that are greater than 44 μm are considered sand-sized particles (regardless of their material). These can be subcategorized as coarse (greater than 2 mm), intermediate (between 2 mm and 250 μm), medium (between 250 and 74 μm), and fine (between 74 and 44 μm). Particles sized between 44 and 2 μm are silt-sized. And particles less than 2 μm are called colloidal. Clay particles are colloidal in size. While sand- and silt-sized particles can be physically separated in a liquid, a colloidal-sized particle cannot. It must be removed using a chemical reaction, which typically enlarges the particle and makes it susceptible to physical separation. The range of particle sizes are illustrated in **Fig. 3.3**.

The surface area of a clay particle is remarkable. For example, a 1 cm cube of clay has a surface area of $6 \times 10^{-4} \text{ m}^2$. Chop that same 1 cm cube into 1- μm cubes (the size of a clay particle) and the result would be $10,000^3$ (10^{12}) particles. Each particle would have a surface area of $6 \times 10^{-12} \text{ m}^2$; 10^{12} of those particles would yield a surface area of 6 m^2 —this is an increase of 10,000 in the available surface area. And, because the chemical reactivity of clay is partially dependent on its surface area, the more dispersed a clay is, the more reactive it becomes.

The surface area of a clay particle typically has an ion associated with it. This cation links the platelet structure of the clay together. The strength of the cation, as well as other environmental conditions, dictates whether the platelets separate or not.

Hydration occurs as clay platelets absorb water and swell. **Fig. 3.4** illustrates the various forms of clay behavior. Dispersion (or disaggregation) causes clay platelets to break apart and disperse into the water because of loss of attractive forces as water forces the platelets farther apart. Aggregation—a result of ionic or thermal conditions—alters the hydration of a layer around the clay platelets, removes the deflocculant from positive-edge charges, and allows platelets to assume a face-to-face structure. Flocculation begins when mechanical shearing stops and platelets that previously dispersed come together because of the attractive force of surface charges on the platelets. Deflocculation, the opposite effect, occurs by addition of chemical deflocculant to flocculated mud; the positive-edge charges are covered and attraction forces are greatly reduced.

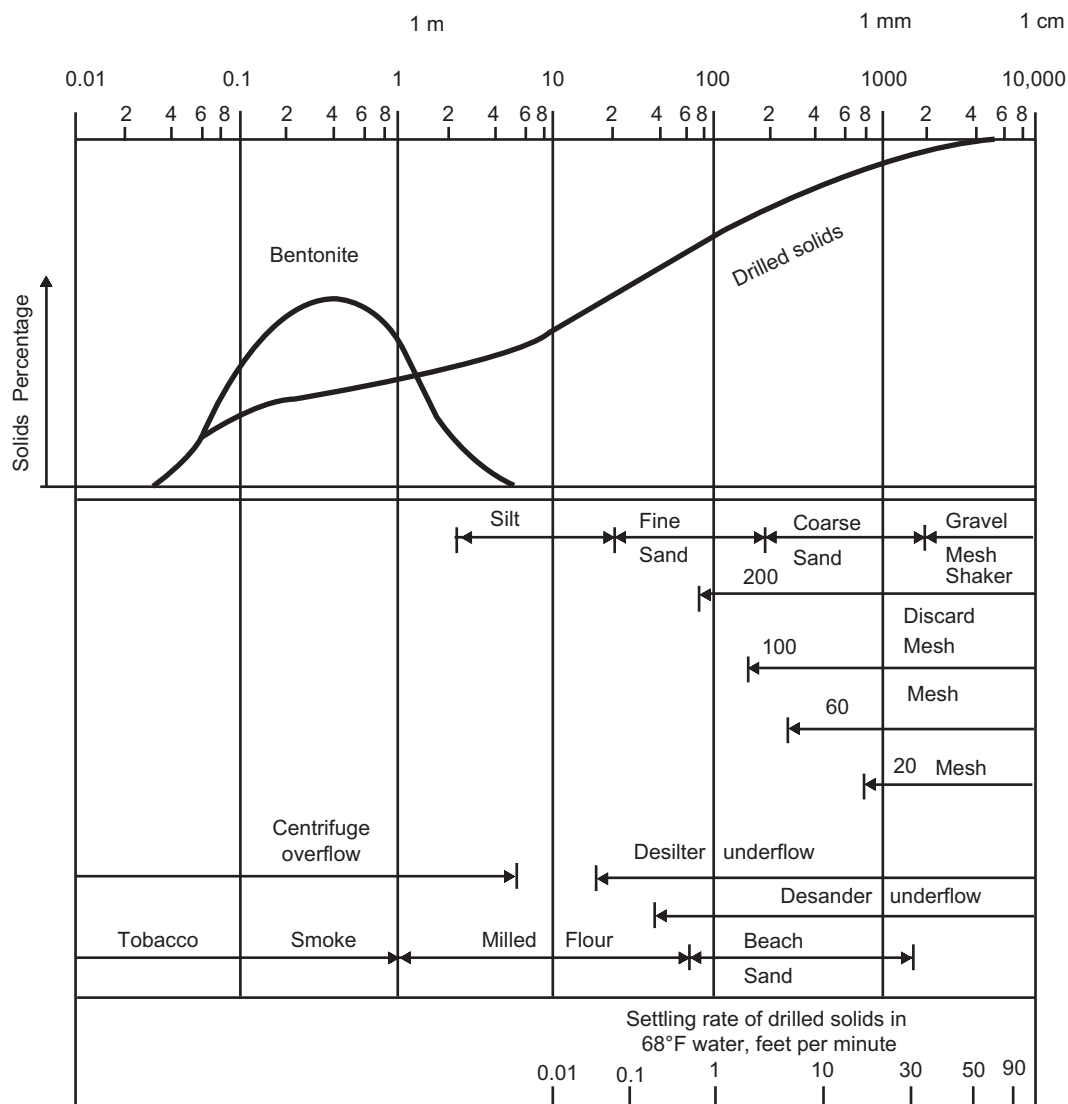


Fig. 3.3—Particle size of solids (Annis 1974). Reprinted courtesy of ExxonMobil.

3.5.2 Clay Types. From the standpoint of geology, clay (sediments less than 0.0039 mm in size) is a group of rock-forming, hydrous aluminum silicate minerals that are layered in morphology and can form by the alteration of silicate minerals. On the other hand, from the standpoint of drilling-fluid technology, clay is a large family of complex minerals containing the elements magnesium, aluminum, silicon, and oxygen (magnesium, aluminum silicates) combined in a sheetlike structure (Darley and Gray 1991).

Various clays react to water at differing levels known as activity levels. The smectites are the most reactive with water, easily disassociating. The best known clay is sodium montmorillonite, better known as bentonite or gel. Calcium montmorillonite is sometimes called subbentonite. And vermiculite is the least active of the smectites. The next less-reactive clays are the illites, followed by the chlorites, and the kaolinites. Each of these clays is present in differing proportions in formations, a fact that can seriously complicate drilling-fluid selection.

Wyoming bentonite is composed primarily of three-layer clays called montmorillonite (a mineral found near Montmorillon, France). The term now is reserved usually for hydrous aluminum silicates approximately represented by the formula $4\text{SiO}_2 \cdot \text{Al}_2\text{O}_3 \cdot \text{H}_2\text{O} + \text{water}$, but with some of the aluminum cations Al^{3+} being replaced by magnesium cations Mg^{2+} . This replacement of Al^{3+} by Mg^{2+} causes the montmorillonite structure to have an excess of electrons. This negative charge is satisfied by loosely held cations from the associated water. The name sodium montmorillonite refers to a clay mineral in which the loosely held cation is the Na^+ ion.

Montmorillonite, a hydrophilic and dispersible clay mineral of the smectite group, is a mineral that tends to swell when exposed to water. This clay has the extraordinary capacity of exchanging cations, typically sodium

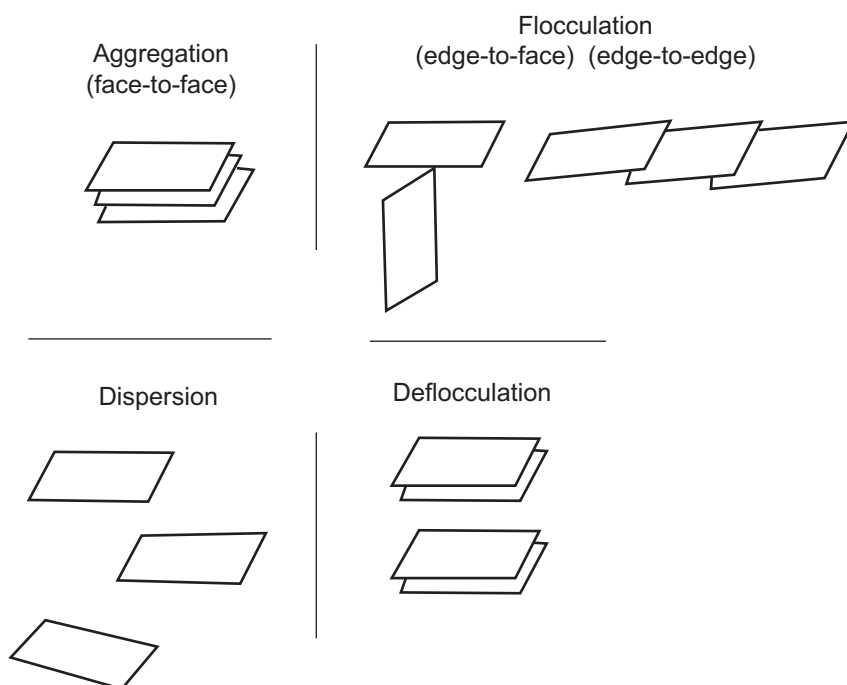


Fig. 3.4—Association of clay particles (after Bourgoyne et al. 1991).

(Na⁺) and calcium (Ca⁺²). Sodium montmorillonite is known as a premium mud additive. It is considered higher-quality swelling clay, while calcium-type montmorillonite is of lower quality and is treated during grinding by adding more additives for various commercial applications. Sodium montmorillonite is capable of swelling to approximately 10 times its original volume when mixed with fresh water. Calcium montmorillonite will swell only two to four times its original volume when mixed with water. In mud parlance, bentonite is classified as sodium bentonite and calcium bentonite, depending on the exchangeable cation (Darley and Gray 1991).

Montmorillonite clay has a mica-type crystal structure made up of a crystal lattice of silica and aluminum, and the lattice is loosely bound with a cation such as sodium or calcium. In the presence of water, the crystal lattice absorbs water, allowing the crystal to swell. The covalent calcium ion holds the crystal lattice together tighter, allowing less swelling. A model representation of the structure of sodium montmorillonite is shown in **Fig. 3.5** (Grim 1968). A central alumina octahedral sheet has silica tetrahedral sheets on either side. These sheetlike structures are stacked with water and the loosely held cations between them. Polar molecules such as water can enter between the unit layers and increase the interlayer spacing. This is the mechanism through which montmorillonite hydrates or swells. A photomicrograph of montmorillonite particles in water is shown in **Fig. 3.6** (Grim 1968). Note the platelike character of the particles.

In addition to the substitution of Mg²⁺ for Al³⁺ in the montmorillonite lattice, many other substitutions are possible. Thus, the name montmorillonite often is used as a group name including many specific mineral structures. However, in recent years, the name smectite has become widely accepted as the group name, and the term montmorillonite has been reserved for the predominantly aluminous member of the group shown in **Fig. 3.5**. This recent naming convention has been adopted in this text.

The ability of smectite clays to swell when exposed to water is considerably affected when the salinity of the water is too great. In the particular case of salt water, a fibrous, needlelike clay mineral called attapulgite is used. Attapulgite (a mineral found near Attapulgis, Georgia, USA) is composed of magnesium-aluminum silicate and is incapable of controlling the filtration properties of the mud. Attapulgite is approximately represented by the formula (Mg,Al)₂Si₄O₁₀·4H₂O, but with some pairs of the magnesium cations (2Mg²⁺) being replaced by a single trivalent cation. A photomicrograph of attapulgite in water is shown in **Fig. 3.7a**. The ability of attapulgite to build viscosity is thought to be a result of interaction between the attapulgite fibers rather than the hydration of the water molecules. A longer period of agitation is required to build viscosity with attapulgite than with smectite clays. However, with continued agitation, viscosity decreases are observed eventually because of the mechanical breakage of the long fibers. This can be offset through the periodic addition of a new attapulgite material to the system.

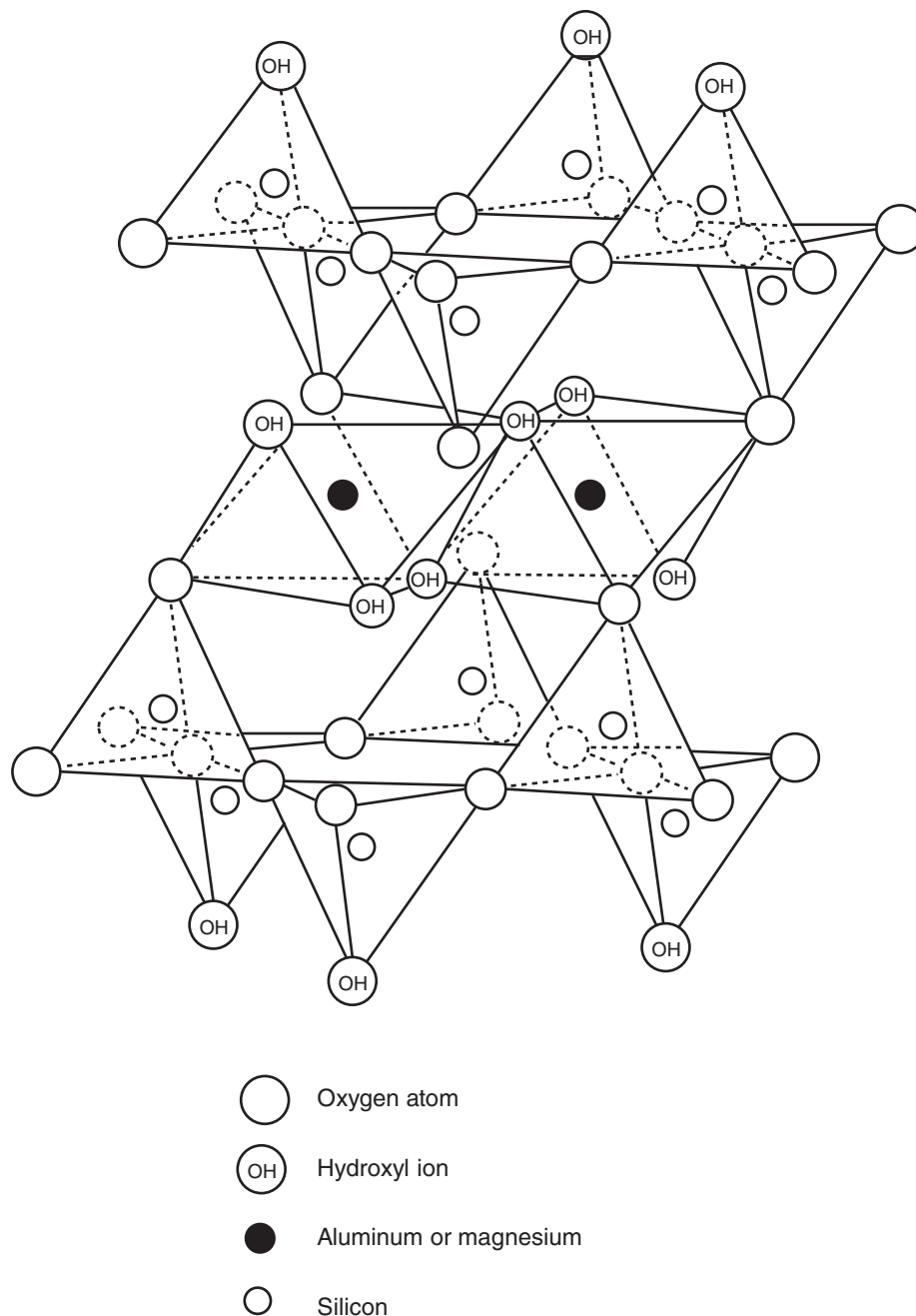


Fig. 3.5—Structure of sodium montmorillonite (Grim 1968). Used with permission of McGraw-Hill.

The clay mineral sepiolite, a magnesium silicate with a fibrous texture, has been proposed as a high-temperature substitute for attapulgite. A photomicrograph of sepiolite in water is shown in Fig. 3.7b. The idealized formula can be written $\text{Si}_{12}\text{Mg}_8\text{O}_{32} \cdot n\text{H}_2\text{O}$. X-ray diffraction techniques and scanning-electron-microscope studies have established that the crystalline structure of this mineral is stable at temperatures up to 800°F. Slurries prepared from sepiolite exhibit favorable rheological properties over a wide range of temperatures.

3.6 Estimating Drilling Fluid Properties

Two principal properties of interest in drilling fluids are density (mud weight) and viscosity. Reasonably accurate densities can be estimated from basic principles, but viscosity can be estimated within a broad range, at best. Fortunately, drilling-fluid viscosity usually is not specified in a narrow range, but testing and adjusting mud viscosity usually is desirable.

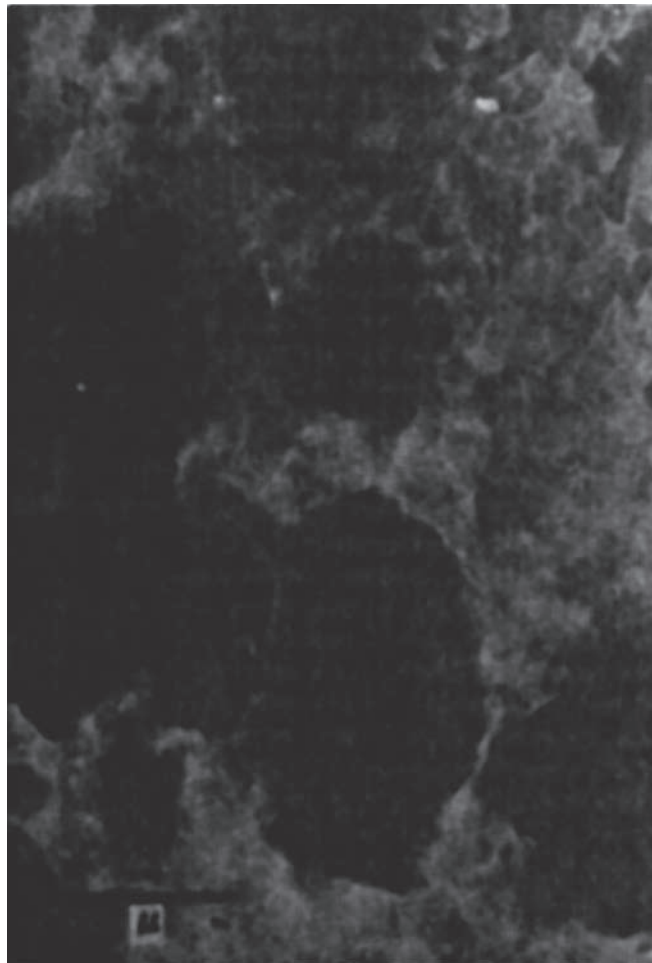


Fig. 3.6—Transmission electron photomicrograph of montmorillonite (Grim 1968). Used with permission of McGraw-Hill.



(a)



(b)

Fig. 3.7—Transmission electron photomicrograph of attapulgite (left) and sepiolite (right) (Grim 1968). Used with permission of McGraw-Hill.

3.6.1 Calculating Mud Weight. Generally speaking, drilling mud is composed of four major components: water or brine phase, an oil phase, low density solids, and high density solids. These four components are immiscible, that is, no component dissolves in any other component to any significant degree. This means that the four components form an *ideal mixture*. In an ideal mixture, the sum of the component volumes equals the total volume of the mixture:

$$V_f = V_w + V_o + V_{ls} + V_{hs}, \quad \dots \quad (3.1)$$

where V_f is the total fluid volume, V_w is the volume of the water phase, V_o is the volume of the oil phase, V_{ls} is the volume of the low density solids, and V_{hs} is the volume of the high density solids. This volume sum may seem obvious, but there are common mixtures that are not ideal. For instance, a mixture of table salt and fresh water does not obey Eq. 3.1, and therefore, the prediction of the volume of salt/water mixtures is extremely complex (Rogers and Pitzer 1982).

The total weight of a fluid mixture is simply the sum of the weights of the components. Conservation of mass ensures that the total weight calculation is always correct:

$$m_f = \rho_w V_w + \rho_o V_o + \rho_{ls} V_{ls} + \rho_{hs} V_{hs}, \quad \dots \quad (3.2)$$

where m_f is the mass of the fluid mixture, ρ_w is the density of the water phase, ρ_o is the density of the oil phase, ρ_{ls} is the density of the low-density solids, and ρ_{hs} is the density of the high-density solids. The overall density of the fluid mixture, then, is

$$\begin{aligned} \rho_f &= \frac{m_f}{V_f} = \frac{\rho_w V_w}{V_f} + \frac{\rho_o V_o}{V_f} + \frac{\rho_{ls} V_{ls}}{V_f} + \frac{\rho_{hs} V_{hs}}{V_f} \\ &= \rho_w f_w + \rho_o f_o + \rho_{ls} f_{ls} + \rho_{hs} f_{hs}, \quad \dots \quad (3.3) \end{aligned}$$

where f_w is the volume fraction of the water phase, f_o is the volume fraction of the oil phase, f_{ls} is the volume fraction of the low density solids, and f_{hs} is the volume fraction of the high density solids. Note that the sum of the volume fractions equals 1. The specific gravities of typical drilling-fluid solids are given in **Table 3.1**. Changes in temperature and pressure will change the volumes of the components. While the solid phases show little change over typical ranges of temperature and pressure, water does show some change with temperature, and oil shows considerable change with pressure and temperature. Water is relatively incompressible, while oils are much more compressible. If we review Eq. 3.2, we see that the volume of the fluid changes as the volume of the water phase and oil phase changes. As a result, the volume fractions, computed at a given pressure and temperature, are not constants and vary with changes in pressure and temperature. If we measure volume fractions at a specified temperature, the following formula gives the density of the mixture at new temperatures and pressures:

$$\rho_f(P, T) = \frac{\rho_f(P_r, T_r)}{1 - \frac{f_o \Delta \rho_o}{\rho_o(P, T)} - \frac{f_w \Delta \rho_w}{\rho_w(P, T)}}, \quad \dots \quad (3.4)$$

$$\Delta \rho_w = \rho_w(P, T) - \rho_w(P_r, T_r)$$

$$\Delta \rho_o = \rho_o(P, T) - \rho_o(P_r, T_r),$$

where P_r is the reference pressure and T_r is the reference temperature used to calculate the volume fractions f_w and f_o .

Water and Oil Densities. The effect of temperature and pressure on the density of water, the density of diesel oil, and the density of typical synthetic oil is shown in **Figs. 3.8 through 3.10**, respectively. For an accurate

TABLE 3.1—DENSITY OF SOLIDS IN DRILLING FLUIDS (SG)							
Bentonite	2.6	Limestone	2.8	Hematite	5.05	Galena	7.50
Barite	4.2	Siderite	3.08	Ilmetite	4.6	Cuttings	~2.6
Attapulgit	2.89	Sand	2.63	NaCl	2.16	CaCl ₂	1.96

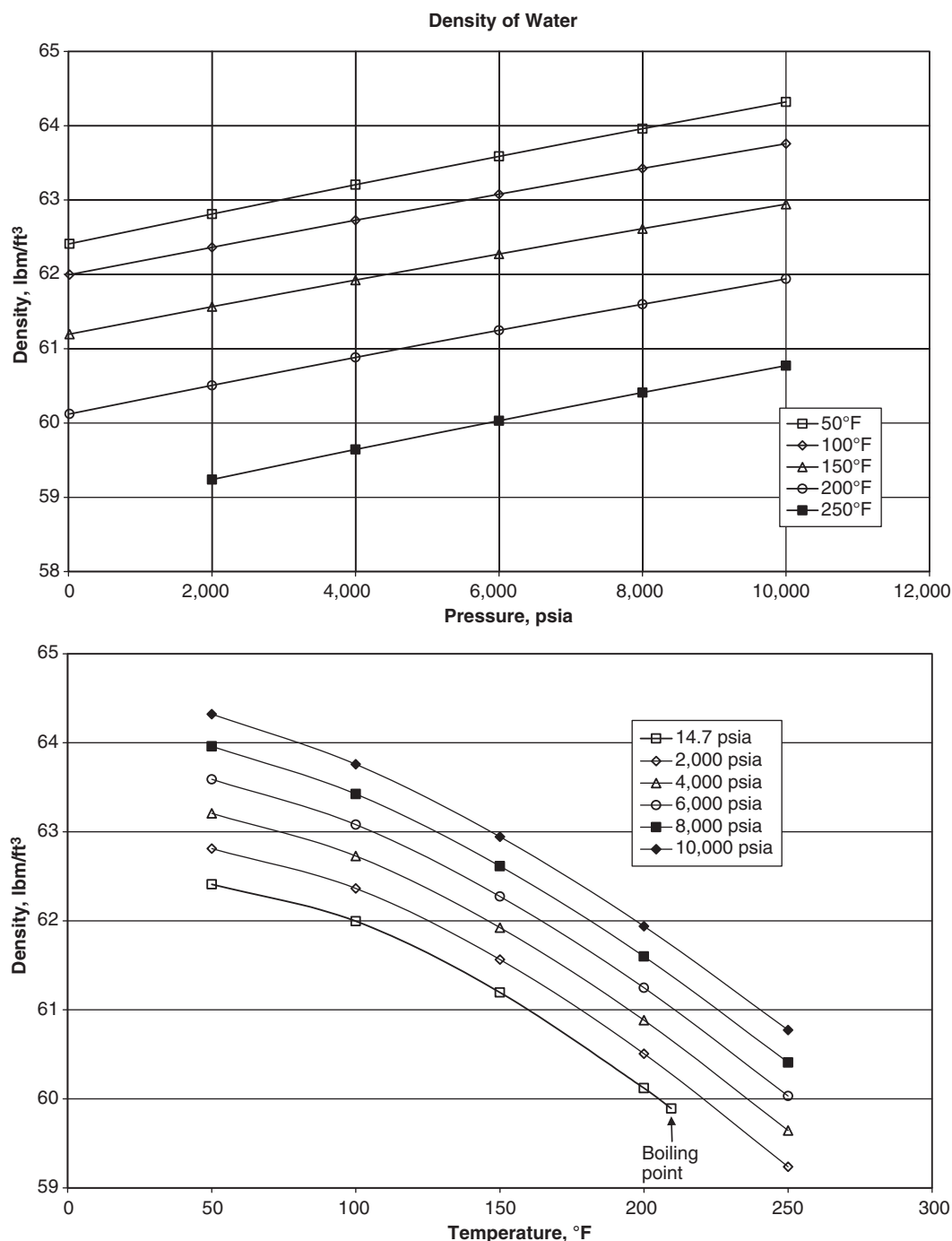


Fig. 3.8—Density of fresh water as a function of pressure and temperature.

analytic formula for water density, we recommend the correlation in Parry et al. (2000). Sorelle et al. (1982) gives the following simplified formula:

$$\rho_w = 8.63186 - 3.31977 \times 10^{-3} T + 2.37170 \times 10^{-5} P, \quad \dots \quad (3.5)$$

where ρ_w is water density in lbm/gal, T is temperature in °F, and P is pressure in psia. A general correlation for oil density has been proposed by Zamora et al. (2000):

$$SG_0 = (a_0 + b_0 T) + (a_1 + b_1 T) P + (a_2 + b_2 T) P^2, \quad \dots \quad (3.6)$$

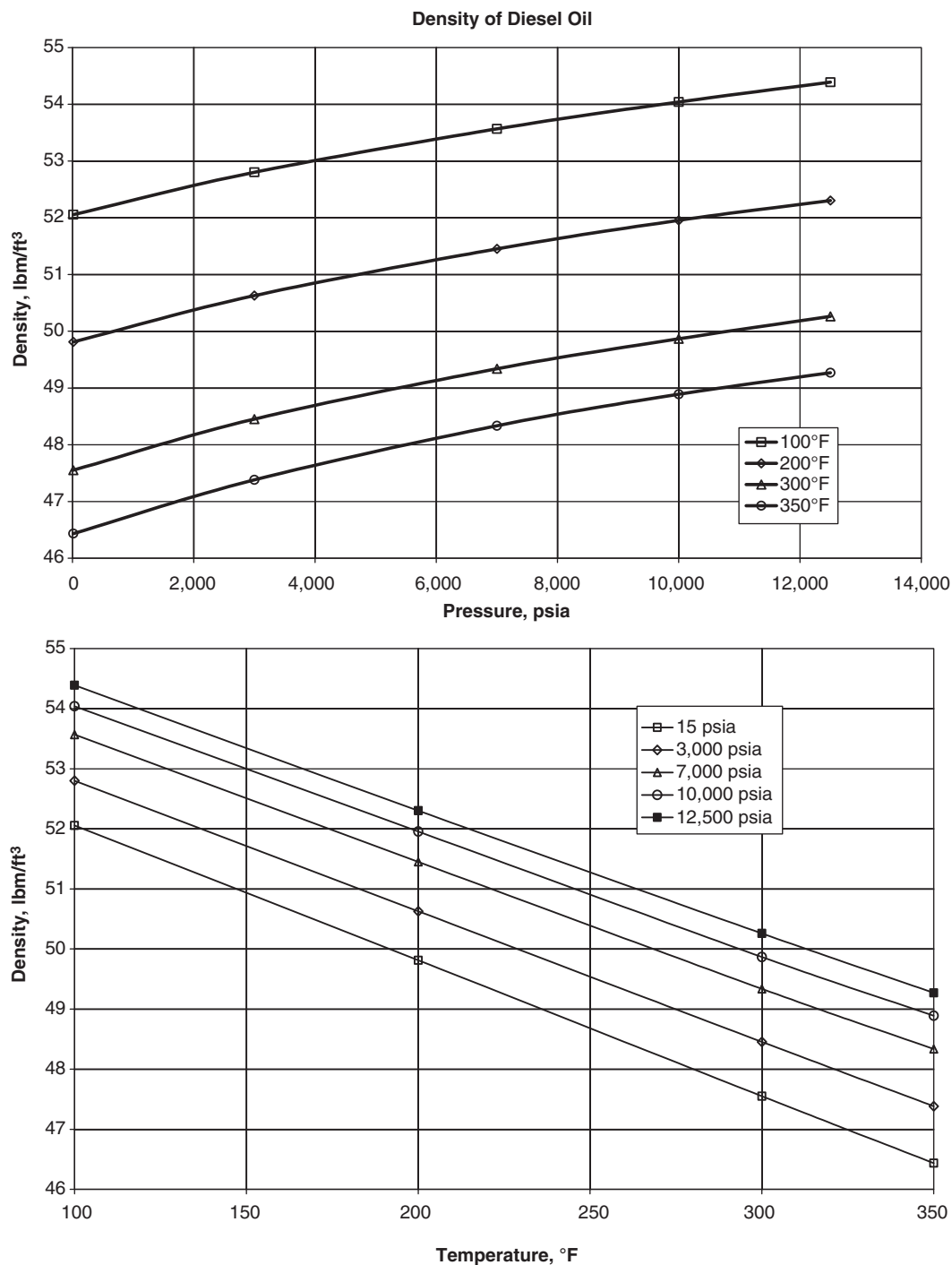


Fig. 3.9—Density of diesel oil as a function of pressure and temperature.

where SG_0 is the oil specific gravity, T is temperature in °F, and P is pressure in psia. Specific gravity is converted to lbm/gal by multiplying by 8.34. **Table 3.2** gives coefficient values for diesel oil and four synthetic oils.

Brine Density. As mentioned earlier, mixtures of water and salts, such as NaCl, KCl, and $MgCl_2$ are not ideal solutions and do not obey the mixing rules given in Eqs. 3.1 through 3.4. The calculation of brine density is extremely difficult and beyond the scope of this book. The interested student is referred to Rodgers and Pitzer (1982) and Kemp and Thomas (1987). The usual method for calculating brine density is to refer to tables, such as **Table 3.3** from Halliburton's cementing tables (Halliburton 2001).

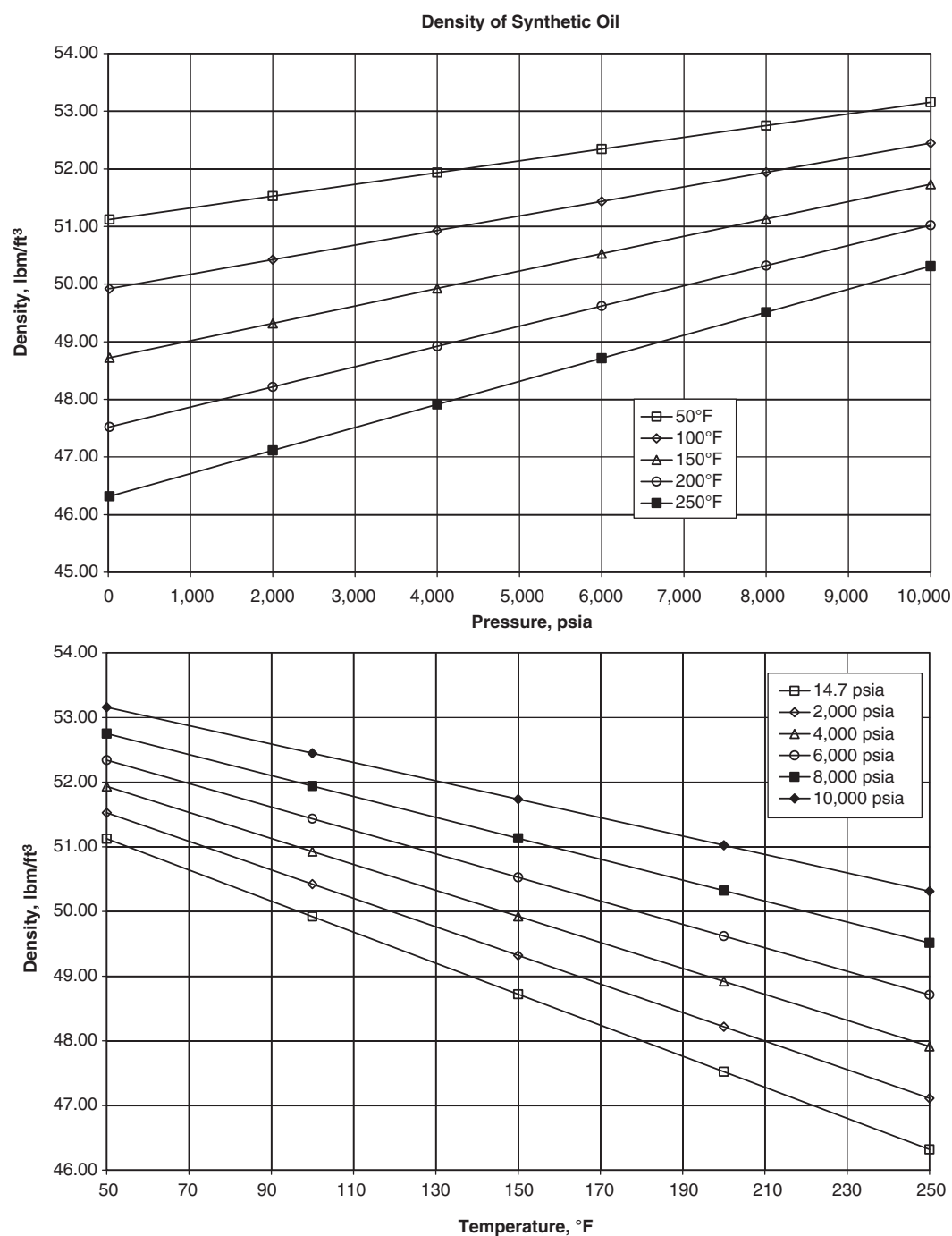


Fig. 3.10—Density of synthetic oil as a function of pressure and temperature.

	$a_0 \times 10^4$	$b_0 \times 10$	$a_1 \times 10^8$	$b_1 \times 10^6$	$a_2 \times 10^{13}$	$b_2 \times 10^{12}$
Diesel	-3.6058	8.7071	0.4640	3.6031	-1.6843	-72.465
LVT 200	-3.8503	8.3847	1.5695	2.4817	-4.3373	6.5076
LAO C16C18	-3.5547	8.1304	1.2965	3.1227	-2.7166	-28.894
Saraline 200	-3.7621	8.0019	1.5814	2.3560	-4.3235	10.891
EMO-4000	-3.7799	8.4174	1.3525	2.8808	-3.1847	-17.697

TABLE 3.3—BRINE PROPERTIES (HALLIBURTON 1981)											
PHYSICAL PROPERTIES OF SODIUM CHLORIDE SOLUTIONS											
Percent Sodium Chloride by Weight		Density of Solution		Specific Gravity	Weight of Salt			Yield of Solution	Freeze Point		
of Solution	of Water	lbm/gal	kg/m ³	@ 20°C	lbm/gal of Water	lbm/bbl of Water	kg/m ³ of Water		°F	°C	
0		8.34	998	0.998				1.000			
1	1.01	8.38	1005	1.005	0.08	3.54	10.08	1.005	30.9	−0.6	
2	2.04	8.45	1013	1.013	0.17	7.15	20.36	1.008	29.9	−1.2	
3	3.09	8.51	1020	1.020	0.26	10.82	30.85	1.011	28.8	−1.8	
4	4.17	8.57	1027	1.027	0.35	14.61	41.63	1.015	27.7	−2.4	
5	5.26	8.62	1034	1.034	0.44	18.42	52.51	1.018	26.2	−3.0	
6	6.38	8.68	1041	1.041	0.53	22.35	63.69	1.022	25.3	−3.7	
8	8.70	8.81	1056	1.056	0.73	30.47	86.85	1.029	22.9	−5.1	
10	11.11	8.93	1071	1.071	0.93	38.92	110.90	1.038	20.2	−6.6	
12	13.64	9.06	1086	1.086	1.14	47.78	136.16	1.047	17.3	−8.2	
14	16.28	9.18	1101	1.101	1.36	57.03	162.51	1.056	14.1	−9.9	
16	19.05	9.31	1116	1.116	1.59	66.73	190.16	1.067	10.6	−11.9	
18	21.95	9.44	1132	1.132	1.83	76.89	219.11	1.077	6.7	−14.0	
20	25.00	9.57	1148	1.148	2.09	87.57	249.56	1.089	2.4	−16.5	
22	28.21	9.71	1164	1.164	2.35	98.81	281.60	1.101	−2.5	−19.2	
24	31.58	9.84	1180	1.180	2.63	110.62	315.24	1.115	+1.4*	−17.0*	
26	35.14	9.98	1197	1.197	2.93	123.09	350.78	1.129	+27.9**	−2.3**	
* Precipitation @ −17°C, 1.4°F; ** Precipitation @ −2.3°C, 27.9°F											
PHYSICAL PROPERTIES OF POTASSIUM CHLORIDE SOLUTIONS											
Percent Potassium Chloride by Weight		Density of Solution		Specific Gravity	Weight of Potassium Chloride			kg of Potassium per m ³ of Water	kg of Chloride per m ³ of Water	Freeze Point	
of Solution	of Water	lbm/gal	kg/m ³	@ 20°C	lbm/gal of Water	lbm/bbl of Water	kg/m ³ of Water			°F	°C
0	—	8.34	998	0.998	—	—	—	—	—	—	—
1	1.01	8.38	1005	1.005	0.08	3.54	10.08	5.27	4.78	31.2	−0.44
2	2.04	8.43	1011	1.011	0.17	7.15	20.36	10.6	9.6	30.3	−0.94
3	3.09	8.48	1017	1.017	0.26	10.82	30.85	16.0	14.5	29.5	−1.39
4	4.17	8.54	1024	1.024	0.35	14.61	41.63	21.5	19.5	28.7	−1.83
6	6.38	8.65	1037	1.037	0.53	22.35	63.69	32.6	29.6	27.0	−2.78
8	8.70	8.75	1050	1.050	0.73	30.47	86.85	44.0	39.8	25.2	−3.78
10	11.11	8.87	1063	1.063	0.93	38.92	110.90	55.8	50.0	23.3	−4.83
12	13.64	8.98	1077	1.077	1.14	47.78	136.16	67.8	61.4	21.4	−5.89
14	16.28	9.10	1091	1.091	1.36	57.03	162.51	80.0	72.5	19.3	−7.06
16	19.05	9.21	1104	1.104	1.59	66.73	190.16	92.6	84.0	17.4	−8.11
18	21.95	9.33	1119	1.119	1.83	76.89	219.11	105.4	95.5	14.9	−9.50
20	25.00	9.45	1133	1.113	2.09	87.57	249.56	118.8	107.8	15.0	−9.44
22	28.21	9.57	1147	1.147	2.35	98.81	281.60	132.1	119.8	32.6	10.33
24	31.58	9.69	1162	1.162	2.63	110.62	315.24	146.3	132.6	52.0*	11.11*
26.5	36.05	9.82	1178	1.178	3.10	126.28	359.86	163.7	148.5	78.3*	25.72*
* Precipitates											

Example 3.1 Determine the volume and density of brine composed of 110.6 lbm of NaCl and 1 bbl of fresh water at 68°F.

Solution. From Table 3.3, the total volume is 1.115 bbl, and the solution density is 9.84 lbm/gal. Note that if ideal mixing is assumed, the total volume calculated, using Table 3.1 for the specific gravity of NaCl, is given by

$$V = V_w + V_{\text{NaCl}} = 1.0 \text{ bbl} + \frac{110.6 \text{ lbm}}{(2.16 \text{ SG})(8.34 \text{ lbm/gal})(42 \text{ gal/bbl})} = 1.146 \text{ bbl.}$$

This volume corresponds to a density of

$$\rho = \frac{(8.34 \text{ lbm/gal})(42 \text{ gal/bbl}) + 110.6 \text{ lbm}}{1.1462 \text{ bbl}} = 401.76 \text{ lbm/bbl} = 9.57 \text{ lbm/gal}.$$

This value does not compare favorably with the true value shown in Table 3.3. As previously stated, salt solutions do not obey ideal mixture assumptions.

Mud Weight Calculations. This section provides five example problems that are very typical of day-to-day mud-engineering calculations. The equations are helpful in the sense that if you are working in a location where barite specific gravity is not always 4.2, or you are using some other type of high-density weighting material, accurate values can still be calculated. Remember that published charts are usually based on barite with specific gravity of 4.2.

Example 3.2 In this problem we will calculate the barite requirements for a weighted mud. We are not concerned with the volume increase of our mud. How much API barite (SG = 4.2) is needed?

Solution. First we look at the volume and mass balances:

$$\begin{aligned} V^f - V^i &= \Delta V \\ \rho^f V^f &= \rho^i V^i + \rho_{hs} \Delta V, \end{aligned}$$

where V^i is the initial volume, V^f is the final volume, ρ^i is the initial mud density of 11 lbm/gal, ρ^f is the final mud density of 11.5 lbm/gal, and ΔV is the volume of barite added. We then solve for V^f , assuming initially 200 bbl mud; from Table 3.1, we know the specific gravity of barite is 4.2, so the density of barite = (4.2)(8.34) = 35 lbm/gal:

$$V^f = V^i \left(\frac{\rho_{hs} - \rho^i}{\rho_{hs} - \rho^f} \right) = (200 \text{ bbl}) \left(\frac{35 - 11}{35 - 11.5} \right) = 204.3 \text{ bbl}.$$

Note that you will need to have an additional 4.3-bbl tank volume to be able to accommodate the increase. While this is not much in this case, weighting up to large volumes and higher densities would strain the capacity of a rig.

Next we calculate how much barite we need to add to get the increase:

$$m_{hs} = (V^f - V^i) \rho_{hs} = (204.3 - 200)(35)(42 \text{ gal/bbl}) = 6,255 \text{ lbm} \approx 63 \text{ sacks},$$

where m_{hs} is the mass of high density solids (barite) to be added.

Now that the basic principle has been illustrated, we can move on to a slightly more complex situation.

Example 3.3 The volume of the mud system is currently 800 bbl. The mud weight is 12 lbm/gal and needs to be increased to 14 lbm/gal. Because the mud system is full, we need to throw out some mud before we weight up the remainder.

Usually, when adding a large amount of barite to a system, the dry barite tends to rob the system of its water. It is good practice to add about 1 gal of water for every sack (100 lbm) of barite to compensate for this issue.

We need to calculate the volume of old mud to throw away and how much barite we need to add to the system.

Solution. This problem is similar to the previous problem, with two exceptions:

1. The final volume is known.
2. Additional water is added proportional to the barite added.

Because the additional water is proportional to the added mass of the barite,

$$\Delta V_w = m_{hs} V^{wb} = \rho_{hs} \Delta V_{hs} V^{wb},$$

where $V^{wb} = 1$ gal of water per 100 lbm of barite. Rewriting the volume and mass balances:

$$V^f - V^i = \Delta V_{hs} + \rho_{hs} V^{wb} \Delta V_{hs}$$

$$\rho^f V^f = \rho^i V^i + \rho_{hs} \Delta V_{hs} + \rho_w \rho_{hs} V^{wb} \Delta V_{hs}.$$

The volume of old mud to be thrown away is simply the difference in the desired initial volume V^i and the actual initial volume. We solve the above equations for the desired initial volume, where we have been given the desired final volume:

$$V^i = V^f \left[\frac{\rho_{hs} \left(\frac{1 + \rho_w V^{wb}}{1 + \rho_{hs} V^{wb}} \right) - \rho^f}{\rho_{hs} \left(\frac{1 + \rho_w V^{wb}}{1 + \rho_{hs} V^{wb}} \right) - \rho^i} \right] = 800 \left[\frac{35 \left(\frac{1 + 8.33(0.01)}{1 + 35(0.01)} \right) - 14}{35 \left(\frac{1 + 8.33(0.01)}{1 + 35(0.01)} \right) - 12} \right] = 700.5 \text{ bbl.}$$

V^i is the initial volume we need to start with so that when we finish weighing up, we will maintain the 800-bbl system volume. Note that the equation is the inverse of the one in Example 3.2 with only the additional factor to take into account the additional water added in with the dry barite.

The volume of mud we need to throw out V^{discard} is

$$V^{\text{discard}} = V^f - V^i = 800 - 700.53 = 99.47 \text{ bbl.}$$

Next, we calculate how much barite we need:

$$m_{hs} = \frac{\rho_{hs}}{1 + \rho_{hs} V^{wb}} (V^i - V^f) = \left[\frac{35}{1 + 35(0.01)} (800 - 700.53) \right] (42 \text{ gal/bbl}) = 108,309 \text{ lbm}$$

$$\approx 1,083 \text{ sacks.}$$

Remember also to add in 1 gal of water per sack of barite (i.e., 1,083 gal or 25.8 bbl water).

So the procedure is to

1. Throw out 99.47 bbl of mud.
2. Add 1,083 sacks of barite and 25.8 bbl water.
3. Mix it up, and you are ready to go.

Example 3.4 This example will illustrate another common situation. Suppose we have just set intermediate casing and are ready to drill ahead. We have been informed that we are to hit a high pressure zone 50 ft below the shoe and need to weigh up the mud to 14 lbm/gal. Currently we have 9.5 lbm/gal unweighted mud in the hole with 5% solids content.

Because there is a large distance to drill, it is necessary to lower the solids content of the mud to 3%. The mud volume is 1,000 bbl, which is too much, and we determine that an 800-bbl volume is sufficient. (It costs more to weigh up 1,000 bbl than 800 bbl.)

This scenario requires a mass operation on the mud, getting it into first-class condition so that the next section can be drilled without any problems. The first step is to lower the solids content of the mud using dilution. Because the final mud volume must be 800 bbl, 200 bbl are thrown out. Additionally, more mud will need to be removed and water added to reach the 3% solids content.

Solution. The initial start volume is determined:

$$V^i = V^f \left(\frac{f_{ls}^f}{f_{ls}^i} \right) = 800 \left(\frac{0.03}{0.05} \right) = 480 \text{ bbl,}$$

where f_{ls}^i is the initial low density solids fraction and f_{ls}^f is the final low-density solids fraction. Therefore, an additional 320 bbl of mud must be thrown out to leave the 480 bbl. Next, determine how much water must be added to the system:

$$V_w = \frac{(\rho_{hs} - \rho^f)V^f - (\rho_{hs} - \rho^i)V^i}{\rho_{hs} - \rho_w} = \frac{(35 - 14)800 - (35 - 9.5)480}{35 - 8.33} = 171 \text{ bbl water,}$$

where V_w is the volume of water added. Finally, determine the amount of barite to be added:

$$m_{hs} = (V^f - V^i - V_w)\rho_{hs} = (800 - 480 - 171)35(42 \text{ gal/bbl}) = 219,000 \text{ lbm} \\ \approx 2,190 \text{ sacks.}$$

This will result in 800 bbl of 14 lbm/gal mud.

Example 3.5 To drop the weight of a drilling fluid, calculate the volume of dilution fluid required to decrease the density of the drilling fluid when a volume increase can be tolerated:

Solution.

$$V^f = V^i \left(\frac{\rho^i - \rho^f}{\rho_{hs} - \rho^f} \right) = 200 \left(\frac{11.5 - 11}{35 - 11} \right) = 4.2 \text{ bbl.}$$

So, in this case, adding 4.2 bbl will dilute 200 bbl of mud from 11.5 lbm/gal to 11.0 lbm/gal. The total volume would end up at 204.2 bbl.

Example 3.6 To drop the weight of a drilling fluid without a change in volume, calculate the volume of dilution fluid required to decrease the density of a drilling fluid, and calculate the volume of old mud to throw away.

Solution. The volume of old mud to be thrown away:

$$V^i = V^f \left(\frac{\rho_{hs} - \rho^f}{\rho_{hs} - \rho^i} \right) = 200 \left(\frac{35 - 11}{35 - 11.5} \right) = 195.8 \text{ bbl.}$$

V^i is the initial volume to start with so that when density reduction is finished, the 200-bbl system volume is maintained. The volume of mud to be thrown out (V^{discard}) and the amount of water to be added is

$$V^{\text{discard}} = V^f - V^i = 200 - 195.8 = 4.2 \text{ bbl.}$$

3.6.2 Estimating Mud Viscosity. Correlations for the viscosity of fresh water and of various oils are available from many sources. For example, Parry et al. (2000) provide correlations for fresh water, and Poling et al. (2000) provide correlations for oils. The effect that pressure and temperature have on the water viscosity is shown in **Fig. 3.11** and for diesel oil in **Fig. 3.12**. The viscous properties of a mixture of liquid and solid components, however, are not well understood. **Fig. 3.13** shows the effect of low density solids on the viscosity of water, and the variation for different types of solids is quite pronounced. A formula for dilute mixtures of spherical, noninteracting particles has been developed by Einstein (Govier and Aziz 2008):

$$\mu_M = \mu(1 + 2.5f_{ls}), \quad \dots\dots\dots (3.7)$$

where μ is the fluid viscosity, μ_M is the viscosity of the mixture, and f_{ls} is the solid volume fraction. This formula is valid only up to 1–2% of solids by volume. Guth and Simha (Govier and Aziz 2008) extended Einstein's results:

$$\mu_M = \mu(1 + 2.5f_{ls} + 14.1f_{ls}^2), \quad \dots\dots\dots (3.8)$$

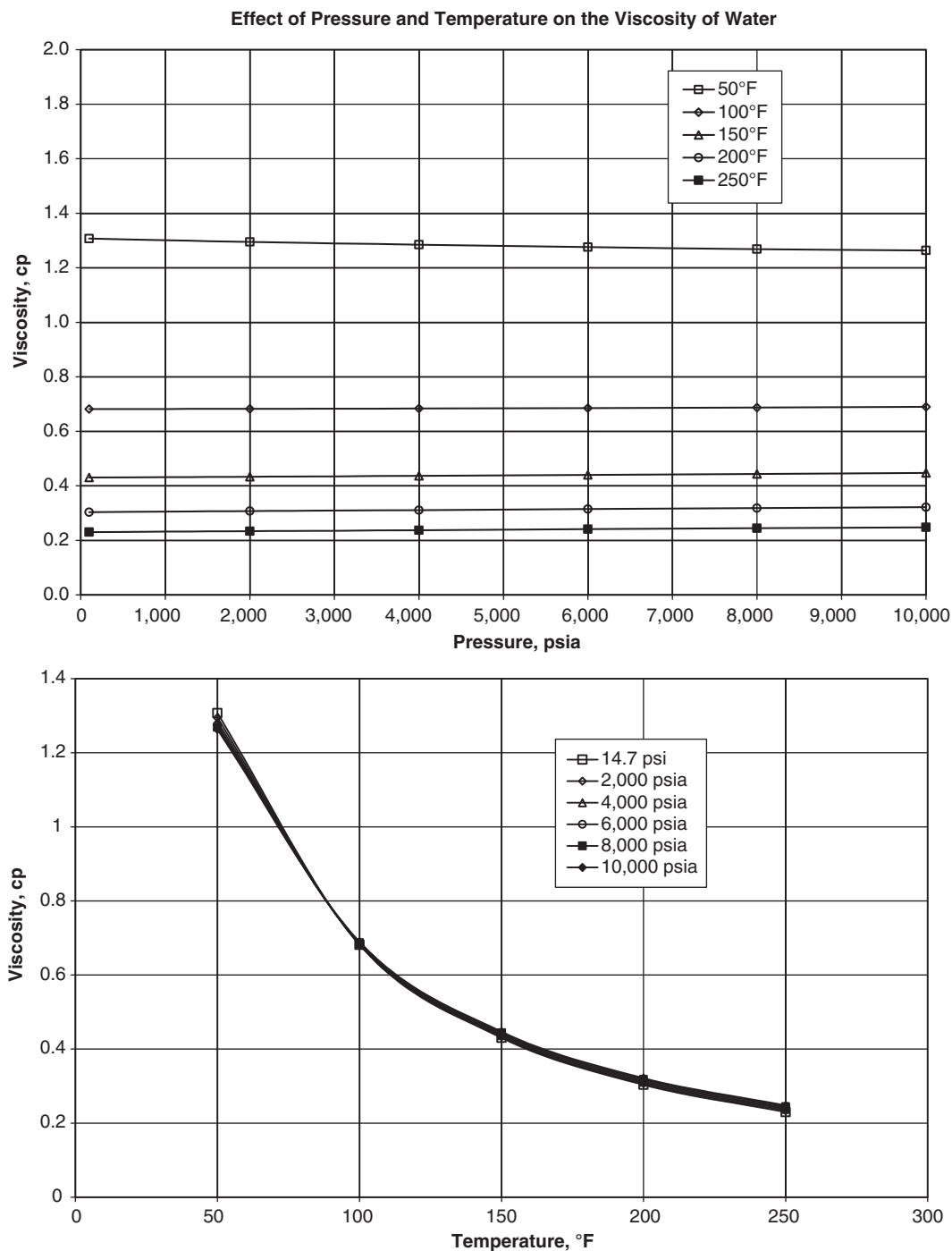


Fig. 3.11—Viscosity of fresh water as a function of pressure and temperature.

which is valid up to about a volume fraction of 20% with about a 10% error. Unfortunately, the assumptions of spherical and noninteracting particles are not generally valid for drilling fluids and are especially untrue for brines and water-bentonite mixtures.

Generally speaking, drilling fluids are mixed from basic components, the viscosity of the fluid is tested, and the viscous properties are then adjusted, if necessary, using chemical additives. The variation in drilling-fluid viscous properties as a function of pressure and temperature have been correlated by Alderman et al. (1988) for water-based muds and Houwen and Geehan (1986) for oil-based muds.

3.7 Testing of Drilling Fluids

During the drilling process, the physical and rheological properties of a drilling fluid have to be controlled accurately to ensure the fluid's appropriate performance. These properties are regularly tested and recorded on the

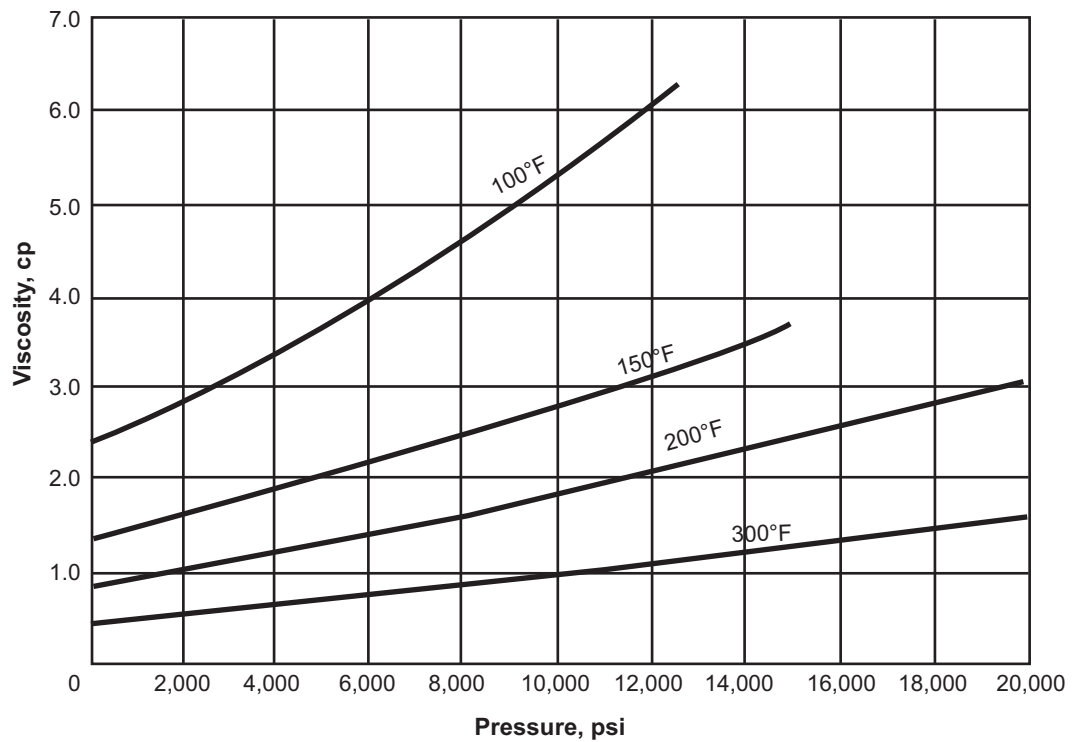


Fig. 3.12—Viscosity of diesel oil as a function of pressure and temperature (Annis 1974). Reprinted courtesy of ExxonMobil.

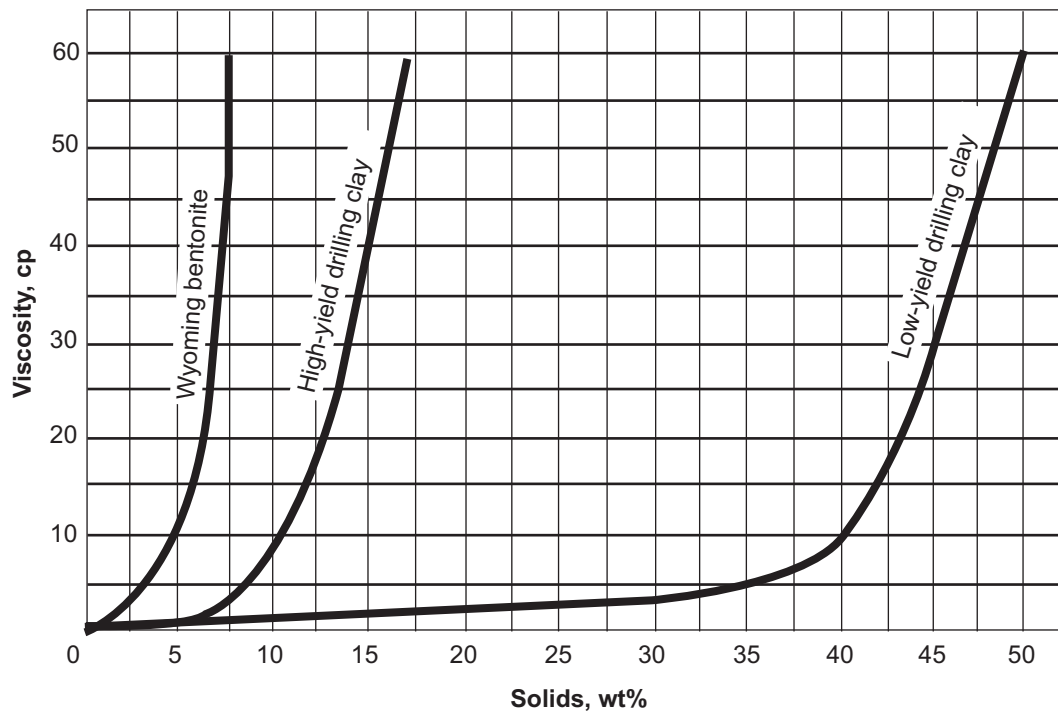


Fig. 3.13—Viscosity of fresh water/solids mixtures (from Bourgoyne et al. 1991).

drilling-mud report, which is presented by the API (*API Spec. 13B-1* 2009). The drilling-fluid technicians carry out the field tests at the wellsite where the mud properties are routinely monitored.

Because the chemical tests conducted upon the water phase are only semiquantitative, the control of the water's ionic balance is quite complicated. Thus, a persistent question arises: How accurate are the test results? From a chemical standpoint, most of the chemical test results are sufficient for interpretation of drilling-fluid behavior. But, occasionally, no chemical balance is present and the interpretation of those results does not point to the actual problem.

A water-based mud is composed of a three-phase system: water, active solids, and inert solids. The active solids (hydrophilic) such as hydratable clays react with the water phase by dissolving chemicals and by providing viscosity to the mud. On the other hand, the inert solids (hydrophobic) such as sand and shale do not react with the water and chemicals to any significant degree. Basically, the inert solids make difficult the analyses and control of the solids in the drilling fluid (i.e., inert solids produce undesirable effects).

3.7.1 Properties of Drilling Fluids. There are many physical and chemical properties of drilling fluids that are useful to know or even critical to determine. The physical properties of a drilling fluid, the density, and the rheological properties are examined continuously to optimize the rotary-drilling process. These properties contribute to preventing an influx of formation fluid, providing wellbore stability, providing hydraulic energy at the drilling bit, removing drilled solids (cuttings) from the well and suspending them during static periods, and permitting segregation of solids and gas at the surface. The chemical properties of a drilling fluid provide the chemical effects associated with formation damage, rheological-property changes, and cuttings-transport issues.

3.7.2 Testing for Density. The mass per unit volume of a drilling fluid, density, is commonly reported either in pounds per gallon (lbm/gal), in kilograms per cubic meter (kg/m^3), grams per cubic centimeter (also called specific gravity [SG]), or in hydrostatic gradient, lbm/in²/ft (psi/ft) or psi/1,000 ft. The mud density and the depth of the well control the hydrostatic pressure exerted by a static drilling-fluid column. The mud density prevents inflow of formation fluid into the well and collapse of the open hole and the casing. To prevent inflow, the hydrostatic pressure of a mud column must exceed the formation or pore pressure. However, excessive mud weight can cause lost circulation and considerably affect the rate of penetration.

The mass per unit volume (density or mud weight) of the drilling fluid is determined by the use of the mud balance. A typical pressurized mud balance is illustrated in **Fig. 3.14**. It is important to note that fresh water weighs 8.34 lbm/gal. Therefore, to calibrate a mud balance, fresh water must be used. If brine is used, the calibration will be incorrect unless one knows precisely the salt concentration and can determine the actual weight of the calibration fluid.



Fig. 3.14—Pressurized mud balance. Courtesy of Halliburton.

3.7.3 Testing for Flow Properties. The flow properties of the drilling fluid play a very important role in the success of the rotary-drilling operation and they must be controlled if the fluid is to perform its various functions properly.

Viscosity. The resistance to flow of a fluid and the resistance to the movement of an object through a fluid are usually stated in terms of the viscosity of the fluid. Experimentally, under conditions of laminar flow, the force required to move a plate at constant speed against the resistance of a fluid is proportional to the area of the plate and to the velocity gradient perpendicular to the plate. The constant of proportionality is called the viscosity. In the oil field, the following terms are used to describe the drilling-fluid viscosity: funnel viscosity, apparent viscosity, plastic viscosity, and effective viscosity. Viscosity is the rheological property of the drilling fluid that indicates its resistance to flow. Viscosity is defined as the ratio of shear stress to shear rate:

$$\mu = \frac{\tau}{\dot{\gamma}}, \quad \dots \dots \dots (3.9)$$

where τ is the shear stress, $\dot{\gamma}$ is the shear rate, and μ is the viscosity. The shear rate is the velocity gradient or fluid velocity/length. The shear stress is the force over an area exerted on the fluid ($\tau = \text{force/area}$), and μ is the constant of proportionality, or viscosity, of the fluid. Viscosity, in the drilling industry, is expressed in centipoise (cp), where 1 cp = 0.01 poise = 0.01 dyne-sec/cm² = 0.01 g/cm-sec. The shear rate ($\dot{\gamma}$, sec⁻¹) of a fluid is defined as the velocity change divided by the width of a canal through which it is moving in laminar flow. The shear stress (τ , lbf/100 ft²) is the force per unit area needed to move a fluid at a given shear rate. When the proportionality between shear stress and shear rate is independent of shear rate, the fluid is called Newtonian, and many common fluids have this behavior. However, most of the drilling fluids are characterized as non-Newtonian fluids, where the proportionality is shear-rate dependent.

Testing for Viscosity. A simple test for viscosity at the wellsite is the Marsh-funnel test. The Marsh funnel, shown in Fig. 3.15a, is a cone-shaped tool with a small bore tube on the bottom end through which drilling mud flows due to gravity action. The resulting value is not a true viscosity value but a relative comparison one. The qualitative measurement indicates how thick the drilling mud sample is measuring a timed rate of flow. This viscosity is the number of seconds it takes for 1 quart of drilling mud to flow through the funnel. For example, the fluid would be described as a “43 viscosity fluid” if its flowing from the funnel reaches the 1-quart line in 43 seconds. However, no useful engineering information can be derived from this test.

The shear stress-shear rate relationship of a drilling mud is determined by conducting tests in a concentric viscometer (Fig. 3.15b). This consists of concentric cylinders, one of which rotates (usually the outer one). A sample of fluid is placed between the cylinders and the torque on the inner cylinder is measured, as illustrated in Fig. 3.16. Assuming an incompressible fluid, with flow in the laminar-flow regime, the equation of motion can be solved for t to give:

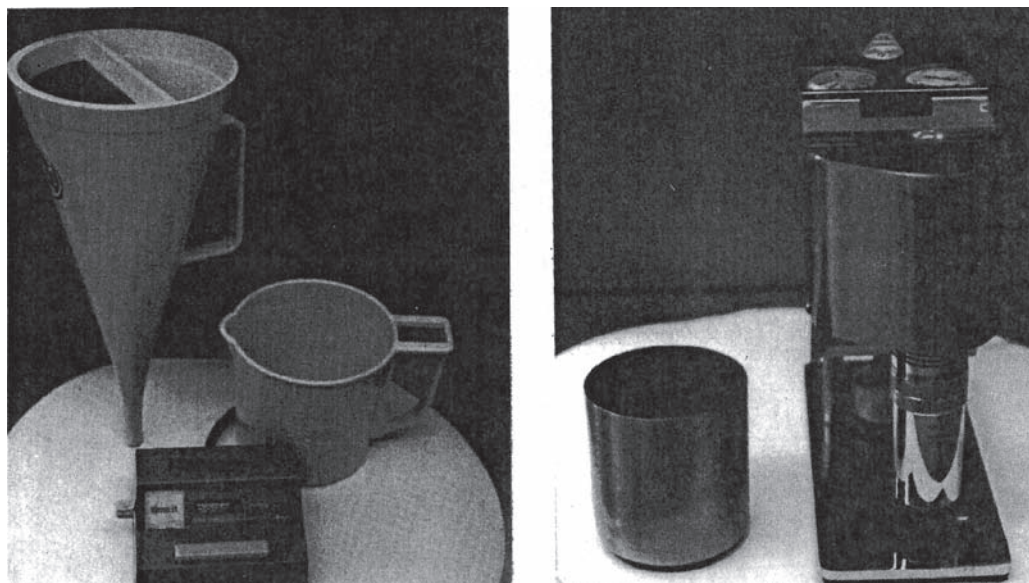


Fig. 3.15—Marsh funnel (left) and rotational viscometer (right) (Bourgoyne et al. 1991).

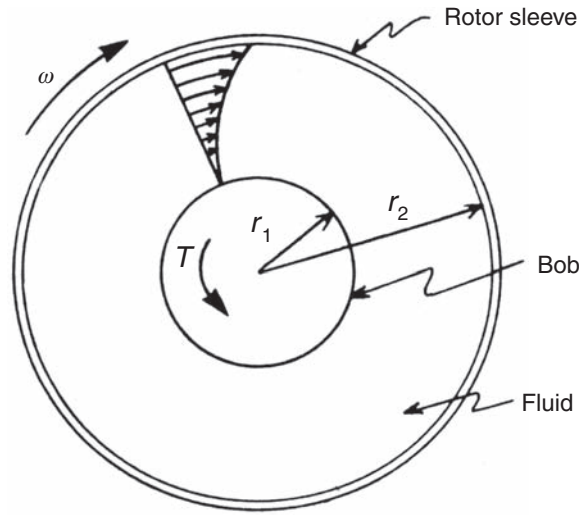


Fig. 3.16—Rotational-viscometer geometry (Bourgoyne et al. 1991).

$$\tau = \frac{M_t}{2\pi r_1^2 L}, \quad \dots \dots \dots (3.10)$$

where M_t is the torque, r_1 is the radius of the bob, and L is the length of the cylinders. In a concentric viscometer, torque M_t is measured at different rotational speeds of the outer cylinder.

Shear stress is then calculated from Eq. 3.10 and shear rate is given by:

$$\dot{\gamma} = \frac{4\pi r_2^2 \omega}{r_2^2 - r_1^2}, \quad \dots \dots \dots (3.11)$$

where r_2 is the inside radius of the outer cylinder and ω is the angular velocity of the outer cylinder. A number of commercially available concentric-cylinder rotary viscometers are suitable for use with drilling muds. They are similar in principle to the viscometer already discussed. All are based on a design by Savins and Roper (1954)—a two-speed viscometer that enabled the determination of the parameters of a fluid model called a Bingham plastic model. A Bingham plastic fluid model assumes that no flow occurs for shear stresses below τ_y , called the yield point. For shear stresses above the yield point, a Bingham plastic fluid behaves as a Newtonian fluid with viscosity μ_p , called the plastic viscosity. The formula for the Bingham plastic model is given by

$$\tau = \tau_y + \mu_p \dot{\gamma}. \quad \dots \dots \dots (3.12)$$

Fig. 3.17 shows the result of a typical viscometer test, with the Bingham-plastic curve shown as a solid line and the actual fluid response shown as a dashed line. We can see that the Bingham plastic model does not fit this fluid very well except for high shear rates, and that the true yield point falls well below the calculated yield point. For this reason, many other fluid models have been devised, which will be studied in Chapter 5. For our current purposes, we will only consider the Bingham plastic model, but note that the viscometer results can be used in other ways. Viscometers are built so that

- 1° dial reading = $1.067 \text{ lbf}/100 \text{ ft}^2 = 5.109 \text{ dynes}/\text{cm}^2$ shear stress
- $1 \text{ rev}/\text{min} = 1.703 \text{ reciprocal seconds}$, shear rate

Therefore, the plastic viscosity and yield point are calculated very simply from two dial readings at 600 rev/min and 300 rev/min, respectively.

$$\text{PV} = \theta_{600} - \theta_{300}, \quad \dots \dots \dots (3.13)$$

$$\text{YP} = \theta_{300} - \text{PV}, \quad \dots \dots \dots (3.14)$$

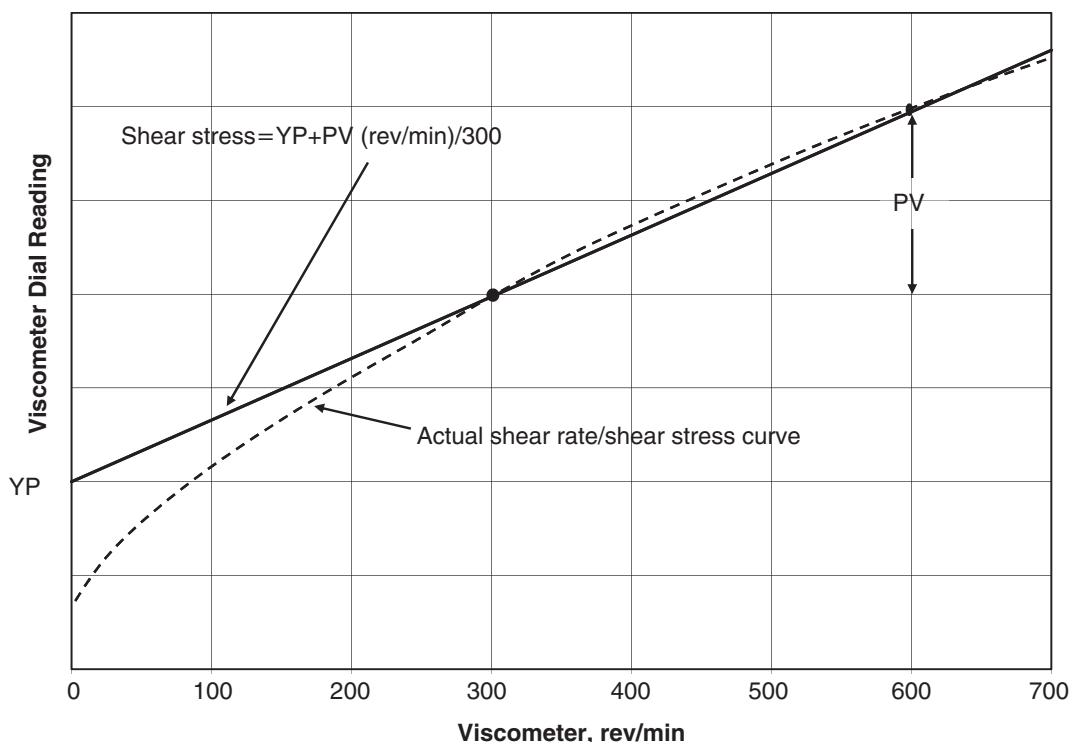


Fig. 3.17—Rotational-viscometer results.

where PV is plastic viscosity and YP is yield point. The units of plastic viscosity come out conveniently as centipoise (cp). Yield point results are reported using the units lbf/100 ft². Apparent viscosity μ_a may be calculated from the Savins and Roper (1954) viscometer reading as follows:

$$\mu_a = \frac{300 \theta}{\omega} \quad (3.15)$$

$\mu_a = \tau/\gamma = 5.109/1.703$ poise/degree per rev/min = 300 cp/degree per rev/min = $300 \theta/\omega$, where θ is the dial reading at ω rev/min. Apparent viscosity is usually reported at the 600 rev/min reading.

Notice that real fluids are not ideally any of the models shown above, but generally are close to one model or another. The selection of the model may be motivated by a particular fluid velocity of interest. Using a direct reading concentric-cylinder rotary viscometer, a more meaningful measurement of rheological properties is obtained. This rotational cylinder and bob instrument is largely known in the drilling industry as a V-G meter. In 1951, Melrose and Lilienthal (Rogers 1963) developed this multispeed viscometer for laboratory or field use in measuring the rheological properties. The rotational viscometer is capable of providing plastic viscosity, apparent viscosity, yield point, and gel strength.

Although most models operate at six different speeds, only two dial readings are converted to the rheological parameters plastic viscosity and yield point—the 300- and 600-speed readings. The shear speed—that is 300 rev/min and 600 rev/min—is the rotational speed on a standard oil-field viscometer on which the shear rate is measured. The V-G meter is called a direct reading viscometer because at a given speed, the dial reading is a true centipoise viscosity. For example, the dial reading (511 sec⁻¹) at 300 rev/min (θ_{300}) represents the true viscosity.

Plastic Viscosity. For a plastic fluid, the plastic viscosity is the shear stress in excess of the yield stress that will induce a unit rate of shear. In other words, it is that part of the flow resistance in a drilling fluid mainly produced by the friction of the suspended particles and by the viscosity of the liquid phase (IMCO 1981). It is given by Eq. 3.13. Recommended ranges of plastic viscosity are given in Fig. 3.18 as a function of mud density.

Yield Point. The yield point of clay in fresh water is defined as the number of barrels of 15-cp mud that can be obtained from 1 ton of dry material. Above 15 cp, small additions of clay have a significant effect on viscosity. The yield point is given by Eq. 3.14. Recommended ranges of yield point are given in Fig. 3.19 as a function of mud density.

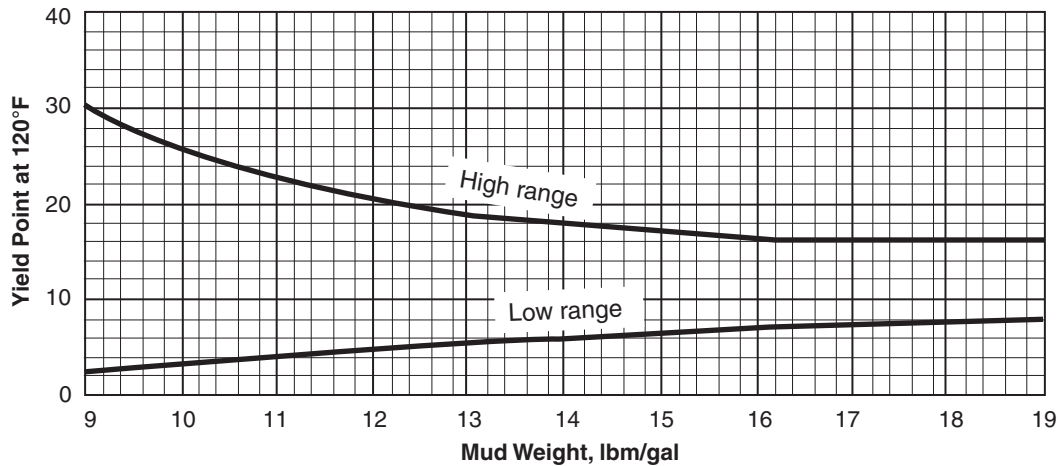


Fig. 3.18—Recommended range of yield point (Annis 1974). Reprinted courtesy of ExxonMobil.

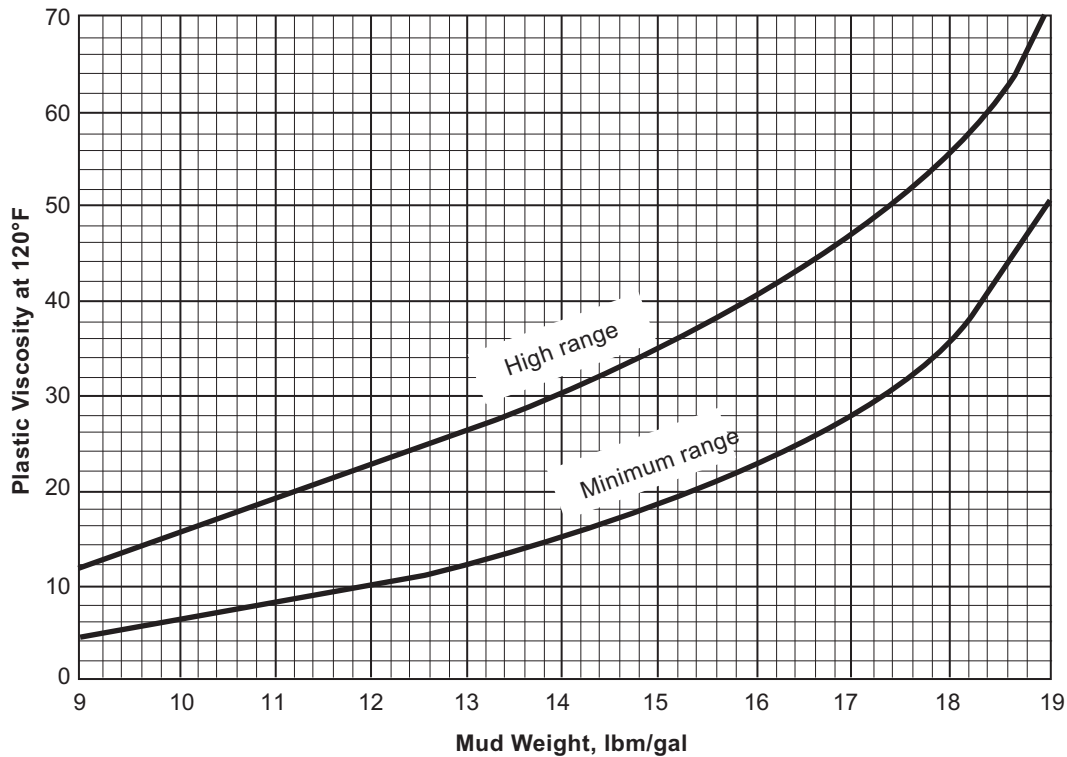


Fig. 3.19—Suggested range of plastic viscosity (Annis 1974). Reprinted courtesy of ExxonMobil.

Apparent Viscosity. In evaluating drilling fluids, it is common practice to report the effective viscosity at 600 rev/min using Eq. 3.15. This quantity is called the apparent viscosity, and is given by

$$AV = \frac{300 \theta_{600}}{600} = \frac{1}{2} \theta_{600}, \quad \dots \dots \dots (3.16)$$

where AV is apparent viscosity.

Effective Viscosity. Effective viscosity is defined as the viscosity of a Newtonian fluid that exhibits the same shear stress at the same rate of shear as the actual fluid being tested. Although it is a very useful parameter in hydraulic equations when the shear rate is known, the value of the effective viscosity is meaningless unless the rate of shear at which it is measured is specified. Furthermore, it is not a reliable parameter for comparing the viscous properties of two fluids; at least two parameters are necessary for that purpose.

Gel Strength. Gel strength is the third rheological parameter commonly used to describe non-Newtonian fluids. The gel strength is the shear stress measured at low shear rate after a mud has set quiescently for a period of time. In other words, it is the measure of ability of a colloidal solid at rest to form a gel. A colloid is a finely divided solid that does not deposit by gravity when dispersed in a liquid medium. Gel strength has the unit of pressure usually reported in lbf/100 ft². It is a measure of the same interparticle forces of a fluid as determined by the yield point, except that gel strength is measured under static conditions.

This rheological parameter is useful in drilling operations for determining the swabbing effect on pulling the drillpipe, the pressure required to break circulation, the ease of release of gas, and the settling of particles in the mud pits. The common gel strength measurements are initial and 10-min gels, which can be measured with a V-G meter as follows:

The fluid is stirred at 600 rev/min until a stable dial reading is achieved. Then the instrument is turned off. After 10 seconds of rest, the cylinder is rotated at 3 rev/min and the highest dial reading is recorded. This is called the “initial gel strength.” The same procedure is applied to measure the 10-min gel strength using a resting time of 10 minutes after stirring the mud.

Example 3.7 A mud sample in a rotational viscometer equipped with a standard torsion spring gives a dial reading of 46 when operated at 600 rev/min and a dial reading of 28 when operated at 300 rev/min. Compute the apparent viscosity of the mud at each rotor speed. Also compute the plastic viscosity and yield point.

Solution. Use of Eq. 3.15 for the 300-rev/min dial reading gives

$$\mu_a = \frac{300(28)}{300} = 28 \text{ cp.}$$

Similarly, use of Eq. 3.15 for the 600-rev/min dial reading gives

$$\mu_a = \frac{300(46)}{600} = 23 \text{ cp.}$$

Note that the apparent viscosity does not remain constant but decreases as the rotor speed is increased. This type of non-Newtonian behavior is shown by essentially all drilling muds.

The plastic viscosity of the mud can be computed using Eq. 3.13:

$$\mu_a = \frac{300(46)}{600} = 23 \text{ cp.}$$

The yield point can be computed using Eq. 3.14:

$$\tau_Y = \theta_{300} - \mu_p = 28 - 18 = 10 \text{ lbf/100 ft}^2.$$

3.7.4 Lubricity Testing. Increasing the lubricity of a drilling fluid is a technique used to help prevent stuck pipe. In this application, lubricity is the coefficient of friction between the drillpipe and the mud filter cake. The API recommended practices for mud testing do not include a specification for lubricity. Lubricity testing has undergone developmental changes to obtain a more accurate correlation between test results and actual wellbore conditions.

In 1999, a specially designed fully automated device to accurately measure the coefficient of friction between metal and mud filter cake was tested on several drilling-fluid types (Isambourg 1999). To simulate downhole conditions, drilling fluid is circulated inside a pressurized cell with a temperature capability of 100°C. The cell is also equipped with an internal porous cylinder to simulate filtrate invasion and filter cake buildup across a permeable formation. Lubricity measurements are obtained through sensors on the rotating captor, which represents the drillstring.

Once the filter cake has been deposited on the metal screen, the rotating captor moves laterally to make contact with the cake. At this point, cake thickness can be determined and recorded, and the captor can be further embedded in the cake at a preselected speed. The outer cell can be rotated at one-quarter intervals to obtain measurements at four points on the filter cake. The apparatus and procedure produced accurate and

reproducible coefficients of friction existing between the filter cake and “drill pipe” under simulated down-hole conditions. A schematic of the lubricity tester is illustrated in **Fig. 3.20**. The test measures the applied force F and the applied torque M_t . The coefficient of friction is μ_f calculated on the basis of the three following formulas:

$$M_t = F_f r_{cp}, \quad \dots \dots \dots (3.17a)$$

$$F_f^2 + F_N^2 = \vec{F} \cdot \vec{F} = F^2, \quad \dots \dots \dots (3.17b)$$

$$F_f = \mu_f F_N, \quad \dots \dots \dots (3.17c)$$

where r_{cp} is the radius of the captor, F_N is the normal force and F_f is the friction force. Moment equilibrium gives the value of F_f in Eq. 3.17a. The sum of the friction force and the normal force equals the applied force \vec{F} , so their magnitudes are equal, as given in Eq. 3.17b. Having determined F_N , we can now calculate the friction coefficient μ_f with Eq. 3.17c.

Similar apparatuses were used to analyze differential sticking forces, pull forces, and associated mud-cake pore pressures. This leads to the conclusion that filter-cake compaction and permeability have a greater impact on the likelihood of differential sticking than cake thickness alone. The type and amount of solids affect filter-cake characteristics, the degree of pipe sticking, and the pull-out force to get it free. Potassium chloride concentration in the mud may play an important role in the pull-out force because it changes the mud-cake strength through the potassium-inhibitive effect on clays.

3.7.5 Filtration Properties. The filtration and wall-building properties of drilling fluids are acknowledged as being the most significant in the good drilling of wells. This ability of the mud to seal permeable zones with a thin, low-permeability filter cake represents the key for successful completion of the hole. The mud would continuously invade the permeable formations allowing the filtrate to enter if a filter cake were not formed.

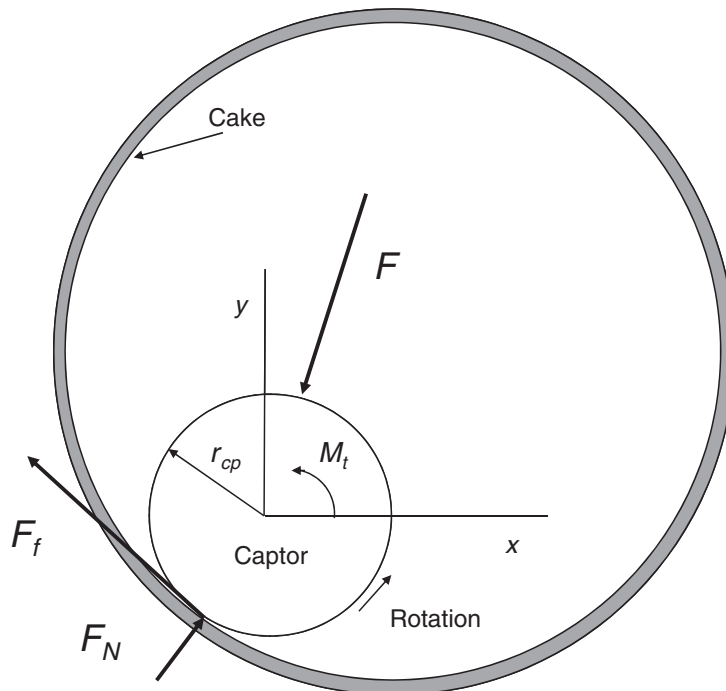


Fig. 3.20—Lubricity-test geometry.

The API Filter Press—Static Filtration. The filter press (**Fig. 3.21**) is used to determine the filtration rate through a standard filter paper and the rate at which the mudcake thickness increases on the standard filter paper under standard test conditions. This test is indicative of the rate at which permeable formations are sealed by the deposition of a mudcake after being penetrated by the bit.

The flow of mud filtrate through a mudcake is described by Darcy's law. Thus, the rate of filtration is given by

$$\frac{dV_f}{dt} = \frac{kA \Delta P}{\mu_{mf} h_{mc}}, \quad \dots \dots \dots (3.18)$$

where

dV_f/dt = the filtration rate, cm³/s

k = the permeability of the mudcake, darcies

A = the area of the filter paper, cm²

ΔP = the pressure drop across the mudcake, atm

μ_{mf} = the viscosity of the mud filtrate, cp

h_{mc} = the thickness of the filter cake (mudcake), cm

At any time t during the filtration process, the volume of solids in the mud that has been filtered is equal to the volume of solids deposited in the filter cake:

$$f_{sm} V_m = f_{sc} h_{mc} A,$$

where f_{sm} is the volume fraction of solids in the mud, and f_{sc} is the volume fraction of solids in the cake, or

$$f_{sm} (h_{mc} A + V_f) = f_{sc} h_{mc} A.$$

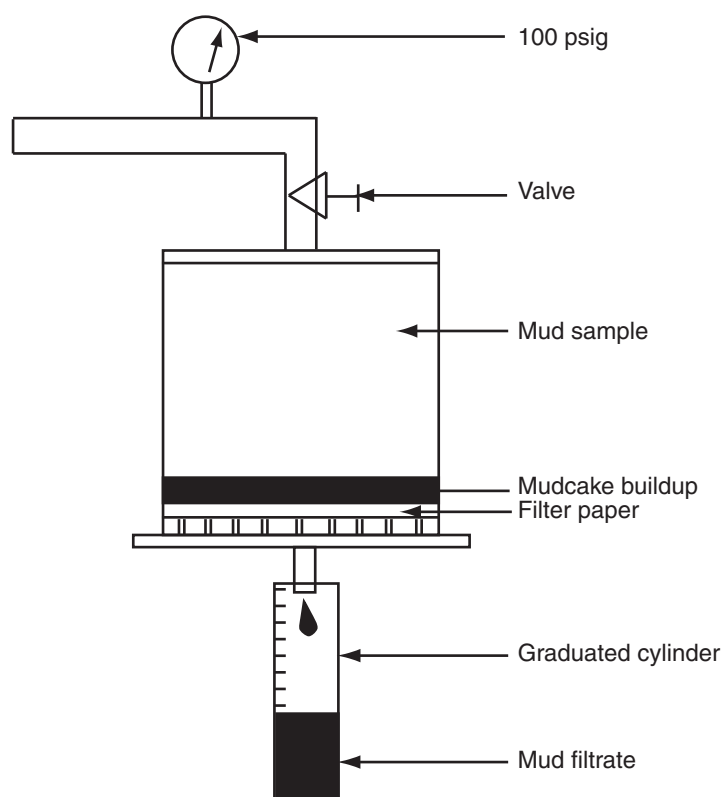


Fig. 3.21—API filter-press schematic (Bourgoyne et al. 1991).

Therefore,

$$h_{mc} = \frac{f_{sm} V_f}{A(f_{sc} - f_{sm})} = \frac{V_f}{A \left(\frac{f_{sc}}{f_{sm}} - 1 \right)}. \quad \dots \dots \dots (3.19)$$

Inserting this expression for h_{mc} into Eq. 3.18 and integrating

$$\int_0^{V_f} V_f dV_f = \int_0^t \frac{kA\Delta P}{\mu_{mf}} A \left(\frac{f_{sc}}{f_{sm}} - 1 \right) dt$$

$$\frac{1}{2} V_f^2 = \frac{k}{\mu_{mf}} A^2 \left(\frac{f_{sc}}{f_{sm}} - 1 \right) \Delta P t,$$

or

$$V_f = \sqrt{2k\Delta P \left(\frac{f_{sc}}{f_{sm}} - 1 \right) A} \frac{\sqrt{t}}{\sqrt{\mu_{mf}}}. \quad \dots \dots \dots (3.20)$$

The standard API filter press has an area of 45 cm² and is operated at a pressure of 6.8 atm (100 psig). The filtrate volume collected in a 30-minute time period is reported as the standard water loss. Note that Eq. 3.20 indicates that the filtrate volume is proportional to the square root of the time period used. Thus, the filtrate collected after 7.5 minutes should be approximately half the filtrate collected after 30 minutes. It is common practice to report twice the 7.5-minute filtrate volume as the API water loss when the 30-minute filtrate volume exceeds the capacity of the filtrate receiver. However, as shown in **Fig. 3.22**, a spurt-loss volume of filtrate, V_{sp} , often is observed before the porosity and permeability of the filter cake stabilize and Eq. 3.20 becomes applicable. If a significant spurt loss is observed, the following equation should be used to extrapolate the 7.5-minute water loss to the standard API water loss:

$$V_{30} = 2(V_{7.5} - V_{sp}) + V_{sp}. \quad \dots \dots \dots (3.21)$$

The best method for determining spurt loss is to plot V vs. \sqrt{t} and extrapolate to zero time as shown in **Fig. 3.22**.

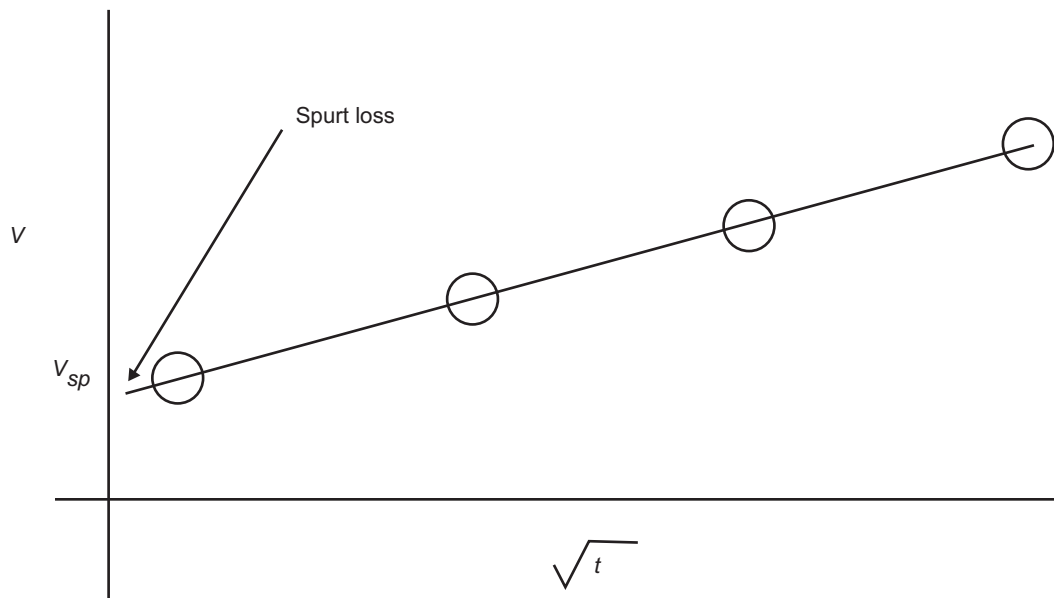


Fig. 3.22—Filtration spurt loss (Bourgoyne et al. 1991).

In addition to the standard API filter press, a smaller filter press capable of operating at elevated temperatures and pressures also is commonly used. The filtration rate increases with temperature because the viscosity of the filtrate is reduced. Pressure usually has little effect on filtration rate because the permeability of the mudcake tends to decrease with increasing pressure, and the term $\sqrt{k\Delta P}$ in Eq. 3.20 remains essentially constant. However, an elevated pressure is required to prevent boiling when operating above 212°F. The area of the filter paper used in the high-pressure/high-temperature (HP/HT) filter press is one-half the area of the standard filter press. Thus, the volume of filtrate collected in 30 minutes must be doubled before reporting as API water loss. An example HP/HT filter press is shown in Fig. 3.23.

Example 3.8 Using the following data obtained by using an HP/HT filter press, determine the spurt loss and API water loss.

Time (minutes)	Filtrate Volume (cm ³)
1.0	6.5
7.5	14.2

Solution. The spurt loss of the cell can be obtained by extrapolating to zero time using the two data points given:

$$6.5 - \frac{14.2 - 6.5}{\sqrt{7.5} - \sqrt{1}} \sqrt{1} = 2.07 \text{ cm}^3.$$

However, since the standard API filter press has twice the cross-sectional area of the HP/HT filter press, the corrected spurt loss is 4.14 cm³. The 30-minute filtrate volume can be computed using Eq. 3.8:

$$\begin{aligned} V_{30} &= 2(V_{7.5} - V_{sp}) + V_{sp} \\ &= 2(14.2 - 2.07) + 2.07 = 26.33 \text{ cm}^3. \end{aligned}$$

Adjusting for the effect of the filter press cross-sectional area, we obtain an API water loss of 52.66 cm³ at the elevated temperature and pressure of the test.

Both low-temperature and high-pressure API filter presses are operated under static conditions—that is, the mud is not flowing past the cake as filtration takes place. Other presses have been designed to model more accurately the filtration process wherein mud is flowed past the cake, as it does in the wellbore. Such presses that model *dynamic filtration* have shown that, after a given period of time, the mudcake thickness remains constant—that is, the cake is eroded as fast as it is being deposited. Thus, dynamic-filtration rates are higher than static-filtration rates. With a constant-thickness cake, integrating Eq. 3.18, we have

$$V_f = \frac{kA \Delta P t}{\mu_{mf} h_{mc}}. \quad (3.22)$$

A standard dynamic-filtration test has not been developed to date. Field mud testing uses the static filtration test to characterize the filtration quality of the mud. Unfortunately, there are no reliable guidelines for correlating static- and dynamic-filtration rates. Our ability to predict quantitatively filtration rates in the wellbore during various drilling operations remains questionable.

3.7.6 Testing for Chemical Properties. Again, a solid understanding of drilling fluids requires a sound understanding of their chemistry. Drilling-fluid engineers deal with mud chemistry daily because the mud's water-phase complexity requires control to keep the desired ionic balance. Simple water chemistry cannot provide an accurate prediction of ionic behavior that results from the interaction and reaction of various ions with solids in mud systems. Standard chemical tests have been elaborated for determining the concentration of certain ions present in the drilling fluid, such as OH⁻, Cl⁻, and Ca⁺².

Acids, Bases, and Salts. Acids are sour-tasting solutions that cause effervescence in contact with carbonates, cause corrosion to metals, turn blue litmus (a dye extracted from lichens) paper red, and react with bases to form

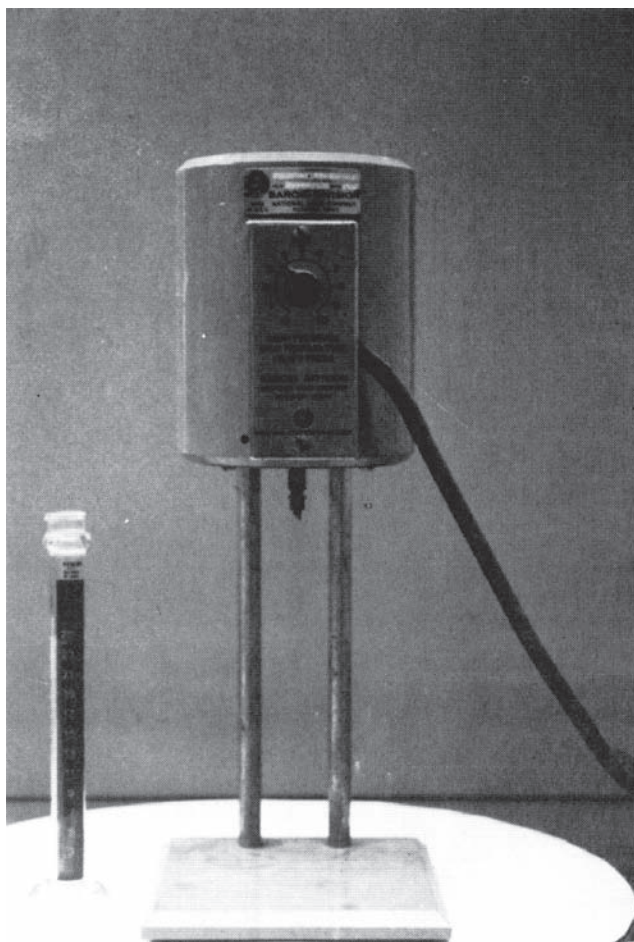


Fig. 3.23—HP/HT filter press (Bourgoyne et al. 1991).

salts. Acid comes from the Latin word “acidus” which means “sharp.” Because acids are substances considered to have an excess of hydrogen ions (H^+), they are termed *strong* (pH from 0 to 4) or *weak* (pH from 3 to 6) according to hydrogen-ion concentration. A weak acid is an acid that only partially ionizes in an aqueous (mainly water) solution (i.e., not every molecule breaks apart).

Bases are bitter-tasting solutions that feel slippery in solution, turn red litmus blue, and become less basic when mixed with acids. The weakness of a base depends on the quantity of the molecule that dissociates into hydroxyl ions (OH^-) in solution. A strong base is a base that has a very high pH (from 10 to 14). A weak base is a base that only partially ionizes in an aqueous solution. Weak bases usually have a pH close to 7 (from 8 to 10).

Salts are any compound other than water formed by the reaction of an acid and a base. In other words, salts are combinations of the negative ion from an acid, known as an anion, and the positive ion from a base, known as cation. Depending on the relative strengths of the particular ions, a salt may be neutral or have a tendency in the direction of the acid or the base. For example, an alkaline salt is the combination of a weak acid with a strong base, whereas a neutral salt is the mixture of both strong acid and strong base.

Acidity and Alkalinity. A solution is considered acidic when the hydrogen-ion concentration (H^+) is greater than the hydroxyl-ion concentration (OH^-); the opposite is called an alkaline solution. The relative acidity or alkalinity of a liquid (drilling fluid) is conveniently expressed as pH. Drilling-fluid pH considerably affects the mud-rheological properties, the dispersability of clays, the solubility of chemical products, and the corrosion of steel-based materials.

Buffer Solutions. A buffer solution is one that resists large pH changes when small quantities of a base or acid are added to the solution. In other words, a buffer solution contains components that will remove any hydrogen ions or hydroxide ions that might be added to it. Acidic buffer solutions have a pH less than 7 and are commonly a combination of a weak acid (i.e., carbonic acid, H_2CO_3) with one of its salts—often a sodium salt. On the other hand, base-buffer solutions have a pH greater than 7 and are the combination of a weak base (i.e., ammonium

hydroxide, NH_4OH) with one of its salts. In either case, a buffer solution is a mixture of a weak acid or weak base and its salt.

Triethanolamine, lime, and magnesium oxide are all solutions used to buffer pH-sensitive drilling-fluid systems. To maintain stable mud properties and to resist the negative effect of many contaminants, buffering is highly advantageous.

Electrolytes. An electrolyte is a nonmetallic substance that dissociates into ions in aqueous solution. Electrolytes conduct electric currents in solutions by moving ions rather than electrons. In other words, electrolytes provide the ion-transport mechanism between the positive and negative electrodes of an electrochemical cell. All acids, bases, and salts are electrolytes.

Strong electrolytes are completely ionized solutions (having a high concentration of ions), while weak electrolytes are not completely ionized solutions. Salts are commonly strong electrolytes, whereas water is a weak electrolyte and not as conductive as salt solutions.

Titration. Chemical analysis by titration is used to test drilling fluids. Titration is a technique used to determine the concentration of a solute (a dissolved substance) in a solution. One solution is added to another solution until the chemical reaction between the two solutes is complete. The concentration and volume of one solution is known (N_1 and V_1 , respectively), and a sample volume of a different solution (V_2) is used to determine the unknown concentration (N_2). That is,

$$N_2 = \frac{V_1 N_1}{V_2}.$$

API Specification 13I (2009) explains the titration process used in drilling-fluid chemical tests.

Concentration of Solutions. There are several different ways of specifying the concentration of solutions. The reason for these multiple definitions is that some definitions are more convenient than others, depending on the materials being studied.

Molality (m): The molality of a solution is the concentration expressed as number of moles of solute (the material dissolved) per kilogram of solvent. For example, 1 mol (molal) of NaOH = 40 g NaOH /kilogram water. This unit of concentration is not used commonly for mud laboratory testing.

Molarity (M): This unit of concentration is used commonly for laboratory testing and analytical reagents, expressed in units of g mol/L. The molar concentration of a solution is expressed as the number of moles of solute per liter of solution. For example, 1M HCl = 36.5 g/L because 1M HCl contains 36.5 g (molecular weight) of HCl dissolved in 1 liter of solution. If the normality concentration of a solution is known, the molarity can be determined using $\text{molarity} = \text{normality} \div \text{net positive valence}$.

Normality (N): Equivalent concentration or normality is commonly used with acid/base reactions (laboratory reagents), expressed as gram equivalent weight per liter, gew/L. Normality is the concentration unit expressed in equivalent weights of solute per liter of solution. A one normal solution (1N) contains 1 mole of solute, divided by its ionic charge, in 1 liter of solution. A gram equivalent weight is the mass of the substance that contains a 1-gram atom of available hydrogen or its equivalent. In other words, the equivalent weight of an element or ion is

Atomic weight/charge of the ion formed,

whereas the equivalent weight of a compound is

Molecular weight/total charges of cations (positive ions).

For example, sulfuric acid (H_2SO_4) has a molecular weight of 98 and a total cation charge of 2 (2H^+). Because the equivalent weight of sulfuric acid is 49 g, the 1N concentration is 49 g/L.

Milligrams per liter (mg/L): This “weight-volume-relationship” concentration unit is commonly improperly reported as the “weight-weight relationship” unit called parts per million (ppm). In fact some sources define it as equivalent to 1 ppm. As a weight per volume relationship, a 10 mg/L solution contains 10 milligrams of solute per liter of solution. Milligrams per liter can be easily converted to ppm if solution density is known.

Parts per million (ppm): This weight-weight relationship is the parts by weight of a solute per million parts of solution.

Example 3.9 A CaCl_2 solution is prepared at 68°F by adding 11.11 g of CaCl_2 to 100 cm^3 of water. At this temperature, water has a density of 0.9982 g/cm^3 and the resulting solution has a density of 1.0835 g/cm^3 . Express the concentration of the solution using (1) molality, (2) molarity, (3) normality, (4) milligrams per liter, and (5) parts per million. The molecular weight of CaCl_2 is 111.0 g/g-mole.

Solution.

1. For a water density of 0.9982 g/cm³, the molality of the solution is

$$\frac{11.11 \text{ g}}{111.0 \text{ g/g} \cdot \text{mole}} \times \frac{1,000 \text{ g/kg}}{(0.9982 \text{ g/cm}^3)(100 \text{ cm}^3)} = 1.003 \text{ g} \cdot \text{mol/kg}.$$

The volume of the solution can be computed from the mass of solute and solvent and the density of the solution. Because 11.11 g of CaCl₂ added to 100 cm³ of water gave a solution density of 1.0835 g/cm³, the solution volume is

$$\frac{(11.11 + 99.82) \text{ g}}{1.0835 \text{ g/cm}^3} = 102.38 \text{ cm}^3.$$

2. Thus, the molarity of the solution is

$$\frac{11.11 \text{ g}}{102.38 \text{ cm}^3} \times \frac{1 \text{ g mol}}{111 \text{ g}} \times \frac{1,000 \text{ cm}^3}{1 \text{ L}} = 0.978 \text{ g mol/L}.$$

3. Because 0.5 mol of CaCl₂ would tend to react with 1 mol of hydrogen, the gram-equivalent weight of CaCl₂ is half the molecular weight. The normality of the solution is

$$\frac{11.11 \text{ g}}{102.38 \text{ cm}^3} \times \frac{1 \text{ gew}}{55.5 \text{ g}} \times \frac{1,000 \text{ cm}^3}{1 \text{ L}} = 1.955 \text{ gew/L}.$$

4. Concentration of CaCl₂ in milligrams per liter is

$$\frac{11.11 \text{ g}}{102.38 \text{ cm}^3} \times \frac{1,000 \text{ mg}}{1 \text{ g}} \times \frac{1,000 \text{ cm}^3}{1 \text{ L}} = 108,517 \text{ mg/L}.$$

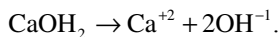
5. The concentration of CaCl₂ in parts per million is given by

$$\frac{11.11 \text{ g}}{(11.11 + 99.8) \text{ g}} \times \frac{1 \text{ ppm}}{10^{-6}} = 100,153 \text{ ppm}.$$

Alkalinity and Lime Content. Alkalinity is not the same as pH; it refers to the ability of a solution to react with an acid. In other words, alkalinity is the concentration of excess hydroxyl (OH⁻), bicarbonate (HCO₃⁻), and carbonate (CO₃⁻²) ions in a water-based solution. Alkalinity is a chemical property of an aqueous system that implies that there are more hydroxyl ions (OH⁻) in the system, or a potential to produce more hydroxyl ions, than there are hydrogen ions (H⁺), or potential to produce hydrogen ions.

In drilling-fluid engineering, the phenolphthalein alkalinity (*P*) refers to the amount of acid (ml of 0.02 N H₂SO₄ for water-based mud) required to titrate 1 ml of filtrate fluid (*P_f*) or mud (*P_m*) and reduce the pH to 8.3, the phenolphthalein endpoint, whereas the methyl orange filtrate alkalinity (*M_f*) measures the acid required to reduce pH to 4.3, the methyl orange endpoint. The alkalinity test is a well-known water-analysis procedure to estimate the concentration of the ions OH⁻, HCO₃⁻, and CO₃⁻² in the aqueous phase of the mud.

When drilling fluid is saturated by calcium hydroxide (CaOH₂)—commercially called lime—it is named lime-treated mud. The lime suspended in the mud will go into and tends to stabilize the pH. Once lime is added it becomes primarily an alkalinity source producing hydroxyl ions:

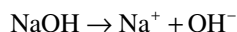


The hydroxyl ions are immediately active in the drilling-fluid system. The free-lime content, ρ_{FL} , is calculated as

$$\rho_{FL} = 0.26(P_m - F_w P_f),$$

where F_w is the volume fraction of water in the mud.

Caustic soda, a strong base, represents another alkalinity source:



Alkalinity testing allows measuring of P_m , M_{ff} , and P_f by determining the amount of a standard acid solution necessary to neutralize the alkalinity present. Measurements of P_m , M_{ff} , and P_f can indicate the source and the amount of alkalinity. In addition, these measurements help monitor and identify CO_2 , HCO_3^- , and CO_3^{2-} contamination, and give the mud engineer a better understanding of the ionic and buffering environment of the drilling-fluid system.

Solid-Content Analysis. In addition to the effects of solids (e.g., sand) on drilling-fluid properties such as density, viscosity, gel strength, fluid loss, and temperature stability, sand is highly abrasive to the fluid-circulating system. For this reason, the solid content in the drilling mud must be maintained at a low level. Formations containing silica and quartz add sand to the mud after being penetrated by the drilling bit.

Solid-content tests determine the content of sand, total solids, oil, and water and the cation-exchange capacity of the drilling mud. The sand content of mud is measured by the use of a 200-mesh sand-screen set, while the mud retort test determines the volume fraction of oil, water, and total solids in drilling mud. Although there is not a standardized value for the sand-content test, the presence of such solids should be noted and reported in volume percentage (vol%).

Hydrogen-Ion Concentration (pH). The pH value is always used to describe the acidity or basicity of solutions and is defined as the negative log of the hydrogen-ion concentration. Currently, there are two methods for measuring the hydrogen-ion (H^+) concentration (pH) of drilling fluids: colorimetric method, using pH paper test strips, and the electrometric method, using a pH meter with a glass electrode.

From the chemical-dissociation reaction of hydrogen, pH is denoted as follows:

$$\text{pH} = -\log[\text{H}^+],$$

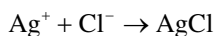
where $[\text{H}^+]$ is the hydrogen-ion concentration. For pure water at 75°F, $\text{pH} = 7$ and the pure-water system is called neutral. Systems with pH less than 7 (from 1 to 6) are called acidic, while those with pH greater than 7 (from 8 to 14) are called basic or alkaline.

A change of one pH unit corresponds to a tenfold increase in hydrogen-ion concentration. Water is a weak electrolyte that exists in nature as molecules of H_2O . It can ionize to form hydronium (H_3O^+) ions and hydroxyl (OH^-) ions. The equilibrium of water with these ions ($2\text{H}_2\text{O} \rightleftharpoons \text{H}_3\text{O}^+ + \text{OH}^-$) may be affected by dissolved acid solutions when hydrogen ions (H^+) are added. Hydrogen ions increase the hydronium concentration $[\text{H}_3\text{O}^+]$.

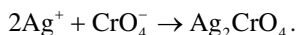
Because mud pH affects mud rheological properties, the dispersibility of clays, the corrosion of steel materials (drillstring and completion equipment), and the solubility of various chemicals and products, routine adjustments to the mud pH are fundamental to drilling-fluid control. For example, a proper pH level permits bentonite to yield faster and fully and to remain in suspension.

Alkalinity refers to the acid-neutralizing ability of a solution or mixture. In other words, it is a chemical property of a solution indicating that there are more hydroxyl ions (OH^-) than hydrogen ions (H^+). Standardized acids are used to determine the total amount of hydroxyl ions in the solution by titration. The phenolphthalein alkalinity refers to the quantity of acid needed to reduce the mud pH to 8.3, which is the phenolphthalein endpoint (Bourgoyne 1991). Because pH readings become rather insensitive at higher values (due to the logarithmic scale), the analysis of the mud filtrate for determining the alkalinity of the drilling fluid is preferable. The phenolphthalein alkalinity test reports the number of ml of 0.02N (N/50) acid needed per ml of drilling mud.

Chlorine Concentration (Salt). In areas where salt (sodium chloride) can enter and contaminate drilling fluids, the chlorine or salt analysis is extremely important. Salt enters the mud when either salt-containing formations are drilled or salt-water (formation water) enters the wellbore. This includes most of the world's oil and gas fields. The chlorine-ion (Cl^-) concentration is determined by titration using a silver-nitrate solution as titrant and potassium chromate as the endpoint indicator. For the titration to work correctly, the pH of the filtrate must be slightly basic (e.g., $\text{pH} = 8.3$). The titrant causes the chlorine ion to be removed from the solution as silver chloride (white precipitate), while the silver chromate will not start to precipitate until all chloride ions are tied up as silver chloride. Two chemical reactions take place as follows, first the precipitation of silver chloride:



and then the precipitation of silver chromate:



Calcium Concentration (Total Hardness). The presence of calcium and magnesium ions determines the total hardness of drilling-mud filtrate. These contaminants—the divalent cations Ca^{2+} and Mg^{2+} —are frequently present in the water used to prepare the mud, in the cement used for the cementing process, and in anhydrite or gypsum formations. The total Ca^{2+} and Mg^{2+} concentration is determined by titration. The process termed *water softening* is used to remove hardness.

In some oil fields, the water available for use in the drilling fluid is fairly hard. The harder the water, the more bentonite it takes to produce an acceptable gel mud because the clays have low yields when mixed in hard water (Magcobar 1972).

3.8 Solids Control

Solids-control equipment is designed to control the buildup of undesirable solids in a mud system. Rheological and filtration properties can become difficult to control when the concentration of drilled solids (low-gravity solids) becomes excessive. Penetration rates and bit life decrease and hole problems increase with a high concentration of drill solids.

In an ideal situation, all drill solids are removed from a drilling fluid. Under typical drilling conditions, low-gravity solids should be maintained below 6 vol%. How serious is the added mass of the drilled solids? The volume of rock fragments generated by the bit per hour of drilling is given by

$$V_{ls} = \frac{\pi(1-\phi)d^2}{4} \text{ROP}, \quad \dots\dots\dots (3.23)$$

where V_{ls} is the solids volume of rock fragments entering the mud, ϕ is the average formation porosity, d is the bit diameter, and ROP is the rate of penetration of the bit. The first few thousand feet of hole drilled in the US Gulf Coast area usually has a diameter of approximately 15 in. and is drilled in excess of 100 ft/hr. Thus, for an average formation porosity of 0.25, V_{ls} would be given approximately by

$$V_{ls} = \frac{\pi(1-0.25)(15/12)^2}{4} \times (100) = 122.7 \text{ ft}^3/\text{hr}.$$

From Table 3.1, the average specific gravity of drilled solids is approximately 2.6, so the density is $2.6 \times 62.4 \text{ lbm/ft}^3$ (density of water) = 162.2 lbm/ft^3 . At a rock solids inlet volume rate of $122.7 \text{ ft}^3/\text{hr}$, the drilled solids mass rate is:

$$162.2 \text{ lbm/ft}^3 \times 122.7 \text{ ft}^3/\text{hr} \times 1 \text{ ton}/2000 \text{ lbm} = 9.95 \text{ tons/hr}.$$

Thus, the volume of drilled solids that must be removed from the mud can be quite large.

Formation-friendly low density solids and solids-free water-based fluid systems can be formulated with a brine base (for density) and polymers for viscosity and fluid-loss control. The introduction of a clay-free SBF system has further enhanced the well-respected performance of SBFs by providing a flat rheological profile that responds quickly to treatment in cold and high-temperature environments. However, achieving the maximum benefit from running these fluid systems depends to a great extent on the efficiency of the rig's solids-control equipment. **Fig. 3.24** shows a typical solids-removal system. Four devices are illustrated:

- Screen shaker
- Desander
- Desilter
- Centrifuge

Desanders and desilters are similar devices called hydrocyclones. **Fig. 3.25** shows the various solids-particle sizes and the range of sizes that each device can remove from the drilling fluid. Note that “mesh” refers to the screen shaker, also called a shale shaker. Not shown is a settling pit where solids are allowed to settle out of the drilling fluid.

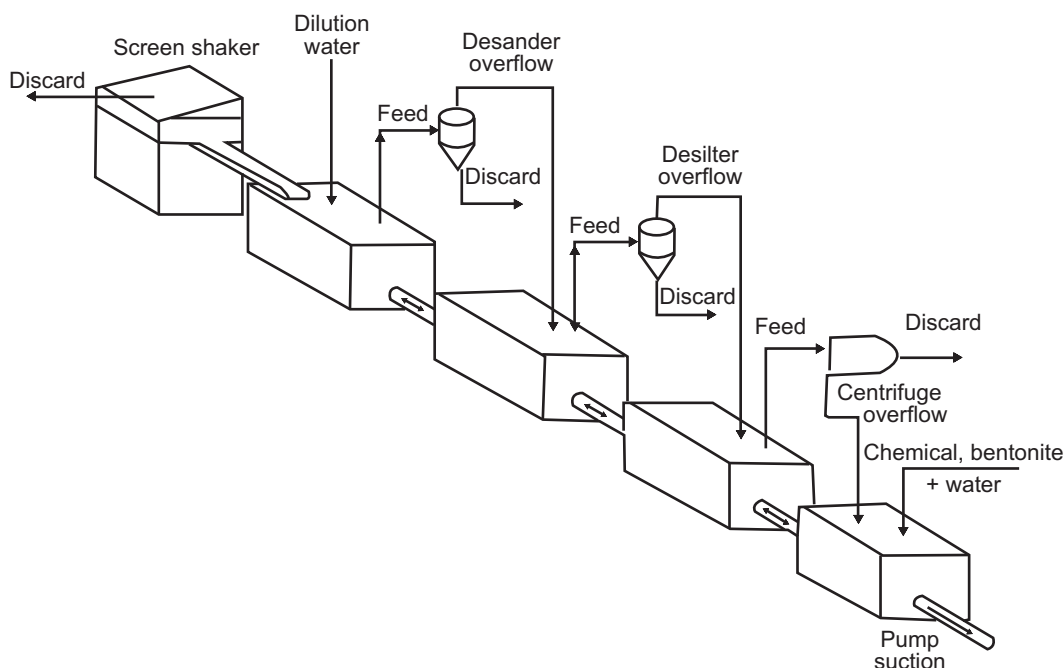


Fig. 3.24—Solids-control system (Bourgoyne et al. 1991).

The two primary sources of solids are chemical additives and formation cuttings. Formation cuttings are contaminants that degrade the performance of the drilling fluid. If the cuttings are not removed, they will be ground into smaller and smaller particles that become more difficult to remove from the drilling fluid. Keep in mind—the smaller the drill-solid particle to be removed, the more difficult it is to remove.

Most formation solids can be removed by mechanical means at the surface. Small particles are more difficult to remove and have a greater effect on drilling-fluid properties than large particles. Solids-processing efficiency is determined by the last piece of equipment processing 100% of the flow.

Solids control is accomplished either mechanically with a screen or with the application of time and gravity. Mechanically with a screen means a shale shaker. Time and gravity means either a settling pit or a hydrocyclone. If time is not available, then increasing gravity through centrifugal separation devices is effective. Dilution is another form of solids control, but is generally considered to be a much less efficient and much more expensive option, which we have already addressed earlier in this chapter.

3.8.1 Settling Pit. One inexpensive solids-control method is to allow a drilling fluid time to settle. That means circulating through a settling pit. Particles above colloidal size will eventually settle out if in a quiescent condition. However, the smaller the particle, the longer it will take to settle. In some cases, for silt-sized particles, it may take days. Particle-settling velocities are given in Fig. 3.25.

3.8.2 Shale Shakers. The most common screen device is a shale shaker (**Fig. 3.26**), which contains one or more vibrating screens through which mud passes as it circulates out of the hole. Shale shakers are classified as circular/elliptical or linear-motion shale shakers.

Mesh Size. Mesh screen size is the number of openings per linear inch as measured from the center of the wire. For example, a 70×30 oblong screen has 70 openings across a 1-in. segment, with 30 openings along the 1-in. line perpendicular to the first segment. A 20×20 mesh screen has 20 openings per inch of screen on mutually perpendicular sides. It has relatively large openings. A 220×220 mesh screen has 220 openings per inch on both sides. It has relatively small openings. In addition, the mesh material in this case is much smaller in diameter than in the 20×20 mesh screen, potentially making tearing more likely.

Circular/Elliptical-Motion Shaker. This shaker, also known as a “rumba” shaker, uses elliptical rollers to generate a circular rocking motion to provide better solids removal through the screens.

Linear-Motion Shaker. The development of the linear-motion shaker has made the use of a desander/desilter almost unnecessary. If 220 mesh screens can be run on the shaker, the fluid can go directly from the shaker to the mud cleaner (that has 250 mesh screens for a finer cut of particles).

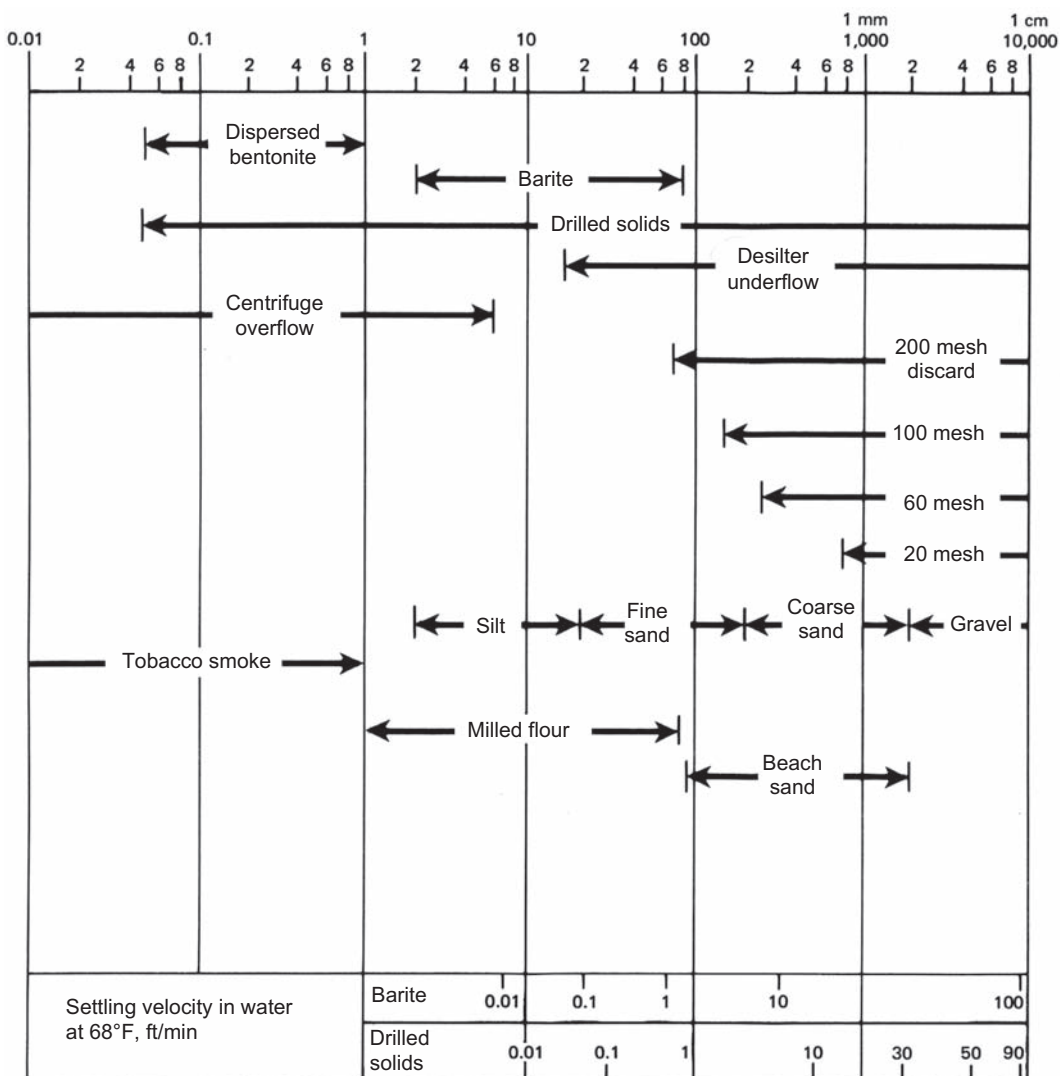


Fig. 3.25—Particle size for solids-control devices (Annis 1974). Reprinted courtesy of ExxonMobil.

A linear-motion shaker uses a straight back-and-forth rocking motion to keep the fluid circulating through the screens. Four-screen linear-motion shakers configured in a series currently provide extremely efficient removal of drill solids. Very fine mesh screens can be run on these shakers, constrained only by the need to preserve the barite in a weighted system.

Actual separation sizes are determined by factors such as particle shape, fluid viscosity, feed rates, and particle cohesiveness. Some drilling fluids can form a high surface-tension film on the wires of the screen and reduce the effective opening size of the screen.

Screens are available in 2D and 3D designs. 2D screens can be classified as panel screens, with two or three layers bound at each side by a one-piece, double-folded hook strip, or they can be classified as perforated-plate screens, with two or three layers bonded to a perforated metal plate that provides support and is easy to repair.

3D screens are perforated plate screens with a corrugated surface that runs parallel to the flow of fluid, providing more screen area than the 2D screen configuration. On a properly designed screen, the fluid will pass through the openings about midway down the screen surface.

3.8.3 Hydrocyclones. Hydrocyclones are a means to circulate a drilling fluid around a cylinder at a high rate of speed. In effect, the gravitational field on the drilling fluid is artificially increased, greatly speeding up the settling time of the particles. A typical hydrocyclone is illustrated in Fig. 3.27. Hydrocyclones have been used by the drilling industry for decades, and it is amusing that they were only recently discovered for use in home vacuum cleaners.

Hydrocyclones come in various sizes and shapes. They are usually specified by the size particles they are designed to remove. There are desanders, desilters, mud cleaners, and centrifuges. A desander typically has a few



Fig. 3.26—Typical shale shaker [from *Oilfield Glossary* (2011)]. Courtesy of Mark Ramsey/Texas Drilling Associates.

large diameter cones (greater than 6 in. diameter), whereas a desilter has a larger number of small diameter cones (less than 6 in. in diameter). Desanders are designed to remove sand-sized particles and desilters are designed to remove silt-sized particles. Mud cleaners are a combination of a fine-screened (roughly 320 mesh) shale shaker under a desilter. It is used for weighted muds because barite tends to be removed with silt-sized particles. By using a mud cleaner, barite can be recovered and reused.

Example 3.10 A mud cup is placed under one cone of a hydrocyclone being used to process an unweighted mud. Thirty seconds were required to collect 1 qt of ejected slurry. The density of the slurry was determined (using a mud balance) to be 17.4 lbm/gal. Compute the mass of solids and volume of water being ejected by the cone per hour.

Solution. The density of the slurry ejected from the desilter can be expressed in terms of the volume fraction of low-specific-gravity solids by

$$\bar{\rho} = \frac{m_{ls} + m_w}{V_{ls} + V_w} = \frac{\rho_{ls}V_{ls} + \rho_wV_w}{V_{ls} + V_w} = \rho_{ls}f_{ls} + \rho_wf_w,$$

where $\bar{\rho}$ is the density of the slurry, m_{ls} is the mass of the low density solids, and m_w is the mass of the water. Using the values given in Table 3.1, the average density of low-specific-gravity solids is $2.6 \times 8.33 = 21.7$ lbm/gal, and the density of water is 8.33 lbm/gal. Substituting these values in the above equation yields

$$17.4 = 21.7f_{ls} + 8.33(1 - f_{ls}).$$

Solving for the volume fraction of solids gives

$$f_{ls} = \frac{17.4 - 8.33}{21.7 - 8.33} = 0.6784.$$

Because the slurry is being ejected at a rate of 1 qt per 30 seconds, the mass rate of solids is

$$\frac{0.6784 \text{ qt}}{30 \text{ sec}} \times \frac{1 \text{ gal}}{4 \text{ qt}} \times \frac{21.7 \text{ lbm}}{\text{gal}} \times \frac{3,600 \text{ sec}}{\text{hr}} = 441.6 \text{ lbm/hr},$$

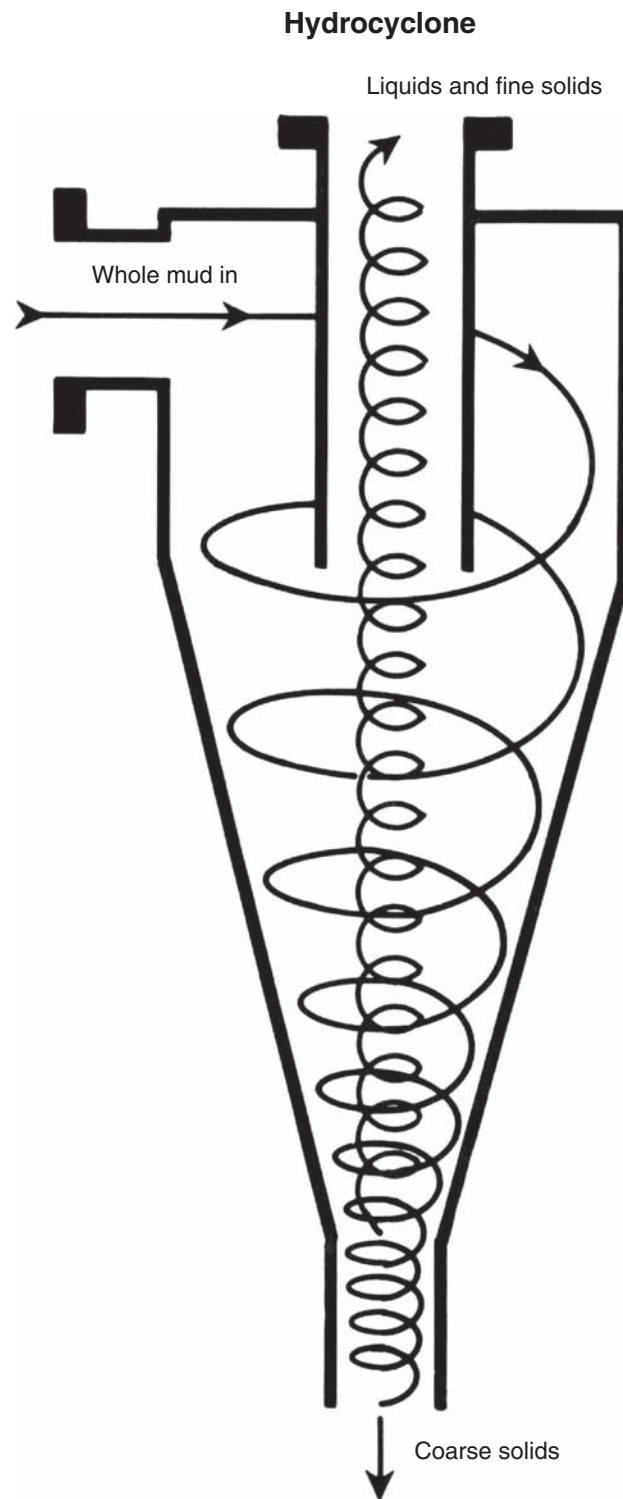


Fig. 3.27—Hydrocyclone schematic (Annis 1974). Reprinted courtesy of ExxonMobil.

and the volume rate of water ejected is

$$\frac{(1.0 - 0.6784) \text{ qt}}{30 \text{ sec}} \times \frac{1 \text{ gal}}{4 \text{ qt}} \times \frac{3,600 \text{ sec}}{\text{hr}} = 9.65 \text{ gal/hr.}$$

Note that to prevent the gradual loss of water from the mud, 9.65 gal of water must be added each hour to make up for the water ejected by this single cone.

3.8.4 Centrifuge. When installed downstream of properly configured shakers, a decanter centrifuge efficiently removes most of the fine particles that traditional solids-removal equipment cannot capture. Typically, the decanter centrifuge features slender cylindrical- or conical-bowl sections with a relatively large aspect (length/diameter) ratio, as shown in **Fig. 3.28**. A screw conveyor is fitted inside the bowl for continuous removal of separated solids. Typical bowl speeds are 1,800 to 4,000 rev/min and the developed G-force is between 644 and 3,100 Gs.

The drilling fluid is fed into the rapidly spinning cylindrical section. Through centrifugal force, the solids form a layer around the bowl wall. The thickness of this layer is determined by a series of discharge weirs at the end of the cylindrical section through which the clean liquid is decanted. The solids, being heavier, collect at the bowl wall. From there they are continuously removed by the screw conveyor. The solids are transported along the conical section (the beach) where they are dried, and then discarded out the discharge ports.

The separation result, solids recovery, solids dryness, and liquid clarity can be optimized during operation. Parameters influencing the result are easily regulated and include feed rate, rev/min (G-force), pond depth, and differential conveyor speed.

3.8.5 Summary. A high-efficiency system for drill-solids removal means drastically reduced mud cost and significantly increased penetration rates, as well as a significantly decreased risk of differential sticking and other associated hole problems. The dilution costs for maintaining a drilling fluid in perfect condition are directly related to the drill solids remaining in the system after processing by the solids-control equipment. A small increase in solids-removal efficiency can result in large savings.

3.9 Health, Safety, and Environmental (HSE) Considerations

A prime objective in all drilling operations is to minimize safety and environmental risks while maintaining drilling performance. Operators and service companies alike take a proactive stance to reduce the potential for

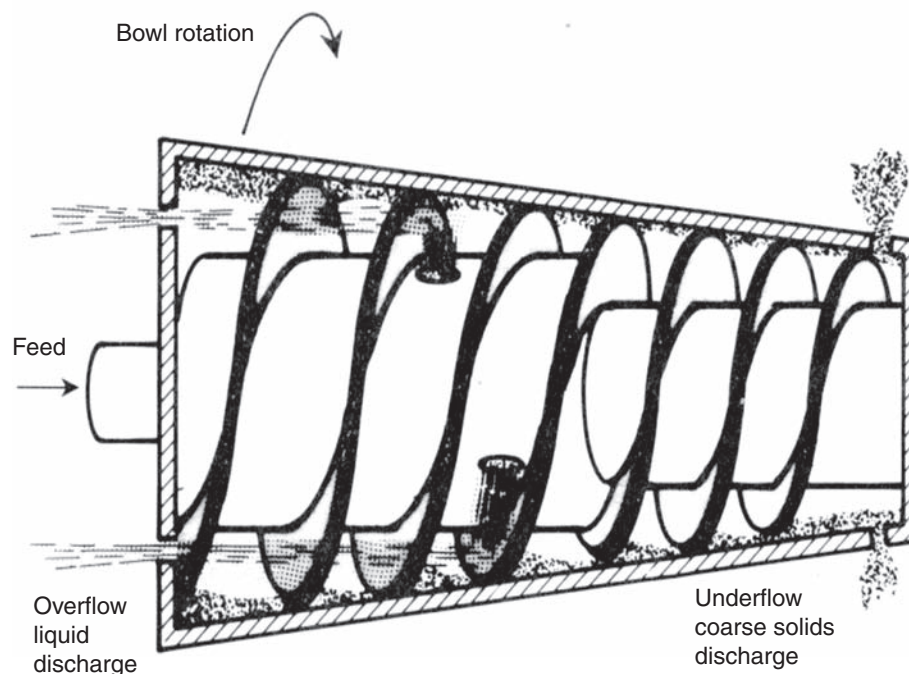


Fig. 3.28—Decanting-centrifuge schematic (Annis 1974). Reprinted courtesy of ExxonMobil.

hazardous incidents and to minimize the impact of any single incident. The HSE policies of many companies are more stringent than those required by national governments and the various agencies charged with overseeing drilling operations. All personnel who take part in the well-construction process must comply with these standards to ensure their own safety and the safety of others. On most locations, a zero-tolerance policy is in effect concerning behaviors that may endanger workers, the environment, or the safe progress of the operation. Additionally, all personnel are encouraged to report any potentially hazardous activities or circumstances through a variety of observational safety programs.

The packaging, transport, and storage of drilling-fluid additives and/or premixed-fluid systems are subject to close scrutiny regarding HSE issues. Personnel who handle drilling fluid and its components are required to wear personal protective equipment (PPE) to prevent inhalation and/or direct contact with potentially hazardous materials. Risk-assessed ergonomic programs have been established to reduce the potential for injuries related to lifting and operating mud-mixing equipment.

3.9.1 Protecting the Environment. In addition to the obvious benefits of minimizing, if not totally eliminating, sources of pollution and related threats to the ecosystem, the oil and gas industry recognizes that governmental permission to acquire and develop commercial reserves worldwide is more easily obtained if drilling-related accidents are few and far between.

Drilling fluid companies strive to achieve and maintain an “econoecological” balance with each drilling-fluid system and additive. A “green” drilling-fluid system that performs poorly will seldom be used; poor performance extends drilling time and increases the likelihood of hole problems as well as the cost of well construction. Conversely, using a properly managed high-performance SBF can shorten the duration of the drilling operation and/or help maintain wellbore stability, thereby reducing opportunities for environmental damage. These and other factors must be weighed in the design and selection of any drilling-fluid system.

3.9.2 Sources of Contamination. Both land- and offshore-drilling locations are subject to regulations addressing the disposal of whole mud, drill cuttings and other solids, and run-off, if any, generated by rainfall, wave action, or water used at the rigsite. Industrywide efforts to eliminate environmental hazards resulting from accidents or the negligent handling of drilling fluids and/or drill cuttings encompass several contamination issues related to drilling fluids:

- Formulation: chlorides, base oils, heavy metals, corrosion inhibitors
- Natural sources: crude oil, salt water, or salt formation
- Rigsite materials: pipe dope, lubricants, fuel

In some cases, reformulating drilling-fluid systems makes them more benign to the environment. For example, chrome lignosulfonate water-based fluid is available in a chrome-free formulation. The development of SBFs resulted from the need to replace diesel and mineral OBFs due to environmental restrictions.

The discharge of conventional OBFs and drill cuttings was effectively prohibited in the North Sea in 2000. Cuttings generated by drilling with certain compliant SBFs may be discharged overboard in the western GOM if they comply with the retention on cuttings (ROC) limits introduced in 2002. Neither traditional OBFs nor the drill cuttings produced while using them can be discharged in the GOM; the rare offshore operation using a diesel- or mineral-based fluid must include a closed-loop process for continuously capturing all drill cuttings and returning them to shore for regulated disposal.

3.9.3 Drilling Fluids and Waste-Stream Reduction. As a result of the increasing emphasis on environmental protection and efficient use of resources, the concept of Total Fluids Management® (TFM) has emerged as a means of conserving materials, improving operational performance, and generating the appropriate documentation to verify that a given well-construction project was completed in compliance with governmental and corporate regulations.

The key focus of TFM is to cover the interface between all aspects of the drilling operation and to exploit the natural synergies between different service specialties. The mission of the TFM supervisors is to guide and focus all members of the team on their individual targets in order to achieve the collective goal. The mission also addresses the means and resources required to achieve the goals, measure the improvement, and refine the expectations for further project stages. The examples of TFM discussed here represent practices in the North Sea and the GOM.

During the late 1990s, a major Norwegian operator analyzed current practices related to the control and management of drilling and well fluids and the associated waste generation (Paulsen et al. 2001). A TFM model

was developed to improve environmental performance by reducing waste, maintaining or improving drilling performance, and preserving the profitability of contractor and service-company participants. The model was designed to reward performance according to Key Environmental Performance Indicators (KEPIs), so that any reduction in materials usage (i.e., sales) was offset. Once all participants agreed to the criteria, a TFM program was implemented to address the following areas:

- Measurement and management of drilling fluids, completion fluids, and drill cuttings
- Waste minimization
- Performance assessment
- Report formats and protocols
- Scheduled performance and target reviews
- Continuous improvement

In the GOM, regulations covering the discharge of synthetic-based drilling fluids and drill cuttings have increased the complexity, number, and types of measurements along with the potential for noncompliance. This has created the need for checks and balances in the daily monitoring and in the end of well report issued by the environmental testing company on location. The resulting environmental-compliance document must be provided to the operator and must be verifiable and auditable by governmental and environmental oversight groups.

3.9.4 Waste Management. The use of inhibitive drilling-fluid systems and good performance from solids-control equipment are key factors in the effort to reduce the volume of solids and liquids generated at the rigsite. Studies indicate that the greatest impact on waste-minimization strategies and capabilities is achieved through close monitoring and control of the drilling-fluid system, though other fluid-related operations such as completion, cementing, and rig-wastewater handling should also be part of the TFM program. Implementation of these policies resulted in overall well-construction-cost reductions and increased drilling performance.

Because of the inherent value of synthetic-based drilling fluids and the restrictions applied to their discharge, the reuse of these fluids has long been an industry standard. The various TFM programs currently implemented worldwide ensure that the recovery of reusable fluids is optimized through close attention to

- Fluid quality assurance/quality control (QA/QC)
- Fluid transport
- Fluid flow at the rigsite
- Solids-control-equipment operation
- Cuttings processing

Documentation requirements for these processes provide quantifiable indicators of environmental and economic performance of a specific TFM program.

In areas where drill cuttings must be returned to shore, recently improved pneumatic-transfer systems allow the cuttings to be captured below the shale shakers and pumped with compressed air to rigsite-storage units (Martin 2002). Supply boats equipped with the same pneumatic system receive the cuttings from the rig, transport them to shore, and then pump them into large storage tanks for eventual disposal. Auger-type conveyances are also commonly used to move drilled cuttings from the rig to vessels for treatment and/or transport to shore.

3.9.5 Treatment and Disposal of Drilled Cuttings. Where offshore discharge of cuttings is not sanctioned by regulatory and environmental agencies, there are many possible disposal options. Waste segregation at the rigsite is a key factor in the success of zero-discharge programs. Drilling-fluid waste, drill cuttings, waste generated by cementing or completion operations, and waste water from the rig must be handled and stored separately.

Another option is minimizing the initial volume of cuttings through installation and careful maintenance of high performance solids-control equipment. An effective cuttings-drying process should be established at the rigsite so that any cuttings transported to shore have the lowest possible fluid retention. At present, thermal desorption is considered one of the most effective methods of processing cuttings. Thermal desorption results in a 0.1 to 0.5% ROC rate and recovers the liquid oil for possible reuse. In thermal desorption, cuttings are heated to a very high temperature so that oil and water are boiled into gases. The water is released as steam and the oil is condensed to liquid.

However, the recovered oil may not have the same properties as the original base fluid because of the possibility of high temperatures breaking the heavier hydrocarbon molecules into lighter compounds. This may lower the oil flash point and alter its rheological properties. Though these changes are generally slight, they are

sufficient to prevent most operators from attempting to reuse the oil in a drilling-mud formulation. The oil is typically used as heating oil or to fuel the thermal desorption process. Salts or heavy metals are not removed from the cuttings.

3.9.6 Encapsulation. Recommended primarily for the treatment of oil-wet cuttings (but also efficient in solidifying liquid oil-based mud, water-based-mud cuttings, or solids discharge from flocculation systems), the typical encapsulation process is capable of treating up to 20 bbl/hr. The cuttings are mixed with calcium or silicate materials to produce a low-permeability cementitious matrix that reduces the mobility of oil. Kiln dust, an inexpensive waste by-product of cement factories, can be used, as can standard cement. The generator-powered system consists of one hopper for cuttings/sludge and one hopper for chemical treatment. Both feed to a central mixing area by means of screw conveyors. The speed of each conveyor can be adjusted, allowing the operator to control the ratio of chemical to sludge (generally from 30 to 50 % by weight).

A silica-calcium oxide-encapsulating agent is mixed with the raw cuttings and thorough mixing is ensured. Water is added as demanded by the process. The cuttings are recirculated in the mixing device (auger, auger tank, and ribbon blender) until satisfactory appearance is observed and field scale tests (sheen/can test) are passed. Specialized laboratory tests are required and compliance with the applicable regulations ensured before following a customer's instructions for disposal.

3.9.7 Bioremediation. Bioremediation is the process of using micro-organisms in a controlled, engineered environment to reclaim soil, sludge, and water polluted by hazardous and nonhazardous substances that can affect human health and/or the environment. These micro-organisms may be native to the contaminated media, genetically developed/enhanced, or they may be isolated from natural processes, selectively adapted to degrade a specific contaminant and brought to the contaminated site.

Land farming is the use of native bacteria, helped with additions of nutrients, water, and aeration, to break down harmful substances into environmentally-safe compounds. The broad metabolic capabilities of the micro-organisms enable them to remove or to reduce pollutant concentrations to levels that no longer present a risk to human health or the environment. In addition, the use of micro-organisms is not capital intensive, making bioremediation a cost-effective and feasible solution for small- and large-scale applications.

For bioremediation to successfully occur, the contaminants in question must be degradable by the involved micro-organisms. The breakdown of these contaminant molecules is accomplished by enzymes produced by the microbes. Enzymes can be added to the solids to increase the rate of breakdown.

Hydrocarbons are biodegradable. N-alkanes and n-alkylaromatics between C10 and C22 are generally considered low toxic. Compounds between C5 and C9 are biodegradable at low concentrations. Gaseous alkanes from C1 to C4 are biodegradable, but this is not the usual removal mechanism. Alkanes, n-alkylaromatics, and aromatics over C22 show low toxicity, but their physical characteristics, including their low solubility in water and their solid state at 35°C (optimum bioremediation-process temperature), are a problem, affecting their biodegradability.

Biodegradation is not always a successful process; sometimes the substance remains unaltered for one or more of the following reasons:

- The chemical concentration is high enough to kill micro-organisms.
- The number and type of micro-organisms is inadequate to carry out the process.
- The soil acidity or alkalinity may be inappropriate.
- The micro-organisms may suffer from a lack of nutrients such as nitrogen, phosphorous, potassium, sulphur, or other micronutrients necessary for their normal metabolism.
- The moisture conditions may be inadequate.
- The micro-organisms may suffer from a lack of oxygen, nitrate, or sulphate, which are their main energy source.

Bioremediation is one of the most cost-effective treatment methods available for destroying certain categories of hazardous and nonhazardous waste, offering the following advantages:

- Proven technology for on-site destruction of many organic contaminants to concentrations below the cleanup standards
- Cost savings associated with the on-site treatment and low-capital cost (typically requires simple and readily available equipment)
- Reduced future liability associated with possible leaching of lime-fixed material

- Flexibility to perform treatment on-site rather than transporting cuttings to a central facility
- The ability to use treated material as filling material or base material to be mixed with untreated cuttings

Certain considerations apply to the use of bioremediation. These include high levels of oxygen, which facilitate bacteria growth. In the case of land farming, the soil is aerated by mechanical tilling of the soil. The biodegradation rate is directly proportional to the oxygen level in the soil.

The bioremediation process can be adversely affected by high rain conditions; therefore it is necessary to install appropriate drainage systems to direct, collect, use, and/or dispose of rain water. Proper roofing should be provided for bioremediation facilities. The field capacity is the amount of water held in the soil after the excess gravitational water has drained away and after the rate of downward movement of water has materially decreased. A moisture level between 50 and 70% is best for bioremediation.

The optimum temperature for bioremediation ranges from 75°F to 98°F. Lower temperatures slow or stop bacteria activity, while temperatures above 135°F can destroy most bacteria. The optimal pH range for hydrocarbon-eating bacteria is from 6 to 8. Below 5, fungi become the predominant soil microbe and the bacteria population is reduced. A pH greater than 6 is recommended to minimize hazardous metal migration.

Bioreactors are designed to reduce the cuttings to a benign soil-like material that can be disposed of without risk at any onshore location. Small bioreactors have been developed for use in laboratories, but at present there are no units with sufficient capacity to handle the volumes of cuttings typical of offshore drilling operations.

Problems

- 3.1 Discuss the functions of a drilling fluid.
- 3.2 An 11.4-lbm/gal freshwater mud is found to have a solids content of 16.2 vol%.
 - (a) Compute the volume fraction of API barite and low-specific-gravity solids.
Answer: 0.068 and 0.094.
 - (b) Compute the weight fraction of API barite and low-specific-gravity solids in the mud.
Answer: 0.209 and 0.179.
 - (c) Compute the API barite and low-specific-gravity solids content in pounds per barrels of mud.
Answer: 100 and 85.5 lbm/bbl.
- 3.3 Compute the density of a mud mixed by adding 30 lbm/bbl of clay and 200 lbm of API barite to 1 bbl of water.
Answer: 11.8 lbm/gal.
- 3.4 Determine the density of a brine mixed by adding 150 lbm of CaCl_2 to 1 bbl of water.
Answer: 10.7 lbm/gal.
- 3.5 Discuss the desirable and undesirable aspects of a high mud viscosity.
- 3.6 Compute the yield of a clay that requires addition of 35 lbm/bbl of clay to 1 bbl of water to raise the apparent viscosity of water to 15 cp (measured in a Fann viscometer at 600 rev/min).
Answer: 59.3 bbl/ton.
- 3.7 A mud cup is placed under one cone of a hydrocyclone unit being used to process an unweighted mud. Twenty seconds were required to collect 1 qt of ejected slurry having a density of 20 lbm/gal. Compute the mass of solids and water being ejected by the cone per hour.
Answer: Solids: 852 lbm/hr and water: 47.6 lbm/hr.
- 3.8 A 1,000-bbl unweighted freshwater-mud system has a density of 9.5 lbm/gal. What mud treatment would be required to reduce the solids content to 4% by volume? The total mud volume must be maintained at 1,000 bbl and the minimum allowable mud density is 8.8 lbm/gal.
Answer: Discard 544 bbl of mud, add 544 bbl of water.
- 3.9 The density of 600 bbl of 12-lbm/gal mud must be increased to 14 lbm/gal using API barite. One gallon of water per sack of barite will be added to maintain an acceptable mud consistency. The final volume is not limited. How much barite is required? *Answer:* 92,800 lbm.
- 3.10 The density of 800 bbl of 14-lbm/gal mud must be increased to 14.5 lbm/gal using API barite. The total mud volume is limited to 800 bbl. Compute the volume of old mud that should be discarded and the weight of API barite required.
Answer: Discard 19.05 bbl of mud, add 28,000 lbm of barite.
- 3.11 The density of 900 bbl of a 16-lbm/gal mud must be increased to 17 lbm/gal. The volume fraction of low-specific-gravity solids also must be reduced from 0.055 to 0.030 by dilution with water. A final mud volume of 900 bbl is desired. Compute the volume of original mud that must be discarded and the amount of water and API barite that should be added.
Answer: Discard 409 bbl of mud, add 257.6 bbl of water and 222,500 lbm of barite.

- 3.12 Assuming a clay and chemical cost of USD 10/bbl of mud discarded and a barium sulfate cost of USD 0.10/lbm, compute the value of the mud discarded in Problem 3.11. If an error of + 0.01% is made in determining the original volume fraction of low-specific-gravity solids in the mud, how much mud was unnecessarily discarded?
Answer: USD 16,697; 191 bbl.
- 3.13 Derive expressions for determining the amounts of barite and water that should be added to increase the density of 100 bbl of mud from ρ_1 to ρ_2 . Also derive an expression for the increase in mud volume expected upon adding the barite and the water. Assume a water requirement of 1 gal per sack of barite.
Answer: $M_B = 109,000 (\rho_2 - \rho_1) / (28.08 - \rho_2)$; $V_w = M_B / 4,200$; $V = 0.0091 M_B$.
- 3.14 A 16.5-lbm/gal mud is entering a centrifuge at a rate of 20 gal/min along with 8.34 lbm/gal of dilution water, which enters the centrifuge at a rate of 10 gal/min. The density of the centrifuge underflow is 23.8 lbm/gal while the density of the overflow is 9.5 lbm/gal. The mud contains 25 lbm/bbl bentonite and 10 lbm/bbl deflocculant. Compute the rate at which bentonite, deflocculant, water, and API barite should be added downstream of the centrifuge to maintain the mud properties constant.
Answer: 10.02 lbm/min of bentonite, 4.01 lbm/min of deflocculant, 9.78 gal/min of water, and 20.81 lbm/min of barite.
- 3.15 A well is being drilled and a mud weight of 17.5 lbm/gal is predicted. Intermediate casing has just been set in 15 lbm/gal freshwater mud that has a solids content of 29%, a plastic viscosity of 32 cp, and a yield point of 20 lbf/100 ft² (measured at 120°F). What treatment is recommended upon increasing the mud weight to 17.5 lbm/gal?
- 3.16 Define an inhibitive mud. Name three types of inhibitive water-based muds.
- 3.17 Discuss why prehydrated bentonite is used in high-salinity muds.
- 3.18 Discuss the advantages and disadvantages of using oil muds.
- 3.19 Compute the pounds per barrel of CaCl_2 that should be added to the water phase of an oil mud to inhibit hydration of a shale having an activity of 0.8. If the oil mud will contain 30% water by volume, how much CaCl_2 per barrel of mud will be required?
Answer: 98.7 lbm/bbl of water and 29.6 lbm/bbl of mud.
- 3.20 Define these terms: (1) emulsifier, (2) wetting agent, (3) preferentially oil wet, (4) fatty-acid soap, and (5) balanced activity mud.
- 3.21 A saline solution contains 175.5 g of NaCl per liter of solution. Using a water density of 0.9982 g/cm³, express the concentration of NaCl in terms of (1) molality, (2) molarity, (3) normality, (4) parts per million, (5) milligrams per liter, (6) weight percent, and (7) pounds per barrel of water.
Answer: (1) 3.198 mol; (2) 3.00 g mol/L; (3) 3.00 gew/L; (4) 157,440 ppm; (5) 175,500 mg/L; (6) 15.7 wt%; (7) 65.4 lbm/bbl.
- 3.22 Discuss the difference between these alkalinity values: (1) P_m and P_f , and (2) P_f and M_f .
- 3.23 One liter of solution contains 3.0 g of NaOH and 8.3 g of Na_2CO_3 . Compute the theoretical values of P_f and M_f .
Answer: 7.7 cm³; 11.6 cm³.
- 3.24 Alkalinity tests on a mud give a P_m value of 5.0 and a P_f value of 0.7. Determine the approximate amount of undissolved lime in the mud. The volume fraction of water in the mud is 80%.
Answer: 1.154 lbm/bbl.
- 3.25 A volume of 20 mL of 0.0282 N AgNO_3 was required to titrate 1 mL of saline water in the API test for salinity. Determine the concentration of Cl^- and NaCl in the solution in mg/L assuming only NaCl was present.
Answer: 20,000 mg/L and 33,000 mg/L.
- 3.26 Name the three common causes of flocculation. Also name four types of mud additives used to control flocculation.

Nomenclature

- A = area of the filter paper, cm²
 AV = apparent viscosity, cp
 d = bit diameter, in.
 dV/dt = filtration rate, cm³/s
 f_{hs} = volume fraction of the high-density solids
 f_{ls} = volume fraction of the low-density solids
 f_o = volume fraction of the oil phase
 f_{sc} = volume fraction of solids in the cake

f_{sm}	=	volume fraction of solids in the mud
f_w	=	volume fraction of the water phase
\bar{F}	=	applied force in the lubricity test, lbf
F_f	=	friction force in the lubricity test, lbf
F_N	=	normal force in lubricity test, lbf
h_{mc}	=	thickness of the filter cake (mudcake), cm
k	=	permeability of the mudcake, darcies
L	=	length of the cylinders in a concentric viscometer, in.
m_f	=	the mass of the fluid mixture, lbm
m_{ls}	=	mass of low density solids, lbm
m_w	=	mass of water, lbm.
M_f	=	methyl orange filtrate alkalinity
M_t	=	torque, ft-lbf
P	=	phenolphthalein alkalinity, ml of 0.02 N H_2SO_4
P_f	=	phenolphthalein alkalinity of filtrate fluid, ml of 0.02 N H_2SO_4
P_m	=	phenolphthalein alkalinity of mud, ml of 0.02 N H_2SO_4
P	=	pressure, psia
P_r	=	reference pressure, psia
PV	=	plastic viscosity, cp
r_{cp}	=	radius of the captor in the lubricity test, in.
r_1	=	radius of the bob in a concentric viscometer, in.
r_2	=	inside radius of the outer cylinder in a concentric viscometer, in.
ROP	=	rate of penetration of the bit, ft/hr
SG_o	=	oil specific gravity
t	=	time in filtration test, s
T	=	temperature, °F
T_r	=	reference temperature, °F
V_f	=	total fluid volume, ft ³
V_{hs}	=	volume of the high-density solids, ft ³
V_{ls}	=	volume of the low-density solids, ft ³
V_o	=	volume of the oil phase, ft ³
V^{sp}	=	spurt-loss volume, cm ³
V_w	=	volume of the water phase, ft ³
$V_{7.5}$	=	15-minute filtrate volume, cm ³
V_{30}	=	30-minute filtrate volume, cm ³
YP	=	yield point, lbf/100 ft ²
$\dot{\gamma}$	=	shear rate, s ⁻¹
ΔP	=	pressure drop across the mudcake, atm
θ	=	dial reading on a viscometer, degrees
θ_{300}	=	dial reading on a viscometer at 300 rev/min, degrees
θ_{600}	=	dial reading on a viscometer at 600 rev/min, degrees
μ	=	viscosity, cp
μ_a	=	apparent viscosity, cp
μ_f	=	friction coefficient measured in lubricity test
μ_{mf}	=	viscosity of the mud filtrate, cp
μ_M	=	viscosity of a mixture, cp
μ_p	=	plastic viscosity, cp
$\bar{\rho}$	=	slurry density from desilter, lbm/gal
ρ_{FL}	=	free lime content, ppb
ρ_{hs}	=	density of the high-density solids, lbm/gal
ρ_{ls}	=	density of the low-density solids, lbm/gal
ρ_o	=	density of the oil phase, lbm/gal
ρ_w	=	density of the water phase, lbm/gal
τ	=	shear stress, psia
τ_Y	=	yield point (YP), lbf/100 ft ²
ϕ	=	the average formation porosity
ω	=	angular velocity of the outer cylinder, rev/min

Acknowledgments

The author would like to recognize Joe Billingsley, Jim Fisk, John Hall, Edgardo Hernandez, Tim Haggerty, Uday Tare, Rob Valenziano, Tim Wright, and Francisco Sanchez-Nodar for their significant contributions to this chapter.

References

- Alderman, N.J., Gavignet, A., Guillot, D., and Maitland, G.C. 1988. High-Temperature, High-Pressure Rheology of Water-Based Muds. Paper SPE 18035 presented at the SPE Annual Technical Conference and Exhibition, Houston, 2–5 October. DOI: [10.2118/18035-MS](https://doi.org/10.2118/18035-MS).
- Annis, M.R. 1974. *Drilling Fluids Technology*. Houston: ExxonMobil.
- API Specification 13A, *Specification for Drilling-Fluid Materials*, 16th edition. 2004. Washington, DC: API.
- API Specification 13B-1, *Recommended Practice for Field Testing Water-Based Drilling Fluids*, fourth edition. 2009. Washington, DC: API.
- API Specification 13B-2, *Recommended Practice for Field Testing Oil-Based Drilling Fluids*, fourth edition. 2009. Washington, DC: API.
- API Specification 13I, *Recommended Practice for Laboratory Testing Drilling Fluids*, eighth edition. 2009. Washington, DC: API.
- Beart, R. 1845. Apparatus for Boring in the Earth and in Stone, England, Patent No. 10,258.
- Bland, R.G., Waughman, R.R., Halliday, W.S., Tomkins, P.G., Pessier, R.C., and Isbell, M.R. 2002. Water-Based Alternatives to Oil-Based Muds: Do They Actually Exist? Paper SPE 74542 presented at the IADC/SPE Drilling Conference, Dallas, 26–28 February. DOI: [10.2118/74542-MS](https://doi.org/10.2118/74542-MS).
- Bleier, R., Leuterman, A.J., and Stark, C. 1993. Drilling Fluids: Making Peace with the Environment. *J Pet Technol* **45** (1): 6–10. SPE-24553-PA. DOI: [10.2118/24553-PA](https://doi.org/10.2118/24553-PA).
- Bourgoyne, A.T., Millheim, K.K., Chenevert, M.E., and Young, F.S. 1991. *Applied Drilling Engineering*. SPE Textbook Series, SPE, Richardson, Texas **2**: 42–53; 131–137.
- Clark, J.A. and Halbouty, M.T. 1980. *Spindletop*. Houston: Gulf Publishing.
- Darley, H.C.H. and Gray, G.R. 1988. *Composition and Properties of Drilling and Completion Fluids*. Houston: Gulf Publishing.
- Drilling Fluid Engineering Manual*. 1972. Houston: Dresser Industries, Magcobar Division.
- Govier, G.W. and Aziz, K. 2008. *The Flow of Complex Mixtures in Pipes*, SPE, Richardson, Texas.
- Grim, R.E. 1968. *Clay Mineralogy*. New York City: McGraw-Hill Books.
- Halliburton. 2001. *The Red Book: Halliburton Cementing Tables*, Duncan, Oklahoma: Halliburton Company.
- Halliburton. 1981. *The Red Book: Halliburton Cementing Tables*, Section 240, 11–13. Duncan, Oklahoma: Halliburton Company.
- Houwen, O.H. and Geehan, T. 1986. Rheology of Oil Base Muds. Paper SPE 15416 presented at the SPE Annual Technical Conference and Exhibition, New Orleans, 5–8 October. DOI: [10.2118/15416-MS](https://doi.org/10.2118/15416-MS).
- IMCO Services. 1981. *Applied Mud Technology*, seventh edition, 8–10. Houston: IMCO Services Division of Halliburton Company.
- Isambourg, P., Ottesen, S., Benaissa, S., and Marti, J. 1999. Down-Hole Simulation Cell for Measurement of Lubricity and Differential Pressure Sticking. Paper SPE 52816 presented at the SPE/IADC Drilling Conference, Amsterdam, 9–11 March. DOI: [10.2118/52816-MS](https://doi.org/10.2118/52816-MS).
- Kemp, N.P. and Thomas, D.C. 1987. Density Modeling for Pure and Mixed-Salt Brines as a Function of Composition, Temperature, and Pressure. SPE Paper 16079 presented at the SPE/IADC Drilling Conference, New Orleans, 15–18 March. DOI: [10.2118/16079-MS](https://doi.org/10.2118/16079-MS).
- Magcobar Operations. 1972. *Drilling Fluid Engineering Manual*, sixth edition. Houston: Dresser Industries Magcobar Operations, Oilfield Products Division.
- Martin, N., Krukowski, F., Bingham, R., and Logan, G. 2002. Processing Oil-Contaminated Cuttings. *Drilling*, AADE (June 2002): 32–34.
- Mody, F.K. and Hale, A.H. 1993. Borehole Stability Model to Couple the Mechanics and Chemistry of Drilling Fluid/Shale Interaction. *J Pet Technol* **45** (11): 1093–1101. SPE-25728-PA. DOI: [10.2118/25728-PA](https://doi.org/10.2118/25728-PA).
- Paulsen, J.E., Saasen, A., Jensen, B., and Grinrod, M. 2001. Key Environmental Performance Indicators in Drilling Operations. Paper SPE 71839 presented at Offshore Europe, Aberdeen, 4–7 September. DOI: [10.2118/71839-MS](https://doi.org/10.2118/71839-MS).
- Parry, W.T., Bellows, J.C., Gallagher, J.S., and Harvey, A.H. 2000. *ASME International Steam Tables For Industrial Use: Based on the IAPWS Industrial Formulation 1997 for the Thermodynamic Properties of Water and Steam (IAPWS-IF97)*. CRTD, **58**. New York: ASME Press.

- Poling, B.E., Prausnitz, J.M., and O'Connell, J.P. 2000. *The Properties of Gases and Liquids*, fifth edition. New York: McGraw-Hill.
- Rogers, P.S.Z. and Pitzer, K.S. 1982. Volumetric Properties of Aqueous Sodium Chloride Solutions. *J. Physical and Chemical Reference Data* **11** (1): 15–81.
- Rogers, W.F. 1963. *Composition and Properties of Oil Well Drilling Fluids*, third edition, Gulf Publishing Company, Houston, 33–34, 122–159.
- Savins, J.G. and Roper, W.F. 1954. A Direct Indicating Viscometer for Drilling Fluids, *API Drill. Prod. Prac.*, 7–22. Washington, DC: API.
- Sorelle, R.R., Jardioli, A., Buckley, P., and Barrios, J.R. 1982. Mathematical Field Model Predicts Downhole Density Changes in Static Drilling Fluids. Paper SPE 11118 presented at the SPE Annual Technical Conference and Exhibition, New Orleans, 26–29 September. DOI: [10.2118/11118-MS](https://doi.org/10.2118/11118-MS).
- Stroud, B.K. 1926. Application of Mud-Laden Fluids to Oil or Gas Wells, U.S. Patent No. 1,575,944.
- Tare, U., Mody, F.K., and Tan, C.P. 2002. New Generation of Membrane Efficient Water-Based Drilling Fluids: Pragmatic and Cost-Effective Solutions to Borehole Stability Problems. Paper 2002-166 presented at the Canadian International Petroleum Conference, Calgary, 11–13 June. DOI: [10.2118/2002-166](https://doi.org/10.2118/2002-166).
- Whitson, C.D. and McFadyen, M.K. 2001. Lessons Learned in the Planning and Drilling of Deep, Subsalt Wells in the Deepwater Gulf of Mexico. Paper SPE 71363 presented at the SPE Annual Technical Conference and Exhibition, New Orleans, 30 September–3 October. DOI: [10.2118/71363-MS](https://doi.org/10.2118/71363-MS).
- World Oil. 2002. *Drilling Completion & Workover Fluids* **223** (6): D1–D34.
- Zamora, M., Broussard, P.N., and Stephens, M.P. 2000. The Top 10 Mud-Related Concerns in Deepwater Drilling Operations. Paper SPE 59019 presented at the SPE International Petroleum Conference and Exhibition in Mexico, Villahermosa, Mexico, 1–3 February. DOI: [10.2118/59019-MS](https://doi.org/10.2118/59019-MS).

Further Reading

- Baroid Drilling Fluids. 1990. In *Manual of Drilling Fluids Technology*. Houston: Baroid Corporation.
- Brantly, J.E. 1971. *History of Oilwell Drilling*. Houston: Gulf Publishing.
- Burke, C.J. and Veil, J.A. 1995. Synthetic Drilling Muds: Environmental Gain Deserves Regulatory Confirmation. Paper SPE 29737 presented at the SPE/EPA Exploration and Production Environmental Conference, Houston, 27–29 March. DOI: [10.2118/29737-MS](https://doi.org/10.2118/29737-MS).
- Burnett, D.B. and Hodge, R.M. 1996. Laboratory and Field Evaluation of the Role of Drill Solids in Formation Damage and Reduced Horizontal Well Productivity. Paper SPE 37125 presented at the SPE International Conference on Horizontal Well Technology, Calgary, 18–20 November. DOI: [10.2118/37125-MS](https://doi.org/10.2118/37125-MS).
- Cameron, C. 2001. Drilling Fluids Design and Management for Extended Reach Drilling. Paper SPE 72290 presented at the SPE/IADC Middle East Drilling Technology Conference, Bahrain, 22–24 October. DOI: [10.2118/72290-MS](https://doi.org/10.2118/72290-MS).
- Chenevert, M.E. 1970. Shale Control With Balanced-Activity Oil-Continuous Muds. *J Pet Technol* **22** (10): 1309–1316; *Trans.*, AIME, **249**. SPE-2559-PA. DOI: [10.2118/2559-PA](https://doi.org/10.2118/2559-PA).
- Cobianco, S., Bartosek, M., Lezzi, A., and Guarneri, A. 1999. How To Manage Drill-In Fluid Composition to Minimize Fluid Losses During Drilling Operations. *SPE Drill & Compl* **16** (3): 154–158. SPE-73567-PA. DOI: [10.2118/73567-PA](https://doi.org/10.2118/73567-PA).
- Darley, H.C.H. 1969. A Laboratory Investigation of Borehole Stability, *J Pet Technol* **21** (7): 883–892; *Trans.*, AIME, **246**. SPE-2400-PA. DOI: [10.2118/2400-PA](https://doi.org/10.2118/2400-PA).
- Davison, J.M., Jones, M., Shuchart, C.E., and Gerard, C. 2001. Oil-Based Muds for Reservoir Drilling: Their Performance and Cleanup Characteristics. *SPE Drill & Compl* **16** (2): 127–134. SPE-72063-PA. DOI: [10.2118/72063-PA](https://doi.org/10.2118/72063-PA).
- Hemphill, T., Murphy, B., and Mix, K. 2001. Optimization of Rates of Penetration in Deepwater Drilling: Identifying the Limits. Paper SPE 71362 presented at the SPE Annual Technical Conference and Exhibition, New Orleans, 30 September–3 October. DOI: [10.2118/71362-MS](https://doi.org/10.2118/71362-MS).
- MacEachern, D.P., Hudson, C.E., and Touns, B. 2001. Intensive Evaluation of a Rig's Fluid Handling System Shown to Dramatically Improve Efficiency, Lower Costs. Paper SPE 67738 presented at the SPE/IADC Drilling Conference, Amsterdam, 27 February–1 March. DOI: [10.2118/67738-MS](https://doi.org/10.2118/67738-MS).
- OSPAR Commission. 2001. Annual Report 2000–2001, 30. London: OSPAR Commission.
- Paulsen, J.E., Jensen, B., Løklingholm, G., and Saasen, A. 2000. Cost-Benefit Decisions Integrating Business and Eco-Management Results in Best Environmental Practice in Drilling and Well Operations. Paper SPE 61147 presented at the SPE International Conference on Health, Safety, and Environment in Oil and Gas Exploration and Production, Stavanger, 26–28 June. DOI: [10.2118/61147-MS](https://doi.org/10.2118/61147-MS).

- Sheffield, J.S., Collins, K.B., and Hackney, R.M. 1983. Salt Drilling in the Rocky Mountains. Paper SPE 11374 presented at the IADC/SPE Drilling Conference, New Orleans, 20–23 February. DOI: [10.2118/11374-MS](https://doi.org/10.2118/11374-MS).
- Valentine, A.V. 2002. Accurately Measuring Discharged Drilled Cuttings and Retained Fluids. Paper SPE 73933 presented at the SPE International Conference on Health, Safety, and Environment in Oil and Gas Exploration and Production, Kuala Lumpur, 20–22 March. DOI: [10.2118/73933-MS](https://doi.org/10.2118/73933-MS).
- Whitfill, C.D., Rachal, G., Lawson, J., and Armagost, K. 2002. Drilling Salt—Effect of Drilling Fluid on Penetration Rate and Hole Size. Paper SPE 74546 presented at the IADC/SPE Drilling Conference, Dallas, 26–28 February. DOI: [10.2118/74546-MS](https://doi.org/10.2118/74546-MS).

SI Metric Conversion Factors

atm	×	1.013 250*	E + 05 = Pa
bbl	×	1.589 873	E – 01 = m ³
cp	×	1.0*	E – 03 = Pa.s
ft	×	3.048*	E – 01 = m
ft ²	×	9.290 304*	E – 02 = m ²
ft ³	×	2.831 685	E – 02 = m ³
°F		(°F – 32)/1.8	= °C
gal	×	3.785 412	E – 03 = m ³
in.	×	2.54*	E + 00 = cm
in. ²	×	6.451 6*	E + 00 = cm ²
in. ³	×	1.638 706	E + 01 = cm ³
lbf	×	4.448 222	E + 00 = N
lbm	×	4.535 924	E – 01 = kg
mL	×	1.0*	E + 00 = cm ³
ppb	×	2.85300	E + 00 = kg/m ³
psi	×	6.894 757	E + 00 = kPa

*Conversion factor is exact.

Chapter 4

Cementing

Ron Sweatman, Halliburton

This chapter is an updated version of the Cementing chapter that first appeared in Bourgoyne et al. (1991). The purposes of this chapter are to present (1) the primary objectives of cementing, (2) the test procedures used to determine if the cement slurry and set cement have suitable properties for meeting these objectives, (3) the additives used to obtain the desirable properties under various well conditions, and (4) the techniques used to place the cement at the desired location in the well. Many advances have been made in laboratory testing, engineering design, and cement placement technologies during the last 25 years. Summaries of key improvements are presented, with references cited for detailed information. The mathematical modeling of the flow behavior of the cement slurry is not discussed in this chapter but is presented in detail in Chapter 5.

Cementing is used in the drilling operation to prevent the movement of fluid through the annular space outside the casing, protect and support the casing, stop the movement of fluid into vugular or fractured formations, and close an abandoned portion of the well. Cementing is the process of placing a cement slurry in a well by mixing powdered cement, additives, and water at the surface and pumping it by hydraulic displacement to the desired location. Thus, the hardened, or reacted, cement slurry becomes “set” cement, a rigid solid that exhibits favorable strength characteristics. The rigidity of hard-set cement must be designed to allow enough ductility to maintain a seal under expected load conditions including those in deep, high-pressure/high-temperature (HP/HT) wells; see *API RP 65-Part 2* (2010) for additional information.

The drilling engineer is concerned with the selection of the best cement composition and placement technique for each required application. A deep well that encounters abnormally high formation pressure may require several casing strings to be cemented properly in place before the well can be drilled and completed successfully. The cement composition and placement technique for each job must be chosen so that the cement will achieve an adequate strength soon after being placed in the desired location. This minimizes the waiting period after cementing and before commencing rig operations to change the BOP, wellhead, hydrostatic pressures, and drill out the casing shoe. However, the cement must remain pumpable long enough at high temperatures to allow placement to the desired location. Also, each cement job must be designed so that the density and length of the unset cement column results in sufficient subsurface pressure to prevent the movement of formation pore fluids into the wellbore while not causing formation fractures and lost circulation. As this initial overbalanced pressure slowly becomes underbalanced during the cement curing period, cement properties such as rapid static-gel-strength (SGS) development must take over to prevent formation-fluid influx and potential blowouts; for more details, see *API RP 65-Part 2* (2010). Consideration also must be given to the composition of subsurface contaminating fluids to which the cement will be exposed.

Poor cement jobs may result in delayed production, flow from unintended intervals behind casing, sustained annular pressure, and loss of casing integrity due to corrosion. Remedial operations are possible; however, they are costly and time consuming. In some instances, a poor cement job may cause a loss of the well.

4.1 Composition of Portland Cement

The main ingredient in almost all drilling cements is *Portland cement*, an artificial cement made by burning a blend of limestone and clay. This is the same basic type of cement used in making concrete. A slurry of Portland cement in water is ideal for use in wells because it can be pumped easily and hardens readily in an underwater environment. The name “Portland cement” was chosen by its inventor, Joseph Aspdin, because he thought the produced solid resembled a stone quarried on the Isle of Portland off the coast of England.

A schematic representation of the manufacturing process for Portland cement is shown in **Fig. 4.1**. The oxides of calcium, aluminum, iron, and silicon react in the extreme temperature of the kiln (2,600 to 2,800°F), resulting in balls of cement *clinker* upon cooling. After aging in storage, the seasoned clinker is taken to the grinding mills where gypsum ($\text{CaSO}_4 \cdot 2\text{H}_2\text{O}$) is added (1 to 3% by weight of cement) to control setting time and hardening of cement (strength). The units sold by the cement company are the *barrel*, which contains 376 lbm or four 94-lbm sacks, or by U.S. tons (2,000 lbm) and metric tonnes (2,205 lbm).

Cement chemists have found that there are four crystalline compounds in the clinker that hydrate to form or aid in the formation of a rigid structure. These are tricalcium silicate ($3\text{CaO} \cdot \text{SiO}_2$ or C_3S), dicalcium silicate ($2\text{CaO} \cdot \text{SiO}_2$ or C_2S), tricalcium aluminate ($3\text{CaO} \cdot \text{Al}_2\text{O}_3$ or C_3A), and tetracalcium aluminoferrite ($4\text{CaO} \cdot \text{Al}_2\text{O}_3 \cdot \text{Fe}_2\text{O}_3$ or C_4AF). The hydration reaction is exothermic and generates a considerable quantity of heat, especially the hydration of C_3A .

The chemical equations representing the hydration of the cement compounds when they are mixed with water are as follows.

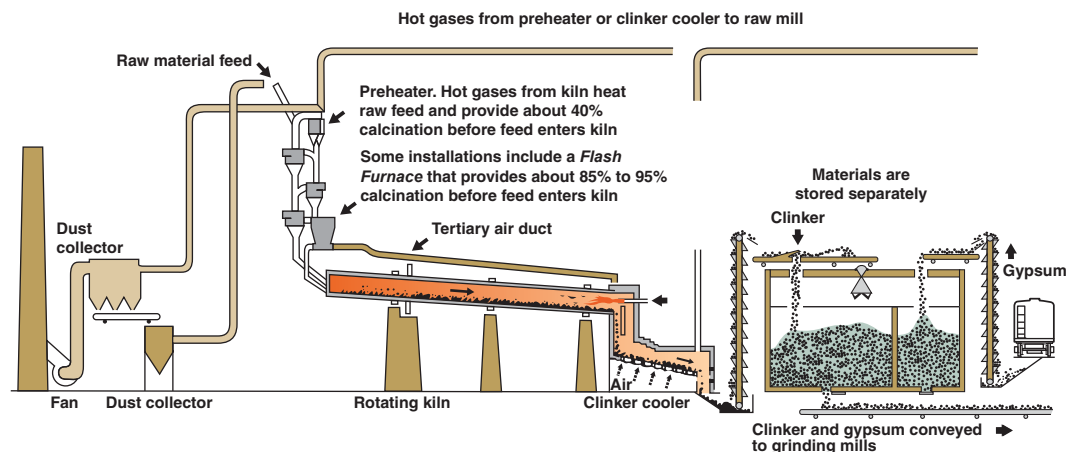
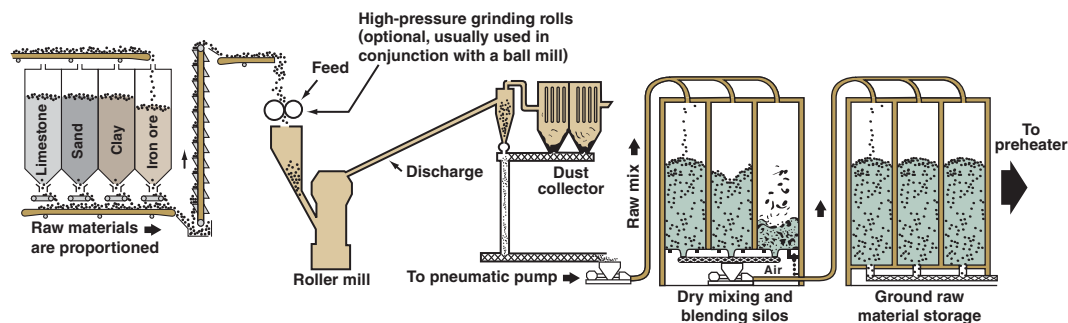
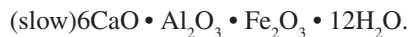
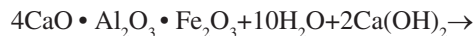
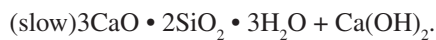
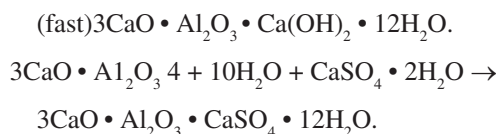


Fig. 4.1—Manufacture of Portland cement [after Kosmatka and Wilson (2011)]. Courtesy of Portland Cement Association.



The main cementing compound in the reaction products is $3\text{CaO} \cdot 2\text{SiO}_2 \cdot 3\text{H}_2\text{O}$, which is called tobermorite gel. The gel has an extremely fine particle size and, thus, a large surface area. Strong surface attractive forces cause the gel to adsorb on all crystals and particles and bind them together. Excess water that is not hydrated reduces cement strength and makes the cement more porous and permeable.

C_3S is thought to be the major contributor to strength, especially during the first 28 days of curing. C_2S hydrates very slowly and contributes mainly to long-term strength. C_3A hydrates very rapidly and produces most of the heat of hydration observed during the first few days. The gypsum added to the clinker before grinding controls the rapid hydration of C_3A . The C_3A portion of the cement also is attacked readily by water containing sulfates. C_4AF has only minor effects on the physical properties of the cement.

The chemical composition of Portland cement generally is given in terms of oxide analysis. The relative amounts of the four crystalline compounds present are computed from the oxide analysis. *API Spec. 10A/ISO 10426-1* (2002) uses the following equations for calculating the weight percent of the crystalline compounds from the weight percent of the oxides present.

$$\text{C}_3\text{S} = 4.07\text{C} - 7.6\text{S} - 6.72\text{A} - 1.43\text{F} - 2.85\text{SO}_3 \quad (4.1)$$

$$\text{C}_2\text{S} = 2.87\text{S} - 0.754\text{C}_3\text{S} \quad (4.2)$$

$$\text{C}_3\text{A} = 2.65\text{A} - 1.69\text{F} \quad (4.3)$$

$$\text{C}_4\text{AF} = 3.04\text{F} \quad (4.4)$$

These equations are valid as long as the weight ratio of Al_2O_3 to Fe_2O_3 present is greater than 0.64.

Example 4.1 Calculate the percentages of C_3S , C_2S , C_3A , and C_4AF from the following oxide analysis of a standard Portland cement.

Oxide	Weight Percent
Lime (CaO or C)	65.6
Silica (SiO_2 or S)	22.2
Alumina (Al_2O_3 or A)	5.8
Ferric oxide (Fe_2O_3 or F)	2.8
Magnesia (MgO)	1.9
Sulfur trioxide (SO_3)	1.8
Ignition loss	0.7

Solution. The A/F ratio is $5.8/2.8 = 2.07$. Thus, using Eqs. 4.1 through 4.4 yields

$$\begin{aligned}
 \text{C}_3\text{S} &= 4.07(65.6) - 7.6(22.2) - 6.72(5.8) \\
 &\quad - 1.43(2.8) - 2.85(1.8) = 50.16 \%.
 \end{aligned}$$

$$\text{C}_2\text{S} = 2.87(22.2) - 0.754(50.16) = 25.89\%.$$

$$\text{C}_3\text{A} = 2.65(5.8) - 1.69(2.8) = 10.64\%.$$

$$\text{C}_4\text{AF} = 3.04(2.8) = 8.51\%.$$

4.2 Cement Testing

API Spec. 10A/ISO 10426-1 (2002), *RP 10B-2/ISO 10426-2* (2005), *RP 10B-3/ISO 10426-3* (2004), *RP 10B-4/ISO 10426-4* (2004); other API, ISO, and ASTM standards; and some nonstandard publications such as SPE

papers may present state-of-the-art, recommended procedures for testing well cements. All of these tests were devised to help drilling personnel determine if a given cement composition will be suitable for specific well conditions. Cement slurry design specifications almost always are stated in terms of these laboratory tests. The test equipment needed to perform many of the types of tests include:

- A pressurized mud balance for determining the slurry density
- An HP/HT filter press for determining the filtration rate of the slurry
- A rotational viscometer for determining the rheological properties of the slurry
- A consistometer for determining the thickening rate characteristics of the slurry under downhole pressure and temperature conditions
- Cement HP/HT curing and strength testing machines for determining the compressive strength of the cement
- A graduated cylinder for determining the free fluid of the setting cement
- An HP/HT SGS testing device to measure the time period for the fluid cement slurry to convert into a high-enough SGS to inhibit formation-fluid influx and migration [see more in *ISO 10426-6* (2008)]
- A triaxial load cell for determining the ductility of the cement

The first six types of tests are commonly performed for well cementing operations. The seventh type is needed for cement placed across potential flow zones to contain formation fluids during cement curing periods, and the eighth one is needed to ensure sustainable cement sealing and support integrity under life of the well-load cases. Unlike drilling-fluid testing, routine testing of the cement slurry normally is not done at the rig site except for cement slurry density, which is required to calibrate density measuring devices on the cement mixing and pumping equipment. However, it is imperative for the drilling engineer to understand the nature of these tests if he or she is to interpret cement specifications and reported test results properly.

The pressurized mud balance, filter press, and rotational viscometer used for cement testing are basically the same equipment described in Chapter 3 for testing drilling fluids, except that an HP/HT filter press is used instead of the low-pressure version. An HP/HT version of the rotational viscometer is often used for applications in deep, hot hole sections. When measuring the density of cement slurries, entrained air in the sample is more difficult to remove. The pressurized mud balance shown in **Fig. 4.2** can be used to minimize the effect of the entrained air. Cement slurry density should be determined by use of a pressurized mud balance described in *ISO 10426-2* (2005).

4.2.1 Cement Consistometer. The pressurized and atmospheric-pressure consistometers used in testing cement are shown in **Figs. 4.3a and 4.3b**. The pressurized consistometer consists essentially of a rotating cylindrical slurry container equipped with a stationary paddle assembly, all enclosed in a pressure chamber capable of withstanding temperatures and pressures encountered in well cementing operations. The cylindrical slurry chamber is rotated at 150 rev/min during the test. The slurry consistency is defined in terms of the torque exerted on the paddle by the cement slurry. The relation between torque and slurry consistency is given by

$$B_c = \frac{T - 78.2}{20.02}, \quad \dots \dots \dots (4.5)$$



Fig. 4.2—Mud balance. Courtesy of Halliburton.



Fig. 4.3—Examples of (a) pressurized and (b) atmospheric consistometers. Courtesy of Halliburton.

where T = the torque on the paddle in g-cm and B_c = the slurry consistency in API consistency units designated by B_c . The thickening time of the slurry is defined as the time required to reach a consistency of 100 B_c . This value is felt to be representative of the upper limit of pumpability. The temperature and pressure schedule followed during the test must be given with the thickening time for the test results to be meaningful. API periodically reviews field data concerning the temperatures and pressures encountered during various types of cementing operations and publishes recommended schedules for use with the consistometer. *API Spec. 10A* (2002), *RP 10B-2* (2005)/*ISO 10426-2* (2003), *RP 10B-3* (2004)/*ISO 10426-3* (2003), and *RP 10B-4* (2004)/*ISO 10426-4* (2004) provide procedures for a number of schedules for simulating various casing and liner cementing operations. While some standards provide “test schedules” for testing thickening times for different well depths and temperature gradients, the test schedule for a given job needs to be calculated using the actual well conditions and the anticipated pump rates.

The atmospheric-pressure consistometer is frequently used to simulate a given history of slurry pumping before performing certain tests on the slurry, such as tests for free fluid, rheology, fluid loss, and compressive strength. For example, the rheological properties of cement slurries are time dependent because the cement thickens with time. The history of shear rate, temperature, and pressure before measuring the cement rheological properties using a rotational viscometer can be specified in terms of a schedule followed using the consistometer. The consistometer also is sometimes used to determine the maximum, minimum, and normal water ratios [% BWOC (by weight of cement)] for various types of cements and is most often used to condition the slurry for the free fluid content test. In the water-ratio tests, the sample is placed first in the consistometer and stirred for a period of 20 minutes at 80°F and atmospheric pressure. The *minimum water content (or water ratio in % BWOC)* is the amount of mixing water per sack of cement that will result in a consistency of 30 B_c at the end of this period. The *normal water content* is the amount of mixing water per sack of cement that will result in a consistency of 11 B_c at the end of the test. The *free fluid (original name: water) content* is determined by pouring a 250-mL sample from the consistometer into a glass graduated cylinder and noting the amount of free supernatant water that separates from the slurry over a 2-hour period. The *maximum water content* is defined as the amount of water per sack of cement that will result in 3.5 mL of free water. However, these water-ratio tests often can have varying results when additives are used in the cement slurry. A consistometer designed to operate only at atmospheric pressure is frequently used in conjunction with the determination of the slurry rheological, free fluid, and filtrate loss properties and water content.

Example 4.2 The torque required to hold the paddle assembly stationary in a cement consistometer rotating at 150 rev/min is 520 g-cm. Compute the slurry consistency.

$$B_c = \frac{T - 78.2}{20.02} = \frac{520 - 78.2}{20.02} = 22 \text{ consistency units}$$

4.2.2 Strength Tests. The standard tests for cement compressive strength are published in *API Spec. 10A* (2002)/*ISO 10426-1* (2002), *RP 10B-2* (2005)/*ISO 10426-2* (2003), *RP 10B-3* (2004)/*ISO 10426-3* (2003), and *RP 10B-4* (2004)/*ISO 10426-4* (2004) for drilling cements. The compressive strength of the set cement is the compressional force required to crush the cement divided by the cross-sectional area of the sample. Test schedules for curing strength test specimens are recommended by API. These schedules are based on average conditions encountered in different types of cementing operations and are updated periodically on the basis of current field data. The compressive strength of the cement is usually about 12 times greater than the tensile strength at any given curing time. Thus, frequently only the compressive strength is reported.

Nondestructive Sonic Strength Testing of Cement. A sonic nondestructive testing procedure is used to correlate cement compressive strength to sonic travel time and is performed by a testing device commonly called an ultrasonic cement analyzer (UCA). Strength correlations are specific to certain cement slurry compositions, and some cement compositions may not fit the correlations supplied by the UCA manufacturer. Custom correlations may be needed for some cement system formulations. The UCA test is the most frequently used test for compressive strength. More information on the UCA test can be found in *ISO 10426-2* (2005).

4.2.3 Nonstandard Tests and Modeling. Parr et al. (2009) used a variety of nonstandard tests and numerical models to find the root cause for abnormally high cement-displacement pressures in liner cementing. The test and mathematical model conclusions are listed next.

1. Slurry dewatering and filter-cake buildup were successfully simulated to show an annular restriction effect caused by a high-permeability formation interval.
2. Solids settling was demonstrated within the drilling mud and spacer fluids. The mud was shown to build a soft layer of low-mobility solids, but not a hard layer of solids. The effect of the low-mobility solids on cement placement would be to make the mud difficult to remove completely from the hole, thereby allowing the mud and cement to mix.
3. Using ultralow shear and HP/HT downhole conditions, the static-gel-strength (SGS) development of the drilling fluid was measured, showing that mud erodibility was low, meaning that subsequent mud displacement by cement would be difficult.
4. Film buildup on interior liner pipe walls was measured and shown to be minor relative to issues with cement placement.
5. Results of mud/spacer/cement compatibility laboratory test data and numerical modeling showed the means by which mixing of mud and cement as incompatible fluids might occur and contribute greatly to the abnormal cementing job pressures.

4.2.4 Permeability Testing. Routine permeability testing of cement has been abandoned by the oil and gas industry. Further, the old method of cement permeability testing (Bourgoyne 1991) is not commonly practiced today. The following discussion explains this change in procedure.

In Sutton et al. (1984a, 1984b), the authors discuss the time period for natural gas to migrate through cement with a very high (e.g., 12 md) permeability in a long cement column. For example, the time of gas migration through 2,000 linear ft of 12-md cement was found to be in excess of 72 years. The realization that cement permeability was relatively unimportant for annular gas flow was recognized as early as the early 1960s (Goode 1962). This is one reason why the *API RP-65* Task Group focused on other reasons for both short-term (during well construction) and long-term (most cases in < 10 years) annular flows. Instead of cement permeability, the main focus is on some of the following reasons or causes for flows:

- Poor cement placement
- Cement channeling through mud, leaving bypassed mud that forms a gas flow path
- Lost circulation during cementing, resulting in cement channeling or top of cement below a flow zone
- Poor removal of mudcake that later converts into an annular flow path
- Poor control of cement SGS development that causes an underbalanced condition before cement sets
- Formation of a microannulus at the cement/pipe and/or cement/borehole wall interfaces
- Stress cracking in hard-set, brittle cements that are not designed for certain cyclic well loads (temperature and pressure changes)

The *API RP-65* Task Group did not propose any maximum value for cement permeability in *RP 65-Part 2* (2010), as it is not a concern and routinely is much lower than the 12-md example. Gas migration travel-time

periods calculated with typically low cement permeability values may be several hundreds or thousands of years, depending on cement column lengths and differential pressures. Further, geochemical reactions over these time periods have been shown to deposit scale that seals the cement pores indefinitely. However, when these calculations predict problems, special cements (such as those used in low pH, corrosive environments) are used to ensure sealing by the cement.

For instance (Sweatman et al. 2009b), most scientists agree that 1,000 years of CO₂ containment in an injection reservoir is sufficient to ensure permanent sequestration. Well-abandonment cement plugs with relatively short lengths of Portland type cements can seal CO₂ inside the well under the most severe corrosive conditions for much greater time periods than 1,000 years, regardless of CO₂-induced degradation. Consequently, the consensus of opinion has now shifted from cement permeability to other issues such as cement slurry placement assurance (100% mud removal, etc.) and long-term mechanical integrity (stress resistance) to prevent annular leak pathways like channels, microannuli, and cracks.

Accordingly, the API Task Group discounted cement permeability as a cause for natural gas migration occurrences. This is why routine permeability testing of cement has been abandoned by the oil and gas industry. During the industry's evaluation, the old API cement permeability test under ambient pressure and temperature conditions was found technically invalid because it could not simulate the downhole conditions that affected cement permeability, such as geochemical effects and confining stresses in the annulus. Consequently, new laboratory tests have been developed to measure gas flow through cement permeability under downhole conditions. Discussion of these tests is considered to be beyond the scope of this textbook, but details may be found in many references, such as papers concerning sealing CO₂ injection wells with cement [e.g., Carey et al. (2006), Huerta et al. (2008), Kutchko et al. (2009), Rodot and Garnier (2009), Santra et al. (2009), and Sweatman et al. (2009b)].

4.3 Standard and Nonstandard Drilling Cements

API Spec. 10A (2002) and its equivalent standard, *ISO 10426-1* (2006), have defined eight (six in *ISO 10426-1*) standard classes and three standard types of cement for use in wells. The more recent ISO standard drops Classes E and F, and API may likely follow suit in the next edition of *Spec. 10A*. The six classes specified are designated Class A, B, C, D, G, and H. The intended meanings of the various classes are defined in **Table 4.1**. The three types specified are (1) ordinary, "O"; (2) moderate sulfate-resistant, "MSR"; and (3) high sulfate-resistant, "HSR." The chemical and physical requirements for the various types and classes are given in *API Spec. 10A*. The majority of oilwell cements are Class G and Class H.

The physical requirements of the various classes of cement given in *API Spec. 10A* apply to cement samples prepared according to API specifications. To provide uniformity in testing, it is necessary to specify the amount of water to be mixed with each type of cement. These water-content ratios, shown in **Table 4.2**, often are referred to as the normal water content or "API water" of the cement class. As will be discussed in the next section, Wyoming bentonite sometimes is added to the cement slurry to reduce the slurry density, or barium sulfate is added to increase the slurry density. For example, the water content may be increased 5.3 wt% for each weight percent of bentonite added and 0.2 wt% for each weight percent of barium sulfate added.

4.3.1 Construction Industry Cement Designations. Five basic types of Portland cements are used commonly in the construction industry in the USA. The ASTM classifications and international designations for these five cements are shown in **Table 4.3**. Note that ASTM Type I, called normal, ordinary, or common cement, is similar to API Class A cement. Likewise, ASTM Type II, which is modified for moderate sulfate resistance, is similar to API Class B cement. ASTM Type III, called high early strength cement, is similar to API Class C cement. Other types of construction cements can be found in standards by other countries.

4.3.2 Nonstandard Cements. Nonstandard cements are often used for special applications and do not fall into any specific API, ISO, or ASTM classification. Some of these cements are dry blends of API, ISO, or ASTM cements and additives for well applications in primary or remedial cementing operations. These cement materials' quality and uniformity are generally controlled by the supplier and include the following types:

- Pozzolan/Portland cements
- Pozzolan/lime cements
- Resin or plastic cements
- Gypsum cements
- Microfine cements
- Expanding cements

<p align="center">TABLE 4.1—STANDARD CEMENT CLASSES AND GRADES</p> <p align="center">[from <i>API Spec. 10A</i> (2002)] Reproduced courtesy of the American Petroleum Institute.</p>
<p>Class A</p> <p>The product obtained by grinding Portland cement clinker, consisting essentially of hydraulic calcium silicates, usually containing one or more forms of calcium sulfate as an interground additive. At the option of the manufacturer, processing additives may be used in the manufacture of Class A cement, provided such materials in the amounts used have been shown to meet the requirements of ASTM C 465. This product is intended for use when special properties are not required. Available only in ordinary (O) Grade (similar to ASTM C 150, Type I).</p>
<p>Class B</p> <p>The product obtained by grinding Portland cement clinker, consisting essentially of hydraulic calcium silicates, usually containing one or more forms of calcium sulfate as an interground additive. At the option of the manufacturer, processing additives may be used in the manufacture of Class B cement, provided such materials in the amounts used have been shown to meet the requirements of ASTM C 465. This product is intended for use when conditions require moderate or high sulfate-resistance. Available in both moderate sulfate-resistant (MSR) and high sulfate-resistant (HSR) Grades (similar to ASTM C 150, Type II).</p>
<p>Class C</p> <p>The product obtained by grinding Portland cement clinker, consisting essentially of hydraulic calcium silicates, usually containing one or more forms of calcium sulfate as an interground additive. At the option of the manufacturer, processing additives may be used in the manufacture of Class C cement, provided such materials in the amounts used have been shown to meet the requirements of ASTM C 465. This product is intended for use when conditions require high early strength. Available in ordinary (O), moderate sulfate-resistant (MSR) and high sulfate-resistant (HSR) Grades (similar to ASTM C 150, Type III).</p>
<p>Class D</p> <p>The product obtained by grinding Portland cement clinker, consisting essentially of hydraulic calcium silicates, usually containing one or more forms of calcium sulfate as an interground additive. At the option of the manufacturer, processing additives may be used in the manufacture of Class D cement, provided such materials in the amounts used have been shown to meet the requirements of ASTM C 465. Further, at the option of the manufacturer, suitable set-modifying agents may be interground or blended during manufacture. This product is intended for use under conditions of moderately high temperatures and pressures. Available in moderate sulfate-resistant (MSR) and high sulfate-resistant (HSR) Grades.</p>
<p>Class E</p> <p>The product obtained by grinding Portland cement clinker, consisting essentially of hydraulic calcium silicates, usually containing one or more forms of calcium sulfate as an interground additive. At the option of the manufacturer, processing additives may be used in the manufacture of Class E cement, provided such materials in the amounts used have been shown to meet the requirements of ASTM C 465. Further, at the option of the manufacturer, suitable set-modifying agents may be interground or blended during manufacture. This product is intended for use under conditions of high temperatures and pressures. Available in moderate sulfate-resistant (MSR) and high sulfate-resistant (HSR) Grades.</p>
<p>Class F</p> <p>The product obtained by grinding Portland cement clinker, consisting essentially of hydraulic calcium silicates, usually containing one or more forms of calcium sulfate as an interground additive. At the option of the manufacturer, processing additives may be used in the manufacture of Class F cement, provided such materials in the amounts used have been shown to meet the requirements of ASTM C 465. Further, at the option of the manufacturer, suitable set-modifying agents may be interground or blended during manufacture. This product is intended for use under conditions of extremely high temperatures and pressures. Available in moderate sulfate-resistant (MSR) and high sulfate-resistant (HSR) Grades.</p>
<p>Class G</p> <p>The product obtained by grinding Portland cement clinker, consisting essentially of hydraulic calcium silicates, usually containing one or more forms of calcium sulfate as an interground additive. No additives other than calcium sulfate or water, or both, shall be interground or blended with the clinker during manufacture of Class G well cement. This product is intended for use as a basic well cement. Available in moderate sulfate-resistant (MSR) and high sulfate-resistant (HSR) Grades.</p>
<p>Class H</p> <p>The product obtained by grinding Portland cement clinker, consisting essentially of hydraulic calcium silicates, usually containing one or more forms of calcium sulfate as an interground additive. No additives other than calcium sulfate or water, or both, shall be interground or blended with the clinker during manufacture of Class H well cement. This product is intended for use as a basic well cement. Available in moderate sulfate-resistant (MSR) and high sulfate-resistant (HSR) Grades.</p>

TABLE 4.2—NORMAL WATER CONTENT OF CEMENT[from *API Spec. 10A* (2002)] Reproduced courtesy of the American Petroleum Institute.

API Cement Class	Water % by Weight of Cement	Water	
		Gallon per sack	Liter per sack
A and B	46	5.19	19.6
C	56	6.32	23.9
D, E, F, and H	38	4.29	16.2
G	44	4.97	18.8

TABLE 4.3—BASIC ASTM CEMENT TYPES [*ASTM Standards on Cement* (1975)]*

ASTM Type	International Designation	API Class	Common Name	Typical Composition			
				C ₃ S	C ₂ S	C ₃ A	C ₄ AF
I	OC	A	Normal Ordinary Common	53	24	8	8
II		B	Modified	47	32	3	12
III	RHC	C	High early strength	58	16	8	8
IV	LHC		Low heat	26	54	2	12
V	SRC		Sulfate-resistant	—	—	—	—

* Reprinted, with permission, from the *Annual Book of ASTM Standards, Part 13*, 1975, copyright ASTM International, 100 Barr Harbor Drive, West Conshohocken, PA 19428.

- High-alumina cements
- Latex cements
- Cements for permafrost environments
- Sorel cements

Some of these cements that are commonly used are described below:

Pozzolan-Portland Cements. Pozzolan materials are often dry blended with Portland cements including API, ISO, or ASTM cements to produce “lightweight” (low-density) slurries for well cementing applications. Pozzolan materials include any natural or industrial siliceous or silica-aluminous material, which, though not cementitious in itself, will combine with lime in the presence of water at ambient temperatures to produce strength-developing insoluble compounds similar to those formed from hydration of Portland cement. Typically, pozzolan materials are categorized as natural or artificial and can be either processed or unprocessed. The most common sources of natural pozzolan materials are volcanic materials and diatomaceous earth. Diatomaceous earth is composed of diatom fossil remains consisting of opaline silica. Artificial pozzolan materials are produced by partially calcining natural materials such as clays, shales, and certain siliceous rocks, or are more usually obtained as an industrial byproduct. Artificial pozzolan materials include metakaolin, fly ash, microsilica (silica fume), and ground granulated blast-furnace slag. As explained by Santra (2009) and Sweatman (2009a, 2009b), the addition of pozzolan materials to API, ISO, or ASTM (Portland) cements reduces permeability and protects cement from chemical attack by corrosive formation waters with the buffered pH found in CO₂ injection zones. In most cases, pozzolan materials also can reduce the effect of sulfate attack, though this is somewhat dependent on the slurry design.

Gypsum Cements. Gypsum cement is a blended cement composed of API Class A, C, G, or H cement and the hemihydrate form of gypsum (CaSO₄ · 0.5H₂O). In practice, the term “gypsum cements” normally indicates blends containing 20% or more gypsum. Gypsum cements are commonly used in low-temperature applications for primary casing or remedial cementing work. This combination is particularly useful in shallow wells to minimize fallback after placement. The unique properties of gypsum cement are its capacity to set rapidly, its high early strength, and its positive expansion (approximately 2.0%). This is caused by the “plaster of Paris” reaction in which the hemihydrate rehydrates to form gypsum.

A cement with high gypsum content has increased ductility and acid solubility. It is usually used in situations of high lateral stress or in temporary plugging applications. A 50:50 gypsum cement is frequently used in fighting lost circulation, to form a permanent insoluble plug. These blends should be used cautiously because they have very rapid setting properties and could set prematurely during placement. A limitation of gypsum cements is that they are nonhydraulic and are not stable in contact with external water sources, including corrosive formation waters.

Microfine Cements. Microfine cements are composed of very finely ground (1) sulfate-resisting Portland cements, (2) Portland cement blends with ground granulated blast furnace slag, and (3) alkali-activated ground granulated blast furnace slag. The specific surface area for microfine cements is 500 to 1,000 m²/kg (and sometimes higher). Microfine cements have an average particle size of 4 to 6 microns and a maximum particle size of 15 microns. They hydrate in the same manner as normal Portland cements, though at a significantly faster rate because of the greater surface area. The blends of Portland cement and ground granulated blast furnace slag cement are equivalent to a finely ground pozzolanic cement, resulting in a faster hydration reaction. Such cements have a high penetrability and ultrarapid hardening. Applications for such cements include consolidation of unsound formations and repair of casing leaks in squeeze operations, particularly “tight” leaks that are inaccessible by conventional cement slurries because of their penetrability. Ultrafine alkali-activated ground blast furnace slag is used in the mud-to-cement technology in which water-based drilling mud is converted to cement.

Expanding Cements. Expansive cements are available primarily for improving the bond of cement to pipe and formation. If expansion is properly restrained, its magnitude will be reduced, and a prestress will develop. Expansion can also be used to compensate for shrinkage in neat Portland cement. Expansive cements were developed in the 1950s and 1960s that are hydraulic in nature and have controlled expansion that occurs just after setting. These cements were based on either the formation of considerable quantities of ettringite (C₆AS₃H₃₂) after set, or on hydration of anhydrous polyvalent metal oxides such as MgO or hard-burned CaO. In the late 1970s, in-situ gas-generating additives were developed; these additives produce microsize gas bubbles that cause the cement to expand while still in the plastic state.

Other formulations of expanding cement include the following:

- API and ISO Class A or H (Portland cement) containing 5 to 10% of the hemihydrate forms of gypsum
- API and ISO Class A, G, or H cements containing sodium chloride in concentrations ranging from 5% to saturation
- Cement additives that create in-situ gas generation within the cement matrix based primarily on the reaction of finely ground alumina powder with the alkalis present in the cement aqueous solution to produce hydrogen gas. Although alumina powder is the most commonly used additive, zinc, magnesium, and iron powders are potential alternatives.

At this time, the API and ISO standards contain no test procedures or specifications for measuring the expansion forces in cement. There are, however, an API Technical Report (*API 10TR2, Shrinkage and Expansion in Oil-well Cements*) and an *ISO 10426-5* standard (2005) that describe some of the test procedures used for expansion. Hydraulic bonding tests also have been used to evaluate cement expansion.

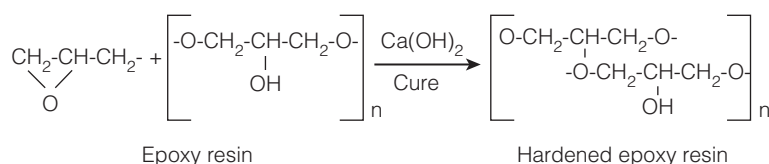
Calcium Aluminate Cements. High-alumina cement (HAC) was first developed for industrial use as a solution to the degradation of mortars and concretes in ground containing large quantities of sulfate. Today, these cements are used primarily in refractory concretes, but they are also widely used in construction for rapid setting and controlled expansion or shrinkage compensation. In well-cementing operations, they are used at both temperature extremes in permafrost zones with temperatures at 32°F or below; in in-situ combustion wells (fireflood), where temperatures may range from 750 to 2,000°F; and in thermal recovery wells, where temperatures can exceed 1,300°F and fluctuate dramatically.

Several high-alumina cements have been developed with alumina contents of 35 to 90 percent, and there is a move to term these collectively as calcium aluminate cements (CACs) because the reactive phase in all cases is calcium aluminate. CAC is manufactured by blending bauxite (aluminum ore) and limestone and heating the mixture above 2,640°F in reverberatory open-hearth furnaces until it is liquefied. The molten clinker is continuously removed through a tap hole, collected in molds, cooled, and ground in ball mills. The setting time for CAC is controlled by the composition, and no materials are added during grinding.

The manufacturer usually controls standards for CACs because few national standards address these cements. These cements can be accelerated or retarded to fit individual well conditions; however, the retardation characteristics differ from those of Portland cements. The addition of Portland cement to a refractory cement will cause a flash set; therefore, when both are handled in the field, they must be stored separately.

Latex Cement. Latex cement, although sometimes identified as a special cement, is actually a blend of API and ISO Class A, G, or H with latex. Latex is a colloidal suspension of polymer in water; the latex blends found in latex cements are generally copolymer systems that incorporate more than one type of polymer to optimize film formation and flexibility. The copolymers are based on polyvinyl acetate, polyvinylidene chloride-polyvinyl chloride, polyacrylate copolymers, or styrene-butadiene and are spherical with diameters of 0.01 to 1.0 μm . In general, a latex emulsion contains only 50% by weight of solids and is usually stabilized by an emulsifying surface-active agent. The latex particles coalesce to form a continuous film around the cement hydration products in the set cement and effectively coat the walls of the capillary pores. A well-distributed latex film may protect the cement from chemical attack by some types of corrosive conditions such as formation waters containing carbonic acid. Latex also imparts elasticity to the set cement and improves the bonding strength and filtration control of the cement slurry.

Resin or Plastic Cements. Resin and plastic cements are specialty materials used for selectively plugging open holes, squeezing perforations, and primary cementing of waste-disposal wells, especially in highly aggressive, acidic environments. These cements may be composed of resins and catalysts alone or contain fillers such as silica sand. Other systems are mixtures of water, liquid resins, and a catalyst blended with API Class A, B, G, or H cement. For example:



A unique property of these cements is their capability to be squeezed under applied pressure into a permeable zone to form a seal within the formation. These specialty cements are used in relatively small volumes and are generally effective at temperatures from 60 to 200°F (15 to 93°C). Some types of resin cements can be applied in wells with higher temperature conditions.

Sorel Cement. Sorel cement is a magnesium-oxychloride cement used as a temporary plugging material in well cementing. The cement is made by mixing powdered magnesium oxide with a concentrated solution of magnesium chloride. The complex hydration reactions include at least eight different primary reactions. Carbonates are generally incorporated into the formulation to reduce the solubility of the magnesium hydroxide chloride hydrates that are normally formed by producing carbonated hydrates. The main phases formed are $\text{Mg}_2\text{OHClCO}_3 \cdot 3\text{H}_2\text{O}$ and $\text{Mg}_3(\text{OH})_2(\text{CO}_3)_4 \cdot 4\text{H}_2\text{O}$. Sorel cements have been used on occasion in the Commonwealth of Independent States (CIS) for cementing oil wells at temperatures up to 1,400°F (752°C). An acid-soluble magnesia cement that reacts as a complex Sorel cement has been set across production perforations as a temporary abandonment plug and used to protect water-injection zones during workover operations (Sweatman and Scoggins 1990). The same system has been used to squeeze lost-circulation zones during drilling operations. A more finely ground version is available for applications requiring short cement times.

Acid-soluble Sorel cements are not recommended for permanent sealing in corrosive environments, such as well cementing applications across formations containing carbonic acid waters or “wet” CO_2 gas.

4.4 Cement Additives

Typically, cement additives are free-flowing powders that either can be dry blended with the cement before transporting it to the well or can be dispersed in the mixing water at the job site. At present, the cement classes G and H can be modified easily through the use of additives to meet almost any job specifications economically. The use of modified Class H cement has become extremely popular.

The cement additives available can be subdivided into these functional groups: (1) density-control additives, (2) setting-time-control additives, (3) lost-circulation additives, (4) filtration-control additives, (5) viscosity-control additives, and (6) special additives for unusual problems. The first two categories are perhaps the most important because they receive consideration on almost every cement job. Some additives serve more than one purpose and, thus, would fit under more than one of the classifications shown above.

It should be well understood that all additives have both primary and secondary effects. For example, an additive that affects slurry density may also influence slurry viscosity and setting time. In fact, the mechanisms of acceleration and retardation are still not completely understood. It should be noted that most of additives are strongly influenced by the chemical and physical properties of the cement, which may vary considerably even for a given API class of cement.

The nomenclature used by the petroleum industry to express the concentration of cement additives often is confusing to the student. However, most of the confusion can be cleared up by pointing out that the reference basis of cement mixtures is a unit weight of cement. When the concentration of an additive is expressed as a “weight percent” or simply “percent,” the intended meaning is usually that the weight of the additive put in the cement mixture is computed by multiplying the weight of cement in the mixture by the weight percent given by 100%. The concentration of liquid additives sometimes is expressed as gallons per sack of cement. A sack of cement contains 94 lbm unless the cement product is a blend of cement and some other material. The water content of the slurry is sometimes expressed as the water/cement ratio in gallons per sack and sometimes expressed as a weight percent. The term “percent mix” is used for water content expressed as a weight percent. Thus,

$$\text{percent mix} = \frac{\text{water weight}}{\text{cement weight}} \times 100.$$

Many components are used in low concentration and have very minor effects on slurry volume. Physical properties of cement components needed to perform the ideal mixing calculations are given in **Table 4.4**.

The volume of slurry obtained per sack of cement used is called the *yield* of the cement. This term should not be confused with the yield of clay or the yield point of a fluid as discussed in Chapter 3.

Example 4.3 It is desired to mix a slurry of Class A cement containing 3% bentonite, using the normal mixing water as specified by API (Table 4.2). Determine the weight of bentonite (specific gravity = 2.65) and volume of water to be mixed with one 94-lbm sack of cement (specific gravity = 3.14). Also, compute the percent mix, yield, and density of the slurry.

Solution. The weight of bentonite to be blended with one sack of Class A cement is

$$0.03(94) = 2.82 \text{ lbm}.$$

The normal water content for Class A cement is 46% (Table 4.2). However, 5.3% water must be added for each percent of bentonite. Thus, the percent mix is

$$46 + 3(5.3) = 61.9\%.$$

The water volume to be added per sack of Class A cement is given by

$$\frac{0.619 (94 \text{ lbm/sack})}{8.33 \text{ lbm/gal}} = 6.98 \text{ gal}.$$

The specific gravities of cement and bentonite are 3.14 and 2.65, respectively. The volume of the slurry is given by

$$\frac{94 \text{ lbm}}{3.14(8.33) \text{ lbm/sack}} + \frac{2.82 \text{ lbm}}{2.65(8.33) \text{ lbm/sack}} + 6.98 \text{ gal/sack} = 10.7 \text{ gal/sack}.$$

The yield of the slurry is

$$\frac{10.7 \text{ gal/sack}}{7.48 \text{ gal/ft}^3} = 1.43 \text{ ft}^3/\text{sack}$$

The density of the slurry is the total mass divided by the total volume or

$$\frac{94 + 2.82 + 8.33(6.98)}{10.7} = 14.5 \text{ lbm/gal}.$$

4.4.1 Density Control. The density of the cement slurry must be high enough to prevent the higher-pressured formations from flowing into the well during cementing operations, yet not so high as to cause fracture of the

TABLE 4.4—PHYSICAL PROPERTIES OF CEMENTING MATERIALS (Halliburton 2001)

Material	Bulk Weight, lbm/ft ³	Specific Gravity	Absolute Volume	
			gal/lbm	ft ³ /lbm
API Class A cement	94	3.15	0.0380	0.0051
API Class C cement	94	3.19	0.0376	0.0050
API Class G cement	94	3.18	0.0377	0.0050
API Class H cement	94	3.18	0.0377	0.0050
Ciment Fondu	90	3.20	0.0375	0.0050
Activated Charcoal	14	1.57	0.0765	0.0102
Gilsonite	50	1.07	0.1122	0.0150
Micro-Fly Ash	65	2.54	0.0473	0.00630
Calcium Chloride	saturated liquid	1.32	0.0908	0.0121
Potassium Chloride	saturated liquid	1.18	0.1017	0.0136
Sodium Chloride	saturated liquid	1.20	0.0999	0.0134
Latex	30	0.997	0.1202	0.0167
Attapulgite	40	2.58	0.0465	0.0062
Barite	135	4.23	0.0284	0.0038
Bentonite	60	2.65	0.0453	0.0061
Calcium Carbonate	22.3	2.71	0.0443	0.0059
Calcium Chloride (dry)	50.5	1.96	0.0612	0.0082
Hydrated Lime	31	2.34	0.0513	0.0069
Iron Carbonate	114.5	3.7	0.0324	0.0043
Hematite	193	5.02	0.0239	0.0032
Perlite (0 psi)	8	0.67	0.1792	0.0240
Perlite (3000 psi)		2.2	0.0546	0.0073
Sodium Chloride (dry)	71	2.17	0.0553	0.0074
Sand 35% porosity	106.6	2.63	0.0456	0.0061
Sand 39% porosity	100	2.63	0.0456	0.0061
Silica Flour	70	2.63	0.0456	0.0061
Diesel Oil No. 1		0.82	0.1461	0.0195
Diesel Oil No. 1		0.85	0.1410	0.0189
Sea Water		1.025	0.1169	0.0156
Fresh Water		1.0	0.1198	0.0160
Potassium Chloride 3%		1.019	0.0443	0.0059
Potassium Chloride 5%		1.031	0.0450	0.0060
Sodium Chloride 6%		1.041	0.0372	0.0050
Sodium Chloride 12%		1.078	0.0391	0.0052
Sodium Chloride 18%		1.112	0.0405	0.0054
Sodium Chloride 24%		1.145	0.0417	0.0056

weaker formations. In most cases, the density of the cement slurry obtained by mixing cement with the normal amount of water will be too great for the formation fracture strength, and it will be desirable to lower the slurry density.

Reducing the cement density also tends to reduce the overall cost of the cement slurry. Slurry density is reduced by using nitrogen as an additive to mix foam cement. In recent years, low-density microspheres have been added to foam cement. Other common methods use nonfoamed cement with a higher water/cement ratio or with added low-specific-gravity solids, or both. The higher water/cement ratio approach that uses bentonite or silicate additives has been found to cause poor sealing results, leading to formation-fluid influx and migration between zones or up the annulus to the wellhead, and is not recommended for applications across potential flow zones or where unknown flow zones may exist.

The low-specific-gravity solids commonly used to reduce slurry density include (1) nitrogen plus foaming agents, (2) microspheres, (3) pozzolans, (4) sodium silicates, and (5) bentonite (sodium montmorillonite). The last two solids in this list are not recommended for certain applications, including those that control gas migration.

When extremely weak formations are present, it may not be possible to reduce slurry density sufficiently to prevent fracture. In this case, the mud column in front of the cement slurry can be aerated with nitrogen to reduce hydrostatic pressure further. However, nitrogen and foaming agents added to cement slurries are often the best method for reducing cement density while maintaining other good properties.

4.4.2 Foamed Cement. It is possible to make slurries ranging in density from 4 to 18 lbm/gal using foamed cement. Foamed cement is a mixture of cement slurry, foaming agents, and a gas. Foamed cement is created when a gas, usually nitrogen, is injected at high pressure into a base slurry that incorporates a foaming agent and foam stabilizer. Nitrogen gas can be considered inert and does not react with or modify the cement hydration product formation. Under special circumstances, compressed air can be used instead of nitrogen to create foamed cement. In general, because of the pressures, rates, and gas volumes involved, nitrogen-pumping equipment provides a more reliable gas supply. The process forms an extremely stable, lightweight slurry that looks like gray shaving foam. When foamed slurries are properly mixed and sheared, they contain tiny, discrete bubbles that will not coalesce or migrate. Because the bubbles that form are not interconnected, they form a low-density cement matrix with low permeability and relatively high strength.

Virtually any oilwell-cementing job can be considered a candidate for foamed cementing, including primary and remedial cementing functions onshore and offshore, and in vertical or horizontal wells. Although its design and execution can be more complex than standard jobs, foamed cement has many advantages that can overcome these concerns. Foamed cement is lightweight, provides excellent strength-to-density ratio, is ductile, enhances mud removal, expands, helps prevent gas migration, improves zonal isolation, imparts fluid-loss control, is applicable for squeezing and plugging, insulates, stabilizes at high temperatures, is compatible with non-Portland cements, simplifies admix logistics, enhances volume, has low permeability, is stable to crossflows, and forms a synergistic effect with some additives, which enhances the property of the additive. The disadvantage of foamed cement is the need for specialized cementing equipment both for field application and for laboratory testing. See *API RP 65-Part 1* (2002), *RP 65-Part 2* (2010), and *RP 10B-4* (2004) or its equivalent, *ISO 10426-4* (2004), for recommended practices on using and testing foam cements.

4.4.3 Microspheres. Microspheres are used when slurry densities from 8.5 to 11 lbm/gal are required. They are hollow spheres obtained as a byproduct from power-generating plants or are specifically formulated. The byproduct microspheres are essentially hollow fly-ash glass spheres. They are present, typically, in Class F fly ashes, but usually in small amounts; however, they are obtained in substantial quantities when excess fly ash is disposed of in waste lagoons. The low-density hollow spheres float to the top and are separated by a flotation process. These hollow spheres are composed of silica-rich aluminosilicate glasses typical of fly ash and are generally filled with a mixture of combustion gases such as CO_2 , NO_x , and SO_x . The synthetic hollow spheres are manufactured from a soda-lime borosilicate glass and are formulated to provide a high strength-to-weight ratio—they are typically filled with nitrogen. The synthesized microspheres provide a more consistent composition and exhibit better resistance to mechanical shear and hydraulic pressure.

The primary disadvantage of most microspheres is their susceptibility to crushing during mixing and pumping and when exposed to hydrostatic pressures above the average crush strength. This can lead to increased slurry density, increased slurry viscosity, decreased slurry volume, and premature slurry dehydration.

However, crushing effects can be minimized by the suitable choice of microspheres. These effects can be predicted and taken into account in slurry design calculations to produce a slurry with the required characteristics for the well conditions. Lightweight systems incorporating microspheres can provide excellent strength development and can help control fluid loss, settling, and free water.

4.4.4 Pozzolan. Pozzolans are siliceous and aluminous mineral substances that will react with calcium hydroxide formed in the hydration of Portland cement to form calcium silicates that possess cementitious properties. Diatomaceous earth, which has been discussed previously, is an example of a pozzolan. However, the term *pozzolan* as used in marketing cement additives usually refers to finely ground pumice or fly ash (flue dust) produced in coal-burning power plants. The specific gravity of pozzolans is only slightly less than the specific gravity of Portland cement, and the water requirement of pozzolans is approximately the same as for Portland cements. Thus, only slight reductions in density can be achieved with this material. The range of slurry densities possible using various concentrations of one type of pozzolan is about 13 to 16 lbm/gal. Because of this relatively low cost, considerable cost savings can be achieved through the use of pozzolans.

4.4.5 Sodium Silicates. Sodium silicate liquid and metasilicate particulates are used as accelerators and for lightening the density of cement. They are used in concentrations from 0.1% BWOC up to approximately 4% by weight.

4.4.6 Bentonite (Specific Gravity = 2.65). The use of bentonite (sodium montmorillonite) clay for building drilling-fluid viscosity has been discussed previously in Chapter 3. This same clay mineral is used extensively as an additive for lowering cement density; however, bentonite marketed for use in drilling fluid sometimes is treated with an organic polymer that is undesirable for use in cement slurries because it tends to increase slurry viscosity. The addition of bentonite lowers the slurry density because of its lower specific gravity and because its ability to hydrate permits the use of much higher water concentrations. Bentonite concentrations as high as 25% by weight of cement have been used. The bentonite usually is blended dry with the cement before mixing with water, but it can be prehydrated in the mixing water. Much higher increases in water content can be obtained for each percent bentonite added when the bentonite is prehydrated in the mixing water. The ratio of bentonite dry blended to bentonite prehydrated is approximately 3.6:1 for comparable slurry properties.

In addition to lowering slurry density, the addition of bentonite lowers slurry cost; however, a high percentage of bentonite in cement also will cause a reduction in cement strength and thickening time. Also, the higher water content lowers the resistance to sulfate attack and increases the permeability of the set cement. At temperatures above 230°F, the use of bentonite promotes retrogression of strength in cements with time; however, test results have been found to vary significantly from batch to batch. When exact data are needed, tests should be conducted with the same materials and mixing water that will be used in the cementing operations.

In areas in which the formation pore pressure is extremely high, it may be necessary to increase the slurry density. Slurry density usually is increased by using a lower water content or adding high-specific-gravity solids. The high-specific-gravity solids commonly used to increase slurry density include hematite and barite (barium sulfate). The specific gravity values of selected cement additives are shown in Table 4.4. The water requirements for the various additives are shown in Table 4.5.

4.4.7 Hematite. Hematite is reddish iron oxide ore (Fe_2O_3) having a specific gravity of approximately 5.02. Hematite can be used to increase the density of a cement slurry to as high as 19 lbm/gal. Metallic powders having a higher specific gravity than hematite have been tried but were found to settle out of the slurry rapidly unless they were ground extremely fine. When ground fine enough to prevent settling, the increased water requirement results in slurry densities below those possible with hematite. The water requirement for hematite is approximately 0.36 gal/100 lbm hematite. The effect of hematite on the thickening time and compressive strength

TABLE 4.5—WATER REQUIREMENTS OF CEMENTING MATERIALS
(Halliburton 2001)

Material	Minimum gal/lbm	Maximum gal/lbm
API Class A cement	0.05532	0.05532
API Class C cement	0.06702	0.06702
API Class G cement	0.05319	0.05319
API Class H cement	0.04574	0.04574
Ciment Fondu	0.04787	0.04787
Activated Charcoal	none	none
Gilsonite	0.04	0.04
Calcium Chloride	none	none
Potassium Chloride	none	none
Sodium Chloride	none	none
Latex	0.0	0.8/sack
Attapulgate	0.69	0.69
Barite	0.0264	0.0264
Bentonite	0.69	0.69
Calcium Carbonate	none	none
Calcium Chloride (dry)	none	none
Hydrated Lime	0.153	0.153
Hematite	0.0036	0.0036
Perlite (0 psi)	0.5	0.5
Sand	none	none
Silica Flour	0.049	0.049

of the cement has been found to be minimal at the concentrations of hematite generally used. The range of slurry densities possible using various concentrations of hematite is approximately 16 to 19 lbm/gal.

4.4.8 Barite (Specific Gravity = 4.23). The use of barite, or barium sulfate, for increasing the density of drilling fluids has been discussed previously in Chapter 3. This mineral also is used extensively for increasing the density of cement slurry. The water requirements for barite are considerably higher than for hematite or ilmenite, requiring approximately 2.4 gal/100 lbm of barite. The large amount of water required decreases the compressive strength of the cement and dilutes the other chemical additives. The range of slurry densities possible using various concentrations of barite is about 16 to 19 lbm/gal.

Example 4.4 It is desired to increase the density of a Class H cement slurry to 17.5 lbm/gal. Compute the amount of hematite that should be blended with each sack of cement. The water requirements are 4.5 gal/94 lbm Class H cement and 0.36 gal/100 lbm hematite.

Solution. Let x represent the pounds of hematite per sack of cement. The total water requirement of the slurry then is given by $4.5 + 0.0036x$. Expressing the slurry density, ρ , in terms of x yields

$$\rho = \frac{\text{total mass, lbm}}{\text{total volume, gal}},$$

$$17.5 = \frac{94 + x + 8.34(4.5 + 0.0036x)}{\left[\frac{94}{3.14(8.34)} + \frac{x}{5.02(8.34)} + (4.5 + 0.0036x) \right]}$$

Solving this expression yields $x = 18.3$ lbm hematite/94 lbm cement.

A summary of oilwell cementing additives is shown in **Tables 4.6a and 4.6b**. **Table 4.7** shows the effects of some additives on the physical properties of cement.

4.4.9 Setting-Time Control. The cement must set and develop sufficient strength to support the casing and seal off fluid movement behind the casing before drilling or completion activities can be resumed. The exact amount of compressive strength needed is difficult to determine, but a value of 500 psi commonly is used in field practice. Experimental work by Farris (1946) has shown that a tensile strength of only a few psi was sufficient to support the weight of the casing under laboratory conditions; however, some consideration also must be given to the dynamic loading imposed by the rotating drillstring during subsequent drilling operations. It is possible for the drillstring to knock off the lower joint of casing and junk the hole if a good bond is not obtained. The cement strength required to prevent significant fluid movement behind the casing was investigated by Clark (1953). His data show that tensile strengths as low as 40 psi are acceptable, with maximum bonding being reached at a value of approximately 100 psi. Because the ratio of compressive strength to tensile strengths usually is approximately 12:1, 40- and 100-psi tensile strengths correspond to compressive strengths of 480 and 1,200 psi.

When cementing shallow, low-temperature wells, it may be necessary to accelerate the cement hydration so that the waiting period after cementing is minimized. The commonly used cement accelerators are calcium chloride, sodium chloride, the hemihydrate form of gypsum, and sodium silicate. Cement setting time also is a function of the cement composition, fineness, and water content. For example, API Class C cement is ground finer and has a higher C3A content to promote rapid hydration. When low water/cement ratios are used to reduce setting time, friction-reducing agents (dispersants) sometimes are used to control rheological properties; however, the dispersant must be chosen with care because many dispersants tend to retard the setting of the cement. Organic dispersants such as tannins and lignins already may be present in the water available for mixing cement, especially in swampy locations; thus, it often is important to measure cement thickening time using a water sample taken from the location.

4.4.10 Calcium Chloride. Calcium chloride in concentrations up to 4% by weight commonly is used as a cement accelerator in wells having bottomhole temperatures of less than 125°F. It is available in a regular grade (77% calcium chloride) and an anhydrous grade (96% calcium chloride). The anhydrous grade is in more general use because it absorbs moisture less readily and is easier to maintain in storage.

TABLE 4.6—SUMMARY OF OILWELL CEMENTING ADDITIVES (Lake 2006)

Type of Additive	Use	Chemical Composition	Benefit	Type of Cement
Accelerators	Reducing WOC time Setting surface pipe Setting cement plugs Combating lost circulation	Calcium chloride Sodium chloride Gypsum Sodium silicate Dispersants Seawater	Accelerated setting High early strength	All API classes Pozzolans Diacel systems
Retarders	Increasing thickening time for placement Reducing slurry viscosity	Lignosulfonates Organic acids CMHEC Modified lignosulfonates	Increased pumping time Better flow properties	API Classes D, E, G, and H Pozzolans Diacel systems
Weight-reducing additives	Reducing weight Combating lost circulation	Bentonite/attapulgite Gilsonite Diatomaceous earth Perlite Pozzolans Microspheres (glass spheres) Nitrogen (foam cement)	Lighter weight Economy Better fill-up Lower density	All API classes Pozzolans Diacel systems
Heavyweight additives	Combating high pressure Increasing slurry weight	Hematite Limenite Barite Sand Dispersants	Higher density	API Classes D, E, G, and H
Additives for controlling lost circulation	Bridging Increasing fill-up Combating lost circulation Fast-setting systems	Gilsonite Walnut hulls Cellophane flakes Gypsum cement Bentonite-diesel oil Nylon fibers Thixotropic additives	Bridged fractures Lighter fluid columns Squeezed fractured zones Treating lost circulation	All API classes Pozzolans Diacel systems
Filtration-control additives	Squeeze cementing Setting long liners Cementing in water-sensitive formations	Polymers Dispersants CMHEC Latex	Reduced dehydration Lower volume of cement Better fill-up	All API classes Pozzolans Diacel systems
Dispersants	Reducing hydraulic horsepower Densifying cement slurries for plugging Improving flow properties	Organic acids Polymers Sodium chloride Lignosulfonates	Thinner slurries Decreased fluid loss Better mud removal Better placement	All API classes Pozzolans Diacel systems
Special cements or additives	Salt	Sodium chloride	Better bonding to salt, shales, sands	All API classes

TABLE 4.6—SUMMARY OF OILWELL CEMENTING ADDITIVES (Lake 2006) (Continued)				
Type of Additive	Use	Chemical Composition	Benefit	Type of Cement
Silica flour	High-temperature cementing	Silicon dioxide	Stabilized strength	All API classes
Radioactive tracers	Tracing flow patterns Locating leaks	$^{131}_{53}\text{I}$, $^{192}_{77}\text{Ir}$		All API classes
Pozzolan lime	High-temperature cementing	Silica-lime reactions	Lighter weight Economy	
Silica lime	High-temperature cementing	Silica-lime reactions	Lighter weight	
Gypsum cement	Dealing with special conditions	Calcium sulfate Hemihydrate	Higher strength Faster setting	
Latex cement	Dealing with special conditions	Liquid or powdered latex	Better bonding Controlled filtration	API Classes A, B, G, and H
Thixotropic additives	Covering lost-circulation zones Preventing gas migration	Organic additives Inorganic additives	Fast setting and/or gelation Less fallback Reduces lost circulation	All API classes

4.4.11 Sodium Chloride. Sodium chloride is an accelerator when used in low concentrations. Maximum acceleration occurs at a concentration of approximately 5% (by weight of mixing water) for cements containing no bentonite. At concentrations above 5%, the effectiveness of sodium chloride as an accelerator is reduced. Saturated sodium chloride solutions tend to act as a retarder, rather than an accelerator. Saturated sodium chloride cements are used primarily for cementing through salt formations and through shale formations that are highly sensitive to fresh water. Potassium chloride is more effective than sodium chloride for inhibiting shale hydration and can be used for this purpose when the additional cost is justified.

Seawater often is used for mixing cement when drilling offshore. The sodium, magnesium, and calcium chlorides at the concentrations present in the seawater all act as cement accelerators. Typical effects of seawater on cement slurry properties as compared with fresh water are shown in **Table 4.8**.

This thickening time obtained with seawater usually is adequate for cement placement where bottomhole temperatures do not exceed 160°F. Cement retarders can be used to counteract the effect of the seawater at higher temperatures, but laboratory tests always should be performed before this type of application.

4.4.12 Gypsum. Special grades of gypsum hemihydrate cement can be blended with Portland cement to produce a cement with a low thickening time at low temperatures. These materials should not be used at high temperatures because the gypsum hydrates may not form a stable set. The maximum working temperature depends on the grade of gypsum cement used, varying from 140°F for the regular grade to 180°F for the high-temperature grade. A full range of blends, from as little as 1 sack gypsum/20 sacks cement to pure gypsum, have been used for various applications. The water requirement of gypsum hemihydrate is approximately 4.8 gal/100-lbm sack.

For very shallow wells and surface applications at low temperatures, where an extremely short setting time combined with rapid strength development is desired, a small amount of sodium chloride can be used with a gypsum cement blend. For example, a laboratory blend of 90 lbm of gypsum hemihydrate, 10 lbm of Class A Portland cement, and 2 lbm of salt when mixed with 4.8 gal of water will develop more than 1,000 psi of compression strength when cured at only 50°F for 30 minutes.

4.4.13 Cement Retarders. Most of the organic compounds discussed in Chapter 3 for use as drilling-fluid deflocculants tend to retard the setting of Portland cement slurries. These materials also are called thinners or dispersants. Calcium lignosulfonate, one of the common mud deflocculants, has been found to be very effective as a cement retarder at very low concentrations. Laboratory data on the thickening time of cements at various concentrations of calcium lignosulfonate are available from petroleum-industry service companies.

The addition of an organic acid to the calcium lignosulfonate has been found to give excellent retarding characteristics at extremely high temperatures. It also improves the rheological properties of the slurry to a greater

TABLE 4.7—EFFECTS OF CEMENT ADMIXTURES ON THE PHYSICAL PROPERTIES OF CEMENT (Lake 2006)

	Accelerator (Calcium Chloride)	Bentonite	Pozzolan (Fly Ash)	Heavyweight Hematite	Retarders	Friction Reducers (Dispersants)	Filtration Additives	Lost- Circulation Additives	Sand	Salt, 10 to 20%	Silica Flour	Seawater
<u>Water Requirements</u>												
Increases		Y	X			X	X	X			X	
Decreases												
<u>Density</u>												
Increases				Y		Y		Y	X	X		X
Decreases		Y	Y								X	
<u>Viscosity</u>												
Increases		X	X	X	X	Y	X		X	X		
Decreases	X											
<u>Thickening Time</u>												
Accelerates	Y	X			Y	X	X					X
Retards												
<u>Fluid Loss of Slurry</u>												
Increases						X	Y					
Decreases		X										
<u>Early Strength</u>												
Increases	Y	X	X	X	Y	X	X		X		X	X
Decreases												
<u>Final Strength</u>												
Increases		X	X			X					Y	
Decreases												
<u>Durability</u>												
Increases			Y		X						Y	
Decreases	X											
<u>Types of Cementing Job Applications (where mostly used)</u>												
Conductor	X					X		X		X		X
casing												
Surface casing	X		X			X		X		X		X
Intermediate		X	X			X		X		X		X
casing												
Production		X	X	X	X	X	X	X			X	
casing												
Liners				X	X	X	X				X	
Squeezing					X	X	X					
Plugging					X	X	X		X			

Note: For temperature 230°F. X = minor effects and Y = major effects

TABLE 4.8—TYPICAL EFFECT OF SEAWATER ON THICKENING TIME (WATER RATIO: 5.2 GAL/SACK) (Bourgoyne et al. 1991)					
	Thickening Time (Hours: Minutes)		Compressive Strength (psi at 24 hours)		
	6,000 ft*	8,000 ft*	50°F	110°F; 1,600 psi	140°F; 3,000 psi
API Class A Cement					
Fresh water	2:25	1:59	435	3,230	4,025
Seawater	1:33	1:17	520	4,105	4,670
API Class H Cement					
Fresh water	2:59	2:16	—	1,410	2,575
Seawater	1:47	1:20	—	2,500	3,085
*API RP 10B Casing Schedule					

extent than calcium lignosulfonate alone. When the addition of the organic acid increases the effectiveness of the retarder to the extent that less than 0.3% would be used, it may be difficult to obtain a uniform blend. In this case, the use of calcium lignosulfonate is best. The addition of the organic acid also has been found to be effective in Class A cement.

Calcium-sodium lignosulfonate has been found to be superior to a calcium lignosulfonate when high concentrations of bentonite are used in the cement. The use of calcium-sodium lignosulfonate has been found to produce a slurry having a lower viscosity during mixing; it also helps to reduce air entrainment.

Sodium tetraborate decahydrate (borax) can be used to enhance the effectiveness of the organic deflocculants as retarders, especially in deep, high-temperature wells where a large increase in thickening time is needed. The optimum borax concentration is thought to be approximately one-third of the concentration of deflocculant used. Laboratory tests have shown that in addition to increasing the pumping time, the borax reduces the detrimental effect of the deflocculant on the early compressive strength of the cement.

Carboxymethyl hydroxyethyl cellulose (CMHEC) commonly is used for both cement retardation and fluid-loss control. It is used more commonly with cements containing diatomaceous earth, but it is effective as a retarder in essentially all Portland cements. Laboratory data on the thickening time and compressive strength of cements at various concentrations of CMHEC are available from the service companies.

4.4.14 Lost-Circulation Additives. *Lost circulation* is defined as the loss of drilling fluid or cement from the well to subsurface formations. This condition is detected at the surface when the flow rate out of the annulus is less than the pump rate into the well. Lost circulation occurs when extremely-high-permeability formations are encountered (such as a gravel bed, oyster bed, or vugular limestone) or when a fractured formation is encountered or created while drilling or performing other operations such as running casing because of excessive wellbore pressure.

Lost circulation usually occurs while drilling and can be overcome by adding lost-circulation material to the drilling fluid or reducing the drilling-fluid density. In some cases, however, lost-circulation material is added to the cement slurry to minimize the loss of cement to a troublesome formation during cementing and, thus, to ensure placement of the cement in the desired location. The lost-circulation additives are classified as fibrous, granular, or lamellated. In laboratory experiments, fibrous and granular additives are effective in high-permeability gravel beds. In simulated fractures, granular and lamellated additives are found to be effective. The commonly used granular additives include gilsonite, expanded perlite, plastics, and crushed walnut shells. Fibrous materials used include nylon fibers, shredded wood bark, sawdust, and hay. However, the use of wood products can cause cement retardation because they contain tannins. Lamellated materials include cellophane and mica flakes.

Semi-solid and flash-setting slurries are available for stopping severe lost-circulation problems encountered while drilling that cannot be remedied by adding lost-circulation additives to the mud. The placement of these cements and noncement systems in the lost-circulation zone requires a special operation because they are not merely additives to the fluid being circulated while drilling. The slurries most often used for this purpose include

- Gypsum hemihydrate cements
- Mixtures of bentonite and diesel oil (gunk)
- Mixtures of cement, bentonite, and diesel oil

- “WB super-gunks” (WB=water-based) comprised of hydradable clays, crosslinking polymers slurried in aqueous fluids
- “OB super-gunks” (OB=oil-based) with hydradable clays and latex slurried in nonaqueous fluids including diesel, mineral, and synthetic oils

4.4.15 Filtration-Control Additives. Cement filtration-control additives serve the same function as the mud filtration-control additives discussed in Chapter 3. However, cement slurries containing no filtration-control additives have much higher filtration rates than clay/water muds. An untreated slurry of Class H cement has a 30-minute API filter loss in excess of 1000 cm³. It is desirable to limit the loss of water filtrate from the slurry to permeable formations to

- Minimize the hydration of formations containing water-sensitive shales
- Prevent increases in slurry viscosity during cement placement
- Prevent the formation of annular bridges (which can act as a packer and remove hydrostatic pressure holding back potentially dangerous high-pressure zones)
- Reduce the rate of cement dehydration while pumping cement into abandoned perforated intervals and, thus, allow for the plugging of longer perforated intervals in a single operation

The commonly used filtration-control additives include latex, bentonite with a dispersant, CMHEC, and various organic polymers.

4.4.16 Viscosity-Control Additives. Untreated cement slurries have a high effective viscosity at the shear rates present during cement placement. It is desirable to reduce the effective viscosity of the slurry so that (1) less pump horsepower will be required for cement placement, (2) there will be reduction in the annular frictional pressure gradient and, thus, a smaller chance of formation fracture, and (3) the slurry can be placed in turbulent flow at a lower pumping rate. Some evidence indicates that the drilling fluid is displaced with less mixing and, thus, less cement contamination when the flow pattern is turbulent. The required flow rates that result in turbulent flow can be calculated using equations given in Chapter 5. The commonly used viscosity-control additives include organic deflocculants such as calcium lignosulfonate; sodium chloride; and certain long-chain polymers. These additives are also called thinners, dispersants, or friction reducers. Deflocculants reduce cement viscosity in the same manner as discussed previously in Chapter 3 for drilling fluids; however, it should be noted that deflocculants act as retarders as well as thinners. Certain organic polymers are available that will act as thinners without accelerating or retarding the cement.

4.4.17 Other Additives. Miscellaneous additives and slurries not discussed in the previous categories given include

- Paraformaldehyde and sodium chromate, which are used to counteract the effect of cement contamination by organic deflocculants from the drilling mud
- Silica flour, which is used to form a stronger, more stable, and less permeable cement for high-temperature applications
- Hydrazine, an oxygen scavenger used to control corrosion
- Radioactive tracers used to determine where the cement has been placed
- Special fibers such as nylon to make the cement more impact resistant
- Special compounds that slowly evolve into small gas bubbles as the cement begins to harden

The formation of small gas bubbles in the cement is thought to be desirable when there is a danger of gas flow occurring in the newly cemented borehole when the cement begins to harden. There have been several cases of gas flow through the annulus several hours after cementing operations were completed. A gas flow outside the casing can be particularly difficult to stop because conventional well-control procedures cannot be used easily.

The mechanism by which gas blowouts occur shortly after cementing is not fully understood; however, it is known that the formation of a semi-rigid gel structure begins as soon as cement placement is completed. Initially, the formation of the static gel structure is similar to that occurring in a drilling fluid when fluid movement is stopped. Later, as the cement begins to set, the cement gel becomes much more progressive than that of a drilling fluid. As the cement slurry goes through a transition from a liquid to a solid, it begins to lose the ability to transmit

hydrostatic pressure to the lower part of the cemented annulus. If this loss in ability to transmit hydrostatic pressure is accompanied by a cement slurry volume reduction, the wellbore pressure can fall sufficiently to permit gas from a permeable high-pressure formation to enter the annulus. The semi-rigid slurry may not be able to withstand the higher stresses created when gas begins to flow. Gas flow may increase and communicate with a more shallow formation. In an extreme case, gas flow may reach the surface.

Volume reductions occurring while the cement is making the transition from a liquid slurry to a rigid solid can be traced to two sources. A small volume reduction, as measured in the soundness test, occurs as a result of the cement hydration reaction. For most cements used in current practice, this volume reduction (called *plastic-state shrinkage*) is small, generally being on the order of 0.1 to 0.3% (Sabins and Sutton 1991). Much larger volume reductions are thought to be possible due to the loss of water filtrate to the borehole walls.

The magnitude of the pressure loss per unit volume of filtrate loss is controlled primarily by the cement compressibility during the early stages of the hardening process. A cement with a high compressibility is desirable because it will give a small pressure loss per unit volume of filtrate loss. The introduction of a compound that will react slowly to form small gas bubbles as the cement begins to harden will greatly increase the compressibility of the cement. Cement compressibility also can be increased by blending small volumes of nitrogen gas with the cement slurry during mixing.

A high-compressibility cement permits much larger volumes of water filtrate to be lost without greatly increasing the potential for gas flow into the well. Other methods for reducing the potential for gas flow after cementing include use of filtration-control additives to reduce the volume of filtrate loss, shorter cement columns to reduce the effectiveness of the gel strength in blocking the transmission of hydrostatic pressure, and cements that build gel strength quickly after pumping is stopped and harden more rapidly.

4.5 Cement Placement Techniques

Different cementing equipment and placement techniques are used for cementing *casing* strings, cementing *liner* strings, setting cement *plugs*, and *squeeze* cementing. These different types of cementing applications are schematically depicted in **Fig. 4.4**. A casing string differs from a liner in that casing extends to the surface, while the top of a liner is attached to subsurface casing previously cemented in place. Cement plugs are placed in open hole or in casing before abandoning the lower portion of the well. Cement is squeezed into lost-circulation zones, abandoned casing perforations, or a leaking cemented zone to stop undesired fluid movement.

4.5.1 Cement Casing. The conventional method for cementing casing is described in **Fig. 4.5**. The following describes the typical procedure for a single-stage primary cement job.

When the well has been drilled to the planned setting depth for the next string of casing, or the driller has been forced to stop and set a casing for wellbore stability or other reasons, the casing running and cement operations begin.

First, the drillstring is tripped out of the hole, and the casing string is made up and run into the hole. The first item on the casing string is the guide/float shoe. In its simplest form, the purpose of a guide shoe is to direct the casing away from ledges to minimize side-wall caving and to aid in safely passing hard shoulders and passing through crooked holes. If the guide shoe does not have a float, then a float collar is placed above the guide shoe. The original purpose of a float collar was to facilitate running the casing by reducing the load on the derrick. This purpose is accomplished by preventing the drilling fluid from flowing into the casing when it is run into the hole. The derrick design has improved over the years, and now the main purpose of the float collar is to prevent the cement from flowing back into the casing. The interval of casing that is to be cemented may have centralizers attached; centralizers are attached to the casing to keep it off the borehole wall and centralize it as much as possible. Centralizing the casing helps to provide a uniform fluid-flow profile around the annulus and leads to better drilling-fluid removal and proper cement placement. Scratchers, or wall cleaners, are devices that attach to the casing to remove loose filter cake from the wellbore. They are most effective when used while the cement is being pumped. Like centralizers, scratchers help to distribute the cement around the casing. There are two general types of scratchers: those that are used when the casing is rotated, and those that are used when the casing is reciprocated.

Next, the cementing head is installed. A cementing head is designed to attach to the top joint of well casing. The head allows cementing plugs to be released ahead of and behind the cement slurry in order to isolate the cement slurry from wellbore fluids ahead of the cement and from displacing fluids pumped behind the slurry.

Once the casing is at the bottom, the hole is normally circulated to remove the gelled drilling fluid and make it mobile. This step is very important because the drilling fluid is more difficult to remove from the narrow annulus around the casing. Normally, circulation is broken slowly to prevent fracturing the well. The drilling fluid has been static in the well for several hours and may be severely gelled. Moving the pipe during hole conditioning

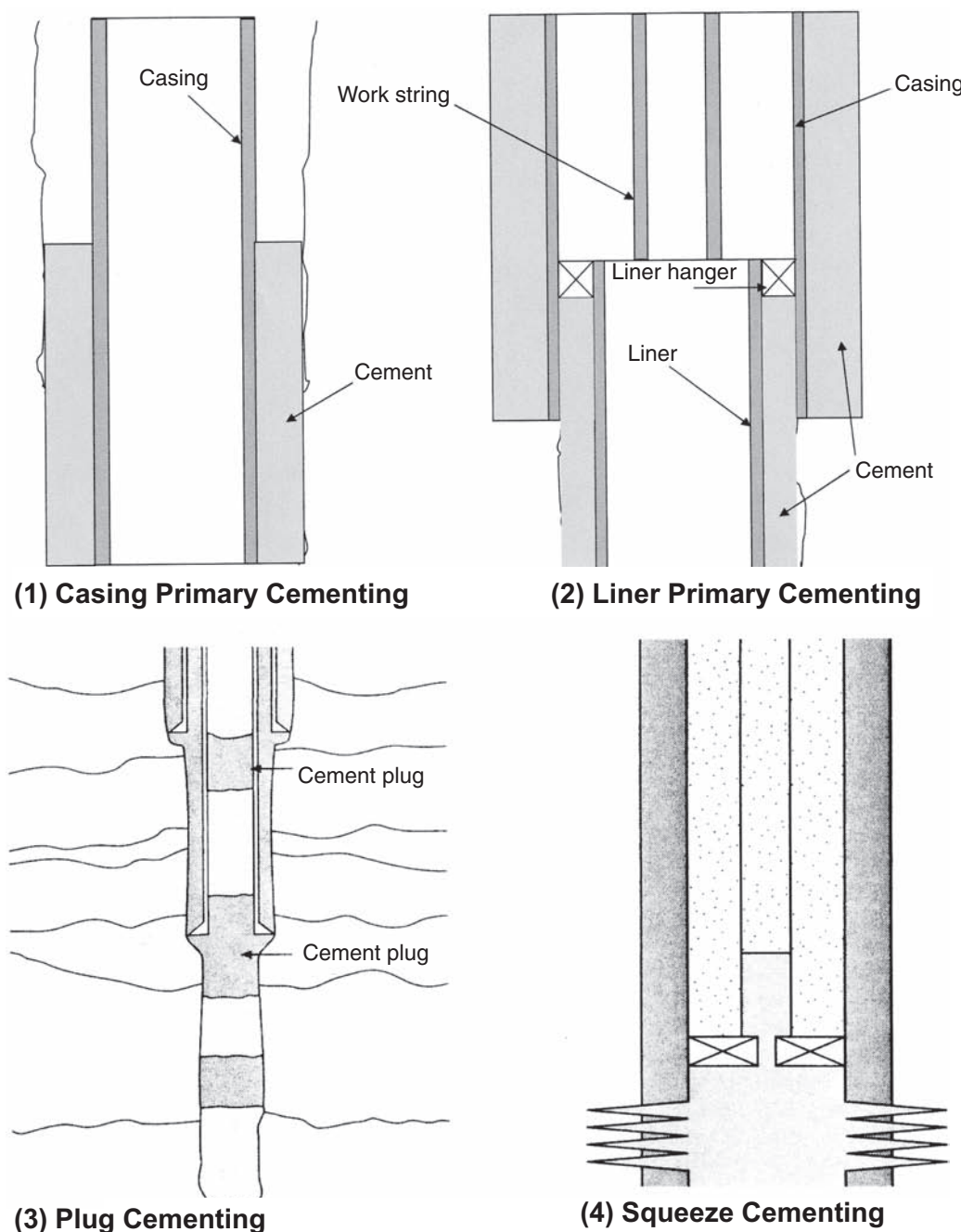


Fig. 4.4—Common cementing applications.

will improve the gelled-drilling-fluid removal. Rotating or reciprocating the pipe helps the flow go into the narrow side of the annulus. Pressure changes resulting from pipe movement must be considered so as not to change the well conditions. A preflush may now be used; preflushes are used to thin and disperse drilling-fluid particles, and they usually go into turbulent flow at low rates, helping to clean drilling fluid from the annulus. Some chemical flushes aggressively attack specific drilling fluids, breaking them down and further enhancing drilling-fluid removal.

Before the cement is pumped, a spacer may be pumped into the casing. A spacer is a volume of fluid injected ahead of the cement but behind the drilling fluid. It can also enhance the removal of gelled drilling fluid, allowing a better cement bond. Spacers can be designed to serve other needs; for example, weighted spacers can help with well control, and reactive spacers can provide increased benefits for removing drilling fluids. The drilling-fluid/spacer interface and the spacer/cement slurry interface must be compatible.

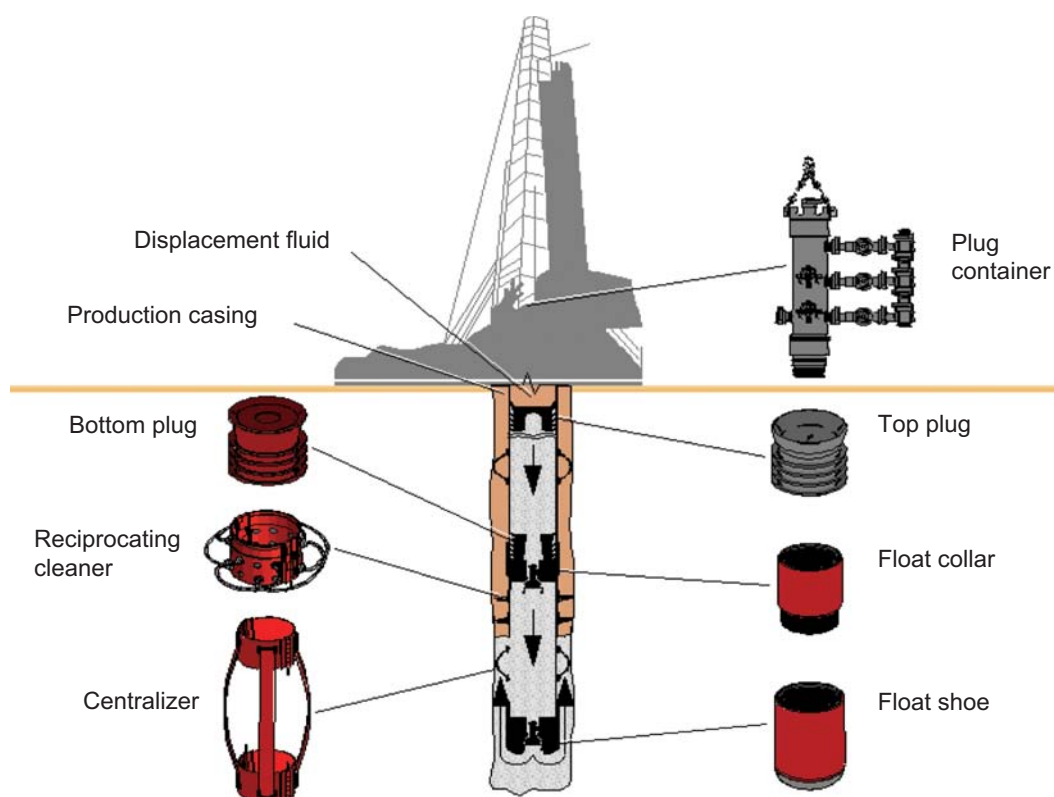


Fig. 4.5—Primary cementing. Courtesy of Halliburton.

Neat cement is introduced in a hopper, where it is thoroughly mixed with water by a high-velocity, recirculating cement mixer (RCM). The resulting slurry is then pumped down the casing between two plugs with wiping fins, which are placed in the system at the proper time by means of a cementing head. When the bottom plug reaches the float collar, it stops; pressure builds up, which quickly ruptures the plug's diaphragm and allows the slurry to continue.

The top plug, however, has a solid core, so that when it seats in the float collar, the surface pump pressure builds up sharply, thereby signaling the pump operator that the job is complete. The position of the top plug may also be checked either by metering the displacing fluid (because the casing volume is known), or by following the plug with a wire measuring line. The casing below the float collar is left full of cement, which can be drilled out if necessary. This latter procedure is commonly called "drilling the plug."

The float collar can act as a check valve to prevent cement from backing up into the casing. Top plugs that have pressure seals and latch in place can be used in addition to the float collar. Fluid movement also can be prevented by holding pressure on the top plug with the displacing fluid; however, it is not good practice to hold excessive pressure in the casing while the cement sets because when the pressure is released, the casing may change diameter sufficiently to break the bond with the cement and form a small annular channel.

Not all operators use a bottom plug when cementing. Indeed, there have been cases in which the solid plug mistakenly was placed below the cement slurry. Also, with some of the first plug designs, the float collar was stopped up by plug fragments before completing the cement displacement. When a bottom plug is not used, however, the cement does not wipe all the mud from the wall of the casing. This results in a contaminated zone being built up in front of the top plug, as shown in Fig. 4.6.

In addition to the conventional placement method for cementing casings, there are several modified techniques used in special situations. These include: (1) stage cementing, (2) inner-string cementing, (3) annular cementing through tubing, (4) multiple-string cementing, (5) reverse-circulation cementing, and (6) delayed-setting cementing.

4.5.2 Stage Cementing. Stage cementing is one of the procedures developed to permit using a cement column height in the annulus that normally would cause the fracture of one or more subsurface formations. It also can be used to reduce the potential for gas flow after cementing. The first stage of the cementing operation is conducted in the conventional manner. After the slurry hardens, a bomb is dropped (Fig. 4.7) to open a side port in a staging tool placed in the casing string. The second-stage cement then is pumped through this side port and into the annulus above the set first-stage cement. Equipment also is available for three-stage cementing.

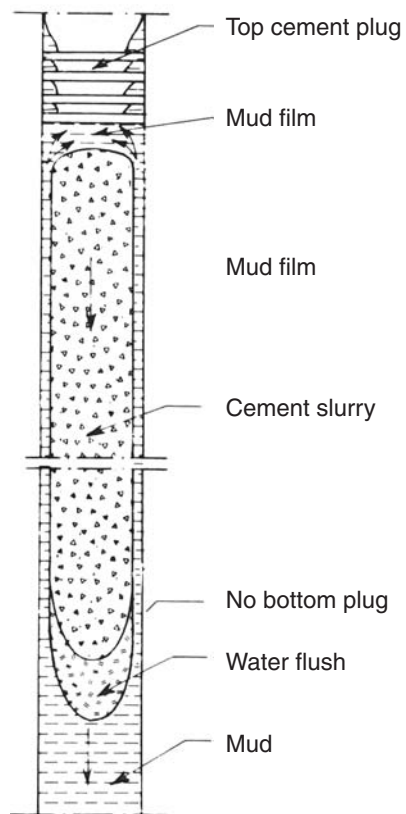


Fig. 4.6—Cement contamination without bottom plug (Bourgoyne et al. 1991).

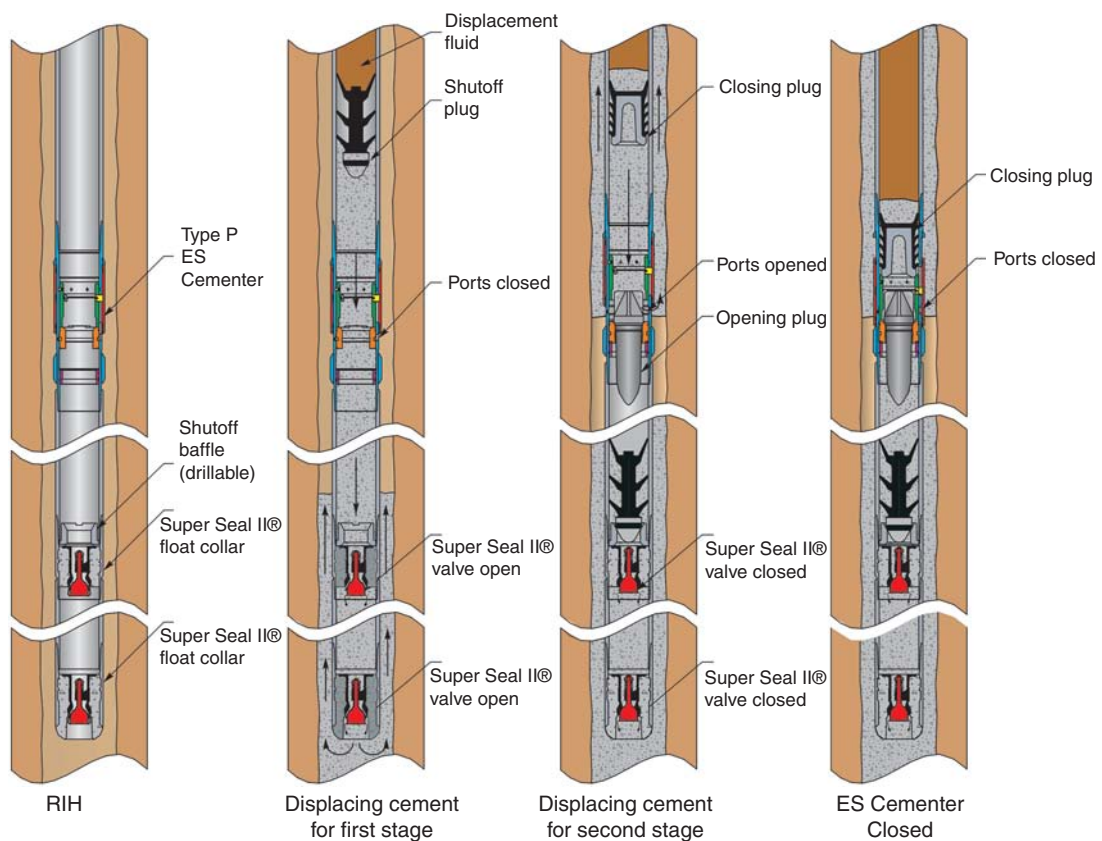


Fig. 4.7—Stage cementing. Courtesy of Halliburton.

4.5.3 Inner-String Cementing. Inner-string cementing was developed to reduce the cementing time and the amount of cement left in the shoe joint of large-diameter casing. The technique uses a float collar or shoe modified with sealing adapters, which permits tubing or drillpipe (work string) to be landed and hydraulically sealed. The cement then is displaced down the inner drillpipe or tubing string rather than the casing. When the float collar or shoe is equipped with a backpressure valve or latch-down plug, the inner string can be withdrawn immediately after displacing the cement.

4.5.4 Annular Cementing Through Tubing. This technique consists of pumping cement through tubing run in the annulus between two casing strings or between the casing and the open hole. It usually is used to bring the top of the previously placed cement to the surface or to repair casing.

4.5.5 Multiple-String Cementing. Multiple-string cementing is a multiple completion method that involves cementing several strings of tubing in the hole without the use of an outer casing string. This type of completion is an alternative to the more conventional multiple-completion method, in which the tubing strings are set using packers inside a larger-diameter casing.

4.5.6 Reverse-Circulation Cementing. Reverse-circulation cementing consists of pumping the slurry down the annulus and displacing the mud back through the casing. This method has been used in some instances in which extremely-low-strength formations were present near the bottom of the hole. A special float collar or shoe as well as a special wellhead assembly is required to use this method. Because wiper plugs cannot be used, it is difficult to detect the end of the cement displacement. The cement usually is overdisplaced at least 300 ft into the bottom of the casing to enhance the probability of a good cement job at the shoe.

4.5.7 Delayed-Setting Cementing. Delayed-setting cementing is used to obtain a more uniform mud displacement from the annulus than is possible with the conventional cement-placement technique. This method consists of placing retarded cement slurry having good filtration properties in the wellbore before running the casing. Cement placement is accomplished down the drillpipe (work string) and up the annulus. The drillpipe then is removed from the well, and casing is lowered into the unset cement slurry. This method also can be modified for multiple-string cementing, with cement displacement being made through the lower string.

4.5.8 Cementing Liners. A liner is a casing that does not extend to the top of the well but overlaps with the previous casing. The amount of overlap depends upon the purpose of the liner and can be in the range of 50 to 500 ft. The liners are classified as production liners (run from the last casing to the total depth), drilling or intermediate liners (run to isolate sloughing shale, lost circulation zones, etc.) and tieback liners that extend from the top of the existing liner uphole to another casing or the top of the hole. The conventional method of liner cementing is illustrated in Fig. 4.8. The liner is attached to the drillpipe using a special liner-setting tool. The liner-setting tool then is actuated so that the liner is attached mechanically to and supported by the casing without hydraulically sealing the passage between the liner and the casing. The cement is pumped down the drillpipe and separated from the displacing fluid by a latch-down plug. This latch-down plug actuates a special wiper plug in the liner-setting tool after the top of the cement column reaches the liner. When the wiper plug reaches the float collar, a pressure increase at the surface signifies the end of the cement displacement. The drillstring then must be released from the liner-setting tool and withdrawn before the cement hardens.

Usually, a volume of cement sufficient to extend past the top of the liner is displaced. When the drillstring is withdrawn, this cement collects at the top of the liner but generally does not fall to the bottom. This cement can be washed out using the drillpipe or drilled out after the cement sets. When cement is not displaced to the top of the liner, cement must be forced into this area using a squeeze-cementing method, which is discussed later in Section 4.5.10.

A large variety of liner-setting tools is available; most of these tools are set with either a mechanical or hydraulic devices. The hydraulically set devices are actuated by drillpipe rotation or by dropping a ball or plug and then set by applying pump pressure. The mechanically set devices are actuated by drillpipe rotation and set by lowering the drillpipe. A liner-setting tool must be selected on the basis of the liner weight, annular dimensions, cement-displacement rate, and liner-cementing procedure. There is a trend toward not setting the liner until after cement displacement; this allows the liner to be moved while cementing to improve mud removal in the annulus. This practice imposes some limitations on the selection of conventional liner-setting tools; however, expandable liner hangers can be moved easily while cementing and can lower cement placement pressures by having a larger cross-sectional flow area in the liner lap. Expandable liners are also available, and their use is increasing for several reasons. First, they can be run as drilling liners without losing the planned hole diameter vs. depth. Second, they

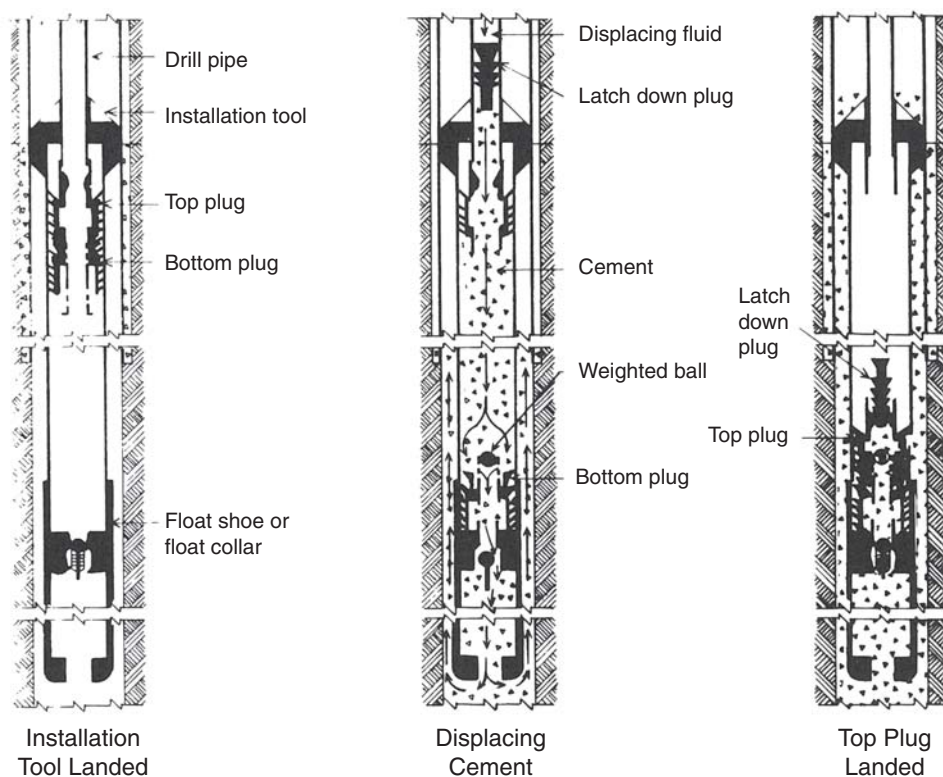


Fig. 4.8—Conventional placement techniques for cementing a liner (Bourgoyne et al. 1991).

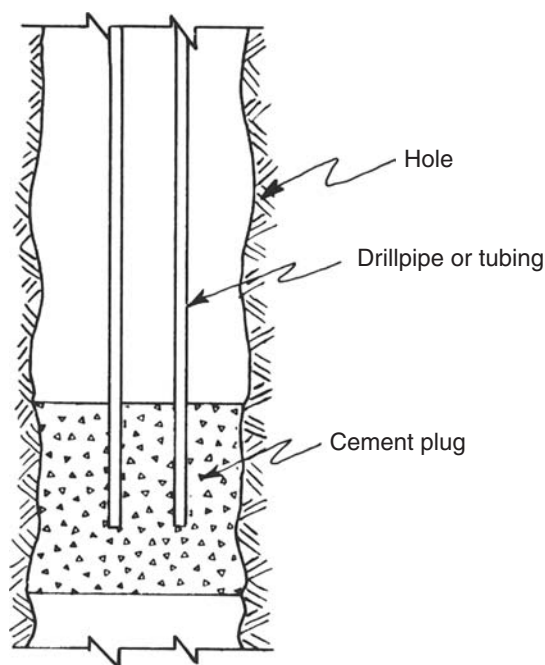


Fig. 4.9—Placement technique used for setting cement plug (Bourgoyne et al. 1991).

have larger cross-sectional flow areas to lower circulating and pumping pressures. Third, their smaller diameter helps running the pipe into the hole under difficult hole conditions without getting stuck. The cementing of expandable liners requires special procedures and cement compositions.

After drilling the well, it may be desirable to extend the liner back to the surface if a commercial hydrocarbon deposit is found and the well is to be completed. As mentioned earlier, this type of casing is called a *tieback liner*. If casing is used to extend the liner up the hole, but not all the way to the surface, it is called a *stub liner*. Stub liners

are used primarily to repair the top of a leaking liner. The reader is encouraged to search the Internet to find some useful animations illustrating running liners developed by various service companies for marketing purposes.

4.5.9 Plug Cementing. Displacement efficiency, slurry stability, fluid compatibilities, and all the issues that are normally considered for a primary cement job must be carefully considered for a cement plug job. Plugging operations are difficult because the work string that is located at a certain depth to place a heavier-density balanced cement plug must be pulled up and removed from its position to a safe distance above the cement plug without causing damage to the cement, either by swabbing the lower lighter-density wellbore fluid into the cement or by stringing out the cement into the wellbore fluid above the cement.

Cement plugs can be set in open hole or in casing. Plugs are set to prevent fluid communication between an abandoned lower portion of the well and the upper part of the well. Plugs also are set to provide a seat for directional drilling tools used to sidetrack the well.

Cement plugs are placed using drillpipe or tubing, as shown in **Fig. 4.9**. When a plug is placed off-bottom in an open hole, a caliper log can be used to locate an in-gauge portion of the hole. Centralizers and scratchers can be placed on the bottom section of the pipe that will be opposite the section of hole to be plugged. Cement is pumped down the drillpipe or tubing and into the hole. The cement slurry has a natural tendency to form a bridge below the tubing, causing the slurry to move up the annular space opposite the drillpipe or tubing. When cementing in casing, a bridge plug (**Fig. 4.10**) sometimes is placed below the cement plug to assist in forming a good hydraulic seal. A new type of bridge plug constructed entirely with “composite” nonmetallic materials is easily drilled out of the wellbore. Like the metal ones, composite bridge plugs are designed to provide zonal isolation of the wellbore.

When the drillpipe or tubing is open-ended, cement displacement is continued until the fluid columns are *balanced* (i.e., they have the same height of slurry inside the pipe and annulus). As shown in **Fig. 4.11**, the pump pressure during the displacement provides a good indication of when the fluid columns are balanced. The drillstring or tubing then is pulled slowly from the cement slurry.

An improved plug placement technique has been described by Doherty (1933) and Goins (1959) as an alternative to the balanced-column method. Mud contamination is minimized by placing a slug of water in front of and behind the cement slurry. The cement is displaced almost completely from the drillpipe or tubing. To prevent backflow while the pipe is being pulled, a special backpressure valve or plug catcher can be used at the bottom of the pipe string. Cement plugs also can be set using a wireline device called a *dump bailer*. After setting a bridge plug at the desired depth, the dump bailer is filled with cement and lowered into the well on a wireline. The dump bailer is designed to empty the slurry into the hole when the bailer reaches the bottom. After the first batch of cement takes an initial set, a second batch can be placed. The dump bailer seldom is used during drilling because of the time required to set a long plug.

4.5.10 Squeeze Cementing. Squeeze cementing requires as much technical, engineering, and operational experience as primary cementing but is often done when wellbore conditions are unknown or out of control, and when wasted rig time and escalating costs force poor decisions and high risk. Before using a squeeze application, a series of decisions must be made to determine (1) if a problem exists, (2) the magnitude of the problem, (3) if squeeze cementing will correct it, (4) if economics will support it, and (5) the risk factors that are present.

Squeeze cementing consists of forcing a cement slurry into an area of the well or formation by means of applied hydraulic pressure. The purpose of squeeze cementing is to form a hydraulic seal between the wellbore and the zone squeezed. If the slurry is placed using sufficient pressure to fracture the formation, the process is called a *high-pressure squeeze*. The pressure required to fracture the formation and allow rapid slurry placement is called the *breakdown pressure*. In the high-pressure squeeze, whole cement slurry is forced into the fractured formation. If the slurry is placed using less than the breakdown pressure, the process is called a *low-pressure squeeze*. The low-pressure squeeze causes a cement cake to plate out against the formation as filtrate is lost to the formation. Common applications of squeeze cementing include plugging abandoned casing perforations, plugging severe lost-circulation zones, improving shoe test results in weak or fractured formations, and repairing annular leaks in previously cemented casing (caused by failure of either the casing or the previously placed cement).

The conventional method for squeeze cementing is shown in **Fig. 4.12**. A squeeze packer and a circulating valve (**Fig. 4.13**) are placed above the perforations and lowered into the well on drillpipe or tubing. A slug of water or preflush is placed opposite the zone to be squeezed, and then the squeeze packer is set just above the zone of interest. The circulating valve is opened above the packer, and the cement slurry is displaced down the drillpipe. A slug of water is used before and after the cement slurry to prevent mud contamination of the slurry and mud plugging of the zone of interest. The circulating valve usually is closed after most of the leading water slug has been pumped into the annulus. The cement then is pumped into the zone of interest until the final desired squeeze pressure is obtained. With the low-pressure squeeze, it is common practice to stop pumping



Fig. 4.10—Bridge plug. Courtesy of Halliburton.

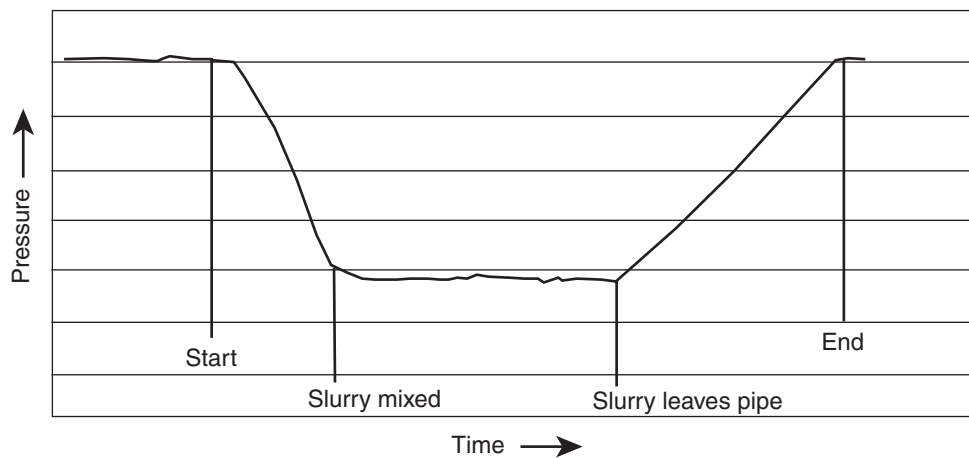


Fig. 4.11—Idealized pressure/time chart for balanced pressure plug (Bourgoyne et al. 1991).

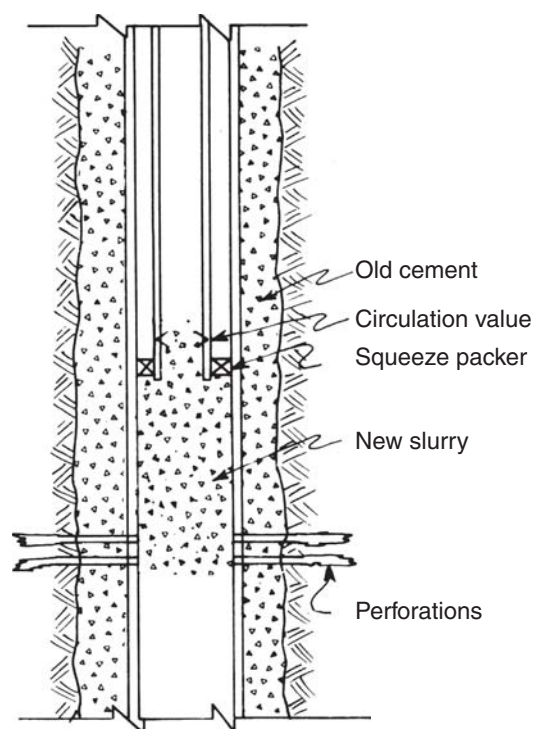


Fig. 4.12—Squeeze cementing technique (Bourgoyne et al. 1991).

periodically, or hesitate, during the squeeze process. This assists in the buildup of filter-cake nodes against the formation or perforations. The circulating valve then is opened, and the excess cement is pumped up the drill-pipe to the surface. This process is called *reversing out*. If the desired squeeze pressure is not obtained, the operation is repeated after waiting for the first batch of cement to take an initial set.

In addition to the conventional squeeze-cementing method, several modified techniques have been developed. In certain instances, it may be necessary to isolate the section below the perforation by placing a bridge plug below the perforations. In other cases, neither a squeeze packer nor a bridge plug is used, and pressure is held against the well by closing the blowout preventers (BOPs). This method is called the *bradenhead squeeze*. A *block squeeze* consists of isolating a production zone by perforating above and below the producing interval and squeezing through both perforated intervals in separate steps.

4.5.11 Cement Volume Requirements. In addition to selecting the cement composition and placement technique, the drilling engineer must determine the volume of cement slurry needed for the job. The volume required usually is based on past experience and regulatory requirements in the area. As little as 300 ft of fill-up has been used behind relatively deep casing strings; however, in some cases, the entire annulus is cemented. It usually is necessary to include considerably more slurry than is indicated by the theoretical hole size because of hole enlargement while drilling. Thus, an excess factor, based on prior experience in the area, usually is applied to the theoretical cement volume. When hole size or caliper logs are available, a more accurate slurry volume can be determined. Example 4.5 illustrates one method of estimating slurry volume requirements for a conventional casing cementing operation.

Example 4.5 Casing having an outside diameter (OD) of 13 $\frac{3}{8}$ in. and an inside diameter (ID) of 12.415 in. is to be cemented at a depth of 2,500 ft. A 40-ft shoe joint will be used between the float collar and the guide shoe. It is desired to place a 500-ft column of high-strength slurry at the bottom of the casing. The high strength slurry is composed of Class A cement mixed using 2% calcium chloride and a water/cement ratio of 5.2 gal/sack. The upper 2,000 ft of the annulus is to be filled with a low-density slurry of Class A cement mixed with 16% bentonite and a 5% sodium chloride and a water/cement ratio of 13 gal/sack. This high water-to-cement ratio slurry should not be used to cement hole sections with potential flow zones or when unknown flow zones may be present. The hole size is 17 in.

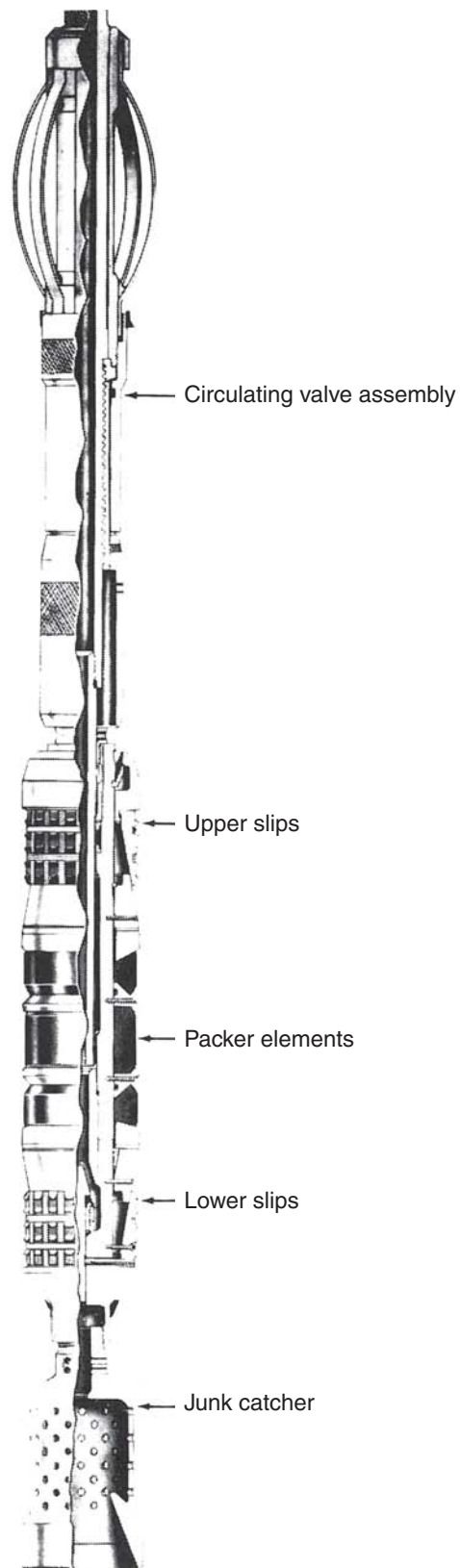


Fig. 4.13—Squeeze packer assembly (Bourgoyne et al. 1991). Image courtesy of Halliburton.

Compute the slurry volume and number of sacks required if the excess factor in the annulus is 1.75.

Solution. Specific gravity of Class A cement is 3.14.

Specific gravity of bentonite is 2.65.

Specific gravity of CaCl_2 is 1.96.

Specific gravity of NaCl is 2.16.

Part I yield of high-strength cement slurry:

$$V_c + V_w + V_{\text{CaCl}_2}$$

Amount of calcium chloride per cement sack:

$$(0.02)(94) = 1.88 \text{ lbm/sack}$$

Volume of calcium chloride:

$$\frac{1.88}{(1.96)(8.34)} = 0.115 \text{ gal/sack}$$

Volume of cement (one sack):

$$\frac{94}{(3.14)(8.34)} = 3.589 \text{ gal/sack}$$

Yield of cement slurry:

$$3.589 + 5.2 + 0.115 = 8.9 \text{ gal/sack} = \frac{8.9}{7.485} = 1.189 \text{ ft}^3/\text{sack}$$

Volume of a 500-ft annular column and a 40-ft column in the casing joint is given by:

$$\frac{\pi}{4}(17^2 - 13.375^2)(500)(12)\frac{1}{1728}(1.75) + \frac{\pi}{4}(12.415^2)(40)(12)\frac{1}{1728} = 559 \text{ ft}^3$$

Slurry volume will require mixing:

$$\frac{559}{1.189} = 470 \text{ sacks of cement}$$

Part II yield of low-density cement slurry:

$$V_c + V_w + V_b + V_{\text{NaCl}}$$

Amount of bentonite per sack of cement:

$$(0.16) 94 = 15.04 \text{ lbm}$$

Volume of bentonite:

$$\frac{15.04}{(2.65)(8.34)} = 0.6805 \text{ gal}$$

Amount of sodium chloride:

$$(0.05)(94) = 4.7 \text{ lbm}$$

Volume of sodium chloride:

$$\frac{4.7}{(2.16)(8.34)} = 0.26 \text{ gal}$$

Yield of cement slurry:

$$3.589 + 13 + 0.6805 + 0.26 = 17.53 \text{ gal} = 2.342 \text{ ft}^3/\text{sack}$$

Volume of 2,000 ft in annulus:

$$\frac{\pi}{4}(17^2 - 13.375^2)(2,000)(12)\frac{1.75}{1728} = 2,100 \text{ ft}^3$$

Slurry volume will require mixing:

$$\frac{2,100}{2.342} = 897 \text{ sacks of cement}$$

$$\text{Total slurry volume} = 2,100 + 559 = 2,659 \text{ ft}^3$$

$$\text{Total number of cement sacks} = 470 + 897 = 1,367 \text{ sacks}$$

4.5.12 Cementing Time Requirements. As discussed previously, the time required to place the cement slurry is one of the more important variables in the engineering design of the slurry properties. The relationships between well depth and cementing time used by API in the specifications for the various cement classes represent average well conditions and may not be applicable in all cases. A more accurate estimation of cementing time can be made on the basis of the actual slurry volume and pumping rates to be used. Also, it is always prudent to allow some extra cementing time for unforeseen operational problems. Example 4.6 illustrates one method of estimating cementing time requirements for a conventional casing cementing operation.

Example 4.6 Estimate the cementing time for the cementing operation if one cementing truck having a mixing capacity of approximately 25 ft³/min is used. The rig pump will be operated at 60 strokes/min and has a pump factor of 0.9674 ft³/stroke.

Solution. Cementing time = mixing time + time required to displace the top plug from the surface to the float collar.

Mixing time (time of placement of cement slurry):

$$= \frac{2,659}{25} = 106 \text{ minutes}$$

Time required to place the drilling fluid:

$$\frac{\text{Volume of mud}}{\text{Mud pump output}} = \frac{\pi}{4}(12.415)^2(2,500 - 40)\left(\frac{12}{1728}\right)\frac{1}{(60)(0.9674)} = 36 \text{ minutes}$$

Total cementing time is:

$$106 + 36 = 142 \text{ minutes}$$

4.5.13 Waiting-on-Cement (WOC) Times. Part of this section is a summary of the recommended WOC practices published in *API RP 65-Part 2*, “Isolating Potential Flow Zones During Well Construction” (2010).

WOC Time Before Nipping Down. Operations to nipple down (i.e., remove) the diverter or BOP stack should wait until the cement is set (50 psi compressive strength) to avoid having an influx of formation fluids that may cause a blowout. Determination of this cement WOC time should take into account several factors, including whether a hydrocarbon zone is exposed in the wellbore or whether there is the possibility that an

unknown zone is exposed. There may be other downhole conditions or cement job results that could modify this guideline. Any plan for nipping down the BOP stack should use a conservative approach to avoid loss of well control or danger to personnel or equipment. Some factors to consider a modified plan to nipple down, such as a longer-than-planned WOC time, include:

- Complete loss of returns while pumping cement
- Delays in getting cement in place, such as pump interruptions that could lead to poor mud removal and poor cement consistency
- Premature returns of cement to surface
- High gas units in the drilling mud prior to cementing

In these cases, the confidence in the cement job would decrease, and waiting on cement for a longer time before nipping down would be prudent, along with other measures discussed below.

Special Considerations. Special considerations exist when determining and applying WOC times:

- Complete a risk assessment and communicate the results to all parties involved.
- Do not run tubing in the annulus between the casing and the diverter, or BOP, prior to completion of cementing operations, and wait until after the cement WOC time has elapsed or until the well has no potential for flow.
- Verify that hydrostatic pressure calculations are performed to ensure sufficient hydrostatic pressure to overbalance all zones in the well prior to washing out the annulus to the mudline suspension hanger (MLSH).

WOC Times for Other Drilling Operations. Operations on the well following cementing should be done so that they will not disturb the cement and damage the seal or cause the cement to set improperly. Any pipe movement to complete hanging the casing and activating seals should be finished before significant gel strength has developed. If done after the cement has developed significant gel strength, such pipe movement may cause a microannulus. There is also a danger of initiating flow if the pipe movement swabs the well in. If the casing is to be hung after cement strength is developed, as when intentionally increasing or decreasing the landed tension in the casing, consideration should be given to the imposed forces on the cement and the cement strength.

Preferably, pressure testing casing should be done before significant gel strength has developed; however, such pressure testing will be limited by the pressure ratings of plugs, floats, cementing heads, and other equipment. Pressure testing can be done after the cement has set, but this can result in microannulus formation or damage to the cement sheath. The pressure should be held on the casing for the shortest length of time required to accomplish the test. The effect of pressure testing will depend on the properties of the cement, the pressure at which the casing is tested (and, consequently, the amount of enlargement of the casing), and the properties of the formation around the cement. Mechanical stress modeling can assist in determining the best time to conduct the pressure tests.

Normally, a minimum compressive strength of 500 psi is recommended before drilling out the shoe of the cemented casing.

The development of strength is also a primary consideration in continued operations such as drillout. Early work has shown that 8 psi tensile strength, or approximately 100 psi compressive strength (compressive strength is approximately 8 to 12 times the tensile strength for most cements), is adequate to support the casing. WOC time before drillout is normally the time that laboratory testing has shown it takes the cement around the casing shoe to develop 500 psi compressive strength. In the past, there has been a practice to maximize compressive strength. This may seem appropriate, with a “more is better” idea for the short term; however, later in the life of the well, load conditions may occur in which high strength may be contrary to good cement sealing and support integrity. High-strength cements are often brittle and lack the ductility needed for sustained well integrity.

WOC Times for Cement Evaluation Logging (excerpt from *API Technical Report 10TR1 2008*). “Historically, many of the guidelines for cement evaluation log interpretation have been based on cement compressive strength. Acoustic impedance, as outlined earlier [in the report], is a better property to use. However, it is important to allow the cement to hydrate sufficiently before running an evaluation log. Generally, at least 48 hours should elapse after the cement is in place prior to running a cement evaluation log.”

4.5.14 Cementing Evaluation. After cementing operations are complete and the cement left in the wellbore, along with portions of the subsurface cementing equipment, has been drilled out, the cement job usually is evaluated to ensure that the cementing objectives have been accomplished. When possible, it is always good practice to positive- and negative-pressure-test cemented casing to the maximum pressure anticipated in

subsequent drilling operations. When pressure testing is not possible, other methods should be used to confirm that the cement has been properly placed in the annulus up to the planned top of cement (TOC). For example, the TOC can be located by making a temperature survey of the well from 6 to 10 hours after completing the cement displacement. When cement is present behind the pipe, heat liberated due to the exothermic hydration reaction will cause an increase in temperature. A noise log can be run to monitor for any formation-fluid influxes. In addition, ultrasonic and acoustic logging tools are available for evaluating the bond between the cement and the pipe and any bypassed mud in the annulus that could allow formation fluids to leak. When the cement is not bonded acoustically to both the pipe and the formation, a strong early sound reflection will be received by the acoustic logging device, indicating sound travel primarily through the casing (**Fig. 4.14**). A comprehensive description of cement evaluation logging technology and best practices can be found in *API Technical Report 10TR1* (2008).

4.6 Well Parameters Affecting Cement Design and Operations

For proper cementing design, it is critical to consider the wellbore conditions such as temperature, pressure, wellbore configuration, well fluid, and formation properties when designing a cement job.

4.6.1 Depth. The depth of the well influences the amount of wellbore fluids involved, the properties of wellbore fluids, the pressures, the temperature, and, thus, the cement slurry design. Wellbore depth is also an influential factor in the selection of hole and casing sizes, in addition to planned well operations parameters such as production or injection rates. Extremely deep wells have their own distinct design challenges because of high temperatures, high pressures, and corrosive formation fluids.

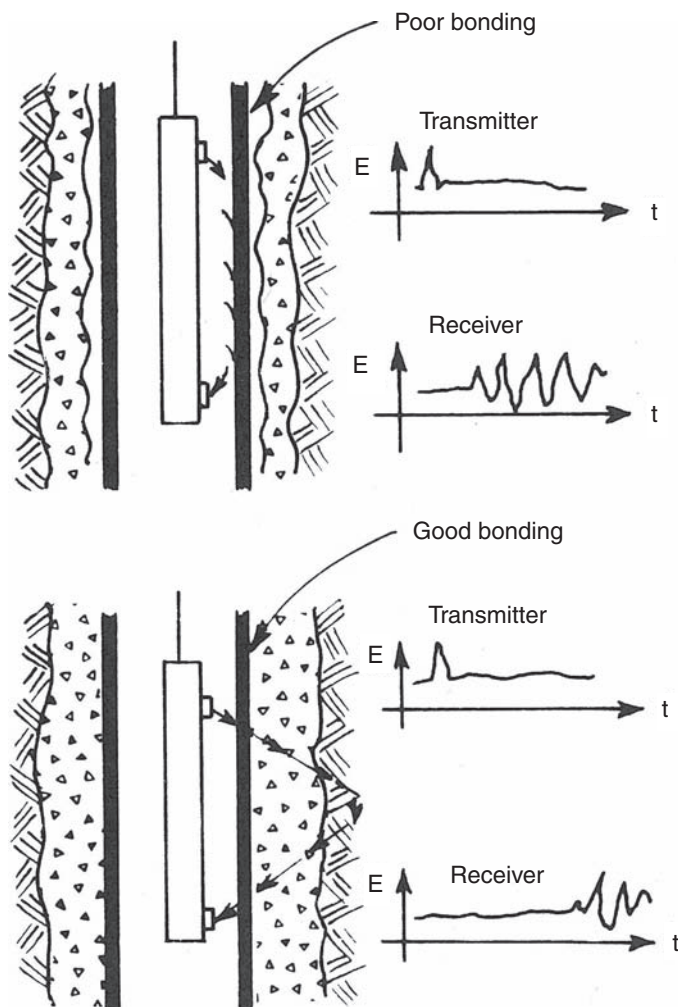


Fig. 4.14—Acoustic energy travel in cased wells (Bourgoyne et al. 1991).

4.6.2 Wellbore Geometry and Drilling-Fluid Removal. The geometry of the wellbore is important in determining the amount of cement required for the cementing operation. The drilled hole's dimensions can be measured using a variety of methods, including acoustic calipers, electric-log calipers, and fluid calipers.

The drilled hole's shape also determines the clearance between the casing and the wellbore, and this annular space influences the drilling-fluid displacement by the cement slurry. A minimum annular space of 1 to 1.5 in. is recommended. Annular clearances that are smaller restrict the flow characteristics and generally make it more difficult for the cement slurry to displace drilling fluids.

Another aspect of borehole geometry is the hole inclination angle. The inclination angle influences the true vertical depth and temperatures. Highly deviated wellbores can be challenging because the casing is not as likely to be centered in the wellbore, and drilling-fluid displacement becomes difficult. In highly inclined wells, it is also difficult to run casing because of high drag forces (see Chapter 8, Section 8.5 for details).

Drilling fluids or muds can become partially dehydrated or gelled when the well is not circulated. Pipe movement (rotation and/or reciprocation) while circulating the well prior to cementing and during cement slurry placement in the annulus can help improve drilling-fluid removal and displacement by the cement slurry.

4.6.3 Temperature. The temperatures of the wellbore are critical in the design of a cement job. There are basically three different temperatures to consider: the bottomhole circulating temperature (BHCT), the bottomhole static temperature (BHST), and the temperature differential, which is the temperature difference between the top and bottom of cement placement.

The BHCT is the temperature at which the cement will be exposed as it circulates past the bottom of the casing. The BHCT controls the time that it takes for the cement to set up. The BHST is the temperature when no fluids are circulating and cooling the wellbore. The BHST plays a vital role in the strength development of the cured cement. The temperature differential becomes a significant factor when the cement is placed over a large depth interval with significant temperature differences between the top and bottom cement locations. Commonly, with a large temperature differential, two different cement slurries may be required to better accommodate the difference in temperatures.

The BHCT can be measured by using temperature probes that are circulated with the drilling fluid. If the actual wellbore temperature cannot be determined, the BHCT can be estimated using the temperature schedules of *API RP 10B-2* (2005) or calculated using analytical or numerical thermal simulations. *API TR 10TR3* (1999), "Temperatures for API Cement Operating Thickening Time Tests" also has relevant information from studies by the API Task Group on Cementing Temperature Schedules. This report's information significantly improved the temperatures in the well-simulation test schedules found in relevant API and ISO standards and offers the largest set of temperature data available to the industry to date. Chapter 10 of Aadnøy et al. (2009) provides the desired theoretical background on the temperature calculations in wells. Knowing the actual temperature that the cement will encounter during placement allows operators to optimize the slurry design.

4.6.4 Formation Pressures. During the planning stages of a cement job, information about the formations' pore pressure, fracture pressure, hole-collapse pressure, lithology, permeability, and other characteristics must be known (see Chapter 2). Generally, these factors will be determined during drilling. The density of the drilling fluids can be a good indication of the equivalent circulating density (ECD) and hydrostatic pressure limitations of the wellbore ($\text{ECD} = \text{wellbore circulating fluid pressure} / \text{true vertical depth}$, expressed as a density such as lbm/gal). The ECD at key depths must be calculated for all fluids, including the drilling fluid, cement spacer, and cement slurries. Wellbore pressure without circulation is called equivalent static density (ESD).

To maintain the integrity of the wellbore, the ECD must not exceed the fracture gradient of the weakest formation in the uncased part of the hole. If the formation breaks down, lost circulation will result. Fluid loss must be controlled for successful primary cementing. The ECD and ESD must not be below the hole-collapse pressure of the weakest formation in the hole. If the ECD or ESD is below the hole-collapse pressure, the hole can cave in, block fluid circulation, and trap the pipe in the hole. Pressures in the wellbore also affect the strength development of the cement.

4.6.5 Formation Chemical Characteristics. The composition (lithology) of formations can present compatibility problems with drilling and cementing fluids. Shale formations are sensitive to fresh water and can slough off or swell if special precautions, such as increasing the salinity of the water, are not taken. Some formations may also contain flowing fluids, high-pressure fluids, and corrosive gases or other complex features that require special attention. Geochemical models are available to predict corrosive conditions by the changes in pH over the life of the well and beyond (for many hundreds of years after well abandonment).

4.6.6 Formation Permeability. When the permeability of formations is high, excessive fluid-filtrate loss and filter-cake buildup (deposits of particle solids carried by the fluids) may occur that can cause poor cementing results. Effects of high permeability include reduced annular cross-sectional-flow areas, inability to remove drill cuttings, partially dehydrated and highly gelled drilling fluids, poor mud conditioning and displacement, inadequate cement placement, lack of zonal isolation, casing damage, and well-control issues. For instance, Parr et al. (2009) reported that a high-permeability (1-darcy) zone caused excessive cement-displacement pressures that prematurely ended the cementing operation, with the top of cement lower than planned and cement left inside the liner. The key problem was a filter-cake-induced hole-diameter decrease that formed an annular-flow restriction across the high-permeability interval. The remaining wells were all successfully cemented by improved mud conditioning to better control filtrate loss and mudcake thickness, as well as lowering of the cement's fluid loss to inhibit excessive cement filter-cake buildup.

Problems

- 4.1 List four steps in the manufacture of Portland cement. What is the approximate weight and bulk volume of Portland cement for 1 bbl and in one sack?
- 4.2 List the equipment needed to perform the standard API tests for drilling cements.
- 4.3 Define the following: minimum water content, normal water content, free water content, and maximum water content.
- 4.4 The torque required to hold the paddle assembly stationary in a cement consistometer rotating at 150 rev/min is 800 g-cm. What is the slurry consistency? *Answer: 36 B_c.*
- 4.5 A Class H cement core sample having a length of 2.54 cm and a diameter of 2.865 cm allows a water flow rate of 0.05 mL/s when placed under a pressure differential of 20 psi. Compute the permeability of the cement. *Answer: 14.5 md.*
- 4.6 The cement tensile strength required to support the weight of a string of casing is estimated to be 8 psi. If the cement is known to have a compressive strength of 200 psi, do you think the casing could be supported by the cement? Why? *Answer: Yes; tensile strength is 17 psi.*
- 4.7 List the eight standard classes and three standard types of API cement. Compare these classes and types with the ASTM cement types used in the construction industry.
- 4.8 How is the composition of a high-sulfate-resistant cement different from a standard Portland cement?
- 4.9 List the normal (API) water content of each class of cement used in slurry preparation. *Answer: 5.19 gal/sack for Classes A and B, 6.32 gal/sack for Class C, 4.29 gal/sack for Classes D through H, and 4.97 gal/sack for Class G.*
- 4.10 Compute the yield and density of each class of cement when mixed with the normal amount of water as defined by API. *Answer: 1.17 ft³/sack and 15.6 lbm/gal for Classes A and B.*
- 4.11 It is desired to reduce the density of a Class A cement to 12.8 lbm/gal by adding bentonite. Using the water requirements for Class A cement and bentonite given in Table 4.5, compute the weight of bentonite that should be blended with each sack of cement. Compute the yield of the slurry. What is the "percent mix" of the slurry? *Answer: 9.3 lbm/sack, 2.09 ft³/sack, 102.9%.*
- 4.12 Repeat Exercise 4.11 using diatomaceous earth instead of bentonite as the low-specific-gravity solid and a water requirement of 3.3 gal/10% diatomaceous earth. *Answer: 11.5 lbm/sack, 1.75 ft³/sack, 84.2%.*
- 4.13 Identify the following cement additives: gilsonite, expanded perlite, and pozzolan.
- 4.14 It is desired to increase the density of a Class H cement to 17.5 lbm/gal using barite. Compute the weight of barite that should be blended with each sack of cement. Use the water requirements for Class H cement (maximum strength) and barite given in Table 4.5. Compute the yield of the slurry. What is the "percent mix" of the slurry? *Answer: 29.4 lbm/sack, 1.26 ft³/sack, 44.3%.*
- 4.15 Repeat Problem 4.14 using sand instead of barite. *Answer: 40.6 lbm/sack, 1.30 ft³/sack, 38.2%.*
- 4.16 List two common cement accelerators.
- 4.17 List two common cement retarders.
- 4.18 List the three types of lost-circulation additives used in cement, and give one example of each type.
- 4.19 List four common filtration-control additives.
- 4.20 Describe in your own words the conventional cement placement techniques used for cementing a casing string, cementing a liner string, setting a cement plug, and squeeze cementing.
- 4.21 What is the purpose of a shoe joint? Why is a shoe joint especially important in a deep cementing job or when no bottom wiper plug is used?

- 4.22 Casing having an OD of 9.625 in. and an ID of 8.535 in. is to be cemented at a depth of 13,300 ft in a 12.25-in. borehole. A 40-ft shoe joint will be used between the float collar and the guide shoe. It is desired to place 2,500 ft of cement in the annulus. Each sack of Class H cement will be mixed with 4.3 gal of water, to which is added 18% salt (by weight of water). A small quantity of dispersant will be blended with the cement, but this additive has no significant effect on the slurry yield or density. Compute the density of the slurry, the yield of the slurry, the number of sacks of cement required, and the cementing time. Assume that cement can be mixed at a rate of 20 sacks/min and displaced at a rate of 9 bbl/min, and use an excess factor of 1.5. The salt will be added to the water phase and, thus, does not blend with the dry cement. *Answer: 16.7 lbm/gal, 1.09 ft³/sack, 1,092 sacks, 159 minutes.*
- 4.23 A 7.0-in. liner having an ID of 6.276 in. is to be cemented at a depth of 15,300 ft in an 8.5-in. hole. Casing is set at 13,300 ft as described in Problem 4.22, and a 300-ft overlap between the casing and liner is desired. A 40-ft shoe joint will be used between the float collar and the guide shoe. It is desired to use 1,000 ft of preflush (in annulus) and then fill the total annular space opposite the liner with cement. Class H cement containing 35% silica flour will be mixed with 5.8 gal of water containing 18% salt (by weight of water). Compute the slurry density, the slurry yield, the volume of cement slurry required if the caliper log shows an average washout of a 2.0-in. increase in hole diameter, and the number of sacks of Class H cement needed. *Answer: 16.3 lbm/gal, 1.61 ft³/sack, 445 sacks.*
- 4.24 Define mixing and displacement time.
- 4.25 Describe in your own words how to evaluate quality of a cement behind casing.
- 4.26 List major parameters that need to consider while designing a cement job.

References

- Aadnoy, B.S., Cooper, I., Miska, S., Mitchell, R.F., and Payne, M.L. eds. 2009. *Advanced Drilling and Well Technology*. Richardson, Texas: SPE.
- API RP 65-Part 1, *Cementing Shallow Water Flow Zones in Deep Water Wells*, first edition. 2002. Washington DC: API.
- API RP 65-Part 2, *Isolating Potential Flow Zones During Well Construction*, first edition. 2010. Washington DC: API.
- API RP 10B-2/ISO 10426-2, *Recommended Practice for Testing Well Cements*, first edition. 2005. Washington DC: API.
- API RP 10B-3/ISO 10426-3, *Recommended Practice on Testing of Deepwater Well Cement Formulations*, first edition. 2004. Washington DC: API.
- API RP 10B-4/ISO 10426-4, *Recommended Practice on Preparation and Testing of Foamed Cement Slurries at Atmospheric Pressure*, first edition. 2004. Washington DC: API.
- API RP 10B-5/ISO 10426-5, *Recommended Practice on Determination of Shrinkage and Expansion of Well Cement Formulations at Atmospheric Pressure*, first edition. 2005. Washington DC: API.
- API RP 13B-1/ISO 10414-1, *Recommended Practice for Field Testing Water-Based Drilling Fluids, Part 1: Water-based Fluids*, third edition. 2003. Washington DC: API.
- API Spec. 10A/ISO 10426-1, *Specification for Cements and Materials for Well Cementing*, 23rd edition, 3–5 and Table 2. 2002. Washington DC: API.
- API TR 10TR1, *Cement Sheath Evaluation*, second edition. 2008. Washington DC: API.
- API TR 10TR2, *Shrinkage and Expansion in Oilwell Cements*, first edition. 1997. Washington DC: API.
- API TR 10TR3, *Temperatures for API Cement Operating Thickening Time Tests*, first edition. 1999. Washington DC: API.
- ASTM Standards on Cement Manual of Cement Testing, Part 13. 1975. Philadelphia, Pennsylvania: ASTM.
- Carey, J.W. et al. 2006. Analysis and Performance of Oil Well Cement with 30 Years of CO₂ Exposure from the SACROC Unit, West Texas, USA. *International J. of Greenhouse Gas Control* 1 (1): 75–85. DOI: [10.1016/S1750-5836\(06\)00004-1](https://doi.org/10.1016/S1750-5836(06)00004-1).
- Clark, R.C. 1953. Requirements of Casing Cement for Segregating Fluid Bearing Formation. *Oil & Gas J.* (1953) 51: 173.
- Doherty, W.T. 1933. Oil-Well Cementing in the Gulf Coast Area. *API Production Bull.* Sec. 4: 60.
- Farris, R.F. 1946. Method for Determining Minimum Waiting-on-Cement Time. *Trans., AIME* 165: 175–188. SPE-946175-G.
- Goins, W.C. 1959. Open-Hole Plugback Operations. In *Oil-Well Cementing Practices in the United States*, 193–197. New York: API.
- Goode, John M. 1962. Gas and Water Permeability Data for Some Common Oilwell Cements. *J. Pet Technol* 14 (8): 851–854. SPE-288-PA. DOI: [10.2118/288-PA](https://doi.org/10.2118/288-PA).

- Halliburton. 2001. *The Red Book: Halliburton Cementing Tables*. Duncan, Oklahoma: Halliburton Company.
- Huerta, N.J., Bryant, S.L., Strazisar, B.R., Kutchko, B.G., and Conrad, L.C. 2008. The Influence of Confining Stress and Chemical Alteration on Conductive Pathways Within Wellbore Cement. *Energy Procedia* **1** (1): 3571–3578.
- ISO 10426-6, *Cements and Materials for Well Cementing, Part 6: Methods for Determining the Static Gel Strength of Cement Formulations*. 2008. Geneva, Switzerland: ISO.
- Kosmatka, S.H. and Wilson, M.L. 2011. *Design and Control of Concrete Mixtures*, 15th edition. Skokie, Illinois: Portland Cement Association.
- Kutchko, B.G., Strazisar, B.R., Huerta, N.J., Lowry, G.V., Dzombak, D.A., and Thaulow, N. 2009. CO₂ Reaction with Hydrated Class H Well Cement Under Geologic Sequestration Conditions: Effects of Flyash Admixtures. *Environ. Sci. Technol.* **43** (10): 3947–3952. DOI: [10.1021/es803007e](https://doi.org/10.1021/es803007e).
- Lake, L.W. 2006. *Petroleum Engineering Handbook, Volume II Drilling Engineering*. SPE, Richardson, Texas: 369–432.
- Parr, I., Sweatman, R., Lee, S., and Farnworth, S. 2009. New Lab Tests and Models Improve Planning for Complex Cementing Jobs Offshore New Zealand. Paper SPE 119386 presented at the SPE/IADC Drilling Conference and Exhibition, Amsterdam, 17–19 March. DOI: [10.2118/119386-MS](https://doi.org/10.2118/119386-MS).
- Rodot, F. and Garnier, A. 2009. Impact of CO₂ on Neat Class G Cement. Paper presented at the IEAGHG Research Program 5th Meeting of the Wellbore Integrity Network, Calgary, 13–14 May.
- Sabins, F.L. and Sutton, D.L. 1991. Interrelationship Between Critical Cement Properties and Volume Changes During Cement Setting. *SPE Drill Eng* **6** (2): 88–94. DOI: [10.2118/20451-PA](https://doi.org/10.2118/20451-PA).
- Santra, A., Reddy, B.R., Liang, F., and Fitzgerald, R. 2009. Reaction of CO₂ with Portland Cement at Downhole Conditions and the Role of Pozzolanic Supplements. Paper SPE 121103 presented at the SPE International Symposium on Oilfield Chemistry, The Woodlands, Texas, USA, 20–22 April. DOI: [10.2118/121103-MS](https://doi.org/10.2118/121103-MS).
- Sutton, D.L., Sabins, F.L., and Faul, R. 1984a. Preventing Annular Gas Flow—1: Annular Gas Flow Theory and Prevention Methods Described. *Oil & Gas J.* **82** (50): 84–92.
- Sutton, D.L., Sabins, F.L., and Faul, Ronald. 1984b. Preventing Annular Gas Flow—2: New Evaluation for Annular Gas-Flow Potential. *Oil & Gas J.* **82** (51): 109–112.
- Sweatman, R.E. and Scoggins, W.C. 1990. Acid-Soluble Magnesia Cement: New Applications in Completion and Workover Operations. *SPE Prod & Eng* **5** (4): 441–447. SPE-18031-PA. DOI: [10.2118/18031-PA](https://doi.org/10.2118/18031-PA).
- Sweatman, R., Parker, M., and Crookshank, S. 2009a. Industry Experience with CO₂ Enhanced Oil Recovery Technology. Paper SPE 126446 presented at the SPE International Conference on CO₂ Capture, Storage, and Utilization, San Diego, California, USA, 2–4 November. DOI: [10.2118/126446-MS](https://doi.org/10.2118/126446-MS).
- Sweatman, R., Santra, A., Kulakofsky, D., and Calvert, J. 2009b. Effective Zonal Isolation for CO₂ Sequestration Wells. Paper SPE 126226 presented at the SPE International Conference on CO₂ Capture, Storage, and Utilization, San Diego, California, USA, 2–4 November, 2009. DOI: [10.2118/126226-MS](https://doi.org/10.2118/126226-MS).

Further Reading and Advanced Topics

- Beirute, R.M., 1984. The Phenomenon of Free Fall During Primary Cementing. Paper SPE 13045 presented at the SPE Annual Technical Conference and Exhibition, Houston, 16–19 September. DOI: [10.2118/13045-MS](https://doi.org/10.2118/13045-MS).
- Beirute, R.M. and Flumerfelt, R.W. 1977. Mechanics of the Displacement Process of Drilling Muds by Cement Slurries Using an Accurate Rheological Model. Paper SPE 6801 presented at the SPE Annual Technical Conference and Exhibition, Denver, 9–12 October. DOI: [10.2118/6801-MS](https://doi.org/10.2118/6801-MS).
- Bourgoyne, A.T., Millheim, K.K., Chenevert, M.E., and Young, F.S. 1991. *Applied Drilling Engineering*. Textbook Series, SPE, Richardson, Texas **2**: 42–53; 131–137.
- Calvert, D.G., Heatman, J., and Griffith, J. 1995. Plug Cementing: Horizontal to Vertical Conditions. Paper SPE 30514 presented at the SPE Annual Technical Conference and Exhibition, Dallas, 22–25 October. DOI: [10.2118/30514-MS](https://doi.org/10.2118/30514-MS).
- Craft, B.C., Holden, W.R., and Graves, E.D. 1962. *Well Design: Drilling and Production*. New Jersey: Prentice Hall.
- Crook, R.J., Faul, R., Bengel, G., and Jones, R.R. 2001. Eight Steps Ensure Successful Cement Placement. *Oil & Gas J.* **99** (27): 37.
- Crook, R.J., Keller, S.R., and Wilson, M.A. 1987. Deviated Wellbore Cementing: Part 2—Solutions. *J. Pet Technol* **39** (8): 961–966. SPE-14198-PA. DOI: [10.2118/14198-PA](https://doi.org/10.2118/14198-PA).
- Davies, D.R., Hartog, J.J., and Cobbett, J.S. 1981. Foamed Cement—A Cement with Many Applications. Paper SPE 9598 presented at the SPE Middle East Technical Conference and Exhibition, Manama, Bahrain, 9–12 March. DOI: [10.2118/9598-MS](https://doi.org/10.2118/9598-MS).
- Hartog, J.J., Davies, D.R., and Stewart, R.B. 1983. An Integrated Approach for Successful Primary Cementations. *J. Pet Technol* **35** (9): 1600–1610. SPE-9599-PA. DOI: [10.2118/9599-PA](https://doi.org/10.2118/9599-PA).

- Jones, R. and Watters, L. 1998. Remedial Cementing. In *Petroleum Well Construction*, Chap. 11. Chichester, New York: John Wiley & Sons.
- Lockyear, C.F., Ryan, D.F., and Cunningham, M.M., 1990. Cement Channeling: How to Predict and Prevent. *SPE Drill Eng* **5** (3): 201–208. SPE-19865-PA. DOI: [10.2118/19865-PA](https://doi.org/10.2118/19865-PA).
- Minear, J.W. and Goodwin, K.J. 1998. Cement-Sheath Evaluation. In *Petroleum Well Construction*, Chap. 10. Chichester, New York: John Wiley & Sons.
- Mitchell, R.F. and Wedelich, H.F. 1989. Prediction of Downhole Temperatures Can Be a Key for Optimal Wellbore Design. Paper SPE 18900 presented at the SPE Production Operations Symposium, Oklahoma City, Oklahoma, USA, 13–14 March. DOI: [10.2118/18900-MS](https://doi.org/10.2118/18900-MS).
- Nelson, E.B. ed. 1990. *Well Cementing*. Developments in Petroleum Science Series, **28**. Amsterdam: Elsevier Science Publishers B.V.
- Ravi, K. and Moran, L. 1998. Primary Cementing. In *Petroleum Well Construction*, Chap. 8. Chichester, New York: John Wiley & Sons.
- Smith, D.K. 1987. *Cementing*. Monograph Series, SPE, Richardson, Texas **4**.
- Sutton, D.L., Sabins, F.L., and Faul, R. 1984. Preventing Annular Gas Flow. *Oil & Gas J.* Part 1 (10 December) and Part 2 (17 December).
- Tinslay, J.M., Miller, E.C., Sabbins, F.L., and Sutton, D.L. 1979. Study of Factors Causing Annular Gas Flow Following Primary Cementing. *J. Pet Technol* **32** (8): 1427–1437. SPE-8257-PA. DOI: [10.2118/8257-PA](https://doi.org/10.2118/8257-PA).
- Watters, L.T. and Beirute, R. 1998. Formation-Fluid Migration After Cementing. *Petroleum Well Construction*, Chap. 9. Chichester, New York: John Wiley & Sons.

SI Metric Conversion Factors

ft	×	3.048*	E – 01 = m
ft ²	×	9.290 304*	E – 02 = m ²
ft ³	×	2.831 685	E – 02 = m ³
°F		(°F – 32)/1.8	= °C
gal	×	3.785 412	E – 03 = m ³
in.	×	2.54*	E + 00 = cm
lbm	×	4.535 924	E – 01 = kg
psi	×	6.894 757	E + 00 = kPa
ton	×	9.071 847	E – 01 = Mg

*Conversion factor is exact.

Chapter 5

Drilling Hydraulics

Vassilios C. Kelessidis, Technical University of Crete, **Roberto Maglione**, Eni Agip, and **Robert F. Mitchell**, Halliburton

The science of fluid mechanics is very important to the drilling engineer. Extremely large fluid pressures are created in the long slender wellbore and tubular pipe strings by the presence of drilling mud or cement. The presence of these subsurface pressures must be considered in almost every well problem encountered.

In this chapter, the relations needed to determine the subsurface fluid pressures will be developed for three common well conditions. These well conditions are (1) a static condition in which both the well fluid and the central pipe string are at rest, (2) a circulating operation in which the fluids are being pumped down the central pipe string and up the annulus, and (3) operations in which a central pipe string is being moved up or down through the fluid. The second and third conditions listed are complicated by the non-Newtonian behavior of drilling muds and cement slurries. Also included in this chapter are the relations governing the transport of rock fragments and immiscible formation fluids to the surface by the drilling fluid.

Applications include (1) calculation of subsurface hydrostatic pressures tending to fracture exposed formations, (2) displacement of cement slurries, (3) bit nozzle size selection, (4) surge pressures due to a vertical pipe movement, and (5) cuttings-carrying capacity of drilling fluids.

The order in which the applications are presented parallels the development of the fundamental fluid-mechanics concepts given in the chapter.

5.1 Introduction to Drilling Hydraulics

The three primary functions of a drilling fluid (the transport of cuttings out of the wellbore, prevention of fluid influx, and the maintenance of wellbore stability) depend on the flow of drilling fluids and the pressures associated with that flow. For instance, if the wellbore pressure exceeds the fracture pressure, fluids will be lost to the formation. If the wellbore pressure falls below the pore pressure, fluids will flow into the wellbore, perhaps causing a blowout. It is clear that accurate wellbore pressure prediction is necessary. To properly engineer a drilling-fluid system, it is necessary to be able to predict pressures and flows of fluids in the wellbore. The purpose of this chapter is to describe in detail the calculations necessary to predict the flow performance of various drilling fluids for the variety of operations used in drilling and completing a well.

Drilling fluids range from relatively incompressible fluids, such as water and brines, to very compressible fluids, such as air and foam. Fluid-mechanics problems range from the simplicity of a static fluid to the complexity of dynamic surge pressures associated with running pipe or casing into the hole. This chapter will first present each specific wellbore flow problem in detail, starting from the simplest and progressing to the most complicated. These problems will be considered in the following order:

1. Hydrostatic pressure calculations
2. Steady flow of fluids

Following these basic problems, we will present a series of special topics:

1. Fluid rheology
2. Laminar flow
3. Turbulent flow
4. Eccentric annulus flow
5. Flow with moving pipe
6. Steady-State wellbore flow
7. Dynamic wellbore pressure prediction
8. Cuttings transport

5.2 Hydrostatic Pressure Calculations

Subsurface well pressures are determined most easily for static well conditions. The variation of pressure with depth in a fluid column can be obtained by considering the free-body diagram (**Fig. 5.1**) for the vertical forces acting on an element of fluid at a depth Z in a hole of cross-sectional area A . The downward force on the fluid element exerted by the fluid above is given by the pressure p times the cross-sectional area of the element, A :

$$F_1 = pA. \quad \dots\dots\dots (5.1)$$

Likewise, there is an upward force on the element exerted by the fluid below, given by

$$F_2 = \left(p + \frac{dp}{dZ} \Delta Z \right) A. \quad \dots\dots\dots (5.2)$$

In addition, the weight of the fluid element is exerting a downward force given by

$$F_3 = \rho g A \Delta Z, \quad \dots\dots\dots (5.3)$$

where ρ is the density of the fluid, and g is the acceleration due to gravity, which at sea level has a value of 9.81 m/s^2 .

Because the fluid is at rest, no shear forces exist and the three forces shown must be in equilibrium; hence,

$$F_1 - F_2 + F_3 = 0,$$

$$pA - \left(p + \frac{dp}{dZ} \Delta Z \right) A + \rho g A \Delta Z = 0.$$

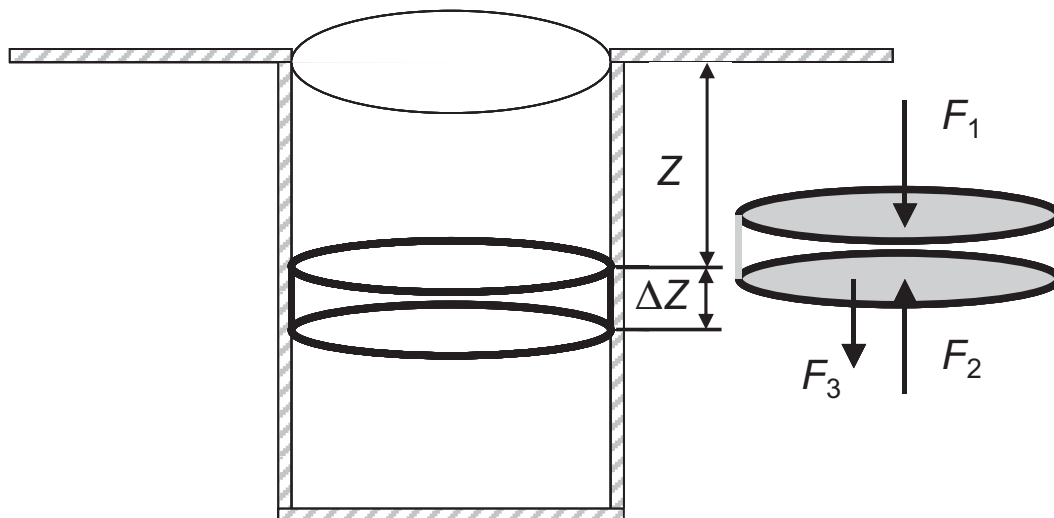


Fig. 5.1—Forces acting on a fluid element.

Expansion of the second term and division by the element volume $A\Delta Z$ gives

$$\frac{dp}{dZ} = \rho g. \quad \dots\dots\dots (5.4a)$$

In SI units, Eq. 5.4 has density ρ in kg/m^3 , depth Z in m, and pressure p is given in Pascals (Pa), while in field units ρ is given in lbm/gal , Z in ft, g is 1 lbf/lbm , and p is lbf/in.^2 (psi). With the conversion factors applied, Eq. 5.4 takes the following form in field units:

$$\frac{dp}{dZ} = 0.05195\rho. \quad \dots\dots\dots (5.4b)$$

A note on units: The drilling industry uses an odd mixture of unconventional English units combined with assorted metric units, depending on where in the world you are drilling. As a result, almost any calculation requires unit conversions, or formulae will have strange coefficients, like 0.05195 in Eq. 5.4b. SI units have the advantage of not needing conversions because the units are consistent, meaning that use of SI units in the equation gives results in SI units. The downside is that no one uses SI units in the drilling industry. When in doubt, convert everything to SI units, calculate, and then convert the result back to field units.

5.2.1 Incompressible Fluids. If we are dealing with a liquid such as drilling mud or salt water, fluid compressibility is negligible for low temperatures, and specific weight can be considered constant with depth. Integration of Eq. 5.4 for an incompressible liquid gives

$$p = \rho g Z + p_0, \quad \dots\dots\dots (5.5a)$$

where p_0 , the constant of integration, is equal to the surface pressure at $Z = 0$. If we are interested in absolute pressure, p_0 will be, at least, atmospheric pressure. Absolute pressure in English units is designated psia. Often, we are interested only in incremental pressure relative to atmospheric, which is called gauge pressure. Gauge pressure in English units is designated psig. In this case, p_0 can be negative. Eq. 5.5a becomes, in field units,

$$p = 0.05195\rho Z + p_0. \quad \dots\dots\dots (5.5b)$$

Normally the static surface pressure p_0 is zero (gauge pressure) unless the blowout preventer of the well is closed and the well is trying to flow.

An important application of the hydrostatic pressure equation is the determination of the proper drilling-fluid density. The fluid column in the well must be of sufficient density to cause the pressure in the well opposite each permeable stratum to be greater than the pore pressure of the formation fluid in the permeable stratum. This problem is illustrated in the schematic drawing shown in **Fig. 5.2**. However, the density of the fluid column must not be sufficient to cause any of the formations exposed to the drilling fluid to fracture. A fractured formation would allow some of the drilling fluid above the fracture depth to leak rapidly from the well into the fractured formation.

Example 5.1 Calculate the static minimum mud density required to prevent flow from a permeable stratum at 12,200 ft if the pore pressure of the formation fluid is 8,500 psig.

Solution. Converting field units to SI units gives

$$p_f = 8,500 \text{ psig} \times 6894.73 \text{ Pa/psi} = 5.86 \times 10^7 \text{ Pa},$$

$$Z = \frac{12,200 \text{ ft}}{3.2808 \text{ ft/m}} = 3.7186 \times 10^3 \text{ m}.$$

Using Eq. 5.3a with $p_0 = 0$ gives

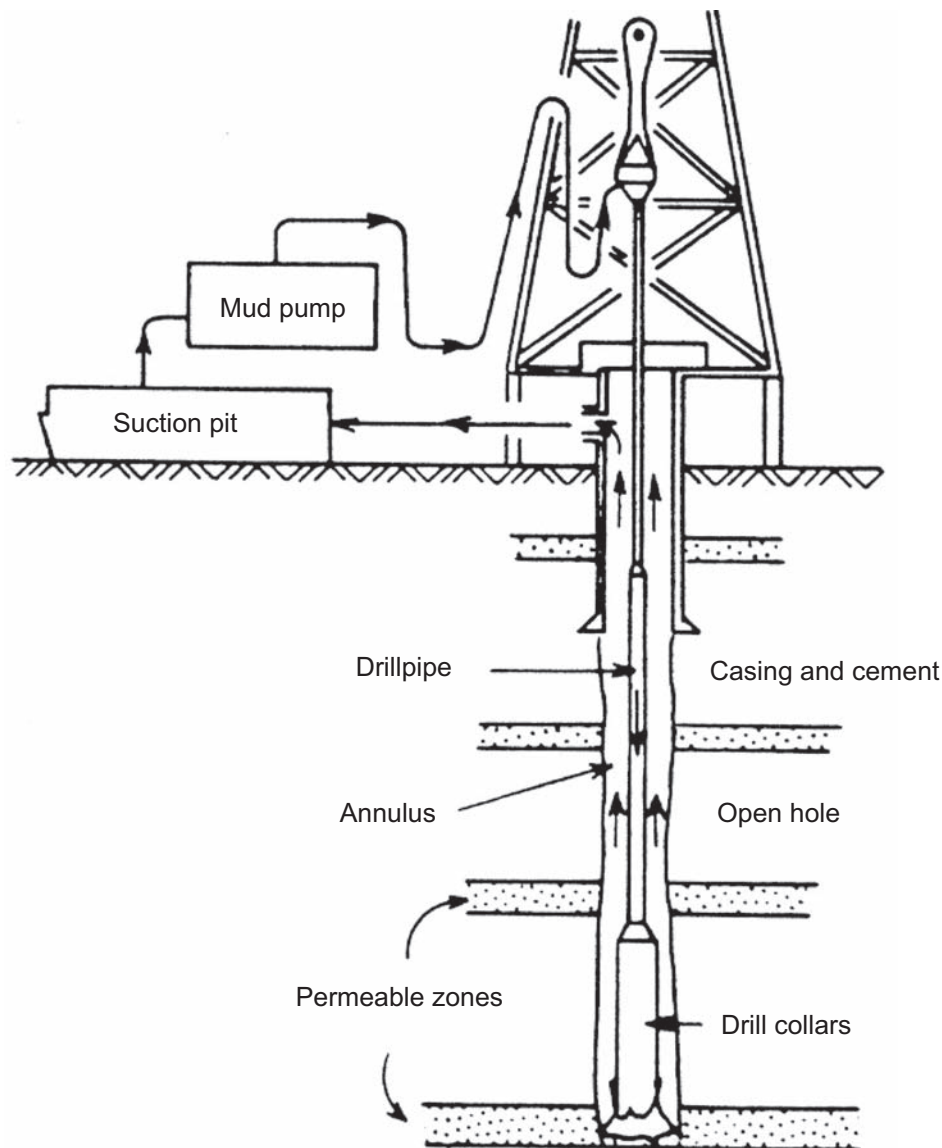


Fig. 5.2—The well-fluid system [from Bourgoyne et al. (1991)].

$$\rho = \frac{p}{gZ} = \frac{5.86 \times 10^7}{(9.81)(3718.6)} = 1606.4 \text{ kg/m}^3,$$

or, in field units,

$$\rho = 1606.4 \text{ kg/m}^3 \times 8.3454 \times 10^{-3} (\text{lbm/gal})/(\text{kg/m}^3) = 13.4 \text{ lbm/gal}.$$

Thus, the mud density must be at least 13.4 lbm/gal to prevent the flow of formation fluid into the wellbore when the well is open to the atmosphere and when there is no mud circulation.

5.2.2 Compressible Fluids. In many drilling and completion operations, a gas is present in at least a portion of the well. In some cases, gas is injected in the well from the surface, while in other cases gas may enter the well from a subsurface formation. The variation of pressure with depth in a static gas column is more complicated than in a static liquid column because the gas density changes with changing pressure.

The gas behavior can be described using the real gas equation, defined by

$$p = \rho z \frac{RT}{M}, \quad \dots \dots \dots (5.6)$$

where p = absolute pressure, ρ = gas density, z = gas compressibility factor, R = universal gas constant, T = absolute temperature, and M = gas molecular weight.

The gas compressibility factor z is a measure of how much the gas behavior deviates from that of an ideal gas, with $z = 1$ for ideal gases. Gas compressibility factors for natural gases have been determined experimentally as a function of temperature and pressure and are readily available in the petroleum and chemical engineering literature [e.g., Standing and Katz (1942), Carr et al. (1954), and Burcik (1957)]. In this chapter the simplifying assumption of ideal-gas behavior will generally be made to assist the student in focusing more easily on the drilling-hydraulics concepts being developed.

The gas density can be expressed as a function of pressure by rearranging Eq. 5.6. Solving this equation for the gas density ρ yields

$$\rho = \frac{pM}{zRT}. \quad (5.7a)$$

Changing units from consistent units to common field units gives

$$\rho = \frac{pM}{80.3zT}, \quad (5.7b)$$

where ρ is expressed in lbm/gal, p is in lbf/in.², M is in lbm/lbm-mol, and T is in degrees Rankine. The gas constant R is given in various unit systems as

$$R = 1,545 \frac{(\text{lbf/ft}^2) \cdot \text{ft}^3}{\text{lbm} \cdot \text{mol} \cdot \text{R}} = 80.3 \frac{\text{psia} \cdot \text{gal}}{\text{lbm} \cdot \text{mol} \cdot \text{R}} = 8.3144 \frac{\text{Pa} \cdot \text{m}^3}{\text{mol} \cdot \text{K}} = 8314.4 \frac{\text{Pa} \cdot \text{m}^3}{\text{kmol} \cdot \text{K}}.$$

When the length of the gas column is not great and the gas pressure is above 6.895×10^6 Pa (1,000 psia), the hydrostatic equation for incompressible liquids given by Eq. 5.3a can be used together with Eq. 5.7a without much loss in accuracy. However, when the gas column is not short or highly pressured, the variation of gas density with depth within the gas column should be taken into account. Using Eqs. 5.4a and 5.7a, we obtain

$$\frac{dp}{dZ} = \frac{g p M}{z R T}. \quad (5.8)$$

If the variation in z within the gas column is not too great, we can treat z as a constant, \bar{z} . Separating variables in the above equation and integrating gives

$$\ln \left(\frac{p}{p_0} \right) = \frac{g M}{\bar{z} R} \int_{z_0}^z \frac{1}{T(\xi)} d\xi. \quad (5.9a)$$

If we assume that T is relatively constant over the depth range, then Eq. 5.9a can be expressed

$$p = p_0 \exp \left(\frac{g M \Delta Z}{\bar{z} R T} \right), \quad (5.9b)$$

or, in field units,

$$p = p_0 \exp \left(\frac{M \Delta Z}{1,544 \bar{z} T} \right), \quad (5.9c)$$

where p is in psi, M in lbm/lbm-mol, ΔZ in ft, and T in degrees R.

Example 5.2 A well contains a tubing filled with methane gas (molecular weight = 16) to a vertical depth of 10,000 ft. The annular space is filled with a 9.0-lbm/gal brine. Assuming ideal gas behavior ($z = 1$), compute the

amount by which the exterior pressure on the tubing exceeds the interior tubing pressure at 10,000 ft if the surface tubing pressure is 1,000 psia and the mean gas temperature is 140°F. If the collapse resistance of the tubing is 8,330 psi, will the tubing collapse due to the high external pressure?

Solution. Converting from field units to SI units gives

$$p_0 = 1,000 \text{ psi} \times 6,894.73 \text{ Pa/psi} = 6.895 \times 10^6 \text{ Pa},$$

$$p_{col} = 8,330 \text{ psi} \times 6,894.76 \text{ Pa/psi} = 57.433 \times 10^6 \text{ Pa},$$

$$\rho = \frac{9 \text{ lbm/gal}}{8.3454 \times 10^{-3} (\text{lbm/gal})/(\text{kg/m}^3)} = 1.078 \times 10^3 \text{ kg/m}^3,$$

$$Z = \frac{10,000 \text{ ft}}{3.2808 \text{ ft/m}} = 3.048 \times 10^3 \text{ m},$$

$$T = \frac{140^\circ\text{F} - 32}{1.8} = 60^\circ\text{C},$$

$$p_0 = 14.7 \text{ psi} \times 6,894.76 \text{ Pa/psi} = 101,353 \text{ Pa}.$$

The pressure in the annulus at a depth of 3048 m is given by Eq. 5.4a:

$$p_a = (9.81)(1078)(3048) + 101,353 = 32.3 \times 10^6 \text{ Pa}$$

The pressure in the tubing at a depth of 3048 m is given by Eq. 5.9a:

$$p_t = 6.895 \times 10^6 \exp\left(\frac{(9.81)(16)(3048)}{(1)(8314.4)(273.3 + 60)}\right) = 8.24 \times 10^6 \text{ Pa}$$

Thus, the pressure difference is given by

$$p_a - p_t = 32.33447 \times 10^6 - 8.2383 \times 10^6 = 24.096 \times 10^6 \text{ Pa}$$

or, in field units,

$$p_a - p_t = \frac{24.096 \times 10^6 \text{ Pa}}{6894.73 \text{ Pa/psi}} = 3,494 \text{ psi},$$

which is considerably below the collapse pressure of the tubing.

The density of the gas in the tubing at the surface could be approximated using Eq. 5.7a as follows:

$$\rho = \frac{(6.895 \times 10^6)(16)}{(1)(8314)(333.3)} = 39.8 \text{ kg/m}^3,$$

or, in field units,

$$\rho = (39.8 \text{ kg/m}^3)(8.3454 \times 10^3) (\text{lbm/gal}) / (\text{kg/m}^3) = 0.332 \text{ lbm/gal}.$$

It is interesting to note that the use of this density in Eq. 5.3a gives

$$p_1 = (39.8)(9.81)(3048) + 6.895 \times 10^6 = 8.09 \times 10^6 \text{ Pa},$$

which is within 150 kPa (22 psi) of the answer obtained using the more complex Eq. 5.9b.

5.2.3 Hydrostatic Pressure in Complex Fluid Columns. During many drilling operations, the well fluid column contains several sections of different fluid densities. The variation of pressure with depth in this type of complex fluid column must be determined by separating the effect of each fluid segment. For example, consider the complex liquid column shown in **Fig. 5.3**.

If the pressure at the top of Section 1 is known to be p_0 , then the pressure at the bottom of Section 1 can be computed from Eq. 5.5a:

$$p_1 = \rho_1 g(Z_1 - Z_0) + p_0.$$

The pressure at the bottom of Section 1 is equal to the pressure at the top of Section 2. Thus, the pressure at the bottom of Section 2 can be expressed in terms of the pressure at the top of Section 2:

$$p_2 = \rho_2 g(Z_2 - Z_1) + p_1 g(Z_1 - Z_0) + p_0.$$

In general, the pressure at any vertical depth Z can be expressed by

$$p = p_0 + g \sum_{i=1}^{i=n} \rho_i (Z_i - Z_{i-1}) + g \rho_n (Z - Z_{n-1}), \quad \dots \dots \dots (5.10)$$

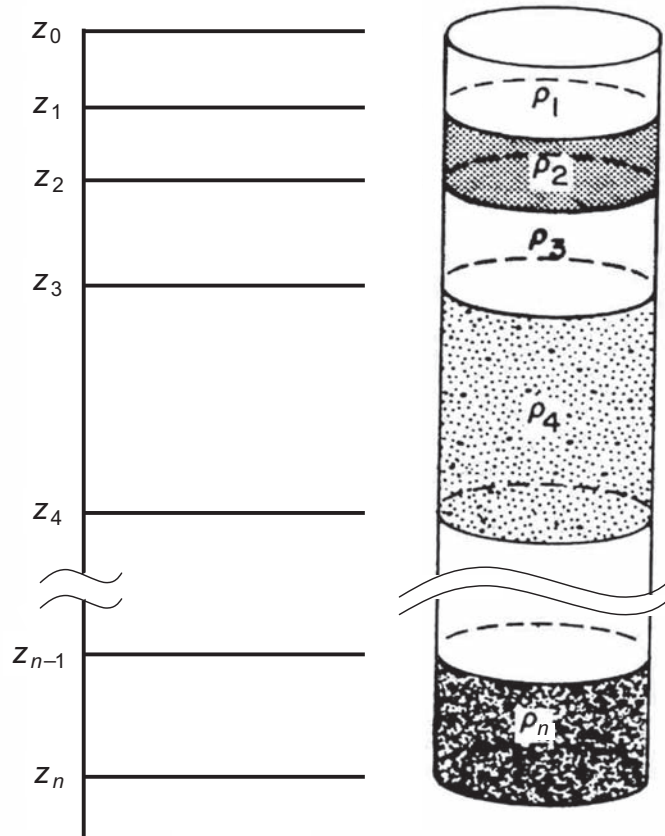


Fig. 5.3—A complex fluid column [from Bourgoyne et al. (1991)].

where $Z_{n-1} < Z < Z_n$. It is frequently desirable to view the well fluid system shown in Fig. 5.3 as a manometer when solving for the pressure at a given point in the well. The drillstring interior usually is represented by the left side of the manometer, and the annulus usually is represented by the right side of the manometer. A hydrostatic pressure balance can then be written in terms of a known pressure and the unknown pressure using Eq. 5.10.

Example 5.3 In intermediate casing string is to be cemented in place at a depth of 10,000 ft. The well contains 10.5-lbm/gal mud when the casing string is placed on bottom. The cementing operation is designed so that the 10.5-lbm/gal mud will be displaced from the annulus by (1) 300 ft of 8.5-lbm/gal mud flush, (2) 1,700 ft of 12.7-lbm/gal filler cement, and (3) 1,000 ft of 16.7-lbm/gal high-strength cement. The high-strength cement will be displaced from the casing with 9-lbm/gal brine. Calculate the pump pressure required to completely displace the cement from the casing.

Solution. Converting from field units to SI units gives

$$\rho_m = \frac{10.5 \text{ lbm/gal}}{8.3454 \times 10^{-3} (\text{lbm/gal})/(\text{kg/m}^3)} = 1.2581 \times 10^3 \text{ kg/m}^3,$$

$$\rho_{fl} = \frac{8.5 \text{ lbm/gal}}{8.3454 \times 10^{-3} (\text{lbm/gal})/(\text{kg/m}^3)} = 1.0185 \times 10^3 \text{ kg/m}^3,$$

$$\rho_{fc} = \frac{12.7 \text{ lbm/gal}}{8.3454 \times 10^{-3} (\text{lbm/gal})/(\text{kg/m}^3)} = 1.5218 \times 10^3 \text{ kg/m}^3,$$

$$\rho_{hc} = \frac{16.7 \text{ lbm/gal}}{8.3454 \times 10^{-3} (\text{lbm/gal})/(\text{kg/m}^3)} = 2.0011 \times 10^3 \text{ kg/m}^3,$$

$$\rho_b = \frac{9.0 \text{ lbm/gal}}{8.3454 \times 10^{-3} (\text{lbm/gal})/(\text{kg/m}^3)} = 1.0784 \times 10^3 \text{ kg/m}^3.$$

The lengths of each fluid column are given by

$$\Delta Z_m = \frac{7,000 \text{ ft}}{3.2808 \text{ ft/m}} = 2.1336 \times 10^3 \text{ m},$$

$$\Delta Z_{fl} = \frac{300 \text{ ft}}{3.2808 \text{ ft/m}} = 91.4 \text{ m},$$

$$\Delta Z_{fc} = \frac{1,700 \text{ ft}}{3.2808 \text{ ft/m}} = 0.5182 \times 10^3 \text{ m},$$

$$\Delta Z_{hc} = \frac{1,000 \text{ ft}}{3.2808 \text{ ft/m}} = 3.048 \times 10^2 \text{ m},$$

$$\Delta Z_b = \frac{10,000 \text{ ft}}{3.2808 \text{ ft/m}} = 3.048 \times 10^3 \text{ m}.$$

The complex well fluid system is understood more easily if viewed as a manometer (**Fig. 5.4**). The hydrostatic pressure balance is written by starting at the known pressure and moving through the various fluid sections to the point of the unknown pressure. When moving down through a section, $Z_{i+1} - Z_i$ is positive and the change in hydrostatic pressure is added to the known pressure; conversely, when moving up through a section, $Z_{i+1} - Z_i$ is negative and the change in hydrostatic pressure is subtracted from the known pressure. Thus,

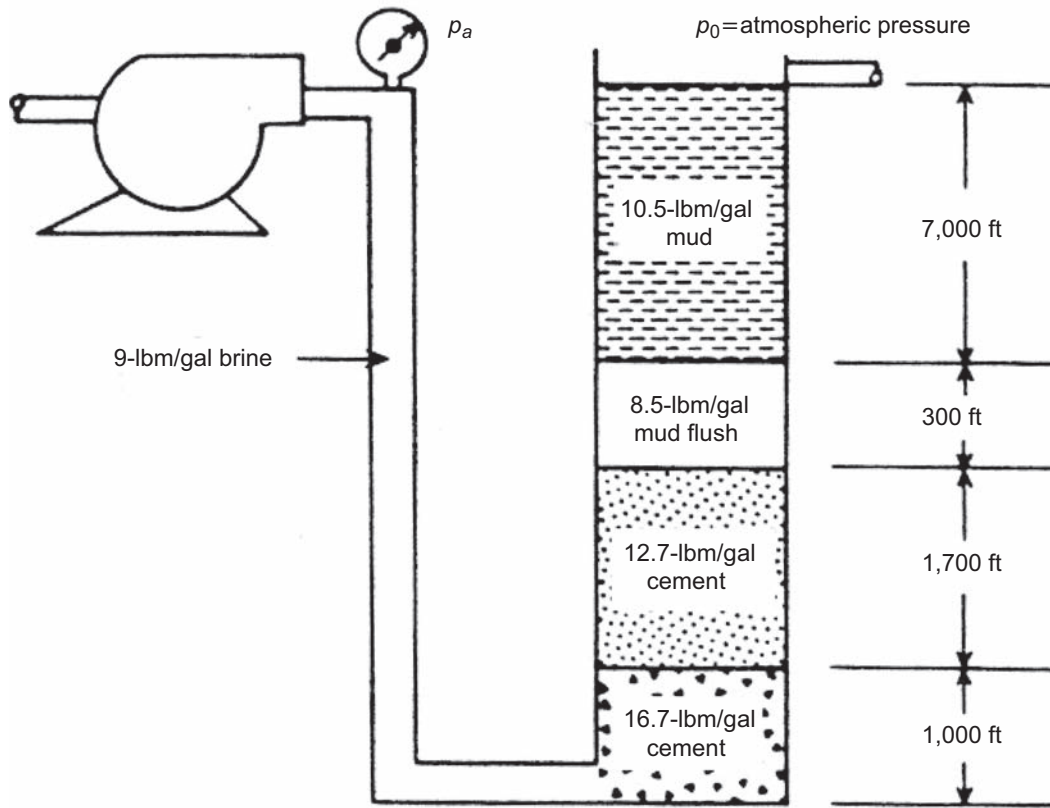


Fig. 5.4—Viewing the well as a manometer [from Bourgoyne et al. (1991)].

$$\begin{aligned}
 p_a &= p_0 + 9.81 \left\{ \begin{aligned} & \left((1.2581 \times 10^3) (2.1336 \times 10^3) + (1.0185 \times 10^3) (0.0914 \times 10^3) \right) \\ & + (1.5218 \times 10^3) (0.5182 \times 10^3) + (2.011 \times 10^3) (0.3048 \times 10^3) \\ & - (1.0784 \times 10^3) (3.048 \times 10^3) \end{aligned} \right\} \\
 &= p_0 + 8.75 \times 10^6 \text{ Pa.}
 \end{aligned}$$

Because the known pressure p_0 is 0 Pa, the gauge pump pressure is

$$p_a = 8.75 \times 10^6 \text{ Pa} = 1,269 \text{ psig.}$$

5.2.4 Equivalent Density Concept. Field experience in a given area often allows guidelines to be developed for the maximum mud density that formations at a given depth will withstand without fracturing during normal drilling operations. It is sometimes helpful to compare a complex-well-fluid column to an equivalent single-fluid column that is open to the atmosphere. This is accomplished by calculating the equivalent mud density ρ_e , which is defined by

$$\rho_e = \frac{p}{gZ} \dots\dots\dots (5.11a)$$

or, in field units,

$$\rho_e = \frac{p}{0.05195Z} \dots\dots\dots (5.11b)$$

The equivalent mud density always should be referenced to a specified depth.

Example 5.4 Calculate the equivalent density at a depth of 10,000 ft for Example 5.3 for static well conditions after the cement has been displaced completely from the casing.

Solution. Converting from field units to SI units gives

$$Z = \frac{10,000 \text{ ft}}{3.2808 \text{ ft/m}} = 3.048 \times 10^3 \text{ m},$$

$$\rho_b = \frac{9 \text{ lbm/gal}}{8.3454 \times 10^{-3} (\text{lbm/gal})/(\text{kg/m}^3)} = 1.0784 \times 10^3 \text{ kg/m}^3.$$

At the end of displacement, the pressure at the bottom of the hole is given by

$$p_{bh} = (1078.4)(9.81)(3048) + 8.75 \times 10^6 = 41.0 \times 10^6 \text{ Pa}.$$

The equivalent density is then

$$\rho_e = \frac{p}{gZ} = \frac{41.0 \times 10^6}{(9.81)(3048)} = 1371 \text{ kg/m}^3,$$

or, in field units,

$$\rho_e = 1371 \times 8.3454 \times 10^{-3} = 11.44 \text{ lbm/gal}.$$

Drilling activity has extended in recent years to high-pressure/high-temperature (HP/HT) wells, where drilling fluids experience both hot and cold temperature extremes, thus undergoing changes in density. The term *mud weight* usually refers to measurements performed at the surface, and while it could be assumed constant at temperatures for standard drilling activity in the past, it certainly does not hold for these HP/HT and deepwater wells. Zamora and Roy (2000) have put forward this issue, and instead of the term *mud weight* they have proposed the use of the term *equivalent static density* (ESD) for static wells and *equivalent circulating density* (ECD) for circulating wells. Simulation results are shown in **Fig. 5.5** for a water-based mud (WBM) and a synthetic-based mud (SBM) in 8,000 ft of water and onshore HP/HT environments.

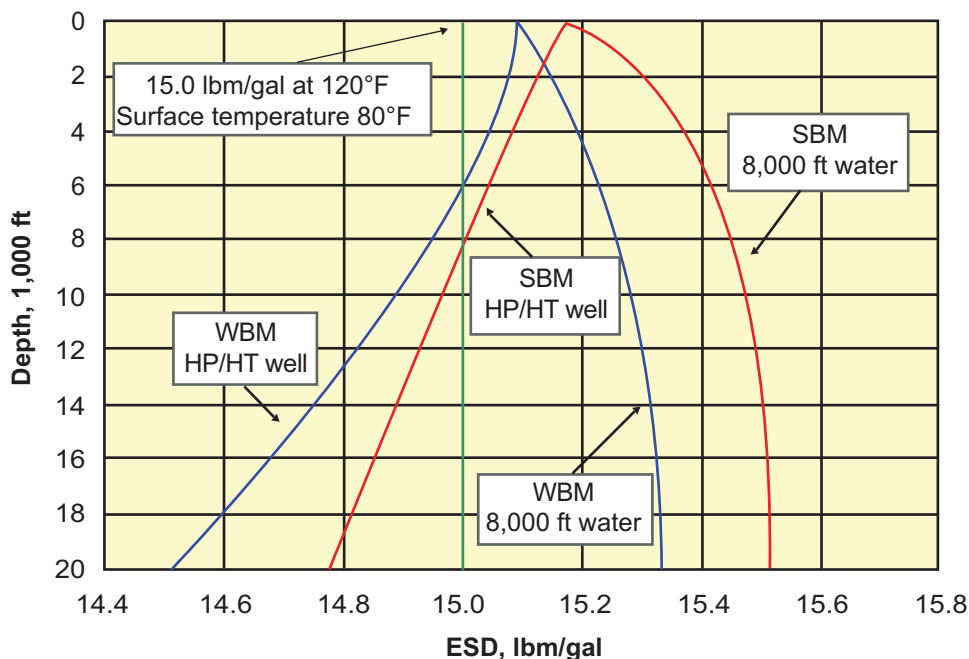


Fig. 5.5—Comparison of equivalent static density for WBM and SBM in 8,000 ft of water and onshore HP/HT environments [from Zamora and Roy (2000)].

The student should be aware of these issues, and appropriate modeling of the temperature and pressure dependence of the drilling fluid density is necessary together with computer simulations for incorporating temperature and pressure profiles into the calculation of ESD.

5.2.5 Effect of Entrained Solids and Gases in Drilling Fluid. Drilling engineers seldom deal with pure liquids or gases. For example, both drilling fluids and cement slurries are primarily a mixture of water and finely divided solids. The drilling mud in the annulus also contains the drilled solids from the rock broken up by the bit and the formation fluids that were contained in the rock. As long as the foreign materials are suspended by the fluid, or settling through the fluid at their terminal velocity, the effect of the foreign materials on hydrostatic pressure can be computed by replacing the fluid density in Eq. 5.5a with the density of the mixture. However, particles that have settled out of the fluid and are supported by grain-to-grain contact do not influence hydrostatic pressure.

The average density of an ideal mixture of N components is given by

$$\rho = \frac{\sum m_i}{\sum V_i} = \frac{\sum \rho_i V_i}{V} = \sum \rho_i \frac{V_i}{V} = \sum \rho_i f_i$$

$$V = \sum_{j=1}^N V_j, \quad f_i = \frac{V_i}{V}, \quad \dots \dots \dots (5.12)$$

where m_i , V_i , ρ_i , and f_i are the mass, volume, density, and volume fraction of component i , respectively, and V is the total volume. As long as the components are liquids and solids, the component density is essentially constant throughout the entire length of the column. Thus, the average density of the mixture also will be essentially constant.

If one component is a finely divided gas, the density of the gas component does not remain constant but decreases with the decreasing pressure. A drilling fluid that is measured to have a low density due to the presence of gas bubbles is said to be *gas-cut*.

The determination of the density of a gas-cut mud can be made in the following way. If N_v moles of gas are dispersed in (or associated with) 1 m^3 of drilling fluid, the volume fraction of gas at a given point in the column is given by

$$f_g = \frac{V_g}{V_m + V_g} = \frac{\frac{zN_v RT}{p}}{1 + \frac{zN_v RT}{p}} = \frac{zN_v RT}{p + zN_v RT} \quad \dots \dots \dots (5.13)$$

In addition, the gas density ρ_g at that point is defined by Eq. 5.7a. Thus, the effective density of the mixture, $\bar{\rho}$, is given by

$$\begin{aligned} \bar{\rho} &= \rho_f(1 - f_g) + \rho_g f_g \\ &= \rho_f \left[1 - \frac{zN_v RT}{p + zN_v RT} \right] + \frac{pM}{zRT} \left[\frac{zN_v RT}{p + zN_v RT} \right] \\ &= \frac{p(\rho_f + MN_v)}{p + zN_v RT}, \quad \dots \dots \dots (5.14) \end{aligned}$$

where M is the average molecular weight of the gas.

Combination of this expression with Eq. 5.4a yields

$$\Delta Z = \int_{p_1}^{p_2} \frac{p + zN_v RT}{g(\rho_f + MN_v)} \frac{dp}{p} \quad \dots \dots \dots (5.15)$$

If the variation of z and T is not too great over the column length of interest, they can be treated as constants of mean values \bar{z} and \bar{T} . Integration of Eq. 5.15 gives

$$\begin{aligned} \Delta Z &= \frac{\Delta p}{a} + \frac{b}{a} \ln \left(1 + \frac{\Delta p}{p_1} \right), \\ \Delta p &= p_2 - p_1, \Delta Z = Z_2 - Z_1, \quad \dots \dots \dots (5.16) \end{aligned}$$

where

$$a = g(\rho_f + MN_v), \quad (5.17)$$

$$b = \bar{z}N_v R\bar{T}. \quad (5.18)$$

It is unfortunate that the pressure Δp appears within the logarithmic term in Eq. 5.16. This means that an iterative calculation procedure must be used for the determination of the change in pressure with elevation for a gas-cut fluid column. However, if the gas-liquid mixture is highly pressured and not very long,

$$\ln\left(1 + \frac{\Delta p}{p_1}\right) \cong \frac{\Delta p}{p_1} - \frac{1}{2}\left(\frac{\Delta p}{p_1}\right)^2 + \frac{1}{3}\left(\frac{\Delta p}{p_1}\right)^3 \dots,$$

which shows that if $\Delta p/p_1 \ll 1$, Eq. 5.16 can be approximated by a linear or a quadratic equation.

Example 5.5 A massive low-permeability sandstone having a porosity of 0.20, a water saturation of 0.3, and a methane gas saturation of 0.7 is being drilled at a rate of 50 ft/hr with a 9.875-in. bit at a depth of 12,000 ft. A 14-lbm/gal drilling fluid is being circulated at a rate of 350 gal/min while drilling. Calculate the change in hydrostatic pressure caused by the drilled formation material entering the mud. Assume that the mean mud temperature is 620 R and that the formation water has a density of 9.0 lbm/gal. Also assume that the gas behavior is ideal and that both the gas and the rock cuttings move at the same annular velocity as the mud. The density of the drilled solids is 21.9 lbm/gal.

Solution. Converting from field units to SI units gives

$$\rho_w = \frac{9 \text{ lbm/gal}}{8.3454 \times 10^{-3} (\text{lbm/gal})/(\text{kg/m}^3)} = 1.0784 \times 10^3 \text{ kg/m}^3,$$

$$\rho_m = \frac{14 \text{ lbm/gal}}{8.3454 \times 10^{-3} (\text{lbm/gal})/(\text{kg/m}^3)} = 1.6776 \times 10^3 \text{ kg/m}^3,$$

$$\rho_s = \frac{21.9 \text{ lbm/gal}}{8.3454 \times 10^{-3} (\text{lbm/gal})/(\text{kg/m}^3)} = 2.6242 \times 10^3 \text{ kg/m}^3,$$

$$d_2 = \frac{9.875 \text{ in.}}{3.937 \times 10^1 \text{ in./m}} = 0.2508 \text{ m},$$

$$Z = \frac{12,000 \text{ ft}}{3.2808 \text{ ft/m}} = 3.658 \times 10^3 \text{ m},$$

$$q = \frac{350 \text{ gal/min}}{1.585 \times 10^4 (\text{gal/min})/(\text{m}^3/\text{s})} = 0.02208 \text{ m}^3/\text{s},$$

$$T = \frac{R}{1.8} = \frac{620}{1.8} = 344.44 \text{ K},$$

$$\text{ROP} = \frac{50 \text{ ft/hr}}{3.2808 \text{ ft/m} \times 3,600 \text{ s/hr}} = 0.004233 \text{ m/s},$$

where ROP = rate of penetration.

The hydrostatic head exerted by the mud is computed as

$$p = 101,325 + (1677.6)(9.81)(3658) = 60.302 \times 10^6 \text{ Pa.}$$

The formation is being drilled at a rate of

$$(0.004233)(\pi \times 0.2508^2/4) = 2.09 \times 10^{-4} \text{ m}^3/\text{s.}$$

Drilled solids are being added to the drilling fluid at a rate of

$$2.09 \times 10^{-4} (1 - 0.2) = 1.672 \times 10^{-4} \text{ m}^3/\text{s.}$$

Formation water is being added to the drilling fluid at a rate of

$$2.09 \times 10^{-4} (0.2)(0.3) = 0.1254 \times 10^{-4} \text{ m}^3/\text{s.}$$

The density of the drilling fluid after the addition of formation water and of drilled solids would be

$$\bar{\rho} = \frac{(1677.6)(0.02208) + (2624.2)(1.672 \times 10^{-4}) + (1078.4)(0.1254 \times 10^{-4})}{0.02208 + 1.672 \times 10^{-4} + 0.1254 \times 10^{-4}} = 1684.4 \text{ kg/m}^3.$$

Methane gas is being added to the drilling fluid at a rate of

$$2.09 \times 10^{-4} (0.2)(0.7) = 0.2926 \times 10^{-4} \text{ m}^3/\text{s.}$$

Assuming that the gas is ideal and that the formation pressure is approximately 38.8×10^6 Pa, the gas density given by Eq. 5.8a is

$$\rho_g = \frac{(60.602 \times 10^6 \text{ Pa})(16 \text{ kg/kmol})}{\left(8314.4 \frac{\text{Pa} \cdot \text{m}^3}{\text{kmol} \cdot \text{K}}\right)(1)(344.44\text{K})} = 336.8 \text{ kg/m}^3.$$

Thus, the gas mass rate entering the well is given by

$$\frac{(336.8 \text{ kg/m}^3)(0.2926 \times 10^{-4} \text{ m}^3/\text{s})}{16 \text{ kg/kmol}} = 6.159 \times 10^{-4} \text{ kmol/s} = 0.6159 \text{ mol/s.}$$

Because the mud is being circulated at a rate of $0.02208 \text{ m}^3/\text{s}$, the moles of gas per m^3 of mud is given by

$$N_v = \frac{0.6159}{0.02208} = 27.894 \text{ mol/m}^3.$$

Using Eqs. 5.17 and 5.18 gives

$$a = (9.81)[1684.4 + (16/1000)(27.894)] = 16,528 \text{ Pa/m}$$

and

$$b = (1)(27.894 \text{ mol/m}^3)[8.3144 \text{ Pa} \cdot \text{m}^3/(\text{mol} \cdot \text{K})](344.44\text{K}) = 79,883 \text{ Pa.}$$

Because the well is open to the atmosphere, the surface pressure p_1 is 101,325 Pa. The bottomhole pressure p_2 must be estimated from Eq. 5.16 in an iterative manner. Eq. 5.16 becomes

$$Z_2 = \frac{p_2 - 101,325}{16,528} + \frac{79,883}{16,528} \ln \frac{p_2}{101,325}.$$

As shown in the table below, various values for p_2 were assumed until the calculated $Z_2 - Z_1$ was equal to the well depth of 3658 m.

p_2 (Pa)	$\frac{p_2 - p_1}{16,528}$ (m)	$4.821 \ln \frac{p_2}{p_1}$ (m)	$Z_2 - Z_1$ (m)
60.329×10^6	3644	30.8	3674.8
59.984×10^6	3623	30.8	3653.8
60.03×10^6	3625.9	30.8	3656.7

Thus, the change in hydrostatic head due to the drilled formation material entering the mud is given by

$$\Delta p = (60.03 - 60.302) \times 10^6 \text{ Pa} = -272,000 \text{ Pa} = -39 \text{ psi}.$$

Example 5.5 indicates that the loss in hydrostatic head due to normal contamination of the drilling fluid is usually negligible. In the past, this was not understood by many drilling personnel. The confusion was caused mainly by a severe lowering of density of the drilling fluid leaving the well at the surface. This lowering of density was due to the rapidly expanding entrained gas resulting from the decrease in hydrostatic pressure on the drilling fluid as it approached the surface. The theoretical surface mud density that would be seen in Example 5.5 is given by Eq. 5.14 as

$$\begin{aligned} \bar{\rho} &= \frac{[1684.4 \text{ kg/m}^3 + (0.016 \text{ kg/mol})(27.89 \text{ mol/m}^3)] \times 101,325 \text{ Pa}}{101,325 \text{ Pa} + (1)(27.89 \text{ mol/m}^3)(8.3144 \text{ Pa} \cdot \text{m}^3/\text{mol} \cdot \text{K})(344.44 \text{ K})} \\ &= 941.83 \text{ kg/m}^3 = 7.9 \text{ lbm/gal.} \end{aligned}$$

In the past, it was common practice to increase the density of the drilling fluid when gas-cut mud was observed at the surface because of a fear of a potential blowout. However, Example 5.5 clearly shows that this should not be done unless the well will flow with the pump off. As shown in **Fig. 5.6**, significant decreases in annular mud density occur only in the relatively shallow part of the annulus. The rapid increase in annular density with depth occurs because the gas volume decreases by a factor of two when the hydrostatic pressure doubles. For example, increasing the hydrostatic pressure at the surface from 101,325 Pa (14.7 psia) to 810,820 Pa (117.6 psia) causes a unit volume of gas to decrease to one-eighth of its original size.

5.2.6 Effect of Well Deviation. Today, drilling engineers seldom deal with vertical wells. For a variety of reasons, wells are deviated from the vertical, often by as much as 90°. We have been considering Z as the true vertical depth (TVD) of the well. In a real well, we use measured depth, s , rather than Z to determine our location in the wellbore. What is even more important is that pressure changes due to friction from fluid flow vary with measured depth, not with TVD. The relationship between TVD and measured depth for a well with constant azimuth is given by:

$$\frac{dZ}{ds} = \cos \varphi, \quad \dots \dots \dots (5.19)$$

where φ is the angle of inclination of the wellbore with the vertical. More-complex geometries will be studied in later chapters, but for our purposes, this will suffice. For $\varphi = 0$, a vertical well, the TVD varies as the measured depth; that is, $Z = s$.

Example 5.6 Calculate the pressure in a deviated well as a function of measured depth. The wellbore is illustrated in **Fig. 5.7**, and the mud weight is 9 lbm/gal. The well is vertical to 2,400 ft, builds angle at 5°/ft, and

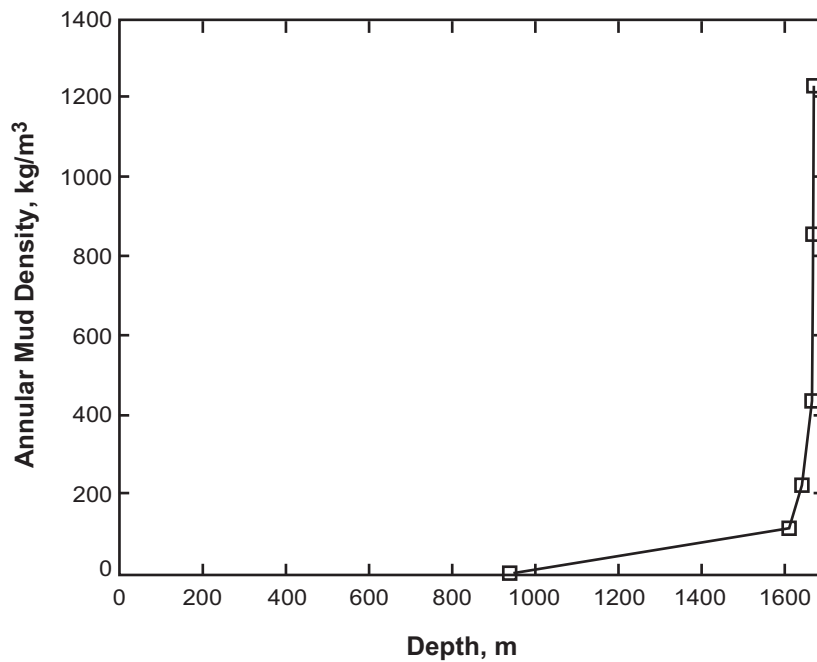


Fig. 5.6—Annular density plot for Example 5.6.

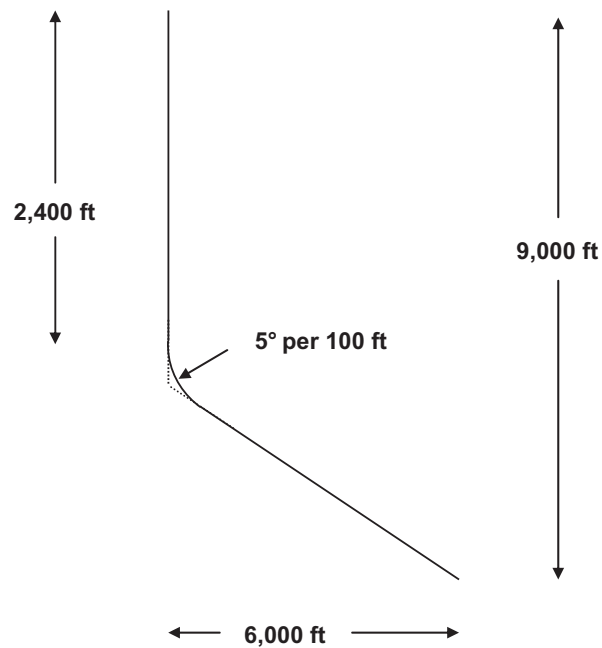


Fig. 5.7—Example of a deviated well.

traverses 6,000 ft laterally, with a TVD at bottomhole of 9,000 ft. From the surface to 2,400 ft measured depth, we know that the TVD corresponds with the measured depth, so the pressure calculation is unchanged from Eq. 5.5b.

Solution. To simplify the calculation, we will ignore the build section and consider the well configuration as two straight lines, as shown by the dotted line in Fig. 5.7. In the deviated section, we see a horizontal displacement of 6,000 ft and a vertical displacement of $9,000 - 2,400 = 6,600$ ft. The approximate angle of inclination is thus:

$$\cos \phi = \frac{6,600}{\sqrt{(6,600)^2 + (6,000)^2}} = 0.740$$

$$\phi = 42.3^\circ.$$

The total measured depth is $2,400 + \sqrt{(6,600)^2 + (6,000)^2} = 11,320$ ft. The pressure as a function of measured depth is

$$p(\text{psig}) = 0.05195(9 \text{ lbm/gal}) \times s \quad s \leq 2,400 \text{ ft}$$

$$= 1,122 \text{ psig} + 0.05195(9 \text{ lbm/gal})(0.740) \times (s - 2,400) \quad s > 2,400 \text{ ft}.$$

Because we know that the TVD of the well is 9,000 ft, the bottomhole pressure is easily calculated using Eq. 5.5b:

$$p(\text{psig}) = 0.05195(9 \text{ lbm/gal}) \times 9,000 \text{ ft} = 4,208 \text{ psig}.$$

If we calculate the bottomhole pressure at measured depth $s = 11,320$ ft, we get

$$p(\text{psig}) = 1,122 \text{ psig} + 0.05195(9 \text{ lbm/gal})(0.740) \times (11,320 \text{ ft} - 2,400 \text{ ft}) = 4,208 \text{ psig}.$$

5.3 Steady Flow of Drilling Fluids

The determination of pressure at various points in the well can be quite complex when either the drilling mud or the drillstring is moving. Frictional forces in the well system can be difficult to describe mathematically. However, in spite of the complexity of the system, the effect of these frictional forces must be determined for the calculation of (1) the flowing bottomhole pressure or ECD during drilling or cementing operations; (2) the bottomhole pressure or ECD during tripping operations; (3) the optimum pump pressure, flow rate, and bit nozzle sizes during drilling operations; (4) the cuttings-carrying capacity of the mud; and (5) the surface and downhole pressures that will occur in the drillstring during well-control operations for various mud flow rates.

The basic physical laws commonly applied to the movement of fluids are conservation of mass, conservation of momentum, and conservation of energy. All of the equations describing fluid flow are obtained by application of these physical laws using an assumed rheological model and an equation of state. Rheological models will be studied in a later section. Example equations of state are the incompressible fluid model, the slightly compressible fluid model, the ideal gas equation, and the real gas equation.

5.3.1 Mass Balance. The law of conservation of mass states that the net mass rate into any volume V is equal to the mass rate out of the volume.

The balance of mass for single-phase flow is given by

$$\dot{m} = \rho v A = \text{constant}. \quad (5.20)$$

\dot{m} = mass flow rate, kg/s,

ρ = density, kg/m³,

v = average velocity, m/s,

A = area, m²,

where *steady-state* flow has been assumed. The drilling engineer normally considers only *steady-state* conditions. Note also that for constant area, which is usually the case, the product of the density and the average velocity is constant. As pressure decreases, so does density, which implies that the average velocity increases. In other words, pressure decreases will accelerate a gas in a constant-area pipe. With the exception of air, gas, or foam drilling, the drilling fluid usually can be considered incompressible. In the absence of any accumulation or leakage of well fluid in the surface equipment or underground formations, the flow rate of an incompressible well fluid must be the same at all points in the well. For an incompressible fluid, Eq. 5.20 takes an even simpler form:

$$q = v A,$$

$$q = \text{volume flow rate, m}^3/\text{s}. \quad (5.21)$$

Knowledge of the average velocity at a given point in the well is often desired. For example, the drilling engineer frequently will compute the average upward flow velocity in the annulus to ensure that it is adequate for cuttings removal.

Example 5.7 A 12-lbm/gal mud is being circulated at 400 gal/min. The 5.0-in. drillpipe has an inside diameter (ID) of 4.33 in., and the drill collars have an ID of 2.5 in. The bit has a diameter of 9.875 in. Calculate the average velocity in the drillpipe, the drill collars, and the annulus opposite the drillpipe.

Solution. Converting to SI units,

$$q = 400 \text{ gal/min} (6.309 \times 10^{-5} \text{ m}^3/\text{s-gal/min}) = 0.0252 \text{ m}^3/\text{s},$$

$$A \text{ inside drillpipe} = \pi/4(4.33 \text{ in.})^2 (0.0254 \text{ m/in.})^2 = 0.00950 \text{ m}^2,$$

$$A \text{ inside drill collar} = \pi/4(2.5 \text{ in.})^2 (0.0254 \text{ m/in.})^2 = 0.00317 \text{ m}^2,$$

$$A \text{ outside drillpipe} = \pi/4[(9.875 \text{ in.})^2 - (5.0 \text{ in.})^2] (0.0254 \text{ m/in.})^2 = 0.0367 \text{ m}^2,$$

$$v \text{ inside drillpipe} = \frac{0.0252 \text{ m}^3/\text{s}}{0.00950 \text{ m}^2} = 2.65 \text{ m/s} = 8.69 \text{ ft/s},$$

$$v \text{ inside drill collars} = \frac{0.0252 \text{ m}^3/\text{s}}{0.00317 \text{ m}^2} = 7.95 \text{ m/s} = 26.1 \text{ ft/s},$$

$$v \text{ drillpipe annulus} = \frac{0.0252 \text{ m}^3/\text{s}}{0.0367 \text{ m}^2} = 0.687 \text{ m/s} = 2.25 \text{ ft/s}.$$

Example 5.8 An interesting calculation is the effect of pressure on the velocity of a flowing gas. Assume that the gas defined in Example 5.2 is flowing at 400 gal/min in the drillpipe annulus of area = 0.00317 m². The density at the surface was 0.332 lbm/gal at a pressure of 14.7 psia. The bottomhole pressure was 1,195 psia. Assume that the temperature at surface and bottomhole are roughly the same.

Solution. The mass flow rate \dot{m} is:

$$\dot{m} = 400 \text{ gal/min} (0.332 \text{ lbm/gal})(7.560 \times 10^{-3} \frac{\text{kg} \cdot \text{min}}{\text{lbm} \cdot \text{sec}}) = 1.00 \text{ kg/s}$$

$$v = \frac{1.00 \text{ kg/s}}{0.00317 \text{ m}^2 (0.332 \text{ lbm/gal})(119.8 \text{ kg} \cdot \text{gal}/\text{m}^3 \cdot \text{lbm})} = 7.93 \text{ m/s}$$

At the same temperature and same z , the densities are proportional to the pressures, so the velocity at bottomhole is

$$v = \frac{14.7 \text{ psia}}{1195 \text{ psia}} 7.93 \text{ m/s} = 0.0976 \text{ m/s}.$$

The student can verify that the mass flow rate is the same at both locations.

5.3.2 Momentum Balance. The balance of momentum for single-phase flow has the form

$$\Delta p + \rho v \Delta v = \int_{\Delta z} \rho g dZ \pm \int_{\Delta s} \left(\frac{dp_f}{ds} \right) ds, \dots\dots\dots (5.22)$$

$$\left(\frac{dp_f}{ds} \right) = \text{pressure change due to fluid friction, Pa/m},$$

$$\Delta s = \text{length of flow increment, m}$$

where steady flow has been assumed again. The Δv term is called the fluid acceleration, and it is nonzero only for compressible fluids. Also note that the term ρv is constant, from Eq. 5.20. The ρg term is the fluid weight term, which has been discussed in detail in Section 5.2. The fluid friction term is often expressed using the friction factor concept:

$$\Delta p + \rho v \Delta v = \int_{\Delta s} \left[\rho g \cos \varphi \pm \frac{2f \rho v^2}{D_h} \right] ds, \quad \dots \quad (5.23)$$

f = Fanning friction factor,
 D_h = hydraulic diameter, m,
 Δs = length of flow increment, m.

We have also used Eq. 5.19 to make everything dependent on measured depth s , though it may be convenient to retain the TVD relationship in some calculations. The Fanning friction factor f depends on the fluid density, velocity, viscosity, fluid type, and pipe roughness. Appropriate models for f , considering a variety of different fluid types, will be considered in detail in the section on rheology. The sign of the friction term is counter to the flow direction (e.g., negative for flow in the positive direction). The hydraulic diameter D_h is defined as

$$D_h = \frac{4 \times \text{Flow Area}}{\text{Wetted Perimeter}} \quad \dots \quad (5.24)$$

For a pipe cross-sectional area:

$$D_h = \frac{4 \times \frac{1}{4} \pi d^2}{\pi d} = d,$$

where d is the ID of the pipe. For the annulus formed by two pipes,

$$D_h = \frac{4 \times \frac{1}{4} \pi (d_o^2 - d_i^2)}{\pi (d_o + d_i)} = d_o - d_i,$$

where d_o is the inside diameter of the outer pipe and d_i is the outside diameter (OD) of the inner pipe. Notice that there is no effect of pipe eccentricity, so that also has to be accounted for in the friction factor. The friction factor we have defined is the Fanning friction factor. The student needs to be aware that there is an alternate definition called the Darcy friction factor that equals four times the Fanning friction factor. Be cautious when using friction factor graphs, tables, or formulas to be sure that you know which friction factor is being defined. For an incompressible fluid, Eq. 5.23 takes the following simple form:

$$\Delta p = \rho g \Delta Z \pm \frac{2f \rho v^2}{D_h} \Delta s, \quad \dots \quad (5.25)$$

where all the coefficients are constant. From his experience with static compressible fluids, the student should expect that solutions to Eq. 5.23 will be solutions to first-order nonlinear differential equations, and that analytic solutions will not, in general, be available.

Example 5.9 Assume that a liquid with density 990 kg/m^3 is flowing down a pipe at a 45° angle. The fluid velocity is 10.0 m/s , and the ID is 0.10 m . The Fanning friction factor has been calculated to be 0.001 . If the surface pressure is atmospheric, what is the gauge pressure at the bottom of a 1000-m pipe?

Solution. The hydrostatic contribution to the bottomhole pressure is

$$\begin{aligned} \Delta p_{\text{hydrostatic}} &= 990 \text{ kg/m}^3 (9.81 \text{ m/s}^2) \cos(45^\circ) (1000 \text{ m}), \\ &= 6.87 \text{ MPa} = 996 \text{ psig}. \end{aligned}$$

The fluid friction contribution is negative because the flow is in the positive s direction:

$$\Delta p_{\text{friction}} = \frac{-2(0.001)(990 \text{ kg/m}^3)(10.0 \text{ m/s})^2}{0.10 \text{ m}}(1000 \text{ m}),$$

$$= -1.98 \text{ MPa} = -287 \text{ psi}.$$

The total pressure at bottomhole is $996 \text{ psig} - 287 \text{ psig} = 709 \text{ psig}$.

5.3.3 Energy Balance. The law of conservation of energy states that the net energy rate out of a system is equal to the time rate of work done within the system. Consider the generalized flow system shown in **Fig. 5.8**. The work done by the fluid is equal to the energy per unit mass of fluid given by the fluid to a fluid engine (or equal to minus the work done by a pump on the fluid). Thus, the law of conservation of energy yields

$$(E_2 - E_1) + (p_2 V_2 - p_1 V_1) - g(Z_2 - Z_1) + \frac{1}{2}(v_2^2 - v_1^2) = W + Q, \quad (5.26)$$

where E is the internal energy of the fluid, W is the work done by the fluid, and Q is the heat per unit mass added to the fluid, with subscript 1 indicating inlet properties and subscript 2 indicating outlet properties. Simplifying this expression using differential notations yields

$$\Delta E - g\Delta Z + \Delta v^2/2 + \Delta(pV) = W + Q. \quad (5.27)$$

Eq. 5.27 is the first law of thermodynamics applied to a steady flow process. This equation is best suited for flow systems that involve either heat transfer or adiabatic processes involving fluids whose thermodynamic properties have been tabulated previously. This form of the equation seldom has been applied by drilling engineers. The change in internal energy of the fluid and the heat gained by the fluid usually is considered using a *friction loss* term, which can be defined in terms of Eq. 5.27 using the following expression:

$$F_{\text{fric}} = \Delta E + \int_1^2 p dV - Q. \quad (5.28)$$

The friction loss term can be used conveniently to account for the lost work or energy wasted by the viscous forces within the flowing fluid. Substitution of Eq. 5.28 into Eq. 5.27 yields

$$\int_1^2 V dp - g\Delta Z + \frac{\Delta v^2}{2} = W - F_{\text{fric}}. \quad (5.29)$$

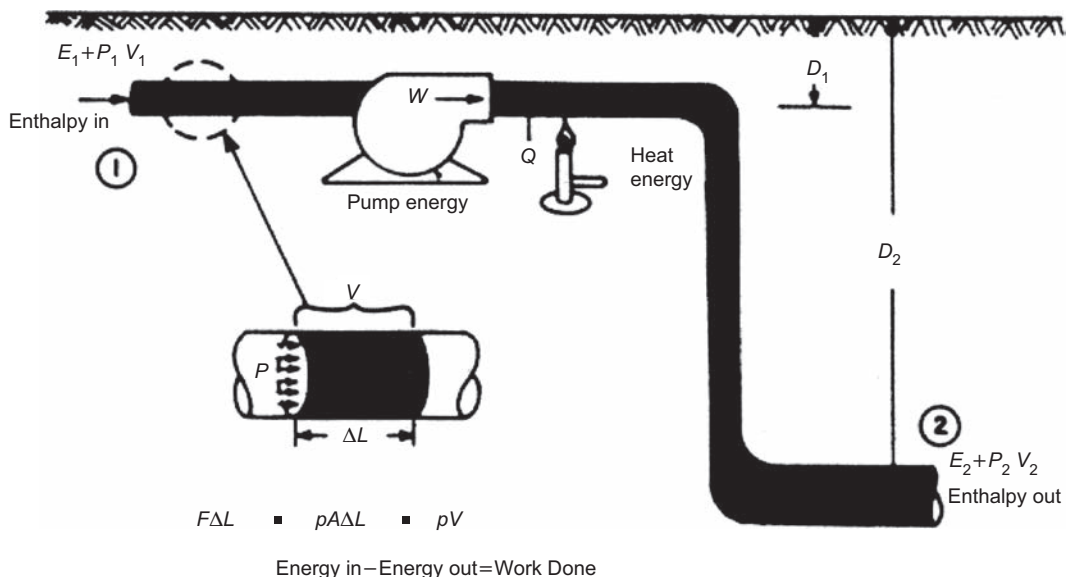


Fig. 5.8—Generalized flow system [from Bourgoyne et al. (1991)].

Eq. 5.29 often is called the mechanical energy balance equation. This equation was in use even before heat flow was recognized as a form of energy transfer by Carnot and Joule and is a completely general expression containing no limiting assumptions other than the exclusion of phase boundaries and magnetic, electrical, and chemical effects. The effect of heat flow in the system is included in the friction loss term F .

The first term in Eq. 5.29,

$$\int_1^2 V dp,$$

may be difficult to evaluate if the fluid is compressible unless the exact path of compression or expansion is known. Fortunately, drilling engineers deal primarily with essentially incompressible fluids having a constant specific volume V .

For incompressible fluids, it holds that

$$\int_1^2 V dp = \frac{\Delta p}{\rho}.$$

Eq. 5.29 also can be expressed by

$$\Delta p/\rho - g\Delta Z + \Delta v^2/2 = W - F_{\text{fric}}$$

or

$$p_1 + 9.81\rho(Z_2 - Z_1) - 0.5(\rho v_2^2 - \rho v_1^2) + \Delta p_p - \Delta p_f = p_2. \quad (5.30)$$

Expressing this equation in practical field units of lbf/in.², lbm/gal, ft/sec, and ft gives

$$p_1 + 0.052\rho(Z_2 - Z_1) - 8.074 \times 10^{-4} \rho(v_2^2 - v_1^2) + \Delta p_p - \Delta p_f = p_2. \quad (5.31)$$

Example 5.10 Determine the pressure at the bottom of the drillstring if the frictional pressure loss in the drillstring is 1,400 psi, the flow rate is 400 gal/min, the mud density is 12 lbm/gal, and the well depth is 10,000 ft. The ID of the drill collars at the bottom of the drillstring is 2.5 in., and the pressure increase developed by the pump is 3,000 psi.

Solution. Converting to SI units gives

$$\rho = \frac{12 \text{ lbm/gal}}{8.3454 \times 10^{-3} (\text{lbm/gal})/(\text{kg/m}^3)} = 1.438 \times 10^3 \text{ kg/m}^3,$$

$$d = \frac{2.5 \text{ in.}}{3.937 \times 10^1 \text{ in./m}} = 0.0635 \text{ m},$$

$$Z = \frac{10,000 \text{ ft}}{3.2808 \text{ ft/m}} = 3.048 \times 10^3 \text{ m},$$

$$q = \frac{400 \text{ gal/min}}{1.585 \times 10^4 (\text{gal/min})/(\text{m}^3/\text{s})} = 2.5236 \times 10^{-2} \text{ m}^3/\text{s},$$

$$\Delta p_f = (1,400 \text{ psi})(6894.73 \text{ Pa/psi}) = 9.6526 \times 10^6 \text{ Pa},$$

$$\Delta p_p = (3,000 \text{ psi})(6894.73 \text{ Pa/psi}) = 20.6814 \times 10^6 \text{ Pa}.$$

The average velocity in the drill collars is

$$v_{dc} = v_2 = \frac{1.274 \times 2.5236 \times 10^{-2}}{(0.0635)^2} = 7.973 \text{ m/s.}$$

The average velocity in the mud pits is essentially zero. Eq. 5.30 then gives

$$(9.81)(1438)(3048) - 0.5(7.973^2) + 20.6814 \times 10^6 - 9.6526 \times 10^6 = p_2,$$

or

$$p_2 = 54.0262 \times 10^6 \text{ Pa} = 7,836 \text{ psig.}$$

Example 5.10 illustrates the minor effect of the kinetic energy term of Eq. 5.30 in this drilling application. In general, the change in kinetic energy caused by fluid acceleration can be ignored, except for the flow of drilling fluid through the bit nozzles.

5.3.4 Flow Through Jet Bits. A schematic of incompressible flow through a short constriction, such as a bit nozzle, is shown in **Fig. 5.9**. In practice, it generally is assumed that (1) the change in pressure due to a change in elevation is negligible; (2) the velocity v_0 upstream of the nozzle is negligible, compared with the nozzle velocity v_n ; and (3) the frictional pressure loss across the nozzle is negligible. Thus, Eq. 5.31 reduces to

$$p_1 - 8.074 \times 10^{-4} \rho v_n^2 = p_2.$$

Substituting the symbol Δp_b for the pressure drop ($p_1 - p_2$) and solving this equation for the nozzle velocity v_n yields

$$v_n = \sqrt{\frac{\Delta p_b}{8.074 \times 10^{-4} \rho}}. \quad \dots \dots \dots (5.32a)$$

In SI units, Eq. 5.32a is given by

$$v_n = \sqrt{2 \frac{\Delta p_b}{\rho}}, \quad \dots \dots \dots (5.32b)$$

where v_n has units of m/s, Δp_b has units of Pa, and ρ has units of kg/m³. Unfortunately, the exit velocity predicted by Eq. 5.32 for a given pressure drop across the bit, Δp_b , never is realized. The actual velocity is always smaller than the velocity computed using Eq. 5.32, primarily because the assumption of frictionless flow is not strictly

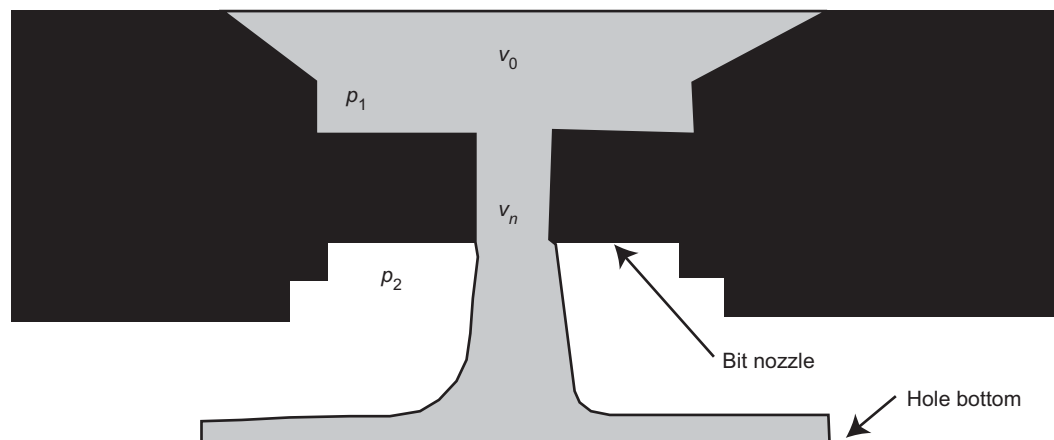


Fig. 5.9—Flow through a bit nozzle [from Bourgoyne et al. (1991)].

true. To compensate for this difference, a correction factor or discharge coefficient C_d usually is introduced so that the modified equation,

$$v_n = C_d \sqrt{\frac{\Delta p_b}{8.074 \times 10^{-4} \rho}}, \quad \dots \dots \dots (5.33a)$$

or, in SI units,

$$v_n = C_d \sqrt{2 \frac{\Delta p_b}{\rho}}, \quad \dots \dots \dots (5.33b)$$

will result in the observed value for nozzle velocity. The discharge coefficient has been determined experimentally for bit nozzles by Eckel and Bielstein (1951). These authors indicated that the discharge coefficient may be as high as 0.98 but recommended a value of 0.95 as a more practical limit.

A rock bit has more than one nozzle, usually the same number of nozzles and cones. When more than one nozzle is present, the pressure drop applied across all of the nozzles must be the same (**Fig. 5.10**).

According to Eq. 5.33, if the pressure drop is the same for each nozzle, the velocities through all nozzles are equal. Therefore, if the nozzles are of different areas, the flow rate q through each nozzle must adjust so that the ratio q/A is the same for each nozzle. If three nozzles are present,

$$\bar{v}_n = \frac{q_1}{A_1} = \frac{q_2}{A_2} = \frac{q_3}{A_3}.$$

Note also that the total flow rate of the pump, q , is given by

$$q = q_1 + q_2 + q_3 = \bar{v}_n A_1 + \bar{v}_n A_2 + \bar{v}_n A_3.$$

Simplifying this expression yields

$$q = \bar{v}_n (A_1 + A_2 + A_3) = \bar{v}_n A_t.$$

Thus, the velocity of flow through each nozzle is also equal to the total flow rate divided by the total nozzle area:

$$\frac{q}{A_t} = \frac{q_1}{A_1} = \frac{q_2}{A_2} = \dots = \frac{q_i}{A_i} \quad \dots \dots \dots (5.34)$$

In field units, the nozzle velocity v_n is given by

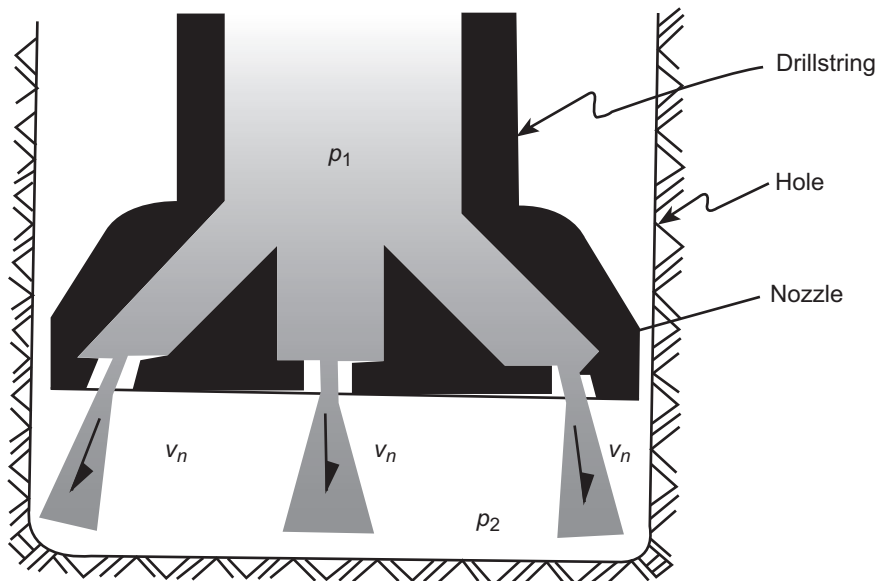


Fig. 5.10—Flow through parallel nozzles [from Bourgoyne et al. (1991)].

$$v_n = \frac{q}{3.117 A_t}, \dots\dots\dots (5.35a)$$

where v_n has units of ft/sec, q has units of gal/min, and A_t has units of in.². In SI units, v_n is given by

$$v_n = \frac{q}{A_t}, \dots\dots\dots (5.35b)$$

where v_n has units of m/s, q has units of m³/s, and A_t has units of m². Combining Eqs. 5.33 and 5.35 and solving for the pressure drop across the bit, Δp_b , yields

$$\Delta p_b = \frac{8.311 \times 10^{-5} \rho q^2}{C_d^2 A_t^2} \dots\dots\dots (5.36a)$$

In SI units, Eq. 5.36a is given by

$$\Delta p_b = \frac{\rho q^2}{2 C_d^2 A_t^2} \dots\dots\dots (5.36b)$$

Because the viscous frictional effects are usually negligible for flow through short nozzles, Eqs. 5.36a and 5.36b are valid for both Newtonian and non-Newtonian fluids, but should be used with caution. For critical applications, experimentally determined discharge coefficients should be determined for a specific mud.

Bit nozzle diameters often are expressed in 32nds of an inch. For example, if the bit nozzles are described as 12-13-13, this denotes that the bit contains one nozzle having a diameter of $12/32$ in. and two nozzles having a diameter of $13/32$ in.

Example 5.11 A 12.0-lbm/gal drilling fluid is flowing through a bit containing three $13/32$ -in. nozzles at a rate of 400 gal/min. Calculate the pressure drop across the bit.

Solution. In SI units, the density ρ , the nozzle diameter d_n , and the flow rate q are given by

$$\rho = \frac{(12 \text{ lbm/gal})}{8.3452 \times 10^{-3} (\text{lbm/gal})/(\text{kg/m}^3)} = 1.438 \times 10^3 \text{ kg/m}^3,$$

$$d_n = \frac{13/32 \text{ in.}}{3.937 \times 10^1 \text{ in./m}} = 1.032 \times 10^{-2} \text{ m},$$

$$q = \frac{400 \text{ gal/min}}{1.585 \times 10^4 (\text{gal/min})/(\text{m}^3/\text{s})} = 2.524 \times 10^{-2} \text{ m}^3/\text{s}.$$

The total area of the three nozzles is given by

$$A_t = 3 \frac{\pi}{4} (1.03 \times 10^{-2})^2 = 2.509 \times 10^{-4} \text{ m}^2$$

or

$$A_t = 0.3889 \text{ in.}^2$$

Using Eq. 5.36b, the pressure drop across the bit is given by

$$\Delta p_b = \frac{(1.438 \times 10^3)(2.524 \times 10^{-2})^2}{2(0.95)^2 (2.509 \times 10^{-4})^2} = 8.062 \times 10^6 \text{ Pa}$$

or

$$\Delta p_b = 1,169 \text{ psi.}$$

5.3.5 Bit Hydraulic Power. Because power is the rate of doing work, pump energy W can be converted to hydraulic power P_H by multiplying W by the mass flow rate ρq . Thus,

$$P_H = \rho W q = \Delta p_p q. \quad (5.37a)$$

In SI units P_H is expressed in watts (W), Δp_p in Pa, and q in m³/s. In field units, if the flow rate q is expressed in gal/min and the pump pressure Δp_p is expressed in lbf/in.², then

$$P_H = \frac{\Delta p_p q}{1,714}, \quad (5.37b)$$

where P_H is expressed in hydraulic horsepower. Likewise, other terms in Eq. 5.31, the pressure balance equation can be expressed as hydraulic horsepower by multiplying the pressure term by $q/1,714$.

Example 5.12 Determine the hydraulic horsepower being developed by the pump discussed in Example 5.10. How much of this power is being lost due to the viscous forces in the drillstring?

Solution. In SI units, the pump pressure Δp_p and the frictional pressure loss in the drillstring are given by

$$\Delta p_p = \frac{3000 \text{ psi}}{1.45 \times 10^{-4} \text{ psi/Pa}} = 2.069 \times 10^7 \text{ Pa},$$

$$\Delta p_{dp} = \frac{1400 \text{ psi}}{1.45 \times 10^{-4} \text{ psi/Pa}} = 9.655 \times 10^6 \text{ Pa}.$$

The pump power being used is given by Eq. 5.37a:

$$P_H = (2.069 \times 10^7)(2.524 \times 10^{-2}) = 5.222 \times 10^5 \text{ W}$$

or

$$P_H = 700 \text{ hp}.$$

The power consumed due to friction in the drillstring is given by

$$P_H = (9.655 \times 10^6)(2.524 \times 10^{-2}) = 2.437 \times 10^5 \text{ W}$$

or

$$P_H = 327 \text{ hp}.$$

5.3.6 Bit Hydraulic Impact Force. The purpose of the jet nozzles is to improve the cleaning action of the drilling fluid at the bottom of the hole. Before jet bits were introduced, rock chips were not removed efficiently, and much of the bit life was consumed regrinding the rock fragments. Further improvements in the cleaning action have been obtained with the introduction of a central nozzle. This avoids the *bit balling* phenomenon in drilling soft formations.

The rheological properties of drilling fluids can affect the hole bottom cleaning, particularly in the area around the bit nozzles and cones. In addition, the apparent viscosity can affect the overall bit performance. An increase in the frictional pressure loss inside the drillstring, because of higher values of the viscosity, reflects in a decrease of the hydraulic power available at the bit. Several investigators have concluded that the cleaning action is maximized by maximizing the total hydraulic impact force of the jetted fluid against the hole bottom. If it is assumed that the jet stream impacts the bottom of the hole in the manner shown in Fig. 5.9, all of the fluid momentum is transferred to the hole bottom.

Because the fluid is travelling at a vertical velocity v_n before striking the hole bottom and is travelling at zero vertical velocity after striking the hole bottom, the time rate of change of momentum (in field units) is given by

$$F_j = \frac{\Delta(m\bar{v})}{\Delta t} \approx \left(\frac{m}{\Delta t} \right) \Delta \bar{v} = \frac{(\rho q)\bar{v}_n}{32.17(60)} = \frac{(\rho q)\bar{v}_n}{1930.2}, \quad \dots\dots\dots (5.38a)$$

or, in SI units,

$$F_j = (\rho q)\bar{v}_n, \quad \dots\dots\dots (5.38b)$$

where ρq is the mass rate of the fluid. Combining Eqs. 5.33a and 5.38a yields

$$F_j = 0.01823 C_d q \sqrt{\rho \Delta p_b}, \quad \dots\dots\dots (5.39a)$$

where F_j is given in lbf. In SI units, Eq. 5.39a is given by

$$F_j = 1.4142 C_d q \sqrt{\rho \Delta p_b}. \quad \dots\dots\dots (5.39b)$$

Example 5.13 Compute the impact force developed by the bit discussed in Example 5.12.

Solution. Using Eq. 5.39b,

$$F_j = 1.4142 (0.95) (2.524 \times 10^{-2}) \sqrt{(1.438 \times 10^3) (8.062 \times 10^6)} = 3651.1 \text{ N}$$

or

$$F_j = 820.8 \text{ lbf.}$$

5.3.7 Jet Bit Nozzle Size Selection. The determination of the proper jet bit nozzle sizes is one of the more frequent applications of the frictional pressure-loss equations by drilling personnel. Significant increases in penetration rate can be achieved through the proper choice of bit nozzles. In relatively competent formations, the penetration rate increase is believed to result from mainly improved cleaning action at the hole bottom. Wasteful regrinding of cuttings is prevented if the fluid circulated through the bit removes the cuttings as rapidly as they are made. In soft formations, the jetted fluid also may aid in the destruction of the hole bottom.

The true optimization of jet bit hydraulics cannot be achieved yet. Before this can be done, accurate mathematical relations must be developed that define the effect of the level of hydraulics on penetration rate, operational costs, bit wear, potential hole problems such as hole washout, and drilling-fluid carrying capacity. At present, there is still disagreement as to what hydraulic parameter should be used to indicate the level of the hydraulic cleaning action. The most commonly used hydraulic design parameters are bit nozzle velocity, bit hydraulic horsepower, and jet impact force. Current field practice involves the selection of the bit nozzle sizes that will cause one of these parameters to be a maximum.

Maximum Nozzle Velocity. Before jet bits were introduced, rig pumps usually were operated at the flow rate corresponding to the estimated minimum annular velocity that would lift the cuttings. To some extent, this practice continues even today. If the jet nozzles are sized so that the surface pressure at this flow rate is equal to the maximum allowable surface pressure, then the fluid velocity in the bit nozzles will be the maximum that can be achieved and still lift the cuttings. This can be proved using Eq. 5.33a, the nozzle velocity equation. As shown in this equation, nozzle velocity is directly proportional to the square root of the pressure drop across the bit.

$$\bar{v}_n \propto \sqrt{\Delta p_b}$$

Thus, the nozzle velocity is a maximum when the pressure drop available at the bit is a maximum. The pressure drop available at the bit is a maximum when the pump pressure is a maximum and the frictional pressure loss in the drillstring and annulus is a minimum. The frictional pressure loss is a minimum when the flow rate is a minimum.

Maximum Bit Hydraulic Horsepower. Speer (1958) pointed out that the effectiveness of jet bits could be improved by increasing the hydraulic power of the pump. Speer reasoned that penetration rate would increase

with hydraulic horsepower until the cuttings were removed as fast as they were generated. After this “perfect cleaning” level was achieved, there should be no further increase in penetration rate with hydraulic power. Shortly after Speer published his paper, several authors pointed out that, because of the frictional pressure loss in the drillstring and annulus, the hydraulic power developed at the bottom of the hole was different from the hydraulic power developed by the pump. They concluded that bit horsepower rather than pump horsepower was the important parameter. Furthermore, it was concluded that bit horsepower was not necessarily maximized by operating the pump at the maximum possible horsepower. The conditions for maximum bit horsepower were derived by Kendall and Goins (1960).

The pump pressure is expended by frictional pressure losses in the surface equipment, Δp_s ; frictional pressure losses in the drillpipe Δp_{dp} and drill collars Δp_{dc} ; pressure losses caused by accelerating the drilling fluid through the nozzle; and frictional pressure losses in the drill collar annulus Δp_{dca} and drillpipe annulus Δp_{dpa} . Stated mathematically,

$$p_p = \Delta p_s + \Delta p_{dp} + \Delta p_{dc} + \Delta p_b + \Delta p_{dca} + \Delta p_{dpa} \quad (5.40)$$

If the total frictional pressure loss to and from the bit is called the *parasitic pressure loss*, Δp_d , then

$$p_d = \Delta p_s + \Delta p_{dp} + \Delta p_{dc} + \Delta p_{dca} + \Delta p_{dpa} \quad (5.41a)$$

and

$$p_p = \Delta p_b + \Delta p_d \quad (5.41b)$$

Because each term of the parasitic pressure loss can be computed for the usual case of turbulent flow,

$$\Delta p_f \propto q^{1.75},$$

we can represent the total parasitic pressure loss using

$$\Delta p_d \propto q^m = cq^m, \quad (5.42)$$

where m is a constant that theoretically has a value near 1.75, and c is a constant that depends on the mud properties and wellbore geometry. Substitution of this expression for Δp_d into Eq. 5.41b and solving for Δp_b yields

$$\Delta p_b = \Delta p_p - cq^m.$$

Because the bit hydraulic horsepower P_{Hb} is given by Eq. 5.37a,

$$P_{Hb} = \frac{\Delta p_b q}{1,714} = \frac{\Delta p_p q - cq^{m+1}}{1,714},$$

using calculus to determine the flow rate at which the bit horsepower is a maximum gives

$$\frac{dP_{Hb}}{dq} = \frac{\Delta p_p - (m+1)cq^m}{1,714} = 0.$$

Solving for the root of this equation yields

$$\Delta p_p = (m+1)cq^m = (m+1)\Delta p_d \quad (5.43a)$$

or

$$\Delta p_d = \frac{\Delta p_p}{(m+1)} \quad (5.43b)$$

Because $(d^2P_{Hb})/dq^2$ is less than zero for this root, the root corresponds to a maximum. Thus, bit hydraulic horsepower is a maximum when the parasitic pressure loss is $[1/(m+1)]$ times the pump pressure.

From a practical standpoint, it is not always desirable to maintain the optimum $\Delta p_d / \Delta p_p$ ratio. It is usually convenient to select a pump liner size that will be suitable for the entire well rather than periodically reducing the liner size as the well depth increases to achieve the theoretical maximum. Thus, in the shallow part of the well, the flow rate usually is held constant at the maximum rate that can be achieved with the convenient liner size. For a given pump horsepower rating P_{HP} this maximum rate is given by

$$q_{\max} = \frac{1,714 P_{HP} E}{p_{\max}}, \quad \dots \dots \dots (5.44)$$

where E is the overall pump efficiency, and p_{\max} is the maximum allowable pump pressure set by the contractor. This flow rate is used until a depth is reached at which $\Delta p_d / \Delta p_p$ is at the optimum value. The flow rate then is decreased with subsequent increases in depth to maintain $\Delta p_d / \Delta p_p$ at the optimum value. However, the flow rate never is reduced below the minimum flow rate to lift the cuttings.

Maximum Jet Impact Force. Some rig operators prefer to select bit nozzle sizes so that the jet impact force is a maximum rather than the bit hydraulic horsepower. McLean (1965) concluded from experimental work that the velocity of the flow across the bottom of the hole was a maximum for the maximum impact force. Eckel (1951), working with small bits in the laboratory, found that the penetration rate could be correlated to a bit Reynolds number group so that

$$\frac{dD}{dt} \propto \left(\frac{\rho \bar{v}_n d_n}{\mu_a} \right)^{a8},$$

where

$\frac{dD}{dt}$ = penetration rate,

ρ = fluid density,

\bar{v}_n = nozzle velocity,

d_n = nozzle diameter,

μ_a = apparent viscosity of the fluid at a shear rate of 10,000 seconds⁻¹, and

$a8$ = constant.

It can be shown that when nozzle sizes are selected so that jet impact force is a maximum, the Reynolds number group defined by Eckel is also a maximum. (The proof of this is left as a student exercise.) The derivation of the proper conditions for maximum jet impact was published first by Kendall and Goins (1960). The jet impact force is given by Eq. 5.39a.

$$\begin{aligned} F_j &= 0.01823 C_d q \sqrt{\rho \Delta p_b} \\ &= 0.01823 C_d q \sqrt{\rho (\Delta p_p - \Delta p_d)}. \end{aligned}$$

Because the parasitic pressure loss is given by Eq. 5.42,

$$F_j = 0.01823 C_d \sqrt{\rho \Delta p_p q^2 - (m+2) \rho c q^{m+1}},$$

using calculus to determine the flow rate at which the bit impact force is a maximum gives

$$\frac{dF_j}{dq} = \frac{\{0.009115 C_d [2 \rho \Delta p_p q - (m+2) \rho c q^{m+1}]\}}{\sqrt{\rho \Delta p_p q^2 - (m+2) \rho c q^{m+1}}}.$$

Solving for the root of this equation yields

$$2 \rho \Delta p_p - (m+2) \rho c q^{m+1} = 0,$$

$$\rho q [2 \Delta p_p - (m+2) \Delta p_d] = 0,$$

or

$$\Delta p_d = \frac{2\Delta p_p}{m+2} \quad \dots\dots\dots (5.45)$$

because $(d^2Fj)/dq^2$ is less than zero for this root, the root corresponds to a maximum. Thus, the jet impact force is a maximum when the parasitic pressure loss is $[2/(w+2)]$ times the pump pressure.

5.4 Rheological Models of Drilling Fluids

The frictional pressure loss term in the pressure balance equation given as Eq. 5.23 is the most difficult to evaluate. However, this term can be quite important because extremely large viscoelastic forces must be overcome to move drilling fluid through the long, slender conduits used in the drilling process. Generally, the elastic properties of drilling fluids and cement slurries and their effects during the flow in the hydraulic circuit of a drilling well are negligible. It is common practice in the computation of the frictional losses to consider only the effects of the viscous forces. However, with the new generations of drilling fluids, with polymers introduced on a regular basis, tests should be conducted to verify the elastic recovery from deformation that occurs during flow.

A mathematical description of the viscous forces present in a fluid is required for the development of friction-loss equations. The rheological models generally used by drilling engineers to approximate fluid behavior are the Newtonian model, the Bingham plastic model, the power-law or Ostwald-de Waele model, and the Herschel-Bulkley model.

5.4.1 Overview of Rheological Models. The viscous forces present in a fluid are characterized by the fluid viscosity. To understand the nature of viscosity, consider a fluid contained between two large parallel plates of area A , which are separated by a small distance L (Fig. 5.11).

The upper plate, which is initially at rest, is set in motion in the x direction at a constant velocity v . After sufficient time has passed for steady motion to be achieved, a constant force F is required to keep the upper plate moving at a constant velocity. The magnitude of the force F was found experimentally to be given by

$$\frac{F}{A} = \mu \frac{v}{L}.$$

The term F/A is called the *shear stress* exerted on the fluid. The constant of proportionality μ is called the *apparent viscosity* of the fluid. Thus, shear stress is defined by

$$\tau = \frac{F}{A}.$$

Note that the area of the plate, A , is the area in contact with the fluid. The velocity gradient v/L is an expression of the *shear rate*:

$$\dot{\gamma} = \frac{dv}{dL} \approx \frac{v}{L} \quad \dots\dots\dots (5.46)$$

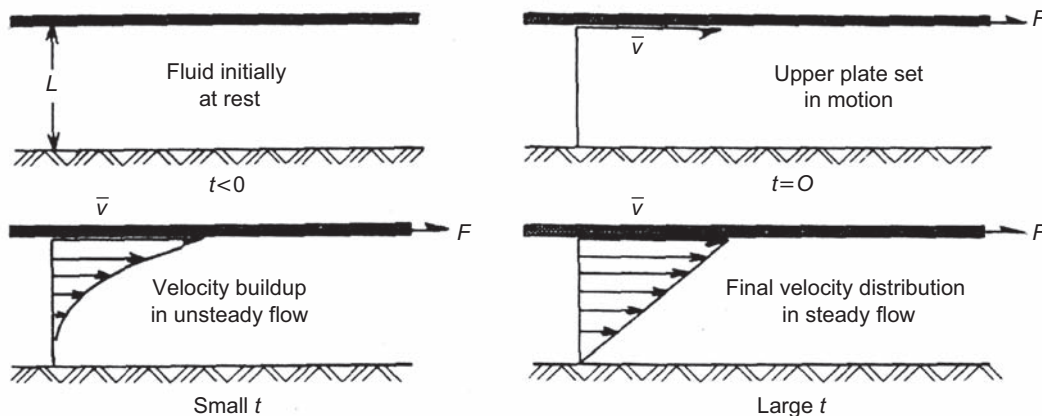


Fig. 5.11—Laminar flow of Newtonian fluids [from Bourgoyne et al. (1991)].

The apparent viscosity is defined as the ratio of the shear stress to the shear rate and depends on the shear rate at which the measurement is made and the prior shear-rate history of the fluid. The viscous forces present in a simple Newtonian fluid are characterized by a constant fluid viscosity. However, most drilling fluids are too complex to be characterized by a single value for viscosity. Fluids that do not exhibit a direct proportionality between shear stress and shear rate are classified as *non-Newtonian*. Non-Newtonian fluids that are shear-dependent are *pseudoplastic* or *yield-pseudoplastic* if the apparent viscosity decreases with increasing shear rate (**Fig. 5.12a**) and are *dilatant* if the apparent viscosity increases with increasing shear rate (Fig. 5.12b). Many drilling fluids and cement slurries are generally pseudoplastic in nature.

The Bingham plastic and the power-law rheological models were used in the past to approximate the pseudoplastic behavior of drilling fluids and cement slurries. The Bingham model was fairly simple, but the power-law model could handle the behavior of pseudoplastic drilling fluids and cement slurries better than the Bingham plastic model, particularly at low shear rates.

However, a typical behavior of the majority of the drilling fluids and of the cement slurries used today includes a yield stress. The behavior of these fluids, called yield-pseudoplastic, is characterized by a trend similar to that of pseudoplastic fluids and by the presence of a finite shear stress at zero shear rate, which is referred to as the

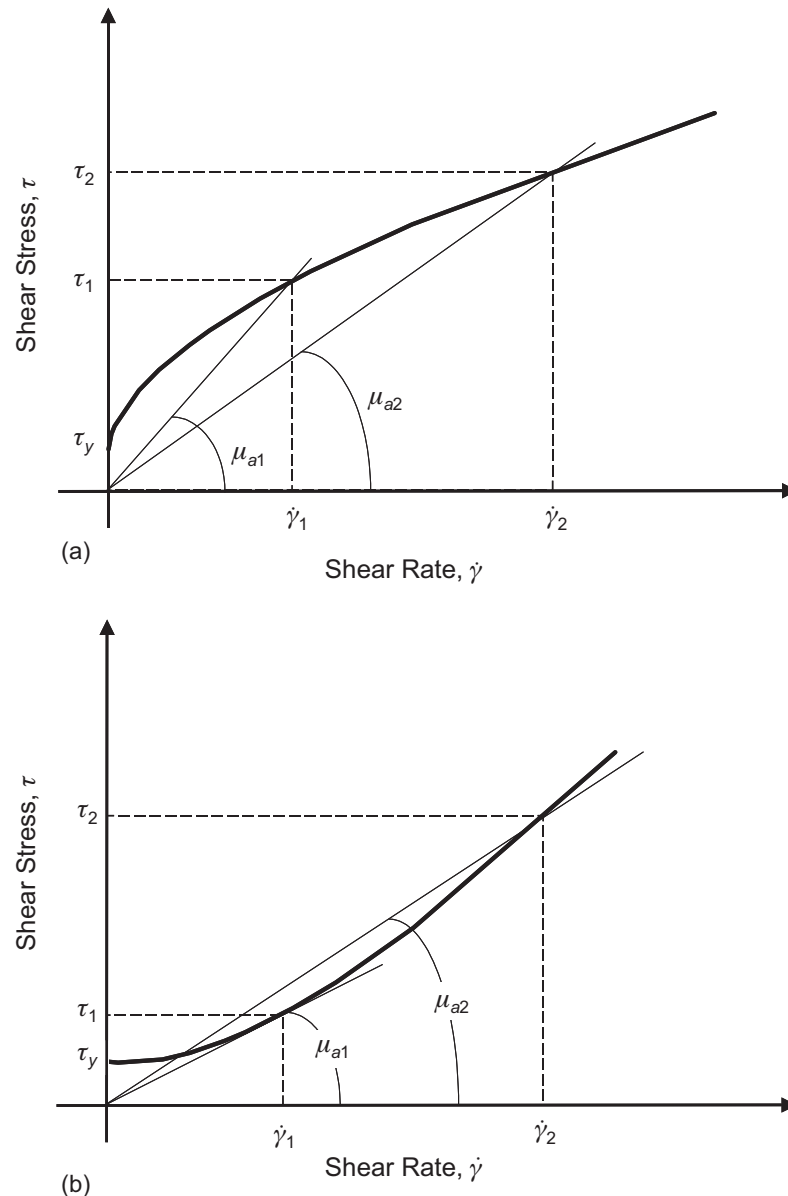


Fig. 5.12—Shear stress vs. shear rate for yield-pseudoplastic and dilatant fluids: (a) yield-pseudoplastic behavior, $\mu_{a2} < \mu_{a1}$, and (b) dilatant behavior, $\mu_{a2} > \mu_{a1}$ [from Bourgoyne et al. (1991)].

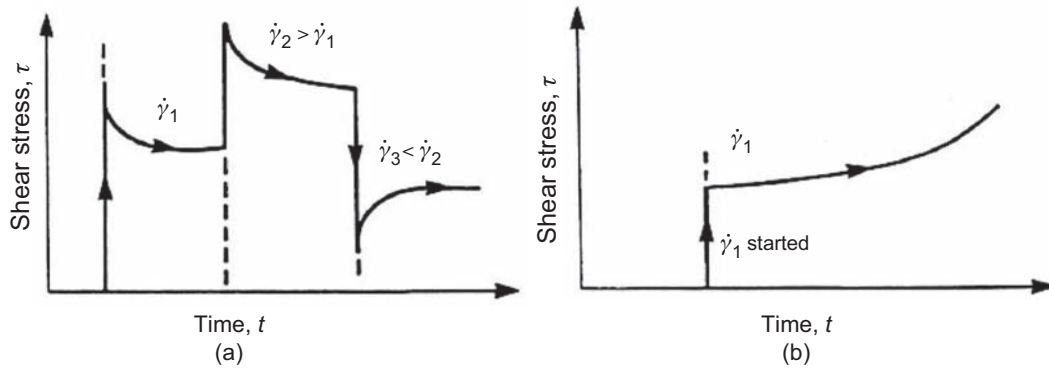


Fig. 5.13—Shear stress vs. time for thixotropic and rheopectic fluids: (a) thixotropic behavior and (b) rheopectic behavior [from Bourgoyne et al. (1991)].

yield stress. One of the rheological models that fits better this kind of behavior, both at low and high shear rates, is the Herschel-Bulkley model.

Non-Newtonian fluids that are dependent on shear time (**Fig. 5.13**) are *thixotropic* if the apparent viscosity decreases with time after the shear rate is increased to a new constant value and are *rheopectic* if the apparent viscosity increases with time after the shear rate is increased to a new constant value. Drilling fluids and cement slurries are generally thixotropic.

At present, the thixotropic behavior of drilling fluids and cement slurries is not modelled mathematically. However, drilling fluids and cement slurries generally are stirred before measuring the apparent viscosities at various shear rates so that steady-state conditions are obtained. Not accounting for thixotropy is satisfactory for most cases, but significant errors can result when a large number of direction changes and diameter changes are present in the hydraulic circuit of the well.

5.4.2 Newtonian Fluid Model. The Newtonian model states that the shear stress τ is directly proportional to the shear rate $\dot{\gamma}$ as follows:

$$\tau = \mu \dot{\gamma}, \quad \dots \dots \dots (5.47)$$

where μ , the constant of proportionality, is known as the apparent viscosity or simply the viscosity of the fluid (**Fig. 5.14**). In terms of the moving plates (**Fig. 5.11**), this means that if the force F is doubled, the plate velocity v also will double. Examples of Newtonian fluids are water, gases, high-gravity oils, and brines.

Viscosity is expressed in poise (P). A poise corresponds to 1 dyne·s/cm² or 1 g/cm·s. In the drilling industry, viscosity generally is expressed in centipoise (cp), where 1 cp = 0.01 poise. In SI units, viscosity is expressed in decapoise (daP), or pascal-seconds (Pa·s), which corresponds to 10 poise. Sometimes, viscosity is expressed in units of lbf·sec/ft². The units of viscosity can be related (at sea level) by

$$1 \frac{\text{lbf} \cdot \text{sec}}{\text{ft}^2} \times \frac{(453.6 \text{ g})(980.7 \text{ cm/s}^2)/\text{lbf}}{(30.48 \text{ cm/ft})^2} = 478.83 \text{ dyne} \cdot \text{s/cm}^2,$$

$$= 47.883 \text{ Pa} \cdot \text{s} = 47,883 \text{ cp}.$$

Example 5.14 An upper plate of 20-cm² area is spaced 1 cm above a stationary plate. Compute the viscosity in cp of a fluid between the plates if a force of 100 dyne is required to move the upper plate at a constant velocity of 10 cm/s.

Solution. In SI units, the area A , the distance L , the force F , and the velocity v are as follows:

$$A = \frac{(20 \text{ cm}^2)}{(10^4 \text{ cm}^2/\text{m}^2)} = 2 \times 10^{-3} \text{ m}^2,$$

$$L = \frac{(1 \text{ cm})}{(10^2 \text{ cm/m})} = 10^{-2} \text{ m},$$

$$F = \frac{(100 \text{ dyne})}{(10^5 \text{ dyne/N})} = 10^{-3} \text{ N},$$

$$v = \frac{(10 \text{ cm/s})}{(10^2 \text{ cm/m})} = 10^{-1} \text{ m/s}.$$

The shear stress τ is given by

$$\tau = \frac{10^{-3} \text{ N}}{2 \times 10^{-3} \text{ m}^2} = 5 \times 10^{-1} \text{ Pa}.$$

The shear rate $\dot{\gamma}$ is given by

$$\dot{\gamma} = \frac{10^{-1} \text{ m/s}}{10^{-2} \text{ m}} = 10 \text{ s}^{-1}.$$

Using Eq. 5.47,

$$\mu = \frac{\tau}{\dot{\gamma}} = \frac{5 \times 10^{-1} \text{ Pa}}{10 \text{ s}^{-1}} = 5 \times 10^{-2} \text{ Pa} \cdot \text{s},$$

or

$$\mu = 50 \text{ cp}.$$

The linear relation between shear stress and shear rate described by Eq. 5.47 is valid only as long as the fluid moves in layers, or lamina. A fluid that flows in this manner is said to be in *laminar flow*. This is true only at relatively low shear rate, and the pressure-velocity relationship is a function of the viscous properties of the fluid. At high shear rates, the flow pattern changes from laminar flow to *turbulent flow*, in which the fluid particles move

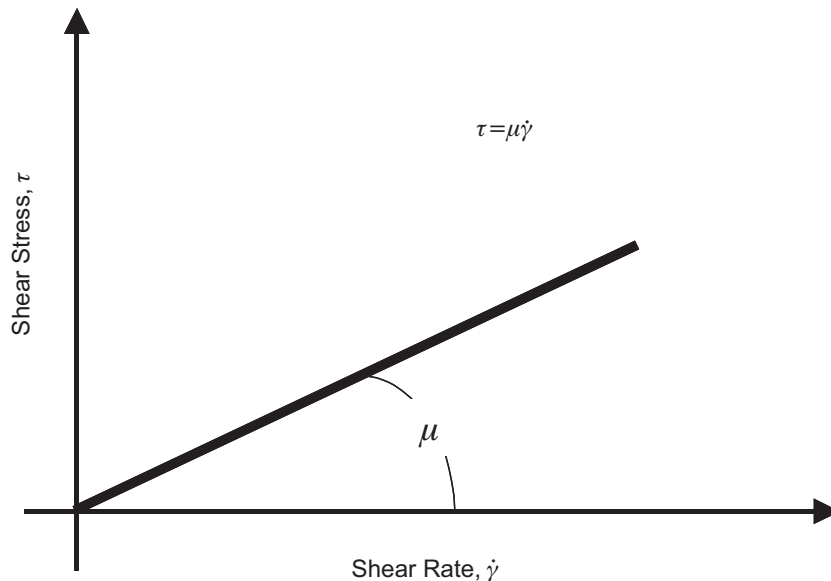


Fig. 5.14—Shear stress vs. shear rate for a Newtonian fluid [from Bourgoyne et al. (1991)].

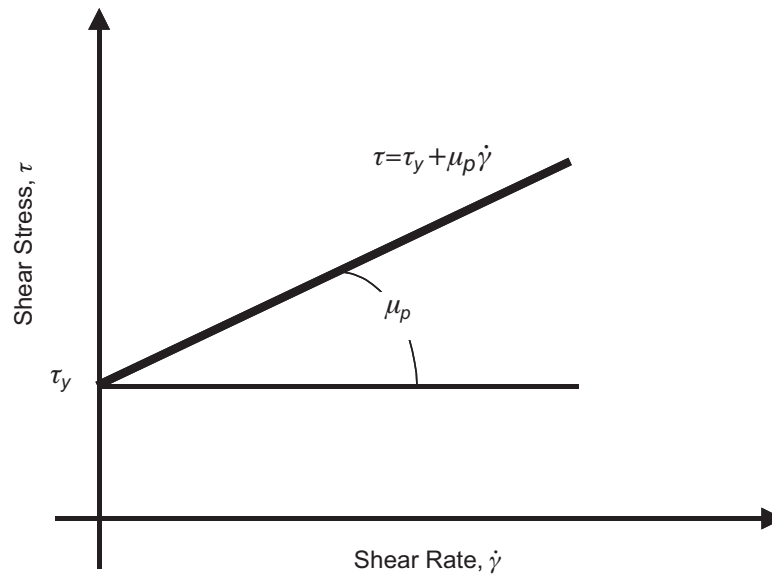


Fig. 5.15—Shear stress vs. shear rate for a Bingham plastic fluid.

downstream in a tumbling, chaotic motion so that vortices and eddies are formed in the fluid. Dye injected into the flow stream thus would be dispersed quickly throughout the entire cross section of the fluid. The turbulent flow of fluids has not been described mathematically. Thus, when turbulent flow occurs, frictional pressure drops must be determined by empirical correlations.

5.4.3 Bingham Plastic Fluids. The Bingham plastic model (Bingham 1922) is defined by

$$\tau = \tau_y + \mu_p \dot{\gamma}, \text{ where } \tau > \tau_y. \quad (5.48)$$

A graphical representation of this behavior is shown in **Fig. 5.15**.

A Bingham plastic fluid will not flow until the applied shear stress τ exceeds a certain minimum value τ_y known as the yield stress. After the yield stress has been exceeded, changes in shear stress are proportional to changes in shear rate, and the constant of proportionality is called the plastic viscosity, μ_p . Eq. 5.48 is valid only for laminar flow. Note that the units of plastic viscosity are the same as the units of Newtonian or apparent viscosity. To be consistent, the units of the yield stress τ_y must be the same as the units for shear stress τ . Thus, the yield stress has consistent units of dyne/cm². In SI units, the yield stress is expressed in N/m² or Pa. However, yield stress usually is expressed in field units of lbf/100 ft². The units can be related (at sea level) by

$$\begin{aligned} \frac{1 \text{ lbf}}{100 \text{ ft}^2} \times \frac{(453.6 \text{ g})(980.7 \text{ cm/s}^2)/\text{lbf}}{100(30.48 \text{ cm/ft})^2} &= 4.788 \text{ dyne/cm}^2, \\ &= 0.4788 \text{ Pa}. \end{aligned}$$

Example 5.15 An upper plate of 20-cm² area is spaced 1 cm above a stationary plate. Compute the yield stress and plastic viscosity of a fluid between the plates if a force of 200 dyne is required to cause any movement of the upper plate and a force of 400 dyne is required to move the upper plate at a constant velocity of 10 cm/s.

Solution. In SI units, the area A , the distance L , the forces F_1 and F_2 , and the velocity v are as follows:

$$A = \frac{20 \text{ cm}^2}{10^4 \text{ cm}^2/\text{m}^2} = 2 \times 10^{-3} \text{ m}^2,$$

$$L = \frac{1 \text{ cm}}{10^2 \text{ cm/m}} = 10^{-2} \text{ m},$$

$$F_1 = \frac{200 \text{ dyne}}{10^5 \text{ dyne/N}} = 2 \times 10^{-3} \text{ N},$$

$$F_2 = \frac{400 \text{ dyne}}{10^5 \text{ dyne/N}} = 4 \times 10^{-3} \text{ N},$$

$$v = \frac{10 \text{ cm/s}}{10^2 \text{ cm/m}} = 10^{-1} \text{ m/s}.$$

The yield stress τ_y is given by Eq. 5.48 with $\dot{\gamma} = 0$:

$$\tau_y = \tau = \frac{2 \times 10^{-3} \text{ N}}{2 \times 10^{-3} \text{ m}^2} = 1 \text{ Pa}.$$

In field units,

$$\tau_y = \tau = \frac{1}{0.479} = 2.09 \text{ lbf/100 ft}^2.$$

The plastic viscosity μ_p is given by Eq. 5.48, with $\dot{\gamma}$ given by

$$\dot{\gamma} = \frac{10^{-1} \text{ m/s}}{10^{-2} \text{ m}} = 10 \text{ s}^{-1}.$$

Thus, μ_p is given by

$$\mu_p = \frac{2-1}{10} = 0.1 \text{ N} \cdot \text{s/m}^2 = 0.1 \text{ Pa} \cdot \text{s},$$

or

$$\mu_p = 100 \text{ cp}.$$

5.4.4 Power-Law Fluids. The power-law model (Ostwald 1925) is defined by

$$\tau = K \dot{\gamma}^n. \quad \dots\dots\dots (5.49)$$

A graphical representation of the model is shown in **Fig. 5.16**.

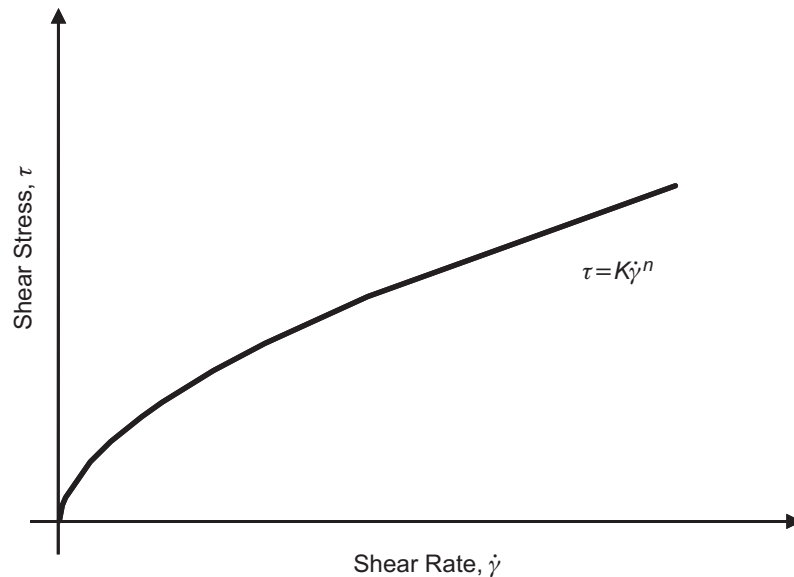


Fig. 5.16—Shear stress vs. shear rate for a pseudoplastic power-law fluid.

Like the Bingham plastic model, the power-law model requires two parameters for fluid characterization. However, the power-law model can be used to represent a pseudoplastic fluid ($n < 1$), a Newtonian fluid ($n = 1$), or a dilatant fluid ($n > 1$). Eq. 5.49 is valid only for laminar flow.

The parameter K usually is called the *consistency index* of the fluid, and the parameter n usually is called either the power-law exponent or the *flow behavior index*. The deviation of the dimensionless flow behavior index from unity characterizes the degree to which the fluid behavior is non-Newtonian. The units of the consistency index K depend on the value of n . K has units of $\text{dyne}\cdot\text{s}^n/\text{cm}^2$ or $\text{g}/\text{cm}\cdot\text{s}^{2-n}$. In SI units, the consistency index is expressed in $\text{N}\cdot\text{s}^n/\text{m}^2$ or $\text{Pa}\cdot\text{s}^n$. In this text, a unit called the equivalent centipoise (eq cp) will be used to represent $0.01 \text{ dyne}\cdot\text{s}^n/\text{cm}^2$. Occasionally, the consistency index is expressed in units of $\text{lbf}\cdot\text{sec}^n/\text{ft}^2$. The units of the consistency index can be related (at sea level) by

$$1 \frac{\text{lbf}\cdot\text{sec}^n}{\text{ft}^2} \times \frac{(453.6 \text{ g})(980.7 \text{ cm/s}^2)/\text{lbf}}{(30.48 \text{ cm/ft})^2} = 478.83 \text{ dyne}\cdot\text{s}^n/\text{cm}^2,$$

$$= 47.883 \text{ Pa}\cdot\text{s}^n = 47,883 \text{ eq cp}.$$

Example 5.16 An upper plate of 20 cm^2 is spaced 1 cm above a stationary plate. Compute the consistency index and flow behavior index if a force of 50 dyne is required to move the upper plate at a constant velocity of 4 cm/s and a force of 100 dyne is required to move the upper plate at a constant velocity of 10 cm/s .

Solution. In SI units, the area A , the distance L , the forces F_1 and F_2 , and the velocities v_1 and v_2 are as follows:

$$A = \frac{20 \text{ cm}^2}{10^4 \text{ cm}^2/\text{m}^2} = 2 \times 10^{-3} \text{ m}^2,$$

$$L = \frac{1 \text{ cm}}{10^2 \text{ cm/m}} = 10^{-2} \text{ m},$$

$$F_1 = \frac{50 \text{ dyne}}{10^5 \text{ dyne/N}} = 5 \times 10^{-4} \text{ N},$$

$$F_2 = \frac{100 \text{ dyne}}{10^5 \text{ dyne/N}} = 10^{-3} \text{ N},$$

$$v_1 = \frac{4 \text{ cm/s}}{10^2 \text{ cm/m}} = 4 \times 10^{-2} \text{ m/s},$$

$$v_2 = \frac{10 \text{ cm/s}}{10^2 \text{ cm/m}} = 10^{-1} \text{ m/s}.$$

Application of Eq. 5.49 at the two rates of shear observed yields the following system of two equations:

$$\begin{cases} \frac{5 \times 10^{-4}}{2 \times 10^{-3}} = K \left(\frac{4 \times 10^{-2}}{10^{-2}} \right)^n \\ \frac{10^{-3}}{2 \times 10^{-3}} = K \left(\frac{10^{-1}}{10^{-2}} \right)^n \end{cases}$$

Dividing the second equation by the first gives

$$\frac{10^{-3}}{5 \times 10^{-4}} = \left(\frac{10^{-1}}{4 \times 10^{-2}} \right)^n.$$

Taking the log of both sides and solving for n yields

$$n = \frac{\log\left(\frac{10^{-3}}{5 \times 10^{-4}}\right)}{\log\left(\frac{10^{-1}}{4 \times 10^{-2}}\right)} = \frac{\log(2)}{\log(5/2)} = 0.756.$$

Substituting this value of n in the first equation of the above system yields

$$K = \frac{5 \times 10^{-1}}{2 \times (4)^{0.756}} = 0.08765 \frac{\text{N} \cdot \text{s}^{0.756}}{\text{m}^2} = 0.8765 \frac{\text{dyne} \cdot \text{s}^{0.756}}{\text{cm}^2},$$

or

$$K = 87.65 \text{ eq cp.}$$

5.4.5 Herschel-Bulkley Fluids. The Herschel-Bulkley model (Herschel and Bulkley 1926) is defined by

$$\tau = \tau_y + K\dot{\gamma}^n, \text{ where } \tau > \tau_y. \quad (5.50)$$

A graphical representation of the model is shown in **Fig. 5.17**. The model combines the characteristics of the Bingham and power-law models and requires three parameters for fluid characterization. The Herschel-Bulkley model can be used to represent a yield-pseudoplastic fluid ($n < 1$), a dilatant fluid ($n > 1$), a pseudoplastic fluid ($\tau_y = 0$, $n < 1$), a plastic fluid ($n = 1$), or a Newtonian fluid ($\tau_y = 0$, $n = 1$). Eq. 5.50 is valid only for laminar flow.

Like the Bingham plastic model, a fluid represented by this model will not flow until the applied shear stress τ exceeds a minimum value τ_y , which is called the *yield stress*. The fluid behaves like a solid until the applied force is high enough to exceed the yield stress. Thus, the yield stress has consistent units of dyne/cm². In SI units, the yield stress is expressed in N/m² or Pa. However, yield stress usually is expressed in field units of lbf/100 ft². The parameter K is called the *consistency index* of the fluid, and the parameter n usually is called the *flow behavior index*. The deviation from unity of the dimensionless flow behavior index characterizes the degree to which the behavior of the fluid is non-Newtonian. Like the power-law model, the units of the parameter K depend on the value of n . K has units of dyne·s ^{n} /cm² or g/cm·s^{2- n} . In SI

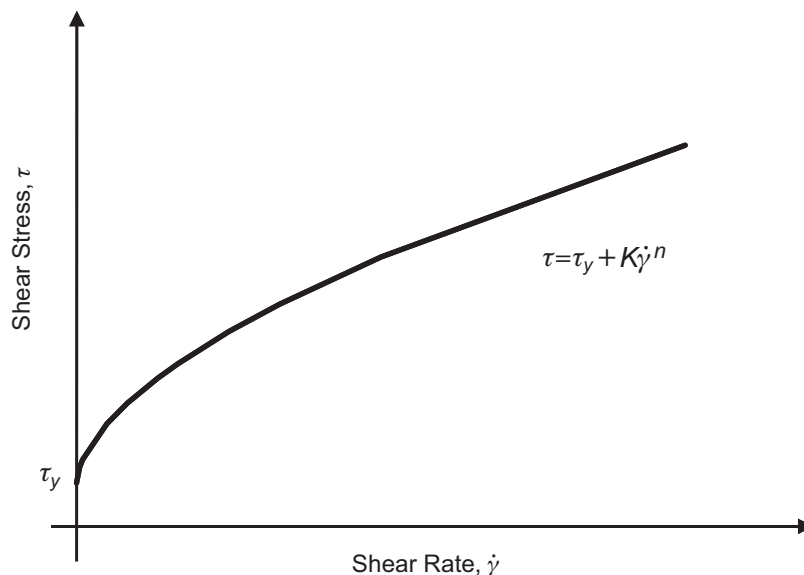


Fig. 5.17—Shear stress vs. shear rate for a yield-pseudoplastic Herschel-Bulkley fluid.

units, the consistency index is expressed in $\text{N}\cdot\text{s}^n/\text{m}^2$ or $\text{Pa}\cdot\text{s}^n$. In this text, a unit called the equivalent centipoise (eq cp) will be used to represent $0.01 \text{ dyne}\cdot\text{s}^n/\text{cm}^2$. Occasionally, the consistency index is expressed in units of $\text{lbf}\cdot\text{sec}^n/\text{ft}^2$.

Example 5.17 An upper plate of 20 cm^2 is spaced 1 cm above a stationary plate. Compute the three rheological parameters of the Herschel-Bulkley model if a force of 60 dyne is required to move the upper plate at a constant velocity of 5 cm/s , a force of 130 dyne is required to move the upper plate at a constant velocity of 12 cm/s , and a force of 250 dyne is required to move the upper plate at a constant velocity of 25 cm/s .

Solution. In SI units, the area A , the distance L , the forces F_1 , F_2 , and F_3 , and the velocities v_1 , v_2 , and v_3 are as follows:

$$A = \frac{20 \text{ cm}^2}{10^4 \text{ cm}^2/\text{m}^2} = 2 \times 10^{-3} \text{ m}^2,$$

$$L = \frac{1 \text{ cm}}{10^2 \text{ cm/m}} = 10^{-2} \text{ m},$$

$$F_1 = \frac{60 \text{ dyne}}{10^5 \text{ dyne/N}} = 6 \times 10^{-4} \text{ N},$$

$$F_2 = \frac{130 \text{ dyne}}{10^5 \text{ dyne/N}} = 1.3 \times 10^{-3} \text{ N},$$

$$F_3 = \frac{250 \text{ dyne}}{10^5 \text{ dyne/N}} = 2.5 \times 10^{-3} \text{ N},$$

$$v_1 = \frac{5 \text{ cm/s}}{10^2 \text{ cm/m}} = 5 \times 10^{-2} \text{ m/s},$$

$$v_2 = \frac{12 \text{ cm/s}}{10^2 \text{ cm/m}} = 1.2 \times 10^{-1} \text{ m/s},$$

$$v_3 = \frac{25 \text{ cm/s}}{10^2 \text{ cm/m}} = 2.5 \times 10^{-1} \text{ m/s}.$$

Application of Eq. 5.50 at the three rates of shear observed yields the following system of three equations:

$$\begin{cases} \frac{6 \times 10^{-4}}{2 \times 10^{-3}} = \tau_y + K \left(\frac{5 \times 10^{-2}}{10^{-2}} \right)^n \\ \frac{1.3 \times 10^{-3}}{2 \times 10^{-3}} = \tau_y + K \left(\frac{1.2 \times 10^{-1}}{10^{-2}} \right)^n \\ \frac{2.5 \times 10^{-3}}{2 \times 10^{-3}} = \tau_y + K \left(\frac{2.5 \times 10^{-1}}{10^{-2}} \right)^n \end{cases}.$$

Solving the equations system yields

$$\tau_y = 0.007 \text{ Pa} = 0.0146 \text{ lbf per } 100 \text{ ft}^2$$

$$K = 0.06903 \frac{\text{N}\cdot\text{s}^{0.898}}{\text{m}^2} = 0.6903 \frac{\text{dyne}\cdot\text{s}^{0.898}}{\text{cm}^2} = 69.03 \text{ eq cp}$$

$$n = 0.898$$

Generally, the rheological parameters that characterize a model are determined by using analytical equations based on a data set of measurements from the rotational viscometer, as reported by the API 13 standards. However, to improve the accuracy of the calculation on the rheological parameters, statistical regression methods are used. They are applied to the complete set $(\tau, \dot{\gamma})$ of measurements performed on a sample of the fluid in the rotational viscometer. Outcomes are a higher accuracy in determining the rheological parameters that characterize the behavior of the tested fluid, and as a consequence a better evaluation of flow parameters such as velocity profile, flow regime, and pressure drop.

Merlo et al. (1995) presented a hydraulic computation model based on the Herschel-Bulkley rheological fluid model. They treated the annulus as a slot and considered also the temperature and pressure influence on drilling hydraulics. Field test circulation results were obtained for 17.5- and 12.25-in. openhole sections at various depths while measuring the rheology of mud. Predictions were made by computing pressure drop using one of the three rheological models [i.e., Bingham plastic—American Petroleum Institute (API) 13 (600 and 300 rev/min readings), power-law—API 13 (600 and 300 rev/min readings), and Herschel-Bulkley based on regression of all six rheological data points]. Their results, presented in tabular form, are represented here graphically.

The authors state that the Herschel-Bulkley rheological model, with parameters derived through regression analysis, gave the best fit to their rheological data and to the pressure-drop data. The errors in predicting the pressure drop and comparing to measurements using the Herschel-Bulkley model were smaller than the errors when using the two-speed models for Bingham plastic and power-law fluids, although the differences, seen in Fig. 5.18, were not that great.

5.4.6 Other Rheological Models. The behavior of drilling fluids and cement slurries also can be simulated by other rheological models. The most used in the practice are the Casson model, for plastic fluids, and the Robertson-Stiff model, for yield-pseudoplastic fluids.

Casson Fluids. The Casson model (Casson 1959) is often used to simulate drilling fluids and cement slurries with plastic behavior, with a higher accuracy than the Bingham plastic model. The model is defined by

$$\sqrt{\tau} = \sqrt{\tau_y} + \sqrt{\mu_p} \sqrt{\dot{\gamma}} \quad \dots \dots \dots (5.51)$$

Eq. 5.51 is valid only for laminar flow. Generally, the model is plotted with coordinates $(\sqrt{\tau}, \sqrt{\dot{\gamma}})$ instead of $(\tau, \dot{\gamma})$ to still maintain the linear trend. A graphical representation is shown in Fig. 5.19.

Like the Bingham plastic model, the Casson model requires two parameters for fluid characterization. A fluid represented by this model requires a finite shear stress, τ_y , below which it will not flow. Above this finite shear stress, referred to as the *yield stress*, changes in shear stress are proportional to changes in shear rate, and the constant of proportionality is called the plastic viscosity, μ_p . Note that the units of plastic viscosity are the same as the units of Newtonian or apparent viscosity. The yield stress has units of dyne/cm². In SI units, the yield stress is expressed in N/m² or Pa. However, yield stress usually is expressed in field units of lbf/100 ft².

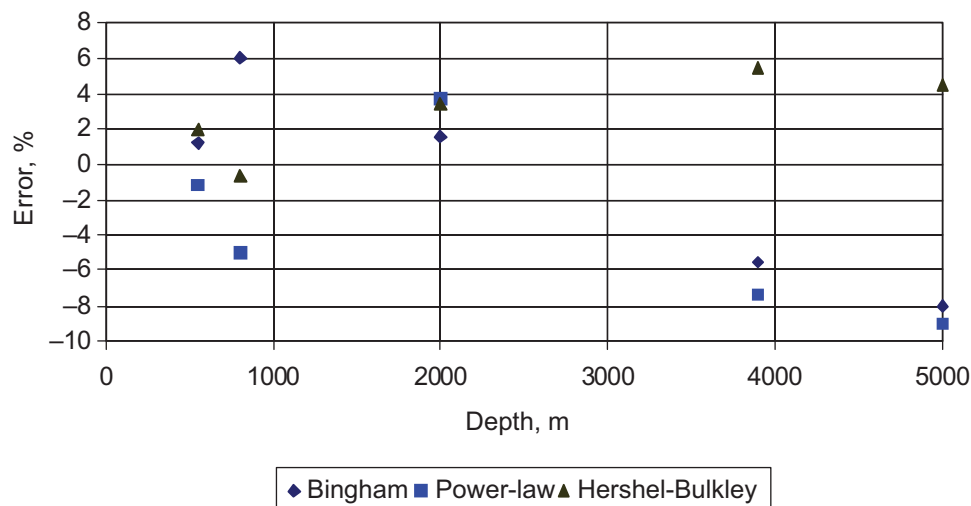


Fig. 5.18—Comparison of Merlo et al. (1995) pressure-drop predictions with their field data.

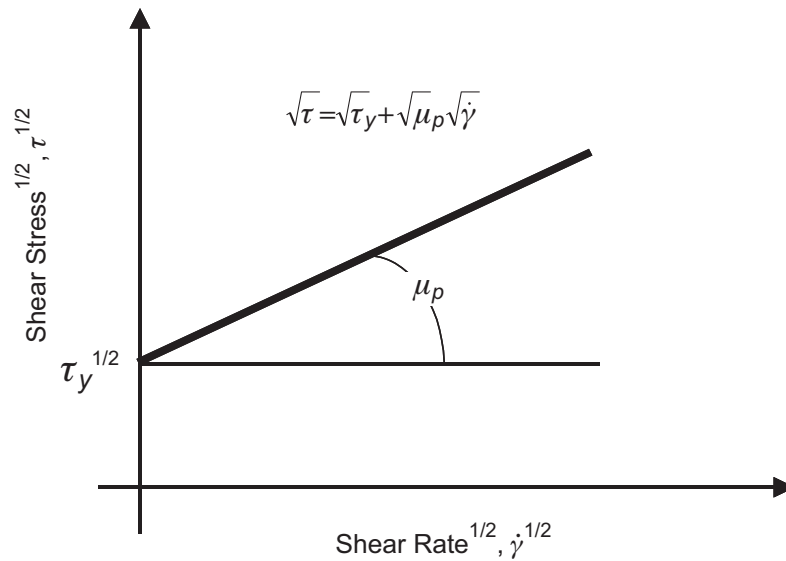


Fig. 5.19—Shear stress vs. shear rate for a Casson fluid.

Example 5.18 An upper plate of 20-cm² area is spaced 1 cm above a stationary plate. Compute the yield stress and plastic viscosity of a fluid between the plates, as seen for Example 5.15, if a force of 200 dyne is required to cause any movement of the upper plate and a force of 400 dyne is required to move the upper plate at a constant velocity of 10 cm/s.

Solution. In SI units, the area A , the distance L , the forces F_1 and F_2 , and the velocity v are the same as in Example 5.15. The yield stress τ_y is given by Eq. 5.51 with $\dot{\gamma} = 0$:

$$\tau_y = \tau = \frac{2 \times 10^{-3} \text{ N}}{2 \times 10^{-3} \text{ m}^2} = 1 \text{ Pa}.$$

In field units,

$$\tau_y = \tau = \frac{1}{0.479} = 2.09 \text{ lbf} / 100 \text{ ft}^2.$$

The plastic viscosity μ_p is given by Eq. 5.51, with $\dot{\gamma}$ given by

$$\dot{\gamma} = \frac{10^{-1} \text{ m/s}}{10^{-2} \text{ m}} = 10 \text{ s}^{-1}.$$

Thus, μ_p is given by

$$\mu_p = \frac{(\sqrt{2} - \sqrt{1})^2}{10} = 0.0171 \text{ N} \cdot \text{s} / \text{m}^2 = 0.0171 \text{ Pa} \cdot \text{s},$$

or

$$\mu_p = 17.1 \text{ cp}.$$

It can be seen that the yield stress calculated by the Casson model is less than that observed with the Bingham plastic model. The plastic viscosity changes according to the model, and here it decreases substantially compared to that calculated by Bingham model.

Robertson-Stiff Fluids. The Robertson-Stiff model (Robertson and Stiff 1976) adequately describes the behavior of yield-pseudoplastic fluids, even though slightly less accurately than the Herschel-Bulkley model. The model is defined by

$$\tau = A(\dot{\gamma} + C)^B. \quad \dots \dots \dots (5.52)$$

Graphical representation of the model is similar to that for the Herschel-Bulkley model. Eq. 5.52 can describe the behavior of yield-pseudoplastic fluids, pseudoplastic fluids ($C = 0$), and Newtonian fluids ($B = 1$, $C = 0$). Eq. 5.52 is valid only for laminar flow. Fluids represented by the Robertson-Stiff model exhibit a yield stress once the flow is initiated. The yield stress is given by AC^B . A , B , and C are constants of the model. The units of the constant A depend on the value of the constant B . A has units of $\text{dyne}\cdot\text{s}^B/\text{cm}^2$ or $\text{g}/\text{cm}\cdot\text{s}^{2-B}$. In SI units, the constant A is expressed in $\text{N}\cdot\text{s}^B/\text{m}^2$ or $\text{Pa}\cdot\text{s}^B$. The constant B is dimensionless, and the units of the constant C are s^{-1} . In this text, a unit called the equivalent centipoise (eq cp) will be used to represent $0.01 \text{ dyne}\cdot\text{s}^B/\text{cm}^2$.

Example 5.19 An upper plate of 20 cm^2 is spaced 1 cm above a stationary plate. Compute the three rheological parameters of the Robertson-Stiff model and the yield stress if a force of 60 dyne is required to move the upper plate at a constant velocity of 5 cm/s , a force of 130 dyne is required to move the upper plate at a constant velocity of 12 cm/s , and a force of 250 dyne is required to move the upper plate at a constant velocity of 25 cm/s .

Solution. In SI units, the area A , the distance L , the forces F_1 , F_2 , and F_3 ; and the velocities v_1 , v_2 , and v_3 are the same as Example 5.17. Application of Eq. 5.52 at the three rates of shear observed yields the following system of three equations:

$$\begin{cases} \frac{6 \times 10^{-4}}{2 \times 10^{-3}} = A \left(\frac{5 \times 10^{-2}}{10^{-2}} + C \right)^B \\ \frac{1.3 \times 10^{-3}}{2 \times 10^{-3}} = A \left(\frac{1.2 \times 10^{-1}}{10^{-2}} + C \right)^B \\ \frac{2.5 \times 10^{-3}}{2 \times 10^{-3}} = A \left(\frac{2.5 \times 10^{-1}}{10^{-2}} + C \right)^B \end{cases}$$

Solving the equations system yields

$$A = 0.06930 \frac{\text{N}\cdot\text{s}^{0.898}}{\text{m}^2} = 0.6930 \frac{\text{dyne}\cdot\text{s}^{0.898}}{\text{cm}^2} = 69.30 \text{ eq cp}$$

$$B = 0.897$$

$$C = 0.12 \text{ s}^{-1}$$

Thus, τ_y is given by

$$\tau_y = AC^B = 0.06930 \times 0.12^{0.897} = 0.0103 \text{ Pa},$$

or

$$\tau_y = 0.0215 \text{ lbf}/100 \text{ ft}^2.$$

The values of parameters A and B are comparable with the consistency index and the flow behavior index of the Herschel-Bulkley model, respectively. The yield stress τ_y determined with the Robertson-Stiff model is slightly higher (+32.0%), but still comparable.

Advanced Models. In addition to the models previously reported, there are many other empirical mathematical descriptions that can describe with high accuracy the behavior of the viscous forces of drilling fluids and cement slurries.

Very often the models have been developed to predict the properties of fluids not properly related to drilling operations, such as polymer solutions, suspensions, and blood. However, they also can be applied successfully to the flow of drilling fluids and cement slurries. They can be classified according to the number of constant parameters that the mathematical description contains. Generally, the higher the number of parameters that characterize the model, the better the approximation of the model to the fluid behavior, but the complexity of the

flow equations becomes higher. Generally, the rheological parameters of these models are determined by non-linear regression techniques, and in very few cases analytical solutions can be available. The equations are valid only for laminar flow.

Three-Parameter Models. These models require three constant parameters for fluid characterization. The Graves-Collins model (Graves and Collins 1978) is defined by

$$\tau = (1 - e^{-\beta \dot{\gamma}})(\tau_0 + \mu \dot{\gamma}). \quad (5.53)$$

The constant parameters of the model are τ_0 , μ , and β . The model can approximate with good accuracy pseudo-plastic fluids at low shear rates and plastic fluids at high shear rates.

The Gucuyener model (Gucuyener 1983) is defined by

$$\tau^{1/m} = \tau_y^{1/m} + \eta \dot{\gamma}^{1/2}. \quad (5.54)$$

The constant parameters of the model are τ_y , η , and m . The model predicts the behavior of yield-pseudoplastic fluids. In addition, it can be used to represent pseudoplastic fluids ($\tau_y = 0$), plastic fluids ($m = 2$), and Newtonian fluids ($\tau_y = 0$, $m = 2$).

The Sisko model (Sisko 1958) is defined by

$$\tau = a \dot{\gamma} + b \dot{\gamma}^c. \quad (5.55)$$

The constant parameters of the model are a , b , and c . The model can describe the behavior of pseudoplastic fluids ($a = 0$), and Newtonian fluids ($b = 0$).

Four-Parameter Models. These models require four constant parameters for fluid characterization. The Shulman model (Shulman 1968) is defined by

$$\tau^{1/n} = \tau_0^{1/n} + (\eta \dot{\gamma})^{1/m}. \quad (5.56)$$

The constant parameters of the model are τ_0 , η , n , and m . The model approximates with high accuracy the properties of yield-pseudoplastic fluids ($n = 1$), pseudoplastic fluids ($\tau_0 = 0$, $n = 1$), plastic fluids ($n = m = 1$ for Bingham plastic fluids, and $n = m = 2$ for Casson fluids), and Newtonian fluids ($\tau_0 = 0$, $n = m = 1$).

The Zhu model (Zhu et al. 2005) is defined by

$$\tau = \tau_0 (1 - e^{-m \dot{\gamma}}) + \eta_1 e^{-t_1 \dot{\gamma}} \dot{\gamma}. \quad (5.57)$$

The constant parameters of the model are τ_0 , η_1 , m , and t_1 . The model can approximate with high accuracy the behavior of yield-pseudoplastic fluids.

Five-Parameter Models. These models require five constant parameters for fluid characterization. The Maglione model (Maglione and Romagnoli 1999a) is defined by

$$\tau^{1/n} = a^{1/n} + (b \dot{\gamma})^{1/m} + (c \dot{\gamma})^{\frac{1}{m}+1}. \quad (5.58)$$

The five constant parameters of the model are a , b , c , n , and m . The parameter a is the yield stress, parameters b and c are related to the fluid viscosity, and n and m are related to the flow behavior index of the fluid. The model approximates with high accuracy the properties of yield-pseudoplastic fluids ($c = 0$, $n = 1$), pseudoplastic fluids ($a = c = 0$, $n = 1$), plastic fluids ($c = 0$ and $n = m = 1$ for Bingham plastic fluids, $c = 0$ and $n = m = 2$ for Casson fluids), and Newtonian fluids ($a = c = 0$, $n = m = 1$).

5.5 Laminar Flow in Pipes and Annuli

The drilling engineer deals primarily with the flow of drilling fluids and cements down the circular bore of the drillstring and up the circular annular space between the drillstring and the casing or open hole. If the pump rate is low enough for the flow to be laminar, the Newtonian, Bingham plastic, or power-law model can be employed to develop the mathematical relation between flow rate and frictional pressure drop. In this development, these simplifying assumptions are made:

- The drillstring is placed concentrically in the casing or open hole.
- The drillstring is not being rotated.
- Sections of open hole are circular in shape and of known diameter.
- The drilling fluid is incompressible.
- The flow is isothermal.
- The flow is 1D.

In reality, none of these assumptions are completely valid, and the resulting system of equations will not describe perfectly the laminar flow of drilling fluids in the well. In addition, the student should keep in mind that the Newtonian, Bingham plastic, and power-law fluid rheological models do not take into account the thixotropic nature of drilling mud and only approximate the actual laminar-flow fluid behavior. Significant research has been conducted on the effect of pipe eccentricity (Luo and Peden 1990; Hacıislamoglu and Laglinois 1990; Nouri and Whitelaw 1997; Uner et al. 1989), pipe rotation (Nouri and Whitelaw 1997; Escudier et al. 2000, 2002), and temperature and pressure variations (Annis 1967; Butts 1972; Merlo et al. 1995) on flowing pressure gradients. State-of-the-art simulators have been developed by many companies that allow numerical computation of velocity profiles and estimation of pressure losses, taking into account the many factors influencing flow of fluids in pipes and annuli (Peng et al. 2003), while with the advent of pressure-while-drilling (PWD) tools, fine tuning of the sophisticated simulators can be done on site (Charlez et al. 1998).

5.5.1. Shear Stress in Laminar Flow. Fluid flowing in a pipe or a concentric annulus does not have a uniform velocity. If the flow pattern is laminar, the fluid velocity immediately adjacent to the pipe walls will be zero, and the fluid velocity in the region most distant from the pipe walls will be a maximum. Typical flow velocity profiles for a laminar flow pattern are shown in **Fig. 5.20**.

Cylindrical Pipe Flow. As shown in this figure, concentric rings of fluid lamina are telescoping down the conduit at different velocities. Pipe flow differs from annular flow because annular flow has a zero velocity boundary condition at the inner pipe radius, r_1 , while pipe flow has zero velocity specified only at the outer radius r_2 .

A relation between radius r , shear stress τ , and frictional pressure gradient dp_f/ds can be obtained from a consideration of Newton's law of motion for a shell of fluid with radius r . Before proceeding, a presentation of the formulation for the shear stress sign convention becomes necessary to develop the appropriate mathematical equations properly. For flow in pipes, only one wall is present and the velocity gradient is positive everywhere (Fig. 5.20a). For flow in an annulus (or a slot), two walls are present, the inner-cylinder wall and the outer-cylinder wall. Close to the inner cylinder, the velocity gradient is positive ($dv/dr > 0$), while close to the outer wall, the velocity gradient is negative ($dv/dr < 0$) (Fig. 5.20b). This fact may create confusion about the proper sign to be used for the developed shear stresses in the two areas of the flow section, and the following analysis and the approach in the rest of the chapter attempt to provide a consistent method to be used.

For a fluid in motion and in contact with a solid surface (**Fig. 5.21**), we always define

$$\tau_{xy} = \mu \frac{dv}{dy}, \quad \dots \dots \dots (5.59)$$

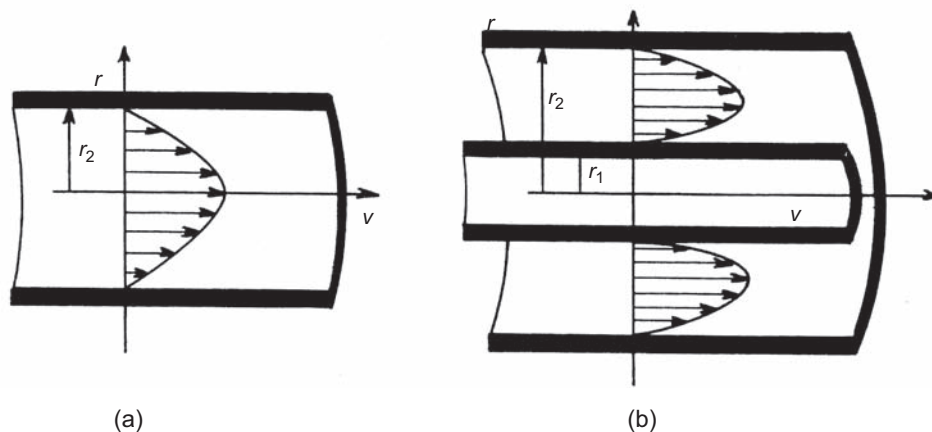


Fig. 5.20—Velocity profiles for laminar flow: (a) pipe flow and (b) annular flow [from Bourgoyne et al. (1991)].

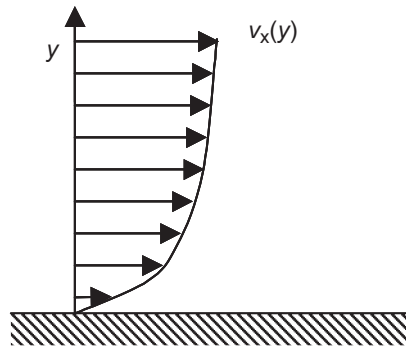


Fig. 5.21—Velocity profile for fluid flowing over a solid surface.

with y the distance from the wall. The direction of the shear stress is defined, by convention, as positive when the outward normal to the surface and the shear stress both act in the same direction. For example, the shear stresses shown in Fig. 5.22 are all positive.

We now examine shear stress distribution in cylindrical coordinates. Shown in Fig. 5.23 is a free-body diagram of a shell of fluid of length Δs and of thickness Δr . The shear stresses are drawn as per the sign convention defined above. Thus, the shear stresses at r and at $r + \Delta r$ are both positive.

The force F_1 applied by the fluid pressure at Point 1 is given by

$$F_1 = p_1 (2\pi r) \Delta r.$$

Likewise, the force F_2 applied by the fluid pressure at Point 2 is given by

$$F_2 = p_2 (2\pi r \Delta r) = \left(p_1 - \frac{dp_f}{ds} \Delta s \right) (2\pi r \Delta r).$$

The negative sign for the dp_f/ds term is required because the frictional pressure change is negative. The frictional force exerted at point r is given by

$$F_3 = \tau 2\pi r \big|_r \Delta s.$$

Similarly, the frictional force exerted at point $r + \Delta r$ is given by

$$F_4 = \tau 2\pi r \big|_{r+\Delta r} \Delta s.$$

If the fluid element is moving at a constant velocity, the sum of the forces acting on the elements must equal zero. Summing forces, we obtain

$$F_1 - F_2 - F_3 + F_4 = 0,$$

or

$$(2\pi r \Delta r) p_1 - (2\pi r \Delta r) \left(p_1 - \frac{dp_f}{ds} \Delta s \right) - \tau 2\pi r \big|_r \Delta s + \tau 2\pi r \big|_{r+\Delta r} \Delta s = 0.$$

Expanding this equation, dividing through by $(2\pi r \Delta r \Delta s)$, and taking the limit as $\Delta r \rightarrow 0$ yields

$$\frac{dp_f}{ds} + \frac{1}{r} \frac{d(\tau r)}{dr} = 0. \quad \dots \dots \dots (5.60)$$

Because dp_f/ds is not a function of r , Eq. 5.60 can be integrated with respect to r . Separating variables and integrating yields

$$\tau = -\frac{r}{2} \frac{dp_f}{ds} + \frac{C_1}{r}, \quad \dots \dots \dots (5.61)$$

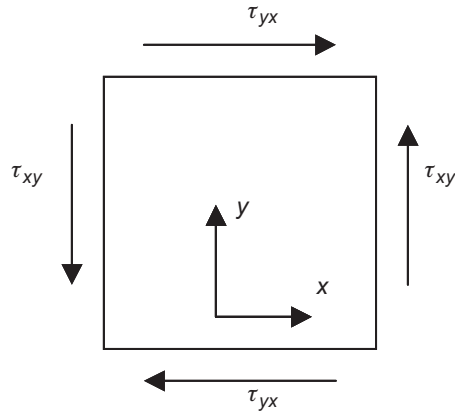


Fig. 5.22—Positive shear stresses acting on a fluid element.

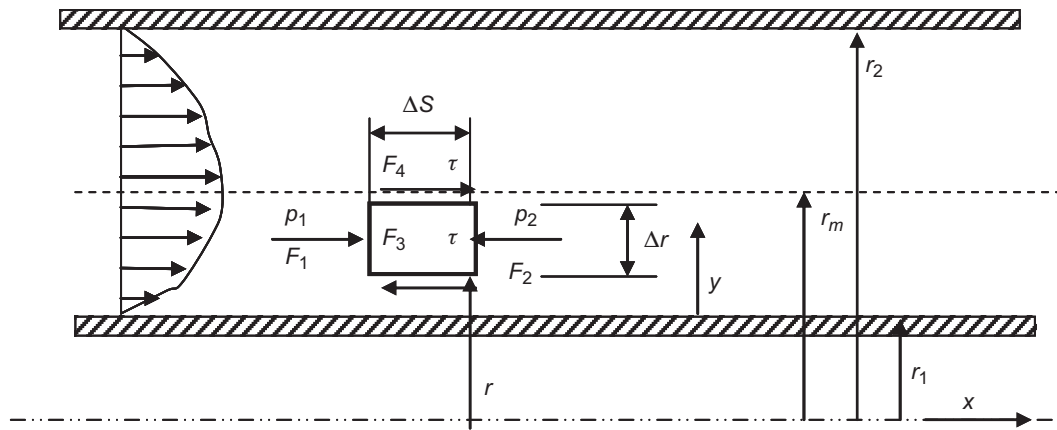


Fig. 5.23—Flow in a cylindrical annulus.

where C_1 is the constant of integration. Eq. 5.61, which relates shear stress and frictional pressure gradient at a given radius, is a consequence of the geometry of the system and does not require any assumption about a fluid rheological model. For pipe flow, the constant C_1 must be zero if the shear stress is not to be infinite at $r = 0$.

The shear rate $\dot{\gamma}$ for the sign convention used is given by

$$\dot{\gamma} = \frac{dv}{dr} \quad \dots \dots \dots (5.62)$$

The shear rate can be related to shear stress using the defining equation for the Newtonian, Bingham plastic, power-law, Herschel-Bulkley, or any other fluid model.

Representing the Annulus as a Slot. Annular flow also can be approximated using equations developed for flow through rectangular slots. The slot flow equations are much simpler to use and are reasonably accurate as long as the ratio $r_p/r_w > 0.3$, where r_p is the outside radius of the pipe and r_w is the wellbore radius. This minimum ratio almost always is exceeded in rotary drilling applications. As shown in Fig. 5.24, an annular space can be represented as a narrow slot having an area A , width w , and height h , given by

$$A = wh = \pi(r_w^2 - r_p^2) \quad \dots \dots \dots (5.63a)$$

and

$$h = r_w - r_p \quad \dots \dots \dots (5.63b)$$

The relation between shear stress and frictional pressure gradient for a slot can be obtained from a consideration of the pressure and viscous forces acting on an element of fluid in the slot (Fig. 5.25).

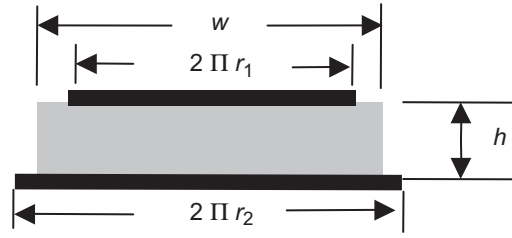


Fig. 5.24—Representing the annulus as a slot [from Bourgoyne et al. (1991)].

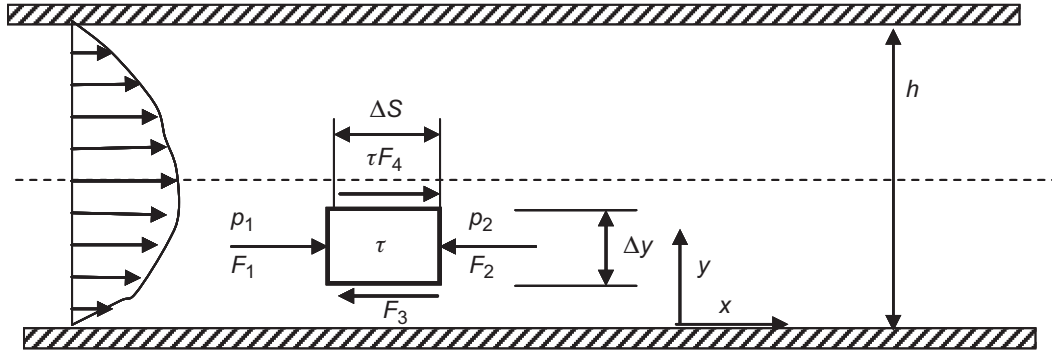


Fig. 5.25—Free-body diagram for fluid element in a narrow slot [from Bourgoyne et al. (1991)].

If we consider an element of fluid having width w and thickness Δy , the forces on the fluid element are drawn as per the sign convention for the shear stresses mentioned above. The force F_1 applied by the fluid pressure at Point 1 is given by

$$F_1 = p_1 w \Delta y.$$

Likewise, the force F_2 applied by the fluid pressure at Point 2 is given by

$$F_2 = p_2 w \Delta y.$$

The frictional force exerted by the adjacent layer of fluid below the fluid element of interest is given by

$$F_3 = \tau|_y w \Delta s.$$

Similarly, the frictional force exerted by the adjacent layer of fluid above the fluid element of interest is given by

$$F_4 = \tau|_{y+\Delta y} w \Delta s.$$

If the flow is steady, the sum of the forces acting on the fluid element must be equal to zero. Summing forces, we obtain

$$F_1 - F_2 - F_3 + F_4 = 0,$$

or

$$p_1 w \Delta y - p_2 w \Delta y - \tau|_y w \Delta s + \tau|_{y+\Delta y} w \Delta s = 0.$$

Expanding this equation, dividing through by $w \Delta s \Delta y$, and letting $\Delta y \rightarrow 0$ yields

$$\frac{dp_f}{ds} + \frac{d\tau}{dy} = 0 \quad \dots\dots\dots (5.64)$$

Because dp_f/ds is not a function of y , Eq. 5.64 can be integrated with respect to y . Separating variables and integrating gives

$$\tau = -y \frac{dp_f}{ds} + \tau_0, \quad \dots\dots\dots (5.65)$$

where τ_0 is the constant of integration that corresponds to the shear stress at $y = 0$.

For the sign convention used, the shear rate is given by

$$\dot{\gamma} = \frac{dv}{dy}.$$

5.5.2 Newtonian Fluid Model. In the following development, the solution for the flow of a Newtonian fluid flowing in a concentric annulus will first be presented, followed by the solution for the flow in a pipe.

If the fluid can be described with the Newtonian fluid model, the shear stress at any point in the fluid in the annulus is given by combining the fluid model with Eq. 5.62:

$$\tau = \mu \dot{\gamma} = \mu \frac{dv}{dr}.$$

Combining this equation with Eq. 5.61, separating variables, and integrating, we obtain

$$v = -\frac{1}{4\mu} \frac{dp_f}{ds} r^2 + \frac{C_1}{\mu} \ln r + C_2, \quad \dots\dots\dots (5.66)$$

where C_1 and C_2 are the constants of integration.

Pipe Flow. The simplest case is pipe flow. We already know that C_1 is zero. The drilling fluid wets the pipe wall, and the fluid layer immediately adjacent to the pipe inside wall ($r = R$) has a velocity of zero. Thus, for pipe flow,

$$v = \frac{1}{4\mu} \frac{dp_f}{ds} (R^2 - r^2). \quad \dots\dots\dots (5.67)$$

For flow of Newtonian fluid in a pipe, the shear stress is given by

$$\tau = \mu \frac{dv}{dr} = -\frac{r}{2} \frac{dp_f}{ds},$$

which is consistent with Eq. 5.61. The velocity profile and the shear stress profile for flow of a Newtonian fluid in a pipe are depicted in **Fig. 5.26**. If the pressure gradient and viscosity are known, Eq. 5.67 can be used to determine the velocity distribution in the pipe. However, a relationship between pressure gradient and total flow rate is needed for most engineering applications. For flow in a pipe, the total flow rate is given by integrating the velocity profile (Eq. 5.67) over the cross-sectional area:

$$q = \int_0^R (v)(2\pi r) dr = \frac{\pi R^4}{8\mu} \frac{dp_f}{ds} \quad \dots\dots\dots (5.68)$$

The flow rate is given in terms of the mean velocity \bar{v} by

$$q = \pi R^2 \bar{v}. \quad \dots\dots\dots (5.69)$$

Combination of Eq. 5.68 and Eq. 5.69 yields

$$\frac{dp_f}{ds} = \frac{8\mu \bar{v}}{R^2}. \quad \dots\dots\dots (5.70a)$$

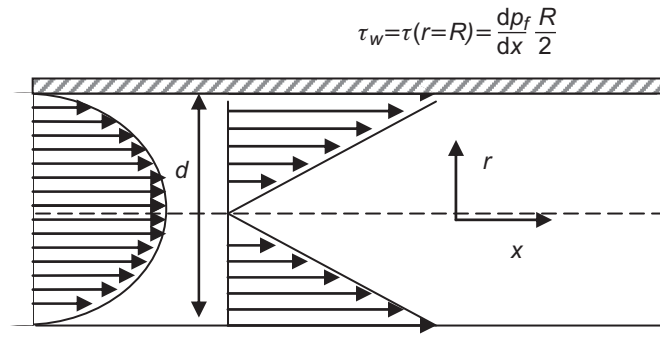


Fig. 5.26—Velocity and shear stress profiles for flow of Newtonian fluid in a pipe.

Expressing Eq. 5.70a in terms of field units gives

$$\frac{dp_f}{ds} = \frac{\mu \bar{v}}{6,000 R^2} \quad (5.70b)$$

Annular Flow. For flow in an annulus, the drilling fluid wets both pipe walls, and the fluid layers immediately adjacent to the pipe walls (at $r = r_p$ and at $r = r_w$) have a velocity of zero. Using these boundary conditions in Eq. 5.66 yields, for the two constants of integration,

$$C_1 = \frac{1}{4} \frac{dp_f}{ds} \frac{(r_w^2 - r_p^2)}{\ln(r_w/r_p)},$$

$$C_2 = -\frac{1}{4\mu} \frac{dp_f}{ds} \frac{\ln(r_p)r_w^2 - \ln(r_w)r_p^2}{\ln(r_w/r_p)}.$$

Substituting these expressions in Eq. 5.66 yields

$$v = \frac{1}{4\mu} \left(\frac{dp_f}{ds} \right) \left[\frac{r_w^2 - r_p^2}{\ln(r_w/r_p)} \ln \frac{r}{r_w} - (r^2 - r_p^2) \right] \quad (5.71)$$

The shear stress for the flow in an annulus is given by

$$\tau = \mu \frac{dv}{dr} = \frac{1}{4} \left(\frac{dp_f}{ds} \right) \left[\frac{r_w^2 - r_p^2}{\ln(r_w/r_p)} \frac{1}{r} - 2r \right] \quad (5.72)$$

The velocity is maximum at a point in the annulus where $r = r_m$. Hence,

$$r = r_m, \quad \tau = 0, \quad v = v_{\max} \quad (5.73)$$

Combination of Eqs. 5.72 and 5.73 gives

$$r_m^2 = \frac{r_w^2 - r_p^2}{2 \ln(r_w/r_p)} \quad (5.74)$$

The equation for the shear stress can be recast in terms of the radius of maximum velocity as follows:

$$\tau = \frac{1}{2} \left(\frac{dp_f}{ds} \right) \left[\frac{r_m^2}{r} - r \right] \quad (5.75)$$

In Fig. 5.27, the profiles of velocity and shear stress together with the forces acting on the fluid elements in the inner region ($r_p \leq r \leq r_m$) and the outer region ($r_m \leq r \leq r_w$) are shown for flow of Newtonian fluid in a concentric annulus, for the coordinate system depicted.

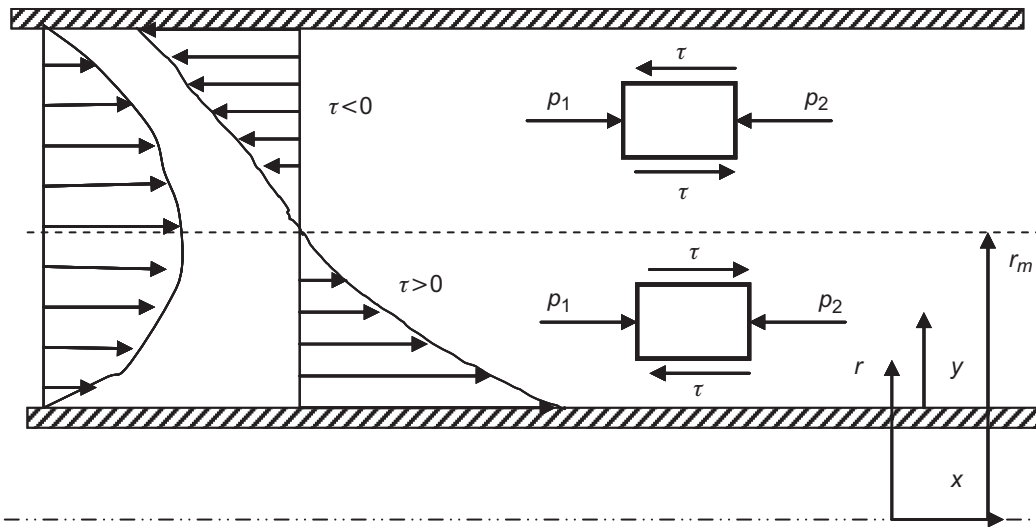


Fig. 5.27—Velocity profile and shear-stress distribution for flow of Newtonian fluid in a concentric annulus.

As with pipe flow, a relation between pressure gradient and total flow rate is needed for most engineering applications. The total flow rate can be obtained by summing the flow contained in each concentric shell of fluid. Thus, for an annulus,

$$q = \int_{r_p}^{r_w} v(2\pi r) dr = \frac{2\pi}{4\mu} \frac{dp_f}{ds} \int_{r_p}^{r_w} \left[\frac{r_w^2 - r_p^2}{\ln(r_w/r_p)} \ln \frac{r}{r_p} - (r^2 - r_p^2) \right] r dr.$$

Upon integration, this equation becomes

$$q = \frac{\pi}{8\mu} \frac{dp_f}{ds} \left[r_w^4 - r_p^4 - \frac{(r_w^2 - r_p^2)^2}{\ln r_w/r_p} \right]. \quad (5.76)$$

This relation was developed first by Lamb (1945).

For annular flow, the flow rate q is the mean velocity \bar{v} multiplied by the annular cross-sectional area:

$$q = \pi(r_w^2 - r_p^2) \bar{v}. \quad (5.77)$$

Substituting this expression for q in Eq. 5.76 and solving for the frictional pressure gradient dp_f/ds gives

$$\frac{dp_f}{ds} = \frac{8\mu\bar{v}}{\left(r_w^2 + r_p^2 - \frac{r_w^2 - r_p^2}{\ln r_w/r_p} \right)}. \quad (5.78)$$

Eq. 5.79a relates mean velocity (flow rate) to developed frictional pressure gradient for the flow of a Newtonian fluid in a concentric annulus in consistent units. Converting from consistent units to field units, Lamb's equation becomes

$$\frac{dp_f}{ds} = \frac{\mu\bar{v}}{6.0 \left(r_w^2 + r_p^2 - \frac{r_w^2 - r_p^2}{\ln r_w/r_p} \right)}. \quad (5.79)$$

where the units are: \bar{v} , ft/s; r_p , ft; r_w , ft; μ , cp; and dp_f/ds , psi/ft.

Example 5.20 A 9-lbm/gal Newtonian fluid having a viscosity of 15 cp is being circulated in a 10,000-ft well containing a 7-in.-ID casing and a 5-in.-OD and 4½-in.-ID drillstring at a rate of 80 gal/min. Compute the static and circulating bottomhole pressure, give the velocity profile in the annulus, and compute the frictional loss in the drillstring. Assume that a laminar flow pattern exists both in the pipe and in the annulus.

Solution. Conversion from field units to SI units gives

$$\rho = \frac{9 \text{ lbm/gal}}{8.3454 \times 10^{-3} (\text{lbm/gal})/(\text{kg/m}^3)} = 1.078 \times 10^3 \text{ kg/m}^3,$$

$$\mu = \frac{15 \text{ cp}}{10^3 \text{ cp}/(\text{Pa} \cdot \text{s})} = 1.5 \times 10^{-2} \text{ Pa} \cdot \text{s},$$

$$r_w = \frac{1}{2} \left(\frac{7 \text{ in.}}{3.937 \times 10^1 \text{ in./m}} \right) = 0.0889 \text{ m},$$

$$r_p = \frac{1}{2} \left(\frac{5 \text{ in.}}{3.937 \times 10^1 \text{ in./m}} \right) = 0.0635 \text{ m},$$

$$R = \frac{1}{2} \left(\frac{4.5 \text{ in.}}{3.937 \times 10^1 \text{ in./m}} \right) = 0.0572 \text{ m},$$

$$Z = \frac{10,000 \text{ ft}}{3.2808 \text{ ft/m}} = 3.048 \times 10^3 \text{ m},$$

$$q = \frac{80 \text{ gal/min}}{1.585 \times 10^4 (\text{gal/min})/(\text{m}^3/\text{s})} = 5.05 \times 10^{-3} \text{ m}^3/\text{s}.$$

The static bottomhole pressure is given by Eq. 5.5a. The annulus is open to the atmosphere at the surface, hence $p_0 = 0 \text{ Pa}$. At the bottom of the hole, the pressure is

$$p = \rho g D + p_0 = 1078 \times 9.81 \times 3048 + 0 = 32.23 \times 10^6 \text{ Pa},$$

or, in field units, the static bottomhole pressure is $p = 4,675 \text{ psig}$.

If fluid acceleration effects are neglected, the circulating bottomhole pressure is the sum of the hydrostatic pressure and the frictional pressure loss in the annulus. The mean velocity in the annulus is given by

$$\bar{v} = \frac{q}{\pi(r_2^2 - r_1^2)} = \frac{5.05 \times 10^{-3}}{(\pi)(0.0889^2 - 0.0635^2)} = 0.415 \text{ m/s}.$$

The frictional pressure gradient is determined using Eq. 5.79a:

$$\frac{dp_f}{ds} = \frac{8(1.5 \times 10^{-2})(0.415)}{\left(0.0889^2 + 0.0635^2 - \frac{0.889^2 - 0.0635^2}{\ln(0.0889/0.0635)} \right)} = 115.6 \text{ Pa/m}.$$

The total frictional pressure loss in the annulus is

$$\Delta p_f = \frac{dp_f}{ds} \Delta s = (115.6 \text{ Pa/m})(3048 \text{ m}) = 0.352 \times 10^6 \text{ Pa},$$

or, in field units,

$$\frac{dp_f}{ds} = \frac{115.57 \text{ Pa/m}}{22,620.2 (\text{Pa/m})/(\text{psi/ft})} = 0.0051 \text{ psi/ft}$$

and

$$\Delta p_f = (352,257 \text{ Pa})/(6894.73 \text{ Pa/psi}) = 51 \text{ psi.}$$

The circulating bottomhole pressure is given by

$$p_c = 32.23 \times 10^6 + 0.35 \times 10^6 = 32.58 \times 10^6 \text{ Pa,}$$

or

$$p_c = 4,725 \text{ psig.}$$

The velocity profile is given in **Fig. 5.28**. The frictional loss in the drillpipe is derived as follows. The mean velocity in the drillpipe is given by

$$\bar{v} = \frac{q}{\pi R^2} = \frac{5.05 \times 10^{-3}}{\pi (0.0572)^2} = 0.492 \text{ m/s.}$$

The frictional pressure gradient is determined using Eq. 5.70a:

$$\frac{dp_f}{ds} = \frac{8(1.5 \times 10^{-2})(0.492)}{(0.0572^2)} = 18.1 \text{ Pa/m,}$$

and total frictional loss is

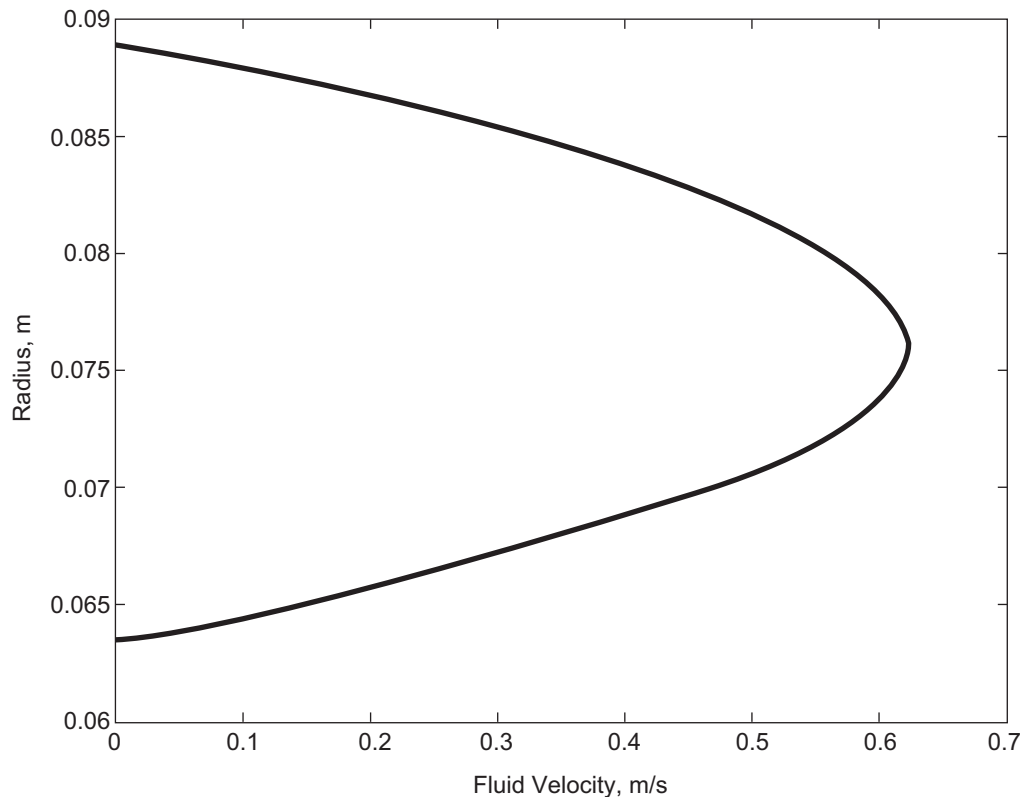


Fig. 5.28—Velocity profile in the concentric annulus of Example 5.22.

$$\Delta p_f = \frac{dp_f}{ds} \Delta s = (18.1 \text{ Pa/m})(3048 \text{ m}) = 55,169 \text{ Pa},$$

or, in field units,

$$\frac{dp_f}{ds} = \frac{18.1 \text{ Pa/m}}{22,620.6 (\text{Pa/m})/(\text{psi/ft})} = .000800 \text{ psi/ft}$$

and

$$\Delta p_f = 55,169 \text{ Pa} / 6894.757 \text{ Pa/psi} = 8.00 \text{ psi}.$$

Slot Flow. For the Newtonian model, we obtain

$$\tau = \mu \dot{\gamma} = \mu \frac{dv}{dy} = -y \frac{dp_f}{ds} + \tau_0.$$

Separating variables and integrating gives

$$v = \frac{\tau_0 y}{\mu} - \frac{y^2}{2\mu} \frac{dp_f}{ds} + v_0, \quad \dots \quad (5.80a)$$

where v_0 is the constant of integration. The fluid wets the pipe walls; therefore, the velocity v is zero for $y = 0$ and for $y = h$. Applying these boundary conditions to Eq. 5.80a yields, for τ_0 and v_0 ,

$$\tau_0 = \frac{h}{2} \frac{dp_f}{ds},$$

$$v_0 = 0.$$

Substituting these values for τ_0 and v_0 in Eq. 5.80a yields

$$v = \frac{1}{2\mu} \frac{dp_f}{ds} (hy - y^2). \quad \dots \quad (5.80b)$$

Similarly, substituting for τ_0 gives, for the shear stress,

$$\tau = \left(\frac{h}{2} - y \right) \frac{dp_f}{ds}. \quad \dots \quad (5.81)$$

The flow rate q is given by

$$q = \int_0^h v dA = \int_0^h v w dy = \frac{w}{2\mu} \frac{dp_f}{ds} \int_0^h (hy - y^2) dy = \frac{h^3}{12} \frac{w}{\mu} \frac{dp_f}{ds}. \quad \dots \quad (5.82a)$$

Substituting the expressions for w and h (given by Eqs. 5.63a and 5.63b) in Eq. 5.82a gives

$$q = \frac{\pi}{12\mu} \frac{dp_f}{ds} (r_w^2 - r_p^2) (r_w - r_p)^2. \quad \dots \quad (5.82b)$$

Expressing the flow rate in terms of the mean flow velocity \bar{v} and solving for the frictional pressure gradient dp_f/ds gives

$$\frac{dp_f}{ds} = \frac{12\mu\bar{v}}{(r_w - r_p)^2} = \frac{48\mu\bar{v}}{(d_w - d_p)^2}. \quad \dots \quad (5.82c)$$

Converting from consistent units to field units of lbf/in.², cp, ft/sec, and in., we obtain

$$\frac{dp_f}{ds} = \frac{\mu \bar{v}}{1,000(d_w - d_p)^2} \quad \dots \dots \dots (5.82d)$$

Example 5.21 Compute the frictional pressure loss for the annulus discussed in Example 5.20 using a slot flow representation of the annulus. Assume that the flow pattern is laminar.

Solution. The ratio d_1/d_2 has a value of 0.714. Because this ratio is greater than 0.3, Eq. 5.82c or 5.82d can be applied. Using Eq. 5.82c we obtain

$$\Delta p_f = \frac{dp_f}{ds} D = \frac{(48)(0.015)(0.415)}{(0.1788 - 0.1270)^2} (3048) = 339,419 \text{ Pa,}$$

or

$$\Delta p_f = (339,419 \text{ Pa}) / (6894.73 \text{ Pa/psi}) = 49 \text{ psi.}$$

Note that this is almost the same value for frictional pressure loss that was obtained using Eq. 5.78 or Eq. 5.79.

5.5.3 Non-Newtonian Fluid Models. Analytical expressions for the isothermal, laminar flow of non-Newtonian fluids can be derived by following essentially the same steps used for Newtonian fluids. The reader is referred to the work of Laird (1957) and Fredrickson and Bird (1958) for a discussion of the development of the annular flow equations for Bingham plastic fluids. However, as in the case of Newtonian fluids, annular flow can be modeled accurately for the usual geometry of interest to drilling engineers through use of the less complex flow equations for a narrow slot. The derivations of the laminar-flow equations for the Bingham plastic, power-law, and Herschel-Bulkley fluid models are given below. The annulus is represented as a narrow slot in these derivations.

Bingham Plastic Model. Developing flow equations for a Bingham plastic fluid (as well as any fluid with a yield stress) is complicated because portions of the fluid having a shear stress less than the yield point must move as a rigid plug down the conduit (**Fig. 5.29**).

Flow in a Slot. We will first investigate the flow of a Bingham fluid in a slot because of its relative simplicity and symmetry. In the region $0 \leq y \leq y_a$, the shear stress in a slot must behave according to Eq. 5.65:

$$\tau = \tau_0 - y \frac{dp_f}{ds}.$$

At $y = 0$, the shear stress is equal to the shear stress at the inner slot wall, $\tau = \tau_{wi}$; hence, $\tau_0 = \tau_{wi}$. At $y = y_a$, the shear stress must be equal to τ_y ; hence

$$\tau = \tau_y = \tau_{wi} - y_a \frac{dp_f}{ds}. \quad \dots \dots \dots (5.83)$$

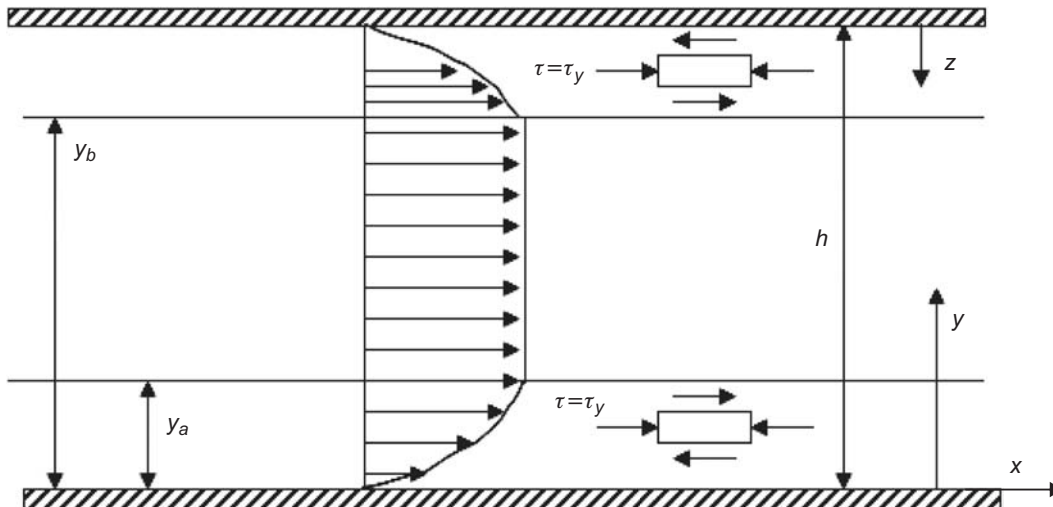


Fig. 5.29—Laminar flow of a Bingham plastic fluid in a slot.

Solving for y_a yields

$$y_a = \frac{\tau_{wi} - \tau_y}{dp_f/ds} \quad \dots\dots\dots (5.84)$$

In the layer between the pipe wall and the plug ($0 \leq y \leq y_a$) (Fig. 5.29), the Bingham model is defined by

$$\tau = \tau_y + \mu_p \frac{dv}{dy} \quad \dots\dots\dots (5.85a)$$

Thus, the shear stress in this fluid region is given by

$$\tau = \tau_y + \mu_p \frac{dv}{dy} = \tau_{wi} - y \frac{dp_f}{ds}.$$

After separating variables and integrating, and noting that v must be zero at $y = 0$, we obtain the following expression for fluid velocity:

$$v = -\frac{y^2}{2\mu_p} \frac{dp_f}{ds} + \frac{(\tau_{wi} - \tau_y)}{\mu_p} y \quad \dots\dots\dots (5.85b)$$

Eq. 5.84 can be used to express $\tau_{wi} - \tau_y$ in terms of y_a and dp_f/ds . Thus,

$$v = \frac{1}{2\mu_p} \frac{dp_f}{ds} (-y^2 + 2y_a y), \text{ where } 0 \leq y \leq y_a \quad \dots\dots\dots (5.85c)$$

The velocity of the plug region can be obtained by evaluating Eq. 5.85c at $y = y_a$, thus giving

$$v_p = \frac{y_a^2}{2\mu_p} \frac{dp_f}{ds} \quad y_a \leq y \leq y_b \quad \dots\dots\dots (5.85d)$$

In the upper layer ($y_b \leq y \leq h$), we expect the same behavior as the lower layer because of the symmetry of the geometry about the center line of the slot. Because the shear stress at the top of the slot ($y = h$) is the same as the shear stress at the bottom of the slot,

$$\tau_{wi} = \tau_{wo} = \tau_w \quad \dots\dots\dots (5.86)$$

we can now relate the shear stress to the frictional pressure drop by a force balance:

$$\tau_w = \frac{h}{2} \frac{dp_f}{ds} \quad \dots\dots\dots (5.87)$$

The velocity profile for the flow in annuli modeled as a slot is then given by

$$\begin{aligned} v &= \frac{1}{2\mu_p} \frac{dp_f}{ds} \left[hy \left(1 - \frac{\tau_y}{\tau_w} \right) - y^2 \right] & 0 \leq y \leq \frac{h}{2} \left(1 - \frac{\tau_y}{\tau_w} \right) \\ v &= v_p = \frac{1}{2\mu_p} \frac{dp_f}{ds} \left[\frac{h}{2} \left(1 - \frac{\tau_y}{\tau_w} \right) \right]^2 & \frac{h}{2} \left(1 - \frac{\tau_y}{\tau_w} \right) \leq y \leq \frac{h}{2} \left(1 + \frac{\tau_y}{\tau_w} \right) \\ v &= \frac{1}{2\mu_p} \frac{dp_f}{ds} \left\{ (y-h) \left[h \left(1 - \frac{\tau_y}{\tau_w} \right) - y \right] \right\} & \frac{h}{2} \left(1 + \frac{\tau_y}{\tau_w} \right) \leq y \leq h \quad \dots\dots\dots (5.88) \end{aligned}$$

The total flow rate through the slot is defined by

$$q = w \int_0^h v dy = w \int_0^{y_a} v dy + w v_p \int_{y_a}^{y_b} dy + w \int_{y_b}^h v dy,$$

where w is the width of the slot. Performing the integrations, the flow rate can be expressed as

$$q = \frac{wh^3}{12\mu_p} \frac{dp_f}{ds} \left[1 - \frac{3}{2} \left(\frac{\tau_y}{\tau_w} \right) + \frac{1}{2} \left(\frac{\tau_y}{\tau_w} \right)^3 \right]. \quad \dots\dots\dots (5.89)$$

In typical situations, the flow rate would be given and the pressure drop would be sought. However, Eq. 5.89 is implicit in pressure drop because of the appearance of the term τ_w in the parenthetical terms. Normally an iteration would be required or a simplification should be made, to be presented later. However, Fordham et al. (1991) have given a relatively unknown solution to Eq. 5.89, which is

$$\frac{\tau_y}{dp_f/ds} \frac{2}{h} = 2 \sqrt{\frac{q}{w(h/2)^2} \frac{\mu_p}{\tau_y} + 1} \times \sin \left\{ \frac{1}{3} \sin^{-1} \left[\left(\frac{q}{w(h/2)^2} \frac{\mu_p}{\tau_y} + 1 \right)^{-3/2} \right] \right\}. \quad \dots\dots\dots (5.90a)$$

Hence, if the flow rate is given, Eq. 5.91a can give the pressure drop directly without requiring an iteration or even an approximation.

For the conditions usually encountered in rotary-drilling applications, the shear stress at the wall, τ_w , is more than twice the yield point, τ_y , and the last term in Eq. 5.90c can be neglected without introducing significant error. Dropping this term and substituting the expression for τ_w given in Eq. 5.86 yields

$$q = \frac{wh^3}{12\mu_p} \frac{dp_f}{ds} - \frac{wh^2}{4\mu_p} \tau_y. \quad \dots\dots\dots (5.90b)$$

Converting w and h into the equivalent dimensions of a concentric circular annulus gives

$$q = \frac{\pi}{12\mu_p} \frac{dp_f}{ds} (r_w^2 - r_p^2)(r_w - r_p)^2 - \frac{\pi}{4\mu_p} \tau_y (r_w^2 - r_p^2)(r_w - r_p). \quad \dots\dots\dots (5.90c)$$

Expressing the flow rate in terms of the mean flow velocity, \bar{v} , and solving for the frictional pressure gradient, dp_f/dL , gives

$$\frac{dp_f}{ds} = \frac{12\mu_p \bar{v}}{(r_w - r_p)^2} + \frac{3\tau_y}{(r_w - r_p)} = \frac{48\mu_p \bar{v}}{(d_w - d_p)^2} + \frac{6\tau_y}{d_w - d_p}. \quad \dots\dots\dots (5.91a)$$

Converting from consistent units to field units of lbf/in.²/ft, cp, ft/sec, in., and lbf/100 ft², we obtain

$$\frac{dp_f}{ds} = \frac{\mu_p \bar{v}}{1,000(d_w - d_p)^2} + \frac{\tau_y}{200(d_w - d_p)}. \quad \dots\dots\dots (5.91b)$$

Pipe Flow. The derivation of the equations for laminar flow of Bingham plastic fluids through a pipe is quite similar to the derivation of the slot flow equation. As in the case of a slot, the portions of the fluid flowing near the center of the conduit that have a shear stress less than the yield point must move as a rigid plug down the conduit (**Fig. 5.30**). At the radius of the plug, r_p , the shear stress, τ_p , must be equal to the yield point, τ_y . Also, the shear stress in a circular tube must behave according to Eq. 5.61. Thus,

$$\tau_p = \tau_y = -\frac{r_p}{2} \frac{dp_f}{ds}. \quad \dots\dots\dots (5.92)$$

In the plug region, the Bingham model is defined by

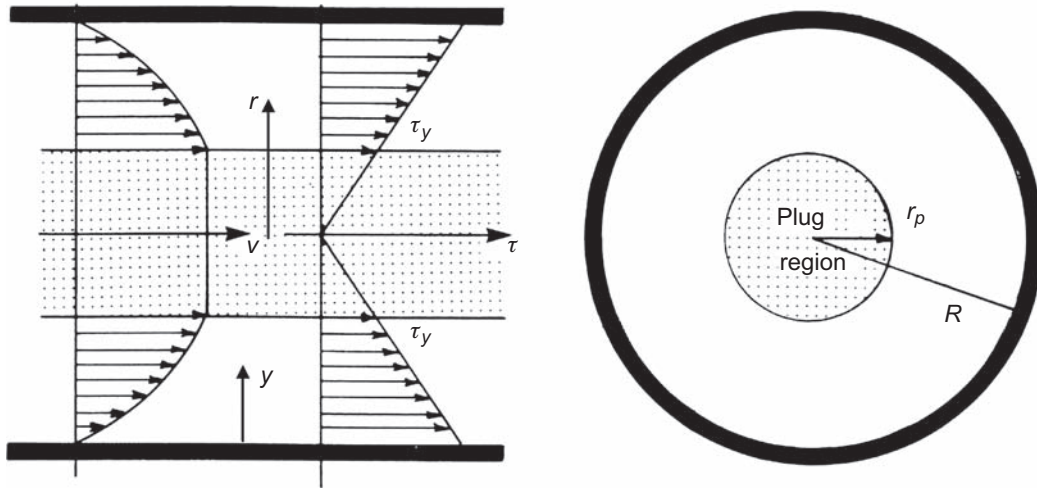


Fig. 5.30—Laminar flow of a Bingham plastic fluid in a pipe.

$$\tau = \tau_y + \mu_p \frac{dv}{dy} = \tau_y + \mu_p \frac{dv}{dr}. \quad (5.93)$$

Thus, the shear stress in the plug region is given by

$$\tau = \tau_y + \mu_p \frac{dv}{dr} = -\frac{r}{2} \frac{dp_f}{ds}.$$

After separating variables and integrating, we obtain the following expression for fluid velocity:

$$v = -\frac{r^2}{4\mu_p} \frac{dp_f}{ds} - \frac{\tau_y}{\mu_p} r + v_0. \quad (5.94a)$$

The constant of integration, v_0 , is obtained using the boundary condition of zero velocity at the pipe wall. Substituting this boundary condition in Eq. 5.94a gives

$$0 = -\frac{R^2}{4\mu_p} \frac{dp_f}{ds} - \frac{\tau_y}{\mu_p} R + v_0.$$

Solving this equation for v_0 gives

$$v_0 = \frac{R^2}{4\mu_p} \frac{dp_f}{ds} + \frac{\tau_y}{\mu_p} R.$$

Substituting this expression for v_0 in Eq. 5.94a yields

$$v = \frac{1}{4\mu_p} \frac{dp_f}{ds} (R^2 - r^2) - \frac{\tau_y}{\mu_p} (R - r) \quad r \geq r_p. \quad (5.94b)$$

The velocity of the plug region can be obtained by evaluating Eq. 5.94b at $r = r_p$ with substitution for τ_y given by Eq. 5.92, which finally yields

$$v_p = \frac{1}{4\mu_p} \frac{dp_f}{ds} (R - r_p)^2 \quad 0 \leq r \leq r_p. \quad (5.94c)$$

The total flow rate through the pipe is defined by

$$q = \int_0^A v dA = 2\pi \int_0^R vr dr = \pi [r^2 v]_0^R - \pi \int_0^R r^2 \frac{dv}{dr} dr.$$

Integration of this equation gives

$$q = \frac{\pi R^4}{8\mu_p} \frac{dp_f}{ds} \left[1 - \frac{4}{3} \left(\frac{\tau_y}{\tau_w} \right) + \frac{1}{3} \left(\frac{\tau_y}{\tau_w} \right)^4 \right] \quad \tau_y \leq \tau_w. \quad (5.95a)$$

Note that this expression reduces to the familiar Hagen-Poiseuille law for τ_y equal to zero. Note also that as τ_y approaches τ_w , the term in brackets approaches zero. This means that the shear stress at the wall must exceed the yield point to cause flow.

It is unfortunate that Eq. 5.95a cannot be solved for the pressure drop in a manner similar to the annulus flow. Hence, when pressure drop is required given the flow rate, Eq. 5.95a should be solved by the use of an iteration procedure. However, for the conditions usually encountered in rotary drilling applications, the shear stress at the wall is more than twice the yield point, and the last term in Eq. 5.95a can be neglected without introducing a significant error. Dropping this term and substituting the expression for τ_w given by Eq. 5.93 evaluated at R yields

$$q = \frac{\pi R^4}{8\mu_p} \frac{dp_f}{ds} - \frac{\pi R^3}{3\mu_p} \tau_y. \quad (5.95b)$$

Expressing the flow rate in terms of the mean flow velocity, \bar{v} , and solving for the frictional pressure gradient, dp_f/dL , gives

$$\frac{dp_f}{ds} = \frac{8\mu_p \bar{v}}{R^2} + \frac{8\tau_y}{3R} = \frac{32\mu_p \bar{v}}{d^2} + \frac{16\tau_y}{3d}. \quad (5.95c)$$

Converting from consistent units to field units of lbf/in.², cp, ft/sec, in., and lbf/100 ft², we obtain, for the pressure drop of a Bingham plastic fluid flowing in a pipe,

$$\frac{dp_f}{ds} = \frac{\mu_p \bar{v}}{1,500d^2} + \frac{\tau_y}{225d}. \quad (5.95d)$$

The shear rate in a Bingham plastic fluid at the pipe wall can be obtained from the shear stress at the pipe wall and the appropriate frictional pressure gradient equation. For a circular pipe and with the approximation represented by Eq. 5.95c, we obtain

$$\begin{aligned} \dot{\gamma}_w &= \frac{\tau_w - \tau_y}{\mu_p} = \frac{R}{2\mu_p} \frac{dp_f}{ds} - \frac{\tau_y}{\mu_p} = \frac{d}{4\mu_p} \left(\frac{16\mu_p \bar{v}}{d^2} + \frac{16\tau_y}{3d} \right) - \frac{\tau_y}{\mu_p} \\ &= \frac{8\bar{v}}{d} + \frac{\tau_y}{3\mu_p}. \end{aligned} \quad (5.96a)$$

Changing from consistent units to field units of sec⁻¹, ft/sec, in., and lbf/100 ft², we obtain, for the approximate wall shear rate for circular pipe,

$$\dot{\gamma}_w = \frac{96\bar{v}}{d} + 159.7 \frac{\tau_y}{\mu_p}. \quad (5.96b)$$

Similarly, for an annulus, the approximate shear rate at the wall, using the approximation from Eq. 5.91b, is given by

$$\begin{aligned} \dot{\gamma}_w &= \frac{h}{2\mu_p} \frac{dp_f}{ds} - \frac{\tau_y}{\mu_p} = \frac{(d_w - d_p)}{4\mu_p} \left[\frac{48\mu_p \bar{v}}{(d_w - d_p)^2} + \frac{6\tau_y}{(d_w - d_p)} \right] - \frac{\tau_y}{\mu_p} \\ &= \frac{12\bar{v}}{d_w - d_p} + \frac{\tau_y}{2\mu_p}. \end{aligned} \quad (5.97a)$$

Changing to field units, we obtain, for the wall shear rate for the annulus,

$$\dot{\gamma}_w = \frac{96\bar{v}}{d_w - d_p} + 239.5 \frac{\tau_y}{\mu_p} \quad (5.97b)$$

Example 5.22 Shah and Sutton (1990) provided a new friction correlation for flow of cement slurries in pipes and annuli. For the 15.6-lbm/gal slurry with rheological data shown below, they found after regression a plastic viscosity of 56.7 cp and a yield stress of 43.3 lbf/100 ft². For flow rates of 2 and 8 bbl/min in a 4.494-in.-ID casing, they found pressure drops of 0.053 and 0.0615 psi/ft, respectively. Similarly, for flow rates of 2 and 8 bbl/min in a 5×7.5-in. annulus, they found pressure drops of 0.096 and 0.1138 psi/ft, respectively.

Compute the corresponding pressure losses in the pipe and the annulus, with the full solution and the approximate solution, and compare with the results given by Shah and Sutton. Assume laminar flow for all situations.

Solution 1—Pipe Computations. We first convert to SI units:

$$d = \frac{4.494 \text{ in.}}{3.937 \times 10^1 \text{ in./m}} = 0.1141 \text{ m,}$$

$$d_p = \frac{5 \text{ in.}}{3.937 \times 10^1 \text{ in./m}} = 0.127 \text{ m,}$$

$$d_w = \frac{7.5 \text{ in.}}{3.937 \times 10^1 \text{ in./m}} = 0.1905 \text{ m,}$$

$$\rho = \frac{15.6 \text{ lbm/gal}}{8.3454 \times 10^{-3} \text{ (lbm/gal)/(kg/m}^3\text{)}} = 1.8693 \times 10^3 \text{ kg/m}^3,$$

$$\mu = \frac{56.7 \text{ cp}}{10^3 \text{ cp/(Pa} \cdot \text{s)}} = 0.0567 \text{ Pa} \cdot \text{s,}$$

$$\tau_y = \frac{43.3 \text{ lbf}}{100 \text{ ft}^2} \times \frac{0.4788 \text{ Pa}}{\text{lbf}/(100 \text{ ft}^2)} = 20.73 \text{ Pa,}$$

$$q_1 = \frac{2 \times 42 \text{ gal/min}}{1.585 \times 10^4 \text{ (gal/min)/(m}^3\text{/s)}} = 0.0053 \text{ m}^3\text{/s,}$$

$$q_2 = \frac{8 \times 42 \text{ gal/min}}{1.585 \times 10^4 \text{ (gal/min)/(m}^3\text{/s)}} = 0.0212 \text{ m}^3\text{/s,}$$

The mean velocity is given by

$$\bar{v}_1 = \frac{0.0053}{(\pi/4)(0.1141)^2} = 0.518 \text{ m/s}$$

and

$$\bar{v}_2 = \frac{0.0212}{(\pi/4)(0.1141)^2} = 2.074 \text{ m/s.}$$

The full solution for pipe flow will be determined through an iteration on τ_w .

Assuming a value for τ_w , then dp_f/ds can be computed from Eq. 5.86, and a new value for q can be computed from Eq. 5.90c. This procedure is continued until the values of τ_w and q converge to a solution. A fast way is to perform computations using the bisection method (Press et al. 1997). A sample of the computations is shown in the following table:

	τ_{w1} (Pa)	q_1 (m ³ /s)	τ_{w2} (Pa)	q_2 (m ³ /s)	τ_{w3} (Pa)	q_3 (m ³ /s)
1st iteration	20.83	2.4×10^{-6}	38.93	0.0317	29.88	0.0117
2nd iteration	20.83	2.4×10^{-6}	29.88	0.0117	25.35	0.0038
3rd iteration	25.35	0.0038	29.88	0.0117	27.617	0.0075
4th iteration	25.35	0.0038	27.617	0.0075	26.486	0.0056
5th iteration	25.35	0.0038	26.486	0.0056	25.92	0.0047
6th iteration	25.92	0.0047	26.486	0.0056	26.20	0.0051
7th iteration	26.20	0.0051	26.486	0.0056	26.34	0.0053

The pressure drop is then

$$\frac{dp_f}{ds} = \frac{4\tau_w}{d} = \frac{4(26.34)}{0.1141} = 923 \text{ Pa/m},$$

or, in field units, $dp_f/ds = 0.0408$ psi/ft, a value that is within 23% of the value predicted by Shah and Sutton.

Applying a similar procedure for $q_2 = 8$ bbl/min, we compute a value of $dp_f/ds = 1204$ Pa/m = 0.053 psi/ft, a value that is within 13% of the value predicted by Shah and Sutton.

Using the approximate solution, Eq. 5.95c, we obtain, for $q_1 = 2$ bbl/min,

$$\frac{dp_f}{ds} = \frac{32(0.0567)(0.518)}{0.1141^2} + \frac{16(20.73)}{3(0.1141)} = 1041 \text{ Pa/m},$$

or, in field units, $dp_f/ds = 0.04602$ psi/ft, a value that is 13% lower than the one predicted by Shah and Sutton and 13% lower than the value predicted using the full solution.

Similarly, for $q_2 = 8$ bbl/min, we obtain

$$\frac{dp_f}{ds} = \frac{32(0.0567)(2.074)}{0.1141^2} + \frac{16(20.73)}{3(0.1141)} = 1258 \text{ Pa/m},$$

or, in field units, $dp_f/ds = 0.0556$ psi/ft, a value that is 10% lower than the one predicted by Shah and Sutton and 5% higher than the value predicted using the full solution.

Solution 2—Annulus Computations. For the annulus computations, we could use the direct equation (Eq. 5.91a) and the approximate solution (Eq. 5.91b).

Using the direct approach, we obtain

$$h = (d_w - d_p)/2 = (0.1905 - 0.127)/2 = 0.03175 \text{ m}$$

and

$$w = \pi(d_w + d_p)/2 = 0.4985 \text{ m}.$$

For the first flow rate, we compute the term

$$\frac{q}{w(h/2)^2} \frac{\mu_p}{\tau_y} = \frac{0.0053}{(0.4975)(0.03175/2)^2} \frac{0.0567}{20.73} = 0.1156,$$

then

$$\frac{20.73}{dp_f/ds} \frac{2}{0.03175} = 2\sqrt{0.1156 + 1} \times \sin \left\{ \frac{1}{3} \sin^{-1} \left[(0.1156 + 1)^{-3/2} \right] \right\} = 0.700.$$

Solving for the pressure drop, we get

$$\frac{dp_f}{ds} = \frac{1305.83}{0.700} = 1865 \text{ Pa/m},$$

or, in field units, $dp_f/ds = 0.08245$ psi/ft, a value that is 14% lower than the one predicted by Shah and Sutton. For the second flow rate, we compute the term

$$\frac{q}{w(h/2)^2} \frac{\mu_p}{\tau_y} = \frac{0.0212}{(0.4975)(0.03175/2)^2} \frac{0.0567}{20.73} = 0.4614,$$

then

$$\frac{20.73}{dp_f/ds} \frac{2}{0.03175} = 2\sqrt{0.4614 + 1} \times \sin \left\{ \frac{1}{3} \sin^{-1} \left[(0.4614 + 1)^{-3/2} \right] \right\} = 0.4817.$$

Solving for the pressure drop, we get

$$\frac{dp_f}{ds} = \frac{1305.83}{0.4817} = 2711 \text{ Pa/m},$$

or, in field units, $dp_f/ds = 0.11985$ psi/ft, a value that is 5% higher than the one predicted by Shah and Sutton.

To use the approximate solution, Eq. 5.91b, we first determine the average velocities for the two flow rates, which are

$$\bar{v}_1 = \frac{0.0053}{(\pi/4)(0.1905^2 - 0.127^2)} = 0.335 \text{ m/s}$$

and

$$\bar{v}_2 = \frac{0.0212}{(\pi/4)(0.1905^2 - 0.127^2)} = 1.34 \text{ m/s}.$$

Then, for the flow rate of 2 bbl/min, we get

$$\frac{dp_f}{ds} = \frac{48(0.0567)(0.335)}{(0.1905 - 0.127)^2} + \frac{6(20.73)}{0.1905 - 0.127} = 2185 \text{ Pa/m},$$

or, in field units, $dp_f/ds = 0.0966$ psi/ft, a value that is 5% higher than the one predicted by Shah and Sutton and 17% higher than the value predicted using the equation for the full solution.

Then for the flow rate of 8 bbl/min, we get

$$\frac{dp_f}{ds} = \frac{48(0.0567)(1.34)}{(0.1905 - 0.127)^2} + \frac{6(20.73)}{0.1905 - 0.127} = 2863 \text{ Pa/m},$$

or, in field units, $dp_f/ds = 0.12658$ psi/ft, a value that is 11% higher than the one predicted by Shah and Sutton and 6% higher than the value predicted using the equation for the full solution.

Power-Law Model. The annular flow of power-law fluids can also be approximated closely using the less complex flow equations for a narrow slot (**Fig. 5.31**).

Slot Flow of Power-Law Model. The shear stress for a power-law fluid in a narrow slot is given by

$$\tau = K \left(\frac{dv}{dy} \right)^n \quad 0 \leq y \leq h/2 \quad \dots \dots \dots (5.98a)$$

and

$$\tau = K \left(\frac{dv}{dz} \right)^n = K \left(-\frac{dv}{dy} \right)^n \quad h/2 \leq y \leq h \quad \dots \dots \dots (5.98b)$$

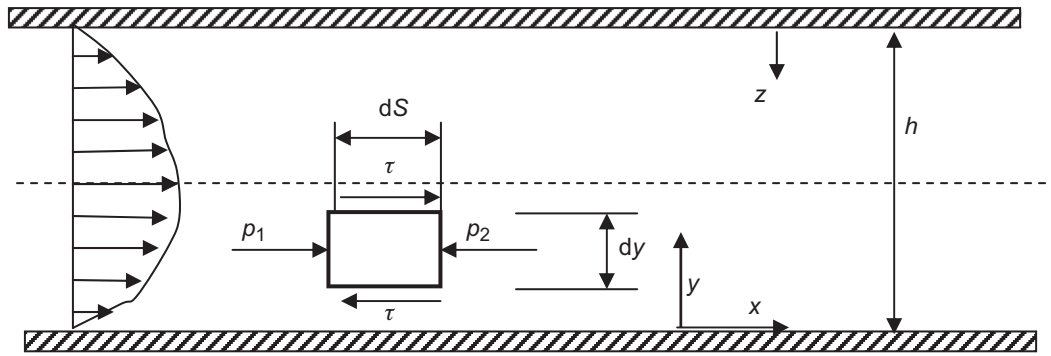


Fig. 5.31—Laminar flow of a power-law fluid in a slot.

In this region, $Z = h - y$. The force balance in the slot (Eq. 5.65) still holds that

$$\tau = -y \frac{dp_f}{ds} + \tau_0.$$

As discussed previously for Newtonian and Bingham plastic models, the shear stress changes linearly with distance, y , in a slot. This is a consequence of the flow geometry and is independent of the rheological models used to describe the flow. Also, by inspection of Fig. 5.31, we see that for a slot, τ is zero at $y = h/2$. Thus,

$$\tau_0 = \frac{h}{2} \frac{dp_f}{ds}.$$

For the $0 \leq y \leq h/2$ region, the shear stress equation can be simplified to

$$\tau = K \left(\frac{dv}{dy} \right)^n = -y \frac{dp_f}{ds} + \frac{h}{2} \frac{dp_f}{ds}.$$

Separating variables and integrating gives

$$v = \frac{-K}{(1+1/n) dp_f/ds} \left[\frac{1}{K} \frac{dp_f}{ds} \left(\frac{h}{2} - y \right) \right]^{1+1/n} + v_0. \quad (5.99a)$$

The constant of integration v_0 can be evaluated using the boundary condition that $v = 0$ at $y = 0$, so that finally

$$v = \frac{-K}{(1+1/n) dp_f/ds} \left\{ \left[\frac{1}{K} \frac{dp_f}{ds} \left(\frac{h}{2} - y \right) \right]^{1+1/n} - \left(\frac{1}{K} \frac{dp_f}{ds} \frac{h}{2} \right)^{1+1/n} \right\} \quad 0 \leq y \leq h/2,$$

which can be written as

$$v = \frac{(dp_f/ds)^{1/n}}{(K)^{1/n}} \frac{1}{(1+1/n)} \left[\left(\frac{h}{2} \right)^{1+1/n} - \left(\frac{h}{2} - y \right)^{1+1/n} \right] \quad 0 \leq y \leq h/2. \quad (5.99b)$$

The velocity profile in the region $h/2 \leq y \leq h$ is determined as follows. In this region, Eq. 5.88 still holds that

$$\tau = \tau' - \frac{dp_f}{ds} (h - y).$$

Noting that at $y = h/2$, $\tau = 0$, it follows that

$$\tau' = \frac{h}{2} \frac{dp_f}{ds}.$$

Hence,

$$\tau = \frac{dp_f}{ds} \left(y - \frac{h}{2} \right) \quad h/2 \leq y \leq h.$$

Combining with Eq. 5.98b and integrating, and noting that $v = 0$ at $y = h$, yields

$$v = \frac{(dp_f/ds)^{1/n}}{(K)^{1/n}} \frac{1}{1+1/n} \left[\left(\frac{h}{2} \right)^{1+1/n} - \left(y - \frac{h}{2} \right)^{1+1/n} \right] \quad h/2 \leq y \leq h. \quad (5.99c)$$

Note that Eqs. 5.99b and 5.99c give the same value at $y = h/2$.

The flow rate in the $0 \leq y \leq h/2$ region is half of the total flow rate and is given by

$$q/2 = v dA = w \int_0^{h/2} v dy.$$

Integration gives

$$q = \frac{\left(\frac{1}{K} \frac{dp_f}{ds} \right)^{1/n} (w)(h)^{(2+1/n)}}{2^{1/n} (4+2/n)}. \quad (5.100a)$$

Substituting the expressions for wh and for h given by Eqs. 5.63a and 5.63b into Eq. 5.100a gives

$$q = \frac{\pi \left(\frac{1}{K} \frac{dp_f}{ds} \right)^{1/n} (r_w^2 - r_p^2)(r_w - r_p)^{1+1/n}}{2^{1/n} (4+2/n)}. \quad (5.100b)$$

Expressing the flow rate in terms of the mean flow velocity, \bar{v} , and solving for the frictional pressure gradient, dp_f/dL , gives

$$\frac{dp_f}{ds} = \frac{2K(4+2/n)^n \bar{v}^n}{(r_w - r_p)^{n+1}} = \frac{4K(8+4/n)^n \bar{v}^n}{(d_w - d_p)^{n+1}}. \quad (5.101a)$$

Converting from consistent units to field units, we obtain

$$\frac{dp_f}{ds} = \frac{K \bar{v}^n}{144,000 (d_2 - d_1)^{n+1}} \left(\frac{2+1/n}{0.0208} \right)^n. \quad (5.101b)$$

The derivation of the pressure-loss equation for the laminar flow of a power-law fluid in a pipe is quite similar to the derivation of the slot flow pressure-loss equation. The shear stress for a power-law fluid in a circular pipe is given by

$$\tau = K \left(-\frac{dv}{dr} \right)^n = \frac{r}{2} \frac{dp_f}{ds}.$$

Separating variables and integrating gives

$$v = \frac{\left(\frac{1}{2K} \frac{dp_f}{ds} \right)^{1/n}}{1+1/n} (R^{1+1/n} - r^{1+1/n}). \quad (5.102)$$

The flow rate, q , is given by

$$q = \int_0^R v dA = \left(2\pi \int_0^R v r dr \right) = \frac{2\pi \left(\frac{1}{K} \frac{dp_f}{ds} \right)^{1/n}}{1 + 1/n} \int_0^R (R^{1+1/n} - r^{1+1/n}) r dr.$$

Integrating this equation yields

$$q = \frac{\pi \left(\frac{1}{2K} \frac{dp_f}{ds} \right)^{1/n}}{(3 + 1/n)} R^2 R^{1+1/n} \dots \dots \dots (5.103)$$

Expressing the flow rate in terms of the mean flow velocity, \bar{v} , and solving for the frictional pressure gradient, dp_f/ds , gives

$$\frac{dp_f}{ds} = \frac{2K \bar{v}^n (3 + 1/n)^n}{R^{n+1}} = \frac{4K \bar{v}^n (6 + 2/n)^n}{d^{n+1}} \dots \dots \dots (5.104a)$$

Converting from consistent units to field units, we obtain

$$\frac{dp_f}{ds} = \frac{K \bar{v}^n}{144,000 d^{n+1} (0.0416)} \dots \dots \dots (5.104b)$$

The shear rate in a power-law fluid at the pipe wall can be obtained from the shear stress at the pipe wall and the appropriate frictional-pressure-gradient equation. For a circular pipe,

$$\begin{aligned} \dot{\gamma}_w &= \left(\frac{\tau_w}{K} \right)^{1/n} = \left(\frac{R}{2K} \frac{dp_f}{ds} \right)^{1/n} = \left[\frac{R}{2K} \frac{2K \bar{v}^n (3 + 1/n)^n}{R^{1+n}} \right]^{1/n} \\ &= \frac{2\bar{v} (3 + 1/n)}{d} \dots \dots \dots (5.105a) \end{aligned}$$

After simplifying and changing from consistent units to field units, we obtain

$$\dot{\gamma}_w = \frac{24\bar{v} (3 + 1/n)}{d} \dots \dots \dots (5.105b)$$

Similarly, for an annulus, the shear rate at the wall is given by

$$\begin{aligned} \dot{\gamma}_w &= \left(\frac{\tau_w}{K} \right)^{1/n} = \left(\frac{h}{2K} \frac{dp_f}{ds} \right)^{1/n} = \left[\frac{d_w - d_p}{2K} \frac{2K \bar{v}^n (4 + 2/n)^n}{(d_w - d_p)^{1+n}} \right]^{1/n} \\ &= \frac{4\bar{v} (2 + 1/n)}{d_w - d_p} \dots \dots \dots (5.106a) \end{aligned}$$

After simplifying and changing from consistent units to field units, we obtain

$$\dot{\gamma}_w = \frac{48\bar{v} (2 + 1/n)}{d_w - d_p} \dots \dots \dots (5.106b)$$

Example 5.23 A cement slurry that has a flow behavior index of 0.3 and a consistency index of 9400 eq cp is being pumped in an 8.097×4.5-in. annulus at a rate of 200 gal/min. Assuming the flow pattern is laminar, compute the frictional pressure loss per 1,000 ft of annulus. Also estimate the shear rate at the pipe wall.

Solution. In SI units, the given data become

$$K = \frac{9400 \text{ eq cp}}{10^3 (\text{eq cp})/(\text{Pa} \cdot \text{s}^n)} = 9.4 \text{ Pa} \cdot \text{s}^n,$$

$$d_w = \frac{8.097 \text{ in.}}{39.37 \text{ in./m}} = 0.2057 \text{ m},$$

$$d_p = \frac{4.5 \text{ in.}}{39.37 \text{ in./m}} = 0.1143 \text{ m},$$

$$q = \frac{200 \text{ gal/min}}{1.585 \times 10^4 (\text{gal/min})/(\text{m}^3/\text{s})} = 0.01262 \text{ m}^3/\text{s},$$

$$\Delta L = \frac{1,000 \text{ ft}}{3.048 \text{ ft/m}} = 328.08 \text{ m}.$$

The mean velocity in the annulus is given by

$$\bar{v} = \frac{q}{(\pi/4)(d_w^2 - d_p^2)} = \frac{0.01262}{(\pi/4)(0.2057^2 - 0.1143^2)} = 0.55 \text{ m/s}.$$

The frictional pressure loss predicted by the power-law model is given by Eq. 5.101,

$$\frac{dp_f}{ds} = \frac{4K(8 + 4/n)^n \bar{v}^n}{(d_w - d_p)^{n+1}} = \frac{4(9.4)(8 + 4/0.3)^{0.3} (0.55)^{0.3}}{(0.2057 - 0.1143)^{1.3}} = 1765.2 \text{ Pa/m},$$

and for 328.08 m of annulus, the total pressure drop is

$$\Delta p_f = (1765.2)(328.08) = 0.58 \times 10^6 \text{ Pa},$$

or, in field units,

$$\frac{dp_f}{ds} = \frac{1765.2 \text{ Pa/m}}{22,620.2 (\text{Pa/m})/(\text{psi/ft})} = 0.078 \text{ psi/ft},$$

$$\Delta p_f = (0.078)(1000) = 78 \text{ psi}.$$

The approximate shear rate at the pipe wall is given by Eq. 5.106a:

$$\dot{\gamma}_w = \frac{4\bar{v}(2 + 1/n)}{d_w - d_p} = \frac{4(0.55)(2 + 1/0.3)}{0.2057 - 0.1143} = 128.4 \text{ s}^{-1}.$$

5.5.4 Herschel-Bulkley Fluids. For the flow of Herschel-Bulkley fluids in an annulus modeled as a slot, the analysis follows that of Bingham plastic fluids.

Slot Flow. The Herschel-Bulkley model is given by

$$\tau = \tau_y + K \left(\frac{dv}{dy} \right)^n \quad \tau > \tau_y \quad \frac{dv}{dy} > 0. \quad \dots \dots \dots (5.107)$$

The geometry is depicted in **Fig. 5.32**. There is a central core of the fluid that moves as a rigid plug if the shear stress levels are smaller than the yield stress of the fluid, similar to the flow of a Bingham plastic fluid in a slot, as described above.

Let y_a be the distance of the lower sheared surface from the bottom plate. As before, the balance of momentum is

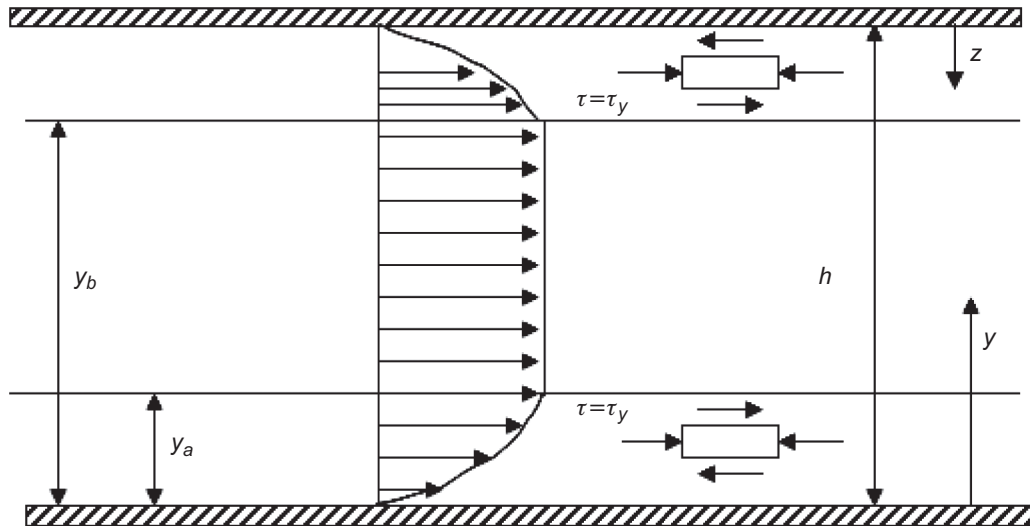


Fig. 5.32—Slot flow of a Herschel-Bulkley fluid.

$$\frac{d\tau}{dy} = \frac{dp_f}{ds}.$$

Integration gives

$$\tau = \tau_0 - y \frac{dp_f}{ds}, \quad \dots \dots \dots (5.108)$$

with τ_0 a constant to be determined.

At the lower side of the plug, y_a , the shear stress τ_a must be equal to τ_y , hence

$$y_a = \frac{\tau_0 - \tau_y}{dp_f/ds}. \quad \dots \dots \dots (5.109)$$

The shear stress is given in terms of the velocity gradient by Eq. 5.107a; hence,

$$\tau = \tau_y + K \left(\frac{dv}{dy} \right)^n = \tau_0 - y \frac{dp_f}{ds}.$$

The solution to the differential equation is given by

$$v = \frac{1}{(m+1)(-dp_f/ds)(K)^m} \left[(\tau_0 - \tau_y) - y \frac{dp_f}{ds} \right]^{m+1} + C_0$$

where $m = 1/n$. The constant of integration is determined from the boundary condition $v = 0$ at $y = 0$, so finally the velocity within the region $0 \leq y \leq y_a$ is given by

$$v = -\frac{1}{(m+1)(dp_f/ds)K^m} \left\{ -(\tau_0 - \tau_y)^{m+1} + \left[(\tau_0 - \tau_y) - y \frac{dp_f}{ds} \right]^{m+1} \right\} \quad 0 \leq y \leq y_a. \quad \dots \dots \dots (5.110a)$$

In terms of parameter y_a , this equation becomes

$$v = \left(\frac{dp_f/ds}{K} \right)^m \left(\frac{1}{m+1} \right) \left[(y_a)^{m+1} - (y_a - y)^{m+1} \right] \quad 0 \leq y \leq y_a. \quad \dots \dots \dots (5.110b)$$

The plug velocity, v_p , is the velocity at $y = y_a$; hence,

$$v_p = \frac{y_a^{m+1}}{m+1} \left(\frac{dp_f/ds}{K} \right)^m \quad y_a \leq y \leq y_b \quad (5.110c)$$

By symmetry, the wall shear stress on the lower plate and the wall shear stress on the upper plate are equal:

$$\tau_{wi} = \tau_{wo} = \tau_w, \quad (5.111a)$$

and balance of momentum gives

$$\tau_w = \frac{h}{2} \frac{dp_f}{ds} \quad (5.111b)$$

Hence, the shear stress equations for the flow in the slot become

$$\tau = \left(\frac{h}{2} - y \right) \frac{dp_f}{dL} \quad 0 \leq y \leq y_a, \quad (5.112a)$$

$$\tau = \tau_y \quad y_a \leq y \leq y_b, \quad (5.112b)$$

$$\tau = \left(y - \frac{h}{2} \right) \frac{dp_f}{dL} \quad y_b \leq y \leq h. \quad (5.112c)$$

The shear stress distribution is depicted in **Fig. 5.33**.

The summary of the necessary equations for the flow of the Herschel-Bulkley fluid in a slot is given below. There is fluid flow only if

$$\frac{dp_f}{dL} > \frac{\tau_y}{h/2} \quad (5.113)$$

When there is flow, then

$$\tau_w = \frac{h}{2} \frac{dp_f}{ds}, \quad (5.114a)$$

$$y_a = \frac{h}{2} - \frac{\tau_y}{dp_f/ds} \quad (5.114b)$$

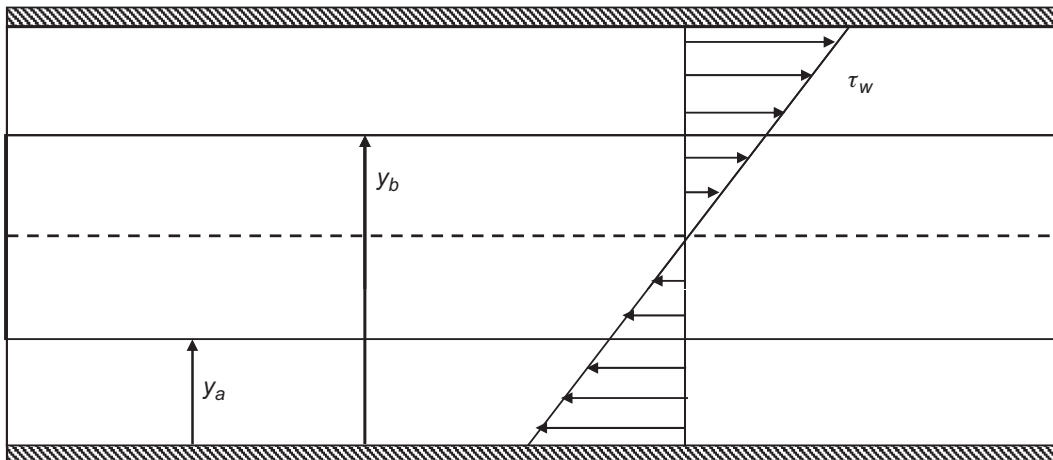


Fig. 5.33—Shear-stress distribution for flow of Herschel-Bulkley fluid in a slot.

The flow rate of the slot is given by

$$q = \frac{2w(h/2)^{2+1/n} \left(\frac{1}{K} \frac{dp_f}{ds} \right)^{1/n} \left(1 - \frac{\tau_y}{(h/2)(dp_f/ds)} \right)^{1+1/n} \left(\frac{\tau_y}{(h/2)(dp_f/ds)} + \frac{1}{n} + 1 \right)}{(1/n+1)(1/n+2)} \quad (5.115)$$

Also, we can express the flow rate in terms of concentric annulus radii as

$$q = \frac{\pi(r_w^2 - r_p^2)(r_w - r_p)^{1+1/n} \left(\frac{1}{K} \frac{dp_f}{ds} \right)^{1/n} \left(1 - \frac{\tau_y}{[(r_w - r_p)/2](dp_f/ds)} \right)^{1+1/n}}{2^{1/n}(1/n+1)(2/n+4)} \times \left(\frac{\tau_y}{[(r_w - r_p)/2](dp_f/ds)} + \frac{1}{n} + 1 \right) \quad (5.116)$$

Eq. 5.100b is implicit in pressure drop. Normally, the flow rate will be available together with the geometry characteristics and the fluid properties, and the pressure drop will be the parameter of interest. In order to solve the above equation, one would have to resort to a trial-and-error solution, in a manner similar to the Bingham plastic fluids, if the full solution (Eq. 5.90c) was retained.

Hanks (1979) has provided the full solution to laminar flow of Herschel-Bulkley fluids in a concentric annulus and presented the results in tabular and graphical form, because explicit equations cannot be derived, relating pressure drop to flow rate for this geometry.

Pipe Flow. For pipe flow of radius R , Eq. 5.87 holds that, for $\tau \geq \tau_y$,

$$\tau = \frac{r}{2} \frac{dp_f}{ds}.$$

The radius at which there is an unsheared portion of the fluid, r_p , is given by

$$\tau_y = \frac{r_p}{2} \frac{dp_f}{ds} \quad (5.117a)$$

The wall shear stress is given by

$$\tau_w = \frac{R}{2} \frac{dp_f}{ds} \quad (5.117b)$$

The Herschel-Bulkley fluid is defined as

$$\tau = \tau_y + K \left(-\frac{dv}{dr} \right)^n \quad (5.118)$$

Hence,

$$\tau_y + K \left(-\frac{dv}{dr} \right)^n = \frac{r}{2} \frac{dp_f}{ds}.$$

The solution to the differential equation is then

$$v = -\frac{2K}{(dp_f/ds)} \frac{1}{m+1} \left(\frac{r}{2K} \frac{dp_f}{ds} - \frac{\tau_y}{K} \right)^{m+1} + v_0,$$

with $m = 1/n$. From the boundary condition $v = 0$ at $r = R$, the constant of integration is easily shown to be

$$v_0 = \frac{2K}{(dp_f/ds)} \frac{1}{m+1} \left(\frac{R}{2K} \frac{dp_f}{ds} - \frac{\tau_y}{K} \right)^{m+1}.$$

The velocity for the laminar flow of a Herschel-Bulkley fluid in a pipe is then given by

$$v = \frac{2K}{(dp_f/ds)} \left(\frac{1}{m+1} \right) \left[\left(\frac{R}{2K} \frac{dp_f}{ds} - \frac{\tau_y}{K} \right)^{m+1} - \left(\frac{r}{2K} \frac{dp_f}{ds} - \frac{\tau_y}{K} \right)^{m+1} \right] \quad r_p = \frac{\tau_y}{(dp_f/ds)/2} \leq r \leq R \dots\dots\dots (5.119a)$$

and

$$v = v_p = \left(\frac{dp_f/ds}{K} \right)^m \left(\frac{1}{m+1} \right) \left(R - \frac{\tau_y}{(dp_f/ds)/2} \right)^{m+1} \quad 0 \leq r \leq r_p \dots\dots\dots (5.119b)$$

This equation can be integrated to give the flow rate:

$$q = \frac{\pi n}{K^{1/n}} \frac{([dp_f/ds] R/2 - \tau_y)^{1/n+1}}{([dp_f/ds]/2)^3} \left[\frac{([dp_f/ds] R/2 - \tau_y)^2}{1+3n} + \frac{2\tau_y ([dp_f/ds] R/2 - \tau_y)}{1+2n} + \frac{\tau_y^2}{1+n} \right] \dots\dots\dots (5.120a)$$

If we now define

$$\phi = \frac{\tau_y}{\tau_w}$$

then Eq. 5.120a becomes

$$q = \pi n R^3 \left(\frac{dp_f/dL}{K} \frac{R}{2} \right)^{1/n} (1-\phi)^{(1+n)/n} \left[\frac{(1-\phi)^2}{3n+1} + \frac{2\phi(1-\phi)}{2n+1} + \frac{\phi^2}{n+1} \right],$$

or

$$q = \pi n R^3 \left(\frac{dp_f/dL}{K} \frac{R}{2} \right)^{1/n} \frac{(1-\phi)^{(1+n)/n}}{(3n+1)(2n+1)(n+1)} \times [(n+1)(2n+1) + 2n(n+1)\phi + 2n^2\phi^2] \dots\dots\dots (5.120b)$$

Eq. 5.120b gives the required flow rate for flow of a Herschel-Bulkley fluid in a pipe of radius R for a given pressure drop dp_f/dL . The equation cannot be simplified further, and the inverse problem of finding the pressure drop for a given flow rate requires iteration, as in the case of Bingham plastic fluids if the full solution was retained.

The velocity profiles can also be given as functions of the parameter ϕ :

$$v = v_p = \frac{nR(\tau_w/K)^{1/n}}{n+1} (1-\phi)^{1/n+1} \quad 0 \leq r \leq \phi R, \dots\dots\dots (5.121a)$$

$$v = \frac{nR(\tau_w/K)^{1/n}}{n+1} \left[(1-\phi)^{1/n+1} - \left(\frac{r}{R} - \phi \right)^{1/n+1} \right] \quad \phi R \leq r \leq R \dots\dots\dots (5.121b)$$

Denoting \bar{v} the mean velocity for flow in a pipe, it can be shown that

$$\bar{v} = \frac{nR(\tau_w/K)^{1/n} (1-\phi)^{1/n+1}}{(3n+1)(2n+1)(n+1)} [(n+1)(2n+1) + 2n(n+1)\phi + 2n^2\phi^2] \dots\dots\dots (5.122)$$

Hence, the velocity profiles can be expressed in terms of the mean velocity as

$$\frac{v_p}{\bar{v}} = \frac{1}{(3n+1)(2n+1)} \frac{(1-\phi)^{1/n+1}}{(n+1)(2n+1)+2n(n+1)\phi+2n^2\phi^2} \quad 0 \leq r \leq \phi R \quad \dots\dots\dots (5.123a)$$

and

$$\frac{v}{\bar{v}} = \frac{1}{(3n+1)(2n+1)} \frac{(1-\phi)^{1/n+1} - \left(\frac{r}{R} - \phi\right)^{1/n+1}}{(n+1)(2n+1)+2n(n+1)\phi+2n^2\phi^2} \quad \phi R \leq r \leq R \quad \dots\dots\dots (5.123b)$$

Example 5.24 Bailey and Peden (2000) presented a comprehensive hydraulic model for flow of drilling fluids in pipes and annuli. They have presented the experimental results of Okafor and Evers (1992) together with their predictions, for both laminar and turbulent flow in a pipe with a 2-in. ID. The laminar data are reproduced in the table below. Using the relationships derived above for Herschel-Bulkley fluids, compute the pressure loss for the various flow velocities indicated in the table and compare with measurements as well as predictions from Bailey and Peden.

The fluid is modeled by the authors as Herschel-Bulkley with parameters $\tau_y = 0.62201$ Pa, $K = 0.11934$ Pa \cdot s n , and $n = 0.75534$.

Velocity (m/s)	Measured $\Delta p/\Delta L$ (Pa/m)	Predicted ¹ $\Delta p/\Delta L$ (Pa/m)	Flow Regime ¹	Predicted ² $\Delta p/\Delta L$ (Pa/m)	Flow Regime ²
0.202	190	206	Laminar	199	Laminar
0.409	283	306	Laminar	295	Laminar
0.562	341	368	Laminar	355	Laminar
0.724	405	429	Laminar	420	Laminar
0.914	470	494	Laminar	489	Laminar
1.076	523	548	Laminar	544	Laminar
1.382	644	641	Laminar	645	Laminar
1.448	700	661	Laminar	665	Laminar

¹ Predicted by Bailey and Peden (2000)

² Predicted using the proposed methodology

Solution. Following the proposed methodology, we get the predictions for pressure drop, which are shown in the table above. The comparison with the data is shown in **Fig. 5.34**.

5.6 Turbulent Flow in Pipes and Annuli

In many drilling operations, the drilling fluid is pumped at too high a rate for laminar flow to be maintained. The fluid lamina become unstable and break into a chaotic diffused flow pattern. The transfer of momentum caused by this chaotic fluid movement causes the velocity distribution to become more uniform across the center portion of the conduit than for laminar flow. However, a thin boundary layer of fluid near the pipe walls generally remains in laminar flow. A schematic representation of laminar and turbulent pipe flow is shown in **Fig. 5.35**.

A mathematical development of flow equations for turbulent flow has not been possible to date. However, a large amount of experimental work has been done in straight sections of circular pipe, and the factors influencing the onset of turbulence and the frictional pressure losses due to turbulent flow have been identified. By applying the method of dimensional analysis, these factors have been grouped so that the empirical data could be expressed in terms of dimensionless numbers.

5.6.1 Newtonian Fluid Models. The experimental work of Reynolds (1883) has shown that the onset of turbulence in the flow of Newtonian fluids through pipes depends on pipe diameter d , density of fluid ρ , viscosity of

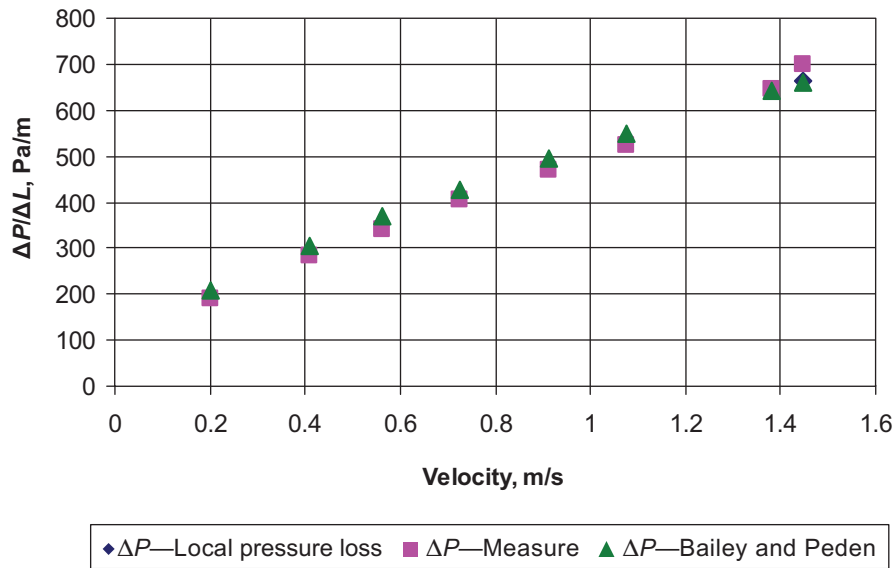


Fig. 5.34—Comparison of predictions with measurements from data of Okafor and Evers (1992) and with predictions of Bailey and Peden (2000).

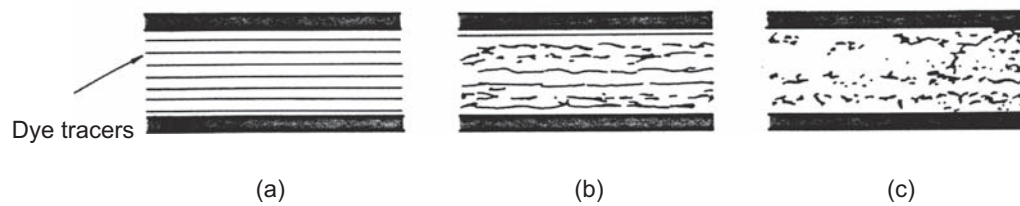


Fig. 5.35—Laminar- and turbulent-flow patterns in a circular pipe: (a) laminar flow, (b) transition between laminar and turbulent flow, and (c) turbulent flow [from Bourgoyne et al. (1991)].

fluid μ , and average flow velocity \bar{v} . In terms of the primary units of mass m , length L , and time t , these variables have the following dimensions:

d, L .

$\rho, m/L^3$.

$\mu, m/(Lt)$.

$\bar{v}, L/t$.

The Buckingham Pi theorem of dimensional analysis states that the number of independent dimensionless groups N that can be obtained from n parameters is given by $N = n - m$, where m is the number of primary units involved. Because all three primary units (m , L , and t) are used in at least one of the four parameters shown previously, $N = 4 - 3 = 1$, and only one independent dimensionless group is possible. The dimensionless grouping commonly used is expressed in consistent units by

$$N_{Re} = \frac{\rho \bar{v} d}{\mu}, \quad \dots \quad (5.124a)$$

where N_{Re} is the Reynolds number. In field units, this equation becomes

$$N_{Re} = \frac{928 \rho \bar{v} d}{\mu}, \quad \dots \quad (5.124b)$$

where ρ = fluid density, lbm/gal; \bar{v} = mean fluid velocity, ft/sec; d = pipe diameter, in.; and μ = fluid viscosity, cp.

For engineering purposes, flow of a Newtonian fluid in pipes usually is considered to be laminar if the Reynolds number is less than 2,100 and turbulent if the Reynolds number is greater than 2,100. However, for Reynolds numbers of approximately 2,000 to 4,000, the flow is actually in a transition region between laminar flow and fully developed turbulent flow. Also, careful experimentation has shown that the laminar region may be made to terminate at a Reynolds number as low as 1,200 by artificially introducing energy into the system (e.g., hitting the pipe with a hammer). Likewise, the laminar flow region can be extended to Reynolds numbers as high as 40,000 by using extremely smooth, straight pipes that are insulated from vibrations. However, these conditions generally are not realized in rotary-drilling situations.

Example 5.25 A 1080-kg/m³ (9.0-lbm/gal) brine having a viscosity of 0.001 Pa·s (1.0 cp) is being circulated in a well at a rate of 0.03787 m³/s (600 gal/min). Determine whether the fluid in the drillpipe is in laminar or turbulent flow if the ID of the drillpipe is 0.1086 m (4.276 in.).

Solution. The cross-sectional area of the pipe is given by

$$A = \pi \frac{d^2}{4} = \frac{(3.14)(0.1086 \text{ m})^2}{4} = 0.009258 \text{ m}^2.$$

The average velocity in the drillpipe is given by

$$\bar{v} = \frac{q}{A} = \frac{0.03787 \text{ m}^3/\text{s}}{0.009258 \text{ m}^2} = 4.088 \text{ m/s},$$

or, in field units,

$$\bar{v} = \frac{4.088 \text{ m/s}}{0.3048 \text{ m/ft}} = 13.4 \text{ ft/s}.$$

Using Eq. 5.123c, the Reynolds number is given by

$$N_{\text{Re}} = \frac{\rho \bar{v} d}{\mu} = \frac{(1,080)(4.088)(0.1086)}{0.001} = 479,473.$$

Because the Reynolds number is well above 2,100, the fluid in the drillpipe is in turbulent flow.

Once it has been established that the flow pattern is turbulent, the determination of the frictional pressure loss must be based on empirical correlations. The most widely used correlations are based on a dimensionless quantity known as the *friction factor*. The friction factor is defined by

$$f = \frac{F_k}{AE_k}, \dots \dots \dots (5.125a)$$

where F_k = force exerted on the conduit walls due to fluid movement, A = characteristic area of the conduit, and E_k = kinetic energy per unit volume of fluid.

For pipe flow, the shear stress on the conduit walls is given by

$$\tau_w = \frac{R}{2} \frac{dp_f}{ds} = \frac{d}{4} \frac{dp_f}{ds}.$$

The force F_k exerted at the pipe wall due to fluid motion is given by

$$F_k = (2\pi R \Delta s) \tau_w = \frac{\pi d^2}{4} \frac{dp_f}{ds} \Delta s.$$

The kinetic energy per unit volume of fluid is given by

$$E_k = \frac{1}{2} \rho \bar{v}^2.$$

Substituting the expressions for F_k and E_k into Eq. 5.124a yields

$$f = \frac{\pi d^2 \frac{dp_f}{ds} \Delta s}{2 \rho \bar{v}^2 A}. \quad \dots\dots\dots (5.125b)$$

If the characteristic area A is chosen to be $A = \pi d \Delta s$, Eq. 5.125b reduces to

$$f = \frac{d}{2 \rho \bar{v}^2} \frac{dp_f}{ds}. \quad \dots\dots\dots (5.125c)$$

Eq. 5.125c is known as the Fanning equation, and the friction factor defined by this equation is called the Fanning friction factor or simply the friction factor. In turbulent flow, the friction factor f is a function of the Reynolds number N_{Re} and a term called the relative roughness, e/d , which is defined as the ratio of the absolute roughness, e , to the pipe diameter, with the absolute roughness representing the average depth of pipe wall irregularities. An empirical correlation for the determination of friction factors for fully developed turbulent flow in circular pipe has been presented by Colebrook (1939). The Colebrook function is given by

$$\frac{1}{\sqrt{f}} = -4 \log \left(0.269 \frac{e}{d} + \frac{1.255}{N_{Re} \sqrt{f}} \right). \quad \dots\dots\dots (5.125d)$$

The friction factor f appears both inside and outside the logarithmic term of Colebrook's equation, requiring an iterative solution technique. This difficulty can be avoided by a graphical representation of the Colebrook function. A plot of friction factor against Reynolds number on log-log paper is called a *Stanton chart*. A Stanton chart for the Colebrook function is shown in **Fig. 5.36**. However, the solution of Eq. 5.125d using an electronic calculator is not difficult and yields more precise results than is possible using the graphical solution.

The selection of an appropriate absolute roughness e for a given application is often difficult. Shown in **Table 5.1** are average roughness values determined empirically for several types of conduits. Also, Cullender and Smith (1956) in a study of published data obtained in clean steel pipes in gas-well and pipeline service found an average pipe roughness of 0.01651 mm (0.00065 in.) to apply to most of the data. Fortunately, in rotary-drilling applications involving the use of relatively viscous drilling fluids, the Reynolds number seldom exceeds 100,000. Also, for most wellbore geometries, the relative roughness is usually less than 0.0004 in all sections. For these conditions, the friction factors for smooth pipe (zero roughness) can be applied for most engineering calculations. For smooth pipe, Eq. 5.124d reduces to

$$\frac{1}{\sqrt{f}} = 4 \log (N_{Re} \sqrt{f}) - 0.395. \quad \dots\dots\dots (5.125e)$$

In addition, for smooth pipe and a Reynolds number range of 2,100 to 100,000, a straightline approximation (on a log-log plot) of the Colebrook function is possible. This approximation, first presented by Blasius (1913), is given by

$$f = \frac{0.0791}{N_{Re}^{0.25}}, \quad \dots\dots\dots (5.125f)$$

where $2,100 \leq N_{Re} \leq 100,000$ and $e/d = 0$.

The Fanning equation (Eq. 5.125c) can be rearranged for the calculation of frictional pressure drop due to turbulent flow in circular pipe as

$$\frac{dp_f}{ds} = \frac{2f \rho \bar{v}^2}{d}, \quad \dots\dots\dots (5.126a)$$

and converting to field units gives

$$\frac{dp_f}{ds} = \frac{f \rho \bar{v}^2}{25.8d}. \quad \dots\dots\dots (5.126b)$$

In addition, the Fanning equation can be extended to the laminar flow region if the friction factor for the laminar region is defined by

$$f = \frac{16}{N_{Re}} \quad (5.126c)$$

The proof of this relation is left as a student exercise.

A simplified turbulent flow equation thus can be developed for smooth pipe and moderate Reynolds numbers by substituting Eq. 5.125d into Eq. 5.126a, which, after simplification, yields

$$\frac{dp_f}{dL} = \frac{0.1582 \rho^{0.75} \bar{v}^{1.75} \mu^{0.25}}{d^{1.25}} = \frac{0.2416 \rho^{0.75} q^{1.75} \mu^{0.25}}{d^{4.75}}, \quad (5.126d)$$

or, in field units,

$$\frac{dp_f}{dL} = \frac{\rho^{0.75} \bar{v}^{1.75} \mu^{0.25}}{1800 d^{1.25}} = \frac{\rho^{0.75} q^{1.75} \mu^{0.25}}{8624 d^{4.75}} \quad (5.126e)$$

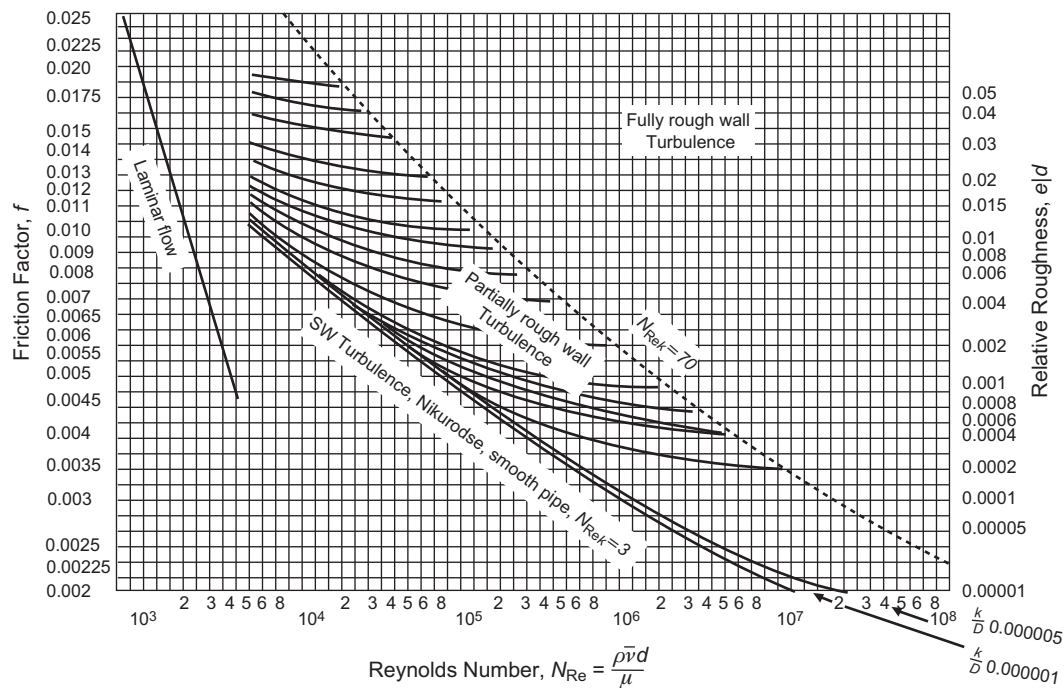


Fig. 5.36—Stanton chart showing Fanning friction factors for turbulent flow in circular pipe [after Moody (1944)].

TABLE 5.1—ABSOLUTE PIPE ROUGHNESS FOR SEVERAL TYPES OF CIRCULAR PIPES [AFTER STREETER (1962)] Reproduced with permission from The McGraw-Hill Companies.		
Type of Pipe	Absolute Roughness, —e (mm)	Absolute Roughness, —e (in.)
Riveted steels	0.00635 to 0.0635	0.00025 to 0.0025
Concrete	0.002108 to 0.02108	0.000083 to 0.00083
Cast iron	0.001803	0.000071
Galvanized iron	0.0010668	0.000042
Asphalted cast iron	0.0008382	0.000033
Commercial steel	0.0003302	0.000013
Drawn tubing	0.0001016	0.000004

Eqs. 5.126d and 5.126e are valid for circular pipes where $e/d = 0$ and N_{Re} is between 2,100 and 100,000. These equations are in a form that readily identifies the relative influence of the various hydraulic parameters on turbulent frictional pressure loss. For example, it can be shown that changing from a drillpipe diameter of 0.143 to 0.1270 m (4.5 to 5 in.) would reduce the pressure loss in the drillpipe by approximately a factor of two.

Example 5.26 Determine the frictional pressure drop in 3048 m (10,000 ft) of 0.143-m (4.5-in.) drillpipe having an ID of 0.09718 m (3.826 in.) if a 0.020-Pa·s (20-cp) Newtonian fluid having a density of 1080 kg/m³ (9 lbm/gal) is pumped through the drillpipe at a rate of 0.0253 m³/s (400 gal/min).

Solution. The mean fluid velocity is given by

$$\bar{v} = \frac{q}{\pi d^2 / 4} = \frac{0.0253}{(3.14/4)(0.09718)^2} = 3.41 \text{ m/s} = 11.2 \text{ ft/s}.$$

The Reynolds number is given by

$$N_{\text{Re}} = \frac{\rho \bar{v} d}{\mu} = \frac{(1080)(3.41)(0.09718)}{0.020} = 17,894.$$

Because the Reynolds number is greater than 2,100, the flow pattern is turbulent. For commercial steel, the absolute roughness is given in Table 5.1 as 0.0003302 mm. Thus, the relative roughness is

$$\frac{e}{d} = \frac{0.0003302 \text{ mm}}{97.18 \text{ mm}} = 0.0000034.$$

Note that this corresponds closely to the smooth pipeline on Fig. 5.36 at a Reynolds number of 17,894. Solving Eq. 5.125d by trial and error, the Fanning friction factor is 0.00666. Thus, the frictional pressure loss is given by

$$\Delta p_f = \frac{dp_f}{dL} \Delta L = \frac{2f\rho\bar{v}^2}{d} \Delta L = \frac{2(0.00666)(1080)(3.41)^2}{(0.09718)} (3048) = 5.211 \times 10^6 \text{ Pa},$$

or, in field units,

$$\Delta p_f = 756 \text{ psi}.$$

It is interesting to note that the use of the simplified turbulent flow equation given by Eq. 5.126c gives

$$\begin{aligned} \Delta p_f = \frac{dp_f}{dL} \Delta L &= \frac{0.1582 \rho^{0.75} \bar{v}^{1.75} \mu^{0.25}}{d^{1.25}} \Delta L = \frac{0.1582 (1080)^{0.75} (3.41)^{1.75} (0.020)^{0.25}}{(0.09718)^{1.25}} (3048) \\ &= 5.3876 \times 10^6 \text{ Pa} = 781 \text{ psi}. \end{aligned}$$

The student should be warned that the Fanning friction factor presented in this text and commonly used in the drilling industry may be different from the friction factor used in other texts. A common friction factor used in many engineering texts is the *Darcy-Weisbach friction factor*, usually presented in graphical form by Moody. The Moody friction factor is four times larger than the Fanning friction factor. Thus, a friction factor read from a Moody chart must be divided by four before being used with the equations presented in this text.

A large amount of experimental work has been done in circular pipe. Unfortunately, this is not true for flow conduits of other shapes. When noncircular flow conduits are encountered, a common practice is to calculate an effective conduit diameter such that the flow behavior in a circular pipe of that diameter would be roughly equivalent to the flow behavior in the noncircular conduit. This concept, called the *hydraulic diameter*, is given in Eq. 5.24.

5.6.2 Non-Newtonian Fluid Models. When the flow becomes turbulent, no analytical solutions exist for flow of non-Newtonian fluids in pipes and annuli, and resort is made to experimental data. Determination of the q - Δp relationship is performed through the use of the friction-factor concept. Several equations have been proposed for the friction factor for turbulent flow of Bingham plastic, power-law, and Herschel-Bulkley fluids. Several investigators have tried to assess the accuracy of these correlations, either comparing the individual predictions or comparing predictions with experimental data. In a study by Harnett and Kostic (1990), referenced by Chabra and Richardson (1999), it was found that the best approach was through the use of the Metzner and Reed graph (Metzner and Reed 1955). Variations of predictions of the different proposed correlations were found to differ by as much as $\pm 50\%$ in a study by Heywood and Cheng (1984) for turbulent flow of Herschel-Bulkley fluids in pipes.

Bingham Plastic Model. The frictional pressure loss associated with the turbulent flow of a Bingham plastic fluid is affected primarily by density and plastic viscosity. While the yield point of the fluid affects both the frictional pressure loss in laminar flow and the fluid velocity at which turbulence begins, at higher shear rates corresponding to a fully turbulent flow pattern, the yield point is no longer a highly significant parameter. It has been found empirically that the frictional pressure loss associated with the turbulent flow of a Bingham plastic fluid can be predicted using the equations developed for Newtonian fluids if the plastic viscosity is substituted for the Newtonian viscosity. This substitution can be made in the Reynolds number used in the Colebrook function defined by Eq. 5.124e or in the simplified turbulent flow equation given by Eq. 5.126c.

Example 5.27 A 10-lbm/gal mud having a plastic viscosity of 40 cp and a yield point of 15 lbf/100 ft² is being circulated at a rate of 600 gal/min. Estimate the frictional pressure loss in the annulus opposite the drill collars if the drill collars are in a 6.5-in. hole, have a length of 1,000 ft, and have a 4.5-in. OD. Assume turbulent flow.

Solution. Converting to SI units, we get

$$\rho = \frac{10 \text{ lbm/gal}}{8.3454 \times 10^{-3} (\text{lbm/gal})/(\text{kg/m}^3)} = 1.198 \times 10^3 \text{ kg/m}^3,$$

$$\mu_p = \frac{40 \text{ cp}}{10^3 \text{ cp}/(\text{Pa} \cdot \text{s})} = 4.0 \times 10^{-2} \text{ Pa} \cdot \text{s},$$

$$\tau_y = \frac{15 \text{ lbf}}{100 \text{ ft}^2} \times \frac{0.4788 \text{ Pa}}{\text{lbf}/(100 \text{ ft}^2)} = 7.182 \text{ Pa},$$

$$d_w = \frac{6.5 \text{ in.}}{3.937 \times 10^1 \text{ in./m}} = 0.1651 \text{ m},$$

$$d_p = \frac{4.5 \text{ in.}}{3.937 \times 10^1 \text{ in./m}} = 0.1143 \text{ m},$$

$$s = \frac{1,000 \text{ ft}}{3.2808 \text{ ft/m}} = 3.048 \times 10^2 \text{ m},$$

$$q = \frac{600 \text{ gal/min}}{1.585 \times 10^4 (\text{gal/min})/(\text{m}^3/\text{s})} = 3.785 \times 10^{-2} \text{ m}^3/\text{s}.$$

The average velocity is given by

$$\bar{v} = \frac{3.785 \times 10^{-2}}{(\pi/4)(0.1651^2 - 0.1143^2)} = 3.397 \text{ m/s}.$$

Computing the hydraulic diameter using Eq. 5.24 yields

$$d_e = 0.1651 - 0.1143 = 0.0508 \text{ m}.$$

The Reynolds number using the plastic viscosity is then

$$N_{Re} = \frac{\rho \bar{v} d_e}{\mu_p} = \frac{(1198)(3.397)(0.0508)}{0.04} = 5,168.$$

The Colebrook function for smooth pipe (Eq. 5.125e) gives a friction factor of 0.0093 for a Reynolds number of 5,168. Thus, the pressure drop is given by

$$\Delta p_f = \frac{dp_f}{ds} \Delta s = \frac{2f \rho \bar{v}^2}{d_e} \Delta s = \frac{2(0.0093)(1198)(3.397)^2(304.8)}{(0.0508)} = 1,542,809 \text{ Pa},$$

or, in field units,

$$\Delta p_f = \frac{1,542,809 \text{ Pa}}{6894.73 \text{ Pa/psi}} = 224 \text{ psi}.$$

It is interesting to note that the use of the laminar flow equation gives

$$\Delta p_f / \Delta s = \frac{48 \mu_p \bar{v}}{(d_w - d_p)^2} + \frac{6 \tau_y}{(d_w - d_p)} = \frac{48(0.04)(3.397)}{(0.1651 - 0.1143)^2} + \frac{6(7.182)}{(0.1651 - 0.1143)} = 3375.6 \text{ Pa/m},$$

or

$$\Delta p_f = (3375.6)(304.8) = 1,028,883 \text{ Pa} = 149 \text{ psi},$$

which is less than the value predicted by the turbulent flow relations. Thus, the flow pattern giving the greatest frictional pressure loss is turbulent flow.

Power-Law Model. Dodge and Metzner (1959) extended the Colebrook equation for Newtonian fluids to power-law fluids and showed that the friction factor for the power-law fluids can be given by

$$\frac{1}{\sqrt{f}} = \frac{4}{(n)^{0.75}} \log(N_{ReMR} f^{1-n/2}) - \frac{0.395}{(n)^{1.2}},$$

$$N_{ReMR} = \frac{\rho \bar{v}^{2-n'} d^{n'}}{K' (8)^{n'-1}} \text{ for pipes},$$

$$N_{ReMR} = \frac{\rho \bar{v} (d_2 - d_1)}{\mu_e} \text{ for annuli.} \quad \dots \quad (5.127)$$

Good agreement was found with their data of polymer solutions and clay suspensions, while Guillot and Dennis (1988) have also reported good agreement of predictions of Eq. 5.127 with their data on cement slurries. Irvine (1988) suggested the following Blasius-type equation for power-law fluids flowing in pipes:

$$f = \left[\frac{D(n)}{N_{ReMR}} \right]^{\frac{1}{3n+1}}, \quad \dots \quad (5.128a)$$

where

$$D(n) = \frac{2^{n+4}}{7^{7n}} \left(\frac{4n}{3n+1} \right)^{3n^2}, \quad \dots \quad (5.128b)$$

which readily reduces to the Blasius equation for $n = 1$. This equation gave $\leq 8\%$ error when compared to data covering a range of $0.35 \leq n \leq 0.89$ and $2,000 \leq N_{ReMR} \leq 50,000$. Guillot (1990) has also suggested a power-law relationship between the friction factor and Reynolds number valid for $N_{ReMR} < 10^5$ of the form

$$f = a(n)N_{\text{Re}MR}^{b(n)}, \quad \dots \quad (5.129a)$$

with $a(n)$ and $b(n)$ having different forms for a pipe and an annulus. For a pipe,

$$a(n) = 0.079 + 0.0207 \log(n), \quad \dots \quad (5.129b)$$

$$b(n) = -0.251 + 0.141 \log(n), \quad \dots \quad (5.129c)$$

while, for the annulus, he gives

$$a(n) = 0.0893 + 0.0246 \log(n), \quad \dots \quad (5.129d)$$

$$b(n) = -0.263 + 0.138 \log(n). \quad \dots \quad (5.129e)$$

The above analysis shows that for power-law fluids flowing either in a pipe or in an annulus, the approach using the apparent Newtonian viscosity gives the same pressure-drop relationships as the approach of using the local power-law fluids, as it should.

Example 5.28 A 15.6-lbm/gal cement slurry having a consistency index of 335 eq cp and a flow behavior index of 0.67 is being pumped at a rate of 672 gal/min between a 9.625-in.-diameter hole and a 7.0-in.-diameter casing. Determine the frictional pressure loss per 100 ft of slurry. Use Eq. 5.175a to obtain the equivalent diameter.

Solution. Converting from field units to SI units, we get

$$\rho = \frac{15.6 \text{ lbm/gal}}{8.3454 \times 10^{-3} (\text{lbm/gal})/(\text{kg/m}^3)} = 1.869 \times 10^3 \text{ kg/m}^3,$$

$$K = \frac{335 \text{ eq cp}}{10^3 (\text{eq cp})/(\text{Pa} \cdot \text{s}^n)} = 0.335 \text{ Pa} \cdot \text{s}^n,$$

$$d_w = \frac{9.625 \text{ in.}}{3.937 \times 10^1 \text{ in./m}} = 0.2445 \text{ m},$$

$$d_p = \frac{7.0 \text{ in.}}{3.937 \times 10^1 \text{ in./m}} = 0.1778 \text{ m},$$

$$D = \frac{100 \text{ ft}}{3.2808 \text{ ft/m}} = 30.48 \text{ m},$$

$$q = \frac{672 \text{ gal/min}}{1.585 \times 10^4 (\text{gal/min})/(\text{m}^3/\text{s})} = 42.397 \times 10^{-3} \text{ m}^3/\text{s}.$$

The equivalent diameter is computed from Eq. 5.24:

$$d_e = d_w - d_p = 0.2445 - 0.1778 = 0.0667 \text{ m}.$$

The mean fluid velocity is given by

$$\bar{v} = \frac{q}{(\pi/4)(d_w^2 - d_p^2)} = \frac{42.397 \times 10^{-3}}{(\pi/4)(0.2445^2 - 0.1778^2)} = 1.917 \text{ m/s}.$$

The Reynolds number is given by Eq. 5.203a:

$$N_{Re} = \frac{\rho \bar{v}^{2-n} (d_w - d_p)^{n-1} d_e}{12^{n-1} K [(2n+1)/3n]^n} = \frac{(1869)(1.917)^{2-0.67} (0.2445-0.1778)^{0.67-1} (0.0667)}{12^{0.67-1} (0.335) [(2 \times 0.67 + 1)/(3 \times 0.67)]^n} = 4,431.$$

From **Fig. 5.37**, the friction factor for $n = 0.67$ and $N_{Re} = 4,431$ is 0.00763. This can be verified using Eq. 5.127. Thus, the frictional pressure drop is given by

$$\frac{dp_f}{ds} = \frac{f \rho \bar{v}^2}{d_e} = \frac{2(0.00763)(1869)(1.917)^2}{[0.816(0.2445-0.1778)]} = 1574 \text{ Pa/m},$$

or, in field units,

$$\frac{dp_f}{ds} = \frac{1.574 \text{ Pa/m}}{22.6202 \text{ (Pa/m)/(psi/ft)}} = 0.0696 \text{ psi/ft},$$

and for 100 ft, the pressure drop is $\Delta p_f = 6.7$ psi.

If we compute the friction using the Irvine equation, we get

$$D(n) = \frac{2^{n+4}}{7^{7n}} \left(\frac{4n}{3n+1} \right)^{3n^2} = \frac{2^{4.67}}{7^{4.69}} \left(\frac{4 \times 0.67}{3 \times 0.67 + 1} \right)^{1.3467} = 0.002368,$$

thus giving

$$f = \left[\frac{0.002368}{4,431} \right]^{0.3322} = 0.00825,$$

which is 8% higher than the one computed with the full Metzner and Reed equation.

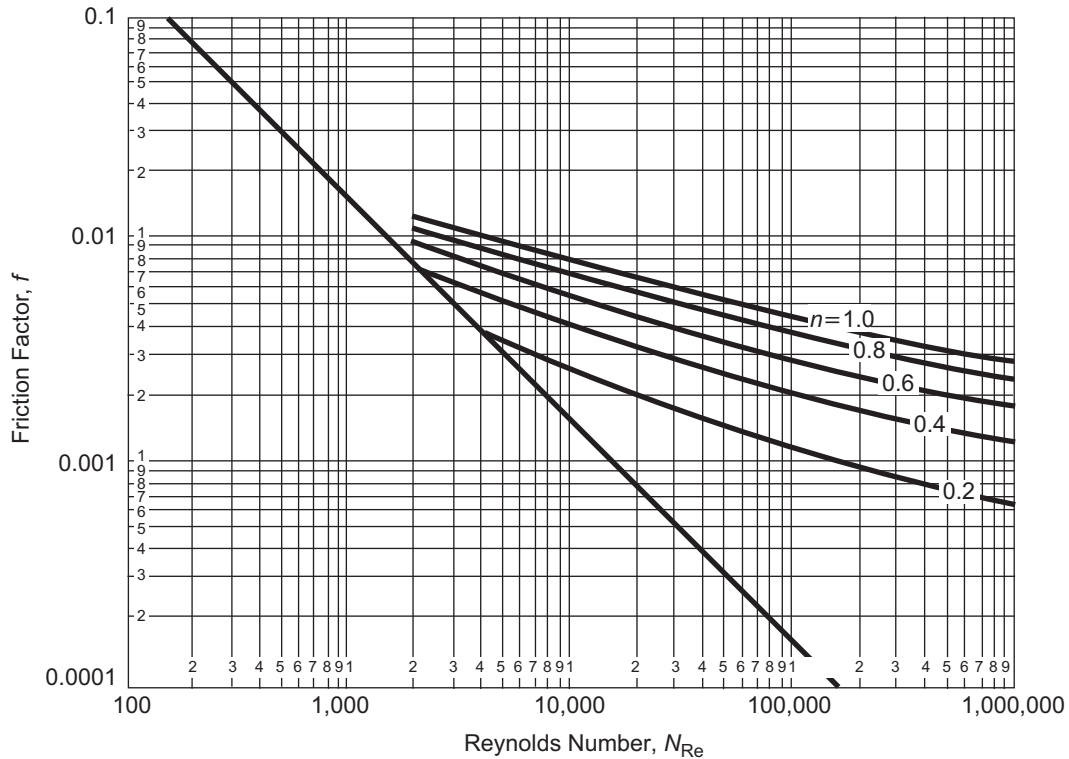


Fig. 5.37—Friction factors for power-law-fluid model [from Bourgoyne et al. (1991)].

Similarly, we can estimate the friction factor using the approach of Guillot; hence,

$$a(n) = 0.0893 + 0.0246 \log(0.67) = 0.08502,$$

and

$$b(n) = -0.263 + 0.138 \log(0.67) = -0.2870.$$

Hence,

$$f = a(n) N_{ReMR}^{b(n)} = (0.08502)(4,431)^{-0.287} = 0.0076,$$

which is within only 1% of the friction factor computed with the full Metzner and Reed equation.

Herschel-Bulkley Model. Various approaches have been suggested to compute the friction factor for turbulent flow of Herschel-Bulkley fluids. In a study by Heywood and Cheng (1984) for turbulent flow of Herschel-Bulkley fluids in pipes, the authors proposed that computation of the friction factor for turbulent flow of power-law fluids can be done either by using the Metzner and Reed approach (Metzner and Reed 1955) by deriving the local power-law parameters of Herschel-Bulkley fluids, thus taking into account the effect of the yield stress, or by neglecting the effect of the yield stress, because at the high shear rates encountered during turbulent flow, the yield stress should have minimal impact. For this situation, the equation proposed for power-law fluids, Eq. 5.127, should be used, with the K and n values being the same values as the parameters of the Herschel-Bulkley fluid. This was further supported in a recent paper by Brand et al. (2001) through measurements of pressure drop in a pipe in turbulent flow. These results indicate that in turbulent flow, the plug zone completely disappears, and the yield stress of the fluid does not play any role in the pressure-drop generation.

Reed and Pilehvari (1993) presented a model for laminar, transitional, and turbulent flow of drilling muds using the Herschel-Bulkley rheological model. They proposed modifications to the diameter(s) of the conduit to account for the non-Newtonian effect and the use of the approach of Metzner and Reed (1955) with the generalized power-law model.

Subramanian and Azar (2000) compared predictions of the Bingham plastic approach, the power-law approach, and the Reed and Pilehvari approach for Herschel-Bulkley fluids with their experimental data for a series of experiments with bentonite, glycol mud, polymer mud, and petroleum-free vegetable-oil mud flowing in a pipe and an annulus. In many cases, the Reed and Pilehvari approach with the Herschel-Bulkley fluid gave the most satisfactory results. For some cases with polymer mud (turbulent flow and rough pipe) and for the petroleum-free vegetable-oil mud, the predictions from all models were at odds with the measurements.

5.6.3 Recommended Friction Models. The *Petroleum Engineering Handbook, Volume II: Drilling Engineering* (Lake 2006) recommends the following friction factor calculations:

Rheological Model 1: Newtonian Fluids.

Pipe Flow.

Frictional pressure drop:

$$\frac{dp_f}{ds} = \frac{2f\rho v^2}{D} \quad \dots\dots\dots (5.130)$$

Reynolds number:

$$N_{Re} = D\rho v/\mu, \quad \dots\dots\dots (5.131)$$

where D is the pipe ID.

Laminar flow:

$$f = 16/N_{Re}, \quad \dots\dots\dots (5.132)$$

for $N_{Re} < 2100$.

Turbulent flow:

$$\frac{1}{\sqrt{f}} = -4 \log_{10} \left[\frac{k/D}{3.7065} + \frac{1.2613}{\text{Re} \sqrt{f}} \right], \quad \dots \quad (5.133)$$

for $N_{\text{Re}} > 3000$, where k is the absolute pipe roughness in the same units as D .

Annular Flow.

Frictional pressure drop:

$$\frac{dp_f}{ds} = \frac{2f \rho v^2}{d_w - d_p}. \quad \dots \quad (5.134)$$

Reynolds number:

$$N_{\text{Re}} = (d_w - d_p) \rho v / \mu, \quad \dots \quad (5.135)$$

where d_w is the annulus OD, and d_p is the ID.

Laminar flow:

$$f = 16/N_{\text{Re}} \text{ (approximate)}, \quad \dots \quad (5.136)$$

for $N_{\text{Re}} < 2100$.

Turbulent flow:

$$\frac{1}{\sqrt{f}} = -4 \log_{10} \left[\frac{k/D}{3.7065} + \frac{1.2613}{\text{Re} \sqrt{f}} \right], \quad \dots \quad (5.137)$$

for $N_{\text{Re}} > 3000$, where k is the absolute pipe roughness in the same units as D .

Rheological Model 2: Bingham Plastic Fluids.

Pipe Flow.

Frictional pressure drop:

$$\frac{dp_f}{ds} = \frac{2f \rho v^2}{D}. \quad \dots \quad (5.138)$$

Reynolds number:

$$N_{\text{Re}} = D \rho v / \mu_p, \quad \dots \quad (5.139)$$

where D is the pipe ID, and μ_p is the plastic viscosity.

Laminar flow:

$$f = 16 \left[(1/N_{\text{Re}}) + (N_{\text{He}} / (6N_{\text{Re}}^2)) - (N_{\text{He}}^4 / (3f^3 N_{\text{Re}}^8)) \right], \quad \dots \quad (5.140)$$

for $N_{\text{Re}} < N_{\text{ReBP1}}$, where

$$N_{\text{He}} = \tau_o \rho D^2 / \mu_p^2.$$

$$N_{\text{ReBP1}} = N_{\text{ReBP2}} - 866(1 - \alpha_c).$$

$$N_{\text{ReBP2}} = N_{\text{He}} [(0.968774 - 1.362439\alpha_c + 0.1600822\alpha_c^4) / (8\alpha_c)].$$

$$\alpha_c = \frac{3}{4} \left[\left((2N_{\text{He}} / 24,500) + (3/4) \right) - \left\{ \left((2N_{\text{He}} / 24,500) + (3/4) \right)^2 - 4(N_{\text{He}} / 24,500)^2 \right\}^{1/2} \right] / (2(N_{\text{He}} / 24,500)).$$

Turbulent flow:

$$f = A(N_{\text{Re}})^{-B}, \quad \dots \quad (5.141)$$

for $N_{Re} > N_{ReBP2}$, where

For $N_{He} \leq 0.75 \times 10^5$, $A = 0.20656$ and $B = 0.3780$.

For $0.75 \times 10^5 < N_{He} \leq 1.575 \times 10^5$, $A = 0.26365$ and $B = 0.38931$.

For $N_{He} > 0.75 \times 10^5$, $A = 0.20521$, $B = 0.35579$, and $N_{He} = \tau_o \rho D^2 / \mu_p^2$.

Annular Flow.

Frictional pressure drop:

$$\frac{dp_f}{ds} = \frac{2f \rho v^2}{d_w - d_p} \quad (5.142)$$

Reynolds number:

$$N_{Re} = (d_w - d_p) \rho v / \mu_p \quad (5.143)$$

where d_w is the annulus OD, d_p is the ID, and μ_p is the plastic viscosity.

Laminar flow:

$$f = 16[(1/N_{Re}) + (N_{He}/(6N_{Re}^2)) - (N_{He}^4/(3f^3 N_{Re}^8))], \quad (5.144)$$

for $N_{Re} < N_{ReBP1}$, where

$$N_{He} = \tau_o \rho (d_w^2 - d_p^2) / \mu_p^2.$$

$$N_{ReBP1} = N_{ReBP2} - 866(1 - \alpha_c).$$

$$N_{ReBP2} = N_{He} [(0.968774 - 1.362439\alpha_c + 0.1600822\alpha_c^4)/(8\alpha_c)].$$

$$\alpha_c = \frac{3}{4} [((2N_{He}/24,500) + (3/4)) - \{((2N_{He}/24,500) + (3/4))^2 - 4(N_{He}/24,500)^2\}^{1/2}] / (2(N_{He}/24,500)).$$

Turbulent flow:

$$f = A(N_{Re})^{-B} \quad (5.145)$$

for $N_{Re} > N_{ReBP2}$, where

For $N_{He} \leq 0.75 \times 10^5$, $A = 0.20656$ and $B = 0.3780$.

For $0.75 \times 10^5 < N_{He} \leq 1.575 \times 10^5$, $A = 0.26365$ and $B = 0.38931$.

For $N_{He} > 0.75 \times 10^5$, $A = 0.20521$, $B = 0.35579$, and $N_{He} = \tau_o \rho (d_w^2 - d_p^2) / \mu_p^2$.

Slit Flow.

Frictional pressure drop:

$$\frac{dp_f}{ds} = \frac{2f \rho v^2}{d_w - d_p} \quad (5.146)$$

Reynolds number:

$$N_{Re} = (d_w - d_p) \rho v / (1.5\mu_p) \quad (5.147)$$

where d_w is the annulus OD, d_p is the ID, and μ_p is the plastic viscosity.

Laminar flow:

$$f = 16[(1/N_{Re}) + ((9/8) N_{He}/(6N_{Re}^2)) - (N_{He}^4/(3f^3 N_{Re}^8))], \quad \dots \quad (5.148)$$

for $N_{Re} < N_{ReBP1}$, where

$$N_{He} = \tau_o \rho (d_w^2 - d_p^2) / (1.5 \mu_p)^2.$$

$$N_{ReBP1} = N_{ReBP2} - 577(1 - \alpha_c).$$

$$N_{ReBP2} = N_{He} [(0.968774 - 1.362439\alpha_c + 0.1600822\alpha_c^4)/(12\alpha_c)].$$

$$\alpha_c = \frac{3}{4} [(((2 N_{He}/24,500) + (3/4)) - \{((2 N_{He}/24,500) + (3/4))^2 - 4(N_{He}/24,500)^2\}^{1/2}) / (2(N_{He}/24,500))].$$

Turbulent flow:

$$f = A(N_{Re})^{-B}, \quad \dots \quad (5.149)$$

for $N_{Re} > N_{ReBP2}$, where

$$\text{For } N_{He} \leq 0.75 \times 10^5, A = 0.20656 \text{ and } B = 0.3780.$$

$$\text{For } 0.75 \times 10^5 < N_{He} \leq 1.575 \times 10^5, A = 0.26365 \text{ and } B = 0.38931.$$

$$\text{For } N_{He} > 0.75 \times 10^5, A = 0.20521, B = 0.35579, \text{ and } N_{He} = \tau_o \rho (d_w^2 - d_p^2) / (1.5 \mu_p)^2.$$

Rheological Model 3: Power Law Fluids.

Pipe Flow.

Frictional pressure drop:

$$\frac{dp_f}{ds} = \frac{2f \rho v^2}{D}. \quad \dots \quad (5.150)$$

Reynolds number:

$$N_{Re} = D^n v^{2-n} \rho / (8^{n-1} [(3n+1)/4n]^n K), \quad \dots \quad (5.151)$$

where D is the pipe ID.

Laminar flow:

$$f = 16/N_{Re}, \quad \dots \quad (5.152)$$

for $N_{Re} \leq 3250 - 1150n$.

Turbulent flow:

$$1/f^{1/2} = \{[(4.0/n^{0.75}) \log(N_{Re} f^{(1-n/2)})] - (0.4/n^{1.2})\}, \quad \dots \quad (5.153)$$

for $N_{Re} \geq 4150 - 1150n$.

Annular Flow.

Frictional pressure drop:

$$\frac{dp_f}{ds} = \frac{2f \rho v^2}{d_w - d_p}. \quad \dots \quad (5.154)$$

Reynolds number:

$$N_{Re} = (d_w - d_p)^n v^{2-n} \rho / (8^{n-1} [(3n+1)/4n]^n K), \quad \dots \quad (5.155)$$

where d_w is the annulus OD and d_p is the ID.

Laminar flow:

$$f = 16/N_{\text{Re}} \text{ (approximate),} \quad \dots \quad (5.156)$$

for $N_{\text{Re}} \leq 3250 - 1150n$.

Turbulent flow:

$$1/f^{1/2} = \{[(4.0/n^{0.75}) \log(N_{\text{Re}} f^{(1-n/2)})] - (0.4/n^{1.2})\}, \quad \dots \quad (5.157)$$

for $N_{\text{Re}} \geq 4150 - 1150n$.

Slit Flow.

Frictional pressure drop:

$$\frac{dp_f}{ds} = \frac{2f\rho v^2}{d_w - d_p}. \quad \dots \quad (5.158)$$

Reynolds number:

$$N_{\text{Re}} = (d_w - d_p)^n v^{2-n} \rho / (12^{n-1} [(2n+1)/3n]^n K). \quad \dots \quad (5.159)$$

Laminar flow:

$$f = 24/N_{\text{Re}}, \quad \dots \quad (5.160)$$

for $N_{\text{Re}} \leq 3250 - 1150n$.

Turbulent flow:

$$1/f^{1/2} = \{[(4.0/n^{0.75}) \log(N_{\text{Re}} f^{(1-n/2)})] - (0.4/n^{1.2})\}, \quad \dots \quad (5.161)$$

for $N_{\text{Re}} \geq 4150 - 1150n$.

Rheological Model 4: Yield Power Law Fluids.

Pipe Flow.

Frictional pressure drop:

$$\frac{dp_f}{ds} = \frac{2f\rho v^2}{D}. \quad \dots \quad (5.162)$$

Reynolds number:

$$N_{\text{ReYPL}} = 8\rho v^2 / (\tau_y + K\dot{\gamma}e^n), \quad \dots \quad (5.163)$$

where

$$\dot{\gamma}e = 8v/D_e.$$

$$D_e = \frac{4n}{3n+1} C_c D.$$

$$C_c = (1-x) \left[\frac{2n^2 x^2}{(1+2n)(1+n)} + \frac{2nx}{1+2n} + 1 \right].$$

$$x = \frac{\tau_y}{\tau_w}.$$

$$\tau_w = \frac{D}{4} \frac{dp_f}{ds}.$$

Laminar flow:

$$f = 16/N_{\text{ReYPL}}, \quad \dots \quad (5.164)$$

for $N_{\text{Re}} \leq 3250 - 1150n$.

Turbulent flow:

$$1/f^{1/2} = \{[(4.0/n^{0.75}) \log(N_{\text{Re}} f^{(1-n/2)})] - (0.4/n^{1.2})\}, \quad \dots \quad (5.165)$$

for $N_{\text{Re}} \geq 4150 - 1150n$.

Slit Flow.

Frictional pressure drop:

$$\frac{dp_f}{ds} = \frac{2f \rho v^2}{d_w - d_p}. \quad \dots \quad (5.166)$$

Reynolds number:

$$N_{\text{ReYPL}} = 12 \rho v^2 / (\tau_y + K \dot{\gamma} e^n), \quad \dots \quad (5.167)$$

where

$$\gamma_e = 12v/D_e,$$

$$D_e = \frac{3n}{2n+1} C_c (d_w - d_p),$$

$$C_c = (1-x) \left[\frac{nx}{1+n} + 1 \right],$$

$$x = \frac{\tau_y}{\tau_w},$$

$$\tau_w = \frac{(d_w - d_p)}{4} \frac{dp_f}{ds}, \quad \dots \quad (5.168)$$

Laminar flow:

$$f = 24/N_{\text{Re}}, \quad \dots \quad (5.169)$$

for $N_{\text{Re}} \leq 3250 - 1150n$.

Turbulent flow:

$$1/f^{1/2} = \{[(4.0/n^{0.75}) \log(N_{\text{Re}} f^{(1-n/2)})] - (0.4/n^{1.2})\}, \quad \dots \quad (5.170)$$

for $N_{\text{Re}} \geq 4150 - 1150n$.

5.7 Frictional Pressure Drop in an Eccentric Annulus

In general, the pipe in the wellbore is usually not concentric with the wellbore. Only in special cases, such as a casing string with centralizers or a “packed” bottomhole assembly, will there be near-concentric annuli. The frictional pressure drop in an eccentric annulus is known to be less than the frictional pressure drop in a concentric annulus. For laminar flow of Newtonian fluids, the pressure drop in a fully eccentric annulus is approximately half the pressure drop in a concentric annulus. For turbulent flow, the difference is about 30%. For non-Newtonian fluids, the effect is less, but still significant. In deviated wells, the drillpipe should be fully eccentric over much of the deviated wellbore, resulting in reduced fluid friction.

Define the correction factor for eccentricity:

$$C_e = \frac{\left(\frac{dp_f}{ds}\right)_e}{\left(\frac{dp_f}{ds}\right)_c}, \quad \dots \quad (5.171)$$

where subscript e denotes eccentric, and subscript c denotes concentric. The geometry of an eccentric annulus and the definition of the degree of eccentricity δr_e are shown in **Fig. 5.38**. The eccentricity N_e , a dimensionless number that ranges from zero (concentric annulus) to one (fully eccentric annulus), is given by

$$N_e = \frac{\delta r_e}{r_w - r_p}. \quad \dots \quad (5.172)$$

5.7.1 Newtonian Fluid Model. The laminar-flow analytic solution (Piercy et al. 1933) is not easy to derive and is very complex. For those interested, it is given on page 126 of White (1974). Fortunately, there is a simple solution for a narrow annulus:

$$\frac{q_e}{q_c} = 1 + \frac{3}{2} N_e^2. \quad \dots \quad (5.173)$$

Note that full eccentricity increases the flow rate by a factor of $2\frac{1}{2}$. The laminar flow solution for an annulus shows that the frictional pressure drop is proportional to the volume flow rate, so

$$C_e = \frac{2}{2 + 3N_e^2}. \quad \dots \quad (5.174)$$

For turbulent flow, Tao and Donovan (1955) have determined experimentally that, roughly,

$$\frac{q_e}{q_c} = 1 - .1975N_e + 1.8N_e^2 - 1.0625N_e^3, \quad \dots \quad (5.175)$$

which is a cubic fit to **Fig. 5.39** for curve $r_p/r_w = 0.01$. At full eccentricity, the flow rate is approximately 1.54 times the concentric rate. C_e for turbulent flow is

$$C_e = \frac{1}{1 - .1975N_e + 1.8N_e^2 - 1.0625N_e^3}. \quad \dots \quad (5.176)$$

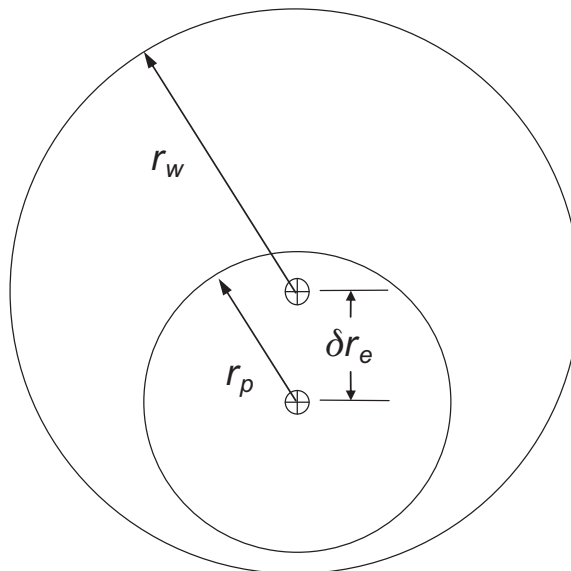


Fig. 5.38—Definition of an eccentric annulus.

5.7.2 Power-Law Model. C_e for laminar flow is determined on the basis of the methods used by Uner et al. (1989). The flow rate through a concentric annulus is given by

$$q_c = \frac{\pi r_w^3}{2} \frac{n}{2n+1} \left| \frac{dp_f}{ds} \frac{r_w}{2K} \right|^{1/n} (1+R_r)(1-R_r)^{2+1/n}, \quad (5.177)$$

where $R_r = r_p/r_w$. The flow rate through an eccentric annulus was determined to be

$$q_c = \frac{\pi r_w^3}{2} \frac{n}{2n+1} \left| \frac{dp_f}{ds} \frac{r_w}{2K} \right|^{1/n} \frac{(1-R_r^2)}{[2E(\lambda) - \pi R_r]} F(\lambda, n, R_r), \quad (5.178)$$

where

$$F(\lambda, n, R_r) = \int_0^\pi \left(\sqrt{1 - \lambda^2 \sin^2 \xi} + \lambda \cos \xi - R_r \right)^{2+1/n} d\xi, \quad (5.179)$$

$$E(\lambda) = \int_0^{\pi/2} \sqrt{1 - \lambda^2 \sin^2 \xi} d\xi, \quad (5.180)$$

and

$$\lambda = \delta r \frac{(1-R_r)}{r_w - r_p}. \quad (5.181)$$

The function $E(\lambda)$ is the complete elliptic integral of the second kind. $E(\lambda)$ and the function F must be evaluated using numerical methods (Press et al. 1997). C_e for laminar flow of a power-law fluid is then

$$C_e = (1-R_r)^{n+1} \left[\frac{2E(\lambda) - \pi R_r}{F(\lambda, n, R_r)} \right]^n. \quad (5.182)$$

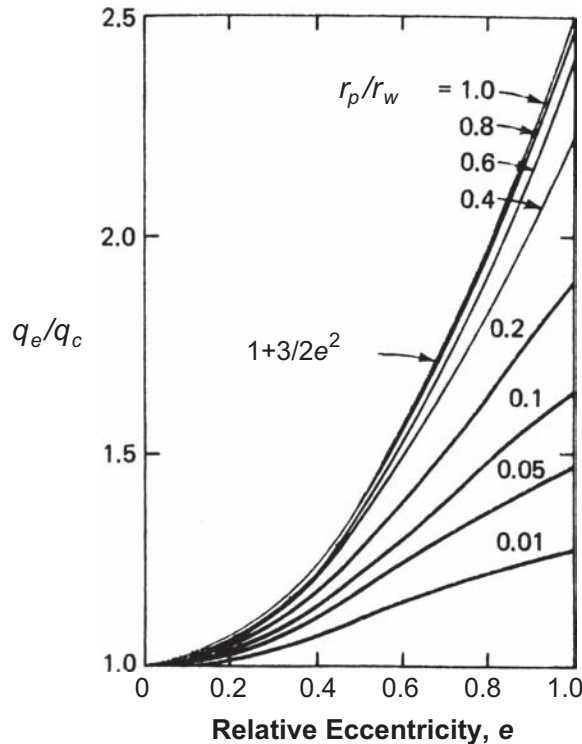


Fig. 5.39—Volume flow through an eccentric annulus [from White (1974)]. Reproduced with permission from The McGraw Hill Companies.

Because C_e depends only on λ , n , and R_p , C_e need be calculated only once, then used for all future frictional pressure drop calculations, as long as the property n does not vary.

A simpler alternate expression for C_e was given by Hacıislamoglu and Langlinais (1990). The equation is as follows:

$$C_e = 1 - 0.072 \left(\frac{N_e}{n} \right) \left(\frac{r_p}{r_w} \right)^{0.8454} - 1.5 N_e^3 \sqrt{n} \left(\frac{r_p}{r_w} \right)^{0.1852} + 0.96 N_e^3 \left(\frac{r_p}{r_w} \right)^{0.2527} \quad (5.183)$$

Eq. 5.183 is valid for eccentricities ranging from 0 to 0.95, inner- to outer-pipe diameter ratios of 0.3 to 0.9, and flow behavior indices from 0.4 to 1.0.

Example 5.29 Before cementing, mud is circulating in a deviated well, with a centralized 9 $\frac{5}{8}$ -in. casing string in a 12 $\frac{1}{4}$ -in. hole. The diameter of the centralizers is 11 $\frac{1}{8}$ in., and the drilling mud has a flow behavior index of 0.65 and a consistency index of 155 eq cp. The pressure-loss gradient in a concentric annulus is estimated to be 0.0442 psi/ft. Determine the frictional-pressure-loss gradient for the eccentric annulus.

Solution. In SI units, the hole size r_w , the outside casing diameter r_p , the centralizer diameter r_c , the consistency index, K , and the pressure gradient dp_f/dL are given by

$$r_w = \frac{(12.25 \text{ in.})}{2(3.937 \times 10 \text{ in./m})} = 0.156 \text{ m,}$$

$$r_p = \frac{(9.625 \text{ in.})}{2(3.937 \times 10 \text{ in./m})} = 0.122 \text{ m,}$$

$$r_c = \frac{(11.125 \text{ in.})}{2(3.937 \times 10 \text{ in./m})} = 0.141 \text{ m,}$$

$$K = \frac{(155 \text{ eq cp})}{(10^3 \text{ eq cp/Pa} \cdot \text{s}^n)} = 1.55 \cdot 10^{-1} \text{ Pa} \cdot \text{s}^n$$

$$\frac{dp_f}{dL} = \frac{(0.0442 \text{ psi/ft})}{(4.4207 \cdot 10^{-4} \text{ psi/ft/Pa/m})} = 10^2 \text{ Pa/m}$$

Assuming the centralizers are touching the low side of the hole, the eccentricity is

$$N_e = \frac{r_w - r_c}{r_w - r_p} = \frac{0.156 - 0.141}{0.156 - 0.122} = 0.44$$

The correlation factor for eccentricity is given by Eq. 5.183:

$$C_e = 1 - 0.072 \left(\frac{0.44}{0.65} \right) \left(\frac{0.122}{0.156} \right)^{0.8454} - 1.5 (0.44)^3 \sqrt{0.65} \left(\frac{0.122}{0.156} \right)^{0.1852} + 0.96 (0.44)^3 \sqrt{0.65} \left(\frac{0.122}{0.156} \right)^{0.2527},$$

$$C_e = 1 - 0.0396 - 0.0984 + 0.0620 = 0.924.$$

The frictional-pressure-loss gradient in the deviated annular section is given by

$$\left(\frac{dp_f}{ds}\right)_e = C_e \left(\frac{dp_f}{ds}\right)_c = 0.924(100 \text{ Pa/m}) = 92.4 \text{ Pa/m} = 0.041 \text{ psi/ft}.$$

C_e for turbulent flow is determined by applying the same techniques to the turbulent velocity profile determined by Dodge and Metzner (1959):

$$\frac{u}{u^*} = \lambda_1 |y| + \lambda_2 \ln(u^*) + \lambda_3, \quad \dots \quad (5.184)$$

where

$$\lambda_1 = 2.458n^{1/4}, \quad \dots \quad (5.185)$$

$$\lambda_2 = 2.458(2-n)n^{-3/4}, \quad \dots \quad (5.186)$$

$$\lambda_3 = 2.458 \ln\left(\frac{\rho}{K}\right)n^{-3/4} + 3.475n^{-3/4} \left[1.960 + 0.815n - 0.707n \ln\left(3 + \frac{1}{n}\right)\right], \quad \dots \quad (5.187)$$

and

$$u^* = \sqrt{\frac{\tau}{\rho}}. \quad \dots \quad (5.188)$$

The volume flow rate through the concentric annulus is given by

$$\begin{aligned} q_c &= u_c^* \int_0^w \int_{-h/2}^{h/2} \left\{ \lambda_1 \ln(y) + \lambda_2 \ln(u_c^*) + \lambda_3 \right\} dy dx, \\ h &= r_w - r_p, \\ w &= \pi(r_w + r_p). \quad \dots \quad (5.189) \end{aligned}$$

Integrating Eq. 5.188 gives

$$q_c = u_c^* A \left\{ \lambda_1 [\ln(h/2) - 1] + \lambda_2 \ln(u_c^*) + \lambda_3 \right\}, \quad \dots \quad (5.190)$$

where A is the flow area. The equivalent integral to Eq. 5.188 for eccentric flow is given by

$$\begin{aligned} q_e &= u_e^* \left\{ \left[B \int_0^{2\pi} \int_{-h(\theta)/2}^{h(\theta)/2} \lambda_1 \ln(y) dy d\theta \right] + A [\lambda_2 \ln(u_e^*) + \lambda_3] \right\}, \\ B &= \frac{\pi r_w^2 (1 - R_r^2)}{2 [2E(\lambda) - \pi R_r]}, \\ h(\theta) &= r_w \left(\sqrt{1 - \lambda^2 \sin^2 \theta} + \lambda \cos \theta - R_r \right). \quad \dots \quad (5.191) \end{aligned}$$

The integral in Eq. 5.190 must be evaluated numerically. C_e can then be determined:

$$C_e = \left(\frac{u_c^*}{u_e^*} \right)^2, \quad \dots \quad (5.192)$$

where u_c^* is determined from the concentric solution given by Dodge and Metzner (1959). The resulting nonlinear equation must be solved for C_e numerically (e.g., by using Newton's method). Because C_e depends only on λ_1 , λ_2 , λ_3 , n , and R_r , C_e need be calculated only once, then used for all future frictional-pressure-drop calculations, as long as the properties ρ , K , and n do not vary.

5.7.3 Bingham Plastic and Herschel-Bulkley Models. For fluid models with a yield stress, neither laminar flow nor turbulent flow models have been developed. For low flow rates, however, one would expect that the sheared fluid layer would be relatively thin, so that it would be similar to a concentric flow. For fully turbulent flow, the Bingham Plastic model should mimic the behavior of a turbulent Newtonian fluid. The fully turbulent Herschel-Bulkley Model should mimic the power-law turbulent model. The intermediate cases, with merging sheared fluid zones, are currently not well understood.

5.8 Frictional Pressure Drop With Pipe Movement

In Sections 5.3 through 5.7, equations that described the movement of fluids through conduits were developed. However, when running casing or making a trip, a slightly different situation is encountered in that the conduit is moved through the fluid rather than the fluid through the conduit.

As pipe is moved downward in a well, the drilling fluid must move upward to exit the region being entered by the new volume of the extending pipe. Likewise, an upward pipe movement requires a downward fluid movement. The flow pattern of the moving fluid can be either laminar or turbulent, depending on the velocity at which the pipe is moved. It is possible to derive mathematical equations for surge and swab pressures only for the laminar flow pattern. Empirical correlations must be used if the flow pattern is turbulent.

5.8.1 Newtonian Fluid Model. The basic differential equations derived in Section 5.11 to describe laminar flow in circular pipes and annuli apply to conduit movement through the fluid as well as fluid movement through the conduit. Only the boundary conditions are different.

A typical velocity profile for laminar flow caused by pulling pipe out of the hole at velocity $-v_p$ is shown in **Fig. 5.40**. Note that the velocity profile inside the inner pipe caused by a vertical pipe movement is identical to the velocity profile caused by pumping fluid down the inner pipe. If the mean fluid velocity in the pipe is expressed relative to the pipe wall, the pipe-flow equation developed in Section 5.5 can be applied. Substituting the term $\bar{v}_i - (-v_p)$ for \bar{v} yields

$$\frac{dp_f}{ds} = \mu \frac{\bar{v}_i + v_p}{1500d^2}, \quad \dots \dots \dots (5.193)$$

or, in SI units,

$$\frac{dp_f}{ds} = 32\mu \frac{\bar{v}_i + v_p}{d^2}. \quad \dots \dots \dots (5.193a)$$

The velocity profile in the annulus caused by vertical pipe movement differs from the velocity profile caused by pumping fluid through the annulus in that the velocity at the wall of the inner pipe is not zero. The slot-flow representation of the annular geometry usually is preferred because of its relative simplicity:

$$q = \frac{\pi}{12\mu} \frac{dp_f}{dL} (r_2^2 - r_1^2)(r_2 - r_1)^2 - \frac{\pi v_p}{2} (r_2^2 - r_1^2). \quad \dots \dots \dots (5.194)$$

Expressing the flow rate in terms of the mean flow velocity in the annulus, \bar{v}_a , and solving for the frictional pressure gradient dp_f/ds gives

$$\frac{dp_f}{ds} = \frac{12\mu(\bar{v}_a + \frac{1}{2}v_p)}{(r_2 - r_1)^2}. \quad \dots \dots \dots (5.195)$$

5.8.2 Non-Newtonian Fluid Model. It is possible to derive laminar-flow surge-pressure equations using non-Newtonian fluid models such as the Bingham plastic and power-law models. This can be accomplished by changing the boundary conditions at the pipe wall from $v = 0$ to $v = -v_p$ in the annular-flow derivations for the Bingham plastic model and power-law model given in Section 5.5. However, the resulting surge-pressure equations are far too complex for field application.

A simplified technique for computing surge pressures was presented by Burkhardt (1961). The simplified method is based on the use of an effective fluid velocity in the annular-flow equations. The suitability of the annular-flow equations for predicting surge pressure is suggested by the similarity of the annular flow and surge pressure equations for the Newtonian fluid model. For example, the Newtonian equation (Eq. 5.195) is obtained if an effective mean annular velocity \bar{v}_{ae} , defined by

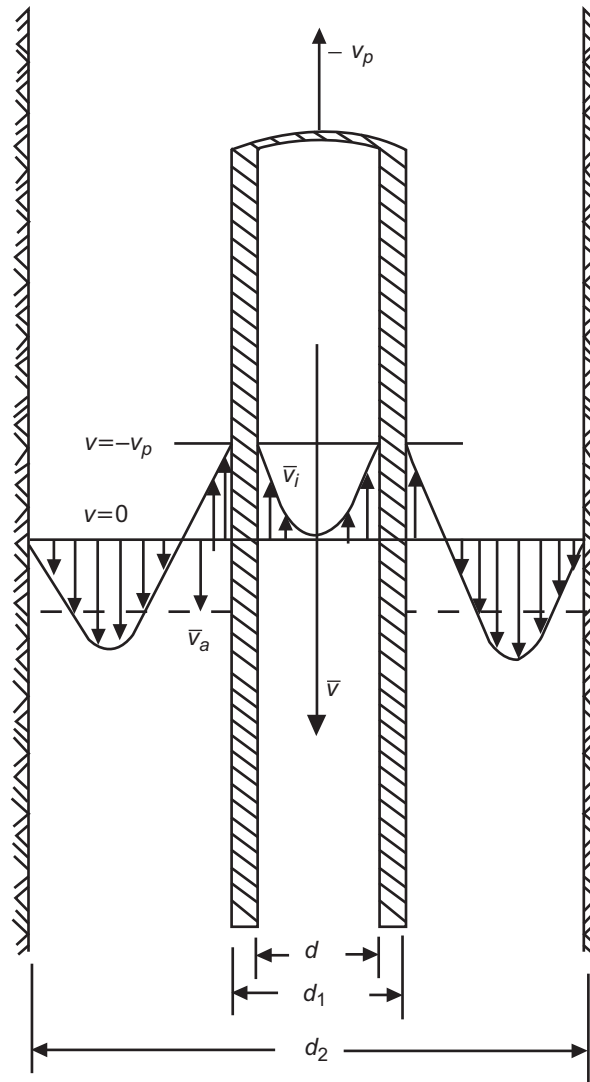


Fig. 5.40—Velocity profiles for laminar-flow pattern when pipe is pulled out of hole [from Bourgoyne et al. (1991)].

$$\bar{v}_{ae} = \bar{v} + 0.5v_p, \quad \dots \dots \dots (5.196)$$

is used in the slot-flow equation. Burkhardt suggested using an effective mean annular velocity given by

$$\bar{v}_{ae} = \bar{v} + Kv_p, \quad \dots \dots \dots (5.197)$$

where the constant K , called the *mud-clinging constant*, is obtained for a given annular geometry using Fig. 5.41.

Burkhardt obtained the correlation for K using complex equations derived for the Bingham plastic model using a slot-flow representation of the annulus. Note that for small annular clearances, where surge and swab pressures will be most significant, the value of K approaches 0.5.

Mud-clinging-constant values also can be obtained from the work of Schuh (1964) for the power-law fluid model and a slot approximation of annular geometry. The resulting curve is used irrespective of flow pattern and falls between Burkhardt's curves for laminar and turbulent flow.

Brooks (1982) developed a series of curves reporting the mud-clinging constant for laminar flow for Bingham plastic and power-law fluids. Assumptions in developing the analytical calculations were a concentric annulus and incompressible fluids. Curves to determine the mud-clinging constant were proposed as a function of the annulus

diameter ratio, the ratio of actual fluid displacement to the maximum or closed-end pipe displacement, and the Bingham number relative to the pipe velocity or the power-law flow behavior index. The Bingham number relative to the pipe velocity is defined as follows:

$$N_{Bip} = \frac{\tau_y (d_2 - d_1)}{\mu_p v_p} \dots \dots \dots (5.198)$$

where μ_p is the plastic viscosity and τ_y is the yield point for Bingham plastic fluids.

Figs. 5.42 and 5.43 show an example of the mud-clinging-constant graphs reported by Brooks (1982) for a Bingham plastic fluid with Bingham number of 100 and for a power-law fluid with flow behavior index of 0.5, respectively.

For Newtonian fluids, the mud-clinging constant is not dependent on the flow velocity ratio, v/v_{\max} , and the related curve follows the one reported by Burkhardt (1961), while the analytical expression is that given by Fontenot and Clark (1974). However, the effect of the non-Newtonian behavior of a drilling fluid reduces the value of the mud-clinging constant, and this effect is more remarkable for low values of the ratio of bulk-fluid velocity to bulk velocity displaced by closed-end pipe, v/v_{\max} . This results in a considerable error when making surge-pressure evaluations.

5.8.3 Turbulent Flow. Empirical correlations have not been developed specifically for the calculations of surge and swab pressures when in turbulent flow. However, Burkhardt (1961) and Schuh (1964) have presented correlations for the mud-clinging constant K applicable for turbulent flow and for commonly used annular geometries (Fig. 5.41). Recall that these annular flow equations, in turn, are based on an empirical correlation developed for circular pipes. Unfortunately, no published criteria for establishing the onset of turbulence are available. The usual procedure is to calculate surge and swab pressures for both the laminar and turbulent flow patterns and then to use the larger value.

5.9 Calculating Steady-State Pressures in a Wellbore

Assuming we can calculate ΔP for each constant area section of drillpipe or annulus (Sections 5.5 through 5.8) and can calculate ΔP for nozzles and area changes (Section 5.3), we are now ready to evaluate the pressures in a wellbore.

5.9.1 Circulating Wellbore Pressures. A typical wellbore fluid system is illustrated in Fig. 5.2. Summing all pressure drops gives the standpipe pressure:

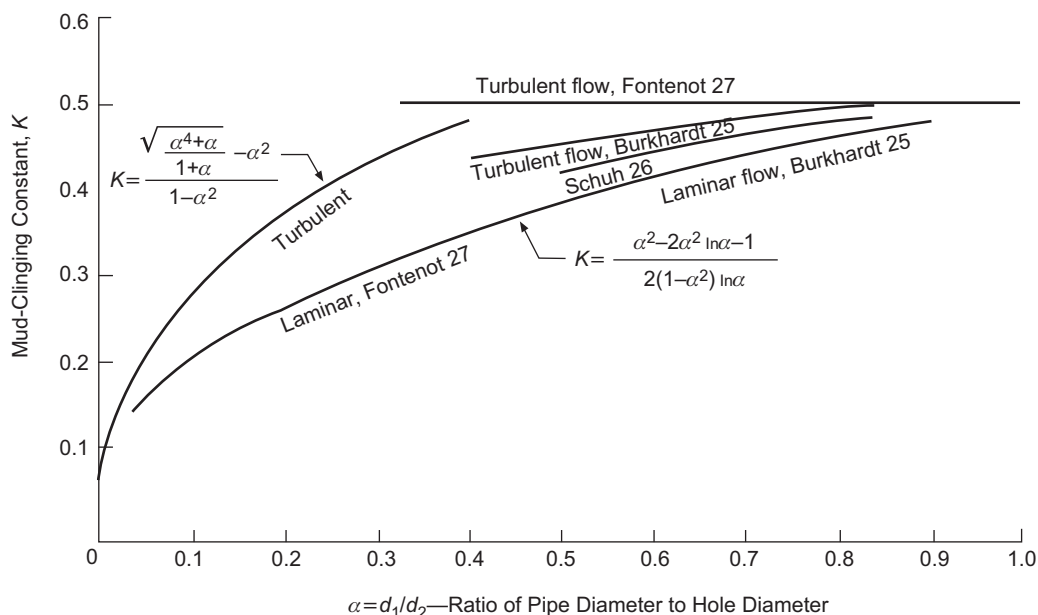


Fig. 5.41—Mud-clinging constant, K , for computing swab/surge pressures [from Bourgoyne et al. (1991)].

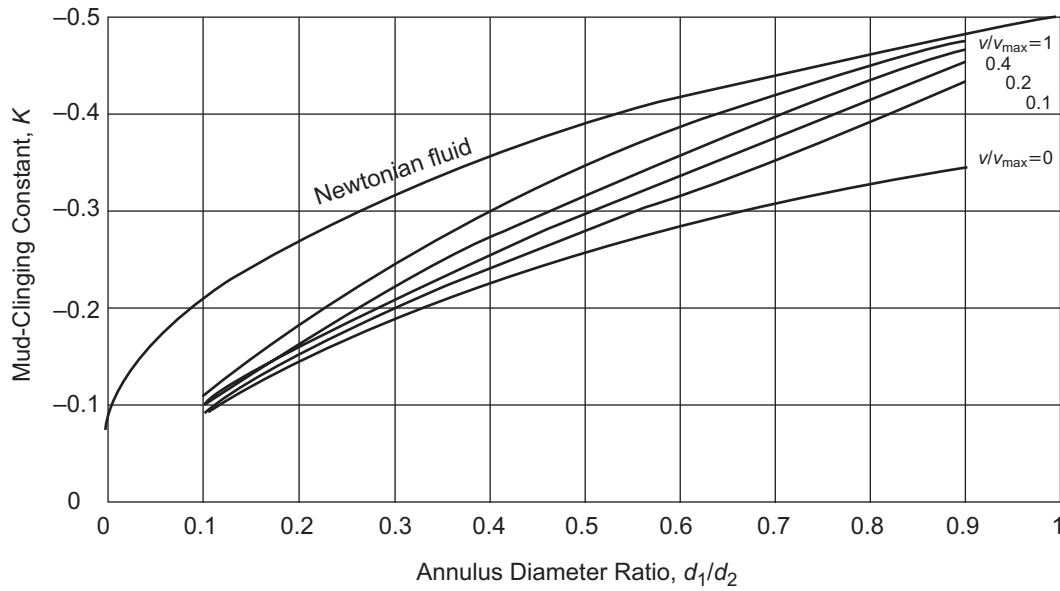


Fig. 5.42—Mud-clinging constant plotted against annulus-diameter ratio for a Bingham plastic fluid and Bingham number equal to 100 [from Bourgoyne et al. (1991)].

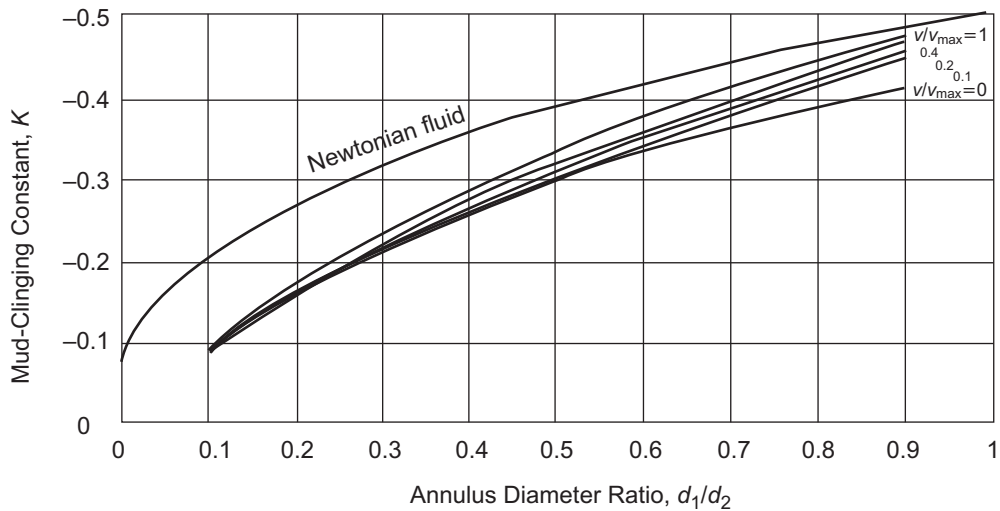


Fig. 5.43—Mud-clinging constant plotted against annulus-diameter ratio for a power-law fluid with flow-behavior index of 0.5 [from Bourgoyne et al. (1991)].

$$P_{\text{standpipe}} = \Delta P(\text{pipe joints}) + \Delta P(\text{internal upsets}) + \Delta P(\text{area changes}) + \Delta P(\text{bit}) \\ + \Delta P(\text{annulus}) + \Delta P(\text{tool joints}) + \Delta P(\text{misc}) + \Delta P(\text{choke}) + P_{\text{atm}} \quad (5.199)$$

In this calculation, we assume that the calculations are started from a known pressure value, most conveniently the atmospheric pressure at the exit of the annulus. This choice is particularly suitable if air or foam drilling is being considered because “choked” gas flow will almost never occur. For this choice of “boundary condition,” flow calculations proceed backward from the annulus exit to the standpipe pressure. For flow in the annulus, both fluid density and fluid friction will increase pressure going down the annulus. Where fluid type changes, the pressure and flow velocity are continuous:

$$P(\text{fluid}_a) = P(\text{fluid}_b) \\ v(\text{fluid}_a) = v(\text{fluid}_b) \text{ at the interface.} \quad (5.200)$$

Notice that mass flow rate may not be continuous at the interface between two fluids because the densities may be different. When calculating from the bit to the standpipe, inside the drillstring, fluid density will decrease pressure and fluid friction will increase pressure. Pressure changes due to internal upsets and tool joints consist of two area changes and a short flow section, as shown in **Fig. 5.44**.

Pressure drop across the bit consists of two area changes, into the nozzles and exit from the nozzles into the open hole annular area. Miscellaneous pressure drops are drops through tools, mud motors, floats, or in-pipe chokes. Sometimes, the manufacturer will have this pressure loss information tabulated; otherwise, one must estimate the pressure loss through use of the tool internal dimensions.

If the standpipe pressure is given, then the flow exiting the annulus must be choked back to atmospheric pressure:

$$\begin{aligned} \Delta P(\text{exit choke}) = & P_{\text{standpipe}} - \Delta P(\text{pipe joints}) - \Delta P(\text{internal upsets}) - \Delta P(\text{area changes}) \\ & - \Delta P(\text{bit}) - \Delta P(\text{annulus}) - \Delta P(\text{tool joints}) - \Delta P(\text{misc}) - P_{\text{atm}} \end{aligned} \quad (5.201)$$

5.9.2 Surge Pressure Prediction. An exceptional flow case is the operation of running pipe or casing into the wellbore. Moving pipe into the wellbore displaces fluid, and the flow of this fluid generates pressures called surge pressures. When the pipe is pulled from the well, negative pressures are generated, and these pressures are called swab pressures. In most wells, the magnitude of the pressure surges is not critical because proper casing design and mud programs leave large enough margins between fracture pressures and formation-fluid pressures. Typically, dynamic fluid flow is not a consideration, so a steady-state calculation can be performed. A certain fraction of wells, however, cannot be designed with large surge-pressure margins. In these critical wells, pressure surges must be maintained within narrow limits. In other critical wells, pressure margins may be large, but pressure surges may still be a concern. Some operations are particularly prone to large pressure surges (e.g., running of low-clearance liners in deep wells). The reader is referred to papers on dynamic surge calculations, and a later section on dynamic pressure calculation will give a taste of this type of calculation.

The surge-pressure analysis consists of two analytical regions: the pipe-annulus region and the pipe-to-bottom-hole region (**Fig. 5.45**). The fluid flow in the pipe-annulus region should be solved using techniques already discussed, but with the following special considerations: frictional pressure drop must be solved for flow in an annulus with a moving pipe, and in deviated wells, the effect of annulus eccentricity should be considered. The analysis of the pipe-to-bottomhole region should consist of a static pressure analysis, with pressure boundary condition determined by the fluid flow at the bit, or pipe end if running casing. The pipe-annulus model and the pipe-to-bottomhole model then are connected through a comprehensive set of force and displacement compatibility relations.

Surface Boundary Conditions. There are six variables that can be specified at the surface:

- p_1 = pipe pressure,
- v_1 = pipe fluid velocity,
- p_2 = annulus pressure,

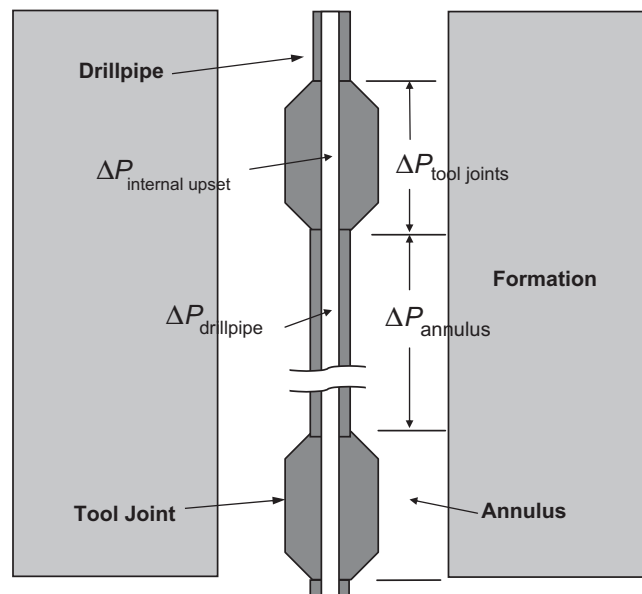


Fig. 5.44—Pressure-drop calculation sections.

$$\begin{aligned} v_2 &= \text{annulus fluid velocity,} \\ v_3 &= \text{pipe velocity.} \end{aligned} \quad (5.202)$$

A maximum of three boundary conditions can be specified at the surface. For surge without circulation, the following boundary conditions hold:

$$\begin{aligned} p_1 &= \text{atmospheric pressure,} \\ p_2 &= \text{atmospheric pressure,} \\ v_3 &= \text{specified pipe velocity.} \end{aligned} \quad (5.203)$$

For a closed-end pipe, the following boundary conditions hold:

$$\begin{aligned} v_1 &= v_3, \text{ fluid velocity equals pipe velocity;} \\ p_2 &= \text{atmospheric pressure;} \\ v_3 &= \text{specified pipe velocity.} \end{aligned} \quad (5.204)$$

For circulation with circulation rate q , the boundary conditions are

$$\begin{aligned} v_1 &= v_3 + q/A_1 \text{ (i.e., fluid velocity equals pipe velocity plus circulation velocity),} \\ p_2 &= \text{atmospheric pressure,} \\ v_3 &= \text{specified pipe velocity.} \end{aligned} \quad (5.205)$$

End of Pipe Boundary Conditions. There are 11 variables that can be specified at the moving pipe end (see Fig. 5.46):

- p_1 = pipe pressure,
- v_1 = pipe velocity,
- p_2 = pipe annulus pressure,
- v_2 = pipe annulus velocity,
- p_n = pipe nozzle pressure,
- v_n = pipe nozzle velocity,
- p_r = annulus return area pressure,
- v_r = annulus return area velocity,
- p = pipe-to-bottomhole pressure,

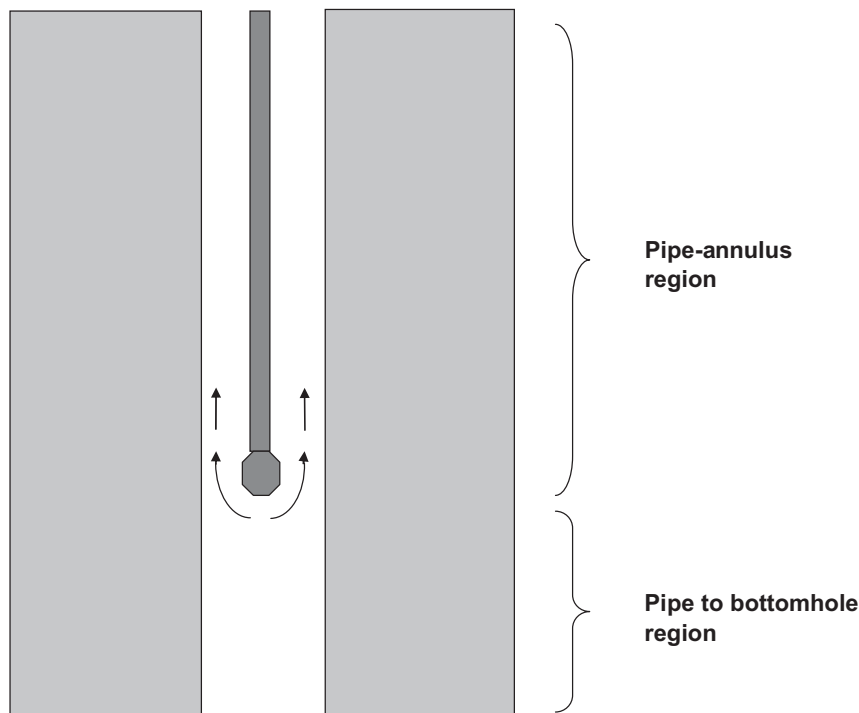


Fig. 5.45—Surge-pressure calculation regions.

$$\begin{aligned} v &= \text{pipe-to-bottomhole velocity,} \\ v_3 &= \text{pipe velocity.} \end{aligned} \quad (5.206)$$

A total of seven boundary conditions can be specified at the moving pipe end with bit, as shown in **Fig. 5.47**.

For the surge model, three mass-balance equations and four nozzle-pressure relations were used:

Pipe-to-bottomhole mass balance:

$$A_r v_r + A_n v_n + A_b v_3 - A v = 0 \quad (5.207)$$

Pipe annulus mass balance:

$$A_2 v_2 - (A_2 - A_r) v_3 - A_r v_r = 0 \quad (5.208)$$

Pipe mass balance:

$$A_1 v_1 - (A_1 - A_n) v_3 - A_n v_n = 0 \quad (5.209)$$

Pipe nozzle pressures:

$$P_1 - P_n = \frac{\rho}{2C_d} (v_n^2 - v_1^2), \quad (5.210)$$

$$P - P_n = \frac{\rho}{2C_d} (v_n^2 - v^2).$$

Annulus return pressures:

$$P_2 - P_r = \frac{\rho}{2C_d} (v_r^2 - v_2^2), \quad (5.211)$$

$$P - P_r = \frac{\rho}{2C_d} (v_r^2 - v^2).$$

The boundary conditions are greatly simplified for a pipe without a bit:

$$A_1 v_1 + A_2 v_2 + A_3 v_3 - A v = 0 \quad (5.212)$$

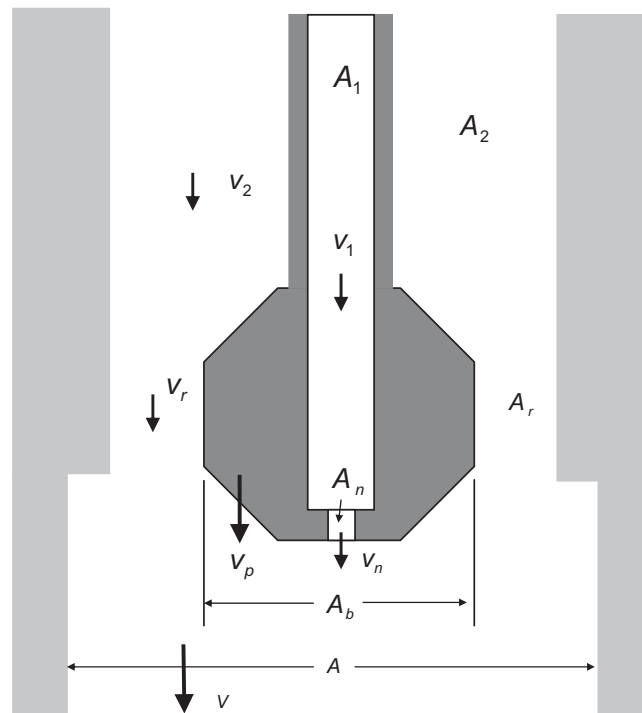


Fig. 5.46—Balance of mass at the bit.

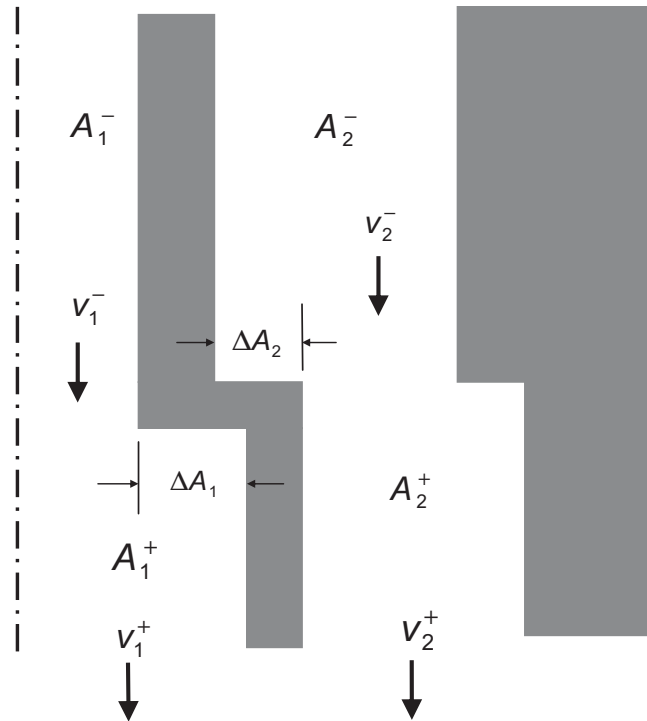


Fig. 5.47—Balance of mass for cross-sectional area changes.

and

$$\begin{aligned} p_1 &= p_2 = p_r = p_n = p, \\ v_1 &= vn, \\ v_2 &= v_r. \end{aligned} \quad (5.213)$$

The boundary condition imposed by a float is the requirement that

$$v_1 - v_3 < 0. \quad (5.214)$$

If the solution of the boundary conditions does not satisfy this condition, the boundary conditions must be solved again with the new requirement:

$$v_1 = v_3. \quad (5.215)$$

Change of Cross-Sectional Area. Changes in the cross-sectional area of the moving pipe generate an additional term in the balance of mass equations due to the fluid displaced by the moving pipe, as shown in Fig. 5.47:

$$\begin{aligned} A_1^+ v_1^+ &= A_1^- v_1^- + \Delta A_1 v_3, \\ A_2^+ v_2^+ &= A_2^- v_2^- + \Delta A_2 v_3 \end{aligned} \quad (5.216)$$

where

$$\begin{aligned} \Delta A_1 &= A_1^+ - A_1^-, \\ \Delta A_2 &= A_2^+ - A_2^-. \end{aligned} \quad (5.217)$$

The superscript minus sign (−) denotes upstream properties and the superscript plus sign (+) denotes downstream properties.

Surge Pressure Solution. Because of the complex boundary conditions, the solution of a steady-state surge pressure is most easily solved with a computer program. For closed-pipe and circulating cases, the flow is defined so that

pressures can be calculated from the annulus exit to the standpipe, as discussed previously. For open pipe surges, the problem is finding how the flow splits between the pipe and the annulus, so that the pressures for both the pipe and the annulus match at the bit. One strategy for solving this problem is

1. Calculate all pressures with all flow in the annulus, then check pressures at the bit; annulus pressure will be lower because of fluid friction.
2. Calculate all pressures with all flow in the pipe, then check pressures at the bit; pipe pressure will be lower because of fluid friction.
3. Calculate a division of flow between the pipe and annulus that will equalize the pressures at the bit.
4. Repeat Step 3 until the two pressures match within an acceptable tolerance.

The efficiency of this calculation will depend on the method chosen for Step 3. With modern computers, this is not a particularly critical problem, so a simple interval halving technique would work. At the i^{th} step, χ_i is the fraction of flow in the pipe and $(1-\chi_i)$ is the fraction in the annulus. Previous steps show that χ_p gives a higher annulus pressure and χ_m gives a lower annulus pressure. Our new choice for χ_i is $\frac{1}{2}(\chi_p + \chi_m)$. We perform the pressure calculation and find that the annulus pressure is higher, so we assign $\chi_p = \chi_i$. If the pressure difference is less than our tolerance, which we choose to be 1 psi, then the calculation is complete. Otherwise, we try another step. How do we establish χ_p and χ_m ? The initial two steps in the solution step should give us $\chi_p = 0$ and $\chi_m = 1$, respectively. In some cases, such as small nozzles or restricted flow around the bit, fluid must flow into either the pipe or the annulus, or the fluid level must fall. For these cases, χ may be negative or greater than one. It may be necessary to repeat Steps 1 and 2 to establish the initial set χ_m and χ_p .

5.10 Dynamic Surge and Swab Pressures

5.10.1 Introduction. Pressure surges in critical wells are commonly calculated using steady-state flow surge models, such as those proposed by Burkhardt (1961) and Schuh (1964). Since these models do not consider the inertia of the fluid or the compressibility of the fluid-wellbore system, the validity of the steady flow assumption was questioned.

When a tubular (such as drillstring or casing) is moved in a hole filled with a fluid, transient pressure fluctuation can occur, causing the fluid pressure at a given depth to oscillate above and below the hydrostatic pressure. Transients occur while either pulling out of the hole or tripping in the hole. It is natural to associate a pressure surge with tripping in, and a pressure swab with pulling out. However, due to the nature of transient pressure, both surges and swabs could occur in either case. For instance, while pulling out, the string is first accelerated to the maximum trip speed, held at that speed for some time, and finally decelerated to rest for each stand pulled. **Fig. 5.48** shows a typical trip-in velocity profile while tripping one stand of drillpipe in the hole. The graph includes picking up off the slips, lowering the stand in the hole, and stopping the stand to set the slips.

Although the pipe has been brought to rest at the surface, the bit does not come to rest at the same time, due to the longitudinal elasticity of the pipe. Therefore the pipe alternately stretches and shortens. Similarly, the fluid inertia causes the fluid to alternately compress and expand. Also, the wellbore contracts and expands, in response to the fluid pressure and its own elasticity. As a result of these transient effects, the local pressure can go above as well as below the static pressure, causing both a surge and a swab. Eventually, the wellbore returns to its original shape, the pipe is back to its original length, the pressure is hydrostatic everywhere, and the pipe and fluid are at rest everywhere.

At the end of the 1970s Lubinski (1977) introduced a dynamic model that included the compressibility and density of the drilling mud. Later, Lal (1983) further improved the model, providing a useful analysis of the factors affecting surge and swab pressures, including formation elasticity or borehole expansion. Mitchell (1988) refined the previous model with the addition of the axial drillstring elasticity and the coupling between the pressure inside and outside the drillstring via the circumferential stiffness of the pipe wall. Bizanti et al. (1991) performed a sensitivity study to quantify the differences between steady-state and unsteady-state models. Rudolf and Suryanarayana (1998) reported field measurements of surge pressures to validate a fully dynamic surge model, as shown in **Fig. 5.49** and **Fig. 5.50**. **Fig. 5.49** shows a typical transient swab/surge pressure against time while tripping in the hole one stand. The graph shows transient pressure behavior over 60 seconds as seen at the bottom of the open hole, starting with the bit 9,366 ft above the hole bottom. The time of 0.00 seconds is when the drillstring is picked up off the slips to trip in one stand. The pressure in the wellbore drops below the pore pressure for approximately 10 seconds (between 17 and 27 seconds), because of pressure transients. In this length of time the hydrostatic pressure is below the pore pressure value of 12.0 lbm/gal (in this example). The pressure transients continue long after the stand has been set in the slips (near

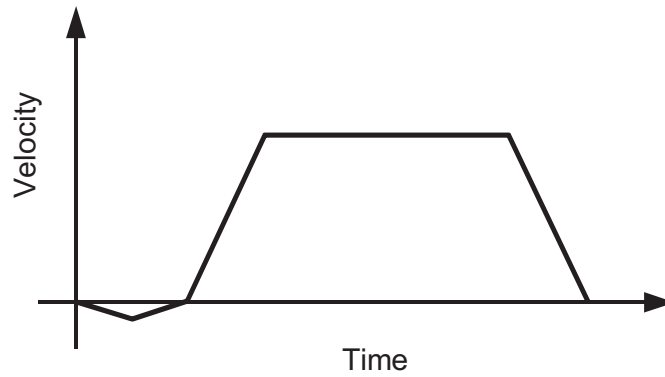


Fig. 5.48—Typical velocity profile while tripping in the hole.

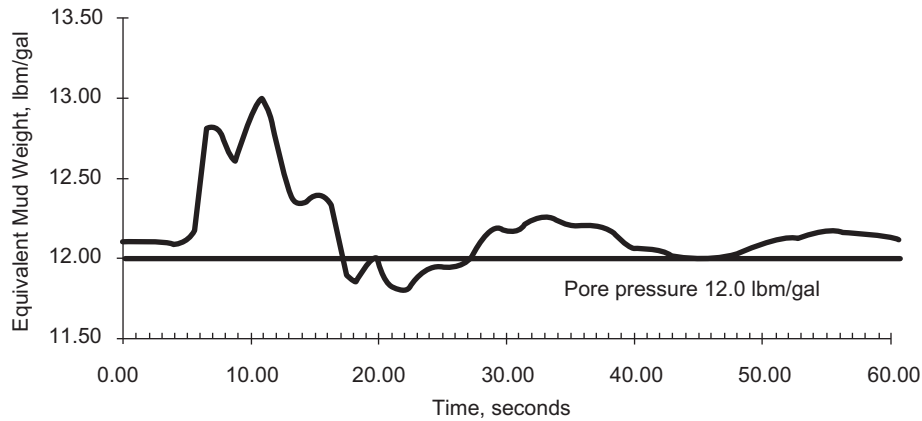


Fig. 5.49—Typical transient swab/surge pressure against time while tripping in one stand [after Rudolf and Suryanarayana (1998)].

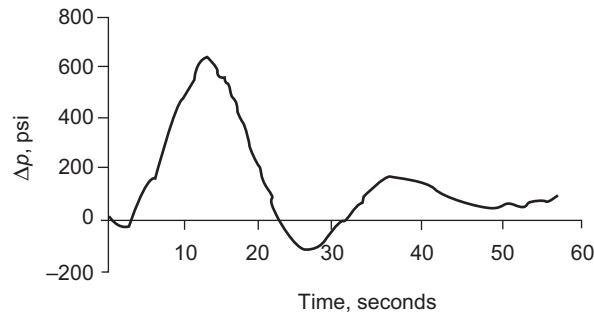


Fig. 5.50—Normalized transient pressures while tripping in one stand [after Rudolf and Suryanarayana (1998)].

the 10-second mark) and are almost completely damped out after 60 seconds. This occurs for each stand lowered into the hole.

Steine et al. (1996) reported on surge and swab experiments performed in an inclined onshore slimhole well. **Fig. 5.51** shows the downhole (1936 m measured depth) pressure development during tripping with plain drill water circulating at 150 L/min. In a successive paper, Bach et al. (1997) reported on a sensitivity study performed on the data obtained from the tests. Wang et al. (1997) studied the effect of unsteady motion of closed-end casing strings in concentric annuli on wellbore surge and swab pressures. Recently, Mitchell (2004) carried out a study on the dynamic surge pressures with high viscous forces in a low-clearance liner annulus. It is well known that, due to narrow margins between pore pressures and fracture gradients, low clearance produces large fluid friction effects, and as a consequence surge pressures can strongly affect casing design. The low clearance between hole and liner restricts return flow to such an extent that all the displaced fluid flows inside the liner, and the annulus

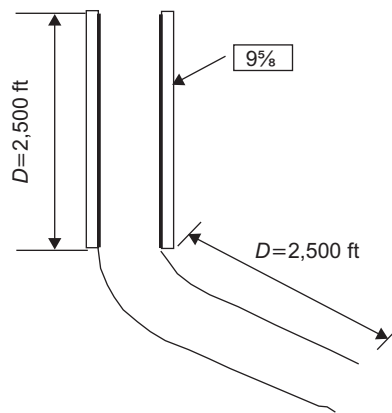


Fig. 5.51—Surge/swab data measured downhole in plain drill water [after Steine et al. (1996)].

fluid is swabbed behind the liner. The possibility of taking a kick while tripping in this kind of well may be significant.

While surge pressures are the primary concern while tripping into a well, two mechanisms have been identified for creating swabs: transient swabs caused by deceleration of the fluid at the end of a trip, and swabs caused by restricted annular flow due to low clearance. The second mechanism is possibly more serious because steady-state swab pressures are possible.

5.10.2 Dynamic Pressure Prediction. Calculating dynamic pressures in a wellbore are significantly more difficult than calculating steady-state flowing conditions. In a dynamic calculation, there are two effects not considered in steady flow: fluid inertia and fluid accumulation. In steady-state mass conservation, flow of fluid into a volume was matched by an equivalent flow out of the volume. In the dynamic calculation, there may not be equal inflow and outflow, but instead, fluid may accumulate within the volume. For fluid accumulation to occur, either the fluid must compress or the wellbore must expand. When considering the momentum equation, the fluid at rest must be accelerated to its final flow rate, and then decelerated when pipe motion stops. The fluid inertia resists this change in velocity.

Typically, dynamic fluid flow is not a consideration. The major exception is the operation of running pipe or casing into the wellbore, where dynamic pressure variation may be as important as pressures caused by fluid friction.

Governing Equations—Dynamic Pressure Prediction . The fluid pressures and velocities in open hole are determined by solving two coupled partial differential equations: the balance of mass and the balance of momentum.

Balance of Mass.

$$\left(\frac{1}{A} \frac{dA}{dP} + \frac{1}{K_b} \right) \frac{dP}{dt} + \frac{\partial v}{\partial z} = 0, \quad \dots \quad (5.218)$$

where

A = cross-sectional area, m²;

P = pressure, Pa;

K_b = fluid bulk modulus, Pa; and

v = fluid velocity, m/s.

The term

$$\left(\frac{1}{A} \frac{dA}{dP} + \frac{1}{K_b} \right) = C \quad \dots \quad (5.219)$$

is the compressibility, C , of the wellbore/fluid system (i.e., the change in wellbore volume per unit change in pressure). The balance of mass consists of three effects: the expansion of the hole because of internal fluid pressure, the compression of the fluid because of changes in fluid pressure, and the influx or outflux of the fluid. The expansion of the hole is governed by the elastic response of the formation and any casing cemented between the fluid and the formation. The fluid volume change is given by the bulk modulus K_b . For drilling muds, K_b varies as a

function of composition, pressure, and temperature. The reciprocal of the bulk modulus is called the compressibility.

Balance of Momentum.

$$\rho \frac{dv}{dt} = -\frac{\partial P}{\partial z} + dP_f + \rho g \cos \varphi = 0 \quad \dots\dots\dots (5.220)$$

where

ρ = fluid density, kg/m³;

dP_f = friction pressure loss, Pa/m;

g = gravitational constant, m/s²;

φ = angle of inclination from the vertical;

and

$$\frac{d}{dt} = \frac{\partial}{\partial t} + v \frac{\partial}{\partial z}$$

The balance of momentum equation consists of four terms. The first term in Eq. 5.220 represents the inertia of the fluid [i.e., the acceleration of the fluid (left side of Eq. 5.220) equals the sum of the forces on the fluid (right side of Eq. 5.220)]. The last three terms are the forces on the fluid. The first of these terms is the pressure gradient. The second is the drag on the fluid because of frictional or viscous forces. The friction pressure drop is a function of the type of fluid and the velocity of the fluid. Frictional drag is discussed in the section on rheology. The last force is the gravitational force.

The balance equations for flow with a pipe in the wellbore are similar to the equations for the openhole model with two important differences. First, the expansivity terms in the balance of mass equations depend on the pressures both inside and outside the pipe. For instance, increased annulus pressure can decrease the cross-sectional area inside the pipe, and increased pipe pressure can increase the cross-sectional area because of pipe elastic deformation. The second major difference is the effect of pipe speed on the frictional pressure drop in the annulus, as discussed in the steady-state surge article. Consult papers on dynamic surge pressures for more detail concerning the wellbore/pipe problem, such as Lubinski (1977) and Mitchell (1988).

Borehole Expansion. The balance of mass equation contains a term that relates the flow cross-sectional area to the fluid pressures. This section discusses the application of elasticity theory to the determination of the coefficients in the balance of mass equation. If we assume that the formation outside the wellbore is elastic, then the displacement of the borehole wall because of change in internal pressure is given by the elastic formula.

$$u = \frac{D_h}{2E_f}(1 + \nu_f)\Delta P, \quad \dots\dots\dots (5.221)$$

where

u = radial displacement, m;

ν_f = Poisson's ratio for the formation; and

E_f = Young's modulus for the formation, Pa.

The cross-sectional area of the annulus is given by

$$A = \pi \left(\frac{1}{2} D_h + u \right)^2 \quad \dots\dots\dots (5.222)$$

If we assume u is small compared to D_h , we can calculate the following formula from Eqs. 5.221 and 5.222.

$$\frac{1}{A} \frac{dA}{dP} = \frac{2(1 + \nu_f)}{E_f} \quad \dots\dots\dots (5.223)$$

Using typical values of formation elastic modulus, the borehole expansion term is the same order of magnitude as the fluid compressibility and cannot be neglected.

Solution Method—Fluid Dynamics. The method of characteristics is the method most commonly used to solve the dynamic pressure-flow equations (Courant et al. 1953). This method has been extensively used in the

analysis of dynamic fluid flow. The characteristic equations are developed using the methods given in Chapter 1 of Lapidus and Pindar (1982). For the open hole below the moving pipe, the fluid motion is governed by the system of equations shown in Eq. 5.224.

$$\begin{bmatrix} 1 & 0 & 0 & C \\ 0 & \rho & 1 & 0 \\ a & 1 & 0 & 0 \\ 0 & 0 & a & 1 \end{bmatrix} \begin{bmatrix} \partial v / \partial z \\ \partial v / \partial t \\ \partial p / \partial z \\ \partial p / \partial t \end{bmatrix} = \begin{bmatrix} 0 \\ h \\ dv/d\xi \\ dp/d\xi \end{bmatrix} \quad \dots\dots\dots (5.224)$$

where the first two equations are the balance of mass, with C equal to the wellbore-fluid compressibility, and the balance of momentum, with friction and gravitation terms lumped together as h :

$$h = dP_f + \rho g \cos \phi \quad \dots\dots\dots (5.225)$$

The last two equations describe the variation of p and v along the characteristic curve $\xi = z \pm a^*t$, where a is the acoustic velocity. We have neglected the fluid velocity relative to the acoustic velocity a in Eq. 5.224. This system of equations is overdetermined; that is, there are more equations than unknowns. For this system to have a solution, the following condition must hold.

$$\det \begin{bmatrix} 1 & 0 & 0 & C \\ 0 & \rho & 1 & 0 \\ a & 1 & 0 & 0 \\ 0 & 0 & a & 1 \end{bmatrix} = 0 \quad \dots\dots\dots (5.226)$$

Evaluating the determinant (Eq. 5.226) defines the acoustic velocity.

$$a^2 = \frac{1}{\rho C} \quad \dots\dots\dots (5.227)$$

The second condition that the equations have a solution requires

$$\det \begin{bmatrix} 1 & 0 & 0 & 0 \\ 0 & \rho & 1 & h \\ a & 1 & 0 & dv/d\xi \\ 0 & 0 & a & dp/d\xi \end{bmatrix} = 0 \quad \dots\dots\dots (5.228)$$

This determinant produces the following differential equations along the characteristic curves.

$$\frac{d}{d\xi}(p \pm \rho a v) = \pm a h \quad \dots\dots\dots (5.229)$$

The characteristic equations are solved to give $p(x,t)$ and $v(x,t)$ in the following way. Eq. 5.229 is integrated along the characteristics for timestep Δt .

$$\begin{aligned} p(z, \Delta t) + \rho a v(z, \Delta t) &= p(z - a \Delta t, 0) + \rho a v(z - a \Delta t, 0) + \int_0^{\Delta \xi} h d\xi^- \\ &= c^+(z, \Delta t) \quad \dots\dots\dots (5.230) \end{aligned}$$

$$\xi^- = z - at$$

and

$$\begin{aligned} p(z, \Delta t) - \rho a v(z, \Delta t) &= p(z + a \Delta t, 0) - \rho a v(z + a \Delta t, 0) - \int_0^{\Delta \xi} h d\xi^+ \\ &= c^-(z, \Delta t) \quad \dots\dots\dots (5.231) \end{aligned}$$

$$\xi^+ = z + at$$

Eqs. 5.230 and 5.231 can be solved simultaneously to give

$$p(z, \Delta t) = \frac{1}{2}(c^+ + c^-) \quad \dots\dots\dots (5.232)$$

and

$$v(z, \Delta t) = \frac{(c^+ - c^-)}{2\rho a} \quad \dots\dots\dots (5.233)$$

Generally, c^+ and c^- must be interpolated to give values at the points of interest (Streeter 1962).

Example 5.30 Consider a well with a rigid wellbore of depth 3000 m by 0.30 m diameter wellbore full of water at 35°C. The density of the water is 994 kg/m³ and the bulk modulus is 2.24×10⁹ Pa. At $t = 0$, a closed end pipe with diameter of 0.194 m begins moving at 1 m/s. Calculate the acoustic velocity, and predict wellbore pressure transients for 2 seconds. Neglect the hydrostatic and frictional pressure drop terms ($h = 0$).

Solution. The acoustic velocity is $\sqrt{2.24 \times 10^9 / 994} = 1,500$ m/s. If we calculate at 1 second intervals, the wellbore is divided into two sections with nodes at 0, 1500, and 3000 m. Boundary conditions are $p = 0$ at the surface and v defined by the pipe movement at $z = 3000$ m.

The volume displaced by the pipe is $\frac{\pi}{4}(0.194\text{m})^2 (1 \text{ m/s}) = 0.118 \text{ m}^3 / \text{s}$. The velocity of the fluid in the annulus at 3000 m is $v = -0.118 \text{ m}^3 / \text{s} / \left[\frac{\pi}{4}(0.3^2 - 0.194^2) \right] = -3.05 \text{ m/s}$, that is, 3.05 m/s upward. At $t = 0$, all of the c^+ and c^- are zero, so the transient pressure at the bottom of the well is given by Eq. 5.230, $p = -\rho a v = (994)(1500)(3.05) = 4.55 \times 10^6 \text{ Pa} = 660 \text{ psi}$.

The formulas for c^+ and c^- for this case become:

$$c^+(z, t + \Delta t) = p(z - 1500, t) + \rho a v(z - 1500, t)$$

$$c^-(z, t + \Delta t) = p(z + 1500, t) - \rho a v(z + 1500, t)$$

For $t = 1$ second,

$$c^-(0, 1) = p(1500, 0) - \rho a v(1500, 0) = 0$$

$$c^+(1500, 1) = p(0, 0) + \rho a v(0, 0) = 0$$

$$c^-(1500, 1) = p(3000, 0) - \rho a v(3000, 0) = 4.55 \times 10^6 + (994)(1500)(3.05) = 9.10 \times 10^6$$

$$c^+(3000, 1) = p(1500, 0) + \rho a v(1500, 0) = 0$$

$$p(0, 1) = 0$$

$$v(0, 1) = 0$$

$$p(1500, 1) = 4.55 \times 10^6 \text{ Pa}$$

$$v(1500, 1) = -3.05 \text{ m/s}$$

$$p(3000, 1) = 4.55 \times 10^6 \text{ Pa}$$

$$v(3000, 1) = -3.05 \text{ m/s}$$

$$c^-(0, 2) = p(1500, 1) - \rho a v(1500, 1) = 4.55 \times 10^6 + (994)(1500)(3.05) = 9.10 \times 10^6$$

$$c^+(1500, 2) = p(0, 1) + \rho a v(0, 1) = 0$$

$$c^-(1500, 2) = p(3000, 1) - \rho a v(3000, 1) = 4.55 \times 10^6 + (994)(1500)(3.05) = 9.10 \times 10^6$$

$$c^+(3000, 2) = p(1500, 1) + \rho a v(1500, 1) = 0$$

$$p(0, 2) = 0$$

$$v(0, 2) = -9.10 \times 10^6 / (994) / (1500) = -6.1 \text{ m/s}$$

$$p(1500, 2) = 4.55 \times 10^6 \text{ Pa}$$

$$v(1500, 2) = -3.05 \text{ m/s}$$

$$p(3000, 2) = 4.55 \times 10^6 \text{ Pa}$$

$$v(3000, 2) = -3.05 \text{ m/s}$$

Notice that the pressure of 660 psi is released at the surface, doubling the flow rate. The student is encouraged to continue this calculation to see how the fluid pressure and velocity change with time. Interpret what is happening with regard to fluid inertia and fluid compressibility.

5.11 Cuttings Transport

5.11.1 Introduction. Of the many functions that are performed by the drilling fluid, the most important is to transport cuttings from the bit up the annulus to the surface. If the cuttings cannot be removed from the wellbore, drilling cannot proceed for long. In rotary drilling operations, both the fluid and the rock fragments are moving. The situation is complicated further by the fact that the fluid velocity varies from zero at the wall to a maximum at the center of annulus. In addition, the rotation of the drillpipe imparts centrifugal force on the rock fragments, which affects their relative location in the annulus. Because of the extreme complexity of this flow behavior, drilling personnel have relied primarily on observation and experience for determining the lifting ability of the drilling fluid. In practice, either the flow rate or effective viscosity of the fluid is increased if problems related to inefficient cuttings removal are encountered. This has resulted in a natural tendency toward thick muds and high annular velocities. However, increasing the mud viscosity or flow rate can be detrimental to the cleaning action beneath the bit and cause a reduction in the penetration rate. Thus, there may be a considerable economic penalty associated with the use of a higher flow rate or mud viscosity than necessary. Transport is usually not a problem if the well is near vertical. However, considerable difficulties can occur when the well is being drilled directionally, because cuttings may accumulate either in a stationary bed at hole angles above about 50° or in a moving, churning bed at lower hole angles. Drilling problems that may result include stuck pipe, lost circulation, high torque and drag, and poor cement jobs. The severity of such problems depends on the amount and location of cuttings distributed along the wellbore.

Vertical Wells. The problem of cuttings transport in vertical wells has been studied for many years, with the earliest analysis of the problem being that of Pigott (1941). Several authors have conducted experimental studies of drilling-fluid carrying capacity. Williams and Bruce (1951) were among the first to recognize the need for establishing the minimum annular velocity required to lift the cuttings. In 1951, they reported the results of extensive laboratory and field measurements on mud carrying capacity. Before their work, the minimum annular velocity generally used in practice was about 200 ft/min. As a result of their work, a value of about 100 ft/min gradually was accepted. More recent experimental work by Sifferman and Becker (1974, 1992) indicates that while 100 ft/min may be required when the drilling fluid is water, a minimum annular velocity of 50 ft/min should provide satisfactory cutting transport for a typical drilling fluid.

The transport efficiency in vertical wells is usually assessed by determining the settling velocity, which is dependent on particle size, density and shape; the drilling fluid rheology and velocity; and the hole/pipe configuration. Several investigators have proposed empirical correlations for estimating the cutting slip velocity experienced during rotary-drilling operations. While these correlations should not be expected to give extremely accurate results for such a complex flow behavior, they do provide valuable insight in the selection of drilling-fluid properties and pump-operating conditions. The correlations of Moore (1974), Chien (1971), and Walker and Mayes (1975) have achieved the most widespread acceptance.

Deviated Wells. Since the early 1980s, cuttings transport studies have focused on inclined wellbores. And an extensive body of literature on both experimental and modeling work has developed. Experimental work on cuttings transport in inclined wellbores has been conducted using flow loops at the University of Tulsa and elsewhere. Different mechanisms, which dominate within different ranges of wellbore angle, determine cuttings bed heights and annular cuttings concentrations as functions of operating parameters (flow rate and penetration rate), wellbore configuration (depth, hole angle, hole size or casing ID, and pipe size), fluid properties

(density and rheology), cuttings characteristics (density, size, bed porosity, and angle of repose), and pipe eccentricity and rotary speed.

Laboratory experience indicates that the flow rate, if high enough, will always remove the cuttings for any fluid, hole size, and hole angle. Unfortunately, flow rates high enough to transport cuttings up and out of the annulus effectively cannot be used in many wells because of limited pump capacity and/or high surface or downhole dynamic pressures. This is particularly true for high angles with hole sizes larger than 12¼ in. High rotary speeds and backreaming are often used when flow rate does not suffice.

5.11.2 Particle Slip Velocity. The earliest analytical studies of cuttings transport considered the fall of particles in a stagnant fluid, with the hope that these results could be applied to a moving fluid with some degree of accuracy. Most start with the relation developed by Stokes (1845) for creeping flow around a spherical particle (**Fig. 5.52**).

$$F_d = 3\pi\mu d_s v_{sl}, \quad \dots\dots\dots (5.234)$$

where

μ = Newtonian viscosity of the fluid, Pa·s;

d_s = particle diameter, m;

v_{sl} = particle slip velocity, m/s; and

F_d = total drag force on the particle, N.

When the Stokes drag is equated to the buoyant weight of the particle W ,

$$W = \frac{\pi}{6}(\rho_s - \rho_f)gd_s^3. \quad \dots\dots\dots (5.235)$$

Then, the slip velocity is given by

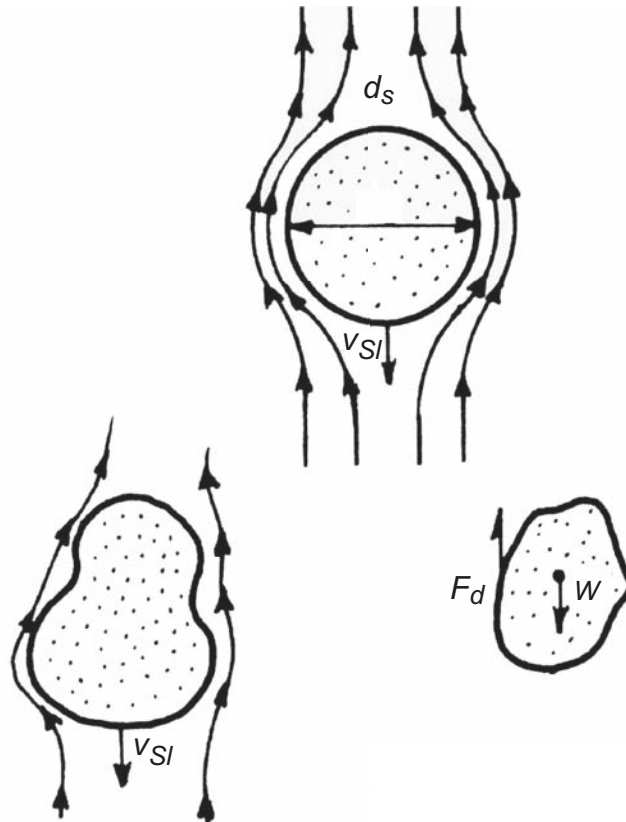


Fig. 5.52—Fluid movement about a settling particle (Bourgoyne et al. 1986).

TABLE 5.2—SPHERICITIES FOR VARIOUS PARTICLE SHAPES (Bourgoyne et al. 1991)

Shape	Sphericity
Sphere	1.0
Octahedron	0.85
Cube	0.81
Prism	
$\ell \cdot \ell \cdot 2\ell$	0.77
$\ell \cdot 2\ell \cdot 2\ell$	0.76
$\ell \cdot 2\ell \cdot 3\ell$	0.73
Cylinders	
$h = r/15$	0.25
$h = r/10$	0.32
$h = r/3$	0.59
$h = r$	0.83
$h = 2r$	0.87
$h = 3r$	0.96
$h = 10r$	0.69
$h = 20r$	0.58

$$v_{sl} = \frac{d_s^2 g (\rho_s - \rho_f)}{18\mu} \quad \dots\dots\dots (5.236)$$

where

ρ_s = solid density, kg/m³;

ρ_f = fluid density, kg/m³; and

g = acceleration of gravity, m/s².

Stokes' law is accurate as long as turbulent eddies are not present in the particle's wake. The onset of turbulence occurs for

$$\text{Re}_p > 0.1 \quad \dots\dots\dots (5.237)$$

where the particle Reynolds number is given by

$$\text{Re}_p = \frac{\rho_f v_{sl} d_s}{\mu} \quad \dots\dots\dots (5.238)$$

For turbulent slip velocities, the drag force is given by

$$F_d = \frac{\pi}{8} f \rho_f v_{sl}^2 d_s, \quad \dots\dots\dots (5.239)$$

where f is an empirically determined friction factor. The friction factor is a function of the particle Reynolds number and the shape of the particle given by Ψ , the sphericity. **Table 5.2** gives the sphericity of various particle shapes.

The friction factor/Reynolds number relationship is shown in **Fig. 5.53** for a range of sphericity. The particle slip velocity for turbulent flow is given by

$$v_{sl} = \frac{2}{3} \sqrt{\frac{3gd_s(\rho_s - \rho_f)}{f\rho_f}} \quad \dots\dots\dots (5.240)$$

If we define a laminar friction factor, $f = 24/\text{Re}_p$, then Eq. 5.240 is valid for all Reynolds numbers.

Example 5.31 How much sand having a mean diameter of 0.025 in. and a sphericity of 0.81 will settle to the bottom of the hole if circulation is stopped for 30 minutes? The drilling fluid is 8.33 lbm/gal water, having a viscosity of 1 cp and containing approximately 1% sand by volume. The specific gravity of the sand is 2.6.

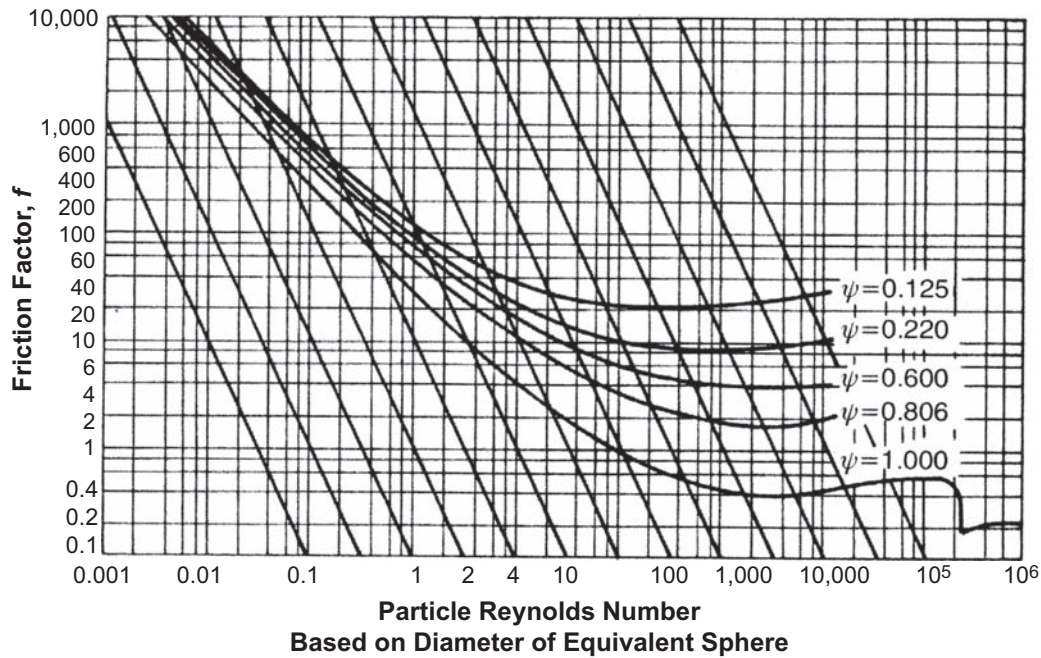


Fig. 5.53—Friction factors for computing particle slip velocity (Bourgoyne et al. 1986).

Solution. In SI units the particle diameter d_s , the fluid density ρ_f , the fluid viscosity μ , and the solid density ρ_s are

$$d_s = \frac{0.025 \text{ in.}}{3.937 \cdot 10 \text{ in./m}} = 0.000635 \text{ m}$$

$$\rho_f = \frac{8.33 \text{ lbm/gal}}{8.3454 \cdot 10^{-3} (\text{lbm/gal}) / (\text{kg/m}^3)} = 0.9981 \cdot 10^3 \text{ kg/m}^3$$

$$\mu = \frac{1 \text{ cp}}{10^3 \text{ cp}/(\text{Pa} \cdot \text{s})} = 1.0 \cdot 10^{-3} \text{ Pa} \cdot \text{s}$$

$$\rho_s = \frac{2.6 \cdot 8.33 \text{ lbm/gal}}{8.3454 \cdot 10^{-3} (\text{lbm/gal}) / (\text{kg/m}^3)} = 2.5952 \cdot 10^3 \text{ kg/m}^3$$

A slip velocity first must be assumed to establish a point on the drag coefficient plot shown in Fig. 5.53. The first guess is by assuming Stokes' law is applicable, hence, Eq. 5.236 gives

$$V = \frac{1}{18} \frac{d_s^2}{\mu} (\rho_s - \rho_f) g = \frac{1}{18} \frac{(0.000635)^2}{0.001} (2.6 - 1)(998.1)(9.81) = 0.351 \text{ m/s.}$$

This slip velocity corresponds to a drag coefficient of

$$C_D = \frac{4}{3} g \frac{d_s}{V^2} \left(\frac{\rho_s - \rho_f}{\rho_f} \right) = \frac{4}{3} (9.81) \frac{0.000635}{0.351^2} \left(\frac{2,595.2 - 998.1}{998.1} \right) = 0.109,$$

and a Reynolds number of

$$\text{Re} = \frac{\rho_f V d_s}{\mu} = \frac{(998.1)(0.351)(0.000635)}{0.001} = 222.$$

Entering Fig. 5.53 at the point ($C_D = 0.109$, $\text{Re} = 222$) and moving parallel to the slant lines to the curve for $\psi = 0.81$ yields an intersection point at ($C_D = 5$, $\text{Re} = 40$). Thus, the slip velocity is given by

$$V = \sqrt{\frac{4}{3} \frac{g d_s (\rho_s - \rho_f)}{C_D \rho_f}} = \sqrt{\frac{4}{3} \frac{9.81 * 0.000635 \left(\frac{2,595.2 - 998.1}{998.1} \right)}{5}} = 0.0516 \text{ m/s} = 0.17 \text{ ft/s}.$$

If circulation is stopped for 30 minutes, the sand will settle from approximately

$$(30 \text{ min})(0.0516 \text{ m/s})(60 \text{ s/min}) = 92.88 \text{ m} = 304.7 \text{ ft}$$

From the bottom portion of the hole. If the sand packs with a porosity of 0.40, the fill on bottom is approximately

$$304.7 \frac{0.01}{(1-0.4)} = 5 \text{ ft}.$$

Non-Newtonian fluids introduce new factors into particle-settling calculations. For a Bingham fluid, the particle will remain suspended with no settling if

$$\tau_y \geq \frac{d_s}{6} (\rho_s - \rho_f), \quad \dots \dots \dots (5.241)$$

where τ_y is the fluid YP. Otherwise, because no other analytic solutions exist, an “apparent” or “equivalent” viscosity is determined from the non-Newtonian fluid parameters. For example, Moore (1974) used the apparent viscosity proposed by Dodge and Metzner (1959) for a pseudoplastic fluid.

$$\mu_a = \frac{K}{144} \left(\frac{D_o - D_i}{v} \right)^{n-1} \left(\frac{2n+1}{0.0208n} \right)^n, \quad \dots \dots \dots (5.242)$$

where

- μ_a = apparent viscosity, Pa·s;
- K = consistency index for pseudoplastic fluid, Pa·s;
- n = power law index;
- D_o = annulus OD, m;
- D_i = annulus ID, m; and
- v = annulus average flow velocity.

Chien (1971) determines apparent viscosity for a Bingham plastic fluid as shown in Eq. 5.243.

$$\mu_a = \mu_p + 5 \frac{\tau_y d_s}{v}, \quad \dots \dots \dots (5.243)$$

where μ_p is the plastic viscosity. The apparent viscosity models with most widespread acceptance are those of Moore (1974).

5.11.3 A Cuttings Transport Model for Vertical Wells. The following model was taken from Clark and Bickham (1994), and is an example of what is called *mechanistic modeling*. For vertical well conditions, **Fig. 5.54** shows a schematic of the cuttings transport process in a YPL fluid under laminar-flow conditions. The area open to flow is characterized as a tube instead of an annulus. This simplifies the wellbore geometry. The tube diameter is based on the hydraulic diameter for pressure-drop calculations.

Because drilling fluid often exhibits a yield stress, there may be a region, near the center of the cross section, where the shear stress is less than the yield stress. There, the mud will move as a plug (i.e., rigid body motion). The plug velocity is v_p . The average cuttings concentration and velocity in the plug are c_p and v_{cp} , respectively. In the annular region around the plug, the mud flows with a velocity gradient and behaves as a viscous fluid. The average annular velocity of the mud in this region is v_a . In addition, for the cuttings in this region, the average concentration and velocity are c_a and v_{ca} , respectively.

Cross-Sectional Geometry. First, let us define the basic wellbore geometry. The hydraulic diameter is defined as four times the flow area divided by the length of the wetted perimeter; namely,

$$D_{\text{hyd}} = \frac{4 \times \text{cross-sectional area}}{\text{wetted perimeter}} \quad \dots \dots \dots (5.244)$$

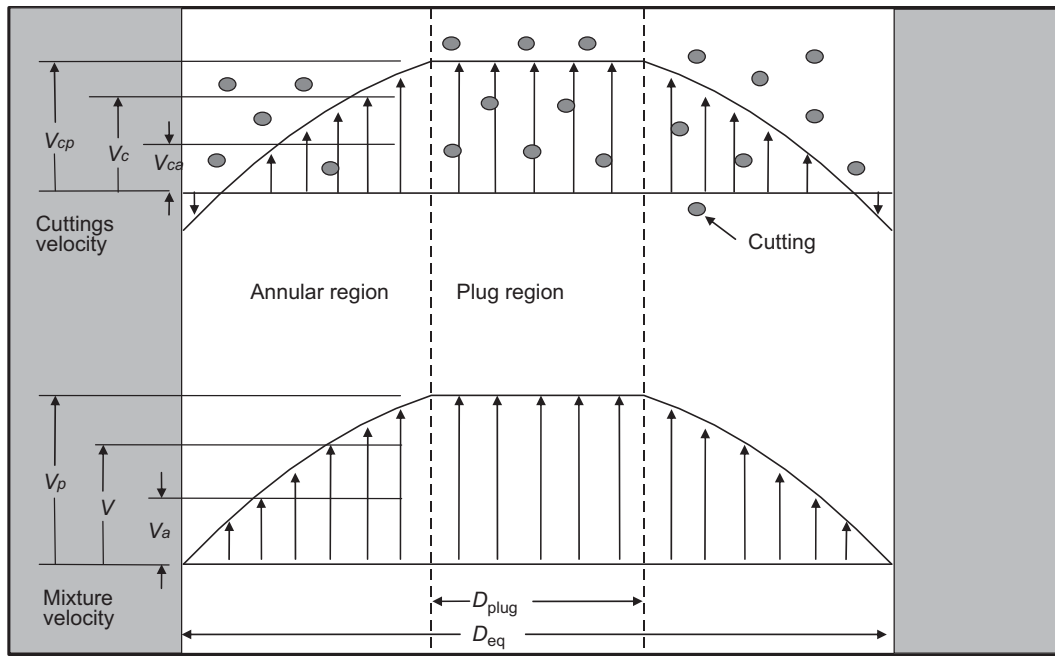


Fig. 5.54—Cuttings-velocity profile: YPL fluid (from Lake 2006).

For the wellbore annulus, the hydraulic diameter of the wellbore cross section is

$$D_{\text{hyd}} = D_h - D_p, \quad (5.245)$$

where D_h is the wellbore diameter, and D_p is the drillpipe O.D. The equivalent diameter is defined as

$$D_{\text{eq}} = \sqrt{4A/\pi}, \quad (5.246)$$

where A is the area open to flow. For the wellbore annulus, the equivalent diameter is

$$D_{\text{eq}} = \sqrt{D_h^2 - D_p^2}. \quad (5.247)$$

The plug diameter ratio is

$$\lambda_p = D_{\text{plug}} / D_{\text{eq}}. \quad (5.248)$$

Flow Conditions. The mixture velocity is

$$v_{\text{mix}} = \frac{Q_c + Q_m}{A}, \quad (5.249)$$

where Q_m is the volumetric flow rate of the mud and Q_c is the volumetric flow rate of the cuttings, which depends on the bit size and the penetration rate. In addition, the mixture velocity can be calculated from the average plug and annulus velocities in the equivalent pipe; namely,

$$v_{\text{mix}} = v_a (1 - \lambda_p^2) + v_p \lambda_p^2, \quad (5.250)$$

where we have used

$$Q_{\text{mix}} = v_a \pi/4 (D_{\text{eq}}^2 - D_{\text{plug}}^2) + v_p \pi/4 D_{\text{plug}}^2,$$

with v_p the plug velocity, v_a the average velocity outside the plug, and Eq. 5.248. See Fig. 5.54 for an illustration of these definitions.

Cuttings Concentration. The feed concentration is defined as

$$c_0 = \frac{Q_c}{Q_c + Q_m} \quad (5.251)$$

The average concentration, c , of cuttings can be calculated as

$$Q_c = cQ_{\text{mix}} = c_a Q_a + c_p Q_p \text{ or} \\ c = c_a (1 - \lambda_p^2) + c_p \lambda_p^2 \quad (5.252)$$

where c_a is the cuttings concentration in the annular region and c_p is the cuttings concentration in the plug region. The cuttings concentrations in the plug and annular regions are now assumed equal. This means that the suspended cuttings are uniformly distributed across the area open to flow. Obviously, this assumption has a major impact, and the actual distribution is probably a function of wellbore geometry, fluid properties, cuttings properties, and operating conditions. With this assumption, the volume flow rate of cuttings is:

$$Q_c = c(v_m - v_s)A, \quad (5.253)$$

where v_m is the average velocity of the mud, and v_s is the average settling velocity of the cuttings. The velocity of a cutting is going to be the velocity of the mud less the settling velocity. We multiply by the concentration c because the cuttings do not fill the entire volume of the annulus, but rather the fraction c of the volume. The volume flow rate of mud is

$$Q_m = (1 - c)v_m A. \quad (5.254)$$

We use $(1 - c)$ because the mud fills the volume of the annulus that is not filled with cuttings. Using Eqs. 5.249, 5.251, 5.253, and 5.254, we obtain

$$v_{\text{mix}} = \frac{cv_s(1 - c)}{c - c_0}, \quad (5.255)$$

where

$$v_s = v_{sa}(1 - \lambda_p^2) - v_{sp}\lambda_p^2 \quad (5.256)$$

is the average settling velocity in the axial direction. At this point, we have used all the principles of mass balance, but we are still left with unknowns. To finish the problem, we need correlations for the unknown quantities in terms of known quantities. The components of the settling velocities in the axial direction are given by correlations

$$v_{sa} = V_1(c, \text{Re}_p, v'_{sa}), \quad (5.257)$$

and

$$v_{sp} = V_2(v'_{sp}, Y_a), \quad (5.258)$$

where

$$v'_{sa} = \sqrt{\frac{4d_s g(\rho_s - \rho)}{3\rho C_D}},$$

$$v'_{sp} = \cos \varphi \sqrt{\frac{4}{\rho C_D} \left\{ \frac{d_s g(\rho_s - \rho)}{3} - \pi \tau_y \right\}},$$

$$\text{Re}_p = \frac{d_s \rho v}{\mu_a},$$

and

$$Y_a = \frac{3\tau_y}{d_s g(\rho_s - \rho)} \quad (5.259)$$

C_D is the drag coefficient of a sphere, τ_y is the yield stress of the mud, and μ_a is the apparent viscosity of the mud at the shear rate resulting from the settling cuttings.

Perry and Chilton (1973) provide the following correlation for V_1 :

$$V_1 = v'_{sa} (1 - c)^n, \quad (5.260)$$

while Clark and Bickham correlated their graphical method with the following equations:

$$\begin{aligned} n &= \exp(0.0811y - 1.19), \\ y &= \frac{-\operatorname{sgn}(x)}{(0.0001 + 0.865|x|^{-6})^{1/6}} \quad (5.261) \\ x &= 1.24 \ln(\operatorname{Re}_p) - 4.59 \end{aligned}$$

The following correlation was developed by Clark and Bickham to model cuttings settling in a mud with a yield stress:

$$V_2 = v'_{sp} (1 - Y_a^{0.94}). \quad (5.262)$$

The value calculated using Eq. 5.255 is the minimum acceptable mixture velocity required for a cuttings concentration. Pigott (1941) recommended that the concentration of suspended cuttings be a value less than 5%. With this limit ($c = 0.05$), Eq. 5.255 becomes

$$v_{\text{mix}} = \frac{0.0475v_s}{0.05 - c_0}, \quad (5.263)$$

where $c_0 < 0.05$. This implies that the penetration rate must be limited to a rate that satisfies this equality.

For near-vertical cases, the critical mud-cuttings mixture velocity equals the value of Eq. 5.263. If the circulation rate exceeds this value, the suspended cuttings concentration will remain less than 5%. However, if the mud circulation velocity is less than the cuttings' settling velocity, the cuttings will eventually build up in the wellbore and plug it.

Example 5.32 An 8¾-in. vertical hole is being drilled at an ROP of 20 ft/hr into a formation with 15% porosity. The drill collar OD is 6½ in. and the mud circulation rate is 100 gal/min. Assume that the settling velocity of the cuttings is the same as that in Example 5.31 (0.17 ft/sec). What is the feed concentration of the cuttings and the actual concentration of the cuttings? Should you change any of your operating parameters?

Solution. The formation is porous with fluid in the pores, so drilling produces both a solids volume flow rate and an additional fluid volume flow rate. Assume the cuttings consist only of solids. Then,

$$A_{\text{hole}} = \pi/4(8.75)^2 = 60 \text{ in.}^2;$$

$$\begin{aligned} Q_c &= (1 - 0.15) \times \text{ROP} \times A_{\text{hole}} = 0.85(20 \text{ ft/hr})(12 \text{ in./ft})/60 \text{ min/hr}(60 \text{ in.}^2) \\ &= 204 \text{ in.}^3/\text{min}; \end{aligned}$$

$$\begin{aligned} \text{Added fluid} &= .15 \times \text{ROP} \times A_{\text{hole}} = 0.15(20 \text{ ft/hr})(12 \text{ in./ft})/60 \text{ min/hr}(60 \text{ in.}^2) \\ &= 36 \text{ in.}^3/\text{min}; \end{aligned}$$

and

$$Q_m = 36 \text{ in.}^3/\text{min} + 100 \text{ gal/min} \times 231 \text{ in.}^3/\text{gal} = 23,140 \text{ in.}^3/\text{min}.$$

$$\text{The feed concentration } c_0 = Q_c/(Q_m + Q_c) = 0.00874.$$

The mixture velocity = $(Q_c + Q_m)/A = (204 + 23,140)/60 = 389$ in./min.

The settling velocity = $0.17 \text{ ft/sec} \times 12 \text{ in./ft} \times 60 \text{ sec/min} = 122$ in./min.

Using these results in Eq. 5.255, we get a quadratic equation in c , with the positive root equal to 0.0127. The actual concentration is higher than the feed concentration because the cuttings travel at a slower speed than the fluid. Pigott (1941) recommended that the concentration of suspended cuttings be a value less than 5%, so we are operating in a safe area, with potential to increase ROP.

5.11.4 Cuttings Transport in Deviated Wells. A comprehensive cuttings transport model should allow a complete analysis for the entire well, from surface to the bit. The different mechanisms which dominate within different ranges of wellbore angle should be used to predict cuttings-bed heights and annular cuttings concentrations as functions of operating parameters (flow rate and penetration rate), wellbore configuration (depth, hole angle, hole size, or casing ID, and pipe size), fluid properties (density and rheology), cuttings characteristics (density, size, bed porosity, and angle of repose), pipe eccentricity, and rotary speed. Because of the complexity, extensive experimental data were necessary to help formulate and validate the new cuttings transport models.

New Experimental Data. Large-scale cuttings transport studies in inclined wellbores were initiated at the Tulsa U. Drilling Research Projects (TUDRP) in the 1980s with the support of major oil and service companies. A flow loop was built that consisted of a 40-ft length of 5-in. transparent annular test section and the means to vary and control

- The angles of inclination between vertical and horizontal
- Fluid pumping flow rate
- Drilling rate
- Drillpipe rotation and eccentricity

Tomren et al. (1986) found marked differences between the cuttings transport in inclined wellbores and that of vertical wellbores. A cuttings bed was observed to form at inclination angles of more than 35° from vertical, and this bed could slide back down for angles up to 50° . Eccentricity, created by the drillpipe lying on the low side of the annulus, was found to worsen the situation. Analysis of annular fluid flow showed that eccentricity diverts most of the fluid flow away from the low side of the annulus, where the cuttings tend to settle, to the more open area above the drillpipe. Okrajni and Azar (1986) investigated the effect of fluid rheology on hole cleaning. They observed that removing a cuttings bed with a high-viscosity fluid (a remedy for the hole-cleaning problem in vertical wells) may in fact be detrimental in high-angle wellbores (assuming a zero to low drillpipe rotation), and that a low-viscosity fluid that can promote turbulence is more helpful. On the basis of this finding and on the previous study, hole cleaning was found to depend on the angle of inclination, hydraulics, fluid rheological properties, drillpipe eccentricity, and rate of penetration. Becker et al. (1991) then showed that the cuttings transport performance of the fluids tested correlated best with the low-end-shear-rate viscosity, particularly the 6-rev/min Fann V-G viscometer dial readings.

By the mid-1980s, a general qualitative understanding of the hole-cleaning problem in highly inclined wellbores had been gained. Because more directional and horizontal wells with longer lateral reaches were being drilled, the need for more and new experimental data created a demand for additional flow loops. In partnership with Chevron, Conoco, Elf Aquitaine, and Philips, TUDRP built a new and larger flow loop, with a 100-ft-long test section of 8-in. annulus, while construction of new flow loops was also done at Heriot-Watt U., BP, Southwest Research, M.I. Drilling Fluids, and the Inst. Français du Pétrole. All the flow loops had a transparent part of the annular test section that allowed observation of the cuttings transport mechanism. These flow loops provided the necessary tools for collecting the badly needed experimental data.

Because of the new flow loops, a significant amount of experimental data was collected on the effect of different parameters on cuttings transport under various conditions. The observations made, and subsequent analysis of, the data collected provided the basis for work toward formulating correlations/models.

Larsen (1993) conducted extensive studies on cuttings transport, totaling more than 700 tests with the TUDRP's 5-in. flow loop. Tests were performed for angles from vertical to horizontal under critical as well as subcritical flow conditions. Critical flow corresponds to the minimum annular average fluid velocity that would prevent stationary accumulation of cuttings bed. Subcritical flow refers to the condition in which a stationary cuttings bed forms. Analysis of the experimental data shows that when the fluid velocity is below the critical value, a cuttings bed starts to form and grows in thickness until the fluid velocity above the bed reaches the

critical value. The critical velocity was reported in the range of 3 to 4 ft/sec, depending on the value of various parameters, such as the fluid rheology, drilling rate, pipe eccentricity, and rotational speed. There were several new findings:

- Under subcritical flow conditions, a medium-rheology mud ($PV = 14$ and $YP = 14$) consistently resulted in slightly smaller cuttings beds than those obtained with the low-rheology ($PV = 7$ and $YP = 7$) or the high-rheology ($PV = 21$ and $YP = 21$) muds. Calculation of the Reynolds number for the tests suggests that the flow regime for this fluid is neither turbulent nor laminar but in the transition range.
- The small cuttings size used (0.1 in.) in the study was more difficult to clean than the medium (0.175 in.) and the large (0.275 in.) sizes (drillpipe rev/min 0 to 50). The small cuttings formed a more packed and smooth bed.
- The height of the cuttings bed (between 55 and 90°) remained nearly the same, but there was a slight increase at 65 to 70°.
- Significant backsliding of the cuttings bed was observed for angles from 35 to 55°.

Seeberger et al. (1989) reported that elevating the low-shear-rate viscosities enhances the cuttings-transport performance of oil muds. Sifferman and Becker (1992) conducted a series of hole-cleaning experiments in an 8-in. flow loop. Statistical analysis of the data showed interaction among various parameters; thus, simple relationships could not be derived. For example, the effect of drillpipe rotation on cuttings transport depended also on the size of the cuttings and the fluid rheology. The effect of rotation was more pronounced for smaller particles and for more viscous muds. Bassal (1995) completed a study of the effect of drillpipe rotation on cuttings transport in inclined wellbores. The variables considered in his work were drillpipe rotary speed, hole inclination, fluid rheology, cuttings size, and fluid flow rate. Results have shown that drillpipe rotation has a significant effect on hole cleaning in directional-well drilling. The level of enhancement in cuttings removal as a result of rotary speed is a function of a combination of fluid rheology, cuttings size, fluid flow rate, and the manner in which the drillstring behaves dynamically.

Flow Patterns. When solid-liquid mixtures flow in inclined and horizontal conduits, we observe specific flow patterns within which the basic characteristics of the two-phase mixture remain the same. The parameters determining the type of the flow pattern are the liquid velocity, the solids loading, the rheology, and the density of the liquid, and the density, diameter, and sphericity of the solids. It is very important to analyze solid-liquid flow in horizontal and inclined annuli from the perspective of the flow patterns because, then, modeling the phenomenon is not only more appropriate but also more accurate.

In the direction of decreasing flow rate (or velocity) we can define the following flow patterns for solid-liquid mixtures flowing in pipes or annuli, as shown in **Fig. 5.55** (Govier and Aziz 1972; Ford et al. 1990; Peden et al. 1990; Kelessidis and Mpandelis 2003).

- Homogeneous (or pseudohomogeneous) suspension or fully suspended symmetric flow pattern. At high liquid velocities, the solids are more or less uniformly distributed in the liquid and there is no slip between the two phases. This flow pattern normally is observed with fairly fine solids, less than 1 mm in diameter, which does not normally occur during drilling applications.
- Heterogeneous suspension or suspended asymmetric flow pattern. As the liquid flow rate is reduced, there is a tendency for the solids to flow near the bottom of the pipe (or the outer pipe of the annulus), but still suspended, thus creating an asymmetric solids concentration. Larger particles tend to segregate towards the bottom, while only the much smaller particles are in suspension higher up the annulus. A subpattern has also been defined, the suspension/saltation pattern, in which the cuttings are still in suspension but are densely populated near the bottom wall, and, in fact, they are transported by jumping forward or saltating on the bottom wall surface.
- Continuous moving bed. At even-lower flow rates, the solids form a continuous bed, which is moving in the direction of the flow, while there may be some nonuniformly distributed solids in the liquid layer above, particularly if solids exist with smaller diameters than the ones forming the bed. The liquid velocity below which this is happening has been given different names like *limit deposit velocity*, *minimum suspension velocity*, or *critical velocity*.
- Separated moving beds (dune or blob flow). As the flow rate is further decreased, separated cuttings beds, sometimes called dunes or blobs, are formed on the low side of the annulus with fairly large thickness and length. Cuttings on the surface of the bed move forward while cuttings inside the bed remain static, but the whole blob moves in the direction of the flow, so that the appearance is as if the bed is transported and moving like a caterpillar.

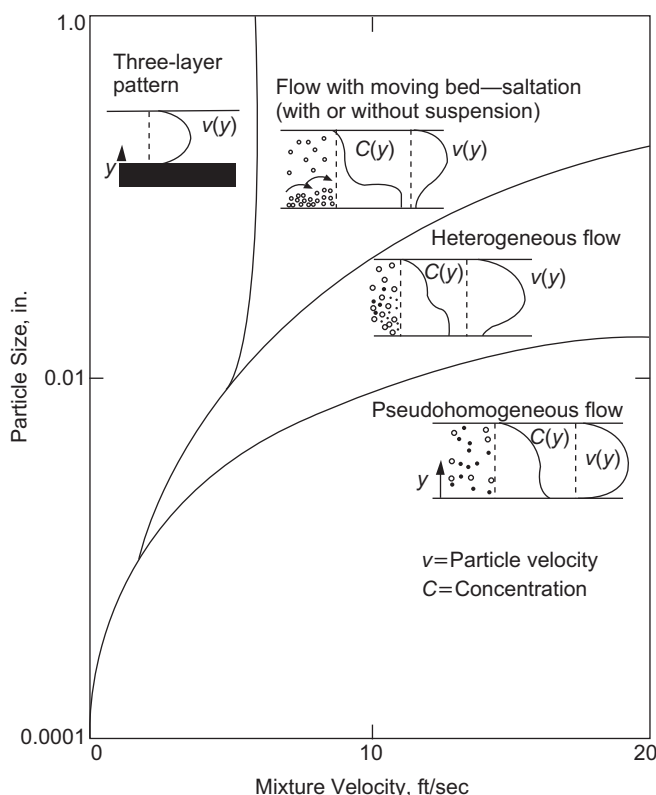


Fig. 5.55—Qualitative description of flow patterns for solid-liquid flow [from Iyoho (1980)].

- **Three-layer pattern.** Further reduction in liquid velocity results in more and more solids depositing on the low side, resulting in three layers: a bed of solids that is not moving, forming a stationary bed, a moving bed of solids on top of the stationary bed, and a heterogeneous liquid-solid mixture above. There is a strong interaction between the heterogeneous solid-liquid mixture and the moving bed, with solids deposited on the bed and re-entrained in the heterogeneous solid-liquid mixture. There is a point of equilibrium where, with the increase in height of the solids bed, the available area for flow of the heterogeneous mixture is decreased, resulting in higher mixture velocities and, hence, an increase in the erosion of the bed by the heterogeneous solid-liquid mixture.

At even lower liquid velocities, the solids pile up in the pipe (or annulus) and full blockage may occur. Experimental evidence and theoretical analysis indicate that this may occur at relatively high solids concentration, not normally encountered during normal drilling operations. However, if cuttings transport is inefficient, resulting in high solids concentration, especially in sections where large cross-sectional areas exist (e.g., in annulus wash-outs), this flow pattern may occur, resulting in considerable problems for the drilling process.

5.11.5 Factors Affecting Cuttings Transport. Field evidence, laboratory testing, and theoretical modeling have provided significant information concerning the major factors that affect cuttings-transport efficiency in horizontal and inclined wellbores. These factors are the annulus flow rate, hole inclination, fluid density and rheology, drillpipe rotation and eccentricity, cuttings size, fluid type, annular clearance, and solids volumetric concentration. Their significance is analyzed below, based on reported experimental and modeling results.

Flow Rate. The velocity in the annulus is one of the major factors affecting hole cleaning ability in horizontal and inclined wellbores, both for cuttings-carrying capacity of the fluid and for bed erosion (Tomren et al. 1986; Sifferman and Becker 1992), and the recommendation is to use the highest flow rates that will not erode the wellbore (Hemphill and Larsen 1993). If a bed is formed, in order to erode it we should resort to either mechanical action, with wiper trips, or hydraulic action, either by increasing the flow rate or by reducing the viscosity in order to achieve turbulent flow (Li and Walker 1999, 2001; Leising and Walton 2002). Modeling and field data show that pump output is the key factor in enhancing hole cleaning potential, and more so for extended-reach wells. If the pump capacity is low, changes in rheology will not affect hole cleaning (Hemphill and Pogue 1999). Computer simulations and modeling of the process, together with comparison with experimental data, produced results

showing that efficient cuttings transport in inclined eccentric annuli is strongly related to computed mean viscous shear stresses averaged over the lower half of the annulus, which of course are related to the flow rate, fluid rheology, and annular hole clearance (Chin 2001).

Hole Inclination. Hole angle has a profound effect on the minimum velocity, defined above (Tomren et al. 1986; Peden et al. 1990; Ford et al. 1990; Sifferman and Becker 1992; Bassal 1995). There appears to exist a critical range of hole inclination angles for which hole cleaning is more difficult compared to other angles, but there is some disagreement among various investigators. Some find that the critical angles were between 35 and 55° from the vertical, because at these angles there is always bed formation and the bed slides downward against the flow (Tomren et al. 1986). Others find them between 40 and 60° (Ford et al. 1990; Peden et al. 1990), while others find that angles between 60 and 90° are the most difficult to clean (Sifferman and Becker 1992; Larsen et al. 1993).

Density. Mud weight has been determined as one of the major factors (Sifferman and Becker 1992) or as the second most significant factor after mud velocity (Hemphill and Larsen 1993) affecting hole cleaning in full-scale inclined wellbores, because of the buoyancy effect, which reduces the cuttings settling velocity. Field data have demonstrated improved efficiencies when weighted sweeps were used instead of high-viscosity sweeps for hole cleaning in deviated wellbores. Minimization of cuttings buildup in the annulus was achieved by allowing regular circulation periods with rotation and with the bit off bottom and utilizing engineered sweeps. Weighted sweeps with weights of 3.0 to 3.5 lbm/gal (360 to 420 kg/m³) above the mud weight, with volumes of approximately 50 bbl (4.5 m³), in 10.625-in. (0.27-m) holes, had a profound effect in improving the cuttings transport efficiency compared with plain drilling fluids or high-viscosity sweeps (Power et al. 2000).

Pipe Rotation. The effect of drillpipe rotation on cuttings transport efficiency has been studied by several investigators, both experimentally and using field data, with mixed results, most of them stating that pipe rotation is very beneficial for cuttings transport. Some investigators believe that pipe rotation has a very small effect when mud flows in turbulent flow, but when flow is laminar the effect of rotation on cuttings transport ability is significant.

Peden et al. (1990) and Ford et al. (1990) report data in which pipe rotation resulted in a smaller minimum velocity when using medium- or high-viscosity liquids, while this was not the case for water, for which no effect of rotation was observed. **Fig. 5.56** shows some of their results depicting the combined effect of pipe rotation and hole inclination. For 120 rev/min (data points with the “D” symbol) and the conditions stated, the minimum velocity is very small with no effect on the minimum velocity of hole inclination between 15 and 90° from the vertical. On the other hand, for the case of no rotation (data points with the “+” symbol) and for the same conditions, the minimum velocity was very large, on the order of 1.1 m/s, with hole inclination influencing the minimum velocity as well. At a pipe rotation of 60 rev/min (data points with the “▲” symbol) the minimum velocity was approximately 2/3 of the minimum velocity at no rotation and eight times more than the minimum velocity at 120 rev/min.

Tomren et al. (1986) found that pipe rotation produced only a slight effect on transport performance in inclined annuli, although they studied only one rotational speed (50 rev/min) and the flow was laminar. Drillpipe rotation was found to be a major factor for the efficiency of cuttings transport by Sifferman and Becker (1992). Laboratory and full-scale tests have shown that critical velocities on the order of 4 to 6 ft/sec (1.22 to 1.83 m/s) are necessary for steady hole cleaning, while field experience shows that for large inclined holes the need is for 2- to 3-ft/sec (0.61- to 0.92-m/s) annular mud velocities (Bassal 1995). In his study, Bassal has shown that the discrepancy between laboratory testing results and field observations was due to the underestimation of the effect of pipe rotary speed, particularly at high rotational speeds.

While drillpipe rotation has a significant effect on hole cleaning during directional drilling, there is a synergistic effect by mud rheology, cuttings size, and mud velocity. For horizontal wells, at low flow rates, the higher the rotational speed, the better the cuttings transport efficiency, while at high flow rates, lower rotational speeds had the most effect (Sanchez et al. 1997).

Field data show that when drilling angle sections, periods of rotation with circulation should be applied so that any cuttings that may have deposited on the hole walls will be agitated into the liquid and therefore enhance cleaning performance (Power et al. 2000). Cuttings erosion in extended-reach wells required extensive circulation at several bottom-up hole volumes, and cuttings removal was greatly improved by rapid string rotation and reciprocation, especially at hole inclinations larger than 70° (Naegel et al. 1998). The authors state that hole cleaning was poor while in sliding mode, thus indicating the positive effect of pipe rotation, and that either low- or high-viscosity pills proved ineffective.

Lockett et al. (1993) studied the importance of rotation effects for efficient hole cleaning using numerical simulation for both vertical and horizontal wellbores through the use of the Taylor number, N_{Ta} . If N_{Ta} is greater than a critical number, which is a function of the Reynolds number, the geometry, and the fluid properties for

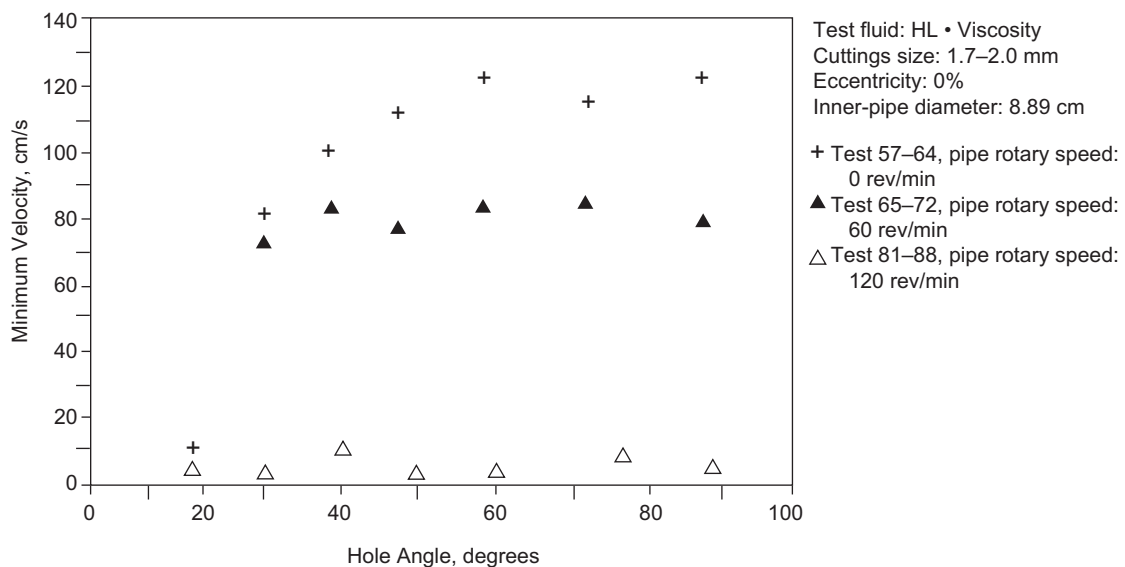


Fig. 5.56—The significant effect of pipe rotation on minimum velocity for laminar flow [from Ford et al. (1990)].

non-Newtonian fluids, the flow becomes unstable and pairs of toroidal counterrotating vortices are formed that aid cuttings lifting much like turbulent eddies do in turbulent flow. Although the presence of Taylor vortices in drilling simulations has not been demonstrated conclusively, the computer simulations of Lockett et al. (1993) indicated that should Taylor vortices be present in a drilling annulus, rock cuttings in the low side of the annulus will experience an oscillatory force due to these vortices with the peak of oscillations sufficient to lift the particles with mass less than a critical value.

Rheology. Rheology appears to affect cuttings transport efficiency, but its significance is controversial. It has been studied extensively, since it is one of the factors that can be both manipulated and monitored during drilling. It is clear that if mud rheological properties are such that the fluid is in turbulent flow in the annulus and the cuttings are in suspension, then the cuttings transport efficiency is at the highest possible levels. In horizontal or near-horizontal wellbores, hole cleaning has been found to be more efficient if a low-viscosity fluid is pumped in turbulent flow rather than a high-viscosity fluid in laminar flow (Okrajni and Azar 1986; Leising and Walton 1998, 2002; Walker and Li 2000).

The problems arise when the cuttings form a bed and the transport efficiency depends then on the cuttings erosion rate, which may be governed by fluid rheology. Contributing to the controversy is the inability of the industry to standardize on the most appropriate rheological model that best describes the drilling fluids used in the field today. While there are still research reports that model the drilling fluids as Bingham plastic or power-law fluids, more and more investigators opt for the use of the more complex but apparently more accurate Herschel-Bulkley fluid model across the shear rate spectrum encountered while flowing up the annulus and particularly in the low-shear-rate zone ($1\text{--}50\text{ s}^{-1}$) where drilled cuttings are usually found to settle (Hemphill et al. 1993; Kenny et al. 1998).

If the annulus is eccentric and the drilling fluid behaves as a yield-pseudoplastic fluid (Bingham plastic or Herschel-Bulkley), then if flow conditions are such that there is plug formation in the low side of the eccentric annulus, trapping of the solids may occur on the low side. Hence, by changing (reducing) the yield point value of the fluid, bed erosion may be enhanced (Martins and Santana 1990).

Some investigators find that for inclined wells, low-viscosity muds clean better than high-viscosity muds (Sanchez et al. 1997), while others find that rheology has a moderate effect on cuttings transport (Sifferman and Becker 1992). If there are constraints on the pump output, hole cleaning can be enhanced through optimization of all rheological parameters of the drilling fluid: K , n , and τ_y (Hemphill and Pogue 1999).

Peden et al. (1990) and Ford et al. (1990) found a mixed effect of rheology on cuttings transport when coupled with the other factors that affect cuttings transport efficiency. For the rolling condition of cuttings (moving-bed pattern) and small annulus clearance, water was the best fluid for hole cleaning, giving smaller minimum velocities, while the high-viscosity fluid was second best and the worst situation was with the low-viscosity fluid. However, for the suspension pattern (heterogeneous flow pattern) and the small annulus clearance, the high-viscosity fluid was the best, followed by water and then by the low-viscosity fluid. Hence, the worst

situation for the small clearance was the low-viscosity fluid with $K = 0.392 \text{ Pa} \cdot \text{s}^n$ and $n \approx 0.65$, with apparent viscosity of $\mu_a \approx 65 \text{ cp}$ at a shear rate of 170 s^{-1} . For the rolling pattern (moving bed) and the large annulus clearance, the high-viscosity fluid was the best, with the low-viscosity fluid and water behaving in a similar manner. However, for the suspension pattern, it appears that fluid rheology does not have any significant effect. These results prompted the authors to observe that turbulence in the annulus has a significant effect on the hole cleaning process, an issue that is dealt with in more detail later on. These findings are illustrated in **Fig. 5.57**.

Hemphill and Larsen (1993) suggest that the Herschel-Bulkley rheological model should be adopted for drilling fluids. For higher angles of inclination it is the power-law flow behavior index n that significantly affects cuttings transport because flow diversion from under the drillpipe is controlled by n . This conclusion is also derived when the drilling fluid is modeled as a power-law fluid by Kenny et al. (1998), with higher values of n promoting more flow under eccentric drillpipes. Experiments have shown that most pronounced vortices and higher velocities close to a stationary wall were obtained with fluids having higher n values (Philip et al. 1998). These observations indicate that it is important to balance the need to minimize the settling velocities of cuttings with more viscous fluids (requiring low n values) and the need to promote fluid velocity close to the walls (requiring higher n values).

The viscoelastic and time-independent yield-pseudoplastic characteristics of biopolymer fluids when examined for hole cleaning efficiency showed that, when in laminar flow, these fluids provided superior cuttings suspension properties and hole cleaning, which were aided by pipe rotation for a horizontal eccentric annulus (Zamora et al. 1993).

The ability of the liquid to erode the cuttings bed once it is formed depends also on the way the cuttings pack and form the bed (Saasen 2002; Kjosnes et al. 2003). If the bed is loose and porous, it is possible to remove single cuttings particles, thus requiring smaller shear stresses and, hence, lower flow rates. If the bed is well consolidated by internal cohesive forces, then it becomes very difficult to erode and to remove single cuttings particles, so larger shear stresses are required. In order to accommodate these findings, the authors propose to minimize gel-strength formation and to keep the low-shear-rate viscosity as low as possible in the drilling fluids so that cuttings bed consolidation is prevented, a suggestion also proposed by Leising and Walton (1998, 2002) for promoting turbulent flow.

Eccentricity. Most of the researchers mention the significant negative impact of eccentricity on hole cleaning ability, but there are not many quantitative studies addressing this parameter. Okrajni and Azar (1986) note that for hole angles between 55 and 90° from vertical, the eccentricity effect is moderate in turbulent flow but significant in laminar flow. For the smaller hole inclination angles, the effect is small for both laminar and turbulent flow. Others found eccentricity to have only a moderate effect on cuttings transport (Sifferman and Becker 1992). Clark and Bickham (1994) found that for small cuttings there was no eccentricity effect, while for larger cuttings the minimum velocity was 30% higher for the eccentric annulus.

Cuttings Size. Drilling action produces a range of cuttings sizes and shapes, which may all coexist at any given time in the annulus, with the majority of cuttings covering a range of US mesh sizes from 4 to 8, which is equivalent

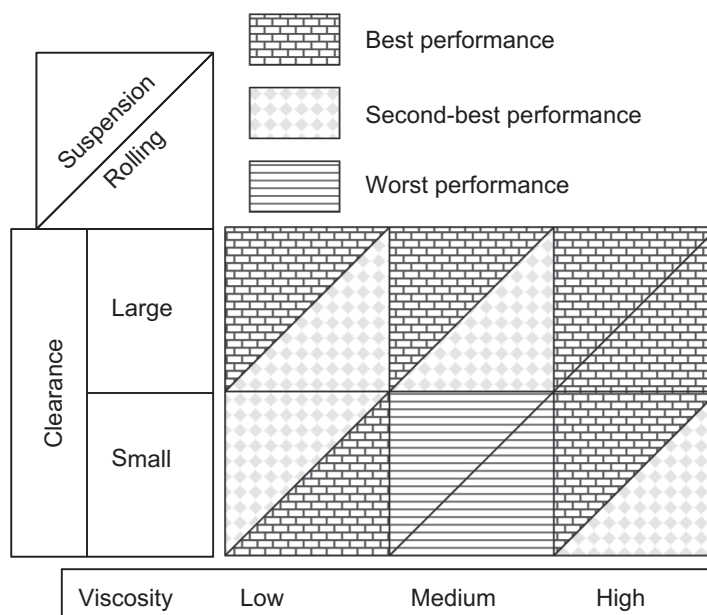


Fig. 5.57—Schematic of experimental findings for the combined effects of annular clearance and viscosity for the suspension and moving bed patterns [composed from data of Peden et al. (1990) and Ford et al. (1990)].

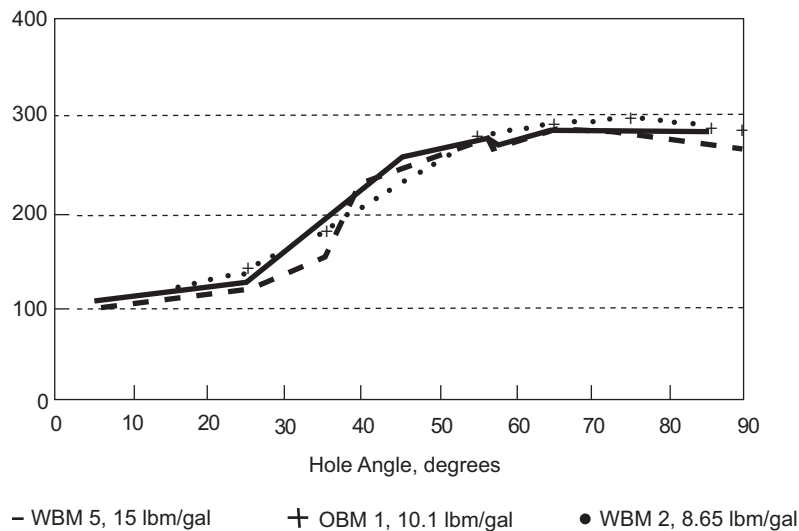


Fig. 5.58—Critical flow rates (velocities) vs. hole angle for two WBMs and one OBM with similar rheological properties [from Hemphill and Larsen (1996)].

to 2.36 to 4.75 mm (Aremu 1998; Cho et al. 2001a). Larger cuttings have been found more difficult to clean with the low-viscosity fluids at all angles of inclination. However, with the high-viscosity fluids, larger cuttings were easier to transport at angles less than 50° (Peden et al. 1990); but Sifferman and Becker (1992) found that cuttings size had only a moderate effect. On the contrary, Sanchez et al. (1997) found that smaller cuttings are more difficult to transport.

If cuttings are in suspension, then smaller cuttings are easier to transport since the larger cuttings tend to settle at higher velocities in the same fluid. Many investigators have reported that once a cuttings bed is formed, smaller cuttings are more difficult to erode than larger cuttings (Pilehvari et al. 1999; Ozbayoglu et al. 2004) because they form beds that are more packed and have smoother surfaces. On the other hand, Martins et al. (1996b) provided experimental results showing the opposite—that larger cuttings are more difficult to erode than smaller cuttings. If the cuttings are small but the drilling fluid contains additives allowing them to bind together, they may form larger clusters that settle more readily, thus reducing hole cleaning efficiency. While this situation may not be observed in laboratory testing because of the small time that cuttings are in contact with the liquid, such occurrences have been reported in the field (Kjosnes et al. 2003). These authors suggest replacing the high-molecular-weight polymers with low-molecular-weight polymers to give lower viscosities and lower gel strengths to induce turbulence.

Solids Volumetric Concentration. Sifferman and Becker (1992) found that solids concentration, which varied from 1 to 4 vol%, had insignificant effect on minimum velocity. Similar results were presented by Larsen et al. (1993), who found a maximum of 25% variation in the minimum velocity (defined above) when they tripled the solids volumetric concentration from 0.65 to nearly 2 vol%. This should be expected because at these low concentrations particle-to-particle interactions are minimal, thus having no effect on hole cleaning. Particle-to-particle interactions appear to be significant for cuttings concentrations larger than approximately 10% by volume.

Mud Type (Water- or Oil-Based). Mud type, water- or oil-based but of the same rheology, normally should have insignificant effect, and such results have been reported by Sifferman and Becker (1992) and Hemphill and Larsen (1993). For similar properties, there were no significant differences in hole cleaning ability of water- and oil-based muds, with a maximum of 10% variation among them, with oil-based muds providing slightly better hole cleaning. Fig. 5.58 shows results of critical flow rate as a function of inclination angle for three fluids having similar API yield point values, similar τ_y values from Herschel-Bulkley modeling, and close values of n , noting, however, that the densities of the three fluids are different. For hole angles greater than 50° from the vertical, the critical flow rates for no cuttings accumulation in the annulus were approximately the same for the two fluid types, and also they remained constant with a very small effect of hole inclination.

Annular Clearance. Investigators examined the effect of annular clearance on hole cleaning ability. Peden et al. (1990) and Ford et al. (1990) studied two annular clearances, 0.95 in. and 1.95 in. They found that it was easier to clean the smaller annular clearance, requiring lower minimum velocity, for both the rolling (moving bed) and suspension patterns. Jalukar et al. (1996) found a linear dependence of critical velocity on annular gap width (hydraulic diameter), as shown in Fig. 5.59.

5.11.6 New Cuttings Transport Models. Larsen et al. (1993) developed a model for highly inclined (50 to 90° angle) wellbores. The model predicts the critical velocity as well as the cuttings-bed thickness when the flow rate is below that of the critical flow. Hemphill and Larsen (1996) showed that oil-based muds with comparable rheological properties performed about the same. Jalukar et al. (1996) modified this model with a scaleup factor to correlate with the data obtained with the 8-in. TUDRP flow loop.

Zamora and Hanson (1991), on the basis of laboratory observations and field experience, compiled 28 rules of thumb to improve high-angle hole cleaning. Luo and Bern (1992) presented charts to determine hole-cleaning requirements in deviated wells. These empirical charts were developed on the basis of the data collected with the BP 8-in. flow loop, and they predicted the critical flow rates required for prevention of cuttings-bed accumulation. The predictions have also been compared with some field data.

Mechanistic Modeling. The existing cuttings-transport correlations and/or models have a few empirical coefficients, determined based on laboratory and/or field data. There is a need for developing comprehensive cuttings transport mechanistic models that can be verified with experimental data. Different levels of the mechanistic approach are possible and can be built on gradually. Ideally, a fluid/solids interaction model, which would be coupled and integrated with a fluid-flow model to simulate the whole cuttings-transport process, is needed. Campos et al. (1995) recently made such an attempt, but much more work is needed to develop a comprehensive solids/liquid flow model.

Ford et al. (1990) published a model for the prediction of minimum transport velocity for two modes: cuttings suspension and cuttings rolling. The predictions were compared with laboratory data.

Gavignet and Sobey (1989) presented a cuttings transport model based on physical phenomena, similar to that published by Wilson (1970), for slurry flow in pipelines that is known as the double-layer model. The model has many interrelated equations and a substantial number of parameters, a few of which are difficult to determine.

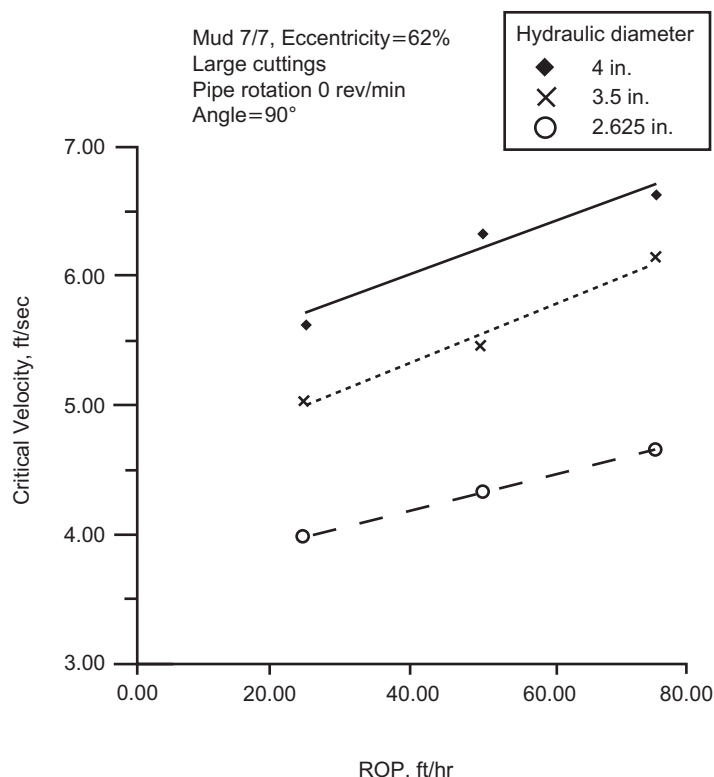


Fig. 5.59—Effect of hydraulic diameter on critical velocity [from Jalukar et al. (1996)]. Courtesy of ASME.

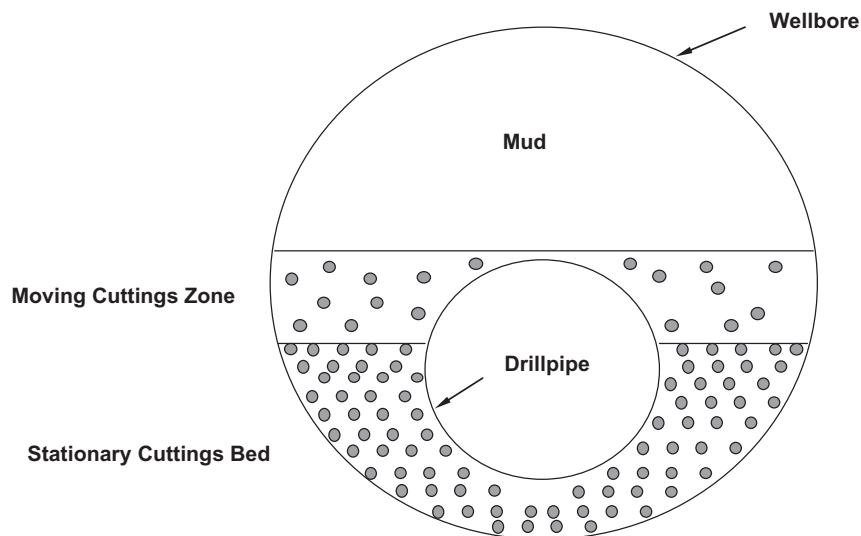


Fig. 5.60—Wellbore cross section with cuttings bed.

Martin et al. (1987) developed a numerical correlation based on the cuttings-transport data that they had collected in the laboratory and in the field.

Clark and Bickham (1994) presented a cuttings-transport model based on fluid mechanics relationships, in which they assumed three cuttings-transport modes: settling, lifting, and rolling—each dominant within a certain range of wellbore angles. Predictions of the model were compared with critical and subcritical flow data they had collected with the TUDRP's 5- and 8-in. flow loops. A prediction of the model was also used to examine several situations in which poor cuttings transport had been responsible for drilling problems.

Campos et al. (1995) developed a mechanistic model for predicting the critical velocity as well as the cuttings-bed height for subcritical flow conditions. Their work was based on earlier work by Oraskar and Whitmore for slurry transport in pipes. The model's predictions are good for thin muds, but the model needs to be further refined to account for thick muds and pipe rotation.

Kenny et al. (1998) defined a lift factor that they used as an indicator of cuttings-transport performance. The lift factor is a combination of the fluid velocity in the lower part of the annulus and the mud-settling velocity determined by Chien's correlation (1971).

Fig. 5.60 illustrates the basic flow configuration for mechanistic cuttings transport modeling. There are three distinct zones in this model: stationary cuttings bed, moving cuttings zone, and "cuttings free" mud-flow zone.

The cuttings-free mud flow creates a shear force at the interface with the moving cuttings bed, which drags the moving cuttings zone along with it. In the moving cuttings zone, gravity forces tend to make the cuttings fall onto the fixed cuttings bed, while aerodynamic and gel forces tend to keep the cuttings suspended. At the interface between the moving cuttings zone and the stationary cuttings bed, fluid friction is trying to strip off cuttings, which are held by gravity and cohesive forces. The balance of these forces determines whether the cuttings bed increases or decreases in depth. The critical flow rate for cuttings transport leaves the cuttings bed unchanged. For effective hole cleaning, the desired flow rate exceeds the critical flow rate.

5.11.7 Field Application. When the results of cuttings transport research and field experience are integrated into a drilling program, hole-cleaning problems are avoided, and excellent drilling performance follows. This has certainly been the case when engineers achieved two new world records in extended-reach drilling.

Guild and Hill (1995) presented another example of integration of hole-cleaning research into field practice. They reported trouble-free drilling in two extended-reach wells after they lost one well because of poor hole cleaning. Their program was designed to maximize the footage drilled between wiper trips and eliminate hole-cleaning back-reaming trips before reaching the casing point. They devised a creative way to avoid significant cuttings accumulation by carefully monitoring the pickup weight, rotating weight, and slackoff weight as drilling continued. They observed that cuttings accumulation in the hole caused the difference between the pickup weight and the slackoff weight to keep increasing, while cleaning the hole decreased the difference. By observing the changes in these parameters and by the use of other readily available information, they were able to closely monitor hole cleaning and control the situation.

Problems

- 5.1 Calculate the hydrostatic pressure at the bottom of the fluid column for each case shown in Fig. 5.4.
Answer: 5,460 psi for Case A.
- 5.2 Calculate the mud density required to fracture a stratum at 5,000 ft if the fracture pressure is 3,800 psig.
Answer: 14.6 lbm/gal.
- 5.3 A mud program is designed for a development well with the following characteristics: target depth 11,700 ft, vertical well, pore pressure at well depth estimated at 6,450 psia; average capacity of the drill pipe and of the annulus is 0.0704 bbl/ft, minimum mud velocity based on prior experience is 110 ft/min. Based on the above determine: (a) the appropriate mud weight, (b) the pressure gradient for the static mud, and (c) the minimum flow rate.
Answer: (a) 11.05 ppg; (b) 0.575 psi/ft; (c) 7.74 bbl/min.
- 5.4 A well is being drilled with a mud weight of 11 ppg at 8,000 ft with previous casing at 2,500 ft. (a) Determine the hydrostatic pressure at 8,000 ft and at 2,500 ft; (b) determine the pressure gradient at 8,000 ft and at 2,500 ft; and (c) if the pore pressure gradient at 8,000 ft is 0.57 psi/ft, do you think you may have a problem while drilling and why?
- 5.5 An ideal gas has an average molecular weight of 20. What is the density of the gas at 2,000 psia and 600 R?
Answer: 0.8 lbm/gal.
- 5.6 The mud density of a well is being increased from 10 to 12 lbm/gal. If the pump is stopped when the interface between the two muds is at a depth of 8,000 ft in the drillstring, what pressure must be held at the surface by the annular blowout preventers to stop the well from flowing? What is the equivalent density in annulus at 4,000 ft after the blowout preventers are closed? *Answer:* 832 psig; 14 lbm/gal.
- 5.7 A well contains methane gas occupying the upper 6,000 ft of annulus. The mean gas temperature is 170°F, and the surface pressure is 4,000 psia. (a) Estimate the pressure exerted against a sand below the bottom of the surface casing at a depth of 5,500 ft. Assume ideal gas behavior. *Answer:* 4,378 psia. (b) Calculate the equivalent density at a depth of 5,500 ft. *Answer:* 15.3 lbm/gal.
- 5.8 A casing string is to be cemented in place at a depth of 10,000 ft. The well contains 10-lbm/gal mud when the casing string is placed on bottom. The cementing operation is designed so that the 10-lbm/gal mud will be displaced from the annulus by 500 ft of 8.5-lbm/gal mud flush, 2,000 ft of 12.7-lbm/gal filler cement, and 1,500 ft of 16.7-lbm/gal high-strength cement. The high-strength cement will be displaced from the casing by 9-lbm/gal brine. Calculate the minimum pump pressure required to completely displace the casing. Assume no shoe joints are used. *Answer:* 1,284 psig.
- 5.9 The penetration rate of the rotary-drilling process can be increased greatly by lowering the hydrostatic pressure exerted against the hole bottom. In areas where formation pressures are controlled easily, the effective hydrostatic pressure sometimes is reduced by injecting gas with the well fluids. Calculate the volume of methane gas per volume of water (scf/gal) that must be injected at 5,000 ft to lower the effective hydrostatic gradient of fresh water to 6.5 lbm/gal. Assume ideal-gas behavior and an average gas temperature of 174°F. Neglect the slip velocity of the gas relative to the water velocity. *Answer:* 0.764 scf/gal.
- 5.10 In order to determine annulus volume prior to cementing, it often is good practice to add CaC_2 in the drillpipe and to detect the produced acetylene (C_2H_2) with the gas chromatograph and the gas trap. A combination of the mud flow rate and of detection time allows for the computation of total volume and, thus, the well diameter. In one such test in a 5,000 ft well (**Fig. 5.61**) drilled with an 8.5-in. bit, we add a $t = 0$, CaC_2 that is detected after 0.9 hr at the surface. Compute the average well diameter and discuss

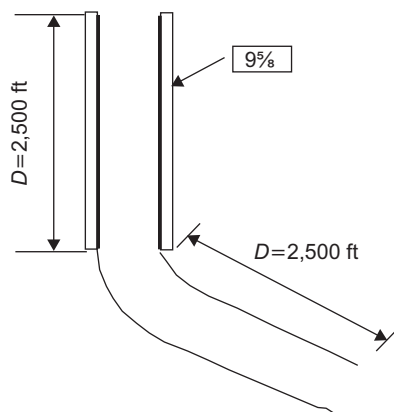


Fig. 5.61—Problem 5.10.

- your findings. How can we use such information? Given data: 9 $\frac{5}{8}$ -in. casing with an ID of 9.063 in., and 5.5-in. drillpipe with a 4.892-in. ID. Mud flow rate = 480 gal/min.
- 5.11 A massive gas sand at 10,000 ft having a porosity of 0.30 and a water saturation of 0.35 is being drilled at a rate of 80 ft/hr using a 9.875-in. bit. The drilling mud has a density of 12 lbm/gal and is being circulated at a rate of 400 gal/min. The annular capacity is 2.8 gal/ft. The mean temperature of the well is 600 R. Ignore the slip velocity of the gas bubbles and rock cuttings. (a) After steady-state conditions are reached, what is the effective bottomhole pressure? Assume that the gas is pure methane and behaves as an ideal gas. *Answer:* 6,205 psia. (b) What is the equivalent mud weight in the annulus? *Answer:* 11.9 lbm/gal. (c) What is the mud density of the mud leaving the annulus at the surface at atmospheric pressure? *Answer:* 5.8 lbm/gal. (d) Make a plot of the density of the drilling fluid in the annulus vs. depth. (e) Can the gas-cut mud at the surface be eliminated completely by increasing the mud density? *Answer:* No.
 - 5.12 A 10-lbm/gal mud is flowing at a steady rate of 160 gal/min down a drillpipe having an ID of 4.33 in. and an OD of 5 in. The diameter of the hole is 10 in. (a) Compute the average flow velocity in the drillpipe. *Answer:* 3.49 ft/sec. (b) Compute the average flow velocity in the annulus opposite the drillpipe. *Answer:* 0.871 ft/sec.
 - 5.13 Determine the pressure at the bottom of the drill collars if the frictional loss in the drillstring is 900 psi, the flow rate is 350 gal/min, the mud density is 10 lbm/gal, and the well depth is 8,000 ft. The ID of the drill collars is 2.75 in. and the pressure developed by the pump is 2,600 psig. *Answer:* 5,860 psig.
 - 5.14 We are drilling an 8.5-in vertical well after installing 9 $\frac{5}{8}$ in. casing at 6,000 ft. We know that the pore pressure, p_f , at 8,000 ft is 6,000 psia. (a) Compute the mud weight for safe drilling at 8,000 ft. (b) If the plastic viscosity is 15 cp and the YP is 10 lbf/100 ft² for this mud weight, compute the bottomhole pressure, p_{bh} , if the minimum mud flow rate is 250 gal/min. (c) Compare p_{bh} with p_f and discuss the implications of the differences observed. Given data: drill pipe OD/ID = 5.5 in./5.0 in., drill collars of 600 ft with OD/ID of 7.5 in./5.5 in.
 - 5.15 A well is being drilled at 10,000 ft. Drilling has stopped and the mud is being circulated for hole cleaning. In a given time, the following parameters have been recorded: $Q = 400$ gal/min, $\rho = 12$ lbm/gal, $\mu_p = 20$ cp, $\tau_y = 10$ lbf/100 ft² and pressure at the drillpipe is 2,980 psig. Drillpipe is 4.5 in. with 4.0 in. ID; the bit is 8.15 in. and has three nozzles— $1\frac{1}{32}$, $1\frac{2}{32}$, and $1\frac{2}{32}$. Prior casing shoe is at 6,000 ft with a casing diameter of 9 $\frac{5}{8}$ in. Determine the average well diameter. Analyze possible factors for being different than expected.
 - 5.16 A 10-lbm/gal mud is being circulated at a rate of 600 gal/min. If the bit contains two $1\frac{5}{32}$ -in. nozzles and one $1\frac{7}{32}$ -in. nozzle and the pump pressure is 3,000 psi, what is the total frictional pressure loss in the well system? *Answer:* 1,969 psig.
 - 5.17 While drilling a well, a drill bit is to be selected together with 3 nozzles. We have available 3 nozzles of $1\frac{4}{32}$ in. and 2 nozzles of $1\frac{3}{32}$ in. It is desirable to have a bit pressure loss between 1,000 and 1,200 psi when mud flows, with a mud weight of 12 lbm/gal and a flow rate of 400 gal/min. State which nozzles you would choose and why.
 - 5.18 Compute the pump pressure required to pump a 9-lbm/gal fluid from sea level to an elevation of 1,000 ft. Assume that inertial and viscous (frictional) pressure changes are negligible. *Answer:* 468 psig.
 - 5.19 A pump is being operated at a rate of 800 gal/min and a pressure of 3,000 psig. The density of the drilling fluid is 15 lbm/gal, and the total nozzle area of the bit is 0.589 in.² (a) Compute the power developed by the pump. *Answer:* 1,400 hp. (b) Compute the power loss to viscous effects. What happens to this energy? *Answer:* 210 hp. The energy is dissipated as heat. (c) Compute the impact force of the jets of fluid against the bottom of the hole. *Answer:* 2,709 lbf.
 - 5.20 Define (a) Newtonian, (b) non-Newtonian, (c) shear stress, (d) shear rate, (e) pseudoplastic, (f) dilatant, (g) thixotropic, and (h) rheopectic.
 - 5.21 A shear stress of 5 dyne/cm² is measured in a fluid for a shear rate of 20 sec⁻¹. Compute the Newtonian or apparent viscosity in cp. *Answer:* 25 cp.
 - 5.22 Fann35 viscometer readings are 20 at 300 rev/min and 40 at 600 rev/min. Would you consider the fluid Newtonian? What is the apparent viscosity at 300 rev/min? What is the apparent viscosity at 600 rev/min? The following shear-stress-rate behavior was observed.

Shear Rate (sec ⁻¹)	Shear Stress (dyne/cm ²)
20	11.0
30	15.2
40	19.1
50	22.9
60	26.5

- (a) Plot shear stress (ordinate) vs. shear rate (abscissa). Make a second plot of shear stress (ordinate) vs. shear rate (abscissa) using log-log scales.
 - (b) Can the fluid behavior be accurately modeled by the Newtonian, Bingham plastic, or power-law model? *Answer:* The fluid appears to be a power-law fluid, but considering possible error in the measurements, a Bingham model is also not unreasonable. The fluid does not appear to be Newtonian.
 - (c) Compute the apparent viscosity for each shear rate. *Answer:* 55 cp at 20 sec⁻¹.
 - (d) Compute the YP and plastic viscosity using data taken at shear rates of 20 and 60 sec⁻¹. *Answer:* $\tau_y = 3.3$ dyne/cm²; $\mu_p = 39$ cp.
 - (e) Compute the consistency index and flow-behavior index using data taken at shear rates of 20 and 60 sec⁻¹. *Answer:* $n = 0.8$; $K = 100$ eq cp.
- 5.23 A fluid is reported as having a plastic viscosity of 40 cp and a YP of 7 lbf/100 ft². Compute a consistency index and flow-behavior index for this fluid. *Answer:* $n = 0.888$; $K = 94$ eq cp.
- 5.24 A 40-cp oil is flowing through 9,000 ft of 3-in. tubing at a rate of 2,500 B/D. Compute the frictional pressure loss in the tubing. Assume that the flow pattern is laminar. *Answer:* 88 psig.
- 5.25A 9.2-lbm/gal Newtonian fluid having a viscosity of 30 cp is being circulated at a rate of 100 gal/min in a vertical well containing a 6-in.-ID casing and a 4.5-in.-OD drillstring. Compute the static and circulating pressure in the annulus of 15,000 ft. Assume that the flow pattern is laminar. *Answer:* 7,176 psig; 7,694 psig.
- 5.26 A Bingham plastic fluid has a plastic viscosity of 50 cp and a YP of 12 lbf/100 ft². Assuming that the flow pattern is laminar, compute the frictional pressure gradient resulting from (a) a flow rate of 50 gal/min through a drillstring having a 3.826-in. ID and (b) a flow rate of 90 gal/min through a 10×7-in. annulus. *Answer:* (a) 0.0171 psi/ft, (b) 0.0240 psi/ft.
- 5.27 Compute the equivalent density below the casing seat at 4,000 ft when a mud having a density of 10 lbm/gal and a gel strength of 70 lbm/100 ft² just begins to flow. The casing has an ID of 7.825 in., and the drillpipe has an OD of 5 in. *Answer:* 11.6 lbm/gal.
- 5.28 A 10-lbm/gal Newtonian fluid having a viscosity of 25 cp is being circulated in a 12,000-ft well containing an 8.30-in.-ID casing and a 5 1/2-in.-OD and 4.67-in.-ID drillstring at a rate of 75 gal/min. Compute the static and circulating bottomhole pressure, give the velocity profile in the annulus, and compute the frictional loss in the drillstring. Assume that a laminar flow pattern exists both in the pipe and in the annulus. Ignore the effects of bit and bit nozzles.
- 5.29 Compute the frictional pressure loss for the annulus discussed in Example 5.28 using a slot flow representation of the annulus. Assume that the flow pattern is laminar.
- 5.30 A cement slurry that has a flow behavior index of 0.35 and a consistency index of 8,000 eq cp is being pumped in a 12.515×5.5-in. annulus at a rate of 300 gal/min. Assuming the flow pattern is laminar, compute the frictional pressure loss per 1,000 ft of annulus. Also estimate the shear rate at the pipe wall.
- 5.31 An 8.5-lbm/gal brine having a viscosity of 3.0 cp is being circulated in a well at a rate of 400 gal/min. Determine whether the fluid in the drillpipe is in laminar or turbulent flow if the ID of the drillpipe is 4.670 in.
- 5.32 Determine the frictional pressure drop in 9,000 ft of 5-in. drillpipe having an ID of 4.408 in. if a 10 cp Newtonian fluid having a density of 9.5 lbm/gal is pumped through the drillpipe at a rate of 300 gal/min.
- 5.33 An 11.5-lbm/gal mud having a plastic viscosity of 55 cp and a YP of 27 lbf/100 ft² is being circulated at a rate of 550 gal/min. Estimate the frictional pressure loss in the annulus opposite 5 in. casing in a 6.5-in. hole, having a length of 1,000 ft. Assume turbulent flow.
- 5.34 A 16-lbm/gal cement slurry having a consistency index of 300 eq cp and a flow-behavior index of 0.75 is being pumped at a rate of 500 gal/min between a 9.5-in.-diameter hole and a 7 3/4-in.-OD casing. Determine the frictional pressure loss per 100 ft of slurry using the power-law fluid model. Use Eq. 5.175a to obtain the equivalent diameter.
- 5.35 A well is being drilled at a depth of 5,000 ft using water with a density of 8.33 lbm/gal and a viscosity of 1 cp as the drilling fluid. The drillpipe has an OD of 4.5 in. and an ID of 3.826 in. The diameter of the hole is 6.5 in. The drilling fluid is being circulated at a rate of 500 gal/min. Assume a relative roughness of zero. (a) Determine the flow pattern in the drillpipe. *Answer:* turbulent. (b) Determine the frictional pressure loss per 1,000 ft of drillpipe. *Answer:* 51.3 psi/1,000 ft. (c) Determine the flow pattern in the annular opposite the drillpipe. *Answer:* turbulent. (d) Determine the frictional pressure loss per 1,000 ft of annulus. *Answer:* 72.9 psi/1,000 ft.
- 5.36 Work Exercise 5.28 for a Bingham plastic fluid having a density of 10 lbm/gal, a plastic viscosity of 25 cp, and a YP of 5 lbf/100 ft². *Answer:* turbulent; 132 psi/1,000 ft; 185 psi/1,000 ft.
- 5.37 Work Exercise 5.28 for a power-law fluid having a density of 12 lbm/gal, a flow-behavior index of 0.75, and a consistency index of 200 eq cp. *Answer:* turbulent; 144 psi/1,000 ft; turbulent; 205 psi/1,000 ft.

- 5.38 A 15-lbm/gal cement slurry has a flow-behavior index of 0.3 and a consistency index of 9,000 eq cp. Compute the flow rate required for turbulent flow in an 8.097×4.5 -in. annulus. Estimate the frictional pressure loss and the shear rate at the wall for this flow rate. Answer: for $N_{Re} = 3,200$, $\bar{v} = 11.5$ ft/sec, and $q = 1,294$ gal/min; 130 psi/1,000 ft; $\dot{\gamma} = 817$.
- 5.39 Mud is circulating in a deviated well, with a centralized $7\frac{5}{8}$ -in. casing string in a $9\frac{1}{2}$ -in. hole. The diameter of the centralizers is $8\frac{1}{8}$ in., and the drilling mud has a flow-behavior index of 0.65 and a consistency index of 155 eq cp. The pressure-loss gradient in a concentric annulus is estimated to be 0.0442 psi/ft. Determine the frictional-pressure-loss gradient for the eccentric annulus.
- 5.40 A $13\frac{3}{8}$ -in. casing is being run into a $17\frac{1}{2}$ -in. gauge vertical wellbore at 5 ft/sec. The wellbore is filled with fresh water of 8.34 lbm/gal, with Newtonian viscosity of 1 cp. The casing has a float, so no fluid flows into the casing. What is the steady-state surge pressure increment at 2,000 ft. caused by frictional pressure drop? Answer: 0.55 psi.

Nomenclature

- a, b = coefficients in gas pressure calculation
- $a(n)$ = Guillot function, dimensionless, Eq. 5.129
- $b(n)$ = Guillot function, dimensionless, Eq. 5.129
- A = area, (L^2), ft^2 , (m^2)
- A_t = total nozzle area, (L^2), $in.^2$, (m^2)
- a = Sisko viscosity, ($m/L \cdot s$), cp, ($Pa \cdot s$)
- A = Robertson-Stiff coefficient, ($m/L \cdot s^{2+B}$), $Pa \cdot s^B$
- b = Sisko parameter, ($m/L \cdot s^{2-c}$), centipoise- sec^{c-1} , ($Pa \cdot s^c$)
- B = Robertson-Stiff coefficient, dimensionless
- c = Sisko parameter, dimensionless
- C = Robertson-Stiff coefficient, ($1/s$), s^{-1}
- C_d = discharge coefficient, dimensionless
- C_e = correction factor for eccentricity, dimensionless
- C_1 = constant of integration, shear stress, Eq. 5.61
- C_s = solids concentration, dimensionless
- d = diameter, (L), in. (m)
- d_n = nozzle diameter, (L), in. (m)
- d_p = inner diameter of annulus, (L), in. (m)
- d_p = particle diameter, (L), in. (cm)
- d_w = outer diameter of annulus, (L), in. (m)
- D_h = hydraulic diameter, (L), in. (m)
- $D(n)$ = Irvine "Blasius" formula, dimensionless, Eq. 5.128
- e = absolute roughness, (L), in. (cm) Eq. 5.125d
- E = internal energy per unit volume, (mL/s^2), Btu/lbm, (J/kg)
- E_k = kinetic energy per unit fluid volume, (mL/s^2), Btu/lbm, (J/kg)
- $E(\lambda)$ = complete elliptic integral of the second kind, Eq. 5.182
- f = Fanning friction factor, dimensionless
- f_s = suspension Fanning friction factor, dimensionless
- f_{sw} = coefficient of friction between cuttings and annulus wall, dimensionless
- f_i = volume fraction of component i , dimensionless
- f_g = volume fraction of gas, dimensionless
- F_1 = downward force on fluid element, (mL/s^2), lbf, (N)
- F_2 = upward force on fluid element, (mL/s^2), lbf, (N)
- F_{ds} = downward sedimentation force, (mL/s^2), lbf, (N)
- F_{fric} = energy loss due to friction per unit mass, (mL/s^2), Btu/lbm, (J/kg)
- F_j = bit hydraulic impact force, (mL/s^2), lbf, (N)
- F_k = force on pipe wall due to fluid motion, (mL/s^2), lbf, (N)
- F_{ue} = upward eddy force, (mL/s^2), lbf, (N)
- g = gravity constant, (L/t^2), lbf/lbm, (m/s^2)
- h = height of slot, (L), ft, (m)
- K = consistency index, ($m/L \cdot s^{2-n}$), lbf- sec^n/ft^2 , $Pa \cdot s^n$
- K = mud-clinging constant, dimensionless
- L = length, (L), ft, (m)

m	=	mass, (m), lbm, (kg)
m_i	=	mass of component i , (m), lbm, (kg)
\dot{m}	=	mass flow rate, (m/s), lbm/sec, (kg/sec)
m	=	Gucuyener, Shulman, or Maglione exponent, dimensionless, Eq. 5.56
m	=	$1/n$, n = flow behavior index, dimensionless
m	=	Zhu parameter, (s), sec, (sec)
M	=	gas molecular weight, lbm/lbm-mol, kg/kg-mole
n	=	number of sections
n	=	flow behavior index, dimensionless
N_e	=	eccentricity, dimensionless
N_{Ga}	=	Galileo number, dimensionless
N_{He}	=	Hedstrom number, dimensionless
N_{Peo}	=	Peclet number based on the outer-pipe diameter, dimensionless
N_{Re}	=	Reynolds number, dimensionless
N_{ReMR}	=	Metzner-Reed Reynolds number, dimensionless
N_{Ta}	=	Taylor number, dimensionless
N_v	=	moles of gas per volume, (m-mol/L ³), lbm-mole/gal, (kg-mole/m ³)
p	=	pressure, (m/L-s ²), psi, (Pa)
p_0	=	pressure at Z_0 , surface pressure, (m/L-s ²), psi, (Pa)
p_a	=	pressure in the annulus, (m/L-s ²), psi, (Pa)
p_{col}	=	collapse pressure, (m/L-s ²), psi, (Pa)
p_t	=	pressure in the tubing, (m/L-s ²), psi, (Pa)
P_H	=	hydraulic power, (mL ² /s ³), hp, (W)
q	=	volume flow rate, (m ³ /s), gal/min, (m ³ /s)
q_c	=	volume flow rate in a concentric annulus, (m ³ /s), gal/min, (m ³ /s)
q_e	=	volume flow rate in a eccentric annulus, (m ³ /s), gal/min, (m ³ /s)
Q	=	heat per unit mass added, (mL/s ²), Btu/lbm, (J/kg)
r	=	radius, (L), in. (m)
r_p	=	inside radius of annulus, (L), in. (cm)
r_w	=	outside radius of annulus, (L), in. (cm)
R	=	universal gas constant, psi-gal/lbm-mole/R, Pa-m ³ /kg-mole/K
R	=	pipe inside radius, (L), ft (m)
R_r	=	r_p/r_w , dimensionless
s	=	measured depth, (L), ft (m)
t_s	=	settlement time for cuttings, (s), second, (sec) Eq. 5.229
t_l	=	Zhu parameter, (s), second, (sec), Eq. 5.57
T	=	absolute temperature, (T), R, (K)
u^*	=	turbulent flow velocity, (L/s), ft/sec, (m/s)
u_c^*	=	turbulent flow velocity for concentric annulus, (L/s), ft/sec, (m/s)
u_e^*	=	turbulent flow velocity for eccentric annulus, (L/s), ft/sec, (m/s)
v	=	velocity, (L/s), ft/sec, (m/s)
\bar{v}	=	average velocity, (L/s), ft/sec, (m/s)
\bar{v}_M	=	mean velocity of fluid-solid mixture, (L/s), ft/sec, (m/s)
v_{MTV}	=	minimum transport velocity, (L/s), ft/sec, (m/s) Eq. 5.225–5.227
v_n	=	nozzle velocity, (L/s), ft/sec, (m/s)
\bar{v}_n	=	average nozzle velocity, (L/s), ft/sec, (m/s)
v_p	=	plug velocity, (L/s), ft/sec, (m/s)
v'_p	=	liquid fluctuating velocity, (L/s), ft/sec, (m/s)
v'_p	=	damped liquid fluctuating velocity, (L/s), ft/sec, (m/s) Eq. 5.221
V	=	total volume, (L ³), gal (m ³)
V_i	=	volume of component i , (L ³), gal (m ³)
V_m	=	volume of mud, (L ³), gallon, (m ³)
V_g	=	volume of gas, (L ³), gal (m ³)
\bar{W}	=	work done per unit mass, (mL/s ²), Btu/lbm, (J/kg)
w	=	width of slot, (L), ft (m)
y	=	coordinate direction along width of slot, (L), ft (m)
y_a	=	thickness of sheared layer in slot, (L), ft (m)

Z	=	TVD, (L), ft (m)
Z_i	=	TVD of section i , (L), ft (m)
Z	=	gas compressibility factor, dimensionless
α	=	damping coefficient, dimensionless, Eq. 5.221
β	=	Graves-Collins parameter, (s), second, (sec)
$\dot{\gamma}$	=	shear rate, (s^{-1}), s^{-1} , (s^{-1})
$\dot{\gamma}_{Nw}$	=	Newtonian wall shear rate, (s^{-1}), s^{-1} , (s^{-1}) Eq. 5.223
Δp	=	pressure increment, (m/L- s^2), psi, (Pa)
Δp_b	=	pressure drop through bit, (m/L- s^2), psi, (Pa)
Δp_f	=	total frictional pressure drop, (m/L- s^2), psi, (Pa)
δr_e	=	degree of eccentricity, (L), ft (cm)
δr_m	=	lowest distance between the inner and outer wall of an inclined annulus
Δs	=	measured depth increment, (L), ft (m)
\bar{v}_{ae}	=	effective mean annular velocity, (L/s), ft/sec, (m/s)
Δv	=	velocity increment, (L/s), ft/sec, (m/s)
ΔZ	=	TVD increment, (L), ft (m)
λ	=	parameter in eccentric annulus calculations, dimensionless
λ_j	=	parameters in eccentric annulus calculations, $j = 1 \dots 3$, dimensionless, Eq. 5.185
$\hat{\lambda}$	=	scaling parameter, dimensionless, Eq. 5.230
η	=	Gucuyener or Shulman viscosity, (m/L-s), cp, (Pa·s)
η_1	=	Zhu viscosity, (m/L-s), cp, (Pa·s), Eq. 5.57
μ	=	viscosity, (m/L-s), cp, (Pa·s)
μ_p	=	plastic viscosity, (m/L-s), cp, (Pa·s)
ρ	=	density, (m/L ³), lbm/gal, (kg/m ³)
ρ_e	=	equivalent mud density, (m/L ³), lbm/gal, (kg/m ³)
ρ_i	=	density of component i , (m/L ³), lbm/gal, (kg/m ³)
ρ_f	=	fluid density, (m/L ³), lbm/gal, (kg/m ³)
τ	=	shear stress, (m/L- s^2), psi, (Pa)
τ_y	=	yield stress, (m/L- s^2), lbf/100 ft ² , (Pa)
τ_{xy}	=	shear stress, xy component, (m/L- s^2), lbf/100 ft ² , (Pa)
τ_w	=	shear stress at wall of slot, (m/L- s^2), lbf/100 ft ² , (Pa)
τ_{wi}	=	shear stress at inner wall of slot, (m/L- s^2), lbf/100 ft ² , (Pa)
τ_{wo}	=	shear stress at outer wall of slot, (m/L- s^2), lbf/100 ft ² , (Pa)
τ_0	=	Graves-Collins yield stress, (m/L- s^2), lbf/100 ft ² , (Pa)
ϕ	=	τ_y / τ_w , dimensionless
φ	=	wellbore inclination, (radians)
Ω	=	pipe rotation rate, (s^{-1}), rev/min, (radians/sec)

Subscripts

b	=	brine, bit
dc	=	drill collars
f	=	friction
fc	=	filler cement
fl	=	flush
hc	=	high-strength cement
m	=	mud
p	=	pump
s	=	solids
w	=	formation water
1,2	=	1 = initial, 2 = final

References

- Annis, M.R. 1967. High-Temperature Flow Properties of Water-Base Drilling Fluids. *JPT* **19** (8): 1074–1080; *Trans.*, AIME, **240**. DOI: [10.2118/1698-PA](https://doi.org/10.2118/1698-PA).
- Aremu, K.J. 1998. Evaluation of Shale Drilling Fluid Interaction Using Specific Surface Area Approach. MS thesis, University of Oklahoma, Norman, Oklahoma.

- Azar, J.J. and Sanchez, R.A. 1997. Important Issues in Cuttings Transport for Drilling Directional Wells. Paper SPE 39020 presented at the Latin American and Caribbean Petroleum Engineering Conference and Exhibition, Rio de Janeiro, 30 August–3 September. DOI: [10.2118/39020-MS](https://doi.org/10.2118/39020-MS).
- Bach, G.F., Bjorkevoll, K., Rommetveit, R., Steine, O.G., and Maglione, R. 1997. Surge and Swab in a Slim Hole Configuration: Full Scale Experiments, Simple Models, and a Computer Verification. E&P Forum, Offshore Mediterranean Conference, Ravenna, Italy, 19–21 March; OMC 97 2: 899–908.
- Bailey, W.J. and Peden, J.M. 2000. A Generalized and Consistent Pressure Drop and Flow Regime Transition Model for Drilling Hydraulics. *SPEDC* 15 (1): 44–56. SPE-62167-PA. DOI: [10.2118/62167-PA](https://doi.org/10.2118/62167-PA).
- Bassal, A.A. 1995. A Study of the Effect of Drillpipe Rotation on Cuttings Transport in Inclined Wellbores. MS thesis, University of Tulsa, Tulsa, Oklahoma.
- Becker, T.E., Azar, J.J., and Okrajni, S.S. 1991. Correlations of Mud Rheological Properties With Cuttings-Transport Performance in Directional Drilling. *SPE Drill Eng* 6 (1): 16–24.
- Bingham, E.C. 1922. *Fluidity and Plasticity*, New York City: McGraw-Hill.
- Bizanti, M.S., Mitchell, R.F., and Letruno, R.E. 1991. Are Improved Surge Models Needed? Paper SPE 22057 available from SPE, Richardson, Texas.
- Blasius, H. 1913. Das Aehnlichkeitsgesetz bei Reibungsvorgängen in Flüssigkeiten. *VDI Mitteilungen Forschungsarbeit Gebiete Ingenieurs*, No. 131: pp. 1–34.
- Brand, F., Peixinho, J., and Nouar, C. 2001. A Quantitative Investigation of the Laminar-to-Turbulent Transition: Application to Efficient Mud Cleaning. Paper SPE 71375 presented at the SPE Annual Technical Conference and Exhibition, New Orleans, 30 September–3 October. DOI: [10.2118/71375-MS](https://doi.org/10.2118/71375-MS).
- Brooks, A.G. 1982. Swab and Surge Pressures in Non-Newtonian Fluids. Paper SPE 10863 available from SPE, Richardson, Texas.
- Butts, H.B. 1972. The Effect of Temperature on Pressure Losses During Drilling. MS thesis, Louisiana State University, Baton Rouge, Louisiana.
- Burcik, E.J. 1957. *Principles of Petroleum Reservoir Fluids*. London: John Wiley and Sons.
- Burkhardt, J.A., 1961. Wellbore Pressure Surges Produced by Pipe Movement. *JPT* 13 (6): 595–605, *Trans.*, AIME, 222. SPE-1546-G. DOI: [10.2118/1546-G](https://doi.org/10.2118/1546-G).
- Carr, N.L., Kobayashi, R., and Burrows, D. 1954. Viscosity of Hydrocarbon Gases Under Pressure. *JPT* 6 (10): 47–55; *Trans.*, AIME 201: 264–272. SPE-297-G. DOI: [10.2118/297-G](https://doi.org/10.2118/297-G).
- Casson, N. 1959. A Flow Equation for Pigment-Oil Suspensions of the Printing Ink Type. *Rheology of Disperse Systems*, 59. London: Pergamon Press.
- Charlez, P.A., Easton, M., and Morrice, G. 1998. Validation of Advanced Hydraulic Modeling Using PWD Data. Paper 8804 presented at the Offshore Technology Conference, Houston, 4–7 May. DOI: [10.4043/8804-MS](https://doi.org/10.4043/8804-MS).
- Chabra, R.P. and Richardson, J.F. 1999. *Non-Newtonian Flow in Process Industries*. Oxford: Butterworth-Heinemann.
- Chien, S.F. 1994. Settling Velocity of Irregularly Shaped Particles. *SPEDC* 9 (4): 281–289. SPE-26121-PA. DOI: [10.2118/26121-PA](https://doi.org/10.2118/26121-PA).
- Chin, W.C. 2001. *Computational Rheology for Pipeline and Annular Flow*. Boston: Gulf Publishing Company.
- Cho, H., Shah, S.N., and Osisanya, S.O. 2000a. A Three-Layer Modeling for Cuttings Transport With Coiled Tubing Horizontal Drilling. Paper SPE 63269 presented at the SPE Annual Technical Conference and Exhibition, Dallas, 1–4 October. DOI: [10.2118/63269-MS](https://doi.org/10.2118/63269-MS).
- Cho, H., Shah, S.N., and Osisanya, S.O. 2001a. Effects of Fluid Flow in a Porous Cuttings-Bed on Cuttings Transport Efficiency and Hydraulics. Paper SPE 71374 presented at the SPE Annual Technical Conference and Exhibition, New Orleans, 30 September–3 October. DOI: [10.2118/71374-MS](https://doi.org/10.2118/71374-MS).
- Churchill, S.W. 1977. Friction Factor Equation Spans All Fluid Flow Regimes. *Chemical Engineering* 84 (24): 91–92.
- Clark, R.K. and Bickham, K.L. 1994. A Mechanistic Model for Cuttings Transport. Paper SPE 28306 presented at the SPE Annual Technical Conference and Exhibition, New Orleans, 25–28 September. DOI: [10.2118/28306-MS](https://doi.org/10.2118/28306-MS).
- Colebrook, C.F. 1939. Turbulent Flow in Pipes, With Particular Reference to the Transition Region Between the Smooth and Rough Pipe Laws. *Journal of the Institute of Civil Engineering* 11: 133–156.
- Courant, Richard and Hilbert, David 1953. *Methods of Mathematical Physics, Volumes 1 and 2, 2nd Revision*, Wiley-Interscience, New York.
- Cullender, M.H. and Smith, R.V. 1956. Practical Solution of Gas Flow Equations for Wells and Pipelines With Large Temperature Gradients. *Trans.*, AIME, 207: 281–287.
- Davies, J.T. 1987. Calculation of Critical Velocities To Maintain Solids in Suspension in Horizontal Pipes. *Chemical Engineering Science* 42 (7): 1667–1670.
- Doan, Q.T., Oguztoreli, M., Masuda, Y., et al. 2000. Modeling of Transient Cuttings Transport in Underbalanced Drilling. Paper IADC/SPE 62742 presented at the IADC/SPE Asia Pacific Drilling Technology, Kuala Lumpur, 11–13 September. DOI: [10.2118/62742-MS](https://doi.org/10.2118/62742-MS).

- Doan, Q.T., Oguztoreli, M., Masuda, Y., et al. 2003. Modeling of Transient Cuttings Transport in Underbalanced Drilling. *SPEJ* **8** (2): 160–170. SPE-85061-PA. DOI: [10.2118/85061-PA](https://doi.org/10.2118/85061-PA).
- Dodge, D.W. and Metzner, A.B. 1959. Turbulent Flow of Non-Newtonian Systems. *AIChE J.* **5** (2): 189–204.
- Doron, P., Garnica, D., and Barnea, D. 1987. Slurry Flow in Horizontal Pipes: Experimental and Modeling. *International J. of Multiphase Flow* **13** (4): 535–547.
- Eckel, J.R. and Bielstein, W.J. 1951. Nozzle Design and Its Effect on Drilling Rate and Pump Operations. *API Drilling and Production Practices*, 28–46 (API Paper 51-028).
- Escudier, M.P., Gouldson, I.W., Oliveira, P.J., and Pinho, F.T. 2000. Effects of Inner Cylinder Rotation on Laminar Flow of a Newtonian Fluid Through an Eccentric Annulus. *International J. of Heat and Fluid Flow* **21** (1): 92–103.
- Escudier, M.P., Oliveira, P.J., and Pinho, F.T. 2002. Fully Developed Laminar Flow of Purely Viscous Non-Newtonian Liquids Through Annuli, Including Effects of Eccentricity and Inner Cylinder Rotation. *International J. of Heat and Fluid Flow* **23** (1): 52–73.
- Fontenot, J.E. and Clark, R.E. 1974. An Improved Method for Calculating Swab and Surge Pressures and Circulating Pressures in a Drilling Well. *SPEJ* **14** (5): 451–462. SPE-4521-PA. DOI: [10.2118/4521-PA](https://doi.org/10.2118/4521-PA).
- Ford, J.T., Peden, J.M., Oyeneyin, M.B., Gao, E., and Zarrouh, R. 1990. Experimental Investigation of Drilled Cuttings Transport in Inclined Boreholes. Paper SPE 20421 presented at the SPE Annual Technical Conference and Exhibition, New Orleans, 23–26 September. DOI: [10.2118/20421-MS](https://doi.org/10.2118/20421-MS).
- Fordham, E.J., Bittleston, S.H., and Tehrani, M.A. 1991. Viscoplastic Flow in Centered Annuli, Pipes, and Slots. *Industrial and Engineering Chemistry Research* **30** (3): 517–524.
- Fredrickson, A.G. and Bird, R.B. 1958. Non-Newtonian Flow in Annuli. *Industrial and Engineering Chemistry Research* **50** (3): 347–352.
- Gavignet, A.A. and Sobey, I.J. 1989. Model Aids Cuttings Transport Prediction. *JPT* **41** (9): 916–921. SPE-15417-PA. DOI: [10.2118/15417-PA](https://doi.org/10.2118/15417-PA).
- Govier, G.W. and Aziz, K. 1972. *The Flow of Complex Mixtures in Pipes*, 456–461. Van Nostrand Reinhold, New York.
- Graves, W.G. and Collins, R.E. 1978. A New Rheological Model for Non-Newtonian Fluids. Paper SPE 7654 available from SPE, Richardson, Texas.
- Green, M.D., Thomesen, C.R., Wolfson, L., and Bern, P.A. 1999. An Integrated Solution of Extended-Reach Drilling Problems in the Niakuk Field, Alaska: Part II—Hydraulics, Cuttings Transport, and PWD. Paper SPE 56564 presented at the SPE Annual Technical Conference and Exhibition, Houston, 3–6 October. DOI: [10.2118/56564-MS](https://doi.org/10.2118/56564-MS).
- Gucuyener, I.H. 1983. A Rheological Model for Drilling Fluids and Cement Slurries. Paper SPE 11487 presented at the Middle East Oil Technology Conference and Exhibition, Bahrain, 14–17 March. DOI: [10.2118/11487-MS](https://doi.org/10.2118/11487-MS).
- Guillot, D. 1990. The Rheology of Well Cement Slurries. In *Well Cementing*, ed. E.B. Nelson, 93–142. Houston: Schlumberger Educational Services.
- Guillot, D. and Dennis, J.D. 1988. Prediction of Laminar and Turbulent Friction Pressures of Cement Slurries in Pipes and Centered Annuli. Paper SPE 18377 presented at the European Petroleum Conference, London, 18–19 October. DOI: [10.2118/18377-MS](https://doi.org/10.2118/18377-MS).
- Haciislamoglu, M. and Langlinais, J. 1990. Non-Newtonian Flow in Eccentric Annuli. *J. of Energy Resources Technology* **112** (3): 163–169. DOI: [10.1115/1.2905753](https://doi.org/10.1115/1.2905753).
- Hanks, R.W. 1979. The Axial Flow of Yield-Pseudoplastic Fluids in a Concentric Annulus. *Industrial Engineering Chemistry Process Design and Development* **18** (3): 488–493. DOI: [10.1021/i260071a024](https://doi.org/10.1021/i260071a024).
- Harnett, J.P. and Kostic, M. 1990. Turbulent Friction Factor Correlations for Power Law Fluids in Circular and Non-Circular Channel. *International Communications in Heat & Mass Transfer* **17** (1): 59–65.
- Hemphill, A.T. and Pogue, T. 1999. Field Applications of ERD Hole Cleaning Modeling. *SPEDC* **14** (4): 247–253. SPE-59731-PA. DOI: [10.2118/59731-PA](https://doi.org/10.2118/59731-PA).
- Hemphill, T. and Larsen, T.I. 1996. Hole-Cleaning Capabilities of Water- and Oil-Based Drilling Fluids: A Comparative Experimental Study. *SPEDC* **11** (4): 201–207. SPE-26328-PA. DOI: [10.2118/26328-PA](https://doi.org/10.2118/26328-PA).
- Hemphill, T., Pilehvari, A., and Campos, W. 1993. Yield Power Law Model More Accurately Predicts Mud Rheology. *Oil & Gas J.* **91** (34): 45–50.
- Herschel, W.H. and Bulkley, R. 1926. Measurement of Consistency as Applied to Rubber-Benzene Solutions. *Proc., American Society of Testing Materials* **26** (II): 621–633.
- Heywood, N.I. and Cheng, D.C-H. 1984. Comparison of Methods for Predicting Head Loss in Turbulent Pipe Flow of Non-Newtonian Fluids. *Transactions of the Institute of Measurement and Control* **6** (1): 33–45.
- Irvine, T.F. 1988. A Generalized Blasius Equation for Power Law Fluids. *Chemical Engineering Communications* **65** (1): 39–47.
- Iyoho, A.W. 1980. Drilled-Cuttings Transport by Non-Newtonian Drilling Fluids Through Inclined Eccentric Annuli. PhD dissertation, University of Tulsa, Tulsa, Oklahoma.

- Jalukar, L.S., Azar, J.J., Pihlevari, A.A., and Shirazi, S.A. 1996. Extensive Experimental Investigation of the Hole Size Effect on Cuttings Transport in Directional Well Drilling. Paper FED-Vol. 239, ASME Fluids Engineering Division Conference, Vol. 4, San Diego, California, 7–12 July: 573–581.
- Kamp, A.M. and Rivero, S. 1999. Layer Modeling for Cuttings Transport in Highly Inclined Wellbores. Paper SPE 53942 presented at the Latin American and Caribbean Petroleum Engineering Conference, Caracas, 21–23 April. DOI: [10.2118/53942-MS](https://doi.org/10.2118/53942-MS).
- Kelessidis, V.C. and Mpandelis, G. 2003. Flow Patterns and Minimum Suspension Velocity for Efficient Cuttings Transport in Horizontal and Deviated Wells in Coiled-Tubing Drilling. Paper SPE 81746 presented at the SPE/ICoTA Coiled Tubing Conference and Exhibition, Houston, 8–9 April. DOI: [10.2118/81746-MS](https://doi.org/10.2118/81746-MS).
- Kelessidis, V.C. and Mpandelis, G.E. 2004a. Hydraulic Parameters Affecting Cuttings Transport for Horizontal Coiled-Tubing Drilling. Paper presented at the 7th National Congress on Mechanics, Chania, Greece, 24–26 June.
- Kenny, P., Sunde, E., and Hemphill, T. 1998. Hole Cleaning Modeling: What's 'n' Got To Do With It? Paper SPE 35099 presented at the IADC/SPE Drilling Conference, New Orleans, 12–15 March. DOI: [10.2118/35099-MS](https://doi.org/10.2118/35099-MS).
- Kjosnes, I., Loklingholm, G., Saasen, A., Syrstand, S.O., Agle, A., and Solvang, K.-A. 2003. Successful Water Based Drilling Fluid Design for Optimizing Hole Cleaning and Hole Stability. Paper SPE/IADC 85330 presented at the SPE/IADC Middle East Drilling Technology Conference and Exhibition, Abu Dhabi, UAE, 20–22 October. DOI: [10.2118/85330-MS](https://doi.org/10.2118/85330-MS).
- Knudsen, J.G. and Katz, D.L. 1958. *Fluid Dynamics and Heat Transfer*, New York City: McGraw-Hill Book Company.
- Laird, W.M. 1957. Slurry and Suspension Transport. *Industrial and Engineering Chemistry* **49** (1): 138–141.
- Lake, L.W. 2006. *Petroleum Engineering Handbook, Volume II Drilling Engineering*. SPE, Richardson, Texas: 141–148.
- Lal, M. 1983. Surge and Swab Modelling for Dynamic Pressures and Safe Trip Velocities. Paper IADC/SPE 11412 presented at the IADC/SPE Drilling Conference, New Orleans, 20–23 February. DOI: [10.2118/11412-MS](https://doi.org/10.2118/11412-MS).
- Larsen, T.I., Pilehvari, A.A., and Azar, J.J. 1993. Development of a New Cuttings Transport Model for High-Angle Wellbores Including Horizontal Wells. *SPEDC* **12** (2): 129–136. SPE-25872-PA. DOI: [10.2118/25872-PA](https://doi.org/10.2118/25872-PA).
- Leising, L.J. and Walton, I.C. 1998. Cuttings Transport Problems and Solutions in Coiled Tubing Drilling. Paper IADC/SPE 39300 presented at the IADC/SPE Drilling Conference, Dallas, 3–6 March. DOI: [10.2118/39300-MS](https://doi.org/10.2118/39300-MS).
- Leising, L.J. and Walton, I.C. 2002. Cuttings Transport Problems and Solutions in Coiled Tubing Drilling. *SPEDC* **17** (1): 54–66. SPE-77261-PA. DOI: [10.2118/77261-PA](https://doi.org/10.2118/77261-PA).
- Li, J. and Walker, S. 1999. Sensitivity Analysis of Hole Cleaning Parameters in Directional Wells. Paper SPE 54498 presented at the 1999 SPE/ICoTA Coiled Tubing Roundtable, Houston, 25–26 May. DOI: [10.2118/54498-MS](https://doi.org/10.2118/54498-MS).
- Li, J. and Walker, S. 2001. Sensitivity Analysis of Hole Cleaning Parameters in Directional Wells. *SPEJ* **6** (4): 356–363. SPE-74710-PA. DOI: [10.2118/74710-PA](https://doi.org/10.2118/74710-PA).
- Lockett, T.J., Richardson, S.M., and Worraker, W.J. 1993. The Importance of Rotation Effects for Efficient Cuttings Removal During Drilling. Paper SPE/IADC 25768 presented at the SPE/IADC Drilling Conference, Amsterdam, 23–25 February. DOI: [10.2118/25768-MS](https://doi.org/10.2118/25768-MS).
- Lubinski, A., Hsu, F.H., and Nolte, K.G. 1977. Transient Pressure Surges Due to Pipe Movement in an Oil Well. *Oil & Gas Science and Technology - Rev. IFP* **32** (3): 307–348.
- Luo, Y. and Peden, J.M. 1990. Flow of Non-Newtonian Fluids Through Eccentric Annuli, *SPE Prod Eng* **5** (2): 91–96.
- Martins, A.L. and Santana, C.C. 1990. Modeling and Simulation of Annular Axial Flow of Solids and Non-Newtonian Mixtures. Presented at the III Encontro Nacional de Ciencias Termicas (ENCIT), Itapema, SC, Brazil, 10–12 December: 709–714.
- Martins, A.L. and Santana, C.C. 1992. Evaluation of Cuttings Transport in Horizontal and Near Horizontal Wells—A Dimensionless Approach. Paper SPE 23643 presented at the SPE Latin American Petroleum Engineering Conference, Caracas, 8–11 March. DOI: [10.2118/23643-MS](https://doi.org/10.2118/23643-MS).
- Masuda, Y., Doan, Q., Oguztoreli, M., et al. 2000. Critical Cuttings Transport Velocity in Inclined Annulus: Experimental Studies and Numerical Simulation. Paper SPE 65502 presented at the SPE/CIM International Conference on Horizontal Well Technology, Calgary, 6–8 November. DOI: [10.2118/65502-MS](https://doi.org/10.2118/65502-MS).
- Merlo, A., Maglione, R., and Piatti, C. 1995. An Innovative Model for Drilling Fluid Hydraulics. Paper SPE 29259 presented at the SPE Asia Pacific Oil and Gas Conference, Kuala Lumpur, 20–22 March. DOI: [10.2118/29259-MS](https://doi.org/10.2118/29259-MS).
- Metzner, A.B. and Reed, J.C. 1955. Flow of Non-Newtonian Fluids—Correlations of the Laminar, Transition and Turbulent-Flow Regions. *AIChE J.* **1** (4): 434–440.
- Mitchell, R.F. 1988. Dynamic Surge/Swab Pressure Predictions. *SPEDE* **3** (3): 325–333. SPE-16156-PA. DOI: [10.2118/16156-PA](https://doi.org/10.2118/16156-PA).
- Mitchell, R.F. 2004. Surge Pressures in Low-Clearance Liners. Paper SPE 87181 presented at the IADC/SPE Drilling Conference, Dallas, 2–4 March. DOI: [10.2118/87181-MS](https://doi.org/10.2118/87181-MS).

- Moody, L.F., 1944. Friction Factors for Pipe Flow. *Transactions of the ASME* **66**: 671. The American Society of Mechanical Engineers.
- Nguyen, D. and Rathman, S.S. 1996. A Three-Layer Hydraulic Program for Effective Cuttings Transport and Hole Cleaning in Highly Deviated and Horizontal Wells. Paper SPE 36383 presented at the IADC/SPE Asia Pacific Drilling Technology, Kuala Lumpur, 9–11 September. DOI: [10.2118/36383-MS](https://doi.org/10.2118/36383-MS).
- Nouri, J.M. and Whitelaw, J.H. 1997. Flow of Newtonian and Non-Newtonian Fluids in an Eccentric Annulus With Rotation of the Inner Cylinder. *International J. of Heat and Fluid Flow* **18** (2): 236–246.
- Okafor, M.N. and Evers, J.F. 1992. Experimental Comparison of Rheology Models for Drilling Fluids. Paper SPE 24086 presented at the Western Regional Meeting, Bakersfield, California, 30 March–1 April. DOI: [10.2118/24086-MS](https://doi.org/10.2118/24086-MS).
- Okrajni, S.S. and Azar, J.J. 1986. The Effects of Mud Rheology on Annular Hole Cleaning in Directional Wells. *SPEDE* **1** (4): 297–308.
- Oraskar, A.D. and Whitmore, R.L. 1980. The Critical Velocity in Pipeline Flow of Slurries, *AIChE. J.* **26** (4): 550–558.
- Ostwald, W. 1925. Ueber die Geschwindigkeitsfunktion der Viskosität disperser Systeme. *Kolloid-Zeitschrift* **36** (4): 99–117.
- Ozbayoglu, E.M., Miska, S.Z., Reed, T., and Takach, N. 2004. Analysis of the Effects of Major Drilling Parameters on Cuttings Transport Efficiency for High-Angle Wells in Coiled Tubing Drilling Operations. Paper SPE 89334 presented at the SPE/ICoTA Coiled Tubing Conference and Exhibition, Houston, 23–24 March. DOI: [10.2118/89334-MS](https://doi.org/10.2118/89334-MS).
- Peden, J.M., Ford, J.T., and Oyeneyin, M.B. 1990. Comprehensive Experimental Investigation of Drilled Cuttings Transport in Inclined Wells Including the Effects of Rotation and Eccentricity. Paper SPE 20925 presented at the European Petroleum Conference, The Hague, 22–24 October. DOI: [10.2118/20925-MS](https://doi.org/10.2118/20925-MS).
- Peng, S., Hodder, M., Kay, M., and Milton, A. 2003. Real-Time, Downhole Hydraulics Modelling Helps Operator Drill the Well and Run Liner Under a Narrow Fracture/Pore Pressure Window Condition. Paper SPE 85309 presented at the SPE/IADC Middle East Drilling Technology Conference and Exhibition, Abu Dhabi, United Arab Emirates, 20–22 October. DOI: [10.2118/85309-MS](https://doi.org/10.2118/85309-MS).
- Perry, R.H. and Chilton, C.H. 1973. *Chemical Engineers' Handbook*, 5th Edition, McGraw-Hill Book Company, New York City.
- Philip, Z., Sharma, M., and Chenevert, M.E. 1998. The Role of Taylor Vortices in the Transport of Drill Cuttings. Paper SPE 39504 presented at the SPE India Oil and Gas Conference and Exhibition, New Delhi, India, 17–19 February. DOI: [10.2118/39504-MS](https://doi.org/10.2118/39504-MS).
- Piercy, N.A.V., Hooper, M.S., and Winny, H.F. 1933. *Phil. Mag.* **15** (7): 647–676.
- Pigott, R.J.S. 1941. Mud Flow in Drilling. *API Drilling and Production Practice*. Paper no. 41-091, 13 pp.
- Pilehvari, A.A., Azar, J.J., and Shirazi, S.A. 1996. State-of-the-Art Cuttings Transport in Horizontal Wellbores. Paper SPE 37079 presented at the SPE International Conference on Horizontal Well Technology, Calgary, 18–20 November. DOI: [10.2118/37079-MS](https://doi.org/10.2118/37079-MS).
- Pilehvari, A.A., Azar, J.J., and Shirazi, S.A. 1999. State-of-the-Art Cuttings Transport in Horizontal Wellbores. *SPEDE* **14** (3): 196–200. SPE-57716-PA. DOI: [10.2118/57716-PA](https://doi.org/10.2118/57716-PA).
- Power, D.J., Hight, C., Weisinger, D., and Rimer, C. 2000. Drilling Practices and Sweep Selection for Efficient Hole Cleaning in Deviated Wellbores. Paper SPE 62794 presented at the 2000 IADC/SPE Asia Pacific Drilling Technology, Kuala Lumpur, 11–13 September. DOI: [10.2118/62794-MS](https://doi.org/10.2118/62794-MS).
- Press, W.H., Teukolsky, S.A., Vetterling, W.T., and Flannery, B.P. 1997. *Numerical Recipes: The Art of Scientific Computing*. Cambridge University Press, New York.
- Reed, T.D. and Pilehvari, A.A. 1993. A New Model for Laminar, Transitional, and Turbulent Flow of Drilling Muds. Paper SPE 25456 presented at the SPE Production Operations Symposium, Oklahoma City, Oklahoma, 21–23 March. DOI: [10.2118/25456-MS](https://doi.org/10.2118/25456-MS).
- Reynolds, O. 1883. An Experimental Investigation of the Circumstances Which Determine Whether the Motion of Water Shall Be Direct or Sinuous, and the Laws of Resistance in Parallel Channels. *Trans.*, Royal Society of London, **174**.
- Robertson, R.E. and Stiff, H.A. Jr. 1976. An Improved Mathematical Model for Relating Shear Stress to Shear Rate in Drilling Fluids and Cement Slurries. *SPEJ* **16** (1): 31–36. SPE-5333-PA. DOI: [10.2118/5333-PA](https://doi.org/10.2118/5333-PA).
- Rudolf, R.L. and Suryanarayana, P.V.R. 1998. Field Validation of Swab Effects While Tripping-In the Hole on Deep, High Temperature Wells. Paper SPE 39395 presented at the IADC/SPE Drilling Conference, Dallas, 3–6 March. DOI: [10.2118/39395-MS](https://doi.org/10.2118/39395-MS).
- Saasen, A. and Loklingholm, G. 2002. The Effect of Drilling Fluid Rheological Properties on Hole Cleaning. Paper SPE 74558 presented at the IADC/SPE Drilling Conference, Dallas, 26–28 February. DOI: [10.2118/74558-MS](https://doi.org/10.2118/74558-MS).

- Sanchez, R.A., Azar, J.J., Bassal, A.A., and Martins, A.L. 1997. The Effect of Drillpipe Rotation on Hole Cleaning During Directional Drilling. Paper SPE 37626 presented at the SPE/IADC Drilling Conference, Amsterdam, 4–6 March. DOI: [10.2118/37626-MS](https://doi.org/10.2118/37626-MS).
- Schuh, F.J. 1964. Computer Makes Surge Pressure Calculations Useful. *Oil & Gas J.* **52** (31): 96.
- Shah, S.N. and Sutton, D.L. 1990. New Friction Correlation for Cements From Pipe and Rotational-Viscometer Data. *SPE Prod Eng* **5** (4): 415–424. SPE-19539-PA. DOI: [10.2118/19539-PA](https://doi.org/10.2118/19539-PA).
- Shulman, Z.P. 1968. One Phenomenological Generalisation of Viscoplastic Rheostable Disperse System Flow Curves. *Teplo-Massoperenos* **10**: 3–10.
- Sifferman, T.R. and Becker, T.E. 1992. Hole Cleaning in Full-Scale Inclined Wellbores, *SPEDE* **7** (2): 115–120. SPE-20422-PA. DOI: [10.2118/20422-PA](https://doi.org/10.2118/20422-PA).
- Sisko, A.W. 1958. Flow of Lubricating Grease. *Industrial Engineering Chemistry* **50** (12): 1789–1792.
- Standing, M.B. and Katz, D.L. 1942. Density of Natural Gases. *Trans., AIME* **146**: 140–149.
- Steine, O.G., Rommetveit, R., Maglione, R., and Sagot, A. 1996. Well Control Experiments Related to Slim Hole Drilling. Paper SPE 35121 presented at the SPE/IADC Drilling Conference, New Orleans, 12–15 March. DOI: [10.2118/35121-MS](https://doi.org/10.2118/35121-MS).
- Subramanian, R. and Azar, J.J. 2000. Experimental Study on Friction Pressure Drop for Non-Newtonian Drilling Fluids in Pipes. Paper SPE 64647 presented at the SPE International Oil and Gas Conference and Exhibition, Beijing, 7–10 November. DOI: [10.2118/64647-MS](https://doi.org/10.2118/64647-MS).
- Tao, L.N. and Donovan, W. F. 1955. *ASME Trans.*, vol. 77, 1291–1301.
- Televantos, Y., Shook, C.A., Carleton, A., and Streat, M. 1979. Flow of Slurries of Coarse Particles at High Solids Concentrations. *Canadian J. of Chemical Engineering* **57** (3): 255–262.
- Tomren, P.H., Iyoho, A.W., and Azar, J.J. 1986. Experimental Study of Cuttings Transport in Directional Wells. *SPEDE* **1** (1): 43–56. SPE-12123-PA. DOI: [10.2118/12123-PA](https://doi.org/10.2118/12123-PA).
- Uner, D. Ozgen, C. and and Tosun, I. 1989. An Approximate Solution for Non-Newtonian Flow in Eccentric Annulus, *Ind. Eng. Chem. Res.* **27** (4): 698.
- Walker, S. and Li, J. 2000. The Effects of Particle Size, Fluid Rheology, and Pipe Eccentricity on Cuttings Transport. Paper SPE 60755 presented at the SPE/ICoTA Coiled Tubing Roundtable, Houston, 5–6 April. DOI: [10.2118/60755-MS](https://doi.org/10.2118/60755-MS).
- Walton, I.C. 1995. Computer Simulator of Coiled Tubing Wellbore Cleanouts in Deviated Wells Recommends Optimum Pump Rate and Fluid Viscosity. Paper SPE 29491 presented at the SPE Production Operations Symposium, Oklahoma City, Oklahoma, 2–4 April. DOI: [10.2118/29491-MS](https://doi.org/10.2118/29491-MS).
- Wang, Y. and Chukwu, A. 1997. Application of Unsteady Couette Flow for Non-Newtonian Power-Law Fluid in Concentric Annular Wellbore. *J. of Petroleum Science and Engineering* **17** (3–4): 229–235.
- White, F.M. 1974. *Viscous Fluid Flow*, page 196. New York City: McGraw-Hill Book Company.
- Wilson, K.C. 1970. Slip Point of Beds in Solid-Liquid Pipeline Flow. *ASCE Journal of Hydraulics* **96** (1): 1–12.
- Zamora, M. and Hanson, P. 1991. More Rules of Thumb to Improve High Angle Hole Cleaning. *Petroleum Engineering International* **64** (9): 22–27.
- Zamora, M. and Roy, S. 2000. The Top 10 Reasons To Rethink Hydraulics and Rheology. Paper SPE 62731 presented at the 2000 IADC/SPE Asia Pacific Drilling Technology Conference, Kuala Lumpur, 11–13 September.
- Zamora, M., Jefferson, D.T., and Powell, J.W. 1993. Hole-Cleaning Study of Polymer-Based Drilling Fluids. Paper SPE 26329 presented at the SPE Annual Technical Conference and Exhibition, Houston, 3–6 October. DOI: [10.2118/26329-MS](https://doi.org/10.2118/26329-MS).
- Zhu, H., Kim, Y.D., and de Kee, D. 2005. Non-Newtonian Fluids With a Yield Stress. *J. of Non-Newtonian Fluid Mechanics* **129** (3): 177–181.

Further Reading and Advanced Topics

- Aadnoy, B.S. 1996. *Modern Well Design*, Rotterdam: A.A. Balkema.
- Atapattu, D.D., Chhabra, R.P., and Uhlherr, P.H.T. 1995. Creeping Sphere Motion in Herschel-Bulkley Fluids: Flow Field and Drag. *J. of Non-Newtonian Fluid Mechanics* **59** (2–3): 245–265. DOI: [10.1016/0377-0257\(95\)01373-4](https://doi.org/10.1016/0377-0257(95)01373-4).
- Bagnold, R.A. 1954. Experiments of a Gravity Free Dispersion of Large Solid Spheres in a Newtonian Fluid Under Shear. *Proc., Royal Society A225*, 49–63.
- Bagnold, R.A. 1957. The Flow of Cohesionless Grains in Fluids. *Philosophical Transactions of the Royal Society of London, Series A, Mathematical and Physical Sciences*, **249** (964): 235–297.
- Beck, F.E., Powell, J.W., and Zamora, M. 1995. The Effect of Rheology on Rate of Penetration. Paper SPE/IADC 29368 presented at the SPE/IADC Drilling Conference, Amsterdam, 28 February–2 March. DOI: [10.2118/29368-MS](https://doi.org/10.2118/29368-MS).

- Becker, T.E., Morgan, R.G., Chin, W.C., and Griffith, J.E. 2003. Improved Rheology Model and Hydraulics Analysis for Tomorrow's Wellbore Fluid Applications. Paper SPE 82415 presented at the SPE Production and Operations Symposium, Oklahoma City, Oklahoma, 22–25 March. DOI: [10.2118/82415-MS](https://doi.org/10.2118/82415-MS).
- Bible, M.J., Hedayati, Z., and Choo, D.K. 1991. State-of-the-Art Trip Monitor. Paper SPE 21965 presented at the SPE/IADC Drilling Conference, Amsterdam, 11–14 March. DOI: [10.2118/21965-MS](https://doi.org/10.2118/21965-MS).
- Bizanti, M.S. and Alkafeef, S.F. 2003. A Simplified Hole Cleaning Solution to Deviated and Horizontal Wells. Paper SPE 81412 presented at the Middle East Oil Show, Bahrain, 9–12 June. DOI: [10.2118/81412-MS](https://doi.org/10.2118/81412-MS).
- Blackery, J. and Mitsoulis, E. 1997. Creeping Motion of a Sphere in Tubes Filled With a Bingham Plastic Material. *J. of Non-Newtonian Fluid Mechanics* **70** (1–2): 59–77. DOI: [10.1016/S0377-0257\(96\)01536-4](https://doi.org/10.1016/S0377-0257(96)01536-4).
- Bourgoynne, A.T., Chenevert, M.E., Millheim, K.K., and Young, F.S. Jr. 1991. *Applied Drilling Engineering*. Textbook Series, SPE, Richardson, Texas **2**: 113–189.
- Campos, W. 1995. Mechanistic Modeling of Cuttings Transport in Directional Wells. PhD dissertation, University of Tulsa, Tulsa, Oklahoma.
- Cheremisinoff, N.P. and Gupta, R. 1983. *Handbook of Fluids in Motion*. Ann Arbor, Michigan: Ann Arbor Science.
- Chhabra, R.P. and Peri, S.S. 1991. Simple Method for the Estimation of Free-Fall Velocity of Spherical Particles in Power Law Liquids. *Powder Technology* **67** (33): 287–290.
- Chhabra, R.P. and Ulherr, P.H.T. 1988. Static Equilibrium and Motion of Spheres in Viscoplastic Liquids. In *Encyclopedia of Fluid Mechanics*, ed. N.P. Cheremisinoff, Vol. 7, 611–633. Houston: Gulf Publishing Company.
- Chhabra, R.P., Agarwal, L., and Sinha, N.K. 1999. Drag on Non-Spherical Particles: An Evaluation of Available Methods. *Powder Technology* **101** (33): 288–295.
- Chien, S.F. 1969. Annular Velocity for Rotary Drilling Operations. Paper SPE 2786 available from SPE, Richardson, Texas.
- Cho, H., Shah, S.N., and Osisanya, S.O. 2000b. A Three-Segment Hydraulic Model for Cuttings Transport in Horizontal and Deviated Wells. Paper SPE/PS CIM 65488 presented at the SPE/CIM International Conference on Horizontal Well Technology, Calgary, 6–8 November. DOI: [10.2118/65488-MS](https://doi.org/10.2118/65488-MS).
- Cho, H., Shah, S.N., and Osisanya, S.O. 2001b. Selection of Optimum Coiled-Tubing Parameters Through the Cuttings Bed Characterization. Paper SPE 68436 presented at the SPE/ICoTA Coiled Tubing Roundtable, Houston, 7–8 March. DOI: [10.2118/68436-MS](https://doi.org/10.2118/68436-MS).
- Chugh, C.P. 1992. *High Technology in Drilling and Exploration*, Rotterdam: A.A. Balkema.
- Chukwu, A. and Blick, E.F. 1990. Surge and Swab Pressure Model. Part 1—Surge and Swab Pressure Computed for Couette Flow of Power-Law Fluids Through a Slot. *Petroleum Engineering International* **62** (6): 48–51.
- Crittendon, B.C. 1959. The Mechanics of Design and Interpretation of Hydraulic Fracture Treatment. *JPT* **11** (10): 21–29. SPE-1106-G. DOI: [10.2118/1106-G](https://doi.org/10.2118/1106-G).
- Dodge, N.A. 1963. Friction Losses in Annular Flow. ASME Paper No. 63-WA-11.
- Doron, P. and Barnea, D. 1993. A Three Layer Model for Solid-Liquid Flow in Horizontal Pipes. *International J. of Multiphase Flow* **19** (6): 1029–1043.
- Doron, P. and Barnea, D. 1995. Pressure Drop and Limit Deposit Velocity for Solid-Liquid Flow in Pipes. *Chemical Engineering Science* **50** (10): 1595–1604.
- Doron, P. and Barnea, D. 1996. Flow Pattern Maps for Solid-Liquid Flow in Pipes. *International J. of Multiphase Flow* **22** (2): 273–283.
- Durand, R. 1953. Basic Relationships of the Transportation of Solids in Pipes—Experimental and Modeling. *Proc.*, 5th Minneapolis International Hydraulics Convention, Minneapolis, Minnesota: 89–103.
- Eckel, J.R. 1967. Microbit Studies of the Effect of Fluid Properties and Hydraulics on Drilling Rate. *JPT* **19** (4): 541–546.
- Fang, P., Manglik, R.M., and Jog, M.A. 1999. Characteristics of Laminar Viscous Shear-Thinning Fluid Flows in Eccentric Annular Channels. *J. of Non-Newtonian Fluid Mechanics* **84** (1): 1–17.
- Feenstra, R. and Zijssling, D.H. 1984. The Effect of Bit Hydraulics on Bit Performance in Relation to the Rock Destruction Mechanism at Depth. Paper SPE 13205 presented at the SPE Annual Technical Conference and Exhibition, Houston, 16–19 September. DOI: [10.2118/13205-MS](https://doi.org/10.2118/13205-MS).
- Founargiotakis, K., Kelessidis, V.C., and Maglione, R. 2008. Laminar, Transitional and Turbulent Flow of Herschel-Bulkley Fluids in Concentric Annulus. *Journal of Canadian Chemical Engineering* **86**: 676–683.
- Gallino, G., Guarneri, A., Poli, G., and Xiao, L. 1996. Scleroglucan Biopolymer Enhances WBM Performances. Paper SPE 36426 presented at the SPE Annual Technical Conference and Exhibition, Denver, 6–9 October. DOI: [10.2118/36426-MS](https://doi.org/10.2118/36426-MS).
- Grinchik, I.P. and Kim, A.K. 1972. Axial Flow of a Non-Linear Viscoplastic Fluid Through Cylindrical Pipes. *J. of Engineering Physics* **23** (2): 1039–1041.
- Grindrod, J., Rayton, C., Sim, C., Biggs, N., Brown, A., and Taylor, P. 2002. The Introduction of New-Generation Positive Displacement Motor Technology in Combination With Application Specific PDC Bits: A Step

- Improvement in Drilling Performance on Horizontal Rotliegendes Sandstone Sections. Paper IADC/SPE 74455 presented at the IADC/SPE Drilling Conference, Dallas, 26–28 February. DOI: [10.2118/74455-MS](https://doi.org/10.2118/74455-MS).
- Gu, D. and Tanner, R.I. 1985. The Drag on a Sphere in a Power Law Fluid. *J. of Non-Newtonian Fluid Mechanics* **17** (1): 1–12.
- Guarneri, A., Carminati, S., Zamora, M., and Roy, S. 2005. Determining Mud Rheology for Optimum Hydraulics. *Proc.*, 7th Offshore Mediterranean Conference, Ravenna, Italy, Session 1, Paper 018.
- Haider, A. and Levenspiel, O. 1989. Drag Coefficient and Terminal Velocity of Spherical and Nonspherical Particles. *Powder Technology* **58** (1): 63–70.
- Hanks, R.W. and Pratt, D.R. 1967. On the Flow of Bingham Plastic Slurries in Pipes and Between Parallel Plates, *SPEJ* **7** (4): 342–346; *Trans.*, AIME, **240**.
- Hutchinson, M. and Rezmer-Cooper, I. 1998. Using Downhole Annular Pressure Measurements To Anticipate Drilling Problems. Paper SPE 49114 presented at the SPE Annual Technical Conference and Exhibition, New Orleans, 27–30 September. DOI: [10.2118/49114-MS](https://doi.org/10.2118/49114-MS).
- Iyoho, A.W. and Takahashi, H. 1993. Modeling Unstable Cuttings Transport in Horizontal Eccentric Wellbores. Paper SPE 27416 available from SPE, Richardson, Texas.
- Kahn, A.R. and Richardson, J.F. 1987. The Resistance to Motion of a Solid Sphere in a Fluid. *Chemical Engineering Communications* **62** (1–6): 135–151.
- Kelessidis, V.C. 2003. Terminal Velocity of Solid Spheres Falling in Newtonian and Non-Newtonian Liquids. *Technika Chronika Science, Journal of the Technical Chamber of Greece V* (1–2): 43–54.
- Kelessidis, V.C. 2004a. An Explicit Equation for the Terminal Settling Velocity of Solid Spheres Falling in Pseudoplastic Fluids. *Chemical Engineering Science* **59** (2): 4437–4447.
- Kelessidis, V.C. and Mpandelis, G.E. 2004b. Hydraulic Parameters Affecting Cuttings Transport for Horizontal Coiled-Tubing Drilling. Paper presented at the 7th National Congress on Mechanics, Chania, Greece, 24–26 June: 95–103.
- Kelessidis, V.C. and Mpandelis, G. 2004c. Measurements and Prediction of Terminal Velocity of Solid Spheres Falling Through Stagnant Pseudoplastic Liquids. *Powder Technology* **147** (1–3): 117–125.
- Kelessidis, V.C., Founargiotakis, K., and Brouzos, C. 2006. Laminar, Turbulent and Transitional Flows of Herschel-Bulkley Fluids in Annuli. Paper presented at the 3rd Annual European Rheology Conference, Hersonisos, Crete, 27–29 April.
- Kendall, W.A. and Goins, W.C. 1960. Design and Operation of Jet Bit Program for Maximum Hydraulic Horsepower, Impact Force, or Jet Velocity. *Trans.*, AIME **219**: 238–247.
- Lali, A.M., Khare, A.S., Joshi, J.B., and Migam, K.D.P. 1989. Behavior of Solid Particles in Viscous Non-Newtonian Solutions: Falling Velocity, Wall Effects and Bed Expansion in Solid-Liquid Fluidized Beds. *Powder Technology* **57** (1): 47–77.
- Lamb, H. 1945. *Hydrodynamics*, sixth edition. New York City: Dover Publications.
- Langlinais, J. and Hacıislamoglu, M. 1991. Effect of Pipe Eccentricity on Surge Pressures. *Journal of Energy Resources Technology* **113** (3): 157–161.
- Luo, Y., Bern, P.A., and Chambers, B.D. 1992. Flow-Rate Predictions for Cleaning Deviated Wells. Paper SPE 23884 presented at the SPE/IADC Drilling Conference, New Orleans, 18–21 February. DOI: [10.2118/23884-MS](https://doi.org/10.2118/23884-MS).
- Machac, I., Ulbrichova, I., Elson, T.P., and Cheesman, D.J. 1995. Fall of Spherical Particles Through Non-Newtonian Suspensions. *Chemical Engineering Science* **50** (20): 3323–3327.
- McLean, R.H. 1965. Velocities, Kinetic Energies, and Shear on Crossflow Under Three-Cone Jet Bits. *JPT* **17** (12): 1443–1448; *Trans.*, AIME, **234**. SPE-1306-PA. DOI: [10.2118/1306-PA](https://doi.org/10.2118/1306-PA).
- Maglione, R. 1998. Rheology Optimisation While Drilling Oil and Gas Wells. *Proc.*, Joint Conference of Italian, Austrian, Slovenian Rheologists, Trieste, Italy, 20–23 May: 149–154.
- Maglione, R. and Kelessidis, V.C. 2006. Choosing the Best Rheological Model for Bentonite Suspensions. Paper presented at the 3rd Annual European Rheology Conference, Hersonisos, Crete, 27–29 April.
- Maglione, R. and Robotti, G. 1996a. Field Rheological Parameters Improve Stand Pipe Pressure Prediction While Drilling. Paper SPE 36099 presented at the SPE Latin American and Caribbean Petroleum Engineering Conference, Port-of-Spain, Trinidad, 23–26 April. DOI: [10.2118/36099-MS](https://doi.org/10.2118/36099-MS).
- Maglione, R. and Robotti, G. 1996b. Numerical Procedure for Solving a Non-Linear Equations System for Determining the Three Rheological Parameters of a Drilling Mud From Experimental Data. *Proc.*, 4th International Conference on Integral Methods in Science and Engineering, Oulu, Finland **II**: 144–149.
- Maglione, R. and Romagnoli, R. 1999 2nd edition. *Reologia e Idraulica dei Fluidi di Perforazione*, pp. 470. Torino: Edizioni: CUSL
- Maglione, R. and Romagnoli, R. 1999b. *Reologia ed Idraulica dei Fluidi di Perforazione*. Turin, Italy: Cusl Edition.

- Maglione, R., Robotti, G., and Romagnoli, R. 1997. Annular Flow Optimisation: A New Integrated Approach. *Proc. 3rd Annual ASME/API Energy Week International Conference*, Houston, 28–30 January, 121–127.
- Martins, A.L., de Sa, C.H.M., Lourenco, A.M.F., and Campos, W. 1996a. Optimizing Cuttings Circulation in Horizontal Well Drilling. Paper SPE 35341 presented at the International Petroleum Conference and Exhibition of Mexico, Villahermosa, Mexico, 5–7 March. DOI: [10.2118/35341-MS](https://doi.org/10.2118/35341-MS).
- Martins, A.L., de Sa, C.H.M., Lourenco, A.M.F., Freire, L.G.M., and Campos, W. 1996b. Experimental Determination of Interfacial Friction Factor in Horizontal Drilling With a Bed of Cuttings. Paper SPE 36075 presented at the SPE Latin American and Caribbean Petroleum Engineering Conference, Port-of-Spain, Trinidad, 23–26 April. DOI: [10.2118/36075-MS](https://doi.org/10.2118/36075-MS).
- Martins, A.L., Santana, M.L., and Gaspari, E.F. 1999. Evaluating the Transport of Solids Generated by Shale Instabilities in ERW Drilling. *SPEDC* **14** (4): 254–259. SPE-59729-PA. DOI: [10.2118/59729-PA](https://doi.org/10.2118/59729-PA).
- Martins, A.L., Lourenco, A.M.F., and de Sa, C.H.M. 2001. Foam Property Requirements for Proper Hole Cleaning While Drilling Horizontal Wells in Underbalanced Conditions. *SPEDC* **16** (4): 195–200. SPE-74333-PA. DOI: [10.2118/74333-PA](https://doi.org/10.2118/74333-PA).
- McCann, R.C., Quigley, M.S., Zamora, M., and Slater, K.S. 1993. Effects of High Speed Pipe Rotation on Pressure in Narrow Annuli. *SPEDC* **10** (2): 96–103. SPE-26343-PA. DOI: [10.2118/26343-PA](https://doi.org/10.2118/26343-PA).
- Metzner, A.B. 1957. Non-Newtonian Fluid Flow. Relationships Between Recent Pressure-Drop Correlations. *Industrial and Engineering Chemistry* **49** (9): 1429.
- Mishra, P. and Tripathi, G. 1971. Transition From Laminar to Turbulent Flow of Purely Viscous Non-Newtonian Fluids in Tubes. *Chemistry Engineering Science* **26** (6): 915–921.
- Miura, H., Takahashi, T., Ichikawa, J., and Kawase, Y. 2001. Bed Expansion in Liquid-Solid Two-Phase Fluidized Beds With Newtonian and Non-Newtonian Fluids Over the Wide Range of Reynolds Numbers. *Powder Technology* **117** (3): 239–246.
- Molerus, O. 1993. *Principles of Flow in Disperse Systems*. Berlin: Chapman and Hall.
- Monicard, R. 1982. *Drilling Mud and Cement Slurry Rheology Manual*. Paris: Editions Technip.
- Moore, P.L. 1974. *Drilling Practices Manual*. Tulsa: Petroleum Publishing Company.
- Moore, P.L. 1986. *Drilling Practices Manual*. Tulsa: PennWell Books.
- Naegel, M., Pradie, E., Beffa, K., Ricaud, J., and Delahaye, T. 1998. Extended Reach Drilling at the Uttermost Part of the Earth. Paper SPE 48944 presented at the SPE Annual Technical Conference and Exhibition, New Orleans, 27–30 September. DOI: [10.2118/48944-MS](https://doi.org/10.2118/48944-MS).
- Naganawa, S., Oikawa, A., Masuda, Y., Yonezawa, T., Hoshino, M., and Acuna, P. 2002. Cuttings Transport in Directional and Horizontal Wells While Aerated Mud Drilling. Paper SPE 77195 presented at the IADC/SPE Asia Pacific Drilling Technology, Jakarta, 9–11 September. DOI: [10.2118/77195-MS](https://doi.org/10.2118/77195-MS).
- Nguyen, D. and Rathman, S.S. 1998a. A Three-Layer Hydraulic Program for Effective Cuttings Transport and Hole Cleaning in Highly Deviated and Horizontal Wells. *SPEDC* **13** (3): 182–189. SPE-51186-PA. DOI: [10.2118/51186-PA](https://doi.org/10.2118/51186-PA).
- Nguyen, D. and Rathman, S.S. 1998b. A Three-Layer Hydraulic Program for Effective Cuttings Transport and Hole Cleaning in Highly Deviated and Horizontal Wells (Supplement to SPE 51186). Paper SPE 51320 available from SPE, Richardson, Texas.
- Okafor, M.N. 1982. Experimental Verification of the Robertson-Stiff Rheology Model for Drilling Fluids. MS thesis, University of Wyoming, Laramie, Wyoming.
- Ooms, G., Burgerscentrum, J.M., and Kampman-Reinhart, B.E. 1999. Influence of Drillpipe Rotation and Eccentricity on Pressure Drop Over Borehole During Drilling. Paper SPE 56638 presented at the SPE Annual Technical Conference and Exhibition, Houston, 3–6 October. DOI: [10.2118/56638-MS](https://doi.org/10.2118/56638-MS).
- Ozbayoglu, E.M., Miska, S.Z., Reed, T., and Takash, N. 2002. Analysis of Bed Height in Horizontal and Highly Inclined Wellbores by Using Artificial Neural Networks. Paper SPE 78939 presented at the SPE International Thermal Operations and Heavy Oil Symposium and International Horizontal Well Technology Conference, Calgary, 4–7 November. DOI: [10.2118/78939-MS](https://doi.org/10.2118/78939-MS).
- Pinelli, D. and Magelli, F. 2001. Solids Falling Velocity and Distribution in Slurry Reactors With Dilute Pseudoplastic Suspensions. *Industrial Engineering Chemistry Research* **40** (2): 4456–4462.
- Rabia, H. 1985. *Oilwell Drilling Engineering: Principles and Practice*. London: Graham and Trotman.
- Robeiro, P.R., Podio, A.L., and Sepehrnoori, K. 1994. The Effect of Rotational Speed and Eccentricity on Annular Flows With Application to Slim Hole Drilling Hydraulics. Paper SPE 26958 presented at the SPE Latin American and Caribbean Petroleum Engineering Conference, Buenos Aires, 27–29 April. DOI: [10.2118/26958-MS](https://doi.org/10.2118/26958-MS).
- Roy, S. and Zamora, M. 2000. Step Improvements in Accurate Real Time Wellsite Hydraulics. Paper 2000 presented at the AADE Technical Conference, Houston, 9–10 February.

- Rudolf, R.L. and Suryanarayana, P.V.R. 1997. Kicks Caused by Tripping-In the Hole on Deep, High Temperature Wells. Paper SPE 38055 presented at the SPE Asia Pacific Oil and Gas Conference and Exhibition, Kuala Lumpur, 14–16 April. DOI: [10.2118/38055-MS](https://doi.org/10.2118/38055-MS).
- Ryan, N.W. and Johnson, M.M. 1959. Transition From Laminar to Turbulent Flow in Pipes. *AIChE J.* **5** (4): 433–435.
- Sample, K.J. and Bourgoyne, A.T. Jr. 1978. Development of Improved Laboratory and Field Procedures for Determining the Carrying Capacity of Drilling Fluids. Paper SPE 7497 presented at the SPE Annual Technical Conference and Exhibition, Houston, 1–4 October. DOI: [10.2118/7497-MS](https://doi.org/10.2118/7497-MS).
- Sanchez, R.A., Azar, J.J., Bassal, A.A., and Martins, A.L. 1999. The Effect of Drillpipe Rotation on Hole Cleaning During Directional Drilling. *SPEJ* **4** (2): 101–108. SPE-56406-PA. DOI: [10.2118/56406-PA](https://doi.org/10.2118/56406-PA).
- Santana, M., Martins, A.L., and Sales, A. Jr. 1998. Advances in the Modeling of the Stratified Flow of Drilled Cuttings in High Angle and Horizontal Wells. Paper SPE 39890 presented at the International Petroleum Conference and Exhibition of Mexico, Villahermosa, Mexico, 3–5 March. DOI: [10.2118/39890-MS](https://doi.org/10.2118/39890-MS).
- Sifferman, T.R., Myers, G.M., Haden, E.L., and Wahl, H.A. 1974. Drill Cutting Transport in Full-Scale Vertical Annuli. *JPT* **26** (11): 1295–1302. SPE-4514-PA. DOI: [10.2118/4514-PA](https://doi.org/10.2118/4514-PA).
- Siginer, D.A. and Bakhtiyarov, S.I. 1998. Flow of Drilling Fluids in Eccentric Annuli. *J. of Non-Newtonian Fluid Mechanics* **78** (2–3): 119–132.
- Silva, M.A. and Shah, S.N. 2000. Friction Pressure Correlations of Newtonian and Non-Newtonian Fluids Through Concentric and Eccentric Annuli. Paper SPE 60720 presented at the SPE/ICoTA Coiled Tubing Roundtable, Houston, 5–6 April. DOI: [10.2118/60720-MS](https://doi.org/10.2118/60720-MS).
- Slatter, P.T. 1996. The Laminar/Turbulent Transition—An Industrial Problem Solved. *Proc.*, 13th International Conference (Slurry Handling and Pipeline Transport) Hydrotransport 13, Johannesburg, South Africa, September 1996. BHR Group, Cranford, UK: 97–113.
- Speer, J.W. 1958. A Method for Determining Optimum Drilling Techniques. *API Drilling & Production Practice*: 130–147. API paper 58-130.
- Stokes, G.O. 1845. Transactions of the Cambridge Philosophical Society. **8**: 287–305.
- Streeter, V.L. 1962. *Fluid Mechanics*, New York City: McGraw-Hill.
- Sutko, A. 1973. Drilling Hydraulics—A Study of Chip Removal Force Under a Full-Size Jet Bit. *SPEJ* **13** (4): 233–238; *Trans.*, AIME, **255**. SPE-3985-PA. DOI: [10.2118/3985-PA](https://doi.org/10.2118/3985-PA).
- Thomas, D.G. 1963. Transport Characteristics of Suspensions: Relation of Hindered Settling Flow Characteristics to Rheological Parameters. *AIChE J.* **9** (3): 310–316.
- Tosun, I., Uner, D., and Ozgen, C. 1989. Flow of a Power-Law Fluid in an Eccentric Annulus. *SPE Drill Eng* **4** (3): 269–272.
- Turton, R. and Clark, N.N. 1987. An Explicit Relationship To Predict Spherical Particle Terminal Velocity. *Powder Technology* **53** (2): 127–129.
- Valentik, L. and Whitmore, R.L. 1965. The Terminal Velocity of Spheres in Bingham Plastics. *British J. of Applied Physics* **16** (8): 1197–1203.
- Venu Madhav, G. and Chhabra, R.P. 1994. Settling Velocities of Non-Spherical Particles in Non-Newtonian Polymer Solutions. *Powder Technology* **78** (1): 77–83.
- Walker, R.E. and Holman, H.E. 1971. Computer Program Predicts Drilling Fluid Performance. *Oil & Gas J.* **69** (13): 80–90.
- Walker, R.E. and Korry, D.E. 1974. Field Method of Evaluating Annular Performance of Drilling Fluids. *JPT* **26** (2): 167–173. SPE-4321-PA. DOI: [10.2118/4321-PA](https://doi.org/10.2118/4321-PA).
- Walker, R.E. and Mayes, T.M. 1975. Design of Muds for Carrying Capacity. *JPT* **27** (7): 893–900; *Trans.*, AIME, **259**. SPE-4975-PA. DOI: [10.2118/4975-PA](https://doi.org/10.2118/4975-PA).
- Walker, R. 1976a. Annular Calculations Balance Cleaning With Pressure Loss. *Oil & Gas J.* **74** (42): 82–88.
- Walker, R.E. 1976b. Hydraulic Limits Are Set by Flow Restrictions. *Oil & Gas J.* **74** (40): 86–90.
- Walker, S. and Li, J. 2001. Coiled-Tubing Wiper Trip Hole Cleaning in Highly Deviated Wellbores. Paper SPE 68435 presented at the SPE/ICoTA Coiled Tubing Roundtable, Houston, 7–8 March. DOI: [10.2118/68435-MS](https://doi.org/10.2118/68435-MS).
- Wan, S., Morrison, D., and Bryden, I.G. 2000. The Flow of Newtonian and Inelastic Non-Newtonian Fluids in Eccentric Annuli With Inner-Cylinder Rotation. *Theoretical and Computational Fluid Dynamics* **13** (5): 349–359.
- Whittaker, A. ed. 1985. *Theory and Application of Drilling Fluid Hydraulics*. Dordrecht, The Netherlands: Kluwer Academic Publishers.
- Williams, C.E. and Bruce, O.H. 1951. Carrying Capacity of Drilling Muds. *Trans.*, AIME **192**: 111–120.
- Wilson, K.C. and Tse, J.K.P. 1984. Deposition Limit for Coarse Particle Transport in Inclined Pipes. Proceedings Ninth International Conference (Hydraulic Transport of Solids in Pipes,) Hydrotransport 9, Rome, Italy, October 17–19, BHR Group, Cranfield, UK.: 149–161.

Chapter 6

Rotary Drilling Bits

Evren Ozbayoglu, University of Tulsa

This chapter is an updated version of the Rotary Drilling Bits chapter that first appeared in Bourgoyne et al. (1991). The purpose of this chapter is to introduce the student to the selection and operation of drilling bits. Included in the chapter are discussions of (1) various bit types available, (2) criteria for selecting the best bit for a given application or drilling program, (3) standard methods for evaluating the performances of dull bits, (4) factors affecting bit wear and rate of penetration (ROP), and (5) optimization of drilling parameters such as weight on bit (WOB) and revolutions per minute (RPM).

6.1 Introduction

A drilling bit is the major tool that conducts the cutting action located at the end of the drillstring. The bit generates the drilling action by scraping, chipping, gouging, or grinding the rock. Drilling fluid is circulated through the bit to remove the drilled cuttings generated inside the wellbore.

There are many variations of bit designs available. The selection of the bit for a particular application will depend on the type of formation to be drilled as well as the expected operating conditions during the drilling process. The performance of a bit is a function of several operating parameters including WOB, RPM, mud properties, and hydraulic efficiency. The drilling engineer must be aware of the design variations, the impact of the operating conditions on the performance of the bit, and the wear generated on the bit in order to be able to select the most appropriate bit for the formation to be drilled.

6.1.1 Historical Development. *Roller-Cone Bits.* Throughout the early 1900s, the performance of roller-cone bits was superior to other bit types and, as a result, their popularity grew as they became the most widely used drill-bit type. The first roller-cone bits were invented by and evolved from a patent by Howard Hughes in 1909 (Hughes 1909) that described a rotary drill bit with two rotating cones. In the early 1930s, the tricone bit was introduced, with cutters designed for hard and soft formations (**Fig. 6.1**).

By the late 1940s, the industry was venturing into deep drilling, which means harder rocks such as limestone and chert, slow penetration rates, and reduced bit life. Because conventional milled-tooth bits were simply inadequate for these drilling environments, in 1949, Hughes Tool Company introduced the first three-cone bit using tungsten carbide inserts in the cutting structure. This bit was characterized by short and closely spaced inserts. Failure in the roller cones was mostly from bearing failure, and not to structure failure. Still, developments achieved mostly focused on bearing enhancements, leg and cutter metallurgy, and hydraulics. Today, modern insert bits are used routinely in many areas from top to bottom in low-solids drilling-mud systems.

Fixed-Cutter Bits. In the early 1900s, fishtail bits or drag bits, which were the early versions of fixed-cutter bits, were introduced. They were made of steel and were configured with two blades or paddles usually covered with harder alloy coatings or cutting tips to extend life. Their major application was mainly to drill very soft rock formations (**Fig. 6.2**).

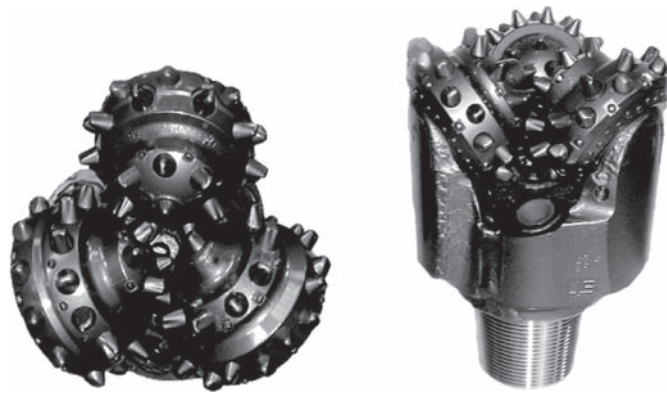


Fig. 6.1—Three-cone bit.



Fig. 6.2—Drag bits (Torquato Drilling Accessories 2011). Reprinted with permission.

The first bits to use diamond for oilwell drilling were dubbed natural-diamond bits because they used natural diamonds as their cutting elements. These bits were first used in the 1940s and were commonly used through the 1980s. There was a significant increase of interest in the natural-diamond industry in the late 1970s, when thermally stable polycrystalline (TSP) bits and polycrystalline-diamond-compact (PDC) technology was developed. Both of these bits use small disks of synthetic diamond to provide the scraping/cutting surface (**Fig. 6.3**). The TSP bit was the first synthetic-diamond component used by the drill-bit industry and represents the evolutionary link to the modern PDC cutter, but it is tolerant of much higher temperatures than a conventional PDC bit.

By the mid-1980s, the PDC drill bit had evolved. In these years, the PDC-bit industry experimented with a wide variety of bit configurations and cutters. Both roller-cone and PDC bits underwent tremendous material and technological advances in the 1990s. Increasing reliability levels combined with more-efficient rock-shearing action have pushed PDC bits to the technological forefront.

6.2 Bit Types

Rotary drilling uses two types of drill bits: roller-cone bits and fixed-cutter bits. Roller-cone bits have one or more cones containing cutting elements, usually referred to as inserts, which rotate about the axis of the cone as the bit is rotated at the bottom of the hole. Milled-tooth (or steel-tooth) bits are typically used for drilling relatively soft formations. Tungsten-carbide-insert (TCI) bits (or button bits) are used in a wider range of formations, including the hardest and most abrasive drilling applications. Fixed-cutter bits, including PDC, impregnated, and diamond bits, can drill an extensive array of formations at various depths. All fixed-cutter bits consist of fixed blades that are integral with the body of the bit and rotate as a single unit.

6.2.1 Roller-Cone Bits. Roller-cone bits are classified as milled-tooth or insert. In milled-tooth bits, the cutting structure is milled from the steel making up the cone. In insert bits, the cutting structure is a series of inserts pressed into the cones. Roller cone bits have a large variety of tooth designs and bearing types, and are suited for a wide variety of formation types and applications.

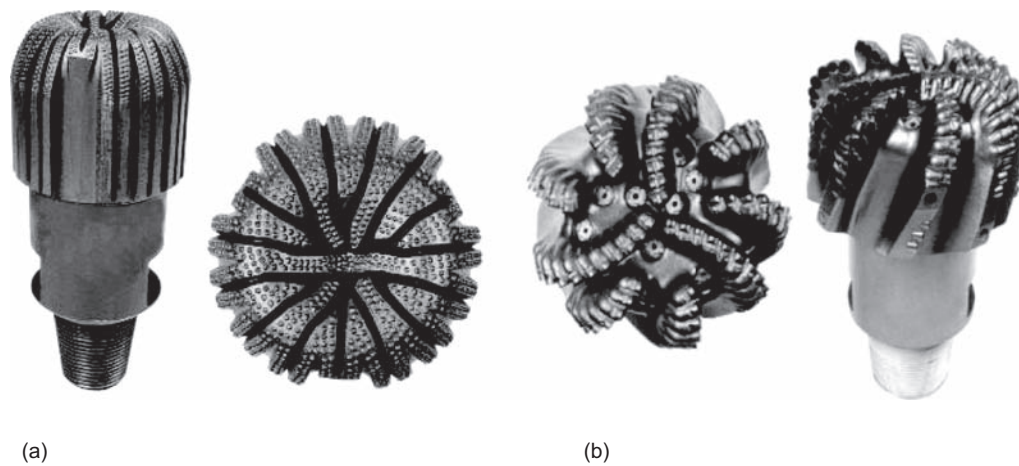


Fig. 6.3—(a) Diamond bits; (b) PDC bits (Mensa-Wilmot et al. 2006).

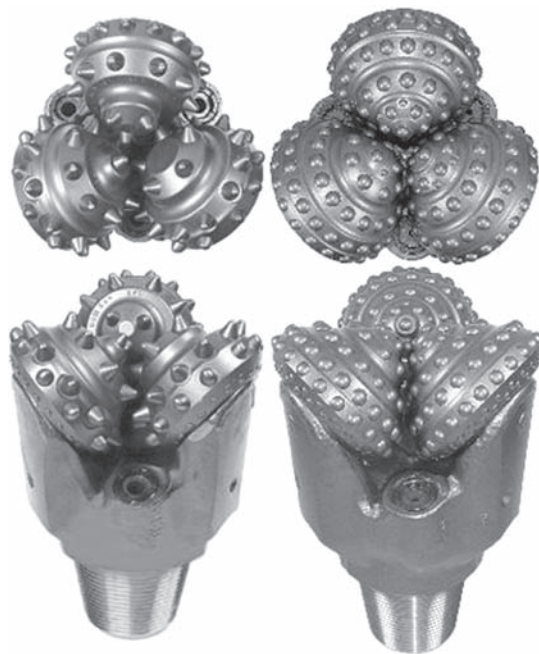


Fig. 6.4—Soft- (left) and hard- (right) formation roller-cone bits (Wamsley and Ford 2007).

The drilling action of a roller-cone bit depends to some extent on the offset of its cones. The offset of the bit is a measure of how much the cones are moved so that their axes do not intersect at a common point on the centerline of the hole. Offsetting causes the cone to stop rotating periodically as the bit is turned and scrapes the hole bottom much like a drag bit. This action tends to increase drilling speed in most formation types. However, it also promotes faster tooth wear in abrasive formations. Cone offsets vary between 0.5 and 0.375 in. for soft-formation roller-cone bits, and are usually between 0.0325 and 0.0 in. for hard-formation bits.

The shape of the bit teeth also has a large effect on the drilling action of a roller-cone bit. Long, widely spaced steel teeth are used for drilling soft formations. As the rock type becomes harder, the tooth length and the cone offset must be reduced to prevent tooth breakage. The drilling action of a bit with zero cone offset is essentially a crushing action. The smaller teeth also allow more room for the construction of stronger bearings (**Fig. 6.4**).

Because formations are not homogeneous, sizable variations exist in their drillability and this has a large impact on cutting-structure geometry. For a given WOB, wide spacing between inserts or teeth results in improved penetration and relatively higher lateral loading on the inserts or teeth. Closely spacing inserts or teeth reduces

TABLE 6.1—RELATIONSHIP BETWEEN INSERTS, TEETH, CUTTINGS-PRODUCTION RATE, HYDRAULIC REQUIREMENTS, AND THE FORMATION (Wamsley and Ford 2007)

Formation Characteristics	Insert/Tooth Spacing	Insert/Tooth Properties	Penetration and Cuttings Generation	Cleaning Flow-Rate Requirements
Soft	Wide	Long and sharp		
Medium	Relatively wide	Shorter and stubbier	Relatively high	Relatively high
High	Close	Short and rounded	Relatively low	Relatively low

loading at the expense of reduced penetration. The design of inserts and teeth themselves depends largely on the hardness and drillability of the formation. Penetration of inserts and teeth, cuttings-production rate, and hydraulic requirements are interrelated, as shown in **Table 6.1**.

The action of bit cones on a formation is of prime importance in achieving a desirable penetration rate. Soft-formation bits require a gouging/scraping action. Hard-formation bits require a chipping/crushing action. These actions are governed primarily by the degree to which the cones roll and skid. Maximum gouging/scraping (soft-formation) actions require a significant amount of skid. Conversely, a chipping/crushing (hard-formation) action requires that cone roll approach a “true roll” condition with very little skidding. For soft formations, a combination of small journal angle, large offset angle, and significant variation in cone profile is required to develop the cone action that skids more than it rolls. The journal is the load-carrying surface of the bearing on a bit, and journal angle is the angle subtended between the axis of rotation of the roller cones and a plane perpendicular to the axis of rotation of the drill bit. Hard formations require a combination of large journal angle, no offset, and minimum variation in cone profile. These will result in cone action closely approaching true roll with little skidding.

6.2.2 Fixed-Cutter Bits. In general, fixed-cutter bits are categorized under two groups: PDC bits (fail the rock through a shearing process) and diamond bits made up of impregnated, natural-diamond and TSP elements (fail the rock through a grinding process). There does exist a third category, which also fails the rock through a shearing process and which is referred to as a *tool steel-bladed bit* or a *drag bit* (Fig. 6.2); however, drag bits are rarely used in the industry today.

The major difference between fixed-cutter bits and roller-cone bits is that fixed-cutter bits do not have any moving parts, which is an advantage, especially with small hole sizes in which space is not available for the cone/bearing systems with proper teeth structure. The introduction of hardfacing to the surface of the blades and the design of fluid passageways greatly improved the performance of fixed-cutter bits. Because of the dragging/scraping action of the fixed-cutter bits, high RPM and low WOB are applied.

PDC Bits. PDC bits use small disks of synthetic diamond to provide the scraping/cutting surface. The small discs may be manufactured in any size and shape and are not sensitive to failure along cleavage planes as natural-diamond bits are. PDC bits have been run very successfully in many fields all around the world. TSP bits are manufactured similarly to PDC bits, except TSP bits can resist much higher operating temperatures than PDC bits.

One commonly used PDC bit is the dual-diameter bit. Dual-diameter bits have a unique geometry that allows them to drill and underream. To achieve this, the bits must be capable of passing through the drift diameter (i.e., the smallest inner diameter of a tubular material) of a well casing and then drilling an oversized (larger than casing diameter) hole. State-of-the-art dual-diameter bits are similar to conventional PDC drill bits in the way that they are manufactured. They typically incorporate a steel-body construction and a variety of PDC and/or diamond-enhanced cutters. They are unitary and have no moving parts (**Fig. 6.5**).

The maximum benefit of dual-diameter bits is realized in swelling or flowing formations in which the risk of sticking pipe can be reduced by drilling an oversized hole. They are commonly used in conjunction with applications requiring increased casing, cement, and gravel-pack clearance; they also can eliminate the need for extra trips and can avoid the risk of moving-part failure in mechanical underreamers in high-cost intervals.

Impregnated Bits. Impregnated-bit bodies are PDC matrix materials that are similar to those used in cutters. The working portions of impregnated bits are unique, such that they contain matrix impregnated with diamonds (**Fig. 6.6**).



Fig. 6.5—Dual-diameter PDC bit.

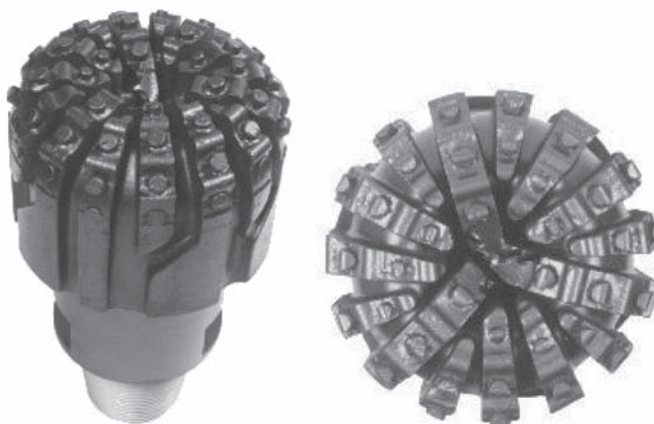


Fig. 6.6—Impregnated bit.

Both natural and synthetic diamonds are prone to breakage from impact. When embedded in a bit body, they are supported to the greatest extent possible and are less susceptible to breakage. However, because the largest diamonds are relatively small, cut depth must be small and ROP must be achieved through increased rotational speed. They are most frequently run in conjunction with turbo drills and high-speed positive-displacement motors that operate at several times normal rotational velocity for rotary drilling (500 to 1,500 rev/min). During drilling, individual diamonds in a bit are exposed at different rates. Sharp, fresh diamonds are always being exposed and placed into service (Fig. 6.7). Better bit performance and reduction in the number of required bits have been reported in abrasive and heterogeneous formations when impregnated bits with turbines are used instead of roller-cone bits and PDCs (Botelho et al. 2006).

Diamond Bits. The term “diamond bit” normally refers to bits incorporating surface-set natural diamonds as cutters. Diamond bits are used in abrasive formations. The cutting action of a diamond bit is developed by scraping away the rock. Diamond bits drill by a high-speed plowing action that breaks the cementation between rock grains. Fine cuttings are developed in low volumes per rotation. To achieve satisfactory ROPs with diamond bits, they must, accordingly, be rotated at high speeds. Despite its high wear resistance, diamond is sensitive to shocks and vibrations. Thus, caution must be taken when running a diamond bit. Effective fluid circulation across the face of the bit is also very important to prevent overheating of the diamonds and the matrix material, and to prevent bit

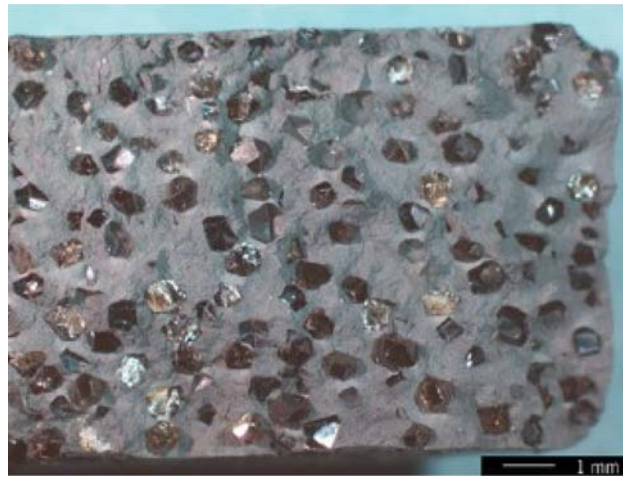


Fig. 6.7—Presentation of diamonds impregnated in a cross-sectional view of a matrix body [from Botelho et al. (2006)].



Fig. 6.8—Hybrid bit (Pessier and Damschen 2010).

balling (i.e., cuttings agglomerating on the bit). The cutting elements are typically placed among and along shallow waterways intended to provide some level of cooling and cleaning.

Diamond bits are described in terms of the profile of their crown, the size of diamond stones (stones per carat), total fluid area incorporated into the design, and fluid-course design (radial or crossflow). Diamonds do not bond with other materials. They are held in place by partial encapsulation in a matrix bit body. Diamonds are set in place on the drilling surfaces of bits (Fig. 6.3a).

6.2.3 Hybrid Bits. Significant advances have been made in PDC-cutter technology, and fixed-blade PDC bits have replaced roller-cone bits in numerous operations. However, in some applications for which the roller-cone bits are uniquely suited—such as drilling hard, abrasive and interbedded formations; complex directional-drilling applications; and, in general, applications in which the torque requirements of a conventional PDC bit exceed the capabilities of a given drilling system—the hybrid bit can substantially enhance the roller-cone bit's performance while generating a lower level of harmful dynamics compared to a conventional PDC bit.

In a hybrid bit, the intermittent crushing of a roller-cone bit is combined with the continuous shearing and scraping of a fixed-blade bit (Fig. 6.8). The central portion of the borehole is cut solely by PDC cutters on the primary blades, while the more-difficult-to-drill outer portion is being disintegrated by the combined action of the cutting elements on the rolling cutters and the fixed blades. The rolling cutters are biased toward the backside of the blades to open up a space (or junk slot) in front of the blades for the return of cuttings and the placement of nozzles (Pessier and Damschen 2010). Hydraulically activated expandable hybrid bits having tricones outside and PDC cutters inside perform successfully in hard formations (Gopalsing 2006).

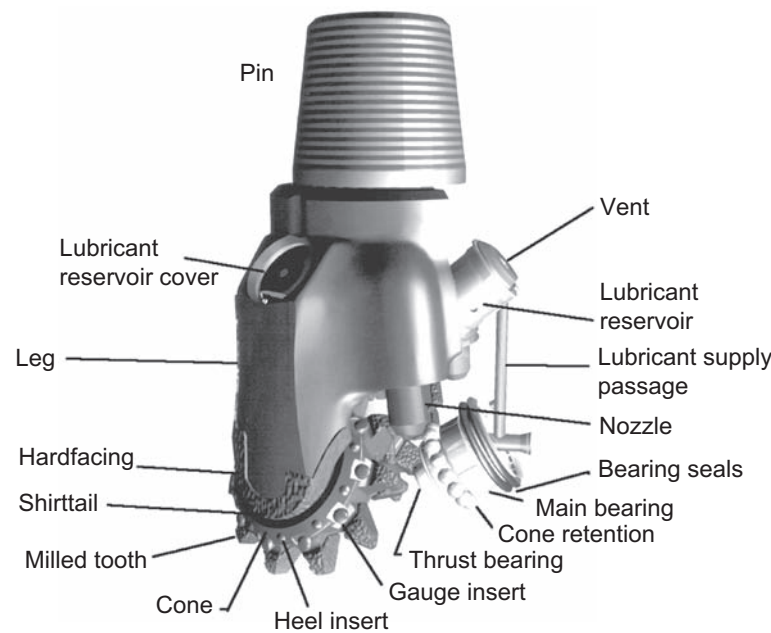


Fig. 6.9—Schematic view of a roller-cone bit (Wamsley and Ford 2007).

6.3 Manufacturing and Design of Bits

Drill-bit performance is influenced by the environment in which the bit operates. Operating choices such as applied WOB, rotary speed, and hydraulic arrangements all have important implications for the way that bits are designed and for their operating performance.

Environmental factors, such as the nature of the formation to be drilled, hole depth and direction, characteristics of drilling fluids, and the way in which a drill rig is operated, are also of critical importance in bit performance and design. Engineers consider these factors for all designs, and every design should begin with close cooperation between the designer and the drilling company to ensure that all applicable inputs contribute to the design.

6.3.1 Roller-Cone Bits. Roller-cone bits generally consist of three similar-sized cones and legs, attached together with a pin connection. Each cone is mounted on bearings. The three legs are welded together to form the cylindrical section, which develops the pin connection. The pin connection provides the connection to the drillstring.

Legs are provided with openings for fluid circulation. The size of these openings can be controlled by inserting nozzles, which provide constraints at the fluid exit in order to obtain high jetting effect for efficient bit and hole cleaning. Mud pumped through the drillstring passes through the nozzles. A schematic view of a roller-cone bit is presented in Fig. 6.9.

The drill-bit design is determined on the basis of the type of rock to be drilled and the size of the hole. Although the legs and journals are identical, the shape and distribution of cutters on the three cones differ. If the bit is a tricone bit, the design should ensure that all three legs must be equally loaded during the drilling process. The journal angle offsets between cones, bearings, and teeth are the major considerations when designing and manufacturing a tricone bit.

Basic Design Principles. Design activities are focused principally on four general areas: material selection for the bit body and cones, geometry and type of cutting structure to be used, mechanical-operating requirements, and hydraulic requirements. The dimensions of a bit at the gauge (outside diameter) and the pin (arrangement for attachment to a drillstem) are fixed, usually by industry standards, and resultant design dimensions always accommodate them.

Hardfacing materials are designed to provide wear (abrasion, erosion, and impact) resistance for the bit. To be effective, hardfacing must be resistant to loss of material by flaking, chipping, and bond failure with the bit. Hardfacing provides wear protection on the lower (shirttail) area of all roller-cone-bit legs and serves as a cutting-structure material on milled-tooth bits. Hardfacing materials containing tungsten carbide grains are the standard for protection against abrasive wear on bit surfaces. To improve the durability of the leg while increasing seal and

bearing reliability, abrasion-resistant hardfacing (**Fig. 6.10**) is incorporated onto the majority of the leg outer diameter (Buske et al. 2008).

Roller-Cone-Bit Components. The first consideration in the physical design of a roller-cone bit is the permissible bit diameter (i.e., the available space). Every element of a roller-cone bit must fit within a circle that is representative of the required well diameter. The sizes of journals, bearings, cones, and hydraulic and lubrication features are collectively governed by the circular cross section of the well. In smaller bits, assembling components are very challenging because of a shortage of space.

The cones of a roller-cone bit are mounted on journals (**Fig. 6.11**). There are three types of bearings used in these bits: roller bearings, which form the outer assembly and help to support the radial loading (or WOB); ball bearings, which resist longitudinal or thrust loads and also help to secure the cones on the journals; and friction bearing in the nose assembly, which helps to support the radial loading.



Fig. 6.10—Left = standard hardfacing; right = enhanced hardfacing (Buske et al. 2008).

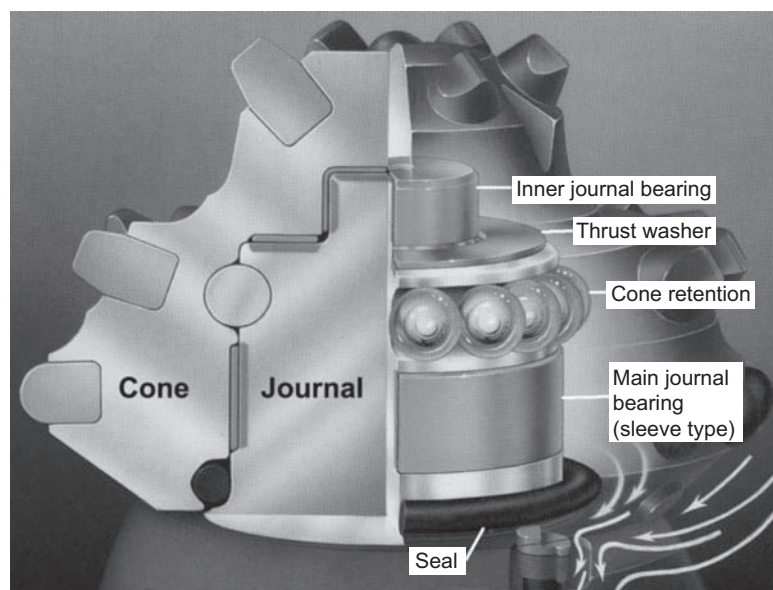


Fig. 6.11—Typical journal-bearing system (Wamsley and Ford 2007).

The bearings should be large enough to support the loads applied. The strength of the journal and cone shell should also be considered. Usually, it is expected that the bearings will not wear out before the cutters. There have been a number of developments in bearing technology used in rock bits (i.e., sealed-bearing bits in which the sealing mechanism prevents abrasive solids in the mud from entering and causing excess frictional resistance in the bearings, and journal-bearing bits in which the cones are mounted directly onto the journal).

All three cones have the same shape except for the first cone, which has a spear point. *Journal angle* describes an angle formed by a line perpendicular to the axis of a bit and the axis of the bit's leg journal (**Fig. 6.12**). Journal angle is usually the first element in a roller-cone-bit design. Because all three cones fit together, the journal angle specifies the outside contour of the bit. It optimizes bit-insert (or tooth) penetration into the formation being drilled; generally, bits with relatively small journal angles are best suited for drilling in softer formations, and those with larger angles perform best in harder formations.

To increase the skidding/gouging action, bit designers generate additional working force by offsetting the centerlines of the cones (**Fig. 6.13**). Basic cone geometry is affected directly by increases or decreases in either journal or offset angles, and a change in one of the two requires a compensating change in the other. When the cone is mounted on a journal, the cone is forced to rotate around the center of the bit. This rotational motion forces the inner-cone profile to skid and the outer-cone profile to gouge. Skidding/gouging improves penetration in soft and medium-formations at the expense of increased insert or tooth wear. In abrasive formations, offset can reduce cutting structure service life to an impractical level. Therefore, bit designers limit the use of offset so that results meet the minimum requirements for formation penetration.

Skidding of a cone is presented in **Fig. 6.14**. The bit rotates around the *bit axis* in a clockwise direction, and the cone rotates around the *cone axis* in counterclockwise direction. These rotational motions can be expressed in terms of instantaneous angular velocities W_1 and W_2 , respectively. Because velocities are vectors, instantaneous

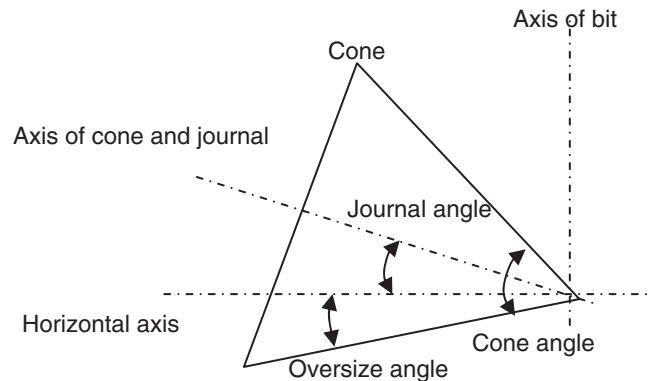


Fig. 6.12—Journal-angle alignment.

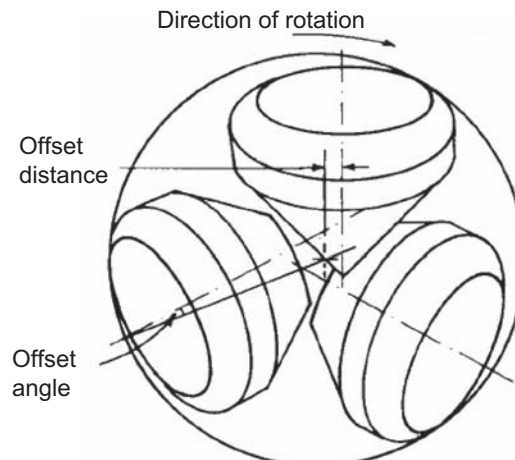


Fig. 6.13—Cone offset (Bourgoyne et al. 1991).

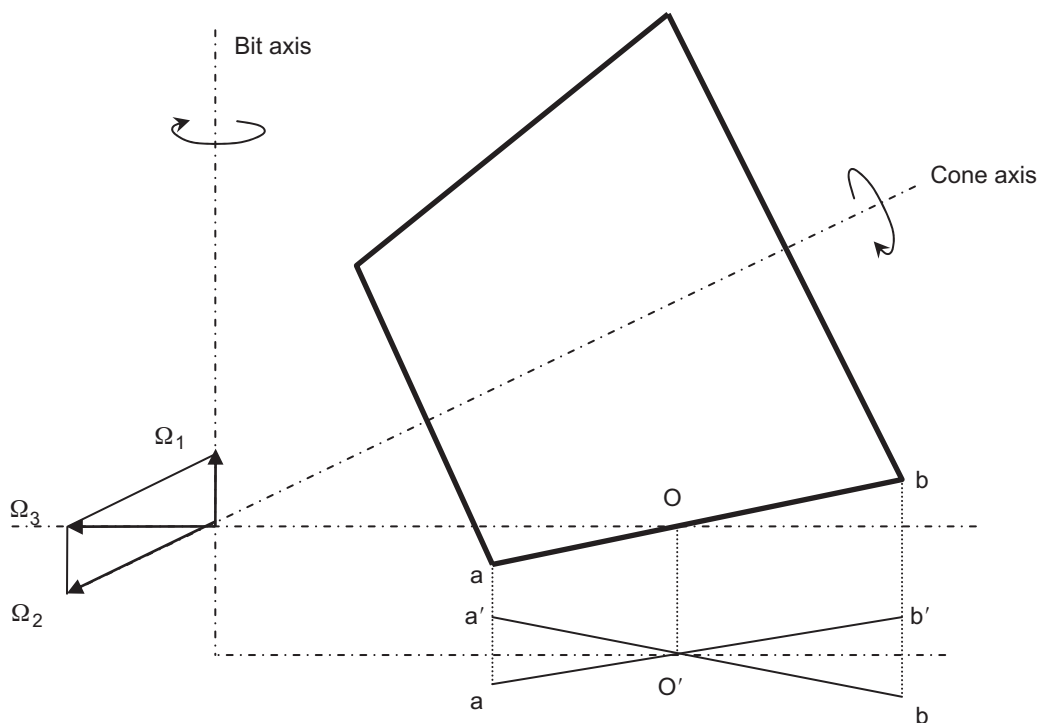


Fig. 6.14—Cone skidding.

rotation is in the direction of the resultant of these two velocities: that is, W^3 . The axis of this vector intercepts the cone at point O, which is motionless. The projection of the cone at this instant is represented by triangles a, a', O' and b, b', O'. These triangles are the grinding/crushing zone at which skidding takes place.

Tooth and insert design is governed primarily by structural requirements for the insert or tooth and formation requirements such as penetration, impact, and abrasion. With borehole diameter and knowledge of formation requirements, the designer selects structurally satisfactory cutting elements that provide an optimum insert/tooth pattern for efficient drilling of the formation. Factors that must be considered to design an efficient insert/tooth and establish an advantageous bottomhole pattern include bearing-assembly arrangement, cone-offset angle, journal angle, cone-profile angles, insert/tooth material, insert/tooth count, and insert/tooth spacing. When these requirements have been satisfied, remaining space is allocated between the insert/tooth contour and the cutting-structure geometry to best suit the formation. The TCIs/teeth designed for drilling soft formations are long and can have various geometries. The TCIs used in bits for hard formations are short and usually have a hemispherical end (Fig. 6.15). These bits are sometimes called button bits.

Drilling fluid circulates inside the drillstring and passes through the bit nozzles. After passing through the nozzles, fluid basically cleans out the face of the bit by carrying the drilled cutting into the annulus. Early bit designs allowed the fluid to leave only through the center of the bit, which was not an effective way of cleaning the cuttings from the bit face. The introduction of nozzles simply created a more efficient method of cleaning the face of the bit because fluid flows through the nozzles and goes around the outside of the bit body. The nozzles are made of tungsten carbide to prevent fluid erosion. The turbulence generated by the jet streams is enough to clean the cutters and allow efficient drilling to continue. The nozzles can be replaced easily. Also, extended nozzles may be preferred for improving the bottomhole cleaning action.

Cone-cleaning-nozzle systems perform best in bit-balling environments, and borehole-cleaning-nozzle systems perform best in bottom-balling environments. Different configurations of nozzle positioning are available for improving drilling performance (Fig. 6.16).

Special Bits. Monocone bits are potentially very advantageous for use in small-diameter systems in which bearing sizing presents significant engineering problems. Monocone bits are also attractive for ultradeep and slimhole drilling operations because of less torsion and longer bearing life (Hu and Liu 2006).

As with monocone bits, two-cone bits have available space for larger bearings and rotate at lower speeds than three-cone bits. Bearing life and seal life for a particular bit diameter are greater than those for comparable three-cone bits. Two-cone bits, although not common, are available and perform well in special applications. For example, an interest has arisen in the industry in using two-cone bits because performances show that improvements

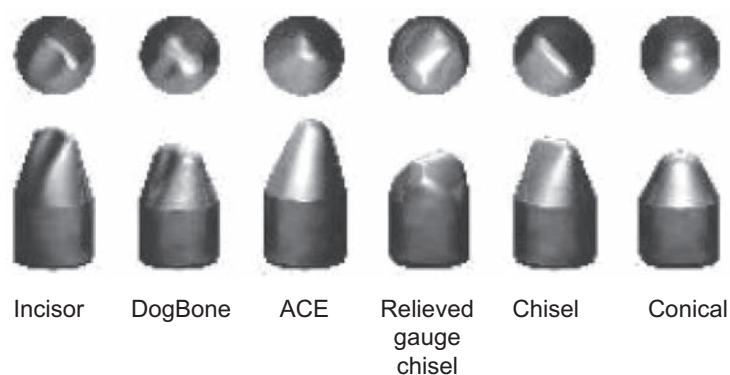


Fig. 6.15—Inserts (Smith Technologies 2005); ACE = asymmetric conical edge.

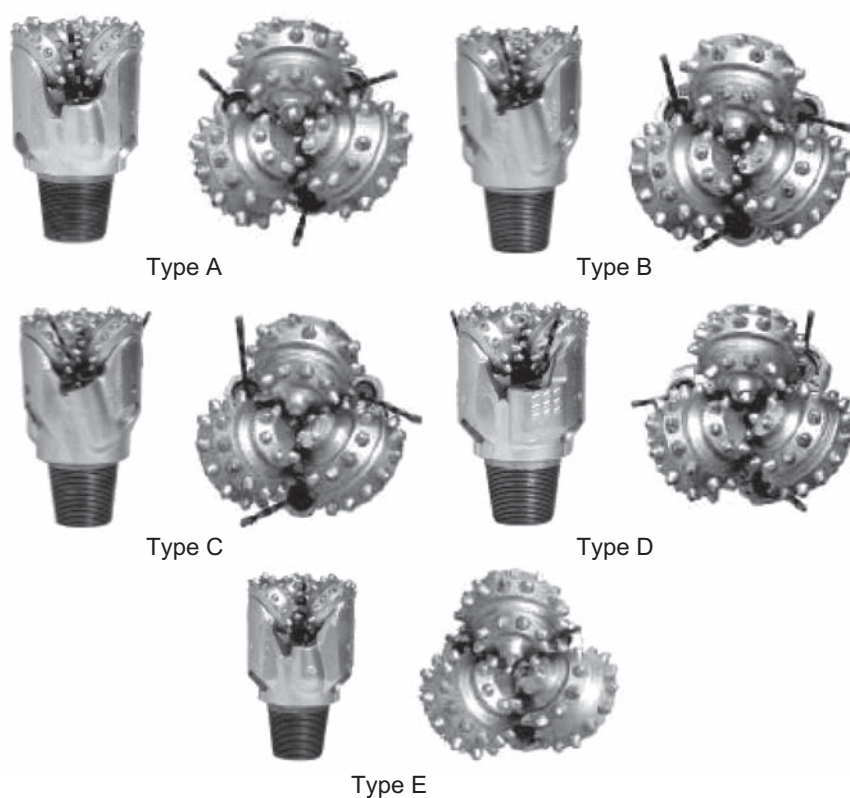


Fig. 6.16—Different nozzle systems: (Type A) the conventional nozzle; (Type B) the nozzles direct the drilling fluid such that it skims the leading edge of the gauge-cutting elements of the cone before impacting the borehole; (Type C) like Type B, but more toward the wall of the borehole; (Type D) a third-cone nozzle is positioned such that the fluid passes between the gauge-cutting surfaces and the borehole wall, on the trailing side of the cone, in the gap created by cone offset (skew angle); and (Type E) the nozzle system developed by using a high-pressure drilling simulator in conjunction with computational fluid dynamics, which maximizes cone and borehole cleaning and cuttings evacuation while minimizing cone erosion (Legderwood et al. 2000).

have been observed in vibrations, directional responsiveness, deviation-free performance, hydraulic aspects of bottomhole cleaning, and free-of-bit balling (Centala et al. 2006). Fig. 6.17 provides photographs of a monocone bit and a two-cone bit.

The cutting action of two-cone bits is similar to that of three-cone bits, but fewer inserts simultaneously contact the hole bottom. Penetration per insert is enhanced, providing particularly beneficial results in applications in which capabilities to place WOB are limited.

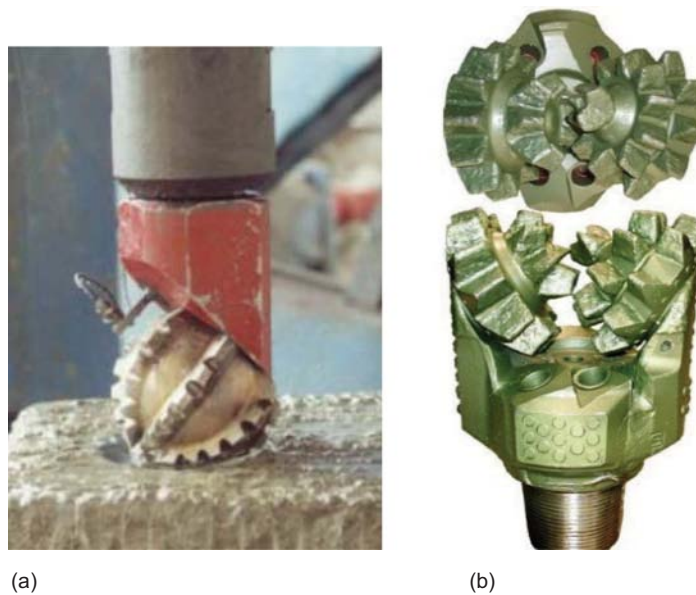


Fig. 6.17—(a) A monocone bit (Hu and Liu 2006); (b) a two-cone bit (Centala et al. 2006).

6.3.2 PDC Bits. A PDC bit has no moving parts—in other words, it has no bearings. The rock-drilling mechanism of PDC bits is shearing rather than crushing (as in roller-cone bits). Rock breakage by shear requires less energy than crushing; hence, less WOB can be applied. However, higher rotational speeds are required.

A PDC bit employs a large number of cutting elements, called PDC cutters. A PDC cutter is constructed by joining a layer of polycrystalline artificial diamond to a cemented tungsten carbide composite under high pressure and temperature. The diamond layer is usually composed of numerous small diamond particles collected together at random orientation for achieving maximum strength and wear resistance.

Basic Design Principles. The design features and constitution of fixed-cutter bits include the number and shape of the blades and the structural body type (matrix or steel) from which the bit body is formed. In addition, these bits are characterized by the shapes and sizes of their cutting elements (PDC cutters) or stones, metallurgic or material makeup, and the sizes and locations of their watercourses (Fig. 6.18).

Two of the important design features of a PDC bit are the number of cutters used and the angle of attack between the cutter and the surface of the formation being drilled. Cutter orientation and bit configuration are defined in terms of backrake, siderake, exposure, and blade height (Fig. 6.19).

Cutter exposure is the amount by which the cutters protrude from the bit body. Backrake is the angle presented by the face of the cutter to the formation and is measured from the vertical. Siderake is the measure of the orientation of the cutter from left to right.

Bit-rake angle is found to have a pronounced effect on the bit forces. The forces acting on a single bit insert increase substantially as the cut depth increases. However, on a fullscale bit, fewer bit inserts are required if each insert takes a deeper bite. Therefore, the total bit force actually may decrease if fewer inserts are employed and deep cuts are made on each bit revolution (Li et al. 1993).

In general, low backrake angles make bits more aggressive (i.e., greater ROP for a given WOB), but more prone to impact damage. High backrake angles reduce aggressiveness, but make the bits less prone to impact damage (i.e., greater resistance to cutter damage). Because of these relationships, backrake angles have to be optimized for specific bit designs and applications.

Siderake angles are classified as negative or positive on the basis of cutter/face orientation. Negative siderake improves bit stabilization but compromises bit cleaning because cuttings tend to be pushed toward the center of the bit. On the other hand, positive siderake increases cleaning efficiency but does not aid in bit stabilization. For a PDC bit, cutter exposure establishes how much a given cutter can bite into a formation before the back of the blades make contact with the formation and prevent efficient WOB use for ROP gains. Under normal conditions, increased exposure, which makes bits more aggressive, is directly dependent on cutter size (Fig. 6.20). Blade height provides room for drilled cuttings to peel off the hole bottom without possibly sticking to the bit body or packing off in front of the cutter and thus reducing ROP.

In general, aggressive bits are defined by large cutter sizes, reduced blade counts, low backrakes, high cutter exposures, and increased blade height, and they are used in soft-formation applications. On the other hand, smaller

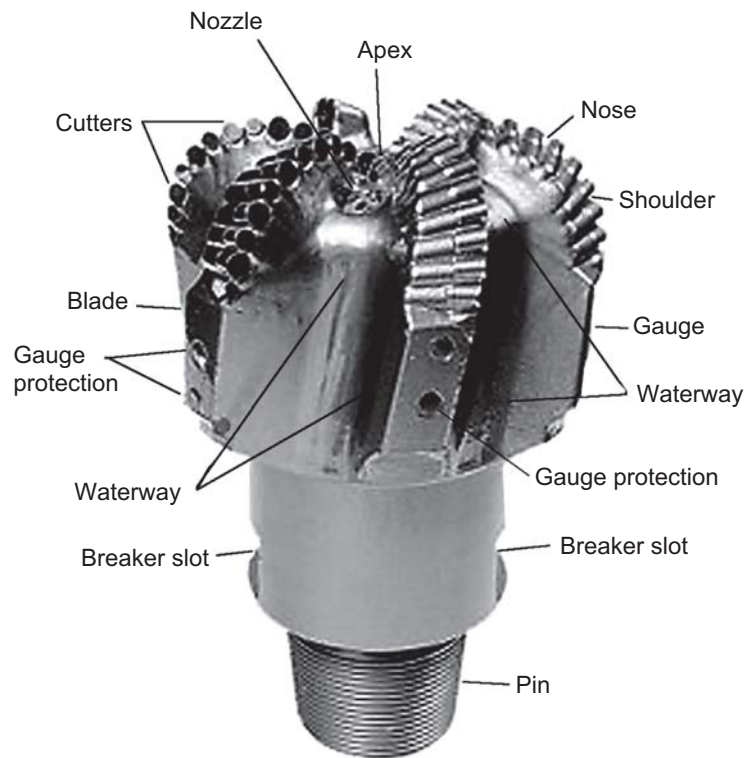


Fig. 6.18—PDC bit (Wamsley and Ford 2007).

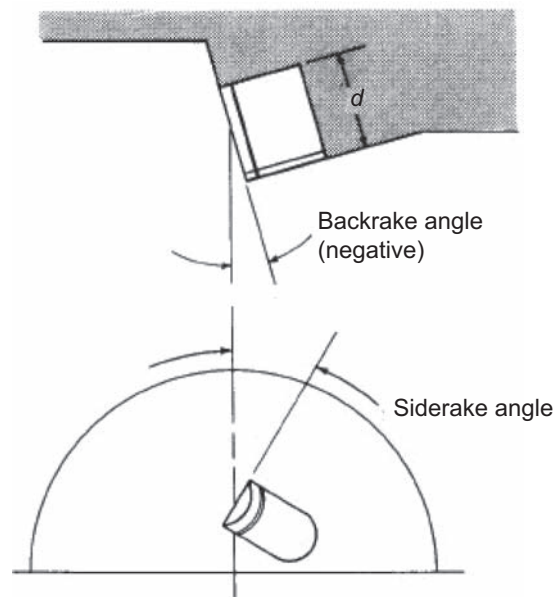


Fig. 6.19—Cutter orientation expressed in terms of exposure, backrake, and siderake (Cerkovnik 1982); d is the height of the cutter visually seen attached to the body.

cutters, high blade counts, high backrakes, reduced cutter exposures, and reduced blade height are used in hard-formation applications.

In the early 1970s, PDC bits incorporated elementary designs without waterways or carefully engineered provisions for cleaning and cooling. By the late 1980s, PDC-bit technology advanced rapidly as the result of a new understanding of bit vibrations and their influence on productivity. Today, cutting structures are recognized as the principal determinant of force balancing for bits and for ROP during drilling.



Fig. 6.20—Soft- (left), medium- (middle), and hard- (right) formation blade/cutter combinations for a PDC bit (Chevron DE Drilling Seminar 2005).

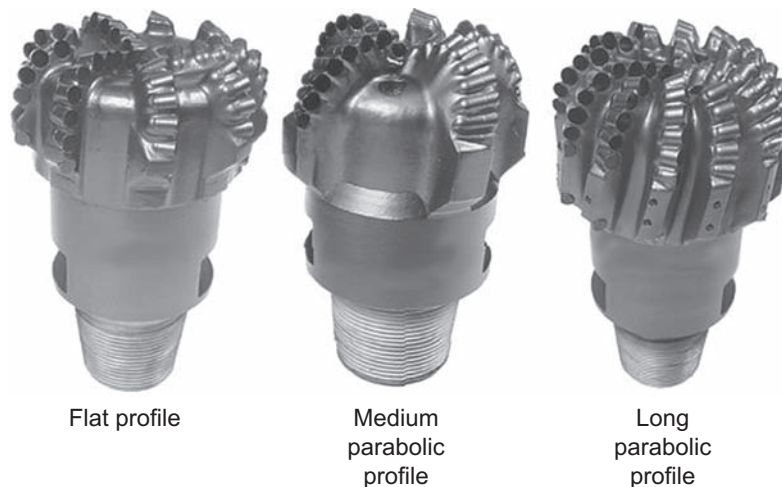


Fig. 6.21—PDC bit profiles (Wamsley and Ford 2007).

Bit Shape. Major crown profiles of PDC bits are flat or shallow cone, tapered or double cone, and parabolic. WOB is distributed homogeneously on the cutters in the flat-or shallow-cone profile. However, this type of crown profile has limited rotational stability and uneven wear. At high rotation speeds, high instantaneous loading, high temperatures, and loss of cooling to the PDC cutters may develop. The tapered- or double-cone profile allows for increased distribution of the cutters toward the outer diameter of the bit, which makes it possible to rotate the bit with greater rotational speeds, which in turn permits better directional stability and wear reduction. The largest surface-area contact and smoothest load distribution can be achieved by the parabolic profile (Fig. 6.21). It offers better rotational and directional stability. Major applications of this profile are typically on downhole motors or turbines.

The design of the watercourse pattern that is cut in the face of the bit and the junk slots that are cut in the side of the bit face controls cuttings removal and diamond cooling. Diamond bits are designed to be operated at a given flow rate and pressure drop across the face of the bit. Experiments conducted by bit manufacturers have indicated the need for approximately 2.0 to 2.5 hp/in.² of hole bottom with an approximate 500- to 1,000-psi pressure drop across the face of the bit to clean and cool the diamond adequately.

Matrix. PDC bits are designed and manufactured in two structurally dissimilar styles: matrix-body bits and steel-body bits. The two provide significantly different capabilities, and because both types have certain advantages, a choice between them would be decided by the needs of the application.

Matrix is a very hard, rather brittle composite material comprising tungsten carbide grains metallurgically bonded with a softer, tougher, metallic binder. Matrix is desirable as a bit material because its hardness is resistant to abrasion and erosion. It is capable of withstanding relatively high compressive loads but, compared to steel, has low resistance to impact loading. Steel is metallurgically the opposite of matrix. Steel is capable of withstanding high impact loads but is relatively soft and without protective features, and will quickly fail by abrasion and

erosion. This makes it possible for steel-body PDC bits to be relatively larger than matrix bits and to incorporate greater height into features such as blades. Matrix-body PDC bits are commonly preferred over steel-body bits for environments in which body erosion is likely to cause a bit to fail. For diamond-impregnated bits, only matrix-body construction can be used. Quality steels are essentially homogeneous, with structural limits that rarely surprise their users.

Cutter Design and Manufacturing. Diamond is the hardest material known. This hardness gives it superior properties for cutting over any other material. Besides their hardness, PDC diamond tables (i.e., the part of a cutter that contacts a formation) have an essential characteristic for drill-bit cutters: they efficiently bond with tungsten carbide materials that can, in turn, be brazed (attached) to bit bodies.

In terms of chemicals and properties, synthetic diamond is identical to natural diamond. Making diamond grit involves a chemically simple process: ordinary carbon is heated under extremely high pressure and temperature. In practice, however, making diamond is far from easy.

Diamond grit is less stable at high temperatures than natural diamond. Because the metallic catalyst trapped in the grit structure has a higher rate of thermal expansion than diamond, differential expansion places diamond-to-diamond bonds under shear and, if loads are high enough, causes failure. If bonds fail, diamonds are quickly lost, so the PDC cutter loses its hardness and sharpness and becomes ineffective. To prevent such failure, PDC cutters must be adequately cooled during drilling. To manufacture a diamond table, diamond grit is sintered with tungsten carbide and metallic binder to form a diamond-rich layer. The tables are wafer-like in shape, and they should be made as thick as structurally possible because diamond volume increases wear life. The highest-quality diamond tables are 2 to 4 mm, and technology advances will increase diamond-table thickness. Tungsten carbide substrates are normally 0.5 in. high and have the same cross-sectional shape and dimensions as the diamond table. The two parts—diamond table and substrate—make up a cutter as shown in **Fig. 6.22a**. PDC-cutter examples are presented in Fig. 6.22b.

The size and number of diamonds used in a diamond bit depend on the hardness of the formation to be drilled. Bits for hard formations have many small (0.07- to 0.125-carat) stones, while bits for soft formations have a few large (0.75- to 2-carat) stones.

Combining advanced PDC-bit designs with state-of-the-art cutter technology has opened up many new applications for PDC bits that, in the past, were appropriate only for International Association of Drilling Contractors (IADC) Series 6, 7, and 8 insert drill bits. Because of this improvement, the PDC bit has become an alternative for drilling hard-rock formations, providing a significant reduction in cost per foot (Schell et al. 2003; Mensa-Wilmot et al. 2003). An advanced series of PDC drill bits incorporating a new highly abrasion-resistant PDC cutter has extended effective PDC-bit application to hard-rock drilling. Bit design has been conducted by considering the optimization of axial, lateral, and torsional forces acting on the bit and by improving cutter thermal resistance (Clayton et al. 2005). New cutting-material developments are at the forefront of the ongoing improvement of PDC bits. A new-generation thermostable cutter is a significant development that shows a step change in cutter and bit performance (Clegg 2006).

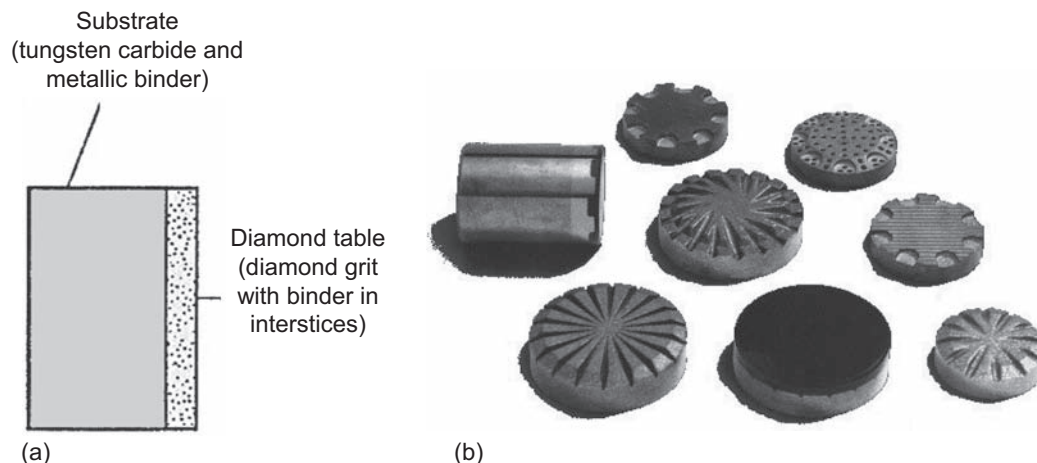


Fig. 6.22—(a) PDC-cutter construction (Wamsley and Ford 2007); (b) example PDC cutters (Chevron DE Drilling Seminar 2005).

		Design Features									
Series	Formations	Types	Standard Roller Bearing	Roller Bearing, Air	Roller Bearing, Gage Protected	Sealed Roller Bearing	Sealed Roller Bearing, Gage Protected	Sealed Friction Bearing	Sealed Friction Bearing, Gage Protected	Directional	Other
			(1)	(2)	(3)	(4)	(5)	(6)	(7)	(8)	(9)
Milled-Tooth Bits	1	Soft formations with low compressive strength and high drillability	1								
			2								
			3								
			4								
	2	Medium to medium-hard formations with high compressive strength	1								
			2								
			3								
			4								
	3	Hard semi-abrasive and abrasive formations	1								
			2								
			3								
			4								
Insert Bits	4	Soft formations with low compressive strength and high drillability	1								
			2								
			3								
			4								
	5	Soft to medium formations with low compressive strength	1								
			2								
			3								
			4								
	6	Medium-hard formations with high compressive strength	1								
			2								
			3								
			4								
	7	Hard semi-abrasive and abrasive formations	1								
			2								
			3								
			4								
	8	Extremely hard and abrasive formations	1								
			2								
			3								
			4								

Fig. 6.23—IADC classification for roller-cone bits [after McGehee et al. (1992)].

6.4 IADC Bit-Classification System

The IADC has developed a system of comparison charts for classifying drill bits according to their design characteristics and their application. There exists a classification system for roller-cone bits and one for fixed-cutter bits.

6.4.1 Roller-Cone-Bit Classification. The IADC roller-cone-bit classification method is an industrywide standard for the description of milled-tooth and insert-type roller-cone bits (Winters et al. 1987). This coding system is based on key design and application-related criteria. The currently used version was introduced in 1992 and incorporates criteria cooperatively developed by drill-bit manufacturers under the auspices of SPE (Fig. 6.23) (McGehee et al. 1992).

The IADC classification system is a four-character design and application-related code. The first three characters are always numeric, and the last character is always alphabetic. The first digit refers to bit series, the second to bit type, the third to bearings and gauge arrangement, and the fourth (alphabetic) character to bit features.

Series, the first character in the IADC system, defines general formation characteristics and divides milled-tooth and insert-type bits. Eight series or categories are used to describe roller-cone rock bits. Series 1 through 3 apply to milled-tooth bits; Series 4 through 8 apply to insert-type bits. The higher the series number, the harder or more abrasive the rock type is. Series 1 represents the softest (easiest) drilling applications for milled-tooth bits; Series 3 represents the hardest and most abrasive applications for milled-tooth bits. Series 4 represents the softest (easiest drilling applications) for insert-type bits, and Series 8 represents very hard and abrasive applications for insert-type bits.

Unfortunately, rock hardness is not clearly defined by the IADC system. The meanings of *soft*, *medium*, or *hard* are subjective and open to a degree of interpretation. The rock types within each category can be described as follows:

- Soft formations are unconsolidated clays and sands, those that can be drilled with a relatively low WOB (3,000–5,000 lbf/in.) and high RPM (125–250 rev/min). High ROPs are expected. Recommended flow rates are 500–800 gal/min to clean the hole effectively, but such rates may cause washouts.

- Medium formations may include shales, gypsum, sand, and siltstone. Usually, a low WOB is sufficient (3,000–6,000 lbf/in.). Medium-rate rotation speeds are recommended (100–150 rev/min). High flow rates are recommended for efficient hole cleaning.
- Hard formations, such as limestone, anhydrite, hard sandstone, and dolomite, have high compressive strength and contain abrasive materials. High WOBs (6,000–10,000 lbf/in.) and lower rotary speeds (40–100 rev/min) are recommended. Hard layers of quartzite or chert are best drilled with insert or diamond bits with higher RPM and lower WOB values. Flow rates are not as critical as in relatively softer formations.

The second character in the IADC categorization system represents bit type—insert or milled tooth—and describes a degree of formation hardness. Types range from 1 through 4.

The third IADC character defines both bearing design and gauge protection. IADC defined nine categories of bearing design and gauge protection:

1. Nonsealed roller bearing (also known as open-bearing bits)
2. Air-cooled roller bearing (designed for air-, foam-, or mist-drilling applications)
3. Nonsealed roller bearing, gauge protected
4. Sealed roller bearing
5. Sealed roller bearing, gauge protected
6. Sealed friction bearing
7. Sealed friction bearing, gauge protected
8. Directional
9. Other

Note that “gauge protected” indicates only that a bit has some feature that protects or enhances bit gauge. It does not specify the nature of the feature. For example, it could indicate special inserts positioned in the heel row location (side of the cone) or diamond-enhanced inserts on the gauge row.

The fourth character used in the system defines features available. IADC considers this category optional. This alphabetic character is not always recorded on bit records but is commonly used within bit manufacturers’ catalogs and brochures. IADC categorization assigns and defines 16 identifying features, as shown in **Table 6.2**.

Only one alphabetic feature character can be used under IADC rules. Bit designs, however, often combine several of these features. In these cases, the most significant feature is usually listed only.

**TABLE 6.2—ADDITIONAL FEATURES
AVAILABLE [after McGehee et al. (1992)]**

A	Air application
B	Special bearing seal
C	Center jet
D	Deviation control
E	Extended reach
F	
G	Extra gauge/body protection
H	Horizontal/steering application
I	
J	Jet deflection
K	
L	Lug pads
M	Motor application
N	
O	
P	
Q	
R	
S	Standard steel tooth model
T	Two-cone bits
U	
V	
W	Enhanced cuttings structure
X	Chisel insert
Y	Conical insert
Z	Other insert shape

Example 6.1 Considering a roller-cone bit, what does “6-3-5-E” stand for?

Solution. “6” shows that the bit is an insert bit for a medium-hard formation. “3” means that the formation should be considered more hard than medium. “5” indicates the category “sealed roller bearing, gauge protected”. Finally, “E” refers to the special feature “extended nozzles.”

6.4.2 Fixed-Cutter-Bit Classification. A large variety of fixed-cutter bit designs are available from several manufacturers. The IADC approved a standard classification system similar to the roller-cone classification system for identifying fixed-cutter bits available from various manufacturers based on a four-character coding system (Winters and Doiron 1987) (**Fig. 6.24**). In 1987, Winters and Doiron introduced another four-character code classification system describing seven bit features.

The first character of the fixed-cutter-classification code describes the primary cutter type and body material (**Fig. 6.25**). Five letters are currently defined:

- D—natural diamond/matrix body
- M—PDC/matrix body
- S—PDC/steel body
- T—TSP/matrix body
- O—other

The distinction of primary cutter types is made because fixed-cutter bits often contain a variety of diamond materials. Typically, one type of diamond is used as the primary cutting element while another type is used as backup material.

Formation	IADC Series Number	Bit Type		Design Feature							
		Drill bit	Step Type	Long Taper	Short Taper	Nontaper	Downhole Motor	Sidetrack	Oil Base	Core Ejector	Other
		Core bit	Conventional Core Barrel	Face Discharge							
			1	2	3	4	5	6	7	8	9
Soft	1	0									
		1									
		2									
		3									
		4									
Medium Soft	2	0									
		1									
		2									
		3									
		4									
Medium	3	0									
		1									
		2									
		3									
		4									
Medium Hard	4	0									
		1									
		2									
		3									
		4									
Hard	5	0									
		1									
		2									
		3									
		4									
Very Hard	6	0									
		1									
		2									
		3									
		4									
Soft	7	0									
		1									
		2									
		3									
		4									
Medium	8	0									
		1									
		2									
		3									
		4									
Hard	9	0									
		1									
		2									
		3									
		4									

Fig. 6.24—IADC classification for PDC and diamond bits [after Bourgoyne et al. (1991) and Winters and Doiron (1987)].

Four-Character Classification Code

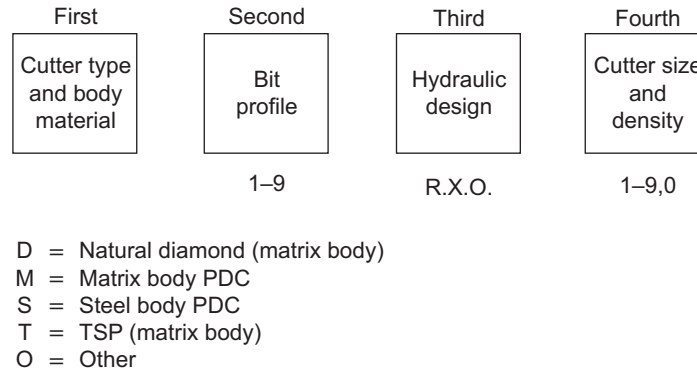


Fig. 6.25—IADC fixed-cutter-bit classification; first character detail [after Winters and Doiron (1987)].

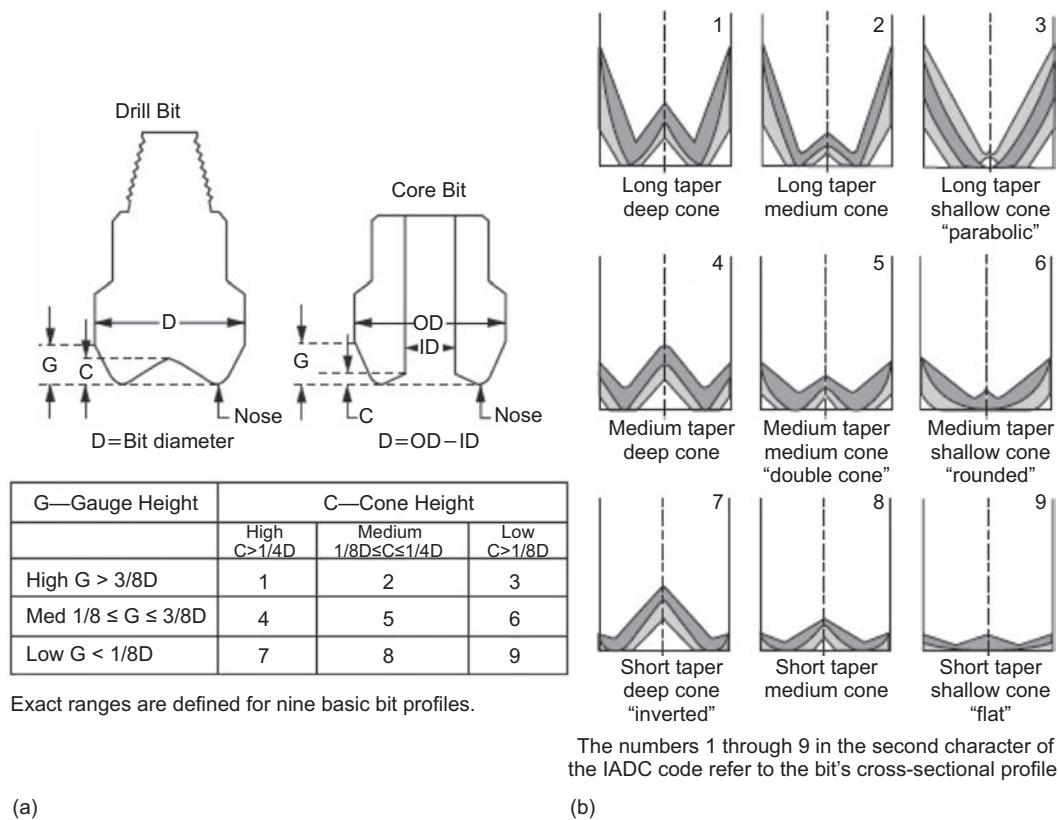


Fig. 6.26—IADC fixed-cutter-bit classification, second character. (a) Bit profile codes; (b) bit profiles [after Winters and Doiron (1987)].

The numbers 1 through 9 in the second character of the fixed-cutter-classification code refer to the bit's cross-sectional profile (**Fig. 6.26**). The term *profile* is used here to describe the cross section of the cutter/bottomhole pattern. This distinction is made because the cutter/bottomhole profile is not necessarily identical to the bit-body profile. Nine basic bit profiles are defined by arranging two profile parameters—outer taper (gauge height) and inner concavity (cone height)—in a 3×3 matrix. The rows and columns of the matrix are assigned high, medium, and low values for each parameter. Gauge height systematically decreases from top to bottom. Cone height systematically decreases from left to right. Each profile is assigned a number. Two versions of the profile matrix are presented. One version (Fig. 6.26a) is primarily for the use of manufacturers

in classifying their bit profiles. Precise ranges of high, medium, and low values are given. These criteria have been selected carefully to provide functional divisions between the numerous popular bit designs. In Fig. 6.26a, gauge-height and cone-height dimensions are normalized to a reference dimension that is taken to be the bit diameter for drill bits and the difference between outer and inner diameters for core bits. Fig. 6.26b provides a visual reference, which is better suited for use by field personnel. Bold lines are drawn as examples of typical bit profiles in each category. Cross-hatched areas represent the range of variation for each category. Each of the nine profiles is given a name. For example, “double cone” is the term used to describe the profile in the center of the matrix (Code 5). The double-cone profile is typical of many natural-diamond and TSP bits. The number 0 is used for unusual bit profiles that cannot be described by the 3×3 matrix of Fig. 6.26a. For example, a *bicenter* bit that has an asymmetrical profile with respect to the bit pin centerline should be classified with the numeral 0.

The numbers 1 through 9 in the third character of the fixed-cutter-classification code refer to the hydraulic design of the bit (**Fig. 6.27**). The hydraulic design is described by two components: the type of fluid outlet and the flow distribution. A 3×3 matrix of orifice types and flow distributions defines nine numeric hydraulic-design codes. The orifice type varies from changeable jets to fixed ports to open throat from left to right in the matrix. The flow distribution varies from bladed to ribbed to open faced from top to bottom. Usually, there is a close correlation between the flow distribution and the cutter arrangement. The term *bladed* refers to raised, continuous-flow restrictions with a standoff distance from the bit body of more than 1.0 in. The term *ribbed* refers to raised continuous-flow restrictions or standoff distance from the bit body of 1.0 in. or less. The term *open faced* refers to nonrestricted flow arrangements. Open-face flow designs generally have a more even distribution of cutters over the bit face than the bladed or ribbed designs. A special case is defined: the numbers 6 and 9 describe the crowfoot/water-course design of most natural-diamond and many TSP bits. Such designs are further described as having either radial flow, cross-flow (feeder/collector), or other hydraulics. Thus, the letters R (radial flow), X (crossflow), or O (other) are used as the hydraulic design code for such bits.

The numbers 1 through 9 and 0 in the fourth character of the fixed-cutter-classification code refer to the cutter size and placement density on the bit (**Fig. 6.28**). A 3×3 matrix of cutter sizes and placement densities defines nine numeric codes. The placement density varies from light to medium to heavy from left to right in the matrix. The cutter size varies from large to medium to small from top to bottom. The ultimate combination of small cutters set in a high-density pattern is the impregnated bit, designated by the number 0. Cutter-size ranges are defined for natural diamonds on the basis of the number of stones per carat. PDC- and TSP-cutter sizes are defined on the basis of the amount of usable cutter height. Usable cutter height rather than total cutter height is the functional measure because various anchoring and attachment methods affect the “exposure” of the cutting structure. The most common type of PDC cutters, which have a diameter that is slightly more than 0.5 in., were taken as the basis for defining medium-sized synthetic-diamond cutters. Cutter-density ranges are not explicitly defined. The appropriate designation is left to the judgment of the manufacturer. In many cases, manufacturers build *light-set* and *heavy-set* versions of a standard product. These can be distinguished by use of the light, medium, or heavy designation which is encoded in the fourth character of the IADC fixed-cutter-bit code. As a general guide, bits with minimal cutter redundancy are classified as having light placement density, and those with high cutter redundancy are classified as having heavy placement density.

	Changeable jets	Fixed port	Open throat
Bladed	1	2	3
Ribbed	4	5	6
Open faced	7	8	9

Alternative codes

R—Radial flow

X—Cross flow

O—Other

The numbers 1 through 9 in the third character of the IADC code refer to the bit's hydraulic design. The letters R, X, and O apply to some types of open-throat bits.

Fig. 6.27—IADC fixed-cutter-bit classification, third character—hydraulic design [after Winters and Doiron (1987)].

Size	Density		
	Light	Medium	Heavy
Large	1	2	3
Medium	4	5	6
Small	7	8	9

O—Impregnated

Cutter size ranges	Natural diamonds stones/carat	Natural diamonds usable cutter height
Large	<3	> $\frac{5}{8}$ in.
Medium	3–7	$\frac{3}{8}$ – $\frac{5}{8}$ in.
Small	>7	$\frac{3}{8}$ in.

- Notes: 1 Cutter density is determined by the manufacturer.
 2 The numbers 1 through 9 and 0 in the fourth character of the IADC code refer to the cutter size and placement density on the bit.

Fig. 6.28—IADC fixed-cutter-bit classification, fourth character—cutter size and density [after Winters and Doiron (1987)].

TABLE 6.3—IADC DULL-GRADING CATEGORIES (Wamsley and Ford 2007)							
T (Cutting Structure)				B	G	Remarks	
1	2	3	4	5	6	7	8
Inner Rows (I)	Outer Rows (O)	Dull Characteristic (D)	Location (L)	Bearing Seal (B)	Gauge $\frac{1}{16}$ (G)	Other Dull (O)	Reason Pulled (R)

Example 6.2 Considering a PDC bit, what does “M-5-4-5” stand for according to the classification system introduced by Winters and Doiron (1987)?

Solution. “M” indicates matrix body, “5” shows that the PDC has a double-cone profile, “4” states that the hydraulic design is ribbed with changeable jets, and “5” refers to medium size cutters with medium cutter density

6.5 IADC Bit Dull-Grading System

The IADC, in conjunction with SPE, has established a systematic method for communication of bit failures. The intent of the system is to facilitate and accelerate product and operational development based on accurate recording of bit experiences. This system is called dull grading. The IADC dull-grading protocol evaluates eight roller-cone- or seven PDC-bit areas, provides a mechanism for systematically evaluating the reasons for removal of a bit from service, and establishes a uniform method for reporting (Brandon et al. 1992; McGehee et al. 1992).

Partly because of dull analyses, bit-design processes and product operating efficiencies evolve rapidly. Engineers identify successful design features that can be reapplied and unsuccessful features that must be corrected or abandoned, manufacturing units receive feedback on product quality, sales personnel migrate performance gains and avoid duplication of mistakes between similar applications, and so forth. All bit manufacturers require collection of dull information for every bit run.

IADC dull grading is closely associated with its bit-classification systems, and the general formats for fixed-cutter- and roller-cone-bit dull grading are similar. There are important differences that must be taken into account, however, and the two approaches are not interchangeable. IADC dull grading reviews four general bit-wear categories: cutting structure (T), bearings and seals (B), gauge (G), and remarks. These categories and their subdivisions are outlined in **Table 6.3**.

6.5.1 Cutting Structure (T). For dull-grading purposes, cutting structures are subdivided into four subcategories: inner rows, outer rows, major dull characteristic of the cutting structure, and location on bit face where the major dull characteristic occurs.

Dull grading begins with evaluation of wear on the inner rows of inserts/teeth (i.e., with the cutting elements not touching the wall of the hole). Outer rows of inserts/teeth are those that touch the wall of the hole. Grading involves measurement of combined inner-row structure reduction and outer-row teeth/insert structure reduction caused by loss, wear, and/or breakage.

Measurement of roller-cone-bit cutting-structure condition requires evaluation of bit tooth/insert wear status. The tooth or cutter wear on all bits is graded in terms of the fractional tooth height that has been worn away. Wear is reported by use of an eight-increment wear scale in which no wear is represented by 0 and completely worn (100%) is represented by 8 (**Fig. 6.29**). For example, if half the original tooth or cutter height has been worn away, the bit will be graded as a T4 (i.e., the teeth are $\frac{1}{2}$, or 50%, worn).

PDC-bit-cutter wear is graded with a 0-to-8 scale in which 0 represents no wear and 8 indicates that no usable cutting surface remains (**Fig. 6.30**). PDC-bit-cutter wear is measured across the diamond table, regardless of the cutter shape, size, type, or exposure. The location of cutter wear is categorized as either the inner two-thirds or outer one-third of the bit radius (**Fig. 6.31**).

For both PDC and surface-set diamond bits, a value is given to cutter wear, as discussed. To obtain average wear for the inner rows of cutters depicted in **Fig. 6.31**, the six included cutters must be individually graded, summed as a group, and averaged to obtain the inner-row wear grade, $(a + b + c + d + e + f)/6$. This analysis is repeated for each blade, and blade results are summed and averaged for the final result. A similar analysis is made for the seven cutters used in the outer bit rows, and the two results are recorded in the first two spaces of the dull grading form.

The cutting-structure dull characteristic (D) is the observed characteristic most likely to limit further use of the bit in the intended application. A two-letter code is used to indicate the major dull characteristics of the cutting structure.

The primary cutter dull characteristic, the third cutting-structure subcategory, is recorded in the third space on the dull-grading record. (Note that noncutting structure or “other” dull characteristics that a bit might exhibit are noted in the seventh grading category.) Category 3 defines only primary cutter wear, whereas Category 7 can be used to describe either secondary cutting-structure wear or wear characteristics that relate to the bit as a whole and are unrelated to cutting structure. Grading codes for the other-dull-characteristics category are the same as those listed in **Table 6.4**.

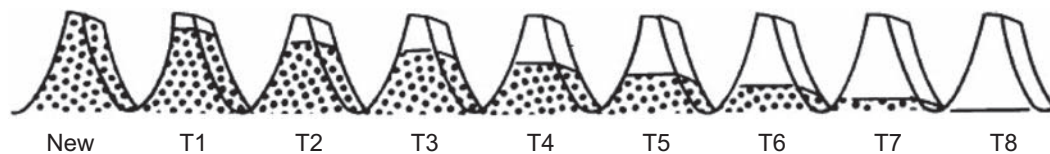


Fig. 6.29—Roller-cone teeth-wear schematic view (0–8 grading) (Bourgoyne et al. 1991).

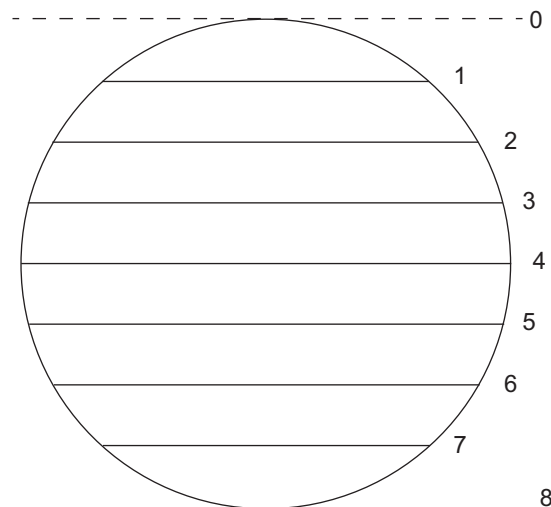


Fig. 6.30—PDC teeth-wear schematic view (0–8 grading) (Wamsley and Ford 2007).

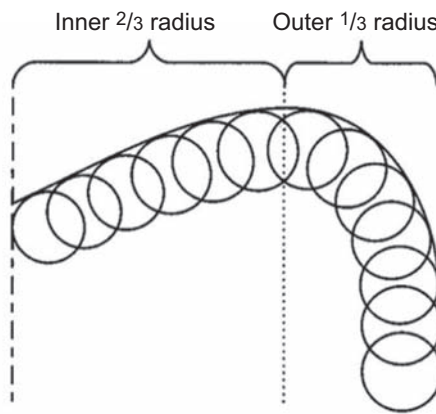


Fig. 6.31—Inner- and outer-body designation for PDC and impregnated bits (Wamsley and Ford 2007).

TABLE 6.4—DULL CHARACTERISTICS (Wamsley and Ford 2007)	
BC	Broken cone
BF	Bond failure
BT	Broken teeth
BU	Balled-up bit
CC	Cracked cone
CD	Cone dragged
CI	Cone interference
CR	Cored
CT	Chipped teeth/cutter
ER	Erosion
FC	Flat crested wear
HC	Heat checking
JD	Junk damage
LC	Lost cone
LN	Lost nozzle
LT	Lost teeth
NR	Not rerunnable (fixed cutter)
OC	Off-center wear
PB	Pinched bit
PN	Plugged nozzle/flow package
RG	Rounded gauge
RO	Ring out
RR	Rerunnable (fixed cutter)
SD	Shirttail damage
SS	Self-sharpening wear
TR	Tracking
WO	Washed-out bit
WT	Worn teeth/cutters
NO	No dull characteristics

The letter codes used to indicate the location of the wear or failure (L) that necessitated removal of the bit from service are listed in **Table 6.5**.

6.5.2 Bearings and Seals (B). Detailed field evaluation of exact bearing wear is very difficult. The bit would have to be disassembled to examine the condition of the bearings and journals. A field evaluation of the dull bit generally will reveal only whether the bearings have failed or are still intact. Bearing failure usually results in one or more *locked* cones that will no longer rotate or in one or more extremely loose cones in which the bearings have become exposed.

TABLE 6.5—DULL LOCATION (Wamsley and Ford 2007)

	Roller Cone		Fixed Cutter
N	Nose row	C	Cone
M	Middle row	N	Nose
G	Gauge row	T	Taper
A	All rows	S	Shoulder
1	Cone no. 1	G	Gauge
2	Cone no. 2	A	All areas/rows
3	Cone no. 3	M	Middle row
		H	Heel row

TABLE 6.6—SEAL/BEARING-EVALUATION CHECKLIST (Wamsley and Ford 2007)

Evaluation/Description	Acceptable Condition
Ability to rotate cone	Rotates normally
Cone springback	Springback exists
Seal squeak	Seal squeak exists
Internal sounds	No internal noises exist
Weeping grease	No lubricant leaks exist
Shale packing	If packing exists, remove before measuring
Gaps at the back face or throat	No bearing gaps exist
Inner or outer bearing letdown	No bearing letdown exists

IADC provides separate protocols for the estimation of bearing and seal wear in nonsealed- and sealed-bearing assemblies. Seal and bearing grading applies only to roller-cone bits. It is always marked X for PDC bits.

A checklist for the seal-and-bearing-system condition is provided in **Table 6.6**. If no seal problems are encountered, use the grading code “E.” If any component in the assembly has failed, use the grading code “F.” If any portion of the bearing is exposed or missing, it is considered an ineffective assembly; again, use the grading code “F.” Use the grading code “N” if it is not possible to determine the condition of both the seal and the bearing. Grade each seal-and-bearing assembly separately by cone number. If grading all assemblies as one, report the worst case.

When bearing wear cannot be detected, it usually is estimated on the basis of the number of hours of bearing life that the drilling engineer thinks the bearings might last. Linear bearing wear with time is assumed in this estimate of bearing life. A bearing-grading chart such as the one shown in **Fig. 6.32** frequently is used in determining the proper bearing-wear code.

6.5.3 Gauge (G). The gauge category of the dull-bit-grading system is used to report an undergauge condition for cutting elements intended to touch the wall of the hole. Gauge is measured with an American Petroleum Institute (API) specified ring gauge.

When the bit wears excessively in the base area of the rolling cones, the bit will drill an undersized hole. Excessive wear on a PDC bit in the shoulder area, and specifically when this wear progresses onto the gauge cutters and gauge pads, will make the bit produce an undergauge hole. Excessive wear on the heel row, gauge row, and shirt-tail area of the insert bit will also produce an undergauge hole. This wear mechanism will typically generate higher than usual drilling torque and may produce a cyclic torque response. In addition, the next bit run may be affected adversely because of the undersized hole created, or—to avoid this—an additional run for reaming may be required.

For three-cone bits, the *two-thirds rule* is applied to measuring the gauge condition. The amount out of gauge, as measured by the ring gauge, is multiplied by two-thirds to give the true gauge condition.

Measurements are taken at either the gauge or heel cutting elements, whichever is closer to the gauge. A ring gauge and a ruler or feeler gauge (shown in **Fig. 6.33**) must be used to measure the amount of gauge wear on a roller-cone bit. Undergauge increments of $\frac{1}{16}$ in. are reported. If a bit is $\frac{1}{16}$ in. undergauge, the gauge report is 1. If

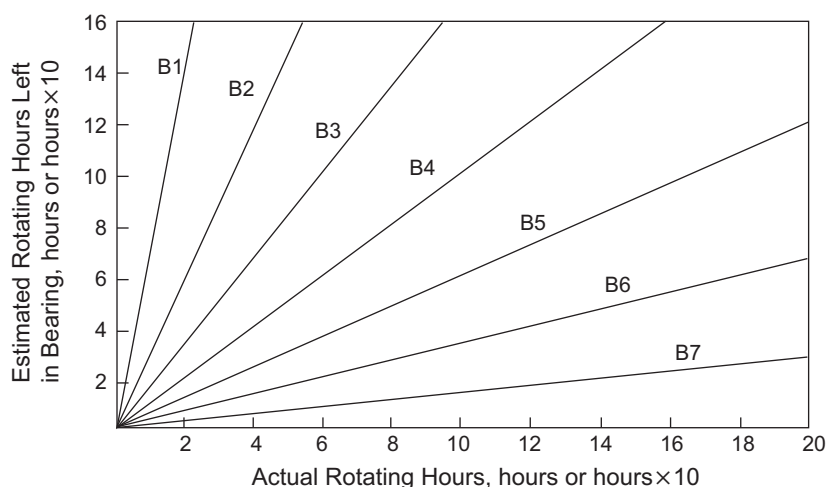


Fig. 6.32—Bearing-grading guide based on a linear scale of 0 to 8 (Bourgoyne et al. 1991).

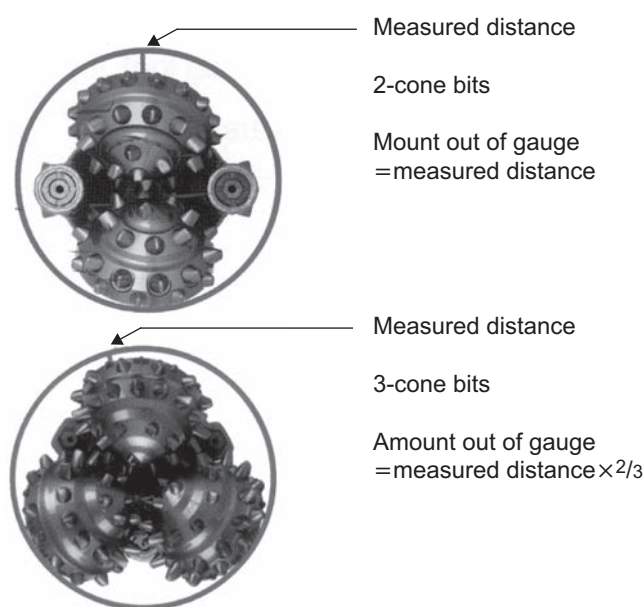


Fig. 6.33—Ring gauge and ruler for measurement of gauge wear (Wamsley and Ford 2007).

a bit is $\frac{1}{8}$ in. ($\frac{2}{16}$ in.) undergauge, the gauge report is 2. If a bit is $\frac{1}{16}$ in. undergauge, the gauge report is 3, and so forth. Round to the nearest $\frac{1}{16}$ -in. Gauge rules apply to cutting-structure elements only.

For diamond and PDC bits, gauge is measured with a nominal ring gauge. Use of an “T” code indicates that the bit remains in gauge. Undergauge increments of $\frac{1}{16}$ in. are reported. If a bit is $\frac{1}{16}$ in. undergauge, the gauge report is 1. If a bit is $\frac{1}{8}$ in. undergauge, the gauge report is 2, and so forth. Round to nearest $\frac{1}{16}$ in. Gauge rules apply to cutting-structure elements only. Measurements are taken at the gauge cutting elements.

6.5.4 Remarks. The “remarks” category allows explanation of dull characteristics that do not correctly fit into other categories and is the category in which the reason a bit was removed from service is recorded.

Other dull characteristics (O) can be used to report dull characteristics other than those reported under cutting-structure dull characteristics (D). Evidence of secondary bit wear is reported in the seventh grading category (O). Such evidence could relate to cutting-structure wear, as recorded in the third space, or may report identifiable wear, such as erosion, for the bit as a whole. The secondary dull characteristic often identifies the cause of the dull characteristic noted in the third space.

The eighth dull-grading category reports the reason that a bit was pulled (R). **Table 6.7** is the list of codes for (R).

TABLE 6.7—REASON PULLED (Wamsley and Ford 2007)

BHA	Change bottomhole assembly
DMF	Downhole motor failure
DTF	Downhole tool failure
DSF	Downhole string failure
DST	Drillstem test
LOG	Run logs
LIH	Left in hole
RIG	Rig repair
CM	Condition mud
CP	Core point
DP	Drill plug
FM	Formation change
HP	Hours on bit
PP	Pump pressure
PR	Penetration rate
TD	Total depth/casing depth
TQ	Torque
TW	Twistoff
WC	Weather conditions

6.6 Rock-Failure Mechanism During Drilling

The method in which rock fails is important in bit design and selection. Formation failure occurs in two modes: brittle failure and plastic failure. The mode in which a formation fails depends on rock strength, which is a function of composition and downhole conditions such as depth, pressure, and temperature.

Formation failure can be depicted with stress/strain curves (**Fig. 6.34**). *Stress*—applied force per unit area—can be tensile, compressive, torsional, or shear. *Strain* is the deformation caused by the applied force. Under brittle failure, the formation fails with very little or no deformation. For plastic failure, the formation deforms elastically until it yields, followed by plastic deformation until rupture.

To operate a given bit properly, the drilling engineer needs to understand as much as possible about the basic mechanisms of rock removal that are at work, including

- Shearing
- Grinding
- Erosion by fluid jet action
- Crushing

To some extent, these mechanisms are interrelated. While one may be dominant for a given bit design, more than one mechanism is usually present. In this discussion, only the two basic rotary-drilling-bit types will be discussed: roller-cone bits and fixed-cutter bits.

6.6.1 Roller-Cone Bits. The action of bit cones on a formation is of prime importance in achieving a desirable penetration rate. Soft-formation bits require a gouging/scraping action. Hard-formation bits require a chipping/crushing action. These actions are governed primarily by the degree to which the cones roll and skid. Maximum gouging/scraping (soft-formation) actions require a significant amount of skid. Conversely, a chipping/crushing (hard-formation) action requires that cone roll approach a “true roll” condition with very little skidding.

Insert bits designed with a large cone-offset angle for drilling soft formations employ all of the basic mechanisms of rock removal. However, the crushing action is the predominant mechanism present for IADC Series 3, 7, and 8 roller-cone bits. Because these bit types are designed for use in hard, brittle formations in which penetration rates tend to be low and drilling costs tend to be high, the crushing mechanism is of considerable economic interest. Maurer (1965) conducted experiments using an original setup of a single-tooth impacting on a rock sample under simulated borehole conditions. He found that the crater mechanism depended to some extent on the pressure differential between the borehole and the rock-pore pressure. At low values of differential pressure, the crushed rock beneath the bit tooth was ejected from the crater, while at high values of differential pressure the crushed rock deformed in a plastic manner and was not ejected

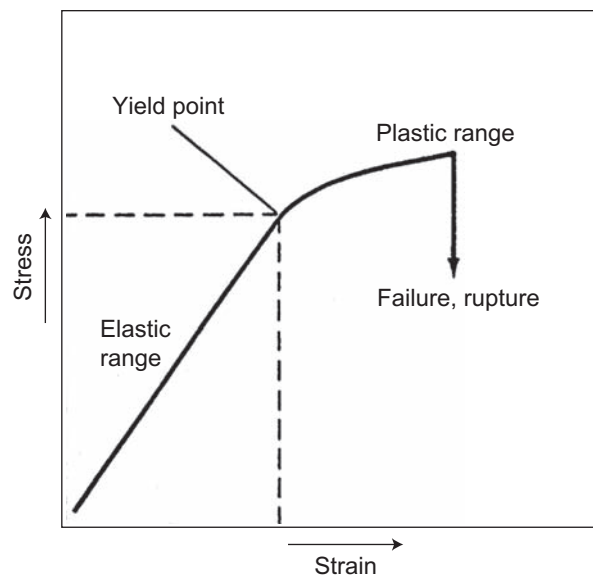


Fig. 6.34—Stress-vs.-strain relation of formations (Wamsley and Ford 2007).

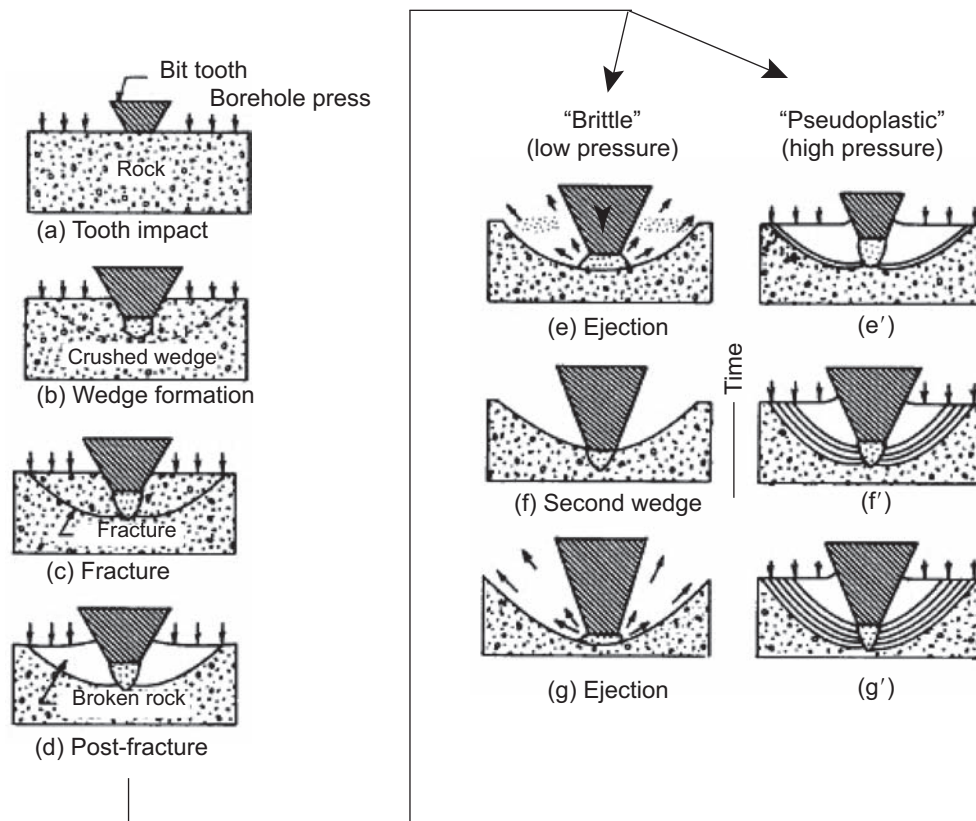


Fig. 6.35—Crater mechanism beneath a bit tooth (Maurer 1965).

completely from the crater. The crater mechanism for both low and high differential fluid pressure is described in Fig. 6.35. The sequence of events shown in this figure is described by Maurer (1965) as follows.

As a load is applied to a bit tooth (A), the constant pressure beneath the tooth increases until it exceeds the compressive strength of the rock, and a wedge of finely powdered rock then is formed beneath the tooth (B). As the force on the tooth increases, the material in the wedge compresses and exerts high lateral forces on the solid rock surrounding the wedge until the shear stress τ exceeds the shear strength S of the solid rock and the rock fractures (C). These fractures propagate along a maximum-shear surface, which intersects the direction

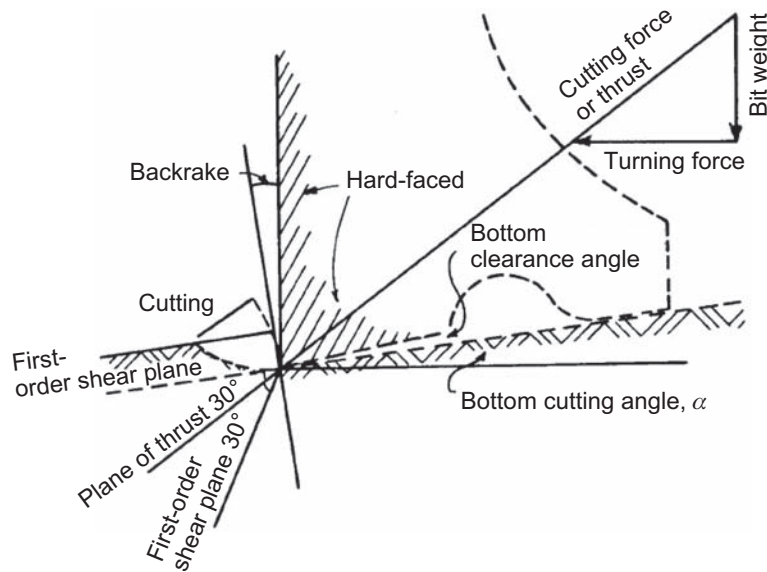


Fig. 6.36—Shear and thrust on a cutter (Hughes 1965).

of the principal stresses at a nearly constant angle as predicted by the Mohr failure criterion (explained in detail in Section 6.2.2). The force at which fracturing begins beneath the tooth is called the *threshold force*. As the force on the tooth increases above the threshold value, subsequent fracturing occurs in the region above the initial fracture, forming a zone of broken rock (D). At low differential pressures, the cuttings formed in the zone of broken rock are ejected easily from the crater (E). The bit tooth then moves forward until it reaches the bottom of the crater, and the process may be repeated (F, G). At high differential pressures, the downward pressure and frictional forces between the rock fragments prevent ejection of the fragments (E'). As the force on the tooth is increased, displacement takes place along fracture planes parallel to the initial fracture (F', G'). This gives the appearance of plastic deformation, and craters formed in this manner are called *pseudoplastic craters*.

High-speed movies (Murray and MacKay 1957) of full-scale bits drilling at atmospheric conditions with air as the circulating fluid have verified that the mechanisms of failure for insert bits with little or no offset is not too different from that observed in single-insert impact experiments. However, the drilling action of insert bits designed with a large offset for drilling soft, plastic formations is considerably more complex than the simple crushing action that results when no offset is used; because each cone alternately rolls and drags, considerable wedging and twisting action is present.

6.6.2 Fixed-Cutter Bits. The cutting mechanism of PDC bits drills primarily by *shearing* such that the cutters have sufficient *axial force* to penetrate into the rock surface and simultaneously have the available torque for bit rotation. The resultant force defines a plane of thrust for the cutter. Cuttings are then sheared off at an initial angle relative to the plane of thrust, which is dependent on rock strength (**Fig. 6.36**). In shear, the energy required to reach the plastic limit for rupture is significantly less than that required by compressive stress. PDC bits, thus, require less WOB than roller-cone bits.

Natural-diamond bits are designed to remove rock primarily by a grinding action. Diamond bits with very large diamonds may possess a shallow plowing action. As the bit is rotating, the exposed diamonds grind against and remove the rock with a very shallow depth of cut. The intent is that as these bits wear, either the exposed diamonds are sharpened because of small fractures during drilling, or new diamonds become exposed as the less-abrasion-resistant body material is worn away. This is a self-sharpening effect that is consistent with other grinding tools where a new grinding surface is continually exposed.

The depth of cut of the bit is determined by the rock strength, the WOB applied, and the dull condition of the bit. The cut geometry at hole bottom is a helix and can be expressed in terms of the bottom-cutting angle or helix angle α . The helix angle α is a function of the cutter penetration per revolution L_p and radius r from the center of the hole. This relation can be defined by

$$\tan \alpha = \frac{L_p}{2\pi r} \quad \dots \dots \dots (6.1)$$

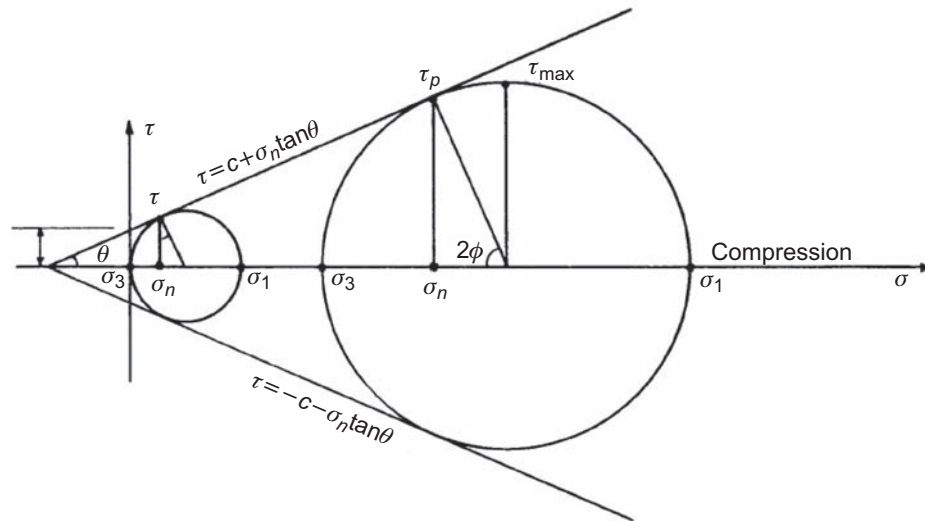


Fig. 6.37—Mohr's circle representation of Mohr failure criterion (Bourgoyne et al. 1991).

Rock-mechanics experts have applied several failure criteria in an attempt to relate rock strength measured in simple compression tests to the rotary-drilling process. One such failure criterion often used is the Mohr theory of failure. The Mohr criterion states that yielding or fracturing should occur when the shear stress exceeds the sum of the cohesive resistance of the material and the frictional resistance of the slip planes or fracture plane. The Mohr criterion is stated mathematically by

$$\tau = \pm(c + \sigma_n \tan \theta), \quad \dots \dots \dots (6.2)$$

where τ is the shear stress at failure, c is the cohesive resistance of the material, σ_n is the normal stress at the failure plane, and θ is the angle of internal friction. As shown in **Fig. 6.37**, this is the equation of a line that is tangent to Mohr's circles drawn for at least two compression tests made at different levels of confining pressure.

To understand the use of the Mohr criterion, consider a rock sample to fail along a plane, as shown in **Fig. 6.38a**, when loaded under a compressive force F and a confining pressure p . The compressive stress σ_1 is given by

$$\sigma_1 = \frac{F}{\pi r^2}.$$

The confining stress is given by

$$\sigma_3 = p.$$

If we examine a small element on any vertical plane bisecting the sample, the element is in the stress state given in **Fig. 6.38b**. Furthermore, we can examine the forces present along the failure plane at failure using the free-body elements shown in **Fig. 6.38b**. The orientation of the failure plane is defined by the angle ϕ between the normal-to-the-failure plane and a horizontal plane. It is also equal to the angle between the failure plane and the direction of the principal stress σ_1 . Both a shear stress τ and a normal stress σ_n must be present to balance σ_1 and σ_3 .

Summing forces normal to the fracture plane (**Fig. 6.38c**) gives

$$\sigma_n dA_n = \sigma_3 dA_3 \cos \phi + \sigma_1 dA_1 \sin \phi$$

The unit area along the fracture plane, dA_n , is related to the unit areas dA_1 and dA_2 by

$$dA_3 = dA_n \cos \phi$$

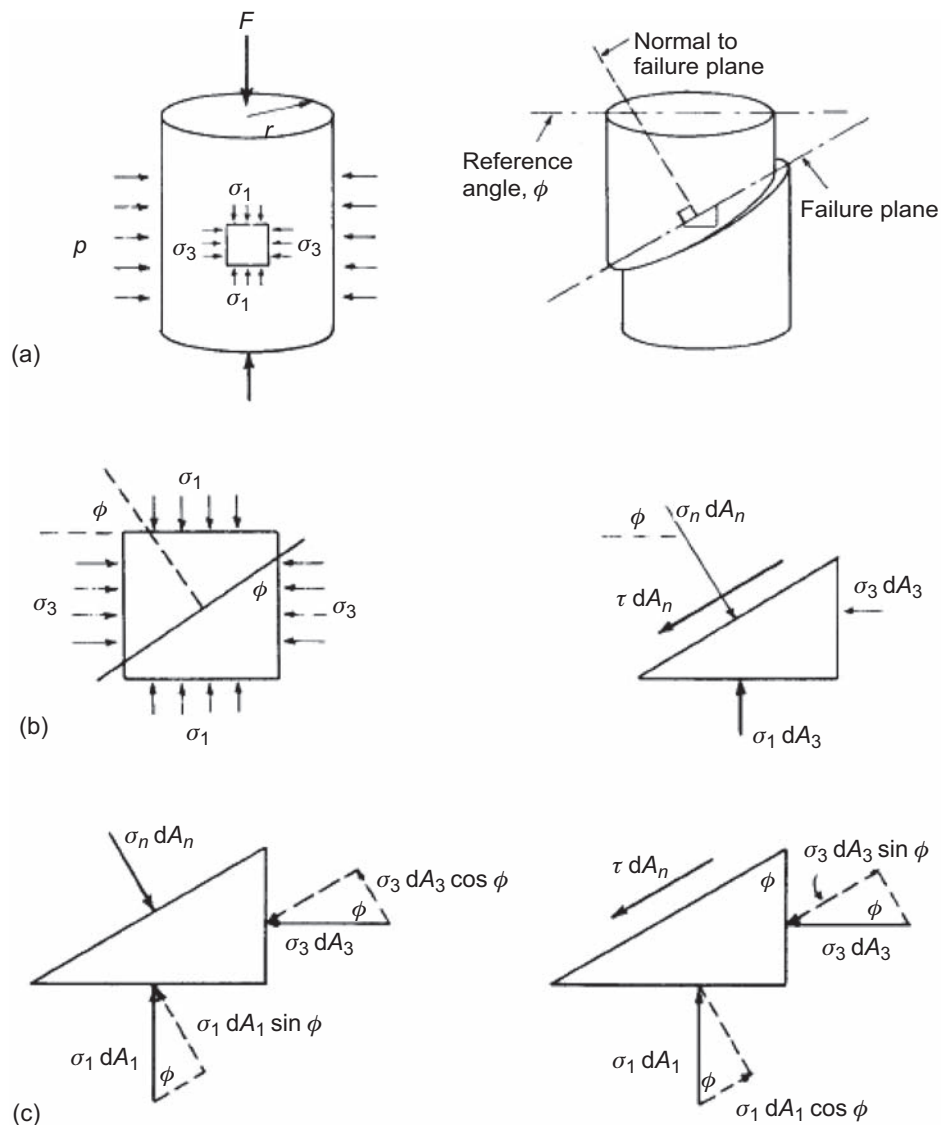


Fig. 6.38—Mohr's circle graphical analysis; (a) reference rock specimen; (b) reference free-body stress element; and (c) force balance normal and parallel to failure plane (Bourgoyne et al. 1991).

and

$$dA_1 = dA_n \sin \phi$$

Making these substitutions in the force-balance equation gives

$$\sigma_n = \sigma_1 \sin^2 \phi + \sigma_3 \cos^2 \phi = \frac{1}{2}(\sigma_1 + \sigma_3) - \frac{1}{2}(\sigma_1 - \sigma_3) \cos(2\phi). \quad \dots \dots \dots (6.3a)$$

Summing the forces parallel to the fracture plane gives

$$\tau dA_n = \sigma_1 dA_1 \cos \phi - \sigma_3 dA_3 \sin \phi$$

Expressing all unit areas in terms of dA_n and simplifying yields

$$\tau = (\sigma_1 - \sigma_3) \sin \phi \cos \phi = \frac{1}{2}(\sigma_1 - \sigma_3) \sin(2\phi). \quad \dots \dots \dots (6.3b)$$

Note that Eqs. 6.3a and 6.3b are represented graphically by the Mohr's circle shown in Fig. 6.37. Note also that the angle of internal friction θ and 2ϕ must sum to 90° . The angle of internal friction for most rocks varies from approximately 30 to 40° .

The Mohr failure criterion can be used to predict the characteristic angle between the shear plane and the plane of thrust for a fixed-cutter bit. Assuming an angle of internal friction of approximately 30° implies

$$2\phi = 90^\circ - 30^\circ$$

or

$$\phi = 30^\circ.$$

This value of ϕ has been verified experimentally by Gray et al. (1962) in tests made at atmospheric pressure.

Example 6.3 A rock sample under a 2,000-psi confining pressure fails when subjected to a compressive loading of 10,000 psi along a plane that makes an angle of 27° with the direction of the compressive load. Using the Mohr failure criterion, determine the angle of internal friction, the shear strength, and the cohesive resistance of the material.

Solution. Given

$$\phi = 27^\circ,$$

$$\sigma_1 = 10,000 \text{ psi},$$

and

$$\sigma_3 = 2,000 \text{ psi},$$

angle of internal friction θ can be determined by using the relation

$$90^\circ = \theta + 2\phi.$$

Thus,

$$\theta = 90 - 2(27) = 36^\circ$$

The shear strength can be determined by using

$$\tau = \frac{1}{2}(\sigma_1 - \sigma_3)\sin(2\phi).$$

Thus,

$$\tau = \frac{1}{2}(10,000 - 2,000)\sin(54) = 3,236 \text{ psi}.$$

The stress normal to the fracture plane σ_n is computed by

$$\sigma_n = \frac{1}{2}(\sigma_1 + \sigma_3) - \frac{1}{2}(\sigma_1 - \sigma_3)\cos(2\phi).$$

Thus,

$$\sigma_n = \frac{1}{2}(10,000 + 2,000) - \frac{1}{2}(10,000 - 2,000)\cos(54) = 3,649 \text{ psi}.$$

The cohesive resistance c can be computed by rearranging

$$\tau = \pm [c + \sigma_n \tan(\theta)].$$

Thus,

$$c = \tau - \sigma_n \tan \theta = 3,236 - 3,649 \tan(36) = 585 \text{ psi.}$$

Graphical Solution. Make a plot of shear strength τ and compression load σ on the y- and x-axes, respectively. Mark 10,000 psi (compressive load) and 2,000 psi (confining pressure) on the x-axis. Develop a circle with a diameter of 8,000 psi with the center at

$$\text{Center} = \frac{10,000 - 2,000}{2} = 4,000 \text{ psi.}$$

Determine the angle of internal friction θ using the correlation

$$90^\circ = \theta + 2\phi,$$

$$\theta = 36^\circ.$$

Draw a tangent line to the circle with an angle of 36° . The tangential point on the circle gives τ . The normal line from τ to the compression line (x-axis) gives σ_n , and the intercept at y-axis gives c .

6.7 Wear Mechanism

The cutting structures of bits often experience catastrophic failures resulting from dynamic-load variations beyond the capacity of the cutting elements. Continuous improvements to cutting structures have steadily increased penetration rates but, at the same time, have elevated their sensitivity to these dynamic effects. Lateral motion of the bit is a major cause of premature cutting-structure wear (Kenner and Isbell 1994).

6.7.1 Cutter Wear. Factors Affecting Wear. The information about the instantaneous rate of bit wear is required for determining the total time interval of bit use. Therefore, it is mandatory to identify the influence of various drilling parameters on the instantaneous rate of bit wear. The *rate* of cutter wear depends primarily on formation abrasiveness, cutting-element size and geometry, bit weight, rotary speed, and the cleaning and cooling action of the drilling fluid.

For roller-cone bits, the major influences on wear on cutters are as follows.

Effect of Tooth Height on Rate of Tooth Wear. Campbell and Mitchell (1959) showed experimentally that the rate at which the height of a steel tooth can be abraded away by a grinding wheel is inversely proportional to the area of the tooth in contact with the grinding wheel. The shape of steel bit teeth is generally triangular in cross section when viewed from either the front or the side. Thus, almost all milled-tooth bits have teeth that can be described using the geometry shown in Fig. 6.39. The bit tooth initially has a contact area given by

$$A_i = w_{x1} w_{y1}.$$

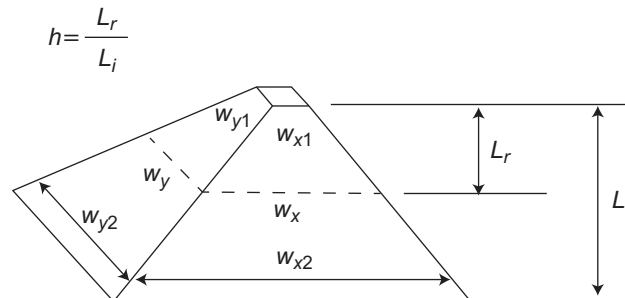


Fig. 6.39—Typical shape of a milled tooth as a function of fractional tooth wear (Bourgoyne et al. 1991).

After removal of tooth height L_r of the original tooth height L_i the bit tooth has a contact area given by

$$A = w_x w_y = \left[w_{x_1} + h(w_{x_2} - w_{x_1}) \right] \left[w_{y_1} + h(w_{y_2} - w_{y_1}) \right].$$

The ratio L_r/L_i is defined as the fractional tooth wear, h :

$$h = \frac{L_r}{L_i}. \quad \dots\dots\dots (6.4)$$

Expressing the contact area A in terms of fractional tooth wear h yields

$$\begin{aligned} A &= \left[w_{x_1} + h(w_{x_2} - w_{x_1}) \right] \left[w_{y_1} + h(w_{y_2} - w_{y_1}) \right] \\ &= (w_{x_1} w_{y_1}) + \left[w_{y_1} (w_{x_2} - w_{x_1}) + w_{x_1} (w_{y_2} - w_{y_1}) \right] h + (w_{x_2} - w_{x_1})(w_{y_2} - w_{y_1}) h^2. \end{aligned}$$

If we define the geometry constants G_1 and G_2 by

$$G_1 = \left[w_{y_1} (w_{x_2} - w_{x_1}) + w_{x_1} (w_{y_2} - w_{y_1}) \right] A_i$$

and

$$G_2 = \left[(w_{x_2} - w_{x_1})(w_{y_2} - w_{y_1}) \right] A_i,$$

the contact area A can be expressed by

$$A = A_i (1 + G_1 h + G_2 h^2).$$

Because the instantaneous wear rate dh/dt is proportional to the inverse of the contact area A ,

$$\frac{dh}{dt} \propto \frac{1}{A_i (1 + G_1 h + G_2 h^2)},$$

the initial wear rate, when $h = 0$, is proportional to A_i . Thus, expressing dh/dt in terms of a standard initial wear rate $(dh/dt)_s$ gives

$$\frac{dh}{dt} \propto \left(\frac{dh}{dt} \right)_s \frac{1}{(1 + G_1 h + G_2 h^2)}. \quad \dots\dots\dots (6.5a)$$

For most bit types, the dimension $w_{x_2} - w_{x_1}$ is small compared with $w_{y_2} - w_{y_1}$. This allows a constant H_2 to be chosen such that the wear rate can be approximated using

$$\frac{dh}{dt} \propto \left(\frac{dh}{dt} \right)_s \frac{1}{(1 + H_2 h)}. \quad \dots\dots\dots (6.5b)$$

The use of Eq. 6.5b in place of Eq. 6.5a greatly simplifies the calculation of tooth wear as a function of rotating time. A case-hardened bit tooth or a tooth with hardfacing on one side often will be self-sharpening as the tooth wears. Even though the mechanism of self-sharpening tooth wear is somewhat different than in the abrasive-wear experiments of Campbell and Mitchell (1959), a constant H_2 usually can be selected such that the instantaneous wear rate can be predicted by use of Eq. 6.5b.

Insert teeth used in roller-cone bits usually fail by fracturing of the brittle tungsten carbide. For this tooth type, fractional tooth wear h represents the fraction of the total number of bit teeth that have been broken. The wear rate (dh/dt) does not decrease with increasing fractional tooth wear h . On the contrary, there is some evidence that the tooth breakage accelerates as the number of broken teeth beneath the bit increases. This type of behavior could be modeled with a negative value for H_2 in Eq. 6.5b. However, this phenomenon has not been studied in detail, and in practice a value of 0 is recommended for H_2 when using insert bits.

Effect of Bit Weight on Rate of Tooth Wear. Galle and Woods (1963) published one of the first equations for predicting the effect of bit weight on the instantaneous rate of tooth wear. The relation assumed by Galle and Woods is

$$\frac{dh}{dt} \propto \frac{1}{1 - \log\left(\frac{W}{d_b}\right)}, \quad \dots\dots\dots (6.6a)$$

where W is the bit weight in 1,000-lbf units and d_b is the bit diameter in inches. Note that $W/d_b < 10.0$.

The wear rate at various bit weights can be expressed in terms of a standard wear rate that would occur for a bit weight of 4,000 lbf per inch of bit diameter. Thus, the wear rate relative to this standard wear rate is given by

$$\frac{dh}{dt} \propto \frac{0.3979\left(\frac{dh}{dt}\right)_s}{1 - \log\left(\frac{W}{d_b}\right)}. \quad \dots\dots\dots (6.6b)$$

Note that dh/dt becomes infinite for $W/d_b = 10$. Thus, this equation predicts that the teeth will fail instantaneously if 10,000 lbf per inch of bit diameter were applied. Later authors (Galle and Woods 1963; Edwards 1964; Young 1969; Reed 1972; Bourgoyne and Young 1974) used a simpler relation between the bit weight and tooth wear rate. Perhaps the most commonly used relation is

$$\frac{dh}{dt} \propto \frac{1}{\left(\frac{W}{d_b}\right)_{\max} - \frac{W}{d_b}}, \quad \dots\dots\dots (6.7a)$$

where $(W/d_b)_{\max}$ is the maximum bit weight per inch of bit diameter at which the bit teeth would fail instantaneously, and $W/d_b < (W/d_b)_{\max}$. Expressing this relation in terms of a standard wear rate at 4,000 lbf per inch of bit diameter yields

$$\frac{dh}{dt} \propto \left(\frac{dh}{dt}\right)_s \left[\frac{\left(\frac{W}{d_b}\right)_{\max} - 4}{\left(\frac{W}{d_b}\right)_{\max} - \frac{W}{d_b}} \right]. \quad \dots\dots\dots (6.7b)$$

Effect of Rotary Speed on Rate of Tooth Wear. The first published relation between the instantaneous rate of tooth wear and the rotary speed N also was presented by Galle and Woods (1963) for milled-tooth bits. The Galle and Woods relation is

$$\frac{dh}{dt} \propto N + 4.34 \times 10^{-5} N^3. \quad \dots\dots\dots (6.8)$$

However, several more-recent authors (Edwards 1964; Young 1969; Reed 1972; Bourgoyne and Young 1974) have shown that essentially the same results can be obtained using the simpler relation

$$\frac{dh}{dt} \propto (N)^{H_1}, \quad \dots\dots\dots (6.9a)$$

where H_1 is a constant. Also, H_1 was found to vary with the bit type used. The Galle and Woods (1903) relation applied only to milled-tooth bit types designed for use in soft formations. Expressing the tooth wear rate in terms of a standard wear rate that would occur at 60 rev/min yields

$$\frac{dh}{dt} \propto \left(\frac{dh}{dt}\right)_s \left(\frac{N}{60}\right)^{H_1}. \quad \dots\dots\dots (6.9b)$$

Effect of Hydraulics on Rate of Tooth Wear. The effect of the cooling and cleaning action of the drilling fluid on cutting-element wear rate (dh/dt) is much more important for fixed-cutter bits (diamond and PDC) than it is for roller-cone bits. Cutting elements on fixed-cutter bits must receive sufficient flow to prevent the buildup of excessive heat, which leads to graphitization of the diamond materials, which thus accelerates the wear process. The flow velocities also must be maintained high enough to prevent clogging of fluid passages with drilled cuttings. The

design of the fluid-distribution passages on a diamond or PDC bit is extremely important and varies considerably among the various bits available. However, the manufacturer will usually specify the total flow area (TFA) needed for specific drill bits based on rig type and capabilities, flow rates, drilling-fluid type and properties, BHA design, formation characteristics, drilling program, and anticipated ROP. Considering a specific TFA, nozzle sizing must also be based on the need to minimize recirculation of the drilling fluid, cuttings regrinding, and stagnation zones on the bit face. In addition to minimizing cutting-element wear rate, efficient fluid distribution and cleaning also improves ROP. It is generally assumed that as long as the flow is present to clean and to cool the drill bit, the effect of hydraulics on cutting-element wear rate can be ignored or can be assumed to be taken care of.

Wear on PDC Cutters. PDC-cutter wear can be divided into two categories, depending on the basic cause of the wear. The first category is steady-state wear that is normally associated with the development of uniform wear flats on the PDC cutter and the gradual degradation in the ROP over the bit life, which is a function of operating parameters applied to the bit and individual cutters, cutter temperature, cutter velocity, formation properties, and cutter properties. The second category of wear is the result of impact loading of the cutters. This type of wear may be caused by dynamic loading of the bit during bit whirl or from drilling through heterogeneous formations (Sinor et al. 1998).

PDC cutters tend to wear in a manner somewhat similar to that of steel-tooth inserts (Hoover and Middleton 1981). Some examples of PDC-cutter wear are presented in **Fig. 6.40**.

The shape of the PDC cutter, which is usually circular, provides a different relationship between fractional tooth wear h and cutter-contact area. For a zero backrake angle, the cutter-contact area is proportional to the length of the chord defined by the lower surface of the cutter remaining after removal of the cutter height L_r (**Fig. 6.41**).

Because the fractional tooth wear h is given by

$$h = \frac{L_r}{d_c}$$

and the dimension y shown in Fig. 6.41 is

$$y = r_c \left(\cos \frac{\beta}{2} \right),$$

then

$$h = \frac{r_c - y}{d_c} = \frac{r_c - \left(r_c \cos \frac{\beta}{2} \right)}{2r_c} = \frac{1 - \cos \frac{\beta}{2}}{2}.$$

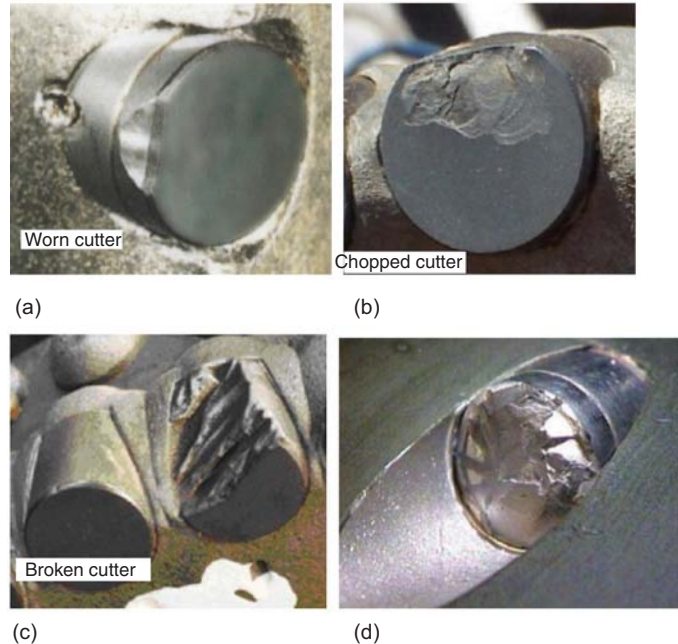


Fig. 6.40—PDC-cutter-wear examples: (a) worn cutter; (b) chipped cutter; (c) broken cutter; (d) failed cutter because of high impact loads (Jaffar et al. 2005).

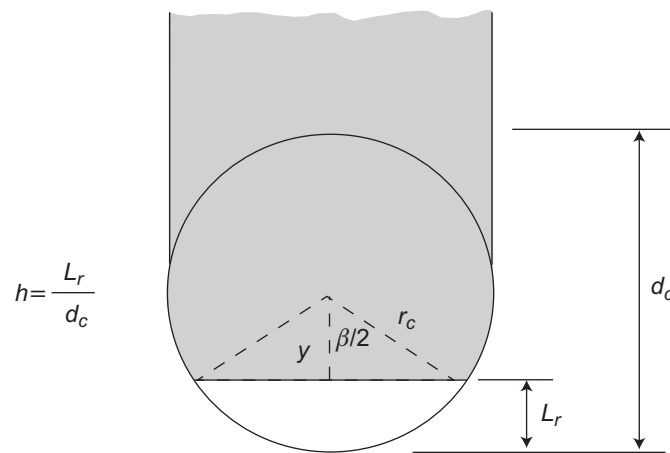


Fig. 6.41—PDC-blank geometry as a function of fractional cutter wear h for a zero backrake angle [from Bourgoyne et al (1991)].

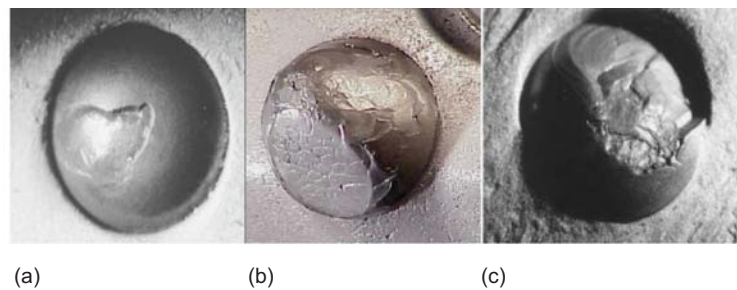


Fig. 6.42—Typical failure modes of PDC inserts: (a) spalling; (b) chipping and heat checking; (c) breakage (Fang et al. 2001).

Solving this expression for the subtended angle β yields

$$\cos \frac{\beta}{2} = 1 - 2h \quad \dots \dots \dots (6.10a)$$

Because the contact area is directly proportional to the chord length subtended by the angle β , then

$$A \propto 2 \left(\frac{d_c}{2} \right) \sin \frac{\beta}{2},$$

and the wear rate (dh/dt) is inversely proportional to this contact area:

$$\frac{dh}{dt} \propto \left(\frac{dh}{dt} \right)_s \frac{1}{d_c \sin \frac{\beta}{2}} \quad \dots \dots \dots (6.10b)$$

The wear rate (dh/dt) decreases with increasing fractional tooth wear h between 0 and 0.5. Above this range, the wear rate increases with increasing h .

For PDC cutters with nonzero backrake angles, the total contact area of the PDC wafer or diamond layer and the tungsten carbide substrate becomes more complex. However, the preceding analysis remains representative of the geometry of the PDC layer, which is believed to be the predominant determinant, in terms of the wear resistance of the PDC cutter. Typical failure modes observed of diamond enhanced inserts are shown in **Fig. 6.42**. Chipping and fracture resistance can be improved at the expense of the hardness and wear resistance of the materials. This tradeoff between wear resistance and chipping resistance hinders the development of super hard materials for demanding drilling applications.

Warren and Sinor (1994) pointed out the effects of bit whirl on PDC cutters. Bit whirl caused the cutters to be damaged by impact loading, even in homogeneous rock, by allowing the cutters to move sideways and backward

so that the diamond cutting edge was damaged. This damage to the cutting edge allowed the carbide substrate to contact the rock and generate heat. This in turn further damaged the diamond and gave the appearance that the cutter had been damaged by heat, when in fact the root cause of the damage was the initial chipping.

Laboratory results for antiwhirl and conventional PDC bits by Dykstra et al. (1994) have shown that vibrations of the former were an order of magnitude less than those of the latter. Backward whirl of the conventional PDC bit was prevalent in both hard and soft formations. Roller-cone-bit tests suggested that they too were subject to backward whirl and that the lateral vibrations that resulted were an order of magnitude worse than the axial vibrations commonly associated with these bits. Johnson (2006) noted that proper blade and cutter alignment during the design stage of PDC bits eliminates whirl. **Fig. 6.43** shows the evidence of the bit whirl by comparing the bottomhole patterns and presents an alternative bit profile to eliminate this problem.

Diamond bits also wear by breakage or loss of the diamond-cutter elements. The wear rate of diamond bits is, thus, not sensitive to the fractional cutter wear. The wear rate of diamond bits is far more sensitive to the amount of cooling provided by the flow of drilling fluid across the face of the bit.

Glowka and Stone (1985) discussed the wear mechanisms for PDC bits and the dependence of wear on cutter temperature. Above 1,382°F (750°C), wear was shown to accelerate because of thermal deterioration on diamond grain pullout, resulting in catastrophic cutter failure. At temperatures below 1,382°F, the primary mode of wear was described as microchipping abrasive wear. Glowka and Stone (1985) have also shown that wear rate increased



Fig. 6.43a—Stable (left) and unstable (right) PDC at high RPM. Instability caused continuous fracturing (Johnson 2006).



Fig. 6.43b— A ring PDC bit, which is very effective in avoiding whirl and in providing high control on steerability (Schell et al. 2003).



Fig. 6.43c—Bit whirl (left) and full-contact gauge ring (right) (Schell et al. 2003).

dramatically above 622°F (350°C). Because of the accelerated wear above 662°F, it is defined as the *critical cutter temperature*. The following equation is derived for wear-flat temperature (i.e., the temperature at the flat surface of the cutter having direct contact with the formation):

$$T_w = T_f + \frac{k_f F_n v f}{A_w} \left[1 + \frac{3\sqrt{\pi}}{4} f k_{hf} \left(\frac{100v}{L_w \alpha_f} \right)^{\frac{1}{2}} \right]^{-1}, \quad \dots \quad (6.11)$$

where T_w is the mean cutter wear-flat temperature, °C; T_f is the fluid temperature, °C; v is the cutting speed, m/s; α_f is the rock thermal diffusivity, cm²/s; A_w is the cutter wear-flat area, cm²; F_n is the normal force on cutter, N; f is the thermal response function, (cm² · °C)/W; k_{hf} is the rock thermal conductivity, W/(cm · °C); k_f is the friction coefficient between rock and cutter; and L_w is the wear-flat length, cm. Thermal response function f is the effective thermal resistance of the cutter and is a function of cutter configuration, thermal properties, and cooling rates.

Wear Equation. Roller-Cone Bits. A composite tooth-wear equation can be obtained by combining the relations approximating the effect of tooth geometry, bit weight, and rotary speed on the rate of tooth wear (Bourgoyne and Young 1974). Thus, the instantaneous rate of tooth wear is given by

$$\frac{dh}{dt} = \frac{1}{\tau_H} \left(\frac{N}{60} \right)^{H_1} \left[\frac{\left(\frac{W}{d_b} \right)_{\max} - 4}{\left(\frac{W}{d_b} \right)_{\max} - \left(\frac{W}{d_b} \right)} \right] \left(\frac{1 + \frac{H_2}{2}}{1 + H_2 h} \right), \quad \dots \quad (6.12)$$

where h is the fractional tooth height that has been worn away; t is the time, hours; H_1 , H_2 , and $(W/d_b)_{\max}$ are constants; W is the bit weight, 1,000-lbf units; N is the rotary speed, rev/min; and τ_H is the formation-abrasiveness constant, hours.

The rock/bit-classification scheme shown in Figs. 6.23 and 6.24 can be used to characterize the many bit types available in the industry from the different bit-manufacturing companies. Recommended values of H_1 , H_2 , and $(W/d_b)_{\max}$ are shown in **Table 6.8** for the various roller-cone-bit classes.

The tooth-wear rate formula given by Eq. 6.12 has been normalized so that the abrasiveness constant τ_H is numerically equal to the time in hours required to completely dull the bit teeth of the given bit type when operated at a constant bit weight of 4,000 lbf/in. and a constant rotary speed of 60 rev/min. The average formation abrasiveness encountered during a bit run can be evaluated using Eq. 6.12, and the final tooth wear h_f can be observed after pulling the bit. If we define a tooth-wear parameter J_2 using

$$J_2 = \left[\frac{\left(\frac{W}{d_b} \right)_{\max} - \frac{W}{d_b}}{\left(\frac{W}{d_b} \right)_{\max} - 4} \right] \left(\frac{60}{N} \right)^{H_1} \left(\frac{1}{1 + \frac{H_2}{2}} \right), \quad \dots \quad (6.13)$$

then Eq. 6.12 can be expressed by

TABLE 6.8—RECOMMENDED TOOTH-WEAR PARAMETERS FOR ROLLER-CONE BITS (Bourgoyne et al. 1991)

Bit Class	H_1	H_2	$\left(\frac{W}{d_b} \right)_{\max}$
1-1 to 1-2	1.9	7	7
1-3 to 1-4	1.84	6	8
2-1 to 2-2	1.8	5	8.5
2-3	1.76	4	9
3-1	1.7	3	10
3-2	1.65	2	10
3-3	1.6	2	10
4-1	1.5	2	10

$$\int_0^{t_b} dt = \tau_H J_2 \int_0^{h_f} (1 + H_2 h) dh. \quad \dots\dots\dots (6.14a)$$

Integration of this equation yields

$$t_b = \tau_H J_2 \left(h_f + H_2 \frac{h_f^2}{2} \right). \quad \dots\dots\dots (6.14b)$$

Solving for the abrasiveness constant τ_H gives

$$\tau_H = \frac{t_b}{J_2 \left(h_f + H_2 \frac{h_f^2}{2} \right)}. \quad \dots\dots\dots (6.15)$$

Although Eqs. 6.12 through 6.15 were developed for use in modeling the loss of tooth height of a milled-tooth bit, they also have been applied with some degree of success to describe the loss of insert teeth by breakage. Insert bits are generally operated at lower rotary speeds than milled-tooth bits to reduce impact loading on the brittle tungsten carbide inserts. In hard formations, high rotary speeds may quickly shatter the inserts (Estes 1974).

Example 6.4 A 9 $\frac{7}{8}$ -in. Class 1-1-1 bit drilled from a depth of 12,000 to 12,200 ft in 12 hours. The average bit weight and rotary speed used for this bit run were 40,000 lbf and 90 rev/min, respectively. When the bit was pulled, it was graded T-6 and B-6. The drilling fluid was a barite-weighted clay/water mixture having a density of 12.0 lbm/gal. Estimate the formation-abrasiveness constant for this depth interval.

Solution. From Eq. 6.15, it is known that

$$\tau_H = \frac{t_b}{J_2 \left(h_f + H_2 \frac{h_f^2}{2} \right)},$$

where

$$J_2 = \left[\frac{\left(\frac{\text{WOB}}{d_b} \right)_{\max} - \frac{\text{WOB}}{d_b}}{\left(\frac{\text{WOB}}{d_b} \right)_{\max} - 4} \right] \left(\frac{60}{N} \right)^{H_1} \left(\frac{1}{1 + \frac{H_2}{2}} \right).$$

From Table 6.8, for a 1-1-1 bit, H_1 is equal to 1.90, H_2 is equal to 7, and

$$\left(\frac{\text{WOB}}{d_b} \right)_{\max} = 7.0 \text{ lbf/in.}$$

Thus, J_2 can be calculated as

$$J_2 = \left[\frac{7.0 - \frac{40}{9.875}}{7.0 - 4} \right] \left(\frac{60}{90} \right)^{1.90} \left(\frac{1}{1 + \frac{7}{2}} \right) = 0.101116.$$

Therefore, the formation-abrasiveness constant can be determined by

$$\tau_H = \frac{12}{(0.101116) \left[\frac{6}{8} + 7 \frac{\left(\frac{6}{8} \right)^2}{2} \right]} = 43.651 \text{ hours.}$$

Wear Equation. Fixed-Cutter Bits. Ziaja and Miska (1982) developed a mathematical model of the diamond-bit drilling process with several limiting assumptions. On the basis of this model, the wear on diamond cutters can be estimated. The wear of diamonds on the face of a diamond bit using a linear-wear model is expressed as

$$X = \sqrt{\frac{240 \tau_s (W) N s (t_b)}{\pi d_d C_d (D_{b_o} - D_{b_i})}}, \quad \dots \dots \dots (6.16)$$

where X is the linear wear, in.; τ_s is the index of rock abrasiveness, in.³/(lbf-in.) W is the weight on bit, lbf; N is the rotary speed, rev/min; s is the average diamond size, carat/stone; t_b is the bit time, hours; d_d is the average diamond diameter, in. (if not known, $d_d = \frac{s^{0.33}}{4.99}$); C_d is the average density of the face stones, carats/in.²; and D_{b_o} and D_{b_i} are outer and inner diameter of the bit, respectively, in. (if the bit is a core bit, $D_{b_i} \neq 0$ but if the bit is a drilling bit, $D_{b_i} = 0$).

Example 6.5 After 6 hours of drilling, a diamond bit with a diameter of $3\frac{2}{3}$ in. is pulled out of the hole. The average linear wear on the diamonds is observed to be 0.05 in. The WOB was 3.8×10^3 , and the rotational speed of the bit was 195 rev/min. Diamond size is 0.358 carats/stone, and average density of the face stones is 4.32 carat/in.² Estimate the index of rock abrasiveness for these drilling conditions.

Solution. From Eq. 6.16, it is known that

$$X = \sqrt{\frac{240 \tau_s (\text{WOB}) N s (t_b)}{\pi d_d C_d (D_{b_o} - D_{b_i})}}.$$

Therefore,

$$\tau_s = \frac{X^2 \pi d_d C_d (D_{b_o} - D_{b_i})}{240 (\text{WOB}) N s (t_b)}.$$

Thus,

$$\tau_s = \frac{0.05^2 \pi \left(\frac{0.358^{0.33}}{4.99} \right) (4.32) (3.333)}{240 (3,800) 195 (0.358) (6)} = 4.227 \times 10^{-11} \text{ in.}^3/\text{lbf-in.}$$

6.7.2 Bearing Wear (Roller Cones Only). The prediction of bearing wear is much more difficult than the prediction of tooth wear. Like tooth wear, the instantaneous rate of bearing wear depends on the current condition of the bit. After the bearing surfaces become damaged, the rate of bearing wear increases greatly. However, because the bearing surfaces cannot be examined readily during the dull-bit evaluation, a linear rate of bearing wear usually is assumed. Also, bearing manufacturers have found that for a given applied force, the bearing life can be expressed in terms of total revolutions as long as the rotary speed is low enough to prevent excessive heat. Thus, bit bearing life usually is assumed to vary linearly with rotary speed.

Factors Affecting Bearing Wear. The effect of bit weight and RPM on bearing life depends on the number and type of bearings used and whether the bearings are sealed. When the bearings are not sealed, bearing lubrication is accomplished with the drilling fluid, in which case the mud properties also affect bearing life.

The hydraulic action of the drilling fluid at the bit is also thought to have some effect on bearing life. As flow rate increases, the ability of the fluid to cool the bearings also increases. However, it is generally believed that flow rates sufficient to lift cuttings will also be sufficient to prevent excessive heat in the bearings. Lummus (1974) has indicated that a jet velocity that is too high can be detrimental to bearing life. Erosion of bit metal can occur, which leads to failure of the bearing grease seals. In the example discussed by Lummus, this phenomenon was important for bit hydraulic-horsepower values greater than 4.5 hp per square inch of hole bottom. However, a general model for predicting the effect of hydraulics on bearing wear was not presented.

Bearing-Wear Equation. Researchers have been putting forward empirical formulas about the bearing wear of roller-cone bits for more than 50 years. One bearing-wear formula used to estimate bearing life is given by Bourgoynne et al. (1991):

$$\frac{db}{dt} = \frac{1}{\tau_B} \left(\frac{N}{60} \right)^{B_1} \left(\frac{W}{4d_b} \right)^{B_2}, \quad \dots \dots \dots (6.17)$$

where b is the fractional bearing life that has been consumed; t is the time, hours; N is the rotary speed, rev/min; W is the bit weight, 1,000 lbf; d_b is the bit diameter, in.; B_1 and B_2 are the bearing-wear exponents; and τ_B is the bearing constant, hours.

Recommended values for the bearing-wear exponents are given in **Table 6.9**. Note that the bearing-wear formula given by Eq. 6.17 is normalized so that the bearing constant τ_B is numerically equal to the life of the bearings if the bit is operated at 4,000 lbf/in. and 60 rev/min. The bearing constant can be evaluated using Eq. 6.17 and the results of a dull-bit evaluation. If we define a bearing-wear parameter J_3 using

$$J_3 = \left(\frac{60}{N} \right)^{B_1} \left(\frac{4d_b}{W} \right)^{B_2}, \quad \dots \quad (6.18)$$

Eq. 6.17 can be expressed by

$$\int_0^{t_b} dt = J_3 \tau_B \int_0^{b_f} db,$$

where b_f is the final bearing wear observed after pulling the bit. Integration of this equation yields

$$t_b = \tau_B J_3 b_f. \quad \dots \quad (6.19)$$

Solving for the bearing constant τ_B gives

$$\tau_B = \frac{t_b}{J_3 b_f}. \quad \dots \quad (6.20)$$

Journal-bearing insert-bit runs without excessive insert breakage or gauge wear typically fail because of seal/bearing wear. The factors affecting seal and bearing surface wear are numerous and complex (Winters and Doiron 1987).

The bearing wear is proportional to the frictional work, which mainly depends on the travel distance and the contact pressure between two surfaces of cone and journal, which are related to rotary speed of the bit and WOB. Also, bearing wear is dependent on bit type, formation, BHA, and downhole conditions. In addition, the wear is related to bit diameter d_b and to time. The equation for bearing dull grade, b_f (0–8), is assumed as follows (Hareland et al. 2009):

$$b_f = K (d_b)^a (t)^b (W)^c (N)^d, \quad \dots \quad (6.21)$$

where K , a , b , c , and d are constants that need to be determined using offset data.

Example 6.6 Field data obtained on $7/8$ -in. Series-6 roller-cone bits at a rotary speed of 60 rev/min show an average bearing life of 32 hours for a bit weight of 5,700 lbf/in. and 45 hours for a bit weight of 3,800 lbf/in. Compute the apparent bearing weight exponent B_2 and the bearing constant, τ_B for this bit type.

TABLE 6.9—RECOMMENDED BEARING-WEAR EXPONENT FOR ROLLER- CONE BITS (Bourgoyne et al. 1991)			
Bearing Type	Drilling-Fluid Type	B_1	B_2
Nonsealed	Barite mud	1	1
	Sulfide mud	1	1
	Water	1	1.2
	Clay/water mud	1	1.5
	Oil-based mud	1	2
Sealed roller bearings	—	0.7	0.85
Sealed journal bearings	—	1.6	1

Solution. From Eq. 6.19,

$$t_b = \tau_B J_3 b_f,$$

where

$$J_3 = \left(\frac{60}{N} \right)^{B_1} \left(\frac{4 d_b}{\text{WOB}} \right)^{B_2}.$$

Therefore, inserting the given information into these equations will yield

$$32 = \left(\frac{60}{60} \right)^{B_1} \left(\frac{4}{5.7} \right)^{B_2} \tau_B$$

and

$$45 = \left(\frac{60}{60} \right)^{B_1} \left(\frac{4}{3.8} \right)^{B_2} \tau_B.$$

So, there are two equations and two unknowns, because B_1 will not affect the equality. Solving for B_2 and τ_B will yield 0.84 and 43.1 hours, respectively.

6.8 ROP

6.8.1 Factors Affecting ROP. The most important variables affecting penetration rate that have been identified and studied include bit type, formation characteristics, drilling-fluid properties, bit operating conditions (bit weight and rotary speed), bit tooth wear, and bit hydraulics.

Bit Type. The bit type selected has a large effect on penetration rate. For roller-cone bits, the initial penetration rate is often highest in a given formation when using bits with long teeth and a large cone-offset angle. However, these bits are practical only in soft formations because of a rapid tooth destruction and decline in penetration rate in hard formations (Chen et al. 2001).

As discussed previously, fixed-cutter bits give a wedging-type rock failure in which the bit penetration per revolution depends on the number of blades and the bottom-cutting angle. Diamond and PDC bits are designed for a given penetration per revolution by the selection of the size and number of diamond or PDC cutters.

Developments in PDC bits that have helped in achieving higher ROPs and longer bit life involve a compromise between open, light-set bits for speed and heavy-set bits for durability. Hydraulic-design improvements prevent bit balling, while mechanical-design enhancements increase the ROP (Taylor et al. 1999). Steel-bodied drill bits have shown significant improvements in drilling efficiency. These bits allow higher ROP in high-mud-weight applications, increased mechanical efficiency, and enhanced wear/erosion resistance (Beaton et al. 2008).

Formation Characteristics. The elastic limit and ultimate strength of the formation are the most important formation properties affecting penetration rate. The shear strength predicted by the Mohr failure criterion sometimes is used to characterize the strength of the formation. Maurer (1965) reported that the crater volume produced beneath a single tooth is inversely proportional to both the compressive strength of the rock and the shear strength of the rock. Bingham (1965) found that the threshold force required to initiate drilling in a given rock at atmospheric pressure could be correlated to the shear strength of the rock as determined in a compression test at atmospheric pressure. To determine the shear strength from a single compression test, an average angle of internal friction of 35° was assumed. The angle of internal friction varies from approximately 30 to 40° for most rocks. Applying Eq. 6.3b for a standard compression test at atmospheric pressure ($\sigma_3 = 0$) gives

$$\tau_o = \frac{1}{2}(\sigma_1 - 0)\sin(90 - \theta) = \frac{\sigma_1}{2}\cos\theta.$$

The threshold force or bit weight, $(W/d_b)_r$, required to initiate drilling was obtained by plotting drilling rate as a function of bit weight per bit diameter, and then extrapolating back to a zero drilling rate. The laboratory correlation obtained in this manner is shown in **Fig. 6.44**.

The permeability of the formation also has a significant effect on the penetration rate. In permeable rocks, the drilling-fluid filtrate can move into the rock ahead of the bit and equalize the pressure differential, acting on the chips formed beneath each tooth. This would tend to promote the more-explosive elastic mode of crater formation described in Fig. 6.35. It also can be argued that the nature of the fluids contained in the pore spaces of the rock

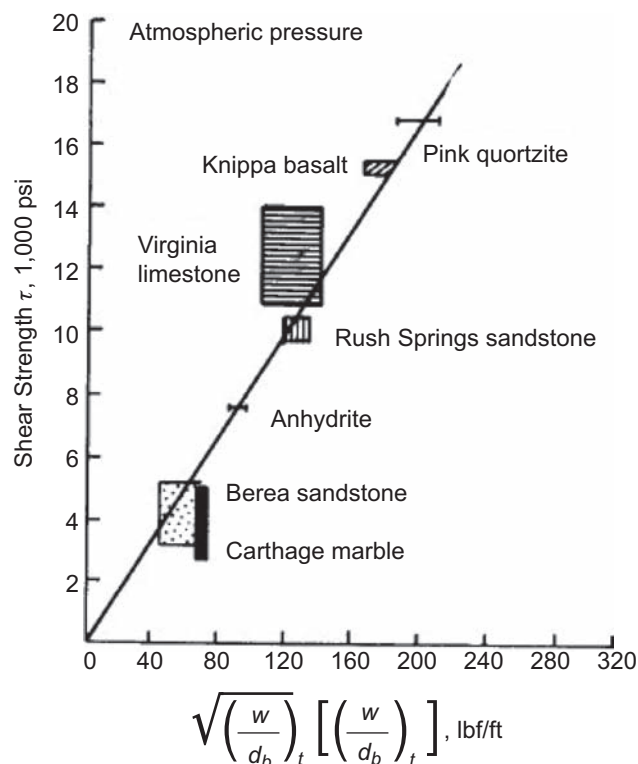


Fig. 6.44—Rock shear strength vs. threshold bit weight (Bingham 1965).

also affects this mechanism because more filtrate volume would be required to equalize the pressure in a rock containing gas than in a rock containing liquid.

The mineral composition of the rock also has some effect on penetration rate. Rocks containing hard, abrasive minerals can cause rapid dulling of a bit's cutting elements. Rocks containing gummy clay minerals can cause the bit to ball up and drill in a very inefficient manner.

Drilling-Fluid Properties. The properties of the drilling fluid reported to affect the penetration rate include density, rheological flow properties, filtration characteristics, solids content and size distribution, and chemical composition.

Penetration rate tends to decrease with increasing fluid density, viscosity, and solids content, and tends to increase with increasing filtration rate. The density, solids content, and filtration characteristics of the mud control the pressure differential across the zone of crushed rock beneath the bit. The fluid viscosity controls the parasitic frictional losses in the drillstring and, thus, the hydraulic energy available through the bit nozzles for cleaning. There is also experimental evidence (Estes 1974) that increasing viscosity reduces penetration rate even when the bit is perfectly clean. The chemical composition of the fluid has an effect on penetration rate in that the hydration rate and bit-balling tendency of some clays are affected by the chemical composition of the fluid.

An increase in drilling-fluid density causes a decrease in penetration rate for roller-cone bits. An increase in drilling-fluid density causes an increase in the bottomhole pressure beneath the bit and, thus, an increase in the pressure differential between the borehole pressure and the formation-fluid pressure. This pressure differential between the borehole pressure and the formation-fluid pressure often is called the *overbalance*. Recall the change in the crater-formation mechanism with increasing overbalance described in Fig. 6.35. The Mohr failure criterion given by Eq. 6.3 predicts a similar effect of overbalance on fixed-cutter bit performance. The normal stress at the failure plane σ_n for a shearing-failure mechanism is directly related to overbalance (Maurer 1965).

Bourgoyne and Young (1974) observed that the relation between overpressure and penetration rate could be represented approximately by a straight line on semilog paper for the range of overbalance commonly used in field practice. In addition, they suggested normalizing the penetration-rate data by dividing the obtained values by the penetration rate achieved at zero overbalance (borehole pressure equal to formation-fluid pressure). Note that a reasonably accurate straight-line representation of the data is possible for moderate values of overbalance. The equation for the straight line shown in Fig. 6.45 is

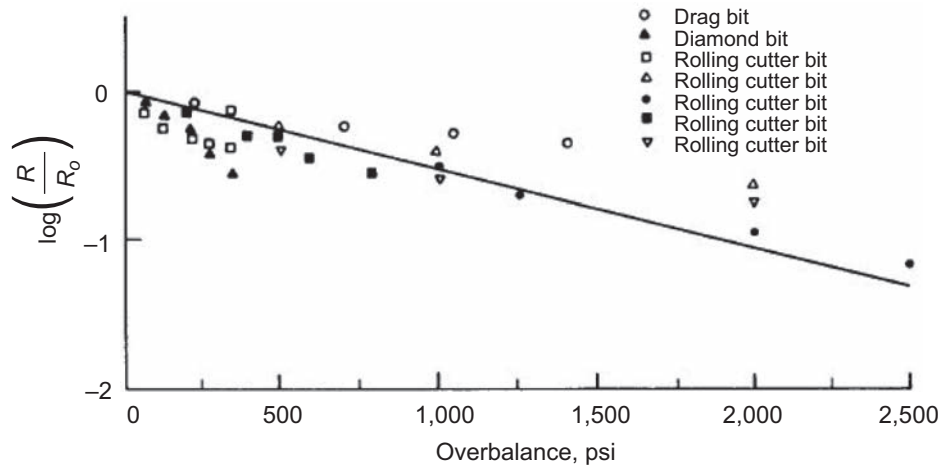


Fig. 6.45—Exponential relation between penetration rate and overbalance for roller-cone bits [from Bourgoyne et al. (1991)].

$$\log\left(\frac{R}{R_0}\right) = -m(p_{bh} - p_f), \quad \dots\dots\dots (6.22a)$$

where R is the penetration rate, R_0 is the penetration rate at zero overbalance, p_{bh} is the bottomhole pressure in the borehole, p_f is the formation-fluid pressure, and m is the slope of the line.

If we express overbalance in terms of equivalent circulating density ρ_c and pore-pressure gradient g_p , we obtain

$$(p_{bh} - p_f) = 0.052 D(\rho_c - g_p).$$

Substituting this expression for overbalance in Eq. 6.22a gives

$$\log\left(\frac{R}{R_0}\right) = -0.052 m D(\rho_c - g_p) = 0.052 m D(g_p - \rho_c).$$

Bourgoyne and Young (1974) chose to replace the combination of constants $(-0.052m)$ by a single coefficient a_4 :

$$\log\left(\frac{R}{R_0}\right) = a_4 D(g_p - \rho_c). \quad \dots\dots\dots (6.22b)$$

This expression is useful for relating changes in mud density or pore-pressure gradient to changes in penetration rate.

Example 6.7 The slope of the shale line in Fig. 6.45 is $-0.000666 \text{ psi}^{-1}$. Evaluate the coefficient a_4 for this value of m , and estimate the change in penetration rate in this shale at 12,000 ft to be expected if the mud density is increased from 12 to 13 lbm/gal. The current penetration rate in this shale is 20 ft/hr.

Solution. The coefficient a_4 is given by

$$a_4 = 0.052(0.000666) = 35 \times 10^{-6}.$$

Eq. 6.22b can be rearranged using the definition of a common logarithm in terms of the initial penetration rate R_1 and mud density ρ_1 to give

$$R_1 = R_0 \times 10^{a_4 D(g_p - \rho_1)} = R_0 e^{2.303 a_4 D(g_p - \rho_1)}.$$

Similarly, for the final penetration rate R_2 and mud density ρ_2 , we obtain

$$R_2 = R_0 \times 10^{a_4 D(g_p - \rho_2)} = R_0 e^{2.303 a_4 D(g_p - \rho_2)}.$$

Dividing the equation for R_2 by the equation for R_1 gives

$$\frac{R_2}{R_1} = e^{2.303 a_4 D(\rho_1 - \rho_2)}.$$

Solving for the final penetration rate R_2 yields

$$R_2 = R_1 e^{2.303 a_4 D(\rho_1 - \rho_2)} = 20 \left[e^{2.303 (35 \times 10^{-6}) (12,000) (12-13)} \right] = 7.60 \text{ ft/hr.}$$

Operating Conditions. Weight on Bit and Rotation Speed. The effect of bit weight and rotary speed on penetration rate has been studied by numerous authors both in the laboratory and in the field. Typically, a plot of penetration rate vs. bit weight obtained experimentally with all other drilling variables held constant has the characteristic shape shown in **Fig. 6.46**. No significant penetration rate is obtained until the threshold formation stress is exceeded (Point b). Penetration rate increases gradually and linearly with increasing values of bit weight for low-to-moderate values of bit weight (Segment ab). A linear curve is again observed at higher bit weights (Segment bc). Although the ROP vs. the WOB correlations for the discussed segments (ab and bc) are both positive, segment bc has a much steeper slope, representing increased drilling efficiency. Point b is the transition point where the rock-failure mode changes from scraping or grinding to shearing. Beyond Point c, subsequent increases in bit weight cause only slight improvements in penetration rate (Segment cd). In some cases, a decrease in penetration rate is observed at extremely high values of bit weight (Segment de). This type of behavior sometimes is called *bit foun-dering*. The poor response of penetration rate at high WOB values is usually attributed to less-efficient hole cleaning because of a higher rate of cuttings generation, or because of a complete penetration of a bit's cutting elements into the formation being drilled, without room or clearance for fluid bypass.

A typical plot of penetration rate vs. rotary speed obtained with all other drilling variables held constant is shown in **Fig. 6.47**. Penetration rate usually increases linearly with rotary speed at low values of rotary speed. At higher values of rotary speed, the response of penetration rate to increasing rotary speed diminishes. The poor penetration-rate response to increasing rotary speeds is also attributed to inefficient bottomhole cleaning.

Maurer (1962) developed a theoretical equation for roller-cone bits, relating penetration rate to bit weight, rotary speed, bit size, and rock strength. The equation was derived from the following observations made in single-insert impact experiments:

1. The crater volume is proportional to the square of the depth of cutter penetration.
2. The depth of cutter penetration is inversely proportional to the rock strength.

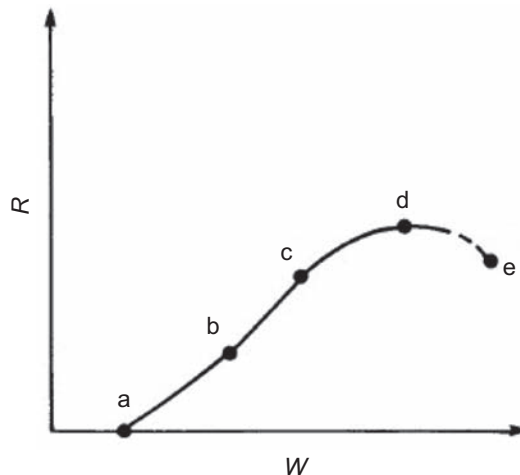


Fig 6.46—Relation between ROP and WOB (Bourgoyne et al. 1991).

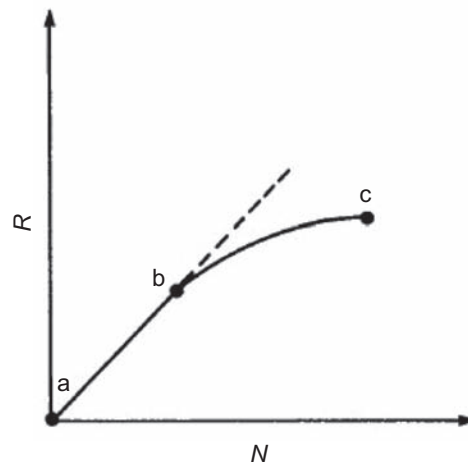


Fig. 6.47—Relation between ROP and rotation speed (Bourgoyne et al. 1991).

For these conditions, the penetration rate R is given by

$$R = \frac{K}{S^2} \left[\frac{W}{d_b} - \left(\frac{W}{d_b} \right)_t \right]^2 N, \quad \dots\dots\dots (6.23)$$

where K is the constant of proportionality; S is the compressive strength of the rock; W is the bit weight; d_b is the bit diameter; $(W/d_b)_t$ is the threshold bit weight per inch of bit diameter; and N is the rotary speed.

This theoretical relation assumes perfect bottomhole cleaning and incomplete bit tooth/insert penetration.

The theoretical equation of Maurer (1962) can be verified using experimental data obtained at relatively low bit weight and rotary speeds corresponding to Segment ab in Figs. 6.46 and 6.47. At moderate values of bit weight, the weight exponent is usually observed to be closer to a value of 1 than the value of 2 predicted by Eq. 6.23. At higher values of bit weight, a weight exponent of less than 1 is usually indicated. Bingham (1965) suggested the following drilling equation on the basis of considerable laboratory and field data:

$$R = K \left(\frac{W}{d_b} \right)^{a_s} N, \quad \dots\dots\dots (6.24)$$

where K is the constant of proportionality that includes the effect of rock strength and a_s is the bit-weight exponent. In this equation the threshold bit weight was assumed to be negligible, and the bit-weight exponent must be determined experimentally for the prevailing conditions. However, a constant rotary-speed exponent of 1 was used in the Bingham equation even though some of his data showed behavior similar to that described by Segment bc in Fig. 6.47.

Several authors have proposed the determination of both a bit-weight exponent and a rotary-speed exponent using data representative of the prevailing conditions. Young (1969) pioneered the development of a computerized drilling-control system in which both the bit weight and rotary speed could be varied systematically when a new formation type was encountered, and the bit-weight and rotary-speed exponents could be computed automatically from the observed penetration-rate response. Values of the bit-weight exponent obtained from field data range from 0.6 to 2.0, while values of the rotary-speed exponent range from 0.4 to 0.9.

Fixed-cutter bits require lower WOB and higher RPM when compared with roller-cone bits. The general recommendation is that the highest RPM that can be achieved should be used. In practice, enough WOB should be supplied for the cutters to penetrate through the formation in order to provide the applied torque to conduct the shearing process properly. Insufficient WOB will cause premature cutter wear, possible diamond chipping, and a slow ROP.

Bit Tooth Wear. Most bits tend to drill slower as the bit run progresses because of cutting-element wear. The tooth length of roller-cone bits is reduced continually by abrasion and chipping. As previously discussed, the teeth are altered by hardfacing or by case-hardening processes to promote a self-sharpening type of tooth wear. However, while this tends to keep the tooth pointed, it does not compensate for the reduced tooth length. The inserts

of tungsten-carbide-type roller-cone bits fail by breaking rather than by abrasion. Often, the entire tooth is lost when breakage occurs. Reductions in penetration rate because of bit wear usually are not as severe for insert bits as for milled-tooth bits unless a large number of teeth are broken during the bit run. Diamond and PDC bits also fail from cutting element breakage or loss of diamonds from the matrix.

Several authors have published mathematical models for computing the effect of cutting-element wear on penetration rate for roller-cone bits. Galle and Woods (1963) published the following model:

$$R \propto \left(\frac{1}{0.928125h^2 + 6h + 1} \right)^{a_7}, \quad \dots \dots \dots (6.25)$$

where h is the fractional tooth height that has been worn away and a_7 is an exponent.

A value of 0.5 was recommended for the exponent a_7 for self-sharpening wear of milled-tooth bits, the primary bit type discussed in Galle and Woods (1963). Bourgoyne and Young (1974) suggested a similar but less complex relationship:

$$R \propto \exp(-a_7 h). \quad \dots \dots \dots (6.26)$$

Bourgoyne and Young suggested that the exponent a_7 be determined on the basis of the observed decline of penetration rate with tooth wear for previous bit runs under similar conditions.

Example 6.8 An initial penetration rate of 20 ft/hr is observed in shale at the beginning of a bit run. The previous bit was identical to the current bit and was operated under the same conditions of bit weight, rotary speed, mud density, and other factors. However, a drilling rate of 12 ft/hr was observed in the same shale formation just before pulling the bit. If the previous bit was graded T-6, compute the approximate value of a_7 .

Solution. The value of h for the previous bit just before the end of the bit run is $9/8$ or 0.75. The value of h for the new bit is zero. Thus, from Eq. 6.26, we have

$$R = K e^{-a_7 h},$$

$$20 = K e^{-a_7(0)},$$

and

$$12 = K e^{-a_7(0.75)}.$$

Dividing the first equation by the second yields

$$\frac{20}{12} = e^{a_7(0.75)}.$$

Taking the natural logarithm of both sides and solving for a_7 gives

$$a_7 = \frac{\ln\left(\frac{20}{12}\right)}{0.75} = 0.68.$$

Bit Hydraulics. The introduction of the nozzle-type roller-cone bits in 1953 showed that significant improvements in penetration rate could be achieved through an improved jetting action at the bit. The improved jetting action promoted better cleaning of the bit teeth as well as improved bottomhole jetting action.

Historically, there have been many positions taken as to the best hydraulics parameter to use in characterizing the effect of hydraulics on bit performance. Bit hydraulic horsepower, jet-impact force, flow rate, and nozzle velocity are all parameters commonly discussed. The level of hydraulics achieved at the bit is thought by many to affect the flounder-point of the bit (i.e., a decrease in rate of penetration although the weight on bit is increased to very high values, which occurs as a result of less-efficient bottomhole cleaning caused by high cuttings generation, or a complete penetration of cutters into the hole bottom.

Eckel (1968), working with microbits in a laboratory drilling machine, has made the most extensive laboratory study to date of the relation between penetration rate and the level of hydraulics. Working at constant bit weight and rotary speed, Eckel found that penetration rate could be correlated to a Reynolds-number group given by

$$N_{Re} = K \frac{\rho v d}{\mu_a}, \quad \dots \dots \dots (6.27)$$

where K is a scaling constant, ρ is the drilling-fluid density, v is the flow rate, d is the nozzle diameter, and μ_a is the apparent viscosity of drilling fluid at $10,000 \text{ sec}^{-1}$.

The shear rate of $10,000 \text{ sec}^{-1}$ was chosen as representative of shear rates present in the bit nozzle. The scaling constant, K , is somewhat arbitrary, but a constant value of $1/1,976$ was used by Eckel (1968) to yield a convenient range of the Reynolds-number group.

The results of Eckel's experiments are summarized in **Fig. 6.48**. Note that penetration rate is increased by increasing the Reynolds-number function for the full range of Reynolds numbers studied. When the bit weight was increased, the correlation curve simply was shifted upward as shown in Fig. 6.48. The behavior at the founder point was not studied by Eckel. It can be shown that, for a given drilling fluid, the Reynolds number function is a maximum when the jet-impact force is a maximum.

Data obtained in full-scale laboratory-drilling experiments conducted under simulated borehole conditions (Tibbitts et al. 1981) have shown that the jet-Reynolds-number group, hydraulic horsepower, and jet-impact force all give similar results when used to correlate the effect of bit hydraulics on penetration rate (i.e., as they increase, ROP also increases). It also has been reported that fluid rheological properties, density, and solid content have influence on ROP (Beck et al. 1995).

6.8.2 ROP Equations. The manner in which the important drilling variables that have been discussed affect penetration rate is quite complex and only partially understood. Several mathematical models that attempt to combine the known relationships have been proposed. These models make it possible to apply formal optimization methods to the problem of selecting the best bit weight and rotary speed to achieve the minimum cost per foot. Many authors (Galle and Woods 1963; Edwards 1964; Young 1969; Reed 1972; Bourgoyne and Young 1974) have reported significant reductions in drilling cost through use of these approximate mathematical models.

Roller-Cone Bits. Penetration-rate equations for roller-cone bits have been proposed by various authors. The approach usually taken is to assume that the effects of bit weight, rotary speed, insert wear, and other factors, on penetration rate are all independent of one another and that the composite effect can be computed using an equation of the form

$$R = (f_1)(f_2)(f_3) \dots (f_n), \quad \dots \dots \dots (6.28a)$$

where $f_1, f_2, f_3, \dots, f_n$ represent the functional relations between penetration rate and various drilling variables. The functional relations chosen usually are based on trends observed in either laboratory or field studies. Some authors

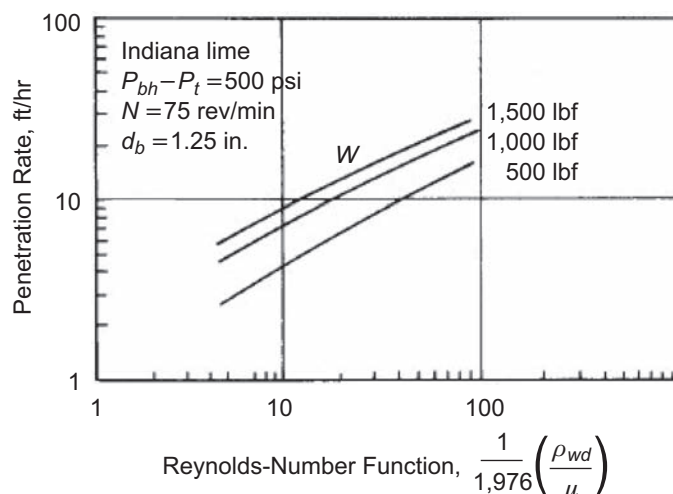


Fig. 6.48—Effect of Reynolds number and WOB on ROP (Eckel 1968).

have chosen to define the functional relation graphically, while others have used curve-fitting techniques to obtain empirical mathematical expressions. Some relatively simple mathematical equations have been used that model only two or three of the drilling variables. An example is the Bingham (1965) model defined by Eq. 6.24.

Perhaps the most complete mathematical drilling model that has been used for roller-cone bits is the model proposed by Bourgoyne and Young (1974). They proposed using eight functions to model the effect of most of the drilling variables discussed in the previous section. The Bourgoyne-Young drilling model can be defined by Eq. 6.28a with the following functional relations:

$$f_1 = e^{2.303 a_1} = K_s \quad \dots \quad (6.28b)$$

$$f_2 = e^{2.303 a_2 (10,000 - D)} \quad \dots \quad (6.28c)$$

$$f_3 = e^{2.303 a_3 D^{0.69} (g_p - 9.0)} \quad \dots \quad (6.28d)$$

$$f_4 = e^{2.303 a_4 D (g_p - \rho_c)} \quad \dots \quad (6.28e)$$

$$f_5 = \left[\frac{\left(\frac{W}{d_b} \right) - \left(\frac{W}{d_b} \right)_t}{4 - \left(\frac{W}{d_b} \right)_t} \right]^{a_5} \quad \dots \quad (6.28f)$$

$$f_6 = \left(\frac{N}{60} \right)^{a_6} \quad \dots \quad (6.28g)$$

$$f_7 = e^{-a_7 h} \quad \dots \quad (6.28h)$$

$$f_8 = \left(\frac{F_j}{1,000} \right)^{a_8} \quad \dots \quad (6.28i)$$

In these equations, D is the true vertical-well depth, ft; g_p is the pore-pressure gradient, lbf/gal; ρ_c is the equivalent circulating density, lbf/gal; $(W/d_b)_t$ is the threshold bit weight per inch of bit diameter at which the bit begins to drill, 1,000 lbf/in.; h is the fractional tooth wear; F_j is the hydraulic impact force beneath the bit, lbf; and a_1 through a_8 are the constants that must be chosen on the basis of local drilling conditions.

The constants a_1 through a_8 can be computed using prior drilling data obtained in the area when detailed drilling data are available. The drilling model can be used both for drilling-optimization calculations and for the detection of changes in formation pore pressure. The function f_1 primarily represents the effects of formation strength and bit type on penetration rate. However, it also includes the effects of drilling variables such as mud type and solids content, which are not included in the drilling model. The exponential expression for f_1 is useful when applying a multiple regression technique presented by Bourgoyne and Young (1974) for computing the values of a_1 through a_8 from prior drilling data obtained in the area. The coefficient 2.303 allows the constant a_1 to be defined easily in terms of the common logarithm of an observed penetration rate.

The functions f_2 and f_3 model the effect of compaction on penetration rate. The function f_2 accounts for the rock-strength increase resulting from the normal compaction with depth, and the function f_3 models the effect of under-compaction experienced in abnormally pressured formations. Note that the $f_2 f_3$ product is equal to 1.0 for a pore-pressure gradient equivalent to 9.0 lbf/gal and a depth of 10,000 ft.

The function f_4 models the effect of overbalance on penetration rate. This function has a value of 1.0 for zero overbalance (i.e., when the formation pore pressure is equal to the bottomhole pressure in the well).

The functions f_5 and f_6 model the effect of bit weight and rotary speed on penetration rate, respectively. Note that f_5 has a value of 1.0 when W/d_b has a value of 4,000 lbf per inch of bit diameter, and f_6 has a value of 1.0 for a rotary speed of 60 rev/min. This was chosen so that the $f_5 f_6$ product would have a value near 1.0 for common

drilling conditions. The threshold bit weight is often quite small and can be neglected in areas such as the US Gulf coast, where the formations are relatively soft. In more-competent formations, the threshold bit weight can be estimated from drilloff tests terminated at very low bit weights. The function f_5 has an upper limit corresponding to the bit founder point, which must be established from drilloff tests. The constants a_5 and a_6 also can be determined from drilloff tests (see Example 6.13). Reported values of a_5 range from 0.5 to 2.0, and reported values of a_6 range from 0.4 to 1.0.

The function f_7 models the effect of tooth wear on penetration rate. The value of a_7 can be estimated from penetration-rate measurements taken in similar formations at similar bit-operating conditions at the beginning and end of a bit run, as shown previously in Example 6.8. The function f_7 has a value of 1.0 for zero insert wear. When tungsten-carbide-insert bits are used and operated at moderate bit weights and rotary speed, insert wear is often insignificant and this term can be neglected. Typical values of a_7 for milled-tooth bits range from 0.3 to 1.5.

The function f_8 models the effect of bit hydraulics on penetration rate. Jet-impact force was chosen as the hydraulic parameter of interest, with a normalized value of 1.0 for f_8 at 1,000 lbf. However, the choice of impact force is arbitrary. Similar results could be obtained with bit hydraulic horsepower or nozzle Reynolds number as the hydraulic parameter affecting penetration rate. Typical values for a_8 range from 0.3 to 0.6.

In practice, it is prudent to select the best average values of a_2 through a_8 for the formation types in the depth interval of interest. However, the value of f_1 varies with the strength of the formation being drilled. The function f_1 is expressed in the same units as penetration rate and commonly is called the *drillability of the formation*. The drillability is numerically equal to the penetration rate that would be observed in the given formation type (under normal compaction) when operating with a new bit at zero overbalance, a bit weight of 4,000 lbf/in., a rotary speed of 60 rev/min, and a depth of 10,000 ft. The drillability of the various formations can be computed with drilling data obtained from previous wells in the area.

Example 6.9 An 8½-in. Class 1-1-1 bit operated at 35,000 lbf and 90 rev/min is drilling in a shale formation at a depth of 9,000 ft at a penetration rate of 30 ft/hr. The formation pore pressure is equivalent to a 9.0-lbm/gal mud, and the equivalent mud weight is 9.7 lbm/gal. The computed impact force beneath the bit is 1,300 lbf, and the computed fractional tooth wear is 0.4. Determine the apparent formation drillability f_1 for this bit type at 9,000 ft using a threshold bit weight of zero and the following values of a_2 through a_8 .

a_2	a_3	a_4	a_5	a_6	a_7	a_8
0.00009	0.000004	0.00002	1.2	0.6	0.4	0.4

Solution. It has been proposed that rate of penetration can be expressed as the multiplication of several exponential functions in the form

$$R = (f_1)(f_2)(f_3) \dots (f_8).$$

For this equation, f_2 through f_8 are presented by Eq. 6.28. Thus, calculation of these functions will yield the determining f_1 .

$$f_2 = e^{2.303 a_2 (10,000 - D)} = e^{2.303 (0.00009) (10,000 - 9,000)} = 1.2303.$$

$$f_3 = e^{2.303 a_3 D^{0.69} (g_p - 9.0)} = e^{2.303 (0.000004) 9,000^{0.69} (9.0 - 9.0)} = 1.0.$$

$$f_4 = e^{2.303 a_4 D (g_p - ECD)} = e^{2.303 (0.00002) (9,000) (9.0 - 9.7)} = 0.74813.$$

$$f_5 = \left[\frac{\left(\frac{\text{WOB}}{d_b} \right) - \left(\frac{\text{WOB}}{d_b} \right)_t}{4 - \left(\frac{\text{WOB}}{d_b} \right)_t} \right]^{a_5} = \left[\frac{\left(\frac{35}{8.5} \right) - 0}{4 - 0} \right]^{1.2} = 1.0354.$$

$$f_6 = \left(\frac{N}{60} \right)^{a_6} = \left(\frac{90}{60} \right)^{0.6} = 1.2754.$$

$$f_7 = e^{-a_7 h} = e^{-(0.4)(0.4)} = 0.85214.$$

$$f_8 = \left(\frac{F_j}{1,000} \right)^{a_8} = \left(\frac{1,300}{1,000} \right)^{0.4} = 1.11065.$$

Therefore, using Eq. 6.28a,

$$30 = (f_1)(1.2303)(1.00494)(0.74813)(1.0354)(1.2754)(0.85214)(1.11065).$$

Thus, f_1 can be calculated as

$$f_1 = 26.08 \text{ ft/hr.}$$

In this example, detailed drilling data were available at a given point in time. This requires the use of a modern well-monitoring and data-recording system. In many instances, data of this quality are not available and an average drillability for an entire bit run must be computed. For bits that show significant insert wear over the life of the bit, the change in the insert-wear function f_7 with time over the life of the bit must be taken into account. If we define a composite drilling variable J_1 using

$$J_1 = (f_1)(f_2)(f_3)(f_4)(f_5)(f_6)(f_8), \quad \dots \quad (6.29)$$

Eq. 6.28a can be expressed by

$$R = \frac{dD}{dt} = J_1 f_7 = J_1 \exp(-a_7 h).$$

Separating variables in this equation yields

$$dD = J_1 \exp(-a_7 h) dt. \quad \dots \quad (6.30)$$

The evaluation of this integral requires a relation between time t and tooth wear h . Recall that Eqs. 6.12 and 6.13 give

$$dt = J_2 \tau_H (1 + H_2 h) dh.$$

Substituting this expression into Eq. 6.30, we obtain

$$dD = J_1 J_2 \tau_H \exp(-a_7 h) (1 + H_2 h) dh. \quad \dots \quad (6.31a)$$

Finally, integration of this equation leads to the following expression of bit footage in terms of the final tooth wear observed.

$$\Delta D = J_1 J_2 \tau_H \left[\frac{1 - e^{-a_7 h_f}}{a_7} + \frac{H_2 (1 - e^{-a_7 h_f} - a_7 h_f e^{-a_7 h_f})}{a_7^2} \right]. \quad \dots \quad (6.31b)$$

This equation can be used to determine the footage corresponding to a given final tooth wear h_f and composite drilling parameter J_1 . Conversely, it also can be used to compute an apparent or average value of J_1 for an observed footage ΔD and final tooth wear h_f . The formation drillability then can be computed from J_1 using Eq. 6.29.

In some cases, it is desirable to compute the footage drilled after a given time interval t_b of bit operation. To use Eq. 6.31 for this purpose, it is necessary to know the insert condition, in terms of dull grade, at the drilling time of interest. Recall that the time required to obtain a given tooth wear is given by Eq. 6.14b. Expressing this equation in terms of h_f , we obtain

$$\left(\frac{H_2 J_2 \tau_H}{2}\right) h_f^2 + (J_2 \tau_H) h_f - t_b = 0.$$

Solving this quadratic equation for h_f gives

$$h_f = \sqrt{\left(\frac{1}{H_2}\right)^2 + \left(\frac{2t_b}{H_2 J_2 \tau_H}\right)} - \frac{1}{H_2}. \quad (6.32)$$

Fixed-Cutter Bits. Diamond bits, as well as other types of fixed-cutter bits, are designed to achieve a given maximum penetration per revolution. Under ideal conditions, the bit weight and RPM are such that the bit is kept feeding into the formation at a constant rate. The penetration rate of a fixed-cutter PDC bit, for a given penetration of the cutting element into the formation, is given by

$$R = L_{pe} n_{be} N, \quad (6.33)$$

where L_{pe} is the effective penetration of each cutting element, n_{be} is the effective number of blades, and N is the rotary speed.

Peterson (1976) developed theoretical equations for the effective penetration L_{pe} and the effective number of blades n_{be} for diamond bits. The equations were derived for a simplified model that assumed the following:

1. The bit has a flat face that is perpendicular to the axis of the hole.
2. Each blade is formed by diamonds laid out as a helix, as shown in **Fig. 6.49a**.
3. The stones are spherical in shape, as shown in Fig. 6.49b.
4. The diamonds are spaced so that the cross-sectional area removed per stone is a maximum for the design depth of penetration.
5. The bit is operated at the design depth of penetration.

The bit hydraulics is sufficient for perfect bottomhole cleaning.

For these conditions, the effective penetration L_{pe} and the effective number of blades n_{be} are given by

$$L_{pe} = 0.67 L_p \quad (6.34a)$$

and

$$n_{be} = 1.92 \left(\frac{C_c}{s_d}\right) d_b \sqrt{d_c L_p - L_p^2}, \quad (6.34b)$$

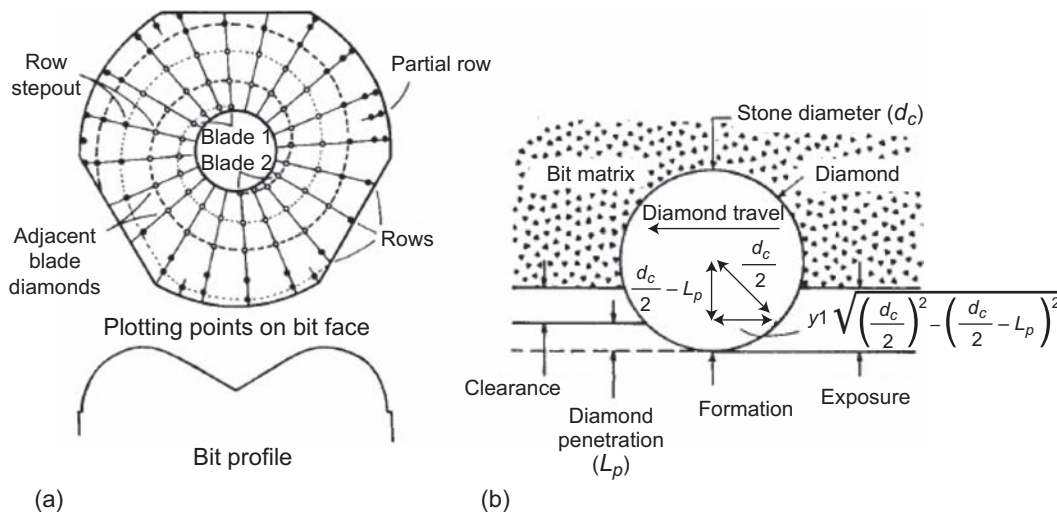


Fig. 6.49—Diamond-bit-stone layout assumed in penetration-rate equation (Peterson 1976).

where C_c is the concentration of diamond cutters, carats/in.²; L_p is the actual depth of penetration of each stone, in.; d_b is the bit diameter, in.; d_c is the average diameter of the face stone cutters, in.; and s_d is the diamond size, carats/stone.

A formation property called the *formation resistance* r_f is used to compute the bit weight required to obtain the design penetration L_p . The formation resistance is the pressure needed to overcome the formation strength, allowing the stone to penetrate the rock.

$$r_f = \frac{W_e}{A_{dt}}, \quad \dots \dots \dots (6.34c)$$

where W_e is the effective weight applied to the bit after the hydraulic pumpoff forces have been taken into account and A_{dt} is the total diamond area in contact with the formation. The formation resistance can be computed from an observed penetration rate after a bit is operated in the formation of interest.

For a spherical stone as shown in Fig. 6.49b, the contact area is given by

$$A_{dt} = \frac{\pi^2 d_b^2}{4} \left(\frac{C_c}{s_d} \right) (d_c L_p - L_p^2). \quad \dots \dots \dots (6.34d)$$

Ziaja (1985) conducted a study on describing the drilling model for PDC core bits and its application to determining the indices of rock properties that affect the bit performance. The model described the mechanical aspects of any PDC core bit, taking into account the wear of PDC cutters that results in penetration-rate reduction.

Example 6.10 A 5.585-in. diamond bit contains 200 stones of 1.0 carats that have a width of 0.0848 in. for a penetration of 0.01 in. Compute the expected ROP if sufficient bit weight for a 0.01-in. depth of a diamond penetration could be maintained at a rotary speed of 100 rev/min.

Solution. ROP can be estimated using Eq. 6.33:

$$\text{ROP} = L_{pe} n_{be} N.$$

Thus, in order to calculate ROP, effective penetration length L_{pe} and effective number of blades n_{be} should be determined.

It is assumed that the bit has a flat face that is perpendicular to the axis of the hole. Therefore,

$$\frac{C_c}{s_d} = \frac{200}{\frac{\pi}{4} d_b^2} = \frac{200}{\frac{\pi}{4} (5.585^2)} = 8.1638 \text{ stone/in.}^2$$

So, the effective number of blades can be calculated using Eq. 6.34b:

$$\begin{aligned} n_{be} &= 1.92 \left(\frac{C_c}{s_d} \right) d_b \sqrt{d_c L_p - L_p^2} \\ &= 1.92 (8.1638) (5.585) \sqrt{0.0848 (0.01) - (0.01^2)} \\ &= 2.39. \end{aligned}$$

Effective penetration length can be obtained with Eq. 6.34a:

$$L_{pe} = 0.67 L_p = 0.67 (0.01) = 0.0067 \text{ in.}$$

Thus, ROP can be calculated by

$$\text{ROP} = L_{pe} n_{be} N = (0.0067) \left(\frac{1 \text{ ft}}{12 \text{ in.}} \right) (2.53) (100) \left(\frac{60 \text{ min}}{1 \text{ hr}} \right) = 8.01 \text{ ft/hr.}$$

6.9 Economics

For those in administration, engineering, manufacturing, and sales, cost calculations are used to evaluate the effectiveness of any product or method, new or old. Because drilling costs are so important, everyone involved should know how to make a few simple cost calculations.

For example, the cost of a PDC bit can be up to 20 times the cost of a milled-tooth bit and up to 4 times the cost of a TCI bit. The choice of a PDC bit, a milled-tooth bit, or an insert roller-cone bit must be economically justified by its performance. Occasionally, this performance justification is accomplished by simply staying in the hole longer. In such cases, the benefits of using that particular bit are intangible.

The main reason for using a bit, however, is that it saves money on a cost-per-foot basis. To be economical, a PDC bit must make up for its additional cost by either drilling faster or staying in the hole longer. Because the bottom line on drilling costs is dollars and cents, bit performance is based on the cost of drilling each foot of hole.

One of the most important aspects of an economic evaluation of a bit is the break-even analysis. A break-even analysis is necessary to determine whether the added bit cost can be justified for a particular application.

The break-even point for a bit is simply the footage and hours needed to equalize the cost-per-foot that would be obtained on a particular well if the bit was not used. To break even, a good offset well must be used for comparative purposes.

6.9.1 Selection of a Bit. As mentioned previously, IADC bit-comparison charts are typically used for selecting the best bit for a particular application (Figs. 6.23 and 6.24). During the planning stage, an in-depth review of offset-well data, records of previous bit performance, and bit-grading characteristics in comparable formations should be conducted. This will help determine the suitable bit types for the formations to be drilled. Data required for a proper bit selection include

- Geological properties and lithological characteristics of the formations to be drilled
- Drilling fluid to be used
- Well profile and equipment to be used

Aggressiveness and wear resistance are two fundamental properties that must be considered when selecting a bit for a specific application. For simplicity's sake, these two bit properties, while not totally independent, may be considered separately. The aggressiveness of the bit is determined by the depth of cut that it is designed to take. In roller-cone bits, aggressiveness is determined by projection, pitch of the teeth, and cone offset. In PDC bits, aggressiveness is determined by the exposure of the cutters and the cutter angle (backrake). Wear resistance, on the other hand, is determined by the density of the cutters, especially those on and near the gauge. In roller-cone bits, increasing wear resistance is accomplished by adding more gauge cutters; using more-durable shapes of cutters; applying diamond to the cutters that contact the gauge; and modifying carbide grade (at the expense of making cutters more brittle) or increasing the number of carbide inserts on the shirrtail. The wear resistance of PDC bits is improved by increasing the length of the gauge so that more cutters can be placed on and near the gauge and by increasing the carbide or diamond content of the gauge pad. Some of the tradeoffs that make a bit more wear resistant also make it more susceptible to cutter breakage and whirl. It is generally accepted that a flat profile is more resistant to off-center bit whirl than a tapered profile, which is more resistant to wear. Typically, bits designed with a specific degree of aggressiveness are available with or without gauge wear enhancement (Spaar et al. 1995).

6.9.2 Cost-Per-Foot Calculation. The performance of a bit may be analyzed on the basis of how much footage it drilled, ft; how fast it drilled (ROP); and how much it cost during the run (the initial cost of the bit and the total operational costs) per foot of the hole drilled. Because the aim of bit selection is to obtain the lowest cost per foot, an analysis is required to achieve this goal. The following equation is usually preferred to estimate the cost per foot for a single bit run:

$$C = \frac{C_b + C_r(t_b + t_t + t_o)}{\Delta D}, \quad \dots \dots \dots (6.35)$$

where C is the overall cost per foot, USD/ft; C_b is the cost of bit, USD; t_b is the rotating time with bit on bottom, hours; t_t is the round-trip time, including connection time, hours; t_o is the other time, which is not rotating time or trip time, hours; C_r is the cost of operating the rig USD/hr; and ΔD is the total footage determined by the particular bit, ft.

As seen from Eq. 6.35, cost per foot is expressed considering the initial cost of the bit, ROP, and the total footage. This equation can be used for many practical purposes, such as conducting a post-drilling analysis to compare one bit run with another in a similar well, or a real-time analysis to decide when to pull the bit out of the hole.

6.9.3 Run-Cycle Speed. The performance of a bit can also be determined by using run-cycle speed (RCS). RCS can be considered as the effective ROP, including the effect of trip time and nonrotating time. RCS (ft/hr) is defined as

$$\text{RCS} = \frac{\Delta D}{t_b + t_t + t_o}, \quad \dots \dots \dots (6.36)$$

where ΔD , t_t , t_b , and t_o are as described in Eq. 6.35. Because rig cost cannot be defined clearly to be used in Eq. 6.35, RCS may give a better understanding of how efficient the drilling operation under consideration is.

6.9.4 Break-Even Analysis. The break-even analysis is usually preferred for conducting an economic analysis of replacing a current bit with a relatively more expensive new bit. The comparison is normally based on a graphical analysis plotting footage vs. rotation time. This analysis is a variation of the cost-per-foot equation. The procedure for developing the plot is as follows:

1. Calculate equivalent rig hours by comparing the initial bit cost C_b (USD) and rig cost C_r (USD/ft) by use of

$$t_{eq} = \frac{C_b}{C_r}. \quad \dots \dots \dots (6.37a)$$

2. Add trip time t_t to t_{eq} to obtain the total number of rig hours corresponding to the cost of the new bit:

$$t_{total} = t_t + t_{eq}. \quad \dots \dots \dots (6.37b)$$

Mark this point on the x-axis of a footage-vs.-time plot, as shown in **Fig. 6.50**.

3. Calculate the footage at break-even cost using

$$\Delta D_{b-e} = \frac{C_b + (t_t)C_r}{C_r}. \quad \dots \dots \dots (6.37c)$$

Mark this point on the y-axis of footage vs. time plot, as shown in Fig. 6.50.

4. Plot a straight line passing through the points obtained in Steps 2 and 3, as shown in Fig. 6.50. This line is the break-even line—that is, any footage and time combination on this line is a break-even point, where cost per foot is constant on any point on this line. Above this line, the new bit will produce lower USD/ft than the offset bit, and below this line, the new bit will be more expensive to run.

6.9.5 Mechanical-Specific-Energy Concept. The concept of mechanical specific energy (MSE) is defined as the work required to destroy a given volume of rock. The MSE-monitoring process can provide the ability to detect changes in drilling efficiency that possibly can be used to optimize operating parameters. Power is defined as

$$P = T \omega + W R,$$

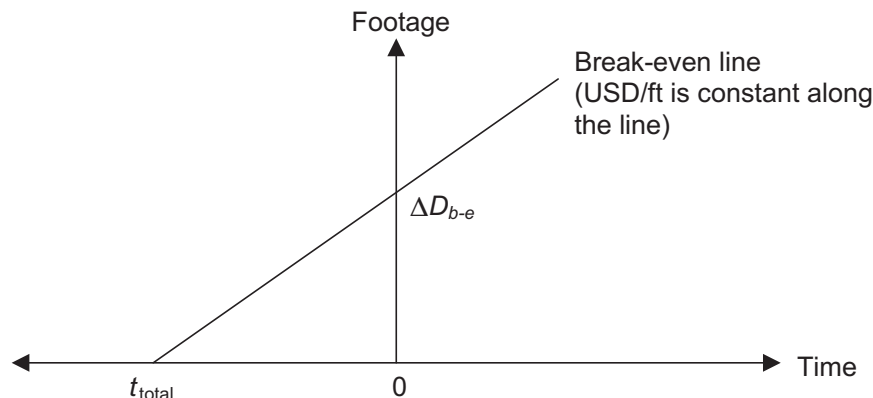


Fig. 6.50—Break-even analysis.

where P is the energy input, W is the WOB, T is the torque, ω is the angular velocity, and R is the ROP. MSE can be expressed in terms of power as

$$\text{MSE} = \frac{P \Delta t}{V}, \quad \dots\dots\dots (6.38a)$$

where Δt is the time interval and V is the volume of rock, which is equal to

$$V = A_b R \Delta t$$

Inserting the definitions of “power” and “volume of rock” into Eq. 6.38a yields

$$\text{MSE} = \frac{T \omega}{A_b R} + \frac{W}{A_b} \quad \dots\dots\dots (6.38b)$$

The MSE equation (Dupriest and Koederitz 2005; Dupriest 2006) can be expressed in terms of drilling parameters as

$$\text{MSE} = \frac{W}{A_b} + \frac{120 \pi N T}{A_b R}, \quad \dots\dots\dots (6.38c)$$

where MSE is in psi, A_b is the bit area, in.²; T is the torque, lbf-ft; W is the WOB, lbf; and N is the rotation speed, rev/min. In Eq. 6.38c, torque is used as a variable in the MSE calculation formula. Torque at the bit can be measured by a measurement-while-drilling system but in most cases no bit-torque measurements exist. The bit-specific coefficient of sliding friction (μ) is introduced to express torque as a function of the WOB and to allow for calculation of the MSE equation in the absence of a reliable torque measurement:

$$T = \frac{\mu d_b \text{WOB}}{36}.$$

Finally, Eq. 6.38c and the torque equation are coupled to form the new form of the MSE equation, which is called the modified MSE and can be shown as

$$\text{MSE}_{\text{mod}} = \text{WOB} \left(\frac{1}{A_b} + \frac{13.33 \mu N}{d_b \text{ROP}} \right) \quad \dots\dots\dots (6.38d)$$

6.9.6 Termination of a Bit Run. There is almost always some uncertainty about the best time to terminate a bit run and begin tripping operations. The use of the tooth-wear equation (Eq. 6.12) and the bearing-wear equation (Eq. 6.17) will provide, at best, a rough estimate of when the bit will be completely worn. In addition, it is helpful to monitor the rotary-table torque. In the case of a roller-cone bit, when the bearings become badly worn, one or more of the cones frequently will lock and cause a sudden increase or large fluctuation in the rotary torque needed to rotate the bit. With a PDC or fixed-cutter bit, when cutter elements are heavily worn or broken, or the bit becomes undergauge, the bit will exhibit much lower than expected ROP and cyclic or elevated torque values.

When the penetration rate decreases rapidly as bit wear progresses, it may be advisable to pull the bit before it is completely worn. If the lithology of the formation is homogeneous, the total drilling cost can be reduced by minimizing the cost of each bit run. In this case, one way to determine when to terminate the bit run is by keeping a current running calculation of the cost per foot for the run, assuming that the bit would be pulled at the current depth. Even if significant bit life remains, the bit should be pulled when the computed cost per foot begins to increase.

However, if the lithology of the formation is not uniform, this procedure will not always result in the minimum total well cost. In this case, an effective criterion for determining optimum bit life can be better established after offset wells are drilled in the area, thus defining the lithological variations, and the contribution of the rock properties can be studied and understood better.

Example 6.11 Determine the optimum bit life for the bit run described in the table below. The lithology of the formation is known to be essentially uniform in this area. The tooth-wear parameter J_2 has a value of 0.4,

the constant H_2 has a value of 6.0, and the bearing-wear parameter J_3 has a value of 0.55. The formation abrasiveness constant τ_H has a value of 50 hours, and the bearing constant τ_B has a value of 30 hours. The bit cost is USD 5,000; the rig cost is USD 4,000/hr; and the trip time is 10 hours.

Footage, ΔD (ft)	Drilling Time, $t_b + t_o$ (hours)	Remarks
0	0	New bit
30	2.0	
50	4.0	
65	6.0	
77	8.0	
87	10.0	
96	12.0	
104	14.0	
111	16.0	Torque increased

Solution. The time required to wear out the teeth can be computed with Eq. 6.14b:

$$t_b = (0.4)(50) \left[(1) + (6) \frac{(1)^2}{2} \right] = 80 \text{ hours.}$$

The time required to wear out the bearings can be computed with Eq. 6.19.

$$t_b = (0.55)(30)(1) = 16.5 \text{ hours.}$$

The cost per foot of the bit run at various depths can be computed with Eq. 6.35. Thus, the overall cost per foot of the bit run that would result if the bit were pulled at the various depths shown are as follows:

Footage, ΔD (ft)	Drilling Time, $t_b + t_o$ (hours)	Drilling Cost, C (USD/ft)
0	0	0.0
30	2.0	1,766.67
50	4.0	1,220.00
65	6.0	1,601.54
77	8.0	1,000.00
87	10.0	977.01
96	12.0	968.75
104	14.0	971.15
111	16.0	981.98

Note that the lowest drilling cost would have resulted if the bit were pulled after 12 hours.

Example 6.12 Recall Example 6.11. Determine the optimum bit life using the break-even analysis and the RCS.

Solution. In order to apply the break-even analysis for determining the optimum bit life, the break-even line must be compared with the RCS. Using Eq. 6.37b,

$$t_{\text{total}} = 10 + \frac{5,000}{4,000} = 11.3 \text{ hours.}$$

A footage (y-axis) vs. time (x-axis) plot is required, which can be obtained using the information given in Example 6.11. On the same plot, t_{total} will be marked. Optimum bit life can be determined by drawing a line that will start from t_{total} , and it will be tangential to the footage-vs.-time curve. Note that the tangential line will have the maximum slope for this case. The result should look like **Fig. 6.51**.

From this graph, it is determined that the bit should be pulled out after 12 hours.

6.10 Bit-Operation Practices

In addition to selecting the best bit for the job, the drilling engineer must see that the bit selected is operated as efficiently and effectively as possible. Items of primary concern include

- Optimizing the BHA
- Preventing premature bit damage
- Bit weights and rotary speeds
- Proper hydraulics
- Bit-run termination criteria

Proper attention must be given to all of these items to maximize drilling performance and minimize drilling costs.

6.10.1 Optimizing the BHA. The BHA used with the bit often has a significant effect on bit performance. The type or size of drill collars used should be effective at preventing the development of bending moments in the drillpipe for the range of bit weight needed during drilling. Also, stabilizers should be used as required to prevent bending of the lower portion of the drill collars. If the drill collars above the bit are not properly centralized in the borehole, the bit rotation and cutting action can be affected adversely. This can result in damaged teeth, bearings, and seals because of cyclic loading on roller-cone bits; chipped or broken cutters on PDC bits; poor borehole quality; directional-drilling problems; much lower performance than anticipated; and increased frequency of drillstring-component failures.

The use of stabilizers having a diameter near the hole size can reduce the severity of these problems greatly. Special shock-absorbing devices called *shock subs* also can be used above the bit to dampen the shock loads further. The additional cost of shock subs is justified more easily for more-expensive bits or for those runs in which success is dependent on achieving a long bit run.

6.10.2 Selection of WOB and Rotation Speed. Drilloff Tests. Frequent changes in formation lithology with depth can make it difficult to evaluate the bit-weight and the rotary-speed exponents from a series of penetration-rate measurements made at various bit weights and rotary speeds. In many cases, the formation lithology may change before the tests are completed. To overcome this problem, a drilloff test can be performed. A drilloff test consists of applying a large weight to the bit and then locking the brake and monitoring the decrease in bit weight with time while maintaining a constant rotary speed. Hooke's law of elasticity then can

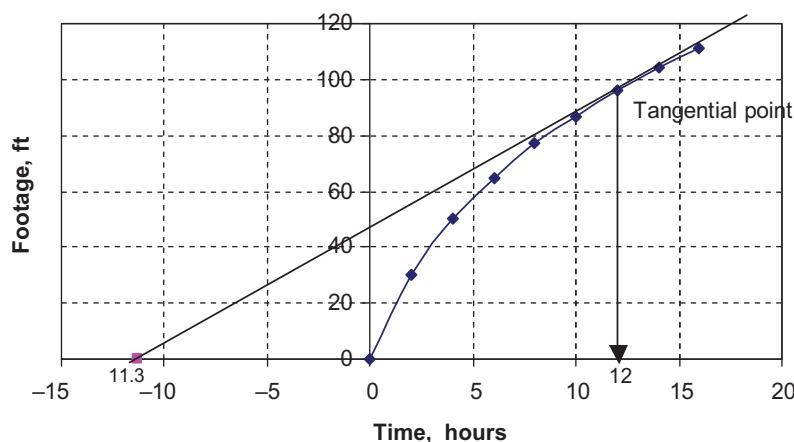


Fig. 6.51—Determination of optimum bit life by use of RCS and break-even analysis.

be applied to compute the amount that the drillstring has stretched as the WOB decreased and the hook load increased. In this manner, the penetration-rate response to changing bit weight can be determined over a very short depth interval.

Hooke's law states that the change in stress is directly proportional to the change in strain:

$$\Delta\sigma = E \Delta\varepsilon. \quad \dots\dots\dots (6.39)$$

For the case of axial tension in a drillstring, the stress change is equal to the change in bit weight divided by the cross-sectional area of the drillpipe. The change in strain is equal to the change in drillpipe length per unit length. Thus, Hooke's law becomes

$$\frac{\Delta W}{A_s} = E \frac{\Delta L}{L}.$$

Solving this expression for ΔL gives

$$\Delta L = \frac{L}{E A_s} \Delta W.$$

The average penetration rate observed for the change in bit weight ΔW can be obtained by dividing this equation by the time interval Δt required to drill off ΔW (Lubinski 1988):

$$R = \frac{\Delta L}{\Delta t} = \frac{L}{E A_s} \frac{\Delta W}{\Delta t}.$$

Range-2 drillpipe has tool-joint upsets over approximately 5% of its length that have a much greater cross-sectional area than the pipe body and essentially do not contribute to the length change observed. Replacing L by $0.95L$ gives

$$R = 0.95 \frac{L}{E A_s} \frac{\Delta W}{\Delta t}. \quad \dots\dots\dots (6.40)$$

The length change of the drill collars is also small and can be ignored.

Example 6.13 Using the following drilloff-test data, evaluate the bit-weight exponent and the rotary-speed exponent. The length of drillpipe at the time of the test was 10,000 ft, and the drillpipe has a cross-sectional area of 5.275 in.² Young's modulus for steel is 30×10^6 . Assume that the threshold bit weight is zero.

Test No. 1 (rotary speed = 150 rev/min)

Bit Weight (1,000 lbf)	Elapsed Time (seconds)
76	0
72	52
68	105
64	160
60	218
56	281
52	352
48	432
44	522
40	626
36	746

Test No. 2 (rotary speed = 100 rev/min)

Bit Weight (1,000 lbf)	Elapsed Time (seconds)
76	0
72	54
68	114
64	180
60	253
56	334
52	424
48	525
44	641
40	773

Solution. The penetration rate can be evaluated using Eq. 6.40:

$$R = 0.95 \frac{L}{E A_s} \frac{\Delta W}{\Delta t}$$

$$= 0.95 \frac{10,000}{(30 \times 10^6) 5.275} \frac{4,000}{\Delta t} = \frac{0.24}{\Delta t}.$$

If we express R in units of ft/hr and Δt in seconds, this expression becomes

$$R = \frac{0.24}{\Delta t} \left(\frac{3,600 \text{ seconds}}{1 \text{ hour}} \right) = \frac{864}{\Delta t}.$$

The drilloff-test data have been evaluated by use of this expression in **Table 6.10**.

A plot of penetration rate vs. average bit weight can be constructed on log-log paper from the results of the drilloff-test analysis. Graphical evaluation of the slope of the straight-line portions of both the $N=150$ rev/min and the $N=100$ rev/min cases yields a value of 1.6. Thus, the observed bit-weight exponent is approximately 1.6 for values of bit weight below the founder region. The rotary-speed exponent can be evaluated from the spacing between the lines in the parallel region.

For example, a penetration rate of 13.7 ft/hr is observed for a bit weight of 58,000 lbf and a rotary speed of 150 rev/min. Reducing the rotary speed to 100 rev/min resulted in a penetration rate of 10.7 ft/hr at the same bit weight. Thus, we have

$$R = K N^{a_6},$$

$$13.7 = K (150)^{a_6},$$

and

$$10.7 = K (100)^{a_6},$$

where K is the constant of proportionality and a_6 is the rotary-speed exponent. Dividing the top equation by the bottom equation gives

$$\frac{13.7}{10.7} = \left(\frac{150}{100} \right)^{a_6}.$$

TABLE 6.10—EXAMPLE OF DRILL-OFF-TEST ANALYSIS (Bourgoyne et al. 1991)

Bit Weight (1,000 lbf)	Average Bit Weight (1,000 lbf)	N=150 rev/min			N=100 rev/min		
		Elapsed Time (seconds)	Δt (seconds)	R (ft/hr)	Elapsed Time (seconds)	Δt (seconds)	R (ft/hr)
76		0			0		
	74		52	16.6		54	16.6
72		52			54		
	70		53	16.6		60	14.4
68		105			114		
	66		55	15.7		66	13.1
64		160			180		
	62		58	14.9		73	11.8
60		218			253		
	58		63	13.7		81	10.7
56		281			334		
	54		71	12.2		90	9.6
52		352			424		
	50		80	10.8		101	8.6
48		432			525		
	46		90	9.6		116	7.4
44		522			641		
	42		104	8.3		132	6.5
40		626			733		
	38		120	7.2			
36		746					

Taking the logarithm of both sides and solving for a_6 yields

$$a_6 = \frac{\log\left(\frac{13.7}{10.7}\right)}{\log\left(\frac{150}{100}\right)} = 0.6.$$

In this example, a good straight-line fit was obtained below the founder region assuming the threshold bit weight was zero. When the threshold bit weight is not zero, it may be necessary to subtract the threshold bit weight from the bit-weight column before plotting the data. If the threshold bit weight is not known, it can be determined by trial and error as the value that gives the best straight-line fit.

WOB and Rotation-Speed Optimization. The weight applied to the bit and the rotational speed of the drill-string have a major effect on both the performance and the life of the bit. These parameters are usually changed during the drilling operation to improve ROP as dictated by formation hardness, to mitigate bit vibrations, to improve directional-drilling efficiency, and to minimize rate of cutter wear. Thus, the determination of the optimum bit weight and rotary speed for a given bit run is one of the routine challenges faced by the drilling engineer.

For roller-cone bits, there are several published methods for computing optimum combinations of bit weight and rotary speed that ensure improved overall drilling performance and reduced drilling costs (Galle and Woods 1963; Edwards 1964; Young 1969; Reed 1972; Bourgoyne and Young 1974; Estes 1974; Lummus 1974). All of these methods require the use of mathematical models to define the effect of bit weight and rotary speed on penetration rate and bit wear. Methods are available for computing both the best variable bit-weight/rotary-speed

schedule and the best constant bit weight and rotary speed for the entire bit run. Galle and Woods (1963) have reported that the simpler constant-weight/-speed methods result in only slightly higher costs per foot than the methods allowing the bit weights and rotary speeds to vary as the bit dulls or encounters different formation characteristics. Reed (1972) indicated a difference of less than 3% in cost per foot between the variable-weight/-speed and the constant-weight/-speed schedules for the cases studied.

One straightforward technique used with roller-cone bits to determine the best constant-weight/-speed schedule is to generate a cost-per-foot table. The cost per foot for various assumed bit weights and rotary speeds can be computed using the penetration-rate and bit-wear models. The best combination of bit weight and rotary speed, the best bit weight for a given rotary speed, or the best rotary speed for a given bit weight then can be read from the table, which corresponds to the minimum cost per foot. The use of the best bit weight for a given rotary speed may be desirable when the rotary-speed selection is limited by the rotary-power transmission system. The best rotary speed for a given bit weight may be desirable when the bit weight is limited because of hole-deviation problems.

Example 6.14 A Class 1-3-1 bit will be used to drill a formation at 7,000 ft having a drillability of 20 ft/hr. The abrasiveness constant τ_H has a value of 15.7 hours, the bearing constant τ_b has a value of 22 hours, and the bearing exponents B_1 and B_2 are equal to 1.0. The formation pore-pressure gradient is equivalent to a 9.0-lbm/gal fluid, and the mud density is 10 lbm/gal. The bit costs USD 4,000, the operating cost of the drilling operation is USD 5,000/hr, the time required to trip for a new bit is 6.5 hours, and 3 minutes are required to make a connection. Using a threshold bit weight per inch $(W/db)_t$ of 0.5 and the values of a_2 through a_8 as given, compute the cost per foot that would be observed for $W/db = 4.0$, $N = 60$ rev/min, and a jet-impact force of 900 lbf.

a_2	a_3	a_4	a_5	a_6	a_7	a_8
0.000087	0.000005	0.000017	1.2	0.6	0.9	0.4

Solution. Using Table 6.8 for a Class 1-3-1 bit, we obtain $H_1 = 1.84$, $H_2 = 6$, and $(W/d_b)_{\max} = 8.0$. The value of J_2 as a function of bit weight and the rotary speed is given by Eq. 6.13:

$$J_2 = \frac{\left[\left(\frac{W}{d_b} \right)_{\max} - \left(\frac{W}{d_b} \right) \right]}{\left[\left(\frac{W}{d_b} \right)_{\max} - 4 \right]} \left(\frac{60}{N} \right)^{H_1} \left(\frac{1}{1 + \frac{H_2}{2}} \right),$$

$$J_2 = \frac{\left[8 - \left(\frac{W}{d_b} \right) \right]}{8 - 4} \left(\frac{60}{N} \right)^{1.84} \left(\frac{1}{1 + \frac{6}{2}} \right),$$

$$J_2 = 0.250 \left(2 - \frac{W}{4d_b} \right) \left(\frac{60}{N} \right)^{1.84}.$$

For $W/d_b = 4$ and $N = 60$, J_2 has a value of 0.250. Using a final tooth dullness of 1.0, Eq. 6.14b gives

$$t_b = J_2 \tau_H \left[(1) + 6 \frac{(1)^2}{2} \right] = 4 J_2 \tau_H.$$

Substituting the values of τ_H and J_2 into this equation yields

$$\begin{aligned} t_b &= 4(15.7)(0.25) \left(2 - \frac{W}{4d_b} \right) \left(\frac{60}{N} \right)^{1.84} \\ &= 15.7 \left(2 - \frac{W}{4d_b} \right) \left(\frac{60}{N} \right)^{1.84}. \end{aligned}$$

For $W/d_b = 4$ and $N = 60$, the time required to reach a tooth dullness of 1.0 predicted by this equation is 15.7 hours.

The bearing life can be computed using Eqs. 6.18 and 6.19:

$$J_3 = \left(\frac{60}{N} \right) \left(\frac{4d_b}{W} \right)^{1.0},$$

$$t_b = J_3 \tau_B b_f = J_3 (22)(1) = 22 \left(\frac{60}{N} \right) \left(\frac{4d_b}{W} \right).$$

For $W/d_b = 4$ and $N = 60$, the time required to completely wear the bearings predicted by this equation is 22 hours. Evaluation of the multipliers f_1 through f_4 and f_8 yields the following:

$$f_1 = 20.$$

$$f_2 = e^{2.303 a_2 (10,000 - D)} = e^{2.303 (0.000087)(10,000 - 7,000)} = 1.83.$$

$$f_3 = e^{2.303 a_3 D^{0.69} (g_p - 9.0)} = 1.0 \text{ for } g_p = 9.0.$$

$$f_4 = e^{2.303 a_4 D (g_p - \rho_c)} = e^{2.303 (0.000017)(7,000)(9.0 - 10.0)} = 0.76.$$

$$f_8 = \left(\frac{F_j}{1,000} \right)^{a_8} = \left(\frac{900}{1,000} \right)^{0.4} = 0.959.$$

Substitution of these values into Eq. 6.29 gives

$$J_1 = (f_1)(f_2)(f_3)(f_4)(f_5)(f_6)(f_8);$$

$$J_1 = (20)(1.83)(1.0)(0.76)(f_5)(f_6)(0.959) = 26.7(f_5)(f_6).$$

For $W/d_b = 4$ and $N = 60$, both the bit-weight function f_5 and the rotary-speed function f_6 have a value of 1.0; thus, J_1 has a value of 26.7.

The footage drilled before tooth failure at 15.7 hours is given by Eq. 6.31b:

$$\Delta D = J_1 J_2 \tau_H \left[\frac{1 - e^{-a_7 h_f}}{a_7} + \frac{H_2 (1 - e^{-a_7 h_f} - a_7 h_f e^{-a_7 h_f})}{a_7^2} \right].$$

Because the bit teeth will fail first, the final tooth dullness h_f is known to be 1.0. When the bearings fail first, it is necessary to compute h_f for the known value of t_b using Eq. 6.32. Solving the above equation for ΔD , we obtain

$$\Delta D = (26.7)(0.250)(15.7) \left\{ \frac{1 - e^{-(0.9)}}{(0.9)} + \frac{6 [1 - e^{-(0.9)} - (0.9)e^{-(0.9)}]}{(0.9)^2} \right\} = 246 \text{ ft.}$$

This footage corresponds to approximately eight joints of drillpipe at 3 minutes per connection. The total connection time is

$$t_o = \frac{3}{60}(8) = 0.4 \text{ hours.}$$

The cost per foot for the bit run is given by Eq. 6.35

$$C = \frac{C_b + C_r (t_b + t_l + t_o)}{\Delta D} = \frac{(4,000) + (5,000)(15.7 + 6.5 + 0.4)}{(246)} = \text{USD } 475.61/\text{ft.}$$

This is the predicted cost per foot that corresponds to ending the bit run just before bit failure and is usually the minimum cost per foot for the bit weight and rotary speed assumed. However, to ensure that this is true, the cost per

foot corresponding to a slightly shorter bit life should be checked. For example, if the bit was pulled after 15 hours, the final tooth dullness, as computed from Eq. 6.32, is given by

$$h_f = \sqrt{\left(\frac{1}{H_2}\right)^2 + \left(\frac{2t_b}{H_2 J_2 \tau_H}\right)} - \frac{1}{H_2}.$$

$$h_f = \sqrt{\left(\frac{1}{6}\right)^2 + \left[\frac{2(15)}{6(0.25)(15.7)}\right]} - \frac{1}{6} = 0.974.$$

The footage drilled for this value of h_f would be

$$\Delta D = (26.7)(0.250)(15.7) \left\{ \frac{1 - e^{-(0.9)(0.974)}}{(0.9)} + \frac{6 \left[1 - e^{-(0.9)(0.974)} - (0.9)(0.974)e^{-(0.9)(0.974)} \right]}{(0.9)^2} \right\} = 238 \text{ ft.}$$

The cost per foot after 15 hours of drilling time is given by

$$C = \frac{(4,000) + (5,000)(15.7 + 6.5 + 0.4)}{(238)} = \text{USD } 491.60/\text{ft.}$$

Note that this cost per foot is slightly greater than the cost per foot corresponding to the maximum possible bit life.

Analytical expressions for the best constant bit weight and rotary speed were derived by Bourgoyne and Young (1974) for the case in which tooth wear limits bit life. Eq. 6.35, the cost-per-foot equation, can be rearranged to give

$$C = \frac{C_r}{\Delta D} \left(\frac{C_b}{C_r} + t_b + t_t \right).$$

Substituting Eq. 6.14a for t_b and Eq. 6.31a for ΔD in this cost-per-foot formula yields

$$C = \frac{C_r}{\int_0^{h_f} e^{(-a_5 h)} (1 + H_2 h) dh} \left[\frac{\frac{C_b}{C_r} + t_t}{J_1 J_2 \tau_H} + \frac{\int_0^{h_f} (1 + H_2 h) dh}{J_1} \right].$$

Taking $\frac{\partial C}{\partial \left(\frac{W}{d_b}\right)} = 0$ and solving yields

$$\left(\frac{C_b}{C_r} + t_t \right) \left\{ a_5 - \frac{\frac{W}{d_b} - \left(\frac{W}{d_b}\right)_t}{\left[\left(\frac{W}{d_b}\right)_{\max} - \frac{W}{d_b}\right]} \right\} + a_5 J_2 \tau_H \int (1 + H_2 h) dh = 0. \quad \dots \quad (6.41a)$$

Taking $\frac{\partial C}{\partial N} = 0$ and solving yields

$$\left(\frac{C_b}{C_r} + t_t \right) \left(1 - \frac{H_1}{a_6} \right) + J_2 \tau_H \int (1 + H_2 h) dh = 0. \quad \dots \quad (6.41b)$$

Solving these two equations simultaneously for W/d_b gives the following expression for optimum bit weight:

$$\left(\frac{W}{d_b} \right)_{\text{opt}} = \frac{a_5 H_1 \left(\frac{W}{d_b} \right)_{\max} + a_6 \left(\frac{W}{d_b} \right)_t}{a_5 H_1 + a_6}. \quad \dots \quad (6.42)$$

If the optimum bit weight predicted by this equation is greater than the flounder bit weight, then the flounder bit weight must be used for the optimum. The optimum bit life is obtained by solving either Eq. 6.41a or Eq. 6.41b for $J_2 \tau_H \int (1 + H_2 h) dh$:

$$t_b = \left(\frac{C_b}{C_r} + t_i + t_c \right) \left(\frac{H_1}{a_6} - 1 \right). \quad \dots\dots\dots (6.43)$$

The optimum rotary speed N_{opt} is obtained using the known value of t_b , in Eq. 6.14b, and solving for J_2 . N_{opt} then can be obtained from J_2 using Eq. 6.13. This leads to the following expression for N_{opt} :

$$N_{\text{opt}} = 60 \left[\frac{\tau_H}{t_b} \frac{\left(\frac{W}{d_b} \right)_{\text{max}} - \left(\frac{W}{d_b} \right)_{\text{opt}}}{\left(\frac{W}{d_b} \right)_{\text{max}} - 4} \right]^{\frac{1}{H_1}} \quad \dots\dots\dots (6.44)$$

Unfortunately, for the case where bit life is limited by bearing wear or penetration rate, such simple expressions for the optimum conditions have not been found, and the construction of a cost-per-foot table is the best approach. This type of calculation is most easily accomplished using a computer.

Example 6.15 Compute the optimum bit weight and rotary speed for a Class 1-1-1 bit, which will be used to drill a formation at 9,000 ft that has a drillability of 40 ft/hr. The abrasiveness constant τ_H has a value of 38 hours. The threshold bit weight per inch is given as 0.5×10^3 lbf/in. and the flounder bit weight is known to be 60,000 lbf at 60 rev/min. Bit cost is USD 6,000 and the cost of the drilling operation is USD 8,000/hr. Required time to trip is 7 hours, and connection time per triple stand is 4 minutes. Determine the optimum WOB and rotary speed for this well if a_5 and a_6 are given as 1.2 and 0.6, respectively.

Solution. Optimum bit weight (Eq. 6.42) and rotary speed (Eq. 6.44) can be determined using

$$\left(\frac{W}{d_b} \right)_{\text{opt}} = \frac{a_5 H_1 \left(\frac{W}{d_b} \right)_{\text{max}} + a_6 \left(\frac{W}{d_b} \right)_i}{a_5 H_1 + a_6}$$

and

$$N_{\text{opt}} = 60 \left[\frac{\tau_H}{t_b} \frac{\left(\frac{W}{d_b} \right)_{\text{max}} - \left(\frac{W}{d_b} \right)_{\text{opt}}}{\left(\frac{W}{d_b} \right)_{\text{max}} - 4} \right]^{\frac{1}{H_1}}.$$

Because the bit is Class 1-1-1 (from Table 6.8), H_1 is equal to 1.90 and $\left(\frac{W}{d_b} \right)_{\text{max}}$ is equal to 7.0. Therefore, optimum bit weight can be calculated as

$$\left(\frac{W}{d_b} \right)_{\text{opt}} = \frac{(1.2)(1.90)(7.0) + (0.6)(0.5)}{(1.2)(1.90) + (0.6)} = 5.65 \text{ klbf/in.}$$

Because the flounder WOB is 60,000 lbf, bit diameter can be estimated as

$$d_b = \frac{60,000}{7,000} = 8.571 \text{ in.}$$

Thus, optimum WOB is equal to 48,390 lbf.

In order to estimate the optimum rotary speed, bit time t_b has to be evaluated using Eq. 6.43. Bit time is given by

$$t_b = \left(\frac{C_b}{C_r} + t_i + t_o \right) \left(\frac{H_1}{a_6} - 1 \right) = \left[\frac{6,000}{8,000} + 7 + \frac{9000}{(90)4} \frac{1 \text{ hr}}{60 \text{ min}} \right] \left(\frac{1.9}{0.6} - 1 \right) = 17.69 \text{ hours.}$$

Thus, optimum rotary speed is equal to

$$N_{\text{opt}} = 60 \left[\left(\frac{38}{17.69} \right) \left(\frac{7.0 - 5.65}{7.0 - 4} \right) \right]^{\frac{1}{1.90}} = 59.03 \text{ rev/min.}$$

So, the optimum WOB and rotation speed combination is 48,390 lbf and 59.03 rev/min, respectively.

For PDC bits, optimization of drilling parameters is also possible. Wojtanowicz and Kuru (1987) introduced an optimization methodology for PDC bits, assuming a footage and determining the optimum operating conditions to maximize the ROP. Footage is defined as a function of rate of penetration R , which depends on many drilling parameters.

$$\Delta D = \int_0^{t_b} R(W, N, K, \omega, \dots) dt = \text{constant}, \quad \dots \quad (6.45)$$

where W is weight on bit, N is rotation speed, K is drillability of the formation, and ω is dimensionless wear on cutters. Values of W and N are considered to be within the practical limits. The ROP equation defined in Wojtanowicz and Kuru (1987) has the form

$$R = K(W - W_t)f(\omega)N^a, \quad \dots \quad (6.46)$$

where W_t is the threshold bit weight to maintain shearing, $f(\omega)$ is the linear wear function of the cutters, and a is constant. The model proposed by Wojtanowicz and Kuru (1987) focuses on the minimum cost that will be achieved by using multiple bits, such that

$$C = \sum_{n=1}^M [C_{b_n} + C_r(t_{b_n} + t_{o_n})] = \min, \quad \dots \quad (6.47)$$

where n is the current bit and M is the total number of bits used. It is known that

$$t_b = \frac{\Delta D}{R}. \quad \dots \quad (6.48)$$

Optimum WOB and rotation speeds are selected on the basis of an iterative procedure that satisfies the condition for Eq. 6.47 of being minimum.

Problems

- 6.1 List the two main types of bits in use today. Also, list two subclassifications of each basic bit type and discuss the conditions considered ideal for the application of each subclassification given.
- 6.2 Discuss how cone offset, tooth height, and number of teeth differ between soft- and hard-formation insert-cutter bits.
- 6.3 Discuss how blade count, cutter density, and cutter structure differ between soft- and hard-formation PDC bits.
- 6.4 Discuss the primary mechanism of drilling for roller-cone bits and fixed-cutter bits.
- 6.5 A rock sample is placed in a strength-testing machine at atmospheric pressure and compressed axially to failure. A force of 12,000 lbf was required for rock failure, and the cross-sectional area of the sample was 2.0 in.² The sample failed along a plane that makes a 35° angle with the direction of the compressional loading.
 - (a) Construct a Mohr's circle using the two principal stresses present.
 - (b) Compute the shear stress present along the plane of failure.
 - (c) Compute the stress normal to the plane of failure.
 - (d) Compute the angle of internal friction.
 - (e) Compute the cohesive resistance of the material.
 - (f) Label the parameters computed in the Steps (b) through (e) on the Mohr's-circle construction. Using the Mohr criterion, compute the compressional force required for rock failure if the sample is placed under a 5,000-psi confining pressure.
- 6.6 What is the best basis of comparison when trying to choose between two different bit types?
- 6.7 The bit type currently used to drill a given formation consistently yields a drilling cost of approximately USD 500/ft. You are sending a new experimental bit type to the field for evaluation in this formation. The new bit is expected to have a bit life of approximately 150 hours as compared with the usual bit life of 50 hours. The new bit costs USD 10,000 and the operating cost of the drilling operation is USD 7,500/hr. Trip time is

approximately 10 hours for the depth of interest. Prepare a graph that shows the break-even cost of USD 500/ft as a function of penetration rate and bit life to assist in the field evaluation of the new bit. Label the region of the graph that shows combinations of penetration rate and bit life that are not acceptable. If the initial penetration rate of the new bit during the first hour is 10 ft/hr, what would you recommend?

6.8 Grade the bit shown in the photograph below (West et al. 2004).



- 6.9 A 9.875-in. Class 1-1-1 bit drilled from a depth of 12,000 to 12,200 ft in 12 hours. The average bit weight and rotary speed used for the bit run were 40,000 lbf and 90 rev/min, respectively. When the bit was pulled, it was graded T-6, B-6. The drilling fluid was a barite-weighted clay/water mud having a density of 12 lbm/gal.
- Compute the average formation-abrasiveness constant for this depth interval.
 - Estimate the time required to completely dull the bit teeth using a bit weight of 45,000 lbf and a rotary speed of 100 rev/min.
 - Compute the bearing constant for this depth interval.
 - Estimate the time required to completely dull the bearings using a bit weight of 45,000 lbf and a rotary speed of 100 rev/min.
- 6.10 Why is cooling the cutters of PDC bits one of the major considerations during an operation?
- 6.11 Compute the bearing constant τ_B for the bit of Example 6.4. Use values of B_1 and B_2 recommended in Table 6.9.
- 6.12 Field data obtained on 7.875-in., Series 6, roller-bearing bits at a rotary speed of 60 rev/min show an average bearing life of 32 hours for a bit weight of 5,700 lbf/in. and 45 hours for 3,800 lbf/in. Compute the apparent bearing weight exponent B_2 and the bearing constant τ_B for this bit type.
- 6.13 Field data observed on 7.875-in., Series 6, sealed journal-bearing bits operating at a rotary speed of 60 rev/min show an average bearing life of 67 hours at 5,700 lbf/in. and 100 hours at 3,800 lbf/in. Compute the apparent bearing weight exponent B_2 and the bearing constant τ_B for this bit type.
- 6.14 Field data observed on 7.875-in., Series 6, sealed journal-bearing bits operated with 4,000 to 5,000 lbf of bit weight per inch of bit diameter showed a medium bit life of 95 hours at a rotary speed of 60 rev/min and 185 hours at 40 rev/min. Using an assumed value of 1.0 for B_2 compute the apparent values for B_1 and τ_B from these observations.
- 6.15 Field data obtained using 7.875-in., Series 6, sealed roller-bearing insert bits operated at 4,000 lbf per inch of bit diameter indicated an average bit life of 42 hours at a rotary speed of 60 rev/min and 55 hours at 40 rev/min. Compute the apparent values of B_1 and τ_B .
- 6.16 Recommend values of B_2 and t_B for 7.875-in., nonsealed, roller-bearing bits operated in oil muds, weighted clay/water muds (barite muds), and a clay/water mud containing H_2S (sulfide mud). The recommendation should be based on the laboratory bearing-wear data shown in the following table and conducted at a rotary speed of 60 rev/min. The bearing life was determined on the basis of 0.1-in. wear in the bearing races.

Laboratory Bearing-Life Data Obtained at 60 rev/min			
Bit Weight/in.	Bearing Life (hours)		
(1,000 lbf/in.)	Sulfide Mud	Barite Mud	Oil Mud
3	14.0	48.0	—
6	7.5	17.5	80.0
9	—	—	25.0

- 6.17 Field data obtained on 8.5-in. sealed roller-bearing insert bits are shown below. Use these data to obtain representative values of B_1 , B_2 , and τ_B for this bit type.

Bit Weight (1,000 lbf/in.)	Rotary Speed (rev/min)	Bearing Life (hours)
4	60	41
6	60	30
4	40	81

- 6.18 Upon completing the drilling run using a diamond-core bit, the following data were recorded: outer diameter of bit = $4\frac{7}{16}$ in.; inner diameter of bit = $3\frac{1}{8}$ in.; diamond size = 0.4 carat/stone; average diamond density = 3.5 carat/in.²; total rotation time = 20 hours; WOB = 7,000 lbf; rotation speed = 250 rev/min; and index of rock abrasiveness is 5.0×10^{-10} in.³/lbf-in. Calculate the linear wear on the diamonds.
- 6.19 Determine the optimum bit life for the bit run described in the following table. The lithology is known to be uniform for the depth range of interest. The tooth wear parameter J_2 has a value of 0.15, the constant H_2 has a value of 7.0, and the bearing-wear parameter J_3 has a value of 0.56. The formation abrasiveness constant τ_H has a value of 40 hours, and the bearing constant τ_B has a value of 40 hours. The bit cost is USD 6,000, the rig-operating cost is USD 5,000/hr, and the trip time is 6 hours.

Drilling Time $t_b + t_o + t_t$ (hours)	Total Footage DD (ft)	Remarks
0	0	New bit
2	30	
4	54	
6	73	
8	88	
10	104	
12	117	
14	127	
16	135	
18	142	
20	147	
22	151	Torque increase

- 6.20 List the factors affecting penetration rate in Problem 6.19.
- 6.21 A penetration rate in shale of 20 ft/hr was obtained using a mud density of 12 lbm/gal at a depth of 10,000 ft. When the mud density was increased to 13 lbm/gal, the penetration rate was decreased to 9.5 ft/hr for similar drilling conditions. Compute the apparent value of the overbalance exponent a_4 .
- 6.22 The penetration rate in shale is observed to increase from 12 to 18 ft/hr when the bit weight is increased from 30,000 to 50,000 lbf. Compute the bit-weight exponent a_5 .
- 6.23 Using the following drilloff-test data, evaluate the bit-weight exponent a_5 and the rotary-speed exponent a_6 . The length of the 4.5-in., 16.6-lbm/ft drillpipe is 12,000 ft.
Test No. 1 (rotary speed = 120 rev/min)

Bit Weight (1,000 lbf)	Elapsed Time (seconds)
80	0
76	104
72	210

Bit Weight (1,000 lbf)	Elapsed Time (seconds)
68	320
64	436
60	562
56	704
52	864
48	1,045

Test No. 2 (rotary speed = 80 rev/min)

Bit Weight (1,000 lbf)	Elapsed Time (seconds)
80	0
76	108
72	228
68	360
64	506
60	668
56	848
52	1,050

- 6.24 The average penetration rate in shale is observed to drop from 18 ft/hr for a new bit to 11 ft/hr at the end of the bit run. The bit was graded T-6, B-7. Assuming that all variables other than tooth wear remained constant, evaluate the tooth-wear exponent a_7 .
- 6.25 A bit contains three $1\frac{1}{32}$ -in. nozzles, and the mud, which has a density of 10 lbm/gal, is being circulated at a rate of 600 gal/min. The penetration rate is observed to decrease from 15 to 11 ft/hr when one of the two pumps is stopped temporarily, causing the circulation rate to fall from 600 to 400 gal/min. Compute the apparent hydraulics exponent a_8 .
- 6.26 An 8.5-in. Class 1-1-1 bit operated at 35,000 lbf and 90 rev/min is drilling in a shale formation at a depth of 9,000 ft at a penetration rate of 30 ft/hr. The formation pore pressure is equivalent to a 9.0-lbm/gal mud, and the equivalent circulating density of the mud on bottom is 9.7 lbm/gal. The computed impact force beneath the bit is 1,300 lbf, and the computed fractional tooth wear is 0.4. Compute the apparent formation drillability f_1 for this bit type at 9,000 ft using a threshold bit weight of zero and the following values of a_2 through a_8 .

a_2	a_3	a_4	a_5	a_6	a_7	a_8
0.00009	0.000004	0.00002	1.2	0.6	0.4	0.4

- 6.27 A diamond bit with a total blade length of 5.585 in. contains 200 stones of 1.0 carats that have a width of 0.0848 in. for a penetration of 0.01 in. Compute the expected penetration rate if sufficient bit weight for a 0.01-in. depth of diamond penetration could be maintained at a rotary speed of 100 rev/min. Assume that the diamonds are shaped and arrayed so that the penetration is two-thirds the maximum penetration depth.
- 6.28 A 9.875-in. diameter Class 1-1-1 bit will be used to drill a formation at 9,000 ft that has a drillability of 40 ft/hr. The abrasiveness constant τ_H has a value of 38 hours, and the bearing constant τ_B has a value of 22 hours. The formation pore-pressure gradient is equivalent to a 9.0-lbm/gal fluid gradient, and the weighted clay/water drilling fluid (barite mud) has a density of 9.7 lbm/gal. The bit cost is USD 6,000, the operating cost of the drilling operation is USD 8,000/hr, the time required to trip for a new bit is 7 hours, and 4 minutes is required to make a connection per 30-ft joint of drillpipe. Using a threshold bit weight per inch of 0.5 and the constants a_2 through a_8 given in Problem 6.26, compute the cost per foot that would be observed for $(W/d_b) = 4.5$, $N = 90$ rev/min, and a jet-impact force of 1,100 lbf.

- 6.29 Compute the optimum bit weight and rotary speed for the bit described in Problem 6.28, assuming bit life is limited by tooth wear. Ignore the effect of connection time. The flounder bit weight is known to be 60,000 lbf/in.
- 6.30 After drilling for 24 hours, a footage of 384 ft has been achieved. The bit used has a cost of USD 4,000. The bit will be replaced with a new one. Two different bit candidates are available, which are expected to give an 18-ft/hr and 21-ft/hr ROP. Bit costs are USD 6,000 and USD 10,000, respectively. The average rig-operation cost is USD 1,200/hr. Determine the more economical bit.

Nomenclature

- a_1 – a_8 = exponents in the penetration rate equation
 A = area, in.²
 A_b = area of bit, in.²
 A_{dt} = total diamond area in contact with the formation, in.²
 b_f = final bearing wear at end of bit run
 B_1, B_2 = bearing-wear exponents
 c = cohesive resistance of material, psi
 C = cost per foot, USD/ft
 C_b = initial cost of bit, USD
 C_c = concentration of diamond cutters, carats/in.²
 C_d = average density of the face stones, carats/in.²
 C_r = fixed operating cost of rig per unit time, USD/hr
 d = diameter, in.
 d_b = diameter of bit, in.
 d_c = diameter of cutter, in.
 d_d = average diamond diameter, in. (if not known, $d_d = \frac{s_d^{0.33}}{4.99}$)
 D = depth, ft
 D_{b_i} = inner diameter of the bit, in. (if the bit is a core bit, $D_{b_i} \neq 0$, but if the bit is a drilling bit, $D_{b_i} = 0$)
 D_{b_o} = outer diameter of the bit, in.
 E = Young's modulus of elasticity, psi
 F = force, lbf
 f_1 – f_8 = functions defining effect of various drilling variables
 F_n = normal force on cutter, lbf
 g_p = formation pore-pressure gradient expressed as an equivalent fluid density, lbm/gal
 G = geometry constant for a given tooth design
 h = fractional tooth wear
 h_f = final tooth wear at end of bit run
 H_1 – H_3 = tooth-geometry constants used to predict bit tooth wear
 J_1 – J_3 = composite functions of bit weight and rotary speed used in penetration-rate, tooth-wear, and bearing-wear equations, respectively
 K = scaling constant
 L = length, in.
 L_i = initial height, in.
 L_p = depth of penetration of drag-bit cutter, in.
 L_r = height removed, in.
 L_w = width cut by an individual diamond for a penetration L_p , in.
 m = slope
MSE = mechanical specific energy, psi
 n_b = effective number of blades of drag bit
 n_c = number of cutters
 N = rotary speed, rev/min
 N_{Re} = Reynolds number
 p = pressure, psi
 r = radius, in.
 R = penetration rate, ft/hr
 R_0 = penetration rate at zero overbalance, ft/hr
 r_f = formation resistance, psi
 s_d = average diamond size, carats/stone

S	= compressive strength of rock, psi
s_d	= size of diamond, carats/stone
t	= time, hours
t_b	= bit life, hours
t_c	= nonrotating time during bit run (e.g., connection time), hours
T_f	= fluid temperature, °F
t_t	= time of tripping operations required to change bit, hours
v	= cutting speed, m/s
v	= fluid velocity, ft/sec
w	= width, in.
W	= WOB, lbf
X	= linear wear, in.
x,y	= spatial coordinates
α	= bottom cutting angle, degree
β	= angle subtended by wear surface on PDC blank, degree
ΔD	= depth interval drilled during bit run, ft
ε	= axial strain
θ	= angle of internal friction, degree
μ_f	= viscosity, cp
μ	= Poisson's ratio
μ_a	= apparent viscosity at 10,000 s ⁻¹
ρ	= mud density, lbm/gal
ρ_c	= equivalent circulating density, lbm/gal
σ	= normal stress, psi
τ	= shear stress, psi
τ_B	= bearing-life constant, hours
τ_H	= formation-abrasiveness constant, hours
τ_o	= shear strength, psi
τ_s	= index of rock abrasiveness, in. ³ /(lbf-in.)
ϕ	= angle between failure plane, degree
ϕ	= direction of principal stress
Ω_1	= instantaneous angular velocity in bit axis, m/s
Ω_2	= instantaneous angular velocity in cone axis, m/s
Ω_3	= resultant of Ω_1 and Ω_2 , m/s

Subscripts

a	= apparent
b	= bit
$b-e$	= break-even
be	= effective blade
bh	= bottomhole
c	= cutter
c	= circulating
c	= cone
dp	= drillpipe
e	= effective
eq	= equivalent
f	= formation
i	= initial
j	= jet
j	= journal
max	= maximum
max	= destructive
max	= slope
mod	= modified
n	= normal to plane
opt	= optimum

p	=	penetration
p_e	=	effective penetration
r	=	removed
s	=	steel
s	=	standard
s	=	reference
t	=	threshold
x, y	=	spatial coordinates or directions

References

- Beaton, T., Herman, J.J., Miko, C., and denOuden, B. 2008. New Steel PDC Drill-Bit Technology Redefines Performance Standards in Key Natural-Gas Applications. Paper SPE 115008 presented at the CIPC/SPE Gas Technology Symposium 2008 Joint Conference, Calgary, 16–19 June. DOI: [10.2118/115008-MS](https://doi.org/10.2118/115008-MS).
- Beck, F.E., Powell, J.W., and Zamora, M. 1995. The Effect of Rheology on Rate of Penetration. Paper SPE 29368 presented at the SPE/IADC Drilling Conference, Amsterdam, 28 February–2 March. DOI: [10.2118/29368-MS](https://doi.org/10.2118/29368-MS).
- Bingham, M.G. 1965. A New Approach to Interpreting Rock Drillability. *Oil & Gas J.* **63** (14): 195–200 (reprint). Tulsa: Petroleum Publishing Company.
- Botelho, R., Barreto, J., Bello, S., Anato, W., and Uzcategui, G. 2006. Drilling Optimization at the Aloctono Block in Venezuela With the Utilization of Latest Technologies in Impregnated Bits and Turbines. Paper SPE 99602 presented at the SPE Annual Technical Conference and Exhibition, San Antonio, Texas, USA, 24–27 September. DOI: [10.2118/99602-MS](https://doi.org/10.2118/99602-MS).
- Bourgoyne, A.T., Chenevert, M.E., Millheim, K.K., and Young, F.S. Jr. 1991. *Applied Drilling Engineering*, second edition. Chapter 5. Richardson, Texas, USA: Society of Petroleum Engineers.
- Bourgoyne, A.T. and Young, F.S. Jr. 1974. A Multiple Regression Approach to Optimal Drilling and Abnormal Pressure Detection. *SPE J.* **14** (4): 371–384; Trans. AIME, **257**. SPE-4238-PA. DOI: [10.2118/4238-PA](https://doi.org/10.2118/4238-PA).
- Brandon, B.D., Cerkovnik, J., Koskie, E., Bayoud, B.B., Colston, F., Clayton, R.I., Anderson, M.E., Hollister, K.T., Senger, J., and Niemi R. 1992. First Revision to the IADC Fixed Cutter Dull Grading System. Paper SPE 23939 presented at the SPE/IADC Drilling Conference, New Orleans, 18–21 February. DOI: [10.2118/23939-MS](https://doi.org/10.2118/23939-MS).
- Buske, R., Rickabaugh, C., Bradford, J., Lukasewich, H., and Overstreet, J. 2008. Performance Paradigm Shift: Drilling Vertical and Directional Sections Through Abrasive Formations with Roller Cone Bits. Paper SPE 114975 presented at the CIPC/SPE Gas Technology Symposium Joint Conference, Calgary, 16–19 June. DOI: [10.2118/114975-MS](https://doi.org/10.2118/114975-MS).
- Campbell, J.M. and Mitchell, B.J. 1959. Effect of Tooth Geometry on Tooth Wear Rate of Rotary Rock Bits. Paper presented at the API Mid-Continent Dist. Spring Meeting, March 1959.
- Centala, P., Burley, M., Burnett, T., Ford, R., and Sinesi, J. 2006. Unlocking Two-Cone-Bit Potential: Technology, People, and Planning Make It Possible and the Lessons Learned. Paper SPE 99017 presented at the IADC/SPE Drilling Conference, Miami, Florida, USA, 21–23 February. DOI: [10.2118/99017-MS](https://doi.org/10.2118/99017-MS).
- Cerkovnik, J. 1982. Design, Application, and Future of Polycrystalline Diamond Compact Cutters in the Rocky Mountains. Paper SPE 10893 presented at the SPE Rocky Mountain Regional Meeting, Billings, Montana, USA, 19–21 May. DOI: [10.2118/10893-MS](https://doi.org/10.2118/10893-MS).
- Chen, S.L., Dahlem, J., and Dennis, J. 2001. Development and Application of a New Roller Cone Bit with Optimized Tooth Orientation. Paper SPE 71053 presented at the SPE Rocky Mountain Petroleum Technology Conference, Keystone, Colorado, USA, 21–23 May. DOI: [10.2118/71053-MS](https://doi.org/10.2118/71053-MS).
- Clayton, R., Chen, S., and Lefort, G. 2005. New Bit Design, Cutter Technology Extend PDC Applications to Hard Rock Drilling. Paper SPE/IADC 91840 presented at the SPE/IADC Drilling Conference, Amsterdam, 23–25 February. DOI: [10.2118/91840-MS](https://doi.org/10.2118/91840-MS).
- Clegg, J. 2006. Faster, Longer, and More-Reliable Bit Runs With New-Generation PDC Cutter. Paper SPE 102067 presented at the SPE Annual Technical Conference and Exhibition, San Antonio, Texas, USA, 24–27 September. DOI: [10.2118/102067-MS](https://doi.org/10.2118/102067-MS).
- Dupriest, F.E. 2006. Comprehensive Drill-Rate Management Process To Maximize Rate of Penetration. Paper SPE 102210 presented at the SPE Annual Technical Conference and Exhibition, San Antonio, Texas, USA, 24–27 September. DOI: [10.2118/102210-MS](https://doi.org/10.2118/102210-MS).
- Dupriest, F.E., and Koederitz, W.L. 2005. Maximizing Drill Rates with Real-Time Surveillance of Mechanical Specific Energy. Paper SPE 92194 presented at the SPE/IADC Drilling Conference, Amsterdam, 23–25 February. DOI: [10.2118/92194-MS](https://doi.org/10.2118/92194-MS).
- Dykstra, M.W., Chen, D.C.K., Warren, T.M., and Zannoni, S.A. 1994. Experimental Evaluations of Drill Bit and Drill String Dynamics. Paper SPE 28323 presented at the SPE Annual Technical Conference and Exhibition, New Orleans, 25–28 September. DOI: [10.2118/28323-MS](https://doi.org/10.2118/28323-MS).

- Eckel, J.R. 1968. Microbit Studies of the Effect of Fluid Properties and Hydraulics on Drilling Rate, II. Paper SPE 2244 presented at the SPE Annual Meeting, Houston, 29 September–2 October. DOI: [10.2118/2244-MS](https://doi.org/10.2118/2244-MS).
- Edwards, J.H. 1964. Engineering Design of Drilling Operations. In *Drilling and Production Practice 1964*, 38–55. Washington, DC: API. 38–55.
- Estes, J.C. 1974. Guidelines for Selecting Rotary Insert Rock Bits. *Pet. Eng.* September.
- Fang, Z., Griffo, A., White, B., Belnap, D., Hamilton, R., Portwood, G., Cox, P., Hilmas, G., and Bitler, J. 2001. Chipping Resistant Polycrystalline Diamond and Carbide Composite Materials for Roller Cone Bits. Paper SPE 71394 presented at the SPE Annual Technical Conference and Exhibition, New Orleans, 30 September–3 October. DOI: [10.2118/71394-MS](https://doi.org/10.2118/71394-MS).
- Galle, E.M. and Woods, A.B. 1963. Best Constant Weight and Rotary Speed for Rotary Rock Bits. In *Drilling and Production Practice 1963*, 48–73. Washington, DC: API.
- Glowka, D.A., and Stone, C.M. 1986. Effects of Thermal and Mechanical Loading on PDC Bit Life. *SPE Drill. Eng.* 1 (3): 201–214. SPE-13257-PA. DOI: [10.2118/13257-PA](https://doi.org/10.2118/13257-PA).
- Gopalsing, P.M. 2006. Advanced Drilling Using a Dual-Bit System. Paper SPE 99478 presented at the SPE Western Regional/AAPG Pacific Section/GSA Cordilleran Section Joint Meeting, Anchorage, 8–10 May. DOI: [10.2118/99478-MS](https://doi.org/10.2118/99478-MS).
- Gray, K.E., Armstrong, F., and Gatlin, C. 1962. Two-Dimensional Study of Rock Breakage in Drag-Bit Drilling at Atmospheric Pressure. *J Pet Technol* 14 (1): 93–98. *Trans.*, AIME, 225. SPE-164-PA. DOI: [10.2118/164-PA](https://doi.org/10.2118/164-PA).
- Hareland, G., Wu, A., and James, J. 2009. Bearing Wear Model for Roller Cones. Paper SPE 125644 presented at the SPE/IADC Middle East Drilling Technology Conference and Exhibition, Manama, Bahrain, 26–28 October. DOI: [10.2118/125644-MS](https://doi.org/10.2118/125644-MS).
- Hoover, E.R. and Middleton, J.N. 1981. Laboratory Evaluation of PDC Drill Bits Under High Speed and High Wear Conditions. Paper SPE 10326 presented at the SPE Annual Technical Conference and Exhibition, San Antonio, 4–7 October. DOI: [10.2118/10326-PA](https://doi.org/10.2118/10326-PA).
- Hu, Q., and Liu, Q. 2006. A New Disc One-Cone Bit. Paper SPE 102381 presented at the SPE International Oil and Gas Conference and Exhibition in China, Beijing, 5–7 December. DOI: [10.2118/102381-MS](https://doi.org/10.2118/102381-MS).
- Hughes, H. 1909. Drill. US Patent No. 930759.
- Hughes, R.V. 1965. Drag Bits Rate New Look in Light of Speed Drilling. *World Oil* (March 1965): 94.
- Jaffar, A., Birch, R., Teasdale, P., and Ani, S.A. 2005. New PDC Technology Significantly Improves Performance in Drilling Deep Khuff Wells for a Major Operator in Abu Dhabi. Paper SPE/IADC 96792 presented at the SPE/IADC Middle East Drilling Technology Conference and Exhibition, Dubai, 12–14 September. DOI: [10.2118/96792-MS](https://doi.org/10.2118/96792-MS).
- Johnson, S. 2006. A New Method of Producing Laterally Stable PDC Drill Bits. Paper SPE 98986 presented at the IADC/SPE Drilling Conference, Miami, Florida, USA, 21–23 February. DOI: [10.2118/98986-MS](https://doi.org/10.2118/98986-MS).
- Kenner, J.V., and Isbell, M.R. 1994. Dynamic Analysis Reveals Stability of Roller Cone Rock Bits. Paper SPE 28314 presented at the SPE Annual Technical Conference and Exhibition, New Orleans, 25–28 September. DOI: [10.2118/28314-MS](https://doi.org/10.2118/28314-MS).
- Ledgerwood, L.W., Wells, M.R., Wiesner, B.C., and Harris, T.M. 2000. Advanced Hydraulics Analysis Optimizes Performance of Roller Cone Drill Bits. Paper SPE 59111 presented at the IADC/SPE Drilling Conference, New Orleans, 23–25 February. DOI: [10.2118/59111-MS](https://doi.org/10.2118/59111-MS).
- Li, X., Hood, M., and Xian, X. 1993. Wear and Damage to PDC Bits. Paper SPE 26294 available from SPE, Richardson, Texas, USA.
- Lubinski, A. 1988. *Developments in Petroleum Engineering: Collected Works of Arthur Lubinski, Vol. 2*, ed. S. Miska, 201–210. Houston: Gulf Publishing Company.
- Lummus, J.L. 1974. Analysis of Mud Hydraulics Interactions. *Pet. Eng.*
- Maurer, W.C. 1962. The “Perfect-Cleaning” Theory of Rotary Drilling. *J Pet Technol* 14 (11): 1270–1274; *Trans.*, AIME, 225. SPE-408-PA. DOI: [10.2118/408-PA](https://doi.org/10.2118/408-PA).
- Maurer, W.C. 1965. Bit-Tooth Penetration Under Simulated Borehole Conditions. *J Pet Technol* 17 (12): 1433–1442; *Trans.*, AIME, 234. SPE-1260-PA. DOI: [10.2118/1260-PA](https://doi.org/10.2118/1260-PA).
- McGehee, D.H., Dahlem, J.S., Gieck, J.C., Kost, B., Lafuze, D., Reinsvold, C.H., and Steinke, S.C. 1992. The IADC Roller Bit Classification System. Paper SPE 23937 presented at the IADC/SPE Drilling Conference, New Orleans, 18–21 February. DOI: [10.2118/23937-MS](https://doi.org/10.2118/23937-MS).
- Mensa-Wilmot, G., Soza, R., and Hudson, K. 2003. Advanced Cutting Structure Improves PDC Bit Performance in Hard Rock Drilling Environments. Paper SPE 84354 presented at the SPE Annual Technical Conference and Exhibition, Denver, 5–8 October. DOI: [10.2118/84354-MS](https://doi.org/10.2118/84354-MS).
- Murray, A.S. and MacKay, S.P. 1957. Water Still Poses Tough Problem in Drilling with Air. *Oil and Gas J.* (10 June 1957): 105.

- Pessier, R., and Damschen, M. 2010. Hybrid Bits Offer Distinct Advantages in Selected Roller Cone and PDC Bit Applications. Paper SPE 128741 presented at the IADC/SPE Drilling Conference and Exhibition, New Orleans, 2–4 February. DOI: [10.2118/128741-MS](https://doi.org/10.2118/128741-MS).
- Peterson, J.L. 1976. Diamond Drilling Model Verified in Field and Laboratory Tests. *J Pet Technol* **28** (2): 215–222; Trans., AIME, **261**. SPE-5072-PA. DOI: [10.2118/5072-PA](https://doi.org/10.2118/5072-PA).
- Reed, R.L. 1972. A Monte Carlo Approach to Optimal Drilling. *SPE J.* **12** (5): 423–438; Trans., AIME, **253**. SPE-3513-PA. DOI: [10.2118/3513-PA](https://doi.org/10.2118/3513-PA).
- Schell, E.J., Phillippi, D., and Fabian, R.T. 2003. New, Stable PDC Technology Significantly Reduces Hard Rock Cost Per Foot. Paper SPE/IADC 79797 presented at the SPE/IADC Drilling Conference, Amsterdam, 19–21 February. DOI: [10.2118/79797-MS](https://doi.org/10.2118/79797-MS).
- Sinor, L.A., Powers, J.R., and Warren, T.M. 1998. The Effect of PDC Cutter Density, Back Rake, Size, and Speed on Performance. Paper IADC/SPE 39306 presented at the IADC/SPE Drilling Conference, Dallas, 3–6 March. DOI: [10.2118/39306-MS](https://doi.org/10.2118/39306-MS).
- Smith Technologies. 2005. *Bit Catalog*.
- Spaar, J.R., Ledgerwood, L.W., Goodman, H., Graff, R.L., and Moo, T.J. 1995. Formation Compressive Strength Estimates for Predicting Drillability and HX Bit Selection. Paper SPE/IADC 29397 presented at the SPE/IADC Drilling Conference, Amsterdam, 28 February–2 March. DOI: [10.2118/29397-MS](https://doi.org/10.2118/29397-MS).
- Taylor, M.R., Murdock, A.D., and Evans, S.M. 1999. High Penetration Rates and Extended Bit Life Through Revolutionary Hydraulic and Mechanical Design in PDC Drill Bit Development. *SPE Drill & Compl* **14** (1): 34–41. SPE-55047-PA. DOI: [10.2118/55047-PA](https://doi.org/10.2118/55047-PA).
- Tibbitts, G.A., Sandstrom, J.L., Black, A.D., and Green, S.J. 1981. Effects of Bit Hydraulics on Full Scale Laboratory Drilled Shale. *J Pet Technol* **33** (7): 1180–1188. SPE-8439-PA. DOI: [10.2118/8439-PA](https://doi.org/10.2118/8439-PA).
- Torquato Drilling Accessories. Torquato Drag Bits, <http://www.torquato.com/dragbits.html>. Accessed 11 January 2011.
- Wamsley, W.H. Jr. and Ford, R. 2007. Introduction to Roller-Cone and Polycrystalline Diamond Drill Bits. In *Petroleum Engineering Handbook*, ed. L. Lake, Vol. 2, Chapter 5. Richardson, Texas, USA: Society of Petroleum Engineers.
- Warren, T.M., and Sinor, L.A. 1994. PDC Bits: What's Needed. Paper SPE 27978 presented at the University of Tulsa Centennial Petroleum Engineering Symposium, Tulsa, 29–31 August. DOI: [10.2118/27978-MS](https://doi.org/10.2118/27978-MS).
- West, W.C., Roy, B.J., Knowles, S.P., Wiesner, B.C., and Isbell, M.R. 2004. Application of New Impregnated Diamond Bit Technology Saves Operator \$2 Million Drilling Southern Oklahoma Well. Paper SPE 87096 presented at the SPE/IADC Drilling Conference, Dallas, 2–4 March. DOI: [10.2118/87096-MS](https://doi.org/10.2118/87096-MS).
- Winters, W.J., and Doiron, H.H. 1987. The 1987 IADC Fixed Cutter Bit Classification System. Paper SPE/IADC 16142 presented at the SPE/IADC Drilling Conference, New Orleans, 15–18 March. DOI: [10.2118/16142-MS](https://doi.org/10.2118/16142-MS).
- Winters, W.J., Senger, J., and Oliver, M.S. 1987. Application of the 1987 IADC Roller Bit Classification System. Paper SPE 16143 presented at the IADC/SPE Drilling Conference, New Orleans, 15–18 March. DOI: [10.2118/16143-MS](https://doi.org/10.2118/16143-MS).
- Wojtanowicz, A.K., and Kuru, E. 1987. Dynamic Drilling Strategy for PDC Bits. Paper SPE 16118 presented at the SPE/IADC Drilling Conference, New Orleans, 15–18 March. DOI: [10.2118/16118-MS](https://doi.org/10.2118/16118-MS).
- Young, F.S. Jr. 1969. Computerized Drilling Control. *J Pet Technol* **21** (4): 483–496; Trans., AIME, **246**. SPE-2241-PA. DOI: [10.2118/2241-PA](https://doi.org/10.2118/2241-PA).
- Ziaja, M.B. 1985. Mathematical Model of the Polycrystalline Diamond Bit Drilling Process and Its Practical Application. Paper SPE 14217 presented at the SPE Annual Technical Conference and Exhibition, Las Vegas, Nevada, USA, 22–25 September. DOI: [10.2118/14217-MS](https://doi.org/10.2118/14217-MS).
- Ziaja, M.B. and Miska, S. 1982. Mathematical Model of the Diamond Bit Drilling Process and Its Practical Application. *SPE J.* **22** (6): 911–922. SPE-10148-PA. DOI: [10.2118/10148-PA](https://doi.org/10.2118/10148-PA).

SI Metric Conversion Factors

ft	×	3.048*	E–01 = m
gal/min	×	3.785 412	E–03 = m ³ /min
hp	×	7.460 43	E – 01 = kW
in.	×	2.54*	E+00 = cm
in. ²	×	6.451 6*	E–00 = cm ²
in. ³	×	1.638 706	E + 01 = cm ³
lbf	×	4.448 222	E + 00 = N
lbm	×	4.535924	E–01 = kg
lbm/gal	×	1.198264	E+02 = kg/m ³
M	×	4.448 222	E+00 = N
psi	×	6.894757	E+00 = kPa

*Conversion factor is exact.

Chapter 7

Casing Design

John W. Barker and Jim Powers, ExxonMobil and Robert F. Mitchell, Halliburton

The purpose of this chapter is to present (1) the primary function of oil-well casing, (2) the various types of casing strings used, and (3) the procedures used in the design of casing strings. Tubing string design is not covered in this chapter. Design issues with drillpipe will not be included.

7.1 Introduction

Oil country tubular goods (OCTG) include casing, tubing, line pipe, and drillpipe. Casing serves several important functions in drilling and completing a well. It prevents collapse of the borehole during drilling and hydraulically isolates the wellbore fluids from the subsurface formations and formation fluids. It minimizes damage to the subsurface environment by the drilling process and to the well by the hostile subsurface environment. It provides a high-strength flow conduit that directs the drilling fluid to the surface and, with blowout preventers (BOPs), enables the safe control of formation pressure. Selective perforation of properly cemented casing also permits isolated communication with a particular formation of interest.

Tubing conducts well fluids from the formation to the wellhead. Line pipe is typically used in surface facilities to convey gas, oil, and water in both the oil and natural-gas industries. Line pipe is sometimes used in oil wells because it is available in larger sizes and is often needed for shallow oilwell strings. Drillpipe is used to drill wells, and it functions as a workstring that enables application of torsion, weight, and hydraulics during the drilling process. The function of drillpipe is very different from that of other types of OCTG, and design issues such as fatigue are more important.

As the search for commercial hydrocarbon deposits reaches greater depths, the number and sizes of the casing strings required to drill and complete a well successfully have also increased. Casing has become one of the most expensive parts of a drilling program; studies have shown that the average cost of tubulars is approximately 18% of the average cost of a completed well (Greenip 1978). Therefore, an important responsibility of the drilling engineer is to design the least expensive casing program that will enable the well to be drilled and operated safely throughout its life. The savings that can be achieved through optimal design, as well as the risk of failure from an improper design, justify a considerable engineering effort in this phase of the drilling program.

Fig. 7.1 shows a typical casing program for a well along the United States Gulf Coast. A well that will not encounter abnormal formation pore-pressure gradients, lost-circulation zones, or salt sections may require only *conductor casing* and *surface casing* to drill to the objective for the well.

Conductor casing is needed to circulate the drilling fluid to the shale shakers without eroding the shallow sediments below the rig and rig foundations when drilling is initiated. The conductor casing also protects the subsequent casing strings from corrosion and may be used to support some of the well load structurally. A diverter system can be installed on the conductor to divert flow from rig personnel and equipment in case of an unexpected influx of formation fluids to surface-casing depth during drilling.

Surface casing prevents cave-in of unconsolidated weaker near-surface sediments and protects the shallow freshwater sands from contamination. Surface casing also supports and protects from corrosion any subsequent

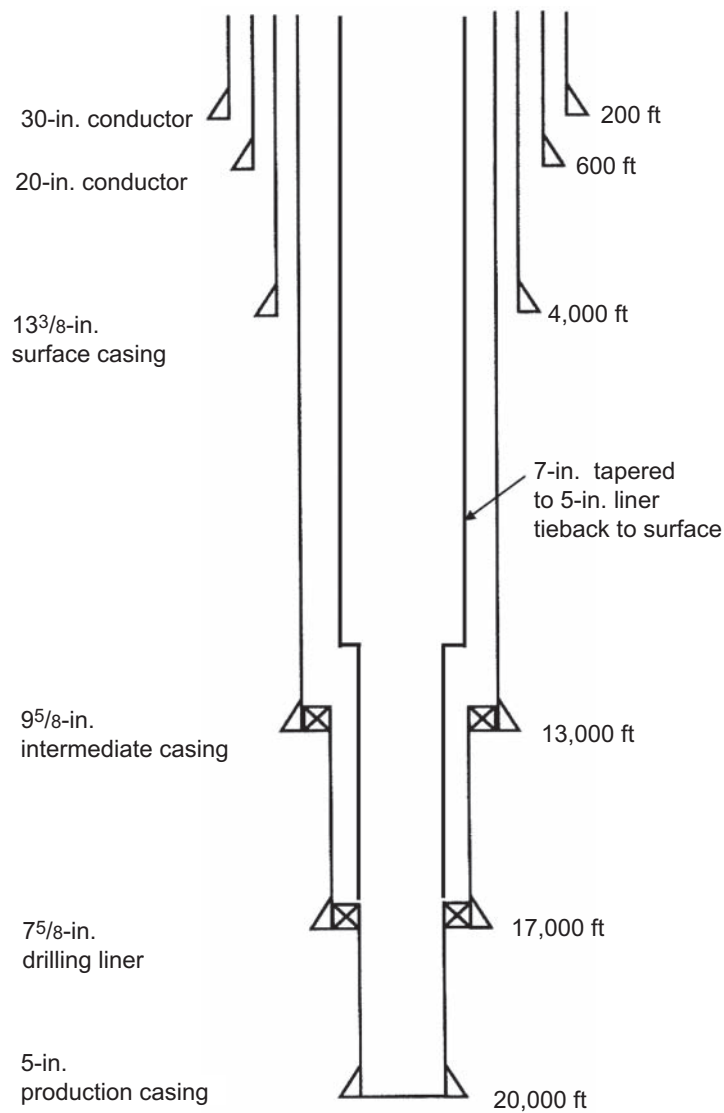


Fig. 7.1—Typical casing program.

casing strings run in the well. In the event of a kick, surface casing generally makes it possible to contain the flow by closing the BOPs.

The BOPs should not be closed unless the casing to which they are attached has been placed deeply enough into the Earth to prevent a pressure-induced formation fracture initiated below the casing seat from reaching the surface or mudline. Subsequent flow through such fractures eventually can erode a large crater, up to several hundred feet in diameter, at the surface or the mudline. Surface-casing setting depths are usually from 300 to 5,000 ft into the sediments. Because of the possibility of contamination of shallow water-supply aquifers, surface-casing setting depths and cementing practices are often subject to government regulations.

Intermediate casing is usually required in deeper wells that penetrate abnormally pressured formations, lost-circulation zones, unstable shale sections, or salt sections. Intermediate casing is often referred to as “protective” or “drilling” casing. Some wells may require one or more strings of intermediate casing between the surface-casing depth and the final well depth. When abnormal formation pore pressures are present in the deeper portions of a well, intermediate casing is needed to protect formations below the surface casing from the pressures created by the required high drilling-fluid density. Similarly, when normal pore pressures are found below sections having abnormal pressure, an additional intermediate casing makes it possible to reduce the mud density to drill deeper formations economically. If a troublesome lost-circulation zone is encountered or an unstable shale or

salt section is penetrated, intermediate casing may also be required to prevent well problems when drilling below these zones.

Liners are casing strings that do not extend to the surface, but are suspended from the bottom of the next larger casing string. A liner hanger (shown as ☒) is used to suspend the top of the liner in the larger casing size; the liner hanger often can seal the annulus between the liner and the larger casing size. Several hundred feet of overlap between the liner hanger and the casing seat is typical and will provide enough length that in the event a seal is not effective in the liner hanger, a cement seal can be obtained in the overlap length. The principal advantage of a liner is its lower cost. However, problems sometimes arise if a hanger fails to suspend the liner correctly or if a seal between the liner and the larger casing is not effective. Moreover, using a liner exposes the casing string above it to additional wear during subsequent drilling. A drilling liner can be used either as an intermediate casing (in that it serves to isolate troublesome zones that tend to cause well problems during drilling operations) or as production casing.

Production casing is usually the final casing string set in a well. It comes in contact with formation fluids below the production packer and with the completion fluid (packer fluid) in the tubing-casing annulus above the production packer. This casing string provides protection for the environment in the event of a failure of the tubing string during production operations and enables the production tubing to be replaced or repaired later in the life of a well. A production liner is a liner that is set at total depth and is usually exposed to formation fluids below the production packer and to packer fluid above the production packer. Production liners are generally connected to the surface wellhead using a tieback casing string when the well is completed. The tieback casing is connected to the top of the liner with a specially designed seal. Production liners with tieback casing strings are advantageous when exploratory drilling below the productive interval is planned. Casing wear resulting from deeper drilling operations then affects only the production liner, not the production tieback. Use of a production liner with a tieback casing string also results in lower-hanging weights in the upper part of the well and thus often enables a more economical design.

7.2 Casing Manufacture

The tubular manufacturing process begins with placing iron ore, limestone, and coke in a blast furnace, where they are heated. Pig iron is produced, which is rich in carbon. The molten pig iron is then placed into a special furnace, often with scrap steel. This special furnace uses oxygen to heat the iron and further reduce its carbon content. Carbon is the primary alloying agent used to increase the strength of iron. Other alloying elements such as molybdenum and chrome are often added to adjust the chemical composition of the molten steel and to impart specific metallurgical properties. The molten metal is then made into billets, which are essentially solid bars. The strength of the final steel depends on its chemical composition as well as on the mechanical and thermal processes used when the billet is formed into a casing tube.

The two basic processes used in the manufacture of OCTG tubes are the seamless process and the electric-resistance-welding (ERW) process. In the seamless process, a hot billet is fed between two obliquely oriented rollers that rotate, advance the billet, and apply a very high compressive load. The center of the billet is fractured by the high compressive stresses induced at the center of the billet by the rollers. Then a central piercing plug is used to open the fracture to form a tube (**Fig. 7.2**). The hot pierced tube is then processed through various plug mills and sizing mills (either hot or cold) to form a tubular of a given wall thickness and with uniform pipe dimensions and roundness. Most types of OCTG are manufactured by the seamless process. The very-high-alloy steels used require unique specialized manufacturing processes.

In the electric-welding process, a billet is formed into flat-sheet steel stock of a specified wall thickness. After being cut to a specified width, the flat stock is then formed into a circular shape by passing it through a series of rollers. A single longitudinal seam is then electric-resistance or electric-induction welded, typically without the addition of filler material. The welding process on the two edges is typically performed by mechanically pressing the two edges together, and the heat for welding is generated by resistance to flow of electric current. Excess material formed in the welding process is then trimmed to leave a uniform OD (OD) and ID (ID). The American Petroleum Institute (API) and International Standards Organization (ISO) have special chemical requirements for the steel used to make higher-strength ERW OCTG.

Low-strength steels can be manufactured solely by adjustment of steel chemistry and may not require additional heat-treatment processes to improve the steel strength and mechanical properties. These steels are typically called carbon steels. Examples of low-carbon steels include common structural steel and railroad rail. Higher-strength steels are manufactured both by adjustment of the steel chemistry and by a heat-treatment process. Sometimes these steels are called carbon steels, but they are technically low-alloy steels because they contain carbon and manganese and frequently other alloying elements such as chromium, nickel, and molybdenum. Higher-strength OCTG usually incorporate some form of heat treatment to achieve the desired strength while maintaining the toughness and ductility of the steel.

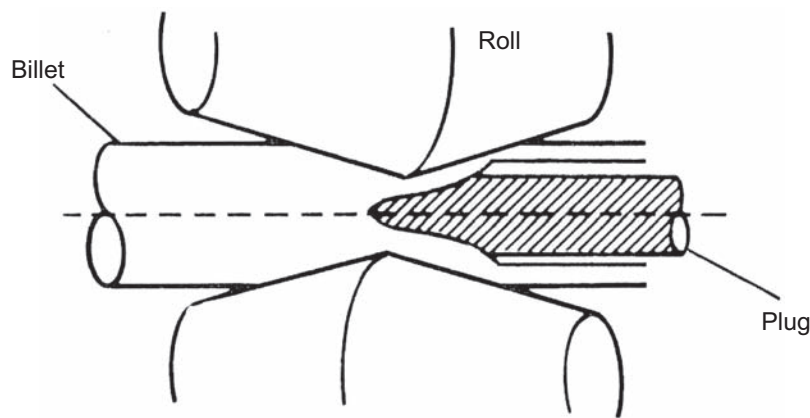


Fig. 7.2—Manufacturing of seamless casing.

Three heat-treatment processes are typically available for carbon and low-alloy steels. These processes can be used for either seamless or ERW tubes and are

- Quench and tempering: heating the tube to roughly 1,600°F, cooling rapidly with water or oil, heating to roughly 1,200°F, and then air-cooling.
- Normalizing and tempering: heating the tube to approximately 1,600°F, air-cooling, heating to approximately 1,000°F, and air-cooling.
- Normalizing: heating the tube to approximately 1,700°F and then air-cooling.

The quenching and tempering process is generally viewed as the best heat-treatment process and is required to achieve higher strength levels.

Very-high-alloy steels are often called corrosion-resistant alloys (CRAs). These steels often are manufactured using particular processes to obtain the desired final material properties. For example, they may be cold-worked rather than heat-treated to increase yield strength.

7.3 Casing Standardization

API and ISO have developed standards for casing and other tubular goods that have been accepted internationally by the petroleum-producing industry. Casing is defined as tubular pipe with an OD range of 4.5 to 20 in. Among the properties included in the API and ISO standards (*API Spec. 5CT/ISO 11960* 2005) for both pipe and couplings are strength, physical dimensions, and quality-control test procedures. In addition to these standards, API and ISO provide bulletins on the recommended minimum performance properties (*API Bull. 5C2* 1999) and formulas (*API TRC 5C3* 2008) for the computation of minimum performance properties.

7.3.1 Grade. API and ISO have adopted a *grade* designation for casing to define the strength characteristics of the pipe. The grade code consists of a letter followed by a number. The number designates the minimum yield strength of the steel in thousands of psi. The yield strength is defined as the tensile stress required to produce a specified total elongation per unit length on a standard test specimen. This strain is slightly beyond the elastic limit. Because there are significant variations in the yield strengths measured for manufactured pipe, a minimum yield-strength criterion, rather than an average yield strength, has been adopted. In addition to specifying the minimum acceptable yield strength of each grade of casing, API and ISO specify the maximum yield strength, the minimum tensile strength, and the minimum elongation per unit length at failure (**Table 7.1**). The letter designation in the grade was selected arbitrarily to provide a unique designation for each grade of casing described in the standards. The letter designation is also used to distinguish between various tensile-strength requirements or different heat-treatment methods used on casing with the same minimum yield strength.

7.3.2 Chemical Requirements. The steel used in casing and couplings must conform to certain chemical requirements. All grades of steel used in API and ISO casing and tubing have a specified maximum sulfur and phosphorus content, expressed as a percentage of total weight. Higher grades of steel can have several additional

TABLE 7.1—API STEEL GRADES

API Grade	Yield Stress (psi)		Minimum Ultimate Tensile Strength (psi)	Minimum Elongation (%)
	Minimum	Maximum		
H-40	40,000	80,000	60,000	29.5
J-55	55,000	80,000	75,000	24.0
K-55	55,000	80,000	95,000	19.5
N-80	80,000	110,000	100,000	18.5
L-80	80,000	95,000	95,000	19.5
C-90	90,000	105,000	100,000	18.5
C-95	95,000	110,000	105,000	18.5
T-95	95,000	110,000	105,000	18.0
P-110	110,000	140,000	125,000	15.0
Q-125	125,000	150,000	135,000	18.0

TABLE 7.2—CHEMICAL REQUIREMENTS FOR SELECTED API CASING GRADES, MASS FRACTION PERCENT

Grade	Type	Carbon	Manganese	Molybdenum		Chromium		Nickel	Copper	Phosphorus	Sulfur	Silicon
		Maximum	Maximum	Minimum	Maximum	Minimum	Maximum	Maximum	Maximum	Maximum	Maximum	Maximum
H-40	—	—	—	—	—	—	—	—	—	0.030	0.030	—
K-55	—	—	—	—	—	—	—	—	—	0.030	0.030	—
N-80	—	—	—	—	—	—	—	—	—	0.030	0.030	—
L-80	1	0.43 ^a	1.90	—	—	—	—	0.25	0.35	0.030	0.030	0.45
C-90	1	0.35	1.00	0.25 ^c	0.75	—	1.20	0.99	—	0.020	0.010	—
C-90	2	0.50	1.90	—	NL	—	NL	0.99	—	0.030	0.010	—
C-95	1	0.45 ^b	1.90	—	—	—	—	—	—	0.030	0.030	0.45
T-95	1	0.35	1.20	0.25 ^d	0.85	0.40	1.50	0.99	—	0.020	0.010	—
T-95	2	0.50	1.90	—	—	—	—	0.99	—	0.030	0.010	—
P-110	—	—	—	—	—	—	—	—	—	0.030 ^e	0.030	—
Q-125	1	0.35	1.00	—	0.75	—	1.20	0.99	—	0.020	0.010	—
Q-125	2	0.35	1.00	—	NL	—	NL	0.99	—	0.020	0.020	—
Q-125	3	0.50	1.90	—	NL	—	NL	0.99	—	0.030	0.010	—
Q-125	4	0.50	1.90	—	NL	—	NL	0.99	—	0.030	0.020	—

Notes: (a) The carbon content for L-80 may be increased up to 0.50% maximum if the product is oil-quenched.
(b) The carbon content for C-95 may be increased up to 0.55% maximum if the product is oil-quenched.
(c) The molybdenum content for C-90, type 1, has no minimum tolerance if wall thickness is less than 0.700 in.
(d) The molybdenum content for T-95 type 1, may be decreased to 0.15% minimum if the wall thickness is less than 0.700 in.
(e) For electric welded grade P-110, the phosphorus content shall be 0.020%.
NL = No limit; elements reported in product analysis.

chemical-composition requirements for carbon, manganese, molybdenum, chromium, nickel, copper, and silicon. **Table 7.2** lists the chemical-composition requirements for several common steels.

Some casing grades have the same numeric code, but a different letter code. Several API and ISO grades are also available in different types, all with the same numeric code. The differences between these grades, which have the same minimum yield strength, include differences in maximum yield strength, chemical requirements, and other properties. In some cases, controlling the often slight variations in these properties is necessary to ensure that the casing will fulfill a special service requirement such as installation in a highly corrosive or cold environment.

Higher steel grades also have hardness specifications and Charpy V-notch impact-test requirements. These requirements ensure that the steel is not brittle and will not fail by brittle cracking. Physical testing of particular specimens taken from specific locations and orientations is necessary to meet this API requirement. Other requirements for grain size, straightness, flatness, and surface condition are included in API and ISO specifications.

API and ISO have additional requirements for special materials containing higher alloying agents than those in the most common types of OCTG. Increased percentages of alloying agents may cause some OCTG to be

more resistant to corrosion. Many downhole environments are very harsh and corrosive. In addition to the API and ISO grades, there are many proprietary steel grades that may or may not conform to all API and ISO specifications and are widely used in the petroleum-producing industry. These steel grades are used for special applications that require very-high-tensile-strength or high-strength steels that are more resistant to corrosion and hostile environments.

7.3.3 Dimensions. The API and ISO standards recognize three length ranges for casing. Range 1 (R-1) includes joint lengths from 16 to 25 ft. Range 2 (R-2) covers the 25- to 34-ft range, and Range 3 (R-3) the 34- to 48-ft range. These standards also specify that when casing is ordered from the mill in amounts greater than one carload, 95% of the pipe must have lengths greater than 18 ft for R-1, 28 ft for R-2, and 36 ft for R-3. In addition, 95% of the shipment must have a maximum length variation no greater than 6 ft for R-1, 5 ft for R-2, and 6 ft for R-3. Casing is run most often in R-3 lengths to reduce the number of connections in the string. Because casing is made up in single joints, R-3 lengths can be handled easily by most rigs. Use of a consistent range of casing lengths in a string is desirable to facilitate casing-running operations. Typically, casing is purchased and used in longer lengths than those of tubing because most drilling rigs have bigger, taller derricks than workover rigs.

To meet API and ISO specifications, the OD of casing must be held within a tolerance of 1.0% larger to 0.5% smaller than the nominal dimension. However, casing manufacturers will generally try to manufacture casing slightly larger than the nominal OD to ensure adequate thread run-out when machining a connection. The minimum permissible pipe-wall thickness permitted by API and ISO specifications is 87.5% of the nominal wall thickness. Casing, however, usually has an average wall thickness close to the nominal wall thickness, resulting in an ID near the nominal ID.

The minimum ID is also controlled by a specified *drift* diameter—the minimum mandrel diameter that must pass unobstructed through the pipe. Drift mandrels have an OD that is determined by subtracting a given tolerance from the calculated ID. The tolerance used to determine the drift-mandrel diameter varies depending on casing size (**Table 7.3**). The length of a casing drift mandrel is 6 in. for casing sizes from 4.5 to 8.625 in. For larger casing sizes, a 12-in.-long drift mandrel must be used. The drift mandrel is not long enough to ensure a straight pipe, but it will ensure the passage of a bit size that is less than the drift diameter.

In some instances, it is desirable to run casing with a drift diameter slightly greater than the API and ISO drift diameter for that casing size. In these instances, casing that has passed an oversized drift mandrel can be specially

TABLE 7.3—CASING DRIFT DIAMETERS

API Standard Drift Diameter	Size (in.)	Nominal weight/ft	API Alternate or Special Drift-In
$d-1/8$ in.	4 1/2		
	5		
	5 1/2		
	6 5/8		
	7	23.0	6.250
	7	32.0	6.000
	7 5/8		
	8 5/8	32.0	7.875
	8 5/8	40.0	7.625
	9 5/8	40.0	8.750
$d-5/32$ in.	9 5/8	53.5	8.500
	9 5/8	58.4	8.375
	10 3/4	45.5	9.875
	10 3/4	55.5	9.625
	11 3/4	60.0	10.625
	11 3/4	65.0	10.625
	13 3/8	72.0	12.250
	13 3/8	76.0	
$d-3/16$ in.	16		
	18 5/8		
	20		

ordered. Some of the more commonly available oversized drift diameters are given in Table 7.3. When non-API and non-ISO drift requirements are specified, they should be made known to the mill, the distributor, and the threading company before the pipe is manufactured.

Casing size (i.e., OD) and nominal wall thickness can be used to specify casing dimensions. However, it is conventional to specify casing dimensions by size and weight per foot. In discussing casing weights, one should differentiate between nominal weight, plain-end weight, and average weight for threads and couplings. The nominal weight per foot is not a true weight per foot, but is useful for identification purposes as an approximate average weight per foot. The plain-end weight per foot is the weight per foot of the pipe body, excluding the threaded portion and coupling weight. The average weight per foot is the total weight of an average joint of threaded pipe with a coupling attached power-tight at one end, divided by the total length of the average joint. In practice, the average weight per foot is sometimes calculated to obtain the best possible estimate of the total weight of a casing string. However, the variation between nominal weight per foot and average weight per foot is generally small, and most design calculations are performed with the nominal weight per foot. Methods to calculate the thread and coupled weight of a casing joint are available in *API TR 5C3* (2008).

Although there are no industry standards for the density of steel used to manufacture casings, low-alloy steels used for this purpose have a density of approximately 490 lbf/ft³ or 0.2836 lbf/in.³. The plain-end weight for API/ISO casing is tabulated in *API Spec. 5CT/ISO 11960* (2005). CRA materials can have a slightly different density than low-alloy steels. For example, API 13 Cr weighs approximately 485 lbf/ft³ or 0.2805 lbf/in.³, and some very-high-alloy steels have specific weights as high as 540 lbf/ft³.

API and ISO also have specifications for some casing connections. These specifications include dimensions, tolerances, manufacturing methods, mechanical properties, and special hostile-service testing. These will be covered in more detail in Section 7.8.

7.4 Line Pipe

Line pipe is typically used in production operations, including pipelines and flowlines, and in refineries and plants. The majority of line pipe is welded into longer lengths rather than using connections. There are API and ISO specifications for couplings used with line pipe up to 20 in. OD. Typically line pipe with couplings are not used in oil wells, but occasionally larger sizes of line pipe are used for conductor strings and even surface-casing strings. Often line pipe used in these applications is welded or has special machined connectors welded to plain-end pipe. API and ISO have specifications for line pipe, and line pipe is manufactured from as small as 1/8 in. OD to as large as 80 in. OD. Line-pipe sizes of 12 in. or less have an actual OD larger than the nominal size. For example, a 6-in. nominal line pipe is actually 6 5/8 in. OD. For line pipe larger than 12 in., the nominal size is the actual OD.

Manufacturing processes and chemical-property requirements for line pipe are different from those for casing. Chemical specifications for line pipe can be more restrictive than for casing because line pipe typically has welded connections. Although some line pipe is manufactured using the seamless process, the majority of line pipe is manufactured with one or more welded seams, which are created by electric welding, submerged-arc welding, or gas-metal arc-welding processes. Heat-treatment processes can be the same as for casing, but can also include other heat-treatment and manufacturing processes such as cold expansion.

Table 7.4 presents a list of the various grades of line pipe specified by API and ISO, along with minimum yield strength and ultimate tensile strength requirements. As for casing and tubing, the OD is specified, and the ID is governed by the OD and the weight tolerances. Unlike the specifications for casing and tubing, *API Spec. 5L* (2007) includes several wall-thickness tolerances for line pipe that are dependent on grade, manufacturing process, and OD. These tolerances are also included in Table 7.4.

API TR 5C3 (2008)/*ISO 10400:2007(E)* (2007) include formulas for calculating the performance properties of casing and line pipe. Generally, the API formulas for the performance properties of casing should provide reasonable estimates for the performance properties of line pipe with yield strength and d_n/t ratio falling within the size and thickness limits given in the API and ISO specifications. However, *API Spec. 5L* addresses line pipe with yield strength and d_n/t ratios that often significantly exceed the casing d_n/t ratios, and therefore the collapse and pipe-body yield-strength formulas developed for casing may not be applicable.

7.5 Strength of Materials

Many of the performance properties of casings are based on the strength of the steel. It is important to understand how the strength of a steel is measured. Moreover, other properties of a steel, such as hardness, toughness, and service temperature, can have an impact on the proper application of a steel. Most oilwell tubulars

TABLE 7.4—API/ISO LINE PIPE SPECIFICATIONS

API/ISO Line Pipe Specifications				Line Pipe Wall Thickness Tolerance		
Grade	Minimum Yield Strength (ksi)	Minimum Ultimate Tensile Strength (ksi)		OD (in.)	Wall Thickness Tolerance %	
		Minimum	Maximum		Grades A,B,A-25	X-42 through X-80
A-25	25	45		2.875 and smaller	+20.0	+15.0
A	30	48			−12.5	−12.5
B	35	60				
X-42	42	60		3.5	+18.0	+15.0
X-46	46	63			−12.5	−12.5
X-52	52	66				
X-56	56	71		4 through 18	+15.0	+15.0
X-60	60	75			−12.5	−12.5
X-65	65	77				
X-70	70	82		> 20 welded	+17.5	+19.5
X-80	80	90	120		−10.0	−8.0
				seamless	+15.0	+17.5
					−12.5	−10.0

Note: Weld area not limited by plus tolerance

are placed into a highly complex combination of many types of loads, which can require special analysis techniques to ensure that the combined stress does not result in failure.

7.5.1 Tensile Test. The strength of a material is its ability to support a load and is generally measured using a uniaxial tensile test. In this test, a machined test specimen with a gauge length of known cross-sectional area is pulled in tension until failure. The applied load and corresponding specimen extension are measured and converted into stress and strain values. The following equations are used to calculate nominal (or engineering) stress and strain and to draw the engineering stress-strain curve. An example of a nominal stress-strain curve for a low-alloy steel is shown in **Fig. 7.3**.

$$\sigma = F/A. \quad \dots\dots\dots (7.1)$$

$$\varepsilon = \Delta L/L. \quad \dots\dots\dots (7.2)$$

Engineering stress and strain are based on the original cross-sectional area and length of the sample. Engineering stress and strain are not the true stress and strain applied to the specimen because they do not account for changes in cross-sectional area or incremental increases in length that occur during the uniaxial tensile test. The true stress is the force applied to the sample divided by the current area of that sample. The true strain is based on the current length of the sample.

At relatively low values of strain, the relation between stress and strain is linear for many materials, including most steels. This relationship is described by Hooke's law:

$$\sigma = E \varepsilon. \quad \dots\dots\dots (7.3)$$

The proportionality constant is the elastic modulus (E), also known as Young's modulus. The elastic modulus is a measure of the stiffness of the material; high-modulus materials require more stress to achieve a given deformation. The elastic modulus of steel is approximately 30,000 ksi.

At the beginning of a tensile test, the deformation (strain) of the specimen increases linearly with the applied load (stress). At these loads, the specimen exhibits elastic behavior; if the load is removed, the specimen returns to its original length along the same stress-strain path. At a certain strain, the specimen deviates from the linear stress-strain relationship, but still exhibits elastic behavior. The point of deviation from linearity is called the

proportional limit. At slightly higher strain, the specimen begins to experience permanent plastic deformation with increasing load. This transition point is called the elastic limit or yield point.

Plastic deformation of a material is known as yielding. Because the yield point can be difficult to determine from load-displacement data, the yield strength or proof stress is an engineering definition of the stress value at which the specimen begins to exhibit plastic deformation. The yield point and the yield strength of a material are different. Two methods are commonly used to calculate yield strength. API and ISO define the yield strength of OCTG as the tensile stress required to produce a specified elongation (or strain), which is typically between 0.5 and 0.65% of total elongation. The other common method is the offset method, which defines yield strength as the tensile stress required to produce a specified plastic strain, most typically 0.2%.

After the specimen passes the yield point, it deforms plastically. A perfectly plastic material would exhibit a plateau at the yield strength, but for metals, the tensile stress applied to the specimen continues to increase, although the specimen is now yielding. The material becomes stronger as it deforms, a behavior known as strain hardening or work hardening. The engineering stress and strain will continue to increase until the stress reaches its peak value—the tensile strength.

The specimen does not break immediately upon reaching its tensile strength. Instead, the strains become highly localized, and the stress required per unit of strain decreases. The local straining of the specimen under this plastic instability condition is called necking. The specimen continues to neck until it finally fractures. The permanent extension, or plastic elongation, of the specimen at failure is a measure of the ductility of the material. For steel OCTG, plastic elongation typically exceeds 20%.

For carbon and low-alloy steels, the mechanical properties are the same in all directions. This condition is called isotropy. Some highly alloyed corrosion-resistant alloys are cold-worked after being formed, and this can result in significantly different yield strengths in different tangential, radial, or axial directions. This condition is called anisotropy.

Most classic design methods never permitted a material to be stressed beyond its yield point. Safety factors were typically used to ensure that working stresses remained below the yield point or yield strength. In more recent years, stresses and deformations in the plastic range of a material have been permitted in certain situations.

Engineering materials are often referred to as either ductile or brittle. Ductility is the property that allows the development of deformation under the application of stress. A ductile material has a relatively large tensile strain up to the point of rupture. A brittle material, on the other hand, has a relatively small strain up to the point of

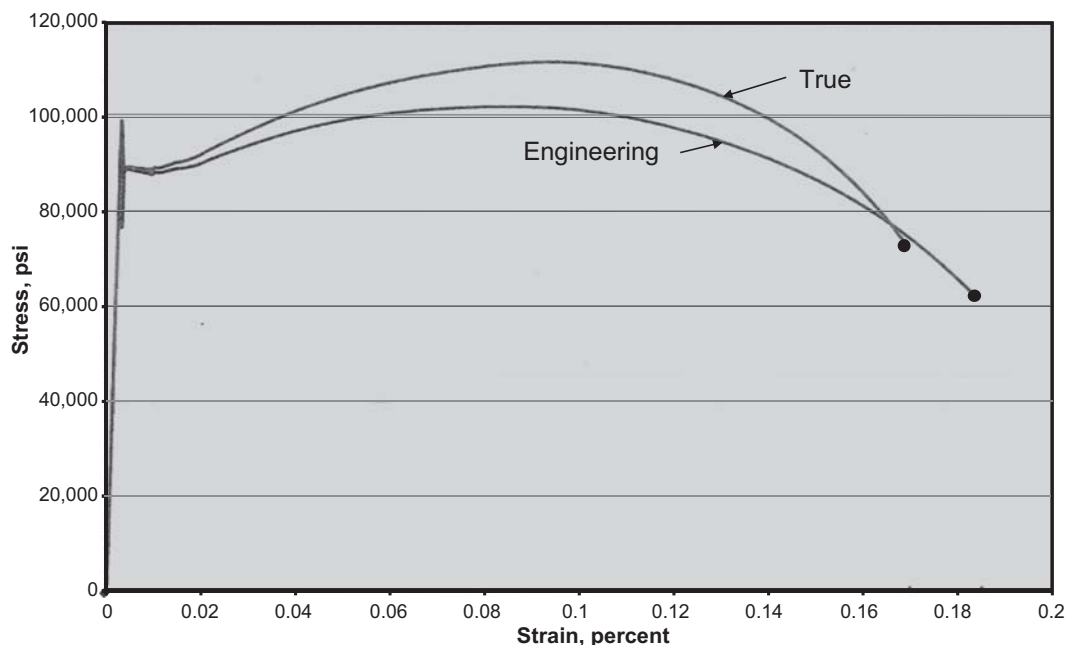


Fig. 7.3—Stress-strain behavior of steel.

failure. A measure of ductility is the percentage elongation of a specified length after fracture. A large percentage elongation indicates high ductility.

7.5.2 Hardness. Technically speaking, hardness is the ability of a material to resist indentation. In a hardness test, a small (~1 mm) indenter is forced into the test material at an applied load. The size of the indentation is used to calculate the hardness value. The hardness scale used depends on the strength of the material; Brinell and Rockwell C (HRC) are the most commonly used scales for OCTG.

Hardness is a useful property because it correlates with tensile strength. High-hardness steels also have high strength. Because hardness indentations are small, hardness measurements are frequently used to characterize local variations in material properties. Consistent hardness measurements indicate consistent tensile properties. API and ISO have requirements for the location and orientation of samples taken from OCTG for hardness testing and specify maximum hardness values as an indicator of fitness for service for some steels. **Table 7.5** includes typical hardness ranges for some API and ISO grades.

7.5.3 Toughness. The toughness of a material is its ability to absorb energy and resist brittle fracture. Brittle fracture is catastrophic and can be manifested at stresses below the yield strength of the material. Brittle materials have low toughness because they experience only small plastic deformations before fracture. Generally, toughness decreases with increasing yield strength. Temperature can have a significant impact on the toughness of carbon and low-alloy steels. Toughness is usually measured using the Charpy impact test at a specified temperature. Elongation requirements are also a measure of ductility and are used to ensure adequate toughness.

The Charpy test measures a material's resistance to a sudden intense impact load. In the test, a heavy pendulum swings through its arc and breaks a V-notched specimen. The impact energy of the sample is a measure of the potential energy absorbed by the sample during failure. This energy is a measure of the toughness of the material and is called the Charpy impact energy or Charpy toughness. Toughness is measured in ft-lbf, and high impact energy indicates high toughness.

Two other specimen characteristics are measured in the Charpy test: percent shear area on the fracture surface, and percent lateral expansion. Percent shear area describes the morphology of the fracture surface—a specimen exhibiting a large percent shear area fractures in a more ductile (rather than brittle) manner. In ductile behavior, a specimen exhibits a relatively large amount of lateral-expansion deformation during fracture. Specifications for

TABLE 7.5—TYPICAL HARDNESS RANGES FOR CASING

Grade (All Types)	Rockwell C-Scale (HRC) Hardness	
	Minimum	Maximum ^(a)
H-40	—	—
K-55	13	24
N-80	15	29
L-80	15	23
C-90	18	25.4
T-95	18	25.4
C-95	17	28
P-110	28	35
Q-125	30	38 ^(b)
Note:		
(a) API requirements shown in bold		
(b) No hardness limits specified for this grade, but maximum hardness variation is restricted during manufacturing. Charpy toughness requirements.		

Charpy testing include required impact energy and percent shear, but typically no requirements for lateral expansion are included.

Although the Charpy impact energy is not a rigorous measurement of fracture toughness, it is very useful for quality-assurance testing of OCTG. Because toughness tends to decrease with increasing strength, Charpy tests are frequently required to verify the toughness of high-strength OCTG such as Q125. API and ISO have requirements for the location and orientation of samples taken from OCTG for Charpy testing and specify a minimum impact toughness as an indicator of fitness for service.

7.5.4 Effect of the Environment on Mechanical Properties. Temperature can have a dramatic effect on the mechanical properties of materials. As temperature increases, yield strength, tensile strength, and stiffness decrease, while ductility increases. Temperature effects on strength need to be considered for high-temperature wells. For example, at 300°F, the yield strength of steel can be reduced to approximately 90% of the room-temperature value. Steel manufacturers can provide more precise information on yield-strength reduction associated with elevated temperature.

Toughness is also strongly affected by temperature. Most low-alloy steels exhibit a nearly constant low toughness value at low temperatures and a nearly constant high toughness value at high temperature, connected by a nearly linear transition region. The transition temperature is the temperature below which a material exhibits 15 ft-lbf impact energy or 50% shear area. Materials are considered brittle when they are below their transition temperature. Because toughness is such a strong function of temperature, toughness is a significant design criterion for cold-temperature design. Charpy tests must be conducted below the coldest anticipated service temperature to verify that the selected materials have sufficient toughness for the application. The presence of hydrogen sulfide (H_2S) also can reduce the toughness of steel OCTG.

7.5.5 Combined Stresses. Loading conditions in an oil well are a highly complex combination of many types of loading, including loads from the environment and loads from temperature changes. Although a tensile test uses a gradually increasing uniaxial loading to determine the strength of a steel, the design problem with tubulars is how to predict the stress in the tubular when the tubular is subjected to biaxial or triaxial stresses, not just uniaxial stresses. **Fig. 7.4** shows the principal stresses that can exist at any point in a tubular as a result of the combined actions of internal, external, and axial loading. In a tubular, the stresses act in three orthogonal directions: axial, radial, and tangential. Axial stresses act parallel with the axis of the tube, radial stresses act through the wall thickness, and tangential stresses act around the tube. The tangential direction is also often referred to as the “hoop” or “circumferential” direction. For a tubular, these three stress directions are the directions of maximum stress and therefore are the maximum principal stresses. The Lamé equations for thick-walled pressure vessels can be used to calculate the radial and tangential principal stresses when there is no bending or torsion (Timoshenko and Goodier 1970). At any radius, r , between the inner radius, r_i , and outer radius, r_o , the Lamé equations are

$$\begin{aligned}\sigma_r &= \frac{r_i^2 P_i - r_o^2 P_e}{r_o^2 - r_i^2} - \frac{(P_i - P_e) r_o^2 r_i^2}{r^2 (r_o^2 - r_i^2)} \\ \sigma_t &= \frac{r_i^2 P_i - r_o^2 P_e}{r_o^2 - r_i^2} + \frac{(P_i - P_e) r_o^2 r_i^2}{r^2 (r_o^2 - r_i^2)}, \dots\dots\dots (7.4)\end{aligned}$$

where σ_r and σ_t are the radial and tangential stresses at radius r . Note that in these equations, the outer radius is typically based on the nominal OD and the inner radius is based on the maximum ID with the permissible wall thickness under tolerance. To be conservative, the inner radius typically is based on the maximum ID according to these calculations.

The total axial stress, σ_z , in a tube is the result of tension or compression loads, σ_a , and bending stresses, σ_b . It can be calculated using the following equation:

$$\begin{aligned}\sigma_z &= \sigma_a \pm \sigma_b \\ \sigma_a &= F_a / A_s \\ F_z &= \sigma_z A_s. \dots\dots\dots (7.5)\end{aligned}$$

The bending stress, σ_b , will be defined later. In most cases, the cross-sectional area of the steel in this equation is based on the nominal inside and OD of the tubular. Bending stresses due to hole deviation, doglegs, or buckling are superimposed on or added to the axial stress. Bending stresses are positive (indicating tension) or negative

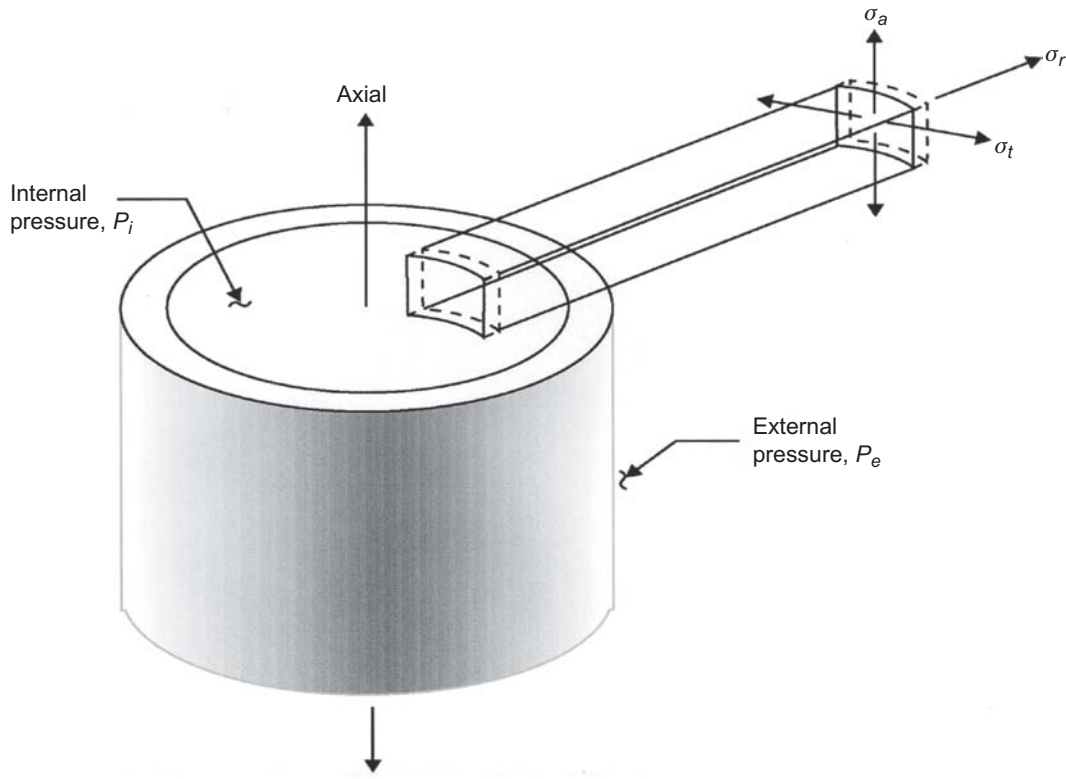


Fig. 7.4—Stresses in a pipe.

(indicating compression), depending on where the stress is computed in the pipe body. Equations for calculating bending stresses will be covered in Section 7.6. Note that the steel cross-sectional area used in this equation is based on the nominal outside and IDs of the tube.

As many as eight theories have been developed that predict a material's failure or yield behavior when several types of loading and the resulting stresses are present (Boresi and Schmidt 2002). One commonly used method is based on the Huber-von Mises-Hencky theory. This theory, also known as the maximum-distortion-energy theory, predicts that failure by yielding will occur when the strain energy of distortion per unit volume of the tube in a triaxial stress state is equal to the strain energy per unit volume that causes yielding in a standard uniaxial test specimen. In simpler terms, this method combines tangential, radial, and axial principal stresses into a single stress-equivalent term, which is then compared to the minimum yield strength of the steel as determined from a simple uniaxial tension test. The stress at a point in the tubular using this theory can be calculated using the following equation:

$$2\sigma_{vm}^2 = (\sigma_z - \sigma_r)^2 + (\sigma_r - \sigma_t)^2 + (\sigma_t - \sigma_z)^2 \quad (7.6)$$

Notice that Eq. 7.6 is independent of hydrostatic pressure, because if we add pressure to each term in Eq. 7.6, the pressures cancel each other out. If we substitute Eqs. 7.4 and 7.5 for the radial and hoop stresses into Eq. 7.6, we get the following result:

$$\sigma_{vm}^2 = \frac{F_e^2}{A_s^2} + \frac{3\pi^2 r_i^4 r_o^4 (P_i - P_e)^2}{A_s^2 r^4} \quad (7.7)$$

$$F_e = F_z - P_i A_i + P_e A_e.$$

F_e is called the effective tension, and we will have further use of it when we study the effects of fluid forces on casing design. We can plot the results of this equation as a graph of effective tension vs. the pressure increment $P_i - P_e$ (Fig. 7.5). Note that the maximum von Mises stress occurs at the inner radius of the pipe, $r = r_i$. When there is bending, however, the bending stress varies with radius, so the inner radius may not be the worst case, as we will see later.

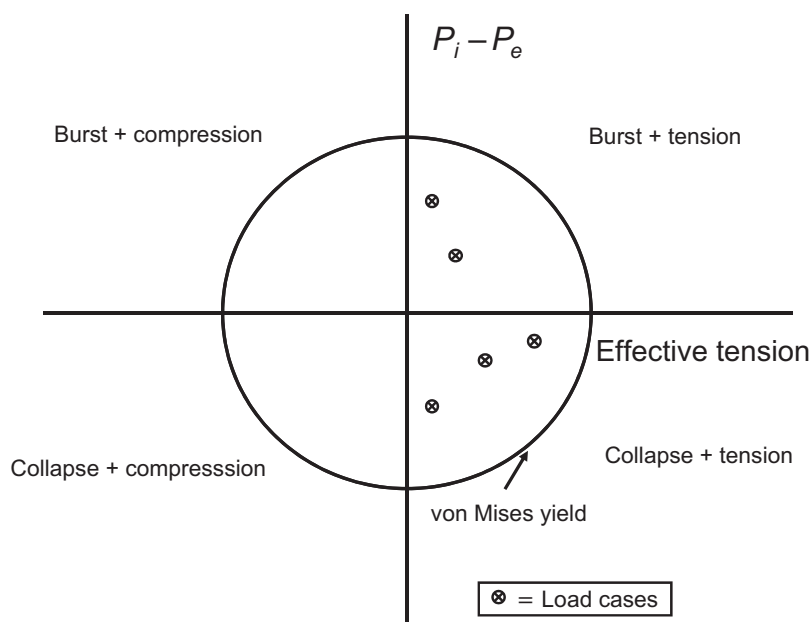


Fig. 7.5—Casing failure criteria.

For a given tubular, it is common to plot the burst, collapse, and axial-load combinations that result in a triaxial equivalent stress equal to the minimum yield strength of the steel, or equal to a reduced maximum working-stress level that is less than the minimum yield strength. All combinations of pressure and axial loads inside the ellipse must result in a triaxial equivalent stress that is less than the maximum desired working stress. A combination of pressure and axial loads outside the ellipse results in a triaxial equivalent stress which is greater than the desired working stress.

Although Eq. 7.7 is accurate for thick-walled pressure vessels, simpler methods to calculate a tubular's performance properties have been used for many years by API and ISO. These methods typically assume uniaxial or biaxial principal stresses and further assume that the radial principal stresses are small, which can be true in thin-walled pressure-vessel design.

7.6 Casing-Tube Performance Properties

The performance properties of tubular goods are a collective term for all the strength and sealability ratings of the tubulars. Casing strength is defined as the maximum load that a tubular can withstand without failure. Failure can be defined in many ways. These include stresses in the tubular exceeding the steel's minimum yield strength, fracture or rupture of the tubular, and a leak in the tubular. Equations, both theoretical and empirical, have been developed by the industry to determine the maximum loading that can be applied to a tubular to ensure that the desired failure criteria will be met. Many of the early equations used by the industry required that the allowable stress in the steel be in the elastic region. Early deterministic approaches to performance ratings were based on calculating a single performance-property value based on material or geometric properties and on the assumption that the stress in the material was below minimum yield strength. Fracture or physical failure of the tubular usually occurred at a much higher loading.

More recently, the industry has moved toward the use of limit-state equations. When used with the measured geometry and properties of the material, they result in a prediction of the failure or rupture performance properties of the tubular. Often this failure occurs in the plastic region, and a method of determining the "limit state" of a tubular was therefore needed. Limit-state equations can be either empirical or probabilistic in nature. For probabilistic limit-state equations, geometric and material properties are typically treated as random, and a statistical approach to determining performance properties is used.

API TR 5C3 (2008)/ISO 10400:1993 (1993) include deterministic equations to calculate the rated performance-property values for *axial tension*, *burst pressure*, and *collapse pressure*. Axial tension loading results primarily from the weight of the casing string suspended below the joint of interest. *Pipe-body yield strength* is the tension force that causes the pipe body to exceed its elastic limit. Similarly, *joint strength* is the minimum tensional force required to cause connection failure. Burst-pressure rating is the calculated minimum internal pressure that will cause the maximum stress in the casing to approach the minimum yield strength in the absence of external

pressure and axial loading. Collapse pressure rating is the minimum external pressure that will cause the casing walls to collapse in the absence of internal pressure and axial loading.

API Bull. 5C2 (1999/ISO 10400:2007(E) (2007) summarize the performance properties for API casing. Several industry publications also include many API and some non-API standard casing-performance properties. These publications include the *Halliburton Cementing Tables* (2001), *BJ-Titan Services Engineering Handbook* (1987), *Baker Oil Tools Tech Facts Engineering Handbook* (1993), and others. Most proprietary connection manufacturers also publish pipe-body performance tables and connection ratings. In addition, some operators have developed proprietary methods and performance-property summaries.

7.6.1 Casing Tension Strength. *API TR 5C3* (2008) defines pipe-body yield strength as the axial load in the tube, which results in the stress being equal to the material's minimum specified yield strength. To calculate the stress in the tube, the specified or nominal OD and the ID are used for API casing. Thus, the pipe-body tensile strength can be expressed as

$$F_{\text{ten}} = \frac{\pi}{4} \sigma_{\text{yield}} (d_n^2 - d^2) \quad \dots \dots \dots (7.8)$$

The pipe-body yield strength computed using Eq. 7.8 is the minimum force that would be expected to cause permanent deformation of the pipe. The expected minimum force required to pull the pipe apart would be significantly higher than this value. Note that nominal OD and ID are used in this equation. Experience has found that for most casings, even with permissible tolerances, the overall wall cross-sectional area will be close to the cross-sectional area obtained if specified or nominal OD and ID are assumed.

Yield strength in compression is typically assumed to be the same as in tension. However, when a casing is loaded in compression, axial buckling may occur, and the casing may fail before reaching the pipe-body yield strength.

Example 7.1 Compute the pipe-body yield strength for 20-in., K-55 casing with a nominal wall thickness of 0.635 in. and a nominal weight per foot of 133 lbf/ft.

Solution. This pipe has a minimum yield strength of 55,000 psi and an ID of

$$d = 20.00 - 2(0.635) = 18.730 \text{ in.}$$

Thus, the cross-sectional area of steel is

$$A_s = \frac{\pi}{4} (20^2 - 18.73^2) = 38.63 \text{ in.}^2,$$

and Eq. 7.8 predicts minimum pipe-body yield strength at an axial load of

$$F_{\text{ten}} = 55,000(38.63) = 2,125,000 \text{ lbf.}$$

The pipe-body yield strength under tensile axial load for both casing and line pipe can be calculated using Eq. 7.8. However, for casing or line pipe in compression, axial buckling can occur before the loading reaches pipe-body yield strength and is dependent on how the tubular is laterally restrained. Axial buckling of a tubular in compression is not considered in Eq. 7.8.

For a particular casing, the limiting case may be governed by the connection rather than the pipe body and does not include any consideration of leak resistance.

7.6.2 Casing Internal Pressure Resistance. *API TR 5C3* (2008)/*ISO/TR 10400:2007(E)* (2007) use the Barlow equation to determine the minimum internal yield pressure for tubulars. The Barlow equation was the first widely accepted formula used for predicting the internal pressure resistance of a thick-walled tube (Seely and Smith 1965). The main difference between the Lamé formula and Barlow's formula lies in the assumptions made concerning how the cylinder as a whole strains under internal pressure. The Barlow formula applies to cylinders subjected to internal pressure only and depends on the assumption that the transverse cross-sectional area remains constant. This assumption is known to be incorrect. The stresses calculated by the Barlow formula are always higher than the stresses calculated by the Lamé formula for the same loading; therefore, Barlow's formula always gives lesser burst-resistance values than the Lamé formula.

Because actual tube failure does not occur until yielding has progressed through the tube wall to the outer diameter and is affected by tensile stress, the API burst resistance typically will be as much as 20% lower than the actual burst-failure rating.

The Barlow equation is easily applied in practice, easily accounts for the acceptable API manufacturing wall-thickness tolerance for casing (which is 12.5% less than nominal wall thickness), and has resulted in acceptable tubular designs in noncritical wells. Sometimes called an “API burst” calculation, the Barlow equation is:

$$P_{br} = f \left[\frac{2\sigma_{\text{yield}} t}{d_n} \right], \quad \dots\dots\dots (7.9)$$

where the wall-thickness correction factor is $f = 0.875$ for standard API tubulars when a 12.5% wall-thickness tolerance is specified. Line pipe has different wall-thickness correction factors, as specified in *API Spec. 5L/ISO 3183* (2009).

API recommends use of this equation with wall thickness rounded to the nearest 0.001 in. and the results rounded to the nearest 10 psi.

Example 7.2 Compute the API burst resistance for 20-in., 133-lbf/ft, K-55 casing with a nominal wall thickness of 0.635 in.

Solution. The API burst resistance is computed using Eq. 7.9:

$$\begin{aligned} P_{br} &= (0.875)[(2)(55,000)(0.635)/20.0] \\ &= 3,056 \text{ psi.} \end{aligned}$$

Rounded to the nearest 10 psi, this value becomes 3,060 psi. This burst-resistance rating corresponds to the minimum expected internal pressure at which permanent pipe deformation could take place if the pipe were subjected to no external pressure or axial loads.

To make the Lamé equations easier to apply, some operators assume that radial stress is insignificant. The radial stress is usually small under moderate design conditions. The Lamé tangential-stress equation (Eq. 7.5) simplifies to this equation when solved for the stress at the minimum specified ID, assuming no internal pressure, the absence of bending and torsion, and no radial stress:

$$P_{br} = \sigma_{\text{yield}} (d_n^2 - d_m^2) / (d_n^2 + d_m^2). \quad \dots\dots\dots (7.10)$$

The specified wall-thickness reduction factor should be used to obtain the maximum pipe-body ID used in this equation. The pipe nominal OD is normally used here.

When design conditions are more stringent and a more accurate tubular design is needed, the von Mises yield theory is often used in conjunction with the Barlow equation or the Lamé equations. The von Mises yield theory is more cumbersome to apply using hand calculations, but computers make this calculation fast and simple. In most cases, a more accurate tubular design is needed where a significant combined load or a hostile service environment is anticipated. Although current API and ISO specifications do not include the formulas and calculations for von Mises analysis, those likely will be included in the next few years.

The internal pressure-resistance formulas discussed so far predict the internal pressure at the point where the stress somewhere in the material starts to exceed the minimum yield strength. The actual burst of a tubular can occur at a much higher internal pressure defined by a limiting-state equation, which can be either empirically or theoretically derived.

Crack propagation due to internal pressure can occur at less than plastic stress when an imperfection or crack in the steel propagates to the point that the material fails. The service environment, defined by temperature, presence of corrosive gases or fluids, pH, and other factors, as well as material properties such as toughness, will govern when this type of failure occurs. Several limiting-state equations have been developed by the industry for brittle fracture.

A ductile rupture or fracture is characteristic of a tubular with adequate toughness for the environment in which it is placed. Failure after deformation of the tube occurs in a ductile manner through to final rupture. The failure is not brittle even in the presence of small imperfections in the steel.

More advanced textbooks include information on limiting-state equations, which can predict rupture pressure using these models.

7.6.3 Casing Collapse Resistance. The collapse of a steel pipe tube from external pressure is a very complex phenomenon and much more difficult to calculate than the bursting of pipe from internal pressure. The reason for this is that collapse is an instability type of failure in many cases and is sensitive to many factors such as ovality, the ratio of tube diameter to wall thickness, yield strength, type of steel heat treatment, and localized wall reduction. There is no simple method of calculating the collapse of a tube because collapse can occur in various modes depending on these parameters. More accurate equations for predicting collapse strength continue to be proposed and studied (Issa and Crawford 1993; Tamano et al. 1983; Ju et al. 1998).

Formulas for calculating collapse-performance properties were first introduced in the late 1960s by the API. Four modes of collapse were recognized, with each mode defined by a separate formula. The ratio of OD to wall thickness and the minimum yield strength are used to determine which collapse-pressure formula should be used.

The four collapse-pressure formulas proposed by the API are listed here in order of increasing d_n/t ratio, as shown in **Fig. 7.6**:

- Yield-strength collapse
- Plastic collapse
- Transition collapse
- Elastic collapse

Five factors (F_1 , F_2 , F_3 , F_4 , and F_5) are used with the tube's d_n/t ratio to determine which of the four collapse-pressure formulas is applicable. The factors are dependent on the yield strength of the tube. They are defined by the following equations:

$$F_1 = c_0 + c_1\sigma_{\text{yield}} + c_2\sigma_{\text{yield}}^2 + c_3\sigma_{\text{yield}}^3, \quad \dots \quad (7.11)$$

$$F_2 = c_4 + c_5\sigma_{\text{yield}}, \quad \dots \quad (7.12)$$

$$F_3 = c_6 + c_7\sigma_{\text{yield}} + c_8\sigma_{\text{yield}}^2 + c_9\sigma_{\text{yield}}^3, \quad \dots \quad (7.13)$$

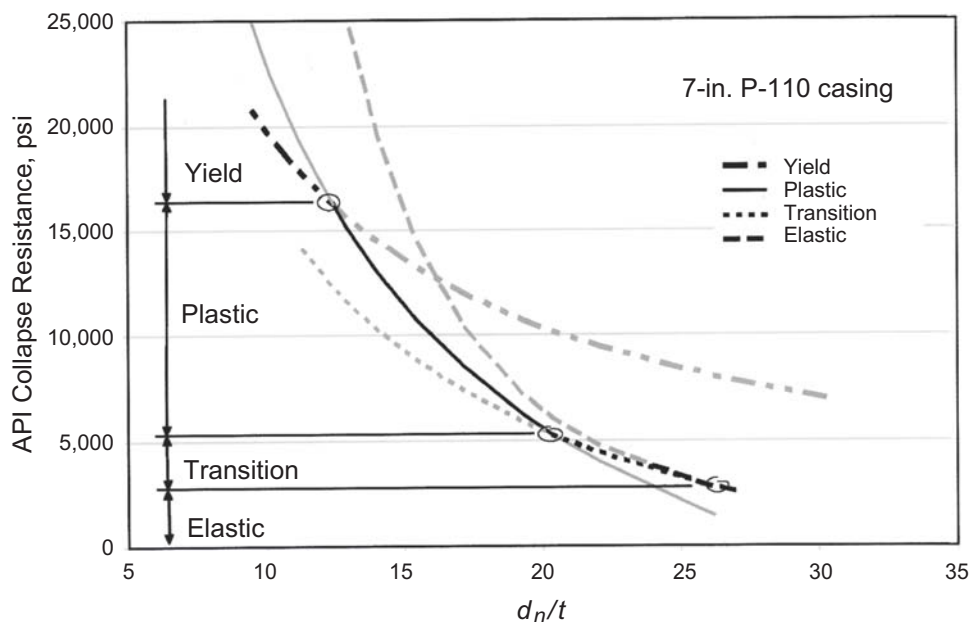


Fig. 7.6—Collapse modes.

$$F_4 = c_{10} \frac{[3R_F/(2 + R_F)]^3}{\sigma_{\text{yield}} [3R_F/(2 + R_F) - R_F][1 - 3R_F/(2 + R_F)]^2}, \quad \dots \quad (7.14)$$

$$F_5 = F_4 R_F, \quad \dots \quad (7.15)$$

where

$$\begin{aligned} c_0 &= 2.8762 & c_1 &= 0.10679 \times 10^{-5} \\ c_2 &= 0.21302 \times 10^{-10} & c_3 &= -0.53132 \times 10^{-16} \\ c_4 &= 0.026233 & c_5 &= 0.50609 \times 10^{-6} \\ c_6 &= -465.93 & c_7 &= 0.030867 \\ c_8 &= -0.10483 \times 10^{-7} & c_9 &= 0.36989 \times 10^{-13} \\ c_{10} &= 46.95 \times 10^6 & R_F &= F_2/F_1 \end{aligned}$$

The d_n/t ranges where the four collapse-pressure equations applicable are separated by three changeover points, which are dependent on casing grade and the values of the factors. The equations used to determine these three changeover points are discussed in the next section.

Yield-Strength Collapse-Pressure Formula. The yield-strength collapse-pressure formula calculates the external pressure that generates the minimum yield stress on the inside wall of a tube and can be derived theoretically using the Lamé equation. Generally, this formula applies to the thickest-walled tubulars used in oil wells. The yield-strength collapse-pressure formula can be written as

$$P_{cr} = 2\sigma_{\text{yield}} \left(\frac{(d_n/t) - 1}{(d_n/t)^2} \right). \quad \dots \quad (7.16)$$

This equation is applicable for d_n/t values up to the value of the d_n/t ratio where the plastic collapse formula becomes applicable. The d_n/t ratio for this changeover point can be calculated using the following equation:

$$\frac{d_n}{t} = \frac{\sqrt{(F_1 - 2)^2 + 8[F_2 + (F_3/\sigma_{\text{yield}})] + (F_1 - 2)}}{2[F_2 + (F_3/\sigma_{\text{yield}})]}. \quad \dots \quad (7.17)$$

Plastic-Collapse Pressure Formula. This equation is based on 2,488 physical-collapse tests of K-55, N-80, and P-110 casings (API TR 5C3 2008). Statistical methods were used to analyze the results of the physical tests, and a plastic-collapse formula was developed to calculate a collapse value with a 95% probability that the actual collapse pressure will exceed the minimum stated with no more than a 0.5% failure rate:

$$P_{cr} = \sigma_{\text{yield}} \left[\frac{F_1}{d_n/t} - F_2 \right] - F_3. \quad \dots \quad (7.18)$$

The d_n/t ratio where the changeover from the plastic-collapse formula to the transition formula occurs can be calculated using the following equation:

$$\frac{d_n}{t} = \frac{2 + \frac{F_2}{F_1}}{\frac{3F_2}{F_1}}. \quad \dots \quad (7.19)$$

Transition-Collapse Pressure Formula. The transition-collapse formula was developed to provide a transition from the plastic-collapse formula to the elastic-collapse formula:

$$P_{cr} = \sigma_{\text{yield}} \left[\frac{F_4}{d_n/t} - F_5 \right] \quad \dots\dots\dots (7.20)$$

The d_n/t range for the changeover from the transition-collapse equation to the elastic-collapse equation can be calculated using the following equation:

$$\frac{d_n}{t} = \left[\frac{\sigma_{\text{yield}}(F_1 - F_4)}{F_3 + \sigma_{\text{yield}}(F_2 - F_5)} \right] \quad \dots\dots\dots (7.21)$$

Elastic-Collapse Pressure Formula. The elastic-collapse pressure formula was theoretically derived and was found to be an adequate upper bound for collapse pressures as determined by testing. The following equation is a modification of the theoretical equation and is used to calculate the minimum elastic-collapse pressure. The API adopted this equation in 1968:

$$P_{cr} = \frac{46.95 \times 10^6}{(d_n/t)[(d_n/t) - 1]^2} \quad \dots\dots\dots (7.22)$$

Note that in elastic collapse, as typically observed in some large tubulars, material yield strength does not affect the collapse resistance of the tubular. Increasing wall thickness is the only available method to increase collapse resistance for tubulars that fall in the elastic-collapse pressure range.

Collapse Resistance of Casing With Combined Loading. As noted in Section 7.5, a tubular material subjected to combined loadings, such as a collapse load, internal pressure, axial tension, or bending, will experience a different stress level from that which would occur if only collapse loads existed. The API offers an equation to calculate the external pressure equivalent when both external and internal pressures are applied to a tubular. The formula is a simple method to account for external pressure and its effect on the collapse rating of a tubular:

$$P_{eq} = P_e - \left[1 - \frac{2}{d_n/t} \right] P_i \quad \dots\dots\dots (7.23)$$

Tension has a detrimental effect on the collapse-pressure rating and a beneficial effect on the burst-pressure rating. By contrast, axial compression has a detrimental effect on burst-pressure rating and a beneficial effect on collapse-pressure rating (Fig. 7.6). In casing design practice for simple wells, it is common to include only the detrimental effects of axial loading.

The current API and ISO method to derate the collapse resistance of a tubular due to tension was developed in the early 1980s. The current API formula accounts for the combined influence of tension and collapse loading on a casing by modifying the minimum yield strength to the yield strength of an axial-stress-equivalent grade. The reduced equivalent yield strength is based on von Mises yield theory. The equivalent yield-strength formula is

$$\sigma_{pa} = \left[\sqrt{1 - 0.75 \left(\frac{\sigma_a}{\sigma_{\text{yield}}} \right)^2} - 0.5 \left(\frac{\sigma_a}{\sigma_{\text{yield}}} \right) \right] \sigma_{\text{yield}} \quad \dots\dots\dots (7.24)$$

The equivalent yield strength due to axial stress is then used in the five collapse-factor equations (Eqs. 7.11–7.15). The appropriate collapse-pressure formula (Eqs. 7.16, 7.18, 7.20, 7.22) is then used to arrive at the reduced collapse-pressure rating due to axial tension.

Example 7.3 Compute the API collapse-pressure rating for 20-in., K-55 casing with a nominal wall thickness of 0.635 in. and a nominal weight per foot of 133 lbf/ft.

Solution. This pipe has a d_n/t ratio given by $d_n/t = 20/0.635 = 31.496$. Eq. 7.21 indicates that this value for d_n/t falls in the range specified for transition collapse. Therefore, the collapse-pressure rating can be computed using Eq. 7.20. Eqs. 7.11–7.15 yield values for factors F_4 and F_5 of 1.989 and 0.036, respectively. The calculation then becomes

$$P_{cr} = 55,000 \left(\frac{1.989}{31.496} - 0.036 \right) = 1,493 \text{ psi}, \quad \dots\dots\dots (7.25)$$

or 1,490 psi rounded to the nearest 10 psi. This collapse-pressure rating is the minimum expected external pressure at which the pipe would collapse if the pipe were subjected to no internal pressure or axial loads.

Special High-Collapse-Resistance Casing. Since the 1970s, manufacturers have produced special tubulars that are “high-collapse” as measured with reference to the API collapse rating. In many cases, the high collapse ratings are achieved by using tubular, mechanical, and dimensional tolerances greater than API standards, thus increasing the yield strength of the steel, and by using superior heat-treatment methods. An API study in the 1980s found that many of these tubulars failed to achieve the claimed design rating (Marlow 1982). This controversial study led to the physical testing of many more samples and some changes in the methods used for physical testing of collapse specimens. Users of “high-collapse” tubulars should therefore consider stricter-than-API dimension and material control and other specifications and testing to ensure the desired product performance. Because API collapse ratings can be improved on significantly with the use of special “high-collapse” tubulars, many operators continue to use them.

Many engineers have found the classic API collapse equations to be conservative. Beginning in the 1980s, several authors developed new methods to predict the collapse of a tubular. These methods are based on finite-element modeling, empirical data, theoretical analysis, and risk-based approaches, such as Issa and Crawford (1993), Ju et al. (1998), Tamano et al. (1983), Brand et al. (1995), and Lewis et al. (1995).

Similarly to the determination of the limit state for burst, methods have been proposed to determine a limit state for collapse, including statistical analysis of physical test results, heat-treatment types, risk analyses, and various mechanical properties of the tubular. The limit-state equations for minimum collapse are presented in *ISO/TR 10400:2007(E)* (2007).

7.6.4 Effect of Bending. In directional wells, the effect of wellbore curvature and vertical deviation angle on axial stress in the casing and couplings must be considered in the casing design. When a casing is forced to bend, the axial tension on the convex side of the bend can increase greatly. On the other hand, in relatively straight sections of hole with a significant vertical deviation angle, the axial stress caused by the weight of the pipe is reduced. Axial stress is also significantly affected by increased friction between the casing and the borehole wall. In current design practice, the detrimental effect of casing bending is considered, but the favorable effect of the vertical deviation angle is neglected. Wall friction, which is favorable to downward pipe movement and unfavorable to upward pipe movement, is generally compensated for by the addition of a minimum acceptable *overpull force* to the free-hanging axial tension.

The curvature of a directional well is generally expressed in terms of the change in the angle of the borehole axis per unit length. The *dogleg severity*, κ , is the change in angle in degrees over the borehole length. The maximum increase in axial stress, σ_b , on the convex side of the pipe is given by Crandall and Dahl (1959). On the concave side of the pipe, the stress magnitude is the same, but the stress is compressive rather than tensile:

$$\sigma_b = \pm \frac{1}{2} E d_n \kappa. \quad \dots\dots\dots (7.26)$$

In oilfield units, where the dogleg severity, κ , is expressed as the change in angle in degrees per 100 ft of borehole length, and the pipe is assumed to be steel, this equation simplifies to

$$\sigma_b = \pm 218 d_n \kappa. \quad \dots\dots\dots (7.27)$$

It is often convenient to express the increased axial stress caused by bending in terms of an equivalent axial force, F_{ab} , where

$$F_{ab} = \pm \sigma_b A_s = \pm 218 \kappa d_n A_s. \quad \dots\dots\dots (7.28)$$

The area of steel, A_s , can be expressed conveniently as the weight per foot of pipe divided by the density of steel. For common field units, Eq. 7.28 becomes

$$F_{ab} = \pm 64 \kappa d_n w_p, \quad \dots\dots\dots (7.29)$$

where F_{ab} , κ , d_n , and w_p have units of lbf, degrees/100 ft, in., and lbf/ft, respectively. Use of a nominal weight per foot for w will generally give acceptable accuracy. Eq. 7.29 is valid when the pipe wall is uniformly in close contact with the borehole wall (i.e., when the size of the upset in OD at the casing connectors is small compared with borehole irregularities).

When the casing is in contact with the borehole wall only at the connectors, the radius of curvature of the pipe is not constant. In this case, the maximum axial stress can be significantly greater than that predicted by Eq. 7.29. Classical beam-deflection theory as stated by Lubinski (1977) can be used in this case to determine the bending stress magnification factor. Lubinski considered only pipe in tension. For pipe in compression, use Paslay and Cernocky (1991) and Mitchell (2003).

In the previous discussion, the effect of bending on casing failure was handled by consideration of the maximum stress present under the combined loading situation experienced. In this analysis, a possibility of failure is indicated when the maximum stress level exceeds the yield strength of the steel. An alternative approach sometimes used is to express the axial strength of the material in terms of combined tension and bending. The approach is used most commonly in rating the tensional joint strength of a coupling subjected to bending. API formulas (API TR 5C3 2008) have been developed for the joint strength of a round-thread casing subjected to bending. When the axial tension strength F_{cr} divided by the cross-sectional area of the pipe wall under the last perfect thread is greater than the minimum yield strength, the joint strength is given by

$$F_{cr} = 0.95A_{jp} \left\{ \sigma_{ult} - \left[\frac{140.5\kappa d_n}{(\sigma_{ult} - \sigma_{yield})^{0.8}} \right]^5 \right\}, \dots\dots\dots (7.30)$$

where

$$F_{cr} / A_{jp} \geq \sigma_{yield},$$

κ is given in degrees/100 ft, and

$$A_{jp} = (\pi/4) \left[(d_n - 0.1425)^2 - (d_n - 2t)^2 \right].$$

When the axial tension strength divided by the cross-sectional area of the pipe wall under the last perfect thread is less than the minimum yield strength, then

$$F_{cr} = 0.95A_{jp} \left(\frac{\sigma_{ult} - \sigma_{yield}}{0.644} + \sigma_{yield} - 218.15\kappa d_n \right). \dots\dots\dots (7.31)$$

These empirical correlations were developed from experimental tests conducted with 5.5-in., 17-lbf/ft, K-55 casing with short round-thread couplings (STC).

Example 7.4 Determine the maximum axial stress for 7.625-in., 39-lbf/ft, N-80 casing if the casing is subjected to a 400,000-lbf axial-tension load in a portion of a directional wellbore having a dogleg severity of 4°/100 ft. Compute the maximum axial stress assuming uniform contact between the casing and the borehole wall.

Solution. Nominal API pipe-body yield strength for this casing is 895,000 lbf, and the ID is 6.625 in. The cross-sectional area of steel in the pipe body is

$$\pi/4(7.625^2 - 6.625^2) = 11.192 \text{ in.}^2$$

The axial stress without bending is

$$400,000/11.192 = 35,740 \text{ psi.}$$

The additional stress level on the convex side of the pipe caused by bending can be computed using Eq. 7.27 under the assumption of uniform contact between the casing and the borehole wall. Eq. 7.27 gives a maximum bending stress of

$$(\Delta\sigma_b)_{\max} = 218(4.0)(7.625) = 6,649 \text{ psi}$$

and a total stress of

$$35,740 \text{ psi} + 6,649 \text{ psi} = 42,389 \text{ psi}.$$

7.6.5 Torsion. For most casing strings, torque is very seldom applied, and when it must be applied, it is limited to the connection makeup torque M_c . The torsional shear stress τ acting in the circumferential direction at a radius at some point in the pipe-body wall thickness is

$$\tau = \frac{M_t r}{J_p}$$

$$J_p = \frac{\pi t^4}{2} \left(\frac{d_n}{t} - 1 \right) \left[\left(\frac{d_n}{t} - 1 \right)^2 + 1 \right]. \quad \dots\dots\dots (7.32)$$

With internal and external pressures, axial force, bending, and torsion, the von Mises equivalent stress equation (Eq. 7.6) becomes

$$2\sigma_{vm}^2 = (\sigma_r - \sigma_t)^2 + (\sigma_t - [\sigma_a \pm \sigma_b])^2 + ([\sigma_a \pm \sigma_b] - \sigma_r)^2 + 6\tau^2. \quad \dots\dots\dots (7.33)$$

7.7 Corrosion

All casing used in wells is susceptible to corrosion. Corrosion can cause failure of a tubular during its design service life, so some sort of protection from corrosion is normally needed. A common application where special corrosion protection may be needed is for production casing below the production packer. This casing will be exposed to corrosive formation fluids. Typically, drilling muds are alkaline, and special corrosion protection for casing exposed only to drilling mud is not needed. The method chosen for corrosion protection is dependent on many factors, including temperature, carbon dioxide, hydrogen sulfide, and other corrosive products such as chlorides, elemental sulfur, and acids. One of the most corrosive gases found in wells is H_2S . A well whose production contains H_2S is called “sour,” and wells without H_2S are called “sweet.”

Carbon dioxide is present in many sweet produced gases. Alone, it is a noncorrosive gas; however, a mixture of water and carbon dioxide is very corrosive. Water and carbon dioxide react to produce carbonic acid, which then reacts with low-alloy steels to form iron carbonate. The resulting dissolution of the steel reduces the wall thickness. This corrosion process is sensitive to temperature and pressure. In addition, high well flow rates typically increase erosion velocity and accelerate the corrosion process because protective films on the steel surface are more rapidly removed. Pitting and steel weight loss are typical results of this type of corrosion.

Normally, when steels corrode, they generate hydrogen atoms, which pair up to become hydrogen gas molecules and bubble off the surface. However, when steel corrodes in an H_2S -containing environment, the sulfide ions retard the formation of hydrogen gas molecules, enabling the hydrogen atoms to diffuse into the steel. The hydrogen atoms in the steel can cause the steel to lose much of its toughness, a phenomenon known as hydrogen embrittlement. Sulfide stress cracking (SSC) is a form of hydrogen embrittlement in which H_2S is the hydrogen source and the material is under tensile stress. Higher-strength low-alloy types of OCTG are generally more susceptible to SSC than are lower-strength grades. For this reason, grades such as C-90 and T-95 have been developed with special metallurgy to resist SSC.

Failures from hydrogen embrittlement often do not occur immediately after exposure to hydrogen sulfide. A time period during which no damage is evident is followed by sudden failure. During this time, hydrogen is being diffused into points of high stress.

Generally, higher-strength low-alloy steels are more susceptible to hydrogen embrittlement than are lower-strength steels. Temperature and applied stress level also play important roles in hydrogen embrittlement. Typically, low temperatures and higher-stress states accelerate hydrogen embrittlement.

For mildly corrosive environments, adequate corrosion protection of carbon and low-alloy steels may be achieved through use of internal plastic coatings or chemical inhibitors. However, these corrosion-prevention methods may have temperature or application restrictions that prevent their use.

Many companies have restrictions on the use of carbon or low-alloy steels in sweet service at moderate to low temperatures. Special restrictions are sometimes specified to mitigate concerns for brittle fracture. These restrictions may include specifications on toughness or API and ISO requirements on steel chemistry. For a specific steel grade, the API and ISO may have several alloying-agent specifications, which are referred to as different types of the same grade. For example, Q-125 casing can be manufactured in any one of four separate types which differ by chemical weight-percentage requirements.

For sour service, tubular-material selection is based on minimum temperature, yield strength, manufacturing process, and application. For example, low-alloy higher-strength ERW grades may not be suitable for sour service. When OCTG are purchased for H_2S applications, test methods as specified by *NACE TM0177-2005* (2005) are often required to verify resistance to SSC.

The industry uses the *NACE MR0175* (1999) specifications to differentiate between sour and sweet service on the basis of total system pressure and partial pressure of H_2S (NACE 1999). Gas systems are sour (**Fig. 7.7**) when the maximum pressure exceeds 65 psi and the partial pressure of H_2S is greater than 0.05 psi. Multiphase systems are considered sour (**Fig. 7.7**) if the maximum gas/liquid ratio is less than 5,000 scf/bbl under any of the following conditions:

- Maximum pressure exceeds 265 psi, and H_2S partial pressure in the gas phase is greater than 0.05 psi.
- Maximum pressure is less than 265 psi, and H_2S partial pressure in the gas phase is greater than 10 psi.
- The gas phase contains more than 15% H_2S .

The following equation can be used to calculate H_2S partial pressure:

$$H_2S \text{ partial pressure} = (\text{pressure} \times \text{volume fraction of } H_2S\text{-ppm})/1,000,000 \quad (7.34)$$

ISO considers pH in addition to H_2S partial pressure to specify sour conditions. This acknowledges that the pH of the environment plays a role in the severity of H_2S attack.

In the 1970s, CRAs began to be used in corrosive well environments. Generally, the corrosion resistance of CRAs is directly proportional to their alloy content. The most commonly used elements that improve the corrosion resistance of CRAs are nickel, chromium, and molybdenum. These are very expensive elements and add greatly to the cost of the tubular.

Two basic types of CRAs are used for casings: stainless steels and high-nickel alloys. Stainless steels use chromium to improve corrosion resistance. When chromium content is increased beyond approximately 12%, a stable

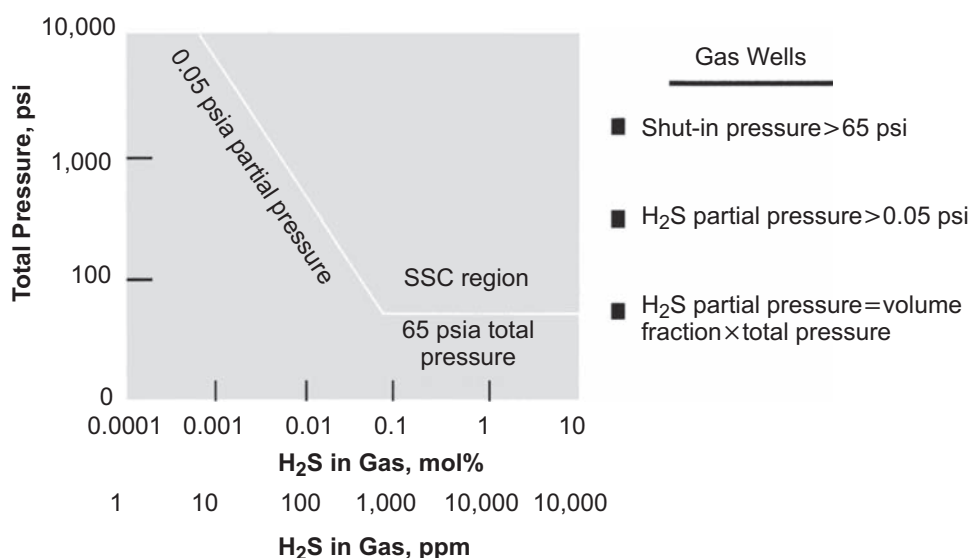


Fig. 7.7—SSC.

chromium-oxide film forms, which helps protect the base metal. Stainless steels contain iron as the primary element, typically 70–88%. Nickel-based alloys contain less than 50% iron and more than 50% nickel, chromium, and molybdenum. Nickel provides strength, toughness, and resistance to stress-corrosion cracking.

Stainless steels are the most commonly used CRAs and are acceptable in many environments. However, stainless steels are susceptible to pitting corrosion and stress-corrosion cracking at elevated temperatures and therefore have maximum chloride and H_2S restrictions and minimum pH restrictions. Inhibitors used to protect the tubular during acidizing are not particularly effective in protecting against corrosion. Visually, CRAs with 12% or more chromium will look like stainless steel and not like carbon or low-alloy steels. These higher-chromium stainless steels are typically manufactured using a different heat-treatment process from that used for carbon or low-alloy steels.

Nickel-based steels can be used in environments with higher H_2S , CO_2 , temperature, and chlorides and with lower pH than can stainless steels. They are even more resistant to corrosion by acidizing fluids than are stainless steels. However, specific acid treatments or other well treatments should be evaluated to determine their tendency to corrode nickel-based alloys. Produced gas with elemental sulfur may cause embrittlement of all CRAs.

There are currently no universally accepted industry manufacturing specifications or material-selection guidelines for most CRA tubulars. *API Spec. 5CT* (2005) includes specifications for both 9 Chrome and 13 Chrome L-80 steels, but additional specifications and usage restrictions should be considered before purchasing this product. Material selection should be based on many factors, including site-specific operating conditions and experience.

CRAs typically have a minimum specified yield strength of more than 80 ksi. Stainless steels are typically available in 80- to 95-ksi yield strength, while nickel-based alloys are available in 65- to 125-ksi yield strength. Often the high yield strength of CRAs is a result of cold working. Cold-worked steels can have anisotropic yield-strength behavior.

7.8 Casing Connections

Oilwell casing is delivered to the rig in approximately 40-ft lengths and must be joined with threaded connectors as each length is run in the well. Casing connections consist of a pin and a box. Connections can be either threaded and coupled or integral-joint (Fig. 7.8). Threaded and coupled connections have pins on both ends of the pipe that screw into a common coupling. For most threaded and coupled casings, the threads are cut into the unaltered diameter of the tubes. Integral-joint casing connections often have the ends of the casing tube thickened (swaged)

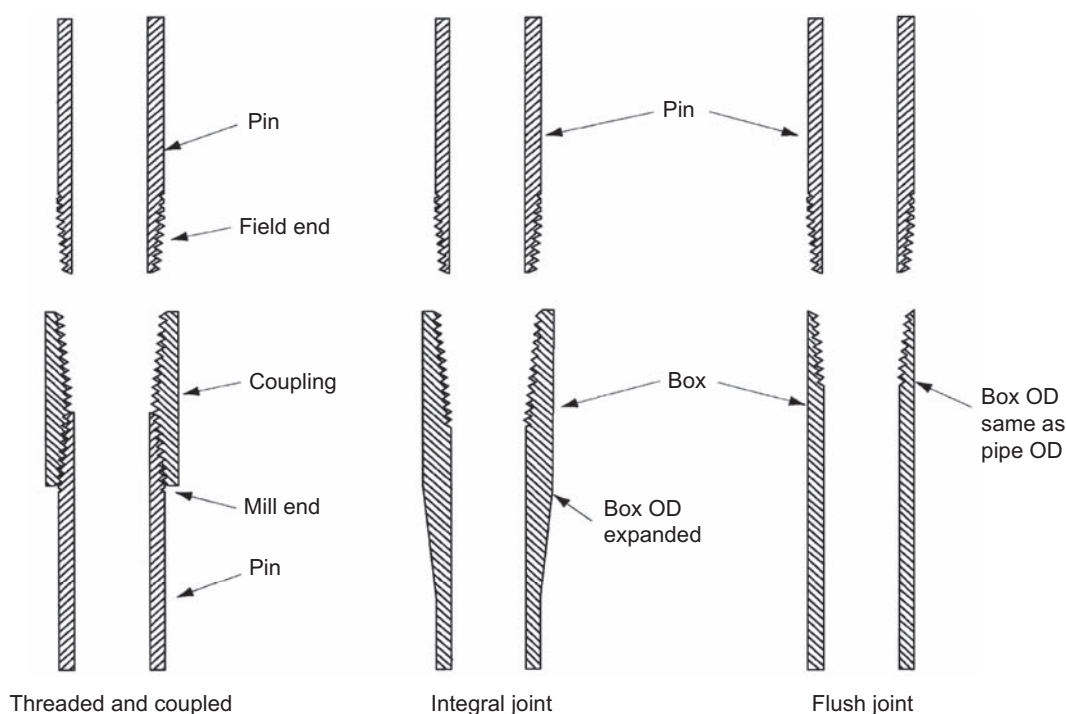


Fig. 7.8—Joints.

on either the tube OD or ID (or both). This provides more metal into which threads can be cut. However, the swaged ends must be heat-treated after swaging to recover the original tube properties before threading.

API and ISO provide several standards for casing connections that are widely used all over the world. They provide specifications for the following four types of casing connectors:

1. STCs
2. Long round threads and couplings (LCs)
3. Buttress threads and couplings (BCs)
4. Extreme line threads and couplings (XCs)

Schematics of each of the API and ISO connections are shown in **Fig. 7.9**.

The most common API and ISO casing connections are the STC, the LC, and the BC. These connections are rugged and reliable when properly made up and have been used by the industry for many years. They are usually cheaper than most alternative connections.

These three connections all use a “tapered-seal” sealing mechanism, which means that the threads on both the coupling and the tube are cut with a taper so that as the connection is made up, the threads are pushed together in a wedging action. The bearing pressure resulting from the wedging action is the sealing mechanism for these connections and is necessary to form a leak-resistant seal. In addition to the thread bearing pressures, it is also necessary to use a thread compound and a suitable coating on the coupling ID to form a leak-resistant connection.

Couplings used on casing are usually manufactured using the forging process or the seamless process and are of the same heat-treatment class and grade as the casing tube. Casing couplings are typically provided with a coating or plating on the threads to prevent galling during makeup and to assist in providing a pressure seal. Generally, coupling threads are surfaced with various forms of metal-phosphate coatings or plated with either tin or zinc using the electroplating process. Typical phosphate platings are very thin, zinc plating is thicker, and tin plating is very thick and soft to provide more sealing capability. Some proprietary connections on CRA materials can also be copper-plated, and some proprietary connections are surface-treated by blasting the pin ends.

7.8.1 Round Threads. STC and LC connectors have the same basic thread design. The threads have a rounded shape and are spaced to give eight threads per inch. Because of this, they are sometimes referred to as 8-round or

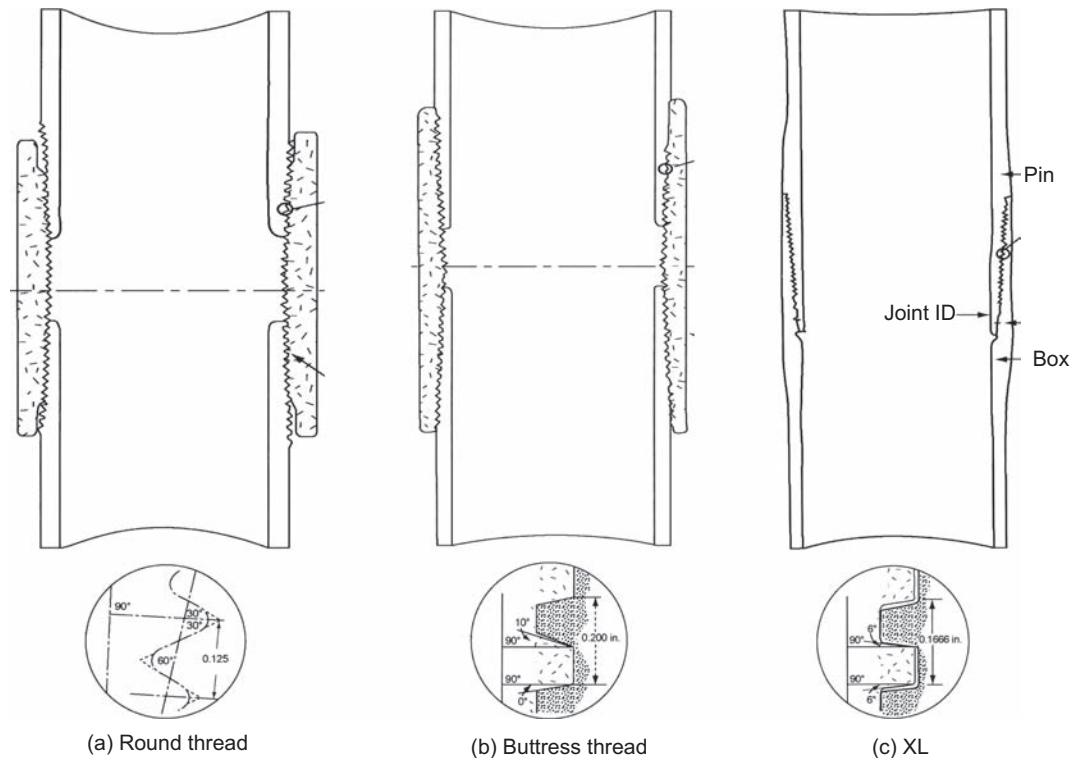


Fig. 7.9—API joints [from Bourgoyne et al. (1991)].

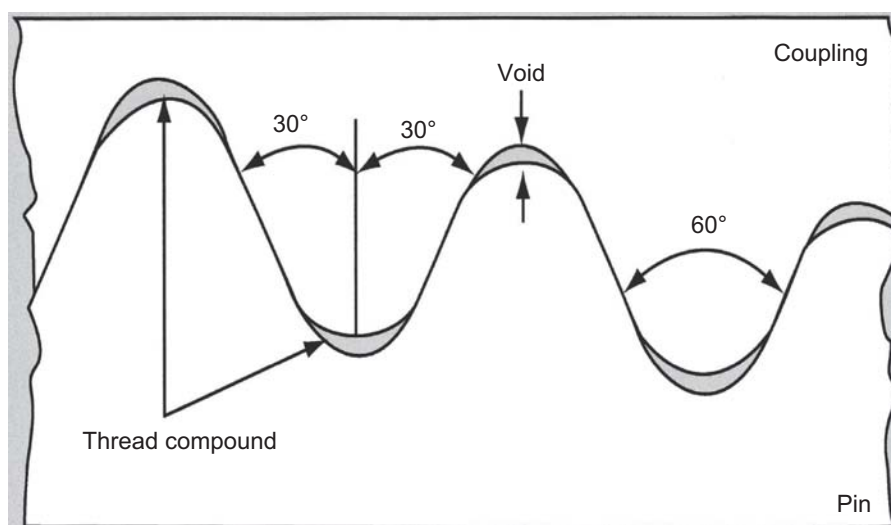


Fig. 7.10—API round threads [from *API Spec. 5B* (2008)]. Reprinted courtesy of the American Petroleum Institute.

round threads. The threads are cut with a taper of $\frac{3}{4}$ in./ft on diameter for all pipe sizes. A longer thread runout and coupling of the LC provide greater tensile strength when needed. These connections are very commonly used because of their proven reliability, ease of manufacture, and low cost.

LC connections have longer couplings and longer thread length than STC connections and are stronger. For casing sizes of $10\frac{3}{4}$ in. and larger, the long taper of an LC connection would result in a very thin wall, which would make the pin end more vulnerable to handling damage. For this reason, only STC connections are typically manufactured for these casing sizes. LC couplings can be used with STC pins, but LC pins cannot be used with STC couplings because the pin ends could meet in the middle, resulting in incomplete engagement of the threads.

As can be seen in **Fig. 7.10**, the round thread is cut with a 60-degree included angle and has rounded peaks and roots. When the coupling is formed, small voids exist at the roots and crests of each thread. A combination of thread compound and plating on the coupling must be used to fill these voids to obtain a seal. If the seal is ineffective, internal pressure acts to separate the threaded surfaces. The sealability of round-thread connections to liquids or gas is sensitive to dimensional variations that can occur depending on the threading order, the thread dope, the plating used on the coupling, the service temperature, high curvature (bending), or the makeup method. Sealability will likely be limited to 70 to 90% of the API internal yield pressure of the coupling or the pipe body.

Threaded connections are often rated according to their *joint efficiency*, which is the tensile strength of the joint divided by the tensile strength of the pipe body. Although the joint efficiency of an LC connection is greater than that of an STC connection, neither is 100% efficient. Because of the taper of the threads and their 60-degree included angle, the threaded end of the casing sometimes begins to yield and then collapses (**Fig. 7.11**). This can produce an unzipping effect in which, upon failure, the pin appears to jump out of the coupling. In addition to this jumpout, fracture of the pin or the coupling can also occur.

In addition to “standard” OD couplings, API and ISO provide dimensional specifications for reduced-OD or “special-clearance” couplings. These couplings have a fixed OD for each pipe size regardless of weight or grade. In general, special-clearance couplings are not used with STC and LC connections. Higher-grade couplings are sometimes used with lower-grade pipe to eliminate the need for an oversized coupling. There are no API or ISO dimensional specifications for oversized couplings as there are for special-clearance couplings.

7.8.2 Buttress Threads. API and ISO both specify a BC that has a more rectangular thread form than the other types. This thread form provides higher tensile strength in the connection, but sealability is more dependent on pipe dope and the coupling plating material. The more rectangular thread form resists pullout loads and enables the connection to approach or even exceed the axial strength of the tube. Typically, buttress connections are slightly more expensive than LC and STC connections.

Fig. 7.9b shows a BC casing thread. The basic thread design is similar to that of the API and ISO round thread in that it is tapered. However, longer coupling and thread runout are used, and the thread shape is squarer, so that the unzipping tendency is greatly reduced. Five threads are cut per inch, and the thread taper is $\frac{3}{4}$ in./ft for casing sizes up to $7\frac{7}{8}$ in. and 1 in./ft for 16-in. or larger casings. As with API round threads, the placement of thread

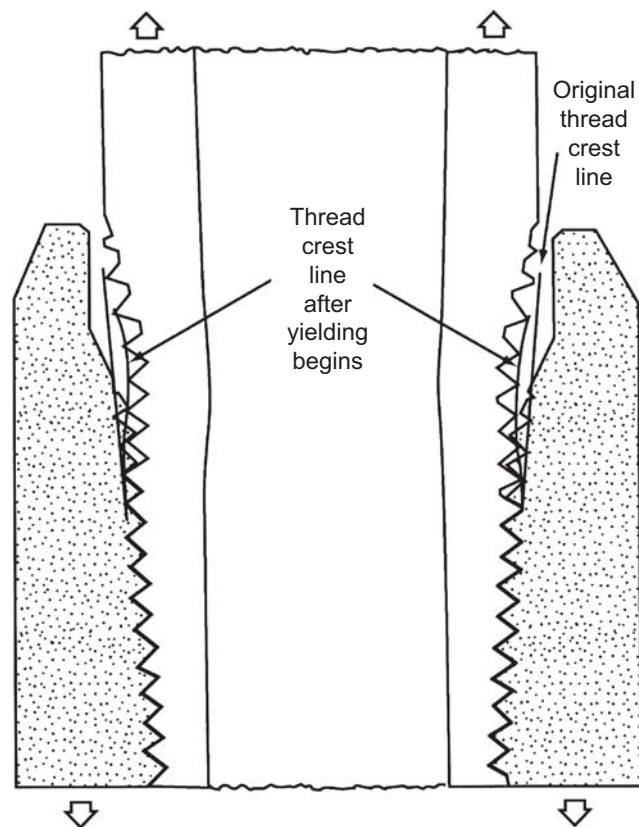


Fig. 7.11—Pull-out [from Bourgoyne et al. (1991)].

compound at the roots of the buttress teeth provides the sealing mechanism. Similarly to API round-thread connections, the sealability of buttress casing connections in liquid or gas service is sensitive to dimensional variations that can occur in the threading order, the thread dope, the plating used on the coupling, the service temperature, the degree of curvature (bending), and the makeup method. The sealability of a buttress connection will likely be limited to 70 to 90 percent of the API internal yield pressure of the coupling or the internal yield pressure of the pipe body in liquid service and can be very low in gas service.

7.8.3 XC Threads. The API XC connector is shown in Fig. 7.9c. It differs from the other API and ISO connectors in that it is an *integral joint* (i.e., the box is machined into the pipe wall). On an integral-joint connection, the pipe wall must be thicker near the ends of the casing to provide enough metal to permit machining of a stronger connection. The OD of an XC connector is significantly less than that of the other API couplings, thus providing an alternative when the largest possible casing size is to be run in a restricted-clearance situation. Moreover, only half as many threaded connections exist as in other connectors; therefore, there are fewer potential sites for leakage. However, the minimum ID will be less for the XC connector than for other types.

The sealing mechanism used in the XC connector is a metal-to-metal seal between the pin and the box (Fig. 7.9c). Metal-to-metal seal connections usually have two precision-machined surfaces that are forced together to resist leakage. This connector does not depend solely on a thread compound for sealing, although a compound is still needed for lubrication. Because of the requirement for thicker pipe walls near the ends and the closer machining tolerances needed for the metal-to-metal seal, XC connectors are much more expensive than the other connectors.

This connection is seldom encountered in oil wells today. Some continue to use this connection in fishing strings where reduced-OD connections are required.

7.8.4 Non-API/ISO Connections. In addition to API/ISO connections, many proprietary connections are available that offer premium features not available on API connections. Among the special features offered are the following:

- Flush joints for maximum clearance
- Smooth bores through connectors for reduced turbulence

- Threads designed for fast makeup with low tendency to cross-thread
- Multiple metal-to-metal seals for improved pressure integrity
- Multiple shoulders for improved torque strength
- High compressive strength for special loading situations
- Resilient rings for secondary pressure seals and connector corrosion protection

Several examples of premium non-API and non-ISO connectors are shown in **Figs. 7.12 through 7.14**, which illustrate the special features listed above.

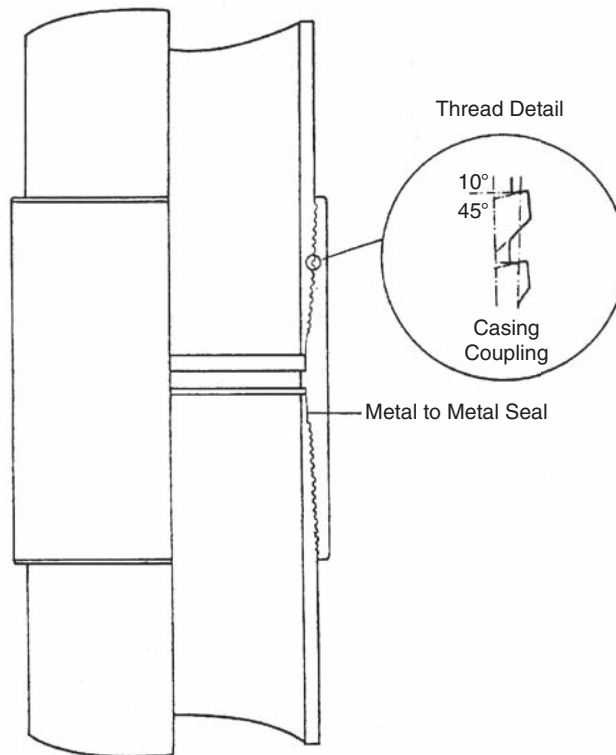


Fig. 7.12—Connector Example 1 [from Bourgoyne et al. (1991)].

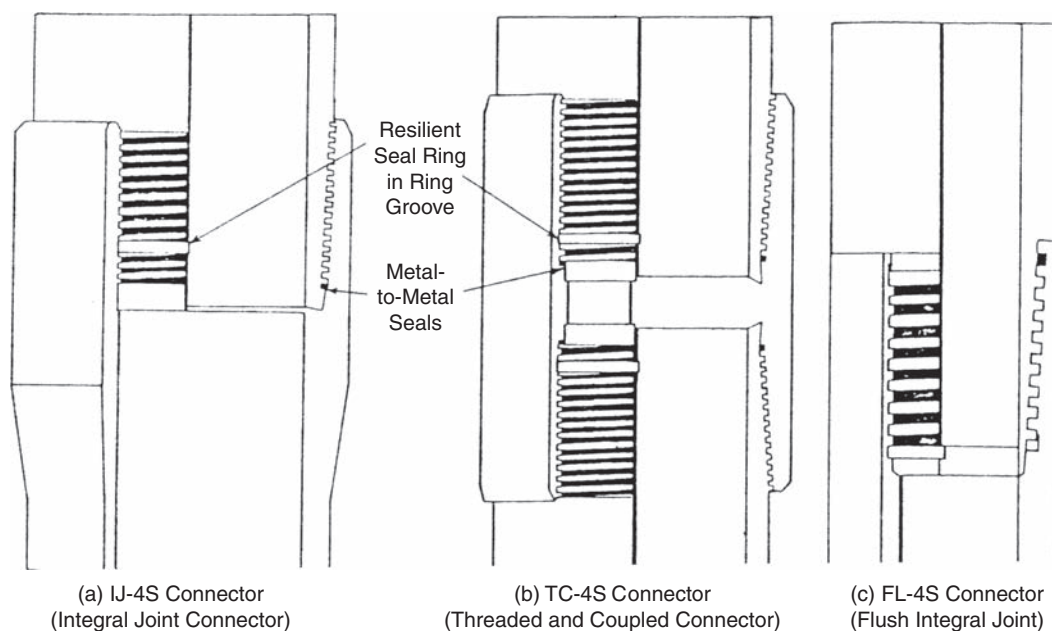


Fig. 7.13— Connector Example 2 [from Bourgoyne et al. (1991)].

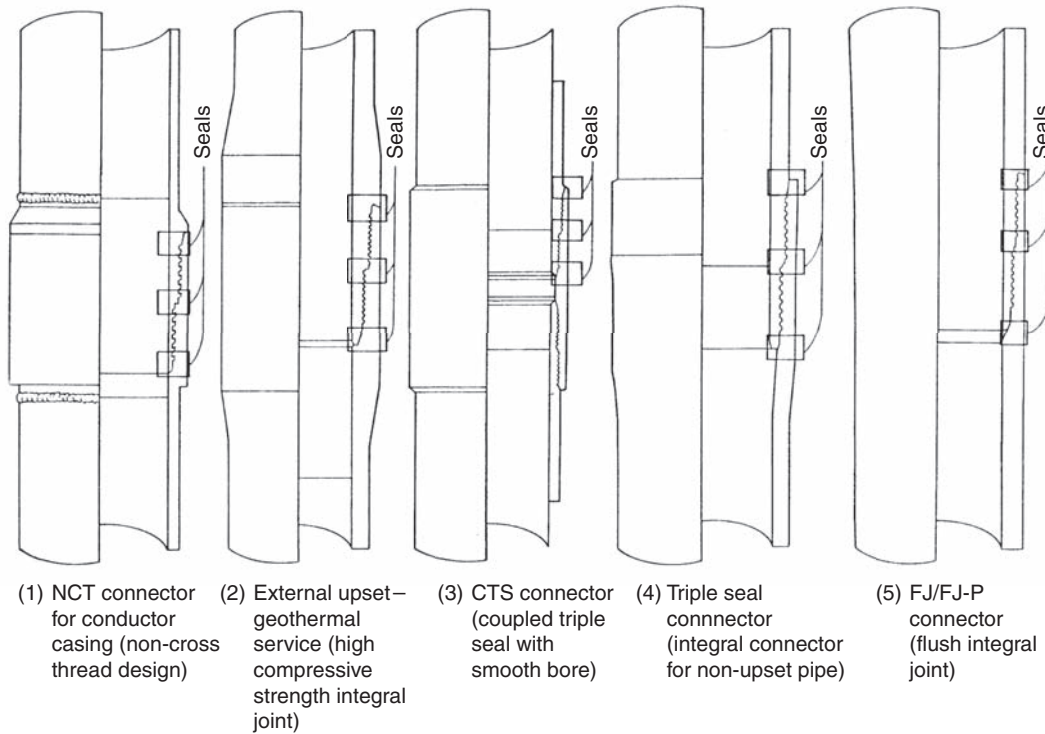


Fig. 7.14— Connector Example 3 [from Bourgoyne et al. (1991)].

Many non-API connections use metal-to-metal sealing mechanisms. Both tapered-seal and metal-to-metal sealing mechanism connections may also use seal rings. An elastomer-type seal ring is placed into grooves machined into the connection to assist sealing. Some connections feature multiple seals for redundancy. Multiple metal-to-metal seals or a combination of a metal-to-metal seal with a seal ring are common. In addition, there are several specialized thread design (e.g., “wedge thread” and “hook thread”) profiles. Many proprietary casing connections have the ends of the casing tube thickened or upset to provide more metal into which threads can be cut.

7.8.5 Thread Compounds. Thread compounds serve three basic purposes: (1) to seal the thread clearances in the thread profile, (2) to lubricate the threads during makeup, and (3) to resist galling resulting from metal-to-metal contact. Most thread compounds consist of particles suspended in a carrier grease. The types and ratios of the particles generally determine the performance of a thread compound. Before 1996, API had two basic specifications for thread-compound formulations. The standard formulation was called the “modified thread compound,” and a silicone-based, high-temperature alternative compound was called “silicone thread compound.” In 1996, API and ISO issued recommended practices and testing and evaluation guidelines for casing thread compounds. These publications suggested performance-based criteria for thread-compound specifications and used the API modified formulation as the reference standard for comparison. The challenge of correlating compound performance derived from bench tests with that observed in full-scale applications has proved to be difficult, and as a result, API does not currently provide performance guidelines or formulations for thread compounds. In July 2003, *API RP 5A3/ISO 13678* were published with editorial corrections and updates.

Many other thread compounds are available, containing various components that aid performance. Some specialty thread compounds are marketed as environmentally acceptable because they rely on constituents other than lead to lubricate and seal. Other thread compounds contain Teflon, which reduces makeup torque and may help provide a seal.

Special thread compounds containing powdered metals are used to reduce frictional forces during connection makeup and to provide filler material to help plug any remaining small voids around the roots and crests of the threads. The choice of compound is of critical importance to prevent galling and to obtain a leak-proof, properly made-up connection. Care must be exercised to ensure that a thread compound appropriate for the connector is used.

Proprietary connection manufacturers frequently offer a recommended type of thread dope that should be used with their connections. At in-service temperatures higher than approximately 300°F, special high-temperature thread compounds may enhance connection performance.

Storage compounds are sometimes applied to casing connections to protect them against corrosion during storage or shipment. These storage compounds should not be used for connection makeup. Storage compounds should be properly removed and the proper thread compound applied for connection makeup.

7.8.6 Connection Makeup. Threaded and coupled casing is normally shipped to the rig with the couplings attached. Each casing joint has a coupling screwed onto one end. The mill end is the end with the coupling installed, so called because the coupling was made up in the pipe mill. The end with no coupling is called the field end because it will be made up in the field. Typically casing is ordered with specifications for mill-end makeup; the requirements may include thread dope, plating, and other preparatory steps. If special makeup is required, then these requirements should be specified in the purchase order. Occasionally, casing is ordered from the mill with the couplings so that makeup of both ends can be controlled and monitored.

API and ISO have issued recommended makeup specifications for connections in their *RP5C1* (1999) specification. These recommendations include how to determine minimum and maximum torque, makeup speed, and position of the coupling face in relationship to the thread vanishing point or the base of the triangle on BTC connections. Other methods of making up API connections have been developed by the industry; these also specify the torque range and coupling position after makeup (Day et al. 1990). Earlier methods that specify makeup torque and number of turns past a reference torque have long been used, but many consider this method to be no longer acceptable for API 8-Round threads (Weiner and Sewell 1967). Advances in thread-manufacturing processes, differences in thread compounds, and variations in coupling coating or plating coefficients have resulted in erratic results when this method is used.

For proprietary connections that use torque shoulders, makeup can be monitored by measuring torque and turns. This approach makes it possible to observe indications of galling and to determine when a connection has reached its recommended torque. The makeup of many proprietary connections with very tight tolerances is sensitive to the amount of thread compound used.

7.8.7 Performance Properties of Connections. Internal Pressure Resistance. The coupling on an API connection can be weaker in burst than one on a plain-end casing. This problem usually occurs with thicker-wall casings and higher grades of casing. The API and ISO equation to calculate the minimum internal yield pressure for round-thread or buttress couplings is based on calculating the coupling wall thickness at the root of the first engaged thread. The internal yield pressures for API round-thread profiles with standard OD couplings and buttress profiles for both standard and special-clearance couplings are tabulated in *API Bull. 5C2* (1999). The API equation for calculating the coupling internal yield pressure is

$$P_{br} = \sigma_{\text{yield}} \left(\frac{d_{c2} - d_{c1}}{d_{c2}} \right) \quad \dots \dots \dots (7.35)$$

The diameter at the root of the coupling thread, d_{c1} , is different for STCs and for BCTs and can be calculated using the following equations:

For an STC,

$$d_{c1} = E_1 - (L_1 + A_1)T_1 + H_1 - S_m, \quad \dots \dots \dots (7.36)$$

where

E_1 is the pitch diameter at the hand-tight plane (in.);

L_1 is the length from the hand-tight plane (in.);

A_1 is the hand-tight standoff (in.) (Note: A_1 in *API Spec. 5B* (2008) is in turns, turns/threads per inch = in.);

T_1 is the taper, 0.0625 in./in. for round threads;

H_1 is the thread height (in.) or 0.10825 in. for eight threads per inch;

S_m is the distance from the root of the coupling thread to the top of the pin thread at the hand-tight position (in.).

API Spec. 5B (2008) includes values for E_1 , L_1 , A_1 , H_1 , and S_m . **Tables 7.6a through 7.6e** summarize the API connection dimensions from *API Spec. 5B*.

TABLE 7.6a—CASING SHORT-THREAD DIMENSIONS [from <i>API Spec. 5B (2008)</i>] Reproduced courtesy of the American Petroleum Institute. All dimensions in inches, except as indicated. See Figure 3.													
(1)	(2)	(3)	(4)	(5)	(6)	(7)	(8)	(9)	(10)	(11)	(12)	(13)	(14)
Size Designation	Major Dia- meter D	Nominal Weight: Thread Coupling (lbm/ft)	Number of Threads per inch	Length: End of Hand- Tight Plane L ₁	Length: Effective Threads L ₂	Total Length: Pipe to End of Vanish Point L ₄	Pitch Diameter at Hand- Tight Plane E ₁	End of Pipe to Center of Coupling, Power- Tight Make- Up J	Length: Face of Coupling to Hand- Tight Plane M	Dia- meter of Coupling Q	Depth of Coupling Recess q	Hand- Tight Stand- off, Thread Turns A	Minimum Length, Full Crest Threads from End of Pipe L _c *
4½	4.500	9.50	8	0.921	1.715	2.000	4.40337	1.125	0.704	4 ¹⁹ / ₃₂	0.500	3	0.875
4½	4.500	Others	8	1.546	2.340	2.625	4.40337	0.500	0.704	4 ¹⁹ / ₃₂	0.500	3	1.500
5	5.000	11.50	8	1.421	2.215	2.500	4.90337	0.750	0.704	5 ³ / ₃₂	0.500	3	1.375
5	5.000	Others	8	1.671	2.465	2.750	4.90337	0.500	0.704	5 ³ / ₃₂	0.500	3	1.625
5½	5.500	All	8	1.796	2.590	2.875	5.40337	0.500	0.704	5 ¹⁹ / ₃₂	0.500	3	1.750
6½	6.625	All	8	2.046	2.840	3.125	6.52837	0.500	0.704	6 ²³ / ₃₂	0.500	3	2.000
7	7.000	17.00	8	1.296	2.090	2.375	6.90337	1.250	0.704	7 ³ / ₃₂	0.500	3	1.250
7	7.000	Others	8	2.046	2.840	3.125	6.90337	0.500	0.704	7 ³ / ₃₂	0.500	3	2.000
7½	7.625	All	8	2.104	2.965	3.250	7.52418	0.500	0.709	7 ²⁵ / ₃₂	0.433	3½	2.125
8½	8.625	24.00	8	1.854	2.715	3.000	8.52418	0.875	0.709	8 ²⁵ / ₃₂	0.433	3½	1.875
8½	8.625	Others	8	2.229	3.090	3.375	8.52418	0.500	0.709	8 ²⁵ / ₃₂	0.433	3½	2.250
9½	9.625	All	8	2.229	3.090	3.375	9.52418	0.500	0.709	9 ²⁵ / ₃₂	0.433	3½	2.250 ^a
9½	9.625	All	8	2.162	3.090	3.375	9.51999	0.500	0.713	9 ²⁵ / ₃₂	0.433	4	2.250 ^b
10¾	10.750	32.75	8	1.604	2.465	2.750	10.64918	1.250	0.709	10 ²⁹ / ₃₂	0.433	3½	1.625 ^a
10¾	10.750	Others	8	2.354	3.215	3.500	10.64918	0.500	0.709	10 ²⁹ / ₃₂	0.433	3½	2.375 ^a
10¾	10.750	Others	8	2.287	3.215	3.500	10.64499	0.500	0.713	10 ²⁹ / ₃₂	0.433	4	2.375 ^b
11¾	11.750	All	8	2.354	3.215	3.500	11.64918	0.500	0.709	11 ²⁹ / ₃₂	0.433	3½	2.375 ^a
11¾	11.750	All	8	2.287	3.215	3.500	11.64499	0.500	0.713	11 ²⁹ / ₃₂	0.433	4	2.375 ^b
13¾	13.375	All	8	2.354	3.215	3.500	13.27418	0.500	0.709	13 ¹⁷ / ₃₂	0.433	3½	2.375 ^a
13¾	13.375	All	8	2.287	3.215	3.500	13.26999	0.500	0.713	13 ¹⁷ / ₃₂	0.433	4	2.375 ^b
16	16.000	All	8	2.854	3.715	4.000	15.89918	0.500	0.709	16 ⁷ / ₃₂	0.366	3½	2.875
18½	18.625	87.50	8	2.854	3.715	4.000	18.52418	0.500	0.709	18 ²⁷ / ₃₂	0.366	3½	2.875
20	20.000	All	8	2.854	3.715	4.000	19.89918	0.500	0.709	20 ⁷ / ₃₂	0.366	3½	2.875 ^c
20	20.000	All	8	2.787	3.715	4.000	19.89499	0.500	0.713	20 ⁷ / ₃₂	0.366	4	2.875 ^d
Include taper on diameter, all sizes, 0.0625 in. per in.													
Note: Hand-tight standoff "A" is the basic allowance for basic power make-up of the joint as shown in Figure 3.													
*L _c = L ₄ - 1.125 in. for 8 round thread casing.													
^a Applicable to coupling grades lower than P110.													
^b Applicable to coupling grades P110 and higher.													
^c Applicable to coupling grades lower than J55 and K55.													
^d Applicable to coupling grades J55 and K55 and higher.													

For buttress casing, the equation is:

$$d_{cl} = E_7(L_7 + I_1)T_1 + 0.062 \quad (7.37)$$

where

E_7 is the pitch diameter (in.);

L_7 is the length of perfect threads (in.);

I_1 is the basic hand-tight position from the triangle stamp (in.);

T_1 is the taper, or 0.0625 in./in. for 13¾-in. and smaller casing and 0.0833 in./in. for 16-in. and larger casing.

For many years, *API TR 5C3* (2008) included an equation to calculate the leak resistance of an API- or ISO-coupled connection. This equation is seldom used now. The equation limited the burst strength or leak resistance of an API or ISO connection on the basis of the interface pressure between the pin and the box. This interface pressure was a result of the makeup and the internal pressure itself.

Connection Joint Strength. Joint strength resists the axial load that causes a coupling or connection to fail. The API and ISO casing-connection joint-strength formulas are based partially on theoretical considerations and partially on empirical observations (*API TR 5C3* 2008). The lesser of the values obtained from the two equations governs for round-thread casing connections. These equations are based on an API test program in the early 1960s

TABLE 7.6b—CASING LONG-THREAD DIMENSIONS [from API Spec. 5B (2008)] Reproduced courtesy of the American Petroleum Institute. All dimensions in inches, except as indicated. See Figure 3.

(1)	(2)	(3)	(4)	(5)	(6)	(7)	(8)	(9)	(10)	(11)	(12)	(13)
Size Designation D	Major Diameter D ₄	Number of Threads per inch	Length: End of Pipe to Hand-Tight Plane L ₁	Length: Effective Threads L ₂	Total Length: Pipe to End of Vanish Point L ₄	Pitch Diameter at Hand-Tight Plane E ₁	End of Pipe to Center of Coupling, Power-Make-Up J	Length: Face of Coupling to Hand-Tight Plane M	Diameter of Coupling Recess Q	Depth of Coupling Recess q	Hand-Tight Stand-off Turns A	Minimum Length, Full Crest Threads from End of Pipe L _c [*]
4½	4.500	8	1.921	2.715	3.000	4.40337	0.500	0.704	4 ¹⁹ / ₃₂	0.500	3	1.875
5	5.000	8	2.296	3.090	3.375	4.90337	0.500	0.704	5 ³ / ₃₂	0.500	3	2.250
5½	5.500	8	2.421	3.215	3.500	5.40337	0.500	0.704	5 ¹⁹ / ₃₂	0.500	3	2.375
6¾	6.625	8	2.796	3.590	3.875	6.52837	0.500	0.704	6 ²³ / ₃₂	0.500	3	2.750
7	7.000	8	2.921	3.715	4.000	6.90337	0.500	0.704	7 ³ / ₃₂	0.500	3	2.875
7¾	7.625	8	2.979	3.840	4.125	7.52418	0.500	0.709	7 ²⁵ / ₃₂	0.433	3½	3.000
8¾	8.625	8	3.354	4.215	4.500	8.52418	0.500	0.709	8 ²⁵ / ₃₂	0.433	3½	3.375
9¾	9.625	8	3.604	4.465	4.750	9.52418	0.500	0.709	9 ²⁵ / ₃₂	0.433	3½	3.625 ^a
9¾	9.625	8	3.537	4.465	4.750	9.51999	0.500	0.713	9 ²⁵ / ₃₂	0.433	4	3.625 ^b
20	20.000	8	4.104	4.965	5.250	19.89918	0.500	0.709	20 ⁷ / ₃₂	0.366	3½	4.125 ^c
20	20.000	8	4.037	4.965	5.250	19.89499	0.500	0.713	20 ⁷ / ₃₂	0.366	4	4.125 ^d

Include taper on diameter, all sizes, 0.0625 in. per in.

Note: Hand-tight standoff "A" is the basic allowance for basic power make-up of the joint as shown in Figure 3.

^{*}L_c = L₄ - 1.125 in. for 8 round thread casing.

^aApplicable to coupling grades lower than P110.

^bApplicable to coupling grades P110 and higher.

^cApplicable to coupling grades lower than J55 and K55.

^dApplicable to coupling grades J55 and K55 and higher.

and predict joint failure rather than the onset of round-thread casing-connection yielding. Note that the equations are based on ultimate strength rather than yield strength. Because the equations are based on joint failure rather than the point at which the stress in the connection reaches yield strength, a design factor (DF) associated with failure rather than yielding should be considered. For API STC connections, the API and ISO formula for computing the minimum coupling fracture strength is

$$F_{\text{ten}} = 0.95A_{jp}\sigma_{\text{ult}}, \quad (7.38)$$

where the area under the last perfect thread for eight-round threads is given by

$$A_{jp} = \pi/4[(d_n - 0.1425)^2 - d^2]. \quad (7.39)$$

The minimum force for joint pullout or thread jumpout is given by

$$F_{\text{ten}} = 0.95A_{jp}L_{et}\left(\frac{0.74d_n^{-0.59}\sigma_{\text{ult}}}{0.5L_{et} + 0.14d_n} + \frac{\sigma_{\text{yield}}}{L_{et} + 0.14d_n}\right). \quad (7.40)$$

For BTC connections, API and ISO have specific equations for minimum coupling-pin and coupling-thread strength. The lesser of the values obtained from the two formulas governs. The tension force for BTC-connection thread failure is given by

$$F_{\text{ten}} = 0.95A_{sc}\sigma_{\text{ult}}\left[1.008 - 0.0396\left(1.083 - \frac{\sigma_{\text{yield}}}{\sigma_{\text{ult}}}\right)d_n\right]. \quad (7.41)$$

The tensile force for coupling-thread failure is given by

$$F_{\text{ten}} = 0.95A_{sc}\sigma_{\text{ult}}, \quad (7.42)$$

TABLE 7.6c—BUTRESS CASING THREAD DIMENSIONS [from *API Spec. 5B (2008)*] Reproduced courtesy of the American Petroleum Institute. All dimensions in inches, except as indicated. See Figure 5.

(1)	(2)	(3)	(4)	(5)	(6)	(7)	(8)	(9)	(10)	(11)	(12)	(13)	(14)
Size	Major Diameter	Number of Threads per inch	Length: Imperfect Threads	Length: Perfect Threads	Total Length: Pipe to Vanish Point	Pitch Diameter ^a	End of Pipe to Center of Coupling, Power-Tight Make-Up	End of Pipe to Center of Coupling, Hand-Tight Make-Up	Length: Face of Coupling to Plane E ₇	Length: End of Pipe to Stamp Angle	Hand-Tight Turns	Counter-bore in Coupling	Minimum Full Crest Threads from End of Pipe
D	D ₄		g	L ₇	L ₄	E ₇	J	J _n	E ₇	A ₁	A	Q	L _c [*]
4½	4.516	5	1.984	1.6535	3.6375	4.454	0.500	0.900	1.884	3 ¹⁵ / ₁₆	½	4.640	1.2535
5	5.016	5	1.984	1.7785	3.7625	4.954	0.500	1.000	1.784	4 ¹ / ₁₆	1	5.140	1.3785
5½	5.516	5	1.984	1.8410	3.8250	5.454	0.500	1.000	1.784	4 ¹ / ₈	1	5.640	1.4410
6½	6.641	5	1.984	2.0285	4.0125	6.579	0.500	1.000	1.784	4 ⁵ / ₁₆	1	6.765	1.6285
7	7.016	5	1.984	2.2160	4.2000	6.954	0.500	1.000	1.784	4½	1	7.140	1.8160
7½	7.641	5	1.984	2.4035	4.3875	7.579	0.500	1.000	1.784	4 ¹¹ / ₁₆	1	7.765	2.0035
8½	8.641	5	1.984	2.5285	4.5125	8.579	0.500	1.000	1.784	4 ¹³ / ₁₆	1	8.765	2.1285
9½	9.641	5	1.984	2.5285	4.5125	9.579	0.500	1.000	1.784	4 ¹³ / ₁₆	1	9.765	2.1285
10½	10.766	5	1.984	2.5285	4.5125	10.704	0.500	1.000	1.784	4 ¹³ / ₁₆	1	10.890	2.1285
11½	11.766	5	1.984	2.5285	4.5125	11.704	0.500	1.000	1.784	4 ¹³ / ₁₆	1	11.890	2.1285
13½	13.391	5	1.984	2.5285	4.5125	13.329	0.500	1.000	1.784	4 ¹³ / ₁₆	1	13.515	2.1285
16	16.000	5	1.488	3.1245	4.6125	15.938	0.500	0.875	1.313	4 ¹³ / ₁₆	7/8	16.154	2.7245
18½	18.625	5	1.488	3.1245	4.6125	18.563	0.500	0.875	1.313	4 ¹³ / ₁₆	7/8	18.779	2.7245
20	20.000	5	1.488	3.1245	4.6125	19.938	0.500	0.875	1.313	4 ¹³ / ₁₆	7/8	20.154	2.7245
Include taper on diameter:							Sizes 13% and smaller—0.0625 in. per in. Sizes 16 and larger—0.0833 in. per in.						

Notes:

- At plane of perfect thread length L₇, the basic major diameter of the pipe thread and plug gage thread is 0.016 in. greater than specified pipe diameter D for sizes 13% and smaller and is equal to the specified pipe diameter for sizes 16 and larger.
- Hand-tight standoff "A" is the basic allowance for basic power make-up of the joint as shown in Figure 5. The ½ in. equilateral triangle stamp located on the pipe at the length A1 from the end of the pipe facilitates obtaining the power make-up provided for by the hand-tight standoff "A"

^aPitch diameter on buttress casing thread is defined as being midway between the major and minor diameters.

*L_c = L₇ – 0.400 in. for buttress thread casing. Within the L_c length, as many as 2 threads showing the original outside surface of the pipe on their crests for a circumferential distance not exceeding 25% of the pipe circumference is permissible. The remaining threads in the L_c thread length shall be full crested threads.

TABLE 7.6d—NON-UPSET TUBING THREAD DIMENSIONS [from *API Spec. 5B* (2008)] Reproduced courtesy of the American Petroleum Institute. All dimensions in inches, except as indicated. See Figure 8.

[illegible]

TABLE 7.6e—EXTERNAL-UPSET TUBING THREAD DIMENSIONS [API Spec. 5B (2008)] Reproduced courtesy of the American Petroleum Institute. All dimensions in inches, except as indicated. See Figure 8.

(1)	(2)	(3)	(4)	(5)	(6)	(7)	(8)	(9)	(10)	(11)	(12)	(13)
Size Designation	Major Dia- meter D ₄	Number of Threads per inch	Length: End of Pipe to Hand-Tight Plane L ₁	Effective Threads L ₂	Total Length: End of Pipe to Vanish Point L ₄	Pitch Dia- meter at Hand-Tight Plane E ₁	End of Pipe to Center of Coupling Power-Tight Make-Up J	Length: Face of Coupling to Hand-Tight Plane M	Dia- meter of Coupling Q	Depth of Coupling q	Hand-Tight Stand-off Turns A	Minimum Length, Full Crest Threads from End of Pipe L _c *
1.050	1.315	10	0.479	0.956	1.125	1.25328	0.500	0.446	1.378	⁵ / ₁₆	2	0.300
1.315	1.469	10	0.604	1.081	1.250	1.40706	0.500	0.446	1.531	⁵ / ₁₆	2	0.350
1.660	1.812	10	0.729	1.206	1.375	1.75079	0.500	0.446	1.875	⁵ / ₁₆	2	0.475
1.900	2.094	10	0.792	1.269	1.438	2.03206	0.500	0.446	2.156	⁵ / ₁₆	2	0.538
2 ³ / ₈	2.594	8	1.154	1.703	1.938	2.50775	0.500	0.534	2.656	³ / ₈	2	0.938
2 ⁷ / ₈	3.094	8	1.341	1.890	2.125	3.00775	0.500	0.534	3.156	³ / ₈	2	1.125
3 ¹ / ₂	3.750	8	1.591	2.140	2.375	3.66395	0.500	0.534	3.813	³ / ₈	2	1.375
4	4.250	8	1.716	2.265	2.500	4.16395	0.500	0.534	4.313	³ / ₈	2	1.500
4 ¹ / ₂	4.750	8	1.841	2.390	2.625	4.66395	0.500	0.534	4.813	³ / ₈	2	1.625
Include taper on diameter, all sizes, 0.0625 in. per in.												
Note: Hand-tight standoff "A" is the basic allowance for basic power make-up of the joint as shown in Figure 8.												
*L _c = L ₄ - 0.900 in. for 10 thread tubing, but not less than 0.300.												
L _c = L ₄ - 1.000 for 8 thread tubing.												

where A_{sc} is given by

$$A_{sc} = \frac{\pi}{4} (d_{c2}^2 - d_{c1}^2) \quad (7.43)$$

API TR 5C3 (2008) and ISO/TR 10400:2007(E) (2007) present a method to calculate the joint strength for a round-thread casing with combined bending and internal pressure. The method is based on physical tests performed in the 1960s.

Connection Collapse. The collapse resistance of API casing couplings is greater than that of the pipe body.

Connection Performance Plot. There is a wide range of designs and performance levels among API connections from various manufacturers, especially for premium connections. Some proprietary connections have strong interactions between sealability and applied tension or axial compression loads. Many vendors provide a von Mises performance envelope for their connections, which in many cases is based on finite-element analysis or physical testing (Fig. 7.15). There are no standards in the industry for these plots, and the envelopes may be based on the onset of yield, a sealability limit, or other criteria. The sealability of a connection will also depend on whether a gastight or a liquid-tight seal is required. Because gas leaks through a connection much more easily than liquid, the sealability of a connection in liquid service is typically much greater than its sealability in gas service. In some cases, vendors will have a different performance envelope for each combination of connection trade name, size, weight, and casing grade.

7.9 Casing-Program Selection and Design

The process of selecting casing-setting depths, hole sizes, number of casing strings, and related parameters is referred to as the casing-program selection process. The casing design process consists of selecting the weight, grade, and connections for the casings that will be used in a string.

The process of casing-program selection begins with specification of the surface and bottomhole well locations and the size of the production casing that will be used if hydrocarbons are found in commercial quantities. The number and sizes of tubing strings and the type of subsurface artificial-lift equipment that may eventually be placed in the well determine the minimum ID of the production casing. These specifications are usually determined for the drilling engineer by other members of the engineering staff. In some cases, the possibility of exploratory drilling below an anticipated productive interval must also be considered. The drilling engineer then must design a program of bit sizes, casing sizes, grades, and setting depths that will enable the well to be drilled and completed safely in the desired producing configuration.

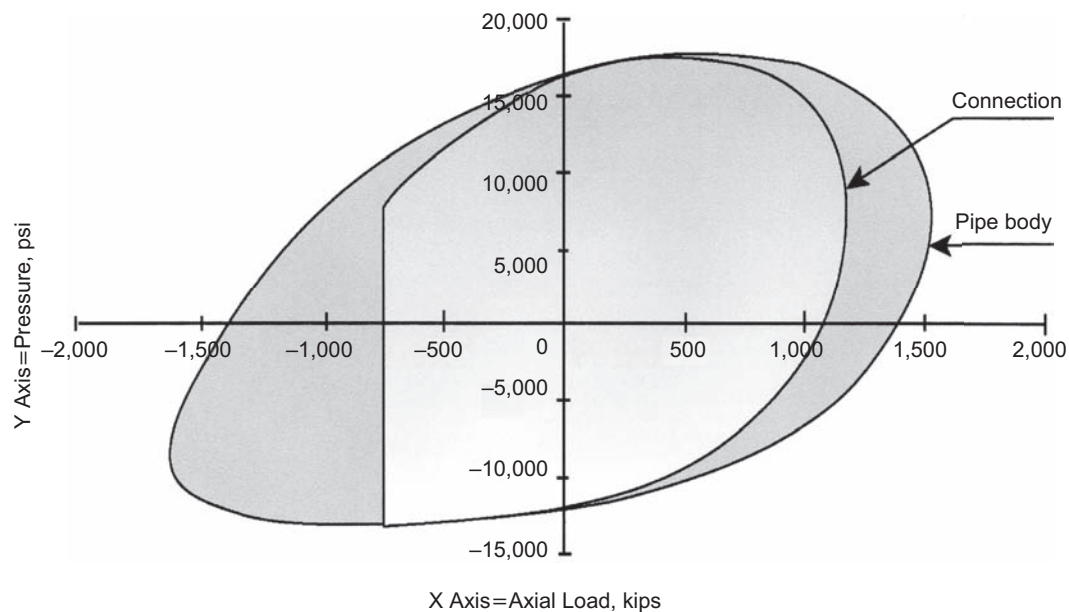


Fig. 7.15—Example of 7-in. 39 lb/ft Q125 connection/pipe body performance envelope (von Mises equivalent).

To obtain the most economical design, casing strings often consist of multiple sections of different steel grades, wall thicknesses, and coupling types. Such a casing string is called a *combination string*. Additional cost savings can sometimes be achieved using liner-tieback combination strings instead of a *full string* run from the surface to the bottom of the hole. When this is done, the reduced tension loads experienced in running the casing in stages often make it possible to use lighter weights or lower grades of casing. The potential savings from use of a liner-tieback combination rather than a full string must be weighed against the additional risks and costs of a successful, leak-free tieback operation. Rig and equipment limitations often make the use of a liner-tieback combination necessary because the tension loads are usually lower than when running a full string.

7.9.1 Selection of Casing-Setting Depths. The selection of the number of casing strings and their respective setting depths is generally based on consideration of the pore-pressure gradients and fracture gradients of the formations to be penetrated. The example shown in **Fig. 7.16** illustrates the relationship between casing setting depth and these gradients. The pore-pressure-gradient and fracture-gradient data are obtained by the methods presented in Chapter 2, expressed as equivalent densities, and plotted against depth. A line representing the planned mud-density program is also plotted. The mud densities are chosen to provide an acceptable *trip margin* above the anticipated formation pore pressures to allow for reductions in effective mud weight caused by upward pipe movement during tripping operations. A commonly used trip margin is 0.5 lbm/gal or one that will provide 200 to 500 psi of excess bottomhole pressure (BHP) over the formation pore pressure.

To reach the depth objective, the effective drilling-fluid density shown at point *a* is chosen to prevent the flow of formation fluid into the well (i.e., to prevent a kick). However, to carry this drilling-fluid density without exceeding the fracture gradient of the weakest formation exposed within the borehole, the protective intermediate casing must extend at least to the depth of Point *b*, where the fracture gradient is equal to the mud density needed to drill to Point *a*. Similarly, to drill to Point *b* and to set intermediate casing, the drilling-fluid density shown at Point *c* will be needed and will require surface casing to be set at least to the depth at Point *d*. When possible, a kick margin is subtracted from the true fracture-gradient line to obtain a design fracture-gradient line. If no kick margin is provided, it is impossible to absorb a kick at the casing-setting depth without causing a hydrofracture and a possible underground blowout.

Other factors, such as the need to protect freshwater aquifers, the presence of vugular lost-circulation zones, the presence of depleted low-pressure zones that tend to cause stuck pipe, the presence of salt beds that tend to flow plastically and close the borehole, and government regulations, can also affect casing-depth requirements. Moreover, experience in an area may show that it is easier to achieve a good casing-seat cement job in some formation types than in others, or that fracture gradients are generally higher in some formation types than in others. Under

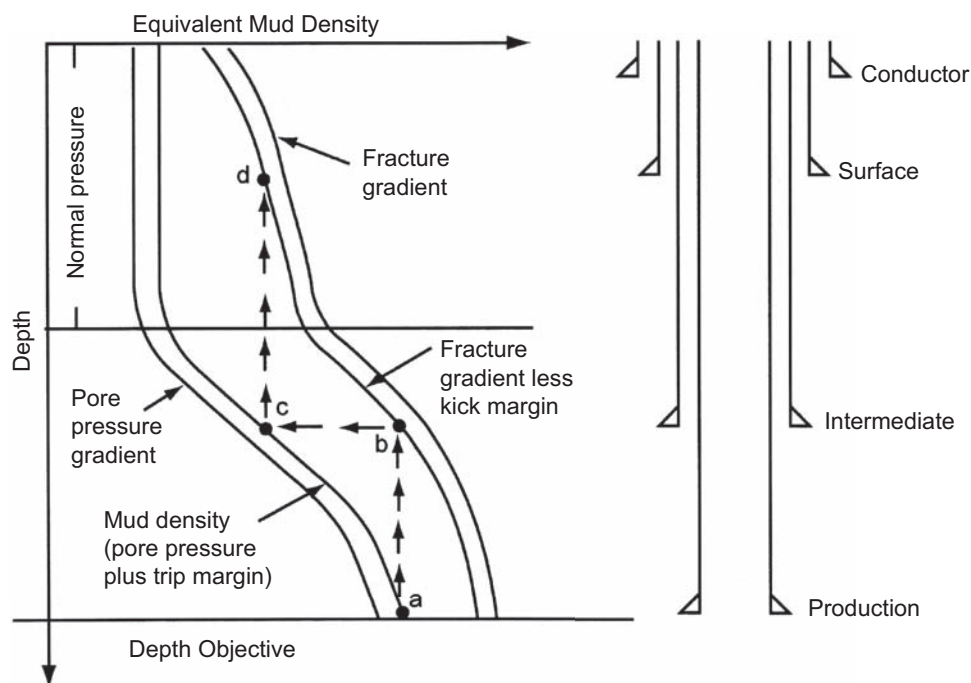


Fig. 7.16—Casing setting depths [from Bourgoyne et al. (1991)].

such conditions, a design must be found that simultaneously will meet these special requirements and the pore-pressure and fracture-gradient requirements outlined above.

The conductor-casing setting depth is based on the mud density required to prevent washout of the shallow borehole when drilling to the depth of the surface casing. The conductor casing must be able to sustain the pressures expected during diverter operations without washing around the outside of the conductor. The conductor casing is often driven into the ground, where soil resistance governs its length. The casing-driving operation is stopped when the number of blows per foot of depth exceeds some specified upper limit. Typically the conductor is not designed to support the weight of the surface casing or of subsequent strings.

Example 7.5 A well is being planned for a location in Jefferson Parish, Louisiana. The intended well completion requires the use of 7-in. production casing set at 15,000 ft. Determine the number of casing strings needed to reach this depth objective safely and select the casing-setting depth of each string. Pore pressure, fracture gradient, and lithology data from logs of nearby wells are given in Fig. 7.17. Allow a 0.5-lbm/gal trip margin and a 0.5-lbm/gal kick margin when making the casing-seat selections. The minimum length of surface casing required to protect the freshwater aquifers is 2,000 ft. Approximately 180 ft of conductor casing is generally required to prevent washout on the outside of the conductor. It is general practice in this area to cement the casing in shale rather than in sandstone.

Solution. The planned mud-density program is first plotted to maintain a 0.5-lbm/gal trip margin at every depth. The design fracture line is then plotted to provide a 0.5-lbm/gal kick margin at every depth. These two lines are shown in Fig. 7.16 by dashed lines. To drill to a depth of 15,000 ft, a 17.6-lbm/gal mud will be required (Point a). This, in turn, requires intermediate casing to be set at 11,400 ft (Point b) to prevent fracture of the formations above 11,400 ft. Similarly, to drill safely to a depth of 11,400 ft to set intermediate casing, a mud density of 13.7 lbm/gal is required (Point c). This, in turn, requires surface casing to be set at 4,000 ft (Point d). Because the formation at 4,000 ft is normally pressured, the usual conductor-casing depth of 180 ft is appropriate.

Only 2,000 ft of surface casing is needed to protect the freshwater aquifers. However, if this minimum casing length were used, intermediate casing would have to be set higher in the transition zone. An additional liner would also have to be set before reaching the total depth objective to maintain the 0.5-lbm/gal kick margin. Because

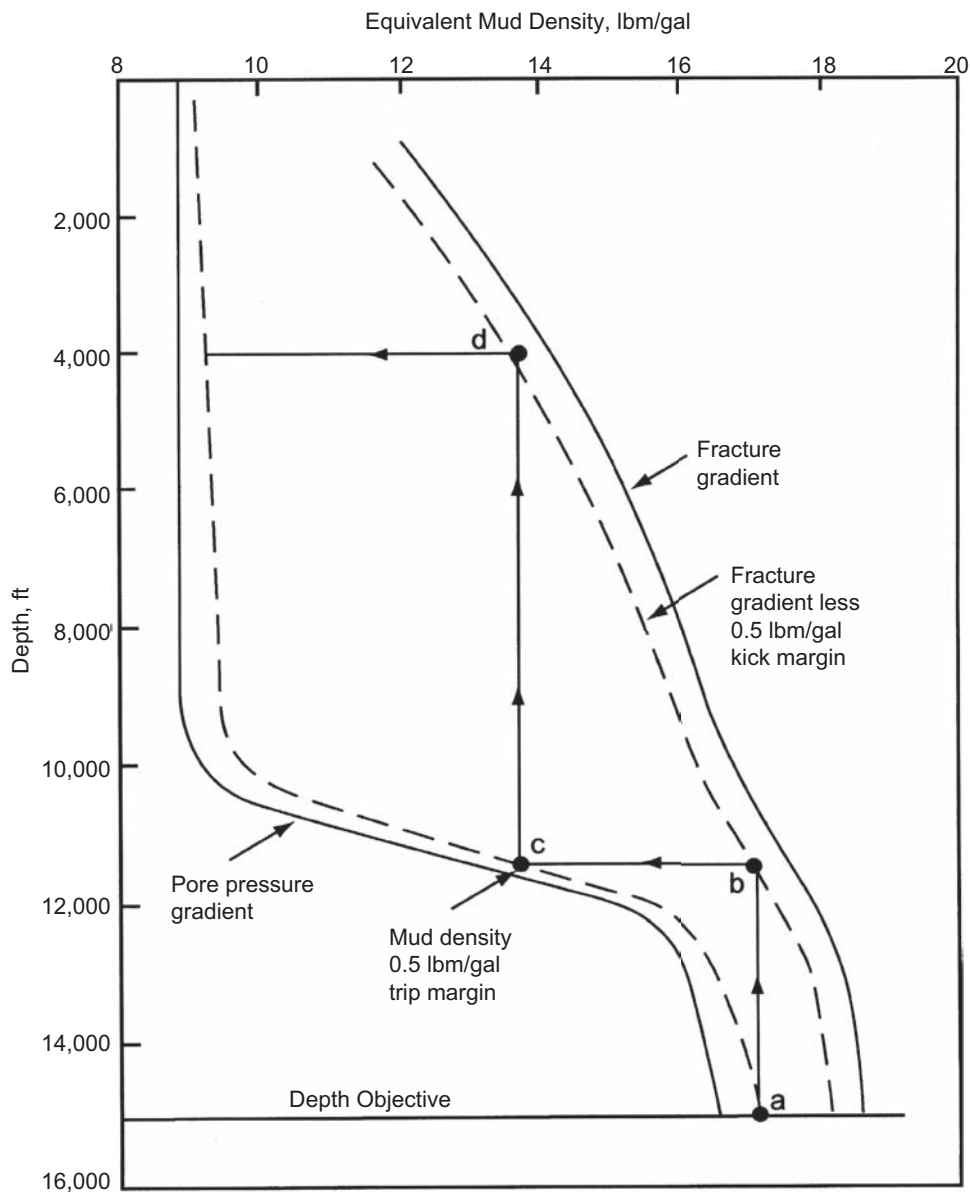


Fig. 7.17—Setting depth example [from Bourgoyne et al. (1991)].

shale is the predominant formation type, only minor variations in casing setting depth are required to maintain the casing seat.

7.9.2 Selection of Casing Sizes. The size of the casing strings is controlled by the necessary ID of the production string and the number of intermediate casing strings required to reach the depth objective. To enable the production casing to be placed in the well, the bit size used to drill the last interval of the well must be slightly larger than the OD of the casing connectors. The selected bit size should provide sufficient clearance beyond the OD of the coupling to allow for mudcake on the borehole wall and for casing appliances such as centralizers and scratchers. This, in turn, determines the minimum size of the second-deepest casing string. Using similar considerations, the bit size and casing size of successively more shallow well segments are selected.

Selection of casing sizes that permit the use of commonly used bits is advantageous because the bit manufacturers make readily available a much larger variety of bit types and features in these common sizes. However, additional bit sizes are available that can be used in special circumstances. Fig. 7.18 shows common hole and bit sizes used to drill wells (Greenip 1978).

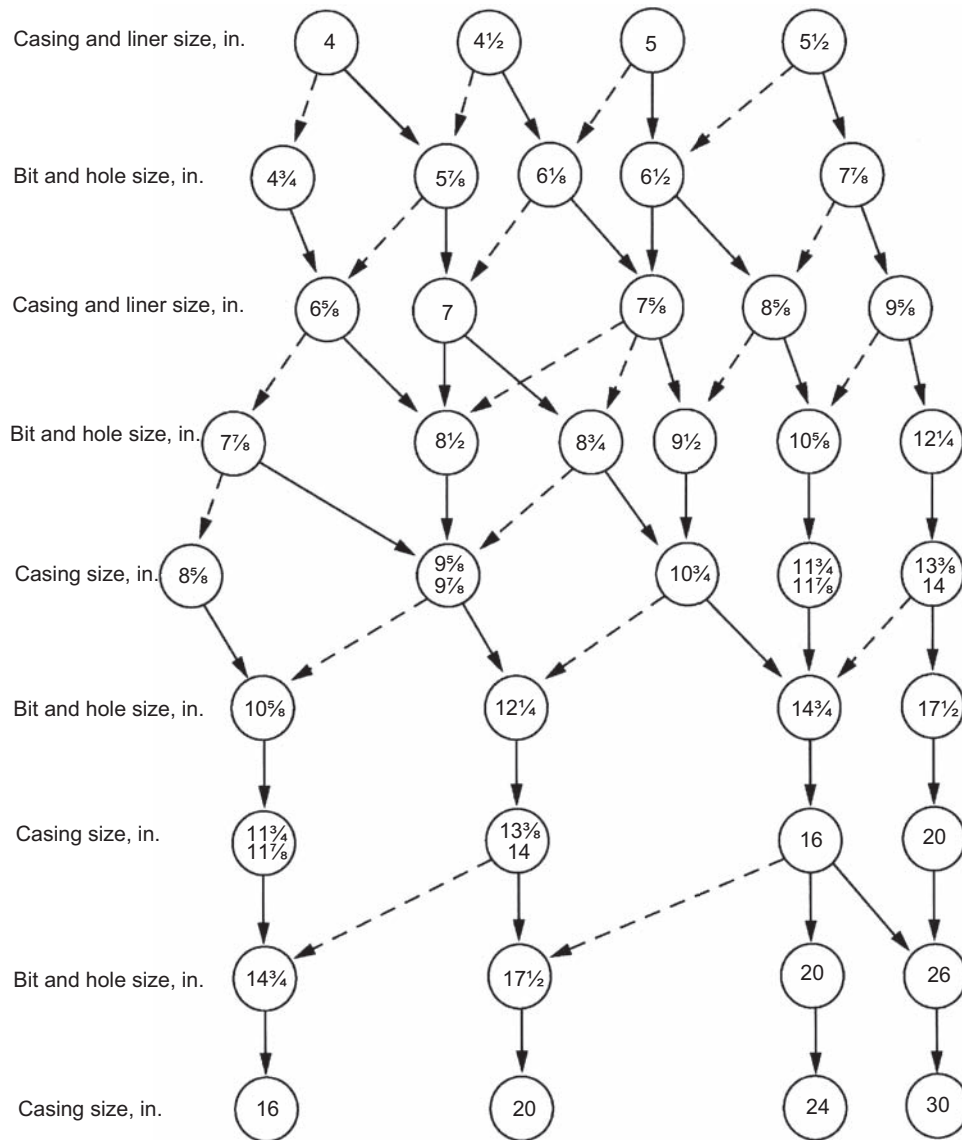


Fig. 7.18—Casing hole size. Solid lines indicate commonly used bits for that size pipe and can be considered adequate clearance to run and cement the casing or liner. The broken lines indicated less common hole sizes used. The selection of one of these broken paths requires that special attention be given to the connection, mud weight, cementing, and doglegs [from Economides et al. (1998)]. Reprinted with permission from John Wiley & Sons.

Example 7.6 Using the data given in Example 7.5, select casing sizes (i.e., OD) for each casing string.

Solution. A 7-in. production casing string is desired. An 8.5-in. bit is selected to drill the bottom section of the borehole. An 8.5-in. bit will pass through most of the available 9.625-in. casings (see Table 7.3). However, a final check will have to be made after the required maximum weight per foot is determined. A 12.25-in. bit is selected to drill to the depth of the intermediate casing. As shown in Fig. 7.18, a 12.25-in. bit will pass through most 13.375-in. casings. A 17.5-in. bit is selected to drill to the depth of the surface casing. Finally, as shown in Fig. 7.18, a 17.5-in. bit will pass through the 20-in. conductor casing, which will be driven into the ground. Some operators would use 18.625-in. conductor casing because a 17.5-in. bit will pass through most commonly used casings of this size.

7.9.3 Selection of Weight, Grade, and Couplings. Once the length and OD of each casing string have been established, the weight, grade, and couplings for each string can be designed. In general, each casing string is designed to withstand the most severe loading conditions anticipated during casing placement and the life of the

well. The loading conditions that are always considered are burst, collapse, and tension. When appropriate, other loading conditions (such as bending or buckling) must also be considered. Because the loading conditions in a well tend to vary with depth, it is often possible to obtain a less expensive casing design using several different weights, grades, and couplings in a single casing string.

It is often impossible to predict the various loading conditions to which a casing string will be subjected during the life of a well. Therefore, the casing design usually is based on an assumed loading condition. The assumed design load must be severe enough that there is a very low probability of a more severe situation actually occurring and causing casing failure. When appropriate, the effects of casing wear and corrosion should be included in the design criteria. These effects tend to reduce the casing thickness and greatly increase the stresses where they occur.

The design loads assumed by the various well operators differ significantly and are too numerous to be exhaustively listed in this text. There are no industry specifications that contain recommendations for design loads. Instead, example design criteria that are felt to be representative of current drilling-engineering practice will be presented. Once the concepts presented in this text are mastered, the reader should be able to apply easily any other criteria used by his particular company.

As mentioned in Section 7.5, most classic design methods never permitted a material to be loaded beyond its design rating, which could be based on a material's yield strength or failure strength. A safety factor is the margin of safety between an applied load and the design rating. A design factor is the minimum safety factor allowed for a particular load; thus, it limits the load that can be safely applied. Design factors are usually based on experience and account for uncertainties in the loads and in the strength or resistance of a tubular. There are no universally accepted design factors, and there are no design factors specified or recommended by industry standards. Design methods based on applying a design factor to the strength or resistance of a tubular to yield the working rating of the tubular are referred to as *working-stress designs*.

To achieve a minimum-cost casing design, the most economical casing and coupling that will meet the design loading conditions must be used for all depths. Because casing prices change frequently, it is not practical to include a detailed price list in a text of this type. In general, minimum cost is achieved when casing with the minimum possible weight per foot in the minimum grade that will meet the design load criteria is selected. For this illustration, only API casing and couplings will be considered in the example applications. It will be assumed that the cost per foot of the casing increases with increasing burst strength and that the cost per connector increases with increasing joint strength.

Casing strings required to drill safely to the depth objective serve different functions from those of the production casing. Similarly, drilling conditions applicable for surface casings are different from those for intermediate casings or drilling liners. For this reason, each type of casing string will have different design load criteria. Design criteria also can vary with the well environment (e.g., wells drilled into permafrost on the north slope of Alaska) and with the well application (e.g., geothermal steam or steam-injection wells). General design criteria will be presented for surface casings, intermediate casings, intermediate casings with a liner, and production casings. Additional criteria for thermal and arctic wells will also be discussed.

7.9.4 Casing Axial Forces. The balance of forces on the casing is shown in **Fig. 7.19**. Adding the forces and taking the limit as Δs goes to zero gives the following equation (Mitchell 2009):

$$\frac{d}{ds} [F_a \bar{t}] + w_p \bar{i}_z + \bar{w}_{if} + \bar{w}_{ef} + \bar{w}_c = 0, \quad \dots \quad (7.44)$$

where w_p is the weight of pipe in air, \bar{w}_{if} is the fluid load on the interior of the pipe, \bar{w}_{ef} is the fluid load on the exterior of the pipe, \bar{w}_c is the contact load, s is the measured depth, \bar{i}_z is the downward direction, and \bar{t} is the vector pointing in the axial direction. The fluid force on the inside of the pipe can be determined with a similar force balance, as shown in **Fig. 7.20**:

$$\bar{w}_{if} = -\frac{d}{ds} [P_i A_i \bar{t}] + \rho_i A_i g \bar{i}_z = 0, \quad \dots \quad (7.45)$$

where ρ_i is the density of the fluid inside the pipe, and g is the gravity constant. The exterior fluid force is somewhat more difficult to determine, but if we assume a static fluid, it is somewhat easier. If we assume a volume of fluid with a missing volume the size of the pipe, then the load on the wall of the hole in the fluid equals the load on the casing. A cylinder of fluid that would fill the hole in this volume of fluid would have a load on it of the opposite sign, since there is no net load on the total fluid volume. Thus, the exterior fluid load has the same form

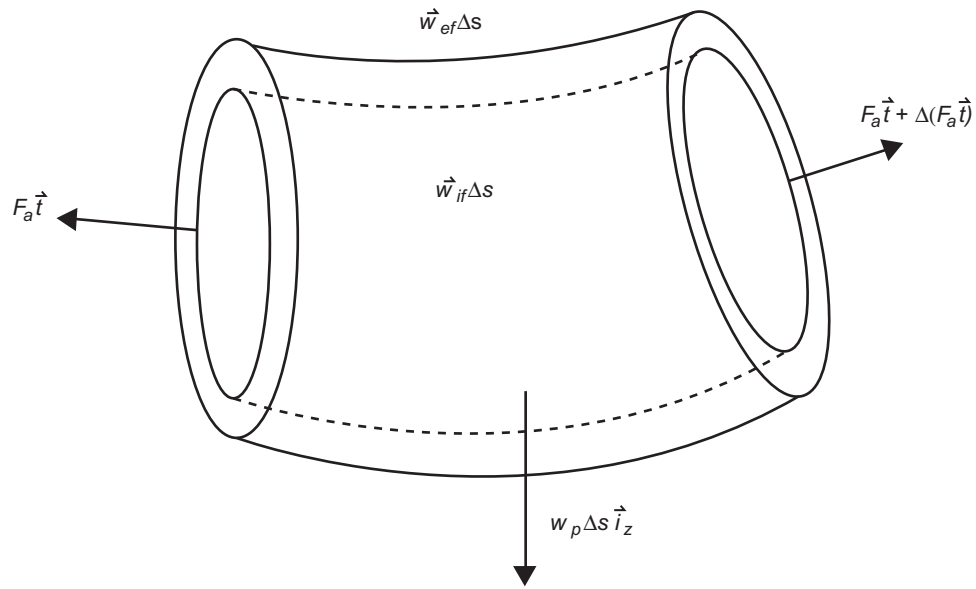


Fig. 7.19—Casing force balance.

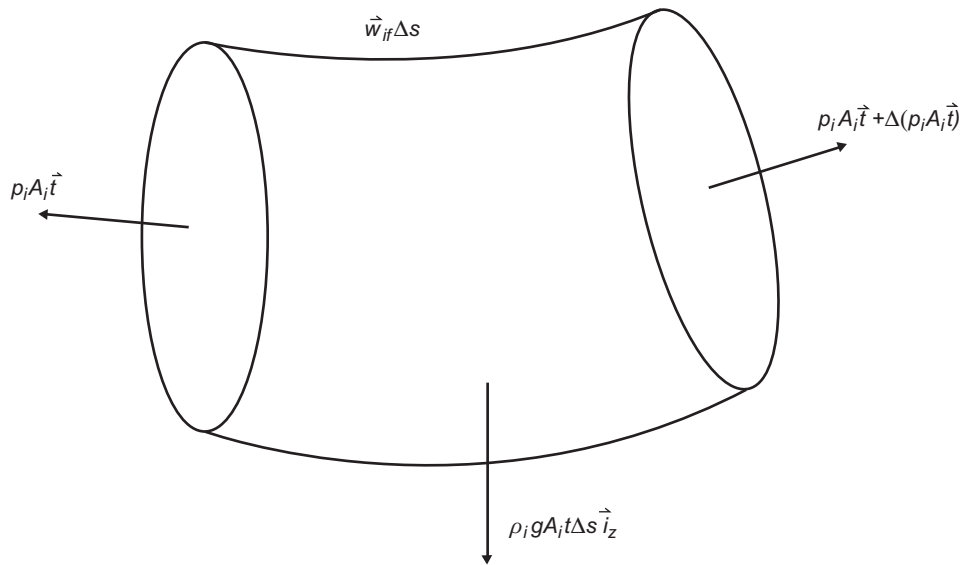


Fig. 7.20—Internal flow force balance.

as Eq. 7.45, but with the opposite sign, the exterior area A_e replacing the interior area A_i and the exterior pressure replacing the interior pressure:

$$\bar{w}_{ef} = \frac{d}{ds} [P_e A_e \vec{t}] - \rho_e A_e g \vec{i}_z = 0, \quad \dots \dots \dots (7.46)$$

where ρ_i is the density outside the casing. Putting loads from Eqs. 7.45 and 7.46 into the pipe force balance gives

$$\frac{d}{ds} [(F_a - P_i A_i + P_e A_e) \vec{t}] + (w_p - \rho_i A_i g + \rho_e A_e g) \vec{i}_z + \bar{w}_c = 0 \quad \dots \dots \dots (7.47)$$

Notice that we can combine terms in Eq. 7.47, and we find that we have again derived the effective tension we found in Section 7.5.5, Eq. 7.7:

$$\begin{aligned} \frac{d}{ds}[F_e \bar{i}] + w_{bp} \bar{i}_z + \bar{w}_c &= 0 \\ F_e &= F_a - P_i A_i + P_e A_e \\ w_{bp} &= w_p - \rho_i A_i g + \rho_e A_e g \end{aligned} \quad (7.48)$$

If we look at only the axial terms in Eq. 7.48, we get the equation for calculating the tension in the casing:

$$\frac{d}{ds} F_e + w_{bp} \cos \varphi = 0 \quad (7.49)$$

where φ is the pipe inclination angle relative to the vertical. Another advantage of using effective tension occurs with a change in cross-section of the pipe. Clearly, pressure forces are generated at changes in area (see **Fig. 7.21**):

$$\begin{aligned} F_a^+ &= F_a^- - P_o \Delta A_e + P_i \Delta A_i \\ \Delta A_i &= A_i^+ - A_i^- \\ \Delta A_o &= A_o^+ - A_o^- \end{aligned} \quad (7.50)$$

The negative superscript denotes upstream of the area change, while the positive superscript denotes downstream. Remember that the sign convention for F is tension positive.

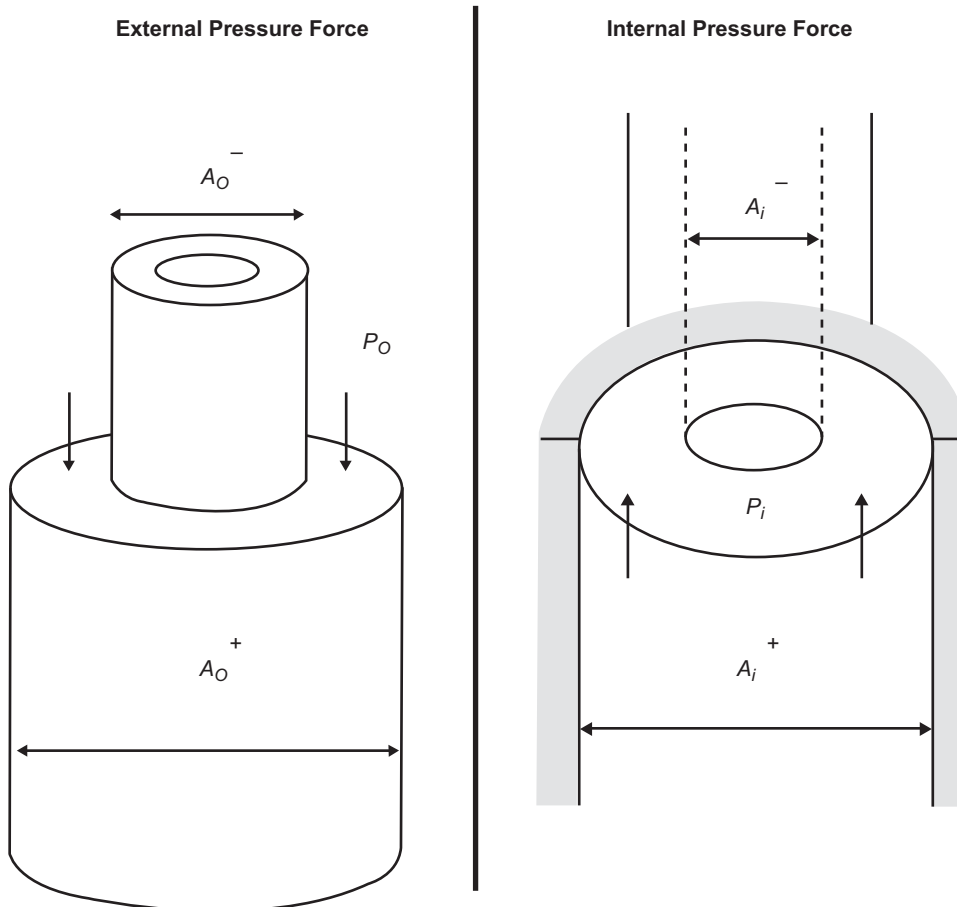


Fig. 7.21—Pressure force due to area change.

$$\begin{aligned}
 F_a^+ &= F_a^- - P_e [A_e^+ - A_e^-] + P_i [A_i^+ - A_i^-] \Rightarrow \\
 F_a^+ - P_i A_i^+ + P_e A_e^+ &= F_a^- - P_i A_i^- + P_e A_e^- \quad \dots \dots \dots (7.51) \\
 \text{or :} \\
 F_e^+ &= F_e^-
 \end{aligned}$$

If we use the effective force, we do not need to account for fluid loads resulting from changes in cross-sectional area.

When designing a casing string, the effect of fluid pressure (buoyancy) is easily included when calculating axial loads by using the effective tension. Because the collapse resistance of a tubular is derated for tension, buoyancy will also affect a tubular's collapse-resistance properties. Drilling engineers sometimes use a simple method to include the buoyancy effect on casing when performing hand calculations. The buoyed weight per foot of casing is obtained by multiplying the air nominal weight per foot of casing by a buoyancy factor. The following equation can be used to calculate the buoyancy factor (BF) in common oilfield units:

$$BF = 1 - \frac{\rho_m}{65.5}, \quad \dots \dots \dots (7.52)$$

where ρ_m is the mud weight in lbm/gal. In this case, w_{bp} can be shown to be

$$\begin{aligned}
 w_{bp} &= w_p - \rho_m g A_i + \rho_m g A_e \\
 &= (\rho_s - \rho_m) g A_s \\
 &= \left(1 - \frac{\rho_m}{\rho_s}\right) w_p \\
 &= BF w_p, \quad \dots \dots \dots (7.53)
 \end{aligned}$$

where ρ_s is the density of steel, and we have converted the density of steel to lbm/gal units.

7.9.5 Surface Casing. Examples of design loading conditions for surface casing are illustrated in **Fig. 7.22** for burst, **Fig. 7.23** for collapse, and **Fig. 7.24** for tension. The high-internal-pressure loading condition used for the burst design is based on a well-control condition which is assumed to occur while circulating out a large kick. The high-external-pressure loading condition used for collapse design is based on a severe lost-circulation problem. The high-axial-tension loading condition is based on an assumption of stuck casing while the casing is being run into the hole before cementing operations.

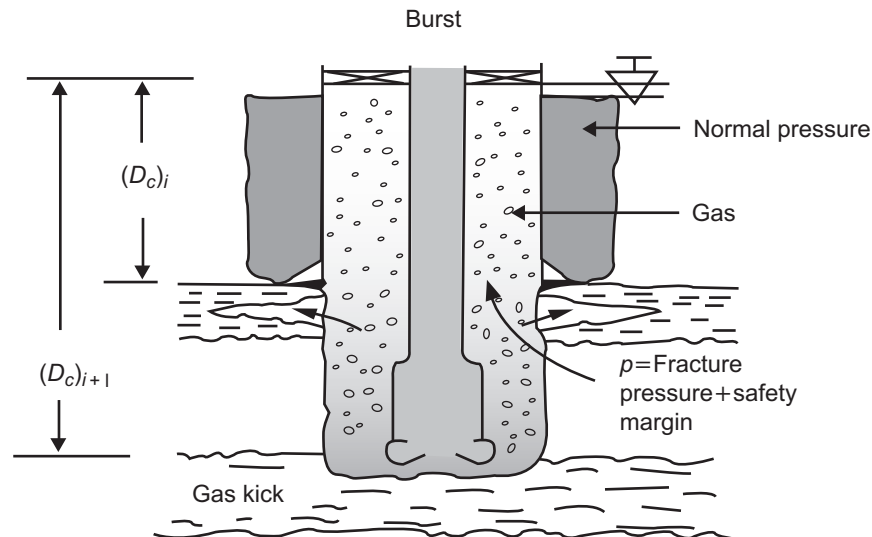


Fig. 7.22—Burst loads [from Bourgoyne et al. (1991)].

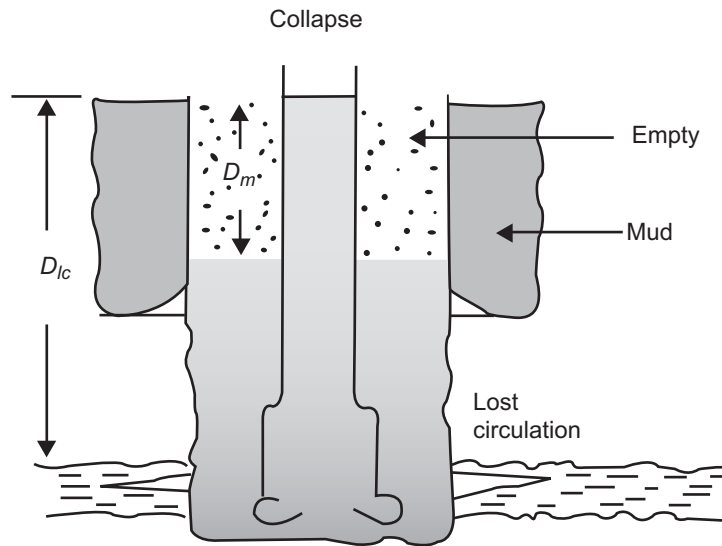


Fig. 7.23—Collapse loads [from Bourgoyne et al. (1991)].

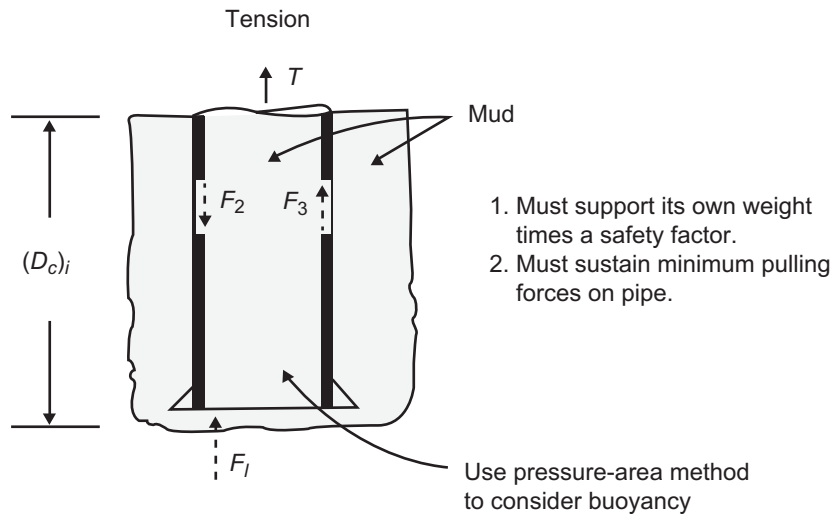


Fig. 7.24—Tension loads [from Bourgoyne et al. (1991)].

The burst design should ensure that the formation-fracture pressure at the casing seat will be exceeded before the casing burst pressure is reached. Therefore, this design uses formation fracture as a safety pressure-release mechanism to ensure that casing rupture will not occur at the surface and endanger the lives of the drilling personnel. The design pressure at the casing seat is equal to the fracture pressure plus a safety margin to allow for an injection pressure that is slightly greater than the fracture pressure. The pressure within the casing is calculated assuming that all the drilling fluid in the casing is lost to the fractured formation, leaving only formation gas in the casing. The external or backup pressure outside the casing, which helps to resist burst, is assumed to be equal to the normal formation pore pressure for the area. The beneficial effect of cement or higher-density mud outside the casing is ignored because of the possibility both of a locally poor cement bond and of mud degradation over time. A safety factor is also used to provide an additional safety margin for possible casing damage during transportation and field handling of the pipe.

The collapse design is based either on the most severe lost-circulation problem that is believed to be possible or on the most severe collapse loading anticipated when the casing is run. For both cases, the maximum possible external pressure, which tends to cause casing collapse, will result from the drilling fluid that is in the hole when the casing is placed and cemented. The beneficial effect of the cement and of possible mud degradation is

ignored, but the detrimental effect of axial tension on the collapse-pressure rating is considered. The beneficial effect of pressure inside the casing can also be taken into account by the consideration of a maximum possible depression of the mud level inside the casing. A safety factor is generally applied to the design loading condition to provide an additional safety margin.

If a severe lost-circulation zone or a pore-pressure regression zone is encountered near the bottom of the next interval of the hole and if no other permeable formations are present above the zone, the fluid level in the well can fall until the BHP is equal to the pore pressure of the zone. Equating the hydrostatic mud pressure to the pore pressure of the lost-circulation zone gives

$$0.052(\rho_{\max})(Z_{lc} - Z_m) = 0.052g_p Z_{lc}, \quad \dots\dots\dots (7.54a)$$

where Z_{lc} is the depth (true vertical) of the lost-circulation zone, g_p is the pore-pressure gradient of the zone, ρ_{\max} is the maximum mud density anticipated in drilling to Z_{lc} , and Z_m is the depth to which the mud level will fall. Solving this expression for Z_m yields

$$Z_m = \frac{(\rho_{\max} - g_p)}{\rho_{\max}} Z_{lc} \quad \dots\dots\dots (7.54b)$$

There is usually considerable uncertainty in the selection of the minimum anticipated pore-pressure gradient and the maximum depth of the zone for use in Eq. 7.54b. In the absence of any previously produced and depleted formations, the normal pore-pressure gradient for the area can be used as a conservative estimate of the minimum anticipated pore-pressure gradient. Similarly, if the lithology is not well known, the depth of the next full-length casing string can be used as a conservative estimate of Z_{lc} .

The minimum fluid level in the casing when it is placed in the well depends on field practices. The casing usually is filled with mud after each joint of casing is made up and run in the hole, and an internal casing pressure that is approximately equal to the external casing pressure is maintained. However, in some cases the casing is *floated in*, or run at least partially empty, to reduce the maximum hook load before reaching bottom. If this practice is anticipated, the maximum depth of the mud level in the casing must be compared to the depth computed using Eq. 7.45b, and the greater value must be used in the collapse-design calculations.

The most difficult part of the collapse design is the correction of the collapse-pressure rating for the effect of axial tension. The difficulty lies in determining the axial tension that is present at the time the maximum collapse load is imposed. If the maximum collapse load is encountered when the casing is run, the axial tension can be readily calculated from a knowledge of the casing weight per foot and the mud hydrostatic pressure in accordance with the principles previously presented. However, if the maximum collapse load is encountered after the cement has hardened and the casing has been landed in the wellhead, the determination of axial stress is much more difficult. In the case of hand calculations, it is common to compute axial tension as the hanging weight for the hydrostatic pressures present when the maximum collapse load is encountered plus any additional tension put in the pipe during and after casing landing. This assumption will result in a maximum tension value and a corrected minimum collapse-pressure rating.

Tension design requires consideration of the axial stresses that are present when the casing is run during cementing operations, when the casing is landed in the slips, and during subsequent drilling and production operations throughout the life of the well. In most cases, the design load is based on conditions that could occur when the casing is run. It is assumed that the casing may become stuck near the bottom and that a maximum amount of pull, in excess of the hanging weight in mud, would then be required to work the casing free. A minimum safety-factor criterion is applied so that the design load will be dictated by the maximum load resulting from the use of either the safety factor or the overpull force, whichever is greater. The minimum overpull force tends to control the design in the upper portion of the casing string, and the minimum safety factor tends to control the design in the lower part of the casing string. Once the casing design is completed, the maximum axial stresses anticipated during cementing, casing loading, and subsequent drilling operations should also be checked to ensure that the design load is never exceeded. In some cases where internal pressure or density has increased and external pressure has decreased because of setting conditions, added tension loads can exceed the overpull force. This phenomenon will be further explained in Section 7.12.

In the design of a combination string of nonuniform wall thickness, the effect of buoyancy is most accurately included using the effective tension concept. The drilling fluid in use at the time the casing is run is used to compute the hydrostatic pressure at each junction between sections of different wall thicknesses, so that the actual

tension can be calculated from the effective tension. For hand calculations, the simpler method shown in Section 7.8.4 is commonly used.

In directional wells, the additional axial stress in the pipe body and connectors caused by bending should be added to the axial stress that results from casing weight and fluid hydrostatic pressure. The directional plan must be used to determine the portions of the casing string that will be subjected to bending when the pipe is run. The lower portion of the casing string will have to travel past all the curved sections in the wellbore, but the upper section of the casing string may not be subjected to any bending.

When the selection of casing grade and weight in a combination string is controlled by collapse, a simultaneous design for collapse and tension will be the most exact. The greatest depth at which the next most economical casing can be used depends on its corrected collapse-pressure rating, which in turn depends on the prior computation of axial tension. An iterative procedure can be used in which the depth of the bottom of the next most economical casing section is first selected on the basis of an uncorrected table value for collapse resistance. The axial tension at this point is then computed, and the collapse resistance is corrected. This procedure enables the depth of the bottom of the next casing section to be updated for a second iteration. Several iterations may be required before the solution converges. A simple graphical method can be used with hand calculations, as shown in Example 7.7, for quicker selection of casing-section depths.

7.9.6 Intermediate Casing. Intermediate casing is similar to surface casing in that its function is to permit the final depth objective of the well to be reached safely. Several methods are used by the industry to ensure that this string is designed for safe handling of formation kicks, lost returns, and other drilling problems that may occur during deep drilling.

Similarly to surface-casing design, internal and external pressure design loads are determined using both burst and collapse analysis. For burst design, the external pressure, or the backup pressure outside the casing that helps resist burst, is typically assumed to be equal to the normal formation pore pressure for the area. The beneficial effect of cement or higher-density mud outside the casing is ignored because of the possibility both of a locally poor cement bond and of mud degradation over time.

Internal-pressure design-load assumptions for burst analysis vary significantly in the industry. Some operators calculate the internal pressure that would result at every depth in a string from circulating out a design kick. The design-kick intensity and volume is chosen to result in well pressures that are equal to (or slightly greater than) the predicted formation pressure at the intermediate-casing shoe. This ensures that the design kick can be successfully circulated past the intermediate-casing shoe without compromising formation integrity at the casing shoe. If the design-kick pressure exceeds the formation strength at the intermediate-casing shoe, a lost return or an underground blowout would likely result, after which the kick could not be circulated to the surface. The maximum surface pressure while circulating out the design kick can also be calculated, and the BOP working pressure is chosen to exceed this maximum surface pressure from the kick-circulation process.

Some operators use the general procedure outlined for surface casing for intermediate-casing strings. However, in some cases, the burst-design requirements dictated by the design-loading condition illustrated in Fig. 7.22 are extremely expensive to meet, especially when the resulting high working pressure is in excess of the working pressure of the surface BOP stacks and choke manifolds for the available rigs. In this case, the operator may accept a slightly larger risk of losing the well and select a less severe design load. The design load remains based on an underground blowout situation which is assumed to occur while a gas kick is being circulated out. However, the acceptable mud loss from the casing is limited to the maximum amount that will cause the working pressure of the surface BOP stack and choke manifold to be reached. If the existing surface equipment is to be retained, it is pointless to design the casing to have a higher working pressure than the surface equipment.

When the surface burst-pressure load is based on the working pressure of the surface equipment, P_{\max} , internal pressures at intermediate depths should be determined, as shown in Fig. 7.22. It is assumed that the upper portion of the casing is filled with mud and the lower portion of the casing is filled with gas. The depth of the mud/gas interface, Z_m , is determined using the following relationship:

$$P_{\text{inj}} = P_{\max} + 0.052\rho_m Z_m + 0.052\rho_g (Z_k - Z_m), \quad \dots \quad (7.55a)$$

where P_{inj} is the injection pressure opposite the lost-circulation zone; ρ_m and ρ_g are the densities of mud and gas, respectively; and Z_{lc} is the depth of the lost-circulation zone. Solving this equation for Z_m gives

$$Z_m = \frac{P_{\text{inj}} - P_{\max}}{0.052(\rho_m - \rho_g)} - \frac{\rho_g Z_{lc}}{(\rho_m - \rho_g)}. \quad \dots \quad (7.55b)$$

The gas behavior can be described using the real gas equation, defined by

$$\rho_g = \frac{pM}{zRT}, \quad \dots \dots \dots (7.56)$$

where p = absolute pressure, ρ_g = gas density, z = gas compressibility factor, R = universal gas constant, T = absolute temperature, and M = gas molecular weight. The gas density is estimated using Eq. 7.56 with $z \approx 1$ (see Chapter 5) and an assumed average molecular weight. The density of the drilling mud is set to the maximum density anticipated while drilling to the depth of the next full-length casing string. This makes it possible to calculate the maximum intermediate pressures between the surface and the casing seat. The depth of the lost-circulation zone is determined from the fracture gradient vs. depth plot as the depth of the weakest exposed formation. The injection pressure is equal to the fracture pressure plus an assumed safety margin to account for a possible pressure drop within the hydraulic fracture.

Collapse-loading design assumptions for intermediate casings are usually similar to those used for surface-casing design, taking lost returns into account. Typically, an intermediate-casing-string design will result in a lower casing grade and weight per foot than those for a production string. As a result, an intermediate string designed only for deep drilling often will not meet production-casing design specifications.

7.9.7 Intermediate Casing With a Liner. The burst-design-load criteria for intermediate casing on which a drilling liner will later be supported must be based on the fracture gradient below the liner. The burst design considers the intermediate casing and liner as a unit. All other design criteria for the intermediate casing are identical to those previously presented.

7.9.8 Production Casing. Example burst-design and collapse-design loading conditions for production casing are illustrated in **Fig. 7.25**. The example burst-design loading condition assumes that a producing well has an initial shut-in BHP equal to the formation pore pressure and a gaseous produced fluid in the well. The production casing must be designed so that it will not fail if the tubing fails. A tubing leak is assumed to be possible at any depth. External pressure for production-casing burst design is generally assumed to be the formation pressure outside the casing. Experience has shown that mud left outside the casing will decrease in density over time if the mud can interact with an open hole. An exception is if the casing annulus outside the production casing is sealed with cement and the mud trapped in the annulus is not free to interact with the open hole. A sealed annulus also creates a fixed-volume annulus, which is subject to annulus mud expansion creating annulus pressure with a temperature increase, a phenomenon which is discussed in Section 7.13.3 and in advanced literature.

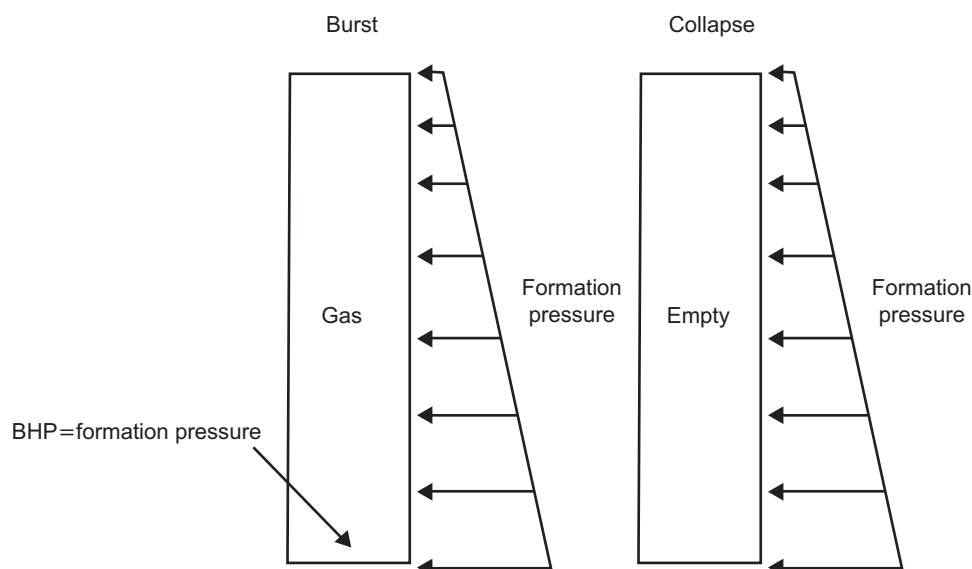


Fig. 7.25—Production casing design and loads.

The collapse design load shown in Fig. 7.25 is based on conditions late in the life of the reservoir, when reservoir pressure has been depleted to a very low (negligible) abandonment pressure. A leak in the tubing or packer could cause loss of the completion fluid, and therefore the low internal pressure is not restricted to the portion of the casing below the packer. Therefore, for design purposes, the entire casing is considered to be empty. For collapse design, the fluid density outside the casing is assumed to be equal to the formation pressure, and the beneficial effect of the cement is ignored.

In the absence of any unusual conditions, the tension design load criteria for production casing are the same as for surface and intermediate casing. When unusual conditions are present, the maximum stresses associated with these conditions must be checked to determine whether they exceed the design load in any portion of the string.

Example 7.7 Design 7-in. production casing for a vertical 16,000-ft sweet service well. The production casing will be set in 10.2-lbm/gal mud. Base the design on the pipe-body performance properties; connections will be chosen later. The operations group has specified a 2,000-ft minimum section length, 100,000-lbf overpull over buoyed casing weight, and a maximum of three sections of casing. A “gauge joint” of the heaviest weight-per-foot casing at the surface is not required. Packer-fluid density is specified as 8.8 lbm/gal salt water, and the expected shut-in tubing pressure (SITP) is 6,000 psi. Minimum pore pressure in the open hole and the BHP is 9.6 lbm/gal. For burst design, assume that a wellhead leak has occurred and that the 6,000-psi tubing pressure has been applied to the top of the 8.8-lbm/gal packer fluid. Assume further that the top of cement in the production casing by the open hole is at 10,500 ft. Use a burst design factor (BDF) of 1.1, a collapse design factor (CDF) of 1.125, and a pipe-body-tension design factor (TDF) of 1.5. Available casing and API pipe-body performance properties with the specified design factor, listed in increasing order of cost, are as follows:

Available Types	Collapse, psi CDF = 1.125	Burst, psi BDF = 1.1	Tension, klbf TDF = 1.5
23.0 lbf, N-80	3,400	5,760	355
23.0 lbf, C-95	3,690	6,850	420
26.0 lbf, C-95	5,235	7,820	478
29.0 lbf, C-95	6,970	8,810	535
32.0 lbf, C-95	8,660	9,780	590
29.0 lbf, P-110	7,580	10,200	620

Solution. Step 1. Determine burst loads:

With 6,000-psi SITP applied on top of the 8.8-lbm/gal packer fluid with a 9.6-lbm/gal external pressure:

Burst load at the surface = 6,000 psi

$$\begin{aligned}\text{Burst load at 16,000 ft} &= (6,000 + (16,000)(8.8)(0.052)) - (16,000)(9.6)(0.052) \\ &= (6,000 + 7,322) - 7,987 \\ &= 5,335 \text{ psi.}\end{aligned}$$

The burst load line is plotted in Fig. 7.26.

Step 2. Determine collapse loads:

Collapse load at the surface = 0 psi

Collapse load at 16,000 ft = 8,000 psi (i.e., BHP)

The collapse load line is plotted in Fig. 7.26. Both burst and collapse loads are plotted on the same figure for convenience.

Step 3. Determine the depth of the neutral plane:

$$BF = 1 - \frac{10.2}{65.5}$$

$$BF = 0.844$$

$$\text{Neutral plane} = (16,000)(0.844) = 13,500 \text{ ft.}$$

The neutral plane is plotted in Fig. 7.26. Note that collapse is the dominant design load below approximately 10,000 ft. Collapse-performance properties will require derating for tension above the neutral plane.

Step 4. Select the bottom Section 1:

The design starts at total depth and moves uphole. To satisfy the collapse load at total depth, 32.0-lbm/ft, C-95 casing will be required. The length of Section 1 will be determined by the setting depth of Section 2.

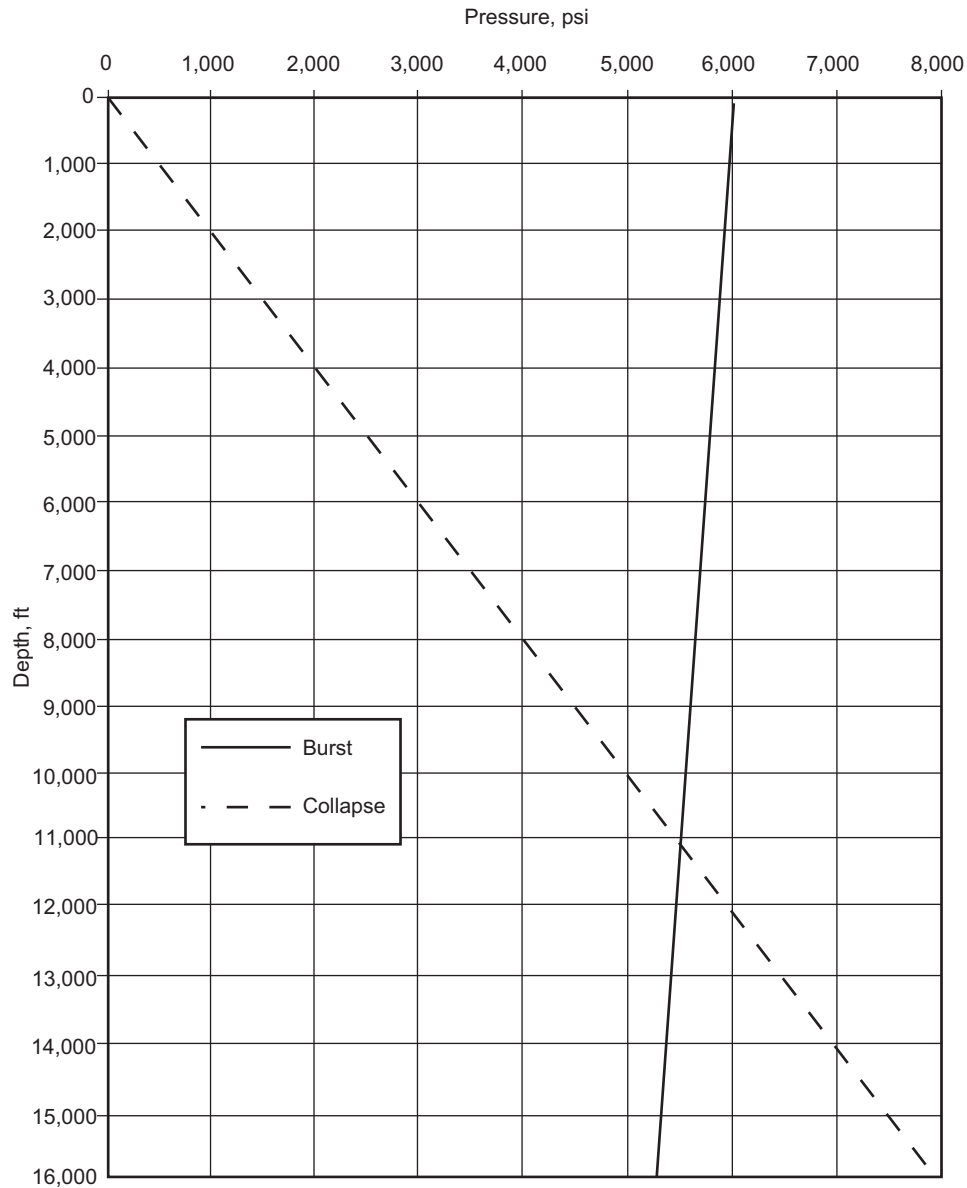


Fig. 7.26—Burst and collapse load lines.

The casing with the next-lowest collapse rating and cost is 29-lbm/ft, C-95 casing. This casing can be set at:

Maximum depth = $6,970 / (8,000 / 16,000) = 13,940$ ft.

Section 1 can be summarized as follows:

Section 1: $16,000 - 13,940 = 2,060$ ft of 32-lbm/ft, C-95 casing.

Because the top of Section 1 is below the neutral plane, collapse resistance for this casing does not need to be reduced for tension.

Step 5. Select Section 2:

The top of Section 2 is dictated by the setting depth of the next uphole section of casing, Section 3. The casing with the next-lowest collapse rating and cost is 26.0-lbm/ft, C-95. The maximum setting depth of this casing, not considering the effect of the reduction in collapse rating for tension, is

Maximum depth = $5,235 \text{ psi} / (8,000 / 16,000) = 10,470$ ft.

Section 2 could be considered to run from 13,940 ft to 10,470 ft; however, the reduction in collapse rating due to tension must be considered for the casing between the neutral plane at 13,500 ft and the top of Section 2. The tensile load at the top of Section 2 (10,470 ft) is

Tension load at 10,470 ft = $(29.0)(13,500 - 10,470) = 87,870$ lbf.

Note that the nominal weight per foot, rather than the buoyed weight per foot for the casing, is used in this calculation. This is because buoyancy was used to calculate the neutral plane, and the casing below the neutral plane is in compression. Using the API equations from Section 7.5.3, the collapse rating for 29.0-lbm/ft, C-95 (Section 2) of 7,840 psi must be reduced to 7,550 psi because of the tensile load of 87.9 kip. The working rating with a 1.125 DF is 6,710 psi. This value is plotted at 10,470 ft, and the full rated collapse resistance is plotted on the neutral plane in Fig. 7.26. Section 2 can be summarized as follows:

Section 2: 13,940 ft – 10,470 ft = 3,470 ft of 29-lbf/ft, C-95 casing.

Step 6. Select Section 3:

From the above calculations, Section 3 will require 26-lbf/ft, C-95 casing. From Fig. 7.26, it is evident that tension and burst loads are becoming the dominant design considerations. Checking the maximum tension loads at the bottom of Section 3 (10,470 ft) with 100,000 lbf overpull:

Maximum tension load at 10,470 ft = $(2,060)(32.0)(0.844) + (3,470)(29.0)(0.844) + 100,000 \text{ lbf} = 240,570 \text{ lbf}$.

Note that the calculated loads for tension use the buoyancy factor (and overpull), while the calculated loads for collapse derating use the air weight above the neutral plane.

The 26.0-lbf/ft, C-95 casing has sufficient burst and tension capacity for a 2,000-ft section. Calculate the maximum possible length of 26.0-lbf/ft, C-95 casing given the desired overpull and DF.

Maximum pipe-body tensile strength with DF (26.0 lbf/ft, C-95) = 478,000 lbf

Maximum tension load at 10,470 ft = 240,570 lbf

Remaining load capacity = 237,430 lbf

$237,430 \text{ lbf} / ((26 \text{ lbf/ft})(0.844)) = 10,820 \text{ ft}$.

Section 3 could extend from 10,470 ft to the surface and not exceed the tension and burst loading requirements. Check the collapse resistance of Section 3 at 10,470 ft.

At 10,470 ft (bottom of Section 3), the tension load is

Load at 0,470 ft in Section 3, 26.0-lbf/ft = $(13,500 - 10,470)(29.0) = 87,870 \text{ lbf}$.

The API collapse rating of Section 3 at 10,470 ft is reduced from 5,890 psi to 5,700 psi because of tension. With a 1.125 DF, the rated collapse loading is 5,070 psi. The required collapse loading at 10,470 ft is

Collapse loading at 10,470 ft = $(8,000 / 16,000)(10,470) = 5,235 \text{ psi}$.

The 29.0-lbf/ft, C-95 casing's tension-reduced collapse rating at 10,470 ft is 5,070 psi, which is less than the required collapse loading of 5,235 psi, so Section 3 cannot begin at 10,470 ft, and Section 2 must extend above 10,470 ft. From Fig. 7.26, it appears that the 29.0-lbf/ft, C-95 casing can begin near 10,000 ft. Check the reduced collapse rating of Section 3 (26.0-lbf/ft, C-95) at 10,000 ft.

At 10,000 ft (bottom of Section 3), the tension load is

Load at 10,000 ft in Section 3, 26.0-lbm/ft = $(13,500 - 10,000)(29.0 \text{ lbf/ft}) = 101,500 \text{ lbf}$.

The API collapse rating of Section 3 at 10,000 ft is reduced from 5,890 psi to 5,670 psi because of the tension value of 101,500 lbf. With the 1.125 DF, the rated collapse loading is 5,040 psi. The required collapse loading at 10,000 ft is 5,000 psi, so Section 3 can begin at 10,000 ft.

The rated collapse loading with no derating for tension is plotted on the neutral plane, and the derated collapse resistance is plotted at 10,000 ft, as shown in Fig. 7.26.

As a check, calculate the collapse load after derating for tension of Section 3 at 3,500 ft:

Load 3,500 ft = load at 10,000 ft + load from 10,000 ft to 3,500 ft
 $= 101,500 \text{ lbf} + (26.0 \text{ lbf/ft})(10,000 - 3,500 \text{ ft})$
 $= 101,500 \text{ lbf} + 169,000 \text{ lbf}$
 $= 270,500 \text{ lbf}$.

Using the API equations from Section 7.5.3, the collapse rating of 5,890 psi for 26.0-lbf/ft, C-95 casing is reduced to 5,100 psi because of the tensile load of 270,500 lbf at 3,500 ft. The working rating with a 1.125 DF is 4,530 psi. This value is plotted in Fig. 7.26.

Check the tension capacity of Section 3 if Section 2 extends to 10,000 ft with 100,000 lbf overpull:

Tension load at 10,000 ft = $(2,060)(32.0)(0.844) + (3,940)(29.0)(0.844) + 100,000 \text{ lbf} = 252,072 \text{ lbf}$.

Pipe-body tensile strength with TDF of Section 3, 26.0-lbf/ft, C-95 = 478,000 lbf, which is adequate.

Check the tensile strength of Section 3 at the surface:

Maximum tension at surface = load at 10,000 ft + load from 10,000 ft to surface
 $= 252,072 + (26.0)(10,000)(0.844)$
 $= 252,072 + 219,440$
 $= 471,510 \text{ lbf}$.

The tension rating of Section 3, using 26.0-lbf/ft, C-95 with TDF, is 478,000 lbf, which is slightly greater than the required tension load at the surface.

Section 3 can be summarized as follows, and the Section 2 length can be changed to

Section 3: 10,000 ft to surface, 26.0-lbf/ft C-95;

Section 2: 13,940 ft – 10,000 ft = 3,940 ft of 29-lbf/ft, C-95 casing.

Step 7. Summarize the final design:

Depth				
Section	Casing Type	Length, ft	Top, ft	Bottom, ft
1 (bottom)	32.0-lbf/ft, C-95	2,060	13,940	16,000
2 (middle)	29.0-lbf/ft, C-95	3,940	10,000	13,940
3 (top)	26.0-lbf/ft, C-95	10,000	0	10,000

This design is based on the pipe-body performance properties. Connection performance properties are not included. To complete the design, connections should be chosen to exceed the pipe-body performance ratings or the casing design checked against connection performance properties.

7.10 Probabilistic Reliability-Based Design of Casings

Load- and resistance-factor design is a reliability-based design philosophy that was developed by the civil-engineering profession beginning in the 1930s in Europe. It is widely accepted today for use in civil engineering projects and is the current basis for many structural-engineering systems (*Manual of Steel Construction* 2001). In the late 1980s and early 1990s, these well-established design techniques began to be applied to oilwell-tubular design (Brand et al. 1995; Payne and Swanson, 1990; Gulati et al. 1994; Lewis et al. 1995).

The traditional working-stress design methods presented previously compare a maximum load with a minimum resistance (or minimum tubular strength), maintaining a safety margin between the two values. The maximum load that a tubular will experience is based on expected operations and historical data and will occur with certainty. Tubular strength is based on specifying minimum manufacturing tolerances for dimensions, steel strength, and stress states such that no failures will occur. **Fig. 7.27** illustrates this design process.

In reliability-based design methods, uncertainties in both the load applied and the strength of a tubular are recognized as being random in nature. The objective of the resulting designs is to account for all uncertainties associated with these design parameters and to determine an appropriate risk level for the particular application. These procedures ensure adequate safety of a tubular design and uniform reliability across many well applications under varying design conditions. For example, for some wells, such as a development well that is drilled after many earlier wells, the actual loads may be known very accurately. For other wells, such as exploration wells, the predicted loads may be less accurate because available offset data may be limited. The final design should ensure that the probability of failure is commensurate with the consequences of failure.

The strength or performance properties of a tubular can vary from joint to joint, and even along the length of a single joint. Many parameters determine the strength of a tubular, including its mechanical properties, manufacturing tolerances and flaws, ease of finding and assessing imperfections, and handling and installation operations. The strength variability inherent in the manufacturing process can be minimized but not eliminated.

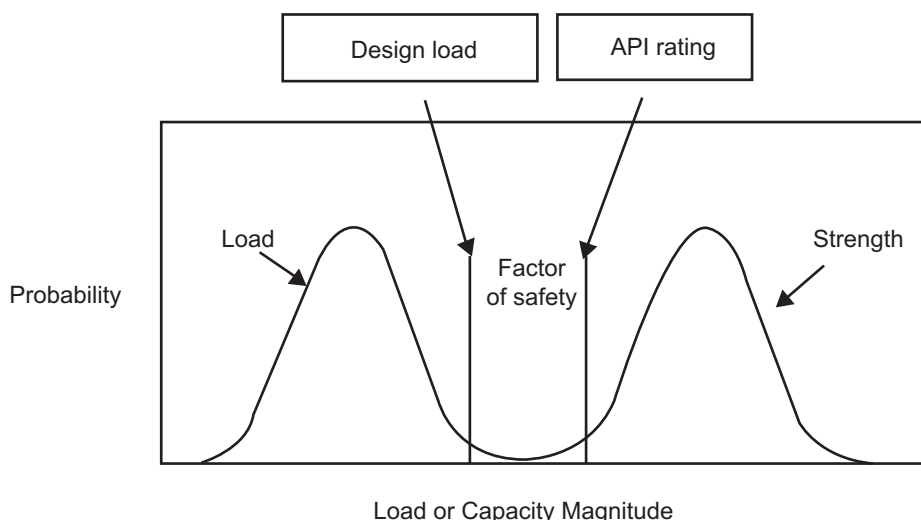


Fig. 7.27—Working stress design.

Actual loads in a well are based on many variables, including drilling loads (kick volume, pore pressure, lost returns) and operational loads (production-fluid density, reservoir pressure). An estimate of the actual loads and their probabilities of occurrence can be made using historical databases or by modeling the load using factors such as the effect that fluid gradients have on kick loads. **Fig. 7.28** illustrates the basic concepts of reliability-based design.

One method used for probabilistic tubular design is to adjust standard load cases and standard tubular performance properties using factors based on statistical methods. These factors are based on the uncertainties in a tubular's loading and determine its performance properties. They are determined so as to provide an acceptable failure probability or risk for the final tubular design and are based on historical data in many cases.

Using this design process, the engineer determines appropriate probabilities of failure or risk levels for a tubular's load and performance properties depending on design conditions. The optimum risk level is not the same for all failure modes because the consequences of failure can vary widely. For example, the cost of a kick resulting in a near-surface blowout can far exceed the cost of a kick below a deep protective string that results in a collapse failure. As a result, a much lower probability of failure would be used to design a surface-casing string than to design a deep intermediate string in a collapse mode. The acceptable probability of failure is chosen considering the consequences of failure, defined as the risk to health, safety, and the environment, as well as the cost of the failure.

Load factors can be selected for each of many specific load situations and can be large or small, depending on whether the case is likely or unlikely. This approach enables the engineer to design for a given level of risk without carrying out cumbersome probabilistic calculations. Performance-property factors can be selected or matched to each of a tubular's performance properties (i.e., burst, collapse, and tension). A shortcoming of this method is that substantial amounts of historical and physical data are necessary to calibrate the load and performance-property factors with the resulting risk. Other parameters, such as casing wear, temperature, and derating for tension, are usually included when determining a tubular's performance-property factors.

The following equation can be used as a check to ensure that a proposed design is acceptable:

Utilization factor = (load × load factor)/(performance-property factor × performance-property value).

7.11 Computer-Based Design of Casings

It is very important for the drilling engineer to understand how to perform casing-design steps manually; however, it would be impractical to analyze every possible load scenario, design an optimized mixed string, or track changing load conditions without using the capabilities of a computer. Furthermore, computers facilitate the calculation of complex combined-load conditions and make it possible to perform routine checks using complex tubular-capacity formulas. Individual users and companies have developed spreadsheets and programs for casing analysis, and several commercially available programs focus on casing-stress analysis and design. This section describes how casing analysis and design programs work, how to use them, and how to interpret the results.

Computer-based analysis of casing and tubing begins with the definition of the stress state of the tubular at the moment it is installed in the well. This stress state is called the *initial condition* and is defined at all points along

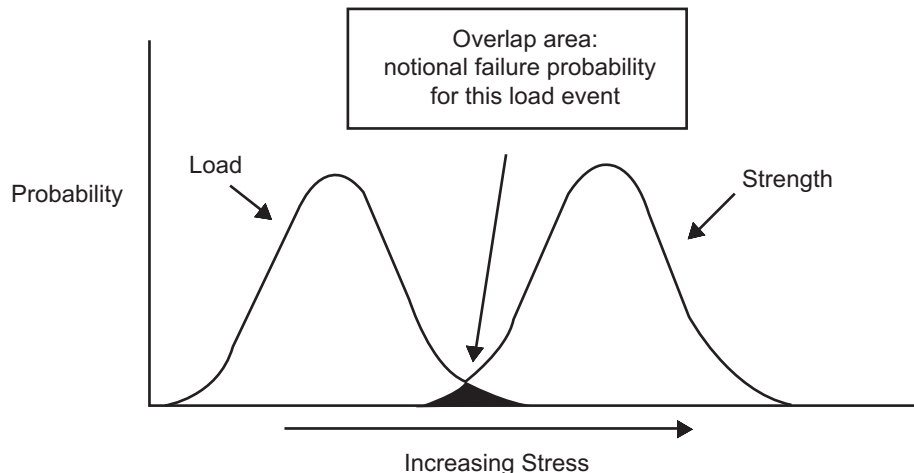


Fig. 7.28—Reliability-based design.

the length of the tubular string. The initial condition and stress state are defined by the *tension load* from dead weight, buoyancy effects, and applied stability loads (see next section); the *internal and external pressures* from hydrostatic fluid columns; *bending* resulting from geometric doglegs in the well path; and a *temperature profile* arising from the installation operation or the presence of geothermal gradients. For casing and liner strings, the initial conditions are typically defined when the cement has been circulated in place and has set and the slips are set in the wellhead. For tubing strings, the initial conditions are typically defined when the packer is set.

Whether commercial software or a custom engineering or corporate program is used, it is essential to understand the assumptions made by the program when the initial conditions are determined. For example, the additional buoyancy effects of the dense lead and tail cement slurries will decrease the tension of a string at the surface compared with that of a string run in mud.

Computer-based analysis continues by considering various operating conditions that result in a new stress state for the tubular. These operating conditions define a *load case*. The software calculates the changes that have occurred from the initial conditions. Changes in internal and external pressure profiles may be caused by changes in the fluid density or gradient. Changes in temperature profile may be caused by cool fluid flowing from the surface or hot fluid flowing from the reservoir. Moreover, the operating conditions may include a pressure imposed at the surface (by pumping operations such as a pressure test or a fracturing operation) or coming from downhole (from the reservoir pressure through perforations or from a kick influx).

Another benefit of using commercial software or an in-house program is that most load cases are predefined. The software user simply selects a load case for analysis from a menu, and the program determines the changes in fluid densities, pressures, and temperatures from other program inputs. As a hypothetical example, if the user selects “hot production” conditions for a tubing string, the program might replace the packer-fluid density present when the tubing was installed by the density of the production fluid, calculate the flowing reservoir pressure, and calculate the temperature profile for a user-specified flow rate.

The program then uses the pressure and temperature changes from initial to operating conditions to calculate the change in tension load and thus the change in stress state. The final load conditions and stress state are compared to the resistance or capacity defined for the tubulars selected for the well. Results are often reported in terms of the ratio of capacity to load or stress (called the *safety factor*) or in terms of the ratio of load to capacity (called the *utilization factor*). The engineer evaluating the selected tubulars for the intended service must compare the safety factor or utilization factor with the design standard imposed by the company or regulatory body. The engineer should review the results carefully and make sure that the pressures and temperatures used in the analysis reflect the intent of the inputs.

The importance of understanding the assumptions made by software when defining the load case to be analyzed, as well as understanding how the inputs are being used in the calculations, cannot be overemphasized. The drilling engineer and the programmer may have slightly different definitions for a load case or an input. Commercial software often incorporates input range checks to provide a warning if an input is inappropriate or not what the programmer intended.

Several input fields require careful attention when the user defines a tubular analysis. The directional survey should have a suitable number of stations to define the well path—one survey station per drillpipe stand is appropriate in long-radius build sections. Too many survey stations may result in unrealistically high calculated dogleg curvatures and bending loads, but too few survey stations may not capture the tension loads from the dead weight of the tubular. Pore pressures and fracture gradients should be defined at each casing point and at the transition to overpressure in the well. Geothermal temperatures may be defined by two or three points or by a simple gradient, but flowing or injecting operating conditions should be modeled using more temperature stations. Some programs calculate and present results at each depth defined by a survey station, a pore-pressure or fracture-pressure station, or a temperature station, so it may be prudent to limit the number of stations to facilitate review of the analysis results.

The initial effort to define the well conditions and the tubular string properly may be difficult, but the effort pays off when a different design must be considered—for example, if the selected tubular does not meet the application requirements or is not available for purchase. “What-if” analysis is easily performed using a computer program. In addition to changing the tubular size, weight, or grade, the user can vary the depth of the top of cement or the amount of tension applied when the slips are set.

For casing designs for directional wells, computer-based analysis is essential. The computer can easily use survey results to interpolate the positions of calculation stations and keep track of the measured depth (which determines the length of pipe above and below each calculation station) and the true vertical depth (which determines the hydrostatic pressure of a column of fluid).

Computer-based analysis typically considers casing strings to be fixed at the wellhead and at the top of cement when it sets. It typically considers tubing strings to be fixed at the wellhead, but they may be fixed at the packer

or allowed to move under operating conditions if a floating-seal configuration is defined. Specialized analysis offered by at least one commercial program allows the wellhead to move under operating conditions (particularly high thermal loads). All the casing and tubing strings defined for the well in this type of analysis must “grow” by the same amount, and axial loads may be redistributed among the strings to satisfy this constraint.

Some commercial programs have optimization capability and can determine the lowest-cost tubular design that meets the load requirements defined by the user. This design capability is a powerful tool that can present options that the user might not have considered. A common limitation of design routines is that the actual cost of a specific tubular is not reflected in the “cost/ton by grade” that is typically specified.

Stress-analysis results from computer programs are a good representation of the pipe body. However, the results do not completely define the stress state of the threaded connections for each joint along the string. The tension, pressure, and temperature results obtained from computer-based analysis can be compared with performance envelopes available from the thread manufacturer or from ISO and API standards. These standards are often available in commercial design programs, and connector manufacturers often have the necessary design data available.

Most computer programs for casing-stress analysis do not consider the suitability of the selected material for the application environment. The potential for stress cracking due to corrosion or sulfides should be evaluated separately from the stress analysis.

7.12 Casing Stability

When a casing string is hanging freely in a vertical well, the burst, collapse, and axial loads can be accurately calculated, and the string will be as straight as the well allows. After the primary cement is pumped, the casing will be hanging freely in the fluid cement, and again the loads in the string can be accurately calculated. After some time waiting for the cement to set, the string is typically landed in a wellhead with a surface tensile load. This essentially fixes the length of the string between the wellhead and the top of cement. With time, the temperature, as well as both the internal and external pressures, change, resulting in changes in the length of the casing.

With a fixed length of casing and the external pressure unchanged from cementing conditions, an increase in internal pressure or a decrease in temperature causes the casing length to contract. Because the casing length is not free to change, axial load increases. If the external pressure around a casing decreases or the temperature increases from the initial setting conditions and the internal pressure remains unchanged, the casing length will increase, and axial stress in the casing will be reduced.

A method is needed to calculate the axial load changes that may result from changes in temperature or from internal or external pressures in the uncemented portion of a string. The general equation for calculating the change in axial load in an uncemented tubular due to changes in temperature or internal or external pressure is

$$\begin{aligned}
 \text{(a) } \Delta L_1 + \Delta L_2 + \Delta L_3 + \Delta L_4 &= 0 \\
 \text{(b) } \Delta L_1 &= \int \frac{\Delta(F_a + \delta F)}{EA_s} ds \\
 \text{(c) } \Delta L_2 &= \int \Delta e_b ds \\
 \text{(d) } \Delta L_3 &= \int \frac{2\nu[\Delta P_e A_e - \Delta P_i A_i]}{EA_s} ds \\
 \text{(e) } \Delta L_4 &= \int \alpha_T \Delta T ds, \dots\dots\dots (7.57)
 \end{aligned}$$

where ν is Poisson’s ratio, δF is the correction load necessary to solve Eq. 7.57a, e_b is the buckling incremental length change, and α_T is the pipe coefficient of thermal expansion. Eq. 7.57a says that the total length change is zero, Eq. 7.57b is the length change due to change in axial force, Eq. 7.57c is the length change due to buckling (addressed later in this section), Eq. 7.57d is the length change due to pressure changes (ballooning), and Eq. 7.57e is the length change due to thermal expansion. All changes are relative to the initial conditions. We must solve for δF to satisfy Eq. 7.57a. The average thermal coefficient of expansion, α_T , for low-alloy steel is approximately $6.9 \times 10^{-6}/^\circ\text{F}$. High-alloy steels typically have a slightly higher coefficient of thermal expansion. Eq. 7.57 should be used only if the axial stress is less than the yield stress and the tubular has not buckled. This equation assumes that the length of the tubular is restrained, which is not always the case in real wells. A tubular inside another tubular with a common length for both tubulars (fixed at top and bottom) will strain and load differently from a single tubular, even with the same average temperature differential. The two tubulars will almost always have different

cross-sectional steel areas. Accurate temperature modeling is best performed using computer programs, which can consider interactions between many casing strings in a well and can even model the change in temperature as the distance from the center of the well increases.

As discussed above, after a string has been cemented, the axial loads in the uncemented portion of the string will change due to changes in internal and external pressures and in temperature. Lubinski et al. (1962) have proved that when pressure acts on the inside walls and not on the ends of a tube, the pressure tends to deflect or bend the tube. Pressure acting on the outside walls and not on the ends tends to prevent deflection. They observed that in some cases an imbalance between internal and external pressures can cause a tubular to buckle or bend. This is called a *loss of stability*. They determined that a loss of stability would occur when the axial load in the tube was below a critical stability load. The critical stability load at a specific vertical well depth can be calculated using the following equation:

$$F_e < 0. \quad (7.58)$$

Remember that F_e is the effective tension, so buckling happens only for compressive (negative) loads. Note that stability can be lost in a string even though axial load is significant; the axial load does not need to be a compressive load. The depth where the axial load equals the critical stability load is called the *stability neutral point*. Why does internal pressure destabilize the casing? If we return to Eq. 7.48, we see that we did not consider all the loads, only the axial loads. A particularly interesting load is the second term in Eq. 7.59:

$$\frac{dF_e}{ds} \bar{t} + F_e \frac{d\bar{t}}{ds} + w_{bp} \bar{t}_z + \bar{w}_c = 0. \quad (7.59)$$

The calculus of a curve in space (Zwillinger 1996) says

$$\frac{d\bar{t}}{ds} = \kappa \bar{n}, \quad (7.60)$$

where κ is the pipe curvature and \bar{n} is the unit vector lying in the plane of the curvature perpendicular to the pipe axial direction, as shown in Fig. 7.29. This means that axial force plus pressure on a curved pipe generates a side load w_{lateral} :

$$w_{\text{lateral}} = F_e \kappa. \quad (7.61)$$

What is the sense of this result? In Fig. 7.29, we can see that there is an excess of area on the side of the pipe on the outside of the bend. The internal pressure on this additional area will generate a side force. Any residual bend in the pipe will generate a load that will increase the bend if Eq. 7.58 is satisfied, and as the bend increases, Eq. 7.61 says that the lateral load increases.

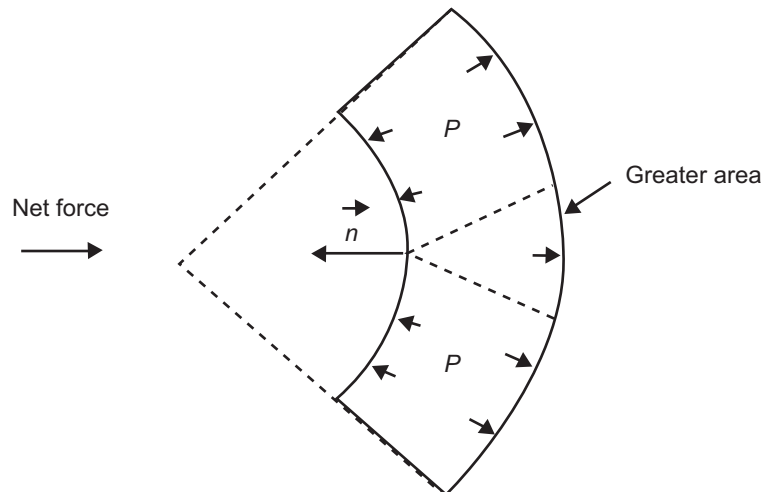


Fig. 7.29—Lateral load from internal pressure.

At the depth where the axial and stability loads are equal, the string is stable, because the lateral load tends to straighten the pipe. As the axial load becomes increasingly less than the stability load, the amount of bending in the string increases (increasing loss of stability). If the axial load is greater than the stability load, the string will remain in its stable unbuckled condition. The degree to which a string can buckle or bend will also depend on the size of the hole or casing in which it is installed.

The minimum axial load in the uncemented portion of a string will typically be at the top of cement. As well depth decreases, effective tension will increase. If a string becomes unstable, loss of stability occurs first at the lowest point, where the effective tension is at a minimum and the string is free to move laterally. Maximum buckling of the string will take place at this depth. With decreasing well depth, the axial load of a buckled string will typically approach the stability load, and the amount of buckling in the string will decrease. At shallower depths, where the axial load exceeds the stability load, the string will not buckle, as illustrated in **Fig. 7.30**.

Dellinger and McLean (1973) have presented evidence that casing wear from drilling in buckled strings is much more severe than in normal drilling, especially when the borehole diameter has been increased due to washout. Today, computer programs are available to calculate casing-string wear related to bending or buckling in a string and to other physical conditions. When drilling under high-pressure, deep, or high-temperature conditions, drilling times are often long. Even a small amount of buckling or bending when rotating time is long may lead to unacceptable levels of wear. Drillstring wear in a short-duration well with minor buckling may be minimal. Wear-mitigation plans should include management of the buckling and bending in a casing string, choice of drillstring hardbanding, use of downhole mud motors or turbines to reduce drillstring rotation, and designing strings with extra wear allowance. Drilling time on many deep critical wells often greatly exceeds original expectations, and the wear-management plan should consider these unplanned events and the future life of the well.

Although stable at the time of installation, a string may become unstable in subsequent operations as changes in pressure occur inside and outside the casing, and as temperatures change. It may be desirable to keep the casing

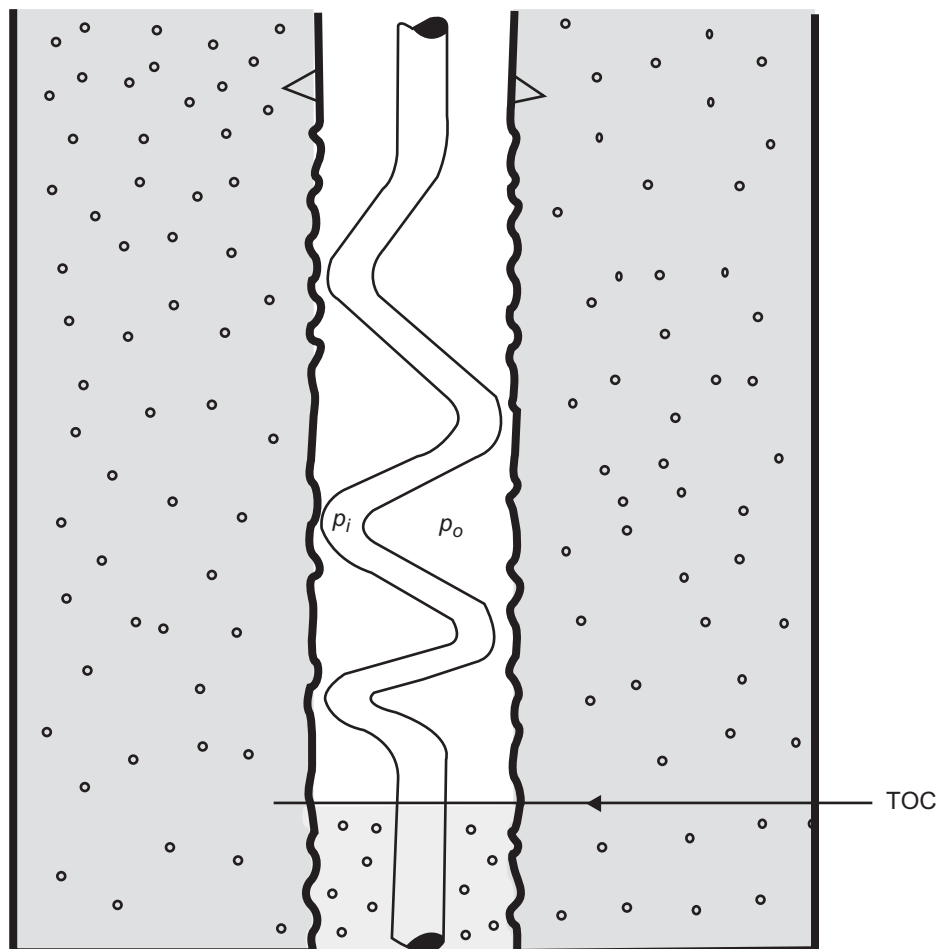


Fig. 7.30—Casing buckling.

in the straight unbuckled condition during some operations, such as when drilling through the casing. In other conditions, such as when internal well pressure is present while circulating out a kick, casing buckling may be limited to low but acceptable levels.

Several options exist to reduce buckling in a string. Any one (or combinations) of these options can be used to increase the axial load where the string is free to move. These methods are generally used to adjust the axial load during or after cementing to result in specified loads at a future time of interest. These methods are

- Adjust cement height.
- Mechanically pull or slack off axial load after the casing below the top-of-cement has become fixed in the cement.
- Apply internal pressure at the surface until both ends of the string become fixed.

The usual procedure used with casing is to adjust cement height. In some cases, an additional axial load is added after the cement has set. Application of internal pressure while the cement sets is usually not desirable with casing. The internal pressure must be applied when the casing is free to respond to pressure—that is, before the casing becomes stuck. With a decrease in the depth to the top of cement or with addition of a mechanical load, the axial load at the top of cement will increase, thus increasing casing stability and discouraging bending.

In an inclined wellbore with angle ϕ , the string lies against the low side of the hole and therefore is supported laterally. This lateral support changes the loads at the points where the string may buckle. A casing will not buckle until the axial compression ($-F_c$, i.e., F_c positive is tension) exceeds the critical force F_c , given by the Paslay-Dawson equation (Dawson and Paslay 1984):

$$F_c = \sqrt{\frac{4EIw_c}{r_c}}, \quad \dots\dots\dots (7.62)$$

where E is Young's modulus (30×10^6 psi for steel), and I is the moment of inertia:

$$I = \pi/4 (r_o^4 - r_i^4), \quad \dots\dots\dots (7.63)$$

r_c is the radial clearance:

$$r_c = r_w - r_o, \quad \dots\dots\dots (7.64)$$

r_w is the wellbore radius, and w_c is the contact force. For a straight pipe, w_c has the simple form:

$$w_c = w_{bp} \cos \phi. \quad \dots\dots\dots (7.65)$$

This equation applies to wellbores that are inclined but not curved (see He and Kyllingstad 1995). Buckling in areas of a wellbore where the angle is changing is more difficult to assess (Mitchell 2008). Initial buckling is lateral (side-to-side) buckling, but when the axial compression exceeds approximately $2F_c$, the buckling is helical (i.e., shaped like a coil spring).

In some cases, it is acceptable to have some degree of instability or buckling in a casing string. The level of acceptable curvature will depend on many well factors, including rotating hours, drillstring tensions, and other wellbore conditions. If buckling is present, then stress may be induced in the casing. Loads due to buckling can be calculated and should be considered as an additional stress in the casing. If a string is unstable (i.e., the axial load is less than the stability load), then the dogleg in the casing at that depth due to instability can be calculated using the following equation:

$$\kappa = \frac{-r_c F_e}{2EI}. \quad \dots\dots\dots (7.66)$$

(The curvature unit in this equation is radians/in., which is convenient for most calculations. For conversion to common field units of degrees/100 ft, multiply by 6.875.) Note that the ID of the wellbore impacts the severity of the dogleg resulting from buckling. An enlarged hole due to washout would increase the dogleg, but if the hole

were of the same diameter as the casing OD, no dogleg would be created. The bending stress at any point r in the cross-section of the pipe can be calculated using the following equation:

$$\sigma_b = \pm Er\kappa. \quad (7.67)$$

Bending stress can be either positive (tension) or negative (compression), depending on whether the stress is calculated for the inside or the outside of the casing bend.

A buckled string is shorter than an unbuckled string. This is easily seen by the example of pulling on a coiled spring. As the spring extends, the wire straightens and elongates. The change in casing length for helical buckling is determined by the following equation (see Eq. 7.57):

$$\Delta L_2 = \int e_b ds$$

$$e_b = \frac{r_c^2 F_e}{4EI}. \quad (7.68)$$

The exact form of the solution depends on how the effective tension varies along the string. For a vertical well,

$$F_e = F_e^0 - w_{bp}(s - s_0). \quad (7.69)$$

Substituting Eq. 7.68 into Eq. 7.69 and integrating over the buckled length from F_e^0 to F_e ,

$$\Delta L_2 = \frac{r_c^2}{2EIw_{bp}} \left[(F_e^0)^2 - (F_e)^2 \right]. \quad (7.70)$$

Example 7.8 A 9.625-in., 53.5-lbf, C-95 grade intermediate casing string is set at 11,600 ft in a vertical well. The top of primary cement (TOC) is planned at 8,000 ft, and only 15-lbm/gal cement will be used. The string had a 9.6-lbm/gal mud inside and outside at the time that the string was cemented. The next step is to hang the 9.625-in. casing in the wellhead without any doglegs in the string due to buckling or temperature changes. The design case is after cementing and during deeper drilling. At the design time of interest, the average temperature increase from the top of cement to the surface has been determined to be 20°F. Also at the design time of interest, the internal mud weight is 16 lbm/gal, and the casing has 2,000 psi surface pressure. Calculate the “as cemented” buoyed weight of the string and how much (if any) tension should be added after the cement sets to prevent buckling from occurring. Calculate the value of the dogleg at the top of cement if this tension were not added after the cement had set.

Solution. The axial load at the top of cement in the “as cemented” condition is

$$F_{8,000 \text{ ft}} = w(Z_c - Z_{\text{TOC}}) + (P_i (\pi d^2)/4) - (P_e (\pi d_n^2)/4),$$

$$F_{8,000 \text{ ft}} = 53.5 (3,600) + (9.6)(0.052)(11,600)(57.21) - ((9.6)(0.052)(8,000) + (15.0)(0.052)(3,600))(72.76),$$

$$F_{8,000 \text{ ft}} = +29,003 \text{ lbf.}$$

The load due to buckling at the time of interest, noting that ν is 0.3 for steel, is:

$$\Delta F_{8,000 \text{ ft}} = (0.052)(0.3)(15.546 \text{ in.}^2)(8,000)[(16 - 9.6) - (9.625/8.535)^2(9.6 - 9.6)/((9.926/8.535)^2 - 1)] + (0.6)(15.546)[(2,000 - 0) - (9.625/8.535)^2(0 - 0)/((9.625/8.535)^2 - 1)],$$

$$\Delta F_{8,000 \text{ ft}} = 114,350 \text{ lbf.}$$

The load change from the “as cemented” condition resulting from an average temperature change of 20°F can be calculated as follows, assuming $\alpha_T = 6.9 \times 10^{-6}$:

$$\Delta F_a = (A_s)(30 \times 10^6)(6.9 \times 10^{-6})(20);$$

$$\Delta F_a = (A_s)(207)(20);$$

$$\Delta F_a = (15.546)(207)(20);$$

$$\Delta F_a = -64,360 \text{ lbf.}$$

The axial load at the time of interest at the top of cement at 8,000 ft would be

$$F_{8,000 \text{ ft}} = (29,003 + 114,350 - 64,360) \text{ lbf},$$

$$F_{8,000 \text{ ft}} = 78,983 \text{ lbf}.$$

The stability load at the top of cement at 8,000 ft is

$$F_r = (2,000 + (16.0 (0.052)(8,000))(57.21)) - (9.6)(0.052)(8,000)(72.76),$$

$$F_r = 204,635 \text{ lbf},$$

$$F_p = F_r - F_a,$$

$$F_p = (204,635 - 78,983) \text{ lbf},$$

$$F_p = 125,650 \text{ lbf}.$$

At the time of interest, it would be necessary to add this amount of tension to the suspended weight of the “as cemented” string to prevent it from buckling due to changes in pressures and temperatures from the “as cemented” conditions.

If this tension were not added after the cement set, the casing would buckle at the top of cement, resulting in a dogleg. If the hole were washed out to 13 in. just above the top of cement, then

$$\kappa = ((1.146 \times 10^{-3})(r)(F_r - F_a))/I,$$

$$\kappa = (1.146 \times 10^{-3}) ((13 - 9.625)/2) (204,635 - 78,983)/160.8,$$

$$\kappa = 1.5 \text{ degrees}/100 \text{ ft}.$$

7.13 Special Casing-Design Considerations

In the previous section, casing-design considerations were based on selected burst, collapse, and axial-tension loading conditions. Although these loading conditions are important in the design of all casing strings, other loading conditions also can be important and should be recognized by the student. These additional loading conditions can be caused by shock loading, cementing operations, and other conditions such as subsidence, permafrost, and formation compaction.

7.13.1 Cementing Casing. Primary and remedial squeeze-cementing operations can also result in design conditions that exceed the conditions based on maximum anticipated pressures during the producing life of the well. During cement pumping, the casing is subjected to internal pressure as the cement is displaced outside the casing. Moreover, the fluid used to displace the cement often has a lower density than the fluid that was pumped ahead of the cement. It is common to bump the wiper plug with sufficient pressure to ensure that the design primary-cement volume is pumped outside the casing. The internal pressure used to bump the wiper plug causes burst loads on the casing and also axial stresses. The surface pressure inside the casing can cause an axial load, which is given by

$$\Delta F_a = \frac{1}{4} p_i \pi d^2. \quad \dots \dots \dots (7.71)$$

Typically, primary cement is composed of a lead and tail cement that are of higher density than the fluid in which the casing is cemented. This can result in the imposition of collapse loads on the casing. In cases with large cement/mud density differences and substantial cement heights, collapse design for cementing operations can present significant challenges. Caution must be exercised during cementing operations to ensure that none of the burst rating, the collapse rating, and the tension rating of the casing is exceeded.

7.13.2 Effect of Field Handling on Casing. The performance properties that a given casing joint will exhibit in the field can be adversely affected by certain field operations. For example, burst strength can be significantly affected by the procedure and equipment used to make up the pipe. Tests have shown that burst strength can be reduced by as much as 70% by combinations of tong marks that penetrate 17% of the wall thickness and 4% out-of-roundness caused by excessive torque.

Mechanical deformations can also occur while the casing is being transported to the well or while it is being run into the hole. Any mechanical deformity in the pipe normally results in a considerable reduction of its collapse resistance. This is especially true for casing with a high d_o/t ratio. Tubulars used in sour service can also be stress-hardened by careless handling. Stress hardening can cause changes in a tube's resistance to certain hostile environments. To mitigate

these problems, special casing-running tools and methods have been developed and are available that will minimize mechanical damage to a string when it is run.

API RP5C1 (1999) lists common problems experienced with tubulars and gives recommendations for good pipe-handling procedures.

7.13.3 Other Special Casing-Design Considerations. Formation subsidence often occurs as pore fluids are produced and reservoir pressures decline. This subsidence can cause significant compressive axial loads which cannot be neglected in casing design. Significant axial loads can occur along the wellbore and also in the reservoir. Some well designers place a section of very-heavy-wall production casing opposite the producing interval to prevent casing damage due to reservoir compaction. Axial stress resulting from subsidence tends to be greatest in soft soil with a low Young's modulus value.

In some areas, the fluids remaining in casing annuli are confined in a fixed volume by cementing operations. When the well heats up, these fluids expand slightly, causing increased pressure in the annulus (Adams 1991). This annular pressure buildup can result in high collapse loads on the inner string or burst loads on outer strings. Computer programs are available to model annulus pressure buildup and its impact on casing burst and design requirements. An example where high strains resulting from heating have an impact on casing designs is that of a subsea well where access to casing annuli is not available; this makes it impossible to vent any pressure resulting from heating.

In wells in Arctic environments, fluids left in casing annuli may freeze due to low ambient temperatures or the presence of permafrost. The resulting loads tend to lead to collapse of tubulars due to expansion of fluids when they freeze. Methods exist to approximate the additional collapse loads due to freezeback; however, they depend upon the accuracy of determination of the wellbore thermal profile during freezeback.

Permafrost can generate casing-string loads as the formation moves outside the casing when pore water outside the casing goes through the freeze/thaw cycle. Both axial loads and collapse loads can be generated in this process. Computer programs have been developed to model loading due to permafrost, which is a very complex interaction.

When casing is set through a salt formation, the salt can plastically deform under stress, resulting in very high collapse loads. Although experience in an area often drives the casing design for salt collapse, many engineers design these strings to withstand a collapse load in the salt that is equal to the overburden. The salt temperature, composition, bedding, inclusions, and purity all factor into how the salt will load a casing string. In some areas, salt in a well does not creep uniformly into the casing, but rather creeps in over a fairly small arc of the wellbore. This type of point loading places very high collapse loads on the casing, which can greatly exceed the overburden pressure.

When casing is being run, the axial stresses resulting from modest running-speed changes are normally not severe. Significant shock loading can develop if a casing string is suddenly stopped while running. Methods to estimate shock loads during casing-running operations form part of advanced drilling technology.

Problems

- 7.1 Discuss the functions of the following casing strings:
 - (a) Conductor casing
 - (b) Surface casing
 - (c) Intermediate casing
 - (d) Production casing
- 7.2 Discuss the advantages of using a liner rather than a full-length casing string.
- 7.3 Name the two basic processes used to manufacture casing.
- 7.4 What is the diameter range of API casing?
- 7.5 Give the three length ranges of casing specified by API.
- 7.6 Define the following terms:
 - (a) Nominal weight
 - (b) Plain-end weight
 - (c) Nominal ID
 - (d) Drift diameter
- 7.7 For each connection, state the number of threads per inch and the pitch:
 - (a) STC
 - (b) LC
 - (c) BC
- 7.8 Consider a 9 $\frac{5}{8}$ -in. 43.5-lbf/ft N-80 production casing in an 11,000 ft vertical well, with top of cement at 8,000 ft. The casing is run in 11 lbm/gal water-based mud.

- (a) What is the hanging weight in air for the casing? *Answer:* 478,500 lbf.
 - (b) What is the hanging weight as run? *Answer:* 394,500 lbf.
 - (c) If we assume 15 lbm/gal cement and 11 lbm/gal displaced mud, what is the surface hanging stress after cementing, and what is the margin of safety for this string? *Answer:* 31,181 psi.
 - (d) Next, consider the effects of a stimulation treatment on this surface stress. Assume that the average temperature change in the surface-to-8,000 ft interval is -50°F , (the coefficient of thermal expansion is $6.9 \times 10^{-6}/^{\circ}\text{F}$, and Young's modulus is 30×10^6 psi for steel). What is the net surface stress in the casing? *Answer:* 41,531 psi.
- 7.9 Calculate the API casing-body burst performance property for 10.75-in., 40.5-lbf, K-55 casing that has a nominal wall thickness of 0.40 in.
- 7.10 Assume that we have 13 $\frac{3}{8}$ -in., 72-lbf/ft N-80 intermediate casing set at 9,000 ft and cemented to surface.
- (a) What is the burst differential pressure for this casing? *Answer:* 5,380 psi. Consider a displacement to gas case, with formation pressure of 6,000 psi, formation depth at 12,000 ft, and a gas gradient equal to 0.1 psi/ft. What is the surface internal pressure? *Answer:* 4,800 psi.
 - (b) If the external pressure is zero, the casing is strong enough to resist this burst pressure. Surface axial stress is the casing weight divided by cross-sectional area (20.77 in.²) less pressure loads when cemented (assume 15 lbm/gal cement). What is the surface axial stress? *Answer:* 24,182 psi tensile.
 - (c) The radial stresses for the internal and external radii are the internal and external pressures. Using the Lamé formula, calculate the internal and external hoop stresses, assuming the external pressure is zero. *Answer:* 60,152 psi and 55,352 psi.
 - (d) What is the von Mises equivalent stress or triaxial stress at the inside radius and at the outside radius? *Answer:* 52,426 psi and 47,905 psi.
 - (e) Compare the burst calculation to the von Mises calculation for this case, and discuss.
- 7.11 Calculate the API collapse rating for 7-in., 38-lbf, N-80 casing with no axial load.
- 7.12 Calculate the API collapse rating of 7-in., 38-lbf, N-80 casing when the casing has an axial load of 400 kip.
- 7.13 Test the collapse resistance of a 7-in., 23-lbf/ft P-110 liner cemented from 8,000 to 12,000 ft. Comparing the 7-in. liner properties against the various collapse regimes, it was found that transition collapse was predicted for this liner. The collapse pressure for this liner is calculated using $F = 2.066$, $G = 0.0532$.
- (a) What is the collapse pressure? *Answer:* 4,440 psi.
 - (b) To evaluate the collapse of this liner, we need internal and external pressures. Internal pressure is determined using the full evacuation above packer. If we assume a 0.1 psi/ft pressure gradient, what is the internal pressure at the base of the liner? *Answer:* 1,200 psi.
 - (c) The external pressure is based on a fully cemented section behind the 7-in. liner. The external pressure profile is given 10 lbm/gal mud above the top of cement with an internal mix-water pressure gradient of 0.45 in the cement column. What is the external pressure at the base of the liner? *Answer:* 5,960 psi.
 - (d) What is the equivalent pressure for comparison with the collapse pressure P_c ? *Answer:* 4,869 psi.
 - (e) Is it appropriate to calculate a von Mises stress for collapse in this case? *Answer:* No, because collapse in the transitional region is not strictly a plastic yield condition.
- 7.14 Assuming typical hole sizes are used, what sizes of intermediate string and surface string would be used if a 5 $\frac{1}{2}$ -in. production string were required?
- 7.15 For 5 $\frac{1}{2}$ -in., 23-lbf casing with either BC or LC standard connections, which grades would fail in axial tension by pipe-body failure before a connection failure occurred?
- 7.16 Develop a spreadsheet to calculate the API round-thread minimum coupling fracture strength and the API minimum joint pullout (or thread jumpout). Does coupling fracture strength or joint pullout result in the lesser connection-joint-strength value for 7-in., 32-lbf, N-80 casing with standard LC connections?
- 7.17 What is the H₂S partial pressure when the maximum pressure is 10,000 psi and the volume fraction of H₂S is 5 ppm?
- 7.18 If a 120-ft length of 16-in., 84-lbf, J-55 casing were restrained from axial movement at both the top and bottom ends, how much force would be imparted to the casing if the average temperature of the casing increased by 20°F?

- 7.19 What is the equivalent axial force caused by a $9\frac{5}{8}$ -in., 43.0-lbf casing bending in a 2.0 deg/100 dogleg? Assume uniform contact between the casing and the borehole wall.
- 7.20 Consider a $2\frac{7}{8}$ -in., 6.5-lbf/ft tubing inside of 7-in., 32-lbf/ft casing. The tubing is submerged in 10 lbm/gal packer fluid with no other pressures applied. The effect of the packer fluid is to reduce the tubing weight per unit length through buoyancy.
- What is the buoyant weight of the tubing? *Answer:* 5.56 lbf/ft, or 0.463 lbf/in.
 - Given that the moment of inertia I is 1.611 in.^4 , the radial clearance is 1.61 in., and Young's modulus = 30×10^6 psi, determine the critical buckling load for the angles 10° , 30° , 60° , and 90° and comment on your results. *Answer:* 3,107 lbf, 5,272 lbf, 6,939 lbf, and 7,456 lbf. Notice how quickly the critical load increases with small angles. At only 10° , the critical load is easily half of the maximum critical load.
 - Assume we have a 10,000-ft vertical tubing string with an effective tension at the bottom of the string of 30,000 lbf compression. Is the string buckled, and what is the maximum bending stress due to buckling? *Answer:* The string is buckled, and the maximum bending stress is 21,550 psi.
 - Where is the neutral point of the string? *Answer:* 4,604 ft.
 - What is the buckled length change of this string? *Answer:* 4.34 ft.

Nomenclature

A	=	area
A_1	=	coupling hand-tight standoff, in.
A_e	=	outer pipe area enclosed by nominal OD
A_i	=	inner pipe area enclosed by nominal ID
A_{jp}	=	steel area under last perfect thread
A_s	=	steel cross-sectional area
A_{sc}	=	steel area in coupling
BF	=	buoyancy factor
c_0 – c_{10}	=	collapse equations coefficients
d	=	nominal ID of pipe
d_{c1}	=	diameter at root of coupling thread at end of pipe in power-tight position
d_{c2}	=	OD of coupling
d_m	=	maximum pipe body ID based on minimum specified wall thickness
d_n	=	nominal OD of pipe
e_B	=	buckling “strain”
E	=	Young's modulus of elasticity
E_1	=	coupling pitch diameter at the hand-tight plane, in.
E_7	=	thread pitch diameter, in.
f	=	wall-thickness correction factor
F	=	force
F_1 ... F_5	=	factors used in the applicable collapse formula
F^a	=	axial force
F^{ab}	=	increased axial force due to bending
F^c	=	critical force to initiate buckling in an inclined hole
F^{cr}	=	axial tension strength of joint
F^e	=	effective tension
F_p	=	required added tension to keep casing in unbuckled condition
F_r	=	stability load
F_{ten}	=	tension force
F_z	=	axial tension including bending
g	=	gravity constant
g_p	=	pore-pressure gradient expressed as equivalent mud density
H_1	=	thread height, in.
\vec{i}_z	=	downward direction vector
I	=	moment of inertia
I_1	=	distance from basic hand-tight position, in.
J_p	=	polar moment of inertia
L	=	length
L_1	=	length from end of pipe to hand-tight plane, in.

L_7	=	length of perfect threads
L_{et}	=	engaged thread length, in.
M	=	gas molecular weight
\bar{n}	=	normal direction vector
P	=	absolute pressure
P_{br}	=	burst pressure rating
P_{cr}	=	collapse pressure rating
P_e	=	external pressure
P_{eq}	=	external pressure equivalent in collapse due to external and internal pressure
P_{max}	=	maximum surface equipment pressure
P_i	=	internal pressure
P_{inj}	=	injection pressure, psi
r	=	radius
r_c	=	radial clearance of annulus
r_i	=	inner radius
r_w	=	wellbore or outer casing radius
r_o	=	outer radius
R	=	universal gas constant
R_F	=	parameter in collapse equations
s	=	measured depth
S_m	=	round-thread distance from pin top of thread to coupling base of thread, in.
t	=	thickness
\bar{t}	=	axial direction vector
T	=	absolute temperature
T_l	=	thread taper, in./in.
w	=	weight per foot
w_{bp}	=	buoyant weight per foot of pipe
\bar{w}_c	=	contact force load vector
\bar{w}_{ef}	=	external fluid load vector on casing
\bar{w}_{if}	=	internal fluid load vector on casing
$w_{lateral}$	=	side load produced by axial force plus pressure on a curved pipe
w_p	=	weight per foot of pipe in air
z	=	gas compressibility factor
Z	=	true vertical depth
Z_c	=	depth of casing
Z_{lc}	=	depth of lost-circulation zone
Z_{toc}	=	depth to top of cement
Z_m	=	depth of mud surface
α_T	=	temperature coefficient of expansion
δF	=	axial force increment to ensure zero length change
Δ	=	change
ΔA_e	=	change in outside area of casing
ΔA_i	=	change in inside area of casing
ΔL	=	length change
ΔL_1	=	length change due to axial forces
ΔL_2	=	length change due to buckling
ΔL_3	=	length change due to ballooning
ΔL_4	=	length change due to thermal expansion
ΔP_e	=	change in external pressure
ΔP_i	=	change in internal pressure
ΔT	=	change in casing temperature
ε	=	strain
κ	=	dogleg severity
ν	=	Poisson's ratio
ρ_e	=	fluid density outside casing
ρ_g	=	gas density
ρ_i	=	fluid density inside casing

ρ_m	=	mud density
ρ_{\max}	=	maximum mud density
ρ_s	=	steel density
σ	=	stress
σ_a	=	total axial stress, not including bending due to hole deviation, doglegs, or buckling
σ_b	=	bending stress
σ_{pa}	=	equivalent yield strength
σ_r	=	radial stress
σ_t	=	tangential stress
σ_{ult}	=	ultimate strength
σ_{yield}	=	yield strength
σ_{vm}	=	von Mises triaxial equivalent stress
σ_z	=	total axial stress including bending
τ	=	shear stress
φ	=	angle of inclination of the wellbore

Subscripts

+	=	upsteam
−	=	downstream

References

- Adams, A.J. 1991. How to Design for Annulus Fluid Heat-up. Paper SPE 22871 presented at the SPE Annual Technical Conference and Exhibition, Dallas, 6–9 October.
- API Bull. 5C2, *Bulletin on Performance Properties of Casing, Tubing, and Drill Pipe*, 21st edition. 1999. Washington, DC: API.
- API RP 5A3/ISO 13678, *Recommended Practice on Thread Compounds for Casing, Tubing, and Line Pipe*, 2nd edition. 2003. Washington, DC: API.
- API RP5C1, 1999. *Recommended Practice for Care and Use of Casing and Tubing*, 18th edition. May 1999. Washington, DC: API.
- API Spec. 5B, *Specification for Threading, Gauging, and Thread Inspection of Casing, Tubing, and Line Pipe Threads*, 15th edition. 2008. Washington, DC: API.
- API Spec. 5CT/ISO 11960, *Specification for Casing and Tubing* (includes Errata dated April 2006), eighth edition, 2005. Washington, DC: API.
- API Spec 5L/ISO 3183, *Specification for Line Pipe*, (includes Errata, January 2009 and Addendum, February 2009), 44th edition. 2007. Washington, DC: API.
- API TR 5C3, *Bulletin on Formulas and Calculations for Casing, Tubing, Drill Pipe, and Line Pipe Properties*, seventh edition. 2008. Washington DC: API.
- Baker Oil Tools. 1993. *Tech Facts: Engineering Handbook*. Houston: Baker Hughes, Inc.
- BJ Titan Services *Engineering Handbook of Technical Information*. 1987. BJ Titan Services, Houston.
- Boresi, A.P. and Schmidt, R.J. 2002. *Advanced Mechanics of Materials*, sixth edition. New York City: John Wiley & Sons.
- Brand, P.R., Whitney, W.S., and Lewis, D.B. 1995. Load and Resistance Factor Design Case Histories. Paper OTC 7937 presented at the Offshore Technology Conference, Houston, 1–4 May.
- Crandall, S.H. and Dahl, N.C. 1959. *An Introduction to the Mechanics of Solids*, 288. New York City: McGraw-Hill Book Company.
- Dawson, R. and Paslay, P.R. 1984. Drillpipe Buckling in Inclined Holes. *J Pet Technol* **36** (10): 1734–1738. SPE-11167-PA. DOI: 10.2118/11167-PA.
- Day, J.B., Moyer, M.C., and Hirshberg, A.J. 1990. New Make-Up Method for API Connections. *SPE Drill Eng* **5** (3): 233–238. SPE-18697-PA. DOI: 10.2118/18697-PA.
- Dellinger, T.B. and McLean, J.C. 1973. Preventing Instability in Partially Cemented Intermediate Casing Strings. Paper SPE 4606 presented at the SPE Annual Meeting, Las Vegas, Nevada, USA, 30 September–3 October. DOI: 10.2118/4606-MS.
- Economides, M.J., Watters, L.T., and Dunn-Norman, S. 1998. *Petroleum Well Construction*, 202, Fig. 7–30. New York: John Wiley & Sons.
- Greenip, J.F. 1978. Designing and Running Pipe. *Oil and Gas J.* (9, 16, and 30 October and 13 and 27 November).

- Gulati, K.C., McKenna, D.L., Maes, M.A., Johnson, R.C., Brand, P.R., Lewis, D.B., Riekels, L., and Maute, R.E. 1994. Reliability-Based Design and Application of Drilling Tubulars. Paper OTC 7557 presented at the Offshore Technology Conference, Houston, 2–5 May. DOI: [10.4043/7557-MS](https://doi.org/10.4043/7557-MS).
- Halliburton, 2001, The Red Book: Halliburton cementing tables, Halliburton Company, Duncan, Oklahoma.
- He, X. and Kyllingstad, A. 1995. Helical Buckling and Lock-Up Conditions for Coiled Tubing in Curved Wells, *SPE Dril & Compl* **10** (1): 10–15. SPE-25370-PA. DOI: [10.2118/25370-PA](https://doi.org/10.2118/25370-PA).
- ISO/TR 10400:2007(E), *Petroleum and Natural Gas Industries—Formulas and Calculations For The Properties Of Casing, Tubing, Drill Pipe and Line Pipe Used as Casing or Tubing*. 2007. ISO TC 67/SC 5/WG 2.
- Issa, J.A. and Crawford, D.S. 1993. An Improved Design Equation for Tubular Collapse. Paper SPE 26317 presented at the SPE Annual Technical Conference and Exhibition, Houston, 3–6 October. DOI: [10.2118/26317-MS](https://doi.org/10.2118/26317-MS).
- Ju, G.T., Power, T.L., and Tallin, A.G. 1998. A Reliability Approach to the Design of OCTG Tubulars Against Collapse. Paper SPE 48332 presented at the SPE Applied Technology Workshop on Risk Based Design of Well Casing and Tubing, The Woodlands, Texas, USA, 7–8 May. DOI: [10.2118/48332-MS](https://doi.org/10.2118/48332-MS).
- Lewis, D.B., Brand, P.R., Whitney, W.S., Hood, M.G., and Maes, M.A. 1995. Load and Resistance Factor Design for Oil Country Tubular Goods. Paper OTC 7936 presented at the Offshore Technology Conference, Houston, 1–4 May. DOI: [10.4043/7936-MS](https://doi.org/10.4043/7936-MS).
- Lubinski, A. 1977. Fatigue of Range 3 Drill Pipe. *Revue de l'Institut Français du Pétrole*, **32** (2): 77011.
- Lubinski, A., Althouse, W.S., and Logan, J.L. 1962. Helical Buckling of Tubing Sealed in Packers, *J Pet Technol* **14** (6): 655–670. DOI: [10.2118/178-PA](https://doi.org/10.2118/178-PA).
- Manual of Steel Construction, Load and Resistance Factor Design*, first edition. 2001. Chicago, Illinois: American Institute of Steel Construction.
- Marlow, R. S. 1982. Collapse Performance of HC-95 Casing. Report on PRAC Project 80-30, 1982 American Petroleum Institute Annual Meeting and Conference.
- Mitchell, R.F. 2003. Lateral Buckling of Pipe With Connectors in Horizontal Wells. *SPE J.* **8** (2): 124–137. SPE-84950-PA. DOI: [10.2118/84950-PA](https://doi.org/10.2118/84950-PA).
- Mitchell, R.F. 2008. Tubing Buckling—The State of the Art. *SPE Dril & Compl* **23** (4): 361–370. SPE-104267-PA. DOI: [10.2118/104267-PA](https://doi.org/10.2118/104267-PA).
- Mitchell, R.F. 2009. Fluid Momentum Balance Defines the Effective Force. Paper SPE 119954 presented at the IADC/SPE Drilling Conference and Exhibition, Amsterdam, 17–19 March. DOI: [10.2118/119954-MS](https://doi.org/10.2118/119954-MS).
- NACE TM0177-2005. Laboratory Testing of Metals for Resistance to Sulfide Stress Cracking and Stress Corrosion Cracking in H₂S Environments. 2005. Houston: National Association of Corrosion Engineers.
- NACE MR0175-1999. NACE Standard Material Requirements. 1999. *Sulfide Stress Cracking Resistant Metallic Materials for Oilfield Equipment*. Houston: National Association of Corrosion Engineers.
- Paslay, P.R. and Cernocky, E.P. 1991. Bending Stress Magnification in Constant Curvature Doglegs With Impact on Drillstring and Casing. Paper SPE 22547 presented at the SPE Annual Technical Conference and Exhibition, Dallas, 6–9 October. DOI: [10.2118/22547-MS](https://doi.org/10.2118/22547-MS).
- Payne, M.L. and Swanson, J.D. 1990. Application of Probabilistic Reliability Methods to Tubular Designs. *SPE Drill Eng* **5** (4): 299–305. SPE-19556-PA. DOI: [10.2118/19556-PA](https://doi.org/10.2118/19556-PA).
- Seely, F.B. and Smith, J.O. 1965. *Advanced Mechanics of Materials*, second edition. New York City: Wiley.
- Tamano, T., Mimaki, T., and Yanagimoto, S. 1983. A New Empirical Formula for Collapse Resistance of Commercial Casing. *Journal of Energy Resources Technology*, ASME, 1983.
- Timoshenko, S.P. and Goodier, J.N. 1970. *Theory of Elasticity*, third edition. New York City: McGraw-Hill Book Company, pp 70–71.
- Weiner, P.D. and Sewell, F.D. 1967. New Technology for Improved Tubular Connection Performance. *J Pet Technol* **19** (3): 337–343. SPE-1601-PA. DOI: [10.2118/1601-PA](https://doi.org/10.2118/1601-PA).
- Zwillinger, D. ed. 1996. *CRC Standard Mathematical Tables and Formulae*, 30th edition, 321–322. Boca Raton, Florida: CRC Press.

SI Metric Conversion Factors

bbl	×	1.589 873	E – 01 = m ³
ft	×	3.048*	E – 01 = m
ft ³	×	2.831 685	E – 02 = m ³
°F		(°F – 32)/1.8	= °C
°F		(°F + 459.67)/1.8	= K
gal	×	3.785 412	E – 03 = m ³
in.	×	2.54*	E + 00 = cm

in. ²	×	6.451 6*	E + 00 = cm ²
in. ³	×	1.638 706	E + 01 = cm ³
kip	×	4.448 222	E + 03 = N
ksi	×	6.894 757	E + 03 = kPa
lbf	×	4.448 222	E + 00 = N
lbm	×	4.535 924	E − 01 = kg
psi	×	6.894 757	E + 00 = kPa

*Conversion factor is exact.

Chapter 8

Directional Drilling

Stefan Miska, University of Tulsa

The objective of this chapter is to present the fundamental concepts of directional drilling. These include directional well trajectory design, determination of the well trajectory from survey data, the control of the wellpath while drilling, and methods for modeling the torque and drag forces on a drillstring.

8.1 Fundamentals of Directional-Well Trajectory Design

8.1.1 Introduction. The term *directional drilling* is a broad term that refers to all activities that are required to design and drill a wellbore to reach a target, or a number of targets, located at some horizontal distance from the top of the hole. In other words, the purpose of directional drilling is to connect the surface location with oil/gas reservoirs that are not located right below it. Any well that is intentionally nonvertical is also called a directional well. Deviation control comprises all activities needed to drill a hole as required by the well plan and geological data.

Historically, the development of directional drilling started about 1920 when some wells crossed their lease boundaries and triggered several lawsuits. The need to know the position of the wellbore in reference to its surface location as well as to the lease boundaries quickly became evident. It soon became standard practice to report the length of the wellbore [the so-called measured depth (MD)], the hole inclination angle (its deviation from vertical), and the hole azimuth (direction from magnetic and geographic north).

In 1929, H. John Eastman developed commercial technology to drill wells from rigs located on land (onshore) to exploit oil reservoirs located beneath the ocean. In 1932, an offshore platform was built in California. At about the same time, offshore drilling platforms were constructed in the Caspian Sea.

Today, much oil and natural-gas production comes from directional wells drilled onshore and offshore, even in environmentally sensitive locations. To enhance production, many wells are drilled with a high inclination angle or even horizontally. At first, horizontal wells were only a few hundred feet long. Thanks to continuous improvements in drilling technology, the horizontal departure was gradually increased to enable drilling of so-called *extended-reach wells* (ERWs). *Extended-reach drilling* (ERD) is commonly used nowadays to reach onshore and offshore oil and gas deposits; the length of such a well can be 20,000 to 40,000 ft or even more. If the stepout is greater than 40,000 ft, the well is classified as *ultra-extended-reach drilling* (uERD). Drilling ERD and uERD wells creates a number of challenges for drilling personnel. To drill such wells effectively required significant improvements in drilling fluids, cuttings transport, and mechanical performance of the drillstring and other elements of a drilling system.

Development of logging-while-drilling (LWD) tools triggered development of so-called *geosteering* methods and *maximum-reservoir-contact* wells. Geosteering involves guiding the wellbore path based on real-time measurements of formation properties rather than following a predetermined trajectory. As the name indicates, the purpose of maximum-reservoir-contact wells is to improve recovery of hydrocarbons by maximizing the contact

area of the well with the formation. To enhance production further, several wells can be drilled from the main well (mother well), resulting in a so-called *multilateral completion*.

Directional wells are also sometimes drilled to control a blowing well or to bypass (sidetrack) a portion of a vertical well that is impossible to drill [e.g., due to wellbore stability problems or loss of portions of a drillstring (fish) in a hole]. Some typical applications of directional drilling are shown schematically in **Fig. 8.1**.

Directional drilling is also widely used for geothermal and civil-engineering applications. Many geothermal projects involve drilling directional wells in hot hard rocks such as granite and other igneous and metamorphic rocks. Civil engineers frequently use directional-drilling techniques for drilling under rivers, highways, and other obstacles. In response to economic and environmental pressures, the use of directional wells is increasing in oil and other industries. Not only has the number of directionally drilled wells increased, but also the well trajectories have become increasingly complex, resulting in a need for more-sophisticated drilling tools and technologies. First, however, some basic concepts will be discussed, followed by some useful mathematical formulations that apply to all directionally drilled wells.

8.1.2 Basic Concepts. The conventional visual representation of a directional well consists of a horizontal and vertical cross-section, as shown in **Fig. 8.2**. For the sake of simplicity, a straight segment A–B is used here to represent the wellbore. The distance from the rotary table [the rotary kelly bushing (RKB)] to Point A or Point B as measured along the wellbore is called a measured depth (MD). The vertical distance from the rotary table to Point A or Point B is called *true vertical depth* (TVD) or simply vertical depth. The vertical and horizontal planes are called the inclination and direction planes respectively. The *inclination angle* ϕ is the angle between the vertical and the wellbore. The *direction angle* ϑ is specified as the azimuth between the geographic north and the projection of the wellbore onto a horizontal plane.

A number of devices exist to measure the hole inclination and azimuth angles. Such devices are called *surveying instruments*. The industry is currently using a number of surveying instruments, ranging from magnetic (single-shot and multishot) to more-sophisticated gyroscopic devices. Magnetic instruments use an inclinometer, a compass, a timer, and a camera, while gyroscopic instruments work on the principle of a spinning mass. The use of magnetic instruments requires installation in the *bottomhole assembly* (BHA) of special drill collars made of stainless steel (approximately 68% nickel and 28% copper, with small additions of iron and manganese—“monel” metals) with nonmagnetic properties. On the other hand, gyroscopic instruments do not require nonmagnetic drill collars because they are immune to magnetic influence. An azimuth reading with a gyrocompass is not distorted by casings and other structures made of steel.

The angle between geographic (true) north and magnetic north is called the *declination angle*. A location where measurements are taken is called a *station*. At each station, an MD, hole inclination angle, and azimuth are recorded.

Modern technology makes it possible to send directional-survey information to the surface using mud-pulse telemetry. Information on hole inclination and azimuth, as well as certain other information (e.g., downhole

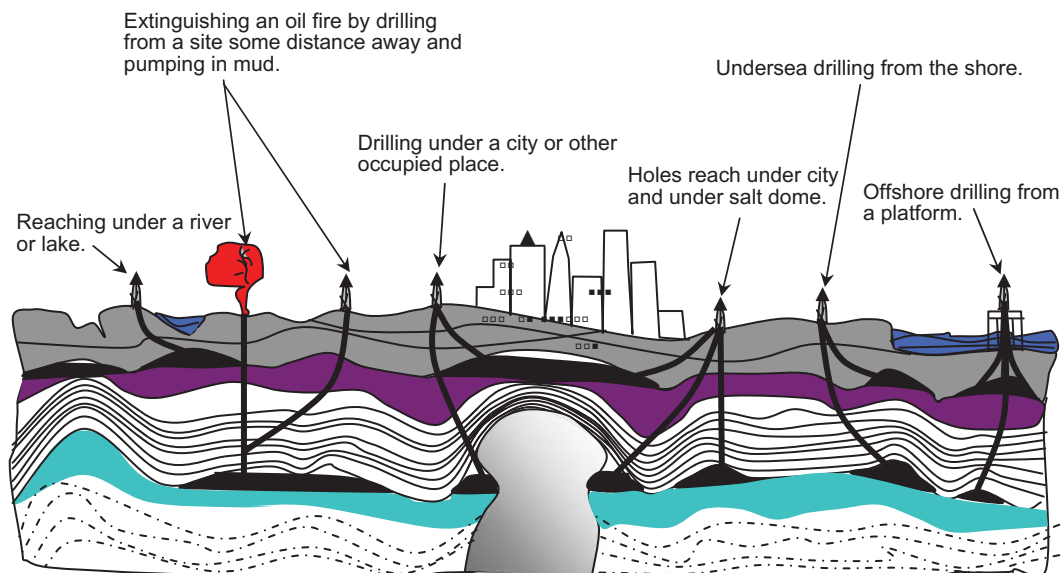


Fig. 8.1—Applications of directional drilling.

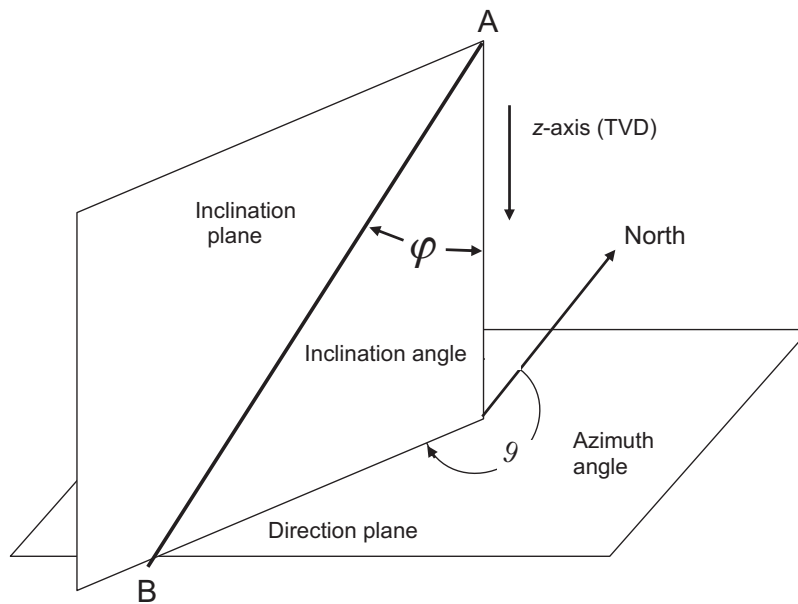


Fig. 8.2—Hole inclination and azimuth angles.

WOB, deflection of tool-face angle), is transmitted as pressure pulses and decoded at the surface while drilling. Typically, the measurements are taken at intervals of between 30 and 300 ft or even less, depending on the complexity of the well path and the purpose of the wellbore.

It is conventional practice to use four 90° quadrants, north, east, south, and west (N-E-S-W) to report well direction. For example, the azimuth angles $\vartheta_1 = 27^\circ$ and $\vartheta_2 = 215^\circ$ can also be reported as $\vartheta_1 = \text{N}27\text{E}$ and $\vartheta_2 = \text{S}35\text{W}$. In other words, if the hole direction is reported as E26S, the azimuth is 116° . **Figs. 8.3a and 8.3b** are examples of a horizontal (plane) view and a vertical (section) view of a wellbore trajectory, represented for the sake of simplicity as straight segments. The x (north) and y (east) axes in Fig. 8.3a intersect in the center of the rotary table (the RKB). The vertical cross section is drawn through the centers of the RKB and the target.

Figs. 8.3a and 8.3b are qualitative in nature to help define some commonly used terms in directional drilling. The *kickoff point* (KOP) is the depth at which the well trajectory departs from the vertical in the direction of the target or is modified by the lead angle. The lead angle is usually to the left of the target horizontal departure line (the line from the initial point O to the target T). The magnitude and direction (left or right) are based on analysis of forces at the drill bit and on local field experience. The *departure* is the horizontal distance between the surface location and the point on the traverse (trajectory). The *closure* is the horizontal distance between the rotary table and the center of the target. **Fig. 8.4** shows a 3D view of a wellbore composed of three segments in x, y, z -coordinates.

The origin of the coordinate system is located at Point P_1 ; Points P_2 , P_3 , and P_4 lie on the trajectory at the coordinates shown in Fig. 8.4. For the sake of simplicity, the segments P_1P_2 , P_2P_3 , and P_3P_4 are assumed to be straight, and their inclination and direction angles are also shown in Fig. 8.4. In reality, a wellbore is composed of curved rather than straight segments, and it is useful to introduce the concepts of build and turn rates as discussed below.

8.1.3 Fundamental Mathematical Formulations. Let us consider a wellbore trajectory as shown schematically in **Fig. 8.5** in a conventional rectangular x, y, z (right-hand) system of coordinates consistent with the north, east, and vertical directions, N, E, and V. The continuous curve O-s in Fig. 8.5 represents the well trajectory (wellbore centerline). Consider a small element ds with components dx , dy , and dz . Because ds is small, it can be approximated as a straight segment with inclination angle φ and azimuth ϑ . The projection of the small element ds onto a horizontal plane is denoted as dl . With motion along the well path, in general, both the inclination angle and azimuth will change. In other words, the hole inclination angle and azimuth are functions of the MD s .

For purposes of directional-well trajectory planning, it is useful to define the following fundamental quantities: Rate of change of the hole inclination angle along the well path, or the so-called *build rate*:

$$B(s) = \frac{d\varphi(s)}{ds} \quad \dots \dots \dots (8.1)$$

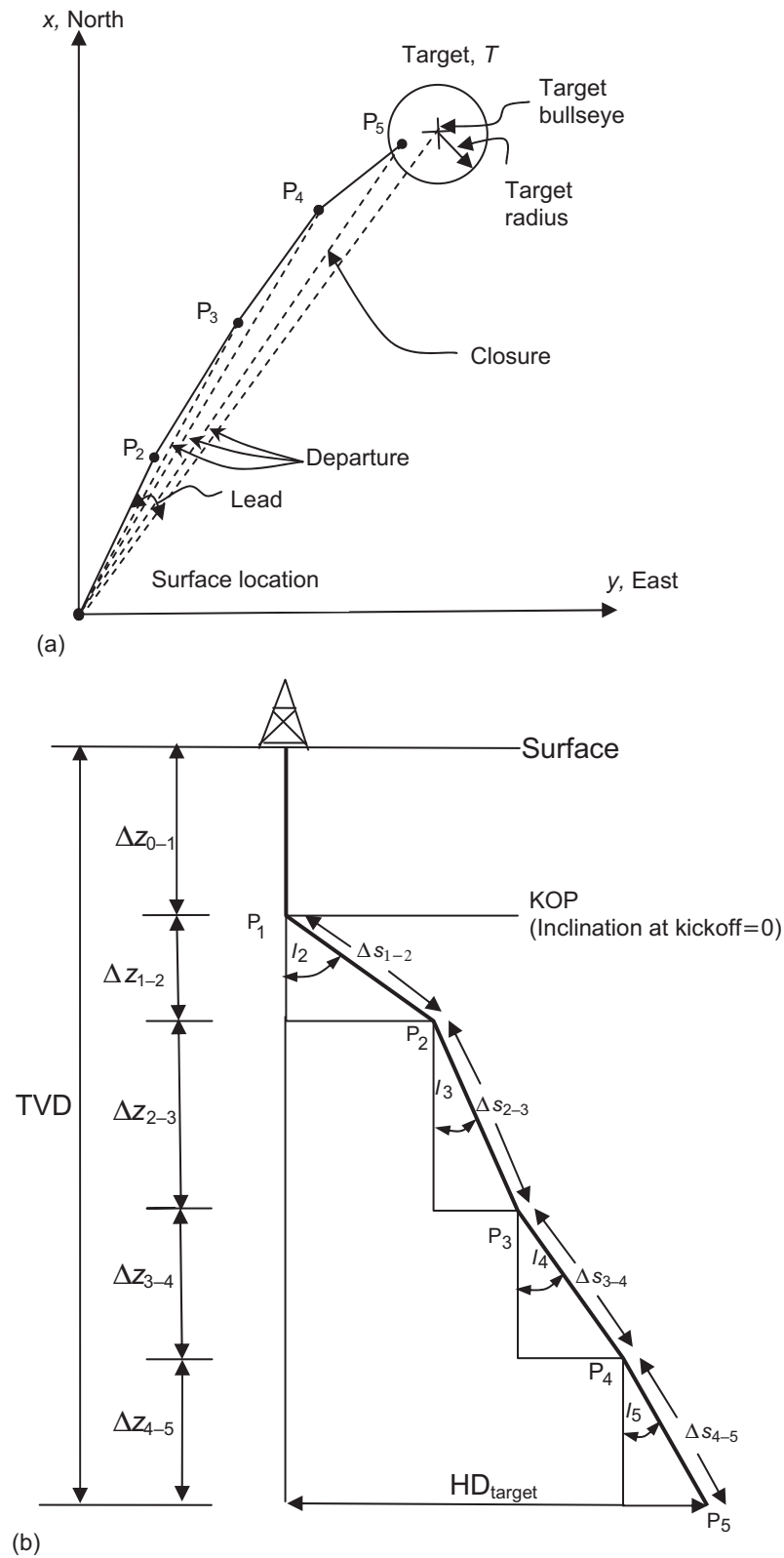


Fig. 8.3—(a) Plane view; (b) side view.

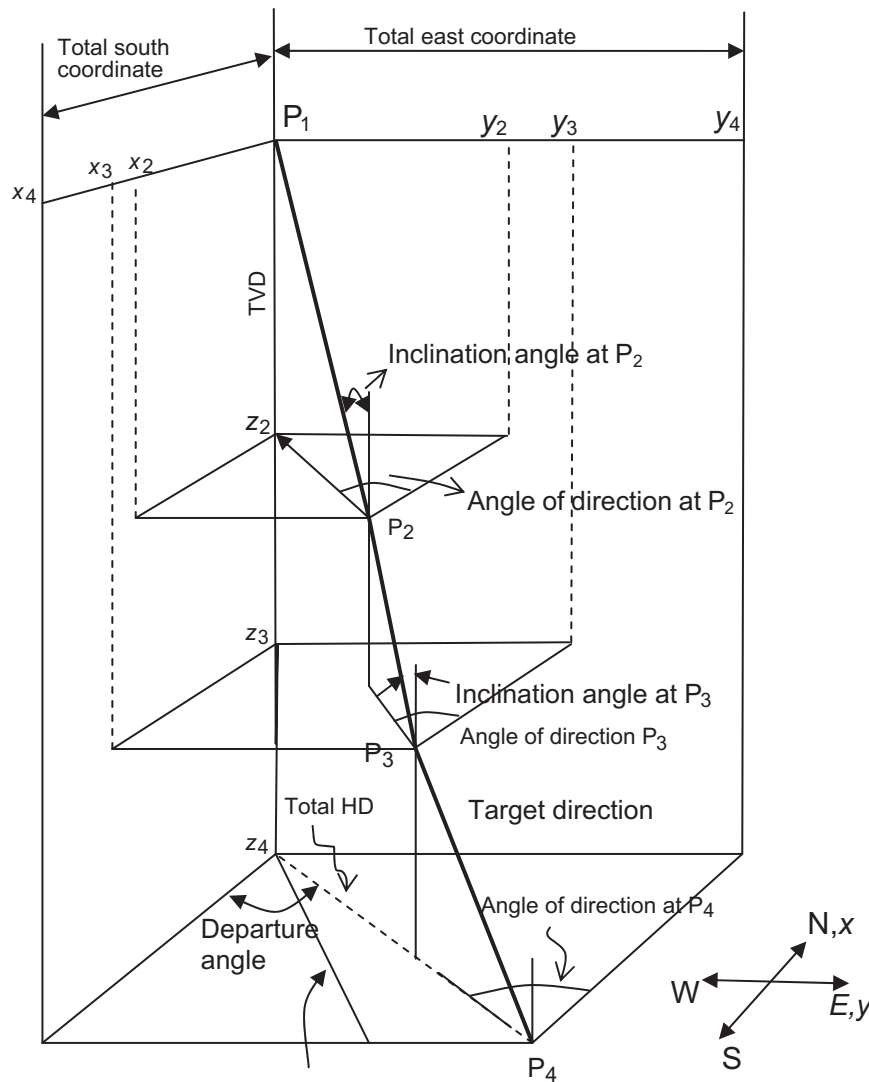


Fig. 8.4—Wellbore composed of three segments.

Rate of change of the azimuth angle along the projection of the well path onto a horizontal plane, or the so-called *horizontal turn rate*:

$$H(s) = \frac{d\theta(s)}{dl} \quad (8.2)$$

Rate of change of the azimuth along the well path, or the *turn rate*:

$$T(s) = \frac{d\theta(s)}{ds} \quad (8.3)$$

In other words, the build and turn rates are the first derivatives of the hole inclination and azimuth angle as functions of MD. In directional drilling, the build and turn rates are usually expressed in degrees/100 ft (or degrees/30 m), and care should be exercised to carry out calculations in a consistent system of units (radians rather than degrees). The rate of change can be positive or negative, depending on whether the angles increase or decrease with MD. For example, a negative build rate indicates that the inclination angle decreases with depth, in which case it is usually called a *drop rate*. Note that, in general, the hole inclination and azimuth angles as well as the build and turn rates are functions of the measured hole depth s .

Examination of the right triangles in Fig. 8.5 immediately reveals the following useful relationships:

$$\frac{dx}{dl} = \cos \theta(s), \quad (8.4)$$

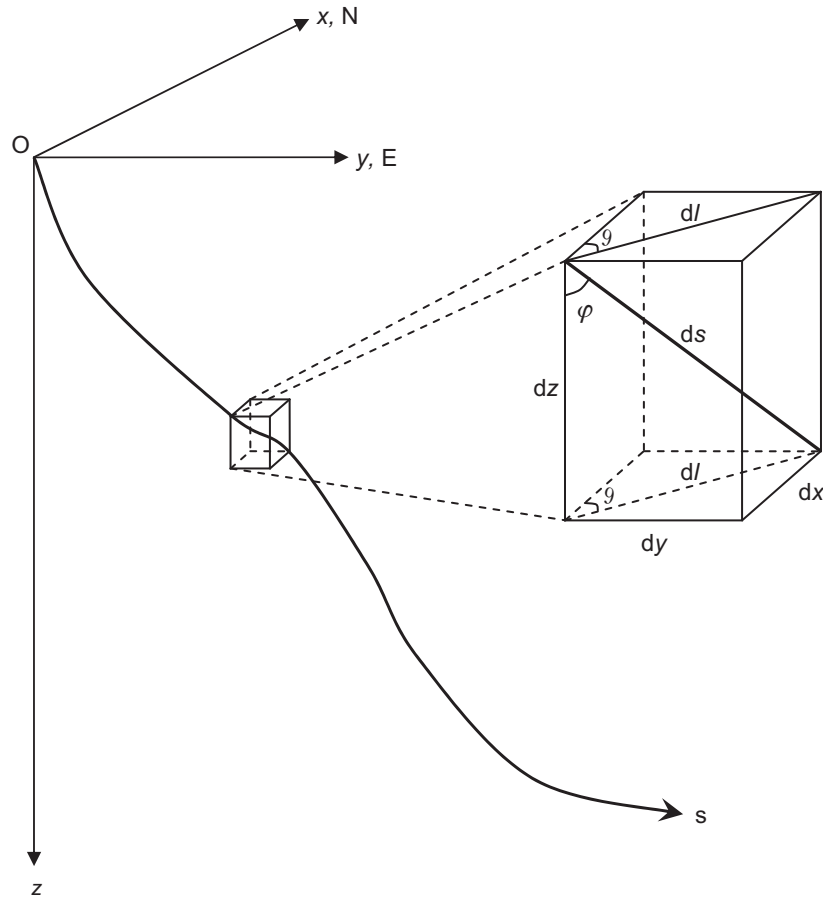


Fig. 8.5—Schematic diagram of a small element of a 3D wellbore trajectory.

$$\frac{dy}{dl} = \sin \vartheta(s), \quad \dots \dots \dots (8.5)$$

$$\frac{dl}{ds} = \sin \varphi(s), \quad \dots \dots \dots (8.6)$$

$$\frac{dz}{ds} = \cos \varphi(s). \quad \dots \dots \dots (8.7)$$

It is also useful to calculate the following derivatives:

$$\frac{dx}{ds} = \frac{dx}{dl} \frac{dl}{ds} = \sin \varphi(s) \cos \vartheta(s), \quad \dots \dots \dots (8.8)$$

$$\frac{dy}{ds} = \frac{dy}{dl} \frac{dl}{ds} = \sin \varphi(s) \sin \vartheta(s). \quad \dots \dots \dots (8.9)$$

In calculus, the quantities defined by Eqs. 8.7, 8.8, and 8.9 are called *directional cosines* and are frequently denoted by the letters l , m , and n . It can be shown that the sum of the squares of the directional cosines is equal to one.

Differentiating Eqs. 8.7, 8.8, and 8.9 yields the second derivatives:

$$\frac{d^2 x}{ds^2} = \cos \varphi \cos \vartheta \frac{d\varphi}{ds} - \sin \varphi \sin \vartheta \frac{d\vartheta}{ds} = B \cos \varphi \cos \vartheta - T \sin \varphi \sin \vartheta, \quad \dots \dots \dots (8.10)$$

$$\frac{d^2 y}{ds^2} = \cos \varphi \sin \vartheta \frac{d\varphi}{ds} + \sin \varphi \cos \vartheta \frac{d\vartheta}{ds} = B \cos \varphi \sin \vartheta + T \sin \varphi \cos \vartheta, \quad (8.11)$$

$$\frac{d^2 z}{ds^2} = -\sin \varphi \frac{d\varphi}{ds} = -B \sin \varphi. \quad (8.12)$$

A good understanding of the definitions formulated above and of their derivatives is essential for solving a number of practical directional-drilling problems.

In well-trajectory design, the coordinates of the initial point are usually known [i.e., the top of the hole (the RKB) or the KOP]. The target-point coordinates are generally also known. In some instances, such as when the well must pass through multiple targets, the directions in terms of inclination and azimuth angles are also specified. The task of the designer is to calculate the coordinates of all other points on the well path. This usually is accomplished in a stepwise manner by selecting a subsequent point on the trajectory a distance Δs (measured along the trajectory) from the initial point (e.g., the KOP). To carry out the required calculations, assumptions frequently must be made about well path build and turn rates as well as hole inclination and direction angles. The calculations are repeated until a smooth well path is obtained that will reach the target or targets. In principle, to obtain the coordinates (x, y, z) of an arbitrary point on a well path, Eqs. 8.7 through 8.9 must be integrated.

Eq. 8.8 provides the difference in x -coordinates:

$$\Delta x = x_2 - x_1 = \int_{s_1}^{s_2} \sin \varphi(s) \cos \vartheta(s) ds. \quad (8.13)$$

Eq. 8.9 provides the difference in y -coordinates:

$$\Delta y = y_2 - y_1 = \int_{s_1}^{s_2} \sin \varphi(s) \sin \vartheta(s) ds. \quad (8.14)$$

Eq. 8.7 the difference in z -coordinates:

$$\Delta z = z_2 - z_1 = \int_{s_1}^{s_2} \cos \varphi(s) ds. \quad (8.15)$$

Clearly, if the coordinates (x_1, y_1, z_1) at Point 1 are known, the coordinates (x_2, y_2, z_2) at Point 2 can be calculated using Eqs. 8.13, 8.14, and 8.15. At times, the integrals are difficult to calculate, and for practical applications, designers use various assumptions to obtain closed-form solutions. Examples of such assumptions are provided in subsequent sections of this chapter. If a closed-form solution is not available, the integrals are evaluated numerically.

8.1.4 Bends in the Vertical and Horizontal Planes. Consider two important special cases of curved wellbore sections located in the vertical and horizontal planes. If a well path is confined to a vertical plane, its azimuth A is constant along the trajectory. Then Eqs. 8.13, 8.14, and 8.15 take the form

$$\Delta x = \cos \vartheta \int_{s_1}^{s_2} \sin \varphi(s) ds = \cos \vartheta \int_{\varphi_1}^{\varphi_2} \frac{1}{B} \sin \varphi d\varphi, \quad (8.16a)$$

$$\Delta y = \sin \vartheta \int_{s_1}^{s_2} \sin \varphi(s) ds = \sin \vartheta \int_{\varphi_1}^{\varphi_2} \frac{1}{B} \sin \varphi d\varphi, \quad (8.16b)$$

$$\Delta z = \int_{\varphi_1}^{\varphi_2} \frac{1}{B} \cos \varphi d\varphi. \quad (8.16c)$$

Furthermore, for the case where a wellbore segment is a circular arc with radius R , the build rate is constant and equal to the reciprocal of the radius ($1/R$). Then, Eq. 8.16 can be integrated to obtain:

$$\Delta x = \frac{\cos \vartheta}{B} (\cos \varphi_1 - \cos \varphi_2) = \xi R \cos \vartheta (\cos \varphi_1 - \cos \varphi_2), \quad (8.17a)$$

$$\Delta y = \frac{\sin \vartheta}{B} (\cos \varphi_1 - \cos \varphi_2) = \xi R \sin \vartheta (\cos \varphi_1 - \cos \varphi_2), \quad (8.17b)$$

$$\Delta z = \frac{1}{B}(\sin \varphi_2 - \sin \varphi_1) = \xi R(\sin \varphi_2 - \sin \varphi_1). \quad (8.17c)$$

The parameter ξ is chosen to be positive (+1) for a positive turn rate and negative (−1) for a negative rate.

Consequently, the horizontal departure, HD, between Points 1 and 2 is

$$\text{HD}_{1-2} = \sqrt{\Delta x^2 + \Delta y^2} = \xi R(\cos \phi_1 - \cos \phi_2). \quad (8.18)$$

Clearly, in this case, the departure is independent of the hole azimuth.

Example 8.1 Consider two points on a curved part of a trajectory located in a vertical plane with azimuth $A = 60^\circ$. The hole inclination angle at Point 1 is $\varphi_1 = 60^\circ$ and at Point 2 is $\varphi_2 = 32^\circ$. The drop-off rate is 6.5/100 ft ($B = -6.5/100$ ft). The rectangular coordinates of Point 1 are $x_1 = 1,650$ ft, $y_1 = 2,858$ ft, and $z_1 = 4,250$ ft.

Calculate:

- the x , y , z coordinates at Point 2
- the radius of curvature R
- the HD between Points 1 and 2
- the length of the segment Δs , the differences in MD between Points 1 and 2

Solution. To make the system of units consistent, the build rate is expressed as

$$(a) \quad B = -(6.5) \left(\frac{\pi}{180} \right) \left(\frac{1}{100} \right) = -(1.1339)(10^{-3}) \text{ 1/ft.}$$

Using Eq. 8.17, the rectangular coordinates can be obtained as

$$(b) \quad x_2 = 1,650 + \frac{\cos 60}{(-1.1339)(10^{-3})}(\cos 65 - \cos 32) = 1,837.6 \text{ ft,}$$

$$(c) \quad y_2 = 2,858 + \frac{\sin 60}{(-1.1339)(10^{-3})}(\cos 65 - \cos 32) = 3,182.9 \text{ ft,}$$

$$(d) \quad z_2 = 4,250 + \frac{1}{(-1.1339)(10^{-3})}(\sin 32 - \sin 65) = 4,581.9 \text{ ft.}$$

The radius of curvature is then

$$(e) \quad R = \frac{1}{B} = \frac{1}{(1.1339)(10^{-3})} = 882 \text{ ft.}$$

The HD between Points 1 and 2 can be calculated as

$$(f) \quad \text{HD}_{1-2} = \sqrt{\Delta x^2 + \Delta y^2} = \sqrt{(187.9)^2 + (324.9)^2} = 375.2 \text{ ft.}$$

For a circular segment in a vertical plane, the differential length of the segment is $ds = R d\varphi$; therefore,

$$(g) \quad \Delta s = \int_{s_1}^{s_2} ds = -R d\varphi = R(\varphi_2 - \varphi_1) = (882) \left(\frac{\pi}{180} \right) (65 - 32) = 508 \text{ ft.}$$

For a bend in a horizontal plane ($\varphi = 90^\circ$), such as a curved horizontal wellbore with constant turn rate H , the difference in vertical coordinates is nil, and the changes in the x - and y -coordinates are given by the following equations:

$$\Delta x = \frac{1}{H}(\sin \vartheta_2 - \sin \vartheta_1) = \xi R(\sin \vartheta_2 - \sin \vartheta_1), \quad (8.19a)$$

$$\Delta y = \frac{1}{H}(\cos \vartheta_1 - \cos \vartheta_2) = \xi R(\cos \vartheta_1 - \cos \vartheta_2). \quad (8.19b)$$

Again, the parameter ξ is chosen to be positive (+1) for a positive turn rate and negative (−1) for a negative rate.

8.1.5 Wellbore Curvature and Dogleg Severity. For several practical reasons, in addition to build and turn rates, it is also useful to determine wellbore curvature and torsion along the well trajectory. In directional-drilling nomenclature, wellbore curvature is frequently called *dogleg severity* (DLS) and expressed in degrees/100 ft, as mentioned earlier. This section presents the concept of curvature; torsion will be defined in Section 8.4.

From calculus, the curvature of a 3D curve can be calculated as

$$\kappa(s) = \left[\left(\frac{d^2x}{ds^2} \right)^2 + \left(\frac{d^2y}{ds^2} \right)^2 + \left(\frac{d^2z}{ds^2} \right)^2 \right]^{\frac{1}{2}} \quad (8.20)$$

Eq. 8.20 gives curvature in any consistent system of units (e.g., 1/ft, 1/m).

In everyday directional-drilling terminology, the term DLS, expressed in degrees per unit length, is often used rather than curvature. If the DLS is expressed in degrees/100 ft, then

$$\text{DLS} = \frac{18,000\kappa(s)}{\pi} \quad (8.21)$$

In other words, Eq. 8.21 gives wellbore DLS in degrees/100 ft if the curvature is expressed as 1/ft. Sometimes the DLS is called the *dogleg rate*.

The radius of curvature R is defined as the inverse of curvature: $R(s) = \kappa(s)^{-1}$. By substituting Eqs. 8.10, 8.11, and 8.12 into Eq. 8.20 and performing some rearrangements, it is possible to obtain the wellbore curvature in terms of build rate, turn rate, and hole inclination angle, as follows:

$$\kappa(s) = \sqrt{B^2 + T^2 \sin^2 \varphi(s)} \quad (8.22)$$

Sometimes the build rate B is called a *vertical build rate* (vertical curvature) and denoted as B_v , and the product $(T \sin \varphi)$ is called a *lateral curvature* and denoted as B_L . The curvature expressed by Eq. 8.22 is called the total curvature.

Because $T = \frac{d\vartheta}{dl} \frac{dl}{ds} = H \sin \varphi(s)$, it is also possible to write the curvature equation in terms of build rate and horizontal turn rate:

$$\kappa(s) = \sqrt{B^2 + H^2 \sin^4 \varphi(s)} \quad (8.23)$$

A good understanding of the concept of curvature is of critical importance for solving many directional-drilling problems, and the reader is strongly encouraged to take a close look at Eqs. 8.22 and 8.23. It should be remembered that curvature is a vector quantity and that Eqs. 8.22 and 8.23 represent only the magnitude of this vector. More information on curvature is provided in Section 8.4 on the use of vectors for well-trajectory calculations based on information obtained from directional surveys.

Wellbore curvature provides information about the rate of overall change in angle due to simultaneous changes in hole inclination and azimuth along the well path. The overall angle change (*dogleg*) between two points on a well path is defined as the angle between the tangent lines at the two points under consideration. The curvature is the rate of change of the overall angle along the trajectory, and therefore the overall angle change β between two neighboring points on the trajectory located Δs apart can be obtained by integrating the curvature along the trajectory as follows:

$$\beta = \int_0^{\Delta s} \kappa(s) ds \quad (8.24)$$

The overall angle change is frequently called a *dogleg*. For example, if the turn rate is nil (no change in azimuth along the well path), the dogleg (DL) will be:

$$\beta = DL = \int_0^{\Delta s} B ds = \int_{\varphi_1}^{\varphi_2} d\varphi = \varphi_2 - \varphi_1 \quad (8.25)$$

Clearly, if the well path is in the vertical plane, the DL is simply equal to the difference between the inclination angles at the two adjacent points.

Lubinski et al. (1953) was the first to derive an equation for DL of the form

$$\beta = 2 \arcsin \sqrt{\sin^2 \left(\frac{\varphi_2 - \varphi_1}{2} \right) + \sin \varphi_1 \sin \varphi_2 \sin^2 \left(\frac{\vartheta_2 - \vartheta_1}{2} \right)}. \quad \dots\dots\dots (8.26)$$

Analysis of Eq. 8.26 shows that for $\vartheta_1 = \vartheta_2$, Eq. 8.26 reduces to Eq. 8.25. Some other useful formulas for DL calculations will be discussed later on.

8.1.6 Directional-Well Profiles. Typically, the design of a directional-well profile consists of two phases. First, a well path is constructed to connect the target with the surface location, and then adjustments are made to account for factors that will eventually influence the final trajectory. In other words, the location of the target and of the drilling rig must be decided before the trajectory shape is designed. The location of the target is the first and most important step. In principle, the well should be placed in the reservoir to optimize production if the purpose of drilling is to recover oil and gas. The optimal wellbore trajectory (traverse) should result in minimum drilling and completion cost or time. Some oil and gas wells are designed to be confined to a vertical plane and are referred to as 2D wells. Such wells are frequently recommended whenever they are possible and economically justified. The well path shape should be considered simultaneously with casing (casing sizes and setting depths, cementing), completion program (perforating, fracturing, gravel packs), wellbore stability, cuttings transport, and any anticipated hole problems. Frequently, to optimize the well path, the geoscientists and engineers must work together from the outset of the project.

After the base well trajectory has been calculated, the designer needs to make corrections to compensate for anticipated effects related to drillpipe rotation (bit walk), formation hardness and dip angle, type of drill bit, and other factors. For example, drillpipe rotation typically results in right-hand bit walk, and therefore a left lead angle is used to compensate for this tendency, as schematically shown earlier in Fig. 8.3a. The optimum lead angle results in the closest approach to the base trajectory. The required information on the directional tendencies of various drilling systems can be obtained by analyzing drilling data from similar wells drilled under similar geological conditions. Lack of such data can lead to considerable discrepancies between calculated well trajectories and those actually observed while drilling the well. This situation places the designer of an exploratory well in a difficult situation. In such cases, as well as during more typical drilling jobs, it is essential to have a contingency plan. Under more complex geological conditions, drilling a pilot hole should be considered to obtain at least some preliminary information about geological conditions, including types of rock, formation dip and strike angles, and possible hole problems. There are three basic 2D directional well trajectories, as shown in Fig. 8.6.

Type 1 consists of a vertical part, a build section, and a tangent that is also called a hold part or slant section. This well profile is also called a *slant well*. Type 2, also called an *S-shaped pattern*, consists of five segments: vertical, buildup, tangent, drop-off, and another vertical at the bottom. A modified S-shaped trajectory has a tangent segment (not vertical) at the bottom of the drop-off part. The S-shaped pattern penetrates the target

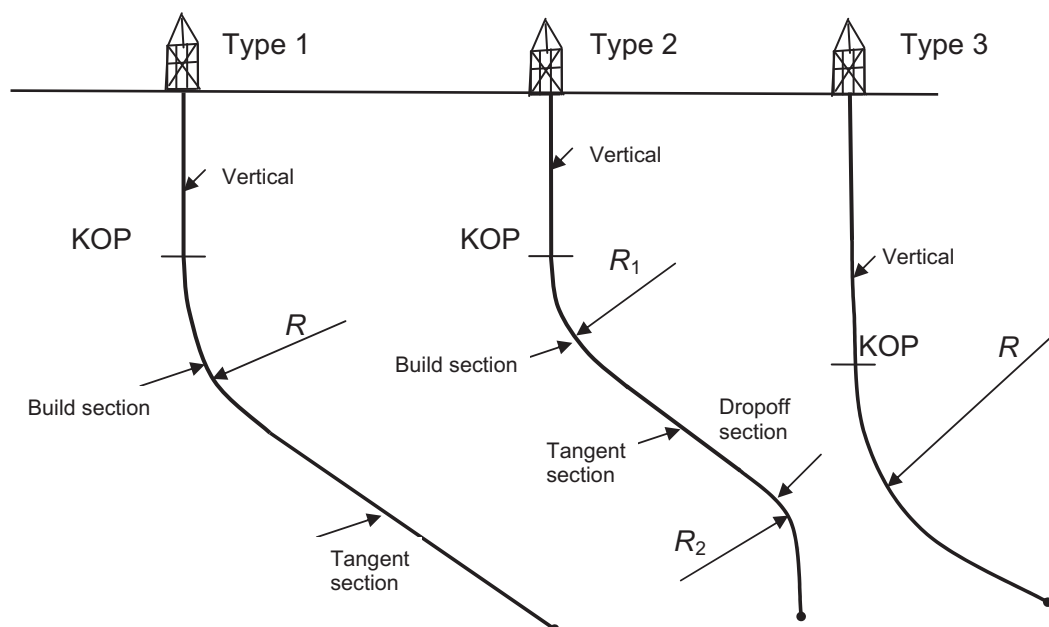


Fig. 8.6—Three major types of 2D wellbore trajectories.

vertically, and the modified S-shaped pattern penetrates the formation at some desired inclination angle. Type 3 is called a *continuous-build trajectory* and consists of a vertical part and a buildup section. Horizontal wells and ERWs are additional types.

The Ideal Slant-Type Well Profile (Type 1). The ideal slant-type well trajectory is confined to a vertical plane, resulting in a 2D well profile. Consider the slant well shown in **Fig. 8.7**, using the following notations: KOP depth; the vertical depth of target (VDT); the horizontal departure of target (HDT); and β [inclination angle of slant part (tangential part)]. For the slant-type well, the tangent angle is equal to the DL of the curved section.

Examination of Fig. 8.7 reveals the following geometric relationships:

- (a) $VDT - KOP = ab + bd$,
- (b) $HDT = de + ef$.

The segments ab , bc , and bd can be calculated as

- (c) $ab = R \sin \beta$,
- (d) $bc = R(1 - \cos \beta)$,
- (e) $bd = ce = \frac{ef}{\tan \beta}$.

Substituting Lines (c), (d), and (e) as calculated above for Lines (a) and (b) gives

$$(f) \quad VDT - KOP = R \sin \beta + \frac{ef}{\tan \beta},$$

$$(g) \quad HDT = R(1 - \cos \beta) + ef. \quad \dots\dots\dots (g)$$

Solving the equation for Line (g) for ef and substituting the result into the equation for Line (f), after some rearrangements, gives

$$(VDT - KOP) \sin \beta + (R - HDT) \cos \beta = R. \quad \dots\dots\dots (8.27)$$

Eq. 8.27 describes the desired relationship between the departure of the tangent, the VDT, the kickoff point (KOP) depth, the radius of curvature, and the inclination angle of the tangent section. The reader is encouraged to use a similar approach and derive the corresponding equation for a Type 2 directional well.

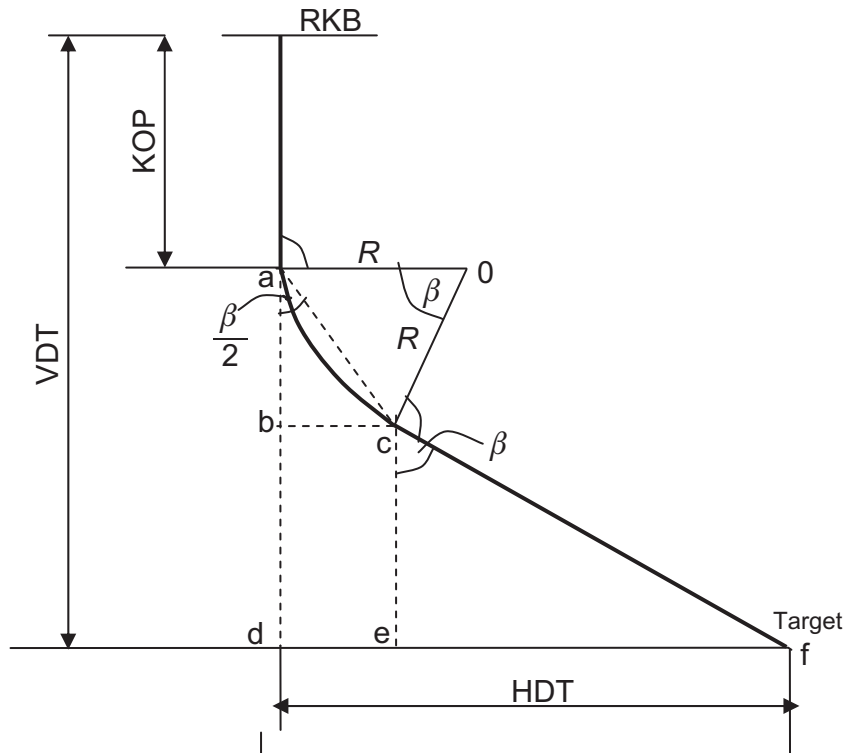


Fig. 8.7—Slant-type well profile.

If the target VDT, the KOP depth, the HDT, and the radius of the build section are given, then Eq. 8.27 can be solved for the DL angle β :

$$\beta = \arcsin\left(\frac{R}{\sqrt{(R - \text{HDT})^2 + (\text{VDT} - \text{KOP})^2}}\right) - \arctan\left(\frac{R - \text{HDT}}{\text{VDT} - \text{KOP}}\right) \quad (8.28)$$

Once the DL angle has been calculated, it is possible to determine the length of the curved section and the build rate in degrees/100 ft.

On the other hand, if the quantities HDT, VDT, KOP, and β are given, then Eq. 8.27 can be solved for the radius of curvature of the build section and subsequently for the required build rate.

Example 8.2 Design the trajectory of a slant-type offshore well for the conditions stated below:

- Elevation (above sea level) of the rotary table = 180 ft
- Target depth (subsea) = -5,374 ft
- Target south coordinate = 2,147 ft
- Target east coordinate = 3,226 ft
- Declination = 6° E
- KOP depth = 1,510 ft
- Buildup rate = 2°/100 ft

A vertical section of this well is shown in **Fig. 8.8a** and a horizontal view in Fig. 8.8b. Find the following:

- Slant angle
- Vertical depth at the beginning of the tangent part
- Departure at the beginning of the tangent part
- MD to the target

Solution.

(a) Target VDT = 180 + 5,374 = 5,554 ft

(b) HDT = $\sqrt{2,147^2 + 3,226^2} = 3,875$ ft

(c) Target direction = $\arctan \frac{3,226}{2,147} = \text{S}56.35\text{E}$ (azimuth 180-56.35=123.65)

(d) Target magnetic direction = 56.35°+6°= S62.35E

(e) Radius of curvature: $R = \frac{180}{(0.02)\pi} = 2,865$ ft

Slant angle:

(f) $\beta = \arcsin\left(\frac{2,865}{\sqrt{(2,865 - 3,875)^2 + (5,554 - 1,510)^2}}\right) - \arctan\left(\frac{2,865 - 3,875}{5,554 - 1,510}\right) = 57.4^\circ$

Further calculations will be performed using a slant angle = 57.4°.

Vertical depth (VD) at the beginning of the tangent part:

(g) $\text{VD}_2 = 1,510 + (2,865)(\sin 57.4) = 3,925$ ft

Departure at the beginning of the tangent part:

(h) $\text{HD}_2 = 2,865(1 - \cos 57.4) = 1,321$ ft

MD at the beginning of the tangent part:

(i) $s_2 = 1,510 + \frac{57.4}{0.02} = 4,380$ ft

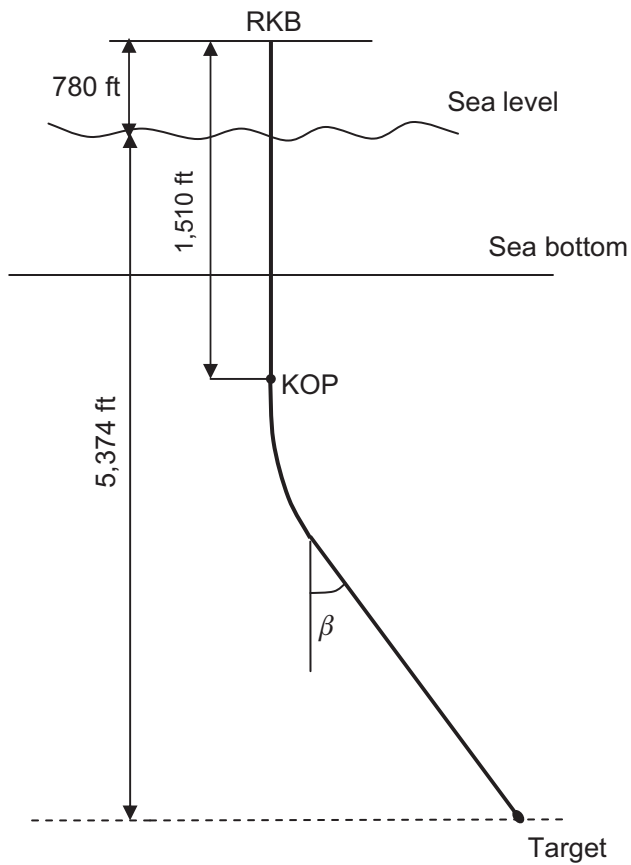


Fig. 8.8a—Offshore slant-well profile.

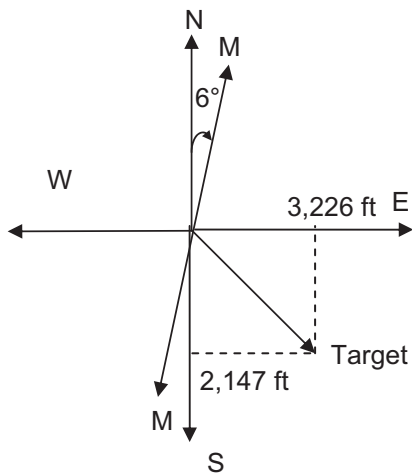


Fig. 8.8b—Horizontal view.

MD at the target:

$$(j) \ s_{\text{target}} = 4,380 + \frac{5,554 - 3,925}{\cos 57.4} = 7,403 \text{ ft}$$

Horizontal Well Profiles. In practical applications, horizontal wells are high-angle wells with inclination angles of approximately 80 to 100°. In an ideal horizontal well, as the name indicates, the inclination angle is equal to 90°. Wells with inclination angles greater than 90° are sometimes drilled to recover oil and gas located in the upper part of a formation as well as to enhance production rates (gravity helps to counteract the frictional pressure losses). Most horizontal wells are drilled in a reservoir partly to maximize wellbore contact with the formation in anticipation of higher-production wells. Horizontal wells are also drilled for enhanced oil recovery purposes (waterflooding) and for water and gas control. **Fig. 8.9** shows a schematic diagram of a horizontal well that consists of a vertical segment, a first buildup segment, a tangent part, and a second buildup segment, followed by a horizontal section. Here, the departure is defined as the displacement from vertical until the well reaches the beginning of the horizontal section. Horizontal displacement is the sum of the length of the horizontal section and the departure. Some horizontal wells consist of one build section connecting the vertical part with a horizontal section.

Typically, horizontal wells are classified by their radius of curvature as:

- Long-radius, with a radius of approximately 1,000–3,000 ft
- Medium-radius, with a radius of 200–1,000 ft
- Short-radius, with a radius of 30–200 ft

There are also ultrashort-radius systems that use high-pressure jetting techniques to turn the well from a vertical to a horizontal orientation.

The distinction between the three horizontal well categories is arbitrary, and in engineering practice, the build rates overlap. Some wells can be a combination of long and medium build rates or of medium and short. For example, a 3°/100 ft build rate may be used in the upper section of a well, followed by a tangent section, with a 10°/100 ft buildup rate below the tangent section to reach a horizontal section.

The build curve can be classified as ideal, simple-tangent, or complex-tangent. The *ideal build curve* connects the KOP with the beginning of the horizontal section using one or two circular arcs. One circular arc located in a vertical plane is possible if $\text{TVD} - \text{KOP} = \text{HD}$. Then the radius of the circular arc is simply equal to $\text{TVD} - \text{KOP}$.

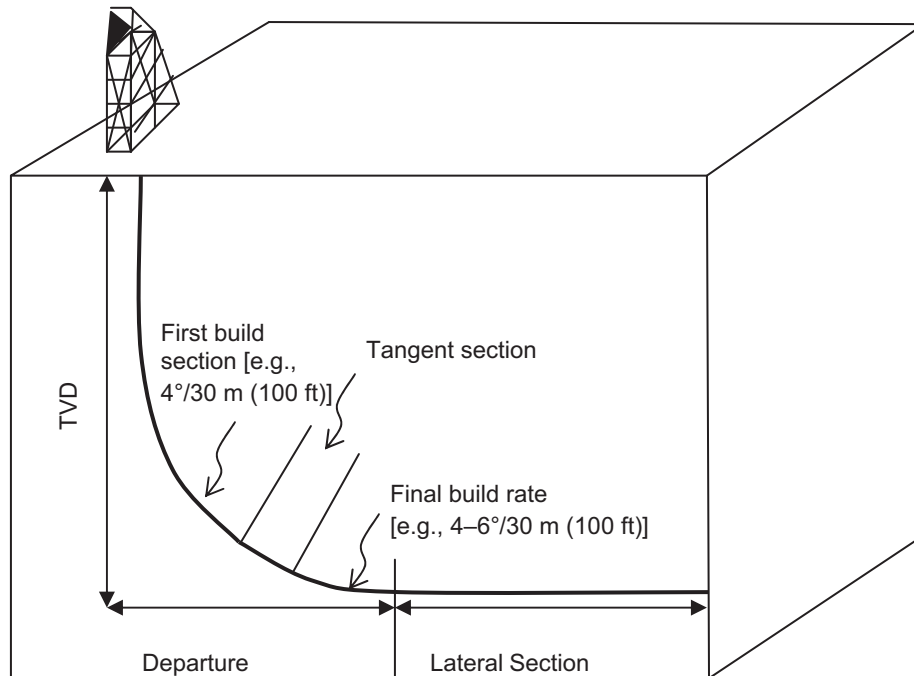


Fig. 8.9—Horizontal well profile consisting of two build sections.

The *simple-tangent build curve* consists of an upper circular arc, a tangent section, and a lower circular arc. The designer must decide on the buildup rates, the angle of the tangent section, and the length of the tangent section. The length of the tangent part should not be less than approximately 120–150 ft so that adjustments can be made if the performance of downhole tools (e.g., mud motors with bent housing) differs from that assumed by the designer.

Example 8.3 Design a simple-tangent horizontal-well profile, given the following:

- KOP = 8,206 ft
- VDT = 9,000 ft
- Tangent length = 120 ft
- Tangent angle = 50°
- Target angle = 90° at VDT
- Expected build rate = 8°/100 ft

Solution. The same build rate will be used for the first and second build segments:

Build radius:

$$(a) \quad R = \frac{5,729}{B} = \frac{5,729}{8} = 716 \text{ ft}$$

Height of first build (Eq. 8.17c):

$$(b) \quad \Delta z_1 = R(\sin \phi_2 - \sin \phi_1) = 716(\sin 50 - \sin 0) = 549 \text{ ft}$$

Height of tangent:

$$(c) \quad \Delta z_{\tan} = s_{\tan} \cos \phi_{\tan} = (120)(\cos 50) = 77 \text{ ft}$$

Height of second build:

$$(d) \quad \Delta z_2 = 716(\sin 90 - \sin 50) = 168 \text{ ft}$$

HD of first build:

$$(e) \quad \Delta HD_1 = R(\cos \phi_1 - \cos \phi_2) = 716(\cos 0 - \cos 50) = 256 \text{ ft}$$

HD of tangent:

$$(f) \quad \Delta HD_{\tan} = s_{\tan} \sin \phi_{\tan} = (120)(\sin 50) = 92 \text{ ft}$$

HD of second build:

$$(g) \quad \Delta HD_2 = (716)(\cos 50 - \cos 90) = 460 \text{ ft}$$

Length of first build:

$$(h) \quad \Delta s_1 = \frac{100(\phi_2 - \phi_1)}{B} = \frac{100(50 - 0)}{8} = 625 \text{ ft}$$

Length of second build:

$$(i) \quad \Delta s_2 = \frac{100(90 - 50)}{8} = 500 \text{ ft}$$

MDs:

At end of first build: 8,206 + 625 = 8,831 ft

At end of tangent: 8,831 + 120 = 8,951 ft

At end of second build: 8,951 + 500 = 9,451 ft

A *complex-tangent build curve* uses the first build interval in a manner similar to the simple-tangent method. However, the second build curve is designed with a lower build rate and also involves turning the curve to the left or right to

reach the desired target. Eventually, a 3D curve is drilled to connect the tangent part with the horizontal segment. This task is accomplished by proper orientation of the tool-face deflection angle, as discussed later in Section 8.3. The well path can be designed to have the entire turn in one direction (right or left) or to turn in one direction for some distance and then in the opposite direction to complete the curve. Of course, turning the well path involves a change in azimuth, which may change the direction (azimuth) of the end of curve. Three-dimensional wellbore segments are discussed later in this book.

In general, the major factors affecting a horizontal-well profile are as follows:

- Anticipated reservoir production performance, existence of fractures and their orientation, depth of gas-oil and water-oil contact (WOC)
- Completion type (open-hole, slotted liner, etc.) and anticipated workover requirements
- Casing and cementing program.
- Drilling fluids and wellbore stability
- Drillstring design (torque and drag)
- Anticipated hole problems (cuttings transport, washouts, others)

8.1.7 Three-Dimensional Well Profiles. In engineering practice, any well trajectory that is not located in a vertical plane is considered to be a 3D well. Under favorable drilling conditions, trajectories can be restricted to a vertical plane; however, in many instances the well path must move in 3D space to meet the well objectives. A 3D well trajectory is designed for a variety of geological and engineering reasons—for example, to avoid some difficult-to-drill subsurface formations (e.g., drilling around salt domes) or to avoid faults. The well path must nearly always be in 3D if the well needs to intersect multiple targets, as is frequently required in horizontal drilling and geosteering applications. Most wells drilled offshore are three-dimensional to avoid intersecting with other wells. An example of the situation that often exists is the 3D view of a multiwell offshore platform as shown schematically in **Fig. 8.10**. Three-dimensional wells are also drilled onshore for environmental reasons (to minimize the footprint of drilling rigs) or when drilling under buildings and other constructions. A group of wells is called a cluster. Frequently, drilling a cluster of wells is not only environmentally friendly, but also more economical because of its higher efficiency and reduced footprint. New generations of onshore drilling rigs that can slide on rails make it easier to implement a multiwell (15–20 wells or more) directional-drilling program.

Another example is the so-called *designer wells*, as shown in **Fig. 8.11**. Such wells originally were drilled in the geologically complex Gullfaks field in the Norwegian sector of the North Sea. The field has a very complex oil reservoir, with many normal and reverse faults. Typically, a designer-type well path involves a strong change in the hole azimuth combined with some change in hole inclination angle. To be classified as a “designer well,”

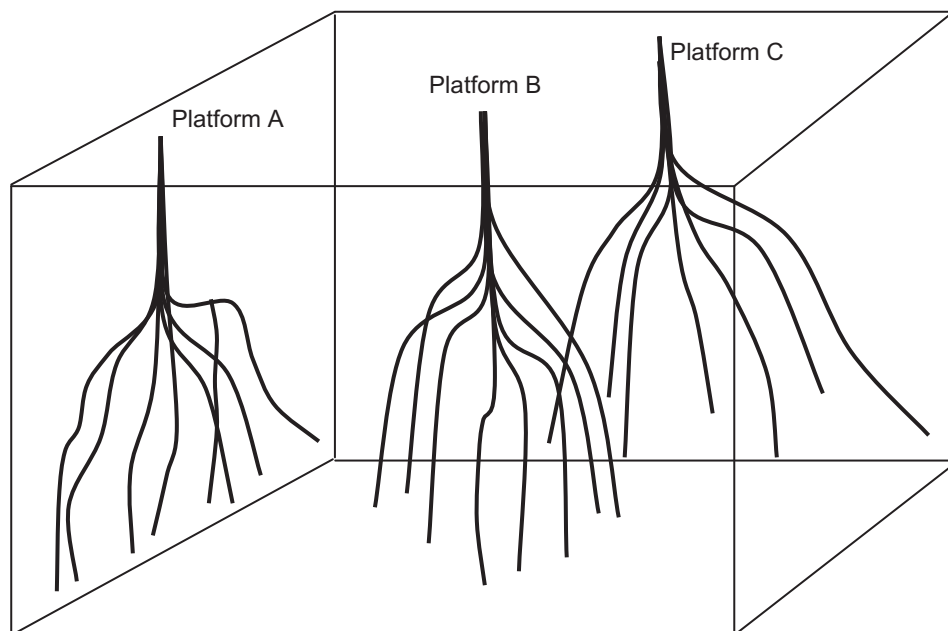


Fig. 8.10—Group of wells drilled for offshore applications.

$$y_2 = y_1 + (\sin \bar{\varphi} \sin \bar{\vartheta}) \Delta s, \quad \dots \quad (8.29b)$$

$$z_2 = z_1 + (\cos \bar{\varphi}) \Delta s, \quad \dots \quad (8.29c)$$

where the average values of the hole inclination and azimuth angles ($\bar{\varphi}$ and $\bar{\vartheta}$) are defined as

$$\bar{\varphi} = \frac{\varphi_2 + \varphi_1}{2} \quad \text{and} \quad \bar{\vartheta} = \frac{\vartheta_2 + \vartheta_1}{2}.$$

In other words, for a given increment in MD Δs between two subsequent points with inclination and azimuth angles φ_{i-1} , ϑ_{i-1} and φ_i , ϑ_i the arithmetic average values and the coordinates x_i , y_i , and z_i can be calculated if the coordinates x_{i-1} , y_{i-1} , and z_{i-1} are known.

Example 8.4 Calculate the rectangular coordinates of a well for the depth range from 8,000 to 8,400 ft. The KOP is at 8,000 ft, and the build rate is $1^\circ/100$ ft, using a lead of 10° and a right-hand walk rate of $1^\circ/100$ ft (the turn rate in a horizontal plane). The direction of the target is N30E. Assume that the first 200 ft is to set the lead, where the direction is held constant to 8,200 ft and then turns right at a rate of $1^\circ/100$ ft.

Solution. The origin of the coordinate system is fixed at the top of the hole ($x_0 = 0$, $y_0 = 0$, $z_0 = 0$), and the first segment is vertical; hence, the inclination angle $\varphi_1 = 0^\circ$ and the azimuth is undetermined. The coordinates of the KOP are $x_1 = 0$ ft, $y_1 = 0$ ft, and $z_1 = 8,000$ ft. For the point located at $\Delta s = 100$ ft from the KOP, the following can be calculated:

$$(a) \quad x_2 = (100) \sin \left(\frac{1+0}{2} \right) \cos 20 = 0.82 \text{ ft}$$

$$(b) \quad y_2 = (100) \sin \left(\frac{1+0}{2} \right) \sin 20 = 0.30 \text{ ft}$$

$$(c) \quad z_2 = 8,000 + (100) \cos \left(\frac{1+0}{2} \right) = 8,099.99 \text{ ft}$$

From 8,100 ft to 8,200 ft, the inclination angle increases to 2° , and the azimuth is N20E:

$$(d) \quad x_3 = 0.82 + (100) \sin \left(\frac{1+2}{2} \right) \cos \left(\frac{20+20}{2} \right) = 3.28 \text{ ft}$$

$$(e) \quad y_3 = 0.30 + (100) \sin \left(\frac{1+2}{2} \right) \sin \left(\frac{20+20}{2} \right) = 1.20 \text{ ft}$$

$$(f) \quad z_3 = 8,099.99 + (100) \cos \left(\frac{1+2}{2} \right) = 8,199.96 \text{ ft}$$

From 8,200 ft to 8,300 ft, the inclination angle increases to 3° , and the azimuth changes to N21E. The following values can then be calculated:

$$(g) \quad x_4 = 3.28 + (100) \sin \left(\frac{2+3}{2} \right) \cos \left(\frac{20+21}{2} \right) = 7.37 \text{ ft}$$

$$(h) \quad y_4 = 1.20 + (100) \sin \left(\frac{2+3}{2} \right) \sin \left(\frac{20+21}{2} \right) = 2.73 \text{ ft}$$

$$(i) \quad z_4 = 8,199.96 + (100) \cos \left(\frac{2+3}{2} \right) = 8,299.86 \text{ ft}$$

From 8,300 ft to 8,400 ft, the inclination and azimuth angles increase to 4° and 22° , resulting in

$$(j) \quad x_5 = 7.37 + (100) \sin \left(\frac{3+4}{2} \right) \cos \left(\frac{21+22}{2} \right) = 13.05 \text{ ft}$$

$$(k) \quad y_5 = 2.73 + (100) \sin\left(\frac{3+4}{2}\right) \sin\left(\frac{21+22}{2}\right) = 4.97 \text{ ft}$$

$$(l) \quad z_5 = 8,299.86 + (100) \cos\left(\frac{3+4}{2}\right) = 8,399.67 \text{ ft}$$

The total HD is

$$(m) \quad HD = \sqrt{(\Sigma \Delta x_i)^2 + (\Sigma \Delta y_i)^2} = \sqrt{(13.05)^2 + (4.97)^2} = 13.96 \text{ ft}$$

$$(n) \quad \text{Departure angle} = \arctan\left(\frac{\Sigma \Delta y_i}{\Sigma \Delta x_i}\right) = \arctan\left(\frac{4.97}{13.05}\right) = 20.8^\circ$$

The Radius-of-Curvature Method (RCM). The RCM was originally proposed by Wilson (1968) to replace earlier methods that used a series of straightline segments to represent the wellbore between survey stations. In this method, it is assumed that the build rate B and the horizontal turn rate H are constant over the trajectory. Typically, a few build and horizontal turn rates must be tried by the designer before finding a well path that will meet the desired objectives. **Fig. 8.12** shows a segment of wellbore between two points on the 3D trajectory. The MD between Points 1 and 2 is Δs .

It should be pointed out that, even if the build and turn rates are constant, the wellbore curvature is not constant between the two points on the well path because the hole inclination angle varies between Points 1 and 2. The assumptions of a constant build rate B and a constant horizontal turn rate H imply that the projections on the vertical plane (the segment between Points 1 and 4) and the horizontal plane (the segment between Points 1 and 3) have constant curvature. The radius of curvature in the vertical plane (R_v) is the reciprocal of the build rate, while the radius of curvature in the horizontal plane (R_h) is the reciprocal of the horizontal turn rate H .

Using the assumption that both build rate and turn rate are constant ($B = \text{constant}$ and $H = \text{constant}$), by integration of Eqs. 8.13, 8.14, and 8.15, the following equations are obtained for calculating the desired rectangular trajectory coordinates:

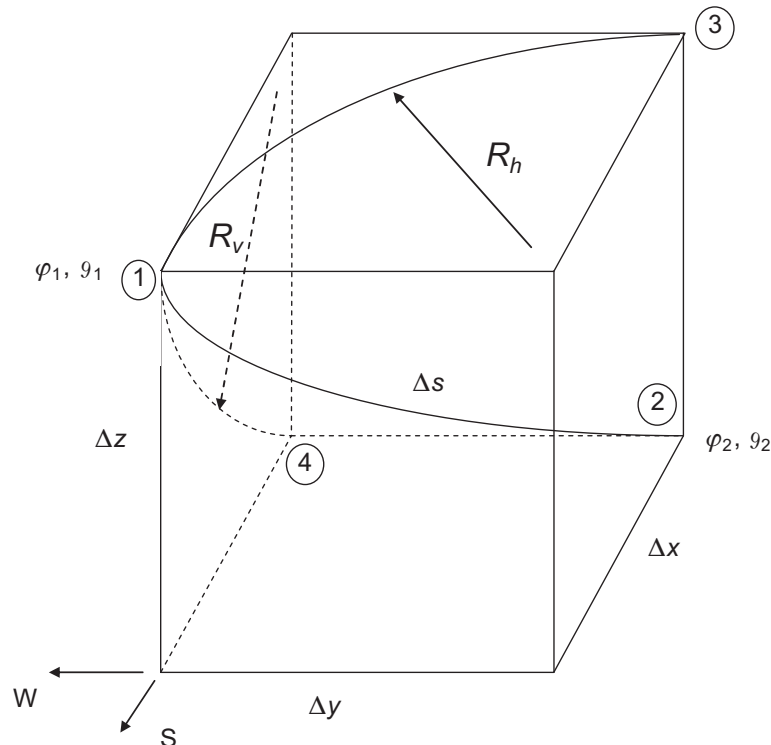


Fig. 8.12—Schematic diagram of a wellbore segment for the radius-of-curvature method.

$$\Delta x = \frac{1}{H} \int_{\vartheta_1}^{\vartheta_2} \cos \vartheta d\vartheta = \frac{\sin \vartheta_2 - \sin \vartheta_1}{H} \quad \dots\dots\dots (8.30a)$$

$$\Delta y = \frac{1}{H} \int_{\vartheta_1}^{\vartheta_2} \sin \vartheta d\vartheta = \frac{\cos \vartheta_1 - \cos \vartheta_2}{H}, \quad \dots\dots\dots (8.30b)$$

$$\Delta z = \frac{1}{B} \int_{\phi_1}^{\phi_2} \cos \phi d\phi = \frac{\sin \phi_2 - \sin \phi_1}{B}. \quad \dots\dots\dots (8.30c)$$

It should be remembered that the above equations are valid in a consistent system of units. The application of this method and some specific cases are given below.

Example 8.5 At a certain point P_1 on a well path, the inclination angle and azimuth are $\varphi_1 = 10.8^\circ$ and $\vartheta_1 = 36.5^\circ$. Assuming an increment in the MD $\Delta s = 200$ ft (the distance between Points 1 and 2), at Point 2 it is necessary to calculate the

- Hole inclination angle φ_2 and azimuth ϑ_2
- Increments in x , y , z coordinates, Δx , Δy , and Δz
- Wellbore curvature (i.e., DLS)
- DL

To perform the calculations, assume a build rate $B = 5.14^\circ/100$ ft and a horizontal turn rate $H = 17^\circ/100$ ft.

Solution. Integrating Eq. 8.1 gives:

$$(a) \int_0^{\Delta s} B ds = \int_{\varphi_1}^{\varphi_2} d\varphi \quad \varphi_2 = \varphi_1 + B\Delta s$$

Hence,

$$(b) \varphi_2 = 10.8^\circ + \frac{5.14^\circ}{100 \text{ ft}}(200 \text{ ft}) = 21.08^\circ.$$

Using Eqs. 8.2 and 8.6,

$$(c) \int_{\vartheta_1}^{\vartheta_2} d\vartheta = \frac{H}{B} \int_{\varphi_1}^{\varphi_2} \sin \varphi d\varphi,$$

and upon integration,

$$(d) \vartheta_2 = \vartheta_1 + \frac{H}{B}(\cos \varphi_1 - \cos \varphi_2).$$

The second term in the equation for Line (d) needs to be expressed in degrees if φ_1 is in degrees. Hence,

$$(e) \vartheta_2 = 36.5^\circ + \frac{17}{5.14} \left(\frac{180}{\pi} \right) (\cos 10.8^\circ - \cos 21.08^\circ) = 45.8^\circ.$$

Now it is possible to calculate the increments of the coordinates using Eqs. 8.30a, 8.30b, and 8.30c as $\Delta x = 41.14$ ft, $\Delta y = 35.95$ ft, and $\Delta z = 192.03$ ft

The wellbore curvature (i.e., DLS) can be calculated using Eq. 8.23:

$$(f) \text{DLS} = \sqrt{(5.14)^2 + (17.0)^2 \sin^4 \varphi(s)} \text{ degrees}/100 \text{ ft}.$$

Clearly, the wellbore curvature is not constant between the two points, but changes with the inclination angle. Using the average inclination angle $\frac{1}{2}(\varphi_1 + \varphi_2)$ to determine the “average DLS,”

$$(g) \text{DLS} = \sqrt{(5.14)^2 + (17.0)^2 \sin^4 (15.94)} = 5.3 \text{ deg}/100 \text{ ft}.$$

This calculation may not be sufficiently accurate because DLS is a nonlinear function of hole inclination angle. If a more accurate calculation were required, it would be necessary to integrate the DLS as a function of MD and to divide the result by the length between the points on the well path (e.g., in the present case, 200 ft).

Using Eq. 8.26:

$$(h) \quad DL = 2 \arcsin \sqrt{\sin^2(5.14) + \sin(10.8) \sin(21.08) \sin^2(4.65)} = 10.56 \text{ degrees.}$$

Example 8.6 Consider Example 8.5, but with the assumption that the designer wants to keep the well path in a vertical plane; in other words, the horizontal turn rate $H = 0$.

Solution. Because $H = 0$, $\vartheta_1 = \vartheta_2 = 36.5^\circ$, and $\varphi_2 = 21.08^\circ$ (build rate = $5.14^\circ/100$ ft). Now Eqs. 8.17a, 8.17b, and 8.17c can be used to calculate the coordinates.

By substituting actual numbers into the above-mentioned equations,

$$\Delta x = 44.1 \text{ ft}, \quad \Delta y = 32.6 \text{ ft}, \quad \Delta z = 192.03 \text{ ft.}$$

The reader is invited to verify the above calculations.

Clearly, four basic cases can be distinguished here (Case 1: B and H are constant along the trajectory; Case 2: $H = 0$ and $B = \text{constant}$; Case 3: $B = 0$ and $H = \text{constant}$; and Case 4: both $B = 0$ and $H = 0$), resulting in four different types of well-trajectory segments. In practical designs, any combination of these can be used to connect the initial point smoothly with the target. A smooth trajectory is achieved if at the connection points (common points), the ends of the two segments have the same inclination and direction angles.

Rivero (1971) used the radius-of-curvature equations to calculate the net thickness of a pay zone of known dip and strike angles. McMillian (1981) provided several examples of use of the RCM to design the well paths of slant and S-shaped wells as well as for 3D well configurations. He proposed a method by which a 3D problem can be transformed into 2D space. Once the 2D well path is determined in 2D space, it can be transferred back into 3D space.

After the base well trajectory is calculated, the designer needs to make corrections to compensate for anticipated effects related to drillpipe rotation (bit walk), formation hardness and dip angle, type of drill bit, and other factors. For example, as mentioned earlier, drillpipe rotation typically results in right-hand bit walk, and therefore a left lead angle is used to compensate for this tendency. The optimum lead angle results in the closest approach to the base trajectory. The required information on the directional tendencies of various drilling systems can be obtained by analyzing drilling data from similar wells drilled under similar geological conditions. Lack of such data can lead to considerable discrepancies between calculated well trajectories and those actually achieved while drilling the well. This situation places the designer of an exploratory well in a difficult situation. In such cases, as well as during more typical drilling jobs, it is essential to have a contingency plan. Under complex geological conditions, drilling a pilot hole should be considered to obtain at least some preliminary information about geological conditions, including types of rock, formation dip and strike angles, and possible hole problems.

Minimum-Curvature/Circular-Arc Method (MCM). An analytical formulation of the minimum-curvature method was originally proposed by Taylor and Mason (1972) and by Zarembo (1973) as a way to improve directional-survey analysis. Zarembo used the term *circular-arc method* and carried out the development using the method of vectors, which will be discussed in the next section of this chapter. More recently, Sawaryn and Thorogood (2003) published a compendium of algorithms useful for directional-well planning and deflection-tool orientation. Currently this method is widely used by the petroleum industry for both well-trajectory planning and directional-survey evaluation.

In this method, two successive points on the trajectory are assumed to lie on a circular arc located in a plane, as shown schematically in Fig. 8.13. In other words, Points 1, 2, and O in Fig. 8.13 lie on the same plane, and the curvature of the segment between Points 1 and 2 is constant. The MD between Points 1 and 2 is Δs , and the radius of the circular arc connecting the two points is R . The angle β is called the DL.

The reader is encouraged to analyze Fig. 8.13 carefully and to prove that the equations for calculating changes in the rectangular coordinates on the trajectory are as given below, with the *ratio factor* quantity is represented by RF:

$$\Delta x = (\sin \varphi_1 \cos \vartheta_1 + \sin \varphi_2 \cos \vartheta_2) RF \quad \dots \quad (8.31a)$$

$$\Delta y = (\sin \varphi_1 \sin \vartheta_1 + \sin \varphi_2 \sin \vartheta_2) RF \quad \dots \quad (8.31b)$$

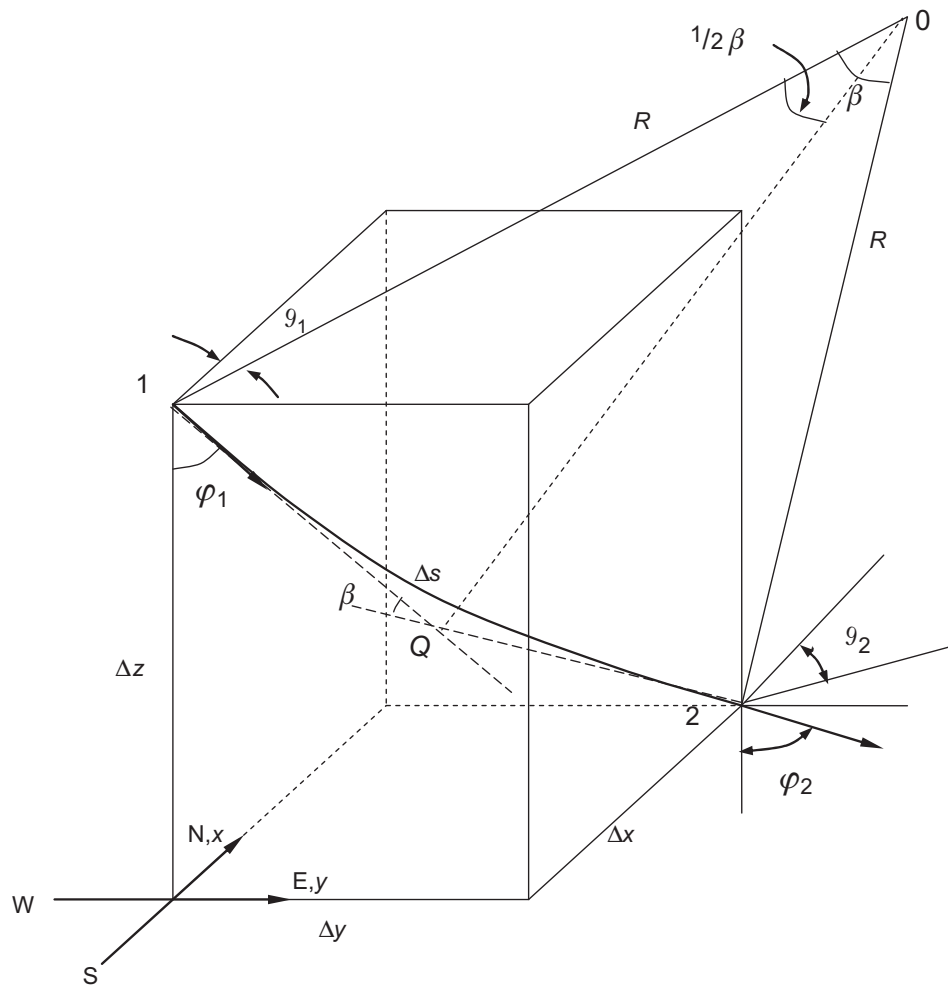


Fig. 8.13—Schematic diagram of a wellbore segment for the minimum-curvature method.

$$\Delta z = (\cos \phi_1 + \cos \phi_2) RF \quad \dots \dots \dots (8.31c)$$

where

$$RF = \frac{\Delta s}{\beta} \tan \frac{\beta}{2} \quad \dots \dots \dots (8.32)$$

Because the well path lies in a plane, this method is also sometimes called the *turn-in-plane method*.

Example 8.7 Given the following data, find the x -, y -, and z -coordinates at Point 2.

Point	MD, ft	Inclination Angle, degrees	Azimuth Angle, degrees	Coordinates		
				x	y	z
Point 1	1,050	3.15	350	102	99	1,044
Point 2	1,627	32.11	76	?	?	?

Solution. Using Eq. 8.26, the DL β can be determined as

$$(a) \quad \beta = 2 \arcsin \sqrt{\sin^2 \left(\frac{32.11 - 3.15}{2} \right) + \sin(3.15) \sin(32.11) \sin^2 \left(\frac{76 - 350}{2} \right)} = 32.03^\circ.$$

From Eq. 8.32, the RF is:

$$(b) \text{ RF} = \frac{577}{32.03} \left(\frac{180}{\pi} \right) \tan \left(\frac{32.03}{2} \right) = 296.1 \text{ ft.}$$

Hence, using Eqs. 8.31a, 8.31b, and 8.31c,

$$(c) \begin{aligned} x_2 &= 102 + (\sin 3.15 \cos 350 + \sin 32.11 \cos 76)(296.1) = 156 \text{ ft,} \\ y_2 &= 99 + (\sin 3.15 \cos 350 + \sin 32.11 \sin 76)(296.1) = 248 \text{ ft,} \\ z_2 &= 1,044 + (\cos 3.15 + \cos 32.11)(296.1) = 1,590 \text{ ft.} \end{aligned}$$

More-detailed derivations and examples are given later in this section when the use of vectors for directional-drilling calculations is discussed.

Constant Build and Turn Rate Method (CBTM). In this method, proposed by Planeix and Fox (1979), it is assumed that the build rate B and turn rate T are constant along the well trajectory. With this assumption, by integrating Eqs. 8.13 and 8.14, the trajectory coordinates can be obtained as:

$$\Delta x = \frac{1}{T^2 - B^2} [T(\sin \varphi_2 \sin \vartheta_2 - \sin \varphi_1 \sin \vartheta_1) + B(\cos \varphi_2 \cos \vartheta_2 - \cos \varphi_1 \cos \vartheta_1)] \quad \dots\dots\dots (8.33)$$

and

$$\Delta y = \frac{1}{T^2 - B^2} [B(\sin \vartheta_2 \cos \varphi_2 - \sin \vartheta_1 \cos \varphi_1) - T(\cos \vartheta_2 \sin \varphi_2 - \cos \vartheta_1 \sin \varphi_1)] \quad \dots\dots\dots (8.34)$$

The equation for calculating the change in a vertical coordinate, Δz , remains the same as for the RCM (Eq. 8.30c) and for this reason is not repeated here. It should be remembered that Eqs. 8.33 and 8.34 are valid only for points on the build and turn curves. As for the RCM, one can consider several special cases such as $T = 0$ and $B = \text{constant}$, $B = 0$ and $T = \text{constant}$ or perhaps $B = 0$ and $T = 0$.

Because the turn rate and the horizontal turn rate are functionally related ($T = H \sin \varphi$), the solutions for Δx , Δy , Δz are all the same as in the RCM. Here a special case of a wellbore trajectory composed of a segment of a circular helix will be discussed. Because a circular helix has constant curvature and constant inclination angle, the build rate is nil ($B = 0$) and the turn rate T is constant.

Example 8.8 Given hole inclination and azimuth angles at two points 100 ft apart on a trajectory composed of a part of a circular helix,

$$\begin{aligned} \varphi_1 &= \varphi_2 = 46.31^\circ, \\ \vartheta_1 &= 65.5^\circ \text{ and } \vartheta_2 = 73.78^\circ, \end{aligned}$$

calculate the:

- DLS and DL
- Pitch and radius of the helix

Solution. To calculate the DLS (curvature), use Eq. 8.22. Because $\varphi = \text{constant}$ and $B = 0$,

$$(a) \text{ DLS} = \sin \varphi \frac{d\vartheta}{ds}.$$

For a circular helix, the curvature is constant, so integrating the above equation yields

$$(b) \text{ DLS} = \sin \varphi \frac{\Delta \vartheta}{\Delta s} = (1.045 \times 10^{-3} \text{ radians/ft} = 5.99^\circ/100 \text{ ft.})$$

Hence, the turn rate $T = 8.28^\circ/100 \text{ ft}$ (0.001445 radians/ft), and the DL is 5.99° .

From calculus, it is known that the x , y , z coordinates of a circular helix with radius r and pitch p are given by the following equations:

$$(c) \text{ } x(s) = r \cos(Ts),$$

$$(d) \ y(s) = r \sin(Ts),$$

$$(e) \ z(s) = \frac{p}{2\pi} Ts.$$

Taking derivatives with respect to s ,

$$(f) \ \frac{dx}{ds} = -rT \sin(Ts),$$

$$(g) \ \frac{dy}{ds} = rT \cos(Ts),$$

$$(h) \ \frac{dz}{ds} = \frac{p}{2\pi} T.$$

It is also known (from Eqs. 8.7 and 8.9) that $\frac{dz}{ds} = \cos \varphi$ and $\frac{dy}{ds} = \sin \varphi \cos \vartheta$. From the above equations, it is possible to obtain the radius of the helix,

$$(i) \ r = \frac{\sin \varphi}{T} = \frac{\sin(46.31)}{0.001446} = 500 \text{ ft},$$

and the pitch of the helix,

$$(j) \ p = \frac{2\pi \cos \vartheta}{T} = \frac{2\pi \cos(46.31)}{0.001446} = 3,000 \text{ ft}.$$

For practical 3D well-path calculations, the designer can assume the radius, the pitch of the helix, and the required hole-inclination angle and calculate the turn rate, the hole azimuth, and the corresponding coordinates x , y , and z along the well path.

Constant Curvature and Build Rate Method (CCBM). The *constant-curvature method* was proposed by Guo et al. (1992) to produce a well path that can be drilled with a constant tool face (as explained in Section 8.3) and to provide more flexibility in 3D well-path trajectory designs. In this method, it is assumed that the wellbore curvature (κ , DLS) and build rate B are constant with the MD s . This method is also known as the *constant tool-face method* and was proposed by Schuh (1992).

Again, to calculate the coordinates, Eqs. 8.13, 8.14, and 8.15 are needed. To perform the required integrations, the inclination and azimuth angles must be determined along the trajectory.

Using Eqs. 8.1 and 8.3,

$$\varphi(s) = \varphi_1 + B(s - s_1) \quad \dots \dots \dots (8.35)$$

and

$$\vartheta(s) = \vartheta_1 + \int_{s_1}^{s_2} T(s) ds. \quad \dots \dots \dots (8.36)$$

The turn rate in Eq. 8.36 can be expressed in terms of DLS and build rate as

$$T(s) = \frac{\sqrt{\text{DLS}^2 - B^2}}{\sin \varphi(s)}. \quad \dots \dots \dots (8.37)$$

With the assumption that the DLS and build rate are constant, integration of Eq. 8.36 yields

$$\vartheta(s) = \vartheta_1 + \frac{\sqrt{\text{DLS}^2 - B^2}}{B} \ln \left[\frac{\tan\{\frac{1}{2}\varphi(s)\}}{\tan(\frac{1}{2}\varphi_1)} \right]. \quad \dots \dots \dots (8.38)$$

It is clear that because of the nonlinear form of Eq. 8.38, the integrals of the trajectory equations (Eqs. 8.13 and 8.14) need to be evaluated numerically. Closed-form solutions can be obtained for a case where the well path is

part of a circular helix. For a circular helix, the build rate is nil, resulting in a constant hole-inclination angle and constant turn rate, as discussed earlier.

Much simpler solutions are possible if the average values of turn rates are used piecewise for calculations. The average values are given by the following equations:

$$\bar{H} = \frac{\sqrt{DLS^2 - B^2}}{B \Delta s} \int_{\varphi_1}^{\varphi_2} \frac{d\varphi}{\sin^2 \varphi} = \frac{\sqrt{DLS^2 - B^2}}{B \Delta s} (\cot \varphi_1 - \cot \varphi_2), \quad \dots \quad (8.39)$$

$$\bar{T} = \frac{\sqrt{DLS^2 - B^2}}{B \Delta s} \int_{\varphi_1}^{\varphi_2} \frac{d\varphi}{\sin \varphi} = \frac{\sqrt{DLS^2 - B^2}}{B \Delta s} \ln \left[\frac{\tan(\frac{1}{2}\varphi_2)}{\tan(\frac{1}{2}\varphi_1)} \right]. \quad \dots \quad (8.40)$$

Once the average values have been determined, the RCM or constant build-and-turn method can be used to calculate the desired rectangular coordinates x , y , and z along the well trajectory.

Example 8.9 In Guo et al. (1992), a practical example is provided for the case of a trajectory that must avoid an underground obstruction at least 90 ft from a vertical passing through the initial and final points of the trajectory. The initial point is located at $x = 100$ ft, $y = 100$ ft, and $z = 1,000$ ft. The endpoint (target point) of the section is at $x = 205$ ft, $y = 445$ ft, and $z = 1,890$ ft. The course length is limited to 1,000 ft.

Solution. The solution requires an iterative approach, and the results are given in **Table 8.1** (radius of curvature), **Table 8.2** (constant turn rate), and **Table 8.3** (constant curvature). The horizontal projection and inclination angle vs. MD plots of the three trajectories are shown in **Figs. 8.14 and 8.15**.

Another method to obtain a smooth 3D curved well path connecting the initial position (e.g., the KOP) with a target involves the use of splines and polynomials. Scholes (1983) was the first to use cubic functions (cubic splines) with four independent parameters to determine the desired rectangular coordinates of the trajectory. Each section of the well path can be described by the following parametric equations:

$$x(t) = A_x s^3 + B_x s^2 + C_x s + D_x, \quad \dots \quad (8.41a)$$

$$y(t) = A_y s^3 + B_y s^2 + C_y s + D_y, \quad \dots \quad (8.41b)$$

$$z(t) = A_z s^3 + B_z s^2 + C_z s + D_z. \quad \dots \quad (8.41c)$$

The task of the designer is to determine the 12 coefficients (A , B , C , and D for x , y , and z) that exist in the above equations, based on given conditions at the initial and final points of the trajectory. More recently, Mitchell (2008) proposed the use of tension and compression splines, and the interested reader is referred to more specific treatments of this subject (Sampaio 2007).

8.1.8 Review Questions and Problems.

1. List major applications of directional wells.
2. Define hole inclination and azimuth angles.
3. Define HD and closure.
4. Define build and turn rates.
5. Consider two points on a curved part of a trajectory located in a vertical plane with the azimuth $\vartheta = 220^\circ$. The hole inclination angle at Point 1 and Point 2 are $\varphi_1 = 38^\circ$ and $\varphi_2 = 46^\circ$. The build rate is $B = 5.5^\circ/100$ ft. The rectangular coordinates of Point 1 are $x_1 = 1,650$ ft, $y_1 = 2,858$ ft, and $z_1 = 4,250$ ft.

Calculate:

- (a) x , y , z coordinates at Point 2
 - (b) Radius of curvature R
 - (c) HD between Point 1 and Point 2
 - (d) The length of the segment (differences in MD at Point 2 and Point 1) Δs
6. The build rate $B = 8.5^\circ/100$ ft and turn rate $T = 3.5^\circ/100$ ft. Calculate the average wellbore curvature between two parts on the trajectory with inclination angles $\varphi_1 = 17^\circ$ and $\varphi_2 = 53^\circ$. Also plot instantaneous curvature vs. hole-inclination angle φ and MD s .
 7. Consider two points on a 3D well trajectory with hole inclination and azimuth angles φ_1 , ϑ_1 and φ_2 , ϑ_2 . Derive Eq. 8.26 for calculating DL.

TABLE 8.1—WELL-PATH SECTION DESIGNED USING THE RCM [After Guo et al. (1998)]

<i>B</i> =4.13°/100 ft; <i>H</i> =20.80°/100 ft								
<i>S</i> (ft)	<i>I</i> (degrees)	<i>A</i> (degrees)	<i>L</i> (ft)	<i>x,N</i> (ft)	<i>y,E</i> (ft)	<i>Z</i> (ft)	DLS (degrees/100 ft)	<i>T</i> (degrees/100 ft)
1,050.0	3.6	31.9	141.0	100.0	100.0	1,000.0	4.13	1.3
1,100.0	5.7	32.7	145.0	103.0	102.0	1,050.0	4.13	2.1
1,150.0	7.7	33.9	151.0	108.0	105.0	1,099.0	4.14	2.8
1,200.0	9.8	35.5	158.0	115.0	110.0	1,149.0	4.17	3.5
1,250.0	11.8	37.5	168.0	122.0	115.0	1,198.0	4.22	4.3
1,300.0	13.9	39.8	179.0	131.0	122.0	1,247.0	4.30	5.0
1,350.0	16.0	42.5	192.0	140.0	131.0	1,295.0	4.42	5.7
1,400.0	18.0	45.5	207.0	151.0	141.0	1,343.0	4.58	6.4
1,450.0	20.1	48.9	223.0	162.0	153.0	1,390.0	4.80	7.1
1,500.0	22.2	52.7	241.0	173.0	167.0	1,437.0	5.08	7.8
1,550.0	24.2	56.8	261.0	185.0	183.0	1,483.0	5.41	8.5
1,600.0	26.3	61.2	282.0	196.0	201.0	1,528.0	5.80	9.2
1,650.0	28.3	66.0	305.0	206.0	222.0	1,572.0	6.25	9.9
1,700.0	30.4	71.1	329.0	215.0	245.0	1,616.0	6.74	10.5
1,750.0	32.5	76.5	355.0	222.0	270.0	1,659.0	7.28	11.2
1,800.0	34.5	82.2	383.0	227.0	297.0	1,700.0	7.86	11.8
1,850.0	36.6	88.3	412.0	230.0	326.0	1,741.0	8.47	12.4
1,900.0	38.7	94.6	443.0	229.0	356.0	1,781.0	9.11	13.0
1,950.0	40.7	101.3	475.0	225.0	388.0	1,819.0	9.77	13.6
2,000.0	42.8	108.2	508.0	216.0	420.0	1,856.0	10.45	14.1
2,050.0	44.8	115.4	542.0	203.0	452.0	1,892.0	11.14	14.7

TABLE 8.2—WELL-PATH SECTION DESIGNED USING THE CONSTANT-TURN-RATE METHOD [After Guo et al. (1992)]

<i>B</i> =4.13°/100 ft; <i>T</i> =11.02°/100 ft								
<i>S</i> (ft)	<i>I</i> (degrees)	<i>A</i> (degrees)	<i>L</i> (ft)	<i>x,N</i> (ft)	<i>y,E</i> (ft)	<i>Z</i> (ft)	DLS (degrees/100 ft)	<i>H</i> (degrees/100 ft)
1,050.0	4.0	2.9	141.0	100.0	100.0	1,000.0	4.20	157.4
1,100.0	6.1	8.4	145.0	104.0	100.0	1,050.0	4.29	104.1
1,150.0	8.1	13.9	152.0	110.0	102.0	1,099.0	4.41	77.8
1,200.0	10.2	19.4	160.0	118.0	104.0	1,149.0	4.56	62.2
1,250.0	12.3	24.9	169.0	127.0	108.0	1,198.0	4.74	51.9
1,300.0	14.3	30.4	181.0	137.0	113.0	1,246.0	4.95	44.5
1,350.0	16.4	35.9	194.0	148.0	120.0	1,295.0	5.17	39.0
1,400.0	18.5	41.5	209.0	160.0	130.0	1,342.0	5.40	34.8
1,450.0	20.5	47.0	226.0	172.0	141.0	1,390.0	5.65	31.4
1,500.0	22.6	52.5	244.0	184.0	155.0	1,436.0	5.91	28.7
1,550.0	24.6	58.0	264.0	195.0	172.0	1,482.0	6.17	26.4
1,600.0	26.7	63.5	286.0	206.0	191.0	1,527.0	6.45	24.5
1,650.0	28.8	69.0	309.0	215.0	212.0	1,571.0	6.72	22.9
1,700.0	30.8	74.5	334.0	223.0	236.0	1,615.0	6.99	21.5
1,750.0	32.9	80.0	360.0	229.0	261.0	1,657.0	7.27	20.3
1,800.0	35.0	85.5	388.0	232.0	289.0	1,698.0	7.54	19.2
1,850.0	37.0	91.0	418.0	233.0	318.0	1,739.0	7.81	18.3
1,900.0	39.1	96.6	448.0	231.0	349.0	1,778.0	8.08	17.5
1,950.0	41.1	102.1	481.0	226.0	381.0	1,817.0	8.34	16.7
2,000.0	43.2	107.6	514.0	217.0	413.0	1,854.0	8.60	16.1
2,050.0	45.3	113.1	549.0	205.0	446.0	1,889.0	8.85	15.5

TABLE 8.3—WELL-PATH SECTION DESIGNED USING CONSTANT-CURVATURE METHOD [After Guo et al. (1992)]								
$B=4.13^{\circ}/100$ ft; $DLS=6.07^{\circ}/100$ ft								
S (ft)	I (degrees)	A (degrees)	L (ft)	x,N (ft)	y,E (ft)	Z (ft)	DLS (degrees/100 ft)	T (degrees/100 ft)
1,050.0	4.1	311.0	141.0	100.0	100.0	1000.0	893.5	63.1
1,100.0	6.1	336.5	145.0	104.0	98.0	1050.0	393.1	41.9
1,150.0	8.2	354.6	152.0	110.0	96.0	1099.0	220.4	31.3
1,200.0	10.2	8.6	160.0	118.0	96.0	1149.0	141.1	25.1
1,250.0	12.3	20.0	169.0	127.0	99.0	1198.0	98.2	20.9
1,300.0	14.4	29.7	181.0	137.0	104.0	1246.0	72.4	18.0
1,350.0	16.4	38.1	194.0	148.0	111.0	1295.0	55.7	15.8
1,400.0	18.5	45.5	209.0	160.0	121.0	1342.0	44.3	14.1
1,450.0	20.6	52.2	226.0	171.0	134.0	1389.0	36.2	12.7
1,500.0	22.6	58.3	244.0	181.0	149.0	1436.0	30.1	11.6
1,550.0	24.7	63.8	264.0	191.0	166.0	1482.0	25.6	10.7
1,600.0	26.7	69.0	286.0	199.0	186.0	1527.0	22.0	9.9
1,650.0	28.8	73.8	309.0	207.0	208.0	1571.0	19.2	9.3
1,700.0	30.9	78.2	334.0	213.0	233.0	1614.0	16.9	8.7
1,750.0	32.9	82.5	361.0	217.0	259.0	1657.0	15.1	8.2
1,800.0	35.0	86.4	389.0	220.0	286.0	1698.0	13.6	7.8
1,850.0	37.1	90.2	418.0	221.0	316.0	1739.0	12.3	7.4
1,900.0	39.1	93.8	449.0	220.0	347.0	1778.0	11.2	7.1
1,950.0	41.2	97.3	481.0	217.0	379.0	1816.0	10.3	6.8
2,000.0	43.2	100.6	515.0	211.0	412.0	1853.0	9.5	6.5
2,050.0	45.3	103.8	550.0	204.0	446.0	1889.0	8.8	6.3

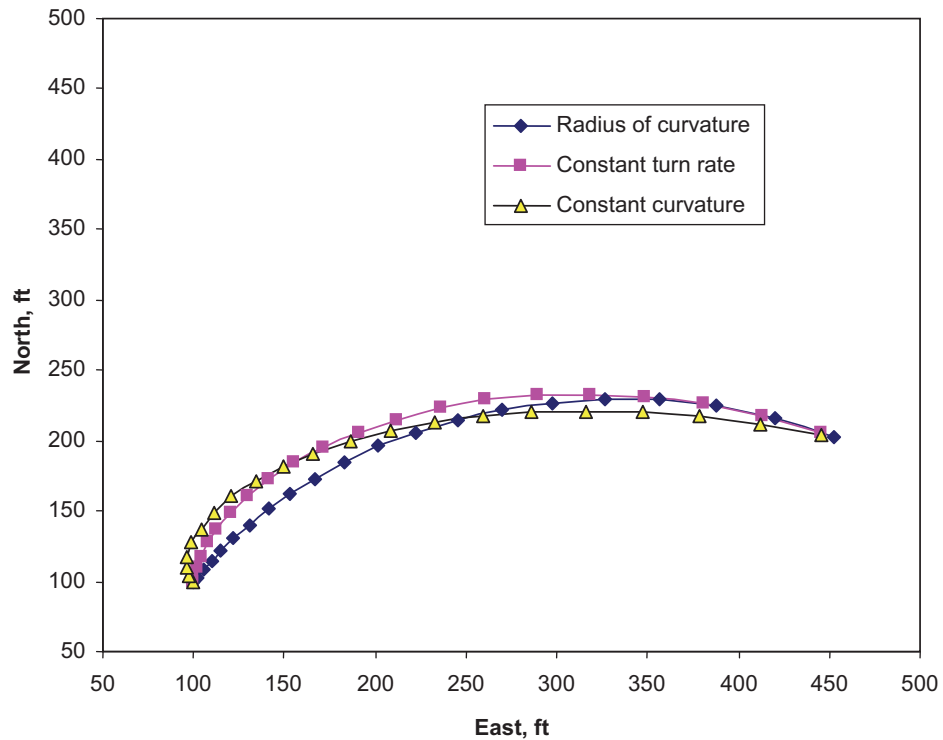


Fig. 8.14—Example 8.9: horizontal projections.

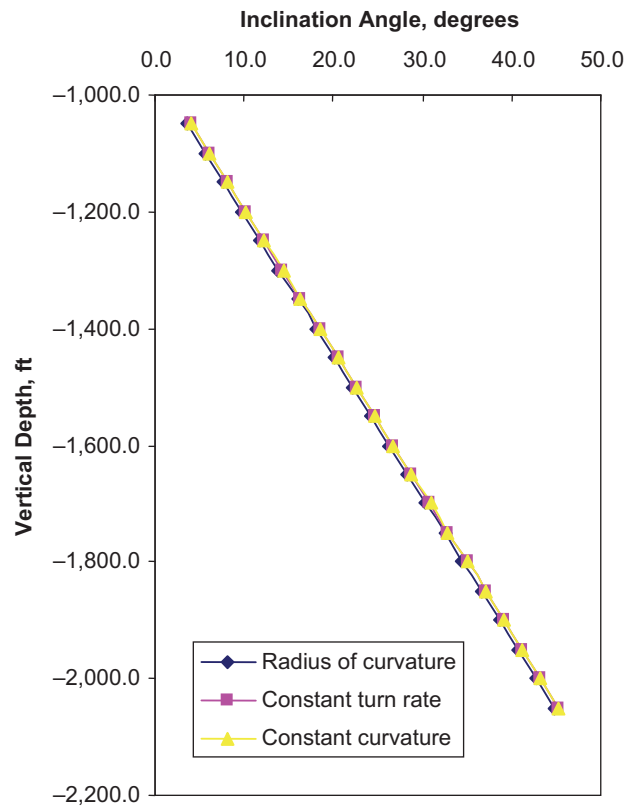


Fig. 8.15—Example 8.9: inclination angles vs. vertical depth.

8. Inclination and azimuth angles at two neighboring points on the well trajectory are as below:

Point	Inclination Angle, degrees	Azimuth Angle, degrees
Point 1	24.2	56.8
Point 2	40.7	101.3

Calculate the DL.

9. Make a schematic diagram of the three basic 2D directional well trajectories.
10. Design trajectory of a slant-type offshore well for the conditions as stated below:
 - Elevation (above sea level) of the rotary table = 80 ft
 - Target depth (subsea) = -6,479 ft
 - Target north coordinate = 3,846 ft
 - Target west coordinate = 4,226 ft
 - Declination = 5.5° E
 - KOP depth = 1,875 ft
 - Build-up rate = 3°/100 ft
11. Design a directional well trajectory using a build, hold and drop segments if the TVD is 14,100 ft and the HD is 9,010 ft. It is recommended that the build and drop is 2°/100 ft. The KOP is at the depth of 1,800 ft.
12. Plan a modified S-shaped trajectory where the target must intersect at a constant inclination of 20°. KOP depth is 1,500 ft, and TVD at the end of drop-off section is 8,500 ft. Rate of drop and build is 2°/100 ft. The desired HD from the surface location is 3,100 ft, and TVD is 9,075 ft.
13. It is desired to design the simple tangent horizontal well profile given:
 - KOP = 1,200 ft
 - VDT = 6,500 ft
 - Minimum tangent length = 150 ft
 - HD = 5,800 ft

14. It is required to find the difference in rectangular coordinates between two points on a well path located $\Delta s = 600$ ft apart given the following:

Point	Inclination Angle, degrees	Azimuth Angle, degrees
Point 1	24.2	56.8
Point 2	40.7	101.3

Perform calculations using:

- AAM
 - RCM
 - MCM
15. Consider data as in Problem 14 above. Calculate the build and turn rates in the middle point of the segment.
16. Derive Eqs. 8.33 and 8.34.
17. Consider two points on a 3D well trajectory with the hole inclination and azimuth angles as follows:

Point	Inclination Angle, degrees	Azimuth angle, degrees
Point 1	45.9	7.5
Point 2	50.0	39.8

The distance between Point 1 and Point 2 is 810 ft. Calculate the hole-inclination angle ϕ and azimuth ϑ at 202 ft and 607 ft from the first point. Assume constant curvature and build rate between Point 1 and Point 2.

18. Given are hole-inclination and azimuth angles at two points 100 ft apart on a trajectory composed of a part of circular helix.

$$\phi_1 = 46.31^\circ \quad \text{and} \quad \phi_2 = 46.31^\circ$$

$$\vartheta_1 = 65.5^\circ \quad \text{and} \quad \vartheta_2 = 73.78^\circ$$

It is required to calculate:

- DLS and DL
- Pitch and radius of the helix

19. Consider data as in Example 8.9. Is it possible to design the well trajectory using the minimum curvature method such that it would meet the prescribed requirements?

8.2 Deviation Control

A number of different methods have been invented to initiate new hole-inclination and azimuth angles (e.g., at KOPs) and to maintain control of a well path while drilling. In some applications, a whipstock or hydraulic jetting can be a cost-effective method to initiate a hole departure from the vertical and to make other required adjustments in hole direction. In buildup or drop-off wellbore segments, as well as in straight-hole drilling (e.g., drilling a tangent section), the inclination angle can be controlled to some extent using a conventional BHA by careful selection of BHA components. Considerable control of a well path, in terms of hole inclination and azimuth angles, can be achieved using downhole motors with a bent sub or bent housing and rotary-steerable tools. Some of these methods are described below.

8.2.1 Whipstocks and Jetting Techniques. Whipstocks and jetting techniques of various types were the principal deflection tools for many years before turbine-type and positive-displacement mud motors were fully developed and made economical for drilling applications. A whipstock is a wedge-shaped steel casting with a tapered concave groove down one side to guide the bit into the wall of the hole to start a deflection. There are two basic types of whipstocks: fixed and removable. The fixed whipstock stays in the hole after the desired deflection (change in hole-inclination and azimuth angles) has been accomplished, while the removable one is pulled out of the hole with the drillstring. A whipstock can be set in an open and cased hole. **Fig. 8.16** shows a removable whipstock in an openhole operation.

The whipstock edge angle is selected according to the desired deflection. A bit of diameter small enough to fit into the hole with the whipstock is then chosen. Initially, the whipstock is fixed to the drillstring above the bit. When the whipstock is positioned at the KOP depth, the center line of the toe is oriented in the desired direction.

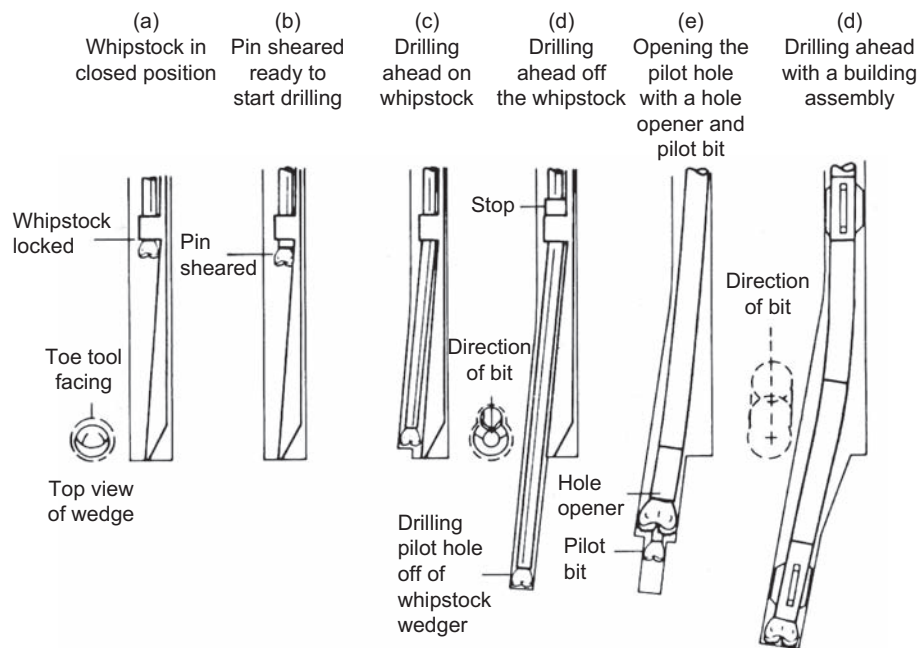


Fig. 8.16—Drilling with retrievable whipstock (Bourgoyne et al. 1986).

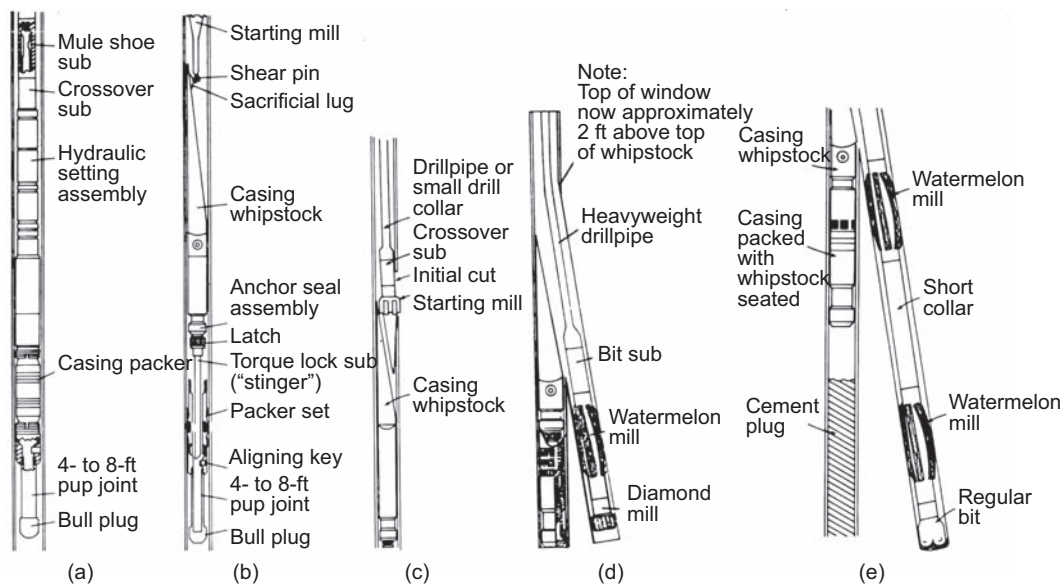


Fig. 8.17—(a) Setting the packer and whipstock seat; (b) locking the whipstock into the packer assembly; (c) cutting the casing with the starting mill; (d) cutting a window in the casing with a side-packing mill; (e) drilling ahead with a tricone bit through a window in the casing (Bourgoyne et al. 1986).

The principles of tool-deflection orientation are described in Section 8.3. With the whipstock assembly oriented, enough weight is applied to the toe of the wedge to prevent whipstock movement when rotation begins. Additional weight is applied to shear the pin that holds the whipstock to the drillstring. As rotation begins, the bit starts to drill forward and sideways according to the shape of the whipstock. Drilling continues until the stop reaches the top of the whipstock, as shown in Fig. 8.16d. Then the whipstock assembly is pulled out, and a pilot bit with a hole opener (reamer) is used to enlarge the wellbore to the desired size. Subsequently, a proper building assembly is run to drill the curved section of the hole. Fixed whipstocks typically are used to sidetrack an existing cased hole, as shown schematically in Fig. 8.17.

Typically, the operation is accomplished in three stages. First, a window is cut with the milling tool. Then the starting mill is replaced by a sidetracking mill, which makes a window approximately 8 to 12 ft long. Then the sidetracking mill is pulled out and replaced by a taper mill and a BHA with watermelon mills to enlarge the casing window to accommodate a conventional BHA. In some applications, a number of trips and many rotating hours are required to make the desired sidetrack.

In soft formations, deflection can be accomplished using a jetting technique, as shown in **Fig. 8.18**. Typically, a rotary three-roller-cone bit with three nozzles, two small and one large, is run into the hole and properly oriented. Drilling-fluid circulation is then initiated to begin the washing action. Rock erosion occurs due to the change in fluid momentum at the bottom of the hole. First, the bit is advanced without rotation for a distance of approximately 3 to 6 ft. Then rotation is started, and conventional drilling proceeds for 20 to 25 ft. A survey is taken to evaluate the inclination and azimuth of the jetted interval. If a change is required, the jetting assembly is oriented again, and the process is repeated until the desired trajectory is achieved. The hardness of the surrounding rocks is the main factor that determines jetting efficiency. Very soft rocks have a tendency to erode too much, making it difficult to maintain the desired direction. Reduction in flow rate may be a good solution if cuttings transport is not a problem. In harder rocks, the rate of jetting is small. However, under some geological conditions, the jetting technique can be the most economical.

8.2.2 Mechanics of BHAs. In conventional rotary drilling, the bottomhole assembly (BHA) is the part of the drillstring that is placed above the drill bit for loading the bit and controlling the wellbore trajectory. The BHA composition can be relatively simple, consisting of only drill collars and a drillpipe, or more complex, consisting of two (or even three) sizes of drill collars, heavyweight drillpipe, and regular drillpipe, as shown in **Fig. 8.19**. For some directional-drilling applications, to drill complex trajectories and to obtain the desired information about subsurface formations, the BHA composition can be very complex, as shown in **Fig. 8.20**.

In general, many parameters influence the performance of BHAs, including

- Bending stiffness (the product of modulus of elasticity and moment of inertia) and weight of each component of the BHA
- Position of each element in the BHA with reference to the drill bit
- Local inclination, azimuth, curvature, and diameter of the hole
- Formation properties and drill-bit type
- WOB and bit rotational speed

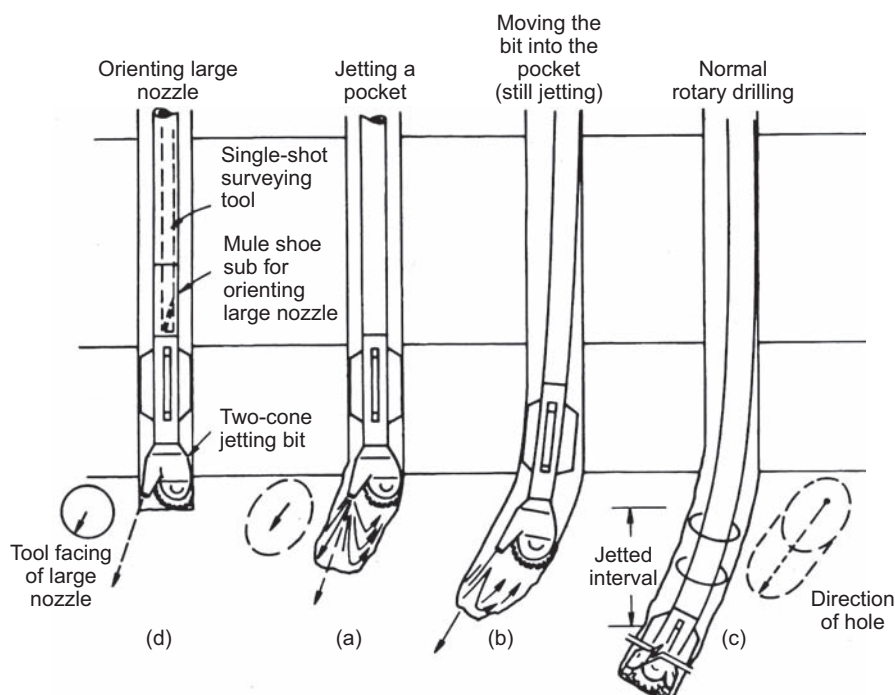


Fig. 8.18—Jetting a trajectory change (Bourgoyne et al. 1986).

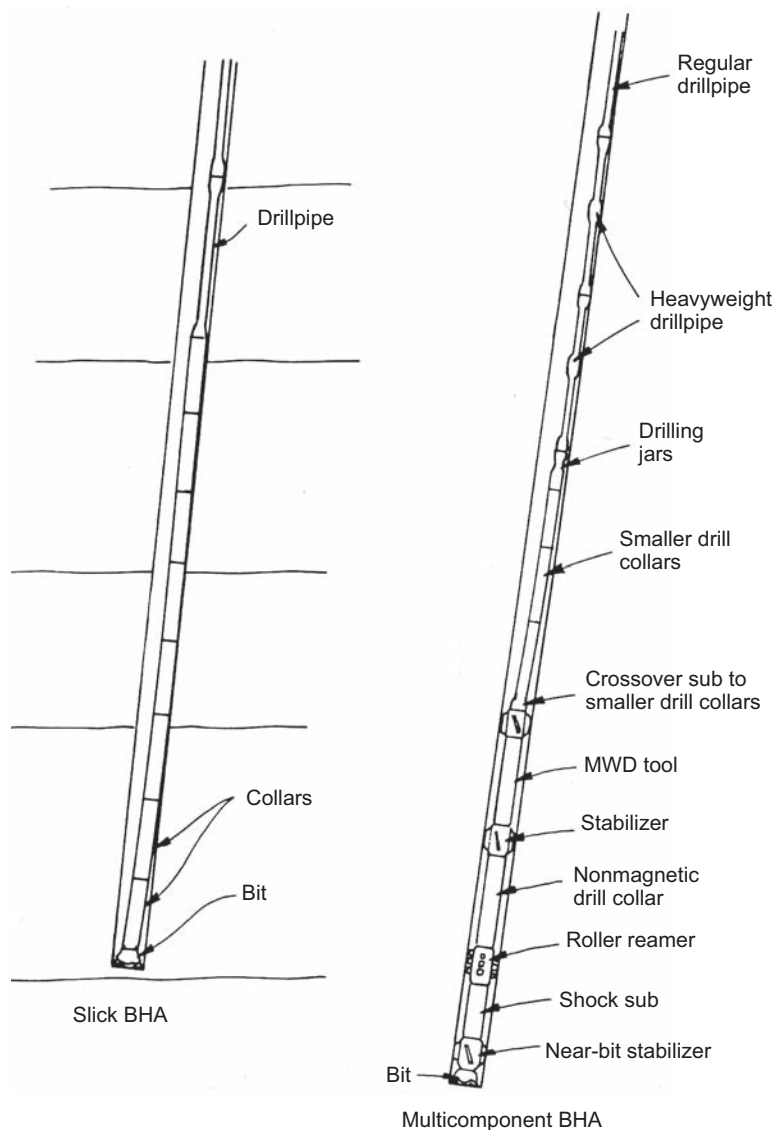


Fig. 8.19—Examples of BHAs (Bourgoyne et al. 1986).

This section presents the major concepts that govern the BHA directional-drilling behavior and mechanical performance. The goal is to find an equilibrium BHA configuration with a known composition in terms of geometric and mechanical properties. Once such an equilibrium configuration has been found, it is possible to determine the forces acting at the bit and to predict the direction of the anticipated drill-bit displacement and consequently that of the wellbore. It is also possible to calculate forces and moments along the BHA and to assess BHA mechanical integrity. Of course, the BHA as designed must not only meet the directional-drilling objectives, but also be strong enough to avoid costly downhole failures.

Here, for the sake of simplicity, a slick assembly will be analyzed first, followed by an assembly with one stabilizer. Developments in straight, inclined, and curved sections of the wellbore will be presented. In all cases, the analysis will be limited to 2D wellbores with the well path confined to a vertical plane. Drill-bit rotation, inertia, and drilling-fluid flow effects are not considered.

Slick Assembly in an Inclined Hole. For the sake of simplicity, consider a slick (uniform inside and outside diameters) BHA in a straight, but inclined, hole, as shown schematically in Fig. 8.21. Also for the sake of simplicity, the system is assumed to be two-dimensional and confined to a vertical plane. At some distance above the bit, the string contacts the low side of the wellbore at a point called the *tangency point*. This discussion will also assume that the string lies on the low side of the hole, as shown in Fig. 8.21. Actually, under some conditions, the string will not lie along the low side, but will buckle and may develop a snaky or even a helical shape.

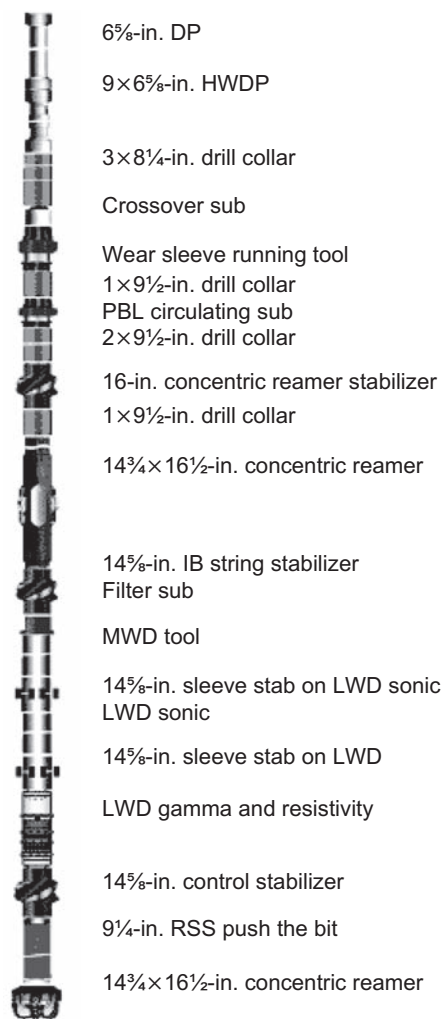


Fig. 8.20—Example of a BHA with a rotary-steerable system and LWD and MWD units (Frenzel and Kull 2008).

Let the axial component of the resultant force R at the bit be defined as the WOB and denote it as W , and let the lateral component be defined as a side force, H_0 (Fig. 8.21). With no WOB, the only force acting on the bit is the side force, which is created by the weight of the string between the bit and the tangency point. This force tends to bring the hole toward the vertical (the pendulum effect). When weight is applied to the bit (a portion of the drill collar is slacked off on the bit by reducing hook load), another force is generated that tends to push the bit toward the upper side of the hole, away from the vertical. With a large enough WOB, the side force is nil ($H_0 = 0$), and the resultant force direction angle, Φ , becomes the same as the hole inclination angle, ϕ . Assuming that the formation and bit do not have a preferential direction for drilling (isotropic drilling conditions), a straight hole is drilled. If the WOB is further increased, the bit is pushed upward, the side force changes direction, and a hole with an inclination angle greater than the original angle will be drilled.

In other words, under isotropic drilling conditions, the BHA may have dropping, holding, or building tendencies, depending on the side force acting on the bit. Moreover, the instantaneous direction of bit penetration into the rock is the same as the direction of the resultant force acting on the drill bit. If a straight hole is drilled, the side force is zero, and it can be said that an equilibrium hole angle has been achieved.

Field experience indicates that formations with bedding planes exhibit better drillability when drilled perpendicular rather than parallel to the bedding planes. In other words, inclined bedding planes make the bit drill up dip, as shown schematically in Fig. 8.22. Consequently, the instantaneous direction of drilling (designated by the symbol ψ in Fig. 8.22) is different from the direction of the resultant force on the drill bit in anisotropic formations.

Lubinski and Woods (1953) introduced the so-called *drilling anisotropy index* for quantitative predictions of drill-bit penetration direction while drilling in anisotropic formations. By definition, the drilling anisotropy index

(h) is the relative difference of drillabilities parallel and perpendicular to bedding planes. If $h = 0$, the formation is isotropic from the standpoint of deviation control. Ho (1986) extended the definition of the anisotropy index to 3D systems.

For a more detailed analysis, differences in the drill bit face- and side-cutting abilities can be included. For example, the face-cutting ability of many rotary tricone roller bits is much better than their side-cutting ability. On the other hand, some diamond bits have similar side- and face-cutting abilities.

It can be shown that the formation dip angle, γ_f , the hole inclination angle, φ , the resultant force angle, Φ , and the drilling anisotropy index, h , are related by the following expression:

$$h = 1 - \frac{\tan(\gamma_f - \varphi)}{\tan(\gamma_f - \Phi)}, \quad \dots \dots \dots (8.42)$$

where φ is the equilibrium hole inclination angle. Eq. 8.42 makes it possible to determine the anisotropy index from actual drilling data if the quantities γ_f , φ , and Φ are known. Examination of Eq. 8.42 reveals that if the resultant-force direction is the same as the hole inclination angle ($\varphi = \Phi$), the value of $h = 0$, and the formation is considered to be isotropic from the standpoint of deviation control.

Because $H_0/W = \tan(\Phi - \varphi)$, it can be shown that the following equation relates side force, H_0 , WOB, W , formation anisotropy index, h , hole inclination angle, φ , and formation dip angle, γ :

$$\frac{H_0}{W} = \frac{h \tan(\varphi - \gamma_f)}{1 - h + \tan^2(\varphi - \gamma_f)} = \tan(\Phi - \varphi). \quad \dots \dots \dots (8.43)$$

Eq. 8.43 couples the interaction between the drill bit and the formation. To use Eq. 8.43, the side force at the bit, H_0 , must be known. This force can be determined from the equilibrium configuration of the BHA.

For this purpose, an idealized system for investigating drill-collar static-equilibrium configurations, but one still useful for practical applications, is presented in **Fig. 8.23**. The borehole is modeled as a cylinder with rigid walls free of any irregularities. Drill collars are represented by an elastic line $Y = Y(X)$, with the unit weight in fluid denoted as w and the bending stiffness denoted as EI . The elastic line of drill collars OT is a plane curve

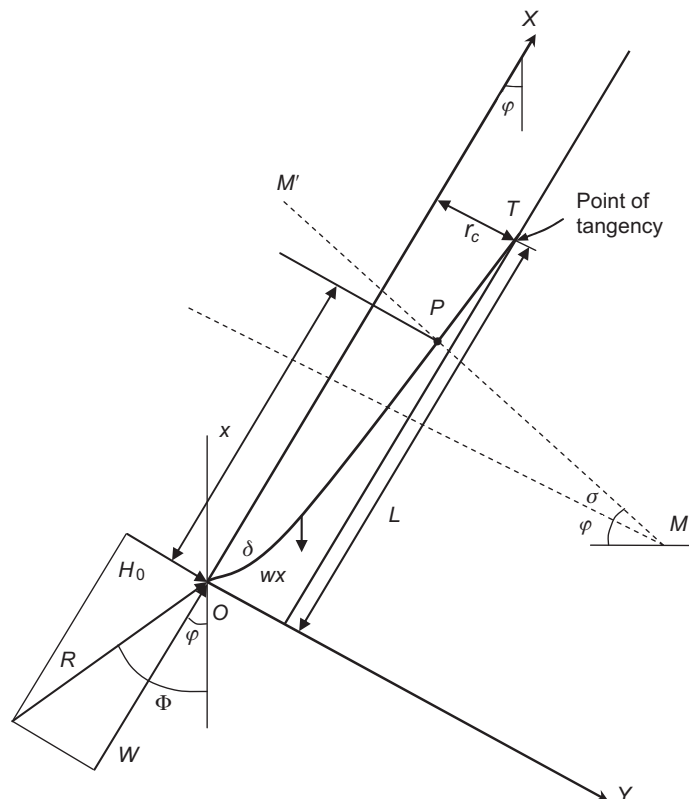


Fig. 8.23—Elastic line of drill collars in an inclined plane.

that lies on the low side of the hole for some interval above the point of tangency, designated as T . The distance from the bit to the point of tangency is denoted as L . In other words, at the point of tangency, $X = L$, both the slope (the first derivative, $\frac{dY}{dX}$) and the curvature are zero. For small deflections, it may be assumed that the elastic-line curvature is equal to the second derivative $\left(\frac{d^2Y}{dX^2}\right)$. In addition, dynamic effects are ignored, and the bit is centered in a borehole at Point 0, which is the origin ($X = 0, Y = 0$) of the orthogonal system of X - Y coordinates. At the point of tangency, the deflection is equal to the radial clearance, r_c , between the wellbore and the drill collars, as shown in Fig. 8.22 [$r_c = 0.5(D_h - OD_{dc})$].

For small deflections, the governing differential equation of the elastic line of drill collars is given by the well-known equation:

$$EI \frac{d^3Y}{dX^3} = S, \quad \dots\dots\dots (8.44)$$

where S = the shearing force at any arbitrary cross section, such as $M'M$ in Fig. 8.23, EI = the bending stiffness (the product of the modulus of elasticity E and the moment of inertia, I) = $\frac{\pi}{64}(OD_{dc}^4 - ID_{dc}^4)$, and OD_{dc} , ID_{dc} = drill-collar outside and inside diameters.

Projecting all the forces onto $M'M$:

$$S = H_0 \cos(\delta) - W \sin \delta + wX \sin(\varphi + \delta). \quad \dots\dots\dots (8.45)$$

Substituting Eq. 8.45 into Eq. 8.44 and noting that for small deflections,

$$\cos \delta \cong 1 \text{ and } \tan \delta \cong \frac{dY}{dX},$$

after some rearrangements,

$$EI \frac{d^3Y}{dX^3} + (W - Xw \cos \varphi) \frac{dY}{dX} = H_0 + Xw \sin \varphi. \quad \dots\dots\dots (8.46)$$

Eq. 8.46 is referred to as Lubinski's equation.

Integration of Eq. 8.46 yields three unknown constants of integration. Because the side force at the bit, H_0 , and the distance to the point of tangency, L , are also unknown, altogether the number of unknowns is five. Consequently, five boundary conditions are needed to obtain the desired solution.

For a slick BHA, the geometric (natural) boundary conditions are as follows:

At the bit:

$$X = 0, Y = 0, \quad \dots\dots\dots (8.47a)$$

And at the point of tangency:

$$Y(L) = r_c, \quad \frac{dY}{dX} = 0 \text{ and } \frac{d^2Y}{dX^2} = 0. \quad \dots\dots\dots (8.47b)$$

Clearly, one more boundary condition is needed to solve the problem. It is typically assumed that the bending moment at the bit is zero, resulting in the following equation:

$$EI \frac{d^2Y}{dX^2} = 0. \quad \dots\dots\dots (8.47c)$$

The governing differential equation, Eq. 8.46, with the boundary conditions given by Eq. 8.47, can be solved using an iterative technique or the power-series method (Lubinski 1987).

The solution, however, may be greatly simplified if $W \gg (wL \cos \varphi)$. This condition is satisfied for large values of WOB, W , and, in wells with high inclination angle, φ ($\varphi \geq 70^\circ$). With this simplification, the governing differential equation can be written as:

$$EI \frac{d^3Y}{dX^3} + W \frac{dY}{dX} = H_0 + Xw \sin \varphi. \quad \dots\dots\dots (8.48)$$

To obtain solutions independent of hole size, drill-collar properties, WOB, and mud weight, the following substitutions can be introduced (Lubinski 1987):

$$Y = m_1 y \text{ and } X = m_2 x, \quad \dots \quad (8.49)$$

where m_1, m_2 = scaling factors in the Y- and X- directions, ft, and x, y = dimensionless coordinates.

Substituting Eq. 8.49 into Eq. 8.48 [to obtain the derivatives, the chain rule of differentiation (e.g., $\frac{dY}{dX} = \frac{m_1}{m_2} \frac{dy}{dx}$, is used)] the result indicates that to obtain the dimensionless form of the governing differential equation, the scaling factors m_1 and m_2 are as follows:

$$m_1 = \frac{EI w \sin \varphi}{W^2}, \quad \dots \quad (8.50a)$$

$$m_2 = \sqrt{\frac{EI}{W}}; \quad \dots \quad (8.50b)$$

consequently, Eq. 8.48 takes the dimensionless form given below:

$$\frac{d^3 y}{dx^3} + \frac{dy}{dx} = h_o + x. \quad \dots \quad (8.51)$$

The corresponding dimensionless boundary conditions are:

At the bit:

$$y(0) = 0, y''(0) = 0 \quad \dots \quad (8.52a)$$

and at the point of tangency:

$$y(\ell) = \frac{r_c}{m_1} = c, \quad y'(\ell) = 0, \quad \text{and} \quad y''(\ell) = 0 \quad \dots \quad (8.52b)$$

The variables h_o, ℓ , and c in Eqs. 8.51 and 8.52b represent the dimensionless side force at the bit, the dimensionless distance to the tangency point, and the dimensionless radial clearance (apparent wellbore radius), respectively.

Solving Eq. 8.51 with the boundary conditions given by Eq. 8.52 yields the desired equation for the centerline of the drill collars in the dimensionless form:

$$y = -1 + \cos x + \left(\frac{1 - \cos \ell}{\sin \ell} \right) \sin x + \frac{1}{2} x^2 + h_o x, \quad \dots \quad (8.53)$$

where

$$h_o = \tan \frac{\ell}{2} - \ell \quad \dots \quad (8.54a)$$

$$\frac{r_c}{m_1} = c = \ell \tan \frac{\ell}{2} - \frac{\ell^2}{2}. \quad \dots \quad (8.54b)$$

Simultaneous solution of Eqs. 8.54a and 8.54b yields the dimensionless side force, h_o , and the dimensionless distance to the point of tangency, ℓ .

The actual (dimensional) side force can now be found from:

$$H_o = m_3 h_o, \text{ where } m_3 = EI \frac{m_1}{m_2^3}. \quad \dots \quad (8.54c)$$

In practical applications, in addition to the side force, it is also necessary to know the so-called *tilt angle*, which describes the direction in which the bit is pointed out. The tilt angle is the angle between the centerline of the hole and the centerline of the bit and is denoted as δ in Fig. 8.23.

To determine the tilt angle, it is first necessary to find the slope of the drill-collar centerline at the bit. The first step is to determine the dimensionless tilt angle by differentiating Eq. 8.53 and setting $x = 0$ in the resulting expression. Then the dimensionless tilt angle needs to be converted to its dimensional form, expressed typically in degrees. For a slick BHA, the tilt angle is fairly small, in the range of approximately 0.1–0.5°.

Using Eqs. 8.42, 8.43, 8.53, and 8.54, several important practical problems can be solved, as illustrated by the following examples. It should be noted that all the above equations are valid in any consistent system of units.

Example 8.10 Consider a 6¼- by 2¼-in. (unit weight 91 lbf/ft) slick BHA in a straight hole, 8½ in. in diameter, with an inclination angle of 25°. The drill collars are made of steel with a modulus of elasticity of $30(10)^6$ lbf/in.². The mud weight is 10 lbf/gal (specific gravity = 1.2) and the WOB is 30,000 lbf. Determine whether this BHA exhibits dropping, holding, or building angle tendencies for the following two cases:

- Case 1: Formation is nondipping and isotropic ($\gamma_f = 0$, $h = 0$).
- Case 2: Formation dip angle is 35° and the formation anisotropy index $h = 0.1$.

Solution. The first step is to calculate the unit weight, w , of the drill collars in the drilling fluid and their moment of inertia, which are equal to 77.1 lbf/ft and $(3.55) 10^{-3}$ ft⁴, respectively.

Then the scaling factors are calculated:

$$(a) \quad m_1 = \frac{(4,320)(10^6)(3.551(10^{-3}))(77.1)(\sin 25)}{(30,000)^2} = 0.555 \text{ ft},$$

$$(b) \quad m_2 = \sqrt{\frac{(4,320)(10^6)(3.551)(10^{-3})}{30,000}} = 22.613 \text{ ft},$$

$$(c) \quad m_3 = (4,320)(10^6)(3.551)(10^{-3}) \frac{0.555}{(22.613)^3} = 736.0 \text{ lbf}.$$

The radial clearance (apparent wellbore radius) is

$$(d) \quad r_c = \frac{0.5}{12}(8.5 - 6.25) = 0.09375 \text{ ft}.$$

Substituting the quantities m_1 and r_c into Eq. 8.54b yields

$$(e) \quad \ell \tan \frac{\ell}{2} - \frac{\ell^2}{2} = 0.1695.$$

By solving the above equation, the desired dimensionless distance to the point of tangency, $\ell = 1.352$, can be obtained. From Eq. 8.54a, the dimensionless side force at the bit can be calculated: $h_0 = -0.552$. Hence, the side force at the bit is $H_0 = (736)(-0.552) = -405$ lbf.

These calculations must be performed carefully because both the magnitude and the direction of the side force are very important for deviation-control applications. The reader is invited to repeat the calculations presented above and to verify both the sign and the magnitude of the side force of the bit.

In conclusion, if the formation is isotropic as stated in Case 1 ($h = 0$), the assembly under consideration will tend to drop because the side force is negative. The rate of change in the angle (the drop rate) depends on the magnitude of the side force, the hardness of the formation, and the side-cutting ability of the bit.

In Case 2, it is necessary to determine the directional tendency of the assembly for the formation dip angle $\gamma_f = 35^\circ$ and anisotropy index $h = 0.1$. For this purpose, the expected bit-displacement direction (with respect to the vertical) is calculated using Eq. 8.42. Setting $\varphi = \Psi$ and solving Eq. 8.42 for ψ :

$$\psi = \gamma_f - \arctan[(1-h)\tan(\gamma_f - \Phi)]. \quad \dots\dots\dots (8.55a)$$

The resultant force angle is:

$$\Phi = \varphi + \arctan\left(\frac{H_0}{W}\right) = 25 + \arctan\left(-\frac{405}{30,000}\right) = 24.23^\circ. \quad \dots\dots\dots (8.55b)$$

Therefore, from Eq. 8.55a, the expected instantaneous bit displacement is

$$\psi = 35 - \arctan[(1-0.1)\tan(35 - 24.23)] = 25.28^\circ. \quad \dots\dots\dots (8.55c)$$

Because the instantaneous rock-bit displacement direction (25.28°) is greater than the initial hole angle (25°), the assembly will exhibit building tendencies. It is therefore apparent that whether a given BHA will have a building or dropping tendency depends not only on the BHA composition and the WOB, but also on the formation-bit interaction.

If the above-calculated angle of 25.28° is used as a new hole inclination angle, a new scaling factor, m_1 , must be calculated, and consequently a new side force and its corresponding angle, ψ . These calculations can be repeated until a new hole-equilibrium angle is found. For anisotropic formations, the side force at the hole-equilibrium angle is not zero. The reader is encouraged to write a computer program to accomplish this evaluation.

For isotropic drilling conditions, a closed-form solution is presented here, as illustrated by Example 8.11 below.

Example 8.11 Consider BHA data as in Example 8.10 above. Assuming that the drilling conditions are isotropic, calculate the expected hole-equilibrium angle.

Solution. For isotropic drilling conditions at hole-equilibrium angle, the side force at the bit is nil. Therefore, Eq. 8.54a takes the form

$$\tan \frac{\ell}{2} - \ell = 0. \quad \dots\dots\dots (8.56a)$$

Solving for the dimensionless distance to the point of tangency, ℓ , the result is $\ell = 2.34$. Hence, from Eq. 8.54b,

$$\frac{r_c}{m_1} = 2.74. \quad \dots\dots\dots (8.56b)$$

Substituting for m_1 in Eq. 8.50a, Eq. 8.56b takes the form

$$\frac{r_c W^2}{EIw \sin \varphi} = 2.74. \quad \dots\dots\dots (8.56c)$$

From Eq. 8.56c, the equilibrium hole angle is

$$\varphi = \arcsin \left(\frac{r_c W^2}{2.74 EIw} \right) = \arcsin \left[\frac{(0.09375)(30,000)^2}{(2.74)(4,320 \times 10^6)(3.551 \times 10^{-3})(77.1)} \right] = 1.5^\circ \quad \dots\dots\dots (8.56d)$$

In conclusion, under isotropic drilling conditions, the assembly under consideration would theoretically be drilling along a certain trajectory with decreasing hole inclination angle to reach 1.5° of equilibrium hole inclination, at which the side force is nil. Once the equilibrium angle is reached, a straight inclined hole is drilled. If the hole inclination angle is given, using Eq. 8.56d, one can calculate the required WOB if the drill-collar bending stiffness, unit weight, and radial clearance are known. The reader is invited to perform a few calculations to develop the desired numerical experience.

Example 8.12 Suppose that while drilling a $12\frac{1}{4}$ -in. hole with an 8-in. by $2\frac{3}{4}$ -in. slick BHA in a formation with dip angle $\gamma_f = 16^\circ$, an hole-equilibrium angle of 11.5° has been established with a WOB of 52,000 lbf. Calculate the drilling anisotropy index, h .

Solution. Performing calculations analogous to those in Example 8.10 above, the side force at the bit can be found to be $H_0 = -397$ lbf. Consequently, the resultant force angle (Eq. 8.55b) is

$$(a) \quad \Phi = \varphi + \arctan \left(-\frac{397}{52,000} \right) = 11.06^\circ.$$

From Eq. 8.42, the drilling anisotropy is

$$(b) \quad h = 1 - \frac{\tan(15-11.5)}{\tan(15-11.06)} = 0.112.$$

Once the drilling anisotropy index has been determined, it is possible to predict a new hole equilibrium angle if the BHA properties (e.g., bending stiffness, effective unit weight) or the WOB were to change.

Slick Assembly in a Curved Hole. Many directionally drilled well profiles (slant type, S-shaped, horizontal wells) consist of straight sections and curved sections of constant curvature, as discussed in Section 8.1.6. Field experience indicates that drilling curved wellbore sections is usually more difficult than drilling slant parts. The following discussion will show how hole curvature will influence the magnitude and direction of the resultant

force as well as the direction in which the drill bit is pointed. However, essentially all the basic concepts of deviation control, as discussed in the part on straight holes, are also valid for curved holes, and the reader is advised to review that section before studying the following material.

A schematic diagram of a slick BHA in a hole with constant curvature is shown in **Fig. 8.24**. The center of the drill bit is at Point O, the line OA represents the centerline of the borehole, and the line OB represents the centerline of the drill collars.

To analyze BHA performance in a curved part of the wellbore, it is convenient to use an S-U system of coordinates, as shown schematically in **Fig. 8.25**. The S-coordinate is defined to coincide with the center of the borehole, and the abscissa, U, is chosen to be perpendicular to S. The function $U(S)$ represents the radial deflection of the centroidal axis of the elastic line of drill collars and is considered to be a positive deflection if directed to the right of the bore-

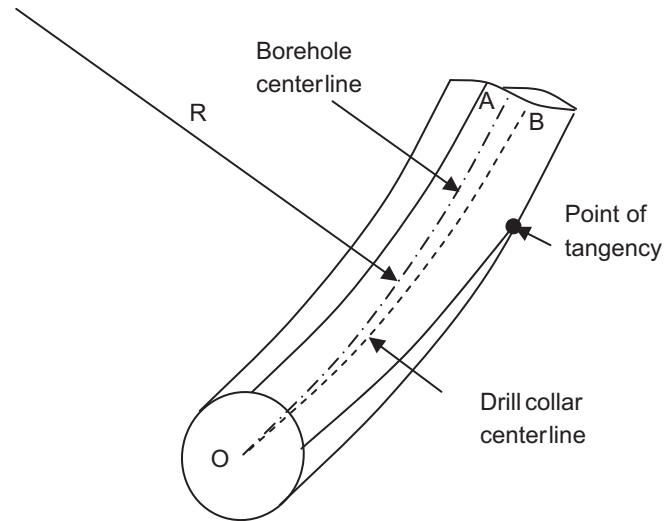


Fig. 8.24—Slick BHA in a curved wellbore with constant curvature [from Miska et al. (1998)]. Reprinted courtesy of the American Society of Mechanical Engineers.

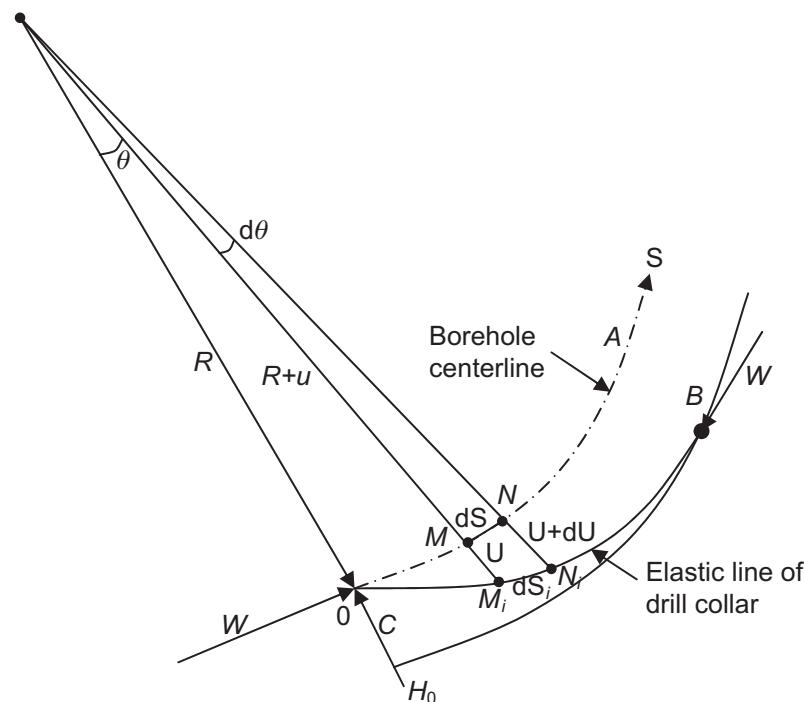


Fig. 8.25—S-U system of coordinates [from Miska et al. (1998)]. Reprinted courtesy of the American Society of Mechanical Engineers.

hole center line. The elastic line of drill collars has its origin at the bit (i.e., zero deflection) and extends to the low side of the borehole, where the point of tangency (i.e., maximum deflection) is eventually reached. Just above the point of tangency, the drill collars are assumed to lie on the low side of the borehole for some finite length.

The drill collars are assumed to be under constant compression between the drill bit and the tangency point. The borehole is modeled as having constant curvature (constant radius of curvature, R) in a 2D vertical plane. It should be noted that if the wellbore curvature goes to infinity, the wellbore become straight. Consequently, all equations discussed in this section are also valid for straight segments of wellbore if the curvature is set to zero (or the radius of curvature is set to infinity).

It can be shown that by transformation of coordinates from the X-Y to the S-U system, the governing differential equation, Eq. 8.48, can be transformed to the following form:

$$EI \frac{d^3 U}{dS^3} + \left(W + \frac{EI}{R^2} \right) \frac{dU}{dS} = H_0 + \left(\frac{W}{R} + w \sin \varphi \right) S. \quad (8.57)$$

In Eq. 8.57, the quantity R represents the wellbore radius of curvature, and all other variables are the same as in Eq. 8.46. Specifically, W is the axial component of the resultant force acting on the bit (i.e., WOB), H_0 is the side force at the bit, EI is the bending stiffness of the drill collars, w is the unit weight of the drill collars in drilling fluid, and φ is the hole inclination. Because the distance to the tangency point is approximately 30–40 ft, it can be assumed that the inclination angle in Eq. 8.57 is constant and equal to the inclination angle at the drill bit. In many practical applications, the term (EI/R^2) is small compared with the WOB, W , and can be neglected. In such cases, Eq. 8.57 assumes the form

$$EI \frac{d^3 U}{dS^3} + W \frac{dU}{dS} = H_0 + \left(\frac{W}{R} + w \sin \varphi \right) S. \quad (8.58)$$

For a slick BHA, the natural (geometric) boundary conditions are

At the drill bit:

$$S = 0, U = 0 \text{ (bit at the center of the wellbore);} \quad (8.58a)$$

at the tangency point:

$$S = L, U(L) = \pm r_c; U'(L) = 0 \text{ and } U''(L) = 0, \quad (8.58b)$$

where r_c and L are the radial clearance and the distance to the point of tangency, respectively.

It can be shown that the bending moment in the S-U system of coordinates is given by

$$EI \frac{d^2 Y}{dX^2} = EI \left(\frac{d^2 U}{dS^2} + \frac{U}{R} - \frac{1}{R} \right). \quad (8.58c)$$

In a manner similar to that for the BHA in a straight inclined hole, it can be assumed that there is no bending moment at the bit ($S = 0$), and, therefore, from Eq. 8.58c,

$$\frac{d^2 U}{dS^2} = \frac{1}{R}. \quad (8.58d)$$

Again, to make the analysis independent of drill-collar dimensions, hole curvature, and drilling-fluid density, the following four scaling factors are introduced:

$$U = n_1 u, S = n_2 s, H_0 = n_3 h_0, R = n_4 r_d. \quad (8.59)$$

Applying the chain rule of differentiation, $\frac{dU}{dS} = \frac{n_1}{n_2} \frac{du}{ds}$ and similarly for the other factors.

The second and third derivatives are evaluated in a similar fashion, leading to the following dimensionless governing differential equation:

$$\frac{d^3 u}{ds^3} + \frac{du}{ds} = h_0 + s. \quad (8.60)$$

It is important to note that the form of the dimensionless governing equation in a curved wellbore (Eq. 8.60) is the same as that of the governing differential equation in a straight inclined hole (Eq. 8.51).

The four scaling factors are defined by the equations:

$$n_1 = \frac{(EI) \left(\frac{W}{R} + w \sin \varphi \right)}{W}, \quad \dots \quad (8.60a)$$

$$n_2 = \sqrt{\frac{EI}{W}}, \quad \dots \quad (8.60b)$$

$$n_3 = \frac{n_1}{n_2} W, \quad \dots \quad (8.60c)$$

$$n_4 = \frac{n_2^2}{n_1}, \quad \dots \quad (8.60d)$$

The corresponding dimensionless boundary conditions become as follows:

At the drill bit:

$$u(s=0) = 0; \quad u''(s=0) = \frac{1}{r_d}; \quad \dots \quad (8.61a)$$

and at the point of tangency:

$$u(\ell) = c; \quad u'(\ell) = 0; \text{ and } u''(\ell) = 0. \quad \dots \quad (8.61b)$$

Solution of the differential equation, Eq. 8.60, with the boundary conditions as given by Eq. 8.61, yields

$$h_0 = \tan\left(\frac{\ell}{2}\right) - \frac{1}{r_d \sin(\ell)} - \ell, \quad \dots \quad (8.62a)$$

$$c = \frac{1}{r_d} - \frac{\ell^2}{2} - \frac{\ell}{r_d \sin(\ell)} + \ell \tan\left(\frac{\ell}{2}\right). \quad \dots \quad (8.62b)$$

It is immediately apparent that if the dimensionless radius of curvature $r_d \rightarrow \infty$ (a straight well), Eqs. 8.62a and 8.62b reduce to the previously derived equations for a slick assembly in a straight but inclined well. Simultaneous solution of Eqs. 8.62a and 8.62b gives the dimensionless side force, h_0 , and subsequently the actual (dimensional) side force.

It can be shown that the dimensionless tilt angle at the bit, δ_d , can be calculated as:

$$\delta_d = \frac{1 + \left(\frac{1}{r_d} - 1 \right) \cos \ell}{\sin \ell} + h_0. \quad \dots \quad (8.63)$$

The following example illustrates the sequence of calculations involved in determining the expected direction of bit penetration under anisotropic drilling conditions.

Example 8.13 Determine the side force at the bit for the BHA data given in Example 8.10 and a hole curvature (i.e., DLS) of $1.1,459^\circ/100$ ft (radius of curvature $R = 5,000$ ft) and inclination angle $\varphi = 10^\circ$.

Solution. The unit weight of the drill collars in mud (77.1 lbf/ft), the flexural rigidity $[(14.821)10^6 \text{ lbf-ft}^2]$, and the radial clearance (0.09375 ft) have already been calculated in Example 8.10. Therefore, the scaling factors can immediately be calculated:

$$(a) \quad n_1 = \frac{(14.821)(10^6) \left[\frac{30,000}{5,000} + (77.1) \sin(10) \right]}{(30,000)^2} = 0.319 \text{ ft},$$

$$(b) \quad n_2 = \sqrt{\frac{(14.821)(10^6)}{30,000}} = 22.2 \text{ ft},$$

$$(c) \ n_3 = \frac{0.319}{22.2}(30,000) = 432 \text{ lbf},$$

$$(d) \ n_4 = \frac{22^2}{0.319} = 1,545 \text{ ft}.$$

The dimensionless radial clearance is then

$$(e) \ c = \frac{0.09375}{0.319} = 0.294$$

and the dimensionless hole curvature is

$$(f) \ \frac{1}{r_d} = \frac{1}{\frac{R}{n_4}} = \frac{n_4}{R} = \frac{1,545}{5,000} = 0.31.$$

Given the dimensionless radial clearance and the curvature, Eqs. 8.62a and 8.62b can be solved simultaneously to obtain the dimensionless side force at the bit: $h_0 = -0.864$. Therefore, the side force at the bit is

$$(g) \ H_0 = (-0.864)(432) = -373.5 \text{ lbf}.$$

The negative value of the side force indicates that this assembly would tend to drop in anisotropic formations. For anisotropic drilling conditions, the expected drill-bit displacement direction would have to be calculated in a manner similar to that in Example 8.10.

8.2.3 Use of Stabilizers To Control Hole Deviation. The practical usefulness of a slick BHA is rather limited because of restrictions related to the WOB and the geometric properties of the drill collars. To achieve a greater degree of control, so-called *stabilizers* are placed at a predetermined distance from the bit. The effective use of stabilizers began in 1953 when Lubinski and Woods published a paper that described a stabilizer in a BHA. They demonstrated that both the distance from the drill bit to the stabilizer and the radial clearance at the stabilizer have a major effect on the side force of the bit and the tilt angle at the bit. However, at that time, the primary purpose of a stabilizer was to increase the distance from the drill bit to the tangency point to maximize the pendulum effect. In fact, this practice is still effectively used today if the purpose of deviation control is to reduce hole inclination angle.

Although the primary purpose of stabilizers is currently to control deviation (the resultant force and its direction at the bit), a near-bit stabilizer is sometimes recommended for keeping the bit rotating about its axis and providing uniform loading on the bit cutting structure and the bearings. A large number of different stabilizer designs are currently available. Selection of the proper type of stabilizer is usually based on analysis of drilling data from holes already drilled under similar geological conditions. *Welded-blade stabilizers* (in which steel blades are welded onto the body of the stabilizer) can be used in soft formations, while *integral-blade stabilizers* (in which the blades are machined from one piece of metal) are recommended in hard formations. Sleeve stabilizers consist of replaceable sleeves that are installed on the stabilizer body. The blades can be furnished with tungsten-carbide inserts for drilling in abrasive formations. Some commonly used types of stabilizers are shown in **Fig. 8.26**. Detailed information on stabilizer dimensions, materials of manufacture, and recommended applicability is readily available from various service-company websites.

More recently, the so-called *adjustable-diameter* (gauge) stabilizers were introduced. These make it possible to control stabilizer OD without tripping the BHA out of the hole. The blades are extended or retracted by special mechanisms to control the clearance between the stabilizer and the wellbore wall. Typically, adjustable stabilizers are activated by WOB or flow of drilling fluid. An example of an adjustable-diameter stabilizer (independent of WOB) used for flow control is shown in **Fig. 8.27**. When the bit is turning, the mud pumps off the piston, which retracts inside the blade diameter. Turning the pumps on again extends the piston, leading to an increase in the diameter of the stabilizer. Various piston positions are indicated by 150- to 250-psi changes in standpipe pressure. Some stabilizers provide communication with the surface by means of the mud-pulse-telemetry system. The stabilizer diameter can be controlled from the surface by a series of flow sequences that are received by the microprocessor located above the stabilizer.

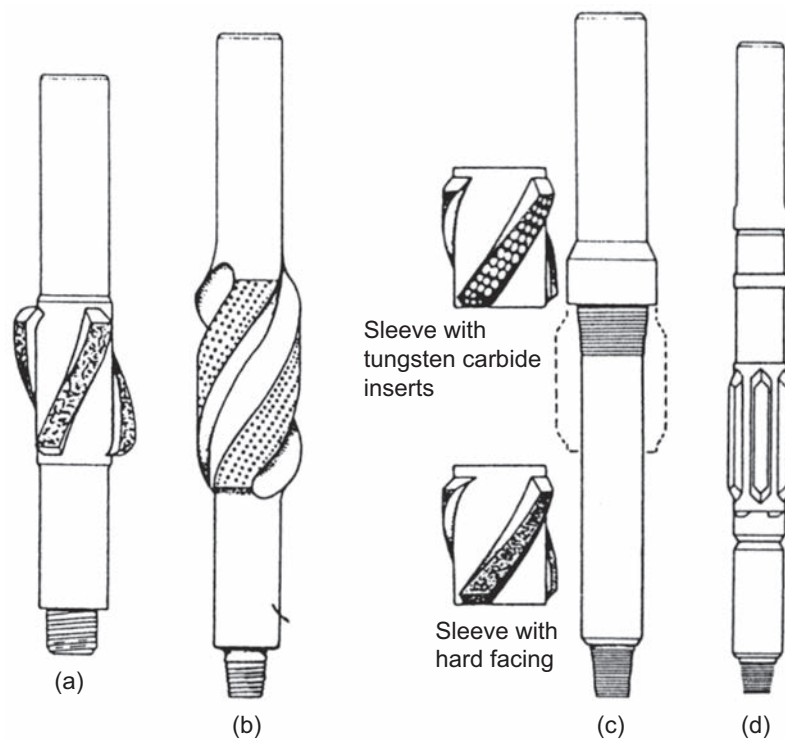


Fig. 8.26—Types of stabilizers: (a) welded-blade; (b) integral-blade; (c) sleeve; (d) nonrotating sleeve (Inglis 1987). Reprinted with kind permission of Springer.

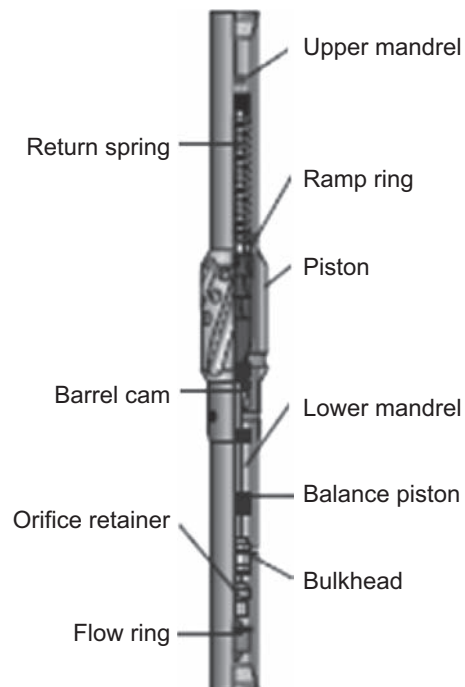


Fig. 8.27—Adjustable-diameter stabilizer (AGS Tool 2010). Courtesy of Halliburton.

When drilling in highly abrasive formations where the bit gauge is wearing fast, a reamer may be placed above the bit. Because the reamer does not provide proper stabilization, a stabilizer may also be required to achieve the desired deviation control. If differential pressure is a problem, drill collars with a helical groove may be needed. Such drill collars are called *spiral drill collars*. When drilling in unstable formations where the hole diameter varies rapidly, a square drill collar may be more effective than a stabilizer. The square drill collar provides long support for wall contact and essentially increases bending stiffness.

Mechanics of a BHA With One Stabilizer in an Inclined Hole. To understand the basic concepts behind the use of a stabilized BHA, let us consider an assembly with one stabilizer, as shown schematically in Fig. 8.28.

The distance to the point of tangency is increased by increasing the distance from the drill bit to the stabilizer. An increase in the unsupported length of the drill collar results in a greater side force at the bit. This tends to bring the hole toward the vertical. This practice is used if drilling personnel want to reduce the inclination angle. In field practice, this is frequently termed the *pendulum effect*. If the stabilizer is placed closer to the bit, then the magnitude of the side forces decreases. Placing the stabilizer even closer may result in a nil side force or a change in the side-force direction. If the bit is pushed toward the high side of the hole, it is said that a so-called *fulcrum effect* is created.

Consider a BHA with one stabilizer, as shown schematically in Fig. 8.28. In a similar manner as for a slick assembly, the elastic line is assumed to be a plane curve. A stabilizer is placed at a distance X_1 from the bit. The radial clearance at the stabilizer is r_{st} . The length of the stabilizer is not considered in this model. In other words, the stabilizer is modeled as a point and simply called a *point stabilizer*. The side force at the stabilizer is denoted as H_{stb} . It is recommended that the reader review the derivation of the governing differential equation for a slick assembly (Section 8.2.2) before studying the following material.

Placing the stabilizer at a distance X_1 from the bit divides the elastic line into two parts: Part A from the bit to the stabilizer and Part B from the stabilizer to the tangency point. The governing differential equations can be formulated for the two parts in a manner similar to that for the slick assembly, using Eq. 8.44 for Parts A and B. Consequently, to determine the equilibrium configuration of the elastic line of the

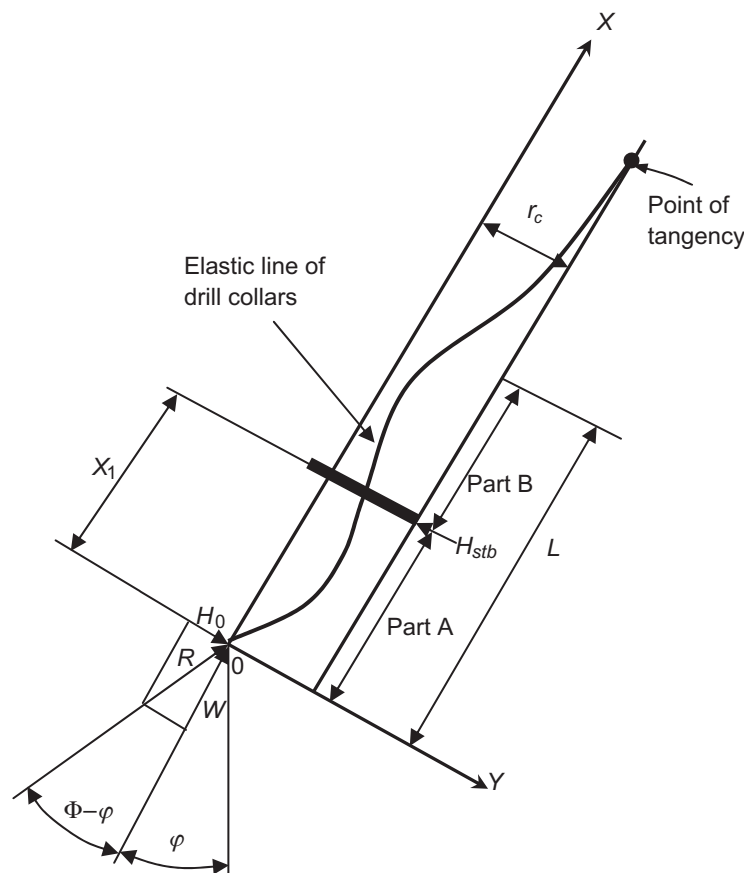


Fig. 8.28—Schematic diagram of BHA with one stabilizer in a straight inclined hole.

BHA with one stabilizer, it is required to solve the following system of two differential equations, of which the first is

$$EI \frac{d^3 Y_A}{dX_A^3} + W \frac{dY_A}{dX_A} = H_0 + X_A w \sin \varphi. \quad (8.64a)$$

Eq. 8.64a is valid for $0 \leq X_A \leq X_1$, and Eq. 8.64b,

$$EI \frac{d^3 Y_B}{dX_B^3} + W \frac{dY_B}{dX_B} = H_0 - H_{stb} + X_B w \sin \varphi, \quad (8.64b)$$

is valid for $X_1 \leq X_B \leq L$.

It should be noted (Fig. 8.28) that a positive side force at the bit, H_0 , occurs if the bit is pushed toward the high side of the hole. For a stabilizer, however, a positive side force means that the stabilizer is pushing on the lower part of the hole. It is also important to note that the sign of the side force and the sign of the deflection at the stabilizer must be consistent. Specifically, both signs must be positive if the stabilizer is on the low side of the hole and both negative if the stabilizer is in contact with the upper side of the hole. For certain equilibrium configurations, the stabilizer does not contact either the upper or the lower side of the hole. In such a case, it is said that the stabilizer is *floating*, and the side force at the stabilizer is nil. Of course, such equilibrium configurations are weak and of little practical importance. In fact, the stabilizer may oscillate between the upper and lower sides of the hole and induce detrimental lateral vibrations.

For a BHA with one stabilizer, the boundary conditions are as follows:

At the bit ($X = 0$):

$$Y_A(0) = 0; \text{ bit in the center of the hole; } \quad (8.65a)$$

$$Y_A''(0) = 0; \text{ no bending moment at the bit. } \quad (8.65b)$$

At the stabilizer ($X = X_1$):

$$Y_A(X_1) = Y_B(X_1) = \pm r_{st}; \text{ continuity of deflection; } \quad (8.65c)$$

$$Y_A'(X_1) = Y_B'(X_1); \text{ continuity of slopes; } \quad (8.65d)$$

$$Y_A''(X_1) = Y_B''(X_1); \text{ continuity of bending moments. } \quad (8.65e)$$

At the tangency point ($X = L$):

$$Y_B(L) = r_c; \text{ deflection equals the apparent radius; } \quad (8.65f)$$

$$Y_B'(L) = 0; \text{ drill collar tangent to borehole wall; } \quad (8.65g)$$

$$Y_B''(L) = 0; \text{ no bending moment at point of tangency. } \quad (8.65h)$$

Introducing the scaling parameters m_1 , m_2 , and m_3 as defined previously (Eqs. 8.50a, 8.50b, and 8.54c), the dimensionless forms of the differential equations can be written as

$$y_a''' + y_a' = h_0 + x_a, \quad (8.66a)$$

$$y_b''' + y_b' = h_0 - h_{stb} + x_b \quad (8.66b)$$

and the corresponding boundary conditions are

At $x = 0$:

$$x = 0, \quad y_a(0) = 0 \quad \text{and} \quad y_a''(0) = 0; \quad \dots\dots\dots (8.67a)$$

at $x = x_1$:

$$y_a(x_1) = y_b(x_1) = \pm r_{st}; \quad \dots\dots\dots (8.67b)$$

$$y_a'(x_1) = y_b'(x_1); \quad \dots\dots\dots (8.67c)$$

$$y_a''(x_1) = y_b''(x_1); \quad \dots\dots\dots (8.67d)$$

at $x = \ell$:

$$y_b(\ell) = r_c/m_1 = c; \quad \dots\dots\dots (8.67e)$$

$$y_b'(\ell) = 0; \quad \dots\dots\dots (8.67f)$$

$$y_b''(\ell) = 0. \quad \dots\dots\dots (8.67g)$$

The lowercase letters in Eqs. 8.66a and 8.66b are dimensionless variables that correspond to the dimensional variables given by Eqs. 8.66a and 8.66b. The same applies to the boundary conditions. For example, $\ell = L/m_2$, $h_0 = H_0/m_3$, $y_a = Y_a/m_1$.

Integrating Eqs. 8.66a and 8.66b yields

$$y_a = C_{1a} + C_{2a} \cos x + C_{3a} \sin x + \frac{1}{2}x^2 + h_0 x, \quad \dots\dots\dots (8.68a)$$

$$y_b = C_{1b} + C_{2b} \cos x + C_{3b} \sin x + \frac{1}{2}x^2 + (h_0 - h_{stb})x. \quad \dots\dots\dots (8.68b)$$

Application of the boundary conditions given by Eq. 8.67 yields:

$$C_{1a} = -1, \quad \dots\dots\dots (8.69a)$$

$$C_{2a} = 1, \quad \dots\dots\dots (8.69b)$$

$$h_0 - h_{stb} = \frac{c_{st} - c + 1 + 0.5(\ell^2 - x_1^2) - \cos(\ell - x_1) - \ell \sin(\ell - x_1)}{x_1 - \ell + \sin(\ell - x_1)}, \quad \dots\dots\dots (8.69c)$$

$$\left(\text{Note : } x_1 = \frac{X_1}{m_2} \text{ and } \ell = \frac{L}{m_2} \right),$$

$$h_0 = \frac{(1 + c_{st} - 0.5x_1^2) - \cos(\ell - x_1) - (\ell + h_1) \sin(\ell - x_1)}{x_1}, \quad \dots\dots\dots (8.69d)$$

$$C_{3a} = \frac{1 + c_{st} - 0.5x_1^2 - \cos x_1 - h_1 x_1}{\sin x_1}, \quad \dots\dots\dots (8.69e)$$

$$C_{1b} = c - 1 - 0.5\ell^2 - (h_0 - h_{stb})\ell, \quad \dots\dots\dots (8.69f)$$

$$C_{2b} = \cos \ell + (\ell + h_0 - h_{stb}) \sin \ell, \quad \dots\dots\dots (8.69g)$$

$$C_{3b} = \sin \ell - (\ell + h_2) \cos \ell, \quad \dots\dots\dots (8.69h)$$

$$(1 - C_{2b}) \sin x_1 + (C_{3b} - C_{3a}) \cos x_1 - h_{stb} = 0. \quad (8.69i)$$

Analysis of Eq. 8.69 leads to the conclusion that Eq. 8.69i actually contains only one unknown, which is the dimensionless distance to the point of tangency, ℓ .

Algebraic rearrangement of Eq. 8.69 yields

$$\sin(x_1 - \ell) + (\ell + h_1) \cos(x_1 - \ell) - \sin x_1 + \cot(x_1) (1 + c_{st} - \cos x_1 - 0.5 x_1^2 - h_0 x_1) + h_{stb} = 0 \quad (8.70)$$

where

$$h_0 = \frac{1 + c_{st} - 0.5 x_1^2 - \cos(x_1 - \ell) + (\ell + h_1) \sin(x_1 - \ell)}{x_1} \quad (8.70a)$$

and

$$h_1 = h_0 - h_{stb} = \frac{c_{st} - c - \cos(x_1 - \ell) + \ell \sin(x_1 - \ell) - 0.5(x_1^2 - \ell^2) + 1}{x_1 - \ell + \sin(\ell - x_1)} \quad (8.70b)$$

Careful examination of Eqs. 8.70, 8.70a, and 8.70b shows that if the dimensionless distance to the stabilizer, x_1 , and the radial clearances, c and c_{st} , are known, then Eq. 8.70 can be solved for the dimensionless distance to the point of tangency, ℓ . Once the value of ℓ has been obtained, the dimensionless side forces at the bit and stabilizers can be found from Eq. 8.70a. Eventually, Eq. 8.70b yields the side force at the stabilizer. Once the forces are determined, the deflections, bending moment, and shear forces along the assembly can be calculated. The bit tilt angle can be calculated from the first derivative at the bit.

The following example illustrates some of the calculations involved.

Example 8.14 Consider a 9-in. by 3-in. drill collar with a unit weight of 192 lbf/ft in a straight hole with inclination angle $\varphi = 25^\circ$. The mud weight is 10.5 lbm/gal, and the WOB = 55,000 lbf. Calculate the side force at the bit if a stabilizer is placed at

Case (a) 15 ft from the bit

Case (b) 60 ft from the bit

The stabilizer clearance = 0.25 in. (OD of stabilizer $D_{o, stb} = 12$ in.). The hole diameter is 12¼ in.

Solution. Unit weight of drill collars in mud:

$$(a) \quad w = (192) \left(1 - \frac{10.5}{65.5} \right) = 161.2 \text{ lbf/ft.}$$

$$(b) \quad \text{Moment of inertia} = \frac{\pi}{64} \left[\left(\frac{9}{12} \right)^4 - \left(\frac{3}{12} \right)^4 \right] = (1.533) 10^{-2} \text{ ft}^4.$$

(c) Drill-collar bending stiffness:

$$EI = (4,320)(10^6)(1.533)(10^{-2}) = (66.23)10^6 \text{ lbf-ft}^2.$$

Now the scaling factors can be calculated:

$$(a) \quad m_1 = \frac{(66.23)(10^6)(161.2)(\sin 25)}{(55,000)^2} = 1.492 \text{ ft,}$$

$$(b) \quad m_2 = \sqrt{\frac{(66.23)(10^6)}{55,000}} = 34.701 \text{ ft,}$$

$$(c) \quad m_3 = (66.3 \times 10^6) \frac{1.492}{(34.701)^3} = 2,365 \text{ lbf.}$$

The dimensionless distance to the stabilizer is:

$$(d) \text{ Case (a) } x_1 = \frac{15}{34.702} = 0.432,$$

$$(e) \text{ Case (b) } x_1 = \frac{60}{34.701} = 1.729.$$

The dimensionless radial clearance at the stabilizer is

$$(f) \ c_{st} = \frac{(0.5)(0.25)}{(12)(1.492)} = 0.00698.$$

The dimensionless radial clearance at the point of tangency is

$$(g) \ c = \frac{0.5(12.25 - 9.0)}{(12)(1.492)} = 0.0908.$$

Solving Eq. 8.70 numerically yields

$$(h) \text{ Case (a) } \ell = 1.835,$$

$$(i) \text{ Case (b) } \ell = 3.267.$$

Consequently, for Eq. 8.51a, the dimensionless side forces are

$$(j) \text{ Case (a) } h_0 = 0.432, \text{ hence } H_0 = 1,035 \text{ lbf;}$$

$$(k) \text{ Case (b) } h_0 = -0.623, \text{ hence } H_0 = -1,472 \text{ lbf.}$$

The results obtained clearly indicate that, for isotropic drilling conditions, the assembly of Case (a) will exhibit building tendencies, while the assembly of Case (b) will have dropping tendencies. In other words, it can be concluded that

1. If the stabilizer is placed 60 ft from the bit, the BHA behaves as a pendulum assembly.
2. If the stabilizer is placed 15 ft from the bit, a fulcrum effect is created.

Clearly, by changing the position of the stabilizer (with all other parameters constant), it is possible to influence the side force at the bit. The reader is invited to calculate the direction of the tilt angle for the two cases.

If the formation is anisotropic and the drilling anisotropy index is known, it is possible to calculate the expected instantaneous bit-displacement angle in a manner similar to that for the slick-type BHA.

In any case, the model and solution presented above are valid only if the drill collars do not contact the wall of the hole between the bit and the stabilizer. A point of contact typically can develop if the distance to the stabilizer is too long or if the WOB is large. Once contact occurs, a side force is created at the contact point, which in turn reduces the effectiveness of the stabilizer for deviation control. If the distance to the stabilizer is even further increased, the drill collars may contact the borehole wall over some finite length, and then the BHA behaves as a slick-type assembly. In other words, the effect of the stabilizer is no longer felt.

Mechanics of a BHA With One Stabilizer in a Curved Wellbore. As discussed earlier, by changing the position of the stabilizer (the distance from the bit), it is possible to control the side force at the bit, as well as the direction in which the bit is pointed out. In general, placing the stabilizer close to the bit yields a fulcrum effect, with the bit pushing on the upper side of the hole. Under isotropic drilling conditions, the fulcrum effect results in building tendencies. Moving the stabilizer away from the bit reduces the fulcrum effect. The side force gradually decreases and eventually becomes negative. A negative side force indicates that the bit is pushed toward the lower side of the hole, which results in a reduction of the hole inclination angle for isotropic drilling conditions. Such a BHA is said to have dropping tendencies. These types of assemblies are called *pendulum assemblies*.

The solution to the problem of determining the equilibrium configuration (the shape of the centerline of the BHA) and consequently the side force at the bit, the tilt angle, and the side force at the stabilizer in a curved wellbore can be obtained in a manner similar to that for an inclined well. Once again, it is necessary to solve a system

of two differential equations with the proper boundary conditions. The solution of this boundary-value problem results in the following equation (Miska et al. 1998):

$$(\sin \ell_1)(C_{2b} - C_{2a}) + (\cos \ell_1)(C_{3a} - C_{3b}) + h_0 - h = 0, \quad (8.71)$$

where

$$C_{2a} = 1 - \frac{1}{r_d}, \quad (8.72a)$$

$$C_{2b} = \cos \ell + (h + \ell) \sin \ell, \quad (8.72b)$$

$$C_{3b} = \sin \ell - (h + \ell) \cos \ell, \quad (8.72c)$$

$$C_{3a} = \frac{\pm c_{stb} + \left(1 - \frac{1}{r}\right)(1 - \cos l_1) - h_0 l_1 - 0.5 l_1^2}{\sin l_1}, \quad (8.72d)$$

$$h = \frac{1 - c \pm c_{stb} + 0.5(\ell^2 - l_1^2) - \cos(\ell - l_1) - \ell \sin(\ell - l_1)}{l_1 - \ell + \sin(\ell - l_1)}, \quad (8.72e)$$

$$h_0 = \frac{1 - \frac{1}{r_d} \pm c_{stb} - 0.5 l_1^2 - \cos(\ell - l_1) - (h + \ell) \sin(\ell - l_1)}{l_1}, \quad (8.72f)$$

where l_1 is the dimensionless distance to the stabilizer. Careful examination of Eq. 8.71 reveals that the only unknown in this equation is the dimensionless distance to the point of tangency. Solving Eq. 8.71 for the distance to the point of tangency (l), the side forces at the bit and the stabilizer can be calculated from Eqs. 8.72f and 8.72e, respectively. The following example illustrates a practical application of the above equations.

Example 8.15 Determine the expected directional tendency of a BHA with one stabilizer in a curved wellbore, given the following data:

- Hole diameter = 12.25 in.
- Hole curvature = 1.9096°/100 ft (radius of curvature $R = 3,000$ ft)
- Hole inclination angle at the bit = 15°
- OD of drill collars = 8.0 in.
- ID of drill collars = 3.0 in.
- WOB = 35,000 lbf
- Mud weight = 10.5 lbm/gal
- Distance from bit to stabilizer = 50 ft
- Stabilizer clearance = 0.25 in.

Solution.

- Unit weight of drill collars: 147 lbf/ft
- Moment of inertia: $(9.505) 10^{-3} \text{ ft}^4$
- Bending stiffness (flexural rigidity): $(41.06) 10^6 \text{ lbf-ft}^2$
- Radial clearance: 0.177 ft
- Scaling factors:
 - $n_1 = 1.4709 \text{ ft}$
 - $n_2 = 34.24 \text{ ft}$
 - $n_3 = 1,503.5 \text{ lbf}$
 - $n_4 = 797.0 \text{ ft}$

- Dimensionless radial clearance: $c = 0.12$
- Dimensionless stabilizer clearance: $c_{sub} = 0.0136$
- Dimensionless distance to stabilizer: $l_1 = 1.46$
- Dimensionless hole curvature: $\frac{1}{r_d} = 0.2657$

Now Eq. 8.71 can be solved numerically to obtain the dimensionless side force at the drill bit: $h_0 = -0.705$.

Consequently, the side force is $H_0 = (-0.705)(1,503.5) = -1,060$ lbf.

Therefore, it can be concluded that the BHA considered in this example would have dropping tendencies under isotropic drilling conditions. For anisotropic drilling, the formation-drill bit interaction must be taken into account, as explained in Section 8.2.2.

Although the concepts discussed above are very useful for obtaining a good understanding of the fundamental principles involved in deviation control, their practical usefulness in the field is limited because most BHAs are fairly complex in composition.

Complex BHAs. If the desired directional-drilling objectives cannot be achieved with one stabilizer, two or even three stabilizers must be used in the BHA and placed in the correct positions relative to the bit. Using more than three stabilizers for deviation control is seldom justified, but it still may be useful for keeping the BHA off the wall of the borehole to avoid differential pressure sticking. In general, in practical applications, only the bottom portion (approximately 120–160 ft) of the BHA affects the forces at the drill bit. Introduction of more than one stabilizer into the BHA makes the problem of determination of BHA equilibrium more difficult because more differential equations must be solved. Several techniques, however, are available to obtain the desired solutions, including analytical solutions (Callas and Callas 1980; Wu and Chen 2006), finite-element methods (Millheim et al. 1979), finite-difference approaches (Fischer 1974), rotation and translation of coordinate systems (Lubinski 1987), and transfer-matrix approaches (Miska 2006).

BHAs generally are designed to a particular build, drop, or hold angle. Classification of BHAs as of build, hold, and drop type is somewhat arbitrary, but still useful for practical purposes. A typical build assembly is shown schematically in Fig. 8.29a.

For a given formation and bit type, the build rate will depend mostly on the distance between the bit and the first stabilizer, the distance between the first and second stabilizers, and the clearances at the stabilizers. A short sub between the bit and the first stabilizer will increase the side force of the bit and result in an increased build rate.

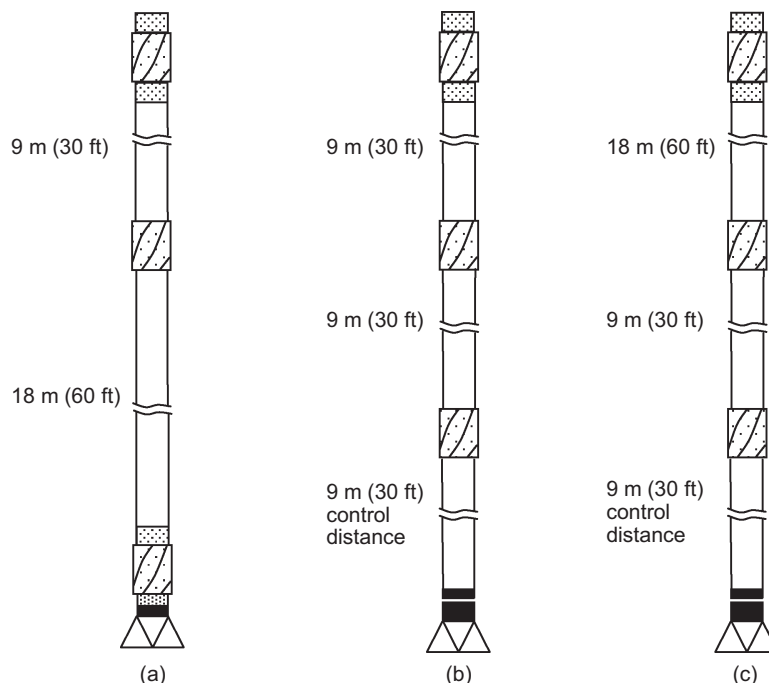


Fig. 8.29—Typical build, hold, and drop BHAs.

As the distance to the first stabilizer increases, the side force of the bit decreases. Typically, the distance between the bit and the first stabilizer should be less than 6 ft to make sure that the BHA remains a build-type assembly.

As the distance between the first and second stabilizers increases, the drill-collar deflection (sag) will also increase, thereby increasing the bit side force (BSF). If the second stabilizer is placed too far from the first, the drill collars may contact the wellbore between the stabilizers, and the building tendency may be lost. For a given bending stiffness, weight of drill collars, and set of radial clearances at the stabilizers and drill collars, the sag of the drill collars depends on the hole inclination angle and the WOB. Generally, it is not recommended to place the second stabilizer more than 60 ft from the first one.

Fig. 8.29b shows a typical hold-angle (packed, locked) assembly. In some applications, four or more stabilizers are closely spaced to increase the overall stiffness of the BHA and thereby drill a straight hole with a constant inclination angle.

A typical pendulum or drop assembly is shown in Fig. 8.29c. In theory, only one stabilizer is needed to develop the pendulum effect that tends to decrease the hole inclination angle, but often three stabilizers are used. Under a given set of drilling conditions (formation, drill bit type, WOB), the drop rate is a strong function of the distance between the bit and the first stabilizer. As the distance to the first stabilizer increases, the lateral component of the weight of the drill collars also increases, and the bit is pushed to the low side of the hole. Generally, the distance between the bit and the first stabilizer is approximately 30 ft. Of course, the radial clearances between the wellbore wall and the stabilizers or drill collars must also be carefully selected.

The BHAs just discussed are sometime called *fixed rotary BHAs* because any adjustments in their composition require tripping operations. For practical purposes, only the WOB can be changed to make the required adjustments in build or drop rates. However, the WOB that is optimum for deviation control may be unacceptable from the viewpoint of drilling rate and bit life. Moreover, changes in the WOB typically result in only minor changes in BHA directional performance for assemblies with two or more stabilizers.

Advancements in adjustable-diameter stabilizers have made it possible to gain more control over build and drop rates without pulling out the BHA. Changes in only the radial clearance at the stabilizers can produce a substantial change in the directional tendencies of the BHA. As shown in Fig. 8.30, the near-bit stabilizer clearance of $\frac{3}{16}$ in. is kept constant, and the BHA directional tendency is controlled by adjusting the clearance at the second stabilizer.

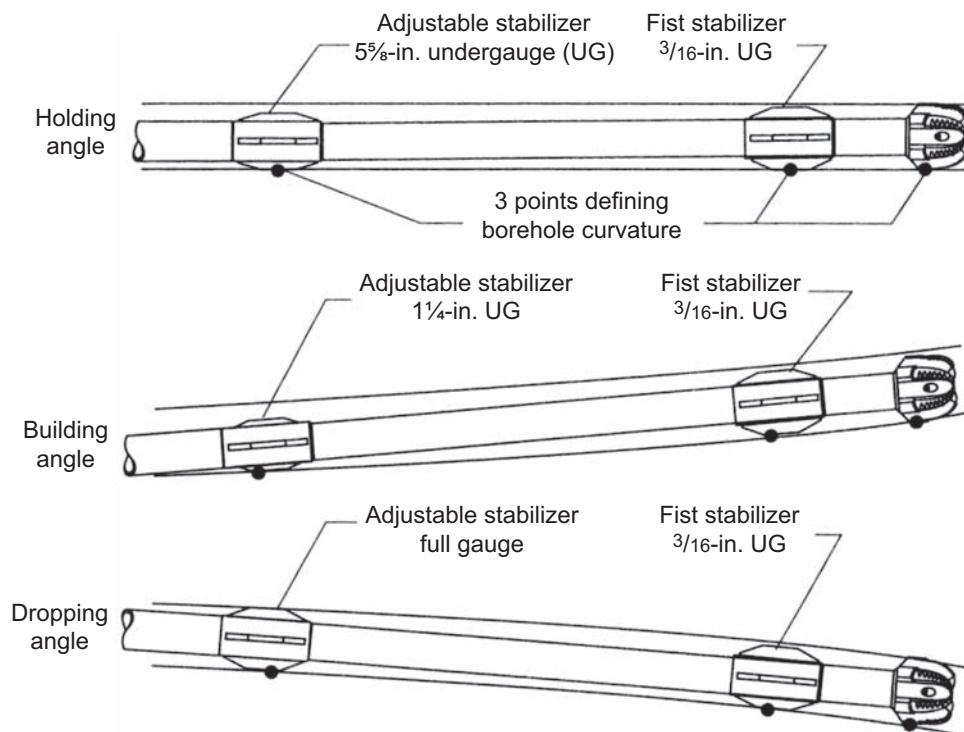


Fig. 8.30—Use of adjustable-diameter stabilizers to control building and dropping tendencies of a BHA (Underwood and Payne 1997). Reproduced with permission of John Wiley & Sons, Ltd.

For practical applications, a BHA computer program is needed to calculate the distances to the stabilizers from the drill bit as well as the desired clearances. It should be well understood that the actual performance of the assemblies illustrated in Fig. 8.30 will depend on the formation and drill-bit directional tendencies, the hole inclination angle, and the quality of the wellbore (washouts, etc.).

In some applications, so-called *continuous stabilization* has been attempted by welding long strips onto drill collars or using closely spaced stabilizers. In this case, the side force at the bit can be estimated simply by considering the clearance between the strips and the wellbore, not between the hole and the collars. Typically such a small clearance results in a larger hole inclination angle and less severe DLs in dipping formations with variable hardness (crooked formations). In other words, using continuous stabilization can be justified in extremely crooked formations.

Frequently, accurate control of hole inclination and azimuth angles is difficult because of formation heterogeneity and variations in BHA and drill-bit loading while drilling. A BHA may include a downhole motor, bent subs, a measurement-while-drilling (MWD) unit, an LWD unit, and other components. The composition of a BHA can be very complex, and its performance analysis requires a sophisticated computer program.

8.2.4 Downhole Drilling Motors. In some applications, it is more effective to rotate only the drill bit rather than the entire drillstring. For this purpose, so-called downhole motors, which provide the torque required to rotate the bit, are used. In other words, the rotational power is localized at the bit, meaning that the wear on drillstring components as well as the energy required for drilling are considerably reduced. There are a number of downhole motors available for drilling. They are usually divided into two groups: the turbine type, also called a *turbodrill*, and the *positive-displacement motor* (PDM). Both types of motors can be used for straight-hole and directional-drilling applications. To achieve more control over trajectory change, motors with bent subs, bent housings, or eccentric stabilizers are recommended.

Turbodrills (also known as dynamic motors) were developed and successfully tested in the first and second decades of the 20th century. In principle, the turbine motor consists of a multistage vane-type rotor and stator section, a bearing section, a drive shaft, and a bit-rotating sub. **Fig. 8.31** shows a turbodrill and its main components.

A single stage composed of a stator and rotor is shown in **Fig. 8.32**. The stator is stationary and deflects the flow of drilling fluid to the rotor, which is attached to the drive shaft and thus transmits the rotary motion to the bit. In other words, the kinetic energy of the drilling-fluid flow stream is converted into kinetic energy of the rotor. This energy is subsequently transferred by means of the drive shaft to the drill bit. In theory, each stage of the turbodrill power section contributes the same amount of torque (power) to the drive shaft. Depending on the turbine design, the number of stages can vary from a few to 400 or even more. In some designs, a gear reducer is also included between the turbine and the drive shaft to slow down the bit rotational speed.

Drilling-fluid flow through the two stages of the turbine is shown in **Fig. 8.33**. For a reaction-type turbine and a constant flow rate, the turbine performance characteristic is shown schematically in **Fig. 8.34**.

If there is no resisting torque at the drive shaft (no WOB), drilling fluid passes freely through the rotor, and the turbine runs at a high rotary speed, which is called the runaway speed (N_{ra}). As the loading on the drill bit is increased (as WOB is added, as torque is increased), the rotational speed is decreased, and eventually the motor

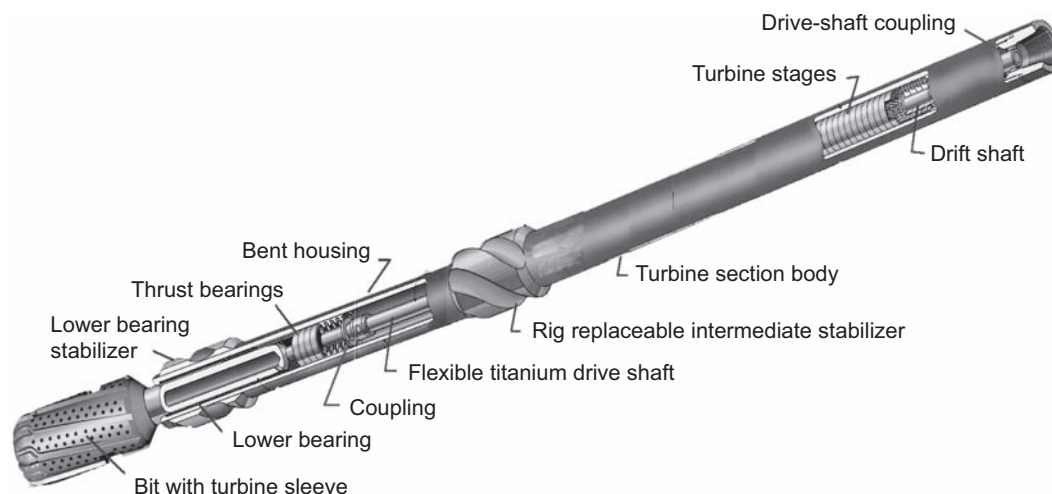


Fig. 8.31—Turbodrill with bent housing (Beaton et al. 2004).

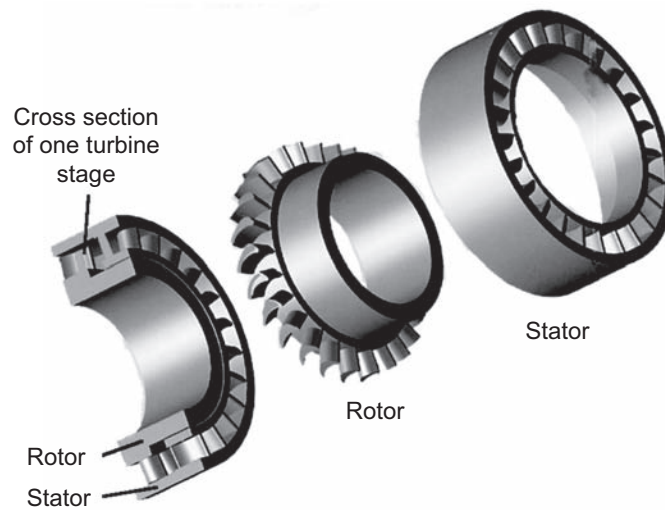


Fig. 8.32—Single stage of turbine (Beaton et al. 2004).

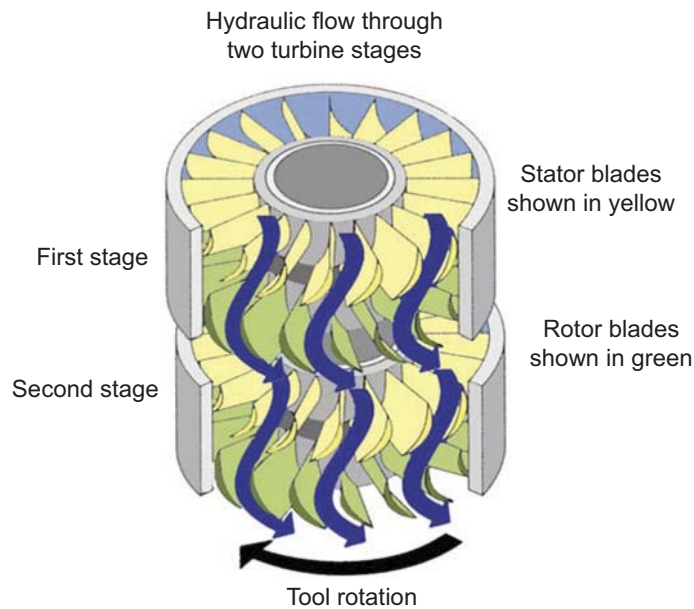


Fig. 8.33—Schematic of drilling-fluid flow through a turbine (Beaton et al. 2004).

stalls ($N = 0$ rev/min). At constant flow rate, the motor torque varies linearly with bit revolutions per minute. Under stall conditions, the turbodrill develops its maximum torque, M_{\max} .

From Fig. 8.34, it is apparent that the relationship between the torque and the bit rotary speed, N , in terms of the stall torque and the runaway speed is

$$M = M_{\max} \left(1 - \frac{N}{N_{ra}} \right) \quad \dots \dots \dots (8.73)$$

The power (product of the moment M and the angular speed ω) can be written as $P = M\omega$, and $\omega = \frac{2\pi N}{60}$:

$$P = \frac{\pi}{30} M_{\max} N \left(1 - \frac{N}{N_{ra}} \right) \quad \dots \dots \dots (8.74)$$

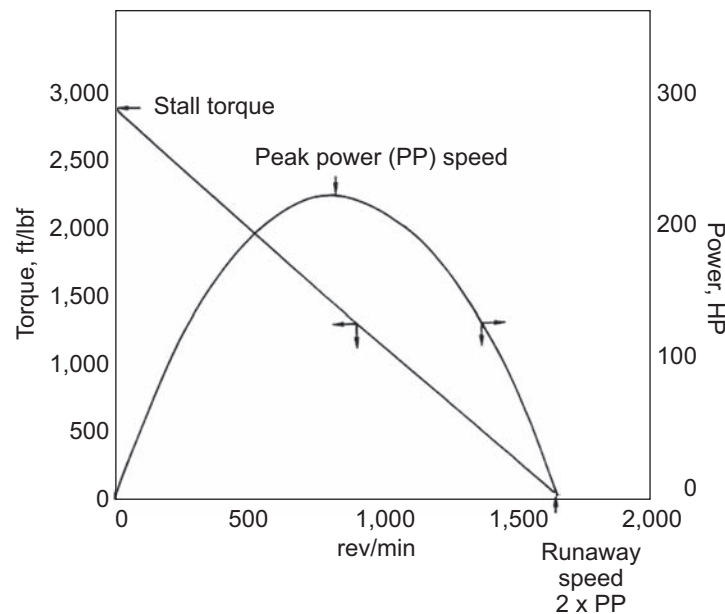


Fig. 8.34—Typical torque and horsepower curves at a flow rate of 500 gal/min and a drilling-fluid density of 10 lbm/gal (Beaton et al. 2004).

From Eq. 8.74, it can be seen that the turbine power is a parabolic function of the bit rotary speed N and that the maximum power is achieved at $N = \frac{N_{ra}}{2}$.

Although the considerations described above are general and useful, for practical applications, the actual turbo-drill performance curves must be developed by bench testing. From bench testing, it is known that the torque vs. rotary-speed relationship is not perfectly linear and that the power vs. rotary-speed relationship is not a perfect parabola at constant flow rate.

PDMs (also known as progressive-cavity motors or helimotors) were developed and introduced to the drilling industry in the mid-1950s; however, the original concepts were presented earlier by René Moineau, a French engineer and inventor who proposed various designs for pumping applications between 1930 and 1948. The conventional PDM (see Fig. 8.35) typically consists of five basic components:

- Dump valve
- Power assembly
- Connecting rod
- Bearing and drive shaft
- Bit sub

The desired torque is generated by the power assembly, which consists of the rotor and stator. Both stator and rotor have helical lobes. The stator is made of an elastomer and is securely fixed in the motor housing. It is very important that the stator material have the resiliency to provide an effective hydraulic seal around the rotor while permitting the rotor to turn freely. The stator always has one more lobe than the rotor, and consequently helical cavities are formed. A half-lobe motor has a rotor with one lobe ($n_r = 1$) and the stator has two lobes, also called teeth ($n_s = 2$).

Fig. 8.36 shows a cross section through the power section of PDMs with various lobe patterns. Forcing drilling fluid to flow through these cavities induces rotation of the rotor. In other words, the fluid will not flow through the power section unless the rotor is turning. Therefore, to allow drilling fluid to enter the drillstring during tripping operations when the motor is not rotating, a dump valve is placed above the power section. The dump valve is furnished with openings that permit the drillstring to fill or empty while the string is being tripped in or out of the hole.

The connecting-rod assembly is attached to the lower end of the rotor and transmits rotational motion to the driveshaft and the bit. It also compensates for orbital motion of the rotor so that the driveshaft rotates about its own axis as it transmits rotary motion to the bit. PDMs are designed to operate with practically all types of drilling

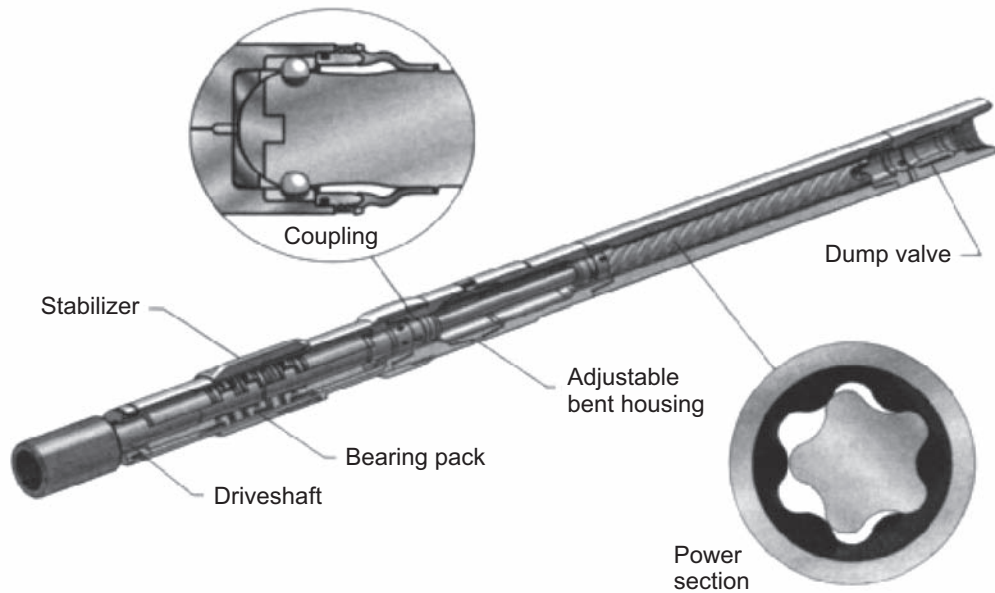


Fig. 8.35—Components of PDM with adjustable bent housing (Underwood and Payne 1997). Reproduced with permission of John Wiley & Sons, Ltd.

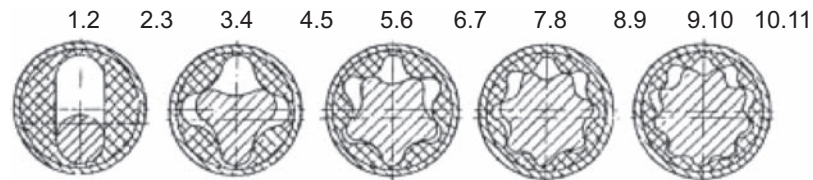


Fig. 8.36—Different lobe patterns (Tiraspolsky 1985). Printed courtesy of Editions Technip.

fluids, including fresh water, salt water, oil-based and synthetic-based fluids, and even foams and air. If the drill bit is off the bottom (no WOB) and drilling fluid is flowing through the power section, the pressure drop across the motor is constant if the flow rate is constant. As the WOB is increased, the pressure drop across the motor increases proportionally, which results in an increase in the standpipe pressure at the surface.

If the pressure drop, Δp (psi), flow rate, Q (gal/min), and motor efficiency are known, it is possible to calculate the motor hydraulic horsepower (US horsepower) using the following equation:

$$HP = \frac{\eta \Delta p Q}{1714} \quad (8.75)$$

The motor efficiency takes into account fluid leaks along contact surfaces between the rotor and stator, various friction losses, and entry and exit effects. For a particular motor design, its volumetric efficiency should be obtained from the manufacturer.

If the bit rotational speed, N (rev/min), is known, the rotary torque can be calculated from the well-known equation

$$T = \frac{5,252 HP}{N} \quad (8.76)$$

At a certain value of WOB, the pressure drop reaches the maximum recommended value, and additional WOB may stall the motor. In a stall condition, the drill bit does not rotate, and pressure builds up rapidly for liquid-based drilling fluids, which in turn may break the seal between the rotor and stator and damage the power assembly. In other words, excessive bit weight should be removed as quickly as possible because major damage to the power section will occur if fluid flows around a nonrotating rotor.

The speed of rotation (rev/min) depends on flow rate and power-section specific displacement per revolution:

$$N = \frac{231Q}{s} \quad (8.77)$$

In Eq. 8.77, the flow rate is in gal/min, and the specific displacement per revolution is in cubic inches. The specific displacement per revolution depends on various geometric factors, including the rotor diameter, its eccentricity, and the configuration of the lobes. In general,

$$s = Ap_r n_r \quad (8.78)$$

where

A = cross-sectional area of the flow path,

p_r = rotor pitch,

n_s = number of lobes in the stator ($n_s = n_r + 1$).

For a single-lobe motor, the flow area is given by

$$A = 2ed_r \quad (8.79)$$

where

e = eccentricity,

d_r = diameter of rotor.

The eccentricity, e , in Eq. 8.79 is the distance between the center of the rotor and the central axis of the stator. From Eq. 8.77, it can be seen that for a given motor configuration, the bit rotational speed is controlled by the drilling-fluid flow rate and increases proportionally with increasing flow rate. The geometric parameters of a particular motor can be obtained from the manufacturer.

A typical PDM performance characteristic curve is shown in **Fig. 8.37**. From Fig. 8.37, it is apparent that at a flow rate of 600 gal/min and a WOB corresponding to a 200-psi pressure drop, the expected bit rotary speed is slightly greater than 180 rev/min. As the pressure drop increases due to added WOB, the bit rotary speed is slightly reduced. Moreover, with an increase in pressure drop, the torque is increased. The maximum torque is obtained at stall conditions. Because the motor turns the bit clockwise (right-hand rotation), for all types of motors, a left-hand (counterclockwise) reactive torque is generated in the motor housing and consequently in the drillstring, which causes the tool joints above the motor to tighten. The left-hand reactive torque also affects the orientation of any bent subs or housings that are used for deviation control.

8.2.5 Steerable Motors. In 1962, a directional-drilling system using a PDM and a bent sub placed above the motor was introduced. The *bent sub* is a short sub placed above the motor. The upper end of the sub is concentric

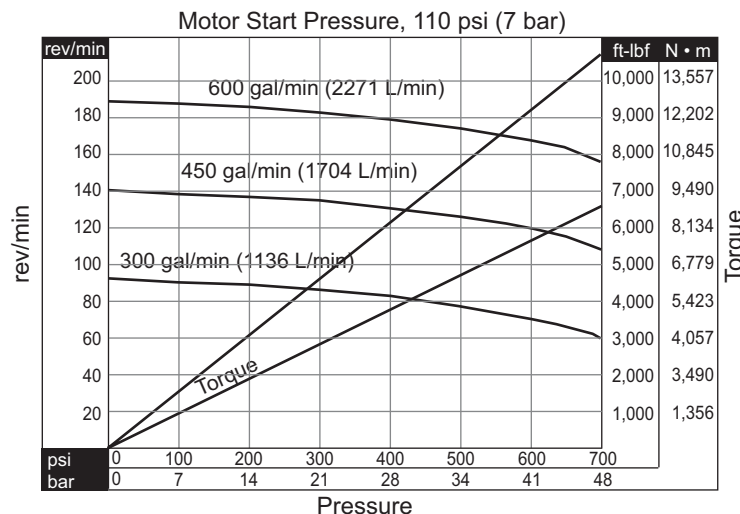


Fig. 8.37—Typical PDM performance characteristic curves (Underwood and Payne 1997). Reproduced with permission of John Wiley & Sons, Ltd.

with the axis of the sub body, and the lower end is inclined in relation to the upper end. The downhole motor is attached directly to the bent sub and oriented to achieve the desired change in hole inclination and azimuth, as shown in **Fig. 8.38**. In some designs, the bent-sub angle can be adjusted from the surface. The effectiveness of the bent sub depends on its location in the BHA (distance from the bit) and the hole inclination angle. A BHA with a straight motor and a bent sub above it is effective in a vertical or nearly vertical hole and is frequently used in a kickoff assembly.

For hole inclination angles of 20° or more, the effectiveness of straight motors with bent subs is poor, and for this reason, downhole motors with bent housings (**Fig. 8.39**) were developed. Fig. 8.39 shows an assembly with two stabilizers and a motor with a bent housing in a nearly vertical and highly inclined hole.

A bent housing, when held stationary (nonrotating), causes the drill bit to drill in the direction of the bend. The bend angle can range from 0° to 3° . Such BHAs are usually furnished with an MWD unit above the motor and are

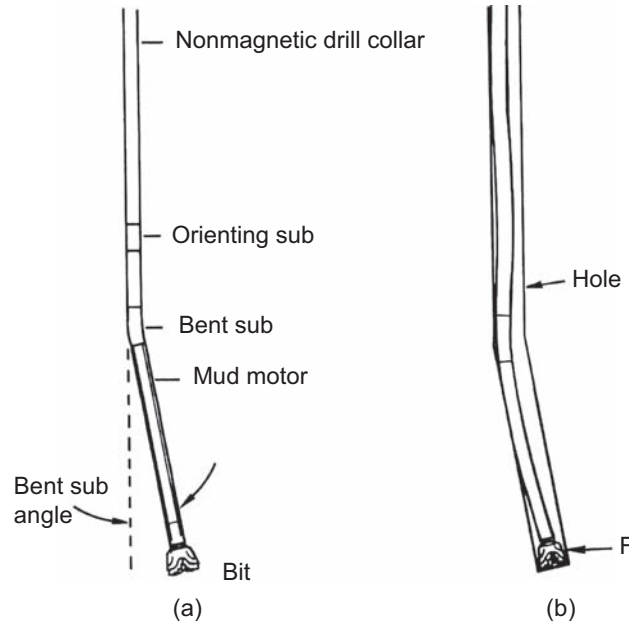


Fig. 8.38—Bent sub above the motor in unconstrained and constrained configurations (Bourgoyne et al. 1986).

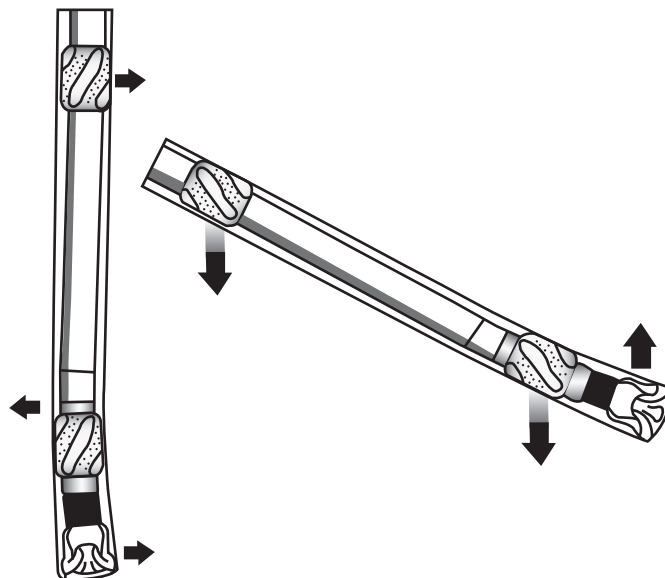


Fig. 8.39—Schematic of bent-housing motor with stabilizers.

called steerable motors (SMs) because they permit the directional driller to orient (steer) the bit in the desired direction. The MWD-unit sensors provide information on the downhole orientation of the bend in terms of tool-face angle. The orientation of the bend is referenced to the high side of the hole. A tool-face angle of 0° indicates that the bent housing is oriented upward and that, consequently, the hole inclination angle will increase while drilling. On the other hand, a tool-face angle of 180° indicates that the hole inclination angle will decrease. A positive tool-face angle of 90° (clockwise rotation) means that the bend is pointed to the right and that therefore the hole will also turn to the right, resulting in an increase in the azimuth angle. Determination of tool-face orientation requires precise information from directional-survey data (inclination and azimuth angles). Information about the tool-face angle is transmitted to the surface and monitored by the directional driller. Several telemetry systems have been developed for this purpose. The calculations involved in determining tool-face orientation are discussed in Section 8.3.

Drilling with SMs involves either active trajectory control in sliding mode or operation in rotating mode, as shown schematically in **Fig. 8.40**. In sliding mode, the drillstring is not rotating, and changes in inclination, azimuth, or both are accomplished by reorientation of the bent housing (tool face), as just mentioned. In rotating mode, the drillpipe is rotated using a rotary table or a topdrive system.

As the drillstring rotates, the bent housing also rotates, which negates the directional effect of the bent housing, and the drill bit drills a slightly overgauge hole. The actual field performance of an SM depends not only on the bent housing angle, but also on the type of formation and the drill-bit type. For example, a bent housing angle of 1.5° may result in a DL of approximately $8^\circ/100$ ft severity (radius of curvature of 719 ft) in competent formations and perhaps only $5^\circ/100$ ft in soft formations (Lesso et al. 2001). Over time, a directional driller develops knowledge of the build, drop, and turn rates for various bent-housing orientations in a given location. The system is used in a rotating mode if there is no need for active directional control and also to make adjustments to the DLS. For example, a well plan may require a $4^\circ/100$ ft DLS (build rate), but the SM delivers $7^\circ/100$ ft. In such a case, the drilling process must be broken into a sequence of sliding and rotating modes to achieve the desired overall build rate of $4^\circ/100$ ft. **Fig. 8.41** shows a segment of a wellbore (500 ft) drilled in both sliding and rotating modes (Lesso et al. 2001).

SMs guided with MWDs can drill more-complex trajectories and are relatively inexpensive. The limitations of SMs are related mostly to the sliding mode of drilling (poor axial-force transfer to the drill bit, inefficient cuttings transport, differential sticking, etc.) and to vibrations in rotary mode. Moreover, considerable time may be spent making tool-face adjustments while switching from rotating to sliding mode in long curved sections and during ERD. These problems led eventually to the development of *rotary-steerable systems* (RSSs).

8.2.6 RSSs. In principle, an RSS enables active well-trajectory control while rotating the drillstring. In other words, unlike SM systems, no sliding drilling is required to change the well-path direction. The desired directional changes (bit steering) can be made while the drillstring is rotating.

Use of an RSS permits effective drilling of wells with complex trajectories and results in a higher rate of drilling in highly inclined wellbore sections. RSSs are particularly effective for drilling long, highly inclined tangent sec-

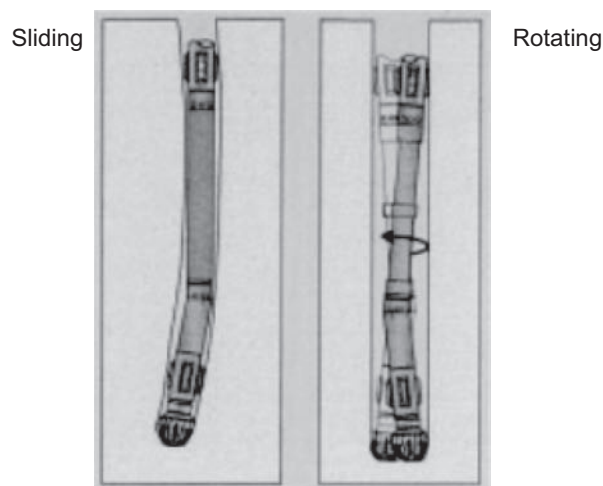


Fig. 8.40—BHA with steerable motor in sliding and rotating mode (Warren 1998).

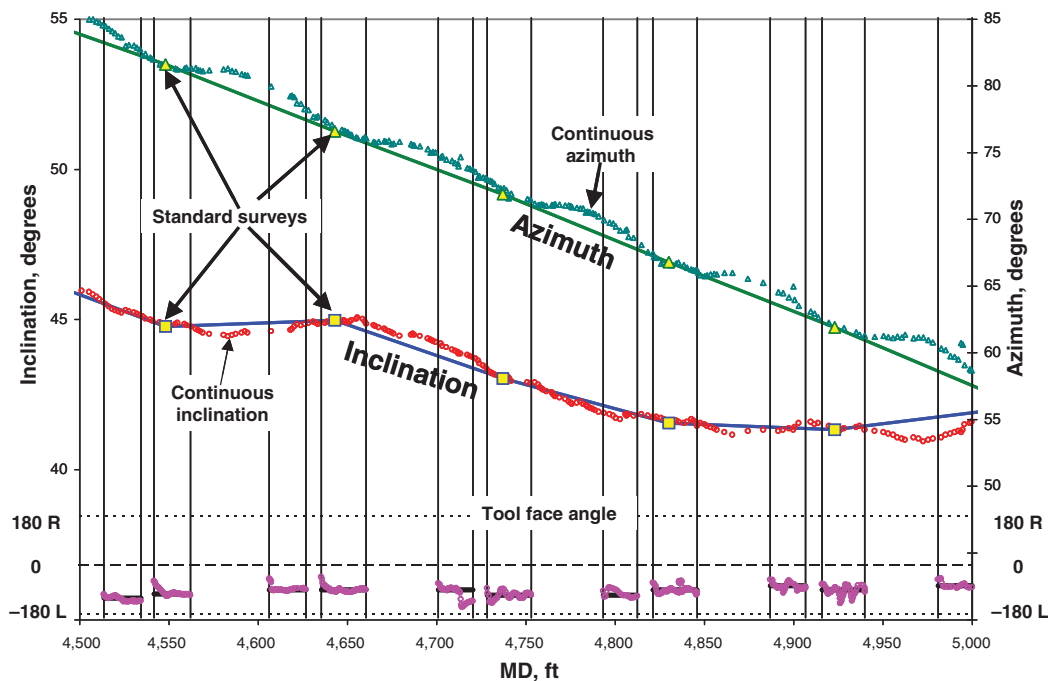


Fig. 8.41—A series of slide-rotate sequences for a 500-ft wellbore section (Lesso et al. 2001).

tions of ERD wells and 3D ERD wells when left and right trajectory turns are performed in a nearly horizontal plane. If the RSS is also used with LWD tools, it can drill wells close to the reservoir top and thus maximize standoff from the water-oil-contact (WOC). Many other applications of RSS in combination with LWD are also possible for optimizing reservoir performance and management.

The first commercially available RSSs were developed in approximately 1995, but the first such tools were proposed much earlier. In fact, the first concepts of deviation control while rotating the drillstring were proposed even before PDMs were commonly used for drilling. In Fig. 8.42a, a system (patented in 1955) is shown based on a nonrotating sleeve placed in the BHA some distance above the bit. Another system (patented in 1959), shown in Fig. 8.42b, uses hydraulically activated guide shoes to control the side force at the bit.

The two systems shown in Fig. 8.42 are just examples of a large number of tools that have been proposed over the years before the tools in use today. Early rotary-steerable BHAs were not commercially successful, however, due to the lack of effective downhole sensors and control systems. Although there is wide variation in the RSS designs now available, they are typically classified as *push-the-bit* or *point-the-bit* systems.

A pure push-the-bit RSS (Fig. 8.43) achieves trajectory change by applying a side load to the bit using nonrotating (stationary) pads or stabilizers that are pushed against the wall of the hole. Because the pads can be pushed out only a certain distance, they become ineffective in borehole sections that easily develop washouts. Systems based on the push-the-bit principle use short-gauge bits (less than 2-in. gauge length) furnished with a good-quality cutting structure capable of active side cutting into the formation.

A point-the-bit RSS (Fig. 8.44) is furnished with a steering assembly that controls the direction of drilling (inclination and azimuth) by orienting a tilted shaft to which a drill bit is attached. The bit is deflected internally using a hydraulic system, which enables the drill bit to be offset and pointed out in the desired direction. Ideally, the face of the bit should be pointing in the desired direction, and the side force at the bit should be nil. The disadvantage of point-the-bit systems is that they are slower to react to required well-path changes and that achievable DLS is less than with a push-the-bit system. In reality, both the push- and point-the-bit systems control side force and tilt angle to a greater or lesser degree.

In the late 1990s, a rotary closed-loop steerable-tool (RCLS) system was developed, which made it possible to make required adjustments automatically and then to maintain a programmed inclination. The RCLS uses near-bit inclination data that are continuously fed to the steering control unit (controller), which in turn automatically adjusts the steering mechanism to maintain the wellbore trajectory as programmed (designed).

Computer-controlled, rather than manual, downhole linking systems facilitate communication from the surface to the downhole unit. Use of automated downlinking permits more precise steering of the drill bit, resulting in a closer match between the programmed (designed) and actually-drilled wellbore trajectories.

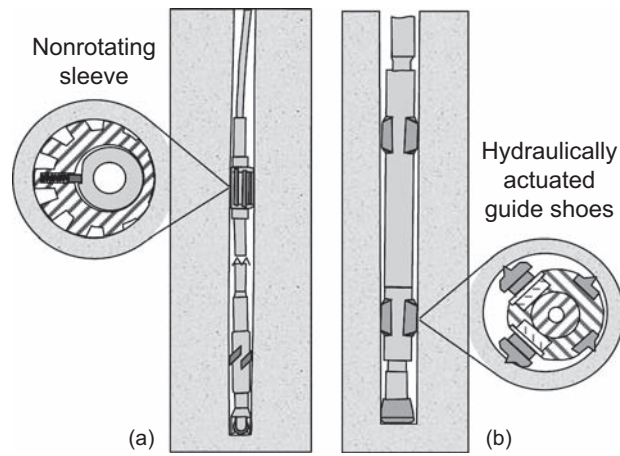


Fig. 8.42—Early rotary-steerable-tool concepts (Warren 2006).



Fig. 8.43—Push-the-bit RSS (Schaaf et al. 2000).

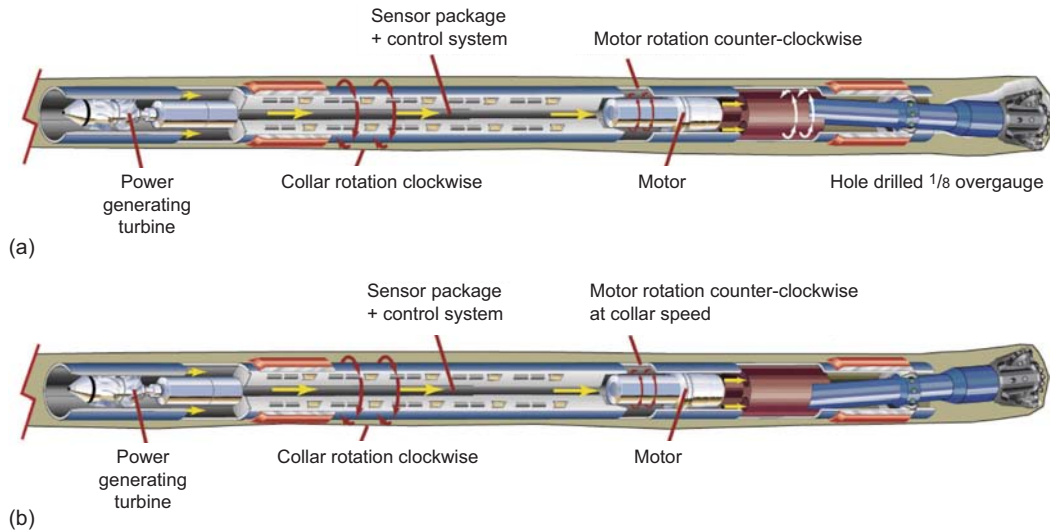


Fig. 8.44—(a) Point-the-bit system in straight mode; (b) point-the-bit system in bent mode (Schaaf et al. 2000).

The well designer must, however, remember the detrimental effects of downhole temperature on electronics and some components (e.g., seals) of RSS and RCLS systems. In high-temperature environments (greater than 250–300°F), a conventional BHA with adjustable-gauge stabilizers may still be the most practical and economical selection for deviation control.

8.2.7 Review Questions and Problems.

1. Make a schematic diagram of a whipstock and explain its applications.
2. Explain why the drill bit of a jetting assembly is furnished with a large nozzle while other nozzles are small or closed off.

3. List the major factors that influence BHA directional and mechanical performance.
4. Explain the concept of an equilibrium hole angle.
5. Define the so-called “drilling anisotropy index.”
6. Derive equations for the scaling factors m_1 , m_2 , and m_3 .
7. Given BHA data as in Example 8.10, calculate:
 - (a) The deflection of the centerline of the drill collars
 - (b) The bending moment
 - (c) The shear force
8. Perform calculations at a distance of 15 ft from the bit.
9. Show that for a slick BHA, the dimensionless tilt angle is given by $\delta_d = 2 \tan \frac{\ell}{2} - \ell$, where ℓ is the dimensionless distance from the bit to the point of tangency.
10. Consider an 8-in. by 3-in. slick BHA in a 12¼-in. hole with an inclination angle of 12°. The WOB is 50,000 lbf, and the mud weight is 10 lbm/gal. Calculate:
 - (a) Distance from the bit to the point of tangency
 - (b) Side force at the bit
 - (c) Bending stress at distances of 5 ft and 10 ft from the bit
11. Using the data specified in Problem 10, calculate the equilibrium hole angle, assuming isotropic drilling conditions.
12. Find the drilling anisotropy index for the following conditions:

Hole diameter = 8 ½ in.
 Drill-collar OD = 6.75 in.
 Drill-collar ID = 2.0 in.
 Unit weight of drill collars = 111 lbf/ft
 Hole equilibrium inclination angle = 10°
 WOB = 20,000 lbf
 Formation dip = 40°
 Mud density = 12 lbm/gal
13. Using the drilling anisotropy index calculated in Problem 12, calculate the expected hole equilibrium angle if the WOB is 32,000 lbf.
14. Using the BHA data specified in Problem 10, calculate the side force at the bit for two cases:
 - (a) The BHA is in a curved hole with a build rate of 5.729°/100 ft.
 - (b) The BHA is in a curved hole with a drop-off rate of 5.529°/100 ft.
15. List the common types of stabilizers.
16. What is the difference between a stabilizer and a reamer?
17. Explain the concepts of the pendulum and fulcrum effects.
18. Using the data from Example 8.14, calculate the side force at the bit for zero clearance at the stabilizer ($c_{st} = 0$).
19. Show that for a BHA with one stabilizer, the dimensionless tilt angle can be calculated using the following equation:

$$\delta_d = h_0 + \frac{c_{st} + 1 - \cos l_1 - 0.5l_1^2 - h_0 l_1}{\sin l_1}$$

where

h_0 = side force at the bit,

c_{st} = clearance at the stabilizer,

l_1 = distance from the bit to the stabilizer.

All quantities in the above equation are dimensionless.

20. Consider a BHA composed of 8-in. by 2³/₁₆-in. drill collars and a stabilizer with OD = 12.22 in. placed in a 12¼-in. hole. The stabilizer is placed 5 ft from the bit, and the WOB is 30,000 lbf. The mud weight is 10.5 lbm/gal, and the hole inclination angle is 55°. Calculate the
 - Side force at the bit
 - Side force at the stabilizer
 - Resultant force angle
 - Bending moment at 3 ft and 9 ft away from the bit
21. Recalculate Problem 20 above assuming distance to the stabilizer of 15, 30, and 45 ft. Also calculate the distance to the stabilizer that results in zero side force at the bit. For this case ($h_0 = 0$), calculate the bit-displacement direction if the formation dip angle $\gamma = 25^\circ$ and the drilling anisotropy index $h = 0.075$.

22. For a BHA as in Problem 20, calculate the expected side force at the bit when the curvature is
 - (a) $4^\circ/100$ ft
 - (b) $8^\circ/100$ ft
 - (c) $12^\circ/100$ ft
 Draw conclusions as appropriate.
23. Create a schematic diagram of a BHA with three stabilizers that is expected to build hole inclination angle under isotropic drilling conditions.
24. Compare the major advantages and disadvantages of turbodrills vs. PDMs for directional-drilling applications.
25. Calculate the power of a turbodrill if at a flow rate of 450 gal/min, a torque of 2,100 lbf-ft is produced at a rotational speed of 480 rev/min.
26. In a single-lobe motor (half-configuration), the rotor diameter is 2.5 in., the eccentricity is 1.125 in., and the rotor pitch is 24 in. At a flow rate of 300 gal/min, the total pressure loss through the motor is 480 psi. Calculate the expected
 - (a) Rotational speed
 - (b) Power output
 - (c) Torque
 Assume that the motor efficiency = 80%.
27. List the advantages and disadvantages of SMs.
28. List the advantages and disadvantages of RSSs.

8.3 Tool-Deflection Orientation

8.3.1 Basic Mathematical Concepts of 3D Trajectory Control. In this discussion, the emphasis will be placed on geometric considerations related to active trajectory control. For the sake of simplicity, let us first consider a deflection tool (e.g., a downhole motor with a bent sub) that is set in a vertical hole.

This tool will produce a deflection (a change in hole inclination angle from the vertical) in the same azimuth (direction) as the tool-deflection setting. For example, if the bent sub angle is 2° , the new hole inclination angle is expected to be 2° as well, and the new hole direction is assumed to be the same as the tool-deflection orientation. This is a purely geometric approach and does not account for the bending effects of the BHA, pipe rotation (if any), formation dip angle, formation anisotropy, or other factors. If a deflection tool is set in a hole that is not vertical and if the tool is oriented in a vertical plane including the hole, the resulting deflection (change in hole inclination angle) will be in the same plane (no change in hole azimuth direction), and the hole inclination angle may build up or drop down, depending on the tool orientation with respect to the high side of the wellbore. For example, if the hole inclination angle is 10° and the tool-deflection angle is 2° , the new hole inclination angle will be 12° if the tool will be pointing up the high side of the wellbore or 8° if the tool will be pointing toward the low side of the wellbore. There is no change in hole direction (azimuth) in this case because the tool is in the same vertical plane as the wellbore.

Now let us consider the situation shown schematically in **Fig. 8.45**. Line AB represents the original hole with inclination angle ϕ . The segment $A'B$ is a projection of AB onto a horizontal plane, and the angle ε is the direction of the original hole with respect to the south direction. In other words, the azimuth of the hole segment AB is $(180 - \varepsilon)^\circ$. A deflection tool with deflection angle β (e.g., a bent sub angle) is placed at the bottom (Point A) and then turned to the left about the AB axis through an angle γ , as shown in Fig. 8.45. The angle γ is called the *tool-face angle*. Segment AC represents a new hole, and $A'C$ is a projection of AC onto a horizontal plane. The new hole direction as measured from the South is $\varepsilon + \Delta\varepsilon$. In other words, by turning the tool face by γ , orienting the tool in the BC direction, the new hole direction has been changed. In Fig. 8.45, the new hole azimuth is less than that of the original hole. It is also clear that the new hole inclination angle will be ϕ_n and that the overall angle change, β , will be the same as the tool deflection angle (e.g., a bent sub angle).

If the tool were to be turned to the right from the high side (case not shown in the figure), then the new hole azimuth would be greater than that of the original hole. If the tool is turned 360° around AB, then a cone would be formed out of lines like AC. Because AB is not vertical, the cross section of the cone on the horizontal plane is an ellipse. The tangents $A'T_1$ and AT_2 define the maximum possible change in the original hole direction for the deflection tool considered in Fig. 8.45.

Ragland Method. The method proposed by Ragland (Ingilis 1987) is valid for small hole inclination angles. For small inclination angles, the ellipse can be approximated by a circle. Such a simplifying assumption was made in the early days of directional drilling and can be effectively used if the hole inclination angle is not more than approximately 20 to 25° . Tool-deflection orientation was determined using graphical techniques or with the aid of

From Fig. 8.49, it can be seen that

$$AB = EA \sin \gamma. \quad (8.81)$$

From triangles EBB' and EAB, it is possible to obtain

$$EB' = EB \cos \phi \text{ and } EB = EA \cos \gamma.$$

Hence,

$$EB' = EA \cos \gamma \cos \phi \quad (8.82)$$

From triangles OEC and OO'E,

$$EA = CE = OE \tan \beta, \quad (8.83)$$

$$O'E = OE \sin \phi, \quad (8.84)$$

$$OE = \frac{AE}{\tan \beta}, \quad (8.85)$$

Combining the above equations, the result is

$$\tan \Delta \varepsilon = \frac{\tan \beta \tan \gamma}{\sin \varphi + \tan \beta \cos \varphi \cos \gamma}. \quad (8.86)$$

Note that if the tool rotation angle γ or the deflection angle β were nil, then there would be no change in the hole direction, $\Delta \varepsilon = 0$.

The new inclination angle φ_n is equal to the angle AOO' or AOD. The Point D (not shown in Fig. 8.47. is obtained by drawing a line from Point A perpendicular to OO':

$$\cos \varphi_n = \frac{OD}{OA} = \frac{OO' - O'D}{OA}. \quad (8.87)$$

From triangles OO'E and EBB',

$$OO' = OE \cos \phi \text{ and } BB' = EB \sin \phi = O'D, \quad (8.88)$$

but $EB = AE \cos \gamma$, hence, $BB' = AE \cos \gamma \sin \phi$.

From triangle OCE,

$$OC = OA = \frac{OE}{\cos \beta}. \quad (8.89)$$

Note also that $EC = AE$ and $AE = OE \tan \beta$.

Combining Eqs. 8.87 through 8.89 yields the desired equation for calculating the new hole inclination angle:

$$\cos \varphi_n = \cos \varphi \cos \beta - \sin \beta \sin \varphi \cos \gamma. \quad (8.90)$$

Note that if the tool-face angle $\gamma = 0$, then the new hole inclination angle is simply $\varphi_n = \varphi + \beta$, and as stated earlier, there is no change in hole direction.

It can also be shown that the overall angle change (the tool-deflection angle or DL) is related to the original and new hole inclination angles (φ and φ_n) and the direction change $\Delta \varepsilon$ as follows:

$$\cos \beta = \sin \varphi \sin \varphi_n \cos \Delta \varepsilon + \cos \varphi \cos \varphi_n. \quad (8.91)$$

Eqs. 8.86, 8.90, and 8.91 form a mathematical model for solving a number of practical problems related to the selection and orientation of deflection tools.

From the directional-drilling engineer's standpoint, the result of the above calculation is three equations that contain five variables. Hence, given any three of the variables, one can calculate the remaining two unknowns. However, one always needs to be careful with the interpretation of the results because multiple solutions are possible due to the periodic nature of the trigonometric functions.

Example 8.17 The hole inclination angle $\phi = 10^\circ$, and the direction is N20°E (azimuth = 20°). It is required to build and turn the hole so that the new hole inclination angle $\phi_n = 12^\circ$ and the new direction is N23E. Calculate the required tool-deflection angle and the tool-face angle γ .

Solution. To obtain the tool-deflection angle, use Eq. 8.91 to get

$$\beta = \arccos(\cos 10 \cos 12 + \sin 10 \sin 12 \cos 3.0) = 2.08^\circ.$$

For the actual deflecting job, a mud motor with a bent housing of 2° can be used.

To increase the hole azimuth angle, the tool needs to be rotated to the right from the high side by the amount obtained from Eq. 8.90:

$$\gamma = \arccos\left(\frac{\cos 10.0 \cos 2.0 - \cos 12.0}{\sin 2.0 \sin 10}\right) = 9.76^\circ.$$

In other words, the tool-deflection direction is N20E + 9.76 = N29.76E.

It is recommended to use the graphical method (Ragland diagram) to solve this problem and compare the solutions.

Example 8.18 The hole inclination angle $\phi = 22^\circ$, and the direction is S36W (azimuth = 216°). It is desired to turn the hole 6° to the right (increase the azimuth) and increase the build angle. For this purpose, a positive-displacement motor with a bent sub of 3° is used. Calculate the expected new hole inclination angle and the required tool direction.

Solution. To solve the problem, again Eq. 8.91 is used, but some rearrangement is needed to calculate ϕ_n . Set $a = \sin \phi \cos \Delta\epsilon$ and $b = \cos \phi$; then Eq. 8.91 can be written as

$$\cos \beta = \sqrt{a^2 + b^2} \cos(\phi_n - \phi),$$

where

$$\phi = \arctan \frac{a}{b} = \arctan \left(\frac{\sin 22 \cos 6}{\cos 22} \right) = 21.89^\circ.$$

Hence,

$$\phi_n = \phi + \arctan \left(\frac{\cos \beta}{\sqrt{a^2 + b^2}} \right) = 21.89 + \arccos \left(\frac{\cos 3}{0.9904} \right) = 23.88^\circ.$$

To find the tool direction, it is necessary to calculate the tool rotation angle γ using Eq. 8.90:

$$\gamma = \arccos \left(\frac{\cos 22 \cos 3 - \cos 23.88}{\sin 3 \sin 22} \right) = 54^\circ.$$

Finally, the required tool direction is obtained as 36 + 54 = S90W, and the azimuth = 270°.

Example 8.19 A survey shows a hole inclination angle of 10° with the direction far off course. A deflection assembly with a bent sub of 2.4° is available on the rig side. Determine the tool rotation angle γ required to obtain the maximum turn. Also find the corresponding hole direction change $\Delta\epsilon$ and the new hole inclination angle ϕ_n .

Solution. As shown in Eq. 8.86 for a given hole inclination angle ϕ and tool-deflection angle β , the change of hole direction $\Delta\epsilon$ is a function only of the angle γ . Hence, it is possible to take the first derivative and equate it to zero:

$$\frac{d\Delta\epsilon}{d\gamma} = \frac{\sin \phi \tan \beta \cos \gamma + \cos \phi \tan^2 \beta}{(\sin \phi + \cos \phi \tan \beta \cos \gamma)^2 + \tan^2 \beta \sin^2 \gamma}$$

Hence,

$$\sin \phi \tan \beta \cos \gamma + \cos \phi \tan^2 \beta = 0. \quad (8.92)$$

Solving for γ yields

$$\gamma = \arccos(-\cot \phi \tan \beta) = \arccos(-\cot(10) \tan(2.4)) = 104^\circ$$

Consequently, the expected maximum change in hole direction is

$$\Delta \varepsilon_{\max} = \arctan \left[\frac{\tan(2.4) \sin(104)}{\sin(10) + \cos(10) \tan(2.4) \cos(104)} \right] = 14^\circ,$$

and the expected new hole inclination angle is

$$\phi_n = \arccos[\cos(10) \cos(2.4) - \sin(10) \sin(2.4)] = 9.7^\circ.$$

Note that if the tool face is turned to the left, the azimuth will decrease, and if it is turned to the right, the azimuth will increase.

8.3.3 Relationships Between Tool-Face Angle, Curvature, and Build and Turn Rates. It is useful to note that for a small tool-deflection angle $d\beta$, the tool-face rotation angle γ is given by

$$\cos \gamma = \frac{\cos \phi \cos d\beta - \cos \phi_n}{\sin d\beta \sin \phi}. \quad (8.93)$$

For small values of $d\beta$, it can be assumed that

$$\cos(d\beta) \cong 1, \quad \sin(d\beta) \cong d\beta, \quad \phi_n - \phi \cong d\phi, \quad \text{and} \quad \cos(d\phi) \cong 1.$$

Hence, after some arrangements, Eq. 8.93 takes the form

$$\cos \gamma = \frac{d\phi}{d\beta} = \frac{B}{DLS}. \quad (8.94)$$

Eq. 8.94 indicates that to drill a hole with a constant build rate and constant curvature, one needs to keep the tool-face angle γ constant with respect to the high side of the hole. Moreover, to drill a well path with a constant inclination angle ($B = 0$), such as a part of a helix, the tool-face angle should be equal to 90° . Continuous adjustments of the tool face are needed to drill a smooth well trajectory.

Now it can be concluded that the lateral curvature is $B_L = DLS \sin \gamma$, and consequently the turn rate T and the horizontal turn rate H are

$$T = \frac{DLS \sin \gamma}{\sin \phi}, \quad (8.95)$$

$$H = \frac{DLS \sin \gamma}{\sin^2 \phi}, \quad (8.96)$$

and the azimuth change can be expressed as

$$\Delta \theta = \tan \gamma \ln \left[\frac{\tan(\frac{1}{2} \phi_2)}{\tan(\frac{1}{2} \phi_1)} \right]. \quad (8.97)$$

8.3.4 Trajectory Calculations for Constant-Curvature and Minimum-Curvature Well Profiles. Using the above equations, well trajectories can be constructed that meet certain geometric constraints (the *drill-ahead* approach). The practical usefulness of the equations presented above will be demonstrated by a numerical example taken from Schuh (1992).

Example 8.20 Design a well trajectory between two points with the inclination, azimuth angles, and coordinates specified below:

$$\begin{aligned}\varphi_{\text{initial}} &= 55^\circ, & \varphi_{\text{final}} &= 90^\circ \\ \mathcal{G}_{\text{initial}} &= 0^\circ, & \mathcal{G}_{\text{final}} &= 20^\circ\end{aligned}$$

Initial coordinates: $x = 0.0$ ft, $y = 0.0$ ft, $z = 3,000$ ft,

Final coordinates: $x = 305$ ft, $y = 60$ ft, $z = 3,100$ ft.

The required hole curvature is $12^\circ/100$ ft.

Solution. First, the calculations will be performed using the constant-curvature (constant tool face) method. Given the initial and final hole inclination angles, a build rate of $10.6^\circ/100$ ft is chosen. This step may require several iterations before the desired value is determined.

Given the build rate and well-path curvature, the tool-face angle γ can be calculated from Eq. 8.94:

$$\gamma = \arccos\left(\frac{10.6}{12}\right) = 28^\circ.$$

Now it is possible to calculate all trajectory parameters for the point located at a distance of 30 ft (3,030 ft of MD) from the initial point.

The inclination angle is

$$\varphi(3,030 \text{ ft}) = \varphi_1 + B\Delta s = 55 + \frac{10.6}{100} 30 = 58.2^\circ,$$

and the azimuth (Eq. 8.97) is

$$\mathcal{G}(3,030 \text{ ft}) = 0 + \left(\frac{180}{\pi}\right)(\tan 28) \ln \left(\frac{\tan \frac{58.2}{2}}{\tan \frac{55.0}{2}}\right) = 2.0^\circ.$$

To calculate the x , y , z coordinates, the piecewise radius-of-curvature equations will be used, so the average value of the horizontal turn rate \bar{H} is needed.

The average value of the horizontal turn rate between the initial point and the point under consideration (30 ft apart) can be obtained by integrating Eq. 8.96:

$$\begin{aligned}\bar{H} &= \frac{DLS \sin \gamma}{\varphi_2 - \varphi_1} \int_{\varphi_1}^{\varphi_2} \frac{d\varphi}{\sin^2 \varphi} = \frac{DLS \sin \gamma}{\varphi_2 - \varphi_1} (\cot \varphi_1 - \cot \varphi_2) \\ &= \frac{(12)(\sin 28)}{(28.2 - 55.0)} \left(\frac{180}{\pi}\right) (\cot 55 - \cot 58.2) = 8.1^\circ/100 \text{ ft}\end{aligned}$$

With Eq. 8.96 and the arithmetic average value of the hole inclination angle

$$\bar{\varphi} = \frac{\varphi_1 + \varphi_2}{2} = \frac{55.0 + 58.3}{2} = 56.6,$$

the result is

$$\bar{H} = \frac{DLS \sin \gamma}{\sin^2 \bar{\varphi}} = \frac{(12)(\sin 28)}{\sin^2 56.6} = 8.08^\circ/100 \text{ ft}.$$

The similarity is due to the small difference in the inclination angles between the two points under consideration. Consequently, the corresponding turn rate (walk rate) is

$$\bar{T} = \frac{DLS \sin \gamma}{\sin \bar{\varphi}} = \frac{(12)(\sin 28)}{\sin 56.6} = 6.75^\circ/100 \text{ ft}.$$

Now the coordinates after drilling $\Delta s = 30$ ft can be calculated using Eqs. 8.30a, 8.30b, and 8.30c:

$$\begin{aligned}x_{30} &= 0 + \frac{1}{0.081} \left(\frac{180}{\pi} \right) (\sin 2.0 - \sin 0) = 24.7 \text{ ft} \\y_{30} &= 0 + \frac{1}{0.081} \left(\frac{180}{\pi} \right) (\cos 0 - \cos 2.0) = 0.43 \text{ ft} \\z_{30} &= 3,000 + \frac{1}{0.106} \left(\frac{180}{\pi} \right) (\sin 58.2 - \sin 55) = 3,016.5 \text{ ft}\end{aligned}$$

In a similar manner, the hole inclination angle, azimuth, and coordinates of subsequent points on the trajectory can be calculated and the results presented in the form of tables and graphs.

Now the sequence of calculations involved in computing a trajectory using the minimum-curvature method will be presented. Given the hole inclination and azimuth angles at the upper and lower end of the well path, Eq. 8.91 can be used to calculate the DL (overall angle change) as

$$DL = \beta = \arccos[(\sin 55)(\sin 90)(\cos 20) + (\cos 55)(\cos 90)] = 39.66^\circ.$$

From Eq. 8.90, the initial tool-face angle γ_1 can be determined as

$$\gamma_1 = \arccos \left[\frac{\cos \varphi_1 \cos \beta - \cos \varphi_2}{\sin \beta \sin \varphi_1} \right] = \arccos \left[\frac{\cos 55 \cos 39.6 - \cos 90}{\sin 39.6 \sin 55} \right] = 32.2^\circ.$$

Here the inclination angles φ_1 and φ_2 correspond to the initial and final inclination angles for the 300-ft section of the wellbore.

After drilling the distance $\Delta s = 30$ ft from the initial point on a circular arc, the corresponding DL is

$$\beta_i = DL_i = \frac{(12)(30)}{100} = 3.6^\circ.$$

The hole inclination angle after drilling 30 ft with the tool-face angle $\gamma = 32.2^\circ$ can be obtained from Eq. 8.90 using 3.6° as the DL:

$$\varphi_1 = \arccos[\cos 55 \cos 3.6 - (\sin 3.6)(\cos 55)(\cos 32.3)] = 58.1^\circ.$$

The corresponding change in azimuth can be calculated from Eq. 8.91:

$$\Delta \theta = \arccos \left[\frac{\cos 3.6 - (\cos 58.1)(\cos 55)}{\sin 55 \sin 58.1} \right] = 2.3^\circ.$$

Now it is possible to calculate the coordinates of the point on the circular-arc trajectory after drilling 30 ft using the minimum-curvature equations (Eqs. 8.31a, 8.31b, and 8.31c).

First, from Eq. 8.32, the RF is

$$RF = \frac{30}{3.6} \frac{180}{\pi} \left(\tan \frac{3.6}{2} \right) = 15 \text{ ft},$$

and the coordinates are

$$\begin{aligned}x_{30} &= 0 + (\sin 55 \cos 0 + \sin 58.1 \cos 2.3)(15) = 25.01 \text{ ft} \\y_{30} &= 0 + (\sin 55 \sin 0 + \sin 58.1 \sin 2.3)(15) = 0.51 \text{ ft} \\z_{30} &= 3,000 + (\cos 55 + \cos 58.1)(15) = 16.54 \text{ ft}.\end{aligned}$$

To calculate the tool-face angle after drilling 30 ft, Eq. 8.90 can be used again to yield

$$\gamma_{30\text{ft}} = \arccos \left[\frac{\cos 58.1 \cos (39.6 - 3.6) - \cos 90}{(\sin 58.1) \sin (39.6 - 3.6)} \right] = 31.05^\circ.$$

Now select a subsequent point ($\Delta s = 30$ ft) on the circular arc and perform the calculations of the new hole inclination angle and azimuth in a similar manner. The calculated tool-face angles vs. MD for the two methods considered are shown in **Fig. 8.50**. The hole inclination angles vs. vertical depth are presented in **Fig. 8.51**. Horizontal projections are shown in **Fig. 8.52**.

The reader is encouraged to write a program to verify the above results and also use the constant-turn-rate method to calculate the corresponding coordinates.

8.3.5 Review Questions and Problems.

1. List three commonly used deflection tools.
2. The hole inclination angle is 46° , and the bend subangle of a deflection tool is 2.0° . If the tool orientation is the same as the hole azimuth, find the expected new hole inclination angle if the tool is pointing
 - (a) To the high side of the wellbore ($\gamma = 0^\circ$)
 - (b) To the low side of the wellbore ($\gamma = 180^\circ$)
3. The following data are given:
 - Hole inclination angle $\phi = 17^\circ$
 - Hole direction N45E ($\vartheta = 45^\circ$)
 - Tool-deflection angle (DL) $\beta = 2.0^\circ$
 - Tool-face angle $\gamma = 35^\circ$ (to the right)

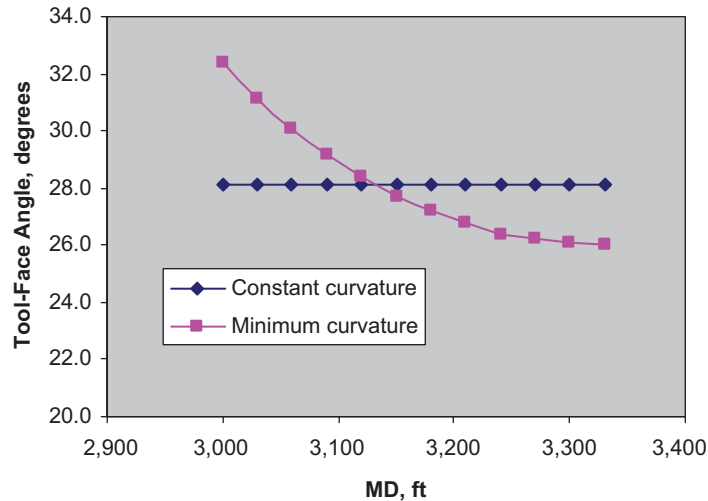


Fig. 8.50—Tool-face angle vs. MD, Example 8.20.

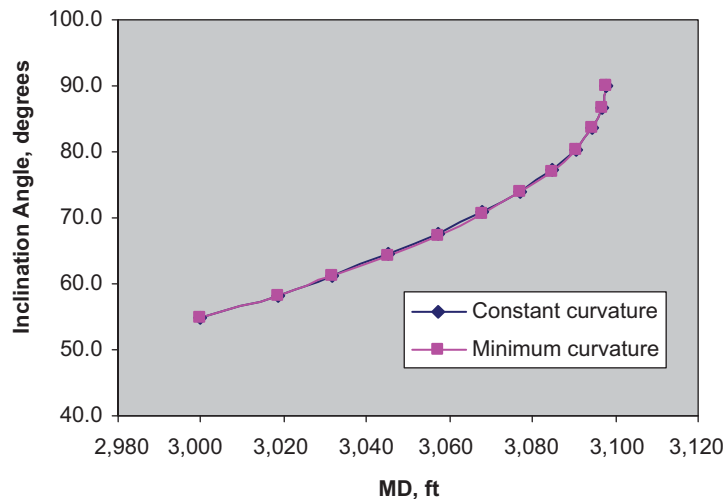


Fig. 8.51—Inclination angle vs. MD, Example 8.20.

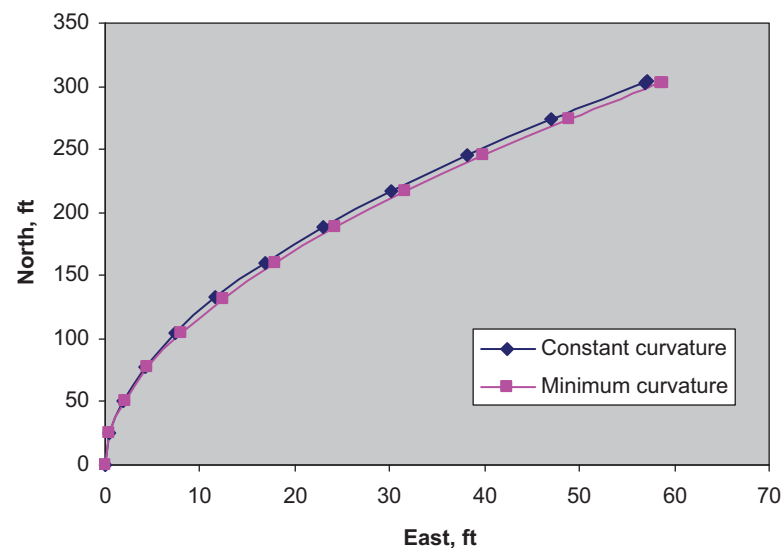


Fig. 8.52—Horizontal projections, Example 8.20.

Construct the Ragland diagram and find the expected new hole inclination and azimuth angles.

4. The original hole inclination and direction angles are $\phi = 10^\circ$ at N30W. It is desired to turn the hole to the left (counterclockwise) and reduce the inclination angle to 8° . Find the tool-deflection angle and tool-face rotation from the high side.
5. The original hole inclination and azimuth angles are $\phi = 6^\circ$ and $\vartheta = 240^\circ$ (S60°W). The desired new hole inclination angle is 7° with $\vartheta = 255^\circ$ (S75°W). To perform this job, a whipstock with a DL of $\beta = 20^\circ$ was used. After drilling some distance, the new hole inclination and azimuth angle were measured to be $6^\circ 30'$ and S72W. Find the amount of rolloff (bit walk) and the actual achieved deflection angle β^* . Note: Because the drillpipe is rotated clockwise, a clockwise rolloff angle is anticipated.
6. Consider the information provided in Problem 5. How should the whipstock be oriented to drill a hole with $\phi_n = 5.5^\circ$ and $\vartheta_n = 217^\circ$ (S37°W)?
7. Carefully review Fig. 8.47 and derive Eq. 8.91. List assumptions.
8. Using the data given in Example 8.16, calculate the new hole angle and azimuth change using Eqs. 8.90 and 8.91. Verify your calculations using Eq. 8.86. Draw conclusions as appropriate.
9. Using the following data, $\phi = 10^\circ$, $\phi_n = 12^\circ$, and $\Delta\epsilon = 20.01^\circ$, find the DL β and the tool-rotation angle γ .
10. Using the following data, $\phi = 10^\circ$ and $\beta = 4.28^\circ$, find $\Delta\epsilon_{\max}$ and the corresponding ϕ_n and tool-face angle γ .
11. Given ϕ , ϕ_n and γ , derive an equation for calculating β .
12. Show that to drill a well path with constant curvature and build rate, one needs to keep the tool-deflection angle γ constant with reference to the high side of the wellbore.
13. It has been determined that at a certain point of a 3D well path, a build rate of $24.5^\circ/100$ ft was achieved with a tool-face angle $\gamma = 47^\circ$ and a hole inclination angle $\phi = 63^\circ$. Calculate the DLS.
14. Show that to drill a well trajectory with constant build (B) and turn (T) rates, one needs to change the tool-face angle as a function of the hole inclination angle ϕ as follows:

$$\gamma = \arctan\left(\frac{T}{B} \sin \phi\right).$$

15. The initial coordinates of a certain 3D well trajectory are $x_1 = 1,450$ ft, $y_1 = 7,160$ ft and $z_1 = 3,785$ ft, and the hole inclination and azimuth angles are $\phi_1 = 35^\circ$ and $\vartheta_1 = 75^\circ$. Predict the hole inclination and azimuth angle after drilling 750 ft with build rate $B = 4.5^\circ/100$ ft if the tool-deflection angle $\gamma = 32^\circ$ is kept constant along the trajectory.
16. Calculate the expected x , y , z coordinates of the endpoint of the trajectory as specified in Problem 15 above.

8.4 Method of Vectors and Its Application to Directional Drilling

8.4.1 Mathematical Preliminaries: Frenet-Serret Equations. A review of the concepts of vectors and vector calculus is recommended before reading this discussion. The position of a point on a curve in three-dimensional space representing the centerline of a well trajectory can be uniquely determined by specifying the rectangular coordinates x, y, z or by a position vector $\vec{r}(s)$ that is a function of the distance measured along the curve from the origin of the coordinate system, as shown schematically in **Fig. 8.53**.

Using the conventional unit vectors \vec{i}, \vec{j} , and \vec{k} and defining s as the distance from the origin of the coordinate system, the position vector $\vec{r}(s)$ can be expressed as

$$\vec{r}(s) = x(s)\vec{i} + y(s)\vec{j} + z(s)\vec{k}. \quad (8.98)$$

The unit tangent vector $\vec{t}(s)$ can be obtained by differentiating the position vector:

$$\vec{t}(s) = \frac{d\vec{r}(s)}{ds} = \frac{dx(s)}{ds}\vec{i} + \frac{dy(s)}{ds}\vec{j} + \frac{dz(s)}{ds}\vec{k}. \quad (8.99)$$

From Eq. 8.99, it is apparent that the tangent vector is indeed a unit vector because the scalar product (dot product) is $\vec{t} \bullet \vec{t} = 1$.

The curvature vector is the second derivative with respect to s of the position vector or the first derivative of the unit tangent vector $\vec{t}(s)$ and is equal to the unit normal vector times the curvature $\kappa(s)$ (the magnitude of the curvature vector):

$$\vec{K}(s) = \frac{d\vec{t}(s)}{ds} = \kappa(s)\vec{n}(s). \quad (8.100)$$

The reciprocal of $\kappa(s)$ is the *radius of curvature*, which is the radius of a circle tangent to the trajectory at a point on the well path. The sign of $\vec{n}(s)$ is defined by the convention that $\kappa(s)$ is positive.

Substituting Eq. 8.99 into Eq. 8.100, the curvature vector can be obtained in terms of the second derivatives of the trajectory coordinates as follows:

$$\vec{K}(s) = \frac{d^2\vec{r}(s)}{ds^2} = \frac{d^2x(s)}{ds^2}\vec{i} + \frac{d^2y(s)}{ds^2}\vec{j} + \frac{d^2z(s)}{ds^2}\vec{k}. \quad (8.101)$$

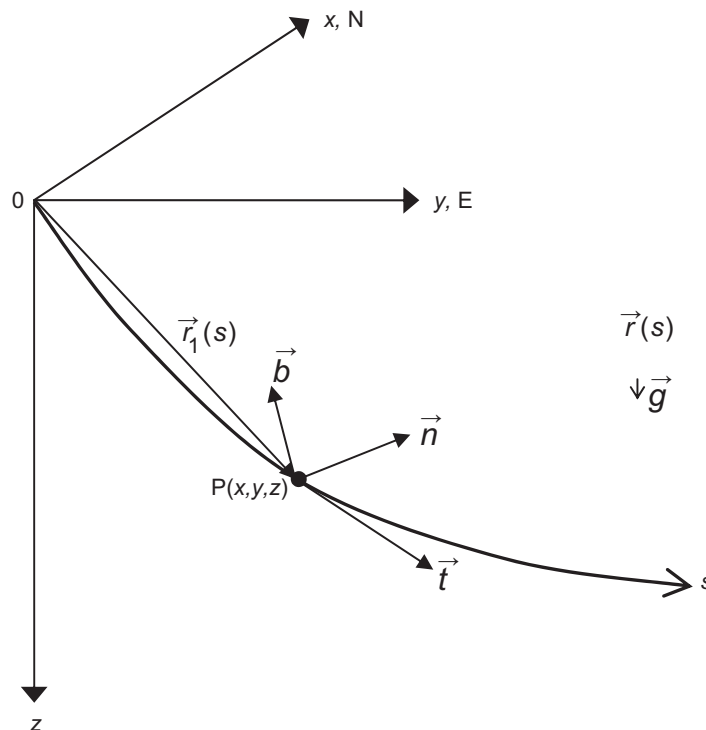


Fig. 8.53—3D segment of wellbore with an arbitrary point $P(x, y, z)$ at distance $\vec{r}(s)$ from the origin.

Hence, the magnitude of the curvature vector is

$$\kappa = \sqrt{\left(\frac{d^2x}{ds^2}\right)^2 + \left(\frac{d^2y}{ds^2}\right)^2 + \left(\frac{d^2z}{ds^2}\right)^2} \quad (8.102)$$

This equation is exactly the same as that used earlier (Eq.8.20) for calculating the wellbore curvature.

To form a set of three mutually perpendicular unit vectors or local coordinates at s , the unit binormal $\vec{b}(s)$ is defined as the cross (vector) product of the unit tangent and normal vectors:

$$\vec{b}(s) = \vec{t}(s) \times \vec{n}(s). \quad (8.103)$$

The unit binormal vector is perpendicular to the plane containing the tangent and normal vectors, and the positive direction is established according to the right-hand rule.

From differential geometry, it is known that the derivative of the unit binormal vector with respect to the arc length (MD) s is

$$\frac{d\vec{b}(s)}{ds} = -\tau(s)\vec{n}(s), \quad (8.104)$$

where $\tau(s)$ is the *torsion* of the curve. It should be pointed out that the torsion represents the rate of change in the unit binormal vector along the well trajectory. For example, if the trajectory is limited to a single plane (mono-plane trajectory), the torsion is zero. In other words, if the well turns in one plane (vertical, inclined, or horizontal), its torsion is zero. However, any 3D well trajectory must be characterized not only by curvature, but also by torsion. In other words, wellbore torsion is an indicator of wellbore departure from a 2D trajectory. The practical usefulness of torsion will be shown later in this chapter in a section on torque-and-drag calculations.

The derivative of the unit normal vector $\frac{d\vec{n}}{ds}$ is given by

$$\frac{d\vec{n}(s)}{ds} = -\kappa(s)\vec{t}(s) + \tau(s)\vec{b}(s). \quad (8.105)$$

The set of Eqs. 8.100, 8.104, and 8.105 is known as the Frenet-Serret equations and is effectively used in modern directional drilling for well-path design, directional-survey evaluations, and torque-and-drag calculations.

8.4.2 DLS, Curvature, and Torsion of a 3D Well Path. The term *wellbore curvature* has already been explained earlier and used for practical calculations. Here it will be shown that same formula can be obtained using vector concepts. In addition, methods to calculate the DL and wellbore torsion will be presented.

Consider a well path in 3D space. If x , y , and z are the rectangular coordinates of an arbitrary point on a trajectory and $\varphi(s)$ and $\vartheta(s)$ are the inclination and azimuth angles along the trajectory, then the unit tangent vector is

$$\vec{t}(s) = \frac{dx(s)}{ds}\vec{i} + \frac{dy(s)}{ds}\vec{j} + \frac{dz(s)}{ds}\vec{k} = (\sin\varphi \cos\vartheta)\vec{i} + (\sin\varphi \sin\vartheta)\vec{j} + \cos\varphi\vec{k}. \quad (8.106)$$

Eq. 8.106 is consistent with the equations of the first derivatives obtained earlier in Section 8.1.3.

It is also useful to note that Eq. 8.106 can also be written in term of the x -, y -, and z -components of the unit tangent vector as $\vec{t}(s) = t_x\vec{i} + t_y\vec{j} + t_z\vec{k}$; hence, for example, the z -component of the unit tangent vector is $t_z = \cos\varphi(s)$.

If the hole inclination and azimuth angles are given at two successive points on the well trajectory, then

$$\vec{t}_1 = (\sin\varphi_1 \cos\vartheta_1)\vec{i} + (\sin\varphi_1 \sin\vartheta_1)\vec{j} + \cos\varphi_1\vec{k}, \quad (8.107a)$$

$$\vec{t}_2 = (\sin\varphi_2 \cos\vartheta_2)\vec{i} + (\sin\varphi_2 \sin\vartheta_2)\vec{j} + \cos\varphi_2\vec{k}. \quad (8.107b)$$

The overall angle change between two arbitrary points on a well path is simply the angle between their two unit tangent vectors.

If the angle between the unit tangent vectors is denoted by β (the DL angle), then the dot product of the unit tangent vectors gives

$$\vec{t}_1 \bullet \vec{t}_2 = \cos\beta. \quad (8.108)$$

Substituting Eqs. 8.107a and 8.107b into Eq. 8.108 and solving for β yields

$$\beta = \arccos \left[\sin \varphi_1 \sin \varphi_2 \cos(\vartheta_1 - \vartheta_2) + \cos \varphi_1 \cos \varphi_2 \right]. \quad (8.109)$$

Differentiating the unit tangent vector given by Eq. 8.106 results in the curvature vector, \vec{K} :

$$\begin{aligned} \vec{K} = & \left[\cos \varphi \cos \vartheta \frac{d\varphi}{ds} - \sin \varphi \sin \vartheta \frac{d\vartheta}{ds} \right] \vec{i} \\ & + \left[\cos \varphi \sin \vartheta \frac{d\varphi}{ds} + \sin \varphi \cos \vartheta \frac{d\vartheta}{ds} \right] \vec{j} - \sin \varphi \frac{d\varphi}{ds} \vec{k}. \end{aligned} \quad (8.110)$$

Hence, the wellbore curvature, which is the magnitude of the curvature vector, is

$$|\vec{K}| = \kappa(s) = \sqrt{\left(\frac{d\varphi}{ds} \right)^2 + \sin^2 \varphi \left(\frac{d\vartheta}{ds} \right)^2}. \quad (8.110a)$$

As anticipated, this is the same equation as Eq. 8.22 used in Section 8.1.5, but obtained in a different manner. Now the unit normal vector can be obtained:

$$\begin{aligned} \vec{n} = & \frac{1}{\kappa} \left[\cos \varphi \cos \vartheta \frac{d\varphi}{ds} - \sin \varphi \sin \vartheta \frac{d\vartheta}{ds} \right] \vec{i} \\ & + \frac{1}{\kappa} \left[\cos \varphi \sin \vartheta \frac{d\varphi}{ds} + \sin \varphi \cos \vartheta \frac{d\vartheta}{ds} \right] \vec{j} - \frac{1}{\kappa} \sin \varphi \frac{d\varphi}{ds} \vec{k}. \end{aligned} \quad (8.111a)$$

In a manner similar to that for the unit tangent vector, the x -, y -, and z -components of the unit normal vector can be distinguished as $\vec{n}(s) = n_x \vec{i} + n_y \vec{j} + n_z \vec{k}$, and the z -component is

$$n_z = -\frac{1}{\kappa} \sin \varphi \frac{d\varphi}{ds} = -\sin \varphi \frac{B}{\kappa} = -\sin \varphi \cos \gamma \quad (8.111b)$$

where B , κ , and γ are the build rate, curvature (i.e., DLS), and deflection tool-face angle. The relationship between build rate, DLS, and tool-face angle is derived in Section 8.3.3.

The unit binormal vector is obtained by taking the cross-product of the unit tangent and unit normal vectors. From Eqs. 8.106 and 8.111a,

$$\begin{aligned} \vec{b} = & \left[-\frac{\sin \vartheta}{\kappa} \left(\frac{d\varphi}{ds} \right) - \frac{\cos \varphi \sin \vartheta \cos \vartheta}{\kappa} \left(\frac{d\vartheta}{ds} \right) \right] \vec{i} \\ & + \left[\frac{\cos \vartheta}{\kappa} \left(\frac{d\varphi}{ds} \right) - \frac{\cos \varphi \sin \vartheta \sin \vartheta}{\kappa} \left(\frac{d\vartheta}{ds} \right) \right] \vec{j} + \frac{\sin^2 \varphi}{\kappa} \left(\frac{d\vartheta}{ds} \right) \vec{k} \end{aligned} \quad (8.112)$$

In a similar manner as before, it can be determined that $\vec{b}(s) = b_x \vec{i} + b_y \vec{j} + b_z \vec{k}$, and the z -component of the unit binormal vector is

$$b_z = \frac{1}{\kappa} \sin^2 \varphi \frac{d\vartheta}{ds} = \sin^2 \varphi \frac{T}{\kappa} = \sin \varphi \sin \gamma, \quad (8.112a)$$

where T is the turn rate (walk rate).

It is known that $\frac{d\vec{b}}{ds} = -\tau \vec{n}$; hence, taking the dot product of both sides yields

$$\frac{d\vec{b}}{ds} \bullet \vec{n} = -\tau \vec{n} \bullet \vec{n} = -\tau,$$

or

$$\tau = -\frac{d\vec{b}}{ds} \bullet \vec{n} = -\left(\frac{d\vec{b}_x}{ds} n_x + \frac{d\vec{b}_y}{ds} n_y + \frac{d\vec{b}_z}{ds} n_z \right). \quad (8.113)$$

Now the derivatives of the unit binormal vector must be obtained:

$$\frac{db_x}{ds} = -\frac{1}{\kappa} \left[\begin{aligned} &2 \cos^2 \varphi \cos \vartheta \left(\frac{d\varphi}{ds} \right) \left(\frac{d\vartheta}{ds} \right) + \sin \vartheta \left(\frac{d^2 \varphi}{ds^2} \right) - \cos \varphi \sin \varphi \sin \vartheta \left(\frac{d\vartheta}{ds} \right)^2 \\ &+ \cos \varphi \sin \varphi \cos \vartheta \left(\frac{d^2 \vartheta}{ds^2} \right) \end{aligned} \right] \dots\dots\dots (8.114)$$

$$\frac{db_y}{ds} = -\frac{1}{\kappa} \left[\begin{aligned} &-2 \cos^2 \varphi \sin \vartheta \left(\frac{d\varphi}{ds} \right) \left(\frac{d\vartheta}{ds} \right) + \cos \vartheta \left(\frac{d^2 \varphi}{ds^2} \right) \\ &-\cos \varphi \sin \varphi \cos \vartheta \left(\frac{d\vartheta}{ds} \right)^2 - \cos \varphi \sin \varphi \sin \vartheta \left(\frac{d^2 \vartheta}{ds^2} \right) \end{aligned} \right], \dots\dots\dots (8.115)$$

$$\frac{db_z}{ds} = \frac{1}{\kappa} \left[2 \sin \varphi \cos \varphi \left(\frac{d\varphi}{ds} \right) \left(\frac{d\vartheta}{ds} \right) + \sin^2 \varphi \left(\frac{d^2 \vartheta}{ds^2} \right) \right]. \dots\dots\dots (8.116)$$

Substituting Eqs. 8.114–8.116 into Eq. 8.113 yields:

$$\tau = \frac{1}{\kappa^2} \left[\begin{aligned} &\cos \varphi \left\{ 2 \left(\frac{d\varphi}{ds} \right)^2 \left(\frac{d\vartheta}{ds} \right) + \sin^2 \varphi \left(\frac{d\vartheta}{ds} \right)^3 \right\} \\ &+ \sin \varphi \left\{ \left(\frac{d\varphi}{ds} \right) \left(\frac{d^2 \vartheta}{ds^2} \right) - \left(\frac{d^2 \varphi}{ds^2} \right) \left(\frac{d\vartheta}{ds} \right) \right\} \end{aligned} \right]. \dots\dots\dots (8.117)$$

Examination of Eq. 8.117 immediately reveals that if the hole azimuth angle is not changing along the wellbore trajectory (e.g., if the well path is in a vertical plane), the wellbore torsion is nil. For a given wellbore curvature, the wellbore torsion is a function of the build and turn rates as well as their derivatives, as stated below:

$$\tau = \frac{1}{\kappa^2} \left[T \cos \varphi (2B^2 + T^2 \sin^2 \varphi) + \sin \varphi \left(B \frac{dT}{ds} - T \frac{dB}{ds} \right) \right]. \dots\dots\dots (8.118)$$

Eq. 8.118 can be simplified for some specific cases by assuming constant build and turn rates.

Example 8.21 Suppose that a well path is part of a circular helix. Calculate the wellbore curvature and torsion if the turn rate $T = 6.5^\circ/100$ ft and the hole inclination angle $\varphi = 65^\circ$.

Solution. To calculate the curvature, Eq. 8.110 is used:

$$\kappa = \sqrt{B^2 + T^2 \sin^2 \varphi} = T \sin \varphi = (6.5) \sin(65) = 5.9^\circ/100 \text{ ft},$$

To calculate the torsion, use Eq. 8.118. Because for a circular helix, $B = 0$ and $\frac{dT}{ds} = 0$

($\varphi = \text{constant}$ and $T = \text{constant}$),

$$\tau = \frac{1}{\kappa^2} (\cos \varphi \sin^2 \varphi) T^3 = T \cos \varphi = (6.5) \cos(65) = 2.75^\circ/100 \text{ ft}.$$

Example 8.22 A wellbore trajectory has been designed using the RCM. For a build rate of $B = 0.12^\circ/\text{ft}$ and a horizontal turn rate of $H = 0.14^\circ/\text{ft}$, calculate the wellbore curvature and torsion at the hole inclination angle $\varphi = 55^\circ$.

Solution. Eq. 8.110 is used (note that $T = H \sin^2 \varphi$) to calculate the wellbore curvature:

$$\kappa = \sqrt{B^2 + H^2 \sin^4 \varphi} = \sqrt{(0.12)^2 + (0.14)^2 \sin^4(55)} = 15.24^\circ/100 \text{ ft},$$

and the wellbore torsion can be obtained from Eq. 8.118:

$$\begin{aligned}\tau &= \frac{H \sin \varphi \cos \varphi}{K^2} (3B^2 + H^2 \sin^4 \varphi) \\ &= \frac{(0.14) \sin(55) \cos(55)}{(0.1524)^2} \left[3(0.12)^2 + (0.14)^2 \sin^4(55) \right] = 14.73^\circ/100 \text{ ft.}\end{aligned}$$

From the above example as well as similar calculations for some other cases, one can conclude that the magnitude of wellbore torsion can fall into a range similar to that of wellbore curvature.

8.4.3 Calculating a Well Trajectory From Survey Data. Once a well is drilled out, its actual position must be evaluated in terms of the three-dimensional coordinates (x, y, z) and the inclination and azimuth angles along the well path. An important issue here is how far the actual wellbore path is from the designed trajectory. Normally, some type of survey instrument, such as a magnetic compass or a gyrocompass, is used to measure the inclination and azimuth angles at various depths, and then the trajectory is calculated using the appropriate equations. **Fig. 8.54** shows the standard way to represent part of a trajectory in the case where surveys have been taken at Points 1 and 2.

The points where the measurements are taken are called the *directional stations* or simply *stations*. The inclination is the angle between the vertical and a tangent to the wellbore at a survey point. The azimuth is the angle between north and the projection of the tangent on a horizontal plane. At each station, the inclination angle φ and azimuth angle ϑ are measured and corrected to true north, in the case of a magnetic survey, or for drift, if a gyroscopic survey was taken. Of course, the MD s at which the surveys were taken is also known. As previously determined, the hole inclination angle and azimuth define the unit tangent vector \vec{t} . The x -, y -, and z -components of the unit tangent vector are

$$\vec{t} \bullet \vec{i} = t_x = \sin \varphi \cos \vartheta, \quad \dots \dots \dots (8.119a)$$

$$\vec{t} \bullet \vec{j} = t_y = \sin \varphi \sin \vartheta \quad \dots \dots \dots (8.119b)$$

$$\vec{t} \bullet \vec{k} = t_z = \cos \varphi. \quad \dots \dots \dots (8.119c)$$

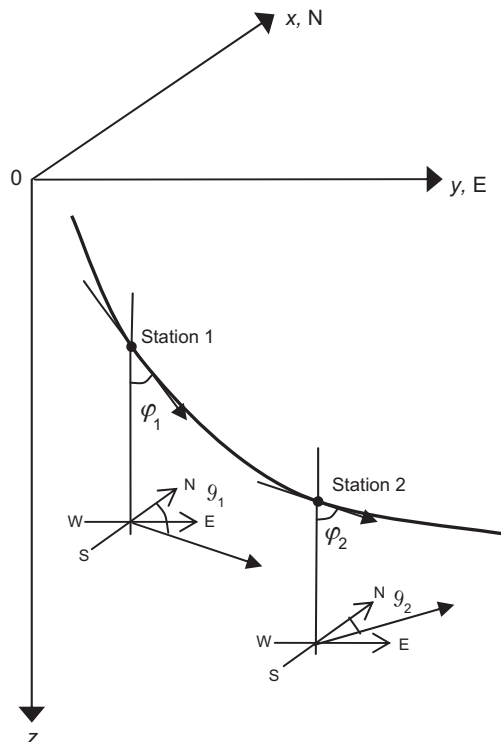


Fig. 8.54—Two survey stations on a 3D wellpath.

If it were known how the angles $\varphi(s)$ and $\vartheta(s)$ vary between stations, then the trajectory could be determined by integrating Eq. 8.119:

$$x_2 = x_1 + \int_{s_1}^{s_2} t_x ds = x_1 + \int_{s_1}^{s_2} \sin \varphi(s) \cos \vartheta(s) ds \quad (8.120a)$$

$$y_2 = y_1 + \int_{s_1}^{s_2} t_y ds = y_1 + \int_{s_1}^{s_2} \sin \varphi(s) \sin \vartheta(s) ds \quad (8.120b)$$

$$z_2 = z_1 + \int_{s_1}^{s_2} t_z ds = z_1 + \int_{s_1}^{s_2} \cos \varphi(s) ds \quad (8.120c)$$

Because at the time the directional survey is performed, it is not known how the inclination and azimuth angles $\varphi(s)$ and $\vartheta(s)$ change between the stations, there is no choice but to introduce some assumptions which will make it possible to carry out the required integrations.

Average-Angle and Tangential Methods. Perhaps the easiest case, although it is not very likely, would be to assume a constant tangent vector between the stations. In other words, if both the inclination angle and azimuth are assumed constant between the stations, then integration of Eq. 8.120 gives a straight line in the (x, y, z) system of coordinates:

$$x_2 = x_1 + (\sin \varphi \cos \vartheta) \Delta s, \quad (8.121a)$$

$$y_2 = y_1 + (\sin \varphi \sin \vartheta) \Delta s, \quad (8.121b)$$

$$z_2 = z_1 + \cos \varphi \Delta s. \quad (8.121c)$$

A fundamental question here is what angles to use in Eq. 8.121. Several versions of Eq. 8.121 have been used by the industry over the years in the early stages of directional drilling. The first method is called the *tangential method*, in which the value of \vec{t} used is the value at s_1 , and, hence, the inclination and azimuth angles in Eq. 8.121 are set to φ_1 and ϑ_1 . If the angles at the lower end are used, the inclination and azimuth angles in Eq. 8.121 are set to φ_2 and ϑ_2 to determine the tangent vector; this approach is called the *terminal-angle method*. In other words, in the terminal-angle method, the straightline path is assumed to have the same inclination angle and azimuth angle as that measured at the lower of the two survey stations. Another method, the AAM or angle-averaging method, determines the constant values using the algebraic average inclination and azimuth angles over the interval between Stations 1 and 2. Hence, for this case,

$$x_2 = x_1 + (\sin \bar{\varphi} \cos \bar{\vartheta}) \Delta s, \quad (8.122a)$$

$$y_2 = y_1 + (\sin \bar{\varphi} \sin \bar{\vartheta}) \Delta s, \quad (8.122b)$$

$$z_2 = z_1 + \cos \bar{\varphi} \Delta s, \quad (8.122c)$$

where the average algebraic values are $\bar{\varphi} = \frac{1}{2}(\varphi_1 + \varphi_2)$ and $\bar{\vartheta} = \frac{1}{2}(\vartheta_1 + \vartheta_2)$ as shown in **Fig. 8.55**.

A potential pitfall in using Eq. 8.122 arises when the angles are close to zero and 2π . For example, if one angle is slightly less than 2π and the other is slightly greater than zero, then the average angle will be near π instead of near 0. To obtain the correct result, either 2π must be subtracted from the first angle or 2π must be added to the second angle. Care must be taken to ensure that a reasonable result is obtained. The second pitfall occurs in the case of nearly vertical wells. In this case, the azimuth angle becomes undefined. Neither of these methods is considered sufficiently accurate for modern use.

RCM. This method uses sets of angles measured at the upper and lower ends of the course length to generate a 3D wellbore path that has a shape of a spherical arc passing through Points 1 and 2, as shown in **Fig. 8.56**.

The unit tangent vectors are as follows:

At Point 1:

$$\vec{t}(s_1) = \sin \varphi_1 \cos \vartheta_1 \vec{i} + \sin \varphi_1 \sin \vartheta_1 \vec{j} + \cos \varphi_1 \vec{k} \quad (8.123)$$

and at Point 2:

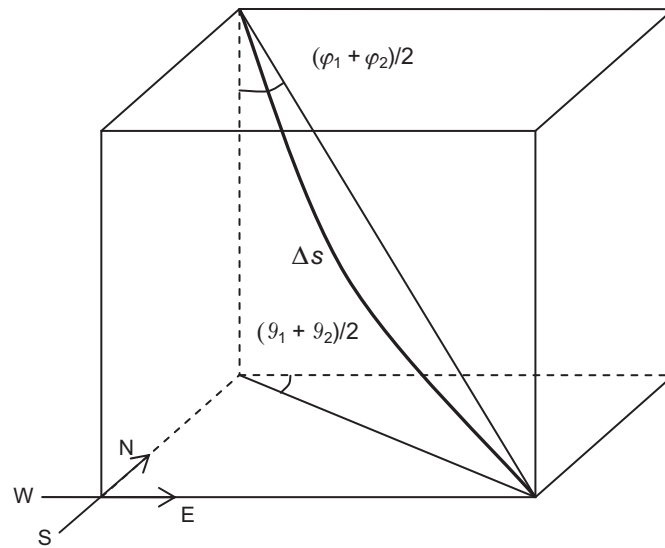


Fig. 8.55—AAM.

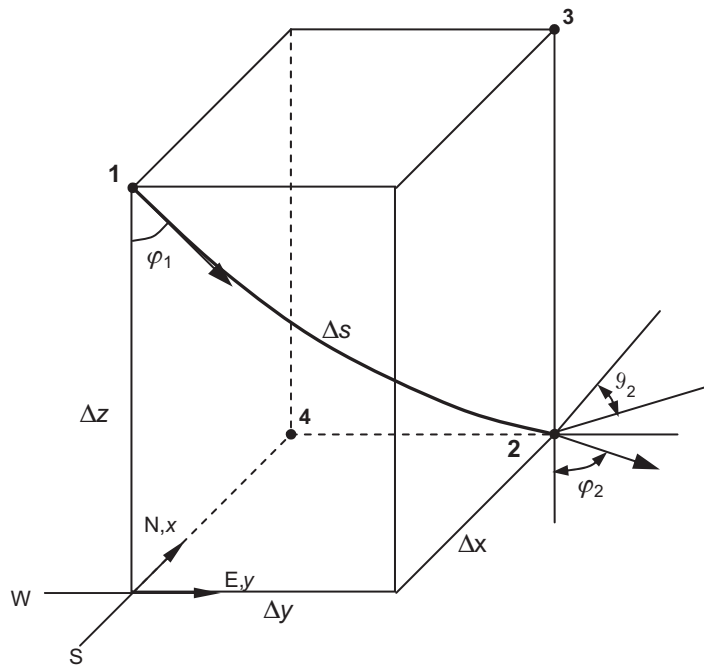


Fig. 8.56—RCM.

$$\vec{i}(s_2) = \sin \varphi_2 \cos \vartheta_2 \vec{i} + \sin \varphi_2 \sin \vartheta_2 \vec{j} + \cos \varphi_2 \vec{k} \quad \dots \quad (8.124)$$

Therefore, the difference between the position vectors, $\Delta \vec{r}$, is

$$\begin{aligned} \Delta \vec{r} = \vec{r}(s_2) - \vec{r}(s_1) = & \left(\int_{s_1}^{s_2} \sin \varphi \cos \vartheta ds \right) \vec{i} + \left(\int_{s_1}^{s_2} \sin \varphi \sin \vartheta ds \right) \vec{j} \\ & + \left(\int_{s_1}^{s_2} \cos \varphi ds \right) \vec{k} \quad \dots \quad (8.125) \end{aligned}$$

Similarly to previous cases, the integrals in Eq. 8.125 can be evaluated for the case where the build and horizontal turn rates are constant between the two survey stations. In this case,

$$\Delta \vec{r} = \vec{r}(s_2) - \vec{r}(s_1) = \left(\int_{s_1}^{s_2} \sin \varphi \cos \vartheta \frac{d\vartheta}{H \sin \varphi} \right) \vec{i} + \left(\int_{s_1}^{s_2} \sin \varphi \sin \vartheta \frac{d\vartheta}{H \sin \varphi} \right) \vec{j} + \left(\int_{s_1}^{s_2} \cos \varphi \frac{d\varphi}{B} \right) \vec{k} \quad \dots \quad (8.126)$$

Upon integration, the x -, y -, and z -components of $\Delta \vec{r}$ can be obtained:

$$\Delta \vec{r} = \left(\frac{\sin \vartheta_2 - \sin \vartheta_1}{H} \right) \vec{i} - \left(\frac{\cos \vartheta_2 - \cos \vartheta_1}{H} \right) \vec{j} + \left(\frac{\sin \varphi_2 - \sin \varphi_1}{B} \right) \vec{k} \quad \dots \quad (8.127)$$

Examination of Eq. 8.127 reveals that, as expected, the same equations were obtained for the rectangular coordinates as for well-path design using the RCM.

Minimum-Curvature Method. In this method, the two tangent vectors are connected by a circular arc, as illustrated in Fig. 8.57.

By imposing the requirement that the arc between \vec{r}_1 and \vec{r}_2 have a minimum curvature, it follows that the arc must be located in a plane. In other words, the minimum-curvature arc is a part of a plane

circle of radius $R = \frac{1}{\kappa}$, as shown in Fig. 8.58.

In Fig. 8.58, the wellbore segment between \vec{r}_1 and \vec{r}_2 is represented by a circular arc of radius R over angle β (the DL) connecting two tangent vectors, \vec{t}_1 at MD s_1 and \vec{t}_2 at MD s_2 . The arc length is $R\beta = s_2 - s_1 = \Delta s$. Note that the angle β is also the angle between the tangents \vec{t}_1 and \vec{t}_2 and is given by Eq. 8.109, which was derived earlier. The corresponding position vectors are $\vec{r}_1(s_1)$ and $\vec{r}_2(s_2)$.

The vector connecting Points 1 and 2 is denoted by $\Delta \vec{r}$ and is equal to $\Delta \vec{r} = \vec{r}_2(s_2) - \vec{r}_1(s_1)$.

If $\Delta \vec{r}$ is known, the change in coordinates Δx , Δy and Δz can be determined as for the RCM. It can be shown that for any point on the arc between Points 1 and 2,

$$\vec{r}(s) = \vec{r}_1(s_1) + \vec{t}_1 R \sin[\kappa(s - s_1)] + \vec{n}_1 R \{1 - \cos[\kappa(s - s_1)]\} \quad \dots \quad (8.128)$$

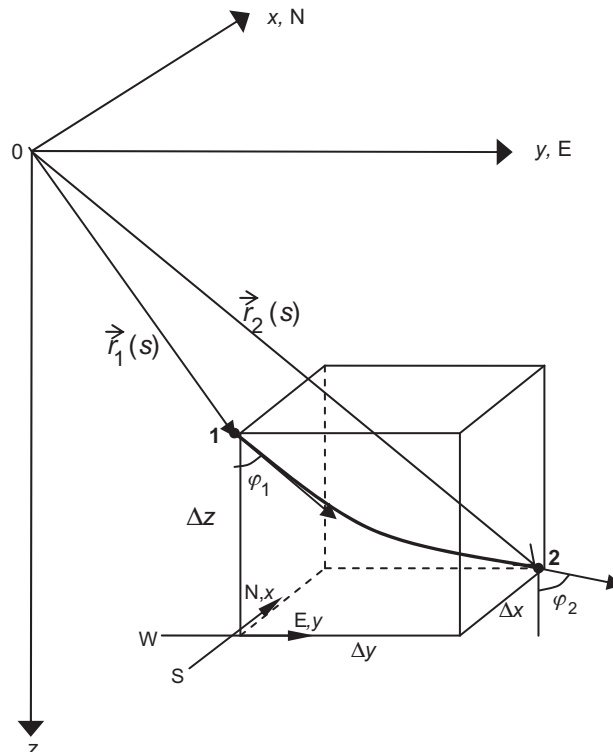


Fig. 8.57—Schematic of minimum-curvature method.

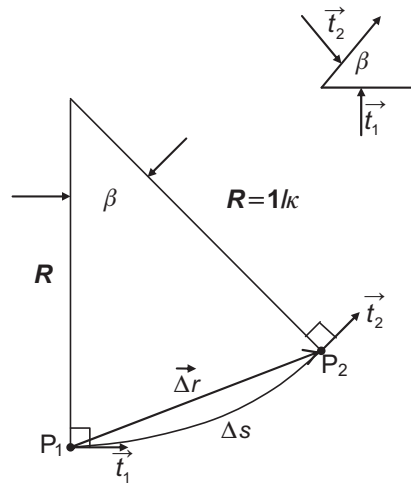


Fig. 8.58—Segment of a circular arc.

Differentiating Eq. 8.128 with respect to s yields the unit tangent vector $\vec{t}(s)$:

$$\vec{t}(s) = \vec{t}_1 \cos[\kappa(s - s_1)] + \vec{n}_1 \sin[\kappa(s - s_1)]. \quad (8.129)$$

Differentiating the unit tangent vector, the unit normal vector is obtained:

$$\vec{n}(s) = \frac{1}{\kappa} \frac{d\vec{t}}{ds} = -\vec{t}_1 \sin[\kappa(s - s_1)] + \vec{n}_1 \cos[\kappa(s - s_1)]. \quad (8.130)$$

Eqs. 8.129 and 8.130 make it possible to calculate the unit tangent and normal vectors at any point along the minimum-curvature trajectory for $s_1 \leq s \leq s_2$. Note that, as expected, at

Also at $s = s_2$

$$\vec{t}_2(s_2) = \vec{t}_2 = \vec{t}_1 \cos(\kappa \Delta s) + \vec{n}_1 \sin(\kappa \Delta s). \quad (8.131)$$

Because the unit tangent vectors \vec{t}_1 and \vec{t}_2 are known (φ and ϑ are known from survey stations), Eq. 8.131 can be solved to obtain the unit normal vector at P_1 :

$$\vec{n}_1 = \frac{\vec{t}_2 - \vec{t}_1 \cos(\kappa \Delta s)}{\sin(\kappa \Delta s)} = \frac{\vec{t}_2 - \vec{t}_1 \cos \beta}{\sin \beta}. \quad (8.132)$$

Note that Eq. 8.132 fails if $\vec{t}_1 = \vec{t}_2$. For this case, Eq. 8.121 for a straight wellbore should be used. For $s = s_2$, Eq. 8.128 can be written as

$$\vec{r}_2(s) - \vec{r}_1(s) = \Delta \vec{r} = (R \sin \beta) \vec{t}_1 + R(1 - \cos \beta) \vec{n}_1. \quad (8.133)$$

Substituting for \vec{n}_1 in Eq. 8.132 and setting $R = \frac{\Delta s}{\beta}$,

$$\Delta \vec{r} = (\vec{t}_1 + \vec{t}_2) \left(\frac{\Delta s}{\beta} \tan \frac{\beta}{2} \right). \quad (8.134)$$

Substituting known survey data for the unit tangent vectors yields the desired equation in rectangular coordinates:

$$x_2 = x_1 + (\sin \varphi_1 \cos \vartheta_1 + \sin \varphi_2 \cos \vartheta_2) RF, \quad (8.135a)$$

$$y_2 = y_1 + (\sin \varphi_1 \sin \vartheta_1 + \sin \varphi_2 \sin \vartheta_2) RF, \quad (8.135b)$$

$$z_2 = z_1 + (\cos \varphi_1 + \cos \varphi_2) \text{RF}, \quad \dots \quad (8.135c)$$

where the ratio factor RF is defined as

$$\text{RF} = \frac{\Delta s}{\beta} \tan \frac{\beta}{2}. \quad \dots \quad (8.136)$$

The reader can immediately notice that Eqs. 8.135 derived above are the same as Eqs. 8.31 and 8.32 for the minimum-curvature method and its application to trajectory design.

Analysis of Eqs. 8.129 and 8.130 shows that if several subsequent survey points are considered, the minimum-curvature trajectory is smooth (its derivatives are continuous) at the survey points. Moreover, because the trajectory between two successive stations is a plane curve, the torsion of each segment is zero. However, although the tangents are continuous in the minimum-curvature method, the normal vectors are discontinuous at the survey locations. In other words, the minimum-curvature trajectory obtained from several survey stations will have discontinuous curvature.

Example 8.23 The following data have been obtained from directional surveys:

MD,ft	Inclination Angle, degrees	Azimuth Angle, degrees
7,100	0	0
7,200	10.1	S68W
7,300	13.4	S65W
7,400	16.3	S75W
7,500	19.6	S61W

Calculate the rectangular coordinates x , y , and z using

- The tangential method
- The AAM
- The minimum-curvature method

At the MD $s = 7,100$ ft, the coordinates are $x = 0$; $y = 0$; and $z = 7,100$ ft.

Solution. The sequence of calculations will be presented for measured-depth values of 7,200 ft and 7,300 ft. The reader is encouraged to complete the calculations for the two remaining stations. The coordinates will be calculated using the tangential method.

According to Eq. 8.121, at $s = 7,200$ ft, $x = 0$, $y = 0$, $z = 7,200$ ft (Note: $\varphi = 0$ because the inclination angle at Station 1 is used).

And at $s = 7,300$ ft,

$$x = 0 + \sin(10.1) \cos(180+68)(100) = -6.57 \text{ ft},$$

$$y = 0 + \sin(10.1) \sin(180+68)(100) = -16.26 \text{ ft},$$

$$z = 7,200 + \cos(10.1)(100) = 7,298.5 \text{ ft}.$$

To use the AAM, the average hole inclination and azimuth angles at $s = 7,200$ ft must first be calculated:

$$\bar{\varphi} = 5.05^\circ \quad \text{and} \quad \bar{\vartheta} = \text{S68W} = 248^\circ$$

Now Eq. 8.122 can be used to calculate the coordinates:

$$x = 0 + \sin(5.05) \cos(248)(100) = -3.30 \text{ ft},$$

$$y = 0 + \sin(5.05) \sin(248)(100) = -8.16 \text{ ft},$$

$$z = 7,100 + \cos(5.05)(100) = 7,199.61 \text{ ft}.$$

In a similar manner, values at $s = 7,300$ ft are obtained:

$$\bar{\varphi} = 11.75^\circ \quad \text{and} \quad \bar{\vartheta} = 246.5^\circ$$

and the corresponding coordinates are

$$x = -3.30 + \sin(11.75) \cos(246.5)(100) = -11.42 \text{ ft},$$

$$y = -8.16 + \sin(11.75) \sin(246.5)(100) = -26.83 \text{ ft},$$

$$z = 7,199.61 + \cos(11.75)(100) = 7,297.51 \text{ ft.}$$

To use the minimum-curvature method, the DL and its corresponding RF must first be calculated. At MD $s = 7,200$ ft, the DL is

$$\beta = \arccos(\sin 0 - 10.1 \cos 0 + \cos 0 \cos 10.1) = 10.1^\circ = 0.176 \text{ radian,}$$

and the RF is

$$\text{RF} = \frac{\Delta s}{\beta} \tan \frac{\beta}{2} = \left(\frac{100}{0.176} \right) \tan \left(\frac{10.1}{2} \right) = 50.21 \text{ ft.}$$

Now the coordinates can be calculated using Eq. 8.135:

$$x = 0 + (\sin 0 \cos 248 + (\sin 10.1) \cos(248)) 50.21 = -3.30 \text{ ft,}$$

$$y = 0 + (\sin 0 \cos 248 + (\sin 10.1) \sin(248)) 50.21 = -8.16 \text{ ft,}$$

$$z = 7,100 + (\cos 0 + \cos 10.1)(50.21) = 7,199.64 \text{ ft.}$$

Consequently, at MD $s = 7,300$ ft,

$$\beta = \arccos(\sin 10.1 \sin 13.4 \cos(-3) + \cos 10.1 \cos 13.4) = 3.355 \text{ deg} = 0.059 \text{ radian,}$$

$$\text{RF} = \frac{100}{(0.059)} \tan \frac{(3.355)}{2} = 49.64 \text{ ft,}$$

$$x = -3.30 + (\sin 10.1 \cos 248 + \sin 13.4 \cos 245)(49.64) = -11.42 \text{ ft,}$$

$$y = -8.16 + (\sin 10.1 \sin 248 + \sin 13.4 \sin 245)(49.64) = -26.66 \text{ ft,}$$

$$z = 7,199.64 + (\cos 10.1 + \cos 13.4)(49.64) = 7,296.8 \text{ ft.}$$

The reader is encouraged to use the RCM and compare the results.

8.4.4 Interpolation Between Survey Stations. If survey stations are not located close enough together, interpolation is frequently required to calculate hole inclination and azimuth angles as well as build and turn rates along the trajectory between two successive stations. Such calculations are particularly important for accurate casing design, torque-and-drag predictions, and hole-cleaning calculations. The following discussion shows how to carry out interpolation calculations for hole inclination and azimuth angles and build and turn rates using the minimum-curvature method. For this purpose, let us consider the following two numerical examples.

Example 8.24 The following are two directional-survey measurements taken 100 ft apart:

Station 1: $\phi_1 = 13.4^\circ$, $\vartheta_1 = \text{S}65\text{W} = 245^\circ$

Station 2: $\phi_2 = 16.3^\circ$, $\vartheta_2 = \text{S}75\text{W} = 255^\circ$

Calculate the hole inclination and azimuth angles at the midpoint (50 ft from the first station), assuming a minimum-curvature well path.

Solution. The unit tangent vector was given by Eq. 8.106 but is repeated below for the reader's convenience:

$$(a) \quad \vec{t}(s) = (\sin \phi \cos \vartheta) \vec{i} + (\sin \phi \sin \vartheta) \vec{j} + (\cos \phi) \vec{k}.$$

For the minimum-curvature well path, the unit tangent vector was given as Eq. 8.129, but again is repeated below:

$$(b) \quad \vec{t}(s) = \vec{t}_1 \cos[\kappa(s - s_1)] + \vec{n}_1 \sin[\kappa(s - s_1)].$$

Multiplying (dot product) Line (a) by \vec{k} yields the z -component of the unit tangent vector:

$$(c) \quad \vec{t} \cdot \vec{k} = \cos \varphi(s)$$

In a similar manner, from Line (b),

$$(d) \quad \vec{t} \cdot \vec{k} = \cos \varphi_1 \cos [\kappa(s - s_1)] + \vec{n}_1 \cdot \vec{k} \sin [\kappa(s - s_1)]$$

Comparing Lines (c) and (d),

$$(e) \quad \cos \varphi(s) = \cos \varphi_1 \cos [\kappa(s - s_1)] + \vec{n}_1 \cdot \vec{k} \sin [\kappa(s - s_1)].$$

Line (e) enables calculation of the hole inclination angle at any arbitrary point of a minimum-curvature trajectory if the dot product $\vec{n}_1 \cdot \vec{k}$ can be determined.

For the minimum-curvature method, the unit normal vector at Station 1 is given by Eq. 8.132:

$$(f) \quad \vec{n}_1 = \frac{1}{\sin \beta} (\vec{t}_2 - \vec{t}_1 \cos \beta).$$

Hence,

$$(g) \quad \vec{n} \cdot \vec{k} = \frac{1}{\sin \beta} (\cos \varphi_2 - \cos \varphi_1 \cos \beta)$$

Substituting Line (g) into Line (e) gives

$$(h) \quad \cos \varphi(s) = (\cos \varphi_1) \cos [\kappa(s - s_1)] + \left(\frac{\cos \varphi_2 - \cos \varphi_1 \cos \beta}{\sin \beta} \right) \sin [\kappa(s - s_1)].$$

Line (h) enables calculation of the hole inclination angle $\varphi(s)$ along the well trajectory between surveying Stations 1 and 2. First, however, it is necessary to calculate the DL angle β and the wellbore curvature κ .

From Eq. 8.109,

$$\beta = \arccos [\sin(13.4) \sin(16.3) \cos(10) + \cos(13.4) \cos(16.3)] = 3.86^\circ.$$

Hence, the wellbore curvature is

$$(i) \quad \kappa = \frac{3.86}{100} = 0.0386^\circ/\text{ft}.$$

Now, using Line (h) at a distance $s - s_1 = 50$ ft from the first station gives

$$\cos \varphi = \cos(13.4) \cos(1.93) + \left[\frac{\cos(16.3) - \cos(13.4) \cos(3.86)}{\sin(3.86)} \right] \sin(1.93) = 0.9668.$$

Consequently, the desired wellbore inclination angle is

$$(j) \quad \varphi = \arccos(0.9668) = 14.79^\circ.$$

The calculations of the azimuth proceed as follows:

From Line (a), the x -component of the unit tangent vector can be obtained:

$$\vec{t} \cdot \vec{i} = \sin \varphi \cos \vartheta$$

Consequently,

$$(k) \quad \vartheta = \arccos \left(\frac{\vec{t} \cdot \vec{i}}{\sin \varphi} \right).$$

The dot product of the \vec{i} and \vec{i} unit vectors is now required.

From Line (b):

$$(l) \quad \vec{i} \cdot \vec{i} = \vec{i}_1 \cdot \vec{i} \cos[\kappa(s-s_1)] + \vec{n} \cdot \vec{i} \sin[\kappa(s-s_1)].$$

It is known that

$$(m) \quad \vec{i}_1 \cdot \vec{i} = \sin \varphi_1 \cos \vartheta_1 = \sin(13.4) \cos(245) = -0.0979,$$

and

$$\begin{aligned} \vec{n}_1 \cdot \vec{i} &= \frac{1}{\sin \beta} (\vec{i}_2 \cdot \vec{i} - \vec{i}_1 \cdot \vec{i} \cos \beta) \\ &= \frac{1}{\sin \beta} (\sin \varphi_2 \cos \vartheta_2 - \sin \varphi_1 \cos \vartheta_1 \cos \beta) \\ (n) \quad &= \frac{1}{\sin(3.86)} (\sin(16.3) \cos(255) - \sin(13.4) \cos(245) \cos(3.86)) = 0.3725 \end{aligned}$$

Substituting Line (m) and Line (n) into Line (l) and the result into Line (k) yields the desired azimuth angle:

$$\vartheta = \arccos\left(\frac{-0.08534}{\sin(14.79)}\right) = \arccos(-0.3342) = 250.47^\circ.$$

Note that two answers are possible for the azimuth angle, but only one is a reasonable choice for the problem under consideration.

The purpose of the next example is to show how to calculate the build and turn rates using the minimum-curvature method.

Example 8.25 For the directional-survey data in Example 8.24, determine the build and turn rates at the midpoint of the minimum-curvature trajectory. The reader is advised to review the Example 8.24 solution before working on the one given below.

Solution. It is known that the z -component of the unit normal vector is given (Eq. 8.111b) by the following equation:

$$(a) \quad n_z = (-\sin \varphi) \frac{d\varphi}{ds} \frac{1}{\kappa} = (-\sin \varphi) \frac{B}{\kappa}.$$

Moreover, the unit normal vector for the minimum-curvature well path (Eq. 8.130) is

$$(b) \quad \vec{n}(s) = -\vec{i}_1 \sin[\kappa(s-s_1)] + \vec{n}_1 \cos[\kappa(s-s_1)].$$

Multiplying (dot product) Line (b) by \vec{k} , the z -component of the unit normal vector is

$$(c) \quad n_z = \vec{n}(s) \cdot \vec{k} = -\vec{i}_1 \cdot \vec{k} \sin[\kappa(s-s_1)] + \vec{n}_1 \cdot \vec{k} \cos[\kappa(s-s_1)].$$

and substituting for the dot products in Line (c) yields

$$(d) \quad n_z = (-\cos \varphi) \sin[\kappa(s-s_1)] + \left[\frac{\cos \varphi_2 - \cos \varphi_1 \cos \beta}{\sin \beta} \right] \cos[\kappa(s-s_1)].$$

By comparing lines (a) and (d), the build rate at any point on the well trajectory between survey Stations 1 and 2 can be determined.

For the midpoint, it is known that

$$\varphi = 14.79^\circ$$

and

$$\kappa(s-s_1) = 1.93^\circ.$$

Consequently, from Line (d), $n_z = -0.1924$, and from Line (a), the build rate $B = 0.0291^\circ/\text{ft} = 2.91^\circ/100 \text{ ft}$.

To calculate the trajectory turn rate (walk rate), the z -component of the unit binormal vector will be needed. It is known (Eq. 8.112a) that

$$(e) \quad b_z = \frac{1}{\kappa} \sin^2 \varphi \frac{d\vartheta}{ds}.$$

For a minimum-curvature trajectory, the unit binormal vector is

$$(f) \quad \vec{b} = \vec{t}_1 \times \vec{n}_1 = \vec{t}_2 \times \vec{n}_2.$$

Substituting for \vec{n}_1 ,

$$(g) \quad \vec{b} = \frac{\vec{t}_1 \times \vec{t}_2}{\sin \beta}$$

Therefore, the z -component of the binormal unit vector is

$$(h) \quad b_z = \vec{b} \cdot \vec{k} = \frac{\sin \varphi_1 \sin \varphi_2 \sin(\vartheta_2 - \vartheta_1)}{\sin \beta}.$$

Hence, $b_z = 0.1678$, and the desired turn rate from Line (e) is

$$\frac{d\vartheta}{ds} = T = \frac{(0.1678)(0.0386)}{\sin^2(14.79)} = 0.0994^\circ/\text{ft} = 9.94^\circ/100 \text{ ft}.$$

8.4.5 Tool-Face Angle Control for a Minimum-Curvature Trajectory. As shown in Examples 8.24 and 8.25, drilling a well that follows a minimum-curvature trajectory involves continuous changes in hole inclination and azimuth angle. Such changes in general result in variable build and turn rates along the minimum-curvature path. The challenge here is to derive an equation for calculation of the instantaneous tool-face angle $\gamma(s)$ along the trajectory if the hole inclination angle $\varphi(s)$ and azimuth $\vartheta(s)$ are known.

To solve this problem, it is convenient to introduce two more unit vectors: the high-side unit vector, \vec{h} , and the right-side unit vector, \vec{v} , as shown in **Fig. 8.59**. As their names indicate, these vectors point out to the high and right sides of the wellbore.

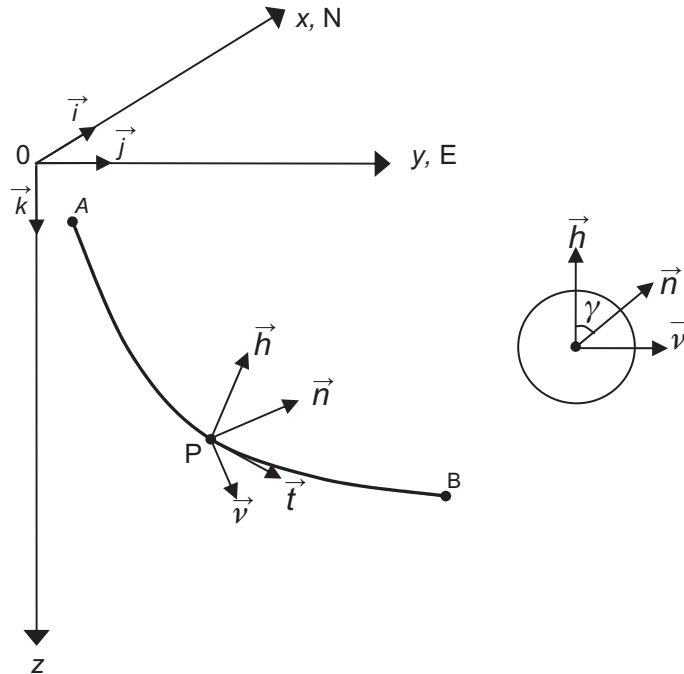


Fig. 8.59—High- and right-side vectors.

In Fig. 8.59, a 3D minimum-curvature well segment is denoted as AB, and at Point P, the unit tangent, normal, high-side, and right-side vectors are denoted as \vec{t} , \vec{n} , \vec{h} , and \vec{v} , respectively. At Point P, the hole inclination angle is φ and the azimuth is ϑ .

The high-side unit vector \vec{h} lies in a vertical plane of the well and is normal to the unit tangential vector \vec{t} ; hence, its inclination angle is $(90^\circ + \varphi)$ and its azimuth is ϑ . The right-side unit vector \vec{v} lies in a horizontal plane perpendicular to both \vec{t} and \vec{h} vectors; hence, its inclination angle is 90° and its azimuth is $(\vartheta + 90^\circ)$.

Consequently, if the unit tangent vector is known, the unit high-side and right-side vectors are

$$\vec{h} = (\cos \varphi \cos \vartheta) \vec{i} + (\cos \varphi \sin \vartheta) \vec{j} + (-\sin \varphi) \vec{k} \quad (8.137)$$

and

$$\vec{v} = (-\sin \vartheta) \vec{i} + (\cos \vartheta) \vec{j}. \quad (8.138)$$

The \vec{v} vector is perpendicular to the \vec{k} vector, and its z -component is nil. The tool-face angle γ is the angle between the unit vectors \vec{h} and \vec{n} ; hence,

$$\vec{h} \cdot \vec{n} = \cos \gamma \quad (8.139)$$

and

$$\vec{v} \cdot \vec{n} = \sin \gamma. \quad (8.140)$$

Consequently, the tool-face angle can also be calculated from the following expression:

$$\gamma = \arctan \left(\frac{\vec{v} \cdot \vec{n}}{\vec{h} \cdot \vec{n}} \right). \quad (8.141)$$

Example 8.26 Consider a segment of a minimum-curvature wellbore as described in Example 8.24. Calculate the tool-face angle γ at the midpoint with $\varphi = 14.79^\circ$ and $\vartheta = 250.47^\circ$.

Solution. Using Eq. 8.137, the components of the unit high-side vector can be calculated as

$$\vec{h}(s = 50 \text{ ft}) = (\cos(14.79) \cos(250.47)) \vec{i} + (\cos(14.79) \sin(250.47)) \vec{j} + (-\sin(14.79)) \vec{k},$$

$$(a) \quad \vec{h} = (-0.3232) \vec{i} + (-0.9112) \vec{j} + (-0.2553) \vec{k}.$$

The unit normal vector $\vec{n}(s)$ is given by Eq. 8.130 and is repeated here for the reader's convenience:

$$(b) \quad \vec{n}(s) = -\vec{t}_1 \sin[\kappa(s - s_1)] + \vec{n}_1 \cos[\kappa(s - s_1)],$$

where

$$(c) \quad \vec{n}_1 = \frac{\vec{t}_2 - \vec{t}_1 \cos \beta}{\sin \beta}.$$

It is necessary to calculate the unit vectors \vec{t}_1 and \vec{t}_2 :

$$(d) \quad \begin{aligned} \vec{t}_1 &= (\sin(13.4) \cos(245)) \vec{i} + (\sin(13.4) \sin(245)) \vec{j} + \cos(13.4) \vec{k} \\ &= (-0.0979) \vec{i} + (-0.2100) \vec{j} + (0.9728) \vec{k}, \end{aligned}$$

$$(e) \quad \begin{aligned} \vec{t}_2 &= (\sin(16.3) \cos(255)) \vec{i} + (\sin(16.3) \sin(255)) \vec{j} + \cos(16.3) \vec{k} \\ &= (-0.0726) \vec{i} + (-0.2711) \vec{j} + (0.9598) \vec{k}. \end{aligned}$$

It is known that $\cos \beta = 0.9977$; substituting Lines (d) and (e) into Line (c) yields the unit normal vector at Point 1:

$$(f) \quad \vec{n}_1 = (0.3724)\vec{i} + (-0.9150)\vec{j} + (-0.1604)\vec{k}.$$

In the present case, $\kappa(s - s_1) = 1.93^\circ$ and substituting Lines (d) and (f) into Line (b) yields the unit normal vector at the midpoint:

$$(g) \quad \vec{n}(s = 50 \text{ ft}) = (0.3755)\vec{i} + (-0.9074)\vec{j} + (-0.1922)\vec{k}.$$

Now the dot product $\vec{h} \cdot \vec{n} = 0.7545$ can be calculated and, using Eq. 8.139, the desired tool-face angle is obtained:

$$\gamma = \arccos(0.7545) = 41^\circ.$$

The deflection tool must be turned 41° to the right from the high-side angle to obtain the required hole inclination and azimuth angles. The reader is encouraged to verify the calculations using Eq. 8.140 and to write a computer program to perform the calculations after every 5 ft of drilling.

The tool-face angle can also be obtained directly from Eq. 8.111b because $n_z = -0.1924$ has already been calculated in Example 8.25. One can easily verify that by using Eq. 8.111b, the tool-face angle is calculated as 41° .

8.4.6 Review Questions and Problems.

1. Define the curvature vector and provide its geometric interpretation.
2. Define the torsion of a 3D curve and provide its geometric interpretation.
3. Explain why torsion is nil if the well path is in a 2D plane.
4. Write the Frenet-Serret equations.
5. Derive Eq. 8.109 for calculating the DL.
6. Show that the z -components of the unit normal and binormal vectors can be expressed in terms of the hole inclination angle φ and the tool-face angle γ by means of the following equations:

$$n_z = -\sin \varphi \cos \gamma,$$

$$b_z = -\sin \varphi \sin \gamma.$$

7. Show that for a minimum-curvature well trajectory with DL β , the z -components of the unit tangential, normal, and binormal vectors can be calculated from the following equations:

$$t_z = \frac{1}{\sin \beta} \left\{ \sin \left(\frac{s_2 - s_1}{\Delta s} \beta \right) \cos \varphi_1 + \sin \left(\frac{s - s_1}{\Delta s} \beta \right) \cos \varphi_2 \right\}$$

$$n_z = \frac{1}{\sin^2 \beta} \left\{ (\sin \varphi_1 \cos \varphi_2 \sin \vartheta_1 - \cos \varphi_1 \sin \varphi_2 \sin \vartheta_2) \right. \\ \left[\sin \left(\frac{s_2 - s}{\Delta s} \beta \right) \sin \varphi_1 \sin \vartheta_1 + \sin \left(\frac{s - s_1}{\Delta s} \beta \right) \sin \varphi_2 \sin \vartheta_2 \right] \\ + (\sin \varphi_1 \cos \varphi_2 \cos \vartheta_1 - \cos \varphi_1 \sin \varphi_2 \cos \vartheta_2) \\ \left. \left[\sin \left(\frac{s_2 - s}{\Delta s} \beta \right) \beta \sin \varphi_1 \cos \vartheta_1 + \sin \left(\frac{s - s_1}{\Delta s} \beta \right) \sin \varphi_2 \cos \vartheta_2 \right] \right\}$$

$$b_z = [\sin \varphi_1 \sin \varphi_2 \sin(\vartheta_2 - \vartheta_1)],$$

where φ_1, ϑ_1 and φ_2, ϑ_2 are the inclination and azimuth angles at the beginning and end points of the wellbore segment; s_1 and s_2 are the MDs at the beginning and end points, $\Delta s = s_2 - s_1$; and s is the MD at any arbitrary point between the limiting points.

8. Calculate the wellbore torsion for a point on a well trajectory with given DLS = 12°/ft and B = 10.6°/ft at hole inclination angles of $\phi = 58.2^\circ$ and $\phi = 86.7^\circ$.
9. Is it true that using the AAM for evaluating directional surveys will result in a wellbore composed of a number of straight segments?
10. For the data in Example 8.23, calculate the trajectory coordinates using the RCM.
11. The following information is available along the well path:

Point	MD, ft	Hole Inclination Angle, degrees	Direction
1	3,424	26.5	N50W
2	3,517	26.75	N48W
3	3,640	27.0	N46W
4	3,734	26.75	N43W
5	3,829	27.5	N41W

The rectangular coordinates at Point 1 are $x = 257.9$ ft, $y = -266.4$ ft, $z = 3368$ ft. Determine the x, y, z coordinates for Points 2 through 5 using the minimum-curvature equations.

12. Consider two points on a well-path segment with the following hole inclination angles and azimuths:

Point	Inclination Angle, degrees	Azimuth Angle, degrees
1	$\phi = 45.9$	$\vartheta = 7.59$
2	$\phi = 50.0$	$\vartheta = 39.8$

The distance between two points as measured along the well path is $\Delta s = 801$ ft. Calculate the hole inclination and azimuth angles at the distance of 202.5 ft and 607.5 ft from the first point, assuming the following:

- (a) minimum-curvature trajectory
- (b) constant curvature and build rate trajectory
13. Wellbore data as in Problem 12. Calculate the build and turn rates at the midpoint, assuming a minimum-curvature trajectory.
14. Data as in Problem 12. Formulate the high-side and right-side unit vectors and calculate the tool-face angle at the midpoint.

8.5 Torque-and-Drag Modeling and Calculations for 2D Well Profiles

In this section, equations are provided for calculating the tension (compression) along a length of drillstring or casing being slowly pulled from or lowered into a directional well. The well path is assumed to be 2D and confined to a vertical plane. Allowance is made for the distributed pipe weight, friction, and hole curvature. On the other hand, the pipe bending stiffness and couplings are not taken into account. In other words, for the sake of simplicity, the string is treated as a continuous flexible cable or rope.

8.5.1 Introduction. For effective drilling, it is necessary to apply a force to the drill bit and to rotate it to obtain the desired rate of drilling. In conventional rotary drilling, the force on the drill bit is achieved by slacking off a part of the weight of the BHA, and the bit rotation is accomplished either by rotating the entire drillstring or by means of a downhole motor. Frequently, even if a downhole motor is used, the drillstring is also rotated to increase the rate of drilling and to improve transport of cuttings from the drill bit to the top of the hole.

In the ideal case of vertical drilling, the hook load (weight indicator at the surface) is attributable to the weight of the drillstring (drillpipe, BHA, and other components) in drilling fluid, reduced by the weight of the portion that is slacked off on the drill bit, which is usually simply called the WOB, that is

$$F_h = W_{dp} + W_{BHA} - \text{WOB}, \dots \dots \dots (8.142)$$

where W_{dp} = weight of drillpipe in drilling fluid, W_{BHA} = weight of BHA (drill collars, downhole motor, MWD unit, stabilizers) in drilling fluid, and WOB = weight on bit.

Usually, the pipe weight in drilling fluid is called the effective weight or *buoyant weight*. For the sake of simplicity, dynamic forces due to acceleration are disregarded in the torque-and-drag analysis.

If the well deviates from the vertical, the drillstring will be in partial contact with the wall of the wellbore, and so-called drag forces will develop due to friction between the contacting surfaces. Because drag forces always oppose the direction of motion, the hook load is at its highest during tripping-out operations. The difference in hook loads during tripping into and tripping out of the well is a very good indicator of the magnitude of the down-hole friction forces. In a good-quality vertical wellbore, the difference in hook loads during tripping-in and tripping-out operations is expected to be small.

The torque (moment) required to rotate the drillstring consists of three major components: torque required for rotating the drill bit, torque for rotating the drillstring to overcome viscous drag due to drilling fluid, and torque due to the contact forces between the drillstring and the wellbore. This can be expressed as

$$M_t = M_{db} + M_{vd} + M_{cd}, \quad \dots \dots \dots (8.143)$$

where M_{db} = torque required to rotate the drill bit, M_{vd} = torque to overcome viscous drag, and M_{cd} = torque to overcome drag resulting from contact forces.

In a good-quality vertical hole, the total torque is controlled by the first two components in Eq. 8.143. In directional drilling and particularly in horizontal wells and ERWs, the third component is dominant and is of great concern for well designers.

Accurate predictions of the forces and torques required for drilling and casing-running operations are very important for calculation of the horsepower needed for drilling (e.g., the selection of rig hoisting and rotary equipment), for evaluation of the mechanical integrity of drillstring and casing components, and for prediction of difficulties with casing running, wellbore stability, and control of penetration rate.

During drilling, the torques and forces are measured at the top of the hole and frequently above the drill bit. These measurements are carried out and recorded in real time and are very useful for detecting potential hole problems such as poor hole cleaning, differential pipe sticking, and hole spiraling. Any significant deviations of the actual measured values from those obtained from well-planning calculations are early indicators of poor hole quality. A good-quality wellbore should be smooth, in gauge, and free of local DLs. Benefits include trouble-free drillstring and casing tripping, logging, and cementing operations.

8.5.2 Axial Drag-Force Calculations. *Straight Inclined Wellbore.* To explain the concept of axial drag, let us consider a smooth pipe (no tool joints) with a unit weight in fluid of w_{bp} in a straight but inclined wellbore with inclination angle ϕ , as shown in Fig. 8.60a. The pipe is pulled out slowly, so acceleration effects can be ignored. The force at the bottom of the pipe is given and equal to F_1 . The task at hand is to calculate the magnitude of the pulling force F_2 at a distance L from the lower end.

To generalize, let us consider the static equilibrium of a small (differential) pipe element with a length of ds and a weight in fluid of $w_{bp} ds$. In other words, the pressure forces attributable to the drilling fluid are not shown on the

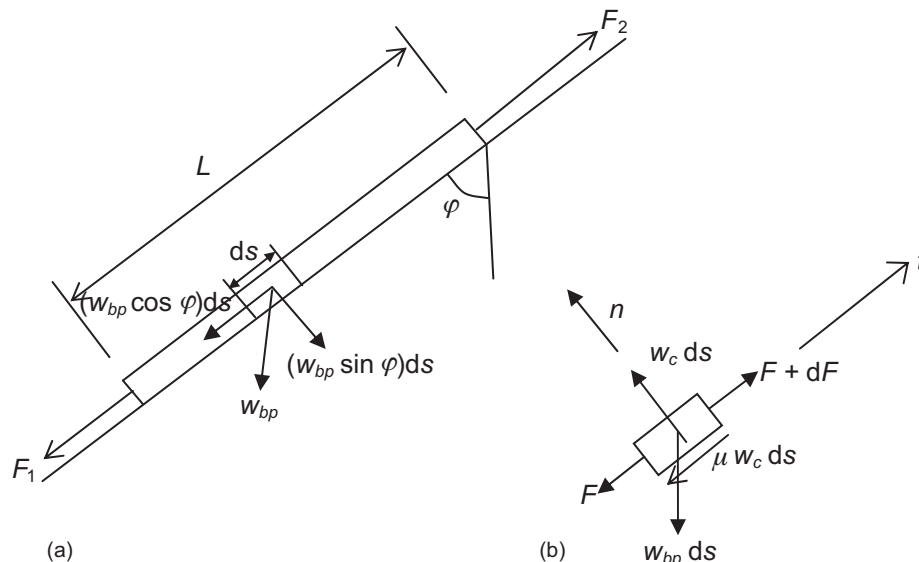


Fig. 8.60—(a) Pipe with length L in a straight inclined hole; (b) free-body diagram for pipe in a straight inclined hole.

free-body diagram (FBD), but their effect results in a pipe unit effective (buoyant pipe) weight w_{bp} . An FBD for this element is shown in Fig. 8.60b. It is convenient to use a t - n coordinate system as shown in Fig. 8.60b, with the positive t acting up the wellbore.

Let F be the tension at the lower end of the differential pipe element and $F+dF$ the tension at the upper end. The force F is also called the *axial effective force*. Let $w_c ds$ and $\mu w_c ds$ be the normal and tangential reactions of the wall of the hole on the differential element of pipe, where. The sliding friction force is pointing downward because the motion is assumed to be upward. Note that the shear forces are not shown on the FBD because they are nil for a straight pipe.

Equilibrium of forces in the normal (perpendicular to the pipe axis) and tangential (parallel to the pipe axis) directions gives the following:

In the normal direction:

$$w_c - (w_{bp}) \sin \varphi = 0. \quad (8.144)$$

In the tangential direction:

$$(F + dF) - F - (w_{bp} ds) \cos \varphi - \mu w_c ds = 0. \quad (8.145)$$

Substituting Eq. 8.144 into Eq. 8.145 yields

$$dF = \mu (w_{bp} \sin \varphi) ds + (w_{bp} \cos \varphi) ds. \quad (8.146)$$

Integrating Eq. 8.146 gives the force at the upper end of the pipe:

$$F_2 = F_1 + \mu (w_{bp} \sin \varphi) L + (w_{bp} \cos \varphi) L. \quad (8.147)$$

Clearly, the axial force F_2 is composed of three terms that represent the force applied at the pipe bottom (e.g., the weight of pipe suspended below the cross section under consideration), the friction force component $[\mu (w_{bp} \sin \varphi) L]$, and the weight of the unsupported part of the string $[(w_{bp} \cos \varphi) L]$. If the pipe is lowered down (tripping in the hole), the sign of the friction component needs to be changed because friction force always opposes motion. Hence,

$$F_2 = F_1 - \mu (w_{bp} \sin \varphi) L + (w_{bp} \cos \varphi) L. \quad (8.148)$$

For example, if the hole inclination angle is 45° , the effective pipe unit weight is 16 lbf/ft, the length of the segment is 300 ft, the coefficient of sliding friction is 0.3, and the force at the lower end is 10,000 lbf, the force at the top of the segment is 14,412 lbf for tripping out and 12,376 lbf for tripping into the wellbore.

Examination of Eq. 8.148 tells us that the force F_2 may be positive (tension), zero, or negative (compression). If the force F_2 is negative, this indicates that the weight of the pipe is not sufficient to move it down. In other words, a negative force indicates that pushing (compression) must be applied to the pipe at the top to slide it into the hole. Application of a pushing force is frequently required in highly inclined wells and is always needed in a horizontal well. If the compressive force is high enough, the string buckles into a 3D snake shape. This is called lateral, snaky, or sinusoidal buckling. Eventually the pipe may even assume a helical shape if the force is large enough, which is called helical buckling.

During drilling operations, the friction coefficient μ in Eqs. 8.147 and 8.148 is determined under actual borehole conditions to match the measured forces at the top of the hole. Consequently, it also includes the effects of poor hole cleaning (cuttings buildup in horizontal and highly inclined parts of the wellbore), tight hole conditions, differential pipe sticking, washouts, keysets, and local wellbore irregularities. Therefore, this quantity is sometimes called the *wellbore friction factor* rather than the friction coefficient. To match the hook loads for tripping into and out of the hole, two different values of wellbore friction factor must sometimes be used. If the wellbore is clean and free of other problems, the sliding friction is the main factor affecting drag forces and torque and is not dependent on the direction of pipe motion.

Typically, well designers assume a sliding friction coefficient between 0.2 and 0.4 (depending mostly on the type of rock and drilling fluids) at the planning stage of well development. However, friction factors of up to 0.8 have been reported in the literature.

Table 8.4 gives friction factors for drilling and casing-running operations in three different regions and using two different drilling-fluid systems.

TABLE 8.4—FRICTION FACTORS FOR DRILLING AND CASING-RUNNING OPERATIONS
(Mason et al. 1999)

Region	Drilling-Fluid System	Drilling 12¼-in. Open Hole	9⅝-in. Casing-Running Open Hole
North Sea	Oil-based	0.10–0.20	0.25–0.40
Caspian Sea	Oil-based	0.20–0.30	0.30–0.50
Alaska	Water-based	0.15–0.25	0.30–0.40

The friction-coefficient values given in Table 8.4 are for a moving drillstring and represent the so-called *dynamic coefficient of friction*. The *static coefficient of friction* is somewhat greater. In other words, a greater force is required to initiate string motion than to keep a string in motion. The difference in the static and dynamic coefficients of friction and the presence of drillstring elasticity result in a slip-stick type of motion that is particularly apparent when the string is being pushed down the hole. This slip-stick motion causes dynamic loading of drillstring components that may be detrimental to the drillbit and to the downhole motor. Uneven loading of the drill bit also causes changes in the deflection tool-face setting that must be frequently corrected to drill the desired well trajectory. Because of the elasticity of the drillstring, some portion of the friction force may be trapped and eventually released, resulting in unexpected string movement.

Over the years, a number of techniques have been developed to reduce longitudinal (sliding) drag. These include various lubricants added to the drilling fluid, rollers, vibrations (hydraulic and mechanical), and special procedures that involve turning the pipe to the right and then to the left through an angle that is sufficiently large to break down most of the axial friction without affecting the orientation of a bent housing or sub that is used for deviation control (Maidla and Hacı 2004).

If the pipe is rotated during tripping operations, the friction is absorbed by the torque, and for the purpose of force calculations, it can be assumed that the sliding friction coefficient is nil. Such an approach is justified because the axial velocity component during drilling is much less than that due to pipe rotation. For practical calculations, the usual approach is still to use Eqs. 8.146 and 8.147 and to set the friction coefficient to zero.

Curved Wellbore of Constant Curvature. In a manner similar to that for a straight inclined well, let us now consider a smooth pipe (free of couplings) in the curved part of a wellbore. For the sake of simplicity, only wellbore segments with constant curvature will be considered here. The case where hole inclination angle decreases with depth will be analyzed first, followed by that where the hole angle increases with depth. It is assumed that the well path lies in a vertical plane, and therefore gravity is acting downward. In other words, the well trajectory is two-dimensional and confined to a vertical plane.

For the sake of simplicity, it is assumed that the pipe has no bending stiffness; it behaves like a flexible cable or rope. At first, this may look like an unrealistic assumption, but field practice indicates that the results obtained using this approach are acceptable for many practical applications. This approach is called a *soft-string model* as opposed to a *stiff-string model* that accounts for pipe bending stiffness.

Drop-Off Bend. First, let us consider the case where the hole inclination angle decreases with depth (a drop-off bend) and the pipe slides on the lower side of the hole.

Fig. 8.61 shows a segment of wellbore with radius R , inclination angle φ , and increase in inclination $d\varphi$. In a similar manner as for the straight inclined wellbore, let F represent the tension at the lower end of the differential pipe element with length ds , and let $F+dF$ represent the tension at the upper end. Let dN and μdN represent the normal (radial) and tangential reactions of the wall of the hole acting on the pipe element. In addition to the forces $F+dF$, F , $w_c R d\varphi$, and $\mu w_c R d\varphi$, the pipe element is subjected to its weight $w_{bp} R d\varphi$, as shown in Fig. 8.61.

Equilibrium of forces in the normal (radial) direction gives

$$w_c R d\varphi - (F + dF) \cos\left(\frac{\pi}{2} - \frac{d\varphi}{2}\right) - F \cos\left(\frac{\pi}{2} - \frac{d\varphi}{2}\right) - (w_{bp} R d\varphi) \cos\left(\frac{\pi}{2} - \varphi\right) = 0. \quad (8.149)$$

The shearing forces are not shown in the FBD because the pipe is assumed to behave as a rope (no bending stiffness).

Assuming $\sin \frac{d\varphi}{2} = \frac{d\varphi}{2}$ and ignoring the higher-order terms such as $\left(dF \frac{d\varphi}{2}\right)$,

$$w_c R d\varphi = F d\varphi + (w_{bp} R d\varphi) \sin \varphi, \quad (8.150)$$

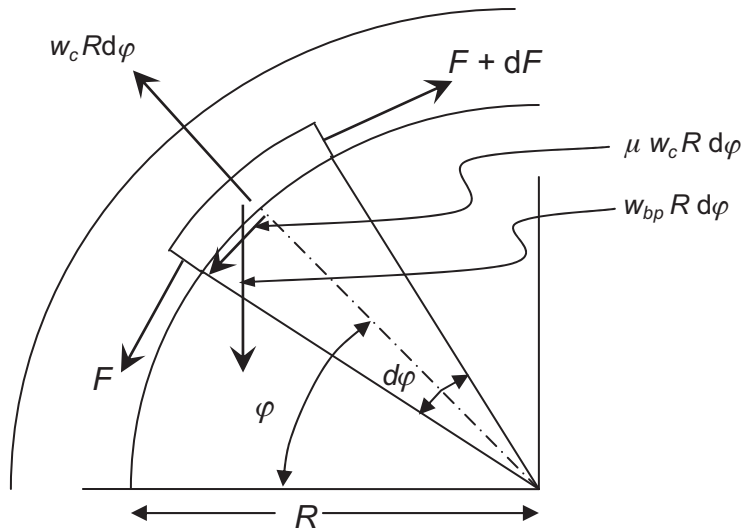


Fig. 8.61—Free-body diagram for a small pipe element in a drop-off bend.

and dividing Eq. 8.150 by $d\varphi$,

$$Rw_c = F + w_{bp} R \sin \varphi, \quad \dots \dots \dots (8.151)$$

or

$$w_c = \frac{F}{R} + w_{bp} \sin \varphi. \quad \dots \dots \dots (8.152)$$

Eq. 8.152 represents the contact force per unit length of pipe w_c . This force consists of two components: the first component, F/R , is due to the pipe force F and the wellbore curvature $\kappa = \frac{1}{R}$, and the second is due to the pipe effective unit weight w_{bp} . Note that even if the pipe unit effective weight w_{bp} is nil (for example, if buoyancy effects counteract the pipe weight), the unit contact force is not nil, but depends on the magnitude of the force F and the wellbore curvature κ . The product κF is called the *capstan force*. It should also be noted that if the pipe is in compression, the first term becomes negative (the direction of the pipe force F is changed), which in turn results in a decrease in the contact force w_c . Eventually, if the contact force is small enough, the pipe can buckle, and then the model described above is no longer valid. This issue is discussed later in this chapter.

Static equilibrium of forces in the tangential direction gives

$$(F + dF) \cos \frac{\varphi}{2} - F \cos \frac{\varphi}{2} - (w_{bp} R d\varphi) \cos \varphi - \mu w_c R d\varphi = 0. \quad \dots \dots \dots (8.153)$$

Assuming $\cos \frac{d\varphi}{2} = 1$,

$$dF = \mu w_c R d\varphi + (w_{bp} R d\varphi) \cos \varphi. \quad \dots \dots \dots (8.154)$$

Substituting Eq. 8.150 into Eq. 8.154 and performing certain rearrangements yields

$$\frac{dF}{d\varphi} - \mu F = \mu w_{bp} R \sin \varphi + w_{bp} R \cos \varphi. \quad \dots \dots \dots (8.155)$$

Solution of Eq. 8.155 gives the desired pipe force F as a function of the hole inclination angle φ :

$$F(\varphi) = (w_{bp} R) \left[\frac{1 - \mu^2}{1 + \mu^2} \sin \varphi - \frac{2\mu}{1 + \mu^2} \cos \varphi \right] + C e^{\mu\varphi}, \quad \dots \dots \dots (8.156)$$

where C is a constant of integration that needs to be determined from the boundary condition at the lower or upper end of the string.

It is useful to note that if the pipe is not sliding (the static case), the dynamic friction force is zero, and Eq. 8.156 reduces to

$$F = w_{bp} R \sin \varphi + C. \quad (8.157)$$

Eq. 8.157 can also be used for calculation of forces if the pipe is rotating. Pipe rotation results in a decrease in the pulling force because the axial drag is absorbed by the rotary torque. It should be remembered, however, that pipe rotation always contributes to pipe fatigue and may lead to drillstring fatigue failures as well as local pipe overheating.

Buildup Bend. If the hole inclination angle is increasing with depth (a buildup bend), two cases must be distinguished depending on the magnitude of the tension in the pipe: the so-called high-tension (Case a) and low-tension (Case b) cases.

Case a (High Tension). If the tension is high enough, the pipe will touch the high side of the wellbore, as shown in Fig. 8.62. For this case, the pulling force F is decreasing while the overall inclination angle φ is increasing. This may lead to some confusion in the derivations. For this reason, it is convenient to consider instead the angle $\beta = \frac{\pi}{2} - \varphi$, which increases as tension increases.

Following similar reasoning as in the case of decreasing hole inclination angle (equilibrium of forces in the radial and tangential directions),

$$w_c R = F - w_{bp} R \cos \beta \quad (8.158)$$

and

$$\frac{dF}{d\beta} - \mu F = w_{bp} R (\sin \beta - \mu \cos \beta). \quad (8.159)$$

Solving Eq. 8.159 and substituting for $\beta = \frac{\pi}{2} - \varphi$, it is possible to obtain the pipe force F as a function of the hole inclination angle φ :

$$F(\varphi) = -\left(w_{bp} R\right) \left[\frac{1-\mu^2}{1+\mu^2} \sin \varphi - \frac{2\mu}{1+\mu^2} \cos \varphi \right] + C e^{\mu \left(\frac{\pi}{2} - \varphi \right)}. \quad (8.160)$$

Eq. 8.160 is valid if the pipe is in contact with the high side of the hole, which requires that the pipe tension satisfy the condition $F \geq w_{bp} R \sin \varphi$.

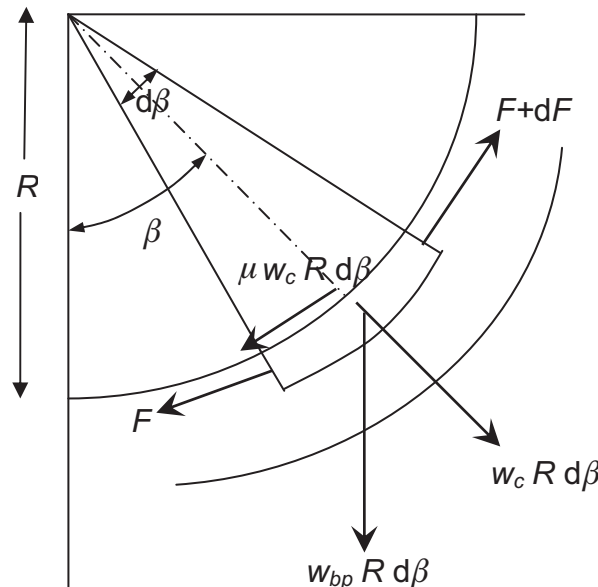


Fig. 8.62—Free-body diagram for a small pipe element in a buildup bend—"high-tension" case.

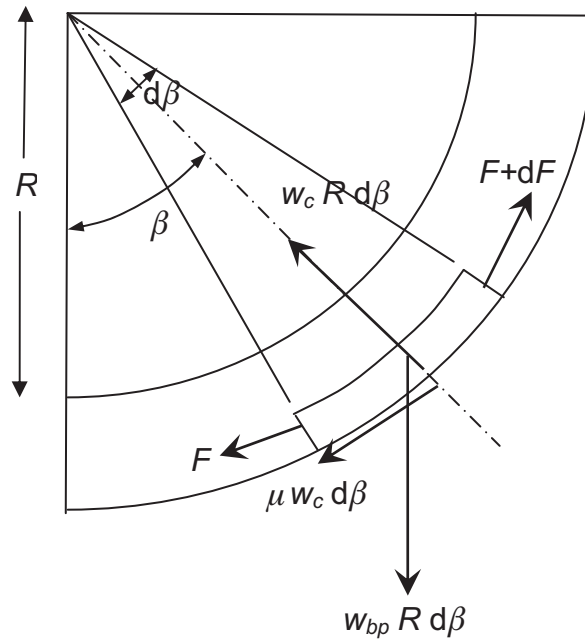


Fig. 8.63—Free-body diagram for a “low-tension” case.

Case b (Low Tension). For the low-tension case ($F \leq w_{bp} R \sin \varphi$), the pipe slides on the lower side of the hole, as shown schematically in Fig. 8.63.

In a manner similar to that for Case a, projecting the forces in the tangential and normal directions, the following equations are obtained:

$$w_c R = w_{bp} R \cos \beta - F \quad \dots \quad (8.161)$$

and

$$\frac{dF}{d\beta} + \mu F = w_{bp} R (\sin \beta + \mu \cos \beta). \quad \dots \quad (8.162)$$

Solving Eq. 8.162 and substituting for $\beta = \frac{\pi}{2} - \varphi$ yields

$$F(\varphi) = \left(w_{bp} R \right) \left[\frac{1 - \mu^2}{1 + \mu^2} \sin \varphi + \frac{2\mu}{1 + \mu^2} \cos \varphi \right] + C \exp \left[-\mu \left(\frac{\pi}{2} - \varphi \right) \right] \quad \dots \quad (8.163)$$

It is important to recall that Eq. 8.163 is valid on condition that $F \leq w_{bp} R \sin \varphi$.

It is self-evident that the string lies on the lower side of the wellbore (due to the effect of gravity) if the pipe is in compression rather than tension. It must be well understood that the equations derived above are valid for a soft-string model and that their practical application will require determination of the constant of integration C from the boundary conditions.

Sometimes well designers use segments with variable rather than constant curvature (parts of a parabola, ellipse, or catenary). A catenary describes the shape of a hanging cable (belt) between two points of suspension.

Example 8.27 Consider a 5-in. drillpipe with a buoyant weight of 20.15 lbf/ft in a wellbore, as shown schematically in Fig. 8.64. It is known that a BHA with a weight of 20,000 lbf is suspended below the drop-off section of the well; the friction coefficient is 0.2. The S-type well trajectory parameters are as follows: KOP is at 1,100 ft; the radius of the buildup section is 558 ft; the length of the buildup section is 439 ft; the tangent length (sail length) is 4,292 ft; the inclination angle for the tangent section is 45° ; the radius of the drop-off section is 558 ft; and the drop-off length is 439 ft.

Calculate the axial force in a drillpipe at Point 4, Point 3, Point 2 and Point 1 on the well trajectory for the following three cases:

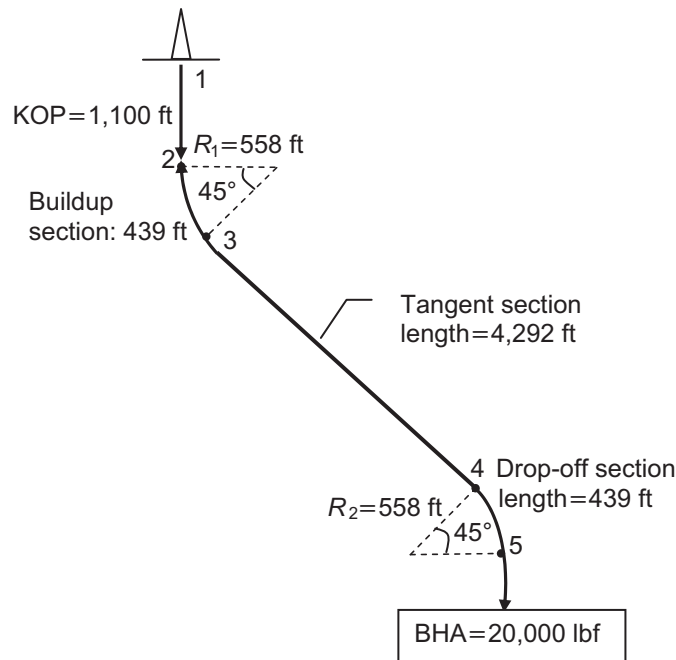


Fig. 8.64—S-type well trajectory for Example 8.27 (drillpipe size = 5 in., unit buoyant weight = 20.15 lbf/ft, friction coefficient = 0.2).

1. Static (frictionless) conditions (assume that the pipe is not moving, set $\mu = 0$)
2. Tripping out of the hole
3. Tripping into the hole

Solution. *Case 1 (Static Conditions).* Assume that the coefficient of friction $\mu = 0$. To obtain the axial force at Point 4, set $\mu = 0$ in Eq. 8.156, which yields

$$F_4 = w_{bp} R \sin \varphi + C.$$

At Point 5, the hole inclination angle $\varphi = 0^\circ$ and $F_h = 20,000$ lbf; hence, the constant $C = 20,000$ lbf, and consequently, the force at Point 4 is

$$F_4 = 20,000 + (20.15)(558) \sin(45^\circ) = 27,950 \text{ lbf.}$$

To calculate the force at Point 3, Eq. 8.147 can be used, setting F_2 (the force at the lower end) equal to the force calculated at Point 4:

$$F_3 = 27,950 + (20.15)(\cos 45^\circ)(4,292) = 89,100 \text{ lbf.}$$

To calculate the force at Point 2, use Eq. 8.160 with $\mu = 0$:

$$F_2 = -w_e R \sin \varphi + C.$$

Because at $\varphi = 45^\circ$, $F = 89,100$ lbf, the constant C is

$$C = 89,100 + (20.15)(\sin 45^\circ)(558) = 97,053 \text{ lbf.}$$

Consequently, at $\varphi = 0$ (Point 2),

$$F_2 = 97,053 \text{ lbf.}$$

At Point 1 (top of the hole),

$$F_1 = 97,053 + (20.15)(1100) = 119,220 \text{ lbf.}$$

Case 2 (Tripping Out of the Hole). To calculate the force F_4 at the top of the drop-off section (Point 4), Eq. 8.156 is used. Because at Point 5 ($\phi = 0$), $F_5 = 20,000$ lbf, the constant C can be calculated as

$$C = 20,000 + \frac{2(0.2)}{1 + (0.2)^2} (20.15)(558) = 24,324 \text{ lbf.}$$

Hence, at Point 4 ($\phi = 45^\circ$),

$$F_4 = (20.15)(558) \left[\frac{1 - 0.2^2}{1 + 0.2^2} \sin 45 - \frac{2(0.2)}{1 + 0.2^2} \cos 45 \right] + (24,324)e^{0.2 \frac{\pi}{4}} = 32,740 \text{ lbf.}$$

Using Eq. 8.147, the force at the bottom of the build section can be calculated as

$$F_3 = 32,740 + (20.15)(4,292)(0.2 \sin 45 + \cos 45) = 106,124 \text{ lbf.}$$

To obtain F_2 at the top of the build section (Point 2), Eq. 8.160 is used. Because the force at the bottom of this section is already known, the constant C can be determined as

$$106,124 = -(20.15)(558) \left[\frac{1 - 0.2^2}{1 + 0.2^2} \sin 45 - \frac{2(0.2)}{1 + 0.2^2} \cos 45 \right] + Ce^{0.2 \left(\frac{\pi}{2} - \frac{\pi}{4} \right)}.$$

Solving for C , the result is $C = 99,524$ lbf.

Therefore, at Point 2 ($\phi = 0$),

$$F_2 = -20.15(558) \left(-\frac{2 - (0.2)}{1 + 0.2^2} \right) + (99,524)e^{0.2 \frac{\pi}{2}} = 132,000 \text{ lbf,}$$

and finally, at the top of the hole,

$$F_1 = 132,000 + (20.15)(1,100) = 154,165 \text{ lbf.}$$

Case 3 (Tripping Into the Hole). To calculate force F_4 , Eq. 8.156 will be used, but with a negative sign for the friction coefficient μ . Because ϕ equals 0° , F_4 equals 20,000 lbf, $C = 15,675$, then at ϕ equal 45° (Point 4):

$$F_4 = (20.15)(558) \left(\frac{1 - 0.2^2}{1 + 0.2^2} \sin 45 + \frac{2(0.2)}{1 + 0.2^2} \cos 45 \right) + (15,675)e^{-0.2 \frac{\pi}{4}} = 23,795 \text{ lbf.}$$

In a similar manner, it is possible to calculate the forces at Points 3, 2, and 1.

The final results for all three cases are given in **Table 8.5**. The magnitude of the effective axial forces along the string is shown in **Fig. 8.65**. The difference between the loads during tripping out and tripping in is due to the direction of the friction force, which always opposes the direction of motion. It is also interesting to note that the static forces are not the average values of the tripping forces.

Once the effective axial force has been calculated, it is possible to calculate the contact force between the pipe (including tool joints or casing couplings) and the wellbore. The unit contact force in the middle of the buildup portion of an S-shaped well (shown in Fig. 8.64) can be calculated using Eq. 8.158. The effective axial force (tripping out) at this point is approximately 130,500 lbf, and the contact force per unit length is approximately 230 lbf/ft. If the spacing between tool joints is 30 ft, the force at each tool joint is approximately 3,450 lbf. The distribution of unit contact forces along the string is shown in **Fig. 8.66**.

In the next step, the designer needs to assess the possible damage to the tool joint, casing, and wellbore. High contact forces can cause grooves in casing or key-seats in the uncased part of the wellbore and serious wear on

TABLE 8.5—AXIAL FORCES ON THE WELL TRAJECTORY; EXAMPLE 8.27

Static Loads (lbf)	Tripping Out (lbf)	Tripping In (lbf)
$F_4 = 27,950$	32,740	23,795
$F_3 = 89,100$	106,124	72,720
$F_2 = 97,053$	132,000	70,084
$F_1 = 119,220$	154,165	92,249

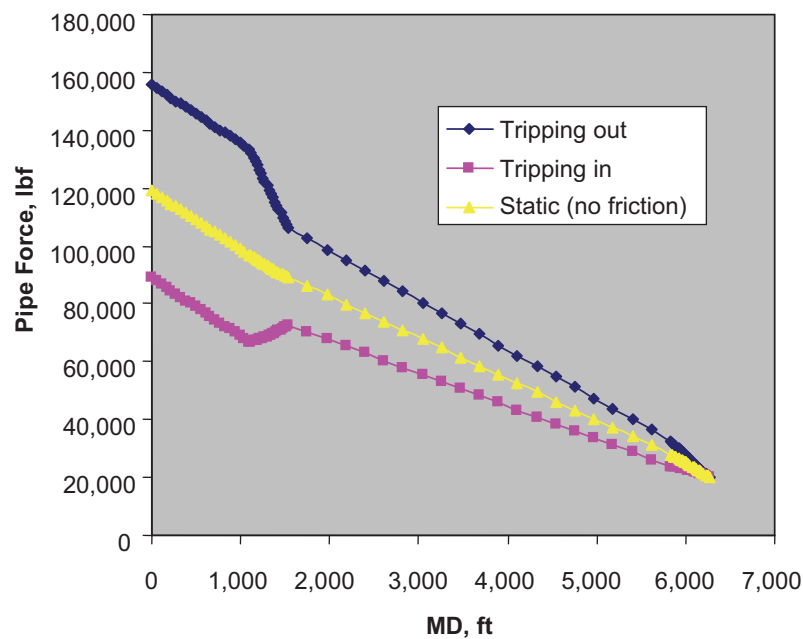


Fig 8.65—Pipe effective force vs. MD, Example 8.27.

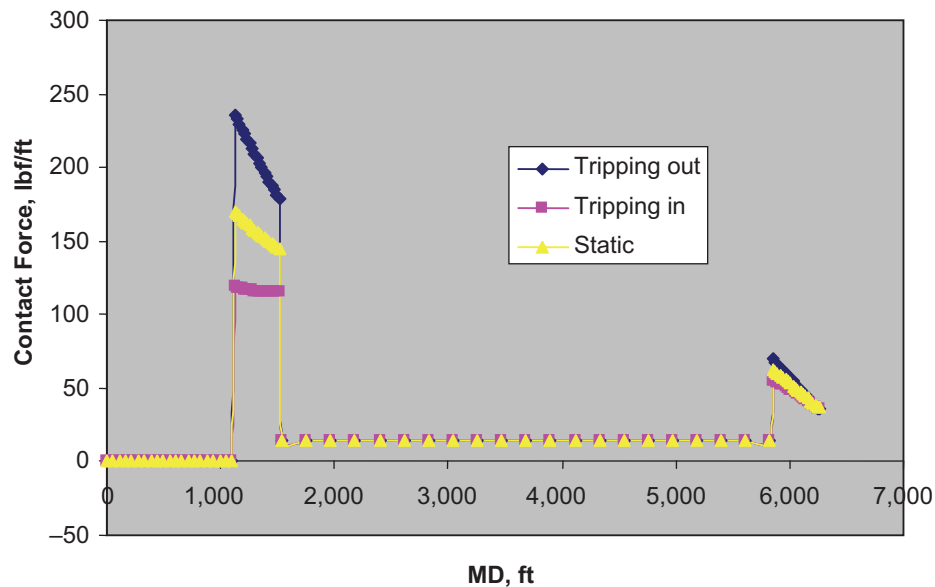


Fig 8.66—Unit contact force vs. MD, Example 8.27.

tool joints. Grooves in a casing reduce its collapse, burst, and tension resistance, and if the groove penetrates through the wall of the casing, it can cause casing failure and possibly fluid leaks into the annular space behind the casing. If the pipe is rotating, a high contact force may result in local pipe overheating, which is detrimental to pipe strength and to the stability of the drilling fluid.

It is difficult to determine maximum acceptable values for contact forces because these depend on formation strength and abrasiveness, casing quality, type of drilling fluid, and many other factors. It is recommended that the force at tool joints should not exceed 2,000 lbf, but forces in the 5,000- to 6,000-lbf range have been reported in some cases.

Example 8.28 Consider three well profiles, each consisting of a vertical part, a buildup segment, and a horizontal section, as shown in Fig. 8.67. The KOPs are at the depths of 3,000, 3,500, and 3,750 ft. The buildup

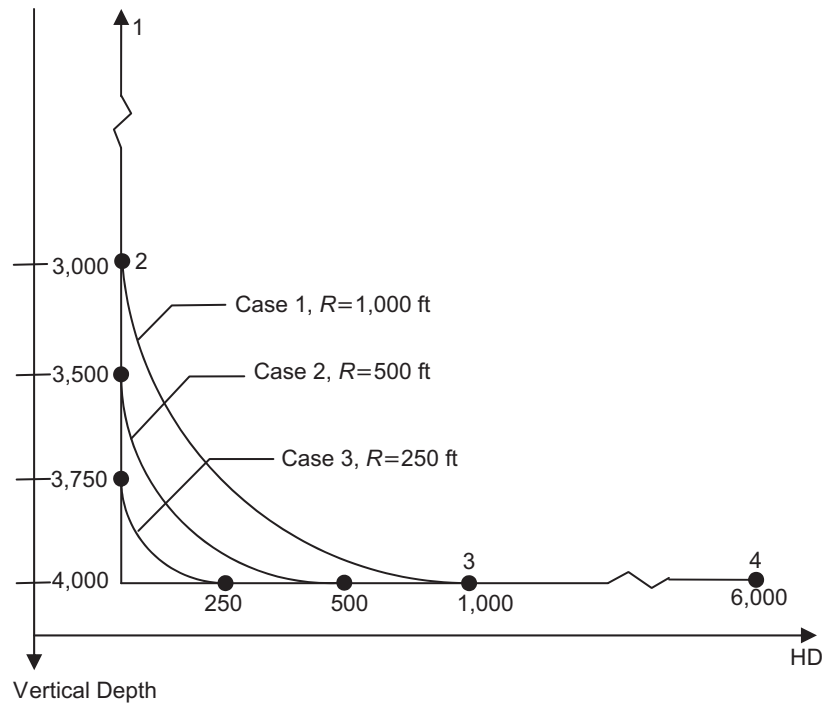


Fig. 8.67—Well profiles for Example 8.28.

rates are $5.73^\circ/100$ ft (long radius), $11.46^\circ/100$ ft (medium radius), and $22.92^\circ/100$ ft (short radius), and the corresponding lengths of the horizontal sections are 5,000, 5,500, and 5,750 ft. Calculate the axial forces during tripping-out and tripping-in operations, assuming a pipe unit weight in fluid of 15 lbf/ft and a coefficient of friction $\mu = 0.3$.

Solution. Let us first consider a long-radius horizontal-well profile (Case 1), in which the pipe is being tripped out of the hole. Using Eq. 8.147, the axial force can be calculated at any distance from the bottom of the horizontal well. Hence, at the end of the buildup section, the force is:

$$F = (0.3)(15.0)(\sin 90)(5000) = 22,500 \text{ lbf.}$$

Because this force is greater than $(15)(1,000)\sin 90 = 15,000$ lbf, this is a “high-tension” case, and Eq. 8.160 must be used to calculate the force while tripping out of the hole.

First, the value of the constant C must be calculated as

$$C = 22,500 + (15)(1,000) \left[\frac{1-0.3^2}{1+0.3^2} (\sin 90) + \frac{2(0.3)}{1+(0.3)^2} (\cos 90) \right] = 35,023 \text{ lbf.}$$

Now Eq. 8.160 is used again to calculate the force at the beginning of the buildup section ($\varphi = 0^\circ$):

$$F = -(15)(1,000) \left[-\frac{2(0.3)}{1+(0.3)^2} \right] + (35,023) e^{0.3 \left(\frac{\pi}{2} - 0 \right)} = 47,836 \text{ lbf.}$$

Hence, the force at the top of the hole is

$$F = 64,350 + (15)(3,000) = 92,836 \text{ lbf.}$$

For tripping in the hole, Eq. 8.148 is used to calculate the force at the end of the buildup segment:

$$F = -(0.3)(15)\sin 90(5,000) = -22,500 \text{ lbf.}$$

A negative sign indicates that a compressive force is needed to push the pipe into the horizontal section of the wellbore.

While tripping in the hole, $F < \omega_{bp} R \sin \phi$ (meaning that the string is sliding on the low side), and Eq. 8.163 is used to calculate the force. Again, the value of C must be calculated as

$$C = -22,500 + (15)(1,000) \left(\frac{1 - 0.3^2}{1 + 0.3^2} \sin 90 \right) = -9,977 \text{ lbf.}$$

Now the force at the top of the buildup segment ($\phi = 0^\circ$) can be calculated

$$F = (15)(1,000) \left(\frac{-2(0.3)}{1 + 0.3^2} \right) + (-9,977) e^{+0.3 \frac{\pi}{2}} = -24,235 \text{ lbf.}$$

Consequently, at the top of the hole, the force is

$$F = -24,235 + (15)(3,000) = 20,764 \text{ lbf.}$$

Axial force profiles along the MD are shown in **Figs. 8.68 through 8.70**.

As expected, in all three cases, the string is under tension while tripping out and partially under tension and partly in compression while tripping in the hole. In the case where the axial friction coefficient is set to zero (the static or frictionless case), the force in the pipe is nil over the horizontal part of the wellbore. In all cases, the static forces are the same because the vertical depth of the hole is 4,000 ft in each case. The difference between the axial force while sliding out or in the hole and the static force is called the *drag force*. According to this model, there is no drag in the vertical part of the wellbore, and consequently the greatest drag force occurs at the top of the buildup section. Another interesting observation is that friction effects are more noticeable for tripping-out than for tripping-in operations.

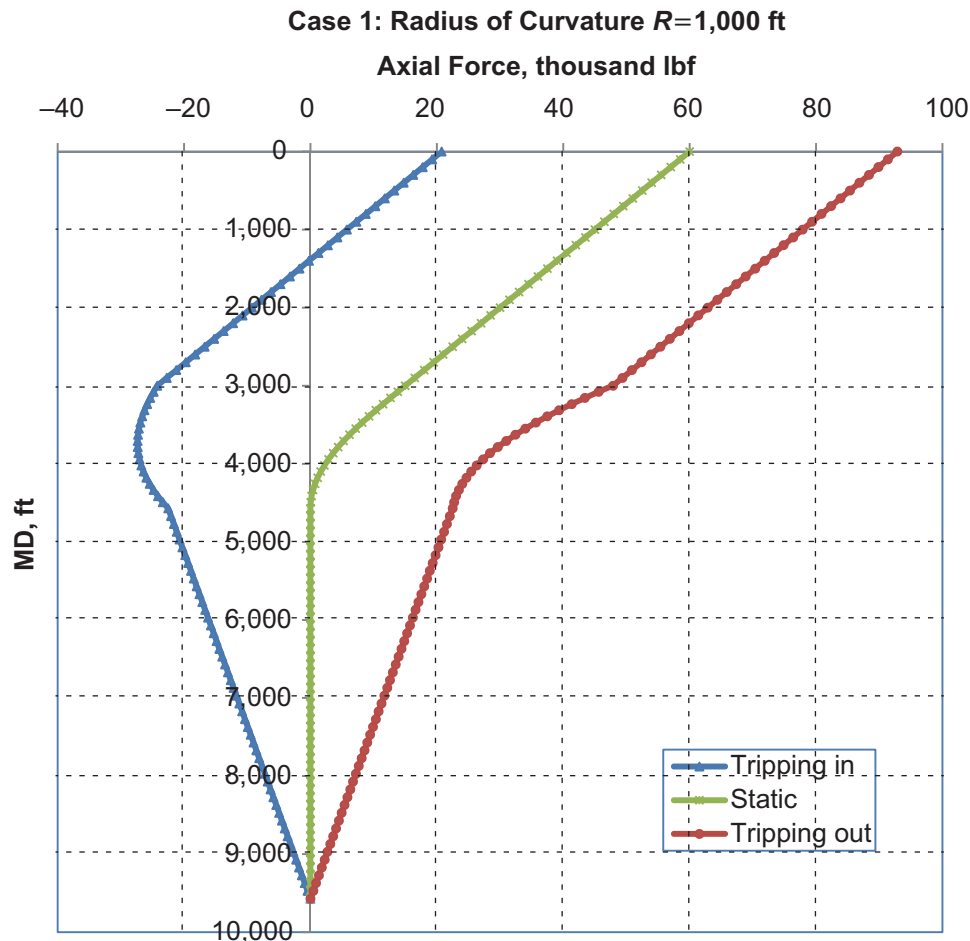


Fig. 8.68—Axial-force profile for Case 1 of Example 8.28.

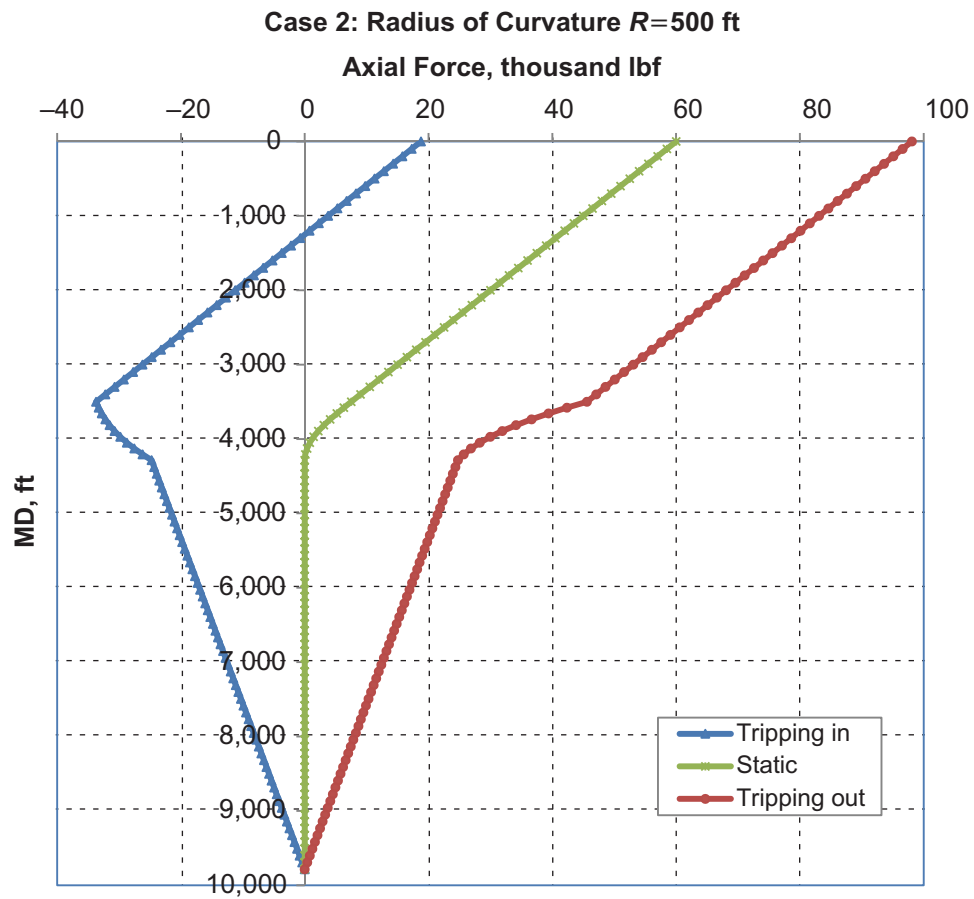


Fig. 8.69—Axial-force profile for Case 2 of Example 8.28.

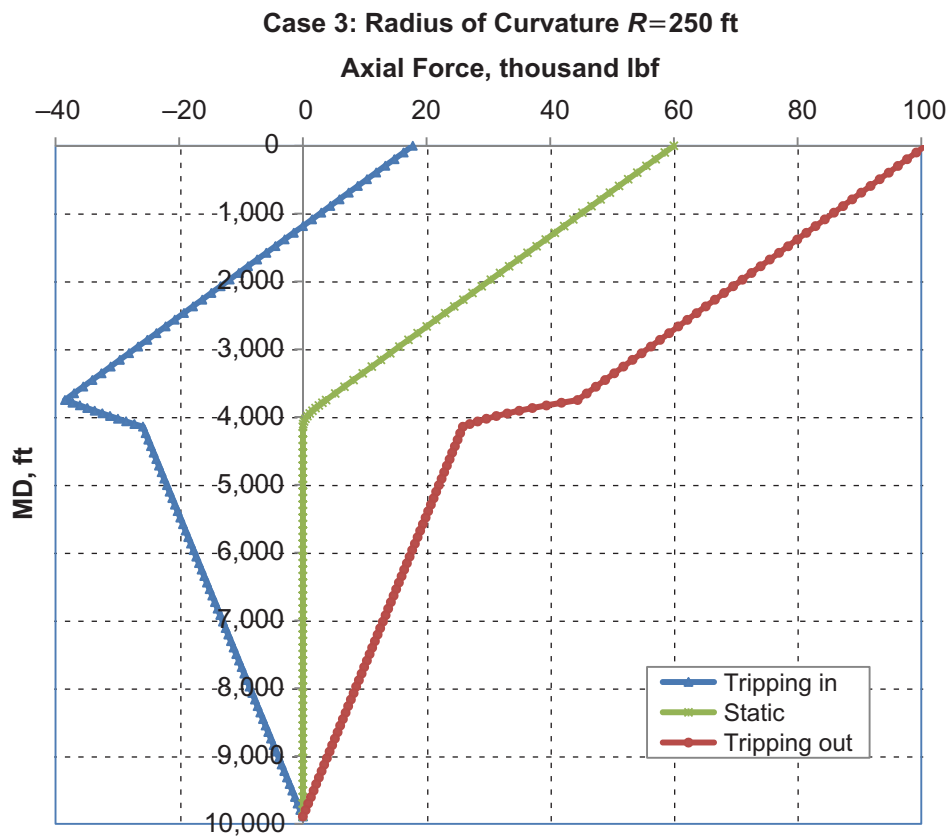


Fig. 8.70—Axial-force profile for Case 3 of Example 8.28.

A unit contact-force profile for Case 1 is shown in **Fig. 8.71**. A positive contact force indicates that the string lies on the low side of the wellbore, while a negative value indicates contact with the upper side. The highest absolute value of the unit contact force (approximately 48 lbf) occurs at the top of the buildup section while the string is being pulled out of the well. Still another interesting finding is that the maximum unit contact force at the bottom of the buildup section (approximately 43 lbf) occurs while tripping into the hole.

8.5.3 Torque Calculations for Pipe Rotation. Field evidence indicates that pipe rotation considerably improves axial force transfer to the bit in highly inclined and horizontal wellbores. In addition, pipe rotation results in less hook load during tripping operations using topdrive systems.

Consider two points on a drillstring segment at MDs s_1 and s_2 , with $s_2 > s_1$ and corresponding inclination angles φ_1 and φ_2 in a drop-off portion of a wellbore. The moment (torque) required to overcome the drag force on the segment is

$$M_{1-2} = \int_{s_1}^{s_2} r_p \mu w_c ds. \quad \dots\dots\dots (8.164)$$

Because $ds = R d\varphi$, and if $\varphi_2 < \varphi_1$, then

$$M_{1-2} = \int_{\varphi_2}^{\varphi_1} r_p \mu w_c R d\varphi. \quad \dots\dots\dots (8.165)$$

If the pipe force at the bottom of the segment is F_2 , then Eq. 8.157 yields the following expression for pipe force as a function of hole inclination angle:

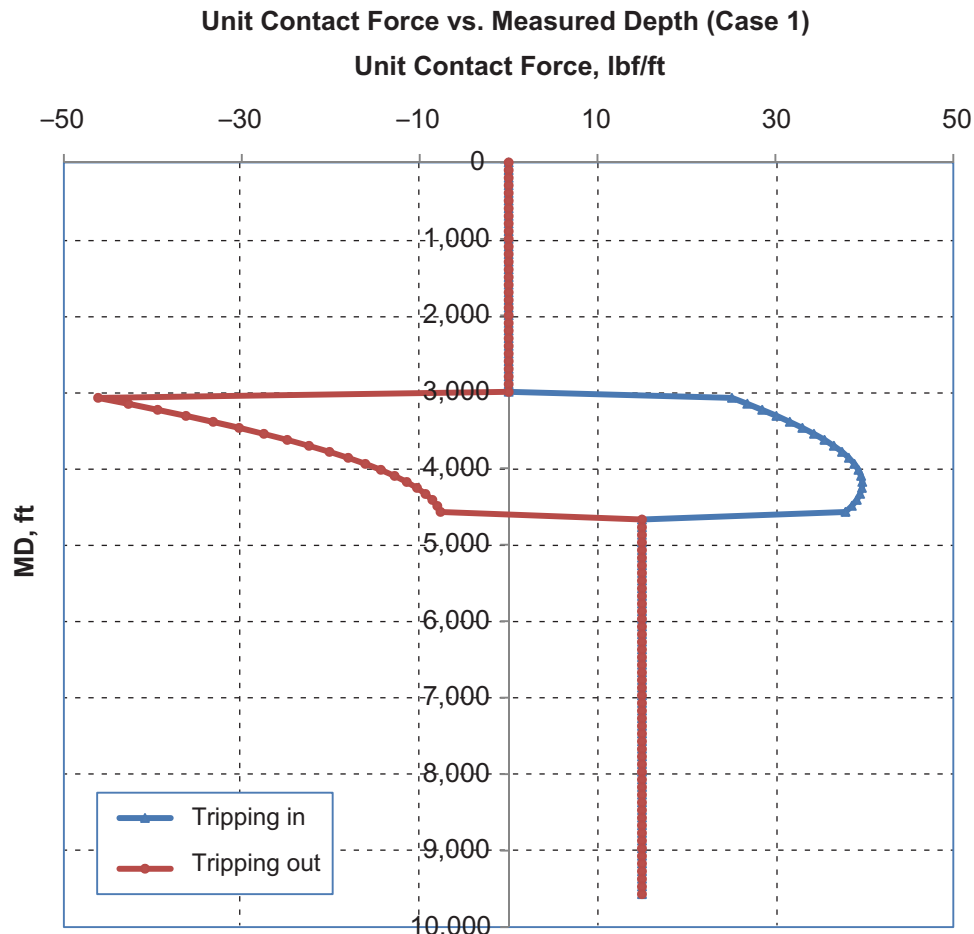


Fig. 8.71—Unit contact force for Example 8.28.

$$F(\varphi) = F_2 + w_{bp}R(\sin \varphi - \sin \varphi_2). \quad (8.166)$$

If Eq. 8.152 is used as a first approximation to calculate the unit contact force, then substituting Eq. 8.166 into Eq. 8.152 gives

$$w_c = \frac{F_2}{R} + 2w_{bp} \sin \varphi - w_{bp} \sin \varphi_2. \quad (8.167)$$

A more accurate unit-contact-force calculation requires vector analysis and is explained later in this chapter.

Substituting Eq. 8.167 into Eq. 8.165 and integrating gives the torque required to overcome friction for the pipe segment under consideration:

$$M_{1-2} = \mu r_p \left\{ F_2(\varphi_1 - \varphi_2) + w_{bp}R[2(\cos \varphi_2 - \cos \varphi_1) - (\varphi_1 - \varphi_2)\sin \varphi_2] \right\}. \quad (8.168)$$

Example 8.29 Calculate the torque needed to rotate the string in a drop-off portion of an S-shaped well, as shown in Fig. 8.64.

Solution. For this case, $\varphi_1 = 45^\circ$, $\varphi_2 = 0^\circ$, and $F_2 = 20,000$ lbf. It is also known that $w_{bp} = 20.15$ lbf/ft and $R = 558$ ft. Substituting the above numbers into Eq. 8.168 yields

$$M_{1-2} = \frac{(0.2)(5.0)}{(2)(12)} \left\{ 20,000(45 - 0) \left(\frac{\pi}{180} \right) + (2,015)558[2(\cos 0 - \cos 45) - 0] \right\} = 928 \text{ ft-lbf}$$

The torque profile for this well is shown in **Fig. 8.72**. The reader is encouraged to write a computer program to generate this curve.

In the vertical portion of the well, the torque is constant because its viscous component has been ignored. In other words, it is been assumed that the drilling fluid is ideal. A rapid increase in torque is observed in the build segment of the well because of the high value of the contact force.

As stated earlier, rotation of a pipe provides several benefits, such as improved axial-force transfer, reduction in pipe forces while tripping, and improved hole cleaning. However, it should always be remembered that pipe rotation also has a considerable detrimental effect because it contributes to pipe fatigue damage and

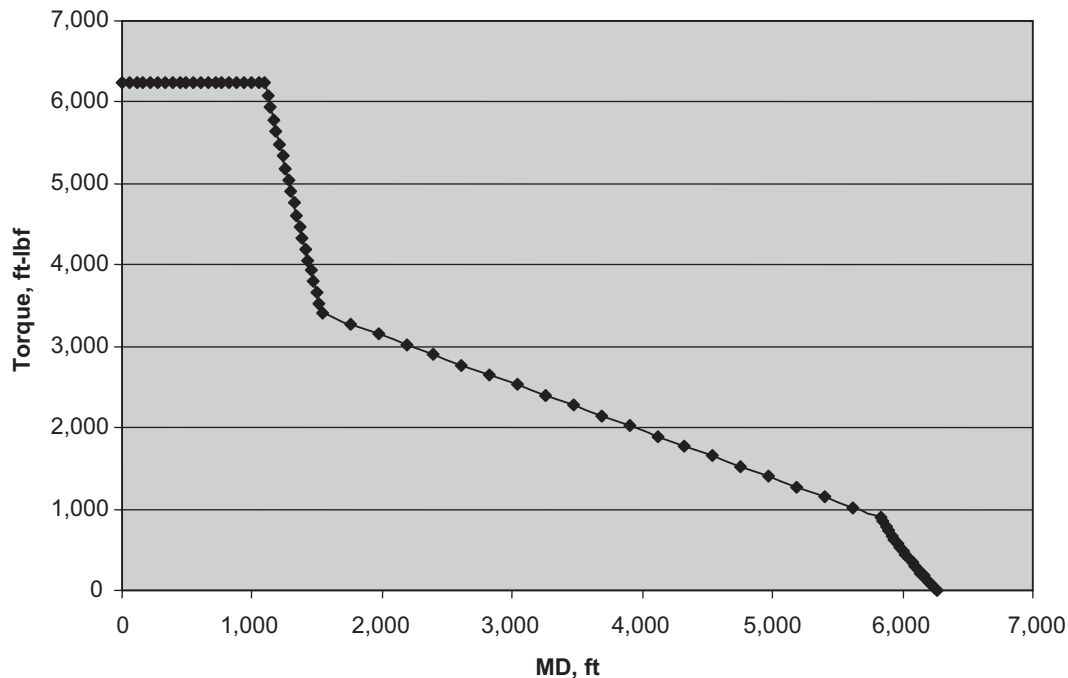


Fig. 8.72—Torque vs. MD, Example 8.29.

casing wear. In particular, rotating the string off-bottom results in an increase in pipe tension (compared to the drilling stage when a part of the string weight is slacked off on the drill bit) and should be kept to the minimum. Field experience shows that at times the torque value also depends on pipe rotational speed. Typically, as the pipe rotational speed is increased, the torque increases also. Hence, it is recommended that values of pipe rotational speed should be specified for a given friction factor. For example, $\mu_{40} = 0.26$ is the friction factor at 40 rev/min.

Because the viscous torque due to drilling fluid is considered to be small, such behavior can be explained by dynamic effects (pipe whirl and precession) and possible cuttings accumulations that are not accounted for in the model presented above.

Example 8.30 Consider the horizontal well profile shown in Fig. 8.67 for Case 1 ($R = 1,000$ ft). Assuming that there is no torque applied at the bottom of the string, it is necessary to calculate the torque at the top of the hole. The pipe unit weight in fluid and the friction coefficient are the same as in Example 8.29; the pipe OD = 4.5 in.

Solution. First, the torque required to rotate the pipe in a horizontal section of a length of 5,000 ft is calculated:

$$M_{3-4} = \int_{4,570}^{9,570} r_p \mu w_c ds = \int_0^{5,000} \left(\frac{4.5}{24} \right) (0.3) (15.0) ds = 4,218 \text{ ft-lbf}$$

The torque required to rotate the pipe in a buildup section ($R = 1,000$ ft) is

$$(a) \quad M_{2-3} = \int_{s_1}^{s_2} r_p \mu w_c ds = \int_{\phi_1}^{\phi_2} r_p \mu w_c R d\phi.$$

The next step is to calculate the unit contact force w_c as a function of hole inclination angle. For this purpose, either Eq. 8.158 or Eq. 8.161 can be used, depending on the amount of tension in the pipe. First, however, the axial force along the string must be calculated. Using Eq. 8.160 or Eq. 8.163 and setting $\mu = 0$,

$$(b) \quad F(\phi) = -w_{bp} R \sin \phi + C.$$

At $\phi = 90^\circ$ the force $F = 0$ lbf, $C = w_{bp} R$, and the axial force in the pipe as a function of hole inclination angle is:

$$(c) \quad F(\phi) = w_{bp} R (1 - \sin \phi).$$

To determine whether a particular case is “low-tension” or “high-tension,” Line (c) must be compared with $w_{bp} R \sin \phi$; hence,

$$(d) \quad w_{bp} R (1 - \sin \phi) = w_{bp} R \sin \phi.$$

Solving Line (d) for ϕ , the value for $\phi = 30^\circ$ is obtained.

To summarize, it can be stated that a string is in “low tension” if $\phi > 30^\circ$ and in “high tension” if $\phi < 30^\circ$.

Consequently, the unit contact force is as follows:

For $90^\circ < \phi < 30^\circ$ (low tension),

$$(e) \quad w_c = w_{bp} (2 \sin \phi - 1);$$

For $30^\circ < \phi < 0^\circ$ (high tension)

$$(f) \quad w_c = w_{bp} (1 - 2 \sin \phi).$$

The torque change on the buildup bend is

$$(g) \quad M_{2-3} = \int_0^{90} r_p \mu w_c R d\phi = (r_p \mu w_{bp} R) \left[\int_0^{30} (1 - 2 \sin \phi) d\phi + \int_{30}^{90} (2 \sin \phi - 1) d\phi \right].$$

Upon integration of Line (g),

$$M_{2-3} = (843)(0.255 + 0.685) = 790 \text{ ft-lbf}.$$

Because viscous torque was ignored, the expected rotary torque at the top of the hole is the summation of the torque components calculated for the horizontal and the buildup sections of the wellbore. The torque at the top = 5,667 + 790 = 6,457 ft-lbf.

8.5.4 Buckling Considerations. It is well known that if a pipe is in high enough compression (e.g., when tripping into a highly inclined and horizontal wellbore), it may buckle, and then the drag models discussed so far in this chapter are no longer applicable.

It can be shown that if friction is ignored, the compressive force required to initiate lateral (sinusoidal) buckling of a long pipe can be calculated from the equation proposed by Dawson and Paslay (1984):

$$F_{cr,s} = 2\sqrt{\frac{EIw_c}{r_c}}, \quad \dots\dots\dots (8.169a)$$

where $F_{cr,s}$ = magnitude of the compressive force in the string required for initiation of lateral buckling, EI = pipe bending stiffness (product of the modulus of elasticity and the moment of inertia), w_c = unit contact force, and r_c = pipe radial clearance [(hole diameter – pipe OD)/2].

Although Eq. 8.169a is strictly valid only for long, frictionless, and perfectly straight and smooth (no tool joints or couplings) pipes, it is still useful for practical design applications. The influence of tool joints, residual pipe bending, and friction is discussed in several SPE papers [e.g., Duman et al. (2003)].

Consistently with the drag-force analysis performed earlier, the unit contact force is

$$w_c = \pm \frac{F}{R} + w_{bp} \sin \phi. \quad \dots\dots\dots (8.169b)$$

A positive sign is associated with a buildup section of the wellbore, while a negative sign is associated with a drop-off section. In the case of a drop-off segment, the contact force can be small, and a relatively small compressive force may buckle the pipe. On the other hand, in a buildup section, the wellbore curvature increases the contact force, and consequently it takes a greater compressive force to buckle the pipe. In other words, positive wellbore curvatures (i.e., DLS) have a stabilizing effect on drillpipe, while in drop-off segments, the buckling resistance is reduced compared with that of a straight inclined hole. Eq. 8.169a is also valid in straight inclined wells. Example 8.31 illustrates the practical usefulness of the above equations.

Example 8.31 Consider Case 1 ($R = 1,000$ ft) for the horizontal wellbore profile discussed in Example 8.29. Calculate whether or not the part under compression during a tripping-in operation will remain straight. Drillpipe bending stiffness is $EI = (345.2)10^6$ lbf/in.², and the hole diameter is 8½ in.

Solution. First consider a horizontal part of the hole. The unit contact force is

$$w_c = w_{bp} \sin \phi = 15 \text{ lbf/ft.}$$

From Eq. 8.169a, the critical force can be calculated as

$$F_{cr,s} = 2\sqrt{\frac{(345.2)10^6 \left(\frac{15}{12}\right)}{\frac{8.5 - 4.5}{2}}} = 29,380 \text{ lbf.}$$

Because the magnitude of the greatest compressive force is 22,500 lbf, it can be concluded that the pipe will not buckle in a horizontal segment of the wellbore.

To calculate the critical force in a curved portion of the wellbore, it is necessary to substitute the contact force given by Eq. 8.169b into Eq. 8.169a and to solve the resulting equation for the force F . Eventually the following equation is obtained:

$$F = \frac{2EI}{r_c R} \left(1 + \sqrt{1 + \frac{(w_{bp} \sin \phi) R^2}{EI}} \right). \quad \dots\dots\dots (8.170a)$$

With all other parameters held constant, the critical lateral buckling force depends on the hole inclination angle φ . For example, at $\varphi = 45^\circ$,

$$F_{cr,s} = \frac{2(345.2)(10^6)}{2(1,000)(12)} \left(1 + \sqrt{1 + \frac{\left(\frac{15}{12}\right)(\sin 45) (1,000(12))^2}{(345.2)10^6}} \right) = 66,684 \text{ lbf.}$$

Clearly the critical lateral buckling force in a buildup part of the wellbore is much higher than in a horizontal section, and the pipe is not buckled there. In conclusion, it can be stated that positive build rates provide more buckling stability for pipe in compression.

In drop-off segments of the wellbore, the critical sinusoidal buckling force can be calculated as

$$F = \frac{2EI}{r_c R} \left(-1 + \sqrt{1 + \frac{w_{bp} \sin \varphi R^2}{EI}} \right) \dots \dots \dots (8.170b)$$

The reader is encouraged to show that as the wellbore radius R goes to very high values (infinity), Eqs. 8.170a and 8.170b reduce to Eq. 8.169a.

The analysis of axial force transfer in post-buckling pipe configurations is beyond the scope of this chapter.

8.5.5 Tortuosity Effects. At the planning stage of well development, the well path is smooth and typically composed of straight and curved segments with constant curvature in two- or three-dimensional space. The actual drilled well trajectory may deviate from the planned path to a lesser or greater degree. The deviations may be a result of changes in geology (type of rock, formation dip angle, faults, etc.) as well as the mechanical behavior of the drill bits and BHAs. For example, drilling with SMs frequently results in a rippling (undulation) effect over a portion of the wellbore. The rippling effect is called *macrotortuosity*. Various tortuosity models have been proposed in the literature. These include simple sine-wave profiles (amplitude and wave length are fitted to directional survey data to simulate the actual wellbore path more closely) and more-sophisticated models involving random changes in inclination and azimuth angles. Practical application of tortuosity models requires a good set of directional-survey data. An example of a segment of wellbore drilled with an SM motor is shown in **Fig. 8.73**.

Wellbore undulation affects not only the torque and drag forces, but also the critical buckling forces. In addition, the wellbore may also exhibit microtortuosity associated with hole spiraling. Hole spiraling can be identified using image logs or good-quality caliper logs. Microtortuosity results in a reduction of the effective wellbore diameter and, consequently, higher torque and drag. Both macro- and microtortuosity may cause significant difficulties in running casing and logging tools into wellbores. Tortuosity factors can be calculated by comparing

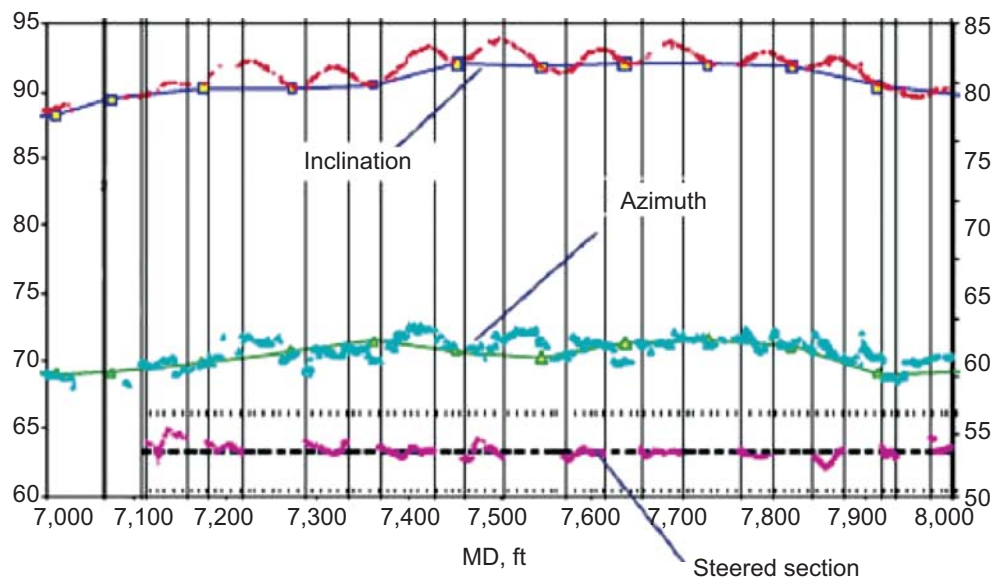


Fig. 8.73—Tortuosity created by a steerable motor (Mason and Chen 2007).

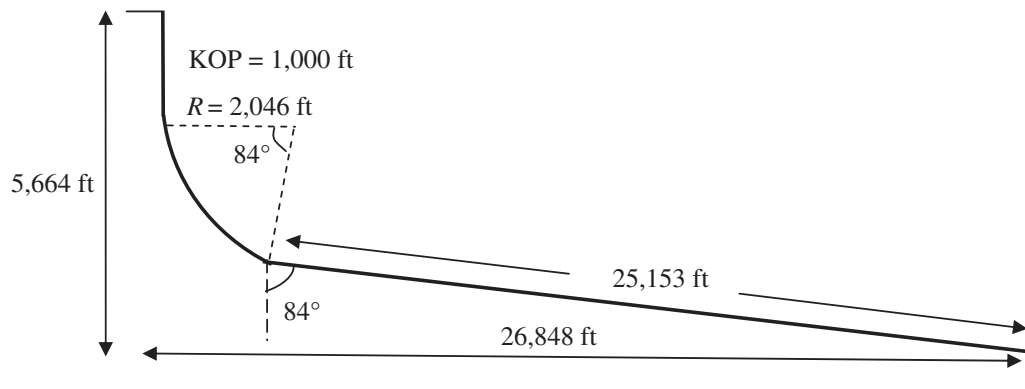
torque and drag values using the results from the planned trajectory and values measured in an “as drilled” well. Some designers will simply increase the value of the friction coefficient to account for tortuosity effects. Because a large number of factors influence torque and drag, this subject is still of great interest to research engineers.

8.5.6 Review Questions and Problems.

1. List the factors that affect torque and drag in vertical and directional drilling.
2. Explain why accurate calculations of torque and drag are important for drilling personnel.
3. Explain why the friction coefficient that exists in a torque-and-drag model is sometimes called a down-hole friction factor.
4. List typical values of the coefficient of friction for oil-based mud and water-based mud drilling fluids.
5. The inclination angle of a hole is 76° . Will the drillstring slide down due to its own weight if the coefficient of friction $\mu = 0.27$?
6. List the major assumptions made in a soft-string model.
7. Create an FBD for a pipe element in a drop-off bend and explain all the forces acting on the element.
8. What is the “capstan force”?
9. A string is pulled out from a drop-off bend. The force at hole inclination angle φ_0 is given and equal to F_0 . Show that the force at hole inclination angle φ can be calculated using the following equation:

$$F(\varphi) = F_0 e^{\mu(\varphi - \varphi_0)} + \frac{w_{bp} R}{1 + \mu^2} \left[(1 - \mu^2) (\sin \varphi - e^{\mu(\varphi - \varphi_0)} \sin \varphi_0 - 2\mu (\cos \varphi - e^{\mu(\varphi - \varphi_0)} \cos \varphi_0)) \right].$$

10. Define “low tension” and “high tension” in buildup bends.



11. Consider the well profile used in Example 8.27. Assuming coefficients of friction $\mu = 0.3$, $\mu = 0.4$ calculate the forces at Point 4, Point 3, Point 2, and Point 1 for tripping-out and tripping-in operations. Write a computer program to solve the problem.
12. Assume the data for the S-shaped well profile described in Example 8.28. The hook load recorded while tripping the string out of the hole is 135,000 lbf. Find the corresponding friction coefficient.
13. Consider a wellbore that consists of a vertical section 4,000 ft in length, a buildup section with radius of curvature $R = 1,000$ ft, and a horizontal section 6,000 ft in length. A 9-in. casing with a unit weight of 40 lbf/ft is to be run into the hole. Calculate the expected force at the top of the hole if the drilling-fluid density is 10 lbm/gal and the coefficient of friction $\mu = 0.25$.
14. Consider an ERW profile as shown in the figure below
 - Hole size: $8\frac{1}{2}$ in.
 - Drillpipe size: $4\frac{1}{2}$ in.
 - Pipe unit weight: 20 lbf/ft
 - Drilling-fluid density: 12 lbm/gal
 - Friction coefficient: $\mu = 0.25$

Calculate:

- (a) The force at the top of the buildup section during tripping-out and tripping-in operations
- (b) The unit contact force in the middle of the buildup section

15. Show that for a high-tension case, the rotary torque in a buildup section of a wellbore can be calculated using the following equation:

$$M(I) = \mu r_p (F_0 + w_e R \sin \varphi_o) [(\varphi - \varphi_o) + 2\mu r_p R (\cos \varphi - \cos \varphi_o)].$$

16. Given the well profile as described in the problem above (an ERW), calculate the torque required to rotate the pipe and the unit contact force at the midpoint of the buildup segment.
17. Calculate the expected force at the top of the ERW described in Problem 14 for running a 9 $\frac{5}{8}$ -in. casing with a unit weight of 40 lbf/ft.
18. Calculate the maximum length of a pipe with unit weight 6.5 lbf/ft (in fluid) that can be pushed into a horizontal section of a wellbore without experiencing lateral buckling if the friction coefficient is $\mu = 0.28$.
19. Calculate the sinusoidal buckling force for a 3 $\frac{1}{2}$ -in. drillpipe in a drop-off segment of a wellbore with a drop rate of 17.5°/100 ft at inclination angles of 35 and 85°.
20. Explain the difference in macro- and microtortuosity effects.

8.6. Torque-and-Drag Modeling for 3D Well Profiles

8.6.1 Equilibrium Equations in 3D. The main purpose of a torque-and-drag model is to develop a system of equations that can be used to calculate forces and moments in the pipe as well as the forces generated by interaction between the pipe and the wellbore. This section presents the development of a three-dimensional model that is subject to several simplifying assumptions, but which is still useful for practical design applications. The major simplifying assumptions are as follows:

- Pipe is in continuous contact with the wellbore (that is, the effects of tool joints, couplings, and wellbore irregularities and tortuosity are ignored).
- Inertial effects due to pipe sliding or rotation are ignored.
- Drilling-fluid flow effects are not considered.
- Friction force is modeled using the Coulomb friction concept.

To derive the force and moment equilibrium equations, consider a differential pipe element as shown in **Fig. 8.74**. For the purpose of this analysis, a right-hand x, y, z system of coordinates was chosen, with the z -axis pointing down and the conventional unit vectors $\vec{i}, \vec{j}, \vec{k}$ as shown in Fig. 8.74. It is also very useful to introduce the right-hand Frenet-Serret local system of coordinates with its unit tangent, normal, and binormal vectors $\vec{t}, \vec{n}, \vec{b}$, as also

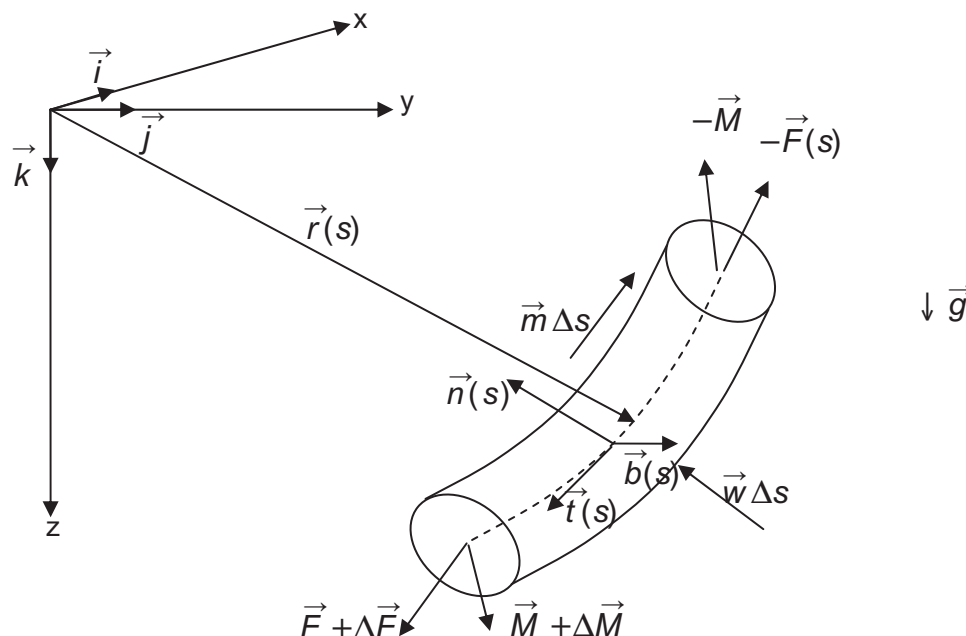


Fig. 8.74—Free-body diagram for a small pipe element in 3D.

shown in Fig. 8.74. The position vector $\vec{r}(s)$ is drawn from the origin of the rectangular coordinates to the pipe element's mass center.

If the pipe is not moving or is moving so slowly that inertial effects can be neglected, the vector sum of all forces on the pipe segment gives:

$$\vec{F} + \Delta\vec{F} + \vec{w}\Delta s - \vec{F} = \vec{0}, \quad (8.171)$$

where \vec{F} is the force in the pipe (internal pipe force), \vec{w} is the total force per unit length applied to the pipe (the resultant of all external forces), and Δs is the length of the pipe segment. In the limit as $\Delta s \rightarrow 0$, the change in force \vec{F} due to the applied load vector \vec{w} is given by the following equation:

$$\frac{d\vec{F}}{ds} + \vec{w} = \vec{0}. \quad (8.172)$$

In general, the pipe force \vec{F} consists of the tangential force F_t (the axial force) and two shear forces in the normal (F_n) and binormal (F_b) directions:

$$\vec{F} = F_t\vec{t} + F_n\vec{n} + F_b\vec{b}. \quad (8.173)$$

Typically, in a torque-and-drag analysis, only three external forces are considered: the force due to the pipe effective weight (the weight of the pipe in fluid) \vec{w}_{bp} , the force normal to the pipe contact force (the side force) \vec{w}_c , and the force due to friction (the drag force) \vec{w}_d . This relationship can be expressed as

$$\vec{w} = \vec{w}_{bp} + \vec{w}_c + \vec{w}_d. \quad (8.174)$$

In the system of coordinates used here, gravity is pointing downward, and so is the z -axis; therefore, the effective unit pipe-weight vector is

$$\vec{w}_{bp} = w_{bp}\vec{k}. \quad (8.175)$$

As already stated earlier, the unit contact force \vec{w}_c is normal to the pipe, and therefore it lies in the $\vec{n}-\vec{b}$ plane. As is known from elementary mechanics, the drag force always opposes the direction of pipe motion. If the pipe is sliding, the drag force is in the tangent \vec{t} direction. If the pipe is rotating, the drag force is also assumed to be tangent to the pipe, but in the $\vec{n}-\vec{b}$ plane.

In a manner similar to that for the force balance, it can be shown that the vector-moment equilibrium equation is

$$\frac{d\vec{M}}{ds} + \vec{t} \times \vec{F} + \vec{m} = \vec{0}, \quad (8.176)$$

where \vec{M} = the internal moment (pipe moment), \vec{m} = the applied moment per unit length (distributed moment) due to the drag force, and \vec{t} = the unit tangent vector.

According to the Bernoulli-Euler theory of elastic beams, for a circular pipe, the moment vector \vec{M} in the pipe consists of the bending moment (pointing in the binormal direction) with a magnitude equal to the product of the pipe bending stiffness (EI), the pipe curvature κ , and the torque (pointing in the tangential direction), which can be expressed as

$$\vec{M} = EI\kappa\vec{b} + M_t\vec{t}, \quad (8.177)$$

where EI = the pipe bending stiffness (the product of modulus of elasticity and moment of inertia), κ = the pipe curvature, and M_t = the magnitude of moment (torque) required for pipe rotation.

The distributed moment \vec{m} associated with the drag force \vec{w}_d is the cross-product of the pipe radius and drag force:

$$\vec{m} = \vec{r}_p \times \vec{w}_d, \quad (8.178)$$

where \vec{r}_p is the pipe radius vector.

For a frictionless system, the moment \vec{m} is nil. It should be well understood that the direction of the unit drag force \vec{w}_d is different for sliding and for rotating pipe.

8.6.2 Pipe in a Straight Section of an Inclined Wellbore. To explain the practical usefulness of the equilibria of forces and moments given by Eqs. 8.172 and 8.176, the wellbore will be assumed to be modeled as straightline segments with given lengths, inclinations, and azimuth angles.

Consider the straight wellbore segment from point i to point $i+1$, shown schematically in **Fig. 8.75**. At Point i , the MD is s_i , and at Point $i+1$, the MD is s_{i+1} .

For a straight segment, the unit tangent vector is constant and is given by

$$\vec{t}_i = (\sin \varphi_i \cos \vartheta_i) \vec{i} + (\sin \varphi_i \sin \vartheta_i) \vec{j} + \cos \varphi_i \vec{k}, \quad \dots \quad (8.179)$$

where φ_i and ϑ_i are the segment's inclination and azimuth angles. The unit normal vector \vec{n} may be selected as any convenient unit vector in the plane normal to the \vec{t} vector. Let it lie in a vertical plane containing segment i so that its inclination angle is $\varphi + \frac{\pi}{2}$ and its azimuth is the same as that of the unit tangent vector. Hence,

$$\vec{n}_i = (\cos \varphi_i \cos \vartheta_i) \vec{i} + (\cos \varphi_i \sin \vartheta_i) \vec{j} - \sin \varphi_i \vec{k}. \quad \dots \quad (8.180)$$

In other words, the unit normal vector is pointing to the high side of the wellbore.

Following the right-hand rule, the unit binormal vector is in a horizontal plane, its inclination angle is equal to $\frac{\pi}{2}$, and its azimuth is $\vartheta_i + \frac{\pi}{2}$, so:

$$\vec{b}_i = (-\sin \vartheta_i) \vec{i} + (\cos \vartheta_i) \vec{j}. \quad \dots \quad (8.181)$$

Clearly, the unit binormal vector is perpendicular to the \vec{k} vector. In other words, the z -component of the binormal vector is zero ($b_z = 0$), and the unit binormal vector is pointing toward the right side of the wellbore.

Now consider two fundamental cases involving a pipe in a sliding mode (tripping in or tripping out) (Case 1) and in a rotating mode (Case 2).

Case 1—Pipe in Sliding Mode. It is assumed that the pipe is sliding slowly in an axial (tangential) direction, as shown in **Fig. 8.76**. The angle θ (Fig. 8.76) is in the $\vec{n} - \vec{b}$ plane and gives the direction of the normal contact force \vec{w}_c . Because the pipe is straight, its curvature and torsion are nil. Taking derivatives of Eq. 8.173 with respect to the MD s ,

$$\frac{d\vec{F}}{ds} = \frac{dF_t}{ds} \vec{t}. \quad \dots \quad (8.182)$$

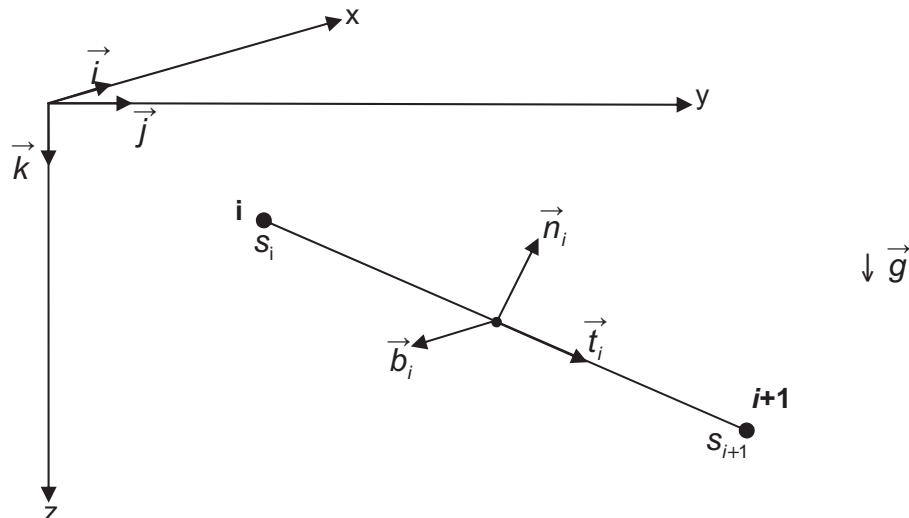


Fig. 8.75—Straight segment of a 3D wellbore.

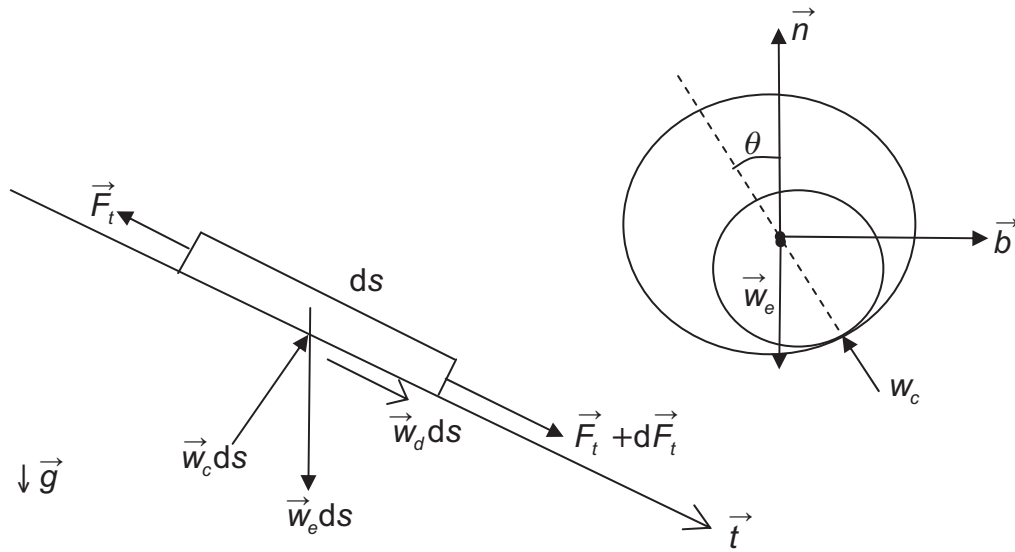


Fig. 8.76—Free-body diagram for sliding pipe.

Examination of the FBDs in Fig. 8.76 reveals that the contact and drag forces can be expressed as

$$\vec{w}_c = (w_c \cos \theta) \vec{n} - (w_c \sin \theta) \vec{b}, \quad (8.183)$$

$$\vec{w}_d = \pm \mu w_c \vec{t}. \quad (8.184)$$

The choice of sign in Eq. 8.184 depends on the direction of pipe motion. The plus sign (+) is for pulling (tripping out), while the negative sign (–) is used when the pipe is moving in a downward direction (tripping into the well). The effective pipe unit weight vector \vec{w}_e is pointing in the z -direction, as given by Eq. 8.175.

The vector force balance can be obtained by substituting Eqs. 8.182, 8.183, and 8.184 into Eq. 8.172:

$$\frac{dF_t}{ds} \vec{t}_i + w_{bp} \vec{k} + (\pm \mu w_c) \vec{t}_i + (w_c \cos \theta) \vec{n}_i - (w_c \sin \theta) \vec{b}_i = \vec{0}. \quad (8.185)$$

The desired scalar components can be obtained by multiplying Eq. 8.185 by the unit vectors \vec{t}_i , \vec{n}_i , and \vec{b}_i (taking dot products). As a result, the three scalar equations can be written as follows:

t -component:

$$\frac{dF_t}{ds} + w_{bp} \vec{t} \cdot \vec{k} \pm (\mu w_c) = 0; \quad (8.186a)$$

n -component:

$$w_{bp} \vec{n} \cdot \vec{k} + w_c \cos \theta = 0; \quad (8.186b)$$

b -component:

$$w_{bp} \vec{b} \cdot \vec{k} - w_c \sin \theta = 0. \quad (8.186c)$$

Using Eqs. 8.179, 8.180, and 8.181, the required unit-vector dot products with Eq. 8.186 can be calculated as

$$\vec{t}_i \cdot \vec{k} = t_{iz} = \cos \varphi_i, \quad (8.187a)$$

$$\vec{n}_i \cdot \vec{k} = n_{iz} = -\sin \varphi_i, \quad \dots \quad (8.187b)$$

$$\vec{b}_i \cdot \vec{k} = b_{iz} = 0. \quad \dots \quad (8.187c)$$

Substituting Eq. 8.187 into Eq. 8.186 yields a system of three equations with three unknowns— F_i , w_c , and θ .

$$\frac{dF_i}{ds} + w_{bp} \cos \varphi \pm \mu w_c = 0, \quad \dots \quad (8.188a)$$

$$-w_{bp} \sin \varphi_i + w_c \cos \theta = 0. \quad \dots \quad (8.188b)$$

$$-w_{bp} \sin \theta = 0. \quad \dots \quad (8.188c)$$

From Eq. 8.188c, it can be concluded that the position angle $\theta = 0$ (that is, the pipe lies on the lower side of the wellbore). From Eq. 8.188b, the unit contact force $w_c = w_{bp} \sin \varphi_i$. Substituting the unit contact force into Eq. 8.188a and integrating the result yields

$$F_{i,i+1} - F_{i,i} + (w_{bp} \cos \varphi_i \pm \mu w_{bp} \sin \varphi_i)(s_{i+1} - s_i) = 0. \quad \dots \quad (8.189)$$

For example, if the force at the bottom of segment i is given and the pipe is pulled out of the wellbore, the force at the top (at Point 1) is

$$F_{i,i} = F_{i,i+1} + (\cos \varphi_i + \mu \sin \varphi_i) w_{bp} (s_{i+1} - s_i). \quad \dots \quad (8.189a)$$

For the case of tripping into the wellbore,

$$F_{i,i} = F_{i,i+1} + (\cos \varphi_i - \mu \sin \varphi_i) w_{bp} (s_{i+1} - s_i). \quad \dots \quad (8.189b)$$

The reader is encouraged to study Eq. 8.176 to verify that all components of the moment-balance equation are nil, indicating that the bending moment and torque are nil for the case of pipe sliding in a straight segment of the wellbore. The results obtained are consistent with basic engineering intuition.

Case 2—Rotating Pipe. Now consider a pipe that is rotating about its own axis. The main task is to calculate the torque required for pipe rotation. The axial effective force in the pipe must also be calculated.

When the pipe is rotated, the drag force (friction force) is no longer in the axial direction, but is now applied opposite to the direction of rotation (friction always opposes motion) in the $\vec{n} - \vec{b}$ plane, as shown in the FBD (Fig. 8.77).

Examination of Fig. 8.77 shows that the drag force \vec{w}_d can be expressed as

$$\vec{w}_d = (w_d \sin \theta) \vec{n}_i + (w_d \cos \theta) \vec{b}_i, \quad \dots \quad (8.190)$$

and that the magnitude of the drag force is

$$w_d = \mu w_c. \quad \dots \quad (8.191)$$

It is important to note that the drag force in the case of pipe rotation has both normal and binormal components. Now the vector sum of forces can be written as

$$\frac{dF_i}{ds} \vec{t}_i + w_c \vec{k} + (\mu w_c \sin \theta) \vec{n}_i + (\mu w_c \cos \theta) \vec{b}_i + (w_c \cos \theta) \vec{n}_i - (w_c \sin \theta) \vec{b}_i = \vec{0}. \quad \dots \quad (8.192)$$

In a manner similar to that for sliding motion (Case 1), multiplying Eq. 8.192 by the unit vectors \vec{t}_i , \vec{n}_i , and \vec{b}_i (taking dot products) yields the desired three scalar components:

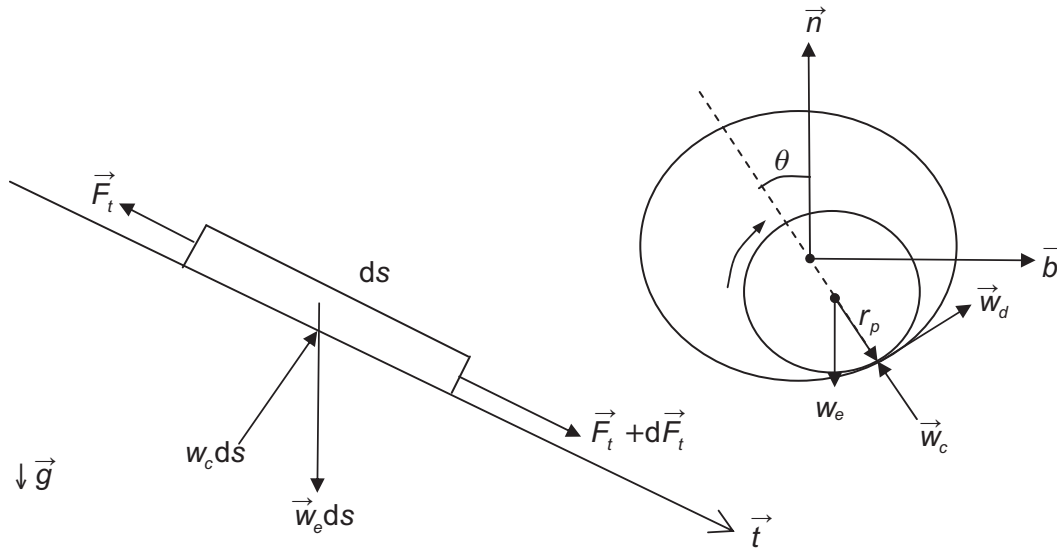


Fig. 8.77—Free-body diagram for rotating pipe.

t -component:

$$\frac{dF_t}{ds} + w_{bp} \vec{t} \cdot \vec{k} = 0; \quad \dots \quad (8.193a)$$

n -component:

$$w_{bp} \vec{n} \cdot \vec{k} + \mu w_s \sin \theta + w_c \cos \theta = 0; \quad \dots \quad (8.193b)$$

b -component:

$$w_{bp} \vec{b} \cdot \vec{k} + \mu w_c \cos \theta - w_s \sin \theta = 0. \quad \dots \quad (8.193c)$$

The dot products in the above equations have already been calculated in Case 1 ($\vec{t}_i \cdot \vec{k} = \cos \varphi_i$, $\vec{n}_i \cdot \vec{k} = -\sin \varphi_i$, and $\vec{b}_i \cdot \vec{k} = 0$); hence, from Eq. 8.193c, the unit contact-force direction angle θ can be obtained as

$$\theta = \arctan(\mu). \quad \dots \quad (8.194)$$

For example, if the friction coefficient is 0.4, then the contact angle is 21.8° . Then, from the n -component equation, the magnitude of the unit contact force is

$$w_c = \frac{w_{bp} \sin \varphi}{\sqrt{\mu^2 + 1}}. \quad \dots \quad (8.195)$$

This result is not intuitively obvious. It is correct, however, due to the effect of the binormal component of the drag force (Eq. 8.190).

In conclusion, if a pipe rotates clockwise about its own axis, it moves up the wellbore through an angle θ counter-clockwise with reference to the low side of the hole. Consequently, the contact force (the side force) is less than the unit contact force due to the normal unit pipe-weight component, $w_{bp} \sin \varphi_i$.

The pipe position angle (contact angle) θ is of essential importance for drilling applications, not only for accurate torque calculations, but also for deviation control and cuttings transport. If it is expected that the pipe will have some cutting ability, then the hole will have a tendency to turn to the right and increase the hole azimuth angle. A similar effect occurs at the drill bit, resulting in bit walk. In actual drilling applications, to determine if the bit walk will be to the right or left, the type of drill bit, its geometry, its face- and side-cutting ability, the formation anisotropy, and the type of BHA would all have to be taken into account.

Bit walk can also be observed if the pipe is not rotating (e.g., when drilling with a downhole motor in a sliding mode). The direction of the walk will depend on the direction of the side force at the bit. For practical applications, the amount of bit walk is determined on the basis of analyses of offset wells that include the mechanical performance of the BHA and drill bits, WOB, rotation speed, and the formation properties and dip and strike angles.

Now the t -component equation can be integrated to obtain the effective axial (tangential) force:

$$F_{t,i+1} - F_{t,i} + w_{bp} \cos \varphi (s_{i+1} - s_i) = 0. \quad (8.196)$$

If $F_{t,i+1}$ is known, the force at the top can be immediately calculated:

$$F_{t,i} = F_{t,i+1} - w_{bp} \cos \varphi (s_{i+1} - s_i). \quad (8.197)$$

To calculate the magnitude of the torque required to rotate the pipe, the balance of moments given by Eq. 8.176 must be used.

For a straight segment of pipe, the curvature $\kappa = 0$ and the moment given by Eq. 8.177 take on the following simple form

$$\vec{M} = M_t \vec{t}_i. \quad (8.198)$$

Because for the case under consideration the force has only a tangential component $\vec{F} = F_t \vec{t}$, the vector product of $\vec{t} \times \vec{F} = 0$ and Eq. 8.176 can be written as

$$\frac{dM_t}{ds} \vec{t}_i + \vec{m} = 0. \quad (8.199)$$

The distributed external moment \vec{m} is attributable to the unit drag force \vec{w}_d acting on the arm \vec{r}_p , as shown in Fig. 8.77:

$$\vec{m} = \vec{r}_p \times \vec{w}_d \quad (8.200)$$

The pipe radius vector \vec{r}_p (with magnitude equal to the pipe radius r_p) is

$$\vec{r}_p = (-r_p \cos \theta) \vec{n}_i + (r_p \sin \theta) \vec{b}_i. \quad (8.201)$$

Substituting Eqs. 8.190 and 8.201 and taking the cross-product gives

$$\vec{m} = (-r_p w_d) \vec{t}_i = (-r_p \mu w_c) \vec{t}_i. \quad (8.202)$$

It is important to point out that the negative sign in Eq. 8.202 indicates that the distributed moment \vec{m} is acting in the direction opposite to that of the unit tangent vector.

Clearly, the equation for the moment consists only of the t -component:

$$\frac{dM_t}{ds} - r_p \mu w_c = 0. \quad (8.203)$$

Integrating Eq. 8.203 yields the equation for the change in torque (ΔM_t) along a pipe segment of length ($s_{i+1} - s_i$):

$$\Delta M_t = r_p \mu w_c (s_{i+1} - s_i). \quad (8.204)$$

For example, if the pipe diameter is 4.5 in., the unit weight in fluid is 16 lbf/ft, the coefficient of friction is 0.3, the length of the segment is 300 ft, the hole inclination angle is 45°, and the torque at the lower end is 1,000 ft-lbf, it is easy to calculate that the unit contact force is 10.8 lbf/ft and the torque at the upper end is 1,183 ft-lbf.

8.6.3 Force and Moment Equilibrium Formulation. This section presents the development of a general system of equations incorporating shear forces, pipe curvature, and torsion. This task will be accomplished in two steps. First, the system of equations for the equilibrium of forces will be derived, and then the system for the equilibrium of moments.

Equilibrium of Forces. Substituting Eqs. 8.173 and 8.174 into Eq. 8.172 gives

$$\frac{d(F_t \vec{t})}{ds} + \frac{d(F_n \vec{n})}{ds} + \frac{d(F_b \vec{b})}{ds} + \vec{w}_{bp} + \vec{w}_c + \vec{w}_d = 0. \quad (8.205)$$

Eq. 8.205 is a general form of the equilibrium of forces for a torque-and-drag model in three dimensions using vector notation. To obtain the corresponding scalar components, the first step is to calculate the derivatives with respect to the MD s and then take the dot products of the tangent, normal, and binomial vectors.

The force derivatives with respect to the MD s are as follows:

$$\frac{d(F_t \vec{t})}{ds} = \frac{dF_t}{ds} \vec{t} + F_t \frac{d\vec{t}}{ds} = \frac{dF_t}{ds} \vec{t} + F_t \kappa \vec{n}, \quad (8.206a)$$

$$\frac{d(F_n \vec{n})}{ds} = \frac{dF_n}{ds} \vec{n} + F_n \frac{d\vec{n}}{ds} = \frac{dF_n}{ds} \vec{n} + F_n (\tau \vec{b} - \kappa \vec{t}), \quad (8.206b)$$

$$\frac{d(F_b \vec{b})}{ds} = \frac{dF_b}{ds} \vec{b} + F_b \frac{d\vec{b}}{ds} = \frac{dF_b}{ds} \vec{b} + F_b (-\tau \vec{n}). \quad (8.206c)$$

Substituting the force components given by Eqs. 8.206a, 8.206b, and 8.206c and also Eqs. 8.174 and 8.175 into Eq. 8.172 and multiplying the resulting equation by the unit tangent, normal, and binormal vectors (taking the dot product) yields the following scalar force equilibrium equations:

t-component

$$\frac{dF_t}{ds} - \kappa F_n + w_{bp} \vec{t} \cdot \vec{k} + \vec{w}_d \cdot \vec{t} = 0; \quad (8.207a)$$

n-component

$$\frac{dF_n}{ds} + \kappa F_t - F_b \tau + w_{bp} \vec{n} \cdot \vec{k} + \vec{w}_d \cdot \vec{n} + \vec{w}_c \cdot \vec{n} = 0; \quad (8.207b)$$

b-component

$$\frac{dF_b}{ds} + F_n \tau + w_{bp} \vec{b} \cdot \vec{k} + \vec{w}_d \cdot \vec{b} + \vec{w}_c \cdot \vec{b} = 0. \quad (8.207c)$$

It should be noted that in addition to the pipe curvature κ in the force balance equations, the pipe torsion τ is also present. In conventional torque-and-drag analysis, it is assumed that the pipe follows the wellbore path; therefore, for practical calculations, the pipe curvature and torsion are usually assumed to be the same as the wellbore curvature and torsion.

Equilibrium of Moments. For a circular pipe with bending stiffness EI , the vector moment \vec{M} in the pipe is given by Eq. 8.176. Differentiating Eq. 8.176 with respect to s yields

$$\frac{d\vec{M}(s)}{ds} = EI \left(\frac{d\kappa}{ds} \vec{b} - \kappa \tau \vec{n} \right) + \frac{dM_t}{ds} \vec{t} + M_t \kappa \vec{n}. \quad (8.208)$$

The vector product of the unit tangent vector and the force in the pipe is

$$\vec{t} \times \vec{F} = \vec{t} \times (F_t \vec{t} + F_n \vec{n} + F_b \vec{b}) = F_n \vec{b} - F_b \vec{n}. \quad (8.209)$$

Substituting Eqs. 8.208 and 8.209 into Eq. 8.176 gives

$$\left(EI \frac{d\kappa}{ds} + F_n \right) \vec{b} + (M_t \kappa - EI \kappa \tau - F_b) \vec{n} + \frac{dM_t}{ds} \vec{t} + \vec{m} = \vec{0}. \quad (8.210)$$

Eq. 8.210 is a general form of the moment balance written in a vector differential form.

Note that Eq. 8.210 contains, not only pipe curvature and torsion, but also the change of curvature $\frac{d\kappa}{ds}$ along the pipe. Note further that all components in Eq. 8.210 have the dimension of force because they represent the moments per unit length of pipe.

To obtain the corresponding three scalar equations, Eq. 8.210 is multiplied by the unit tangent, normal, and binormal vectors (using the dot product).

The three scalar equations are as follows:

t -component

$$\frac{dM_t}{ds} + \vec{m} \cdot \vec{t} = 0; \quad \dots \quad (8.211a)$$

n -component

$$\kappa M_t - EI\kappa\tau - F_b + \vec{m} \cdot \vec{n} = 0; \quad \dots \quad (8.211b)$$

b -component

$$EI \frac{d\kappa}{ds} + F_n + \vec{m} \cdot \vec{b} = 0. \quad \dots \quad (8.211c)$$

In summary, a system of six scalar equations has been obtained that can be solved simultaneously to obtain the desired force and moment components along the pipe. Many practical problems can be solved by skillful application of Eqs. 8.207 and 8.211.

The rest of this chapter will consider some simpler but still useful cases, starting with the soft-string model in three-dimensional space.

8.6.4 Soft-String Model: 3D Formulation. Sliding-Pipe Model. As stated before, a soft-string model assumes that the pipe behaves as a flexible cable with no bending rigidity and no shear forces. In other words, the normal and binormal force components are nil ($F_n = 0$ and $F_b = 0$). A FBD for a pipe element in a sliding mode is shown in Fig. 8.78.

For the case of tripping operations (pipe sliding), the torque $M_t = 0$ along the string, and only the three force equilibria given by Eq. 8.207 are needed; these can be written as:

$$\frac{dF_t}{ds} + w_{bp}t_z + \vec{w}_d \cdot \vec{t} = 0, \quad \dots \quad (8.212a)$$

$$F_t\kappa + w_{bp}n_z + \vec{w}_c \cdot \vec{n} = 0, \quad \dots \quad (8.212b)$$

$$w_{bp}b_z + \vec{w}_c \cdot \vec{b} = 0, \dots \quad (8.212c)$$

where t_z , n_z , and b_z are the z -components of the unit tangential, normal, and binormal vectors as discussed in Section 8.4.

Applying Eqs. 8.183 and 8.184 gives

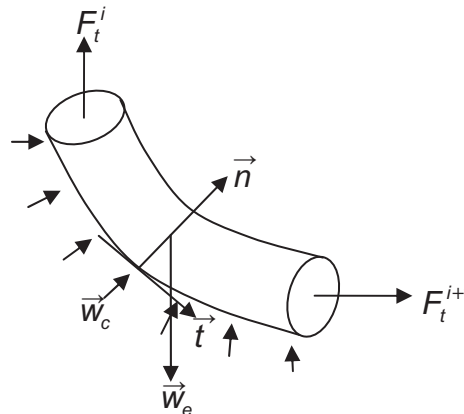


Fig. 8.78—Free-body diagram for a pipe in sliding mode—soft-string model.

$$\vec{w}_d \cdot \vec{t} = \pm \mu w_c, \quad \dots \quad (8.213a)$$

$$\vec{w}_c \cdot \vec{n} = w_c \cos \theta, \quad \dots \quad (8.213b)$$

$$\vec{w}_c \cdot \vec{b} = -w_c \sin \theta, \quad \dots \quad (8.213c)$$

where θ is the contact-force angle as shown in Fig. 8.77.

Substituting Eq. 8.213 into Eq. 8.212 gives

$$\frac{dF_t}{ds} + w_{bp} t_z \pm \mu w_c = 0, \quad \dots \quad (8.214a)$$

$$F_t \kappa + w_{bp} n_z + w_c \cos \theta = 0, \quad \dots \quad (8.214b)$$

$$w_{bp} b_z - w_c \sin \theta = 0. \quad \dots \quad (8.214c)$$

From Eqs. 8.214b and 8.214c, the following formulas can be obtained for the unit contact force (the side force) w_c and the direction angle θ :

$$w_c = \sqrt{(F_t \kappa + w_{bp} n_z)^2 + (w_{bp} b_z)^2}, \quad \dots \quad (8.215a)$$

$$\theta = \tan^{-1} \left(-\frac{w_{bp} b_z}{F_t \kappa + w_{bp} n_z} \right). \quad \dots \quad (8.215b)$$

Substituting Eq. 8.215a into Eq. 8.214a results in the following differential equation for calculating the effective pipe force for tripping operations:

$$\frac{dF_t}{ds} + w_{bp} t_z \pm \mu_f \sqrt{(F_t \kappa + w_{bp} n_z)^2 + (w_{bp} b_z)^2} = 0. \quad \dots \quad (8.216)$$

Because Eq. 8.216 is a first-order differential equation, only one boundary condition is needed to solve for the force along the pipe segment under consideration. If the pipe force at $s=s_i$ is known, the boundary condition is

$$F_t(s=s_i) = F_{s,i}, \quad \dots \quad (8.217)$$

where $F_{s,i}$ is the effective axial force at s_i .

It is also useful to represent the z -components of the unit vectors t_z , n_z , and b_z in terms of wellbore inclination as discussed in Section 8.4.

For the reader's convenience, these equations are repeated below:

$$t_z = \vec{t} \cdot \vec{k} = \cos \varphi, \quad \dots \quad (8.218a)$$

$$n_z = \vec{n} \cdot \vec{k} = -\frac{1}{\kappa} (\sin \varphi) \frac{d\varphi}{ds}. \quad \dots \quad (8.218b)$$

$$b_z = \vec{b} \cdot \vec{k} = \frac{1}{\kappa} \sin^2 \varphi \frac{d\vartheta}{ds}. \quad \dots \quad (8.218c)$$

Now consider the following practical example.

Example 8.32 Calculate the drag force in a segment of a wellbore between two directional surveys as given below:

MD, ft	Inclination Angle, degrees	Azimuth Angle, degrees
7,300	13.4	S65W
7,400	16.3	S75W

The axial force at the bottom of the segment is 30,000 lbf, the pipe unit weight in fluid is 15 lbf/ft, and the coefficient of friction is 0.3. The string is pulled out of the hole.

Solution. Assume a frictionless system (with the friction coefficient $\mu = 0$). Then, from Eq. 8.214a,

$$(a) \quad \frac{dF_t}{ds} + w_{bp} t_z = 0.$$

It is known that

$$(b) \quad t_z = \vec{t} \cdot \vec{k} = \frac{d\vec{r}}{ds} \cdot \vec{k}.$$

Substituting Line (b) into Line (a),

$$dF_t + w_{bp} d\vec{r} \cdot \vec{k} = 0.$$

It is further known that

$$(c) \quad d\vec{r} \cdot \vec{k} = \left[(dx)\vec{i} + (dy)\vec{j} + (dz)\vec{k} \right] \cdot \vec{k} = dz.$$

Substituting Line (c) into Line (b) and integrating yields

$$(d) \quad F_{t1} = F_{t2} + w_{bp} \Delta z.$$

Using the average-angle method as described in Section 8.1.7, it is possible to calculate $\Delta z = 96.7$ ft and then the force at the top of the segment:

$$(e) \quad F_{t1} = 30,000 + (15)(96.7) = 31,450 \text{ lbf}.$$

Now a first approximation of a unit contact force at the midpoint of the segment can be calculated using Eq. 8.215a. First, however, the hole curvature must be determined:

$$(f) \quad \kappa = \sqrt{\left(\frac{16.3 - 13.4}{100} \right)^2 + \sin^2(14.85) \left(\frac{255 - 265}{100} \right)^2} = (3.87)10^{-2} \text{°/ft}.$$

The z -components of the normal and binormal unit vectors can be calculated using Eqs. 8.218b and 8.218c:

$$(g) \quad n_z = -\frac{1}{(3.87)(10^{-2})} \sin(14.85) \left(\frac{2.9}{100} \right) = -0.192,$$

$$(h) \quad b_z = \frac{1}{(3.87)(10^{-2})} \sin^2(14.85) \left(\frac{10}{100} \right) = 0.1697.$$

Substituting Lines (e), (f), (g), and (h) into Eq. 8.215a yields

$$(i) \quad w_c = \sqrt{\left[31450(3.87 \times 10^{-2}) \left(\frac{\pi}{180} \right) + 15(-0.192) \right]^2 + [(15)(0.1697)]^2} = 18.5 \text{ lbf}$$

From Eq. 8.218a, the z -component of the tangent vector at the midpoint is

$$(j) \quad t_z = \cos(14.85) = 0.9666.$$

Substituting Lines (i) and (j) into Eq. 8.214a and integrating yields

$$(k) \quad \begin{aligned} F_{t,1} &= F_{t,2} + w_{bp} t_z \Delta s + \mu w_c \Delta s \\ &= 30,000 + (15)(0.9666)100 + (0.3)(18.5)(100) = 31,450 + 555 \text{ lbf.} \end{aligned}$$

Consequently, the force at the top of the segment is

$$F_{t,1} = 32,005 \text{ lbf.}$$

It should be noted that, as expected, the force obtained from Line (e) is the same as that obtained from Line (k) if $\mu = 0$. Now the direction angle θ of the unit contact force at the midpoint of the segment can be calculated as

$$\theta = \arctan \left(- \frac{(15)(0.1697)}{(31450)(3.87)(10^{-2}) \left(\frac{\pi}{180} \right) + 15(-0.192)} \right) = -7.9^\circ$$

The reader is invited to calculate a second approximation of the forces by repeating the steps described above and eventually writing a program to perform these calculations routinely.

Some alternative useful forms of the governing differential equation (Eq. 8.216) can be obtained by substituting Eq. 8.218 into Eq. 8.216:

$$\frac{dF_t}{ds} + w_{bp} \cos \varphi \pm \mu_f \sqrt{\left(F_t \kappa - \frac{w_e}{\kappa} \sin \varphi \frac{d\varphi}{ds} \right)^2 + \left(w_e \frac{1}{\kappa} \sin^2 \varphi \frac{d\vartheta}{ds} \right)^2} = 0. \quad \dots\dots\dots (8.219)$$

Recall that the quantities $\left(\frac{d\varphi}{ds} \right)$ and $\left(\frac{d\vartheta}{ds} \right)$ are the familiar build rate B and turn (walk) rate T , and that the wellbore curvature is

$$\kappa = \sqrt{\left(\frac{d\varphi}{ds} \right)^2 + \sin^2 \varphi \left(\frac{d\vartheta}{ds} \right)^2}. \quad \dots\dots\dots (8.220)$$

From Eqs. 8.219 and 8.220, after some rearrangements, the following form of the governing differential equation for soft-string model tripping operations can be obtained:

$$\frac{dF_t}{ds} + w_{bp} \cos \varphi \pm \mu_f \sqrt{\left(F_t \frac{d\varphi}{ds} - w_{bp} \sin \varphi \right)^2 + \left(F_t \sin \varphi \frac{d\vartheta}{ds} \right)^2} = 0. \quad \dots\dots\dots (8.221)$$

Eq. 8.221 is the same equation as that presented by Johancsik et al. (1983) and later on by Sheppard et al. (1986).

Note that if the turn rate is nil, the above model reduces to the 2D model discussed earlier in Section 8.5.2. Because the governing differential equation is nonlinear, it does not have an analytical solution, and therefore a numerical approach is required to obtain the pipe effective force along the string. Perhaps the most effective approach is to divide the well path into a number of small elements and carry out calculations in a stepwise manner starting from a point where the force is known.

8.6.5 Drag-Force Calculations for a Minimum-Curvature Well Path. When the wellbore trajectory is modeled using the minimum-curvature method, the z -components of the unit tangential, normal, and binormal vectors are as follows:

$$t_z = (\cos \varphi_1) \cos [\kappa (s - s_1)] + \left(\frac{\cos \varphi_2 - \cos \varphi_1 \cos \beta}{\sin \beta} \right) \sin [\kappa (s - s_1)], \quad \dots\dots\dots (8.222a)$$

$$n_z = (-\cos \varphi_1) \sin [\kappa (s - s_1)] + \left[\frac{\cos \varphi_2 - \cos \varphi_1 \cos \beta}{\sin \beta} \right] \cos [\kappa (s - s_1)], \quad \dots\dots\dots (8.222b)$$

$$b_z = \vec{b} \bullet \vec{k} = \frac{\sin \phi_1 \sin \phi_2 \sin(\vartheta_2 - \vartheta_1)}{\sin \beta} \quad (8.222c)$$

The derivations of Eq. 8.222 are presented in the solutions of Examples 8.24 and 8.25 of Section 8.4.4.

Analysis of Eq. 8.222 shows that if the wellbore inclination and azimuth angles are known at the initial (ϕ_1, ϑ_1) and final (ϕ_2, ϑ_2) points on the minimum-curvature trajectory, the z -component of the binormal vector is constant between the two points, but both t_z and n_z are nonlinear functions of the MD s . Consequently, it is impossible to provide a closed-form solution of Eq. 8.221, and a numerical approach is needed to calculate the drag force.

Although there are several possible options, in this section, the following sequence of calculations is proposed for the minimum-curvature trajectory:

1. Calculate the DL β .
2. Calculate the RF.
3. Calculate Δz , the vertical distance between the stations under consideration.
4. Using Eq. 8.222a, calculate the inclination angle at the midpoint of the trajectory.
5. Calculate the curvature κ .
6. Obtain the z -components t_z, n_z , and b_z at the midpoint of the trajectory using Eq. 8.222.
7. Set $F_t = F_b + w_{bp} \Delta z$ and obtain a first approximation for the unit contact force w_c^1 using Eq. 8.222a.
8. Calculate a first approximation of the axial force at the top of the segment under consideration:

$$F_t^1 = F_b \pm w_{bp} \Delta z + \mu w_c^1 \Delta s \quad (8.223)$$

9. Calculate the average value of the axial force:

$$F_t^a = \frac{F_b + F_t^1}{2}.$$

10. Obtain a second approximation of the unit contact force w_c^{11} using the axial force F_t^a as calculated above.
11. Calculate a second approximation of the axial force:

$$F_t^{11} = F_b \pm w_{bp} \Delta z + \mu w_c^{11} \Delta s.$$

12. Calculate the tolerance $\left| \frac{F_t^1 - F_t^{11}}{F_t^{11}} \right|$, and if the value is less than 1%, terminate the calculations; otherwise, repeat the calculations until the desired accuracy is achieved.

A practical implementation of this procedure is illustrated in Example 8.33.

Example 8.33 Consider a minimum-curvature segment of a wellbore with the parameters given below:

MD, ft	Inclination Angle, degrees	Azimuth Angle, degrees
6,750	30.9	78.2
7,050	43.2	100.6

The force at the bottom of the segment ($s = 7,050$ ft) is 25,000 lbf. The drillpipe size is 5 in., with an effective unit weight of 16 lbf/ft. Calculate the force at the top ($s = 6,750$ ft) of the segment if the pipe is being pulled out of the hole. The coefficient of friction is 0.3.

Solution. Calculate the DL β :

$$\beta = \arccos[(\sin 30.9)(\sin 43.2)\cos(100.6 - 78.2) + (\cos 30.9)(\cos 43.2)] = 18.1^\circ.$$

Calculate the RF:

$$\text{RF} = \frac{300}{0.3157} \tan\left(\frac{18.1}{2}\right) = 151.3 \text{ ft.}$$

Difference in vertical coordinates:

$$\Delta z = (\cos 30.9 + \cos 43.2)(151.3) = 240.1 \text{ ft.}$$

Inclination angle at the midpoint ($s = 6,900$ ft):

$$\cos \bar{\varphi} = 0.8036$$

hence,

$$\bar{\varphi} = 36.52^\circ$$

Calculate the curvature:

$$\kappa = \frac{1}{R} = \frac{18.1}{300} = 6.03^\circ/100 \text{ ft} = (1.052)10^{-3} \text{ ft}^{-1}.$$

Calculate t_z , n_z , and b_z (Eq. 8.222):

$$t_z = \cos 36.8 = 0.8036$$

$$n_z = -0.4018$$

$$b_z = 0.4312$$

Calculate a first approximation of the unit contact force using Eq. 8.218a:

$$w'_c = \sqrt{\left[(25,000 + 16(240.1))(1.052)(10^{-3}) + (16.0)(-0.4018) \right]^2 + \left[(16.0)(0.4312) \right]^2} = 24.9 \text{ lbf/ft.}$$

First approximation of the force at the top of the segment, $s = 6,750$ ft:

$$F'_{t,6,750} = 25,000 + (16.0)(240.1) + (0.3)(24.9)(300) = 31,081 \text{ lbf.}$$

Calculate the average force:

$$F_{t,a} = \frac{31,081 + 25,000}{2} = 28,041 \text{ lbf.}$$

Calculate a second approximation of the unit contact force:

$$w''_c = \sqrt{\left[(28,041)(1.052)(10^{-3}) + (16.0)(-0.4018) \right]^2 + 47.6} = 24.0 \text{ lbf/ft.}$$

Calculate a second approximation for the force at $s = 6,750$ ft:

$$F''_{t,6,750} = 25,000 + 3841.6 + (0.3)(24)(300) = 31,000 \text{ lbf.}$$

Clearly, the relative difference is less than 1%, and the last value can be accepted as the final answer.

For more-accurate calculations, the reader is encouraged to divide the segment into three parts, each 100 ft in length, and repeat the calculations. Useful closed-form solutions can be obtained if Eq. 8.221 is rewritten as follows:

$$\frac{dF_t}{ds} + w_{bp} \cos \varphi \pm \mu F_t \sqrt{\left(\frac{d\varphi}{ds} - \frac{w_{bp} \sin \varphi}{F_t} \right)^2 + \left(\sin \varphi \frac{d\vartheta}{ds} \right)^2} = 0. \quad (8.224)$$

If the term $\frac{d\varphi}{ds}$ is considerably greater than $\frac{w_{bp} \sin \varphi}{F_t}$, then Eq. 8.224 takes the form

$$\frac{dF_t}{ds} \pm \mu \kappa F_t = -w_{bp} \cos \varphi. \quad (8.225)$$

An analytical solution of Eq. 8.225 is possible because the wellbore curvature κ is constant and $\cos \varphi$ is given by Eq. 8.222a for the minimum-curvature method.

8.6.6 Drag-Force Calculations for a Constant Tool-Face Trajectory. For a wellbore trajectory with constant curvature and build rate ($\kappa = \text{constant}$ and $B = \text{constant}$), the tool-face angle γ is also constant, and the following sequence of calculations can be proposed to obtain the unit contact force and the drag force along the pipe:

1. Difference in z -coordinates between final and initial points on the trajectory:

$$\Delta z = \frac{1}{B}(\sin \varphi_2 - \sin \varphi_1)$$

2. Hole inclination angle at the midpoint of the trajectory = $\bar{\varphi} = \frac{1}{2}(\varphi_1 + \varphi_2)$.
3. Tool-face angle:

$$\cos \gamma = \frac{B}{\kappa}.$$

4. z -components of unit tangent, normal, and binormal vectors t_z, n_z, b_z :

$$t_z = \cos \bar{\varphi},$$

$$n_z = -\sin \bar{\varphi} \cos \gamma,$$

$$b_z = \sin \bar{\varphi} \sin \gamma.$$

5. First approximation of $F'_{t,1}$:

$$F'_{t,1} = F_{t,2} + w_{bp} \Delta z,$$

$$\bar{F}_{t,a} = \frac{F'_{t,1} + F_{t,2}}{2}.$$

6. First approximation of the unit contact force using Eq. 8.215a.
7. Second approximation of F''_t , etc.

Example 8.34 Consider a 3D segment of wellbore with a build rate and DLS of $B = 4.13^\circ/100$ ft, DLS = $6.07^\circ/100$ ft. Other data include:

Initial point:

$$\varphi_1 = 4.1^\circ, \vartheta_1 = 311.0^\circ$$

Final point:

$$\varphi_2 = 45.3^\circ, \vartheta_2 = 103.8^\circ$$

MD between the final and initial points:

$$\Delta s = 100 \text{ ft}$$

Force at the final point (bottom of the segment):

$$F = 50,000 \text{ lbf.}$$

Pipe unit weight in fluid:

$$w_{bp} = 15 \text{ lbf/ft}$$

Calculate the force at the top of the segment if the coefficient of friction $\mu = 0.3$.

Solution. Because the build rate is constant, the difference in z -coordinates between the final and initial points on the trajectory is

$$\Delta z = \frac{1}{B}(\sin \varphi_2 - \sin \varphi_1) = \frac{1}{4.13} \left(\frac{18,000}{\pi} \right) [\sin(45.3) - \sin(4.1)] = 887 \text{ ft.}$$

The hole inclination angle at the midpoint of the trajectory is

$$\bar{\varphi} = \frac{1}{2}(4.1 + 45.3) = 24.7^\circ$$

The cosine of the tool-force angle γ is

$$\cos \gamma = \frac{B}{\kappa} = \frac{4.13}{6.07} = 0.6804.$$

The z -components of the unit tangent, normal, and binormal vectors are

$$t_z = \cos \bar{\varphi} = 0.9081,$$

$$n_z = -\sin \bar{\varphi} \cos \gamma = -(0.4186)(0.6804) = -0.2848,$$

$$b_z = \sin \bar{\varphi} \sin \gamma = (0.4186)(0.7328) = 0.3067.$$

If the friction coefficient is ignored, a first approximation of the force at the top of the segment is

$$F'_{t_1} = F_2 + w_{bp} \Delta z = 50,000 + (887)(15) = 63,305 \text{ lbf},$$

and the “average” force is

$$\frac{50,000 + 63,305}{2} = 56,652 \text{ lbf}$$

Now a first approximation of the contact force w_c can be calculated as

$$w'_c = \sqrt{\left[(56,652)(1.059)(10^{-3}) + (15)(-0.2848) \right]^2 + \left[(15)(0.3067) \right]^2} = 55.9 \text{ lbf/ft}.$$

The next step involves calculation of a second approximation of the force at the top of the segment:

$$F''_{t_1} = F_2 + w_{bp} \Delta z + \mu w'_c \Delta s = 50,000 + (15)(887) + (0.3)(55.9)(1,000) = 80,075 \text{ lbf}.$$

A second approximation of the unit/constant force is

$$w''_c = 64.8 \text{ lbf},$$

and the corresponding force at the top of the segment is

$$F''_{t_1} = 82,735 \text{ lbf}.$$

The reader is invited to divide the segment into four parts and repeat the calculations.

8.6.7 Torque Calculations for the Soft-String Model. As the pipe rotates, the drag-force direction is opposite to the direction of pipe rotation in the $\bar{n} - \bar{b}$ plane, as shown schematically in **Fig. 8.79**. For the soft-string model, it is known that the shear force is nil ($F_n = 0$ and $F_b = 0$) and the bending stiffness $EI = 0$. Consequently, the general force (Eq. 8.207) and moment (Eq. 8.211) equilibrium equations reduce to

$$\frac{dF_t}{ds} + w_{bp} t_z = 0, \quad \dots \dots \dots (8.226a)$$

$$F_t \kappa + w_{bp} n_z + w_c \cos \theta + \mu w_c \sin \theta = 0, \quad \dots \dots \dots (8.226b)$$

$$w_{bp} b_z - w_c \sin \theta + \mu w_c \cos \theta = 0, \quad \dots \dots \dots (8.226c)$$

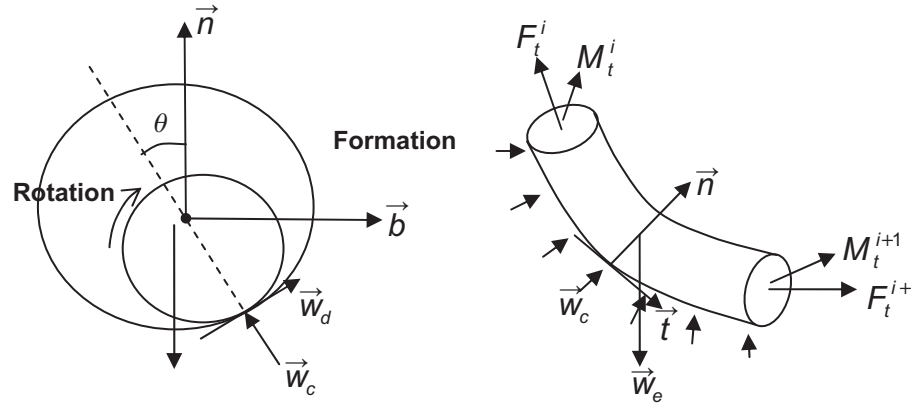


Fig. 8.79—Free-body diagram for the case of pipe rotation.

$$\frac{dM_t}{ds} - \mu w_c r_p = 0, \quad (8.226d)$$

$$M_t \kappa = 0. \quad (8.226e)$$

It is clear that the conceptual weakness of this model is that Eq. 8.226e cannot be satisfied. From Eqs. 8.226b and 8.226c, the unit contact force can be obtained as

$$w_c = \sqrt{\frac{(F_t \kappa + w_{bp} n_z)^2 + (w_{bp} b_z)^2}{1 + \mu^2}}, \quad (8.227a)$$

and the contact-force (side-force) direction angle is

$$\theta = \arctan \mu - \arctan \frac{w_{bp} b_z}{(F_t \kappa + w_{bp} n_z)}. \quad (8.227b)$$

Therefore, it can immediately be concluded that, in contrast to the sliding case, pipe rotation results not only in a decrease in the axial force, but also in the unit contact force, by the factor $\frac{1}{\sqrt{1 + \mu^2}}$,

which depends on the coefficient of friction. The same factor was calculated for the case of a straight inclined wellbore. The side-force direction angle θ is a function, not only of the friction coefficient, but also of the wellbore geometry, the pipe effective unit weight, and the magnitude of the drag force.

Now the model can be reduced to two equations:

$$\frac{dF_t}{ds} + w_{bp} t_z = 0, \quad (8.228a)$$

$$\frac{dM_t}{ds} - \frac{\mu r_p}{\sqrt{1 + \mu^2}} \sqrt{(F_t \kappa + w_{bp} n_z)^2 + (w_{bp} b_z)^2} = 0. \quad (8.228b)$$

If the force and torque are known at $(s = s_i)$, the required boundary conditions are

$$F_t(s = s_i) = F_{t,i}, \quad (8.229a)$$

$$M_t(s = s_i) = M_{t,i}. \quad (8.229b)$$

Eq. 8.226a can easily be integrated (see Example 8.33), but Eq. 8.228b requires a numerical solution because of the nonlinear nature of the expressions for the z -components (n_z and b_z) of the unit normal and binormal vectors.

For quick practical engineering calculations, approximations can be used, as illustrated in the following numerical example.

Example 8.35 Consider a wellbore segment as described in Example 8.33. The torque at the bottom of the segment is 4,750 ft-lbf. Calculate the torque at the top of the segment.

Solution. The magnitude of the force [Line (d) of Example 8.32] at the top of the segment is $F_{t,6,750} = 25,000 + (16)(240.1) = 28,842$ lbf, and a first approximation of a force at the midpoint is 26,921 lbf. Therefore, the corresponding unit contact force (Eq. 8.227a) is

$$w_c = \sqrt{\frac{\left[(26,921)(1.052)(10^{-3}) + (16)(-0.4,070) \right]^2 + \left[(16)(0.4,443) \right]^2}{1 + 0.3^2}} = 22.0 \text{ lbf/ft.}$$

From Eq. 8.228b, the change in the moment for the measured length change $\Delta s = 300$ ft can be calculated as

$$\Delta M_t = \mu r_p w_c \Delta s = (0.3) \left(\frac{5}{24} \right) (22.0)(300) = 412.5 \text{ ft-lbf.}$$

Hence, the torque at the top of the segment is 5162.5 ft-lbf. A more accurate solution can be obtained by dividing the segment into shorter elements.

8.6.8 Stiff-String Model for a Minimum-Curvature Trajectory. As discussed earlier, if the well path follows a minimum-curvature trajectory, the geometric torsion τ is nil, and the curvature is constant. Therefore, the change in the rate of curvature, $\frac{d\kappa}{ds}$, is also nil, and the equilibrium equations are as follows:

Equilibrium of forces:

$$\frac{dF_t}{ds} - F_n \kappa + w_{bp} t_z + (\pm \mu w_c) = 0, \quad \dots \quad (8.230a)$$

$$\frac{dF_n}{ds} + F_a \kappa + w_{bp} n_z + w_c \cos \theta = 0, \quad \dots \quad (8.230b)$$

$$\frac{dF_b}{ds} + w_{bp} b_z - w_c \sin \theta = 0. \quad \dots \quad (8.230c)$$

Equilibrium of moments:

$$\frac{dM_t}{ds} + \vec{m} \cdot \vec{t} = 0, \quad \dots \quad (8.231a)$$

$$M_t \kappa - F_b + \vec{m} \cdot \vec{n} = 0, \quad \dots \quad (8.231b)$$

$$F_n + \vec{m} \cdot \vec{b} = 0. \quad \dots \quad (8.231c)$$

If the pipe is sliding without rotation, the torque $M_t = 0$, and the applied unit moment \vec{m} is

$$\vec{m} = \vec{r}_p \times \vec{w}_d = (\pm \mu w_c r_p \cos \theta) \vec{b} - (\pm \mu w_c r_p \sin \theta) \vec{n}. \quad \dots \quad (8.232)$$

Taking the dot products of Eq. 8.232, the tangential, normal, and binormal components of the unit distributed moment can be obtained as:

$$\vec{m} \cdot \vec{t} = 0, \quad \dots \quad (8.233a)$$

$$\vec{m} \cdot \vec{n} = -\mu w_c r_p \sin \theta, \quad \dots \quad (8.233b)$$

$$\vec{m} \cdot \vec{b} = -\mu w_c r_p \cos \theta. \quad \dots \quad (8.233c)$$

Substituting Eqs. 8.233b and 8.233c into Eqs. 8.231a and 8.231b, the components of the shear force can be obtained as

$$-F_b - \mu r_p w_c \sin \theta = 0, \quad \dots \quad (8.234a)$$

$$F_n - \mu r_p w_c \cos \theta = 0. \quad \dots \quad (8.234b)$$

From Eqs. 8.234a and 8.234b, the magnitude and direction of the unit contact force are

$$w_c = \frac{\sqrt{F_n^2 + F_b^2}}{\mu_f r_p}, \quad \dots \quad (8.235a)$$

$$\theta = \tan^{-1} \left(-\frac{F_b}{F_n} \right). \dots \quad (8.235b)$$

Substituting Eqs. 8.234a, 8.234b, and 8.235a into Eq. 8.230 yields

$$\frac{dF_t}{ds} - \kappa F_n + w_{bp} t_z - \frac{\sqrt{F_n^2 + F_b^2}}{r_p} = 0, \quad \dots \quad (8.236a)$$

$$\frac{dF_n}{ds} + \kappa F_t + w_{bp} n_z + \frac{F_n}{\mu_f r_p} = 0, \quad \dots \quad (8.236b)$$

$$\frac{dF_b}{ds} + w_{bp} b_z + \frac{F_b}{\mu_f r_p} = 0. \quad \dots \quad (8.236c)$$

Eventually a system of three differential equations has been obtained, with three unknown forces, F_t , F_n , and F_b . Note that the pipe bending stiffness EI does not exist in this model because it was eliminated by the fundamental assumptions of constant curvature and zero torsion, which are valid for minimum-curvature trajectories. Three boundary conditions are needed to solve Eq. 8.236. The boundary conditions come from the interaction between the pipe segment under consideration and the parts of the string above or below it:

$$F_a(s = s_i) = F_a^i, \quad \dots \quad (8.237a)$$

$$F_n(s = s_i) = F_{n,i}, \quad \dots \quad (8.237b)$$

$$F_b(s = s_i) = F_{b,i}. \quad \dots \quad (8.237c)$$

Mitchell (2008) analyzed Eq. 8.236 and concluded that for a minimum-curvature trajectory, the most reasonable approach is to use as a first approximation the following value for the magnitude of the binormal component of the shear force:

$$F_b = -w_{bp} b_z \mu r_p \quad \dots \quad (8.238a)$$

The binormal component of the shear force can be considered to be constant along the minimum-curvature trajectory. If it can also be assumed that $\frac{dF_n}{ds}$ can be ignored in Eq. 8.236b, then

$$F_n = -\mu r_p (\kappa F_t + w_{bp} n_z). \quad \dots \quad (8.238b)$$

Substituting Eqs. 8.238a and 8.238b into Eq. 8.235a, it can be observed that the unit contact force is the same as that obtained for the soft-string model. In other words, for sliding pipe, the stiff-string model behaves like a soft string as far as the axial force is concerned, but with the shear forces given by Eqs. 8.238a and 8.238b.

Analysis of torque-and-drag problems for stiff strings and well trajectories involving torsion and variable DLS is beyond the scope of this text.

8.6.9 Review Questions and Problems.

1. Derive the equation for the static equilibrium of moments (Eq. 8.176).
2. Consider Eq. 8.176 and show that for a straight pipe segment in sliding mode (tripping in or out), the bending moment is nil.
3. A 4½-in. pipe with a unit weight of 15 lbf/ft is rotated in a horizontal straight section of wellbore. Calculate the unit contact force and its direction if the coefficient of friction is $\mu = 0.3$ and $\mu = 0.45$. Discuss the importance of the direction of the unit contact force (side force).
4. Explain why wellbore torsion does not exist in a 3D soft-string model.
5. Derive Eq. 8.215a for calculating the unit contact force for a 3D soft-string model.
6. Show that for a 2D well profile, the 3D model for a soft string reduces to the following equation for the case of tripping in:

$$\frac{dF_t}{ds} - \mu F_t \kappa + w_{bp} (\cos \varphi + \mu \sin \varphi) = 0$$

if

$$F_t \kappa - w_{bp} \sin \varphi > 0,$$

else

$$\frac{dF_t}{ds} + \mu F_t \kappa + w_{bp} (\cos \varphi - \mu \sin \varphi) = 0,$$

where $\varphi = \varphi_i + \kappa s$,

φ_i = the hole inclination angle at $s = s_i$.

7. Consider a well profile as described below:

Station	MD, ft	Inclination Angle, degrees	Azimuth Angle, degrees
1	3,000	55	0
2	3,055	60.7	4.1
3	3,110	66.4	7.7
4	3,165	72.2	11
5	3,220	78.1	14.1
6	3,275	84.1	17.1
7	3,330	90	20

The force at the bottom segment is $F_b = 10,000$ lbf, and the coefficient of friction is $\mu = 0.3$.

Calculate the expected force at the top of the segment ($s = 3,000$ ft) for tripping-out and tripping-in operations. The pipe unit weight in fluid is 17.5 lbf/ft. To carry out the calculations, assume a minimum-curvature well path between the stations.

8. Wellbore and drillstring data as in Problem 7 above. Calculate the rotary torque at the top of the segment if the torque at the bottom is 2,580 ft-lbf.
9. Wellbore and drillstring data as in Problem 7. Calculate axial force and torque at the top segment using the constant curvature and build rate method (constant tool-face angle, $\gamma = \text{constant}$).

10. Show that by solving Eq. 8.224 with the boundary condition at $s = s_2$ and the force $F_t = F_{t,2}$, the following result can be obtained:

$$F_t(s) = Ae^{\mu\kappa l} + B\cos(\varphi_2 - Bl) + C\sin(\varphi_2 - Bl),$$

where the quantities A , B , and C are

$$A = F_{t,2} - B\cos\varphi_2 - C\sin\varphi_2$$

$$B = -\frac{\mu w_{bp}\kappa}{B^2 + \mu^2\kappa^2},$$

$$C = -\frac{w_{bp}\kappa}{B^2 + \mu^2\kappa^2}$$

The quantity l is a length of wellbore measured from the endpoint, hence $l = s_2 - s$.

Verify the above equations and calculate the axial force at the top of a wellbore segment with build rate $B = 4.13^\circ/100$ ft and curvature DLS = $6.07^\circ/100$ ft. The hole inclination angle at the bottom end is 45.3° , and the length of the segment is 1,000 ft. The force at the bottom is $F_{t,2} = 50,000$ lbf and the friction coefficient is $\mu = 0.3$. The pipe unit weight in fluid is 15 lbf/ft. Assume that the pipe is being tripped out of the hole.

11. Consider a segment of a horizontal wellbore (a wellbore path confined to a horizontal plane) with constant curvature κ . The string's unit weight in fluid is w_{bp} . Assuming the soft-string model, develop an equation for calculating the unit contact force if the tension in the string is F_t .
12. Consider a segment of a horizontal wellbore as described in Problem 11 above. The length of the segment is 450 ft, and the force applied at the lower end is 8,000 lbf (in tension). Assuming that the coefficient of friction is $\mu = 0.27$, the pipe unit weight = 16 lbf/ft, and the turn rate = $21^\circ/100$ ft, calculate the pulling force at the top of the segment.

Nomenclature

A	=	flow area, in. ²
A_e	=	outer pipe area enclosed by nominal OD, in. ²
A_i	=	inner pipe area enclosed by nominal ID, in. ²
A_s	=	steel cross-sectional area, in. ²
A_x, A_y, A_z	=	cubic interpolation constants
\vec{b}	=	binormal direction vector
b_{iz}	=	component of binormal vector in the z coordinate direction
B	=	build rate
B_L	=	lateral curvature
B_v	=	vertical curvature
B_x, B_y, B_z	=	cubic interpolation constants
c	=	dimensionless radial clearance
c_{st}	=	stabilizer radial clearance, m
C	=	constant in force equation
$C_{1a}, C_{1b}, C_{2a}, C_{2b}, C_{3a}, C_{3b}$	=	coefficients in stabilizer calculation
C_x, C_y, C_z	=	cubic interpolation constants
dl	=	horizontal projection of ds
d_r	=	rotor diameter
ds	=	differential MD
dx, dy, dz	=	differential length in the x, y, z coordinate directions
D_h	=	diameter of wellbore, m
$D_{O, stb}$	=	outside diameter of stabilizer
D_x, D_y, D_z	=	cubic interpolation constants
e	=	eccentricity
E	=	Young's modulus of elasticity, psi
F	=	force, lbf
F_b	=	shear force in binormal direction, lbf
$F_{cr, s}$	=	critical buckling force in a straight wellbore, lbf

F_h	=	hook load, lbf
F_n	=	shear force in normal direction, lbf
F_r	=	stability load, lbf
F_t	=	force in the tangent direction, lbf
h	=	anisotropic index
h_0	=	dimensionless side force
h_{stb}	=	dimensionless side force at the stabilizer
\vec{h}	=	horizontal vector
H	=	horizontal turn rate
\bar{H}	=	average horizontal turn rate
H_0	=	side force on bit
H_{stb}	=	side force at the stabilizer
\vec{i}	=	north coordinate vector
I	=	moment of inertia
ID _{dc}	=	drill collar inside diameter, in.
\vec{j}	=	east coordinate vector
\vec{k}	=	downward vertical vector
\bar{K}	=	curvature vector
ℓ	=	dimensionless distance to point of tangency
L	=	length from bit to point of tangency
m_1, m_2, m_3	=	scaling factors
M	=	torque
M_{cd}	=	torque due to contact drag forces
M_{db}	=	torque at drill bit
M_{\max}	=	maximum torque
M_t	=	torque at rotary table
M_{vd}	=	torque due to viscous drag
n_1, n_2, n_3	=	scaling factors
\vec{n}	=	normal direction vector
n_{iz}	=	x component of normal vector at point i
n_r	=	$n_s - 1$
n_s	=	number of lobes in motor
N	=	motor rotary speed
N_{ra}	=	runaway motor rotary speed
OD _{dc}	=	drill collar outside diameter, in.
p	=	pitch of helix, ft
p_r	=	rotor pitch
P	=	power, hp
P_i	=	points on a trajectory
Q	=	flow rate, gal/min
r	=	radius, in.
\vec{r}	=	displacement vector, ft
r_c	=	radial clearance, in.
r_d	=	dimensionless radius of curvature
r_p	=	radius of the pipe, in.
r_s	=	stabilizer radial clearance, in.
R	=	radius of curvature, ft
s	=	measured depth, equivalent to arc length
s_{target}	=	measured depth to target
\vec{S}	=	shear force
S-U	=	special coordinate system for slick assembly analysis (see Fig. 8.25)
\vec{t}	=	axial direction vector, tangent vector
t_{iz}	=	component of the tangent vector in the x coordinate direction
T	=	azimuth turn rate
\bar{T}	=	average azimuth turn rate

v	= unit right-side vector
w	= weight per foot
\bar{w}_c	= contact force load vector
w_d	= friction force vector
w_{bp}	= buoyant weight per foot of pipe
w_c	= contact force magnitude
W	= weight of drill collars in mud
W_{BHA}	= weight of BHA
W_{dp}	= weight of drillpipe
x, y, z	= conventional (right-hand) rectangular system of coordinates consistent with the north, east, and vertical directions, N, E, and V
z	= true vertical depth
β	= angle change between survey points
β^*	= actual achieved deflection angle
γ	= tool face angle
γ_f	= formation dip angle
δ	= tilt angle
δ_d	= dimensionless tilt angle
$\Delta\epsilon$	= change in hole direction
Δp	= pressure increment
Δx	= change in position in the x coordinate direction
Δy	= change in position in the y coordinate direction
Δz	= change in position in the z coordinate direction
Δs	= increment of MD
ΔL	= length change
ϵ	= angle of original hole with respect to the south direction
η	= efficiency
θ	= angle defining the direction of the contact load
κ	= curvature
μ	= friction coefficient
ξ	= turn rate direction (+ if positive, – if negative)
τ	= geometric torsion of a curve
φ	= angle of inclination of the wellbore
$\bar{\varphi}$	= average angle of inclination
φ_n	= new angle of inclination
Φ	= resultant force angle
ψ	= instantaneous direction of drilling
ω	= angular velocity
ϑ	= azimuth angle
$\bar{\vartheta}$	= average azimuth angle

Abbreviations

BHA	bottomhole assembly
DT	departure of target
DL	overall angle change, dogleg
DLS	dogleg severity
ERD	extended reach drilling
HD	horizontal departure
HP	hydraulic horsepower
KOP	kickoff point
MD	measured depth
MCM	minimum curvature method
MWD	measurement while drilling

PDM	positive displacement motor
RCLS	rotary closed-loop system
RCM	radius-of-curvature method
RKB	rotary kelly bushing
RF	ratio factor
RSS	rotary-steerable system
SM	steerable motors
TVD	true vertical depth
WOB	weight on bit
WOC	Water-oil-contact

References

- AGS (Adjustable Gauge Stabilizer) Tool. 2010. Halliburton, http://www.halliburton.com/premium.aspx?content=/premium/ss/contents/Data_Sheets/web/H02487-A4.pdf. Downloaded 8 November 2010, Fig. HAL 14069.
- Bourgoyne, A.T., Millheim, K.K., Chenevert, M.E., and Young, F.S. Jr. 1986. *Applied Drilling Engineering*, first printing. Richardson, Texas, USA: Society of Petroleum Engineers.
- Callas, N.P. and Callas, R.L. 1980. Boundary Value Problem is Solved. *Oil & Gas J.* (15 December 1980): 62–66.
- Dawson, R. and Pasley, P.R. 1984. Drill Pipe Buckling in Inclined Holes. *J Pet Technol* **36** (10): 1734–1738. SPE-11167-PA. DOI: [10.2118/11167-PA](https://doi.org/10.2118/11167-PA).
- Duman, O.B., Miska, S., and Kuru, E. 2003. Effect of Tool Joints on Contact Force and Axial-Force Transfer in Horizontal Wellbores. *SPE Drill & Compl* **18** (3): 267–274. SPE-85775-PA. DOI: [10.2118/85775-PA](https://doi.org/10.2118/85775-PA).
- Fischer, F.J. 1974. Analysis of Drillstrings in Curved Boreholes. Paper SPE 5071 presented at the SPE Annual Meeting, Houston, October 6–9. DOI: [10.2118/5071-MS](https://doi.org/10.2118/5071-MS).
- Guo, B., Miska, S., and Lee, R.L. 1992. Constant Curvature Method for Planning a 3-D Directional Well. Paper SPE 24381 presented at the SPE Rocky Mountain Regional Meeting, Casper, Wyoming, 18–21 May. DOI: [10.2118/24381-MS](https://doi.org/10.2118/24381-MS).
- Ho, H.-S. 1986. General Formulation of Drillstring Under Large Deformation and Its Use in BHA Analysis. Paper SPE 15562 presented at the SPE Annual Technical Conference and Exhibition, New Orleans, 5–8 October. DOI: [10.2118/15562-MS](https://doi.org/10.2118/15562-MS).
- Inglis, T.A. 1987. *Directional Drilling*. London: Graham and Trotman.
- Johancsik, C.A., Friesen, D.B., and Dawson, R. 1983. Torque and Drag in Directional Wells—Prediction and Measurement. *J Pet Technol* **36** (6): 987–992. SPE-11380-PA. DOI: [10.2118/11380-PA](https://doi.org/10.2118/11380-PA).
- Lesso, W.G., Rezmer-Cooper, I.M., and Chau, M. 2001. Continuous Direction and Inclination Measurements Revolutionize Real-Time Directional Drilling Decision-Making. Paper SPE 67752 presented at the SPE/IADC Drilling Conference, Amsterdam, 27 February–1 March. DOI: [10.2118/67752-MS](https://doi.org/10.2118/67752-MS).
- Lubinski, A. and Woods, H.B. 1955. Use of Stabilizers in Controlling Hole Deviation. *API Drilling and Production Practice*, Vol. 165. Washington, DC: API.
- Lubinski, A. 1987. *Developments in Petroleum Engineering, Vol. 1: Stability of Tubulars, Deviation Control*. Ed. Stefan Miska. Houston: Gulf Publishing Company.
- McMillian, W.M. 1981. Planning the Directional Well—A Calculation Method. *J Pet Technol* **33** (6): 952–962. SPE-8337-PA. DOI: [10.2118/8337-PA](https://doi.org/10.2118/8337-PA).
- Maidla, E. and Haci, M. 2004. Understanding Torque: The Key to Slide-Drilling Directional Wells. Paper SPE 87162 presented at the IADC/SPE Drilling Conference, Dallas, 2–4 March. DOI: [10.2118/87162-MS](https://doi.org/10.2118/87162-MS).
- Millheim, K.K., Jordan, S., and Ritter, C.J. 1978. Bottom-Hole Assembly Analysis Using the Finite-Elements Method. *J Pet Technol* **30** (2): 265–274. SPE-6057-PA. DOI: [10.2118/6057-PA](https://doi.org/10.2118/6057-PA).
- Millheim, K.K., Gubler, F.H., and Zaremba, H.B. 1979. Evaluating and Planning Directional Wells Utilizing Post Analysis Techniques and a Three Dimensional Bottom Hole Assembly Program. Paper SPE 8339 presented at the SPE Annual Technical Conference and Exhibition, Las Vegas, Nevada, USA, 23–26 September. DOI: [10.2118/8339-MS](https://doi.org/10.2118/8339-MS).
- Miska, S. and Miska, W. 2006. Modeling of Complex Bottom Hole Assemblies in Curved and Straight Holes. *Archives of Mining Sciences* **51** (1): 35–54.
- Miska, S., Rajtar, J., and Luo, F. 1998. Type Curves for Predicting Directional Tendencies of Simple Bottom-Hole Assemblies. *J. of Energy Resources Technology* **20** (3): 193–201.

- Mitchell, R.F. 2008. Drillstring Solutions Improve the Torque-Drag Model. Paper SPE 112623 presented at the IADC/SPE Drilling Conference, Orlando, Florida, USA, 4–6 March. DOI: [10.2118/112623-MS](https://doi.org/10.2118/112623-MS).
- Planeix, M.Y. and Fox, R.C. 1979. Use of an Exact Mathematical Formulation to Plan Three Dimensional Directional Wells. Paper SPE 8338 presented at the SPE Annual Technical Conference and Exhibition, Las Vegas, Nevada, USA, 23–26 September. DOI: [10.2118/8338-MS](https://doi.org/10.2118/8338-MS).
- Rivero, R.T. 1971. Use of the Curvature Method to Determine True Vertical Reservoir Thickness. *J Pet Technol* **23** (4): 491–496. SPE-3076-PA. DOI: [10.2118/3076-PA](https://doi.org/10.2118/3076-PA).
- Sampaio J.H.B. Jr. 2007. Planning 3D Well Trajectories Using Spline-in-Tension Function. *J. of Energy Resources Technology* **129** (4): 289–300.
- Sawaryn, S.J. and Thorogood, J.L. 2003. A Compendium of Directional Calculations Based on the Minimum Curvature Method. Paper SPE 84246 presented at the SPE Annual Technical Conference and Exhibition, Denver, 5–8 October. DOI: [10.2118/84246-MS](https://doi.org/10.2118/84246-MS).
- Scholes, H. 1983. A Three-Dimensional Well Planning Method for HDR Geothermal Wells. Paper SPE 12101 presented at the SPE Annual Technical Conference and Exhibition, San Francisco, 5–8 October. DOI: [10.2118/12101-MS](https://doi.org/10.2118/12101-MS).
- Schuh, F.J. 1992. Trajectory Equations for Constant Tool Face Angle Deflections. Paper SPE 23853 presented at the SPE/IADC Drilling Conference held in New Orleans, 18–21 February. DOI: [10.2118/23853-MS](https://doi.org/10.2118/23853-MS).
- Sheppard, M.C., Wick, C., and Burgess, T.M. 1987. Designing Well Paths To Reduce Drag and Torque. *SPE Drill Eng* **2** (4): 344–350. SPE-15463-PA. DOI: [10.2118/15463-PA](https://doi.org/10.2118/15463-PA).
- Taylor, H.L. and Mason, M.C. 1972. A Systematic Approach to Well Surveying Calculations. *SPE J.* **12** (6): 474–488. SPE-3362-PA. DOI: [10.2118/3362-PA](https://doi.org/10.2118/3362-PA).
- Underwood, L.D. and Payne, M.L. 1997. Directional Drilling. In *Petroleum Well Construction*, ed. M.J. Economides, L.T. Watters, and S. Dunn-Norman. Chapter 2. Chichester, New York: John Wiley and Sons.
- Warren, T. 1998. Technology Gains Momentum. *Oil & Gas J.* **96** (51): 101–105.
- Warren, T. 2006. Steerable Motors Hold Their Own Against Rotary Steerable Systems. Paper SPE 104268 presented at the SPE Annual Technical Conference and Exhibition, San Antonio, Texas, USA, 24–27 September. DOI: [10.2118/104268-MS](https://doi.org/10.2118/104268-MS).
- Wilson, G.J. 1968. An Improved Method for Computing Directional Surveys. *J Pet Technol* **20** (8): 871–876. SPE-1992-PA. DOI: [10.2118/1992-PA](https://doi.org/10.2118/1992-PA).
- Woods, H.B. and Lubinski, A. 1953. Factors Affecting the Angle of Inclination and Doglegging in Rotary Bore Holes. *API Drilling and Production Practice*, Vol. 222. Washington, DC: API.
- Wu, M. and Chen, D.C.-K. 2006. A Generic Solution to Bottomhole-Assembly Modeling. Paper SPE 101186 presented at the SPE Annual Technical Conference and Exhibition, San Antonio, Texas, USA, 24–27 September. DOI: [10.2118/101186-MS](https://doi.org/10.2118/101186-MS).
- Zaremba, W.A. 1973. Directional Survey by the Circular Arc Method. *SPE J.* **13** (1): 5–11. SPE-3664-PA. DOI: [10.2118/3664-PA](https://doi.org/10.2118/3664-PA).

Further Reading and Advanced Topics

- Aadnoy, B.S. 2006. *Mechanics of Drilling*. Aachen, Germany: Shaker Verlag.
- Aadnoy, B.S. and Andersen, K. 1998. Friction Analysis for Long Reach Wells. Paper SPE 39391 presented at the IADC/SPE Drilling Conference, Dallas, 3–6 March. DOI: [10.2118/39391-MS](https://doi.org/10.2118/39391-MS).
- Aadnoy, B.S., Fabiri, V.T., and Djuhuus, J. 2006. Construction of Ultralong Wells Using a Catenary Well Profile. Paper SPE 98890 presented at the IADC/SPE Drilling Conference, Miami, Florida, USA, 21–23 February. DOI: [10.2118/98890-MS](https://doi.org/10.2118/98890-MS).
- Aleksandrov, M.M. 1959. Quantitative Evaluation of Frictional Force During Movement of the Tool in a Deviated Hole. *Izvest. Vysshikh Ucheb. Zaved., Nefti Gaz.* **2** (4): 41–48.
- An Engineering Approach to Horizontal Drilling*. 1992. Houston, Texas: Sperry Sun Drilling Services.
- Azar, J.J. and Samuel, G.R. 2007. *Drilling Engineering*. Tulsa: Pennwell Corporation.
- Barr, J.D., Clegg, J.M., and Russell, M.K. 1995. Steerable Rotary Drilling With an Experimental System. Paper SPE 29382 presented at the SPE/IADC Drilling Conference, Amsterdam, 28 February–2 March. DOI: [10.2118/29382-MS](https://doi.org/10.2118/29382-MS).
- Beaton, T., Seale, R., Van Den Bos, M., Salomons, G., and Strang, G. 2004. Applications and Case Histories of Geared Turbodrilling in the North Sea. Paper SPE 87970 presented at the IADC/SPE Asia Pacific Drilling Technology Conference and Exhibition, Kuala Lumpur, 13–15 September. DOI: [10.2118/87970-MS](https://doi.org/10.2118/87970-MS).
- Callas, N.P. 1981. Deviation Control for Bored-Raise Pilot Holes. United States Department of the Interior, Bureau of Mines, REPT-082-470.

- Chen, H. Miska, S., and Mitchell, R.F. 2003. Prediction of Transient Wellbore Trajectory Under Anisotropic Drilling Conditions. *Wiertnictwo Nafta Gaz* **20** (2): 317–329.
- Dareing, D.W. and Ahlers, C.A. 1991. Tubular Bending and Pull-Out Forces in High-Curvature Wellbores. *J. of Energy Resources Technology* **113** (2): 133–140.
- Dyna-Drill Handbook*, third edition. 1982. Long Beach, California, USA: Smith International.
- Eck-Olsen, J., Drevdal, K.E., Samuelli, J., and Reynolds, J. 1995. Designer Drilling Increases Recovery. *World Oil* **216** (4): 55–60, Fig. 2.
- Feenstra, R. and Kamp, A.W. 1984. A Technique for Continuously Controlled Directional Drilling. IADC Drilling Technology Conference Transactions: pp 11–28, Houston, 19–21 March.
- Frenzel, M. and Kull, B.J. 2008. Dynamic Balancing of Bit/Reamer Cutters Improves Drilling Performance. *World Oil* (March 2008): 68–72.
- Gaynor, T., Chen, D.C.-K., Maranuk, C., and Pruitt, J. 2000. An Improved Steerable System: Working Principles, Modeling, and Testing. Paper SPE 63248 presented at the SPE Annual Technical Conference and Exhibition, Dallas, 1–4 October. DOI: [10.2118/63248-MS](https://doi.org/10.2118/63248-MS).
- Hertfelder, G.P., Menge, M., Patel, M., and Ruszka, J. 2008. Complex Extended-Reach Drilling to Exploit Reservoirs in Environmentally Sensitive Area, Offshore California. Paper SPE 111647 presented at the IADC/SPE Drilling Conference, Orlando, Florida, USA, 4–6 March. DOI: [10.2118/111647-MS](https://doi.org/10.2118/111647-MS).
- Ho, H.-S. 1988. An Improved Modeling Program for Computing the Torque and Drag in Directional and Deep Wells. Paper SPE 18047 presented at the SPE Annual Technical Conference and Exhibition, Houston, 2–5 October. DOI: [10.2118/18047-MS](https://doi.org/10.2118/18047-MS).
- Lesage, M., Falconer, I.G., and Wick, C.J. 1988. Evaluating Drilling Practice in Deviated Wells With Torque and Weight Data. *SPE Drill Eng* **3** (3): 248–252. SPE-16114-PA. DOI: [10.2118/16114-PA](https://doi.org/10.2118/16114-PA).
- Lesso, W.G. Jr., Mullens, E., and Daudey, J. 1989. Platform Strategy and Predicting Torque Losses for Modeled Directional Wells in the Amauligak Field of the Beaufort Sea, Canada. Paper SPE 19550 presented at the SPE Annual Technical Conference and Exhibition, San Antonio, Texas, USA, 8–11 October. DOI: [10.2118/19550-MS](https://doi.org/10.2118/19550-MS).
- Lubinski, A. 1963. Frictional Forces Acting on a Drilling String Being Lowered Into or Pulled Out of a Deviated Hole. Tulsa: Pan American Petroleum Corporation.
- Maidla, E., Hacı, M., Jones, S., Cluchey, M., Michael, A., and Warren, T. 2005. Field Proof of the New Sliding Technology for Directional Drilling. Paper SPE 92558 presented at the SPE/IADC Drilling Conference, Amsterdam, 23–25 February. DOI: [10.2118/92558-MS](https://doi.org/10.2118/92558-MS).
- Mason, C.J., Allen, F.M., Ramirez, A.A., Wolfson, L., and Tapper, R. 1999. Casing Running Milestones for Extended-Reach Wells. Paper SPE 52842 presented at the IADC/SPE Drilling Conference, Amsterdam, 9–11 March. DOI: [10.2118/52842-MS](https://doi.org/10.2118/52842-MS).
- Mason, C.J. and Chen, D.C.-K. 2007. Step Changes Needed To Modernize T&D Software. Paper SPE 104609 presented at the SPE/IADC Drilling Conference, Amsterdam, 20–22 February. DOI: [10.2118/104609-MS](https://doi.org/10.2118/104609-MS).
- Millheim, K.K. and Warren, T.M. 1978. Side Cutting Characteristics of Rock Bits and Stabilizers While Drilling. Paper SPE 7518 presented at the SPE Annual Technical Conference and Exhibition, Houston, 1–3 October. DOI: [10.2118/7518-MS](https://doi.org/10.2118/7518-MS).
- Mills, P.G. 1986. *Deviated Drilling*. Boston: International Human Resources Development Corporation.
- Miska, S. and Cunha, J.C. 1995. An Analysis of Helical Buckling of Tubulars Subjected to Axial and Torsional Loading in Inclined Wellbore. Paper SPE 29460 presented at the SPE Production and Operations Symposium, Oklahoma City, Oklahoma, USA, 2–4 April. DOI: [10.2118/29460-MS](https://doi.org/10.2118/29460-MS).
- Miska, S., Qiu, W., Volk, L., and Cunha, J.C. 1996. An Improved Analysis of Axial Force Along Coiled Tubing in Inclined/Horizontal Wellbores. Paper SPE 37056 presented at the SPE International Conference on Horizontal Well Technology, Calgary, 18–20 November. DOI: [10.2118/37056-MS](https://doi.org/10.2118/37056-MS).
- Mitchell, R. and Miska, S. 2006. Helical Buckling of Pipe With Connectors and Torque. *SPE Drill & Compl* **21** (2): 108–115. SPE-87205-PA. DOI: [10.2118/87205-PA](https://doi.org/10.2118/87205-PA).
- Mitchell, R.F. 2006. Tubing Buckling—The State of the Art. Paper SPE 104267 presented at the SPE Annual Technical Conference and Exhibition, San Antonio, Texas, USA, 24–27 September. DOI: [10.2118/104267-MS](https://doi.org/10.2118/104267-MS).
- Mitchell, R.F. and Samuel, R. 2007. How Good is the Torque-Drag Model? Paper SPE 105068 presented at the IADC/SPE Drilling Conference, Amsterdam, 20–22 February. DOI: [10.2118/105068-MS](https://doi.org/10.2118/105068-MS).
- Moody, M. and Jones, S. 2004. Development and Field-Testing of a Cost Effective Rotary Steerable System. Paper SPE 90482 presented at the SPE Annual Technical Conference and Exhibition, Houston, 26–29 September. DOI: [10.2118/90482-MS](https://doi.org/10.2118/90482-MS).
- Murphey, C.E. and Cheatham, J.B. 1966. Hole Deviation and Drill String Behavior. *SPE J.* **6** (1) 44–54. SPE-1259-PA. DOI: [10.2118/1259-PA](https://doi.org/10.2118/1259-PA).

- Odell, A.C. II, Payne, M.L., and Cocking, D.A. 1995. Application of a Highly Variable Gauge Stabilizer at Wytch Farm to Extend the ERD Envelope. Paper SPE 30462 presented at the SPE Annual Technical Conference and Exhibition, Dallas, 22–25 October. DOI: [10.2118/30462-MS](https://doi.org/10.2118/30462-MS).
- Paslay, P.R. 1994. Stress Analysis of Drillstrings. Paper SPE 27976 presented at the SPE/University of Tulsa Centennial Petroleum Engineering Symposium, Tulsa, 29–31 August. DOI: [10.2118/27976-MS](https://doi.org/10.2118/27976-MS).
- Payne, M.L. and Abbassian, F. 1997. Advanced Torque-and-Drag Considerations in Extended-Reach Wells. *SPE Drill & Compl* **12** (1): 55–62. SPE-35102-PA. DOI: [10.2118/35102-PA](https://doi.org/10.2118/35102-PA).
- Qui, W., Miska, S., and Volk, L. 1999. Effect of Coiled Tubing Initial Configuration on Buckling Behavior in a Constant-Curvature Hole. *SPE J.* **4** (1): 64–71. SPE-55682-PA. DOI: [10.2118/55682-PA](https://doi.org/10.2118/55682-PA).
- Samuel, G.R. 2007. *Downhole Drilling Tools*. Houston: Gulf Publishing Company.
- Schaaf, S., Pafitis, D., and Guichemerre, E. 2000. Application of a Point the Bit Rotary Steerable System in Directional Drilling Prototype Well-bore Profiles. Paper SPE 62519 presented at the SPE/AAPG Western Regional Meeting, Long Beach, California, USA, 19–23 June. DOI: [10.2118/62519-MS](https://doi.org/10.2118/62519-MS).
- Schuh, F.J. 1989. Horizontal Well Planning—Build Curve Design. Paper NMT 890008 presented at the Centennial Symposium on Petroleum Technology in the Second Century at New Mexico Tech, Socorro, New Mexico, USA, 16–19 October.
- Thorogood, J.L. and Sawaryn, S.J. 1991. The Traveling-Cylinder Diagram: A Practical Tool for Collision Avoidance. *SPE Drill Eng* **6** (1): 31–36. SPE-19989-PA. DOI: [10.2118/19989-PA](https://doi.org/10.2118/19989-PA).
- Tiraspolsky, W. 1985. *Hydraulic Downhole Motors*. Paris: Editions Technip, 220 (Fig. 149).
- Walker, B.H. 1973. Some Technical and Economic Aspects of Stabilizer Placement. *J Pet Technol* **25** (6): 663–672. SPE-4263-PA. DOI: [10.2118/4263-PA](https://doi.org/10.2118/4263-PA).
- Walstrom, J.E., Harvey, R.P., and Eddy, H.D. 1972. A Comparison of Various Directional Survey Models and an Approach to Model Error Analysis. *J Pet Technol* **24** (8): 935–943. SPE-3379-PA. DOI: [10.2118/3379-PA](https://doi.org/10.2118/3379-PA).
- Yonezawa, T., Cargill, E., Gaynor, T., Hardin, J.R. Jr., Hay, R., Ikeda, A., and Kiyosawa, Y. 2002. Robotic Controlled Drilling: A New Rotary Steerable Drilling System for the Oil and Gas Industry. Paper SPE 74458 presented at the IADC/SPE Drilling Conference, Dallas, 26–28 February. DOI: [10.2118/74458-MS](https://doi.org/10.2118/74458-MS).

SI Metric Conversion Factors

ft	×	3.048*	E – 01 = m
ft ²	×	9.290 304*	E – 02 = m ²
ft ³	×	2.831 685	E – 02 = m ³
gal	×	3.785 412	E – 03 = m ³
hp	×	7.460 43	E – 01 = kW
hp-hr	×	2.684 520	E + 00 = MJ
in.	×	2.54*	E + 00 = cm
in. ²	×	6.451 6*	E + 00 = cm ²
lbf	×	4.448 222	E + 00 = N
lbm	×	4.535 924	E – 01 = kg

*Conversion factor is exact.

Page Intentionally Left Blank

Please Keep Scrolling To Continue

Chapter 9

Fundamentals of Drillstring Design

Stefan Miska, University of Tulsa

The objective of this chapter is to present the fundamentals of drillstring design. Included in this chapter are descriptions of the components of a drillstring, determination of the forces and moments in the drillstring, the effect of wellbore pressures on drillstring forces, and overall drillstring design.

9.1 Introduction

The drillstring (drillstem) is the major component of a rotary drilling system. The typical drillstring consists of a kelly, a drillpipe with tool joints, drill collars, and stabilizers. The part of the drillstring above the bit is called the *bottomhole assembly* (BHA). **Fig. 9.1** illustrates the usual arrangement of drillstring components. The bit is attached to the drill collars by means of a bit sub. In conventional rotary drilling, the rotary motion produced by a rotary table is transmitted to the drillpipe by a square or hexagonal pipe called the *kelly*. For effective rock destruction, the lower part of the drill collars is slacked off onto the drill bit to provide the so-called *weight on bit* (WOB). Cuttings generated by the rock bit are removed from the bottom of the hole by the *drilling fluid*, which is circulated inside the drillstring and through the drill bit into the annular space between the drillstring and the borehole wall. As explained in Chapter 8, stabilizers are placed above the bit to control the direction in which the drill bit will penetrate the formation. Downhole motors with bent subs and rotary-steerable tools are also used for controlling the direction in which the bit drills, as discussed in Chapter 8.

The major functions of a drillstring in conventional rotary drilling operations are

- To transmit rotary motion from the rotary table to a drill bit
- To convey drilling fluid to the working face of the bit
- To produce WOB for effective drilling action
- To provide control of borehole direction

In addition to the elements already mentioned, the drillstring may include shock absorbers, junk baskets, drilling jars, reamers, and other equipment. The drillpipe itself may serve for drillstem testing, completion, well stimulation (e.g., fracturing, acidizing), and fishing operations.

New developments involve using the drillstring as a vehicle for sending downhole information to the top of the hole. High-speed-telemetry drillpipe can provide high-quality downhole dynamic data along with logging information (gamma scans, density images, etc.) that can be effectively used for real-time drilling optimization.

9.2 Drill Collars

The *drill collars* are the major part of the BHA. The BHA, if properly designed, serves several purposes, including loading of the drill bit with the WOB, as previously mentioned. The mechanical and geometric properties of the BHA affect bit performance (i.e., drilling rate and bit wear), hole problems (doglegs, key seats, differential pressure sticking), drillstring vibrations, and drillpipe service life.

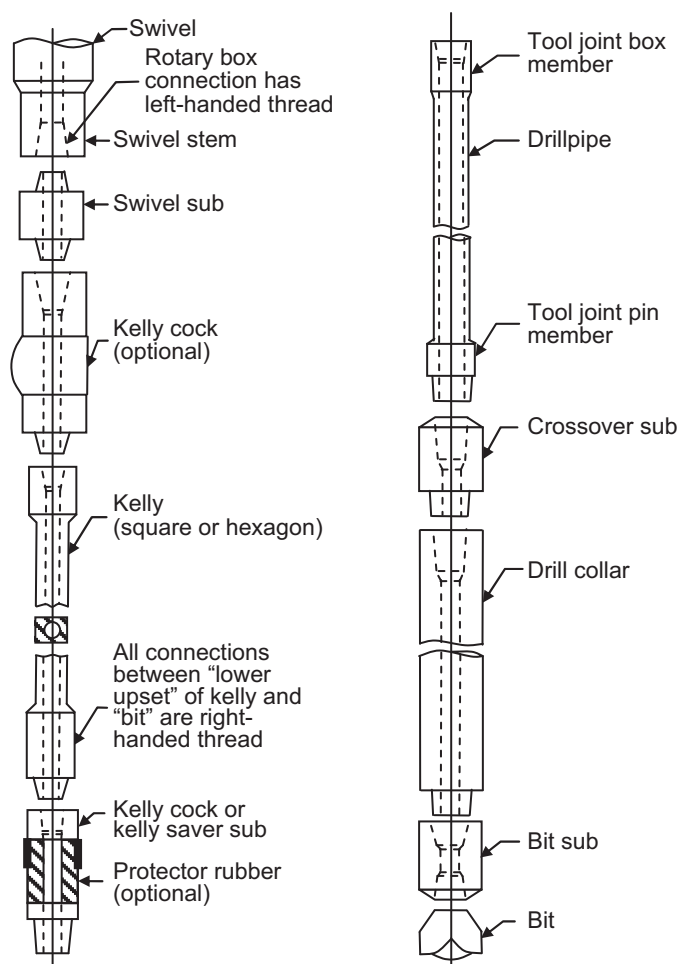


Fig. 9.1—Basic components of a drillstring [after *API Spec. 7:2001 (2001)*]. Reproduced courtesy of the American Petroleum Institute.

Drill collars are manufactured in various sizes and shapes. Conventional drill collars have a round cross section; however, square and spiral drill collars are also used in the drilling industry. Drill collars with a square cross-sectional outside profile are used to increase the stiffness of a BHA, whereas the spiral type is recommended for drilling in areas where differential pressure sticking is a problem. The spiral grooves on the outside surface of these drill collars reduce the contact area between the borehole wall and the drill collars, which, in turn, decreases the sticking force.

The unit weights of new conventional drill collars are given in **Table 9.1**. Corresponding data for non-American-Petroleum-Institute (API) drill collars are available from manufacturers on request. Conventional drill collars are usually made with a uniform outside diameter (OD); however, drill collars with slip and elevator recesses are also available.

The string of drill collars is formed by connecting individual collars (usually with a length of approximately 30 ft) by means of rotary-shouldered connections. Selection charts for drill-collar connections are available from several manufacturers. The connections must be made up with an appropriate amount of makeup torque so that they will not separate under downhole conditions. The recommended makeup torques for different sizes of drill collars are given by *API RP 7G* (1998). Basic physical properties of new drill collars are given in **Table 9.2**.

9.2.1 Selection of Drill-Collar Size and Length. Many factors affect selection of the drill-collar shape and unit weight. The most important factors are

- Bit size
- OD of the casing that is expected to be run in the hole
- Formation dip angle and heterogeneity
- Hydraulic program (i.e., drilling-fluid type, properties, flow rate, and nozzle size)
- Maximum acceptable dogleg (hole curvature)

TABLE 9.1—SIZES AND UNIT WEIGHTS (lbf) OF NEW DRILL COLLARS
 [after API Spec. 7:2001 (2001)] Reproduced courtesy of the American Petroleum Institute.

Drill-Collar ID, in.													
Drill-Collar OD, in.	1	1¼	1½	1¾	2	2¼	2½	2 ¹³ / ₁₆	3	3¼	3½	3¾	4
2⅞	19	18	16										
3	21	20	18										
3⅞		22	22										
3¼		24	25										
3½		29	30										
3¾		33	35										
4	40	39	37	35	32	29							
4⅞	43	41	39	37	35	32							
4¼	46	44	42	40	38	35							
4½	51	50	48	46	43	41							
4¾			54	52	50	47	44						
5			61	59	56	53	50						
5¼			68	65	63	60	57						
5½			75	73	70	67	64	60					
5¾			82	80	78	75	72	67	64	60			
6			90	88	85	83	79	75	72	68			
6¼			98	96	94	91	88	83	80	76	72		
6½			107	105	102	99	96	91	89	85	80		
6¾			116	114	111	108	105	100	98	93	89		
7			125	123	120	117	114	110	107	103	98	93	84
7¼			134	132	130	127	124	119	116	112	108	103	93
7½			144	142	139	137	133	129	126	122	117	113	102
7¾			154	152	150	147	144	139	136	132	128	123	112
8			165	163	160	157	154	150	147	143	138	133	122
8¼			176	174	171	168	165	160	158	154	149	144	133
8½			187	185	182	179	176	172	169	165	160	155	150
9			210	208	206	203	200	195	192	188	184	179	174
9½			234	232	230	227	224	220	216	212	209	206	198
9¾			248	245	243	240	237	232	229	225	221	216	211
10			261	259	257	254	251	246	243	239	235	230	225
11			317	315	313	310	307	302	299	295	291	286	281
12			379	377	374	371	368	364	361	357	352	347	342

- Required WOB
- Possibility of fishing operations (retrieving the string if some of the elements fail and a portion of the BHA is lost in the hole)

If a near-bit stabilizer is not used, to prevent rapid changes in hole deviation (which may make running a casing string difficult or even impossible), the required OD of the drill collars can be calculated as follows:

$$D_{odc} = 2(D_{occ}) - D_b, \quad \dots \dots \dots (9.1)$$

where D_{odc} = outside diameter of drill collars, D_{occ} = outside diameter of casing coupling, and D_b = bit diameter.

The required length of drill collars depends mostly on the desired WOB, the unit weight of the drill collars, and the drilling-fluid density. Assuming that only drill collars will be used to create bit loading, the required length is given by the formula

$$L_{dc} = \frac{(DF)W}{w_{dc} K_b \cos \varphi}, \quad \dots \dots \dots (9.2)$$

TABLE 9.2—PROPERTIES OF NEW DRILL COLLARS		
1	2	3
Drill-Collar OD Range, in.	Minimum Yield Strength, psi	Minimum Tensile Strength, psi
3 1/8 – 6 7/8	110,000	140,000
7 – 10	100,000	135,000

where DF = design factor (DF \cong 1.1 to 1.2); W = WOB, lbf; w_{dc} = unit weight of drill collars (see Table 9.1); K_b = buoyancy factor = $1 - \frac{\gamma_m}{\gamma_{st}}$; γ_m = drilling-fluid specific weight; γ_{st} = drill-collar-material specific weight [steel specific gravity (SG) = 7.85; water = 1.0]; and ϕ = hole inclination angle from the vertical.

A design factor of approximately 1.15 to 1.20 is recommended in nearly vertical holes to ensure that the part of the drillstring above the drill collar is under effective tension. The concept of *effective tension* is explained later in this chapter in the section dealing with axial stress in drillpipe. Maintaining the drillpipe under tension not only prevents it from buckling, but also helps prevent lateral movement of the pipe because of the centrifugal forces that are generated while the pipe is being rotated. Generally, in nearly vertical holes, a higher value of the design factor is recommended for higher rotary speeds of the drillstring and higher flow rates. As the hole inclination angle increases, gravity keeps the drill collars on the lower side of the borehole, which results in drag forces, as discussed in Chapter 8.

The pressure-area method suggested by some authors for calculating the required length of drill collars is not correct and therefore should not be used because it does not consider the tri-axial nature of the stresses that are actually observed when the pipe is immersed in the drilling fluid. It can be shown that hydrostatic forces cannot cause buckling as long as the density of the drilling fluid is less than that of the drill-collar material. In other words, under these conditions, the drill collars will not buckle because of hydrostatic forces, no matter how deep the hole is.

Example 9.1 Select the drill-collar size and length for the following drilling conditions:

Hole size = 8 3/4 in.

Casing size 7 in. with 7.656-in. OD coupling

WOB = 45,000 lbf

Mud SG = 1.2 (water = 1.0, steel = 7.85)

Hole inclination angle = 10°

Design factor = 1.2

Solution. From Eq. 9.1, $D_{odc} = 2(7.656) - 8.75 = 6.562$ in. From Table 9.1, drill collars can be selected with OD = 6 1/2 in. and inside diameter (ID) = 2 in., so that the unit weight $w_u = 102$ lbf/ft. The buoyancy factor is

$$K_b = 1 - \frac{1.2}{7.85} = 0.847,$$

and the length of the drill collars, from Eq. 9.2, is

$$L_{dc} = \frac{(1.2)(45,000)}{(102)(0.847)(\cos 10^\circ)} = 635 \text{ ft.}$$

Assuming that the average length of one joint of drill collar is 30 ft, the required number of joints is 22.

Note that once the ID of the drill collars has been selected (e.g., 2 in.), the unit weight has been determined, and consequently the length of the drill collars can be found from Eq. 9.2. Selecting different IDs gives different corresponding drill-collar string lengths. For each combination of ID and drill-collar length, the

corresponding pressure losses can be calculated. This clearly indicates that the selection of the drillstring should be made in conjunction with the hydraulic program.

9.2.2 Drill-Collar Buckling. To understand the phenomenon of drill-collar buckling, for the sake of simplicity, let us first consider a steel vertical rod with a length $L_r = 5$ ft (60 in.) and a cross-sectional area of 0.5 in.² [diameter = 0.798 in. and moment of inertia = $(1.99)(10^{-2})$ in.⁴]. The lower end is resting on a flat surface, and the upper end is loaded with an axial force. The axial force results in an axial compressive stress equal to the magnitude of the force divided by the cross-sectional area of the rod. By gradually increasing the axial force, it can be observed that at a certain force, the rod buckles. If the hinged types of end conditions (no bending moment) are assumed and the rod weight is neglected, the magnitude of the critical force that causes the rod to buckle can be calculated from the well-known Euler equation [e.g., Popov (1990)] as

$$F_{cr} = \frac{\pi^2 EI}{L_r^2}, \quad \dots \quad (9.3)$$

where EI is a bending stiffness that is a product of modulus of elasticity (E) and the moment of inertia (I), and L_r is the length of the rod. If the rod is made of steel [$E = 30(10)^6$ psi], the critical buckling force from Eq. 9.3 is 1,635 lbf for the case under considerations. Note that in Eq. 9.3, the rod weight is not considered (that is, the rod is assumed to be weightless). In other words, the practical usefulness of Eq. 9.3 is limited to those cases in which the buckling force is much greater than the weight of the compressed elements.

A similar phenomenon may occur if the WOB is increased above a certain value called the *critical WOB*. Because the lateral movement of the drill collar is restricted by the borehole wall, the drill collar will contact the wall, as shown in **Fig. 9.2**.

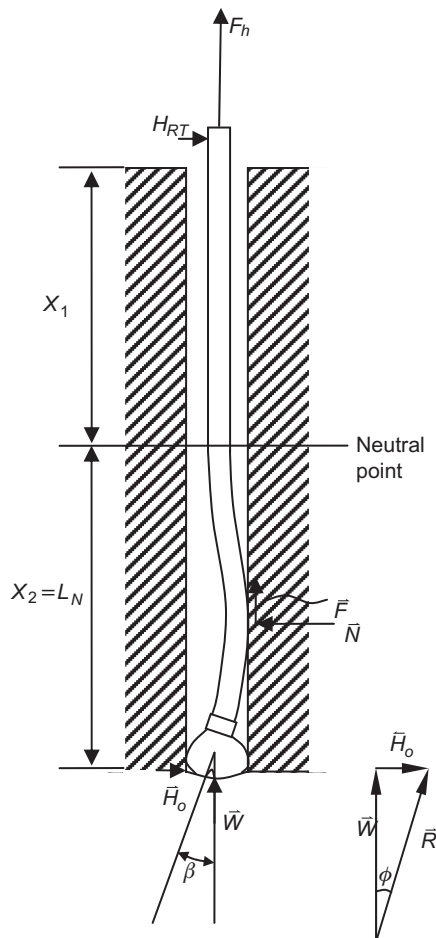


Fig. 9.2—Buckling of collars in a vertical hole [after Lubinski (1987)].

The force W is called the *WOB*, which is the vertical component of the force that the formation exerts on the bit. W is also equal to the weight of the portion of the drill collars in drilling fluid that is below the neutral point, N , reduced by the frictional force, F_f . In other words, the *WOB* force, W , plus the frictional force, F_f , is equal to the weight in mud of the portion of the drill collars that is below the neutral point. The force H_0 is called the side force at the bit. The vertical force equilibrium requires that the F_h (hook load) be equal to the total weight of the drillstring in drilling fluid minus the weight of the drill collars that are used to generate bit loading reduced by the friction force (drag force). In other words, the neutral point divides the drillstring into two parts. The upper part, with length X_1 , is in effective tension, and the lower part, with length X_2 , is in effective compression. Because the buckling of drill collars is attributable to the amount of drill-collar weight that is slacked off onto the drill bit, Eq. 9.3 cannot be used to calculate the critical buckling force.

A theoretical analysis performed by Lubinski (1951, 1987) revealed that for a frictionless system (that is, friction force is neglected), the critical values of *WOB* W_{cr} that cause first- and second-order buckling (meaning that the first or the second buckle contacts the borehole wall) can be calculated from the following expressions:

$$W_{cr,I} = 1.94 w_{bp} m, \quad \dots \dots \dots (9.4)$$

$$W_{cr,II} = 3.75 w_{bp} m, \quad \dots \dots \dots (9.5)$$

where $W_{cr,I}$ = critical value of *WOB* for first-order buckling,

$W_{cr,II}$ = critical value of *WOB* for second-order buckling,

$m = \sqrt[3]{\frac{EI}{w_{bp}}}$, a scaling factor or “dimensionless unit,” which relates actual to dimensionless length, ft,

EI = bending stiffness of the drill collars, and

w_{bp} = unit weight of the drill collars in drilling fluid.

If the *WOB* is less than calculated from Eq. 9.4, the drill collars remain straight and the side force $H_0 = 0$. It can be shown that the coefficient 1.94 in Eq. 9.4 should be replaced with 1.08 for deep wells.

Once the drill collars have buckled, the string is no longer vertical at its lower end, and the bit starts to drill an inclined hole. The direction (inclination) of the force on the bit and the tilt angle are given by (Lubinski 1951, 1987)

$$\Phi = n \frac{r_c}{m}, \quad \dots \dots \dots (9.6)$$

$$\beta = \lambda \frac{r_c}{m}, \quad \dots \dots \dots (9.7)$$

where Φ = inclination of the resultant bit force [note also that $\Phi = \arctan (H_o/W)$],

β = tilt angle (the angle between the tangent to the centerline of the drill collars at the bit and the vertical at the bit) (radians),

r_c = radial clearance (apparent radius of the hole), $r_c = 0.5 (D_b - OD_{dc})$,

n, λ = coefficients that depend on the dimensionless distance, $x_2 = \frac{X_2}{m}$, between the bit and the neutral point, as shown in **Fig. 9.3**.

Assuming that the drill-bit face- and side-cutting abilities are identical and the formation being drilled is isotropic, the expected instantaneous bit-displacement direction is the same as the direction of the resultant force on the bit. If, however, the side-cutting ability of the drill bit is assumed negligible, the bit will penetrate the formation in the direction in which it is pointed out. In other words, the instantaneous hole angle will be equal to the tilt angle. In general, the direction of bit penetration will be neither that of the tilt angle nor that of the resultant force angle, because formation drillability (formation resistance to drilling) is different in different directions.

The magnitude of the force applied by the buckled drill collars on the hole wall is given by

$$N = f w_{bp} r_c, \quad \dots \dots \dots (9.8)$$

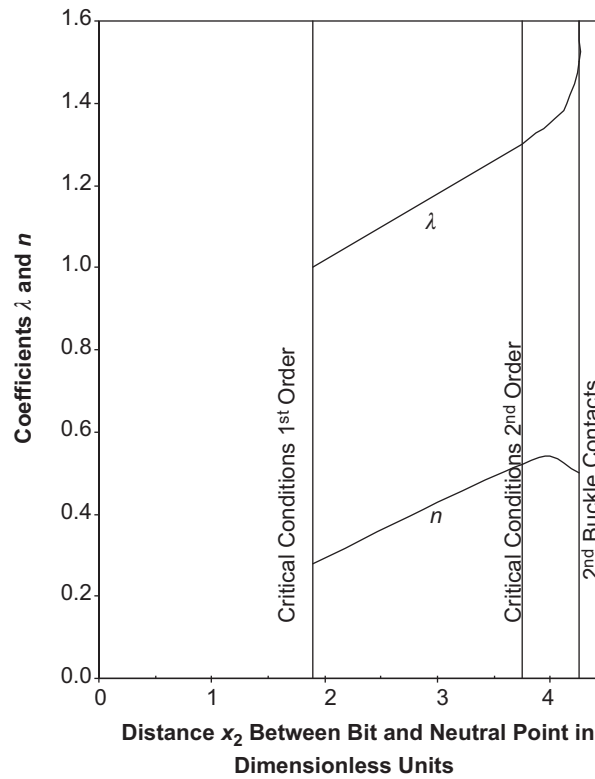


Fig. 9.3—Coefficients λ and n as functions of dimensionless distance from the drill bit to the neutral point, x_2 [after Lubinski (1987)].

where f = a coefficient that depends on the distance from the bit to the neutral point, expressed in dimensionless units, x_2 (Fig. 9.4):

$$x_2 = \frac{L_N}{m}, \quad \dots \dots \dots (9.9)$$

$L_N = X_2$ = distance from the bit to the neutral point, ft:

$$L_N = \frac{W - F}{w_{bp}}, \quad \dots \dots \dots (9.10)$$

$F = \mu N$ = friction force, lbf, and μ = coefficient of friction between the drill collar and the formation at the point of contact.

Analysis of Eqs. 9.8 and 9.10 indicates that if the coefficient of friction (μ) is known or can be estimated, then the force N can be calculated iteratively. If the drillstring is rotating, the friction force is absorbed by the rotary torque, and the axial friction can be ignored in Eq. 9.10.

It is evident that buckling generates a bending moment, which in turn produces a bending stress, which is a tension on one side and a compression on the other. This bending stress affects the compound stress in the inner and outer fibers of the drill collars.

The following expression can be used to calculate the bending moment:

$$M_b = iw_{bp}mr_c, \quad \dots \dots \dots (9.11)$$

where i = the bending-moment coefficient, which is a function of x_2 (Fig. 9.5). There are two points in drill collars where the bending moment reaches a maximum.

In Fig. 9.5, the coefficient i_1 corresponds to the point of maximum bending moment that is nearest to the bit, whereas i_2 corresponds to the point above. The dashed lines M_1M_3 and $M'_1M'_3$ represent the dimensionless distance (the ordinate on the right side of Fig. 9.5) to the two points at which the bending moment is a maximum.

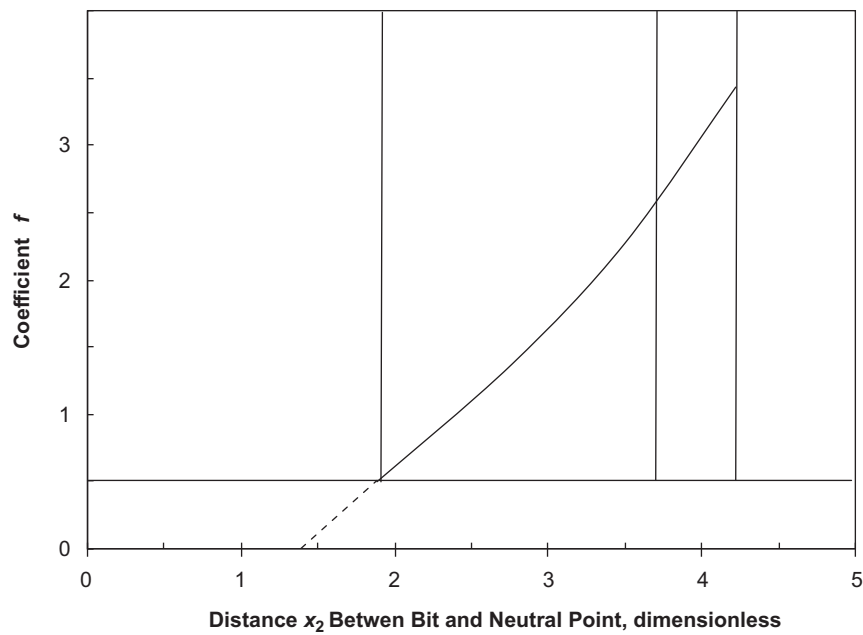


Fig. 9.4—Coefficient f for the force that collars exert on the borehole wall upon buckling [after Lubinski (1987)].

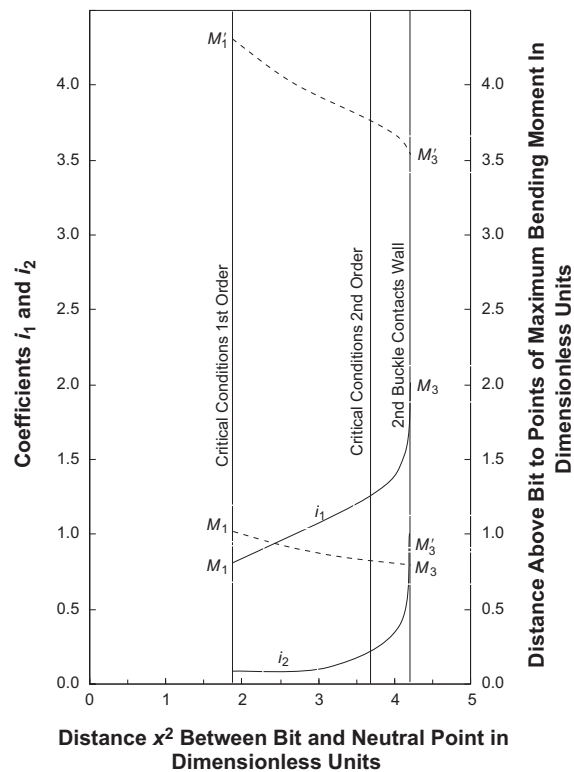


Fig. 9.5—Bending coefficients i_1 and i_2 vs. x_2 [after Lubinski (1987)].

Example 9.2 Consider 7½- by 2½-in. steel drill collars in a 12¼-in. vertical hole. If the WOB $W = 20,000$ lbf and the mud weight = 12 lbm/gal, determine

- Whether drill-collar buckling occurs and, if it does, the distance to the tangency point
- The inclination of the resultant force acting on the bit and the tilt angle
- The side force at the bit

- (d) The force that the buckled drill collar applies to the borehole wall
- (e) The distance from the bit to the point of maximum bending stress and the corresponding bending stress

Solution. The first step is to calculate the moment of inertia:

$$(a) \quad I = \frac{\pi}{64} \left[\left(\frac{7.5}{12} \right)^4 - \left(\frac{2.5}{12} \right)^4 \right] = (7.4)10^{-3} \text{ ft}^4.$$

The unit weight of the drill collars in mud (note that for 7½- × 2½-in. drill collars, the unit weight, $w_{dc} = 133$ lbf/ft):

$$(b) \quad w_{bp} = (133) \left(1 - \frac{12}{65.5} \right) = 108.63 \text{ lbf/ft},$$

$$(c) \quad \text{Dimensionless unit } m = \sqrt[3]{\frac{(4,320)(10^6)(7.4)(10^{-3})}{108.63}} = 66.51 \text{ ft}.$$

The apparent radius of the hole (the radial clearance between wellbore and pipe) is

$$(d) \quad r_c = 0.5 \left(\frac{12.25}{12} - \frac{7.5}{12} \right) = 0.198 \text{ ft}.$$

The WOB that causes first-order buckling is

$$(e) \quad W_{cr,I} = (1.94)(108.63)(66.51) = 14,016.5 \text{ lbf}.$$

The WOB that causes second-order buckling is

$$(f) \quad W_{cr,II} = (3.75)(108.63)(66.51) = 27,093.7 \text{ lbf}.$$

Conclusion: Because the actual WOB is 20,000 lbf, first-order drill-collar buckling will occur. The distance to the neutral point (assuming no friction at the tangency point) is

$$(g) \quad L_N = X_2 = \frac{20,000}{108.63} = 184.11 \text{ ft}.$$

Hence, the dimensionless distance to the neutral point is

$$(h) \quad x_2 = \frac{L_N}{m} = \frac{184.11}{66.51} = 2.768.$$

To calculate the resultant force angle, Φ , and tilt angle, β , the coefficients n and λ can be read from Fig. 9.3 as $n = 0.415$ and $\lambda = 1.14$. Consequently, from Eqs. 9.6 and 9.7,

$$(i) \quad \Phi = (0.415) \frac{0.198}{66.51} = 1.23 \times 10^{-3} \text{ radians} = 0.0708^\circ,$$

$$(j) \quad \beta = (1.14) \frac{0.198}{66.51} = 3.39 \times 10^{-3} \text{ rad} = 0.194^\circ.$$

The side force at the bit (H_0) is

$$(k) \quad H_0 = W \tan \Phi = (20,000)(\tan 0.0708) = 25 \text{ lbf}.$$

Of course, in spite of the relatively small values of the tilt angle β and side force H_0 , the hole will eventually start to deviate from the vertical.

From Fig. 9.4, the coefficient $f = 0.8$. Hence, the side force at the point of tangency is

$$(l) \quad N = (0.8)(108.6)(0.198) = 17.2 \text{ lbf.}$$

To calculate the distance from the bit to the points of maximum bending moment, the values of the dimensionless distances, 0.875 and 4.075, can be read from Fig. 9.5. The corresponding actual distances are $(0.875)(66.51) = 58.2$ ft and $(4.075)(66.51) = 271.05$ ft. To calculate the corresponding bending stresses, coefficients i_1 and i_2 can be obtained from Fig. 9.5 as $i_1 = 0.9$ and $i_2 = 0.15$. Consequently, the bending moments are (Eq. 9.11)

$$(m) \quad M_{b1} = (0.9)(108.63)(66.51)(0.198) = 1287.6 \text{ ft-lbf}$$

and

$$(n) \quad M_{b2} = (0.15)(108.63)(66.51)(0.198) = 214.6 \text{ ft-lbf.}$$

Once the bending moments are known, the corresponding bending stresses can be easily calculated. The reader is invited to complete this calculation.

Buckling in an Inclined Hole. If the hole is straight, but not vertical, the critical WOB that induces buckling can be calculated as follows:

$$W_{cr} = 2mw_{bp}\sqrt{\frac{2m\sin\phi}{r_c}} \dots\dots\dots (9.12)$$

Eq. 9.12 is based on an experimental study performed by H.B. Woods of Hughes Tool Company. However, Dawson and Pasley's (1983) theoretical study of long and frictionless rods provided the following equation:

$$W_{cr} = 2mw_{bp}\sqrt{\frac{m\sin\phi}{r_c}} \dots\dots\dots (9.13)$$

All quantities in Eqs. 9.12 and 9.13 (m , w_{bp} , I , and r_c) have the same meaning as previously. Clearly, the empirical equation (Eq. 9.12) predicts a value of the buckling force greater than that predicted by Eq. 9.13 by a factor of $\sqrt{2}$. This is possibly due to the stabilizing effect of the friction force. In other words, Eq. 9.13 provides a fairly conservative estimate of the buckling force in a straight inclined hole and is frequently used by industry at present. This buckling force is called a sinusoidal, snaky, or *lateral buckling force*. As the compressive force is increased above the lateral buckling force, the pipe eventually develops a 3D helical shape.

Example 9.3 Assuming that the drill-collar properties and the hole size are the same as in Example 9.2, calculate the critical WOB if the hole inclination angle is 5° .

Solution. Using Eq. 9.12,

$$(a) \quad W_{cr} = (2)(66.51)(108.6)\sqrt{\frac{2(66.51)(\sin 5^\circ)}{0.198}} = 110,586 \text{ lbf.}$$

Using Eq. 9.13,

$$(b) \quad W_{cr} = 110,586.4 \frac{1}{\sqrt{2}} = 78,196 \text{ lbf.}$$

Buckling of the drill collars in an inclined hole will require a very high WOB, which is usually outside the range recommended by bit manufacturers for effective drilling. However, because the stiff, heavy drill collars lie on the lower side of the hole, high contact forces are created, which in turn cause increased axial drag, increased rotary

torque, and the possibility of differential sticking. High wall friction can also result in whirling (rolling) of drill collars about the wellbore axis rather than rotation about their own axis. This causes very high rotary torque and additional bending loads that are detrimental to the mechanical integrity of the drillstring.

To reduce the problems associated with stiff, heavy drill collars in directional wells, a regular- or heavyweight drillpipe (i.e., a pipe with increased wall thickness) is used to create the desired WOB. If placed in the BHA above the drill collars, a heavyweight drillpipe provides a gradual change in stiffness between the rigid drill collars and the flexible drillpipe. Naturally, a drillpipe that is much more flexible than the drill collars will buckle under much less force than will the drill collars.

Experiments conducted under static conditions (no pipe rotation) in a horizontal well configuration have shown that a pipe subjected to axial loading first buckles into a “snake” shape (as mentioned earlier, this is also called lateral or sinusoidal buckling), and as the force is increased, the pipe eventually assumes a helical shape. This is the so-called *helical buckling* phenomenon. For pipe with a known bending stiffness (EI), the relationship between the axial force F and the helix pitch p is given by Lubinski (1962, 1987) as

$$\phi^2 = \frac{8\pi EI}{F} \quad (9.14)$$

Once the helix pitch has been obtained, the corresponding pipe curvature (κ_p) can be calculated from Eq. 9.15 and the bending moment (M_b) from Eq. 9.16:

$$\kappa_p = \frac{4\pi^2 r_c}{\phi^2 + 4\pi^2 r_c^2} \quad (9.15)$$

$$M_b = EI\kappa_p \quad (9.16)$$

It can be shown that in a helical pipe configuration, the unit contact force between the pipe and the wellbore is given by Mitchell’s (1986) equation:

$$w_c = \frac{r_c F^2}{4EI} \quad (9.17)$$

Clearly, for a pipe with a known bending stiffness (EI), the radial clearance r_c and the axial force F are the major factors controlling the bending moment (bending stress) and the unit contact force.

Example 9.4 Consider a 3½-in. steel drillpipe with a unit weight of 15.5 lbf/ft (pipe ID = 2.602 in.) in a vertical hole subjected to a compressive force $F = 15,000$ lbf. Calculate the bending moment and the unit contact force if the hole diameter is 7⅞ in. Assume that the pipe is helically buckled.

Solution.

Radial clearance:

$$(a) \quad r_c = \frac{7.875 - 3.5}{2(12)} = 0.1823 \text{ ft.}$$

Bending stiffness:

$$(b) \quad EI = 4,320(10^6) \frac{\pi}{64} \left[\left(\frac{3.5}{12} \right)^4 - \left(\frac{2.602}{12} \right)^4 \right] = (1.065)(10^6) \text{ lbf-ft}^2.$$

Pitch of the helix (Eq. 9.14):

$$(c) \quad \phi = \left[\frac{8\pi(1.065)(10^6)}{15,000} \right]^{1/2} = 42.24 \text{ ft.}$$

Pipe curvature (Eq. 9.15):

$$(d) \kappa_p = \frac{4\pi^2(0.1823)}{42.24^2 + 4\pi^2(0.1823^2)} = (4.027)(10^{-3}) \text{ ft}^{-1}.$$

Bending moment (Eq. 9.16):

$$(e) M_b = (1.065)(10^6)(4.027)(10^{-3}) = 4,288 \text{ ft-lbf}.$$

Contact force per unit length (Eq. 9.17):

$$(f) w_c = \frac{(0.1823)(15000)^2}{4(1.065)(10^6)} = 9.63 \text{ lbf/ft}.$$

9.3 Drillpipe and Tool Joints

The major portion of a drillstring is composed of drillpipe. Drillpipe in common use is made out of steel [steel drillpipe (SDP)]. In some applications (e.g., drilling long extended-reach wells), it may be better to use aluminum drillpipe (ADP) or perhaps titanium drillpipe (TDP). To evaluate the usefulness of ADP and TDP compared with SDP, one would need to consider the wellbore path configuration, the downhole temperatures, the working environment (presence of H_2S and CO_2), and the drag and torque issues discussed in Chapter 8. Hot-rolled, pierced seamless tubing, sometimes with the end threaded (eight threads per inch of thread length), is used for tool-joint attachments. As schematically depicted in Fig. 9.1 *tool joints* provide a means of fastening the individual lengths of pipe together. Currently, threaded connections between the drillpipe and tool joints have been almost completely replaced by butt welds. To reinforce the ends of the pipe, the pipe is upset at both ends. The pipe can be internal-upset (IU), external-upset (EU), or internal-and-external-upset (IEU). These three different designs are shown in Fig. 9.6.

For identification purposes, drillpipe can be classified according to:

- Size (nominal OD)
- Wall thickness (or nominal unit weight)
- Steel grade
- Length ranges

The API standard drillpipe sizes include $2\frac{3}{8}$ in., $2\frac{7}{8}$ in., $3\frac{1}{2}$ in., 4 in., $4\frac{1}{2}$ in., 5 in., $5\frac{1}{2}$ in., and $6\frac{5}{8}$ in. The wall thicknesses and corresponding unit weights for the standardized drillpipe sizes are listed in Table 9.3.

The steel grades used and the corresponding minimum tensile yield strength for each are given in Table 9.4. Usually, drillpipe is available in three length ranges:

Range 1: 16–25 ft

Range 2: 27–30 ft

Range 3: 38–45 ft

In regular rotary-drilling operations, the drillpipe most commonly used is Range 2. The minimum mechanical-performance properties of various kinds of drillpipe are given in Table 9.5.

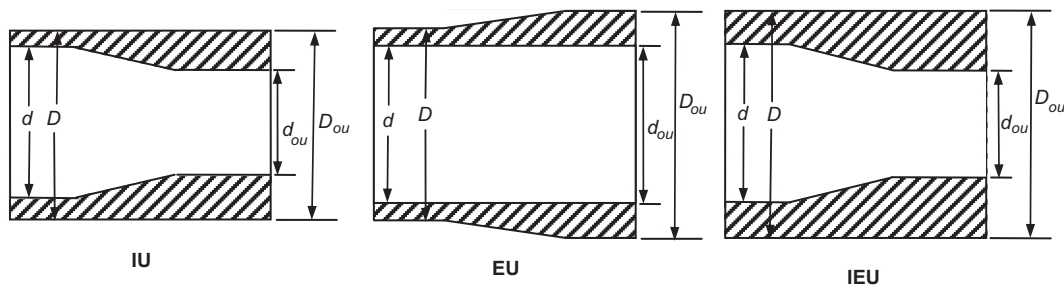


Fig. 9.6—Drillpipe upsets: IU, EU, and IEU.

TABLE 9.3—NEW DRILLPIPE DIMENSIONAL DATA [from <i>API RP 7G</i> (1998)] Reproduced courtesy of the American Petroleum Institute.						
OD, in.	Nominal Weight of Thread Couplings, [lb/ft]	Plain-End Weight, lb/ft	Wall Thickness, in.	ID, in.	Cross-Sectional Area, Body of Pipe, in. ²	Polar Sectional Modulus Z, in. ³
2 $\frac{3}{8}$	4.85	4.43	0.190	1.995	1.3042	1.320
	6.65	6.26	0.280	1.815	1.8429	1.734
2 $\frac{1}{2}$	6.85	6.16	0.217	2.441	1.8120	2.242
	10.40	9.72	0.362	2.151	2.8579	3.204
3 $\frac{1}{2}$	9.50	8.81	0.254	2.992	2.5902	3.922
	13.30	12.31	0.368	2.764	3.6209	5.144
	15.50	14.63	0.449	2.602	4.3037	5.846
4	11.85	10.46	0.262	3.476	3.0767	5.400
	14.00	12.93	0.330	3.340	3.8048	6.458
	15.70	14.69	0.380	3.240	4.3216	7.156
4 $\frac{1}{2}$	13.75	12.24	0.271	3.958	3.6004	7.184
	16.60	14.98	0.337	3.826	4.4074	8.542
	20.00	18.69	0.430	3.640	5.4981	10.232
	22.82	21.36	0.500	3.500	6.2832	11.345
	24.66	23.20	0.550	3.400	6.8251	12.062
5	16.25	14.87	0.296	4.408	4.3743	9.718
	19.50	17.93	0.362	4.276	5.2746	11.416
	25.60	24.03	0.500	4.000	7.0686	14.490
5 $\frac{1}{2}$	19.20	16.87	0.304	4.892	4.9624	12.222
	21.90	19.81	0.361	4.778	5.8282	14.062
	24.70	22.54	0.415	4.670	6.6296	15.688
6 $\frac{3}{8}$	25.20	22.19	0.330	5.965	6.5262	19.572
	27.70	24.22	0.362	5.901	7.1227	21.156

TABLE 9.4—MINIMUM TENSILE YIELD STRENGTH FOR NEW DRILLPIPE	
Steel Grade	Minimum Yield Strength, psi
D	55,000
E	75,000
X – 95	95,000
G – 105	105,000
S – 135	135,000
V – 150	150,000

A tool joint is usually welded onto the drillpipe and consists of a pin and a box, as illustrated in **Fig. 9.7**. It is made from high-alloy steel with a wide thread (4 to 5 threads per inch) on the pin and the box.

Tool joints are classified by style as

- Extra-hole
- Wide-open
- Slimhole
- Full-hole
- Internal-flush

TABLE 9.5—MINIMUM PERFORMANCE PROPERTIES OF NEW DRILLPIPE [from <i>API RP 7G</i> (1998)] Reproduced courtesy of the American Petroleum Institute.							
1	2	3	4	5	6	7	8
OD, in. <i>D</i>	Nominal Weight, lb/ft	Grade	Wall Thickness, in. <i>t</i>	ID, in. <i>d</i>	Collapse Resistance, psi	Internal Yield Pressure, psi	Pipe-Body Yield Strength, 1,000 lb
2½	6.65	E	0.280	1.815	15,600	15,470	138
	6.65	X	0.280	1.815	19,760	19,600	175
	6.65	G	0.280	1.815	21,840	21,660	194
	6.65	S	0.280	1.815	28,080	27,850	249
2¾	10.40	E	0.362	2.151	16,510	16,530	214
	10.40	X	0.362	2.151	20,910	20,930	272
	10.40	G	0.362	2.151	23,110	23,140	300
	10.40	S	0.362	2.151	29,720	29,750	386
3½	9.50	E	0.254	2.992	10,040	9,520	194
	13.30	E	0.368	2.764	14,110	13,800	276
	15.50	E	0.449	2.602	16,770	16,840	323
	13.30	X	0.368	2.764	17,880	17,480	344
	15.50	X	0.449	2.602	21,250	21,330	409
	13.30	G	0.368	2.764	19,760	19,320	380
	15.50	G	0.449	2.602	23,480	23,570	452
	13.30	S	0.368	2.764	25,400	24,840	480
	15.50	S	0.449	2.602	30,190	30,310	581
4	11.85	E	0.262	3.476	8,410	8,600	231
	14.00	E	0.330	3.340	11,350	10,830	285
	14.00	X	0.330	3.340	14,380	13,720	361
	14.00	G	0.330	3.340	15,900	15,160	400
	14.00	S	0.330	3.340	20,170	19,490	514

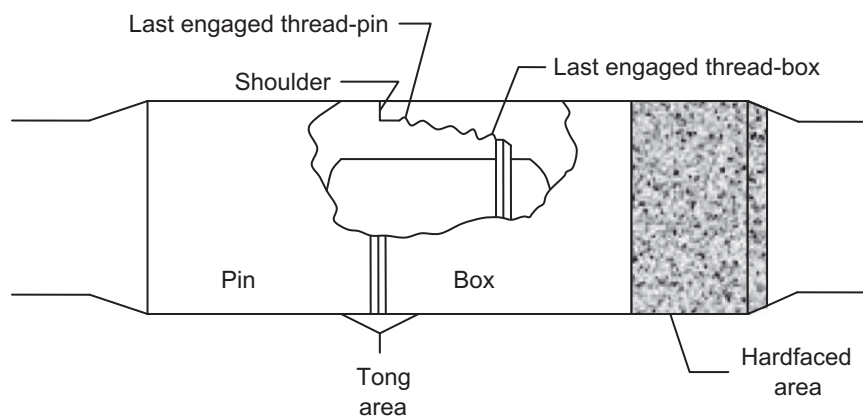


Fig. 9.7—Tool joint: rotary-shouldered connection.

TABLE 9.6—API NUMBERED CONNECTIONS						
[after API RP 7G (1998)] Reproduced courtesy of the American Petroleum Institute.						
API Numbered Connection	NC26	NC31	NC38	NC40	NC46	NC50
Internal flush	2⅝	2⅝	3½		4	4½
Full hole				4		
Extra hole					4½	5
Wide open			3½		4	4½
Slimhole	2⅝	3½	4½			

Table 9.6 shows the corresponding API numbered connections as used in *API RP 7G* (1988). According to the API standard, the mechanical properties of tool joints shall not be lower than the minimum values as specified below:

- Minimum yield strength: 120,000 psi
- Minimum tensile strength: 140,000 psi

For applications that require high rotary torque, double-shoulder tool joints are recommended. A *double-shoulder connection* involves a primary and secondary shoulder (Jellison et al. 2000). In the hand-tight position, only the primary shoulder makes contact. As more makeup torque is applied to the joint in the power-tight position, the box compresses, the pin elongates, and the secondary shoulder engages. The secondary shoulder provides the desired increase in torsional capacity compared with a conventional API rotary-shoulder connection. More technical information on double-shoulder tool joints is available from various manufacturers on the Internet.

Recently, a drillpipe capable of transmitting downhole data and surface control signals has been developed (Jellison and Hall 2003). This drillpipe is frequently called an *intelligent* or *telemetry drillpipe*. It should be noticed, however, that the application of electrical data transmission had been proposed much earlier (Denison 1976). Individual pipe joints include a high-speed data cable that runs along the pipe and terminates at induction coils located in the secondary torque shoulders of double-shoulder tool joints. When two joints are made up under power, the coils are brought into very close proximity, but not into contact with each other. An alternating current flowing through the cable produces a variable electromagnetic field that induces a variable current in the other coil. In other words, the coils create inductive couplings that can transmit signals across the tool-joint interface. Potential applications of telemetry drillpipe include real-time drilling optimization in terms of WOB and bit rotary speed, casing setting depth selection, well control under impending blowout conditions, elimination of wireline logs, and improved control of underbalanced drilling and managed-pressure drilling.

9.3.1 Forces Acting on the Drillstring. A drillstring operating in the borehole is subjected to a number of loads, including tension, compression, torsion, bending, and collapse or burst pressure. These forces can be either static or dynamic. The loads can repeat a number of times (cyclic loads) or can be applied over a relatively short period of time (impact loads). As a result, the stress state of a drillpipe is very complex and difficult to describe analytically. Here, for design purposes, a static stress state is assumed, and an appropriate design factor [safety factor (SF)] is used to arrive at a solution that is acceptable for field conditions.

Axial Tension/Compression Stresses. The largest tension load exists at the top of the drillstring because of the weight of the drill collars, stabilizers, drillpipe, and other string components, and because of forces attributable to fluid pressure acting on surfaces perpendicular to the drillstring axis. The bottom of the string (immersed in a fluid) is subjected to axial compressive force because of the hydrostatic pressure acting at the bottom of the pipe. The stress produced by an axial load, F , on the cross section, A , of a drillstring can be expressed as:

$$\sigma_a = \frac{F}{A}, \quad \dots \dots \dots (9.18)$$

where σ_a = the average axial stress, or simply axial stress (tension or compression), psi; F = axial force, lbf; A = cross-sectional area, $A = 0.785 (D_{op}^2 - D_{ip}^2)$, in.²; D_{op} = pipe OD in.; D_{ip} = pipe ID, in. The axial force, F , which is perpendicular to the cross-sectional area, A , can be determined by generating a free-body diagram, as explained in Example 9.5. Sometimes the stress calculated from Eq. 9.18 is called the *actual (true) axial stress* because it can be measured by strain gauges.

Example 9.5 Suppose that a drillstring is composed of 9,500 ft of 4½-in. drillpipe with a unit weight of 18.3 lbf/ft and a cross-sectional area of 4.4074 in.², and of 600 ft of drill collars with $D_{odc} = 6½$ in., $D_{idc} = 2¼$ in.

($A_{dc} = 29.1922 \text{ in.}^2$), and a unit weight of 99 lbf/ft. The WOB is 28,000 lbf, and the drilling-fluid SG is 1.2 (that of water is 1.0). Calculate the axial stress on a cross section of drillpipe located at a depth of 9,000 ft (500 ft from the top of the drill collars).

Solution. A free-body diagram for this situation is shown in **Fig. 9.8**. Note that only axial forces are considered. System static equilibrium requires that

$$(a) \quad F = W_1 + W_2 + Fp_1 - Fp_2 - W,$$

where F = axial force on the cross section under consideration, lbf; W_1 = weight of drillpipe below the cross section under consideration, lbf; W_2 = weight of drill collars, lbf; Fp_1 = pressure force acting at the top of the drill collars, lbf; Fp_2 = pressure force acting at the bottom of the drill collars, lbf; and W = WOB, lbf.

$$(b) \quad W_1 = (500)(18.3) = 9,150 \text{ lbf}$$

$$(c) \quad W_2 = (600)(99) = 59,400 \text{ lbf}$$

$$(d) \quad Fp_1 = (0.052)(1.2)(8.34)(9,500)(29.1922 - 4.4074) = 122,534 \text{ lbf}$$

$$(e) \quad Fp_2 = (0.052)(1.2)(8.34)(10,100)(29.1922) = 153,440 \text{ lbf}$$

Hence,

$$(f) \quad F = 9,150 + 59,400 + 122,534 - 153,440 - 28,000 = 9,644 \text{ lbf},$$

and the axial stress is a tensile stress ($F > 0$):

$$(g) \quad \sigma_a = \frac{9644}{4.4074} = 2,188 \text{ psi}.$$

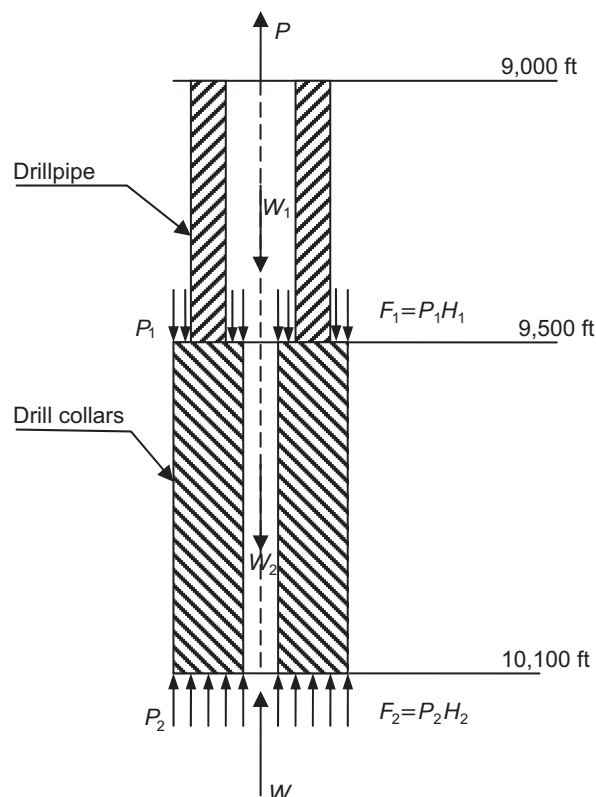


Fig. 9.8—Free-body diagram for Example 9.5.

To determine whether or not a string fails at a given cross section, one must evaluate the 3D stress state that actually exists at the cross section under consideration. Assuming that the drillpipe is a thin-walled pipe, the tangential and radial stresses are the same and equal to the negative of the fluid pressure at a depth of 9,000 ft:

$$(h) \quad \sigma_t = \sigma_r = -(0.052)(1.2)(8.34)(9,000) = -4,683 \text{ psi.}$$

The drilling industry has adopted the maximum-energy-of-distortion theory to assess the strength of tubulars. The theory was originally proposed by Hubert (1904) and was further developed by von Mises (1913). According to the maximum-energy-of-distortion theory (e.g., Popov 1990), yielding begins when the distortion energy reaches the value of the distortion energy at the yield point in a simple tension test.

Assuming that there is no torsion, the following equation can be derived by use of the maximum-energy-of-distortion theory (Budynas 1997; Popov 1990), which is frequently referred to as the Huber-von Mises criterion for yielding:

$$\sigma_Y = \sigma_{vm} = \frac{1}{\sqrt{2}} \left[(\sigma_z - \sigma_t)^2 + (\sigma_t - \sigma_r)^2 + (\sigma_r - \sigma_z)^2 \right]^{1/2}, \quad \dots \quad (9.19)$$

where σ_Y = the yield point (limit of elasticity) as determined in a simple tensile stress test; σ_{vm} = von Mises stress; and $\sigma_z, \sigma_r, \sigma_t$ = axial, radial, and tangential stresses, respectively. The right side of Eq. 9.19 is frequently called a *von Mises stress*. Eq. 9.19 states that yielding occurs if the equivalent stress equals the yield point of the material. If the equivalent stress is less than the yield point, then, theoretically, yielding does not occur. In other words, deformation occurs in the elastic range and disappears when loading is removed.

For the data of Example 9.5, the equivalent stress is

$$\sigma_{vm} = \frac{1}{\sqrt{2}} \left[(2,188 + 4,683)^2 + (4,683 - 4,683)^2 + (4,683 + 2,188)^2 \right]^{1/2} = 6,871 \text{ psi.}$$

In the case under consideration, if the pipe wall is assumed to be thin, the radial and tangential stresses are the same ($\sigma_t = \sigma_r = -p_h$) and equal to the hydrostatic pressure (p_h) of the drilling fluid. Hence, the equivalent stress is

$$\sigma_{vm} = \sigma_z + p_h. \quad \dots \quad (9.20)$$

In general, it should be noted that if there is no WOB, then the axial stress at the bottom of the string is equal to $-p_h$, and consequently the effective stress is nil. At the top of the hole, the hydrostatic pressure term p_h is zero, and the effective stress is equal to the axial stress.

It can also be shown that, for the case under consideration, the effective stress can be calculated by dividing the buoyant weight of the string below the cross section under consideration by the corresponding cross-sectional area:

$$\sigma_e = \frac{(L_{dp} w_{dp} + L_{dc} w_{dc}) K_b}{A}, \quad \dots \quad (9.21)$$

where σ_e = effective axial stress (buoyant stress), psi; L_{dp} = length of drillpipe, ft; w_{dp} = unit weight of drillpipe, lbf/ft; L_{dc} = length of drill collars, ft; w_{dc} = unit weight of drill collars, lbf/ft; and K_b = buoyancy factor.

If the WOB, W , is used, then the effective axial stress is

$$\sigma_e = \frac{(L_{dp} w_{dp} + L_{dc} w_{dc}) K_b - W}{A}. \quad \dots \quad (9.22)$$

Eqs. 9.21 and 9.22 are valid for vertical wells. Appropriate adjustments of the weight components are required for holes that are not vertical.

The quantity calculated using Eq. 9.21 or Eq. 9.22 is called the *effective tensile (compressive) stress*. *API RP 7G* (1988) calls this quantity the *buoyant tensile stress*. Note that this stress does not actually exist because it cannot be measured.

Analysis of Eq. 9.22 reveals that there exists a cross section in the drillstring at which the effective axial stress is nil. Above this cross section, the effective stress is positive, while below it, the effective axial stress is negative. This neutral cross section can be found from the following equation:

$$(L_{dp}w_{dp} + L_{dc}w_{dc})K_b - W = 0.$$

If only the drill collars are used to create WOB, then

$$L_{dc}w_{dc}K_b = W,$$

$$\text{or } L_{dc} = \frac{W}{w_{dc}K_b}. \quad \dots\dots\dots (9.23)$$

It is immediately apparent that Eq. 9.23 may also be obtained by setting $DF = 1$ and $\cos \phi = 1$ in Eq. 9.2.

If the length of drill collars is calculated from Eq. 9.23, then the neutral point resides right at the top of the drill collars. In other words, the drill collars are under effective compression (or just compression), while the drillpipe is under effective tension (or just tension). For the sake of simplicity, in the following discussion, the term “tension/compression” refers to effective tension/compression.

Knowledge of the actual axial stress along the drillstring is useful for calculating the length of the drillstring, while the effective stress indicates whether yielding (loading above yield stress) may occur.

Example 9.6 For the drillstring data of Example 9.5, calculate the total elongation of the drillpipe and the equivalent stress at the top of the hole. Assume that there is no WOB.

Solution. From Hooke’s law, the axial strain is

$$\varepsilon_z = \frac{1}{E}[\sigma_z - \nu(\sigma_t + \sigma_r)]. \quad \dots\dots\dots (9.24)$$

Under hydrostatic pressure conditions and assuming that $\sigma_t = \sigma_r = -p_h$,

$$\varepsilon_z = \frac{1}{E}(\sigma_z + 2\nu p_h), \quad \dots\dots\dots (9.25)$$

where E = modulus of elasticity (for steel, $E = 30 \times 10^6$ psi); ν = Poisson’s ratio (for steel, $\nu \cong 0.28$ – 0.3); σ_z = axial stress, psi; and p_h = hydrostatic pressure of the drilling fluid, psi. The axial stress is

$$(a) \quad \sigma_z = \frac{(9,500 - H)(18.3) + (600)(99) + 122,534 - 153,440}{4.4074} = 45,910 - (4.152) H, \text{ psi},$$

where H = the vertical distance from the top of the hole to the cross section under consideration, in feet. Note that at the top of the hole, $H = 0$ and $\sigma_z = 45,910$ psi.

The hydrostatic pressure is

$$(b) \quad p_h = (0.052)(1.2)(8.34) H = (0.5204) H, \text{ psi}.$$

Substituting the expressions for σ_z and p_h into Eq. 9.25 yields

$$(c) \quad \varepsilon_z = \frac{1}{(30)(10^6)}[45,910 - 3.84(H)].$$

Hence, the drillpipe elongation is

$$(d) \quad \Delta Z = \int_0^{9,500} \frac{[45,910 - (3.84)H]dH}{(30)(10^6)} \cong 8.76 \text{ ft.}$$

To calculate the von Mises stress at the top of the hole ($H = 0$), Eq. 9.22 can be used to obtain

$$(e) \quad \sigma_{vm} = \frac{[(9,500)(18.3) + (600)(99)]0.847}{4,4074} = 44,832 \text{ psi.}$$

The value obtained for the von Mises stress (44,832 psi) is only slightly different from the axial stress (45,910 psi) because of rounding errors. Of course, theoretically, the same number should be obtained. This result is consistent with statements made previously. In fact, the top cross section of the drillpipe is the only point in the drillstring where the value of the axial stress is equal to the effective axial stress. Once again, it must be remembered that while the axial stress is a stress that actually exists in the pipe (and can be measured), the effective axial stress is only a computational device. The magnitude of the effective (equivalent) stress determines whether or not plastic deformation (yielding) occurs.

Torsional Stresses. Torsion in a drillstring is caused by a twisting moment (T) called *torque* and results in a shear or torsional stress (τ) and an angle of twist (ϕ). The shear stress and the differential angle of twist can be calculated as

$$\tau = \frac{Tr}{J}, \quad \dots\dots\dots (9.26)$$

$$\frac{d\phi}{dz} = \frac{T}{GJ}, \quad \dots\dots\dots (9.27)$$

where τ = shear stress, psi

$d\phi/dz$ = differential angle of twist, in.^{-1}

T = torque, in.-lbf

r = distance from the center of the pipe to the point under consideration, in.

$D_{ip} \leq 2r \leq D_{op}$, in.

G = shear modulus of elasticity, $G = \frac{E}{2(1+\nu)}$

J = polar moment of inertia, $J = \frac{\pi}{32}(D_{op}^4 - D_{ip}^4)$

The maximum shear stress occurs at the outer fiber of the pipe, and for this case, Eq. 9.26 can be written as

$$\tau_{\max} = \frac{16 D_{op} T}{\pi (D_{op}^4 - D_{ip}^4)} = \frac{T}{Z}, \quad \dots\dots\dots (9.28)$$

where Z is the polar sectional modulus.

For field engineering calculations, the expected value of rotary torque is calculated as explained in Chapter 8. If the horsepower, HP, to rotate the string is known, the corresponding torque is given by Eq. 9.29:

$$T = \frac{5,250 \text{ HP}}{\text{RPM}}, \quad \dots\dots\dots (9.29)$$

where HP = horsepower required to turn the rock bit and drillstring, hp (1 hp = 550 ft-lbf/s); RPM = drillstring rotary speed, rev/min; and T = rotary torque, ft-lbf. The horsepower to rotate the drillpipe is

$$HP_p = C_d(D_{op}^2)(RPM)(L_{dp})(SG), \quad (9.30)$$

where C_d = an empirical factor that depends on hole inclination angle = $[(4.8(10^{-5}) - (66.5)(10^{-7})]$ for hole angles ranging from 3 to 5°; L_{dp} = length of drillpipe, ft; and D_{op} = OD of drillpipe, in.; SG = drilling-fluid SG (water = 1.0). For hole inclination angles greater than approximately 5°, it is necessary to calculate the torque needed to overcome drag forces (as discussed in Chapter 8) and then eventually the corresponding horsepower.

The horsepower to rotate a rotary-roller rock bit in a vertical hole can be estimated from Eq. 9.31:

$$HP_b = C_f(W)^{1.5} D_b^{2.5} RPM \quad (9.31)$$

where C_f = an empirical factor ranging from $(4)10^{-6}$ for very hard formations to approximately $(14)10^{-5}$ for very soft formations; D_b = bit diameter, in.; and W = WOB, 10^3 lbf. For practical design applications, the coefficient C_f should be obtained from wells drilled under similar drilling conditions.

In addition to the shear stress given by Eq. 9.26, there is a transverse shear stress produced by the shearing force due to changes in bending moment along the pipe. This stress, however, is usually small during regular rotary drilling operations, and for this reason is not usually included in drillstring design calculations.

Example 9.7 Determine the maximum tensile load capacity of 3½-in. drillpipe with unit weight 15.5 lbf/ft, steel grade E with a yield strength of 75,000 psi, if a rotary torque of 6,000 ft-lbf is applied to the pipe.

Solution. Application of the maximum-energy-of-distortion theory for this case yields

$$\sigma_{vm}^2 = \sigma_z^2 + 3\tau^2, \quad (9.32)$$

where σ_z = axial stress (tensile stress).

Because $\sigma_z = \frac{F}{A}$ and $\tau = \frac{T}{Z}$, by substituting the yield strength σ_y of pipe for the effective stress, Eq. 9.32 can be rewritten as

$$\sigma_y^2 = \left(\frac{F}{A}\right)^2 + 3\left(\frac{T}{Z}\right)^2. \quad (9.33)$$

From Eq. 9.33,

$$F = A\sqrt{\sigma_y^2 - 3\left(\frac{T}{Z}\right)^2}. \quad (9.34)$$

Eq. 9.34 provides the static pipe axial-load capacity as a function of rotary torque. Because $Z = 5.846 \text{ in.}^3$ (from Table 9.3) and $\sigma_y = 75,000 \text{ psi}$, the following result can be obtained from Eq. 9.34:

$$F = 4.3037\sqrt{(75,000)^2 - 3\left(\frac{6,000(12)}{5.846}\right)^2} = 309,446 \text{ psi.}$$

Bending Stress. In drilling operations, a drillstring frequently undergoes bending because of hole curvature (dog-legs), transverse loads, and other disturbances. The bending stress can be calculated from the following equation:

$$\sigma_b = \frac{M_b D_{op}}{2I} \quad (9.35)$$

The bending moment in Eq. 9.35 is a product of pipe bending stiffness and curvature κ_p :

$$M_b = EI\kappa_p \quad (9.35a)$$

If, as a first approximation, we assume that the pipe shape parallels the wellbore path (i.e., the pipe is in continuous contact with the wellbore—no tool joints), the magnitude of pipe curvature $\kappa_p = \frac{1}{R}$ and Eq. 9.35 can be written as

$$\sigma_b = \frac{ED_{op}}{2R} \quad (9.36)$$

where R is the wellbore radius of curvature.

As explained in Chapter 8, the hole curvature is usually called the *dogleg severity* (DLS) and is expressed in degrees/100 ft. If, for example, the DLS is 5°/100 ft, this implies that over every foot of hole, the hole curves by 0.05°. The relationship between the radius of curvature and the DLS is

$$R = \frac{5,729.6}{\text{DLS}} \quad (9.37)$$

where DLS = dogleg severity, degrees/100 ft.

Example 9.8 Calculate the maximum torque that can be applied to 4-in. grade E drillpipe with a unit weight of 10.46 lbf/ft (ID = 3.476 in., $A = 3.0767 \text{ in.}^2$, $Z = 5.400 \text{ in.}^3$) if the DLS is 10.0°/100 ft. The tensile load applied to the pipe is $F = 140,000 \text{ lbf}$. To solve this problem, assume that the pipe curvature is the same as the hole curvature.

Solution. Because the bending stress is an axial stress, the effective stress equation is given by

$$\sigma_{vm}^2 = (\sigma_a + \sigma_b)^2 + 3\tau^2 \quad (9.38)$$

where σ_a and σ_b are the axial (tensile or compressive effective stresses) and bending stresses, respectively.

Substituting $\sigma_{vm} = S_y$; $\sigma_a = \frac{F}{A}$; $\sigma_b = \frac{E(D_{op})(\text{DLS})}{(2)(5,729.6)(12)}$; and $\tau = \frac{T}{Z}$ into Eq. 9.38 and solving for T , the following expression for maximum rotary torque results in

$$T_{\max} = \frac{Z}{\sqrt{3}} \sqrt{\sigma_y^2 - \left(\frac{F}{A} + \frac{ED_{op} \text{DLS}}{137,510} \right)^2} \quad (9.39)$$

Eq. 9.39 provides the torsional pipe-load capacity as a function of axial load and DLS.

For the case under consideration, from Eq. 9.39:

$$T_{\max} = \frac{5.4}{\sqrt{3}} \sqrt{(75,000)^2 - \left[\frac{140,000}{3.0767} + \frac{(30)(10^6)(4.0)(10.0)}{137,510} \right]^2} = 161,523 \text{ in.-lbf.}$$

For practical applications, the maximum torque obtained should be divided by a reasonable design factor to account for dynamic effects and other uncertainties. Eq. 9.39 shows that for a given drillpipe material and set of geometric properties, an increase in tensile load and DLS results in a decrease in the torque load capacity of the pipe.

For more accurate calculations, Lubinski (1961, 1987) derived the following expressions, which relate the pipe curvature and the hole curvature that accounts for the presence of tool joints:

Case 1:

$$\kappa_p = \kappa \frac{\alpha \ell_{ij}}{\tanh(\alpha \ell_{ij})} \quad \dots \dots \dots (9.40)$$

Case 2:

$$\kappa_p = \kappa (\alpha \ell_{ij}) \frac{\sinh(\alpha \ell_{ij}) - \alpha \ell_{ij} - \left(\frac{1}{2} + \frac{r_c}{\kappa \ell_{ij}^2} \right) \alpha \ell_{ij} [\cosh(\alpha \ell_{ij}) - 1]}{2 [\cosh(\alpha \ell_{ij}) - 1] - \alpha \ell_{ij} \sinh(\alpha \ell_{ij})}, \quad \dots \dots \dots (9.41)$$

where κ_p = drillpipe curvature at the tool joints, rad/in.; κ = hole curvature over the distance between the tool joints, rad/in.; ℓ_{ij} = half the distance between the tool joints (ℓ_{ij} = 180 in. for Range 2 drillpipe and ℓ_{ij} = 270 in. for

Range 3 drillpipe), in.; $\alpha = \sqrt{\frac{F}{EI}}$; F = tensile force applied to the pipe, lbf; and EI = product of the modulus of elasticity and the moment of inertia, lbf-in.². Eq. 9.40 applies (Case 1) if there is no pipe-to-borehole-wall contact between the tool joints, whereas Eq. 9.41 is used (Case 2) if there is pipe-to-wall contact.

Eq. 9.40 holds true (Case 1) if the hole curvature satisfies the following inequality:

$$\kappa < \frac{r_c / \ell_{ij}^2}{\frac{1}{2} - \frac{\cosh(\alpha \ell_{ij}) - 1}{(\alpha \ell_{ij}) \sinh(\alpha \ell_{ij})}}, \quad \dots \dots \dots (9.42)$$

where $r_c = 0.5(D_{oj} - D_{op})$ and D_{oj} and D_{op} are the tool-joint and drillpipe OD, respectively.

If the hole curvature is greater than the right side of inequality (Eq. 9.42), a pipe-to-wall contact develops, and then Eq. 9.41 must be used. It is also possible that an arc of contact between the pipe and the hole wall may develop (Case 3). This situation, however, is rare for Range 2 drillpipe and for this reason is not described in this text. A complete mathematical model of drillpipe performance in a hole of constant curvature is given by Lubinski (1977, 1987).

Example 9.9 Consider a Range 2 drillpipe with $D_{op} = 4.5$ in. and $D_{ip} = 3.826$ in. in a hole with a dogleg of 5.729°/100 ft. Calculate the bending stress if the weight of the drillstring (buoyant weight) below the dogleg is 70,000 lbf. The tool-joint OD is 6 in.

Solution.

Hole curvature:

$$(a) \quad \kappa = 5.729^\circ/100 \text{ ft} = (8.333)10^{-5} \text{ in.}^{-1}$$

Moment of inertia:

$$(b) \quad I = \frac{\pi}{64} (4.5^4 - 3.826^4) = 9.6105 \text{ in.}^4$$

α , $\alpha \ell_{ij}$, $\tanh(\alpha \ell_{ij})$ can be defined as:

$$(c) \quad \alpha = \sqrt{\frac{70,000}{(30)(10^6)(9.6105)}}, \text{ in.}^{-1},$$

$$(d) \quad \alpha \ell_{ij} = 2.8014,$$

$$(e) \quad \tanh(2.8014) = 0.9926.$$

The right side (RS) of inequality (Eq. 9.42) is:

$$(f) \quad RS = \frac{\frac{0.5(6-4.5)}{180^2}}{0.5 - \frac{\cosh(2.8014) - 1}{(2.8014)\sinh(2.8014)}} = (1.26)10^{-4} \text{ in}^{-1}.$$

Because the RS is greater than the hole curvature, Eq. 9.40 is chosen to calculate the drillpipe curvature:

$$(g) \quad \kappa_p = (8.333)(10^{-5}) \frac{2.8014}{0.9926} = (2.3517)(10^{-4}) \text{ in}^{-1}.$$

Now Eq. 9.36 is used to determine the bending stress:

$$(h) \quad \sigma_b = (0.5)ED_{op}\kappa_p = (0.5)(30)(10^6)(4.5)(2.3517)(10^{-4}) = 15,874 \text{ psi}.$$

Note that if the DLS is used rather than the pipe curvature,

$$(i) \quad R = \frac{5,729.6}{5.729} = 1,000 \text{ ft} = 12,000 \text{ in.},$$

and from Eq. 9.36, the bending stress is:

$$(j) \quad \sigma_b = \frac{(30)(10^6)(4.5)}{(2)(12)(10^3)} = 5,625 \text{ psi}.$$

Therefore, it can be concluded that use of the hole curvature rather than the actual pipe curvature may lead to a significant underestimation of bending stress.

Example 9.9 clearly shows that miscalculation of bending stress may lead to serious overestimation of permissible rotary torque, resulting in possible *twistoff* of the pipe in the immediate vicinity of the tool joints. At this point, the reader is strongly encouraged to recalculate Example 9.8 and draw conclusions.

Consider again the drillpipe of Example 9.9, which is under an effective tensile stress of $70,000/4.4075 = 15,882$ psi. As a result of bending, the outer pipe fiber is actually subjected to a tensile stress of $15,882 + 15,874 = 31,756$ psi, while at the inner fiber, the tensile stress is only $15,882 - 15,874 = 8$ psi. While the drillpipe is rotated about its axis, the outer fiber becomes the inner fiber, and vice versa. Thus, because of rotation, the fiber under consideration undergoes an effective stress variation ranging from 8 psi to 31,756 psi. Such repeated wide fluctuations in stress may result in so-called fatigue failure in the pipe.

The maximum reverse bending stress that will not cause fatigue failure is called the *endurance limit*. The endurance limit depends on a number of factors, the most important being the average tensile stress and the working environment of the pipe. It is known that the greater the average tensile stress, the smaller the endurance limit. The concept of endurance limit applies to noncorrosive environments. In a corrosive drilling fluid (H_2S , CO_2 , etc.), the pipe will always fail after a certain number of stress reversals (rotations), even if the bending stress is small (less than the endurance limit).

For grade E and grade S-135 drillpipe, the endurance limit can be calculated from the following equations:

For grade E:

$$\sigma_b = 19,500 - \frac{10}{67} \sigma_e - \frac{0.6}{(670)^2} (\sigma_e - 33,500)^2, \quad \dots \quad (9.43)$$

which is valid for $\sigma_e < 67,000$ psi.

For grade S-135:

$$\sigma_b = 20,000 \left(1 - \frac{\sigma_e}{145,000} \right), \quad \dots \quad (9.44)$$

which is valid for $\sigma_e < 133,400$ psi. σ_e is the *effective tensional stress*, which is equal to the ratio of the buoyant weight of the drillstring to the cross-sectional area of the pipe. Once the value of σ_e has been determined, the corresponding maximum permissible bending stress can be obtained from Eq. 9.43 or Eq. 9.44. Consequently, the corresponding pipe curvature can be calculated as

$$\kappa_p = \frac{2\sigma_b}{ED_{op}} \quad \dots \quad (9.45)$$

By substituting the value obtained above for κ_p in Eq. 9.40 or Eq. 9.41, finally a value of the so-called *maximum permissible hole curvature* (DLS) can be obtained.

Because the maximum permissible DLS is a decreasing function of the tensile load (the buoyant weight of the drillstring below the dogleg), doglegs are particularly dangerous in the upper part of the hole. If the hole curvature is greater than the maximum permissible curvature, drillpipe fatigue failure may occur. For this reason, it is recommended that, if possible, the DLS should be kept below the maximum permissible value. If the hole curvature is greater than the maximum permissible value, the pipe will accumulate fatigue damage and eventually will fail if rotated for a sufficiently long time. Therefore, to avoid costly drillpipe failures, good records should be kept of the individual pipe segments as they pass through doglegs that exceed the maximum permissible values.

Example 9.10 Calculate the maximum permissible DLS for the following drillstring and hole data: drillpipe steel grade S-135, Range 2, $D_{op} = 4.5$ in. ($D_{ip} = 3.826$, $A = 4.4074$ in.²), unit weight 18.4 lbf/ft (with tool joints). Tool-joint outside diameter $D_{otj} = 6$ in. Drill collars are 7 in. by 2¼ in. with unit weight 117 lbf and total length 550 ft. Drilling-fluid density is 12 lbm/gal. Anticipated depth of the hole below the dogleg is 8,000 ft.

Solution.

- (a) Buoyancy factor: $K_b = 1 - 12/65.4 = 0.815$
- (b) Buoyant weight of drill collars: $(550)(117)(0.815) = 52,445$ lbf
- (c) Buoyant weight of drillpipe: $(8,000 - 550)(18.4)(0.815) = 111,720$ lbf
- (d) Buoyant weight suspended below the dogleg: 164,165 lbf
- (e) Effective tensile stress: $\sigma_e = 164,165/4.4074 = 37,247$ psi

The maximum permissible bending stress can be calculated from Eq. 9.44 as

$$\sigma_b = 20,000 \left(1 - \frac{37,247}{145,000} \right) = 14,862 \text{ psi.}$$

The corresponding pipe curvature (Eq. 9.45) is

$$(f) \quad \kappa_p = \frac{2(14,862)}{30(10^6)4.5} \text{ in.}^{-1} = 2.20 \times 10^{-4} \text{ in.}^{-1}$$

Other related data are

$$(g) \quad I = \frac{\pi}{64}(4.5^4 - 3.826^4) = 9.6 \text{ in.}^4$$

$$(h) \quad \alpha = \sqrt{\frac{F}{EI}} = \sqrt{\frac{164 \ 165}{(30)(10^6)(9.6)}} = 0.02387, \text{ in.}^{-1}$$

$$(i) \quad \alpha \ell_{ij} = (0.02387)(180) = 4.296$$

Maximum permissible DLS:

Using Eq. 9.40,

$$(j) \quad \kappa = \kappa_p \frac{\tanh(\alpha \ell_{ij})}{\alpha \ell_{ij}} = (2.20 \times 10^{-4}) \frac{\tanh(4.296)}{4.296} = 5.12 \times 10^{-5} \text{ in.}^{-1}$$

$$= (5.12)(10^{-5}) \left(\frac{180}{\pi} \right) (12)(100) = 3.52^\circ/100 \text{ ft.}$$

Hence, the maximum permissible DLS is $3.52^\circ/100 \text{ ft.}$

If the pipe is used in a corrosive medium, these calculated values should be somewhat reduced. The choice of design factor should be based on experience from wells with similar drilling conditions.

Pressure-Induced Stresses. Generally, because of drilling-fluid flow, the pressure inside the drillstring is different from the pressure outside. If the drilling fluid is circulated down the drillpipe and up the annular space, the pressure inside the drillstring is greater than the pressure outside. If, however, the drilling-fluid circulation is reversed, the opposite holds true. Consider a certain pipe cross section at which the pressures are P_i inside the pipe and P_o outside the pipe. The pressures P_i and P_o exist because of flow, not because of hydrostatic pressure. These pressures induce axial, tangential, and radial stresses, which can be calculated as

$$\sigma_{an} = \frac{r_i^2 P_i - r_o^2 P_o}{r_o^2 - r_i^2}, \quad \dots \dots \dots (9.46)$$

$$\sigma_t = \frac{(P_i - P_o) r_i^2 r_o^2}{(r_o^2 - r_i^2) r^2} + \sigma_{an}, \quad \dots \dots \dots (9.47)$$

$$\sigma_r = -\frac{(P_i - P_o) r_i^2 r_o^2}{(r_o^2 - r_i^2) r^2} + \sigma_{an}, \quad \dots \dots \dots (9.48)$$

where σ_{an} = axial neutral stress, psi; σ_t = tangential stress, psi; σ_r = radial stress, psi; r_i and r_o = inner and outer radii of the pipe, in.; and r = radial distance to a point in the cross section under consideration, in. (**Fig. 9.9**).

Eqs. 9.47 and 9.48 are known as Lamé's equations. It should be well understood that the neutral axial stress as given by Eq. 9.46 has no effect on bending. It can be shown (Lubinski 1975, 1988), that an increase in the pressure P_i , which results in an increase in the axial stress, does not decrease the pipe tendency to bending. Even a very high value of the inside pressure, P_i , does not prevent bending or buckling of the pipe. On the other hand, an

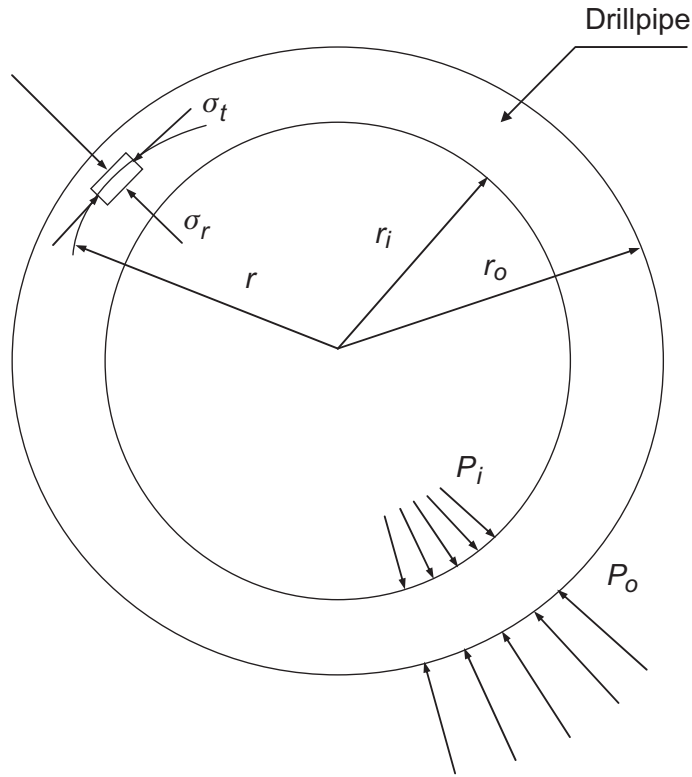


Fig. 9.9—Pipe cross section.

increase in the outside pressure, P_o , although it may produce high compressive stress, does not induce buckling. For this reason, the stress given by Eq. 9.46 is called the *neutral axial stress*.

9.4 Load Capacity of Drillpipe

The proper selection of drillstring components is based on the combined effect of stresses due to tension, torque, bending, and pressures. To evaluate the load capacity of drillpipe (e.g., the maximum allowable tensile load when torque, bending, and pressure are applied simultaneously, or the maximum allowable torque when tensile and other loads are given), once again the maximum-energy-of-distortion theory can be used. According to this theory, yielding occurs when an effective stress that is a function of axial, tangential, radial, and shear stresses reaches the yield point. In the present case, the effective (equivalent) stress may be calculated from the following equation:

$$2\sigma_{vm}^2 = (\sigma_z - \sigma_t)^2 + (\sigma_t - \sigma_r)^2 + (\sigma_r - \sigma_z)^2 + 6\tau^2, \quad \dots \quad (9.49)$$

where σ_z , σ_t , σ_r , and τ are the axial, tangential, radial, and shear stresses, respectively.

If a bending stress exists, it must be added to (or subtracted from) the axial stress, σ_a . The stresses σ_a , σ_t , and σ_r in Eq. 9.49 are calculated without including any isotropic stresses caused by the hydrostatic pressure of the drilling fluid. Once the individual stress components have been determined, the resultant equivalent stress can be calculated:

$$\sigma_{vm} = \frac{1}{\sqrt{2}} \left[(\sigma_z - \sigma_t)^2 + (\sigma_t - \sigma_r)^2 + (\sigma_r - \sigma_z)^2 + 6\tau^2 \right]^{1/2}. \quad \dots \quad (9.50)$$

If the value of σ_{vm} is less than the yield point, the design is theoretically safe. By substituting for $\sigma_{vm} = \sigma_y$ (σ_y = yield strength), Eq. 9.50 can be solved for any one of the stress components if the remaining components are given. In this manner, a number of field problems can be solved by the intelligent application of Eq. 9.50.

For example, consider a drillpipe of known geometric properties that is subjected to an axial stress, σ_a , a bending stress, σ_b , a torsional stress, τ , and internal and external pressures, P_i and P_o , respectively. Substituting for σ_t and σ_r , Eqs. 9.47 and 9.49 (Lamé's equations) after some rearrangements become (Lubinski 1987):

$$\sigma_{vm} = \left\{ \left[\left(\frac{r_i}{r} \right)^2 \frac{\sqrt{3}}{2} (P_i - P_o) f_{td} \right]^2 + \left(\sigma_a - \sigma_{an} \pm \sigma_b \frac{r}{r_o} \right)^2 + 6 \left(\frac{\tau r}{r_o} \right)^2 \right\}^{1/2}, \quad \dots \quad (9.51)$$

where

$$f_{td} = \frac{1}{2} \frac{\left(\frac{D_{op}}{t} \right)^2}{\left(\frac{D_{op}}{t} \right) - 1}, \quad \dots \quad (9.52)$$

where t = pipe-wall thickness ($t = r_o - r_i$). All other notations have already been described.

In regular rotary-drilling operations, the pressure losses in the annular space of the hole are relatively small compared with the losses in other parts of the circulating system and can be ignored in many practical calculations related to drillstring design. Of course, annular pressure losses are very important for accurate calculations of ECD (as discussed in Chapter 5), slimhole, and casing-drilling applications.

The sign (\pm) in Eq. 9.51 accounts for the fact that the bending stress, σ_b , must be added to the average axial stress on one side of the pipe and subtracted from it on the other. It can be shown that for zero bending and torsion, the von Mises effective stress, σ_{vm} , reaches its maximum at $r = r_i$ (i.e., at the inner boundary of the pipe). If, however, the bending and shear stresses are not zero, the von Mises effective stress, σ_{vm} , reaches its maximum at $r_o \geq r \geq r_i$ (i.e., between the inner and the outer boundaries of the pipe).

Example 9.11 Consider the drilling conditions described in Example 9.9. Assuming a drillpipe pressure of 3,500 psi and a tensile load of 165,000 lbf, calculate the maximum allowable rotary torque that can be applied to the pipe if the required SF is 2.0. Ignore the pressure losses in the annular space ($P_o = 0$).

Solution.

- (a) The axial stress is: $\sigma_e = \frac{165,000}{4.4074} = 37,500$ psi.
- (b) The neutral axial stress (Eq. 9.46) is: $\sigma_{an} = \frac{(1.913)^2 (3,500)}{(2.25)^2 - (1.913)^2} = 9,130$ psi.
- (c) Assume that the bending stress is $\sigma_b = 15,000$ psi.
- (d) The quantity $f_{td} = 0.5 \frac{\frac{4.5}{0.337}}{\frac{4.5}{0.337} - 1} = 0.540$.

Substituting for $\sigma_{vm} = 135,000/2.0 = 67,500$ psi, the worst case was found for setting $r = r_o = 2.25$ in., and solving Eq. 9.51 for the maximum allowable shearing stress produces the following result

$$(e) \quad \tau_{max} = \frac{1}{\sqrt{6}} \left\{ (67,500)^2 - \left[\left(\frac{2.25}{1.913} \right)^2 \frac{\sqrt{3}}{2} (3,500)(0.54) \right]^2 - (37,500 - 9,130 + 15,000)^2 \right\}^{1/2} = 21,110 \text{ psi}$$

Hence, the maximum allowable torque is only:

$$(f) \quad T = (21,100)(8.542) = 186,575 \text{ in.-lbf} = 15,548 \text{ ft.-lbf.}$$

Load Capacity of Tool Joints. Individual drillpipe joints are connected together by means of *tool joints*. A tool joint is usually welded onto the drillpipe and consists of a pin and a box, as illustrated in Fig. 9.7.

Not only do the tool joints hold the drillpipe together, but the shoulders of the connections also form a metal-to-metal seal that prevents leakage. The shouldered connections of the drillstring differ in concept from tubing or casing connections. Casing and tubing threads are designed for continuous contact of the thread crest, root, and flanks to provide the desired seal. The threads of tool joints are not designed to provide seals, but are designed to be made up even if the box is overflowing at the time of makeup with drilling fluid laden with solids. Consequently, some clearance must be provided at the crest and root of the thread to accommodate these solids. For this reason, a seal is provided only at the shoulders. In other words, the shoulder is the only area of seal in a rotary shouldered connection. To prevent separation of the shoulders under tension, bending, or both, an appropriate amount of makeup torque is required.

API RP 7G (1998) contains statements such as, “tonging of tool joints properly when going into the hole is one of the most critical of the rig activities in the life of the drillstring and the eventual cost of the operations.” However, fully tested formulas to predict the load capacity of tool joints do not now exist. The following equations describe the major concepts involved in determining the load capacity of a tool joint. If these equations are used for actual design calculations, an appropriate SF must be used.

The makeup torque produces an axial preloading within the pin and the box, as well as torsional stresses. More specifically, the makeup torque induces a tensile stress state within the pin and a compressive stress state within the box. The average magnitude of the axial stress due to the makeup torque can be calculated from the screw-jack equation (Farr 1957):

$$T_m = \frac{\sigma_a A_t}{12} \left(\frac{p_t}{2\pi} + \frac{R_t \mu}{\cos \theta} + R_s \mu \right), \quad \dots \dots \dots (9.53)$$

where T_m = makeup torque, ft-lb; σ_a = axial stress, psi (pin is in tension, box is in compression); A_t = cross-sectional area (for a pin at $\frac{3}{4}$ in. from the shoulder, for a box at $\frac{3}{8}$ in. from the shoulder), in.²; p_t = lead of thread, in.; R_t = mean radius of thread, in.; R_s = mean radius of shoulder, in.; θ = one-half of thread angle, degrees; and μ = coefficient of friction (approximately 0.06–0.08 on average).

The quantity $\sigma_a A_t = W_{pr}$ is called *preloading* and is caused by the torque, T_m . The preloading induced by the makeup torque decreases the total tensile load capacity of the pin. However, the benefit of this design (with its shoulder-to-shoulder contact) considerably outweighs the detrimental effect of the tensile stress induced in the pin. Remember that all connections must be bucked up properly so that the shoulders never separate during drilling or tripping operations. Eq. 9.53 also represents the minimum value of makeup torque required for a given axial load, W , if the product $\sigma_a A$ is replaced by W .

When the tool joint, made up with torque T_m , is subjected to an axial tensional load, its axial load capacity is determined by the tensile strength of the pin. Ignoring the lateral load on the pin created by the axial forces,

$$Q = S_y A_p - W_{pr}, \quad \dots \dots \dots (9.54)$$

where Q = pullout strength of the joint (axial load capacity of tool joint), lbf; W_{pr} = preloading created by the makeup torque, lbf; S_y = minimum yield strength of the pin material, psi; and A_p = pin cross-sectional area, in.².

It can be shown that if lateral load effects are included, the tool-joint pullout strength is

$$Q = \frac{S_y A_p - W_{pr}}{\sqrt{1 + \frac{R_t \cot(\beta + \eta)}{2L_t}} \left[1 + \frac{R_t \cot(\beta + \eta)}{2L_t} \right]}, \quad \dots \dots \dots (9.55)$$

where $\eta = \arctan(\mu)$, degrees; $\beta = 90 - \theta$, degrees; and L_t = length of the threaded portion of the pin, in. All other notations have already been explained.

The maximum value of makeup torque that can be applied to the tool joint for a given axial load, F , is

$$T_{\max} = \frac{(S_y A_p - F)}{12} \left(\frac{p_t}{2\pi} + \frac{R_t \mu}{\cos \theta} + R_s \mu \right). \quad \dots \dots \dots (9.56)$$

Examination of Eqs. 9.53 and 9.56 leads to the conclusion that although the minimum makeup torque increases linearly with the axial load, F (the lateral loading of the pin and the box due to axial force is ignored), the maximum torque decreases linearly with F .

A graphical representation of Eqs. 9.53 and 9.54 is shown in **Fig. 9.10**. This diagram is called a *screw triangle*. By comparing Eqs. 9.53 and 9.56, it is apparent that the intersection of the minimum and maximum makeup-torque lines occurs at $F = 0.5 S_y A_p$. The value of makeup torque corresponding to this point is called the *recommended makeup torque*. For a given type of tool joint, the recommended makeup torque can be found in *API RP 7G*. A good understanding of the screw triangle and the recommended makeup torque is essential for proper use of the drillstring.

Example 9.12 Consider 4.5- × 3.826-in., EU 75 drillpipe (with a yield strength of 75,000 psi) furnished with the new NC 50 (IF) tool joints. According to *API RP 7G* (1998), the recommended makeup torque for this joint is 18,900 ft-lbf. Calculate the pullout strength of the tool joint if $R_t = 2.375$ in., $L_t = 4\frac{1}{2}$ in., $\theta = 30^\circ$, and $A_p = 7.867$ in.². Assume a friction coefficient of 0.08.

Solution. Assuming that the joints are actually made up with a torque equal to the makeup torque, the preloading on the pin is

$$W_{pr} = 0.5 S_y A_p = (0.5)(120,000)(7.867) = 422,000 \text{ lbf.}$$

Before using Eq. 9.55, it is necessary to calculate

$$\eta = \arctan(0.08) = 4.57^\circ,$$

$$\beta = 90 - 30 = 60^\circ.$$

Use of Eq. 9.55 then yields:

$$Q = \frac{422,000}{\sqrt{1 + \frac{(2.375) \cot(64.57)}{(2)(4.5)}} \left[1 + \frac{(2.375) \cot(64.57)}{(2)(4.5)} \right]} = 395,000 \text{ lbf.}$$

Note that the axial load capacity of the drillpipe is $F = (75,000)(4.4074) = 330,555$ lbf. Hence, the tool-joint axial load capacity is greater than that of the drillpipe. It is generally recommended that properly selected drillpipe and tool joints will have this property.

It must be emphasized that the values obtained from the equations shown above are theoretical values. Actual tool joints in field operations are subject to many factors not considered here that may affect tool-joint strength. To withstand higher loads associated with drilling of high-angle extended-reach wells as well as deepwater and

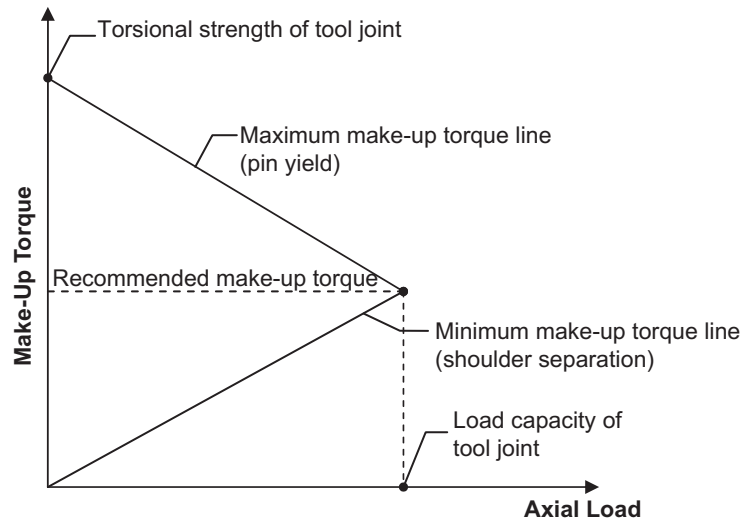


Fig. 9.10—Makeup torque vs. axial load.

ultradeepwater wells, one can use a second-generation, doubled-shoulder connection. Double-shouldered connection provides high torsional strength and gas-tight pressure sealing capacity.

Slip Crushing. The most common method of drillpipe support in the rotary table is the *slip-type mechanism*, shown schematically in **Fig. 9.11**. Once the drillpipe has been suspended from the slips, the wedge's taper produces a transverse force (perpendicular to the pipe axis), which is transmitted into the pipe. It is of critical importance that the pipe be gripped in such a manner that no permanent damage occurs as a result of this transverse force. The distribution of the transverse load is shown in **Fig. 9.11b**. It can be seen that the axial load is greatest at the bottom of the slip. The transverse load diminishes to zero at the bottom and at the top of the slip. The maximum value of the transverse load occurs near the middle of the slip. The critical section of the slip is Section B, where the combined loads (axial and transverse) can cause permanent damage to the pipe.

Theoretically, the maximum allowable static axial load (F_{slip}) that can be supported in the slips can be calculated using the following equation:

$$F_{\text{slip}} = F_{ti} \left[\frac{2}{1 + \left(1 + \frac{2r_o^2 K_s A_{dp}}{(r_o^2 - r_i^2) A_c} \right)^2 + \left(\frac{2r_o^2 K_s A_{dp}}{(r_o^2 - r_i^2) A_c} \right)^2} \right]^{1/2}, \dots \dots \dots (9.57)$$

where F_{ti} = drillpipe tensional load capacity, lbf; A_c = contact area between slips and pipe ($A_c = 2\pi r_o L_s$), in.²; A_{dp} = drillpipe cross-sectional area, in.²; r_o = outside radius of pipe, in.; r_i = inside radius of pipe, in.; L_s = length of slips (12 or 16 in.); and K_s = lateral load factor of slips:

$$K_s = \frac{1 - \mu \tan \psi}{\mu + \tan \psi}, \dots \dots \dots (9.58)$$

where μ = the coefficient of friction between the slips and the bushings and ψ = the taper of the slip in degrees.

If the actual load on the drillstring is less than that calculated from Eq. 9.57, the pipe should not be damaged in the slip area unless the slip itself is improperly supported in the bushings. For practical engineering calculations, an appropriate SF must be used.

Example 9.13 Determine the maximum allowable axial load that can be supported from a set of slips with length 12 in. and taper $\psi = 9^\circ 27' 45''$. The drillpipe data include $D_{op} = 3.5$ in., $D_{ip} = 2.602$ in., $A = 4.3037$ in.², and $S_y = 95,000$ psi. Perform the calculations for $\mu = 0.1$ and $\mu = 0.2$. Assume an SF of 1.8.

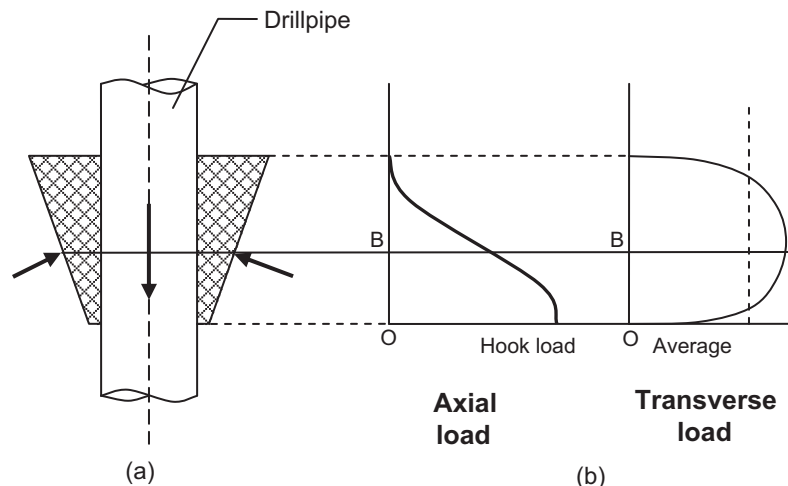


Fig. 9.11—Forces in the slip mechanism.

Solution.

Drillpipe load capacity:

$$(a) \quad F_{ti} = (95,000)(4.3037) = 408,848 \text{ lbf.}$$

Contact area between slips and pipe:

$$(b) \quad A_c = 2\pi(1.75)(12) = 132 \text{ in.}^2.$$

Lateral load factor for $\mu = 0.1$:

$$(c) \quad K_s = \frac{1 - (0.1)\tan(9.5)}{0.1 + \tan(9.5)} = 3.68.$$

Lateral load factor for $\mu = 0.2$:

$$(d) \quad K_s = \frac{1 - (0.2)\tan(9.5)}{0.2 + \tan(9.5)} = 2.63.$$

Use of Eq. 9.58 yields (for $K = 3.68$)

$$F_{\text{slip}} = (408,848) \left\{ \frac{2}{1 + \left[1 + \frac{(2)(1.75)^2 (3.68)(4.3216)}{(1.75^2 - 1.301^2)(132)} \right]^2 + \left[\frac{(2)(1.75)^2 (3.68)(4.3216)}{(1.75^2 - 1.301^2)(132)} \right]^2} \right\}^{1/2}$$

$$= 302,320 \text{ lbf.}$$

In a similar manner, for $K_s = 2.63$, the result is $F_{\text{slip}} = 319,461 \text{ lbf.}$ It is apparent that $\mu = 0.2$ yields a value of F_{slip} greater than that obtained for $\mu = 0.1$. This is not surprising in view of the elementary principles of the wedge mechanism. If the wedge is clean and well lubricated, the coefficient of friction between the wedge and the supporting member is low, producing an increased transverse force. If the wedge is dry and not lubricated, the coefficient of friction increases, and more axial force is required to drive the wedge downward. In conclusion, the contact surface between the bushing and the slips should be clean (free of other bodies), dry, and not lubricated.

9.5 Drillstring Design

The purpose of drillstring design is to determine the optimal size, grade, and length of drillstring components so that they will be sufficiently strong, yet entail minimum cost. Because of the complexity of the problem, an iterative approach is normally used. A design model is initially assumed, the components of the drillstring are selected, and then the design is refined by incorporating factors that were ignored during the first step. The designer must possess a good knowledge of drillstring performance properties (available sizes, grades, etc.), data from wells already drilled in similar conditions to those of the well under consideration, and also current prices of the drillstring components.

The final design should satisfy the following major criteria:

1. The load capacity of any drillstring member (divided by an SF) should be greater than or equal to the maximum permissible load.
2. Neighboring elements must be compatible. This is accomplished by selecting elements with an appropriate *bending-stress ratio* (BSR).
3. The drillstring geometric properties should be selected in conjunction with an optimal hydraulic and casing program.

4. In deviated wells, drillstring rotation should not produce excessive casing damage.
5. The total cost of the string should be kept to a minimum.

Keeping in mind the criteria just mentioned and the fact that the drillstring is subjected to loads that may be cyclic and dynamic, the problem of drillstring design is rather complex. Because of the number and complexity of the calculations involved, obtaining a good design requires the use of high-speed computers. In this chapter, a simplified approach is presented to illustrate the concepts involved and their practical importance.

First, the designer selects the drill-collar size based on the hole and casing diameters. Typically, the components of the BHA are selected on the basis of deviation-control requirements as discussed in Chapter 8. Next, the drillpipe size is selected. To avoid a rapid change in bending stiffness, an intermediate member may be placed between the drill collars and the drillpipe. For best performance, the BSR of adjacent members should be less than approximately 5.0–5.5. The BSR is defined as the ratio of the section moduli of two adjacent members of the drillstring. To satisfy this requirement, more than one size of drill collar may be needed. In addition, a few joints of heavy-walled pipe are often placed above the collars below the regular drillpipe to obtain a BSR < 5.

The maximum allowable length of drillpipe (Section 1) that should be placed above the heavyweight pipe can be calculated as

$$\frac{F_1}{SF} = (L_{dc}w_{dc} + L_{hw}w_{hw} + L_{dp1}w_{dp1})K_b, \quad \dots \quad (9.59)$$

where L_{hw} = length of heavyweight drillpipe (if used in the drillstring), lbf/ft; w_{hw} = unit weight of heavyweight drillpipe, lbf/ft; L_{dp1} = length of Section 1 of the drillpipe, ft; w_{dp1} = unit weight of Section 1 of the drillpipe, lbf/ft; F_1 = tension load capacity of Section 1 of the drillpipe, lbf; and SF = safety factor. Other quantities have already been defined in previous sections of this chapter.

Eq. 9.59 is valid for a vertical hole; however, a corresponding equation can be written for a directional well if the hole shape is known. The tension-load capacity of a particular drillpipe (F_1) can be determined as outlined in Section 9.4. Here, for the sake of simplicity, only axial and torsional loads are assumed, so

$$F_1 = \sqrt{F_{t1}^2 - 3\left(\frac{A_1}{Z_1}T\right)^2}, \quad \dots \quad (9.60)$$

where F_{t1} = tensional axial load capacity of Section 1 of the drillpipe ($F_{t1} = S_y A_1$); A_1 = cross-sectional area of Section 1, in.²; Z_1 = sectional modulus of Section 1, in.³; and T = rotary torque applied to the drillstring, in.-lbf.

The magnitude of the SF depends on the quality of the drillstring, the drilling practices, the working environment, and drilling experience from offset wells. Substituting Eq. 9.60 into Eq. 9.59 and solving for the length of Section 1 of the drillpipe leads to

$$L_{dp1} = \frac{F_1}{(SF)K_b w_{dp1}} - \frac{L_{dc}w_{dc}}{w_{dp1}} - \frac{L_{hw}w_{hw}}{w_{dp1}}. \quad \dots \quad (9.61)$$

If the sum $L_{dc} + L_{hw} + L_{dp1}$ is less than the planned depth of the hole, a stronger pipe must be selected for the portion above Section 1. This stronger pipe will be called Section 2 of the drillpipe.

The maximum length of Section 2 of the drillpipe can be calculated as

$$L_{dp2} = \frac{F_2}{(SF)K_b w_{dp2}} - \frac{L_{dc}w_{dc}}{w_{dp2}} - \frac{L_{hw}w_{hw}}{w_{dp2}} - \frac{L_{dp1}w_{dp1}}{w_{dp2}}, \quad \dots \quad (9.62)$$

$$F_2 = \sqrt{F_{t2}^2 - 3\left(\frac{A_2}{Z_2}T\right)^2}, \quad \dots \quad (9.63)$$

where F_{t2} = tension load capacity of Section 2 of the drillpipe; L_{dp2} = length of Section 2, ft; w_{dp2} = unit weight of Section 2, lbf/ft; A_2 = cross-sectional area of Section 2, in.²; and Z_2 = sectional modulus of Section 2, in.³.

Again, the sum $L_{dc} + L_{hw} + L_{dp1} + L_{dp2}$ is calculated and checked against the total hole depth. If necessary, a third section must be used. Normally, however, to avoid excessive logistical problems, no more than two sections are recommended. A drillstring consisting of more than one size of drillpipe is called a *tapered drillstring*.

Once the drillpipe sizes and lengths have been determined, tool joints should be selected so that their load capacities are greater than that of the drillpipe. The drillstring configuration as obtained must be checked for margin of overpull, bending loads, drilling-fluid pressure, and drillpipe crushing in slips. Usually there are several different drillstring combinations that satisfy the desired strength requirements. To arrive at the final selection, the cost of the various drillstring configurations is calculated, and the design that yields the lowest cost is chosen. In other words, the designer must consider string mechanical integrity, operational difficulties, and economics to select the optimal set of drillstring components.

Example 9.14 Design a drillpipe for the following conditions:

Hole depth = 7,000 ft

Hole size = 7 $\frac{7}{8}$ in.

Mud SG = 1.2 (water = 1.0)

Drill collars: 6 $\frac{1}{4}$ \times 2 $\frac{1}{4}$ in. with unit weight = 91 lb/ft

Length of drill collars = 600 ft

Heavyweight drillpipe = 4 $\frac{1}{2}$ in. by 2 $\frac{3}{4}$ in. with unit weight 41 lb/ft

Length of heavyweight drillpipe = 180 ft

Available drillpipe sizes and grades as given below:

Drillpipe OD (in.)	Cross- Sectional Area (in. ²)	Polar Sectional Modulus (in. ³)	Nominal Unit Weight (lb/ft)	Steel Grade	Tool Joint		
					OD _{ij}	ID _{ij}	Makeup Torque
4 $\frac{1}{2}$	4.4074	8.543	16.60	EU-75	6 $\frac{3}{8}$	3 $\frac{3}{8}$	18,838
4 $\frac{1}{2}$	5.4981	10.232	20.0	EU-75	6 $\frac{3}{8}$	3 $\frac{5}{8}$	20,617

Desired SF = 2.0.

Minimum margin of overpull = 100,000 lbf.

Solution.

Buoyancy factor:

$$K_b = 1 - \frac{1.2}{7.85} = 0.847.$$

Weight of drill collars:

$$w_{dc} L_{dc} = (91)(600) = 54,600 \text{ lbf}$$

Weight of heavyweight drillpipe:

$$w_{hw} L_{hw} = (41)(180) = 7,380 \text{ lbf}$$

Axial load capacity, Section 1 of drillpipe ($w_n = 16.60$ (nominal) lb/ft \rightarrow actual = 17.98 lb/ft):

$$F_{t_1} = (4.4074)(75,000) = 330,555 \text{ lbf.}$$

Axial load capacity, Section 2 of drillpipe [$w_n = 20.0$ (nominal) lb/ft \rightarrow actual = 21.62 lb/ft]:

$$F_{t_1} = (5.4981)(75,000) = 412,358 \text{ lbf.}$$

Load capacity, Section 1 of drillpipe, corrected for torque (Eq. 9.60):

$$F_1 = \left\{ (330,555)^2 - 3 \left[\frac{4.4074}{8.543} (12)(18,838) \right]^2 \right\}^{1/2} = 261,658 \text{ lbf.}$$

Load capacity, Section 2 of drillpipe, corrected for torque (Eq. 9.63):

$$F_2 = \left\{ (412,358)^2 - 3 \left[\frac{5.4981}{10.232} (12)(20,617) \right]^2 \right\}^{1/2} = 342,080 \text{ lbf.}$$

Note that to calculate the load capacity of the drillpipe as corrected for torque, the makeup torque is used. This is reasonable because the rotary torque should not exceed the makeup torque.

Eq. 9.61 can be used to calculate the length of Section 1 of the drillpipe [$w_n = 16.60$ (nominal) lbf/ft]:

$$L_{dp1} = \frac{261,658}{(2.0)(0.847)(17.98)} - \frac{54,600}{17.98} - \frac{7,380}{17.98} = 5,149 \text{ ft.}$$

Assuming that the average joint length is 30 ft, the result is 172 joints with a total length of 5,160 ft. Because the combined length of the drill collars, the heavyweight drillpipe, and Section 1 of the drillpipe (5,880 ft) is less than the total hole depth (7,000 ft), it is necessary to place some stronger pipe above Section 1.

Eq. 9.62 yields

$$L_{dp2} = \frac{342,080.7}{(2.0)(0.847)(21.62)} - \frac{54,600}{21.62} - \frac{7,380}{21.62} - \frac{(5,160)(17.98)}{21.62} = 2,182 \text{ ft.}$$

Because the hole depth is 7,000 ft, the length of drillpipe needed for Section 2 is 1,120 ft, and the total weight of the string is

$$[(600)(91) + (180)(41) + (5160)(17.98) + (1120)(21.62)](0.847) = 151,560 \text{ lbf.}$$

Therefore, the margin of overpull (MOP) is

Section 2:

$$\text{MOP} = 342,080 - 151,560 = 190,520 \text{ lbf.}$$

Section 1:

$$\text{MOP} = 261,140 - 131,079 = 130,061 \text{ lbf}$$

It is clear that the margin of overpull is greater than the required minimum value, and therefore the drillstring configuration as obtained satisfies the design criteria.

Additional calculations should be performed to verify that the design meets the slip-crushing, bending-stress, and drilling-fluid pressure requirements stated in preceding sections of this chapter. Appropriate refinements should be introduced if the predicted stress levels become higher than the maximum acceptable values. In addition, other drillpipe sizes and steel grades should be considered to arrive at other designs. As previously stated, the configuration that meets the safety criteria and yields the least overall cost will become the final drillstring design.

Problems

- 9.1 Name the basic components of a drillstring.
- 9.2 Discuss the major functions of a drillstring.
- 9.3 What is the purpose of using drill collars?
- 9.4 Explain why spiral and square drill collars are sometimes used in a BHA.
- 9.5 List the major factors that affect selection of drill collars.
- 9.6 Select the drill-collar size and length for the following data:
 Hole size = 12¼ in.
 Casing size = 9⅝ in. with 10.625 in. OD coupling
 WOB = 55,000 lbf
 Mud weight = 11.5 lbf/gal
 Hole inclination angle = 15°
 Design factor = 1.1
- 9.7 Define the neutral point from the standpoint of buckling.
- 9.8 Calculate the critical WOB that will result in first-order buckling for the following data:
 Steel drill collars with $OD_{dc} = 7\frac{1}{2}$ in. and $ID_{dc} = 2\frac{1}{2}$ in.
 Mud SG = 1.4 (water = 1.0)
- 9.9 Explain why, after buckling of drill collars, a wellbore deviates from vertical.
- 9.10 Calculate the inclination of the resultant force acting on the bit if $OD_{dc} = 7\frac{1}{2}$ in., $ID_{dc} = 2\frac{1}{2}$ in., mud density = 12.5 lbm/gal, and WOB = 28,000 lbf. The hole diameter is $10\frac{5}{8}$ in.
- 9.11 Calculate the critical axial load that results in buckling of $4\frac{1}{2} \times 2\frac{3}{4}$ in. heavyweight drillpipe with a unit weight of 41 lbf/ft for the following hole inclination angles: 3, 6, 9, and 12°. The mud density is 10 lbm/gal, and the hole size is $8\frac{3}{4}$ in. Draw conclusions.
- 9.12 A drillstring is composed of 5,100 ft of $4\frac{1}{2}$ -in. drillpipe with a unit weight of 18 lbf/ft, 300 ft of $4\frac{1}{2}$ -in. heavyweight drillpipe with a unit weight of 41 lbf/ft, and 660 ft of $6\frac{1}{4}$ -in. drill collars with a unit weight of 91 lbf/ft. If the drilling-fluid density is 14 lbm/gal, find the hook load, assuming that the WOB is 34,000 lbf. Mud weight = 10 lbm/gal. Recalculate this example assuming air as a circulating fluid. To perform the calculations, ignore the hydrostatic head of air.
- 9.13 Using the drillstring composition in Problem 12, calculate the axial stress at the top of the hole and at the cross section located 2,000 ft from the top of the hole.
- 9.14 Calculate the total elongation of the string described in Problem 12 due to its own weight in mud and air.
- 9.15 Explain why an increase in rotary torque leads to a decrease in the load capacity of the drillpipe.
- 9.16 Consider the drillpipe data in Example 9.7. Using the maximum-energy-of-distortion theory, calculate the load capacity of the pipe if the torque is equal to 50% of the twistoff torque.
- 9.17 Recalculate Exercise 9.8 if the DLS is 11.458°/100 ft.
- 9.18 Calculate the maximum permissible DLS for the following drillstring and hole data:
 Drillpipe: Grade E, Range 2, $OD_{dp} = 5$ in., $ID_{dp} = 4.276$ in., actual unit weight = 20.89 lbf/ft;
 Tool joint: NC50 with $OD_{tj} = 6\frac{3}{8}$ in. and $ID_{tj} = 3\frac{3}{4}$ in.
 The buoyant weight of drillstring below the dogleg is 110,000 lbf. Mud weight = 11 lbm/gal.
- 9.19 Suppose that a drillpipe as specified in Example 9.10 is placed in a hole with a DLS of 14.5°/100 ft. The pressure inside the pipe is 3,000 psi, and the torque is 12,000 ft-lbf. Calculate the maximum allowable axial load capacity if the SF is 1.25.
- 9.20 Explain why making up a tool joint with proper torque is of critical importance for drillstring performance while drilling.
- 9.21 Recalculate Example 9.13 assuming that the length of the slips is 16 in. (long slips).
- 9.22 Define the BSR.
- 9.23 Redesign the drillstring discussed in Exercise 9.14 assuming a drillpipe steel grade of S-135.

Nomenclature

- A_t = cross-sectional area in screw-jack equation (9.53), in.²
 A_{dc} = cross-sectional area of drill collars, in.²
 A_{dp} = drillpipe cross-sectional area, in.²
 A_p = pin cross-sectional area, in.²
 A_i = cross-sectional area of Section i, in.²
 C_d = an empirical factor that depends on hole inclination angle
 C_f = an empirical factor ranging from $(4)10^{-6}$ for very hard formations to approximately $(14)10^{-5}$ for very soft formations

$d\phi/dz$	=	differential angle of twist, in. ⁻¹
d	=	nominal inside diameter of connection (Fig. 9.6), in.
D	=	nominal outside diameter of pipe (Fig. 9.6), in.
d_{ou}	=	minimum inside diameter of connection (Fig. 9.6), in.
D_b	=	drill bit diameter, in.
DF	=	design factor
D_{idc}	=	inside diameter of drill collar, in.
D_{ip}	=	inside pipe diameter, in.
DLS	=	dogleg severity, °/100 ft
D_{occ}	=	outside diameter of casing coupling, in.
D_{odc}	=	outside diameter of drill collar, in.
D_{op}	=	outside pipe diameter, in.
D_{otj}	=	OD of tool joint, in.
D_{ou}	=	maximum outside diameter of pipe (Fig. 9.6), in.
E	=	modulus of elasticity (Young's modulus), psi
f	=	coefficient
f_{td}	=	factor in Eq. 9.51
F	=	axial force, lbf
F_{cr}	=	critical buckling force, lbf
F_f	=	friction force, lbf
Fp_1	=	pressure force acting at the top of the drill collars, lbf
Fp_2	=	pressure force acting at the bottom of the drill collars, lbf
F_{cr}	=	critical buckling force, lbf
F_h	=	hook load, lbf
F_{slip}	=	maximum allowable static axial load that can be supported in the slips, lbf
F_{ti}	=	tensional axial load capacity of i th section of drillpipe, lbf
F_i	=	tension load capacity of Section i of the drillpipe, lbf
G	=	shearing modulus of elasticity (modulus of rigidity), psi
H	=	vertical distance, ft
H_0	=	lateral force at the bit, lbf
HP	=	horsepower
HP_b	=	horsepower to rotate a rotary roller rock bit
i	=	bending-moment coefficient
i_1	=	point of maximum bending moment that is nearest to the bit (Fig. 9.5)
i_2	=	point above i_1 (Fig. 9.5)
I	=	moment of inertia, in. ⁴
ID_{dc}	=	inside diameter of drill collars, in.
J	=	polar moment of inertia, in. ⁴
K_b	=	buoyancy factor
K_s	=	lateral load factor of slips
ℓ_{vj}	=	half the distance between tool joints, ft
L_{dc}	=	length of drill collars, ft
L_{dp}	=	length of drillpipe, ft
L_{dp1}	=	length of Section 1 of the drillpipe, ft
L_{hw}	=	length of heavyweight drillpipe, ft
L_N	=	distance from the bit to the neutral point, ft
L_r	=	length of rod, in.
L_s	=	length of slips (12 or 16 in.)
L_t	=	length of the threaded portion of the pin, in.
m	=	$\sqrt[3]{\frac{EI}{w_e}}$, length scaling factor, ft
M_1M_3 and $M'_1M'_3$	=	dimensionless distances to the two points of maximum bending moment
M_b	=	bending moment, ft-lbf
MOP	=	margin of overpull, lbf
n	=	coefficient in Eq. 9.6
N	=	side force at the point of tangency, lbf
OD_{dc}	=	outside diameter of drill collars, in.

ϕ	=	pitch of helix, ft
p_h	=	hydrostatic pressure, psi
P_i	=	pressure inside the pipe, psi
P_o	=	pressure outside the pipe, psi
P_t	=	lead of thread, in.
Q	=	pullout strength of the joint (axial load capacity of tool joint), lbf
r	=	radius, in.
r_c	=	radial clearance, in.
r_i	=	inside radius, in.
r_o	=	outside radius, in.
R	=	wellbore radius of curvature, ft
RPM	=	rotary speed, rev/min
R_s	=	mean radius of shoulder, in.
R_t	=	mean radius of thread, in.
SF	=	safety factor
SG	=	specific gravity
S_y	=	minimum yield strength of the pin material, psi
t	=	pipe thickness, in.
T	=	torque, ft-lbf
T_m	=	make-up torque, ft-lbf
T_{\max}	=	maximum rotary torque, ft/lbf
w_c	=	unit contact force, lbf/ft
w_{dc}	=	unit weight of drill collars, lbf/ft
w_{dp}	=	unit weight of drillpipe, lbf/ft
w_{dp1}	=	unit weight of Section 1 of the drillpipe, lbf/ft
w_{bp}	=	unit buoyant weight of drill collars in drilling fluid, lbf/ft
w_{hw}	=	unit weight of heavy weight drillpipe, lbf/ft
w_n	=	nominal unit weight, lbf/ft
W	=	weight on bit (WOB), lbf
W_1	=	weight of drillpipe below the cross section under consideration, lbf
W_2	=	weight of drill collars, lbf
W_{crI}	=	critical WOB, first order of buckling, lbf
W_{crII}	=	critical WOB, second order of buckling, lbf
W_{pr}	=	preloading created by the make-up torque, lbf
X_1	=	distance from neutral point to the surface, ft
X_2	=	distance from the bit to the neutral point, ft
x_2	=	dimensionless distance from the bit to the neutral point
Z	=	the polar sectional modulus, in. ³
Z_1	=	sectional modulus of Section 1, in. ³
α	=	$\sqrt{\frac{F}{EI}}$
β	=	tilt angle, radians
γ_m	=	drilling fluid specific weight, SG
γ_{st}	=	drill collars specific weight, SG
ΔZ	=	drillpipe elongation due to loading, ft
ϵ_z	=	axial strain, in./in.
η	=	$\arctan(\mu)$, radians
θ	=	one-half of thread angle, radians
κ	=	hole curvature over the distance between tool joints, 1/ft
κ_p	=	pipe curvature, 1/ft
λ	=	coefficient in Eq. 9.7
μ	=	coefficient of friction
ν	=	Poisson's ratio
σ_a	=	average axial stress, psi
σ_{an}	=	axial neutral stress, psi

σ_b	= bending stress, psi
σ_e	= effective axial stress (buoyant stress), psi
σ_r	= radial stress, psi
σ_t	= tangential (hoop) stress, psi
σ_{vm}	= von Mises stress, psi
σ_y	= yield point (limit of elasticity) as determined in a tensile stress test, psi
σ_z	= total axial stress, psi
τ	= shear stress, psi
τ_{max}	= maximum sheer stress, psi
ϕ	= angle of twist, radians
φ	= hole inclination angle, radians
Φ	= inclination of the resultant force at the bit, radians
ψ	= the taper of the slip, radians

References

- API RP 7G, *Recommended Practice for Drill Stem Design and Operation Limits*. 1998. Washington, DC: API.
- API Spec 7:2001 *Specification for rotary drill stem elements*, 40th edition (withdrawn). 2001. Washington, DC: API.
- Budynas, R.G. 1997. *Advanced Strength and Applied Stress Analysis*. New York: McGraw-Hill.
- Dawson, R. and Pasley, P.R. 1983. Drillpipe Buckling in Inclined Holes. Paper SPE 11167 presented at the SPE Annual Technical Conference and Exhibition, New Orleans, 26–29 September. DOI: [10.2118/11167-MS](https://doi.org/10.2118/11167-MS).
- Denison, E.B. 1976. Making Downhole Measurements Through Modified Drill Pipe. *World Oil* (October 1976).
- Farr, A.P. 1957. Torque Requirements for Rotary Shouldered Connections and Selection of Connections Drill Collars. Paper 57-Pet-19 presented at the ASME Petroleum Conference, Tulsa, 22–25 September 1957.
- Jellison, M.J and Hall, D.R. 2003. Intelligent Drill Pipe Creates the Drilling Network. Paper SPE 80454 presented at the SPE Asia Pacific Oil and Gas Conference and Exhibition, Jakarta, 15–17 April. DOI: [10.2118/80454-MS](https://doi.org/10.2118/80454-MS).
- Lubinski, A. 1951. A Study of Buckling Rotary Drilling Strings. In *Drilling and Production Practice*, 178–214. New York: American Petroleum Institute.
- Lubinski, A., Althouse, W.S., and Logan, J.L. 1962. Helical Buckling of Tubing Sealed in Packers. SPE-178-PA. *Trans., AIME* **225**: 655–670.
- Lubinski, A. 1975. Influence of Neutral Axial Stress on Yield and Collapse of Pipe. *J. of Engineering for Industry of ASME* (May 1975).
- Lubinski, A. 1977. Fatigue of Range 3 Drill Pipe. *Revue de l'Institut Français du Pétrole*, March–April.
- Lubinski, A. 1987. *Developments in Petroleum Engineering, Volume I*, ed. S. Miska. Houston: Gulf Publishing.
- Lubinski, A. 1988. *Developments in Petroleum Engineering, Volume II*, ed. S. Miska. Houston: Gulf Publishing.
- Mitchell, R.F. 1986. Simple Frictional Analysis of Helical Buckling of Tubing. *SPE Drill Eng* **1** (6): 457–465. SPE-13064-PA. DOI: [10.2118/13064-PA](https://doi.org/10.2118/13064-PA).
- Popov, E.P. 1990. *Engineering Mechanics of Solids (Prentice-Hall International Series in Civil Engineering and Engineering Mechanics)*. Englewood Cliffs, New Jersey: Prentice-Hall.

Further Reading and Advanced Topics

- Aadnoy, B.S. 2006. *Mechanics of Drilling*. Aachen: Shaker Verlag.
- Azar, J.J. and Samuel, R.G. *Drilling Engineering*. Tulsa: PennWell.
- Belayneh, M. 2006. *A Review of Buckling in Oil Wells*. Aachen: Shaker Verlag.
- Bert, D.R. Storaune, A., and Zheng, N. 2009. Case Study: Drillstring Failure Analysis and New Deep-Well Guidelines Lead to Success. *SPE Drill and Compl* **24** (4): 508–517. SPE-110708-PA. DOI: [10.2118/110708-PA](https://doi.org/10.2118/110708-PA).
- Clark, J., Reynolds, N., Ellies, S., and Stuart, J. 2003. Advances in Fatigue Design: Curvature Index Theory. *World Oil* (October 2003).
- Dareing, D.W. 1984. Drill Collar Length is a Major Factor in Vibration Control. *J Pet Technol* **36** (4): 637–644. SPE-11228-PA. DOI: [10.2118/11228-PA](https://doi.org/10.2118/11228-PA).
- Drilco Drilling Assembly Handbook*. 1982. Houston: Drilco.
- Drilling Manual*, 11th edition. 2007. Chapter B. Houston: International Association of Drilling Contractors.
- Dykstra, M. W. 1996. Nonlinear Drillstring Dynamics. PhD dissertation. University of Tulsa, Tulsa.
- Hill, T., Ellis, S., Lee, K., Reynolds, N., and Zheng, N. 2004. Innovative Design Approach to Reduce Drill String Fatigue. *SPE Drill and Compl* **20** (2): 94–100. SPE-87188-PA. DOI: [10.2118/87188-PA](https://doi.org/10.2118/87188-PA).

- Jellison, M.J., Hassmann, S.P., Snapp, D. 2000. New Developments in Drill Stem Rotary Shoulder Connections. Paper IADC/SPE 62785 presented at the IADC/SPE Asia Pacific Drilling Technology Conference, Kuala Lumpur, 11–13 September. DOI: [10.2118/62785-MS](https://doi.org/10.2118/62785-MS).
- Miska, S. 1996. Drill String: Composition and Design. In *Standard Handbook of Petroleum & Natural Gas Engineering*, Vol. 1, ed. W.C. Lyons, 715–769.
- Mitchell, R. and Miska, S. 2006. Helical Buckling of Pipe with Connectors and Torque. *SPE Drill and Compl* **21** (2): 108–115. SPE-87205-PA. DOI: [10.2118/87205-PA](https://doi.org/10.2118/87205-PA).
- Paslay, P.R. 1994. Stress Analysis of Drilling Strings. Paper SPE 27976 presented at the SPE/University of Tulsa Centennial Symposium in Petroleum Engineering, Tulsa, 29–31 August. DOI: [10.2118/27976-MS](https://doi.org/10.2118/27976-MS).
- Payne, M.L. 1992. Drilling Bottom Hole Assembly Dynamics. PhD dissertation, Rice University, Houston.
- Smith, J.E. 2009. Advanced Drillstring Design. In *Advanced Drilling and Well Technology*, ed. B. Aadnoy, I. Cooper, S. Miska, R.F. Mitchell, and M. Payne. Richardson, Texas: Society of Petroleum Engineers.

SI Metric Conversion Factors

ft	×	3.048*	E – 01 = m
ft ²	×	9.290 304*	E – 02 = m ²
ft ³	×	2.831 685	E – 02 = m ³
in.	×	2.54*	E + 00 = cm
in. ²	×	6.451 6*	E + 00 = cm ²
in. ³	×	1.638 706	E + 01 = cm ³
lbf	×	4.448 222	E + 00 = N
lbm	×	4.535 924	E – 01 = kg
psi	×	6.894 757	E + 00 = kPa

*Conversion factor is exact.

Page Intentionally Left Blank

Please Keep Scrolling To Continue

Chapter 10

Drilling Problems

Neal Adams, Neal Adams Services and **Alfred W. Eustes III**, Colorado School of Mines

The objective of this chapter is to present specific drilling problems and their solutions. Included in this chapter are lost circulation problems, well control and blowout prevention, recovery of broken drillstring components, and preventing stuck drillpipe.

10.1 Lost Circulation

10.1.1 Description. Lost circulation—the significant and continuing loss of whole mud or cement slurry to a formation—is one of the most common and troublesome downhole problems. It has been a hindrance to drilling, completion, and workover operations ever since rotary rigs first came into use, and it continues to have a profound negative impact on well economics. Estimates of the direct and indirect costs of lost-circulation problems in the drilling industry worldwide run into the hundreds of millions of US dollars annually.

Although drilling ahead and primary cementing pose particular risks, lost circulation can occur during any well procedure that involves pumping fluid down the hole. Indications of lost circulation may range from a gradual drop in pit level to a partial or complete loss of returns. In extreme cases, the fluid level in the annulus may drop rapidly, sometimes by hundreds of feet.

Lost circulation invariably results in higher costs for materials, services, and additional rig time. Depending on the timing and severity of its occurrence, it can lead to the loss of formation-evaluation data because the information normally obtained from mud returns and drilled cuttings is no longer available. Lost circulation can also result in reduced well productivity if the loss zone is also a potential pay interval. If the wellbore-fluid level drops far enough and fast enough, the drop can allow fluid to enter the wellbore from a higher-pressure formation. When this influx or kick does occur, it makes well control all the more difficult because of the inability to circulate kill fluid (Ivan et al. 2003).

10.1.2 Occurrence of Lost Circulation. For lost circulation to occur, there must be (1) a formation with flow channels that allow passage of hole fluid from the wellbore and (2) an overbalance or positive pressure differential between the wellbore and the formation. Both of these conditions must be present, although one or the other may predominate. For example, a very small overbalance may be sufficient to drive fluid into a highly porous and permeable rock, while even a relatively nonporous, impermeable rock can accept considerable amounts of fluid if the overbalance is large enough to induce hydraulic fracturing.

Permeable Zones. Some types of rocks, because of their high primary porosity and permeability, almost seem to be designed to cause lost-circulation problems. Unconsolidated formations, gravel beds, loose conglomerates, and shallow or highly depleted sandstones have long been recognized as having natural lost-circulation tendencies. Lost circulation in these rocks most often manifests itself as a gradual drop in pit level, although continued drilling time and additional exposure to the wellbore may result in partial or complete mud losses (see **Fig. 10.1**, the sections marked with an “A”).

Natural Fractures. Secondary porosity and permeability—such as occur in naturally fractured sandstones, shales, and carbonates—are also conducive to lost circulation (**Fig. 10.1**, the section marked with a “C”). Natural

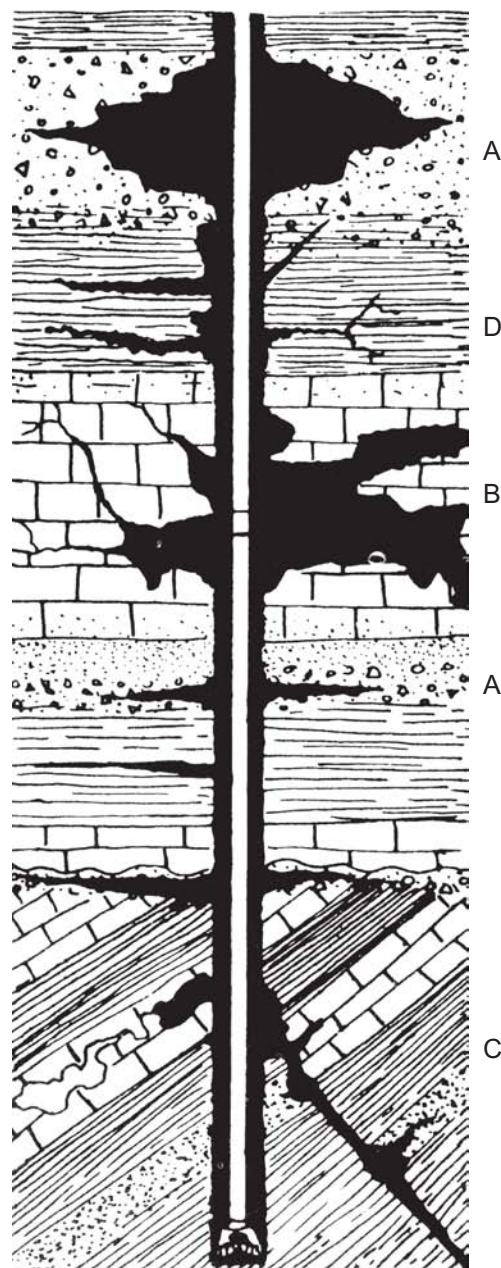


Fig. 10.1—Types of lost circulation. Courtesy of M-I SWACO.

fractures may be either horizontal or vertical depending on a rock's depth, mechanical characteristics, and stress environment. In a horizontal fracture network, lost circulation may first manifest itself as a gradual lowering of the pit level, with a complete loss of returns occurring as additional fractures are encountered. Vertical fractures, on the other hand, will take progressively increasing amounts of mud as drilling progresses and more of the fractures are exposed.

Induced Fractures. If lost returns occur in an area where offset wells have not experienced lost circulation, then the problem is likely the result of fracturing that is induced during well operations, rather than the result of a natural fracture network. Most induced fractures are related in some way to drilling-fluid or cementing programs, although sometimes the well architecture may itself be a contributing factor as, for example, when a surface or intermediate casing string is set too high. Mechanical failures, such as leaks in a shallow casing string, can also result in lost circulation (Fig. 10.1, the section marked with a "D").

Caverns. The most severe lost-circulation problems occur in cavernous or extremely vugular formations (Fig. 10.1, the section marked with a "B"). These are typically limestones that have been leached by water. The void spaces in these formations can be large enough that when they are encountered, the drillstring may actually

drop by as much as several feet preceding a sudden, complete loss of returns. Rough drilling may occur just before a bit encounters a cavernous zone.

10.1.3 Prevention. To prevent or at least minimize lost-circulation problems, it is necessary to address the conditions that cause lost circulation to occur, either by sealing off the problem formation or by reducing the wellbore pressure differential.

Mud System. Prevention of lost circulation starts with the mud system. The best way to seal off a potential loss interval is to keep filtrate losses to a workable minimum and to maintain a thin, firm, impermeable filter cake along the borehole wall. The mud specific density should be as low as possible, but high enough to control the formation pressure (Darley and Gray 1988).

In an area where porous, permeable zones are a known problem, and a low-weight, low-solids mud is being used, it sometimes is a good idea to pretreat the mud with solid LCM. This material should be fine enough to pass through the shale shaker with the other mud components and sized so as to plug small openings in the formation. If mud losses are fracture related, however, such pretreatment will not be effective, especially in weighted-mud systems.

The mud-weight schedule is perhaps the single most important factor in preventing lost circulation. The closer that the hydrostatic pressure of the mud column gets to the formation-fracture pressure, the more likely lost circulation becomes. Local drilling conditions and well parameters will determine how much overbalance is required to optimize drilling performance, control formation pressures, and allow for abnormal or unexpected conditions. If the well cannot be safely drilled using a conventional mud system, then a rig equipped for underbalanced drilling should be considered.

Equivalent Circulating Density (ECD). Even when the mud weight is far less than that required to fracture the formation, lost circulation can still result from a high ECD caused by excessive pump pressure and poor hydraulics practices. The mud's rheological properties (viscosity, yield point, and gel strength) should be specified to maintain its desired cuttings suspension and transport properties, but at the same time should enable the well to be circulated at an optimal pump pressure.

High surge pressure is a major contributor to lost circulation. Surge effects can be minimized by avoiding excessive speed when tripping in the hole, not spudding through bridges or other restrictions, breaking circulation gradually, and maintaining circulation at the minimum pump rate needed to ensure adequate hole cleaning.

Casing Setting Depth. Selection of casing setting depths is crucial to preventing lost circulation and is closely related to the design of the mud program. In many wells, it is necessary to set one or more strings of intermediate casing to protect low-pressure zones from the higher mud weights required for deeper intervals. In selecting these casing points, the well planner should ensure that they are not themselves located in potential loss zones (Moore 1986; Devereaux 1998).

10.1.4 Diagnosis of Lost Circulation. There are a number of methods for combating lost circulation, each of which is effective when properly used. Selecting the best method for a particular situation involves three diagnostic steps:

- Determining at what depth the loss is occurring
- Describing the type of loss zone
- Evaluating the severity of the loss

Depth. Intuitively, one might expect lost circulation to occur at or near the bottom of a well, where the ECD is at its highest. It is far more common, however, for the loss zone to be farther up the hole—typically near the casing shoe—where fractures may have been opened, resealed, and then reopened as the well was drilled deeper with increasing mud weights. Techniques for finding lost-circulation zones commonly involve the use of production-logging devices including spinners, temperature logs, and radioactive-tracer tools.

Methods of Locating Lost-Circulation Zones. The usual way to combat lost circulation during drilling is to monitor the possible presence of LCM across the suspected zone of loss. At shallow depth, the location of the losses into naturally permeable zones need not be known exactly. At greater depths [more than 5,000 ft (1,500 m)] or when severe losses are occurring, the exact location of the “thief” zone must be determined before efficiently sealing the hole and continuing to drill. A number of methods have been developed for this purpose and are discussed below.

Temperature Survey. A temperature-recording device is run twice on wire and records the temperature at various depths (**Fig. 10.2**). First, the device is run under static conditions—when the mud temperature is in equilibrium with the formation—to provide a base log. Enough fresh, cool mud is then pumped into the hole so that the

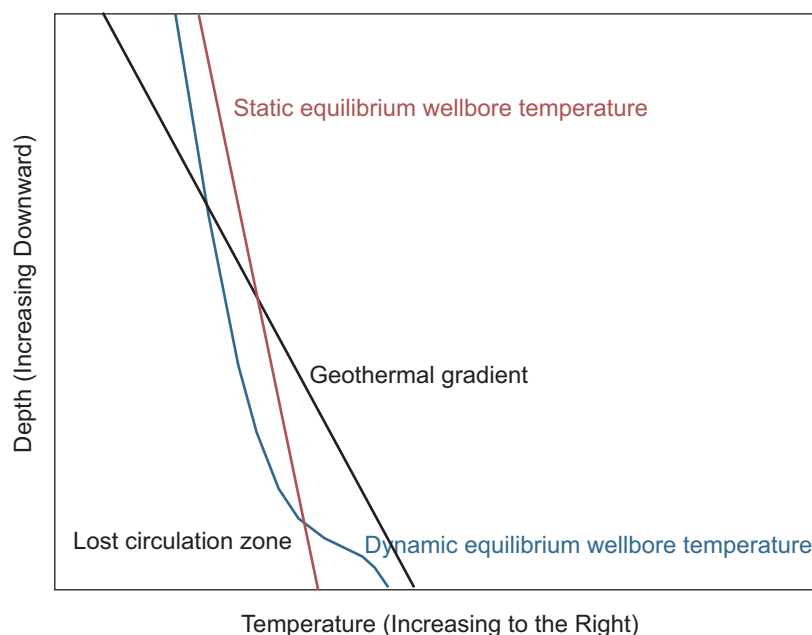


Fig. 10.2—Temperature survey.

change in temperature can be recorded by a second survey. The temperature above the loss zone will be lower than that recorded in the first run. Below the thief zone, the mud remains static and its temperature will be higher than that of the mud flowing into the formation. The new temperature survey will show an anomaly across the zone where the losses are occurring, and their location can be determined by the depth where the recorded line changes its gradient. This method gives good results in areas where the temperature gradient is of the order of $1^{\circ}\text{F}/100\text{ ft}$ ($1.8^{\circ}\text{C}/100\text{ m}$). One benefit of this method is that it can be used with drilling fluids containing large amounts of LCM.

Radioactive-Tracer Survey. Two gamma ray logs are run to determine the exact position of the thief zone. The first is recorded to establish the normal radioactivity of the downhole formation as a basis for comparison. Then, a small amount of radioactive material (e.g., carnotite) is displaced around the hole where losses are suspected to occur. A second gamma ray log is run and compared with the base log. At the thief zone, a steep change of radioactivity can be seen. The precise point of loss can be determined with this method, although it requires special equipment and is expensive.

Hot-Wire Survey. As in the temperature survey, the change in mud temperature is monitored. A calibrated resistance wire that is sensitive to changes in temperature is run to a certain depth, and then fresh, cool mud is pumped into the hole. If a change of temperature at the tool is observed, then the tool is placed above the point of loss. If no change is recorded, then it is placed below the thief zone. This method can be used in any mud system, but a large amount of mud is required to find the exact location of the loss.

Spinner Survey. A small spinner attached to the end of a cable is run in the hole to the location where the losses are suspected to occur. The spinner either spins or turns in response to mud movement, and the revolutions per minute of this response are recorded on film. Near the thief zone, acceleration can be observed as mud flows into the formation. This method delivers the best results when there are no sealing agents in the mud, but it requires large volumes of mud.

Type and Severity of Losses. Once the loss zone is located, it can be described in terms of its lithology and the type of loss that is occurring. For example, if there is a slow but steady decrease in pit level and if mud logs or other data indicate that the loss zone is composed of sandstone, then high permeability and porosity are likely the causes of the problem. On the other hand, if the loss of returns is sudden, induced fracturing is the most likely cause.

The severity of the problem can be expressed in terms of the amount of mud lost and the static fluid-level drop. Seepage causes a gradual lowering of the pit level (generally from 1 to 10 bbl/hr). Losses in the 10- to 50-bbl/hr range are considered partial. Complete losses involve fluid-level drops ranging from 200 to 500 feet (60 to 150 m), while severe complete losses involve drops of more than 500 feet (150 m) where there is evidence of vugs or caverns. In the worst case of lost circulation, an underground blowout, the loss zone is taking not only drilling mud, but also formation fluid from a higher-pressure interval.

Controlling Lost Circulation. Techniques for controlling lost circulation are designed to seal off the loss interval (Howard and Scott 1951). They may entail

- Allowing the formation to heal itself by removing the conditions that caused the lost circulation
- Using LCM or drilled solids to bridge off the interval
- Spotting a high-viscosity plug across the interval
- Squeezing the interval with cement
- Setting pipe across the interval
- Abandoning or sidetracking the loss interval

Depending on the location, type, and severity of the problem, remedial measures may involve a combination of these techniques. No one method is applicable to all types of lost circulation.

Removing the Conditions That Cause Lost Circulation. When lost circulation results from induced fracturing, a pause in operations or a change in drilling practices may help to eliminate the original cause of the fracture.

Healing. In some cases, stopping circulation and allowing solids to build up against the borehole wall may heal an induced fracture. One such procedure involves pulling the pipe into a protective casing or a secure portion of open hole, shutting down the mud pumps for a minimum of six to eight hours, attempting to fill the hole with water, and then gradually resuming circulation in stages.

Reducing the mud weight is an effective way of reducing the hydrostatic pressure of the mud column and, thus, the pressure differential with the formation. This is only feasible, of course, if there is no danger of a kick. Another step would be to adjust the mud viscosity and gel strength based on hole conditions—either increasing the viscosity and gel strength to help slow the flow of mud into permeable zones, or decreasing the viscosity and gel strength to reduce the pump pressure required for circulation, thereby lowering the ECD and reducing losses from induced fractures. Decreasing the pump rate can likewise reduce the circulating pressure.

10.1.5 LCM. In porous, permeable zones, lost circulation most commonly results from inadequate bridging agents or wall-building characteristics. Fixing the problem is, therefore, a matter of adding solids to seal off the interval. In some cases, simply drilling ahead and allowing the formation cuttings to bridge the loss zone may be enough to restore circulation. In other cases, it will be necessary to add solid LCM to the mud system in concentrations not exceeding 10 to 20 lbm/bbl [28 to 57 kg/m³]. **Table 10.1** provides a general classification of solid LCMs and gives examples of each category.

Solid LCMs are most effective when different textures and sizes are used in combination. These materials are suitable only for plugging porous, permeable formations—because of their generic name, operators have often wrongly used them as an all-purpose remedy for all types of lost circulation. Various LCM materials have limits on their bridging capability. This bridging width for a typical LCM is shown in **Figs. 10.3 and 10.4**.

TABLE 10.1—COMMON LOST-CIRCULATION MATERIALS

Classification	Examples	Description
Fibrous materials	Wood fiber (shredded wood, sawdust), paper pulp, glass fiber, cotton fiber, animal hair, leather fiber, straw, and shredded tires	Relatively little rigidity. Can be forced into large openings, where they bridge over and form a mat or base that acts to seal off the formation when solids from the drilling fluid deposit on it. If the openings are too small for the fibers to enter, a bulky, easily removable external cake may form on the walls of the hole. Not recommended for oil-based muds.
Flaky (lamellar) materials	Cellophane, mica (fine and coarse), plastic laminate, wood chips.	Not normally used in cement because they tend to plug surface and downhole cementing equipment. Also may contain organic chemicals that can seriously extend cement-thickening time. Sealing action similar to that of fibrous materials. Cellophane products are not recommended for use in oil-based muds.
Granular materials	Nut shells (fine, medium, coarse, and very coarse), ground plastics, seed grains, coarsely ground rock materials (e.g., bentonite, asphalt, limestone).	Tend to form a bridge just inside the opening of the pore. Must contain particles that approximate the size of the opening, as well as a gradation of smaller particles to form a seal. Granular materials may be used in oil-base muds.
Combination	Selected blends of fibrous and flaky materials and granular LCM.	Blended products containing cellophane flakes are not recommended for use in oil-based muds.

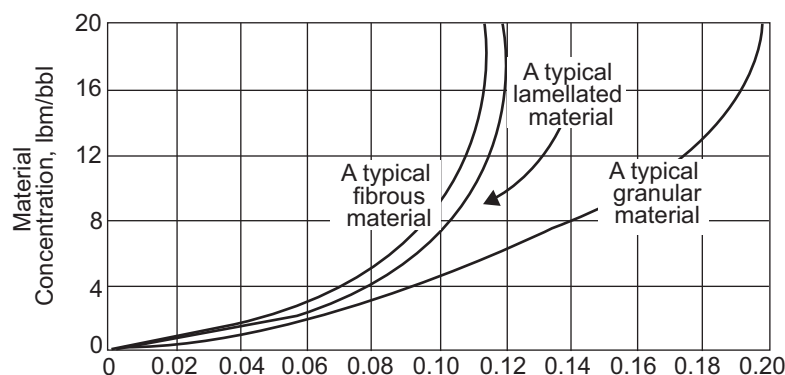


Fig. 10.3—LCM and fracture sizes (Howard 1951).

Material	Type	Description	Concentration, lbm/bbl	Largest Fracture Sealed, in.					
				0	0.04	0.08	0.12	0.16	0.20
Nut shell	Granular	50%— $3/16$ + 10 mesh 50%—10 + 100 mesh	20						
Plastic	"	"	20						
Limestone	"	"	40						
Sulphur	"	"	120						
Nut shell	"	50%—10 + 16 mesh 50%—30 + 100 mesh	20						
Expanded perlite	"	50%— $3/16$ + 10 mesh 50%—10 + 100 mesh	60						
Cellophane	Lamellated	$3/4$ in. flakes	8						
Sawdust	Fibrous	$1/4$ in. particles	10						
Prairie hay	"	$1/2$ in. fibers	10						
Bark	"	$3/8$ in. fibers	10						
Cotton seed hulls	Granular	Fine	10						
Prairie hay	Fibrous	$3/8$ in. particles	12						
Cellophane	Lamellated	$1/2$ in. flakes	8						
Shredded wood	Fibrous	$1/4$ in. fibers	8						
Sawdust	"	$1/16$ in. particles	20						

Fig. 10.4—Types of LCM (Howard 1951).

Slurries and Plugs. An alternative to adding LCM on a system-wide basis, and an effective technique for unconsolidated permeable zones, is to spot a high-filter-loss slurry, consisting of water mixed with conditioning additives and bridging agents, directly in the lost-circulation zone. To spot the slurry, a drill bit (without jet nozzles) is run to the top of the loss zone, and the slurry is displaced to the end of the drillpipe. The slurry is then squeezed into the formation by closing the blowout preventers (BOPs) and pumping at low pressure. As water is squeezed out of the slurry, the bridging agents form a seal across the interval.

In naturally fractured formations, a plug may be pumped across the loss interval. These plugs are designed to be pumpable at the surface and then to develop shear strength when placed downhole. The two main types of plugs are *soft plugs* (also known as reinforcing plugs, viscous pills, or gunk squeezes), and *hard (cement) plugs*.

Soft Plugs. Soft plugs typically consist of a bentonite/diesel-oil base (for water-based muds) or a water base (for oil-based muds), with additives such as LCM, cement, and polymers for special applications. These plugs develop a viscous, gel-like consistency and offer the advantage of deforming under pressure surges, which makes them less likely to break down (Dawson and Goins 1953).

Hard Plugs. Hard plugs can also be used to seal off natural fractures. They have high compressive strength and enough flexibility to enable good control of their flow and setting properties. However, they have a greater tendency to break down under pressure surges than soft plugs and can be harder to drill out. In soft formations, a hard plug may act as a whipstock and cause the bit to sidetrack. Many of the concerns about the use of cement as an LCM have been alleviated in recent years by the development of lightweight slurries and crosslinked cements and by other advances. These same advances have helped prevent lost circulation during primary cement jobs (Mata and Veiga 2004; Romero et al. 2004).

Cavernous formations present a special challenge. If the void spaces are small enough and if the formation can withstand the pressure surges inherent in drilling, it may be possible to seal the caverns. Otherwise, the operator

can attempt to drill blind (i.e., with no returns) or drill underbalanced (using air, foam, mist, or aerated mud as a drilling fluid) and then cement a casing across the loss interval.

Strength-Enhancing Chemicals. As drilling advances into more-difficult areas, the problem of lost circulation often grows worse. When drilling into depleted reservoirs or in deepwater drilling, the trend is to design a mud system that increases the near-wellbore fracture resistance and has low fluid loss. In this situation, the gap between the pore pressure and the fracture gradient must be narrow, or the mud weight required to support the formation (weakened by depleted zones with low pore pressure) will exceed the fracture resistance. The theory behind this approach is to form a stress cage around the borehole, which effectively strengthens the formation with correctly sized bridging particles that prop and seal short fractures as they are created (Aston et al. 2004).

10.1.6 Best Practices. The mud system should have low viscosity and low gel strength and should support proper cuttings transport. When the hole is not properly cleaned, the weight added by loading the annulus with cuttings can overcome the fracture gradient.

When entering areas where losses are known to occur, the mud should be pretreated with 3 to 5 lbm/bbl of LCM that is fine enough to pass the shale shakers.

In shallow formations, adding cement, lime, gyp, or salt can be an inexpensive way to increase viscosity and gel strength and, thus, to slow the flow into the formation and stop losses. Reducing the pump rate can help restore circulation by reducing the ECD. When losses cannot be avoided, drilling blind (without mud returns) is a feasible approach.

Abnormal pressure surges should be avoided, especially while tripping or starting the pumps. Many losses occur when running pipe too fast or applying pressure too rapidly on gelled-up mud.

Pumps should be powered up one at a time at a few strokes per minute and the speed then should be increased smoothly to the desired flow rate. Pumps should be stopped by gradually reducing the flow to 75%, 50%, and 25% before shutting them off completely. Only a small amount of the connection time for a well is due to the running speed of the pipe. Running the pipe more slowly costs only a few seconds, but significantly reduces surge or swabbing pressures, which are the main causes of inducing or opening fractures and initiating fluid loss.

If the fracture gradient is low, using air or foam as a mud system is possible; drilling underbalanced is a way to avoid complete mud loss. If severe losses occur or if circulation cannot be restored after an extended period of trying, abandoning the well may be the most economical solution.

10.2 Well Control

10.2.1 Introduction. Well control and blowout prevention are important topics in the oil industry for a number of reasons: higher drilling costs, possible loss of life, and the waste of natural resources when blowouts occur. One additional reason for concern is the increasing number of government regulations and restrictions that have been placed on the oil industry, partially as a result of recent, much publicized well-control incidents. For these and other reasons, it is important that drilling professionals understand well-control principles and the procedures to be followed to control potential blowouts properly.

The following are key principles for controlling kicks and preventing blowouts:

- Shut in the well quickly.
- When a kick occurs, if in doubt, shut down the well and get help. Kicks happen as frequently while drilling as they do during tripping out of the hole. Many small kicks turn into big blowouts because of improper handling.
- Do not hurry and make mistakes. Take your time and get it right the first time. You may not have an opportunity to do it again.

More details on these topics are presented in this chapter. Unusual problems occurring during kick killing are discussed in other reference sources.

10.2.2 Well-Control Equipment. This section discusses the basic equipment commonly used in well control. The following descriptions are based on onshore operations. For offshore use, the basic principles still apply, although space limitations and the fact that the BOPs are often located on the bottom of the ocean (these are called *subsea BOPs*) do influence some aspects of the procedures. For more details on offshore well-control equipment, special literature should be consulted (Adams 1979a).

Preventer Stack. BOPs are used to seal the wellbore and thereby contain a kick. Two main types of preventers are in use in the industry: the *annular preventer* and the *ram-type preventer* (both types are discussed below).

Preventer stacks are rated to 3,000, 5,000, 10,000, or 15,000 psi. A preventer stack normally consists of an annular preventer on top, followed by one or more (typically up to three) ram-type preventers (**Fig. 10.5**). The inclusion of a full-bore drilling spool makes it possible to connect the kill and choke lines (Adams 1979b, 1980a).

An important consideration for design of the preventer stack is the space it occupies under the rig. Even after setting multiple casings (with each casing head adding to the total height of the equipment), it still must be possible to accommodate the full preventer stack.

Annular Preventers. Annular preventers are able to seal around any object with a circular (or nearly circular) cross section as well as over an empty hole. This means that it can also seal around a kelly (hexagonal shapes are better than square shapes). Because of its variable diameter, it also allows tool joints to pass when pipe is being lowered into the hole while surface pressure is present, an operation called *stripping* (overcoming the pressure area forces with the pipe weight) or *snubbing* (forcing the pipe into the hole because the weight is not enough to overcome the pressure area forces) (**Fig. 10.6**).

Operating pressure is generally lower than that used for ram-type preventers because the piston area is far larger. The pressure can also be adjusted to ease passage of the tubular while stripping into the well by reducing friction. Still, it is necessary to lubricate the pipe while stripping into the well. Drilling-mud or water can be used for lubrication.

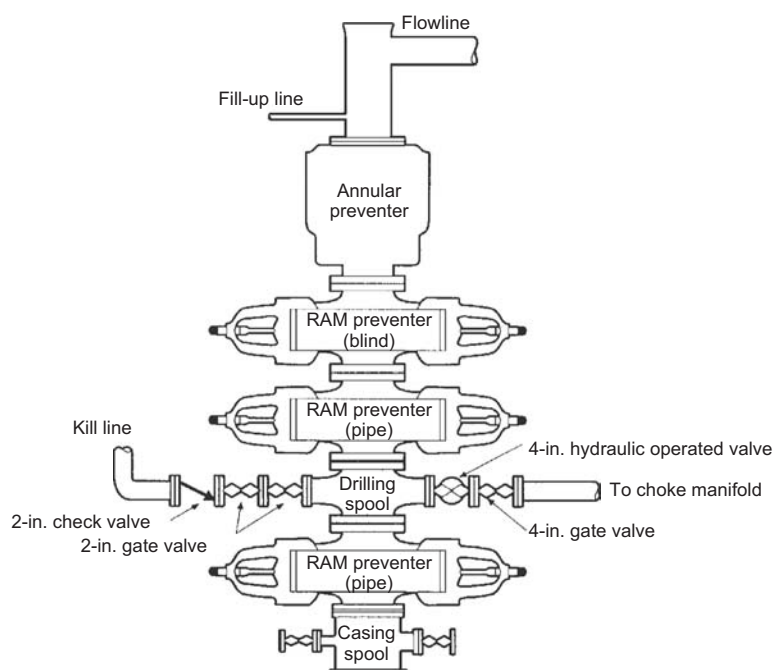


Fig. 10.5—Typical stack arrangement (Watson et al. 2003, page 140).

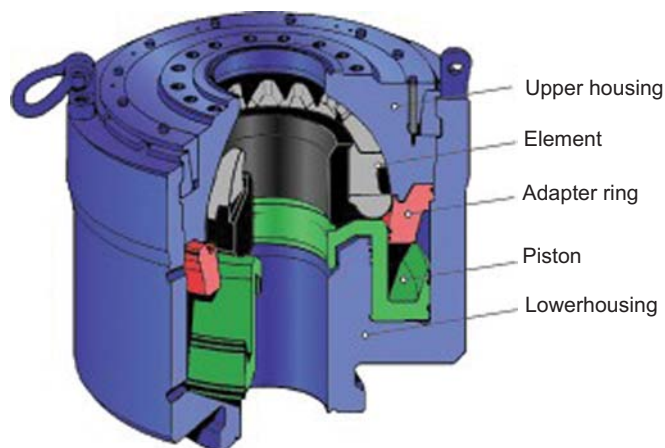


Fig. 10.6—Annular preventer. Courtesy of National Oilwell Varco.

The operating principle of an annular preventer is simple. Hydraulic pressure is applied to the low side of a wedge-shaped piston. The circular wedge then forces the sealing element toward the inside. Frequent closing and opening of the sealing element will significantly shorten its life. In particular, closing over an empty hole has an adverse effect on the sealing element. For this reason, it is common not to test annular preventers as often as ram-type preventers.

Ram-Type Preventers. Rams are found on most BOP stacks, except in some low-pressure applications. They are closed by hydraulic pressure, which forces the set of rams together from both sides. As a backup measure, they can also be manually closed (**Fig. 10.7**).

Sealing is achieved between the upper surface of the ram and the preventer body and between the sealing surfaces of the ram. Different kinds of rams are available. Pipe rams have a semicircular groove that enables sealing around pipe. They are designed for sealing around a specific diameter of pipe. Therefore, changing the rams can be necessary when switching to a different-diameter drillpipe or closing in a well with drill collars or casing (or other equipment) within the preventer stack. Furthermore, while shutting in the well, no tool joints should be located within the preventer stack. This is easily avoided by lowering or lifting the top tool joint of the drillstring to an easily accessible working height at the rig floor.

Variable-bore rams are available with flexible steel fingers that can seal around pipe diameters smaller than that of the ram itself. With a standard pipe ram, it is possible to hang a drillstring on the ram. A variable-bore ram, on the other hand, is not strong enough to support a drillstring.

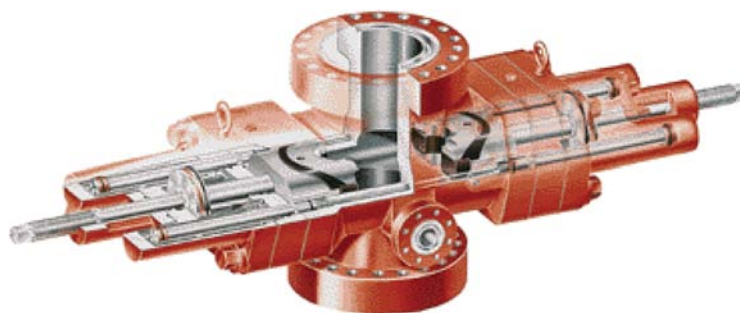
Blind rams are used to seal over an open hole. They have a sealing surface which is pressed together when actuated. A special kind of blind ram is called a *shear ram*. Shear rams have cutting edges and are able to shear through drillpipe (and small-diameter drill collars) and seal over it. Because this option eliminates the possibility of circulating through the drillpipe, the shear ram is considered an option of last resort. Typically these are used offshore.

Most modern ram-type preventers have a built-in secondary seal consisting of a plastic sealing material that is forced against the sealing surfaces by twisting a bolt. This seal is designed as a contingency measure in case the ram preventer starts to leak during a well-control operation (Adams 2005).

Diverter. A diverter assembly is used to divert a gas kick encountered at shallow depth when only a conductor casing is in place. During this phase, the surrounding formation tends to be too weak to contain a shut-in kick. Therefore, the only possibility is to divert the flow in a safe direction. Generally, an annular-type preventer is installed on top of the conductor pipe. Underneath it, a diverter line is run to a pit. This line should be of large diameter to allow the most unrestricted flow possible (**Fig. 10.8**) (Adams 1980a).

Testing. It is of critical importance that the whole well-control system function in the event of an emergency. Therefore, all equipment must be checked for any possible weaknesses *before* installation. Then, testing of the sealing ability and the correct function of every part should occur *after* installation *and* at periodic intervals. Special equipment exists to pressure-test the BOP. The goal of all types of test equipment is to be able to test every single preventer on its own. Therefore, a tool is lowered inside the preventer stack, and a section is sealed off and then pressurized to testing pressure. It is common practice to test equipment first at a low pressure, then at a higher pressure.

Choke Line. The choke line directs flow out of the wellbore to the choke manifold. The choke line is connected to the preventer stack at the drilling spool by two valves. A manually operated master valve sits directly at the spool, followed by a remote-controlled valve. The master valve is used to isolate the choke line should repairs become necessary. During operations, only the hydraulically operated valve is used. The choke line itself should



U Blowout Preventer

Fig. 10.7—U blowout preventer—example of a ram-type preventer (© Cameron 2010).

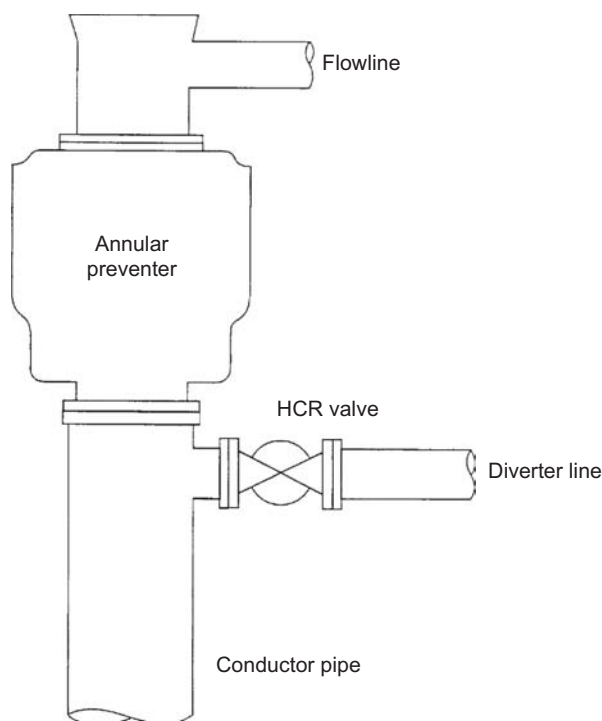


Fig. 10.8—Diverter (Watson et al. 2003, page 261).

be designed with as large a diameter and wall thickness as reasonably possible, because the fluids flowing through it in a well-control situation are likely to be loaded with solids (e.g., drill cuttings) and moving at high velocities, creating a very erosive environment. The choke line should be as straight as possible to minimize turns, which create impacts and erosion at those points. If turns cannot be avoided, they should be designed using targets or T-turns. No threaded connections are acceptable in the choke line. Instead, flanged or welded connections should be used exclusively.

Choke Manifold. The choke manifold is a crucial part of the whole well-control system. The choke manifold makes it possible to control the backpressure on the well while circulating out a kick. The centerline, which runs straight through the manifold and onto a flare pit, is called the *panic line*. It provides the least restricted flow possible in case the well cannot be controlled and must be allowed to blow out. All fluids can then be diverted to a flare pit and flared at a safe distance from other equipment. The manifold generally consists of a manual choke and a remote-controlled choke. This redundancy, as well as the fact that each side can be isolated by the valves, enables continuous operation even if one of the chokes has to be replaced (e.g., as a result of excessive erosion). A pressure gauge, which indicates the casing pressure, should be installed on the choke line at the manifold. Note that during operation, if the choke line is extremely long, the pressure drop within the choke line must be accounted for when reading casing pressure at this point (Fig. 10.9).

Chokes. Drilling chokes used for well-control operations must be built much more sturdily than the standard positive chokes used for production operations. Solids in the mud circulated out of the well will induce erosion, which can wear out a choke relatively quickly. This is one reason to have at least two redundant chokes available. In addition, mud solids can easily plug a choke (Fig. 10.10).

Various choke designs are in use in the industry. The two most common designs either use a plug that moves into and out of an orifice to restrict the flow, or use two rotating carbide plates with circular openings that adjust the flow rate by rotating—and thereby changing—the area available for flow.

Accumulators. The accumulator unit provides the hydraulic power needed to operate the well-control equipment (preventers, automatic valves, and chokes). Accumulators are available with different working-pressure ratings (1,500, 2,000, or 3,000 psi). An accumulator unit consists of several bottles. Each is precharged with nitrogen and loaded with hydraulic fluid. Nitrogen is used because of its noncorrosive and nonflammable properties. The volume of usable hydraulic fluid must be designed so that safe shut-in can be achieved even if the recharge pumps are inoperative. *API RP53* suggests that the volume should be sufficient to close one pipe ram and the annular preventer, and to open the hydraulic choke-line valve. However, these requirements are not widely accepted in the industry. Moreover, some government regulations request higher volumes. Usually, the accumulator

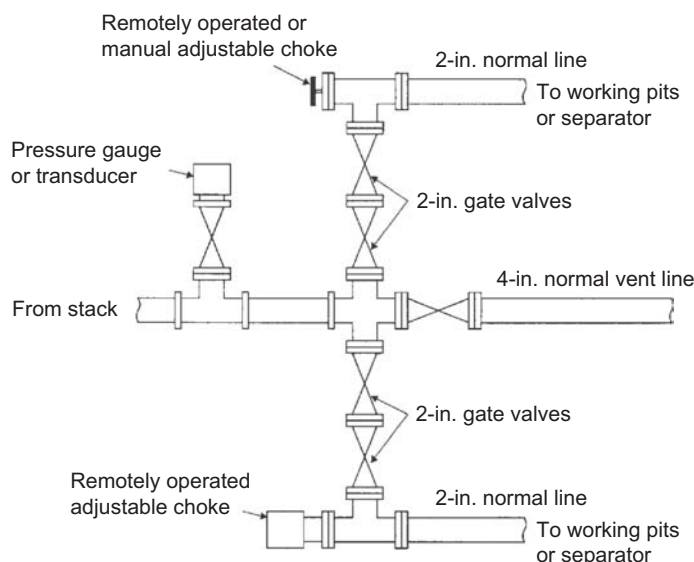


Fig. 10.9—Choke manifold (Watson et al. 2003, page 142).

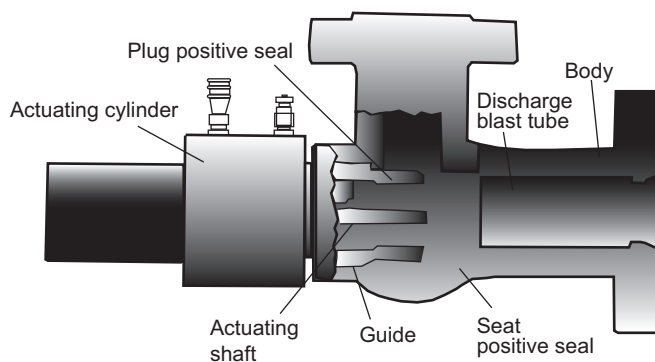


Fig. 10.10—Adjustable choke (Watson et al. 2003, page 252).

unit is charged by two recharge pumps fed from different power sources. One pump is driven electrically, and one is driven by air from the rig pneumatic network. The latter pump can still operate from the compressor air tanks even if there is an electricity outage (Fig. 10.11).

10.2.3 Causes of Kicks. Introduction to Kicks. Different drilling problems confront the operator on a day-to-day basis, including lost circulation, stuck pipe, deviation control, and well control. This discussion focuses on well control; other drilling problems will be considered here only in relation to some aspect of well control.

A *kick* can be defined as a well-control problem in which the pressure encountered within the rock being drilled is greater than the mud hydrostatic pressure acting on the borehole or rock face. When this occurs, the greater formation pressure tends to force formation fluids into the wellbore. The result is an *uncontrolled flow into* a wellbore. This fluid flow is called a kick. If the flow is successfully controlled, the kick has been killed. A *blowout* is an *uncontrolled flow out* of a wellbore and often occurs because a kick was not properly controlled.

For a kick to occur, three things must happen simultaneously. First, a mobile fluid must be present in the porous rock adjacent to the borehole. Second, there must be enough permeability to sustain a flow into the wellbore. Third and most importantly, the pressure exerted in the wellbore, from a combination of hydrostatic, dynamic, and surface pressures, must be less than the pore pressure in the formation. If any one of these factors is missing, the well cannot kick. In one particular situation, gas can be entrained into a wellbore from inside the volume of rock being drilled, and this can lead to a kick even if permeability is not an important issue.

The severity of a kick depends on several factors. One is the ability of the rock to allow fluid flow. The *permeability* of rock describes its ability to allow fluid movement. The *porosity* measures the amount of fluid-containing

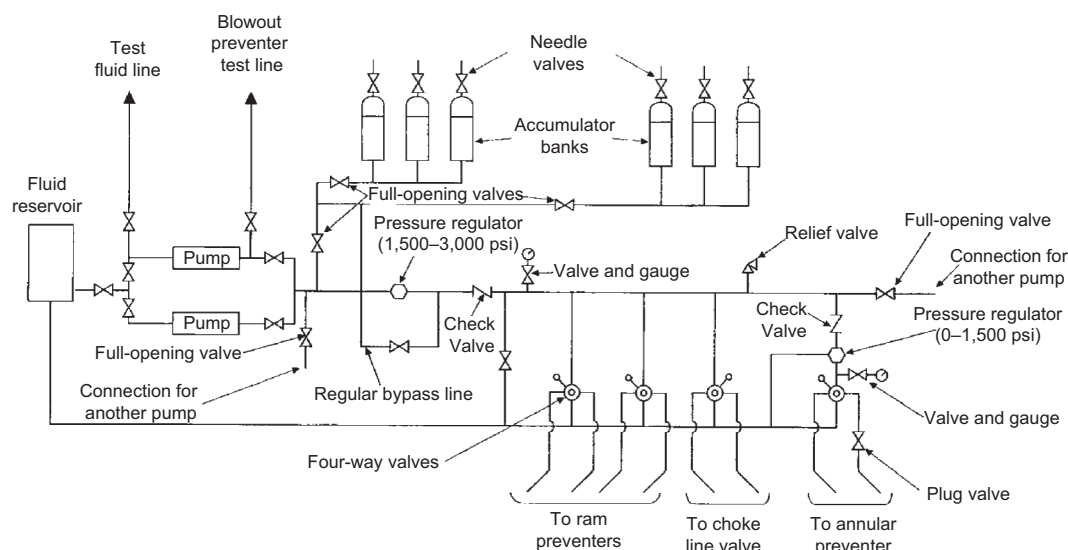


Fig. 10.11—Accumulator schematic (API RP 53 1984). Reproduced courtesy of the American Petroleum Institute.

space in the rock. A rock with high permeability and high porosity has a greater potential to generate a severe kick than a rock with low permeability and low porosity. For example, sandstone is considered to have a greater kick potential than shale because, in general, sand has a greater permeability and porosity than shale.

Another controlling variable for kick severity is the *pressure differential* involved. The pressure differential is the difference between the formation-fluid pressure and the mud hydrostatic pressure. If the formation pressure is much greater than the hydrostatic pressure, a large negative differential pressure exists. If this negative differential pressure is coupled with high permeability and porosity, a severe kick can occur.

A kick can be characterized in several ways. One way is by the type of formation fluid that has entered the borehole. Known kick fluids include gas, oil, salt water, magnesium chloride, water, hydrogen sulfide (sour) gas, and carbon dioxide. If gas has entered the borehole, the kick is called a *gas kick*. Furthermore, if a volume of 20 bbl (3.2 m³) of gas has entered the borehole, the kick could be called a 20-bbl (3.2-m³) gas kick. Another method of characterizing kicks is by the required mud-weight increase necessary to control the well and to kill a potential blowout. For example, if a kick required a 0.7-lbm/gal (84-kg/m³) mud-weight increase to control the well, the kick could be called a 0.7-lbm/gal (84-kg/m³) kick. It is interesting to note that control of an average kick will require a mud-weight increase of approximately 0.5 lbm/gal (60 kg/m³) or even less.

An additional important well-control consideration is the pressure that the formation rock can withstand without generating an induced fracture. This rock strength is often called the *fracture mud weight* or gradient and is usually expressed in lbm/gal equivalent mud weight. The *equivalent mud weight* is the sum of the pressures exerted on the borehole wall and includes mud hydrostatic pressure, pressure surges resulting from pipe movement, frictional pressures applied against the formation as a result of pumping the drilling fluid, and any casing pressure caused by a kick. For example, if the fracture mud weight of a formation has been determined as 16.0 lbm/gal, the well can withstand any combination of these pressures that yields the same total pressure as a column of 16.0-lbm/gal (1,920-kg/m³) mud extending to the depth in question. This combination could be (1) a 16.0-lbm/gal (1,920-kg/m³) mud, (2) a 15.0-lbm/gal (1,800-kg/m³) mud and some amount of casing pressure, (3) a 15.5-lbm/gal (1,860-kg/m³) mud and a smaller amount of casing pressure, or (4) other combinations.

Causes of Kicks. Kicks occur because formation pressure is greater than mud hydrostatic pressure, which causes fluids to flow from the formation into the wellbore. In almost all drilling operations, the operator attempts to maintain a hydrostatic pressure greater than the formation pressure (a relationship that is called an *overbalanced condition*) and, thus, to prevent kicks. However, on occasion (and for various reasons), the formation will exceed the wellbore pressure, and a kick will occur. Following are the key causes of kicks:

- Insufficient mud weight
- Improper hole fill up on trips
- Swabbing
- Cutting of mud by formation fluids
- Lost circulation

Insufficient Mud Weight. Insufficient mud weight is the predominant cause of kicks. A permeable zone is drilled using a mud weight that exerts less pressure than the formation pressure within the zone. Fluids begin to flow into the wellbore, and a kick occurs.

Abnormal formation pressures are often associated with kicks. They are defined as pressures that have an equivalent mud weight greater than normal conditions. *Normal conditions* are defined as equivalent mud weights ranging from a freshwater density of 8.34 lbm/gal (1,000 kg/m³) to a saturated NaCl-water density of 10 lbm/gal (1,200 kg/m³). In well-control situations, greater-than-normal formation pressures are the greatest concern. Because normal formation pressure is equal to a full column of native water, an abnormally pressured formation will exert more pressure than that column of water. If an abnormally pressured formation is encountered while drilling with mud weight that is insufficient to control the zone being drilled, a potential kick situation is present. Whether a kick occurs depends on the permeability and porosity of the rock.

A number of methods can be used to estimate formation pressures in an effort to prevent this type of kick. Some are listed below:

Qualitative Methods:

- Paleontology
- Offset well-log analysis
- Temperature-anomaly analysis
- Gas measurement
- Mud- or cuttings-resistivity analysis
- Cutting-characteristics analysis
- Hole-condition analysis

Quantitative Methods:

- Shale density profile
- *d*-exponent analysis
- Normalized penetration-rate analysis
- Other drilling equations

Kicks caused by insufficient mud weight seem to require the obvious solution of drilling with high mud weight. However, this is not always a viable solution. First, a high mud weight may exceed the fracture mud weight of the formation and induce lost circulation. Second, a mud weight in excess of the formation pressure may significantly reduce penetration rates. In addition, pipe sticking becomes a serious concern when excessive mud weights are used. The best solution is to maintain a mud weight slightly greater than the formation pressure until the mud weight begins to approach the fracture mud weight, thus requiring an additional string of casing.

Tripping Practice. Improperly filling the hole during trips is another predominant cause of kicks. As the drill-pipe is pulled out of the hole, the mud level falls because the pipe steel had displaced some mud. With the pipe no longer in the hole, the overall mud level decreases.

It is necessary to fill the hole with mud periodically to avoid reducing the hydrostatic pressure and thereby allowing a kick to occur. Several methods can be used to fill the hole, but all must be able to measure accurately the amount of mud required. It is not satisfactory under any conditions to allow a centrifugal pump to fill the hole continuously from the suction pit, because with this approach, accurate mud-volume measurement is not possible. The two methods most commonly used to monitor hole fill up are a *trip tank* and *pump-stroke measurement*.

A *trip tank* includes a calibration device to monitor the volume of mud entering the hole. The tank can be placed above the preventer to allow gravity feed into the annulus, or a centrifugal pump can pump mud into the annulus, with the overflow returning to the trip tank. The advantages of a trip tank include ensuring that the hole remains full at all times and providing an accurate measurement of the amount of mud entering the hole. Another method of keeping a full hole is to fill the hole periodically using a positive-displacement pump. A flowline device can be installed to measure the number of pump strokes required to fill the hole and to shut off the pump automatically when the hole is full.

Swabbing. Pulling the drillstring from the borehole creates swab pressures. *Swab pressure* is negative and reduces the effective hydrostatic pressure throughout the hole below the bit. If this pressure reduction lowers the effective hydrostatic pressure below the formation pressure, a potential kick situation has developed. The variables controlling swab pressures include pipe-pulling speed, mud properties, hole configuration, and the effect of “balled” equipment. Some of these effects can be seen in **Table 10.2**.

TABLE 10.2—EXAMPLE SWAB PRESSURES (PSI) IN VARIOUS HOLE SIZES AT VARIOUS PULLING SPEEDS FOR A 14.0-PPG MUD AND 4½-IN. DRILLPIPE (LAKE 2006)

Hole Size, in.	Pulling Speeds, seconds/stand					
	15	22	30	45	68	75
8½	267	167	124	98	84	75
6½	589	344	256	192	159	140
5¾	921	524	294	289	231	200

Cut Mud. Gas-contaminated mud will occasionally cause a kick. The mud-density reduction is usually caused by fluids from the core volume which are cut and released into the mud system. As the gas is circulated to the surface, it expands and reduces the overall hydrostatic pressure sufficiently to allow a kick to occur. Although the mud weight is cut severely at the surface, the hydrostatic pressure is not reduced significantly because most gas expansion occurs near the surface and not at the hole bottom.

Lost Circulation. Occasionally kicks are caused by lost circulation. A decreased hydrostatic pressure occurs because of a shorter mud column. When a kick occurs because of lost circulation, the problem may become severe. A large volume of kick fluid may enter the hole before the rising mud level is observed at the surface. It is a recommended practice to fill the hole with some type of fluid to monitor mud level.

10.2.4 Kick Signs. A number of warning signs and possible kick indicators can be observed at the surface. It is the responsibility of each crew member to recognize and interpret these signs and to take proper action. Not all of these signs will positively identify a kick; some simply warn of potential kick situations. Key warning signs include the following:

- Flow-rate increase
- Pit-volume increase
- Continuing flow in the well with the pumps off
- Pump-pressure decrease along with a pump-stroke increase
- Improper hole fill up on trips
- Change in string weight
- Drilling break
- Decrease in mud weight

Each warning sign is identified in the following paragraphs as being of primary or secondary importance to kick detection.

Warnings Signs of Primary Importance to Kick Detection. *Flow-Rate Increase.* An increase in the flow rate leaving the well while pumping at a constant rate is a primary kick indicator. The increased flow rate can be interpreted to mean that the formation is helping the rig pumps to move fluid up the annulus by forcing formation fluids into the wellbore. This is a key indicator of a kick.

Pit-Volume Increase. If the pit volume has not been changed as a result of control actions from the surface, an increase indicates that a kick is occurring. Fluids entering the wellbore displace an equal volume of mud in the flowline and cause an increase in pit level. However, this change takes some time to manifest itself and does not provide an immediate indication of a kick.

Flowing Well. When the rig pumps are not moving the mud, continued flow from the well indicates that a kick is in progress. An exception is when the mud in the drillpipe is considerably heavier than that in the annulus (for example, in the case of a slug). Care must be taken to determine whether a slug is present. If so, the flow will decrease and eventually stop.

Warnings Signs of Secondary Importance to Kick Detection. *Drilling Break.* An abrupt increase in bit penetration rate, called a *drilling break*, is a warning sign of a possible kick. A gradual increase in penetration rate is an indicator of abnormal pressure and should not be misconstrued as an abrupt rate increase. When the rate suddenly increases, it can be assumed that the rock type has changed. It can also be assumed that the new rock type has the potential to kick (as in the case of a sand), even if the previously drilled rock did not have this potential (as in the case of shale). Although a drilling break may have been observed, it is not certain that a kick will then occur, but only that a new formation that may have kick potential is now being drilled.

When a drilling break occurs, it is a recommended practice that the driller should drill 3 to 5 ft (1 to 1.5 m) into the new formation and then stop to check for flowing formation fluids. Flow checks are not always performed in

tophole drilling or if drilling through a series of stringers where repetitive breaks are encountered; unfortunately many kicks and blowouts have occurred as a result of this failure to perform flow checks.

Pump-Pressure Decrease with Stroke Increase. A pump-pressure change may indicate a kick. Initial fluid entry into the borehole may cause the mud to flocculate, which may increase the pump pressure temporarily. As the flow continues, the low-density influx will displace the heavier drilling fluids, and the pump pressure may begin to decrease. As the fluid in the annulus becomes less dense, the mud in the drillpipe tends to drop, and the pump speed may increase. However, other drilling problems may cause these same signs. A hole in the pipe, called a *washout*, will cause pump pressure to decrease. A twistoff of the drillstring will give the same signs. It is proper procedure, however, to check for a kick if these signs are observed.

Reduced Mud Weight. Reduced mud weight in the flowline has occasionally caused a kick to occur. Some causes for reduced mud weight are core-volume cutting by gas or circulation of connection air or aerated mud from the pits down the drillpipe. Fortunately, the lower mud weights generated by the cutting effect are found near the surface, occur generally as a result of gas expansion, and do not appreciably reduce mud density throughout the hole. **Table 10.3** shows that gas cutting has a very small effect on bottomhole hydrostatic pressure. An important point to remember about gas cutting is that if the well did not kick during the time required to drill the gas zone and to circulate the gas to the surface, only a small possibility exists that it will kick later. Generally, gas cutting indicates that a gas-containing formation has been drilled; it does not mean that the mud weight must be increased.

Improper Hole Fill-Up. When the drillstring is pulled out of the hole, the mud level should decrease by a volume equivalent to that of the steel removed. If the hole does not fill with the volume of mud calculated to bring the mud level back to the surface, it can be assumed that a kick fluid has entered the hole and filled the displacement volume of the drillstring. Even though gas or salt water has entered the hole, the well may not flow until enough fluid has entered to reduce the hydrostatic pressure to a value lower than the formation pressure.

Change in String Weight. Drilling fluid provides a buoyant effect on the drillstring and reduces the actual pipe weight supported by the derrick. Heavier muds have a greater buoyant force than less dense muds. When a kick occurs and low-density formation fluids begin to enter the borehole, the buoyant force of the mud system is reduced. The string weight observed at the surface will increase. However, this change may be small and not readily observable.

10.2.5 Shut-In Procedure. When one or more warning signs of a kick have been observed, steps should be taken to shut in the well. If there is any doubt as to whether the well is flowing, shut it in and check the pressures. Moreover, there is no difference in this context between “just a small flow” and a “full-flowing” well, because both can very quickly turn into a big blowout. There has been some hesitation in the past to close in a flowing well because of the possibility of sticking the pipe. It can be shown that for all types of pipe sticking, including differential pressure, heaving, or sloughing shale, it is better to close in the well quickly and reduce the kick influx. This approach in fact reduces the chances of pipe sticking. The primary concern at this point is to kill the kick safely; when feasible, the secondary concern is to avoid pipe sticking.

Some concern has been expressed about fracturing the well and creating an underground blowout as a result of shutting in a well when a kick occurs. If the well is allowed to flow, it will eventually become necessary to shut in the well, at which time the possibility of fracturing the well will be greater than if the well had been shut in immediately after the initial kick detection. **Table 10.4** shows an example of the higher casing pressures that can result from continuous flow.

Initial Shut-In. There has been considerable discussion about the merits of hard vs. soft shut-in procedures. In a *hard shut-in procedure*, the annular preventer(s) are closed immediately after the pumps are shut down. In a *soft shut-in procedure*, the choke is opened before the preventers are closed, and the choke is closed afterward.

**TABLE 10.3—EXAMPLES OF THE PRESSURE-REDUCTION EFFECT (IN PSI)
OF GAS-CUT MUD ON BOTTOMHOLE HYDROSTATIC PRESSURE (Lake 2006)**

Depth	10 lbm/gal cut to 5 lbm/gal	18 lbm/gal cut to 16.2 lbm/gal	18.0 lbm/gal cut to 9 lbm/gal
1,000	51	31	60
5,000	72	41	82
10,000	86	48	95
20,000	97	51	105

TABLE 10.4—EXAMPLES OF THE EFFECT OF CONTINUOUS INFLUX ON CASING PRESSURE AS A RESULT OF FAILURE TO CLOSE IN THE WELL (Lake 2006)

<u>Volume of Gas Gained, bbl</u>	<u>Casing Pressure, psi</u>
20	1,468
30	1,654
40	1,796

Arguments in favor of a soft shut-in procedure are (1) it avoids water hammer because fluid flow is not stopped abruptly and (2) it provides an alternate means of well control (the low-choke-pressure method) if the casing pressure becomes excessive. The water-hammer concern has been proved to be of no substance, and the low-choke-pressure method of well control is an unreliable procedure. It is best to use the hard shut-in procedure to minimize the kick volume.

Drilling Kicks—Land or Bottom-Supported Offshore Rigs. These rigs do not move during normal drilling operations. They include land and barge rigs, jackups, and platform rigs.

Shut-In Procedures.

- When a primary kick-warning sign has been observed, immediately raise the kelly or top drive until a tool joint is above the rotary table.
- Stop the mud pumps.
- Close the annular preventer.
- Notify company personnel.
- Read and record the shut-in drillpipe pressure, the shut-in casing pressure, and the pit gain. (The *shut-in drillpipe pressure* is referred to as the SIDPP and the *shut-in casing pressure* as the SICP.)

Raising the kelly/top drive is an important part of this procedure. With the kelly/top drive out of the hole, the valve at the bottom of the kelly/top drive can be closed if necessary. Also, the annular preventer members can attain a more secure seal on pipe than against a kelly.

Tripping Kicks—Land or Bottom-Supported Offshore Rigs. A high percentage of well-control problems occur when a trip is in progress. Kick problems may be compounded when the rig crew is preoccupied with the trip mechanics and fails to observe the initial warning signs of a kick.

Shut-In Procedures.

- When a primary warning sign of a kick has been observed, immediately set the top tool joint on the slips.
- Install and make up a full-opening, fully opened safety valve on the drillpipe.
- Close the safety valve and the annular preventer.
- Notify company personnel.
- Pick up and make up the kelly/ top drive.
- Open the safety valve.
- Read and record the SIDPP, the SICP, and the pit gain.

Installing a full-opening safety valve in preference to an inside BOP (float) valve is of prime importance because of the advantages offered by the full-opening valve. If flow occurs up the drillpipe as a result of a trip kick, the fully opened, full-opening valve is physically easier to stab. Also, a float-type inside BOP valve will close automatically when the upward-moving fluid contacts the valve. If wireline work such as drillpipe perforation or logging becomes necessary, the full-opening valve will accept logging tools approximately equal to its inside diameter, whereas the float valve may prohibit wireline work altogether. After the kick is shut in, an inside BOP float valve may be stabbed onto the full-opening valve to enable stripping operations.

Drilling Kicks—Floating Rigs. A floating rig moves during normal drilling operations. The primary types of floating rigs are semisubmersibles and drillships. Several differences in shut-in procedures apply to floaters. Drillstring movement can occur, even with a motion compensator in operation. Moreover, the BOP stack is located on the sea floor. To solve the problem of possible vessel and drillstring movement and resulting wear on the preventers, a tool joint may be lowered onto the closed pipe rams. The string weight is hung on these rams. This procedure may not be necessary if the rig has a functional motion compensator.

When the stack is located a considerable distance from the rig floor, the problem is to ensure that a tool joint does not interfere with the closing of the preventer elements. A spacing-out procedure should be executed

when the BOP is tested, after running the BOP stack. Close the rams, slowly lower the drillstring until a tool joint contacts the rams, and record the position of the kelly/top drive at that point. Spacing-out should occur so that a tool joint and the lower kelly valve are above the rotary table. Spacing should be correlated with tide-measuring equipment on the rig floor.

The following procedure could be altered to use the annular preventer and motion compensator for cases in which (1) the SIDPP and SICP are low and close to the same value (indicating oil or water) or (2) the “kick volume” is less than 20 to 30 bbl and the expected time to kill the well is less than two or three hours. Be sure that the closing pressure on the annular preventer is reduced to within the range recommended by the manufacturer for this situation, to avoid annular-element failure.

Shut-In Procedures.

- When a primary warning sign of a kick has been observed, immediately raise the kelly/top drive to the level previously designated during the spacing-out procedure (tide adjusted).
- Stop the mud pumps.
- Close the annular preventer.
- Notify company personnel.
- Close the upper set of pipe rams.
- Reduce the hydraulic pressure on the annular preventer.
- Lower the drillpipe until the pipe is supported entirely by the rams.
- Read and record the SIDPP, the SICP, and the pit gain.

Tripping Kicks—Floating Rigs. The procedures for kick closure during a tripping operation on a floater are a combination of floating drilling procedures and tripping procedures for immobile rigs.

Shut-In Procedures.

- When a primary warning sign of a kick has been observed, immediately set the top tool joint onto the slips.
- Install and make up a full-opening, fully opened safety valve in the drillpipe.
- Close the safety valve and the annular preventer.
- Notify company personnel.
- Pick up and make up the kelly/top drive.
- Reduce the hydraulic pressure on the annular preventer.
- Lower the drillpipe until it is supported by the rams.
- Read and record the SIDPP, the SICP, and the pit gain.

Diverter Procedures—All Rigs. When a kick occurs in a well with insufficient casing to control a kick safely, a blowout will occur. Because a shallow underground blowout is difficult to control and may cause the loss of the rig, an attempt is usually made to divert a surface blowout away from the rig. This is the common practice on land and on offshore rigs that are not mobile. Special attention must be paid to opening the diverter lines before shutting in the well.

- When a primary warning sign of a kick has been observed, immediately raise the kelly/top drive until a tool joint is above the rotary table.
- Increase the pump rate to maximum output.
- Open the diverter-line valve(s).
- Close the diverter unit (or annular preventer).
- Notify company personnel.

Recent experiences show that shallow gas flows are difficult to control. Industry philosophy is improving, and new handling procedures are being developed.

Crew Member Responsibilities for Shut-In Procedures. Each crew member has different responsibilities during shut-in procedures. These are listed according to job classification.

Floorhand (Roughneck):

- Notify the driller if any warning signs of kicks are observed.
- Assist in installing the full-opening safety valve if a trip is in progress.
- Initiate well-control responsibilities after shut-in.

Derrickman:

- Notify the driller if any warning signs of kicks are observed.
- Initiate well-control responsibilities and begin mud-mixing preparations.

Driller:

- Shut in the well immediately if any of the primary warning signs of kicks are observed.
- If a kick occurs while performing a trip, set the top tool joint onto the slips and direct the crews in the installation of the safety valve before closing the preventers.
- Notify all appropriate company personnel.

Reading and Interpreting Shut-In Pressures. Shut-in pressures are defined as pressures recorded on the drillpipe and the casing when the well is closed. Although both pressures are important, the drillpipe pressure will be used almost exclusively in killing the well. If the SIDPP reads as zero, check to see whether a drillpipe float valve is installed.

During a kick, fluids flow from the formation into the wellbore. When the well is closed to prevent a blowout, pressure builds at the surface because of the entry of formation fluid into the annulus and the difference between the mud hydrostatic pressure and the formation pressure. Because this pressure imbalance cannot exist for long, the surface pressures will build so that, eventually, the surface pressure plus the mud and influx hydrostatic pressures in the well will be equal to the formation pressure. The equations below express this relationship for the drillpipe and the annular side, respectively:

$$\begin{aligned} p_{\text{form}} &= \text{SIDPP} + p_{\text{DP}}, \\ p_{\text{form}} &= \text{SICP} + p_{\text{ann}} + p_{\text{kick}}, \end{aligned} \quad (10.1)$$

where p_{form} is the formation pressure, p_{DP} is the drillstring hydrostatic pressure, p_{ann} is the annulus hydrostatic pressure, and p_{kick} is the kick pressure.

Interpretation of Recorded Pressures. Fig. 10.12 illustrates an important basic principle. It can be observed that the formation pressure is greater than the drillpipe hydrostatic pressure by an amount equal to the shut-in drillpipe pressure. The drillpipe pressure gauge is a bottomhole pressure (BHP) gauge. The casing-pressure reading cannot be considered as a direct BHP gauge measurement because the amount of formation fluid in the annulus is generally unknown.

Constant BHP Concept. Fig. 10.12 can be used to illustrate another important basic principle. The 780-psi (5.4-MPa) reading observed on the drillpipe gauge is the amount of pressure that was necessary to balance the mud pressure at the hole bottom with the pressure in the gas sand at 15,000 ft (4,600 m). A basic law of physics states that formation fluids travel from areas of high pressure to areas of lower pressure only and that they do not travel between areas of equal pressures, assuming that gravity segregation can be neglected. If the drillpipe pressure is controlled so that the total mud pressure at the hole bottom is slightly greater than the formation pressure, then no additional kick influx will enter the well. The concept is the basis of the constant BHP method of well control, in which the pressure at the hole bottom is kept constant and at least equal to the formation pressure.

Effects of Time. After shut-in, a finite amount of time will elapse before both pressures stabilize. The kick flow rate will eventually drop to close to zero when the pressure in the wellbore is almost equal to that in the formation. The amount of time this takes varies with the difference between the wellbore and the formation pressures, the permeability, the fluid viscosity, and the length and diameter of hole in the kicking formation. Stabilization may take a few minutes to several hours depending on the conditions surrounding the kick. In general, 15 minutes are allowed to obtain shut-in pressures. The pressure will typically increase rapidly at first and then level off, although it will not necessarily become stable. The breakpoint in the pressure curve is taken as the SIDPP.

Several other factors affect the time needed for pressures to stabilize. One reason that they may not necessarily stabilize is differences in density between the kick fluid and the drilling fluid. Gas migration involves the movement of low-density fluids up the annulus. The kick may start to migrate up the hole, with an attendant increase in surface pressure (in the absence of any mitigation technique). It will tend to build pressure at the surface if time is allowed for migration. In addition, the influx may tend to degrade hole stability and to cause either stuck pipe or hole bridging. These problems must be considered when reading the shut-in pressures.

Trapped Pressure. Trapped pressure is any pressure recorded on the drillpipe or annulus that is greater than the amount needed to balance the BHP. Pressure can be trapped in the system in several ways. One common way is for gas to migrate up the annulus and expand; another is to shut in the well before the mud pumps have stopped running. Using a pressure reading that includes trapped pressure may result in erroneous kill calculations. There

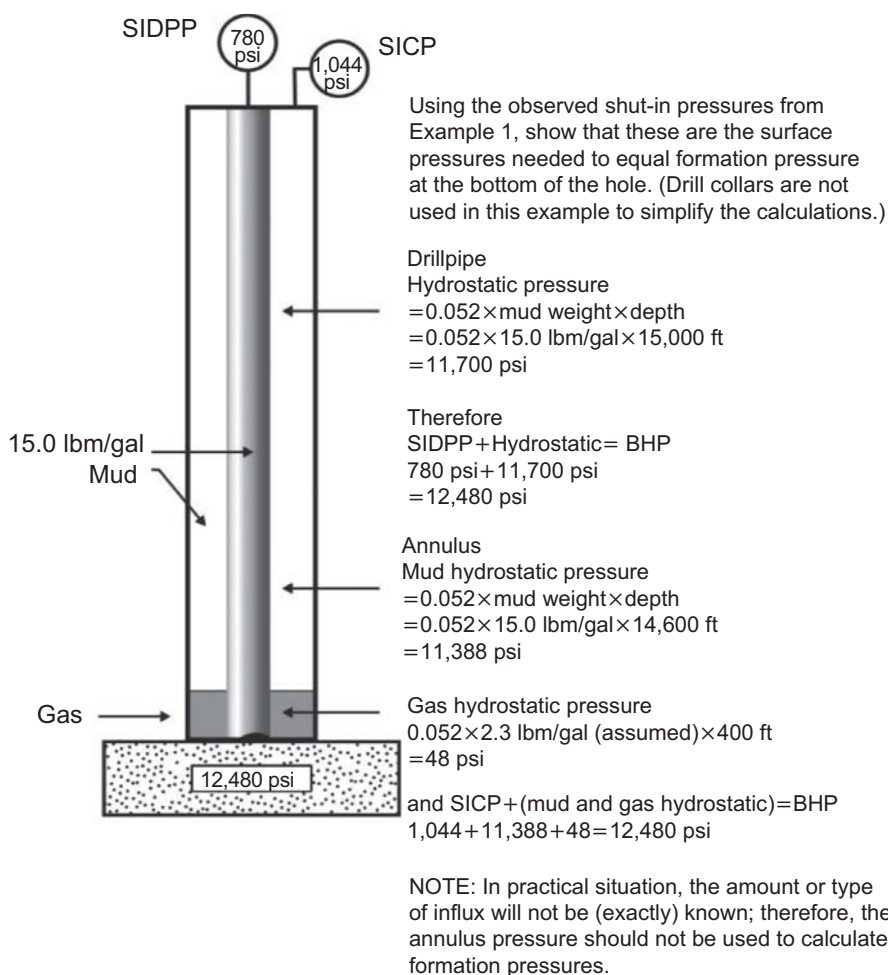


Fig. 10.12—Pressure relationships at shut-in conditions (Lake 2006).

exist guidelines for checking for and releasing trapped pressure. If these are not properly executed, the well will be much more difficult to kill. These guidelines are as follows:

- When checking for trapped pressure, bleed from the casing side only. There are several reasons for this: (1) the choke is located on the casing side; (2) it avoids contamination of the mud in the drillpipe; and (3) it avoids the possibility of plugging the bit jets.
- Use the drillpipe pressure as a guide because it is a direct BHP indicator.
- Bleed small amounts ($\frac{1}{4}$ to $\frac{1}{2}$ bbl) of mud at a time. Close the choke after bleeding and observe the pressure on the drillpipe.
- Continue to alternate the bleeding and subsequent pressure-observation procedures as long as the drillpipe pressure continues to decrease. When the drillpipe pressure ceases to drop, stop bleeding and record the true SIDPP and casing pressure.
- If the drillpipe pressure should decrease to zero during this procedure, continue to bleed and check pressures on the casing side as long as the casing pressure decreases (note: this step will normally not be necessary).

Because the trapped pressure is in excess of that needed to balance the BHP, it can be bled off without allowing any additional influx into the well. However, after the trapped pressure has been bled off, if bleeding is continued, more influx will be allowed into the well, and surface casing pressures will begin to increase. Although bleeding procedures can be implemented at any time, it is advisable to check for trapped pressure when the well is shut in initially and to recheck whether any pressure remains on the shut-in drillpipe after the drillpipe has been displaced with kill mud.

Drillpipe Floats. A kick can occur when a drillpipe float valve is used. Because a float valve prevents movement of fluid and pressure up the drillpipe, a drillpipe pressure reading will not be available after the well has been

shut in. Several procedures are available for obtaining a drillpipe pressure value; the choice depends on the amount of information known when the kick occurs (see **Fig. 10.13**).

The procedure to obtain a drillpipe pressure value if the slow pumping rate (kill rate) is known is as follows:

- Shut in the well, record the SICP, and obtain the kill rate either from the driller or from the daily tour report.
- Instruct the driller to start the pumps and maintain the pumping rate (measured in strokes) at the kill rate.
- As the driller starts the pumps, use the choke to regulate the casing pressure to the same pressure that was originally recorded at shut-in conditions.
- After the pumps are running at the kill rate with the casing pressure properly regulated at shut-in pressure, record the pressure on the drillpipe while pumping.
- Shut down the pumps and close the choke.
- The SIDPP equals the total pumping pressure minus the kill-rate pressure.

If the kill rate is not known, the procedure is as follows:

- Shut in the well.
- Line up a low-volume, high-pressure reciprocating pump on the standpipe.
- Start pumping and fill all the lines.
- Gradually increase the torque on the pumps until they begin to move fluid down the drillpipe.
- The SIDPP is the amount of pressure required to initiate fluid movement. This is assumed to be the amount needed to overcome the pressure acting against the bottom side of the valve.

Kick Identification. When a kick occurs, it may prove useful to know the type of influx (gas, oil, or salt water) entering the wellbore. It must be remembered that the well-control procedures outlined here are designed to kill all types of kicks safely. The equation required to perform the kick-influx calculation is:

$$g_{\text{kick}} = g_{\text{mud}} - \frac{\text{SICP} - \text{SIDPP}}{h_{\text{kick}}} \quad \dots \dots \dots (10.2)$$

where g_{mud} is mud density in psi/ft, h_{kick} is kick height in ft, and g_{kick} is kick density in psi/ft. The influx gradient can be evaluated using the guidelines in **Table 10.5**.

Although both the SIDPP and SICP can be determined accurately, it is difficult to determine the influx height. This requires knowledge of the pit gain and the exact hole size.

Kill-Mud-Weight Calculation. Kill calculations require the mud weight, which will be needed to balance the bottomhole formation pressure. The *kill mud weight* is defined as the weight of mud necessary to balance the formation pressure. It will be shown later in this chapter that using the exact required mud weight without variations reduces downhole stresses. Because the drillpipe pressure has been defined as the reading from a BHP

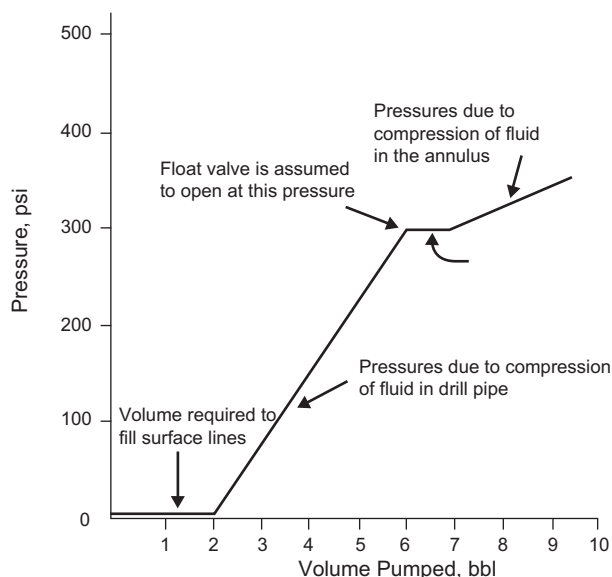


Fig. 10.13—Procedure for establishing SIDPP with a float in the drillstring (Lake 2006).

TABLE 10.5—GRADIENTS FOR DIFFERENT TYPES OF INFLUX (Lake 2006)

Gradient, psi/ft	Type of Influx
0.05–0.2	Gas
0.2–0.4	Probable combination of gas, oil, and/or saltwater
>0.5	Oil or saltwater

gauge, the SIDPP can be used to calculate the mud weight necessary to kill the well. The equation for kill mud weight is

$$\text{KMW} = 19.25 \frac{\text{SIDPP}}{\text{TVD}} + \text{OMW} \quad \dots \quad (10.3)$$

where TVD is true vertical depth in ft, OMW is original mud weight in lbm/gal, and KMW is kill mud weight in lbm/gal. Because the casing pressure does not appear in the above equation, a high casing pressure does not necessarily indicate a high kill mud weight. The same is true for a high pit gain.

Well-Control Procedures. Introduction. Many well-control procedures have been developed over the years. Some have used systematic approaches, while others have been based on logical but perhaps unsound principles. The systematic approaches will be presented in this section.

In previous sections, the constant-BHP approach was described, in which the total pressures (e.g., mud hydrostatic pressure and casing pressure) at the bottom of the hole are maintained at a value slightly greater than the formation pressure to prevent influx of formation fluids into the wellbore. Moreover, because the BHP is only slightly greater than the formation pressure, this approach minimizes the possibility of inducing a fracture and an underground blowout. This concept can be implemented in three ways:

- *One-circulation or wait-and-weight method.* (Another name often used is the *engineer's method*.) After the kick is shut in, weight the mud to kill density and then pump out the kick fluid in one circulation using the kill mud.
- *Two-circulation or driller's method.* After the kick is shut in, the kick fluid is pumped out of the hole before the mud density is increased.
- *Concurrent method.* Pumping begins immediately after the kick is shut in, and pressures are recorded. The mud density is increased as rapidly as possible while pumping the kick fluid out of the well.

If properly used, each method achieves constant pressure at the hole bottom and will not allow additional influx into the well. Procedural and theoretical differences tend to make one procedure more desirable than the others in any particular situation.

Wait-and-Weight Method. Fig. 10.14 illustrates the one-circulation or wait-and-weight method. At Point 1, the SIDPP is used to calculate the kill mud weight. The mud weight is increased to kill density in the suction pit. As the kill mud is pumped down the drillpipe, the static drillpipe pressure is controlled to decrease linearly until, at Point 2, the drillpipe pressure should be zero. At this point, the heavy mud has killed the drillpipe pressure. At Point 3, the initial pumping pressure on the drillpipe is the sum of the shut-in drillpipe pressure and the kill-rate pressure. While kill mud is being pumped down the pipe, the circulating pressure decreases until, at Point 4, only the pumping pressure remains. From the time that kill mud is at the bit until it reaches the flowline, the choke is used to control the drillpipe pressure to the final circulating pressure value. The driller must ensure that the pump continues to operate at the kill speed.

Driller's Method. In the two-circulation or driller's method, the circulation is started immediately. Kill mud is not added to the first circulation. The drillpipe pressure will therefore not decrease during the first circulation (see Fig. 10.15). The purpose of the first circulation is to remove the kick fluid from the annulus. In the second circulation, the mud weight is increased, causing a decrease in pressure from the initial pumping pressure at Point 1 to the final circulating pressure at Point 2. This pressure is held constant while the annulus is displaced with kill mud.

Concurrent Method. This method is the most difficult to execute properly. As soon as the kick is shut in, pumping begins immediately after the pressures have been read. The mud density is increased as rapidly as rig facilities will allow. The difficulty is to determine the density of the mud being circulated and its relative position in the drillpipe. Because this position determines the drillpipe pressures, the rate of pressure decrease may not be as consistent as in the other two methods (see Fig. 10.16). As a new density value arrives at the bit or at some predetermined depth, the drillpipe pressure is decreased by an amount equal to the hydrostatic pressure of the new

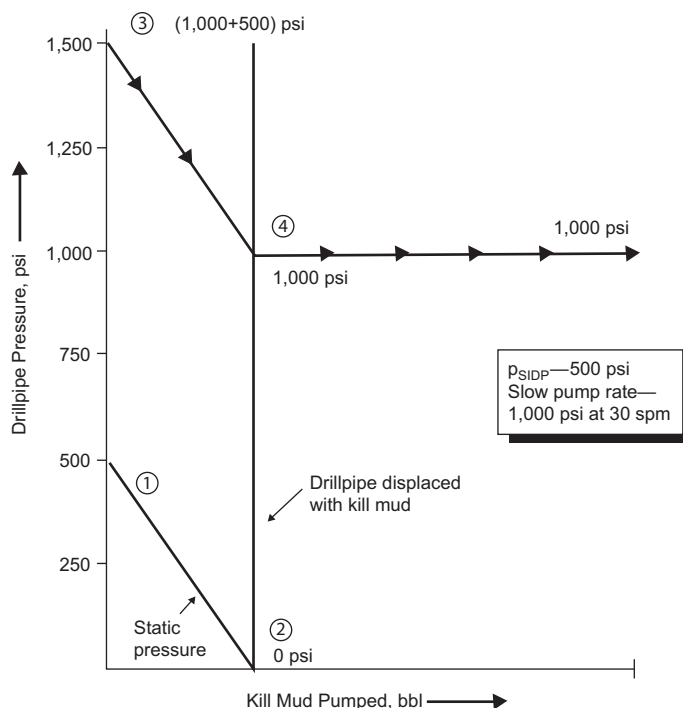


Fig. 10.14—Wait-and-weight method (Lake 2006).

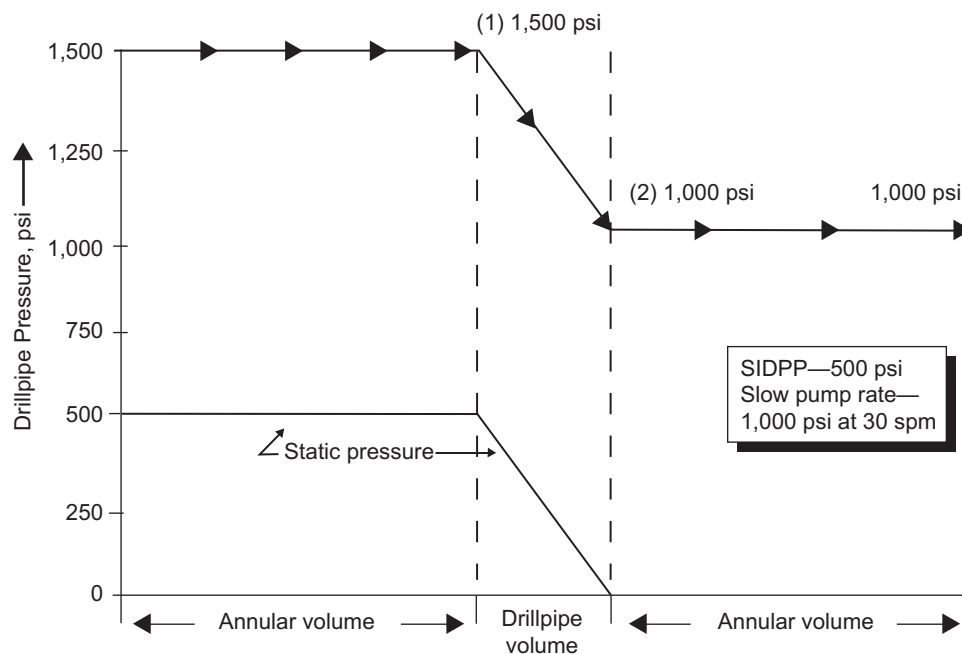


Fig. 10.15—Driller's method (Lake 2006).

mud-weight increment. When the drillpipe is displaced with kill mud, the pumping pressure is maintained constant until the kill mud reaches the flowline.

Constant BHP Methods. Determining the best well-control method for most situations involves several considerations, such as (1) the time required to execute the kill procedure, (2) the surface pressures resulting from the kick, (3) the tradeoff of complexity vs. ease of implementation, and (4) the downhole stresses which will be applied to the formation during the process of killing the kick. All these points must be analyzed before a procedure can be selected. The following list briefly summarizes the general opinion in the industry:

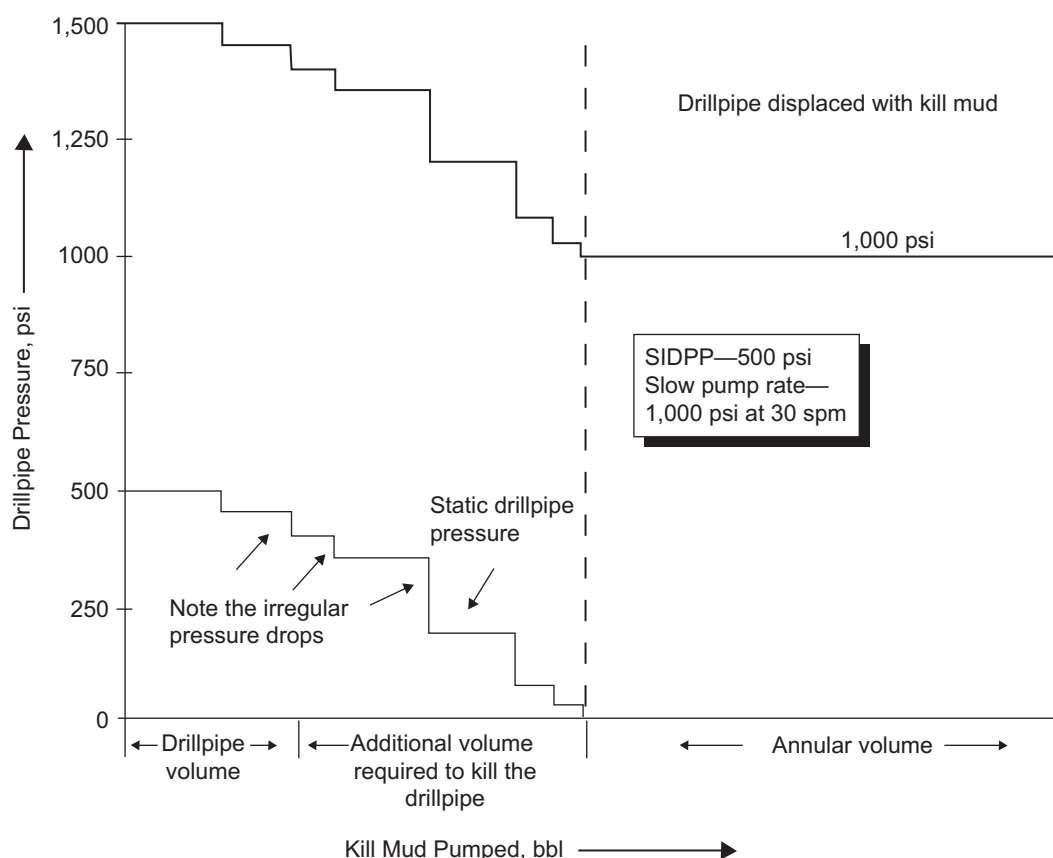


Fig. 10.16—Concurrent method (Lake 2006).

- The wait-and-weight method should be used in most cases.
- The driller's method should be used if a good casing shoe exists and if delays are expected in weighting the system.
- The concurrent method should be used only in rare cases. Its primary use would be for a severe kick (1.5 lbm/gal or greater) with a large influx and a potential problem with development of lost circulation. The pump rate should be kept to a minimum to enable the weight to be increased smoothly.

In the present analysis of kick-killing procedures, emphasis has been placed on the first two circulation methods. Inspection of these procedures will reveal that they are opposite approaches, with the concurrent method falling somewhere in between.

Special Considerations for Well-Control Procedures. Time. Two important time considerations must be attended to in the kill procedure. The first is the time required to increase the mud density from its original weight to the final kill weight. Because some operators become very concerned with pipe sticking during this period, a well-control procedure is often chosen to minimize the waiting time required to increase the mud density. The procedures that involve the shortest initial waiting times are the concurrent method and the two-circulation method. In both procedures, pumping begins immediately after the shut-in pressures have been recorded.

A second important time consideration, however, is the overall time required for the complete procedure to be implemented. The one-circulation method requires one complete fluid displacement (drillpipe and annulus), while the two-circulation method requires that the annulus be displaced twice in addition to the drillpipe displacement. In certain situations, the extra time required for the two-circulation method may be a serious concern with respect to hole stability or preventer wear.

Surface Pressures. During the course of killing a well, surface pressures may reach alarming values. This may be a problem because of gas-volume expansion near the surface. It is important to choose the kill procedure that requires the least possible surface pressure to balance the bottomhole formation pressure.

Figs. 10.17 and 10.18 illustrate the different surface-pressure requirements for several kick situations. The first major difference can be noted immediately after the drillpipe has been displaced with kill mud. The necessary

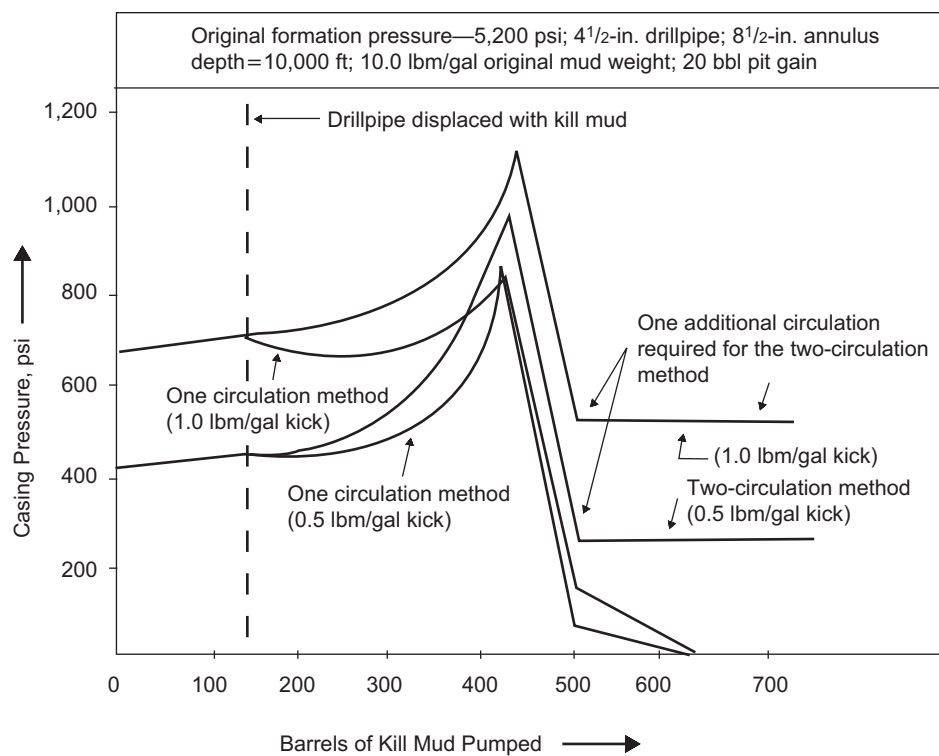


Fig. 10.17—Static annular pressures for one circulation vs. two circulations for a 10,000-ft well (Lake 2006).

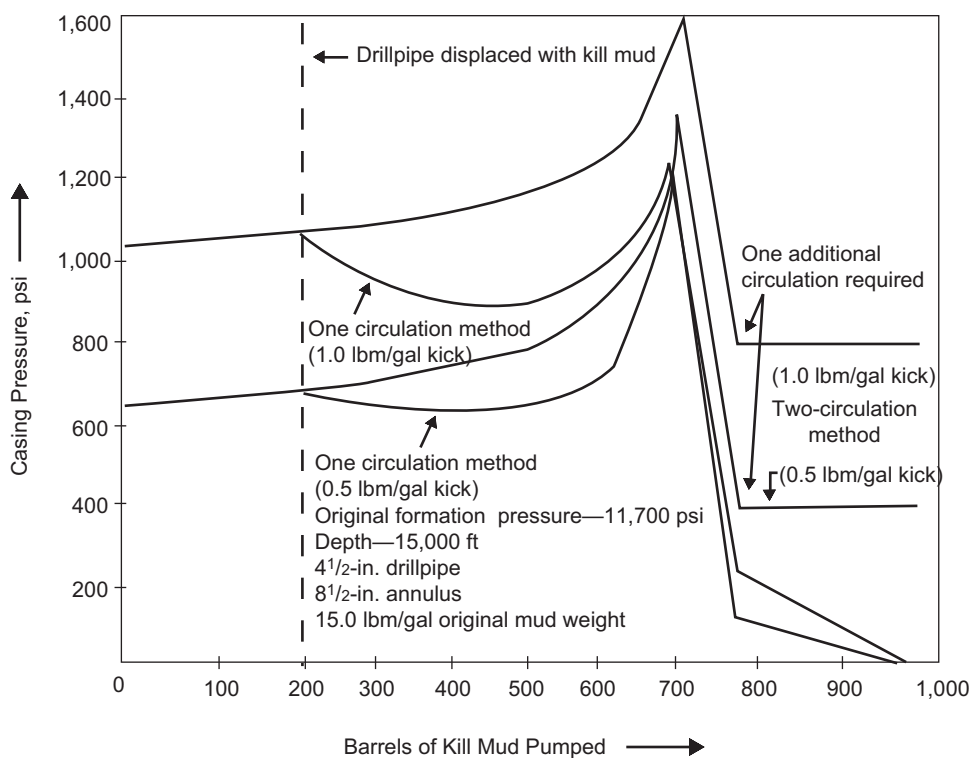


Fig. 10.18—Static annular pressures for one circulation vs. two circulations in a 15,000-ft well (Lake 2006).

casing pressure begins to decrease from the increased kill-mud hydrostatic pressure in the one-circulation procedure. This decrease is not seen in the two-circulation method because this procedure does not circulate kill mud initially. In fact, the casing pressure increases as the expansion of the gas bubble displaces mud from the hole. The second pressure difference occurs as the gas approaches the surface. The two-circulation procedure generates higher pressures as a result of the lower density of the original mud. It is interesting to note that these necessarily high casing pressures suppress the gas expansion to a small degree, resulting in a later arrival of gas at the surface.

Procedural Complexity. In general, the suitability of a process is partially dependent on the ease with which it can be executed. This principle holds true for well control. If a kick-killing procedure is difficult to comprehend and to implement, its reliability will be diminished. The concurrent method is an example of reduced reliability because of procedural complexity. To perform this procedure properly, the drillpipe pressure must be reduced according to the weight of the mud being circulated and its position in the pipe. This implies that (1) the crew will inform the operator when a new mud weight is being pumped, (2) that the rig facilities can sustain this increased mud weight, and (3) that the mud-weight position in the pipe can be determined by pump-stroke counting. Many operators have discontinued using this method because of its complexity.

On the other hand, the one- and two-circulation methods are widely used because of their ease of implementation. In both procedures, the drillpipe pressure remains constant over long intervals of time. Moreover, because the drillpipe is being displaced with kill mud, the drillpipe pressure decrease is essentially a straight-line relationship, not staggered as in the concurrent method.

Downhole Stresses. Although all considerations are important, the primary concern should be the stresses imposed on the borehole wall. If the kick-imposed stresses are greater than the formation can withstand, an induced fracture will occur, creating the possibility of an underground blowout. The procedure that imposes the least downhole stress while maintaining a constant pressure on the kicking zone is considered the safest kick-control method.

Equivalent mud weights are a useful tool to measure downhole stresses. *Equivalent weight* is defined as the total pressure at a depth converted to pounds per gallon of mud weight:

$$EMW = 19.25 \frac{\sum p}{TVD} \dots \dots \dots (10.4)$$

where $\sum p$ is the summation of pressures to TVD in psi and EMW is equivalent mud weight in lbm/gal. The equivalent mud weights for the systems shown in Figs. 10.17 and 10.18 are presented in **Figs. 10.19 and 10.20**, respectively. The one-circulation method has consistently lower equivalent mud weights throughout the killing process after the drillpipe has been displaced. The procedures generally exhibit the same maximum equivalent mud weights from the time the well is shut in until the drillpipe is displaced.

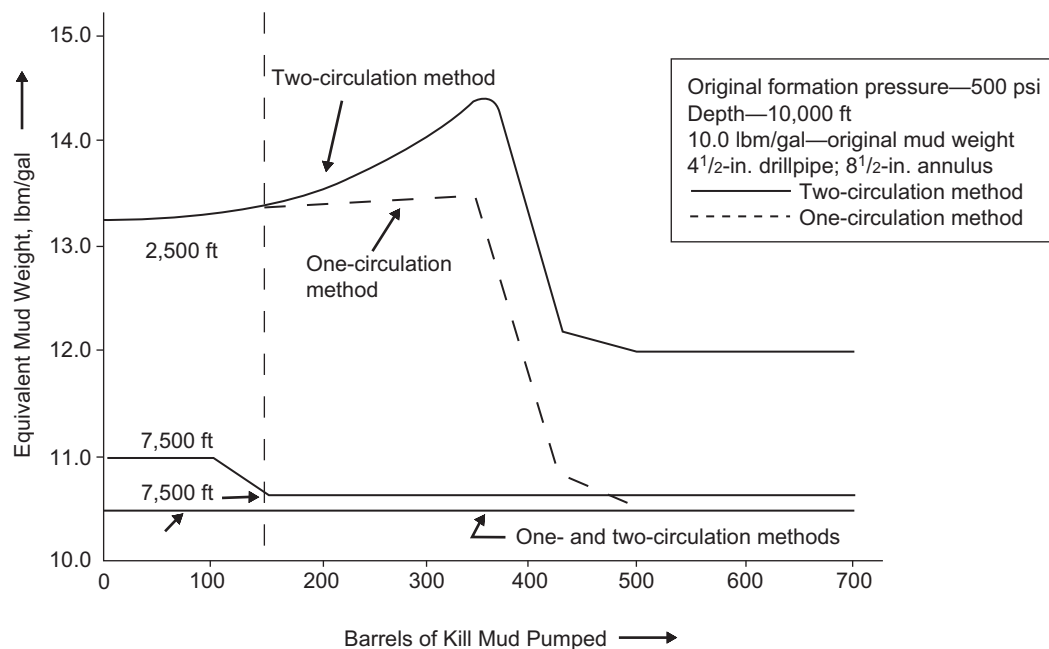


Fig. 10.19—Equivalent mud weights for both circulation methods in a 10,000-ft well (Lake 2006).

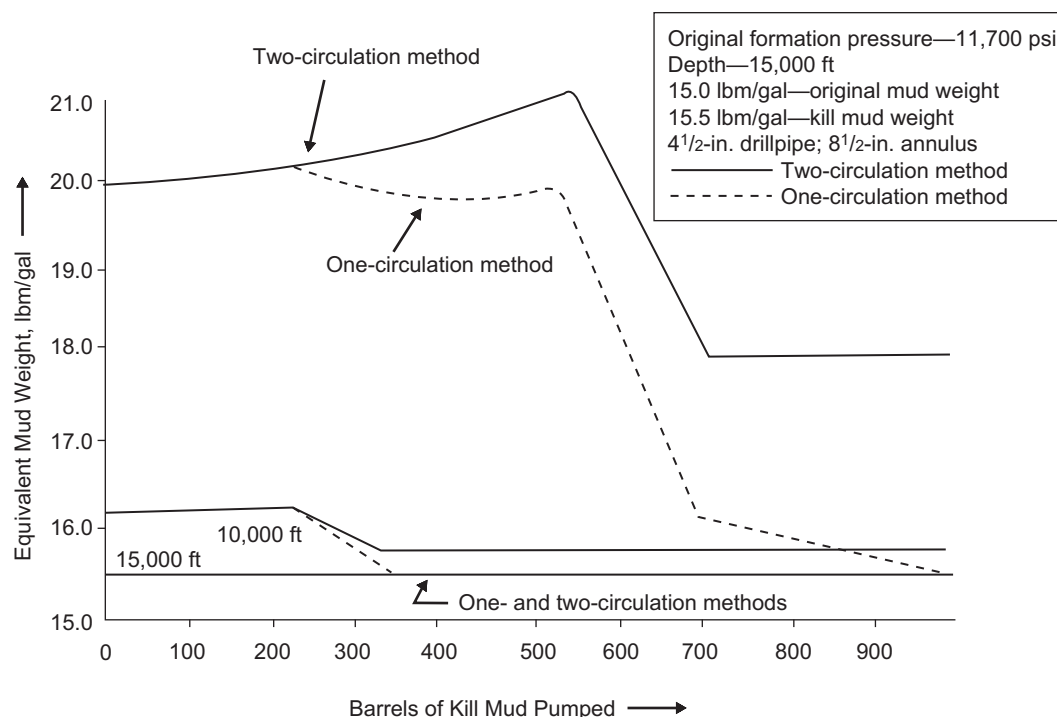


Fig. 10.20—Equivalent mud weights for both circulation methods in a 15,000-ft well (Lake 2006).

These figures illustrate an important principle. The maximum stresses occur very early in the circulation process at deeper depth, not at the maximum-casing-pressure intervals. The maximum lost-circulation possibilities will not occur under gas-to-surface conditions, as might seem logical to the casual observer. If a fracture is not created at shut-in, it will probably not occur throughout the remainder of the process. A full understanding of this behavior may calm operators' concerns about formation fracture as the gas approaches the surface.

Variables Affecting Kill Procedures. Although variables that affect kick-killing do not necessitate a change in the basic procedural structure, they may cause unexpected behavior that can mislead an operator into making bad decisions. The one-circulation method will be used to demonstrate the effect of these variables.

Influx Type. The type of influx entering the wellbore plays a key role in casing-pressure behavior. The influx type can range from heavy oil to fresh water. The most common type is gas or salt water. Each of these has its own characteristic casing-pressure curve and different downhole effects.

Gas kicks are generally more dramatic than other types of influx. Among the reasons are (1) the high rate at which gas enters the wellbore, (2) high casing pressures resulting partially from the low-density fluid, (3) expansion of the gas as it approaches the surface, (4) fluid migration up the wellbore, and (5) fluid flammability. A typical gas-kick casing-pressure curve is shown in Fig. 10.21. Gas expansion from decreased confining pressures as the fluid is pumped up the wellbore affects the kick-killing process. As the gas begins to expand, the previously decreasing casing pressure begins to increase at an accelerating rate. This higher casing pressure may give the false impression that another kick influx is entering the well. Immediately after the gas reaches the surface, the casing pressure decreases rapidly, which may give the impression that lost circulation has occurred.

Both of these casing-pressure changes are expected behaviors and do not indicate an additional influx or lost circulation. The possibility of lost circulation is less under gas-to-surface conditions than under the initial shut-in conditions (see Figs. 10.19 and 10.20).

When gas expands, the increased gas volume displaces fluid from the well, resulting in a pit gain. Fig. 10.22 shows the pit gain for the problem illustrated in Fig. 10.17. This pit gain is in addition to the volume increase from weighting materials. Because the pit gains in volume, it is logical to assume that the flow rate exiting the well will increase (Fig. 10.23).

Saltwater kicks do not pose the same problems as gas kicks. Volume expansion does not occur. Also, because salt water is denser than gas, casing pressures are less than for a comparable volume of gas (see Fig. 10.24). Shut-in pressures for a 50-bbl (7.9-m³) saltwater kick are approximately the same as those shown in Fig. 10.17 for a 20-bbl (3.2-m³) gas kick under the same conditions.

Hole-stability and pipe-sticking problems are generally more severe with a saltwater kick than with gas. The saltwater fluid causes a freshwater mud filter cake to flocculate, creating pipe-sticking tendencies and unstable hole

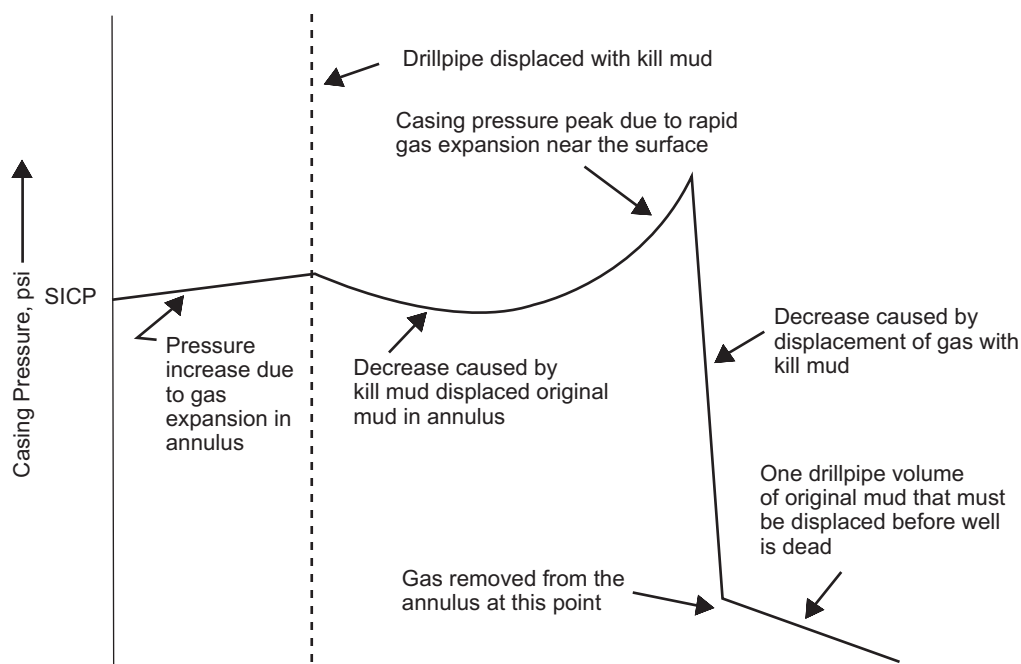


Fig. 10.21—Typical gas-kick casing-pressure curve for the wait-and-weight method (Lake 2006).

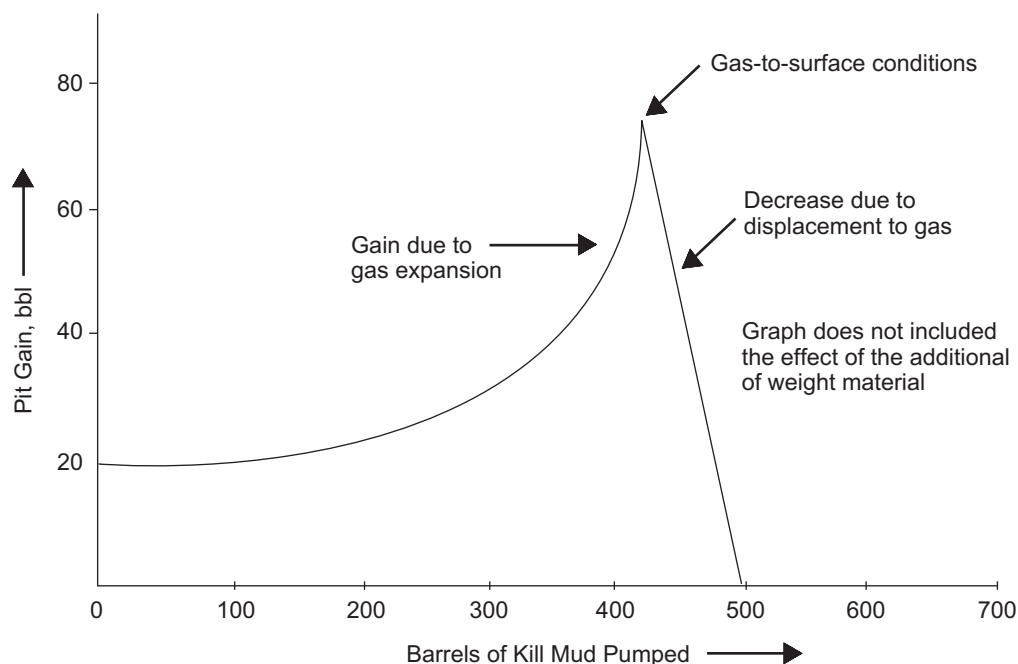


Fig. 10.22—Pit gain curve for the 1-lbm/gal kick illustrated in Fig. 10.17 (Lake 2006).

conditions. The severity of these problems increases with large kick volumes and with extended waiting periods before the fluid is pumped from the hole.

Volume of Influx. The fluid volume entering the well is a controlling variable on the casing pressure throughout the kill process. Increased influx volumes give rise to higher initial SICP values and to greater pressure differences under gas-to-surface conditions (Fig. 10.25). This observation underlines the importance of quick closure rather than hesitation.

Variations in Kill-Weight Increment. The original mud density must be increased in most kick situations to kill the well. This incremental density increase has some effect on casing-pressure behavior (Fig. 10.26). The gas-to-surface pressures are higher than the original shut-in pressures for 0.5-lbm/gal (60-kg/m³) and 1.0-lbm/gal

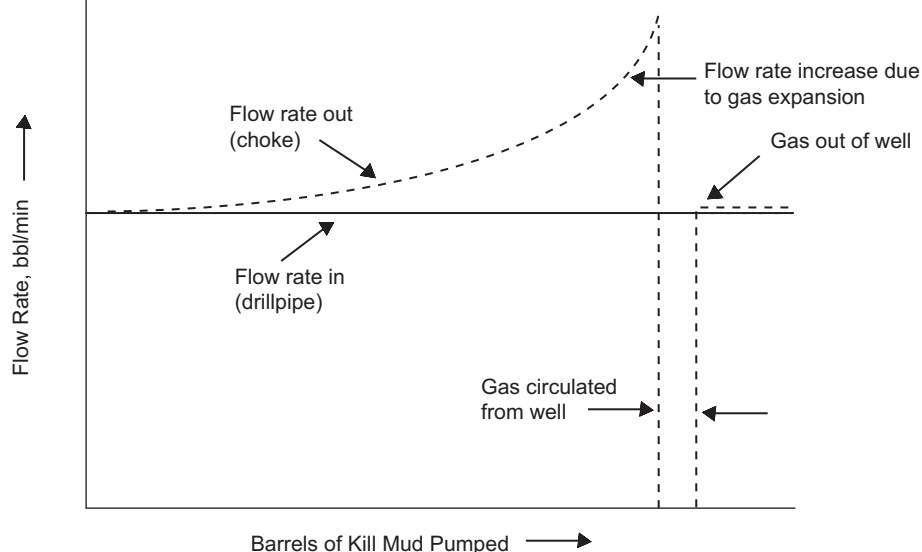


Fig. 10.23—Typical flow rates during kick kill operations (Lake 2006).

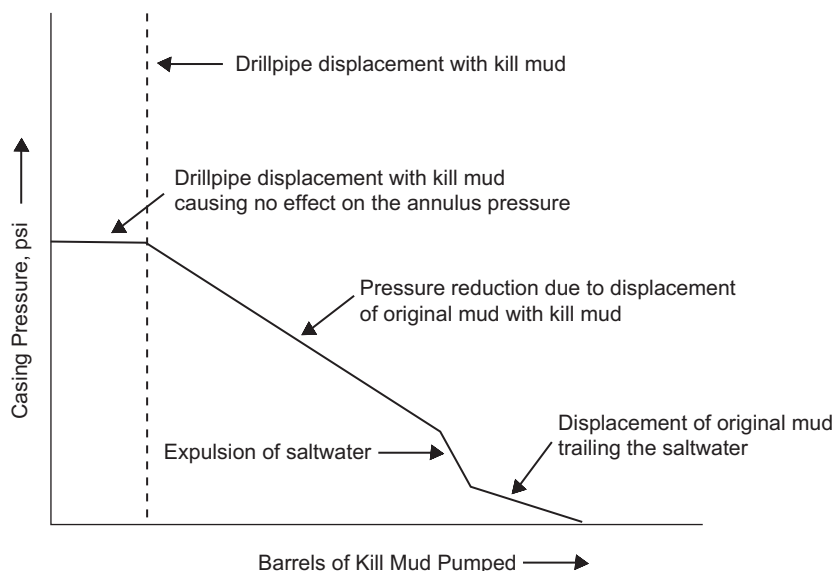


Fig. 10.24—Typical saltwater-kick casing-pressure curve (Lake 2006).

(120-kg/m³) kicks. The 2.0-lbm/gal (240-kg/m³) and 3.0-lbm/gal (360-kg/m³) mud-weight increases do not show this tendency. The 3.0-lbm/gal (360-kg/m³) kick has a lower gas-to-surface pressure than that at initial closure due to suppressed gas expansion, which minimizes the associated pressures. This is generally observed in kicks requiring an incremental increase greater than 2.0 lbm/gal (240 kg/m³).

Another important mud-weight variation is the difference between the kill mud weight necessary to balance BHP and the mud weight actually circulated. If the weight of circulated mud is less than the kill mud weight, the casing pressure will be higher than if the kill mud weight had been used, because of the need to maintain a balanced pressure at the hole bottom (Figs. 10.17 and 10.18). The equivalent mud weights will be greater, which increases the possibility of formation fracture.

Circulated mud weights greater than the calculated kill mud weight do not decrease the casing pressure. This situation is synonymous with mud-weight safety factors and is called *overkill*. As the extra-heavy mud is pumped down the drillpipe, the casing pressure will increase due to the U-tube effect (Fig. 10.27). This U-tube principle states that the pressures on each side of the tube must be equal (Fig. 10.28). These higher casing pressures create associated downhole stresses that increase formation-fracture potential.

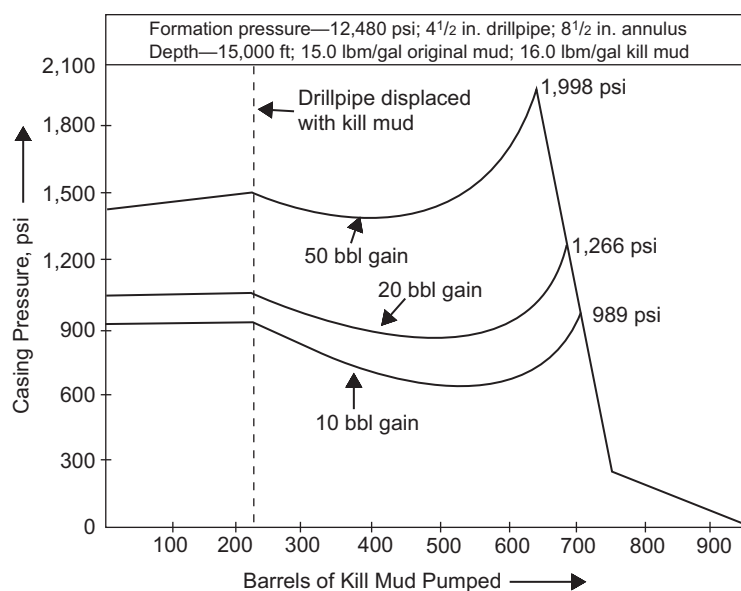


Fig. 10.25—Static casing-pressure curves for 10-, 20-, and 50-bbl kick volumes (Lake 2006).

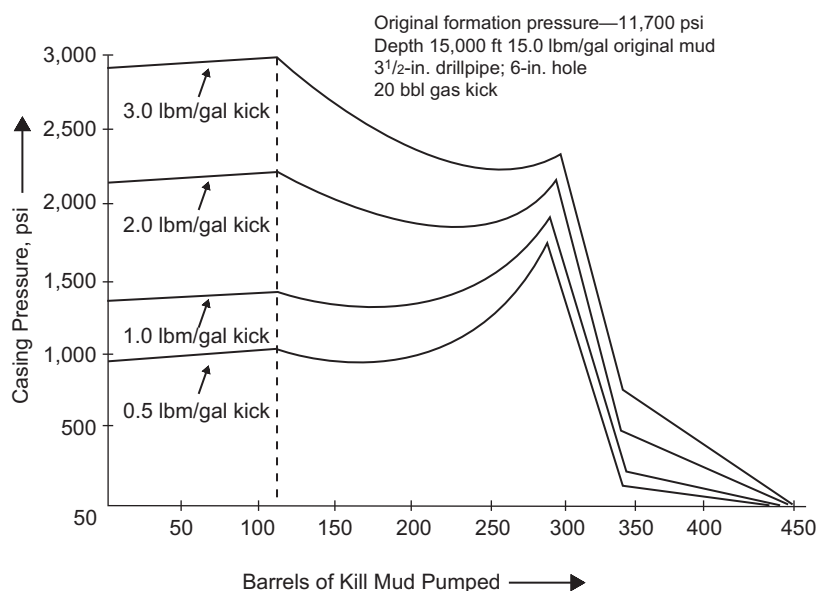


Fig. 10.26—Comparison of required kill mud-weight increments for different sizes of kick (Lake 2006).

Several attempts have been made to achieve the benefits of “safety factors” while avoiding the ill effects of high casing pressures caused by the U-tube effect. The most common approach has been to subtract the hydrostatic pressure supplied by the extra mud-weight increment from the final circulating pressure, creating a zero net effect from the added mud weight. In a static situation, the casing pressure is reduced by an amount equal to the hydrostatic-pressure safety factor, which results in zero net effect. From a theoretical standpoint, the approach is based on sound principles. However, field experience has shown that this procedure is not practical because of its complexity. This procedure is not necessary for proper well control, and only experienced well-control engineers should use it.

Hole-Geometry Variations. In practical kick-killing situations, hole and drillstring size changes will alter the kick-fluid geometry. This is a particular problem in deep tapered holes where several pipe and hole sizes are used. The influx may occupy a large vertical space at the hole bottom, creating a high casing pressure. As the fluid is pumped into the larger annular spaces, the vertical height is decreased, thus increasing the mud-column height and resulting in lower casing pressures. **Figs. 10.29 through 10.31** show a typical tapered hole and its associated casing- and drillpipe-pressure curves.

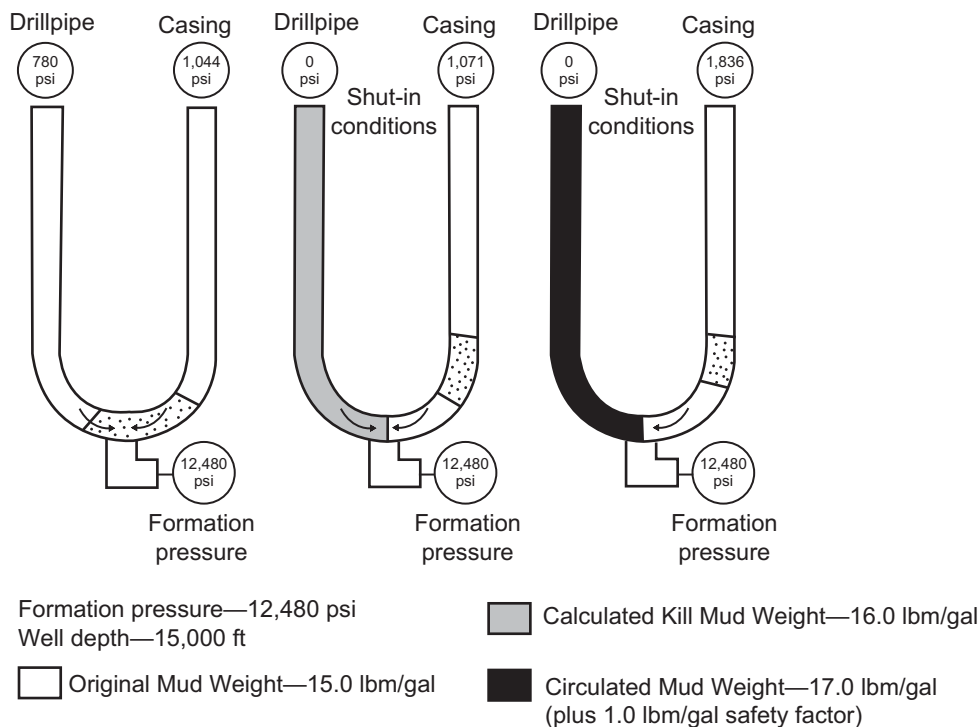


Fig. 10.27—Safety-factor effects (1 lbm/gal) and casing pressures (Lake 2006).

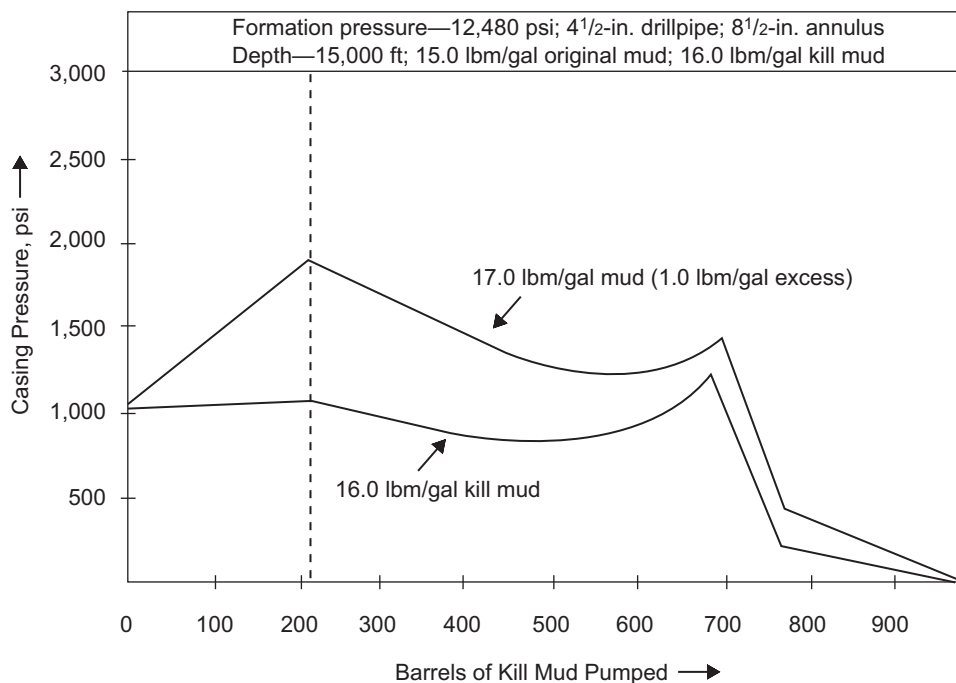


Fig. 10.28—Excess mud-weight effect on annular pressure (Lake 2006).

10.3 Pipe Sticking and Fishing Operations

This section discusses drillstring components, the various ways that a drillstring can become stuck in the borehole, typical fishing techniques, and the mechanics of jarring. This discussion includes a description of the types of jars and other tools used in jarring strings.

In the drilling industry, fishing operations are not pleasant outings by a lake or river. They involve sleepless nights, exhausting days, much time, and a lot of money. It is up to the rig personnel—primarily the drilling engineer

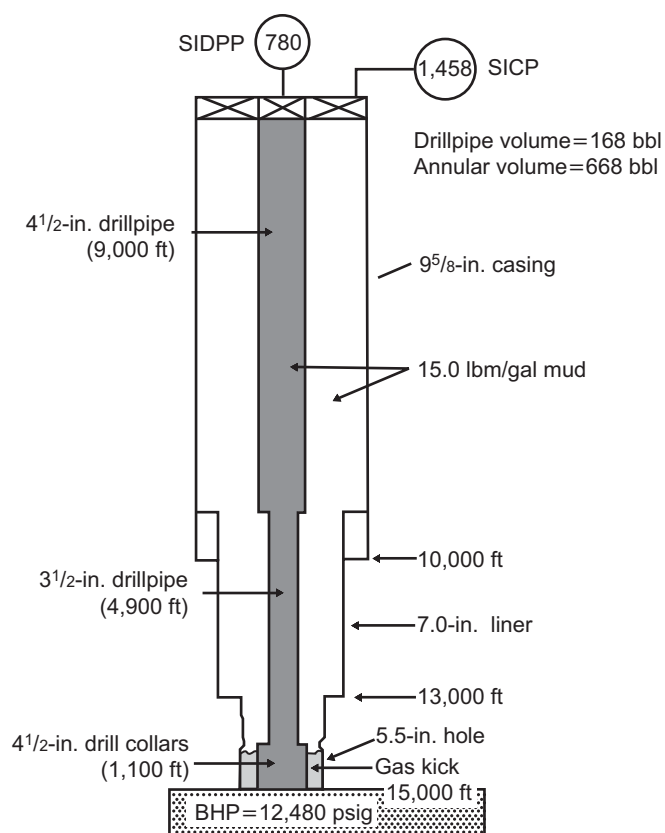


Fig. 10.29—Tapered hole (Lake 2006).

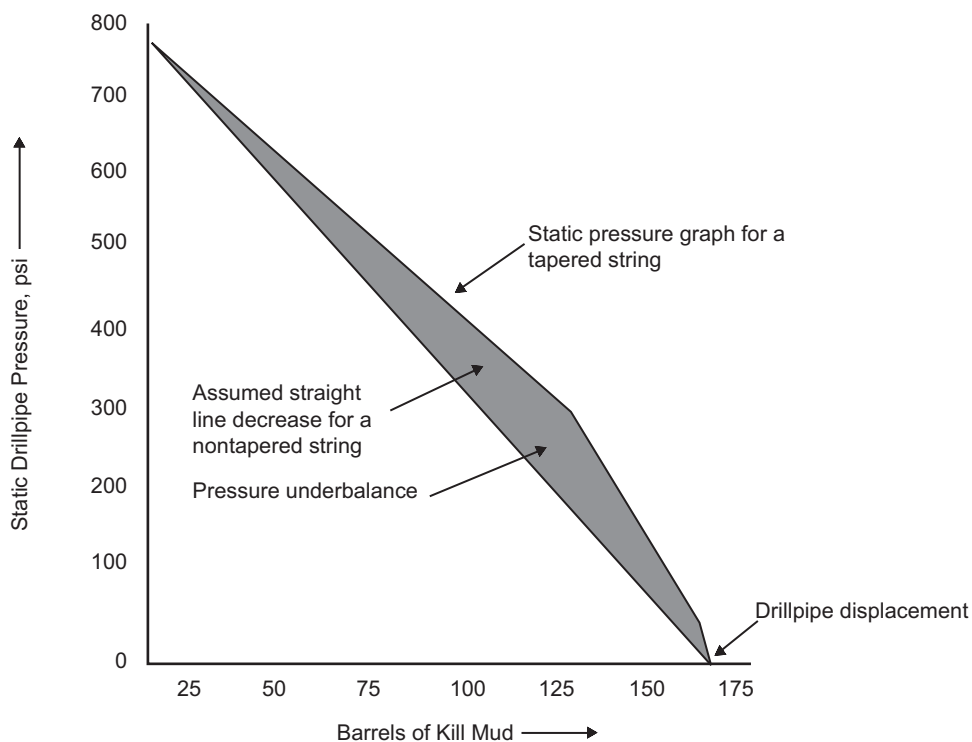


Fig. 10.30—Static drillpipe pressure for tapered string (Lake 2006).

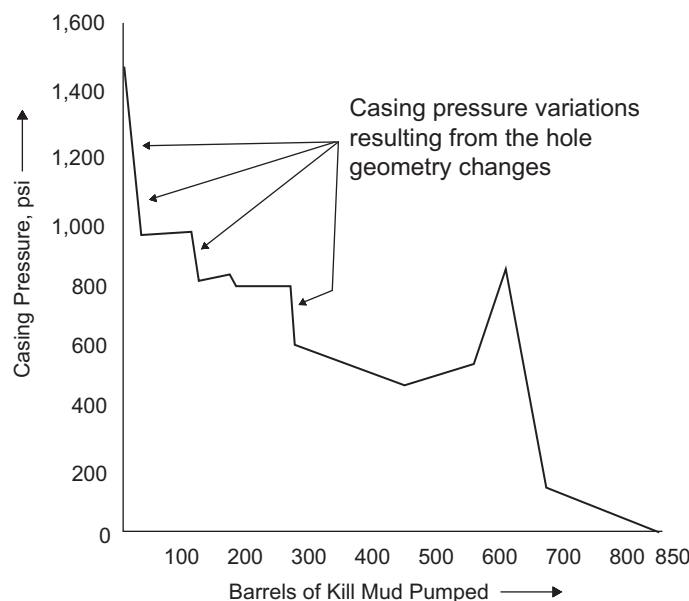


Fig. 10.31—Hole geometry effects on casing pressure (Lake 2006).

involved—to complete the fishing operation as quickly and as economically as possible or to determine that the best course of action is to abandon the hole. *Fishing* is a term coined by the drillers of the cable-tool era. After a cable line broke, the drillers would put a hook on the end of the remaining line and try to “catch” the lost line. Being the innovators that these drillers were, they often devised unique and clever methods of recovering items that were lost in the hole. Many of these items, such as wireline spears and wireline jars (now called bumper subs) still exist and are used daily.

There are many techniques and procedures for fishing, and the drilling engineer must determine the appropriate method for retrieving the lost or stuck item, usually referred to as the *fish*. For example, wireline fishing is considerably different from fishing with drillpipe. The nature of the fish itself may dictate the procedure. A fish may be free or stuck. If the fish is stuck, jarring or washover operations may be needed.

10.3.1 Stuck-Drillstring Problems. There are more ways to get stuck in a hole than there are words to describe the emotions of the driller after this happens. Just about any item that goes into a hole—including drillpipe, drill collars, casing, tubing, and downhole production equipment—can get stuck. This section reviews the most common ways of getting stuck in both open and cased holes (Adams 1977a).

Differential-Pressure Sticking. Differential-pressure sticking, often called differential sticking, is very prevalent in the drilling industry. Differential sticking causes most of the fishing operations that occur in the Gulf of Mexico. Basically, the string is stuck against the side of the well because of a large pressure differential between the fluid in the borehole and that in the formation. Differential-pressure pipe sticking occurs when friction forces in the wellbore acting on the drillstring in a normal direction exceed either the rig’s ability to move the pipe or the strength of the pipe. Hydrostatic pressure creates a differential that forces the pipe into a filter cake across a permeable zone (**Fig. 10.32**). This sticking usually occurs, initially, only across a permeable zone such as sand, where friction resistance is a function of several variables. Forward operations are halted until the stuck pipe can be removed from the wellbore or a sidetrack hole can be drilled. Both of these options are costly in terms of both time and money (Helmick and Longley 1957).

Formation-pressure increases above normal pressure—usually called *abnormal pressure*—require increased mud weights to control the high-pressure formations. Lower-pressure, uncased formations higher in the hole will also be exposed to these higher mud weights and, consequently, to increased pressure differentials. Pressure regressions can sometimes occur in deeper drilling intervals. At these levels, the formation pressure is receding, while the mud weight remains constant to control the high-pressure formations that have already been penetrated and remain uncased. With each newly drilled section, the tendency toward differential pressure and sticking can increase. Properly designed casing programs can significantly reduce stuck-pipe occurrences during changing pressure regimes.

Differential sticking occurs only across a permeable formation and, in fact, the higher the permeability, the higher the probability of differential sticking. As the drilling fluid moves across the permeable zone, it tends to

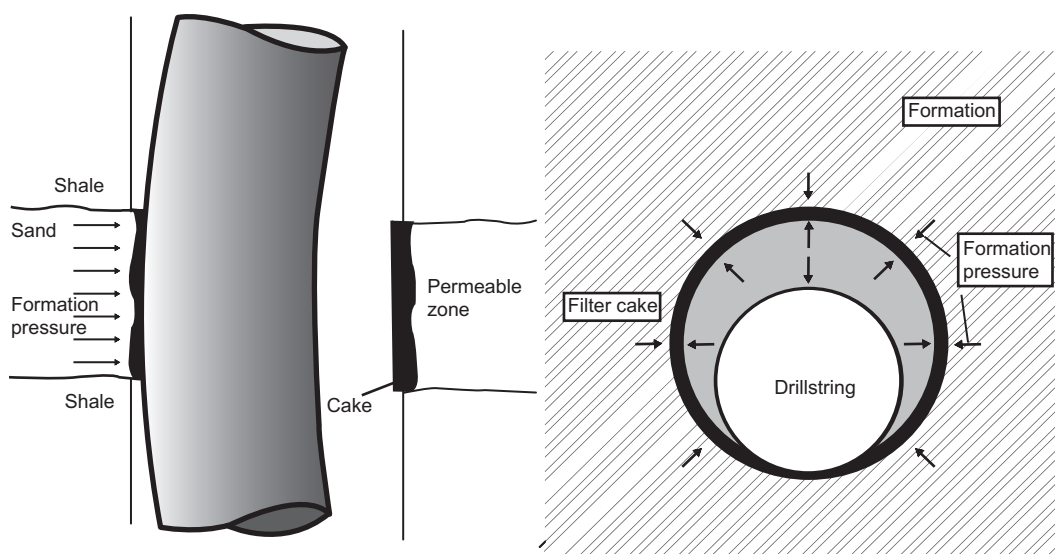


Fig. 10.32—Basic concept of differential pressure sticking: pipe is stuck in the filter cake in a permeable zone (Adams 1977a).

lose its fluid phase to the permeable formation, leaving behind the solid phase. These remaining solids often settle out onto the side of the borehole. This nearly impermeable filter cake can become very thick. Meanwhile, if the hydrostatic pressure of the mud in the permeable zone is much higher than the formation pressure in the permeable zone, there will be a pressure gradient toward the formation across the borehole wall. If, by chance, the drillpipe or collars are lying in the filter cake (which is likely because all boreholes have some degree of deviation), a hydraulic seal can form. Now the pressure gradient lies across the string. Because filter cake has a high friction coefficient, the force required to pull the string tangentially across the filter cake is high. In many cases, the rig is not powerful enough to pull the string or the string is not strong enough to handle the load. Differential sticking is usually the problem if the drillstring cannot be moved up or down or rotated, yet circulation can be maintained. Typically it occurs when the drillstring is lying stationary across a permeable zone.

An equation used in the petroleum industry to describe differential sticking is

$$F_{\text{tangential}} = A\mu P_{\text{normal}}, \quad (10.5)$$

where A is the hydraulically sealed area, μ is the coefficient of friction, P_{normal} is the pressure differential between the wellbore and the formation, and $F_{\text{tangential}}$ is the drag force needed to move up or down the hole.

Unsticking requires the reduction of the normal force, the coefficient of friction of the filter cake, or the hydraulically sealed area—or a combination of these. The sooner these methods can be undertaken, the greater the chance of success. One method used to unstick the string is to spot a lightweight fluid with a filter-cake-destroying chemical and then jar on the string. The fluid reduces the pressure differential, the coefficient of friction of the filter cake, and the hydraulic seal area. An example of this approach would be to spot an oil-based fluid across the stuck point. Another method is to blow nitrogen past the stuck point. This assumes that there are no potential kick zones above or below the stuck point. Well control can easily be lost in such cases.

Undergauge Hole Sticking. An *undergauge hole* is any hole that has a smaller diameter than the bit that drilled that section of hole. One potential cause of an undergauge condition is drilling a high-clay-content plastic shale with a freshwater mud. If an oil-based mud is used, a plastic salt formation can “flow” into the wellbore. If the wellbore fluid has a hydrostatic pressure less than the formation pressure, shale or salt will slowly ooze into the wellbore. This process is slow, but can stick the drilling tools of the unwary.

An undergauge hole can also occur because a drill bit has been worn smaller while drilling through an abrasive formation. In this case, the hole is undergauge because the bit drilled it that way. If a new bit is run, it can jam into the undergauge section of the hole and become stuck. This is often called *tapered-hole sticking*. The presence of a thick filter cake as described above can also cause an undergauge hole. The filter cake can become so thick that tools cannot drag through it. The filter cake shows as a drag load on the weight indicator.

Sloughing-Hole Sticking. Sloughing-hole sticking occurs after a piece of the hole wall sloughs off. For example, water-sensitive shales that have been invaded by water will swell and break. If circulation is stopped, the broken pieces will collect around the drillstring and eventually pack the drillstring in place.

Shales under high formation pressure can slough as well. In this case, the formation pressure is greater than the wellbore hydrostatic pressure. Because shale has very low permeability, no flow is observed. The rock, which has a high pressure differential toward the wellbore, shears off the hole wall. The result can be seen as large cuttings on the shale shaker screen. Sometimes, the borehole curvature can be seen on the cuttings, a classic sign of having entered a high-pressure zone. If too much sloughing occurs, or if the wellbore is not cleaned properly, the drillstring can become stuck. More than likely, circulation will cease, and no string movement will be possible.

Steeply dipping and fractured formations can also slough into the hole. Drilling sites in overthrust belts are notorious for this problem. If there are cavities in the wellbore, cuttings can collect there. After circulation stops, the cuttings in the cavities may fall back into the hole.

Keyseat Sticking. In a deviated hole, or if ledges are present, the drillpipe can wear a slot into the borehole wall. This slot, called a *keyseat*, has essentially the same diameter as the drillpipe. While the drillstring is being pulled, the drill collars or bit will try to run through the keyseat. Because the diameter of the keyseat is smaller than that of the drill collars or bit, these tools become wedged in the keyseat. Circulation can be maintained in this situation. Of course, the usual response of a driller who sees the string start to stick is to pull harder. This exacerbates the situation, sticking the string even more solidly. Keyseat sticking usually occurs while the drillstring is being moved up the hole during a trip.

Sand Sticking and Mud Sticking. Sand sticking and mud sticking are similar. The sand particles or the solids in the mud can settle out of suspension. If there is little or no circulation, the rain of particles settles around the string, sticking the string in place. Sand sticking usually occurs in cased holes, although it can also occur in open holes. In cased holes, a leak can develop in the casing, enabling sand particles to flow into the well. The sand particles will then fall down and eventually pile up either on a packer or on some other restriction in the hole.

Mud sticking is similar. For whatever reason, the solids that form part of the mud can settle out of suspension. These solids can be barite particles or cuttings. In a high-temperature well, the mud can lose its fluid phase (filtrate), leaving the solids packed around the string. In addition, sometimes contaminants such as acids or salts can alter the mud properties leading to loss of the suspension properties of the mud.

Inadequate-Hole-Cleaning Sticking. Inadequate-hole-cleaning sticking can occur if the flow rate of the circulation fluid slows to the point that the solids-carrying capacity of the circulation fluid is exceeded by the force of gravity. If the fluid is not viscous enough or flowing fast enough, the drag forces on the solids are less than the gravity forces. This means that the solids flow down the hole, instead of up and out of the hole. The hole fills up with solids that build up around the string, eventually sticking the string. The flow rate can slow down for a number of reasons, including

- The driller may not be running the pumps fast enough.
- There could be a hole enlargement in the drillstring that slows the flow rate (e.g., a washout).
- The amount of solids may become overwhelming as a result of sloughing shales, unconsolidated formations, or lost circulation.
- There may be a rate of penetration that generates cuttings faster than the drilling fluid can carry.

Cemented Sticking. Cemented sticking can occur if the cement that is being circulated goes somewhere other than where it was intended to go. For example, if a cement plug was being spotted and the cement flowed higher up the string than anticipated, the cement could set before the string could be pulled out of the cement. The string is then stuck. If the cement is not too thick, the string could be jarred loose; otherwise, a washover operation is needed. The causes of cement sticking include

- Mechanical failures (e.g., string leaks)
- Human error (e.g., miscalculating a displacement or losing track of cement being used to remedy a blowout or a lost-circulation zone)
- An oversized hole

Blowout Sticking. During an uncontrolled flow of fluid from a well, called a *blowout*, solids and materials such as drillpipe protector rubbers can flow with the fluids and become lodged against the string. The force of the blowout then wedges these solids and materials against the string. These same solids and materials can also bridge across the hole.

Mechanical Sticking. This is a “catch-all” category for sticking problems. Any drilling or completion tool can become mechanically stuck.

Packers. Sometimes the slips on a packer can become wedged so tightly against the casing that they cannot come free. In addition, retrieval failures can happen. In these cases, sometimes a high-force pulse of short duration can knock the packer loose.

Multiple Strings. Multiple strings can jam in a hole. The two, three, or even four strings in the hole can rotate around each other as they are being run into the hole. The strings become intertwined, in which case they are notoriously difficult to retrieve.

Crooked Pipe. If a drillstring is dropped in a mud-filled hole, the string can become permanently bent. This bend can wedge the string against the side of the hole, making it difficult to retrieve. If a string is dropped in an air-drilled hole, there is no hope of recovery. Think of taking your string up in an airplane and dropping it from some altitude.

Junk in the Hole. Junk in the hole is a description for small pieces of man-made materials that either are dropped down the hole or fall off of a downhole tool. Examples of items dropped down the hole include drill-collar safety clamps, wrenches, and drillstring tools being made up in the rotary table. Items that can fall off of downhole tools include slips from packers, rubber drillpipe protectors, and (especially prevalent) cones off roller-cone bits. This debris can either fall to the bottom of the hole or can wedge against the side of the drillstring. If debris has wedged the string in the hole, then jarring can possibly knock it loose.

10.3.2 What Is The Problem? Recognizing the Problem. As noted, several types of pipe sticking may occur during drilling. Certain identification markers are peculiar to pipe sticking. Recognition of these markers will help in the decision to select the appropriate procedure to free the pipe.

Often, time is an important factor in determining the severity of a sticking problem. For example, in pressure-differential sticking, after the pipe becomes stuck, filtration continues to deposit solids adjacent to the pipe/mudcake interface and increases the contact area. In addition, filtration continues behind the pipe/mudcake interface. This ongoing deposition decreases the water content of the filter cake and increases its friction coefficient (**Fig. 10.33**).

Two early warning signs of differential sticking are increased torque and drag. Both indicate that an increased frictional force is being encountered while either rotating or moving pipe vertically in the hole. These increases may indicate other drilling problems, but they are most often considered the early warning signs of differential sticking. When pipe is differentially stuck, there is no obstruction in the hole to prevent or retard mud circulation, as opposed to the case of a pipe stuck due to hole bridging or caving (**Fig. 10.34**). Continued fluid circulation while the pipe is stuck is a basic indicator of differential sticking. Another characteristic is the inability to rotate or move the pipe in either direction. This is the primary distinction from keyseating, in which the pipe becomes stuck as a result of prolonged wear in a dogleg. Although these two types of pipe sticking appear identical in most respects, pipe stuck in a keyseat can usually be worked downward, which is not possible if the pipe is differentially stuck. Differential sticking usually occurs when the pipe has remained motionless in the hole for a prolonged period of time. Often pipe becomes stuck while making a joint connection. In other cases, long periods of inactivity are necessary for other reasons.

Knowledge of the depth intervals at which sticking is more likely to occur is important in evaluating the remedial procedures to be followed. The intervals most likely to create differential sticking are those with high differential pressures. These can be divided into three categories:

- Drilling through depleted reservoirs
- Pressure progressions
- Pressure regressions

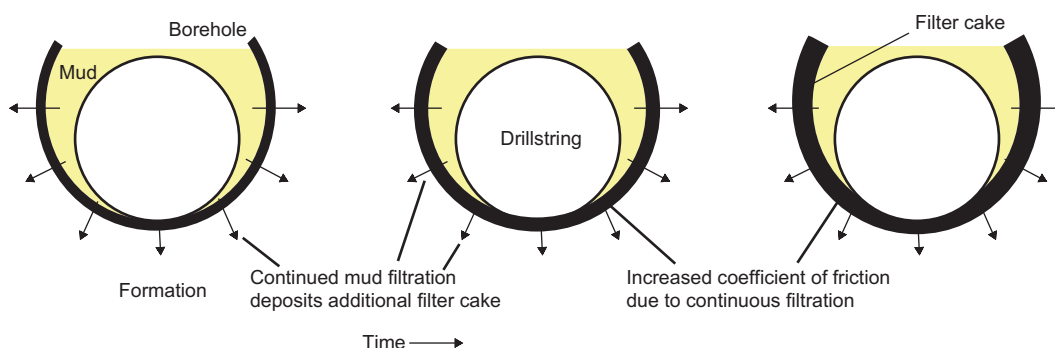


Fig. 10.33—After the pipe is stuck, filtration continues to deposit solids, which build the filter cake and increase the coefficient of friction behind the pipe because of decreased water content (Adams 1977a).

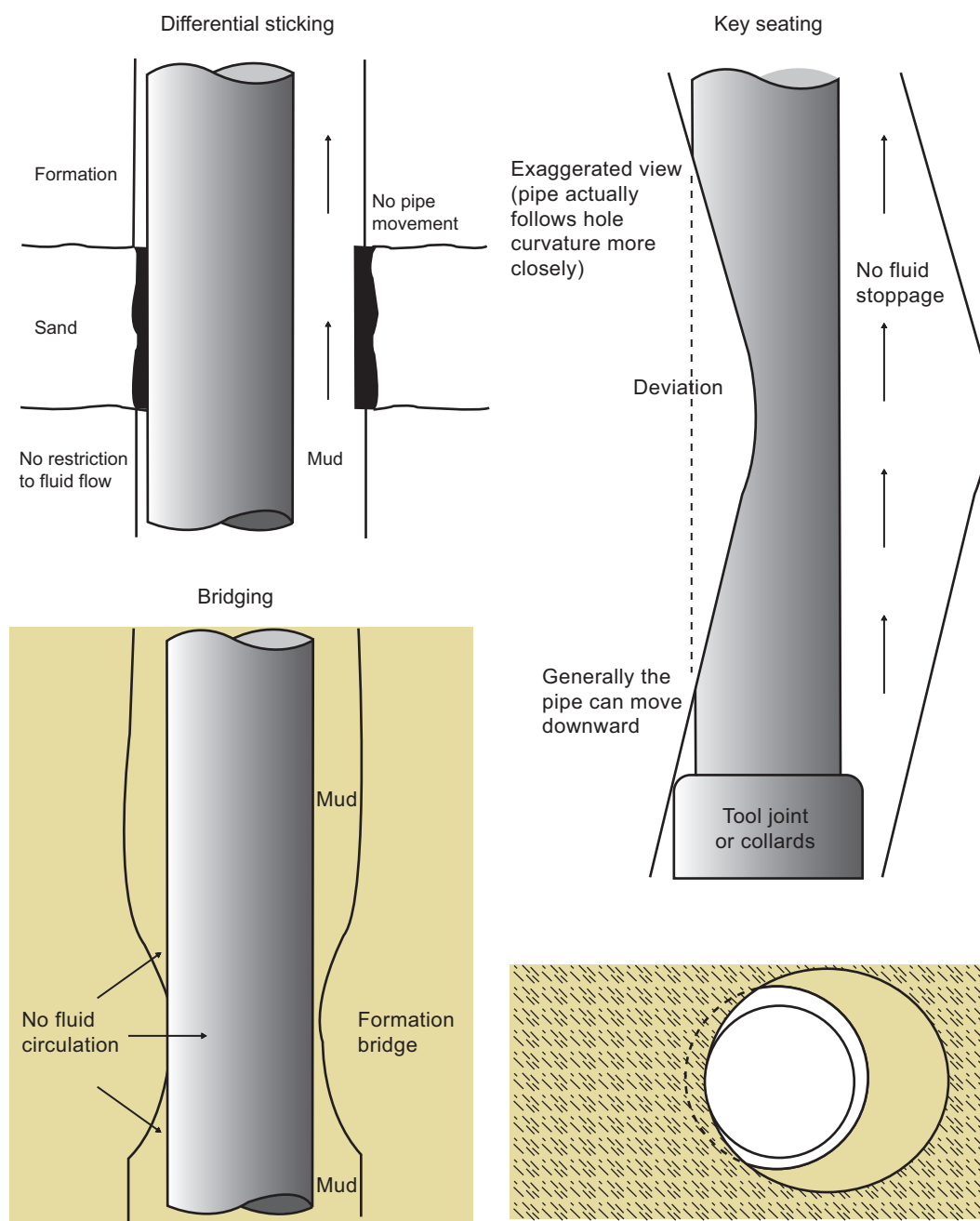


Fig. 10.34—Differential sticking poses no restriction to fluid flow as opposed to bridging; differentially stuck pipe cannot be moved in any direction, as opposed to keyseating (Adams 1977a).

A common drilling situation with a high sticking tendency is drilling through a depleted reservoir, one that is not only hydrocarbon-depleted, but also pressure-depleted. Differential pressures in these cases can range as high as several thousand pounds, compared with a differential of only a few hundred pounds before depletion (see Fig. 10.35).

Minimizing Sticking. Using the proper procedures for preventing stuck pipe in intervals that are expected to be troublesome can significantly reduce the number of stuck-pipe occurrences. Low-water-loss muds reduce the initial contact area because they produce a thin, hard filter cake. A thick, soft filter cake is associated with a high-water-loss mud. Pipe cannot be embedded as deeply in a thin cake and, therefore, the sticking force is reduced (see Fig. 10.36).

Moreover, low-water-loss muds have a reduced filtration rate, which decreases the solids-deposition rate along the pipe/cake interface and minimizes the friction coefficient increase. Oil-based muds offer perhaps the best

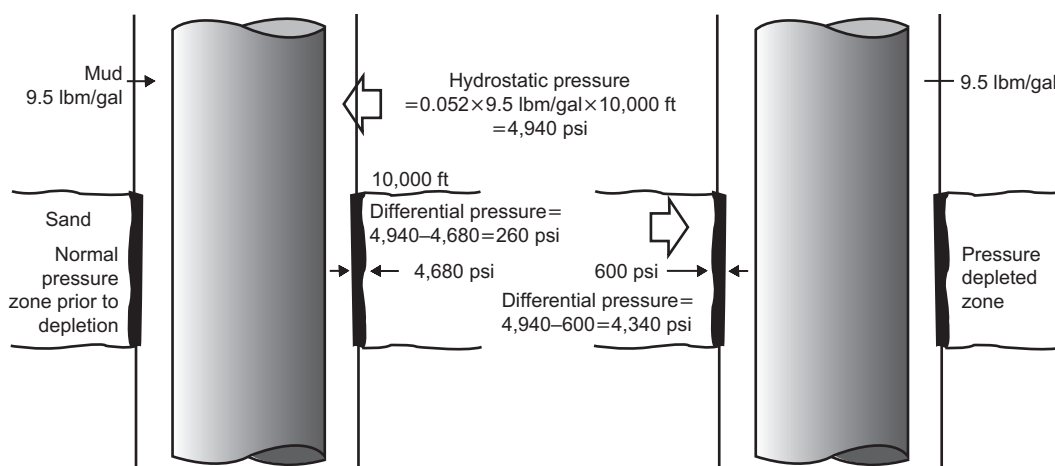


Fig. 10.35—Drilling through a depleted reservoir will create differential pressures greater than drilling the reservoir when it was originally normally pressured (Adams 1977a).

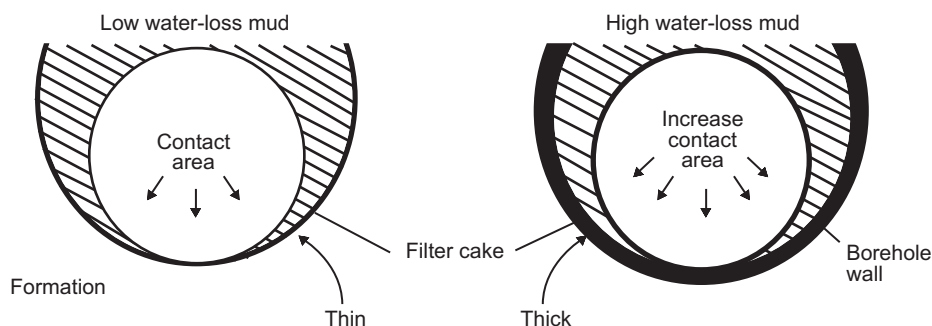


Fig. 10.36—Low-water-loss muds form a thinner, harder filter cake than do high-water-loss muds and are less susceptible to sticking (Adams 1977b).

weapon against stuck pipe. Increased lubricity is most important. These muds develop little or no filter cake, resulting in minimum contact area for the pipe.

Drillstring alterations can reduce sticking tendencies by minimizing the pipe area in contact with the borehole wall. Commonly, stabilizers in the bottomhole assembly (BHA) are used to force pipe standoff. To position the stabilizers properly, the formation of interest must be relatively close to the stabilizer. Another string alteration uses spirally grooved drill collars or heavyweight pipe instead of conventional or smooth pipe. This pipe has a spiraling, shallow but wide groove cut into the outer diameter over the entire length of the joint. Surface area is reduced by approximately 50%, while weight is reduced only by 4%.

A field-developed procedure has been used successfully to minimize (temporarily) the mud friction coefficient along the borehole wall. Addition of walnut hulls or similar specialty products has been found to reduce friction by embedding hulls in the filter cake. This material seems to act like ball bearings for pipe. Although the friction reduction—for both drag and torque—is temporary, it usually alleviates the immediate rigsite situation. The addition of bentonite to the mud system is another temporary measure for reducing the friction coefficient on the borehole wall. The hydration capabilities of the bentonite reduce sticking tendencies. This relief is also temporary because the water film is eventually lost through further filtration or is replaced with drilling solids with a higher friction coefficient (Adams 1977a, 1977b).

Detecting Stuck Sections. This operation involves first determining where the string is stuck in the hole, and then determining the procedure needed to unstuck the string. If a pipe string cannot be quickly worked or jarred free, the next step is to determine the *free point*, or the depth above which the string is free to move.

Freepointing. An initial estimate involves taking a stretch reading to see how far the pipe moves in response to an applied tension. Although not as accurate as the wireline methods that may be used later, stretch readings provide a good first approximation of the free point. Moreover, if the drillstring is plugged, stretch readings may be the only way of obtaining this information.

A procedure for obtaining a stretch reading is as follows:

- Calculate the buoyant weight of the drillstring, including the blocks (or use the hook load recorded immediately before sticking occurred).
- Pick up the pipe to this weight and make a mark on the pipe at the rotary table.
- Apply a predetermined amount of overpull to the drillstring. Service companies provide charts, nomographs, and other tools for estimating this overpull.
- Make another mark on the pipe at the rotary table. The length between these two marks represents the amount of stretch in the pipe.

Once a stretch reading has been recorded, there are two ways of estimating the free point. The first method uses the relationship

$$L = \frac{\Delta LAE}{F}, \quad \dots \dots \dots (10.6)$$

where L is the free-pipe length, ΔL is the stretch length, A is the cross-sectional pipe area, E is the modulus of elasticity, and F is the tension load applied.

A simpler approximation of this equation is

$$L = 735,294 \frac{\Delta L W_p}{F}, \quad \dots \dots \dots (10.7)$$

where W_p is the unit weight of pipe, lbf/in. = $2.67 (OD^2 - ID^2)$, OD is outside diameter in inches, ID is inside diameter in inches, and

$$L = \frac{K}{F}. \quad \dots \dots \dots (10.8)$$

The pipe stretch constant, K , shown in **Table 10.6** can be used with Eq. 10.8.

Although this method is fast, it is not particularly accurate. It can provide an answer to within two or three joints. If the string is to be backed off, a more accurate answer is needed. In addition, if there is more than one type of pipe in the string, the calculations become more complicated. Moreover, if the hole is deviated or dog-legged, the drag from the string rubbing against the hole wall may preclude any stretching of the string below that point.

Freepoint Tool. The freepoint tool (see **Fig. 10.37**) is far more accurate than the stretch method; however, it requires that a wireline tool be run inside the drillstring. The freepoint tool consists of a set of strain gauges and spring-loaded drag blocks or electromagnets that rub against the inside of the string. As the tool is run into the string, torsion or tension is applied to the string. The degree of pipe movement resulting from the application of this torsion or tension is transmitted to the surface through the wireline. After the tool moves below the stuck point, no movement of the string will be detected.

A collar log is also run in conjunction with freepoint tools for positive depth control. A *pipe-recovery log* (**Fig. 10.38**) records acoustic measurements in which high energy readings indicate free pipe and low energy readings indicate stuck pipe. It provides a continuous record of stuck intervals and identifies potential trouble spots or areas where sticking is especially severe.

TABLE 10.6—CONSTANTS USED TO CALCULATE THE FREE POINT

Tubing	K Value
2 in.	3,250,000
2.5 in.	4,500,000
Drillpipe	K Value
2.87 in. (10.4 lbf/ft)	7,000,000
3.5 in. (13.3 lbf/ft)	8,800,000
4.5 in. (16.6 lbf/ft)	10,800,000



Fig. 10.37—Freepoint indication tool. Courtesy of Dia-log (Adams 1977b).

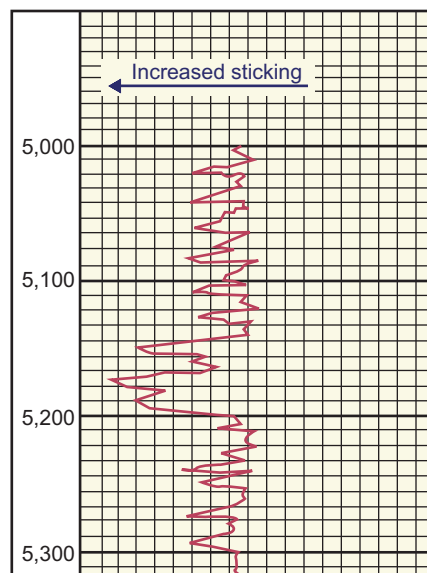


Fig. 10.38—Freepoint log (Adams 1977b).

It is important to understand that the drillstring below the uppermost stuck section is not necessarily stuck. It could be entirely free, or else free at some depths and stuck at others. This information is of critical importance for making decisions about future operations.

The pipe-recovery log provides more decision-making information than the freepoint survey. The log results provide guidance about which downhole intervals are more likely to be free or stuck. The tool functions similarly to cement evaluation logs that identify the various degrees of bonding after a cement job. Interpretation of the results is not unequivocal. Pipe in some hole sections may appear to be free, yet cannot be pulled if backed off with a string shot.

10.3.3 Procedures To Free a Differentially Stuck Drillstring. After a drillstring becomes differentially stuck, three release techniques may be used:

- Spotting fluids
- Hydrostatic reductions
- Mechanical methods

Selection of the appropriate procedure is based on an evaluation of the factors that created the problem in the first place, the time elapsed since initial sticking, mud types and properties, and other issues (Adams 1977b).

Spotting Fluids. A *spotting fluid* is any type of fluid used to cover a section of a well for any reason. Those used for stuck pipe are usually oil-based products positioned or spotted in an open hole to cover a specified interval (Fig. 10.39).

The oil penetrates the filter cake and invades the seal on the drillpipe. In addition, the oil tends to wet the circumference of the pipe, creating a thin layer between the pipe and the mudcake (Fig. 10.40). This reduces the coefficient of friction and may enable the pipe to be pulled free.

Spotting-fluid density is important. Hydrocarbon fluids that are less dense than drilling fluids will migrate or float to the surface. The reverse is true with oil weighted to a density greater than that of the original drilling fluid. To ensure that the spotting fluid will remain where it is placed in the hole, its density should be approximately the same as the mud density. One exception is when pipe is known to be stuck at the bottom of the hole. The spotting-fluid density should then be slightly greater than the mud density to ensure complete encirclement of the pipe in spite of gravity segregation.

One potential problem with weighted spotting fluids is that the mixing time for the chemicals and the barite in oil may appear limited because of the perceived need to spot the fluid as quickly as possible. If the fluid is not mixed properly, the properties necessary to support the barite in suspension may not develop. This can result in barite settling that forms a bridge plug in the pipe or the open hole. Proper fluid mixing is necessary, even if it takes a little longer.

Spotting-fluid success is directly related to the volume used. Larger volumes cover a longer section of the open hole and are therefore more likely to cover the stuck intervals. It is a mistake to assume that the pipe is stuck only in the drill-collar region and to use only enough fluid volume to cover the collars. This conservative tendency in

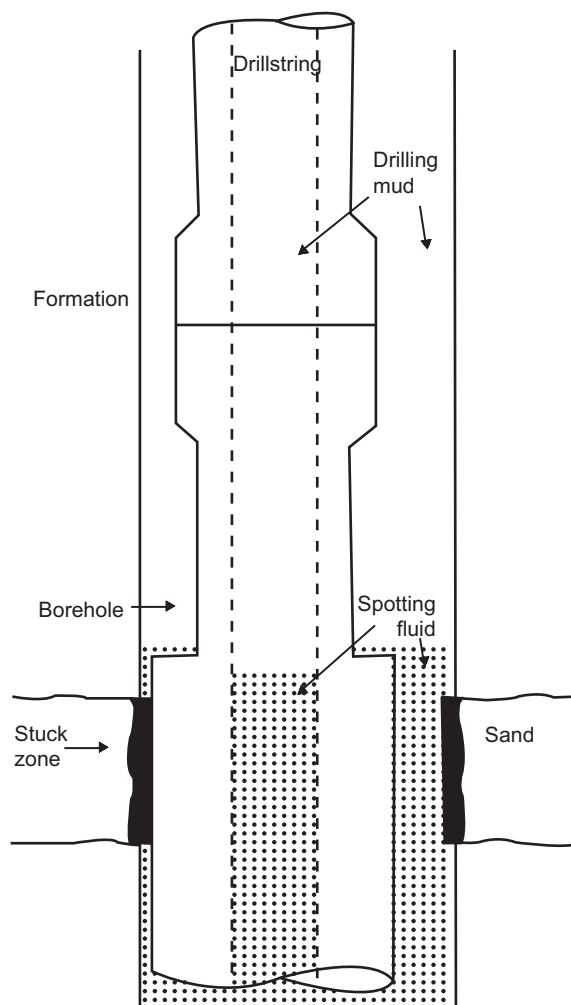


Fig. 10.39—Spotting fluids are usually oil-based muds positioned in the hole to cover a particular interval (Adams 1977b).

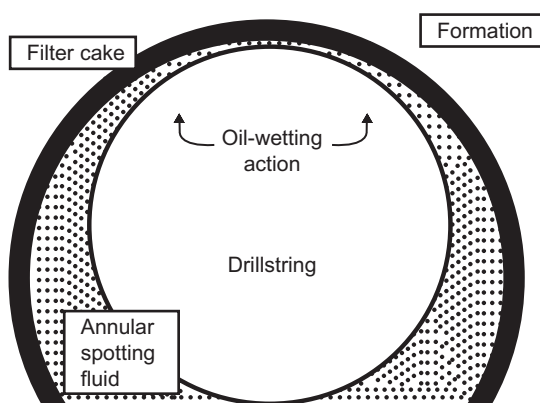


Fig. 10.40—Oil has a tendency to wet the circumference of the pipe, reducing friction (Adams 1977b).

spotting-fluid use probably contributes to a large number of failures. Minimum spotting-fluid volumes can be determined at the rigsite. Using the pipe-stretch calculations described earlier, the uppermost stuck interval can be identified. Once this is done, a sufficient fluid volume should be used to cover this section and all lower open-hole sections.

Pipe sections higher in the hole often become stuck while efforts are being made to free lower sections (**Fig. 10.41**). It is often beneficial to spot enough fluid volume to cover all exposed permeable zones. Although more expensive initially, this technique may be the most economical procedure overall.

After spotting the fluid in the hole, time is required before the pipe can be released. The amount of time depends on a number of factors such as mud properties, mud-displacement efficiencies, hole-to-pipe geometry, and differential pressure. Even though the time cannot be quantified with any degree of precision, raw field data suggest that an average of eight to ten hours is required for release. Many cases, however, have taken longer. A good field rule is to spot enough fluid to cover the open-hole section and wait for at least 12 hours for the fluid to free the pipe.

Correct positioning of the spotting fluid is of critical importance. The volume pumped must be recorded using number of pump strokes or the rig's trip tanks. Fluid should be spotted in the open hole with a volume left in the drillpipe (**Fig. 10.42**). At specific time intervals, small amounts of fluid must be displaced from the pipe to create annular movement. This may increase fluid effectiveness as well as minimizing potential bridges.

While displacing fluid and waiting for the pipe to release, it is important to maintain a rig hookload that is equal to or slightly less than the load before the pipe stuck. Do not hold extra pull on the pipe while using spotting fluid. Extra surface pull does not increase the chemical effectiveness of the spotting fluid, and it places abnormal stresses on the pipe. Pipe should be raised and lowered as conditions permit and at specific intervals, perhaps hourly, to check whether it can be released. Lowering some weight onto the pipe for a short time can also assist in releasing the stuck pipe from the filter cake. If the pipe is not yet free, release the extra surface pull and allow additional time for the fluid to work.

Spotting fluids may be used effectively for preventive as well as remedial purposes. For instance, fluid may be spotted before running casing or tubulars into a well where a sticking potential exists.

Hydrostatic Pressure Reduction. Reducing differential pressure is another technique for releasing stuck pipe. Lowering the differential pressure reduces the restraining force on pipe, and it may become possible to pull it free. Reducing hydrostatic pressure, however, may create problems such as kicks or sloughing in other hole sections. Circulating a lower-density fluid reduces hydrostatic pressure. Another common procedure is a localized pressure reduction to reduce hydrostatic pressure on and below the stuck interval while maintaining full hydrostatic pressure above.

Localized pressure reduction uses stuck-zone detection procedures, conventional backoff procedures, and drill-stem-testing (DST) tools (**Fig. 10.43**). After the stuck interval has been identified, the pipe above that section is unscrewed and pulled from the hole, and a DST tool is attached. The pipe is rerun and screwed into the fish. Water is displaced into the drillpipe to reduce hydrostatic pressure to a precalculated value. The test tool is opened and the pipe is pulled free. This procedure minimizes exposure of the open hole to reduced pressure while decreasing pressure in the zone of interest.

This technique is not universally applicable in all drilling environments. The pressure reduction below the DST tool can create potentially large negative differential pressures. Kicks can occur, or the hole can collapse.

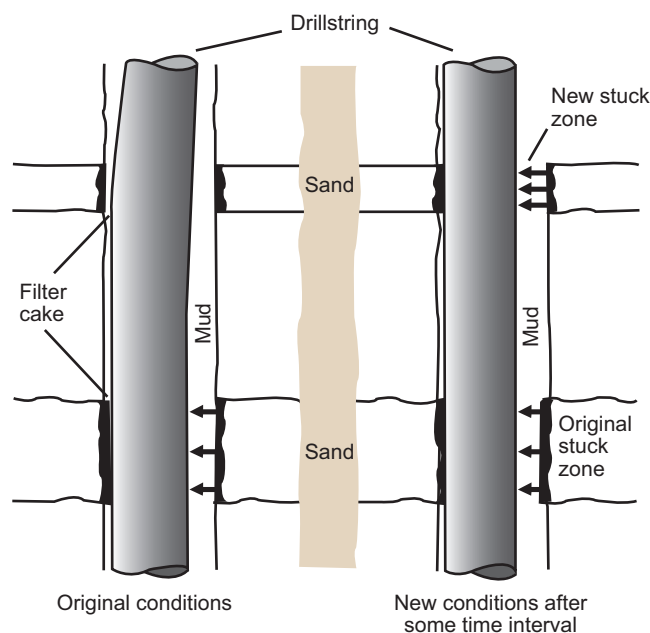


Fig. 10.41—Sections above the original stuck section often become stuck during the time spent trying to free the pipe (Adams 1977b).

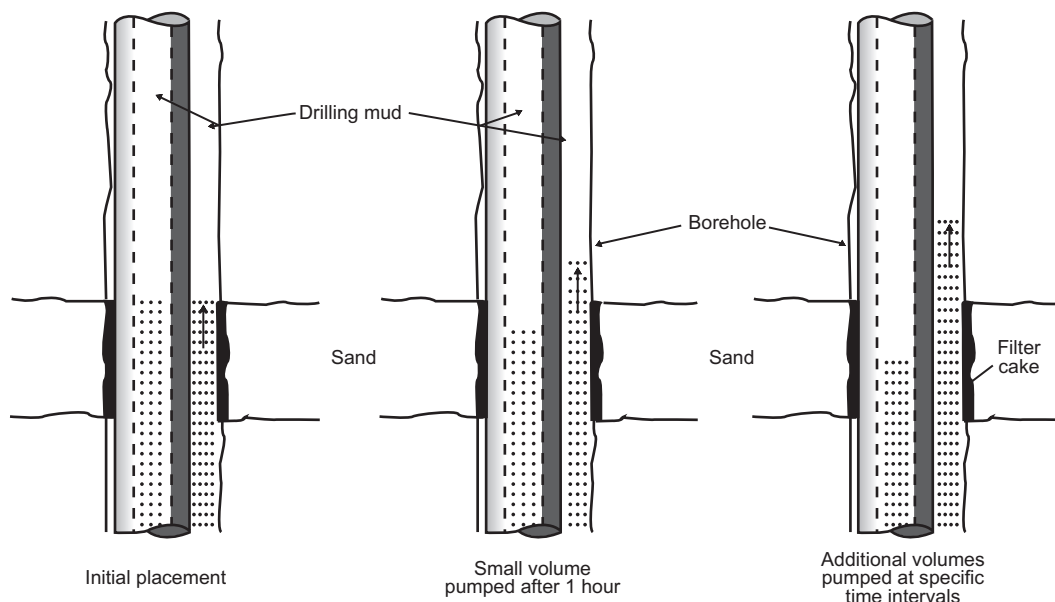


Fig. 10.42—Fluid should be spotted in the open hole with some volume left in the drillpipe for pumping at later intervals (Adams 1977b).

The technique is better suited for hard, low-permeability rocks such as west Texas geology rather than young, high-permeability environments such as the Gulf of Mexico, Indonesia, and large sedimentary basins such as the Niger, Amazon, and Makaham regions.

Mechanical Methods. Mechanical methods physically destroy the bond between the pipe and the filter cake. They are based either on impact loading using jarring devices or on destruction of the cake by grinding procedures. Another method is to wash over the pipe—in essence, coring over the stuck pipe.

With the drillstring out of the hole, the fishing tools are made up. A fishing string with a jar is often called a *jarring string*. A typical jarring string consists of an overshot or screw-in sub, drill collars, a jar, more drill collars, perhaps an accelerator, more drill collars, perhaps a bumper sub, and drillpipe. The makeup of jarring strings varies considerably and depends on the fish and the amount of jarring force needed. There are no hard-and-fast rules

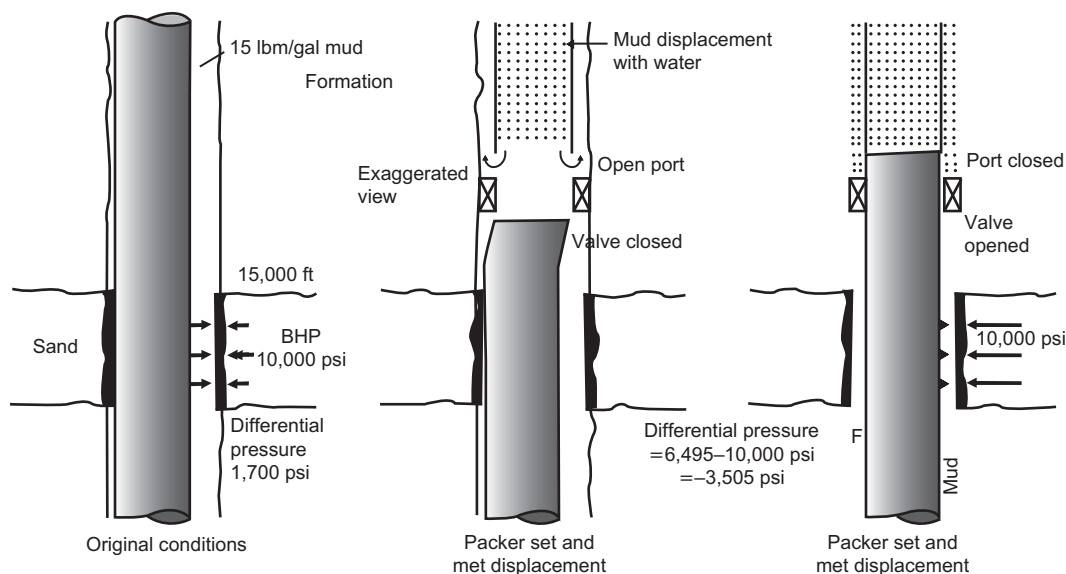


Fig. 10.43—Localized pressure reduction is possible using conventional test tools (Adams 1977b).

for making up a jarring string. The amount of impulse, force, and energy developed and applied by the jar to the string is highly dependent on the makeup of the jarring string.

Jarring. Jarring is simply the process of impacting the fish with a large force impulse. This is not unlike hitting a stuck item with a hammer. For example, if a mechanic finds a cotter pin stuck in its hole, the first thing usually done is to hit the pin with a hammer. The reaction is a longitudinal wave running back and forth in the pin. The longitudinal wave causes the particles of the pin to move as the wave passes through the particles. This, in turn, causes motion along the side of the pin and the hole in which the pin is stuck. If the forces are large enough to overcome the friction loads at the interface of the pin and hole, the pin will move. With enough hammer blows, the pin eventually comes loose (or breaks).

The same phenomenon is true when using jarring to fish for stuck tools. In this case, the hammer is called a *jar*. The jar is placed in the drillstring in a position where it can apply a hammer blow to the fish. This is accomplished in the following manner (Fig. 10.44). The string is stretched, putting strain energy into the string above and below the jar. The amount of tension put into the string over and above the weight of the string above the jar is called the *overpull*. At some predetermined load value, the jar is triggered. The top and bottom parts of the jar disconnect from each other and are free to travel up for the top part (called the hammer) and down for the bottom part (called the anvil). Both parts of the string contract at what is known as the *free contraction velocity* and build kinetic energy. Eventually, after the anvil and hammer have traveled a certain distance (called the stroke), the hammer and anvil will impact. Most of the kinetic energy is converted back into strain energy that then propagates up and down the string. Some of this energy will propagate to the stuck point and hopefully jar the fish loose. The magnitudes of the force, energy, and impulse involved depend on the initial strain energy, the stroke length, and the wave-propagation characteristics of the jarring string. With each hammer blow, this wave propagates to the stuck point to provide a short-duration (milliseconds) pulse of force. Eventually the fish will come loose. The bad news is that this may take days or weeks. At some point, it may be more economical to abandon the hole and drill a new one.

Types of Jars. The original jar used in cable-tool drilling consisted of two links of steel attached to the cable. The links would be loose while attached to the fish. Then the driller would pull on the cable, causing the two links to crash together. This applied a jolt to the fish.

There are two types of jars: fishing jars and drilling jars. *Fishing jars* are used in fishing strings. They are of somewhat lighter construction than drilling jars and are more easily adjusted from the surface. In addition, they are designed to generate a larger impact than the typical drilling jar. *Drilling jars* are part of the drillstring. They are placed in the drillstring to be ready for immediate use in case the drillstring gets stuck. Both types of jar can operate on either a hydraulic or a mechanical principle. Most jars can operate either downward or upward, but are designed to impart a larger impact force upward. The jar is designed to impart a force impulse to the fish.

A review of field case histories suggests that if jarring is to be effective, success will be achieved within the initial few hits of the jars. Jarring operations that are ineffective within the first hour are likely to prove ineffective regardless of the length of the operation. The exception can be when jarring is used after large volumes of spotting fluids have been pumped into the open hole.

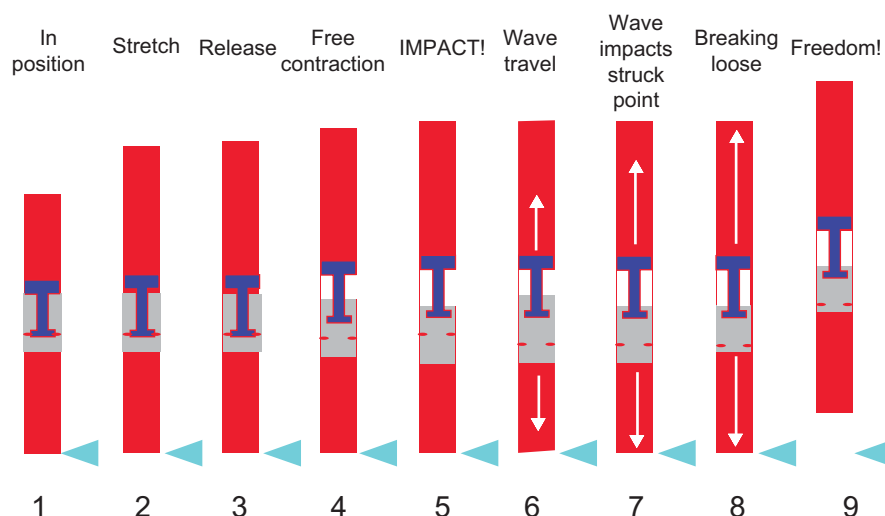


Fig. 10.44—Jarring process (Eustes 1996).

Hydraulic Jars. Hydraulic jars are often called *oil jars* because a hydraulic fluid or light oil is used in the jar. In the cocked position, the jar has a tight-fitting piston (the hammer) inside of a cylinder. There is fluid in a chamber above the piston. As the string is pulled in tension, the piston tries to move up, but the fluid above cannot bypass the piston very quickly. The fluid increases in pressure and slowly bypasses the piston through a bypass hole or channel. At some point, as the piston slowly travels up the cylinder, the tight clearance opens up to a very loose clearance, and the fluid can easily bypass the piston. At this point, the jar is triggered. The sudden reduction in pressure above the piston enables the piston to travel freely up the cylinder until it impacts the anvil. After impact, and after the strain waves have died out, the jar is reset by slowly recompressing the jar and shoving the piston back into the tight-fitting cylinder. This can take a few minutes.

The big advantage of a hydraulic jar is that the impact intensity can be varied from the surface by changing the amount of overpull in the string before triggering the jar. However, heat and too-rapid recocking can destroy the seals in the hydraulic jar. If the seals leak, the jar has failed, and a trip is necessary. Hydraulic fishing jars are of somewhat lighter construction than hydraulic drilling jars.

Some jars can be triggered to provide impact either upward or downward. The upward impact is called an *up hit*. This is the usual operational direction of most jars. However, in some cases, such as when unsticking a keyseated string, the jar should be fired downward. This is called a *down hit*. Most jars do not work as well downward as they do upward.

Mechanical Jars. Mechanical jars trigger differently than hydraulic jars. The triggering mechanism can be a set of rollers or a spring detent that is set at a given load for triggering. The trigger load is set at the surface before running in the hole. Once in the hole, most mechanical jars cannot be reset to a different triggering load. A few mechanical jars enable very limited trigger load changes by using torque from the string to reset the trigger load. These kinds of jars can be recocked up to three times per minute, as opposed to the two- to three-minute delay for hydraulic jars. Mechanical jars tend to be more rugged than their hydraulic counterparts and are used more often in drilling strings.

Accelerator. An accelerator is often called a booster jar or an intensifier. It is run in the jarring string somewhere above the jar and is full of a compressible fluid that acts like a spring. The accelerator can act as a shock absorber for the rest of the jarring string under the impact of the jar, but its main purpose is to intensify the impact force. The force of the jar impact is directly related to the velocities of the hammer and anvil. The accelerator acts to increase the velocity of the hammer by reflecting the free-contraction waves sooner than would have occurred without the accelerator. The position of the accelerator in the jarring string is critical to the success of this intensification. The accelerator makes possible an impact of shorter duration and greater force.

Bumper Sub. A bumper sub is used to impart a downward impact to a jarring string. It is in essence a mechanical slip joint. The impact is generated by allowing the string to fall through the length of the slip joint. After the string travels along the slip joint, it stops with an impact. By maintaining the load such that the slip joint is within its stroke, the only load below the bumper sub is the string below that point. Moreover, if an overshot or a spear is grappled onto a fish, it takes a downward blow to free the grapples.

Jars. Jars are mechanical tools placed in the drillstring to deliver an impact load when triggered. Jars are run in the string during drilling, but may wash out or be located below the stuck interval, negating their use. Placement

of jars in the string after stuck pipe occurs requires backoff procedures, which entail delays and complicate the situation. Jars should never be considered as an all-purpose pipe-release tool, but should be used with other conventional approaches.

Washover Pipe. Wash pipe is perhaps the most widely used procedure to free severely stuck pipe. A *wash pipe* is a large-diameter, thin-walled tubular with a grinding shoe on the bottom. The shoe is used to destroy the bond between the pipe and the cake as the wash pipe is rotated and lowered. After a specific length has been freed in this manner, the previously stuck section can be mechanically unscrewed and retrieved. This procedure is repeated until the entire drill string has been recovered.

A common occurrence when using wash pipe is that it also becomes stuck. Its large OD then prevents further retrieval operations. Sidetracking around the fish (or fishes) is the only remaining viable option. Retrieval presents several problems. Because the borehole is known to have sticking tendencies, the danger of stuck wash pipe is especially great because of the large outer surface area of the pipe. Occasionally, it is impossible to free and remove all pipe in the hole completely. When this occurs, it becomes necessary to sidetrack.

Backoff Procedures. After the stuck point has been found, the method of recovery must be determined. Often, the string is broken just above the stuck point, and a jarring string is run into the hole. The *backoff procedure*, as this is called, involves unscrewing or cutting the string above the stuck point. Unscrewing the string is the preferred method because it leaves the string intact. Breaking the string involves explosive, chemical, or mechanical cutting of the metal.

To unscrew a string that is stuck, a string shot is run into the hole. A *string shot* is a small amount of explosive. The tool joint that is to be unscrewed is found using a collar locator. Then the string shot is run into the middle of the inside of the tool joint. The driller then applies torque and tension to the string. The amount of torque should be sufficient to unscrew the string after the shot, but not before. The string shot is then exploded. The resulting torque in the string should unscrew the string at the explosion point. The approach is similar to hammering a reluctant screw. If all goes well, which it often does not, the string should come loose at that point. The string is then pulled out of the hole, leaving the fish stuck in the hole.

10.3.4 Economics of Avoiding or Freeing Stuck Pipe. Previous discussions have covered various efficient procedures to avoid or free stuck pipe. The economics of each option should be a primary factor when considering various preventive and remedial procedures. From an economic viewpoint, it is better to prevent differential sticking than to be forced to use remedial measures. However, when remedial efforts are necessary, the cost of large volumes of spotting fluids is small compared to rig costs.

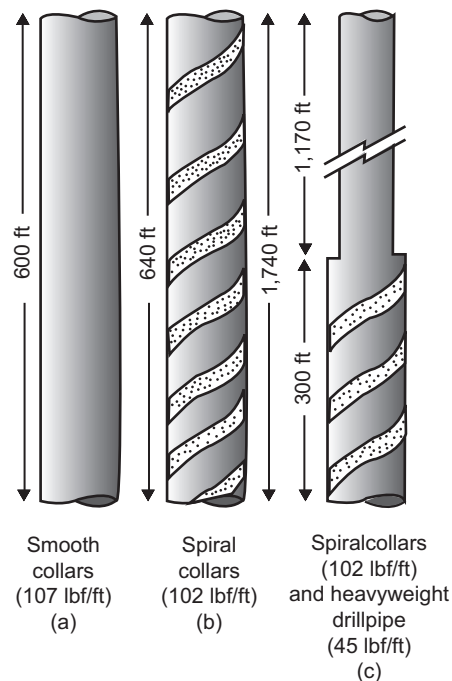


Fig. 10.45—Combining spiral collars and heavyweight drillpipe exposes the minimum area to sticking while maintaining the equivalent buoyed weight.

The use of washover techniques should be based on economics. Drillpipe recovery “at any cost” should be replaced with sound economic judgment. A recent study of stuck pipe at various offshore Louisiana locations revealed that an average cost of USD 393,610 was incurred to resume drilling at the original depth before sticking occurred.

Some confusion exists as to which techniques are best to retrieve pipe when spotting fluid fails. Economics are the controlling factor at this point, and the drilling supervisor must decide whether it is less expensive to fish the stuck pipe or simply to sidetrack and redrill the interval.

Drillstring Economics. Altering the drillstring configuration is an easy and inexpensive technique to avoid stuck pipe. Minimizing the contact area between the pipe and the wellbore can be accomplished using spirally grooved collars and heavyweight drillpipe. **Fig. 10.45** shows several example BHAs which have the same buoyed weight. The assemblies in Figs. 10.45b and 10.45c effectively reduce contact area without sacrificing available bit weight.

Table 10.7 shows rental prices for various types of collars and heavyweight pipe plus the cost of each BHA illustrated in Fig. 10.45. Table 10.7 also shows that if USD 20,000/day is a typical rig cost (including support services), the cost of improved BHAs to avoid stuck pipe represents only a fraction of daily rig costs.

Drilling fluids play an important role in relation to stuck pipe. Water-based muds with low filtration properties, low friction coefficients, thin filter cakes, and low rates of filter-cake buildup can reduce the severity of sticking if it does occur. **Table 10.8** shows the relative costs of building and maintaining muds of various densities and filtration rates.

TABLE 10.7—COST COMPARISONS FOR A BHA TO MINIMIZE CONTACT AREA					
Smooth Wall Collars		Spiral Collars		Heavyweight Drillpipe (HWDP)	
Size (in.)	Cost (USD/day/jt)	Size (in.)	Cost (USD/day/jt)	Size (in.)	Cost (USD/day/jt)
3 ¹ / ₈ –4 ¹ / ₈	8	3 ¹ / ₈ –4 ¹ / ₈	9	3 ¹ / ₂	7
4 ¹ / ₂ –5	9	4 ¹ / ₂ –5	10	4 ¹ / ₂	9
5 ¹ / ₂ –6	10	5 ¹ / ₄ –6	11		
6 ¹ / ₈ –7	11	6 ¹ / ₈ –7	14		
7 ¹ / ₈ –8	12				
8 ¹ / ₄ –10	28				
11	57				
BHA Cost		Percent of Rig Cost for 20,000/day Rig			
Smooth collars (A)		USD 220/day			
Spiral collars (B)		USD 308/day			
Spiral collars with HWDP		USD 413/day			
				1.10%	
				1.50%	
				2.00%	

TABLE 10.8—COSTS FOR FRESHWATER LIGNOSULFONATE MUDS				
Weight (lbm/gal)	Mud System Initial Cost/bbl		Daily Maintenance Cost/bbl	
	6 cm ³ Water Loss	2 cm ³ Water Loss	6 cm ³ Water Loss	2 cm ³ Water Loss
10	7.31	7.67	0.72	0.9
11	7.38	7.75	0.9	1.08
12	9.65	10.1	0.96	1.14
13	12.02	12.62	1	1.18
14	14.51	15.23	1.06	1.24
15	17.1	17.95	1.13	1.31
16	19.83	20.82	1.19	1.34
17	22.72	23.86	1.25	1.34
18	25.7	26.98	1.38	1.5

High-density muds exhibit little variation in cost because of the relative ease of decreasing the filtration properties of muds with high percentages of barite. Lower-density muds exhibit greater variation in the cost to reduce filtration properties, but the difference is small compared to total rig costs, as shown in Table 10.7. The cost data in Table 10.8 are for lignosulfonate muds. Because lime and other inhibited muds are comparable in cost and may provide additional protection against sticking, it would be prudent to use these types of muds if all other mud-programming variables were equal. Oil-based muds provide maximum protection against stuck pipe. Oil-based mud costs (as well as environmental concerns) have historically been considered prohibitive, when in fact these muds may be cheaper compared with water-based muds. Oil-based and synthetic-oil-based muds are becoming standard in many wells to avoid hole problems.

Problems

- 10.1 Calculate the hydrostatic pressure for each of the following:
 - (a) 13,500 ft of 14-lbm/gal mud
 - (b) 8,600 ft of 9-lbm/gal salt water
 - (b) 17,000 ft of 18.5-lbm/gal mud
- 10.2 A well is 15,000 ft deep, true vertical depth. It contains 7,500 ft of 15-lbm/gal mud and 7,500 ft of 16-lbm/gal mud. What are the hydrostatic pressures for each section and the total hydrostatic pressure at 15,000 ft?
- 10.3 A typical kick situation has developed the following arrangement of fluids in the annulus:
 - (a) 2,500 ft, 12-lbm/gal mud
 - (b) 2,500 ft, 8.6-lbm/gal salt water
 - (c) 3,500 ft, 12-lbm/gal mud
 - (d) 4,000 ft, 13.1-lbm/gal mud
- 10.4 Using the solution from Problem 10.2, what is the equivalent mud weight at 15,000 ft?
- 10.5 What is the equivalent mud weight of the system from Problem 10.3 at 2,500 ft; 5,000 ft; 8,500 ft, and 12,500 ft?
- 10.6 A kick situation has developed that shows 500 psi on the annulus pressure gauge. The annulus contains 8,000 ft of 10-lbm/gal mud above 1,000 ft of 9-lbm/gal salt water. What is the equivalent mud weight at 9,000 ft?
- 10.7 If the active mud system of the Louisiana Producer No. 14 contains 1,260 bbl of 12.5-lbm/gal mud, what would be the number of 100-lbm sacks of barite necessary to increase the mud weight to 13.5 lbm/gal? What would be the number of long tons?
- 10.8 In Problem 10.7, if the mud weight was increased from 17.5 lbm/gal to 18.5 lbm/gal, would the sack requirements be the same? If not, how much would be required in 100-lbm sacks?
- 10.9 The AMSCO Oil Company is drilling at 12,675 ft with 13.2-lbm/gal mud. It becomes necessary to increase the bottom hole hydrostatic pressure by 450 psi. What mud weight is required? If the active mud volume is 975 bbl, how much barite is required?
- 10.10 In a blowout situation, the Dry Hole Oil and Gas Co. Wildcat No. 182 must develop a hydrostatic pressure of 7,400 psi over a 5,000-ft interval. What is the required mud weight? Assuming a galena-based mud is used, how many tons are required if the mud system presently contains 460 bbl of 14-lbm/gal mud?
- 10.11 The mud density required to kill an underground blowout is 26 lbm/gal. A total of 500 bbl of 18-lbm/gal mud was used as the base fluid. How many tons of hematite would be required to weight the mud?
- 10.12 If the hydrostatic pressure must be increased by 700 psi in a well that contains 12,600 ft of 11.5-lbm/gal mud, how much barite in 100-lbm sacks is required? If hematite were used instead of barite, how much would be required? The system volume is 1,200 bbl.
- 10.13 Calculate the pressure reduction when 450 ft of 4.5-in., 16.6-lbm/ft pipe is pulled without filling the hole. The hole diameter is 7.875 in. and 15.6-lbm/gal mud is used.
- 10.14 Using data from Problem 10.13, what would be the pressure reduction if 450 ft of 6-in.-OD \times 2-in.-ID collars are pulled without filling the hole? Assume two cases—one in which the drillpipe is plugged and one in which the drillpipe is not plugged.
- 10.15 A well is drilled to 13,000 ft with 13.2-lbm/gal mud. The formation pressure in a gas sand at that depth is 8,710 psi. The intermediate casing is 43.5 lbm/ft, 9.625 in. ID set to 11,000 ft, TVD. The drillpipe is 4.5 in. OD, with collars of 7-in. OD with 2-in. ID. The operator requires that the hole be filled after

- 5 stands of drillpipe and drill collars are pulled. Will the well kick when pulling the drillpipe? Will the well kick when pulling the drill collars? Assume two cases—one in which the drillpipe or drill collar is plugged and one in which it is not plugged.
- 10.16 Calculate the pump strokes required to fill the hole in Problems 10.13, 10.14, and 10.15 for each of the following pumps. Assume 90% efficiency.
- 6.5-in. liner, 18-in. stroke length, duplex
 - 7-in. liner, 14-in. stroke length, duplex
 - 4-in. liner, 10-in. stroke length, duplex
 - 3-in. liner, 6-in. stroke length, triplex
 - 3-in. liner, 10-in. stroke length, triplex
 - 4-in. liner, 18-in. stroke length, triplex
- 10.17 In an effort to measure the output of a 3-in. liner by a 10-in. stroke, triplex pump under actual conditions, a 20-bbl trip tank was filled with mud. A total of 1,274 strokes were required to empty the tank. What is the pump output, volume per stroke? What is the pump efficiency?
- 10.18 A drillstring contains 12,000 ft of 4.5-in., 16.6-lbm/ft drillpipe and 1,000 ft of 7-in. OD \times 2.5-in. ID drill collars. How many strokes would be required to displace the pipe if a 4.5 \times 10-in. triplex pump was used at 90% efficiency? At 80% efficiency?
- 10.19 A kick is taken on a well with the following pressures recorded:

Shut-in (min)	SIDPP (psi)	SICP (psi)	Pit Gain (bbl)
0	250	375	18
5	290	415	18
10	290	415	18
15	295	415	18

- What is the true shut-in pressure to be used in mud calculation?
 - The drillstring contains 10,600 ft, TVD of 12.1-lbm/gal mud. What is the BHP?
- 10.20 Using the data given below, what is the true shut-in pressure?

Increment	Bleed Volume (bbl)	SIDPP (psi)	SICP (psi)
0	-	760	1,160
1	1	700	1,100
2	1	640	1,040
3	0.5	630	1,020
4	0.5	630	1,020
5	0.5	630	1,030
6	0.5	630	1,045

- 10.21 Given the solution from Problem 10.20, what is the BHP for each of the following:

Well	TVD (ft)	Mud (lbm/gal)
1	10,750	10.4
2	13,500	14.6
3	8,300	9.5
4	15,000	11.7
5	5,500	9.9

- 10.22 After a kick is taken, bleeding procedures were implemented to check for trapped pressure. Using the results given below, what is the true shut-in pressure?

Increment	Bleed Volume (bbl)	SIDPP (psi)	SICP (psi)
0	-	250	690
1	1	175	615
2	1	100	540
3	1	50	490
4	1	20	470
5	1	0	450
6	1	0	450
7	1	0	460

- 10.23 Using the solution from Problem 10.22, what is the BHP if the mud weight is 12.1 lbm/gal and the well depth is 13,130 ft, TVD?
- 10.24 A kick was taken on a well in which a float valve was used in the drillstring. The SIDPP was read as 0 psi and the SICP was 675 psi. The kill rate and associated pressure was 32 strokes per minute (spm) and 700 psi, respectively. After implementing the procedures to establish the true SIDPP, the total pumping pressure was 1,150 psi. What was the true SIDPP?
- 10.25 Using the data given below, calculate the BHP of the well.
 SIDPP: 0 psi (float valve in the drillstring)
 SICP: 400 psi
 Pump data: 45 spm, 750 psi
 Total pump pressure, initial: 900 psi
 TVD: 11,000 ft
 Mud: 12.9 lbm/gal
- 10.26 While drilling the Colorado Rover No. 1, a kick was shut in with an SIDPP of 400 psi and an SICP of 550 psi. A kill rate had not been established prior to the kick. The pumps were started after the well was shut in and run at 21 spm while the casing pressure was maintained constant at 550 psi. The total drillpipe pressure was observed to be 1,250 psi. What is the pumping pressure at 21 spm (assuming no kick)?
- 10.27 Using the same conditions from Problem 10.26, the pumps were run at 35 spm with a total pumping pressure of 1,500 psi. What is the kill pump pressure at 35 spm?
- 10.28 While killing the kick in Problem 10.26, Pump 1 washed out a valve while displacing the drillpipe with kill mud. The well was shut in and the pressures recorded as 175 psi SIDPP and 525 psi SICP. Rather than repairing Pump 1, Pump 2 was started at 45 spm while the casing pressure was held at 525 psi. The total drillpipe pressure at 45 spm was observed to be 1,475 psi. What was the kill pressure for Pump 2?
- 10.29 A kick occurred on a well in which the kill rate was not known and a float valve was used in the drillstring. The SIDPP was 0 psi and the SICP was 500 psi. A low-volume pump was connected to the stand pipe and pressure applied. The following results were obtained. What was the SIDPP?

Volume Pumped (bbl)	SIDPP (psi)
0	0
1	0
2	40
3	90
4	140
5	190

6	210
7	215
8	215
9	220

- 10.30 Using the results from Problem 10.29, the rig pump was run at 25 spm with a pressure of 950 psi. The casing pressure was held constant throughout this procedure. What was the kill rate pressure?
- 10.31 What is the probable kick-influx fluid using the following data? (Assume the kick fluid is around the drill collars only.)
 SIDPP: 400 psi
 SICP: 600 psi
 Pit gain: 25 bbl
 Mud: 12.0 lbm/gal
 Collars (OD): 6.0 in.
 Hole: 9.875 in.
- 10.32 Using the data from Problem 10.31, what is the probable influx if the OMW was 17 lbm/gal?
- 10.33 If the following data is known, what fluid type entered the well? (Assume no collars.)
 SIDPP: 800 psi
 SICP: 1,400 psi
 Pit gain: 20 bbl
 Mud: 15.0 lbm/gal
 Pipe (OD): 3.5 in.
 Hole: 6.0 in.
- 10.34 Using the same data from Problem 10.33, what fluid entered the well if the SICP was 1,100 psi?
- 10.35 A kick was taken on a well in which the following data was known. What was the kill mud weight?
 SIDPP: 250 psi
 SICP: 475 psi
 Pit gain: 20 bbl
 Mud: 13.4 lbm/gal
 Measured depth: 12,750 ft
 TVD: 12,000 ft
- 10.36 Calculate the kill mud weight for Problem 10.19.
- 10.37 If the information in Problem 10.20 is known, what must be the mud-weight increase to kill the well if the TVD is 12,300 ft?
- 10.38 Calculate the kill mud weights for the situations developed in Problems 10.20 and 10.21.
- 10.39 What mud-weight increase is necessary for Problem 10.22?
- 10.40 If the following data is known, what is the mud-weight increase necessary to balance each situation?

No.	SIDPP (psi)	SICP (psi)	Pit Gain (bbl)	TVD (ft)
1	300	500	30	14,200
2	300	4,750	108	14,200
3	450	800	18	21,630
4	300	500	unknown	14,200
5	300	unknown	35	14,200
6	unknown	500	35	14,200
7	0	500	35	14,200

- 10.41 A kick was taken on a well in which the following data were known. What was the kill mud weight?
 SIDPP: 250 psi
 SICP: 475 psi
 Measured depth: 12,750 ft
 True vertical depth: 12,000 ft
 Mud weight: 13.4 lbm/gal

10.42 If the following data is known, what is the mud-weight increase necessary to balance each situation?

SIDPP (psi)	SICP (psi)	Pit Gain (bbl)	TVD (ft)
a. 300	500	30	14,200
b. 300	4,750	108	14,200
c. 450	800	18	21,630
d. 300	500	unknown	14,200
e. 300	unknown	35	14,200
f. unknown	500	35	14,200
g. 0	500	35	14,200

Nomenclature

- A = hydraulically sealed area, in.²
 A_p = cross-sectional area of the pipe, in.²
 E = modulus of elasticity
 F_{applied} = applied force to the stuck drillstring, lbf
 $F_{\text{tangential}}$ = drag force needed to move up or down the hole, lbf
 g_{kick} = gradient of kick fluid in annulus, psi/ft
 g_{mud} = mud gradient, psi/ft
 h_{kick} = height of kick fluid in annulus, ft
 L = free pipe length, ft
 p_{ann} = annulus hydrostatic pressure, psi
 p_{DP} = drillpipe pressure, psi
 p_{form} = formation pressure, psi
 p_{kick} = kick-fluid hydrostatic pressure, psi
 p_{normal} = pressure differential between the wellbore and the formation
 w_p = unit weight of the pipe, lbf/in. [2.67(OD²–ID²)]
 ΔL = stretch length, in.
 μ = coefficient of friction, dimensionless

References

- Adams, N.J. 1977a. How to Control Differential Pipe Sticking, Part 3—Field Study Presents New Results. *Petroleum Engineer International* **49** (12): 44–50.
 Adams, N.J. 1977b. How to Control Differential Pipe Sticking, Part 1—What is the Problem? *Petroleum Engineer* **49** (10): 32–42.
 Adams, N.J. 1979a. Pressure Control Equipment Role Vital. *Oil and Gas Journal* **77** (52): 58–66.
 Adams, N.J. 1979b. Well Control Starts with BOPs. *Oil and Gas Journal* **77** (50): 95–99.
 Adams, N.J. 1980a. Choosing, Checking Stack is Key to Safe Blowout Preventer Use. *Oil and Gas Journal* **78** (1): 97–104.
 Adams, N.J. 1980b. Supplemental Rig Equipment Has Vital Job. *Oil and Gas Journal* **78** (3): 83–86.
 Adams, N.J. 1993. *Drilling Problems and Drilling Optimization*. Boston, Massachusetts: IHRDC Publishing.
 Adams, N.J. 2005. Substitute Parts Can Be Fatal. *Pipeline Magazine*, Dubai, UAE.
 API RP 53, *Recommended Practices for Blowout Prevention Equipment Systems for Drilling Wells*, third edition. 1997. Washington, DC: API.
 Aston, M.S., Alberty, M.W., McLean, M.R., de Jong, H.J., and Armagost, K. 2004. Drilling Fluids for Wellbore Strengthening. Paper SPE 87130 presented at the IADC/SPE Drilling Conference, Dallas, 2–4 March. DOI: 10.2118/87130-MS.
 Bourgoyne, A.T., Millheim, K.K., Chenevert, M.E., and Young, F.S. 1986. *Applied Drilling Engineering*. Textbook Series, SPE, Richardson, Texas **2**.
 Cameron. 2010. Drilling Systems-U Blowout Preventer, <http://www.c-a-m.com/forms/Product.aspx?prodID=7e219b5f-bbac-4149-9da2-ef29be9b1d51> (accessed 22 November 2010).

- Darley, H.C. and Gray, G.R. 1988. *Composition and Properties of Drilling and Completion Fluids*. Houston: Gulf Publishing.
- Dawson, D.D. and Goins, W.C. 1953. Bentonite-Diesel Oil Squeeze. *World Oil* **137** (5): 222–223.
- Devereux, S. 1998. *Practical Well Planning and Drilling Manual*. Tulsa: PennWell.
- Eustes, A.W. III. 1996. A Frequency Domain Approach to Drillstring Jarring Analysis. Golden; Colorado: Colorado School of Mines.
- General Electric Company. 2010. Hydril Pressure Control GK Annular Blowout Preventer, http://www.hydrilpressure-control.com/_pdf/pressureControlBrochures/GE_HY_GKBOP_FS_080610.pdf. Downloaded 22 November 2010.
- Helmick, W.E. and Longley, A.J. 1957. Pressure Differential Sticking of Drill Pipe and How It Can Be Avoided or Relieved. *Oil and Gas Journal* **55** (24): 132.
- Howard, G.C. and Scott P.P. 1951. An Analysis of the Control of Lost Circulation. *Trans.*, AIME **192**: 171–182.
- Ivan, C., Bruton, J. and Bloys, B. 2003. Lost Circulation Can Be Managed Better. *World Oil* **224** (6): 73–76.
- Lake, L.W. 2006. *Petroleum Engineering Handbook*, Vol. II, Drilling Engineering. Richardson, Texas: SPE.
- Mata, F. and Veiga, M. 2004. Crosslinked Cements Solve Lost Circulation Problems. Paper SPE 90496 presented at the SPE Annual Technical Conference and Exhibition, Houston, 26–29 September. DOI: [10.2118/90496-MS](https://doi.org/10.2118/90496-MS).
- M-I SWACO Drilling Fluids Engineering Manual, Chap. 14, 1. 2006. Houston: M-I SWACO.
- Moore, P.L. 1986. *Drilling Practices Manual*. Tulsa: PennWell.
- Romero, S.N., Monroy, R.R., Johnson, C., Cardenas, F., and Abraham, G.A.T. 2004. Preventing Lost Circulation by Use of Lightweight Slurries with Reticular Systems: Depleted Reservoirs in Southern Mexico. *SPE Drill & Compl* **21** (3): 185–192. SPE-92187-PA. DOI: [10.2118/92187-PA](https://doi.org/10.2118/92187-PA).
- Watson, D., Brittenham, T., and Moore, P.L. 2003. *Advanced Well Control*. Textbook Series, SPE, Richardson, Texas **10**.

SI Metric Conversion Factors

bbl	×	1.589 873	E – 01 = m ³
ft	×	3.048*	E – 01 = m
°F	×	(°F – 32)/1.8	= °C
gal	×	3.785 412	E – 03 = m ³
in.	×	2.54*	E + 00 = cm
in. ²	×	6.451 6*	E + 00 = cm ²
lbf	×	4.448 222	E + 00 = N
lbm	×	4.535 924	E – 01 = kg
psi	×	6.894 757	E + 00 = kPa
ton	×	9.071 847	E – 01 = Mg
ton (metric)	×	1.0*	E + 00 = Mg
tonf	×	8.896 444	E + 03 = N
tonne	×	1.0*	E + 00 = Mg

*Conversion factor is exact.

Appendix—Proposed Standard Symbols for Drilling Engineering

SPE does not have a set of symbols specific to drilling engineering. The following symbols are consistent with SPE usage, or SPE reserve usage, and ISO usage with the following exceptions:

I is used by SPE for various items, but not moment of inertia.

u is used by SPE for velocity.

ϕ and θ are used by SPE, but not φ and ϑ , unlikely to be confused in context.

φ and ϑ are used by ISO, but not consistent with this usage.

Units are given as standard SI units.

Because there is no standard set of symbols, symbols in the individual chapters may not follow this standard exactly, but each chapter will have a list of symbols to prevent confusion.

A	=	area, m ²
A_i	=	internal cross-sectional area of the pipe, m ²
A_o	=	external cross-sectional area of the pipe, m ²
A_p	=	cross-sectional area of the pipe, m ²
A_w	=	cross-sectional area of the wellbore, m ²
\vec{b}	=	$\vec{t} \times \vec{n}$, the unit binormal vector of the wellbore trajectory
c	=	compressibility, Pa ⁻¹
c_p	=	heat capacity at constant pressure, J/kg-K
c_v	=	heat capacity at constant volume, J/kg-K
d	=	diameter, m
d_i	=	inside diameter, m
d_o	=	outside diameter, m
d_w	=	wellbore diameter, m
D_h	=	hydraulic diameter, m
E	=	Young's elastic modulus, Pa
E	=	energy, J
f	=	fraction
f_D	=	Darcy friction factor
f_F	=	Fanning friction factor
\vec{F}	=	force, N
F_a	=	axial force, N
F_e	=	□effective□force, $F_e = F_a + F_{st}$, N
F_{st}	=	stream thrust force, $(p + \rho v^2)A$, N
g	=	acceleration of gravity, m/s ²
G	=	shear modulus, Pa
h	=	specific enthalpy, J/kg
h	=	height, thickness, m
I	=	moment of inertia (may be tensor), m ⁴
J	=	polar moment of inertia, m ⁴
K	=	bulk modulus, Pa
K	=	consistency index, pseudoplastic fluid, Pa-s ⁿ
L	=	distance or length, m
L_f	=	fracture half-length, m
m	=	mass, kg
\dot{m}	=	mass flow rate, kg/s
\vec{m}	=	applied moment load vector, N-m/m

M_w	=	molecular weight
\vec{M}	=	moment vector, N-m
M_b	=	bending moment, N-m
M_t	=	axial torque, N-m
n	=	flow behavior index, pseudoplastic fluid
\vec{n}	=	unit normal vector of the wellbore trajectory
N_{He}	=	Hedstrom number
N_{Nu}	=	Nusselt number
N_{Re}	=	Reynolds number
p_{break}	=	breakdown pressure in extended leakoff test, Pa
$p_{closure}$	=	closure pressure in extended leakoff test, Pa
p_i	=	fluid pressure internal to the pipe, Pa
p_o	=	fluid pressure external to the pipe, Pa
p_{pore}	=	pore pressure, Pa
p_{reopen}	=	reopening pressure in extended leakoff test, Pa
q	=	heat flow rate, W
q	=	flow rate, m ³ /s
R	=	radius of curvature, m
R	=	ideal gas constant, Pa-m ³ -K/kg
r_c	=	radial clearance, m
r_H	=	hydraulic radius, m
r_i	=	inside radius of pipe, m
r_o	=	outside radius of pipe, m
r_w	=	wellbore radius, m
s	=	measured depth, m
s	=	specific entropy, J/kg-K
t	=	time, s
\vec{t}	=	unit tangent vector to the wellbore trajectory
T	=	temperature, K
\vec{u}	=	displacement, m
\vec{u}_d	=	total drillstring displacement, m
\vec{u}_w	=	wellbore trajectory, m
U	=	energy, J
U_b	=	bending energy, J
v	=	velocity, m/s
v_i	=	fluid velocity internal to the pipe, m/s
v_o	=	fluid velocity external to the pipe, m/s
v_p	=	compressional wave velocity, m/s
v_s	=	shear wave velocity, m/s
V	=	volume, m ³
\vec{w}	=	total load per unit length applied to the pipe, N/m
\vec{w}_{bp}	=	buoyant weight per unit length of the pipe, N/m
\vec{w}_c	=	contact force between the pipe and the wellbore, N/m
\vec{w}_d	=	friction drag force tangent to the wellbore, N/m
\vec{w}_{ef}	=	load on the pipe due to external flow, N/m
\vec{w}_{efw}	=	load on the wellbore due to fluid flow, N/m
\vec{w}_{if}	=	load on the pipe due to internal flow, N/m
\vec{w}_p	=	weight per unit length of the pipe in air, N/m
W	=	work, J
y	=	holdup

z	=	true vertical depth, m
z	=	gas compressibility factor
α	=	coefficient of thermal expansion, K ⁻¹
β	=	buoyancy factor
β_H	=	angle from North to maximum horizontal stress
γ	=	shear strain
γ	=	specific gravity
$\dot{\gamma}$	=	shear rate, s ⁻¹
δ, Δ	=	decrement
ε	=	normal strain, strain
ε_r	=	radial strain
ε_z	=	axial strain
$\varepsilon_\theta, \varepsilon_h$	=	hoop strain
κ	=	curvature = 1/R, m ⁻¹
λ	=	thermal conductivity, W/m-K
μ	=	viscosity, Pa-s
μ_a	=	apparent viscosity, Pa-s
μ_f	=	Coulomb friction coefficient
μ_p	=	plastic viscosity, Pa-s
ρ_i	=	internal fluid density, kg/m ³
ρ_o	=	external fluid density, kg/m ³
φ	=	inclination angle
ϕ	=	porosity
ϑ	=	azimuth angle
σ	=	stress, Pa
σ'	=	effective stress, Pa
σ_h	=	minimum horizontal formation stress, Pa
σ_H	=	maximum horizontal formation stress, Pa
σ_n	=	normal stress, Pa
σ_r	=	radial stress, Pa
σ_t	=	tensile strength of rock, Pa
σ_{ult}	=	ultimate strength, Pa
σ_v	=	overburden (vertical formation) stress, Pa
σ_Y	=	yield stress, Pa
σ_z	=	axial stress, Pa
σ_θ	=	hoop stress, Pa
τ	=	shear stress, Pa
τ_c	=	cohesion of the formation, Pa
τ_y	=	yield point, Pa
θ	=	borehole circumferential angle
θ	=	soil angle of internal friction
ν	=	Poisson's ratio
ω	=	angular frequency, s ⁻¹

Special Cement Chemistry Notation

C ₃ S	=	tricalcium silicate 3CaO•SiO ₂
C ₂ S	=	dicalcium silicate 2CaO•SiO ₂
C ₃ A	=	tricalcium aluminate 3CaO•Al ₂ O ₃
C ₄ AF	=	tetracalcium aluminoferrite 4CaO•Al ₂ O ₃ •Fe ₂ O ₃
CH	=	calcium hydroxide Ca(OH) ₂
C-S-H	=	variable composition of CaO•SiO ₂ •H ₂ O
C \bar{S} H ₂	=	calcium sulfate dihydrate (gypsum) CaSO ₄ •2H ₂ O

C_2AH_8	=	$2CaO \cdot Al_2O_3 \cdot 8H_2O$
C_3AH_6	=	hydrogarnet $3CaO \cdot Al_2O_3 \cdot 6H_2O$
C_4AH_{19}	=	$4CaO \cdot Al_2O_3 \cdot 19H_2O$
$C_6A\bar{S}_3H_{32}$	=	ettringite $6CaO \cdot Al_2O_3 \cdot 3SO_3 \cdot 32H_2O$
$C_4A\bar{S}H_{12}$	=	monosulfate or monosulfoaluminate $4CaO \cdot Al_2O_3 \cdot SO_3 \cdot 12H_2O$
$C\bar{S}H_{1/2}$	=	calcium sulfate hemihydrate (plaster or bassanite)
$\gamma - C\bar{S}$	=	anhydrous calcium sulfate (soluble anhydrite)

Author Index

A

Aadnoy, B.S., 14, 31, 55–85, 174
Abraham, G.A.T., 630
Adams, A.J., 442
Adams, N.J., 625–675
Agle, A., 292–293
Alberty, M.W., 631
Alderman, N.J., 108
Althouse, W.S., 437, 595
Anato, W., 315–316
Anderson, M.E., 331
Ani, S.A., 345
Annis, M.R., 96, 109, 114, 126, 128–129, 219
Aremu, K.J., 293
Armagost, K., 631
Armstrong, F., 341
Aston, M.S., 631
Azar, J.J., 255, 287, 289–294
Aziz, K., 107, 288

B

Bach, G.F., 274
Bailey, W.J., 245–246
Barreto, J., 315–316
Barrios, J.R., 101
Bassal, A.A., 288, 290–291, 293
Bayoud, B.B., 331
Beart, R., 87
Beaton, T., 352
Becker, T.E., 279, 287–293
Beck, F.E., 358
Bello, S., 315–316
Bellows, J.C., 101, 107
Belnap, D., 346
Benaissa, S., 115
Bern, P.A., 294
Bickham, K.L., 283, 286, 292, 295
Bielstein, W.J., 200, 205
Bingham, E.C., 210
Bingham, M.G., 352–353, 356, 359
Bingham, R., 131
Birch, R., 345
Bird, R.B., 229
Bitler, J., 346
Bittleston, S.H., 231
Bizanti, M.S., 273
Bjorkevoll, K., 274
Black, A.D., 358
Bland, R.G., 94
Blasius, H., 248
Bleier, R., 88
Bloys, B., 625
Boresi, A.P., 396
Botelho, R., 315–316
Bourgoyne, A.T. Jr., 7–8, 19–20, 22–23, 42, 48, 87, 91, 93, 97, 109, 111–112, 117–118, 120, 123, 125, 311, 319, 328, 332, 335, 339–340, 344, 346, 348, 350–351, 353–359, 371, 374, 478–480, 506
Bradford, J., 318
Bradley, W.B., 55
Brand, F., 255
Brand, P.R., 403, 433
Brandon, B.D., 331
Brantley, J.E., 3–4
Brittenham, T., 632, 634–635
Brooks, A.G., 266–267
Broussard, P.N., 101

Bruton, J., 625
Bryant, S.L., 145
Buckley, P., 101
Budynas, R.G., 601
Bulkley, R., 213
Burcik, E.J., 183
Burgess, T.M., 568
Burkhardt, J.A., 265–267, 273
Burley, M., 322
Burnett, T., 322
Burrows, D., 183
Buske, R., 318
Butts, H.B., 219

C

Callas, N.P., 499
Callas, R.L., 499
Calvert, J., 145, 147
Campbell, J.M., 342–343
Campos, W., 289–293
Cardenas, F., 630
Carey, J.W., 145
Carlson, J.G., 42
Carr, N.L., 183
Casson, N., 215
Centala, P., 322
Cerkovnik, J., 323, 331
Cernocky, E.P., 404
Chabra, R.P., 251
Charlez, P.A., 219
Chau, M., 507–508
Chen, D.C.K., 347, 499
Chenevert, M.E., 7–8, 19–20, 22–23, 42, 48, 73, 87, 91, 93, 97, 109, 111–112, 117–118, 120, 123, 125, 292, 311, 319, 328, 332, 335, 339–340, 346, 348, 350–351, 354–356, 371, 478–480, 506
Cheng, D.C.H., 251, 255
Chen, S.L., 325, 352
Chien, S.F., 279, 283
Chilton, C.H., 286
Chin, W.C., 290
Cho, H., 293
Christman, S.A., 82
Chukwu, A., 274
Clark, J.A., 87
Clark, R.C., 154
Clark, R.E., 267
Clark, R.K., 283, 286, 292, 295
Clayton, R.I., 325, 331
Clegg, J., 325
Colebrook, C.F., 248
Collins, R.E., 218
Colston, F., 331
Conrad, L.C., 145
Cook, J., 66
Cooper, I., 14, 31, 174
Courant, R., 276
Cox, P., 346
Crandall, S.H., 403
Crawford, D.S., 400, 403
Crookshank, S., 145, 147
Cullender, M.H., 248
Cunha, J.C., 1–52

D

Dahlem, J.S., 326–327, 331, 352
Dahl, N.C., 403

Damschen, M., 316
 Darley, H.C.H., 87–88, 90, 95–97, 627
 Dawson, D.D., 630
 Dawson, R., 439, 554, 568, 594
 Day, J.B., 413
 de Jong, H.J., 631
 de Kee, D., 218
 Dellinger, T.B., 438
 DeLuca, M., 38
 Denison, E.B., 599
 Dennis, J.D., 252, 352
 denOuden, B., 352
 Devereux, S., 627
 Dodge, D.W., 252, 264, 283
 Doherty, W.T., 166
 Doiron, H.H., 328–331, 351
 Donovan, W. F., 261
 Drake, E.L., 2
 Duman, O.B., 554
 Dunn-Norman, S., 421
 Dupriest, F.E., 366
 Dykstra, M.W., 347
 Dzombak, D.A., 145

E

Easton, M., 219
 Eaton, B.A., 82
 Eckel, J.R., 200, 205, 358
 Economides, M.J., 421
 Edwards, J.H., 344, 358, 371
 Edwards, S., 66
 Escudier, M.P., 219
 Estes, J.C., 349, 353, 371
 Eustes, A.W. III., 87–133, 625–675
 Evans, S.M., 352
 Evers, J.F., 245–246

F

Fabian, R.T., 325, 347
 Fang, Z., 346
 Farnworth, S., 144, 175
 Farr, A.P., 612
 Farris, R.F., 154
 Faul, R., 144, 160
 Fischer, F.J., 499
 Fitzgerald, R., 177
 Flannery, B.P., 234, 262
 Fontenot, J.E., 267
 Fordham, E.J., 231
 Ford, J.T., 288, 290–294
 Ford, R., 313–314, 317–318, 323–325, 331–337
 Fox, R.C., 471
 Fredrickson, A.G., 229
 Friesen, D.B., 568

G

Gallagher, J.S., 101, 107
 Galle, E.M., 343–344, 357–358, 371–372
 Gao, E., 288, 290–292, 294
 Garnier, A., 145
 Gatlin, C., 341
 Gavignet, A., 108, 294
 Geehan, T., 108
 Giddens, P.G., 2
 Gieck, J.C., 326–327, 331
 Glowka, D.A., 347
 Goins, W.C., 166, 630
 Goode, J.M., 144
 Goodier, J.N., 395
 Goodman, H., 364
 Gopalsing, P.M., 316

Gouldson, I.W., 219
 Govier, G.W., 107, 288
 Graff, R.L., 364
 Graves, W.G., 218
 Gray, G.R., 87–88, 90, 95–97, 627
 Gray, K.E., 341
 Greenip, J.F., 385, 420
 Green, S.J., 358
 Griffo, A., 346
 Grim, R.E., 97–99
 Grinrod, M., 130
 Gubler, F.H., 499, 512
 Gucuyener, I.H., 218
 Guillot, D., 108, 252
 Gulati, K.C., 433
 Guo, B., 472–475

H

Haciislamoglu, M., 219, 263
 Hacı, M., 541
 Halbouty, M.T., 87
 Hale, A.H., 94
 Hall, D.R., 599
 Halliday, W.S., 94
 Hamilton, R., 346
 Hanks, R.W., 243
 Hanson, P., 294
 Hareland, G., 81, 351
 Harnett, J.P., 251
 Harvey, A.H., 101, 107
 Helmick, W.E., 656
 Hemphill, A.T., 289, 291
 Hemphill, T., 289–295
 Herman, J.J., 352
 Herschel, W.H., 213
 Heywood, N.I., 251, 255
 Hight, C., 290
 Hilbert, D., 276
 Hilmas, G., 346
 Hirshberg, A.J., 413
 Hoberock, L.L., 81
 Hodder, M., 219
 Ho, H.-S., 483
 Hollister, K.T., 331
 Hood, M.G., 322, 403, 433
 Hooper, M.S., 261
 Hoover, E.R., 345
 Houwen, O.H., 108
 Howard, G.C., 629
 Hsu, F.H., 273, 276
 Hubbert, M.K., 82
 Hudson, K., 313, 325
 Huerta, N.J., 145
 Hughes, H., 311
 Hughes, R.V., 338
 Hu, Q., 320, 322

I

Ikoku, C.U., 42
 Inglis, T.A., 492, 511
 Irvine, T.F., 252
 Isambourg, P., 115
 Isbell, M.R., 94, 342, 377
 Issa, J.A., 400, 403
 Ivan, C., 625
 Iyoho, A.W., 287, 289–290

J

Jaffar, A., 345
 Jalukar, L.S., 294
 James, J., 351

Jardioli, A., 101
 Jefferson, D.T., 292
 Jellison, M.J., 599
 Jensen, B., 130
 Johancsik, C.A., 568
 Johnson, C., 630
 Johnson, R.C., 433
 Johnson, S., 347
 Jordan, S., 513–514
 Jorden, J.R., 80
 Ju, G.T., 400, 403

K

Kastor, R., 1–52
 Katz, D.L., 183
 Kay, M., 219
 Kelessidis, V.C., 179–301
 Kelly, J., 82
 Kemp, N.P., 102
 Kenner, J.V., 342
 Kenny, P., 291–292, 295
 Kim, Y.D., 218
 Kjosnes, I., 292–293
 Knowles, S.P., 377
 Kobayashi, R., 183
 Koederitz, W.L., 366
 Koskie, E., 331
 Kosmatka, S.H., 140
 Kost, B., 326–327, 331
 Kostic, M., 251
 Krukowski, F., 131
 Kulakofsky, D., 145, 147
 Kuru, E., 376, 554
 Kutchko, B.G., 145

L

Lafuze, D., 326–327, 331
 Laird, W.M., 229
 Lake, L.W., 15, 155–157, 255, 284, 639–640, 643–656
 Lal, M., 273
 Langlinais, J., 219, 263
 Larsen, T.I., 287, 289–290, 292–294
 Ledgerwood, L.W., 364
 Lee, R.L., 472–475
 Lee, S., 144, 175
 Lefort, G., 325
 Leising, L.J., 289, 291–292
 Lesso, W.G., 507–508
 Letruno, R.E., 273
 Leuterman, A.J., 88
 Lewis, D.B., 403, 433
 Liang, F., 177
 Li, J., 289, 291
 Li, X., 322
 Liu, Q., 320, 322
 Lockett, T.J., 290–291
 Logan, G., 131
 Logan, J.L., 437, 595
 Loklingholm, G., 292–293
 Longley, A.J., 656
 Lowry, G.V., 145
 Lubinski, A., 273, 276, 369, 404, 437, 457, 481–482, 484, 491, 499, 589–592, 595, 606, 609, 611
 Lukasewich, H., 318
 Lummus, J.L., 350, 371
 Luo, F., 488, 498
 Luo, Y., 219

M

Mackay, S.P., 338
 Maglione, R., 179–301

Maes, M.A., 403, 433
 Maidla, E., 541
 Maitland, G.C., 108
 Maksoud, J., 36
 Marlow, R. S., 403
 Marti, J., 115
 Martin, N., 131
 Martins, A.L., 290–291, 293
 Mason, M.C., 469
 Mata, F., 630
 Matthews, W.R., 82
 Maute, R.E., 433
 McFadyen, M.K., 88
 McGehee, D.H., 326–327, 331
 McKenna, D.L., 433
 McLean, J.C., 438
 McLean, M.R., 631
 McMillian, W.M., 469
 Mensa-Wilmot, G., 313, 325
 Merlo, A., 215, 219
 Metzner, A.B., 251–252, 254–255, 264, 283, 300
 Middleton, J.N., 345
 Miko, C., 352
 Millheim, K.K., 7–8, 19–20, 22–23, 42, 48, 87, 91, 93, 97, 109, 111–112, 117–118, 120, 123, 125, 311, 319, 328, 332, 335, 339–340, 346, 348, 350–351, 354–356, 371, 478–480, 499, 506, 512–514
 Milton, A., 219
 Mimaki, T., 400, 403
 Miska, S.Z., 14, 31, 174, 293, 350, 449–576, 585–622
 Miska, W., 499
 Mitchell, B.J., 342–343
 Mitchell, R.F., 14, 31, 174, 179–301, 404, 422, 439, 473, 575, 595
 Mody, F.K., 92, 94
 Monroy, R.R., 630
 Moody, L.F., 249–250
 Moore, P.L., 627, 632, 634–635
 Moo, T.J., 364
 Morrice, G., 219
 Moyer, M.C., 413
 Mpandelis, G.E., 288
 Murdock, A.D., 352
 Murray, A.S., 338

N

Niemi R., 331
 Nolte, K.G., 273, 276
 Nouar, C., 255
 Nouri, J.M., 219

O

O'Connell, J.P., 107
 Okafor, M.N., 245–246
 Okrajni, S.S., 287, 291–292
 Oliveira, P.J., 219
 Oliver, M.S., 326
 Oraskar, A.D., 295
 Osisanya, S.O., 293
 Ostwald, W., 211
 Ottesen, S., 115
 Overstreet, J., 318
 Oyenevin, M.B., 288, 290–294
 Ozbayoglu, E.M., 293, 311–382
 Ozgen, C., 219, 262

P

Parker, M., 145, 147
 Parr, I., 144, 175
 Parry, W.T., 101, 107
 Pasley, P.R., 404, 439, 554, 594

Paulsen, J.E., 130
 Payne, M.L., 14, 31, 174, 433, 500, 504–505
 Peden, J.M., 219, 245–246, 288, 290–294
 Peixinho, J., 255
 Peng, S., 219
 Pennebaker, E.S., 82
 Perry, R.H., 286
 Pessier, R.C., 94, 316
 Peterson, J.L., 362
 Philip, Z., 292
 Phillippi, D., 325, 347
 Piatti, C., 215, 219
 Piercy, N.A.V., 261
 Pigott, R.J.S., 279, 286–287
 Pilehvari, A.A., 255, 287, 289–290, 292–294
 Pilkington, P.E., 82
 Pinho, F.T., 219
 Pitzer, K.S., 100
 Planeix, M.Y., 471
 Pogue, T., 289, 291
 Poling, B.E., 107
 Popov, E.P., 589, 601
 Portwood, G., 346
 Powell, J.W., 292, 358
 Power, D.J., 290
 Powers, J.R., 345
 Power, T.L., 400, 403
 Prausnitz, J.M., 107
 Press, W.H., 234, 262

R

Rajtar, J., 488, 498
 Reddy, B.R., 145, 147
 Reed, J.C., 251, 254–255, 300
 Reed, R.L., 344, 358, 371–372
 Reed, T.D., 255, 293
 Reinsvold, C.H., 326–327, 331
 Reynolds, O., 245
 Rezmer-Cooper, I.M., 507–508
 Richardson, J.F., 251
 Richardson, S.M., 290–291
 Rickabaugh, C., 318
 Riekels, L., 433
 Rimer, C., 290
 Ritter, C.J., 513–514
 Rivero, R.T. 469
 Robertson, R.E., 216–217, 299
 Rodot, F., 145
 Rogers, P.S.Z., 100
 Rogers, W.F., 113
 Romero, S.N., 630
 Rommetveit, R., 274–275
 Roper, W.F., 112–113
 Roy, B.J., 377
 Roy, S., 188
 Rudolf, R.L., 273–274

S

Saasen, A., 130, 292–293
 Sabins, F.L., 144, 160
 Sagot, A., 274–275
 Sahdev, M., 25
 Sampaio, J.H.B. Jr., 473
 Sanchez, R.A., 290–291, 293
 Sandstrom, J.L., 358
 Santana, C.C., 291
 Santra, A., 145, 147
 Savins, J.G., 112–113
 Sawaryn, S.J., 469
 Schell, E.J., 325, 347
 Schmidt, R.J., 396

Scholes, H. 473
 Schuh, F.J., 266–267, 273, 472, 517
 Scoggins, W.C., 145, 147
 Scott, P.P., 629
 Seely, F.B., 398
 Senger, J., 326, 331
 Sewell, F.D., 413
 Shah, S.N., 234–236, 293
 Sharma, M., 292
 Sheppard, M.C., 568
 Shirazi, S.A., 293–294
 Shirley, O.J., 80
 Shulman, Z.P., 218
 Sifferman, T.R., 279, 288–293
 Sinesi, J., 322
 Sinor, L.A., 345–346
 Sisko, A.W., 218, 299
 Smith, J.O., 398
 Smith, R.V., 248
 Sobey, I.J., 294
 Solvang, K.-A., 292–293
 Sorelle, R.R., 101
 Soza, R., 313, 325
 Spaar, J.R., 364
 Standing, M.B., 183
 Stark, C., 88
 Steine, O.G., 274–275
 Steinke, S.C., 326–327, 331
 Stephens, M.P., 101
 Stiff, H.A. Jr., 216–217, 299
 Stone, C.M., 347
 Strazisar, B.R., 145
 Stroud, B.K., 87–88
 Subramanian, R., 255
 Sunde, E., 291–292, 295
 Suryanarayana, P.V.R., 273–274
 Sutton, D.L., 144, 160, 234–236
 Swanson, J.D., 433
 Sweatman, R.E., 139–176
 Syrstand, S.O., 292–293

T

Takach, N., 293
 Tallin, A.G., 400, 403
 Tamano, T., 400, 403
 Tan, C.P., 92
 Tao, L.N., 261
 Tare, U., 92
 Taylor, H.L., 469
 Taylor, M.R., 352
 Teasdale, P., 345
 Tehrani, M.A., 231
 Teplitz, C.J., 42
 Terzaghi, K., 57
 Teukolsky, S.A., 234, 262
 Thaulow, N., 145
 Thomas, D.C., 102
 Thorogood, J.L., 469
 Tibbitts, G.A., 358
 Timoshenko, S.P., 395
 Tomkins, P.G., 94
 Tomren, P.H., 287, 289–290
 Tosun, I., 219, 262

U

Underwood, L.D., 500, 504–505
 Uner, D., 219, 262
 Uzcategui, G., 315–316

V

Veiga, M., 630
 Vetterling, W.T., 234, 262

W

Walker, S., 289, 291
 Walton, I.C., 289, 291–292
 Wamsley, W.H. Jr., 313–314, 317–318, 323–325, 331–337
 Wang, Y., 274
 Warren, T.M., 345–347, 507, 509
 Watson, D., 632, 634–635
 Watters, L.T., 421
 Waughman, R.R., 94
 Weiner, P.D., 413
 Weisinger, D., 290
 West, W.C., 377
 White, B., 346
 White, F.M., 261–262
 Whitelaw, J.H., 219
 Whitmore, R.L., 295
 Whitney, W.S., 403, 433
 Whitson, C.D., 88
 Wick, C., 568
 Wiesner, B.C., 377
 Willis, D.G., 82
 Wilson, G.J., 467
 Wilson, K.C., 294
 Wilson, M.L., 140
 Winny, H.F., 261
 Winters, W.J., 326, 328–331, 351
 Wojtanowicz, A.K., 376
 Woods, A.B., 343–344, 357–358, 371–372
 Woods, H.B., 457, 481, 491
 Worraker, W.J., 290–291
 Wu, A., 351
 Wu, M., 499

X

Xian, X., 322

Y

Yanagimoto, S., 400, 403
 Young, F.S. Jr., 7–8, 19–20, 22–23, 42, 48, 87, 91, 93, 97,
 109, 111–112, 117–118, 120, 123, 125, 311, 319, 328, 332,
 335, 339–340, 344, 346, 348, 350–351, 353–359, 371,
 374, 478–480, 506

Z

Zamora, M., 101, 188, 292, 294, 358
 Zannoni, S.A., 347
 Zaremba, H.B., 499, 512
 Zaremba, W.A., 469
 Zarrough, R., 288, 290–292, 294
 Zhu, H., 218
 Ziaja, M.B., 350, 363
 Zwillinger, D., 53, 437

Page Intentionally Left Blank

Please Keep Scrolling To Continue

Subject Index

A

actual (true) axial stress, 599
aluminum drillpipe (ADP), 596
analytical 3D model
 3D deflection model, 512–513
 inclination angle, 512, 514–515
 MM 'K cross section, 512, 514
 overall angle change, 515
 tool-face plane, 512, 514
 trigonometric functions, 516
apparent viscosity, 206
average-angle method (AAM), 465–466

B

barite, 154
bending-stress ratio (BSR), 615–616
bentonite, 153
BHA. *See* bottomhole assembly
Bingham plastic fluids
 frictional pressure drop, eccentric annulus, 265
 pipe flow
 field units, 233
 flow rate, 232–233
 fluid velocity, 232
 plug region, 231–232
 shear rate, 233–234
 shear stress, 231–232
 rheological models, 207, 210
 slot flow
 flow rate, 231
 plug region, 230
 shear stress, 229–230
 velocity, 230
bioremediation, 132–133
blowout preventers (BOP), 32
borehole stability analysis
 borehole collapse, 78–80
 inclined wells
 failure analysis, 75
 in-situ stresses, 74–75
 Kirsch equations, 73–74
 principal borehole stresses, 76–77
 vertical wells
 borehole pressure, 62–63
 breakout analysis, 66
 caliper logs, 71
 circulation loss, 55
 classical mechanics approach, 61–62
 collapse failure, 66–67
 equivalent density, 56
 fracture gradients, 63–64
 fracture mechanics approach, 61
 gradient equation, 56
 hole enlargement/collapse, 55
 in-situ stresses, 57
 LOT, 63–64
 mechanical borehole collapse, 55
 Mohr-Coulomb shear model (*see* Mohr-Coulomb shear model)
 mud losses, 62
 optimal mud weight, 64–65
 pore pressures, 58–59
 radial, tangential and axial stress, 61–62
 shear failure, 66, 68
 stress concentration factor, 61
 unplanned time spent, 56–57
 water-based vs. oil-based drilling fluids, 73

bottomhole assembly (BHA)
 bit-displacement direction, 486
 curved wellbore, constant curvature, 488
 dimensionless boundary conditions, 485
 dimensionless governing differential equation, 489
 drill collars, 585–586
 drilling anisotropy index, 481, 483
 drilling, dipping formations, 481–482
 drillpipes, 31
 drillstring, 479
 elastic line, drill collars, 483–484, 489
 equilibrium configuration, 480
 face- and side-cutting abilities, 483
 instantaneous bit displacement, 486–487
 isotropic drilling conditions, 481
 Lubinski's equation, 484
 magnetic instruments, 450
 parameters, 479
 resultant force angle, 486
 rotary-steerable system, 479, 481
 scaling factors, 485, 489–490
 shearing force, 484
 side force, 485–486
 slick assembly, inclined hole, 480, 482
 S-U system of coordinates, 488
 tangency point, 480
 tilt angle, 485
breakout analysis, 66
Buckingham Pi theorem, 246
buoyancy factor (BF), 425

C

calcium aluminate cements, 148
calcium chloride, 154
cam-actuated drill-ahead (CADA) tool, 40–41
carbon steels, 387
casing axial forces
 balance, 422–423
 buoyancy factor, 425
 exterior fluid, 422
 internal flow force balance, 422–423
 pressure force, area change, 424
casing design
 casing program, 385–386
 casing-program selection
 axial forces, 422–425
 casing-setting depths, 418–419
 combination string, 418
 intermediate casing, 428–429
 production casing, 429–430
 size, casing strings, 420–421
 surface casing, 425–428
 weight, grade, and couplings, 421–422
 computer-based design
 initial condition, 434–435
 load case, 435
 optimization capability, 436
 safety and utilization factor, 435
 spreadsheets and programs, 434
conductor casing, 385
connections
 API and ISO, 407
 buttress threads, 409–410
 collapse, 417
 connection joint strength, 414–415, 417
 internal pressure resistance (*see* internal pressure resistance)

- makeup, 413
- non-API/ISO, 410–412
- performance plot, 417–418
- round threads, 408–410
- thread compounds, 412–413
- threaded and coupled/integral-joint, 407
- XC threads, 410
- corrosion
 - CRAAs, 406–407
 - gas, H₂S, 405
 - H₂S partial pressure, 406
 - hydrogen embrittlement, 405
 - prevention methods, 406
 - protection, 405
 - SSC, 405–406
 - stainless and nickel-based steels, 407
- intermediate casing, 386–387
- line pipe, 385, 391–392
- liner, 387
- manufacture, 387–388
- OCTG, 385
- performance properties
 - axial tension, 397
 - bending effect, 403–404
 - casing tension strength, 398
 - collapse resistance, 400–403
 - deterministic approach, 397
 - failure/rupture, 397
 - internal pressure resistance, 398–400
 - proprietary methods, 398
 - torsion, 405
- probabilistic reliability, 433–434
- production casing, 387
- special considerations
 - casing annuli, 442
 - cementing, 441
 - field handling effect, 441–442
- stability, 436–440
- standardization
 - chemical requirements, 388–390
 - dimensions, 390–391
 - grade, 388–389
- strength of materials
 - combined stresses, 395–397
 - environment, mechanical properties, 395
 - hardness, 394
 - tensile test, 392–394
 - toughness, 394–395
- surface casing, 385–386
- tubing, 385
- casing strength, 397
- Casson fluids, 215–216
- cementing
 - additives
 - barite, 154
 - bentonite, 153
 - calcium chloride, 154
 - cement retarders, 156, 158
 - definition, 149
 - density control, 150–152
 - filtration-control additives, 159
 - foamed cement, 152
 - gypsum, 156
 - hematite, 153–154
 - hydrazine, 159
 - lost-circulation additives, 158–159
 - materials physical properties, 150–151
 - microspheres, 152
 - nylon, 159
 - paraformaldehyde and sodium chromate, 159
 - percent mix, 150
 - plastic-state shrinkage, 160
 - pozzolans, 152
 - radioactive tracers, 159
 - setting-time control, 154
 - silica flour, 159
 - sodium chloride, 156
 - sodium silicates, 152
 - viscosity-control additives, 159
 - cement testing
 - API Spec. 10A*, 141–142
 - consistometer, 142–143
 - filter press, 142
 - nonstandard tests and modeling, 144
 - permeability testing, 144–145
 - pressurized mud balance, 142
 - rotational viscometer, 142
 - strength tests, 144
 - definition, 139
 - placement techniques
 - annular cementing through tubing, 164
 - casing, 160–163
 - cementing evaluation, 172–173
 - cementing time requirements, 171
 - cement volume requirements, 168, 170–171
 - delayed-setting cementing, 164
 - inner-string cementing, 164
 - liners, 164–166
 - multiple-string cementing, 164
 - plug cementing, 165–167
 - reverse-circulation cementing, 164
 - squeeze cementing, 166, 168–169
 - stage cementing, 162–163
 - WOC times, 171–172
 - Portland cement composition, 140–141
 - standard and nonstandard drilling cements
 - API Spec. 10A*, 145
 - classes and grades, 145–146
 - construction industry cement designations, 145, 147
 - nonstandard cements, 145, 147–149
 - normal water content of cement, 145, 147
 - well parameters
 - depth, 173
 - formation chemical characteristics, 174
 - formation permeability, 175
 - formation pressures, 174
 - temperatures, 174
 - wellbore geometry and drilling-fluid removal, 174
- cement retarders, 156, 158
- Charpy impact energy, 394–395
- Charpy toughness. *See* Charpy impact energy
- clay types
 - activity levels, 96
 - attapulgitite, 97–99
 - bentonite/gel, 96
 - montmorillonite, 96–97, 99
 - sodium montmorillonite, 97–98
 - subbentonite, 96
- Colebrook function, 248
- collapse resistance
 - casing, combined loading, 402
 - collapse modes, 400
 - elastic-collapse pressure formula, 402
 - factors, yield strength, 400–401
 - high-collapse tubulars, 403
 - plastic-collapse pressure formula, 401
 - transition-collapse pressure formula, 401–402
 - yield-strength collapse-pressure formula, 401
- combined stresses
 - axial and radial stresses, 395
 - bending stress, 395–396
 - effective tension, 396

- failure criteria, 396–397
- hoop/circumferential direction, 395
- Huber-von Mises-Hencky theory, 396
- loading condition, 395
- pipe, 395–396
- complex-tangent build curve, 463–464
- consistency index, 212–213
- constant build and turn rate method (CBTM), 471
- constant curvature and build rate method (CCBM), 472–473
- constant tool-face method. *See* constant curvature and build rate method
- corrosion-resistant alloys (CRAs), 388, 406–407
- cutter wear
 - bit weight, 343–344
 - hydraulics, 344–345
 - PDC cutters
 - bit whirl and full-contact gauge ring, 347
 - blank geometry, 345–346
 - chipping and fracture resistance, 346
 - contact area, 346
 - critical cutter temperature, 348
 - dynamic loading, 345
 - failure modes, 346
 - fractional tooth wear, 345
 - ring PDC bit, 347
 - stable and unstable PDC, 347
 - steady-state wear, 345
 - wear-flat temperature, 348
 - rotary speed, 344
 - tooth height, 342–343
 - wear equation
 - fixed-cutter bits, 350
 - roller-cone bits, 348–349
- cuttings transport
 - annular clearance, 294
 - cuttings size, 292–293
 - density, 290
 - deviated wells
 - flow patterns, 288–289
 - flow rates, 280
 - inclined wellbores, 279
 - new experimental data, 287–288
 - eccentricity, 292
 - field application, 295
 - flow rate, 289–290
 - hole inclination, 290
 - mechanistic modeling, 294–295
 - mud type, 293
 - particle slip velocity
 - Bingham fluid, 283
 - friction factor, 281
 - non-Newtonian fluids, 283
 - Reynolds number, 281
 - sphericity, 281
 - stagnant fluid, 280
 - Stokes drag, 280
 - pipe rotation, 290–291
 - rheology, 291–292
 - solids volumetric concentration, 293
 - vertical wells
 - cross-sectional geometry, 283–284
 - cuttings concentration, 285–286
 - drilling-fluid carrying capacity, 279
 - flow conditions, 284
 - transport efficiency, 279
- D**
- Darcy friction factor, 196
- Darcy-Weisbach friction factor, 250
- directional drilling
 - deviation control
 - BHA mechanics (*see* bottomhole assembly)
 - downhole drilling motors (*see* downhole drilling motors)
 - RSSs, 507–509
 - stabilizers (*see* stabilizers, hole deviation control)
 - steerable motors, 505–507
 - whipstocks and jetting techniques, 477–479
 - directional-well trajectory design
 - applications, 450
 - build rate, 451
 - definition and development, 449
 - directional cosines, 454
 - directional-well profiles, 458–464
 - drop rate, 453
 - 3D wellbore trajectory, 451, 454
 - ERW and ERD, 449
 - geosteering methods, 449–450
 - hole inclination and azimuth angles, 450–451
 - horizontal turn rate, 453
 - inclination and direction angle, 450
 - KOP, 451
 - measured depth (MD), 450
 - multilateral completion, 449–450
 - plane and side view, 451–452
 - surveying instruments, 450
 - target-point coordinates, 455
 - three-dimensional well profiles (*see* three-dimensional well profiles)
 - three segments wellbore, 451, 453
 - turn rate, 453
 - TVD, 450
 - vertical and horizontal planes, 455–456
 - wellbore curvature and dogleg severity, 457–458
 - method of vectors
 - 3D well path, 523–525
 - Frenet-Serret equations, 522–523
 - minimum-curvature trajectory, 535–536
 - survey station interpolation, 532
 - well trajectory, survey data, 526–531
 - tool-deflection orientation
 - analytical 3D model, 512–516
 - constant- and minimum-curvature well profiles, 517
 - 3D trajectory control, 511–512
 - face angle, curvature, and build and turn rates, 517
 - torque and drag modeling
 - buckling consideration, 554
 - conventional rotary drilling, 538
 - drag-force calculations, 568–571
 - drag forces, 539
 - effective/buoyant weight, 538
 - equilibrium equations in 3D, 557–559
 - force and moment equilibrium formulation, 563–565
 - inclined wellbore, pipe, 559–563
 - pipe rotation, 551–553
 - soft-string model (*see* soft-string model)
 - stiff-string model, 574–576
 - straight inclined wellbore (*see* straight inclined wellbore)
 - torque (moment), 539
 - tortuosity effect, 555–556
 - vertical drilling, 538
 - WOB, 538
 - directional-well profiles
 - continuous-build trajectory, 459
 - 2D wellbore trajectories, 458
 - 2D wells, 458
 - horizontal well profiles, 462–464
 - ideal slant-type well profile, 459–460
 - slant well, 458
 - S-shaped pattern, 458–459
 - two phases, 458
 - dogleg rate, 457

- dogleg severity (DLS)
 - bending effect, 403
 - bending stress, 605
 - wellbore curvature, 457–458
- downhole drilling motors
 - bit rotary speed, 503
 - connecting-rod assembly, 503–504
 - different lobe patterns, 503–504
 - drilling-fluid flow, 501–502
 - eccentricity, 505
 - flow area, 505
 - motor hydraulic horsepower, 504
 - PDM, 503–504
 - PDM performance characteristic curve, 505
 - power, 502
 - rotary torque, 504
 - specific displacement per revolution, 505
 - torque, 502, 505
 - turbine performance characteristic, 501, 503
 - turbine single stage, 501–502
 - turbodrill, 501
- drag-force calculations
 - constant tool-face trajectory, 571
 - minimum-curvature well path, 568–569
- drill collar buckling
 - axial force, 589
 - bending coefficients, 591–592
 - borehole wall, 591–592
 - coefficients, 590–591
 - Euler equation, 589
 - first- and second-order, 590
 - helical buckling phenomenon, 595
 - inclined hole, 594
 - resultant bit force, 590
 - side force, 590
 - tilt angle, 590
 - vertical hole, 589
 - WOB, 590
- drilling-fluid-handling equipment
 - decanting centrifuge, 27–28
 - hydrocyclone, 26–27
 - mud pits, 25
 - sand trap, 26
 - shale shaker, 26
 - vacuum-chamber degasser, 28–29
- drilling fluids
 - additives, 94–95
 - buoyancy, 90
 - clay chemistry
 - clay types (*see* clay types)
 - particle sizes, 95–97
 - continuous-phase classification
 - OBF, 92–93
 - pneumatic drilling fluids, 93–94
 - silicate-based drilling fluids, 94
 - water-based fluids, 91–92
 - control subsurface pressure, 89–90
 - cuttings transport, 89
 - fluid-loss control, 89
 - health, safety, and environmental considerations
 - bioremediation, 132–133
 - contamination sources, 130
 - encapsulation, 132
 - environmental protection, 130
 - personal protective equipment, 130
 - treatment and disposal, drilled cuttings, 131–132
 - waste management, 131
 - waste-stream reduction, 130–131
 - zero-tolerance policy, 130
 - history, 87–88
 - hydraulic horsepower transmission, 90
 - lubrication and cooling, 89
 - LWD tool, 90
 - mud viscosity estimation, 107–109
 - mud weight calculation
 - brine density, 102, 104
 - specific gravities, drilling-fluid solids, 100
 - water and oil densities, 100–103
 - OBF, 88
 - physicochemical functions, 89
 - solids-control
 - centrifuge, 129–130
 - formation cuttings, 125
 - hydrocyclones, 124–128
 - settling pit, 125
 - shale shakers, 125–127
 - solids-particle sizes, 124, 126
 - solids-removal system, 124–125
 - testing
 - acidity and alkalinity, 120
 - acids, bases, and salts, 119–120
 - alkalinity and lime content, 122–123
 - API filter press—static filtration, 117–120
 - apparent viscosity, 114
 - buffer solutions, 120–121
 - calcium concentration, 124
 - chlorine concentration, 123–124
 - concentration of solutions, 121
 - density, 110
 - effective viscosity, 114
 - electrolytes, 121
 - gel strength, 115
 - hydrogen-ion concentration, 123
 - lubricity testing, 115–116
 - physical and chemical properties, 110
 - plastic viscosity, 113–114
 - solid-content analysis, 123
 - titration, 121
 - viscosity, 111–113
 - water-based mud, 110
 - yield point, 113–114
- drilling hydraulics
 - cuttings transport
 - annular clearance, 294
 - cuttings size, 292–293
 - density, 290
 - deviated wells, 279–280, 287–289
 - eccentricity, 292
 - field application, 295
 - flow rate, 289–290
 - hole inclination, 290
 - mechanistic modeling, 294–295
 - mud type, 293
 - particle slip velocity, 280–283
 - pipe rotation, 290–291
 - rheology, 291–292
 - solids volumetric concentration, 293
 - vertical wells, 279, 283–287
 - dynamic surge and swab pressures
 - axial drillstring elasticity, 273
 - balance of mass, 275–276
 - balance of momentum, 276
 - borehole expansion, 276
 - longitudinal elasticity, 273
 - low-clearance liner annulus, 274–275
 - normalized transient pressures, 273–274
 - solution method—fluid dynamics, 276–278
 - transient swab/surge pressure, 273–274
 - trip-in velocity profile, 273–274
 - frictional pressure drop, eccentric annulus
 - Bingham plastic and Herschel-Bulkley models, 265
 - correction factor, 260–261

- Newtonian fluid model, 261
 - with pipe movement, 265–267
 - power-law model, 262–264
- hydrostatic pressure calculations
 - complex fluid columns, 185–186
 - compressible fluids, 182–183
 - entrained solids and gases, 189–190, 192
 - equivalent density concept, 187–189
 - forces, fluid element, 180
 - incompressible fluids, 181–182
 - SI units, 181
 - subsurface well pressures, 180
 - well deviation, 192
- laminar flow, pipes and annuli
 - annulus as slot, 221–223
 - Bingham plastic model (*see* Bingham plastic fluids)
 - cylindrical pipe flow, 219–221
 - Herschel-Bulkley fluids (*see* Herschel-Bulkley fluids)
 - Newtonian fluid model (*see* Newtonian fluid models)
 - power-law model, 236–239
 - pump rate, 218
 - PWD tools, 219
- rheological models
 - advanced models, 217–218
 - Bingham plastic fluids, 207, 210
 - Casson fluids, 215–216
 - Herschel-Bulkley fluids, 213–215
 - laminar flow, Newtonian fluids, 206
 - Newtonian fluid model, 208–210
 - non-Newtonian fluids, 207–208
 - power-law fluids, 211–212
 - pseudoplastic/yield-pseudoplastic, 207
 - Robertson-Stiff fluids, 216–217
 - shear stress vs. rate, 206–207
 - shear stress vs. time, 207–208
 - viscous forces, 206
 - yield stress, 207–208
- steady flow
 - bit hydraulic impact force, 202–203
 - bit hydraulic power, 202
 - energy balance, 197–198
 - flow through jet bits, 199–201
 - frictional forces, 194
 - jet bit nozzle size selection, 203–206
 - mass balance, 194–195
 - momentum balance, 195–196
- steady-state pressures
 - surge pressure prediction (*see* surge pressure prediction)
 - wellbore pressure circulation, 267–269
- turbulent flow, pipes and annuli
 - Newtonian fluid models (*see* Newtonian fluid models)
 - non-Newtonian fluid models, 251–255
 - recommended friction models (*see* recommended friction models)
- wellbore pressure, 179
- drillstring design
 - BHA, 585–586
 - BSR, 616
- drill collars
 - buckling, 589–592
 - manufacture, 586
 - physical properties, 586, 588
 - size and length, 586–589
 - spiral grooves, 586
 - string, 586
 - unit weights, 586–587
- drilling fluid, 585
- drillpipe and tool joints
 - API numbered connections, 599
 - axial tension/compression stresses, 599
 - bending stress, 604–605
 - dimensional data, 596–597
 - double-shoulder connection, 599
 - intelligent/telemetry drillpipe, 599
 - IU, EU, and IEU, 596
 - minimum performance properties, 596, 598
 - minimum tensile yield strength, 596–597
 - pressure-induced stresses, 609–610
 - rotary-shouldered connection, 597–598
 - torsional stresses, 603–604
 - interactive approach, 615
 - load capacity, drillpipe, 610–611
 - tapered drillstring, 617
 - WOB, 585
- 3D well path
 - unit binormal vector, 524–525
 - unit normal vector, 524
 - unit tangent vector, 523–524
 - wellbore curvature, 524
 - wellbore torsion, 525
- E**
 - effective tensile (compressive) stress, 601–602
 - effective tension, 588
 - effective tensional stress, 608
 - elastic limit/yield point, 393
 - electric-resistance-welding (ERW) process, 387
 - empirical correlations
 - drillability correlations, 80–81
 - fracture pressure correlations, 81–82
 - pore-pressure correlations, 82
 - endurance limit, 607
 - equivalent centipoise, 212, 214, 217
 - Euler equation, 589
 - expanding cements, 148
 - extended-reach drilling (ERD), 449
 - extended-reach wells (ERWs), 449
 - Extreme line and couplings (XCs) threads, 410
- F**
 - Fanning equation, 248–249
 - Fanning friction factor, 248
 - filtration-control additives, 159
 - fixed-cutter bits
 - diamond bits
 - abrasive formations, 315
 - matrix body, 315–316
 - oilwell drilling, 312
 - partial encapsulation, 316
 - profile, crown, 316
 - scraping/cutting surface, 312–313
 - fish tail/drag bits, 311–312
 - IADC bit-classification system
 - bicenter bit, 330
 - bit's cross-sectional profile, 329
 - cutter/bottomhole pattern, 329
 - cutter size and density, 330–331
 - double-cone profile, 330
 - four-character coding system, 328
 - hydraulic design, 330
 - primary cutter type and body material, 328–329
 - impregnated bit, 314–316
 - PDC bits
 - cutter design and manufacturing, 325
 - design principles, 322–324
 - dual-diameter bit, 314–315
 - matrix, 324–325
 - rock-shearing action, 312
 - scraping/cutting surface, 312–313
 - shape, 324
 - rock-failure mechanism
 - angle of internal friction, 341

- axial force, 338
- compressive and confining stress, 339
- force-balance equation, 340
- helix angle, 338
- Mohr criterion, 339–340
- self-sharpening effect, 338
- unit area, 339–340
- ROP, 362–363
- TSP bits, 312
- wear equation, 350
- flow behavior index, 212–213
- fluid acceleration, 196
- foamed cement, 152
- fracture mud weight, 636
- free-body diagram (FBD), 539–540
- G**
- gas kick, 636
- gauge pressure, 181
- geomechanics, drilling
 - borehole stability analysis (*see* borehole stability analysis)
 - empirical correlations, 80–82
- gypsum, 156
- gypsum cements, 147–148
- H**
- health, safety, and environment (HSE) policy, 5
- helitransportable rigs, 7
- hematite, 153–154
- Herschel-Bulkley fluids
 - frictional pressure drop, eccentric annulus, 265
 - pipe flow, 243–245
 - rheological models
 - consistency index, 213–214
 - flow behavior index, 213
 - hydraulic computation model, 215
 - rotational viscometer, 215
 - shear stress vs. rate, 213
 - yield stress, 213
 - slot flow
 - flow rate, 243
 - shear stress, 240–242
 - velocity, 241–242
- hoisting system
 - block and tackle
 - derrick and substructure, 22
 - drilling line, 20–21
 - efficiency factors, 20
 - mechanical advantage, 18–19
 - nominal breaking strength, wire rope, 21
 - schematic diagram, 18–19
 - drawworks, 18–19
- Huber-von Mises-Hencky theory, 396
- hybrid bits, 316
- hydraulic diameter, 250
- hydrazine, 159
- hydrostatic pressure calculations
 - complex fluid columns, 185–186
 - compressible fluids, 182–183
 - entrained solids and gases, 189–190, 192
 - equivalent density concept, 187–189
 - forces, fluid element, 180
 - incompressible fluids, 181–182
 - SI units, 181
 - subsurface well pressures, 180
 - well deviation, 192
- I**
- IADC bit-classification system
 - fixed-cutter bits
 - bicenter bit, 330
 - bit's cross-sectional profile, 329
 - cutter/bottomhole pattern, 329
 - cutter size and density, 330–331
 - double-cone profile, 330
 - four-character coding system, 328
 - hydraulic design, 330
 - primary cutter type and body material, 328–329
 - roller-cone bits, 326–327
- IADC bit dull-grading system
 - bearings and seals, 333–335
 - cutting structure
 - dull characteristics, 332–333
 - dull location, 333–334
 - PDC and surface-set diamond bits, 332–333
 - roller-cone-bit, 332
 - subcategories, 331
 - gauge, 334–335
 - remarks category, 335–336
- ideal build curve, 462
- inclined wellbore, pipe
 - rotating pipe
 - bit walk, 563
 - distributed external moment, 563
 - drag force, 561
 - effective axial (tangential) force, 563
 - FBD, 561–562
 - magnitude, 562
 - moment, 563
 - pipe position angle, 562
 - pipe radius vector, 563
 - scalar components, 561–562
 - unit contact-force direction angle, 562
 - sliding mode, 559–561
 - straight segment, 3D wellbore, 559
 - unit binormal and tangent vector, 559
- internal pressure resistance
 - API burst calculation, 399
 - Barlow equation, 398–399
 - butress casing thread dimensions, 413, 416
 - casing long-thread dimensions, 413, 415
 - casing short-thread dimensions, 413–414
 - coupling internal yield pressure, 413
 - crack propagation, 399
 - diameter, coupling thread, 413
 - ductile rupture, 399–400
 - external-upset tubing thread dimensions, 413, 417
 - Lamé formula, 398
 - non-upset tubing thread dimensions, 413, 416
 - von Mises yield theory, 399
- International Association of Drilling Contractors (IADC), 325
- J**
- jarring string, 666–668
- jet bit nozzle size selection
 - maximum bit hydraulic horsepower, 203–205
 - maximum jet impact force, 205–206
 - maximum nozzle velocity, 203
- joint operating agreement (JOA), 5
- K**
- kelly, 585
- kickoff point (KOP), 451
- L**
- Lamé equations, 395
- latex cement, 149
- leakoff test (LOT), 63–64
- logging-while-drilling (LWD) tool, 90
- loss of stability, 437
- lost circulation
 - caverns, 626–627

diagnosis, 627–629
 induced fractures, 626
 natural fractures, 625–626
 permeable zones, 625–626
 prevention
 casing setting depth, 627
 ECD, 627
 mud system, 627
 shallow formations, 631
 solid LCM
 classification, 629
 fracture sizes, 629–630
 hard plugs, 630–631
 slurries and plugs, 630
 soft plugs, 630
 strength-enhancing chemicals, 631
 types, 629–630
 whole mud/cement slurry loss, 625
 lost-circulation additives, 158–159
 Lubinski's equation, 484

M

macrotortuosity, 555
 margin of overpull (MOP), 618
 maximum-distortion-energy theory. *See* Huber-von Mises-Hencky theory
 maximum permissible hole curvature, 608
 mechanical energy balance equation, 198
 mechanical specific energy (MSE), 365–366
 mechanistic modeling, 283, 294–295
 microfine cements, 148
 microspheres, 152
 microtortuosity, 555
 minimum-curvature/circular-arc method (MCM), 469–470
 minimum-curvature trajectory, 574–576
 modified thread compound, 412
 Mohr-Coulomb shear model
 critical collapse pressure, 67–68
 failure line, 67–68
 fracture angle, 68–69
 Leuders limestone, 67–68
 material properties, 68
 mechanical wellbore collapse, 68
 Moody friction factor, 250
 mud-clinging constant, 266

N

necking, 393
 Newtonian fluid models
 frictional pressure drop, eccentric annulus, 261
 laminar flow
 annular flow, 224–225
 pipe flow, 223–224
 shear stress, 223
 slot flow, 228–229
 rheological models
 pressure-velocity relationship, 209
 shear stress and rate, 208–209
 turbulent flow, 209–210
 viscosity, 208
 turbulent flow
 absolute pipe roughness, 248–249
 Buckingham Pi theorem, 246
 Colebrook function, 248
 Darcy-Weisbach friction factor, 250
 drillpipe diameter, 250
 Fanning equation, 248–249
 friction factor, 247–248
 kinetic energy, 247–248
 Moody friction factor, 250
 primary units, 246

rotary-drilling situations, 247
 shear stress, 247
 Stanton chart, 248–249
 non-Newtonian fluid models
 Bingham plastic model
 pipe flow, 231–234
 slot flow, 229–231
 power-law model
 flow rate, 238–239
 shear rate, 239
 shear stress, 236–237
 velocity, 237–238
 rheological models, 207–208
 turbulent flow
 Bingham plastic model, 251
 Herschel-Bulkley model, 255
 power-law model, 252–253
 nylon, 159

O

oil-based fluids (OBF), 88
 oil country tubular goods (OCTGs), 385, 395
 overkill, 652

P

paraformaldehyde and sodium chromate, 159
 parasitic pressure loss, 204
 percent mix, 150
 pipe sticking
 backoff procedures, 669
 blowout sticking, 658
 cemented sticking, 658
 depth intervals, 659
 differential-pressure sticking, 656–657
 fishing, 656
 freeing stuck pipe, 669–671
 hole bridging/caving, 659–660
 hydrostatic pressure reduction, 665–667
 inadequate-hole-cleaning sticking, 658
 keyseat sticking, 658
 low-water-loss muds, 660–661
 mechanical methods
 accelerator, 668
 bumper sub, 668
 drilling and fishing jars, 667
 hydraulic jars, 668
 jarring string, 666–668
 mechanical jars, 668
 mechanical sticking, 658–659
 mud friction coefficient, 661
 mud sticking, 658
 sand sticking, 658
 sloughing-hole sticking, 657–658
 spotting fluids, 664–666
 stuck section detection, 661–663
 time factor, 659
 torque and drag, 659
 undergauge hole sticking, 657
 walnut hulls, 661
 washover pipe, 669
 plastic-state shrinkage, 160
 plastic viscosity, 210, 215
 point-the-bit system, 508–509
 polycrystalline-diamond-compact (PDC) bits
 cutter design and manufacturing, 325
 design principles, 322–324
 dual-diameter bit, 314–315
 matrix, 324–325
 rock-shearing action, 312
 scraping/cutting surface, 312–313
 shape, 324

positive-displacement motor (PDM), 503–504

power-law fluids

frictional pressure drop, eccentric annulus, 262–264

laminar flow

flow rate, 238–239

shear rate, 239

shear stress, 236–237

velocity, 237–238

rheological models, 211–212

pozzolan-Portland cements, 147

pozzolans, 152

pressure-induced stresses, 609–610

pressure-while-drilling (PWD) tools, 219

progressive-cavity motors/helicopters. *See* positive-displacement motor

push-the-bit RSS, 508–509

R

radioactive tracers, 159

radius-of-curvature method (RCM), 467–469

Ragland method, 511–512

rate of penetration (ROP)

bit hydraulics, 357–358

bit tooth wear, 356–357

bit type, 352

drilling-fluid properties, 353–354

fixed-cutter bits, 362–363

formation characteristics, 352–353

operating conditions, 355–356

roller-cone bits

bit footage, 361

Bourgoyne-Young drilling model, 359–360

composite drilling variable, 361

curve-fitting techniques, 359

final tooth wear, 361–632

penetration-rate equations, 358

recommended friction models

Bingham plastic fluids, 256–258

Newtonian fluids, 255–256

power law fluids, 258–259

yield power law fluids, 259–260

recommended makeup torque, 613

resin and plastic cements, 149

roller-cone bits

bearing wear, 350–351

components

cone-cleaning-nozzle systems, 320–321

cone offset, 319

cone skidding, 319–320

grinding/crushing zone, 320

inserts, 320–321

journal angles, 319

journal-bearing system, 318

skidding/gouging action, 319

cone offset, 313

cutting-structure geometry, 313

design principles, 317–318

historical development, 311–312

IADC bit-classification system, 326–327

journal angle, 314

milled-tooth/insert bits, 312

monocone bits, 320–322

rock-failure mechanism

crater mechanism, 336–337

insert bits, 336

pseudoplastic craters, 338

rock fractures, 337

threshold force, 338

ROP

bit footage, 361

Bourgoyne-Young drilling model, 359–360

composite drilling variable, 361

curve-fitting techniques, 359

final tooth wear, 361–632

penetration-rate equations, 358

soft- and hard-formation bits, 313–314

two-cone bits, 320–322

wear equation, 348–349

rotary closed-loop steerable-tool (RCLS) system, 508–509

rotary drilling, 7–8

BHA, 31

bits (*see* rotary drilling bits)

cable drilling tools, 2–4

cable-tool rig, 2–3

circulating system

centrifugal pumps, 25

drilling-fluid-handling equipment (*see* drilling-fluid-handling equipment)

drilling-fluid path, 23

duplex double-acting pump, 23–24

duplex pump factor, 24

mud pumps, 23

pulsation dampeners, 25

pump suction design, 24–25

triplex single-acting pump, 24

wellbore, pressure, 28

development, 2–3, 5

drilling cost analysis

authorization, expenditure, 41, 45–46

casing, 45

learning curve, 42

time distribution, deepwater well, 46–47

drilling rig organization, 6–7

drillstring stabilizer, 31–32

hoisting system (*see* hoisting system)

HSE policy, 5

JOA, 5

land rigs

cantilever derrick, 9

mobile rigs, 7, 9

rig specification sheet, 9–11

Lucas spindletop well, 2, 4

marine drilling

CADA tool, 40–41

dynamic positioning system, 36–38

heave compensators, 38

MLH mud line suspension system, 38–39

mooring system, 36

pneumatic tensioning system, 37

SS10 subsea system, 39–40

thruster, 36–37

marine rigs

anchored drillship, 14–15

compliant towers, 12

deepwater rigs, 15–16

dynamic positioning system, 14

fixed-platform structure, 12–13

jackup rig, 12–13

semisubmersible drilling unit, 14

spar platform, 15

submersible offshore drilling barges, 10, 12

TLP, 15

offshore operations, 6

oil well, 1

operational standards, 6

rig classification, 7–8

rig power system, 16–17

rotary swivel, 29–30

rudimentary hand tools, 1

steam engine, 2, 4

topdrive, 29–30

well classification, 5

- well construction, 16
 - well-control system
 - annular preventer, 33–34
 - blind rams, 32
 - blowout, 32
 - BOP, 32–34
 - double ram preventer, 32–33
 - kick, 31
 - kill line, 33
 - well-monitoring system, 35–36
 - wildcat, 5
 - rotary drilling bits
 - bit-operation practices
 - BHA optimization, 368
 - drill-off tests, 368–369
 - WOB and rotation-speed optimization, 371–372, 376
 - economics
 - bit run termination, 366
 - bit selection, 364
 - break-even analysis, 365
 - cost calculations, 363
 - cost-per-foot calculation, 364
 - MSE, 365–366
 - run-cycle speed, 365
 - fixed-cutter bits (*see* fixed-cutter bits)
 - hybrid bits, 316
 - IADC bit dull-grading system (*see* IADC bit dull-grading system)
 - roller-cone bits (*see* roller-cone bits)
 - ROP
 - bit hydraulics, 357–358
 - bit tooth wear, 356–357
 - bit type, 352
 - drilling-fluid properties, 353–354
 - formation characteristics, 352–353
 - operating conditions, 355–356
 - wear mechanism
 - bearing wear, 350–351
 - cutter wear (*see* cutter wear)
 - rotary-steerable systems (RSSs), 507–509
- S**
- shear failure, 66
 - shear stress
 - laminar flow, pipes and annuli
 - annulus as slot, 221–223
 - cylindrical pipe flow, 219–221
 - vs. rate, 206–207
 - vs. time, 207–208
 - silica flour, 159
 - silicone thread compound, 412
 - simple-tangent build curve, 463
 - slip crushing, 614
 - sodium chloride, 156
 - sodium montmorillonite, 97
 - sodium silicates, 152
 - soft-string model
 - sliding-pipe model
 - boundary condition, 566
 - free-body diagram, 565
 - governing differential equation, 568
 - tripping operations, 565–566
 - unit contact force and direction angle, 566
 - torque calculations, 572–574
 - Sorel cement, 149
 - stability neutral point, 437
 - stabilizers, hole deviation control
 - adjustable-diameter (gauge) stabilizer, 491–492
 - BHA mechanics, curved wellbore
 - boundary-value problem, 498
 - fulcrum effect, 497
 - pendulum assemblies, 497
 - BHA mechanics, inclined hole
 - boundary conditions, 494–496
 - contact point, 497
 - dimensionless distance, 496
 - equilibrium configurations, 494
 - fulcrum and pendulum effect, 493
 - point stabilizer, 493
 - scaling parameters, 494
 - schematic diagram, 493
 - tilt angle, 496
 - communication, 491
 - complex BHA
 - build assembly, 499–500
 - building and dropping tendencies control, 500–501
 - continuous stabilization, 501
 - fixed rotary BHA, 500
 - hold-angle assembly, 499–500
 - pendulum/drop assembly, 499–500
 - primary purpose, 491
 - spiral drill collars, 493
 - types of, 491–492
 - Stanton chart, 248–249
 - steerable motors
 - actual field performance, 507
 - bent-housing motor, 506
 - bent sub, 505–506
 - definition, 506–507
 - disadvantages, 507
 - 500-ft wellbore section, slide-rotate sequence, 507–508
 - sliding and rotating mode, 507
 - tool-face angle, 507
 - straight inclined wellbore
 - axial effective force, 540
 - buildup bend
 - axial force, 546
 - drag force, 549
 - high tension, 543–544
 - low tension, 544
 - pipe effective force vs. MD, 546–547
 - under tension, 549
 - unit contact force, 551
 - unit contact force vs. MD, 546–547
 - curved wellbore, constant curvature, 541
 - drop-off bend
 - capstan force, 542
 - dynamic friction force, 543
 - small pipe element, 541–542
 - dynamic coefficient of friction, 541
 - FBD, 539–540
 - friction component, 540
 - helical buckling, 540
 - lateral, snaky/sinusoidal buckling, 540
 - static coefficient of friction, 541
 - wellbore friction factor, 540–541
 - sulfide stress cracking (SSC), 405
 - surface casing
 - beneficial effect, 426–427
 - burst design, 426
 - burst loads, 425
 - collapse loads, 425–426
 - directional wells, 428
 - loading condition, 425
 - lost-circulation zone, 427
 - tension loads, 425–426
 - surge pressure prediction
 - definition, 269
 - end of pipe boundary conditions, 270–272
 - pipe-annulus and pipe-to-bottomhole region, 269–270
 - pressure-drop calculation, 269
 - surface boundary conditions, 269–270
 - surge pressure solution, 272–273
 - swab pressures, 269

T

tangential method, 527
 tensile test
 brittle material, 393–394
 ductility, 393
 isotropy condition, 393
 nominal stress-strain curve, 392–393
 offset method, 393
 proportional limit, 392–393
 strain/work hardening, 393
 tension leg platform (TLP), 15
 terminal-angle method, 527
 thermally stable polycrystalline (TSP) bits, 312, 314, 330
 three-dimensional (3D) well profiles
 AAM, 465–466
 CBTM, 471
 CCBM, 472–473
 cluster, 464
 designer wells, Gullfaks field, 464–465
 MCM, 469–470
 offshore applications, 464
 RCM, 467–469
 torque and drag modeling
 drag-force calculations, 568–571
 equilibrium equations in 3D, 557–559
 force and moment equilibrium formulation, 563–565
 inclined wellbore, pipe, 559–563
 soft-string model (*see* soft-string model)
 stiff-string model, 574–576
 titanium drillpipe (TDP), 596
 torque, 603
 torque and drag modeling
 2D well profiles
 buckling consideration, 554
 pipe rotation, 551–553
 straight inclined wellbore (*see* straight inclined wellbore)
 tortuosity effect, 555–556
 3D well profiles
 drag-force calculations, 568–571
 equilibrium equations in 3D, 557–559
 force and moment equilibrium formulation, 563–565
 inclined wellbore, pipe, 559–563
 soft-string model (*see* soft-string model)
 stiff-string model, 574–576
 torsional stresses, 603–604
 true vertical depth (TVD), 450
 tungsten-carbide-insert (TCI) bits, 312, 320, 364

U

unit binormal vector, 523
 U-tube principle, 652–654

V

viscosity-control additives, 159
 von Mises stress, 601

W

waiting-on-cement (WOC) times, 171–172
 weight on bit (WOB), 585
 well control
 accumulators, 634–635
 blowout prevention, 631
 choke line, 633–634
 choke manifold, 634–635
 kicks
 causes, 636–638
 characteristics, 636
 controlling principles, 631
 definition, 635
 equivalent mud weight, 636
 pressure differential, 636
 warning signs, 638–639

preventer stack
 annular preventers, 632–633
 blind rams, 633
 diverters, 633–634
 preventer stack, 631–632
 ram-type preventers, 633
 variable-bore rams, 633
 shut-in procedure
 concurrent method, 645–647
 constant BHP methods, 646–647
 crew member responsibilities, 641–642
 diverter procedures, 641
 downhole stresses, 649–650
 driller's method, 645–646
 drilling kicks, 640–641
 gas kicks, 650–651
 hard vs. soft shut-in procedures, 639–640
 hole-geometry variations, 653, 655–656
 kick identification, 644–645
 kill-mud-weight calculation, 644–645
 kill-weight increment, 651–653
 procedural complexity, 649
 saltwater kicks, 650–652
 shut-in pressures, 642–644
 static casing-pressure curves, 651, 653
 surface pressures, 647–648
 time considerations, 647
 tripping kicks, 640–641
 U-tube principle, 652–654
 wait and weight method, 645–646
 subsea BOP, 631
 testing, 633
 well trajectory, survey data
 average-angle and tangential methods, 527
 directional/simply stations, 526
 inclination and azimuth angles, 526
 minimum-curvature method, 529–531
 RCM, 527–529
 two survey stations, 3D well path, 526
 whipstocks and jetting techniques, 477–479
 working-stress designs, 422, 433

Y

yield strength, 388
 yield stress
 Casson fluids, 215
 drilling fluids, cement slurries, 207–208
 Herschel-Bulkley fluids, 213